Designing α/β-peptide foldamers to target diverse protein surfaces

By

James William Checco III

A dissertation submitted in partial fulfillment of

the requirements for the degree of

Doctor of Philosophy

(Chemistry)

at the

UNIVERSITY OF WISCONSIN-MADISON

2015

Date of final oral examination: 8/19/2015

The dissertation is approved by the following members of the Final Oral Committee:
Samuel H. Gellman, Professor, Chemistry
Helen E. Blackwell, Professor, Chemistry
Katrina T. Forest, Professor, Bacteriology
William L. Murphy, Professor, Biomedical Engineering
Tehshik P. Yoon, Professor, Chemistry

Acknowledgements

I thank my advisor, Sam Gellman, for being an incredible mentor and role model. Sam has taught me so much about research, about problem solving, and about mentorship. Nearly every interaction I have had with Sam has inspired me to be the absolute best scientist and person that I can.

I thank my colleagues in the Gellman laboratory, who have been both mentors and friends. I especially thank former lab members Jay Steinkruger, Aaron Almeida, Holly Haase, and Lisa Johnson for their invaluable training and advice as I started my work in the lab. I thank Ross Cheloha, one of my very best friends, for all of the hours we've spent discussing research, and the hundreds of great ideas that have come from these conversations.

I thank my collaborators, who have worked with me to accomplish research goals that I would never have been able to complete on my own. In particular, Bill Murphy, Katy Forest, and Doug Fairlie have been amazing advisors, and my collaborations with their laboratories have taught me much about areas outside of the Gellman group's expertise.

Finally, I thank the undergraduate coworkers who I have mentored. Collaborating with these young scientists has been one of the most rewarding experiences of my life. I hope that I have taught them as much as they have taught me.

Collaborators
Dr. David Belair (UW-Madison)
Dr. Chelcie Eller (UW-Madison)
Dr. Douglas Fairlie (WEHI)
Prof. Katrina Forest (UW-Madison)
Prof. Ben Hackel (UMN)
Dr. Erinna Lee (WEHI)
Takayuki Miki (Kyoto University)
Prof. William Murphy (UW-Madison)
Prof. Ronald Raines (UW-Madison)

Gellman Lab Collaborators
Geoffrey Eddinger
Dr. Holly Haase
Dale Kreitler
Nicole Thomas

Undergraduate Colleagues
Alexander Chartier
Timothy Choi
Nicholas Rettko
Jeffrey Vinokur
Julia Wilson

Facilities and Instrumentation
Dr. Melissa Boersma – Peptide Synthesis
Dr. Darrell McCaslin – Biophysics Instrumentation Facility
Dr. Martha Vestling – Mass Spectrometry

Dissertation Editorial Assistance
Prof. Sam Gellman
Dr. David Belair
Geoffrey Eddinger
Marlies Hager
Nicholas Rettko
Julia Wilson

Dissertation Committee
Prof. Sam Gellman
Prof. Helen Blackwell
Prof. Katrina Forest
Prof. William Murphy
Prof. Tehshik Yoon

Funding
Biotechnology Training Program (BTP)
National Institutes of Health (NIH)

Table of Contents

Chapter 1: Designing molecules to target protein surfaces and modulate protein-protein interactions 1

1.1 Preface 2

1.2 Targeting protein surfaces and protein-protein interactions 3

1.3 Types of compounds that modulate protein-protein interactions 4

1.4 Targeting protein surfaces with small molecules 6

1.5 Targeting protein surfaces with large proteins 8

1.6 Targeting protein surfaces with peptides and protein scaffolds 10

1.6.1 Peptides derived from natural proteins 10

1.6.2 Peptides with stabilized secondary structures 11

1.6.3 Peptides derived from combinatorial libraries and mini-protein scaffolds 17

1.7 Targeting protein surfaces with foldamers 21

1.7.1 Foldamers 21

1.7.2 D-Peptides 22

1.7.3 Peptoids 23

1.7.4 β-Peptides 24

1.8 α/β-Peptide foldamers as mimics of α-peptides 28

1.8.1 Introduction to α/β-peptides 28

1.8.2 Structure-based design of α/β-peptides 28

1.8.3 Sequence-based design of α/β-peptides 29

1.8.4 Backbone rigidification of α/β-peptides with cyclic β-residues 34

1.8.5 α/β-Peptide agonists of Class B G-protein coupled receptors 36

1.8.6 Beyond α-helix mimicry 40

1.9 Limitations and challenges for α/β-peptides 42

1.10 References 44

Chapter 2: α/β-Peptide antagonists of the VEGF-VEGFR interaction derived from the Z-domain scaffold 64

2.1 Preface 66

2.2 Introduction 67

2.2.1 VEGF-VEGFR interaction and VEGF antagonists 67

2.2.2 α/β-Peptides targeting VEGF 69

2.2.3 Peptides that bind VEGF derived from the Z-domain scaffold 70

2.2.4 Previous efforts to truncate Z-domain derivatives 72

2.2.5 Z-VEGF as a starting point for α/β-peptide design 74

2.3 Design of a helix-loop-helix α-peptide targeting the VEGF receptor binding site 76

2.3.1 Analysis of Z-VEGF binding to VEGF by FP assay 76

2.3.2 Truncation of Z-VEGF 79

2.3.3 Exploration of salt bridging interactions to stabilize helix-loop-helix conformation 85

2.4 α/β-Peptide design using iterative non-natural residue incorporation 89

2.5 Crystal structure of α/β-peptide 2.37 bound to $VEGF_{8-109}$ 99

2.6 Protease susceptibility 103

2.6.1 Susceptibility to proteinase K degradation 103

2.6.2 Susceptibility to degradation in simulated gastric fluid (SGF) 105

2.7 Antagonism of VEGF signaling in cell culture 109

2.8 Conclusions 115

2.9 Future directions 118

2.10 Experimental methods 119

2.10.1 General 119

2.10.2 Peptide synthesis and purification 120

2.10.3 Protein expression and purification 121

2.10.4 VEGF fluorescence polarization assays 123

2.10.5 Circular dichroism spectroscopy 130

2.10.6 Crystallization 130
2.10.7 X-ray data collection and structure determination 131
2.10.8 Proteinase K susceptibility assay 134
2.10.9 Simulated gastric fluid (SGF) susceptibility assay 135
2.10.10 HUVEC proliferation assay 135
2.10.11 LIVE/DEAD viability assay 137
2.10.12 Peptide characterization 138
2.11 References 183

Chapter 3: Targeting diverse protein surfaces with α/β-peptides derived from the Z-domain scaffold 190
3.1 Preface 192
3.2 Introduction 193
3.2.1 Non-immunoglobulin scaffolds for targeting protein surfaces 193
3.2.2 The Z-domain scaffold 193
3.2.3 α/β-Peptide mimicry of the Z-domain scaffold 196
3.3 α/β-Peptide mimicry of Z-IgG 198
3.3.1 Design of α/β-peptide mimics of Z-IgG 198
3.3.2 Evaluation of binding to IgG by ELISA 200
3.3.3 Attempts at co-crystallization 204
3.3.4 Preliminary pharmacokinetics studies 205
3.4 α/β-Peptide mimicry of Z-TNFα 209
3.4.1 Design of α/β-peptide mimics of Z-TNFα 209
3.4.2 Evaluation of binding by competition ELISA 210
3.5 Selectivity of α/β-peptides 211
3.6 α/β-Peptide mimicry of Z-HER2 213
3.6.1 Background 213

3.6.2 Initial designs and evaluation 216
3.6.3 Final designs 222
3.6.4 Proteolysis 224
3.6.5 In vivo tumor imaging 226
3.7 Attempts at α/β-peptide mimicry of Z-EGFR 230
3.8 Conclusions 233
3.9 Future directions 236
3.10 Experimental methods 239
3.10.1 General 239
3.10.2 Peptide synthesis and purification 239
3.10.3 IgG ELISA 240
3.10.4 Crystallization 245
3.10.5 Pharmacokinetics in mice 247
3.10.6 TNFα-TNFR1 competition ELISA 260
3.10.7 $VEGF_{165}$ competition FP 262
3.10.8 HER2 competition ELISA 262
3.10.9 Circular dichroism (CD) spectroscopy 265
3.10.10 Proteolysis 265
3.10.11 In vivo tumor imaging 266
3.10.12 EGFR competition ELISA 266
3.10.13 Peptide characterization 268
3.11 References 312

Chapter 4: Optimization and mechanistic evaluation of α- and α/β-peptide tumor necrosis factor-α antagonists 317
4.1 Preface 319
4.2 Introduction 320

4.2.1 Tumor necrosis factor-α (TNFα) signaling 320
4.2.2 Antagonists of the TNFα-TNFR interaction 321
4.2.3 α/β-Peptides targeting TNFα 323
4.2.4 A note on affinity measurements 324
4.3 Optimization of α/β-peptides derived from Z-TNFα 325
4.3.1 Initial optimization attempts 325
4.3.2 α/β-Peptide analogues lacking a disulfide constraint 328
4.3.3 Exploring alternative disulfide positions and final designs 330
4.4 Protease susceptibility 333
4.5 Z-TNFα is dependent on TWEEN20 for binding to TNFα 335
4.6 Truncation of other Z-domains targeting TNFα 345
4.7 Z-domain analogues synergize with TWEEN20 to block TNFα-mediated cell death 348
4.8 Z-domain analogues synergize with SPD304 351
4.9 Conclusions 356
4.10 Future directions 361
4.11 Experimental methods 363
4.11.1 General 363
4.11.2 Peptide synthesis and purification 364
4.11.3 TNFα-TNFR1 competition ELISA 364
4.11.4 α/β-Peptide 3.5-TNFα competition ELISA 370
4.11.5 IgG1-κ competition ELISA 371
4.11.6 Circular dichroism (CD) spectroscopy 371
4.11.7 Protease digestion assay 371
4.11.8 WEHI-13VAR cell viability assays 372
4.11.9 Monitoring the TNFα oligomer by SEC 374
4.11.10 Peptide characterization 377

4.12 References 402

Chapter 5: Attempts to design membrane-permeable analogues of a high-affinity α/β-peptide targeting Bcl-2 protein-protein interactions 405

5.1 Preface 407

5.2 Introduction 408

5.2.1 Bcl-2 family protein-protein interactions 408

5.2.2 α/β-Peptides targeting Bcl-2 proteins 411

5.2.3 Commonly utilized methods for increasing the membrane-permeability of peptides 413

5.3 Novel cyclic β-amino acid residues with labile ester side chains 415

5.4 Bim-derived α/β-peptides bearing J-amino acid residues for cell permeability 418

5.4.1 Initial α/β-Peptide designs 418

5.4.2 Characterization of α/β-peptides 419

5.5 Evaluation of cellular uptake by confocal microscopy 424

5.6 Evaluation of activity by cell-based assays 427

5.6.1 Initial cell killing assays 427

5.6.2 Second generation α/β-peptide designs 435

5.6.3 MDA-MB-435 cell-killing experiments 436

5.7 Conclusions 438

5.8 Future directions 442

5.9 Experimental methods 443

5.9.1 General 443

5.9.2 Synthesis of J-amino acid monomers 444

5.9.3 Peptide synthesis and purification 462

5.9.4 Bcl-x_L competition FP assay 463

5.9.5 Chemical hydrolysis of α/β-peptide 5.2 464

5.9.6 Solubility experiments 464

5.9.7 Live-cell confocal microscopy 465
5.9.8 Cell-killing assays 466
5.9.9 Peptide characterization 470
5.10 References 492

Chapter 6: α/β-Peptide mimics of cell-penetrating peptides targeting intracellular protein-protein interactions with activity in living cells 498
6.1 Preface 500
6.2 Introduction 501
6.2.1 BH3 domains 501
6.2.2 "Stapled" α-helical mimics of BH3 domains 502
6.2.3 BimSAHB is a crosslinked analogue of the Bim BH3 domain 504
6.2.4 α/β-Peptide mimics of "stapled" peptides 504
6.3 Design and characterization of α/β-peptide mimics of BimSAHB 506
6.3.1 α/β-Peptide design 506
6.3.2 Protein binding by SPR 508
6.3.3 Structural analysis in solution by circular dichroism 509
6.3.4 Crystal structures 510
6.4 Activity in cell culture 512
6.4.1 Cytochrome c release assay from permeabilized cells 512
6.4.2 Cell killing assays 514
6.4.3 Effect of serum on cell killing effect 520
6.4.4 Cytochrome c release assay on unpermeabilized cells 521
6.4.5 Analysis of cellular uptake by live-cell confocal microscopy 522
6.5 Protease susceptibility 526
6.6 Conclusions 527
6.7 Future directions 533

6.8 Experimental methods 534

6.8.1 General 534

6.8.2 Peptide synthesis and purification 539

6.8.3 Recombinant protein expression and purification 540

6.8.4 Surface plasmson resonance (SPR) competition assays 540

6.8.5 Circular dichroism 540

6.8.6 Crystallography 542

6.8.7 Crystal diffraction data collection and structure determination 543

6.8.8 Cytochrome c release assays 545

6.8.9 Cell killing assays 545

6.8.10 Analysis of cell killing by live-cell confocal microscopy 546

6.8.11 Protease susceptibility assay 551

6.8.12 Peptide characterization 552

6.9 References 567

Chapter 1: Designing molecules to target protein surfaces and modulate protein-protein interactions

1.1 Preface

Molecules that bind selectively to specific sites on proteins are useful for probing protein function, for the treatment of diseases caused by misregulated protein-protein interactions, and as diagnostic tools for biomarker detection. However, developing molecules to adequately bind to surfaces at protein-protein interaction interfaces is challenging due to the relatively large size and irregular shape of many of these target protein surfaces. The primary purpose of this chapter is to highlight some of the strategies currently pursued to develop agents that bind protein surfaces and modulate protein-protein interactions. I discuss several different categories of molecules that can target protein surfaces, highlight important examples, and discuss some of the advantages and disadvantages for each category. The latter part of this chapter describes advances in the design of "α/β-peptide" foldamers as a source of high-affinity and protease-resistant molecules to target protein surfaces, along with some of the current limitations and challenges for the α/β-peptide approach. The research projects described in the remaining chapters of this dissertation aim to address these limitations, with the ultimate goal of developing strategies to design α/β-peptides to target a wide variety of protein surfaces.

1.2 Targeting protein surfaces and protein-protein interactions

Proteins play essential roles in almost all biological processes, where they perform diverse functions ranging from signal transduction to the catalysis of complex chemical transformations. Proteins often associate with other proteins, and these protein-protein interactions are critical for normal biological function. Many disease states are associated with the overexpression of particular proteins or misregulated protein-protein interactions. Molecules that can selectively bind to specific surfaces on target proteins may modulate protein-protein interactions for the treatment of disease or serve as diagnostic tools for biomarker detection (Figure 1.1).[1-6]

The interfaces at protein-protein interactions are often very large, usually with >1500 $Å^2$ solvent accessible surface area buried upon complex formation.[7-10] Furthermore, many protein surfaces are relatively flat and irregularly shaped, and are often devoid of "hot spot" regions that can be easily targeted. Designing agents that can selectively modulate protein-protein interactions is a significant challenge due to the large contact surfaces involved.[3] Small molecules, the traditional choice for drug compounds, often fail to target protein-protein interactions due to their size.[3, 11, 12] In contrast, large proteins, such as antibodies, can often recognize protein surfaces with high affinity and selectivity because they can make many more productive contacts over a larger surface. However, large proteins have a number of disadvantages, particularly a high cost of production.[13, 14] Medium-sized peptides can often be developed to bind to protein surfaces with high affinity and selectivity, but also suffer from significant disadvantages, such as rapid degradation by protease enzymes and an inability to cross cell membranes.[15-17] These disadvantages severely limit the utility of peptides in living systems.

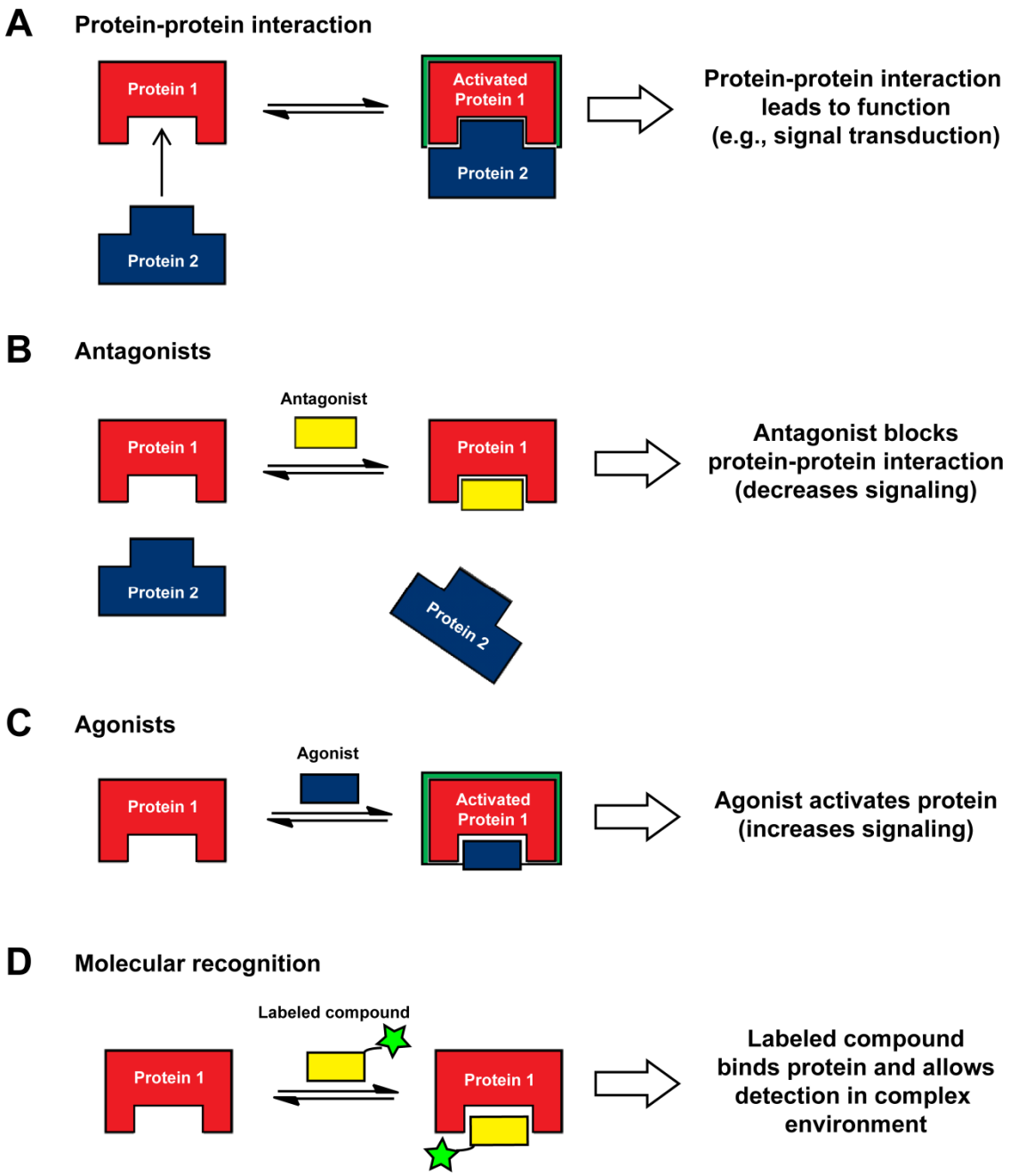

Figure 1.1 Cartoon representation of (A) a protein-protein interaction, (B) blocking a protein-protein interaction with an antagonist, (C) activating a protein with an agonist, and (D) detecting a protein with a labeled compound.

1.3 Types of compounds that modulate protein-protein interactions

Molecules that target protein surfaces and/or modulate protein-protein interactions can be useful for a number of applications. First, compounds that modulate protein-protein interactions can be valuable research tools to interrogate normal or misregulated protein

function. Second, as mentioned above, compounds that can selectively modulate misregulated protein-protein interactions can serve as therapeutic agents for the treatment of disease. Below, I highlight three important ways in which molecules can interact with proteins: as antagonists of protein-protein interactions, as agonists of protein signaling, or as diagnostic tools for protein detection.

Antagonist compounds block protein-protein interactions, generally by binding at the interaction surface of one binding partner. In a therapeutic context, antagonists can be used to treat disease states caused by increased signaling through a given protein-protein interaction. For example, overexpression of the pro-angiogenic protein vascular endothelial growth factor (VEGF) is associated with several forms of cancer and age-related wet macular degeneration.[18-20] In both of these diseases, increased signaling of VEGF through binding to its cell-surface receptors (VEGFRs) leads to aberrant and deleterious blood vessel formation. Blocking the VEGF-VEGFR interaction with a molecule that binds to one of these proteins at the interaction interface (and thus prevents signaling) is a strategy that can be used for therapeutic treatment.[20-22] Similarly, increased signaling of the cytokine tumor necrosis factor-α (TNFα) is associated with a number of autoimmune diseases, and molecules that bind to TNFα to block the binding to its receptors are used to treat these disorders.[23-25] In addition to blocking misregulated signaling in human cells, antagonists of protein-protein interactions can also be used to prevent the formation of other unwanted protein complexes, such those utilized by viruses (e.g., HIV) for the infection of host cells.[26, 27]

Agonist compounds act on protein receptors to increase signaling, often by mimicking the native protein binding partner. Agonists of protein receptors can be used to treat diseases caused by insufficient signaling through a particular protein-protein interaction. For example,

parathyroid hormone (PTH) interacts with its receptors (PTHRs) as the primary regulator of calcium homeostasis.[28, 29] Patients who suffer from osteoporosis have decreased bone density, and stimulation of bone growth can be achieved by activating PTHRs with agonists of these receptors.[30] Similarly, the hormone glucagon-like peptide-1 (GLP-1) interacts with its receptor (GLP-1R) to play an important role in insulin regulation. Agonists of GLP-1R, like the gila monster-derived peptide exendin-4 (Exenatide),[31] are used to treat type 2 diabetes.[32]

In some cases, simply knowing the relative expression level or localization of a protein can aid in the diagnosis of disease, with direct applications for treatment. For example, human epidermal growth factor receptor 2 (HER2) is overexpressed in 25-30% of breast cancer metastases.[33, 34] HER2-overexpressing tumors often respond favorably to treatment by anti-HER2 antibodies (e.g., Herceptin),[35, 36] but these drugs are ineffective against tumors that do not express high levels of HER2. Thus, knowing the level of HER2 expression of a tumor can be valuable for determining if the patient will respond to Herceptin treatment. A molecule that binds selectively to the surface of HER2 and can be detected by imaging can be a valuable tool for non-invasive evaluation of HER2 expression levels and localization of tumors.[37-39]

1.4 Targeting protein surfaces with small molecules

Small molecules are the traditional choice for drug compounds because small molecules are generally cheaper to make and often have better pharmacokinetic properties relative to biomacromolecules.[3, 11, 12] Furthermore, small molecules are attractive as therapeutics because they often have high oral bioavailability and can readily cross cell membranes to reach intracellular targets; neither of these properties is generally available to biologics.[15, 40] However, small molecules generally fail to effectively block protein-protein interactions because of the large size of many protein interaction interfaces. For example, a ligand with molecular weight of

500 Da can cover ~300 Å^2 on a protein surface,[40] but the typical protein-protein interaction buries >1500 Å^2 of surface area upon complex formation.[7-10] In contrast, for other drug targets, such as enzyme active sites, small molecules can relatively easily be designed to bind and block activity. Despite the difficulty in developing small molecule protein-protein interaction inhibitors, there have been several impressive successes in this field. Examples of small molecules targeting two protein-protein interactions are given below, although additional proteins have been successfully targeted with small molecules, as reviewed elsewhere.[3, 11, 12]

The B cell lymphoma-2 (Bcl-2) family of proteins is critically involved in regulating apoptosis (programmed cell death) in cells.[41-43] The Bcl-2 family is made up of both pro-apoptotic and anti-apoptotic family members, and carefully regulated interactions between proteins within this family control the initiation of apoptosis in response to certain damage signals. Some cancers evade apoptosis by overexpressing anti-apoptotic proteins in the Bcl-2 family, which bind and inhibit the action of the pro-apoptotic proteins. Antagonism of the interaction between anti-apoptotic and pro-apoptotic Bcl-2 family members may constitute a viable strategy to reactivate apoptosis and kill cancer cells.[44, 45] Pro-apoptotic Bcl-2 family proteins contain an α-helical BH3 domain that engages a hydrophobic cleft on the anti-apoptotic proteins, and several small molecules have been discovered that can bind in this hydrophobic cleft and antagonize these protein-protein interactions. In 2005, Oltersdorf et al. reported ABT-737 (Figure 1.2), a small molecule discovered through NMR-based screening of fragments that bound anti-apoptotic proteins Bcl-x_L, Bcl-2, and Bcl-w, antagonized Bcl-2 family proteins *in vitro*, and induced the regression of tumors in animal models.[44] An optimized analogue of ABT-737, ABT-263 (Navitoclax),[46] is currently in clinical trials for the treatment of various

cancers (Figure 1.2).[47, 48] A related compound, ABT-199, which selectively targets Bcl-2, is also in clinical trials.[49, 50]

Another interesting example of small molecule antagonism of a protein-protein interaction is the small molecule SPD304 (Figure 1.2), which blocks TNFα signaling through its receptors via an unexpected mechanism of action.[51] The active form of the inflammatory cytokine TNFα is a non-covalent homotrimer. SPD304 blocks TNFα signaling by binding at the TNFα oligomerization interface and dissociating the trimer, rather than directly blocking binding to the receptor. This example highlights that mechanisms of action alternative to directly blocking receptor binding, such as oligomer dissociation or binding at allosteric sites,[52] may be useful for blocking deleterious protein signaling.

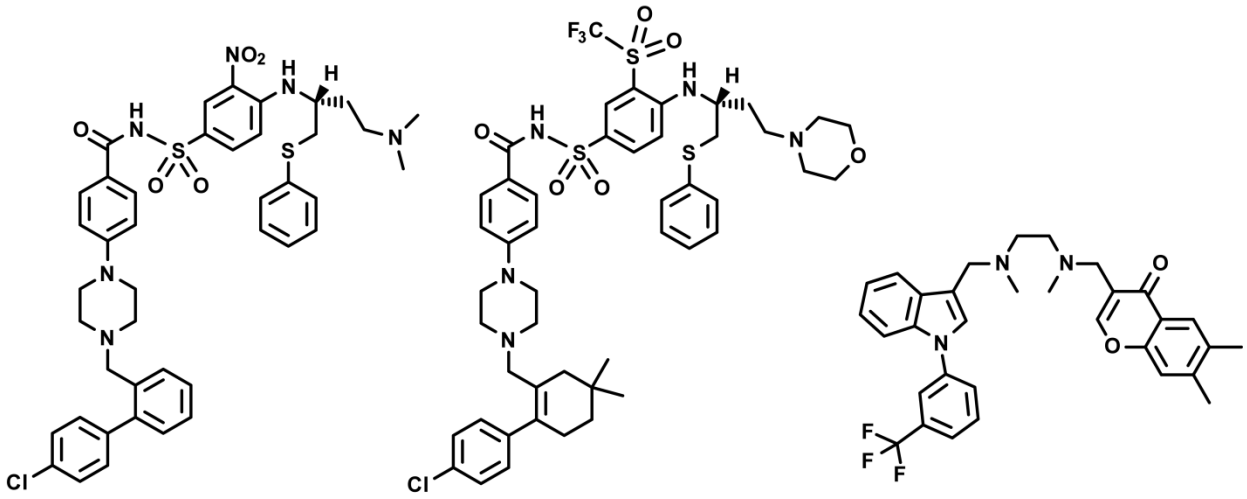

Figure 1.2 Examples of small molecule inhibitors of protein-protein interactions. ABT-737 and ABT-263 target Bcl-2 family anti-apoptotic proteins.[44, 46] SPD304 targets TNFα and dissociates the active TNFα homotrimer.[51]

1.5 Targeting protein surfaces with large proteins

Perhaps one of the most intuitive ways to target a large protein surface is to use another large protein, such as a natural interaction partner (e.g., a fragment of the native receptor) or an

antibody directed against the target surface.[13, 53, 54] Indeed, this strategy has been one of the most successful to date for the development of therapeutic inhibitors of protein-protein interactions, with a number of large protein drugs currently approved for clinical use. For example, bevacizumab (antibody),[55] ranibizumab (antibody fragment),[56] and afibercept (engineered receptor fragment)[57, 58] are protein antagonists of the VEGF-VEGFR interaction approved to treat various cancers or wet age-related macular degeneration.[13, 19, 20, 22] Similarly, adalimumab (antibody), infliximab (antibody), and etanercept (receptor fragment-Fc fusion) are currently approved as TNFα-TNFR antagonists to treat inflammatory diseases such as rheumatoid arthritis and Crohn's disease.[13, 23, 24]

Advances in protein engineering technologies have allowed for redesigning of natural protein ligands with impressive new functions.[53] Naturally occurring VEGF is a homodimeric molecule with two equivalent receptor-binding sites that must both bind a molecule of VEGFR to initiate angiogenesis through receptor dimerization. In a recent example, Cochran et al.[59] altered one of the receptor-binding sites in a single-chain VEGF variant to bind $\alpha_v\beta_3$ integrin, a cell-surface receptor that is known to play a critical role in angiogenesis,[60] but left the other VEGF receptor binding site intact.[59] The resulting VEGF variants, which bound both VEGFR and $\alpha_v\beta_3$ integrin, were antagonists for both pro-angiogenic receptors. One such dual-specific VEGF variant almost completely blocked VEGF-mediated blood vessel formation in Matrigel plugs implanted in mice.[59, 61]

Well-folded proteins generally have very high affinity for protein targets and are fairly stable in biological systems. However, large proteins have a number of disadvantages. Many large proteins are difficult to produce due to extensive post-translational modifications that are often required for activity, and often have a high cost of production. Furthermore, proteins can

have poor solubility, potential immunogenicity, low storage stability, and low membrane permeability.[13, 14]

1.6 Targeting protein surfaces with peptides and protein scaffolds

1.6.1 Peptides derived from natural proteins

Medium-sized peptides derived from natural interaction partners offer a source for the development of ligands targeting a protein surface with high affinity and selectivity.[15, 62, 63] For protein-protein interactions that are mediated primarily through a helical interaction, a synthetic peptide corresponding to the helical segment of one protein partner can be used to block that protein from engaging its natural binding site. One successful example of this strategy is the 36-residue polypeptide enfuvirtide (Fuzeon), derived from the C-heptad repeat (CHR) region of HIV membrane protein gp41, which is clinically approved to treat HIV.[26, 27, 64] The formation of a six-helix bundle involving the CHR and the N-heptad repeat regions (NHR) of gp41 is a critical step in virus-host cell membrane fusion, which is essential for infection of the host cell. Enfuvirtide, which mimics the helical conformation of the CHR, binds to the NHR and prevents gp41 from forming the correct six-helix bundle required for infection.

Class B G-protein coupled receptors (GPCRs) are cell-surface receptors that are activated by peptide hormones.[65] Thus, known ligands of Class B GPCRs can act as starting points targets for deriving agonists of these receptors. For example, the synthetic peptide corresponding to residues 1-34 of PTH, known as teriparatide (Forteo), is approved for the treatment of osteoporosis.[30] Teriparatide mimics the active portion of PTH and acts as an agonist of PTHR signaling, and can increase bone density when injected. Similarly, exendin-4

(Exenatide), a 39-residue synthetic analogue of a peptide from gila monster siliva that acts as an agonist of GLP-1R,[31] is currently approved to treat type 2 diabetes.[32]

Peptides derived from the α-helical BH3 domains of Bcl-2 proteins have been studied as a potential source of antagonists of this family of protein-protein interactions for the treatment of cancer. Indeed, synthetic peptides of ~20 residues can be used to antagonize Bcl-2 protein-protein interactions in protein-binding experiments by occupying the BH3 domain-binding groove on anti-apoptotic Bcl-2 proteins.[66, 67] However, the Bcl-2 family of proteins function inside the cell, and unmodified peptides derived from BH3 domains cannot cross cell membranes.

Although medium-sized peptides derived from natural proteins can offer high-affinity ligands for protein surfaces, they suffer from significant disadvantages. Like large proteins, peptides cannot cross cell membranes. This inability to enter cells limits their applications exclusively to extracellular protein targets. In addition, unmodified peptides are generally not orally bioavailable. Finally, medium-sized peptides often suffer from a high susceptibility to protease degradation due to their low conformational stability. This lowers the half-life of peptides *in vivo*, and is a significant barrier to their use in biological systems.[15-17]

1.6.2 Peptides with stabilized secondary structures

The α-helix secondary structure plays an important role in many protein-protein interactions,[68, 69] and compounds that mimic helices are attractive sources of ligands to modulate these interactions.[2, 70] An α-helical peptide may be one the of most obvious sources of a "helix mimic", but most short peptides are not well folded in solution, which can limit their affinity to protein surfaces. Stabilizing the secondary structure of a peptide ligand can increase its affinity to a target protein relative to flexible counterparts, primarily by decreasing the entropic penalty

associated with folding into the conformation required for binding.[71, 72] Furthermore, because proteases act only on unfolded polypeptide chains,[73] stabilizing the secondary structure of a peptide can decrease susceptibility to protease degradation.[71, 72] Thus, stabilizing the secondary structure of peptides targeting protein surfaces represents an attractive route to deriving compounds with favorable properties that bind target proteins.

There are several methods for stabilizing helical secondary structures. For instance, incorporating residues with high helix propensity, such as alanine or the non-proteinogenic 2-aminoisobutyric acid (Aib),[74] can increase helical structure. Additionally, the incorporation of charged residues that form salt bridges in the folded peptide can increase the conformational stability of short peptides.[75, 76] As an example, the incorporation of several alanine residues, along with pairs of glutamate and arginine residues at *i,i+4* positions, significantly increased the helical content of a peptide derived from the CHR of gp41, as determined by circular dichroism.[77] Importantly, this helix-stabilized peptide (called **T-2635**) was 3600-fold more active than enfuvirtide at inhibiting infection by an enfuvirtide-resistant strain of HIV.

Stabilizing peptide secondary structure through a covalent crosslink is commonly used to increase affinity and decrease protease stability. One example of this approach is side chain crosslinking, in which two amino acid residues are covalently connected through their side chains. Numerous crosslinking functionalities have been employed to stabilize helical structures,[78] such as lactam bridges derived from the side chains of naturally occurring residues (e.g., lysine and glutamate),[79-81] thioether bridges formed by alkylation of cysteine residues with crosslinking groups,[82] and triazole bridges formed by the Huisgen 1,3-dipolar cycloaddition reaction (Figure 1.3).[83, 84]

Crosslinking of unnatural residues bearing alkene side chains using olefin metathesis, first described by Blackwell and Grubbs, has achieved particular attention as a helix-stabilization strategy (Figure 1.3).[85, 86] Although the first examples of this peptide crosslinking approach utilized alkene ethers (e.g., O-allyl serine residues),[85] Verdine et al. used α,α-disubstituted "all-hydrocarbon" alkene residues to crosslink short peptides in a helical conformation.[87] This strategy, which promotes a helical conformation both from the restricted torsion angles of the α,α-disubstituted residues[88] and from the covalent crosslink, decreased the susceptibility of the resulting "stapled" peptides to protease degradation. In a follow-up report from the same group, this crosslinking strategy was used to design "stapled" analogues of the helical BH3 domain from the Bcl-2 pro-apoptotic protein Bid.[89] One crosslinked Bid analogue entered Jurkat leukemia cells and induced apoptosis, showing that the crosslinked Bid peptide could antagonize Bcl-2 protein-protein interactions in living cells. This result was extremely surprising, as peptides and proteins are usually unable to cross cell membranes.

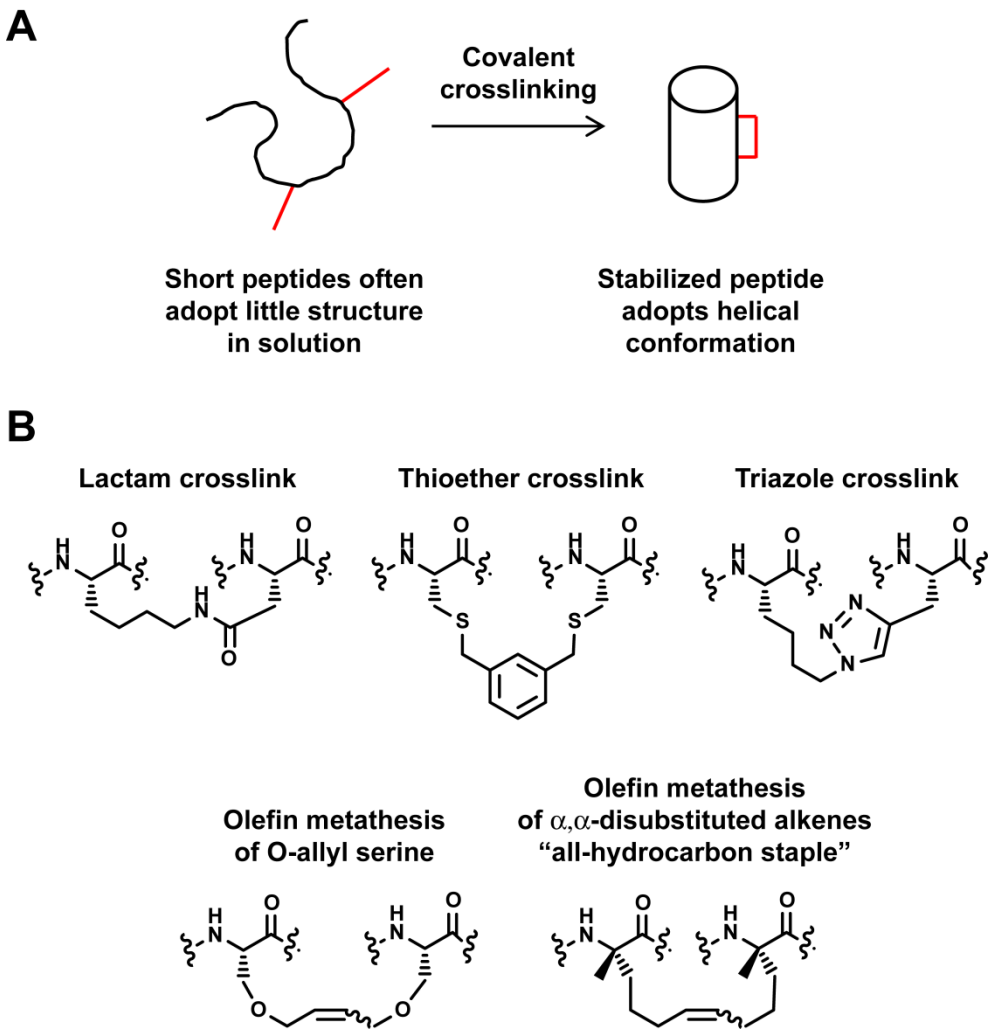

Figure 1.3 Covalent crosslinking can increase the conformational stability of helical peptides. (A) Cartoon representation of side chain crosslinking stabilizing a helical peptide. (B) Examples of different types of side chain crosslinks.

The all-hydrocarbon crosslinking strategy has been utilized to design crosslinked analogues of other helical peptides to modulate a variety of protein-protein interactions, and some of these crosslinked analogues have been shown to enter cells.[90-98] In a recent example, a crosslinked peptide derived from the protein MAML1 was designed to antagonize activation of the NOTCH transcription factor complex. Treatment with this stapled MAML1 analogue reduced the progression of a mouse model of T-cell acute lymphoblastic leukemia (T-ALL), a form of cancer that is characterized by inappropriate NOTCH activation.[99] Similarly, crosslinked

peptides derived from the protein BCL9 were designed to disrupt the BCL9-β-catenin complex, a transcriptional regulator in the Wnt signaling pathway associated with several cancers.[100] As designed, the lead crosslinked BCL-9 analogue from these studies antagonized the BCL-9-β-catenin interaction, had a 26-fold increased stability to chymotrypsin degradation relative to an unstapled analogue, and suppressed tumor growth in two Wnt-driven mouse models of cancer.

In 2010, Walensky et al. designed "double-stabled" crosslinked antagonists of HIV membrane fusion derived from the CHR of gp41 bearing two hydrocarbon crosslinks.[101] Consistent with other examples involving multiple side chain crosslinks,[80] this report found that the incorporation of two crosslinks significantly stabilized helical structure and reduced protease susceptibility relative to peptides containing zero or one side chain crosslink.[101] One "double-stapled" analogue was found to be ~80-fold more resistant to chymotrypsin degradation than was enfuvirtide, the α-peptide antagonist of gp41 signaling used to treat HIV. A variation of this approach, termed helical peptide "stitching", has recently been described, in which two hydrocarbon crosslinks emerge from a common attachment point.[102] Stitched helices were shown to have higher helical content, greater protease stability, and greater cellular permeability than peptides with single crosslinks or unmodified analogues.[102, 103] Finally, Grossmann et al. recently showed that hydrocarbon crosslinking can stabilize a peptide that adopts an irregular secondary structure (in contrast to the helical structures described above) and increase binding to its protein target ~20-fold.[104] This last example highlights the possibility that side chain crosslinking can be used for the stabilization of non-helical secondary structures to provide benefits to a variety of different peptides targeting protein-protein interactions.

At present, it is not clear how the hydrocarbon crosslink confers membrane permeability. The high hydrophobicity of the "staple" likely plays a critical role in the association of these peptides with hydrophobic cell membranes. Studies suggest that crosslinked peptides of this type enter cells through endocytosis rather than passive diffusion.[89, 103] However, the incorporation of an all-hydrocarbon crosslink does not guarantee increased potency or membrane permeability, and many peptides containing hydrocarbon crosslinks are not membrane permeable.[81, 91, 95, 105] Furthermore, some hydrocarbon "stapled" peptides have significant disadvantages, such as low aqueous solubility and inactivation in the presence of serum.[95, 98, 106] The crosslink can also make direct contacts with the target protein, which may alter the peptide's recognition properties and selectivity.[107] All-hydrocarbon side chain crosslinks, and their role in helix stabilization and membrane permeability, are explored in Chapter 6.

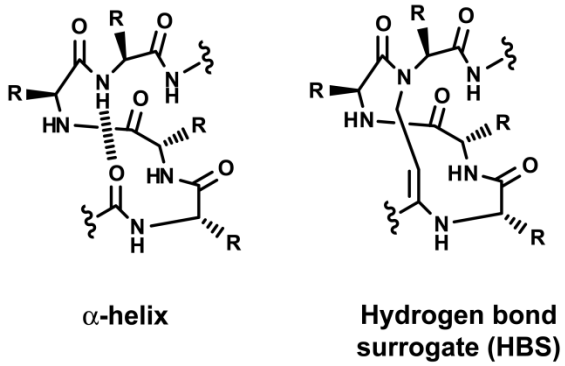

Figure 1.4 The hydrogen bond surrogate (HBS) strategy for helix stabilization replaces a backbone hydrogen bond (dashed line) in a natural α-helix (left) with a carbon-carbon bond through olefin metathesis (right). Figure adapted from Chapman et al.[108]

Another strategy for stabilizing short helical peptides, pioneered by Arora et al., is the hydrogen-bond surrogate (HBS), in which a *i,i+4* backbone hydrogen bond is substituted with a carbon-carbon bond formed by olefin metathesis (Figure 1.4).[108, 109] Covalent connection in the

HBS strategy can increase helical content of the resulting peptide by nucleating helix formation, leading to high affinity peptides with a decreased susceptibility to protease degradation relative to unconstrained analgoues.[110] One key advantage of HBS peptides for targeting protein surfaces is that side chain functionality is not altered, in contrast to side chain crosslinking. The HBS approach has been applied to target a number of therapeutically-relevant targets, including anti-apoptotic protein Bcl-x_L,[111] HIV membrane fusion protein gp41,[112] and MDM2 (which sequesters and inactivates tumor-suppressing protein p53).[113, 114] In a recent example, HBS peptides were designed based on a peptide from hypoxia-inducible factor 1α (HIF-1α), a protein which plays a role in the expression of certain oncogenes.[115] These HBS peptides bound co-activator protein p300, and blocked its interaction with HIF-1, inhibiting transcription of target genes. In a follow-up report, another HBS peptide targeting p300 was shown to suppress tumor growth in a mouse xenograft model of renal cancer.[116] Finally, a HBS peptide derived from the guanine nucleotide exchange factor Sos inhibited the Ras-Sos interaction in living cells.[117] Because many of these examples target protein-protein interactions inside cells, the activity of these HBS peptides in cell and animal models indicates that some HBS peptides are able to cross cell membranes and reach intracellular targets.

1.6.3 Peptides derived from combinatorial libraries and mini-protein scaffolds

An alternative to deriving a high-affinity peptide targeting a specific protein surface from a natural binding partner is to derive a peptide *de novo*. One way to obtain novel high-affinity peptides is through selection from combinatorial libraries.[15, 118] In this approach, large libraries of randomized peptide sequences, created either from combinatorial genetic libraries (e.g., using phage display)[119-122] or from combinatorial synthesis,[123, 124] are screened for their ability to bind to a particular target. “Hit” compounds that bind the target protein are pulled

out of the library mixture, often by affinity-based selection.[122] For example, Cunningham et al. used phage display to derive peptides that bound VEGF at the receptor-binding site and could act as antagonists of VEGF signaling.[125] The peptide with the highest affinity for VEGF, **v114**, attenuated VEGF-induced proliferation of human umbilical vein endothelial cells (HUVECs). An NMR structure of a related peptide, **v107**, in complex with $VEGF_{8-109}$ showed that **v107** binds to the receptor-binding site, as intended.[126] In a more recent example, Keating et al. used yeast display and selection to identify variants of the Bim BH3 domain that bound selectively to anti-apoptotic protein Mcl-1, an important Bcl-2 family target for which there are currently no inhibitors in the clinic.[127]

Mini-protein scaffolds are small proteins that adopt well-defined tertiary structures that either tolerate side chain substitution of multiple residues on a defined surface.[128-134] These scaffolds are usually derived from small, monomeric proteins or from isolated domains from a larger protein.[129] Combinatorial libraries of peptides derived from a particular scaffold can be designed such that each peptide in the library retains the overall three-dimensional fold of the scaffold while displaying randomized segments (e.g., surfaces or loops) that may bind to a target protein (Figure 1.5). This randomization and selection against new target proteins is somewhat analogous to the generation of antibodies: different antibodies share the same overall fold but display variable loop regions that determine binding specificity.

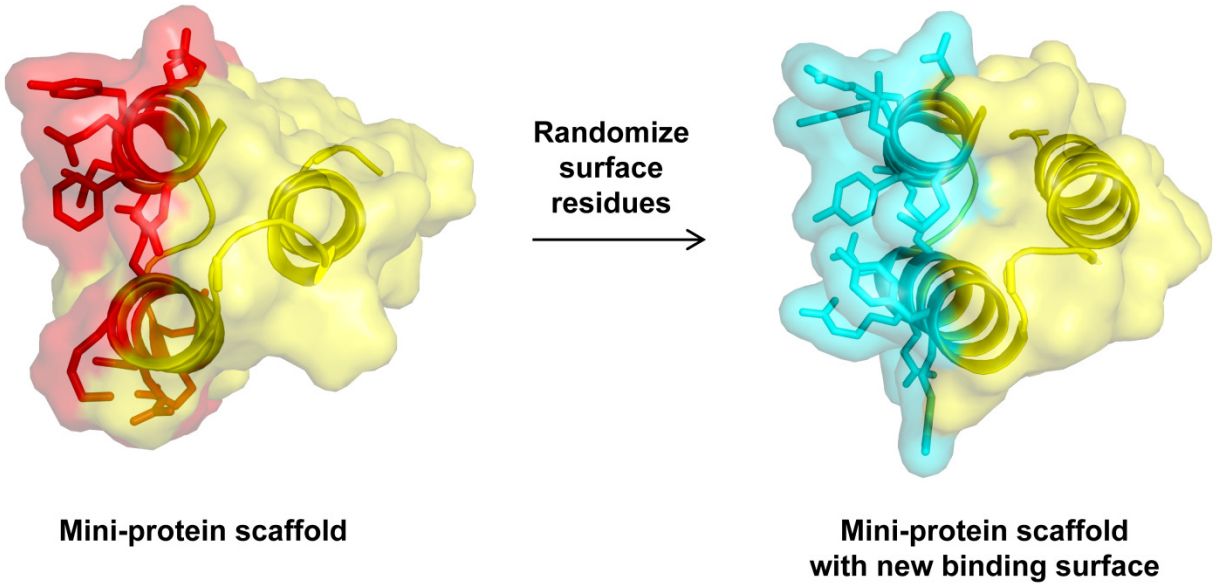

Figure 1.5 Combinatorial randomization on a mini-protein scaffold leads to a peptide that adopts the same overall folded structure but displays a variable region (e.g., surface or loops) that can bind to a protein target. Figure shows two peptides from the "Z-domain" scaffold, one that binds IgG through the surface shown in red (left, PDB: 2SPZ),[135] and one that binds HER2 through the surface shown in teal (right, PDB: 3MZW).[136] Residues in yellow are identical between the two peptides. In this figure, some residues at the N-terminus of each peptide have been omitted for clarity.

One of the most well-studied mini-protein scaffolds is the three-helix Z-domain, or "Affibody", derived from Protein A of *Staphylococcus aureus* (Figures 1.5 and 1.6).[137-139] The Z-domain scaffold has been used to derive high affinity binders to a large number of protein targets of therapeutic interest, including VEGF,[140] VEGFR2,[141] TNFα,[142-145] HER2,[37, 146] and EGFR.[147, 148] Z-domain-derived peptides targeting HER2 have been used to image HER2-overexpressing tumors in breast cancer patients.[38, 39] The Z-domain scaffold is discussed more extensively in Chapters 2-4.

In addition to the Z-domain scaffold, a diverse range of mini-protein scaffolds are explored by a number of research groups as alternatives to antibodies for deriving peptides to target proteins surfaces, including the DARPin scaffold,[149] the Adnectin scaffold,[150] the Anticalin scaffold,[151] and the Avimer scaffold.[152] Each scaffold adopts a distinct fold and thus these scaffolds present different types of binding interfaces relative to one another. This diversity is

likely to be important for targeting different protein surfaces (Figure 1.6). One recent example of a peptide derived from a mini-protein scaffold includes a DARPin-derived peptide that binds IgE and blocks receptor binding through a novel allosteric mechanism.[153] As another example, CT-322, a peptide derived from the Adnectin scaffold that targets VEGFR2 and blocks VEGF signaling,[154, 155] is currently in clinical trials to treat various forms of cancer.[156]

Mini-protein scaffolds offer several advantages over antibodies. A number of scaffolds currently being explored lack post-translational modifications and disulfide bonds, meaning that they can be produced in bacterial expression systems, which are cheaper and higher yielding than the eukaryotic systems required for antibody production.[128-130, 134] The smaller size of many mini-protein scaffolds relative to antibodies allows them to be chemically synthesized, which offers advantages in terms of site-selective modification (e.g., conjugation to fluorophore or a therapeutic agent). Additionally, the smaller size may give therapeutic and diagnostic advantages such as increased tissue penetration and faster plasma clearance time (which is important for imaging applications) through renal filtration compared to the much larger antibodies. However, fast plasma clearance time is likely a disadvantage for mini-proteins in therapeutic applications (such as antagonizing protein-protein interactions), and chemical modifications may be needed to increase plasma residence time of these proteins for such applications.[17, 157] Finally, affinity-based selection from a combinatorial library does not guarantee that a mini-protein binds in the intended binding site on the target or adopts the intended conformation.[158]

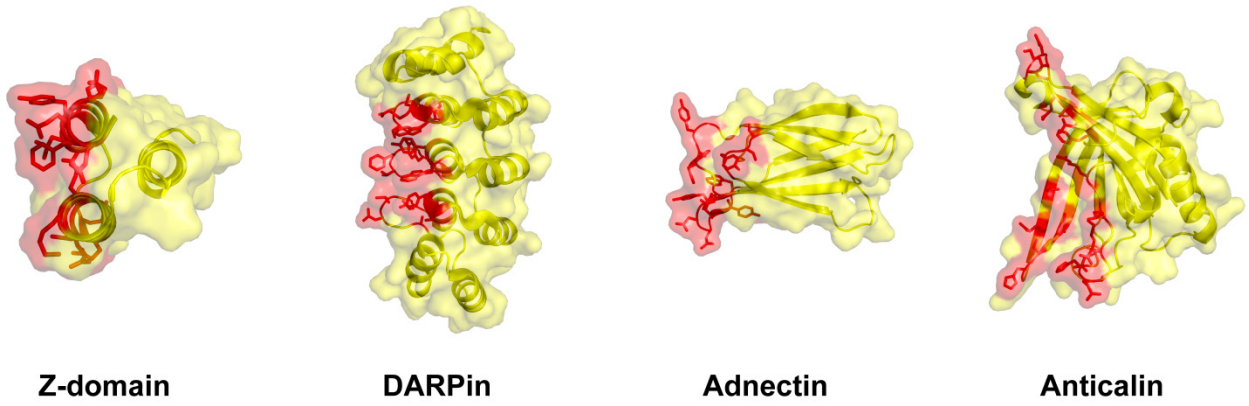

Figure 1.6 High resolution structures of some of the commonly used mini-protein scaffolds. Regions in red are those that are typically randomized to form combinatorial libraries to derive binding to new targets. Structures are the Z-domain scaffold (PDB: 2SPZ),[135] the DARPin scaffold (PDB: 1SVX),[159] the Adnectin scaffold (PDB: 3RZW),[160] and the Anticalin scaffold (PDB: 3BX7).[161]

1.7 Targeting protein surfaces with foldamers

1.7.1 Foldamers

Foldamers are non-natural oligomers that adopt discrete, compact folded structures.[162-164] Foldamers can achieve protein-like functions by displaying chemical functionalities (e.g., side chains) in fixed spatial arrangements, analogous to side chain presentation by well-folded proteins. Peptide foldamers are therefore a promising source of molecules that can bind protein surfaces with high affinity and selectivity to modulate protein-protein interactions. The non-natural elements of foldamers give them advantages over conventional peptides. Perhaps most significantly, whereas peptides made up of natural α-residues are highly susceptible to degradation by proteases, proteases often do not recognize the non-natural backbone of foldamers, which dramatically increases their stability in biological systems.[165, 166] The decreased susceptibility to protease degradation for peptide foldamers may lead to improved pharmacokinetic properties *in vivo* relative to natural peptides. In this section, I highlight a few of the important classes of peptide foldamers that have been utilized to derive high-affinity molecules targeting protein surfaces, along with several examples in each class (Figure 1.7).

α/β-Peptide foldamers, which are the focus of the research described in this dissertation, are discussed in detail in the following section.

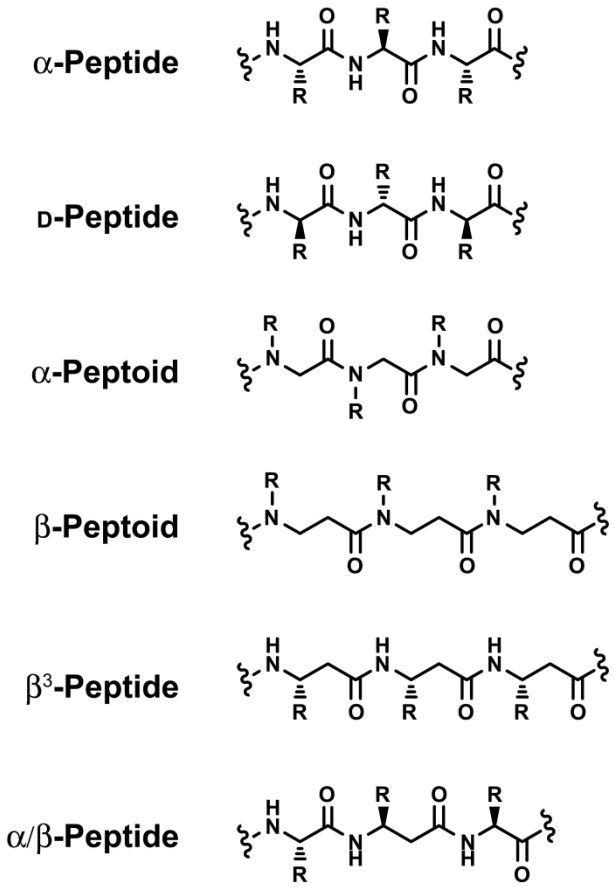

Figure 1.7 Generic backbone structure for an α-peptide, along with several classes of peptide foldamers discussed in this chapter.

1.7.2 D-Peptides

D-Peptides are oligomers comprised exclusively of D-amino acid residues and achiral glycine (Figure 1.7). Although D-peptides contain the same chemical composition of natural L-peptides, the inverted stereochemistry at the α-carbon significantly diminishes the susceptibility of D-peptides to protease degradation relative to natural peptides.[167, 168] However, designing D-peptides to target a particular protein surface is challenging. Phage display is not available for the production of large combinatorial libraries of D-peptides, as the ribosome

cannot incorporate D-amino acids. Mirror-image phage display, first developed by Kim et al.,[169] represents one promising strategy to develop D-peptides to target a particular protein surface.[170] In this technique, the enantiomer of the protein target (a D-protein) is chemically synthesized, and then phage display and selection are performed against the D-protein to derive an L-peptide binder. Because of symmetry, the enantiomer of this phage-derived L-peptide, a D-peptide, will bind to the native L-protein. Using mirror-image phage display, D-peptides have been developed that bind to a variety of therapeutically relevant targets, including gp41,[171-173] MDM2,[174, 175] and VEGF.[176] However, a significant disadvantage of mirror-image phage display is that one must first chemically synthesize the enantiomer of the protein target, which becomes increasingly difficult as the size of the protein target increases.

1.7.3 Peptoids

Peptoids are oligomers of *N*-substituted glycine residues (Figure 1.7).[177, 178] Although the peptoid backbone lacks chirality and secondary amide protons (both of which play important roles in α-peptide secondary structure), properly designed peptoids can adopt stable secondary structures. The ability to adopt folded structures, as well as their high proteolytic stability[168, 177, 179] and increased membrane permeability relative to α-peptides,[180, 181] make peptoid foldamers attractive candidates for modulators of protein-protein interactions in living systems.[178] Indeed, there are several reports of peptoids targeting protein surfaces, such as peptoids that inhibit p53-HDM2 complexation,[182] peptoids targeting VEGFR2 that block tumor growth *in vivo*,[183, 184] and peptoid inhibitors of the protein unfolding activity of the 19S proteasome regulatory particle.[185, 186] In one very recent example, peptoids that bound the ubiquitin receptor Rpn13 on the 26S proteasome with high specificity were found to selectively kill multiple myeloma cells (which heavily rely on the 26S proteasome for survival), but did not kill HEK-293T cells (which

do not rely on the 26S proteasome).[187] In another recent example, "*N*-methyl scanning" and "peptoid residue scanning" were utilized to design peptide-peptoid hybrid analogues of an autoinducing peptide that plays a key role in quorum sensing in *Staphylococcus aureus*.[188] This effort resulted in new structure-activity relationship information about the native peptide ligand, as well as the development of the first selective inhibitor of the group-IV AgrC quorum sensing receptor. Finally, a recent report describes the first oligomers with a β-peptoid backbone (Figure 1.7) that adopt a stable helical structure both in solution and in the solid state.[189] These stably-folded β-peptoids may serve as the starting point for new foldamer designs.

1.7.4 β-Peptides

β-Peptides are oligomers of β-amino acids, which contain an additional carbon atom in the backbone relative to α-amino acids (Figures 1.7 and 1.8).[166, 190-193] β-Peptides can adopt well-folded helix and sheet structures in aqueous solutions.[191, 192, 194] The high folding propensity of β-peptides, along with the observation that they are almost completely resistant to protease degradation,[165, 195-198] have made β-peptides particularly attractive starting points for foldamer design.

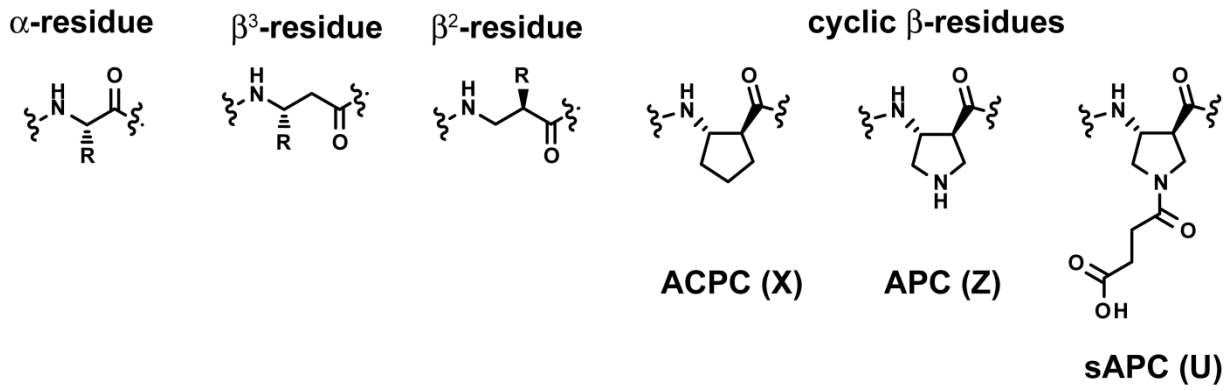

Figure 1.8 Structures of a generic α-residue, a generic β^3-residue, a generic β^2-residue, and several cyclic β-residues utilized in β-peptide and α/β-peptide design.

Early examples of β-peptides with biological functions include inhibitors of fat and cholesterol absorption[199] and antibiotic agents.[200, 201] More recently, β-peptides with anti-fungal properties have been explored.[202-204] These functions rely primarily on these β-peptides' global amphipathic helical structure. In addition to these relatively non-specific interactions, β-peptides targeting specific protein surfaces as modulators of protein-protein interactions have been developed. In early studies, Seebach et al. designed β-peptide analogues of somatostatin that bound to somatostatin receptors, showing for the first time that β-peptides could mimic functions of α-peptides in binding to a specific human protein surface.[205, 206] In 2004, Schepartz et al. reported β-peptides designed to mimic the function of a p53 peptide by projecting three side chains critical for HDM2 binding along one face of a β-peptide 14-helix.[207] One β-peptide, **β53-1**, was found to bind to HDM2 and could compete with labeled p53 for binding to HDM2 in fluorescence polarization (FP) assays, although the affinity was somewhat weaker than that of the parent α-peptide. A solution NMR structure of **β53-1** showed that it adopted the anticipated 14-helix and projected the three side chains critical for HDM2 binding along one face, as designed.[208] Follow-up studies increased the affinity of this β-peptide ~10-fold by incorporating previously identified side chain substitutions.[209, 210] In attempts to increase membrane permeability of these β-peptides, Schepartz et al. reported analogues of their HDM2-binding β-peptides bearing small cationic patches[211] and hydrocarbon crosslinks.[212] Some of these β-peptides were reported to enter cells, and preliminary results suggested that some could modestly antagonize p53-HMD2 interactions in HCT116 cells.[211]

In 2005, Schepartz et al. designed a β-peptide targeting a surface pocket on the N-heptad repeat (NHR) of gp41 by "mapping" three critical binding residues from the native C-heptad repeat (CHR) peptide onto the β-peptide 14-helix, similar to the strategy outlined for p53-HDM2

antagonism described above.[213] Some of the resulting β-peptides developed in this study were found to bind to a gp41 model protein, IZN17, and could inhibit gp41-mediated cell-cell fusion in a model infectivity assay. A subsequent study from the same group found that side chain substitution could be used to modestly increase cell-cell fusion inhibitory potency of the β-peptides and reduce toxicity to human cells.[214] However, these β-peptides were ~500-fold less potent at inhibiting cell-cell fusion than is enfuvirtide (Fuzeon), an α-peptide drug used to treat HIV.

In 2006, our group, in collaboration with Compton and co-workers, reported β-peptides designed to mimic the heptad repeat of human cytomegalovirus (HCMV) surface glycoprotein gB for the inhibition of HCMV infection.[215] The most potent of these β-peptides was able to block HCMV infection in cell-based assays and was specific to HCMV over other viruses, consistent with the design hypothesis. Furthermore, the optimized β-peptide was significantly more potent than α-peptides derived from the gB protein, showing that the β-peptide foldamer is superior to the α-peptide prototype in this context.

More recently, DeGrado et al. used a "computed helical antimembrane protein" (CHAMP) method[216] to design a β-peptide that binds specifically to the transmembrane (TM) domain of membrane protein, α_{IIb}.[217] In the unbound form of the platelet integrin $\alpha_{IIb}\beta_3$, the helical TM domains of α_{IIb} and β_3 interact. When $\alpha_{IIb}\beta_3$ binds to its ligand, fibrinogen, these helix-helix interactions are disrupted. Distruption of the association between α_{IIb} and β_3 by α-peptides that bind to either of these TM segments can lead to integrin activation.[216] Consistent with its intended design, DeGrado's β-peptide bound the α_{IIb} TM domain in DPC micelles, as determined by AUC experiments.[217] Furthermore, the β-peptide activated $\alpha_{IIb}\beta_3$ and facilitated fibrinogen binding, as determined by rupture force spectroscopy and TEM, consistent with its

intended effect as an inhibitor of the α_{IIb}-β_3 interaction. No comparison was made between the β-peptide and any α-peptide known to disrupt the α_{IIb}-β_3 interaction, although the β-peptide disrupted the interaction as well as did a positive control condition of 2 mM Mn^{2+}, which disrupts the α_{IIb}-β_3 association.

In 2013 Schepartz et al. described efforts to derive β-peptide agonists of GLP-1R by replacing the C-terminal segment of exendin-4 with β-peptides hypothesized to mimic the display of side chains known to make important contacts with GLP-1R.[218] This effort resulted in compounds that bound GLP-1R and activated cAMP production in cells expressing GLP-1R, but not other class B GPCRs. However, their potency was about one million-fold lower than that of the parent α-peptide, exendin-4.

β-peptides are attractive scaffolds for foldamer design because of their well-folded and diverse structures, as well as their extreme resistance to protease degradation. However, attempts to design β-peptides that mimic the function of natural α-peptides have yielded mixed results. In many cases, efforts to mimic the side chain display of an α-helix by "mapping" critical contact residues onto one face of a β-peptide helix leads to β-peptides with significantly reduced affinity or potency relative to their parent α-peptides. These results ultimately indicate that β-peptide helices may not adequately recapitulate the side chain display of a natural α-helix. Approaches for *de novo* β-peptide design (e.g., using computational methods such as CHAMP, mentioned above)[216] may be valuable resources for deriving β-peptides with high-affinity for target protein surfaces.

1.8 α/β-Peptide foldamers as mimics of α-peptides

1.8.1 Introduction to α/β-peptides

α/β-Peptides, oligomers of both α- and β-amino acid residues, can be designed as high-affinity compounds targeting protein surfaces.[163, 219-221] Because a β-residue placed within a sequence of α-residues can protect nearby amide bonds from protolysis,[166, 195] α/β-peptides with β-residues spaced throughout their sequence can be significantly more resistant to proteolysis than their α-peptide counterparts. Thus, properly designed α/β-peptides can offer the advantage of being structurally "similar" enough to natural α-peptides to facilitate high-affinity protein recognition, and yet display a significantly reduced susceptibility to proteolytic degradation.

1.8.2 Structure-based design of α/β-peptides

α/β-Peptides comprised of 1:1 alternating α- and β-residues can adopt well-folded helical structures that are different from those of β-peptides.[222, 223] Early studies from our group sought to use the 1:1 α/β-peptide foldamer scaffold as a starting point for the design of α/β-peptides targeting the BH3 recognition cleft on the Bcl-2 family anti-apoptotic protein Bcl-x_L.[224, 225] This structure-based design strategy attempted to recapitulate the display of side chains known to be critical for binding of BH3 ligands to Bcl-x_L onto the α/β-peptide 14/15-helix, similar to the approaches described above for the design of β-peptides. From this effort, a 15-residue α/β-peptide was identified that bound Bcl-x_L with IC_{50} = 40 μM (K_i = 1.5 μM) by competition FP assay. In contrast, evaluating over 150 β-peptide designs for binding to Bcl-x_L led to only very weak binders (IC_{50} > 500 μM by competition FP assay). However, the highest affinity α/β-peptide from this study bound to Bcl-x_L with ~60-fold weaker affinity than did an α-peptide derived from a natural BH3 sequence. High-affinity binding was achieved only by replacing the

six C-terminal residues of this α/β-peptide with natural α-residues, creating a chimeric (α/β+α)-peptide that bound Bcl-x_L with IC_{50} = 0.029 μM (K_i = 0.0007 μM).[224, 225] A crystal structure of the chimeric (α/β+α)-peptide in complex with Bcl-x_L showed that this (α/β+α)-peptide bound to the protein in the BH3 recognition groove, as designed, and made many of the anticipated side chain contacts.[226] However, the natural α-peptide segment at the N-terminal region of the chimeric (α/β+α)-peptide was highly susceptible to degradation by proteases due to the lack of β-residues in this region.[227] These results ultimately suggested that the chimeric (α/β+α)-peptide design approach was not ideal for the development of foldamers that display high affinity for proteins while also displaying a reduced susceptibility to proteolysis.

1.8.3 Sequence-based design of α/β-peptides

The previous section described the design of α/β-peptides targeting the BH3 binding cleft of Bcl-x_L by attempting to display key protein-contacting side chains from the 14/15-helix formed by a 1:1 alternating α/β-peptide scaffold. This strategy, called "structure-based design", starts with a foldamer scaffold and attempts to imbue the foldamer scaffold with function (e.g., protein binding). A fundamentally different design strategy, called "sequence-based design", instead begins with a functional α-peptide, and then replaces a subset of the α-residues with β^3-residues bearing the same side chains in a regular substitution pattern (Figure 1.9). The optimal end result of the sequence-based design strategy is an α/β-peptide that recapitulates enough of the side chain display of the parent α-peptide to provide high-affinity binding to the natural protein target, but has a decreased susceptibility to protease degradation due to the β-residues spaced throughout the sequence.

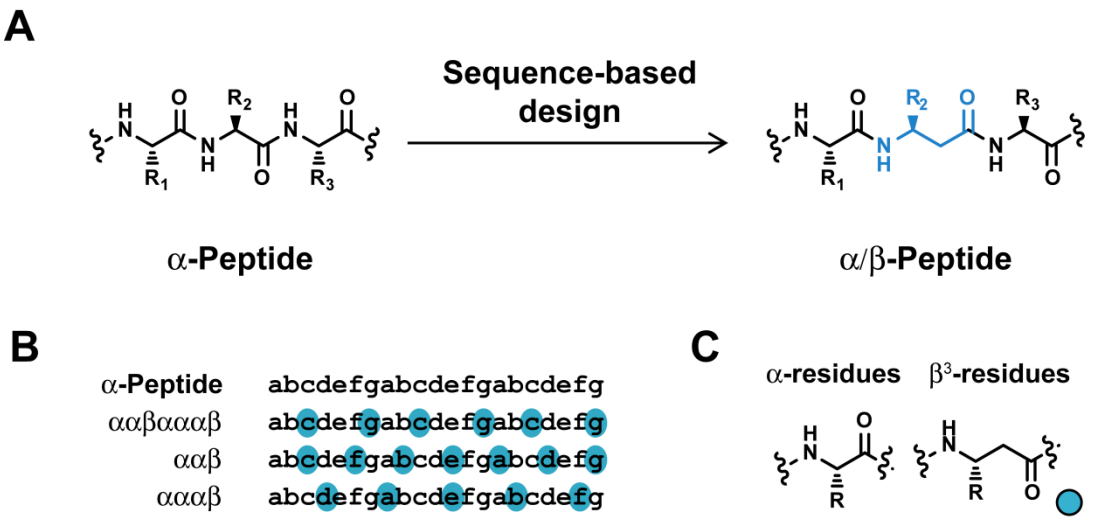

Figure 1.9 Sequence-based design of α/β-peptides to mimic functional α-peptides. (A) Depiction of the sequence-based design strategy, in which select α-residues in an α-peptide are replaced with β^3-residues (teal) with the same side chain. (B) Examples of different patterns of α→β^3-residue substitution. Several generic α- and α/β-peptide sequences are shown, with "abcdefg" representing the heptad repeat of an α-helix. Positions for β^3-residue replacements are indicated by teal circles. (C) Structures of a generic α-residue and a generic β^3-residue (teal).

Crystal structures of α/β-peptides derived from sequence-based design based on the α-helical peptide GCN4-pLI (an engineered peptide that forms a stable four-helix bundle quaternary structure) using ααβ, αααβ, and αααβαααβ substitution patterns showed that each of these patterns of α→β-residue substitution could result in an α/β-peptide that adopted a helical structure closely resembling that of an α-helix.[228, 229] Each of these substitution patterns places β-residues at different positions on the surface of the helical α/β-peptide. For instance, the αααβαααβ pattern places β-residues in a "stripe" along one face of the helix (see Figure 1.10D for an example).

A

Puma	Ac-EEQWAREIGAQLRRMADDLNAQYERR-NH_2
1.1	Ac-EEQWAREIGAQLRRMADDLNAQYERR-NH_2
1.2	Ac-EEQWAREIGAQLRRMADDLNAQYERR-NH_2
1.3	Ac-EEQWAREIGAQLRRMADDLNAQYERR-NH_2
1.4	Ac-EEQWAREIGAQLRRMADDLNAQYERR-NH_2
1.5	Ac-EEQWAREIGAQLRRMADDLNAQYERR-NH_2
1.6	Ac-EEQWAREIGAQLRRMADDLNAQYERR-NH_2
1.7	Ac-EEQWAREIGAQLRRMADDLNAQYERR-NH_2
1.8	Ac-WAREIGAQLRRMADDLNAQYE-NH_2

B

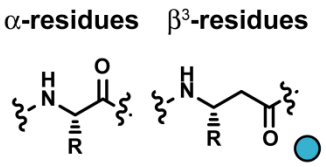

C

	SPR IC_{50} (nM)		Prot. K $t_{1/2}$ (min.)
	Bcl-x_L	Mcl-1	
Puma	18	10	0.7
1.3	18	480	> 3000
1.8	26	8000	-

D

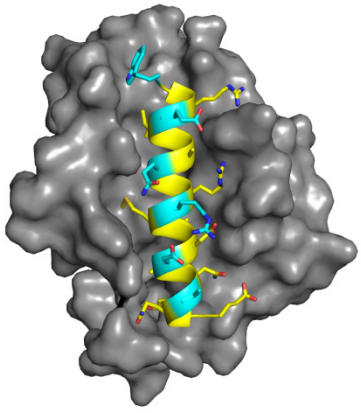

1.8 + Bcl-x_L
(PDB: 2YJ1)

Figure 1.10 Previously reported analogues of α-peptide **Puma**, using sequence-based design.[230, 231] (A) Primary sequences of α- and α/β-peptides derived from the Puma BH3 domain. β^3-residues are indicated by teal circles. (B) Structures of a generic α-residue and a generic β^3-residue. (C) Affinity of **Puma**, **1.3**, and **1.8** for Bcl-x_L and Mcl-1, as determined by competition SPR (from ref.[231]), and susceptibility of 50 μM α-peptide **Puma** or α/β-peptide **1.3** to 10 μg/mL proteinase K (from ref.[230]). (D) X-ray crystal structure of α/β-peptide **1.8** (yellow and teal) in complex with Bcl-x_L (gray) (PDB: 2YJ1).[231] β^3-residues are depicted in teal.

The similarity between the α-peptide helix and the α/β-peptide helices derived from sequence-based design suggested that this strategy may be successfully applied to α/β-peptide mimicry of helical peptides that target protein surfaces. Our group applied sequence-based design to develop α/β-peptides mimicking a 26-residue α-peptide derived from the BH3 domain of Puma, a pro-apoptotic protein from the Bcl-2 family that binds to the BH3 cleft on anti-apoptotic proteins (**Puma**, Figure 1.10).[230] Seven α/β-peptide analogues of **Puma** were synthesized containing α→β^3-residue substitutions in each possible ααβαααβ pattern (α/β-

peptides **1.1-1.7**). These seven α/β-peptides were evaluated for their ability to bind to anti-apoptotic proteins Bcl-x_L and Mcl-1. One α/β-peptide, **1.3**, bound to both Bcl-x_L (IC_{50} = 18 nM, by competition SPR assay) and Mcl-1 (IC_{50} = 480 nM) (Figure 1.10C). Indeed, α/β-peptide **1.3** matched the affinity of the parent α-peptide for Bcl-x_L, but bound Mcl-1 ~50-fold more weakly than did the α-peptide. Importantly, α/β-peptide **1.3** was >4000-fold more stable to degradation by the aggressive protease proteinase K than the parent α-peptide. A crystal structure of a truncated analogue of **1.3** (α/β-peptide **1.8**) in complex with Bcl-x_L showed that α/β-peptide **1.8** very closely mimicked the α-peptide when bound to its protein target, with the β-residues aligned on the solvent-exposed face of the helix, as designed (Figure 1.10D).[231] Collectively, the results from Puma mimicry indicate that α/β-peptides derived from sequence-based design can be good structural and functional mimics of helical α-peptides, while being significantly more stable to proteolytic destruction.

The α/β-peptide mimics of Puma described above utilized the ααβαααβ substitution pattern, which aligns β-residues along one face of the resulting helix. To explore other α/β-peptide backbones derived from sequence-based design, α/β-peptide analogues of the Bim BH3 domain were explored with different α→β^3-residue substitution patterns.[232] Three substitution patterns were surveyed (ααβ, αααβ, and ααβαααβ), and each possible 18-residue α/β-peptide derivative of the Bim α-peptide was synthesized within each pattern family. This strategy resulted in a set of 14 α/β-peptide analogues of the Bim BH3 domain, each with the same side chains as the parent α-peptide, but with additional methylene units in their backbone at various positions arising from the placement of the β^3-residues. The Bim-derived α/β-peptides were evaluated for binding to protein targets Bcl-x_L and Mcl-1, and compared to the parent α-peptide, which binds to both of these anti-apoptotic proteins with high affinity. From this

survey, α/β-peptides were identified that bound both Bcl-x_L and Mcl-1 with high affinity, that selectively bound to only one of these two proteins, or that did not bind to either protein. The variable behavior of the different α/β-peptides is interesting since all of the α/β-peptides described in this study were nearly isomeric. These results indicate that subtle changes in the display of side chains in an α/β-peptide can affect the interaction of α/β-peptides with proteins in different ways. Crystal structures of two of these α/β-peptides in complex with Bcl-x_L, one with an ααβααaβ pattern and one with an αααβ pattern, showed that both of these backbones could be accommodated in the canonical BH3 recognition groove, and that both α/β-peptides accurately mimicked most of the critical binding interactions common to BH3 peptides. Extended analogues of these α/β-peptides (26-residues) bound target proteins with higher affinity and induced cytochrome *c* release from the mitochondria of mouse embryonic fibroblasts (MEFs) with permeabilized membranes, indicating that these α/β-peptides can antagonize target anti-apoptotic proteins in a complex cellular environment devoid of a membrane barrier. Finally, these α/β-peptides were >150-fold more resistant to proteinase K degradation than their parent α-peptide. Together, these results show that diverse backbone patterns, derived through sequence-based design, can be utilized to achieve biostable α/β-peptides that mimic natural α-helical α-peptides.

Arora et al. recently used sequence-based design to derive α/β-peptide mimics of a short peptide derived from the p53 activation domain stabilized in a helical conformation by the HBS approach described above.[114] Using primarily NMR-based experiments, Arora et al. showed that HBS α/β-peptide analogues of p53 containing an αααβ substitution pattern could be more conformationally defined than the parent HBS α-peptide, if the HBS macrocycle is properly designed to template helix nucleation. The most conformationally rigid HBS α/β-peptide from

this study bound to protein target MDM2 with affinity identical to that of the parent HBS α-peptide, indicating that the HBS α/β-peptide is an excellent functional mimic of the α-peptide. Because HBS-stabilized α-peptides can sometimes enter cells,[116, 117] the HBS α/β-peptide analogues of p53 may have activity in cell-based experiments.[114]

1.8.4 Backbone rigidification of α/β-peptides with cyclic β-residues

Having successfully utilized the sequence-based design approach to mimic an α-peptide derived from the Puma BH3 domain, our group next asked if this same approach could be used to mimic a longer α-helical sequence of direct therapeutic relevance. Sequence-based design using $\alpha \rightarrow \beta^3$ substitutions in an ααβααaβ pattern was applied to derive an α/β-peptide analogue of the HIV membrane-fusion inhibitor **T-2635**, a 38-residue α-helical α-peptide which targets the N-heptad repeat (NHR) regions of HIV protein gp41 (Figure 1.11).[233] Although the resulting α/β-peptide (**1.9**) displayed decreased susceptibility to degradation by proteinase K, it bound a gp41 model protein, gp41-5, with affinity >10,000-fold lower than the parent α-peptide, as determined by a competition FP assay. Whereas the far-UV circular dichroism (CD) spectrum of α-peptide **T-2635** indicates that this peptide is predominantly helical in solution, the far-UV CD spectrum of α/β-peptide **1.9** revealed that this α/β-peptide was predominantly unstructured in solution. Together, the FP and CD data suggest that the incorporation of β^3-residues in **1.9** decreased this α/β-peptide's conformational stability relative to α-peptide **T-2635**.

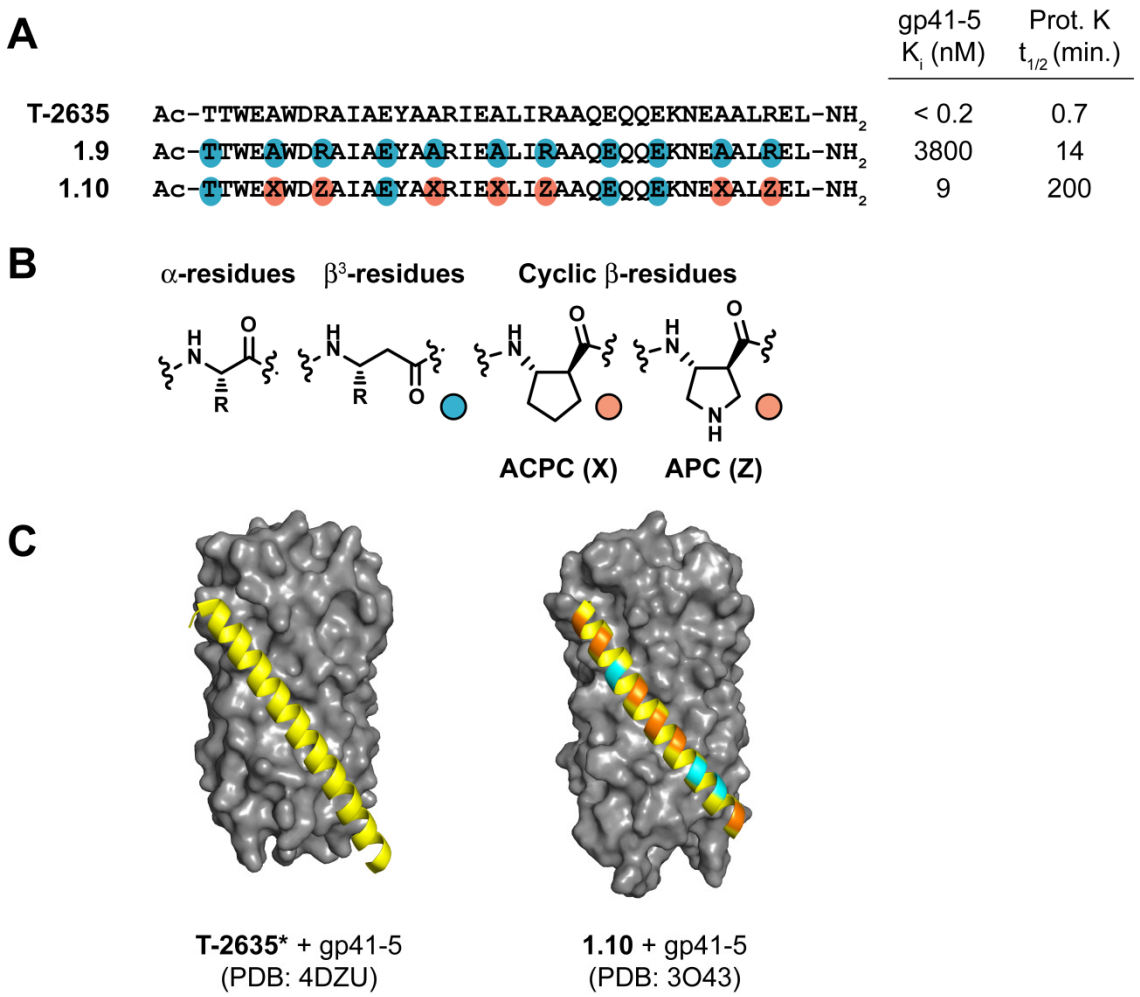

Figure 1.11 Sequence-based design and backbone rigidification of HIV membrane-fusion inhibitor **T-2635**.[233-235] (A) Primary sequences of α-peptide **T-2635** and α/β-peptide analogues, along with affinity for gp41-5 (as determined by competition FP assay) and relative susceptibility of 20 μM α- or α/β-peptide to 10 μg/mL proteinase K (from ref.[233]). Non-natural residues are indicated by colored circles. (B) Structures of a generic α-residue, a generic β^3-residue (teal), and the cyclic β-residues ACPC (X) and APC (Z) (orange). (C) Crystal structure of an analogue of α-peptide **T-2635** (denoted **T-2635***) in complex with gp41-5 (gray) (left, PDB: 4DZU).[235] Crystal structure of α/β-peptide **1.10** in complex with gp41-5 (gray) (right, PDB: 3O43).[234] For **T-2635*** and **1.10**, residues are colored by type, yellow for α-residues, teal for β^3-residues, and orange for cyclic β-residues.

The decrease in affinity of **1.9** for gp41-5 relative to that of α-peptide **T-2635** may have resulted from the addition of many flexible bonds to the backbone from the 11 α→β^3-residue replacements, which should increase the entropic cost of helix formation required for binding to gp41. This affinity decrease upon α→β^3-residue replacement contrasts with the cases described above, in which incorporating β^3-residues in shorter helical sequences did not have a very large

negative impact on α/β-peptide binding.[114, 230] β-Residues containing a five-membered ring (e.g., ACPC, APC, Figure 1.11B), can constrain the Cα-Cβ backbone torsion and preorganize α/β-peptides into a helical structure.[191, 236] Indeed, replacing several of the flexible β^3-residues **1.9** with preorganizing cyclic β-residues, to give **1.10**, led to a significant increase in affinity for gp41-5 (Figure 1.11A).[233] Furthermore, **1.10** was even less susceptible to proteinase K degradation than was α/β-peptide **1.9**. The higher affinity for gp41-5 and the reduced protease susceptibility of **1.10** presumably arise from a greater conformational stability in solution relative to **1.9**. A crystal structure of **1.10** in complex with gp41-5 showed that this α/β-peptide adopts a helical conformation and can interact with the natural six-helix bundle assembly, as intended (Figure 1.11C).[233, 234] Importantly, **1.10** inhibited HIV infection of four different viral strains, with potency comparable to that of the parent α-peptide **T-2635** and better than that of HIV drug enfuvirtide.[233] These experiments show that backbone rigidification, by replacing β^3-residues with conformationally preorganized cyclic β-residues, can increase the affinity and protease stability of helical α/β-peptides.

In a recent report from our group, β^3-residues in the Bim-derived α/β-peptides described above were replaced with cyclic β-residues to yield α/β-peptides with even greater affinity for Bcl-2 family anti-apoptotic proteins and greater protease stability than the analogues with β^3-residues.[237] This last example emphasizes that sequence-based design, followed by backbone rigidification by incorporating cyclic β-residues, may be a general strategy for the development of protease-resistant helical ligands targeting protein surfaces.

1.8.5 α/β-Peptide agonists of Class B G-protein coupled receptors

Class B G protein-coupled receptors (GPCRs) are membrane-bound receptors that regulate many important cellular functions. Class B GPCRs are activated by medium-sized

peptide hormones, and synthetic peptides can be used as therapeutic agonists of these receptors.[65] The parathyroid hormone receptor 1 (PTHR1) is a Class B GPCR that plays a critical role in the regulation of blood calcium levels. A synthetic peptide, **PTH(1-34)**, is an agonist of PTHR1 and is currently used to treat osteoporosis.[30] The C-terminal portion of **PTH(1-34)** forms an α-helix upon binding to PTHR1, while the conformation of the N-terminal portion when bound to the receptor is not known.[238] Inspired by the successes described above for the mimicry of helical α-peptides, our group used sequence-based design to derive α/β-peptide analogues of **PTH(1-34)** with β^3-residues incorporated in the helical C-terminal segment in an ααaβ pattern (α/β-peptides **1.11-1.16**, Figure 1.12).[239] All of the α/β-peptide analogues of **PTH(1-34)** tested were full agonists of PTHR1 with potencies similar to that of the parent α-peptide, as determined by a cell-based GloSensor cAMP assay. The α/β-peptide analogues of **PTH(1-34)** were compared to **PTH(1-34)** itself for binding to both the G protein-coupled state (RG) and G protein-independent state (R^0) of PTHR1; selectivity for either of these receptor states can affect the potency of receptor activation and duration of activation *in vivo*. In these receptor-binding experiments, all of α/β-peptide analogues of **PTH(1-34)** bound to both the RG and R^0 state of PTHR1, but differed in their affinities to these two receptor states when compared to **PTH(1-34)**. For example, α/β-peptide **1.12** (Figure 1.12) bound to the RG state of PTHR1 with affinity nearly identical to that of α-peptide **PTH(1-34)**, but bound to the R^0 state of PTHR1 with affinity ~20-fold lower than **PTH(1-34)**. Another α/β-peptide, **1.15**, bound to both receptor states with affinity within 2-fold of **PTH(1-34)**.

α-Peptide **PTH(1-34)** and α/β-peptides **1.12** and **1.15** were injected into mice, and both α/β-peptides led to an increase in blood calcium levels, consistent with their intended effect as PTHR1 agonists (Figure 1.12C). Interestingly, α/β-peptide **1.15** showed an increased duration of

response, maintaining elevated blood calcium levels longer than did α-peptide **PTH(1-34)**. Pharmacokinetic analysis revealed that **1.15** lasted significantly longer in the blood stream than did **PTH(1-34)** (Figure 1.12D), which is likely the origin of the prolonged signaling resulting from treatment with this compound. The increased plasma residence time of the α/β-peptide relative to the α-peptide may arise from the decrease in protease susceptibility imparted by the β-residues in this sequence. Importantly, this report was the first to show activity of α/β-peptides *in vivo*.

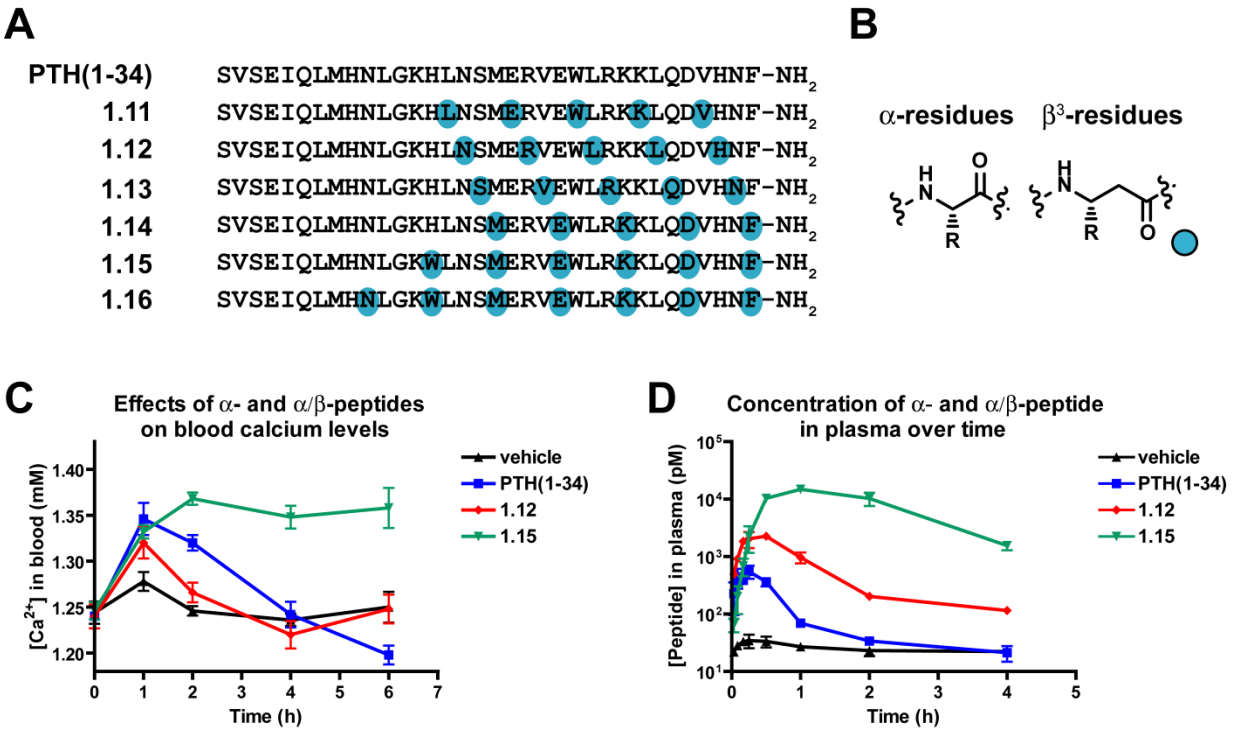

Figure 1.12 α/β-Peptide analogues of PTH(1-34).[239] (A) Primary sequences of **PTH(1-34)** and α/β-peptide analogues. Non-natural residues are indicated by colored circles. (B) Structures of a generic α-residue and a generic β^3-residue (teal). (C) Effects of the indicated α- or α/β-peptide on blood Ca2+ levels in mice (n = 5) at a dose of 20 nmol/kg (from ref.[239]). (D) Concentrations of the indicated α- or α/β-peptide in plasma from blood withdrawn from mice (n = 3) at times post-injection, as in panel C (from ref.[239]).

The glucagon-like peptide-1 receptor (GLP-1R) interacts with the peptide hormone GLP-1 as a key regulator of insulin secretion. GLP-1 is rapidly degraded *in vivo*, but longer-lasting agonists of GLP-1R can be used to treat type 2 diabetes.[32] Like **PTH(1-34)**, the

C-terminal portion of GLP-1 adopts an α-helix when bound to GLP-1R,[240] suggesting that a properly designed α/β-peptide may be able to functionally mimic the activity of this α-peptide. Initial efforts to design α/β-peptide analogues of **GLP-1(7-37)** using a sequence-based design approach were not successful; an α/β-peptide analogue bearing three α→β^3-residue substitutions was only a very weak agonist of GLP-1R.[241] This contrasts with the α/β-peptide mimics of **PTH(1-34)** discussed above, in which α→β^3-residue replacements were generally well-tolerated.[239] However, the incorporation of cyclic β-residues in an ααaβ pattern throughout the C-terminal portion of **GLP-1(7-37),** along with two Aib residue substitutions in the N-terminal portion, led to an α/β-peptide analogue of **GLP-1(7-37)** that was a full agonist of GLP-1R with potency comparable to that of the parent α-peptide. In an *in vitro* protease digestion experiment, an α/β-peptide analogue of **GLP-1(7-37)** displayed a half-life of 83 hours when incubated with neprilysin, an enzyme known to degrade GLP1 *in vivo*. Under the same conditions, **GLP-1(7-37)** displayed a half-life of 0.33 hours. The α/β-peptide analogue of **GLP-1(7-37)** matched the ability of the prototype α-peptide to stimulate the secretion of insulin from mouse pancreatic islets. When the α/β-peptide analogue of **GLP-1(7-37)** was tested for the ability to normalize blood glucose levels in mice by a glucose tolerance test, the α/β-peptide matched the ability of **GLP-1(7-37)** to suppress an increase in blood glucose concentration. When a second glucose tolerance test was performed 5 hours after injection of α- or α/β-peptides, GLP-1(7-37) was unable to suppress blood glucose levels, presumably because this peptide was degraded in the blood stream during the 5 hour period. In contrast, the α/β-peptide was able to suppress an increase in blood glucose concentration during the second glucose tolerance test, consistent with the hypothesis that the incorporation of the Aib and cyclic β-residues leads to prolonged action *in vivo*.

1.8.6 Beyond α-helix mimicry

The examples highlighted above show that properly designed α/β-peptides can mimic the structure and protein recognition functions of α-peptides that adopt a single, contiguous α-helix, while displaying a decreased susceptibility to protease degradation. However, not all protein-protein interactions can be modulated by a single helical ligand. For example, the interaction between vascular endothelial growth factor (VEGF) and its receptors (VEGFRs) is characterized by a large and broad interface that is relatively flat.[242] In an effort to develop α/β-peptide antagonists of the VEGF-VEGFR interaction, our group designed α/β-peptide mimics of the phage-derived α-peptide **v114** (Figure 1.13).[243] A solution structure of a related peptide, **v107**, suggests that **v114** adopts a specific but irregular secondary structure when bound to VEGF, with very little helix content (Figure 1.13B).[126] Because of **v114**'s irregular secondary structure, the sequence-based design principles outlined above, in which β^3-residues are substituted at regular positions throughout the sequence, were unlikely to be successful. Instead, a "β^3-scan"[244] was employed to survey each position of **v114*** (the M10→Nle analogue of **v114**) for tolerance to α→β^3-residue substitution. Several single positions in **v114*** tolerated α→β^3-residue substitutions, with the resulting α/β-peptides binding to the receptor-binding region of VEGF with affinity comparable to that of **v114*** (though always somewhat lower), as determined by competition FP assay. However, incorporating enough β-residue substitutions to significantly decrease the α/β-peptide's susceptibility to proteolysis led to a large decrease in affinity for VEGF relative to **v114*** (>60-fold decrease in affinity for the α/β-peptide that was the most stable to degradation by proteinase K). Nevertheless, the α/β-peptides identified in this study were able to modestly attenuate the VEGF-induced proliferation of human umbilical

endothelial cells (HUVECs), indicating that they act as antagonists of VEGF signaling in cell culture.

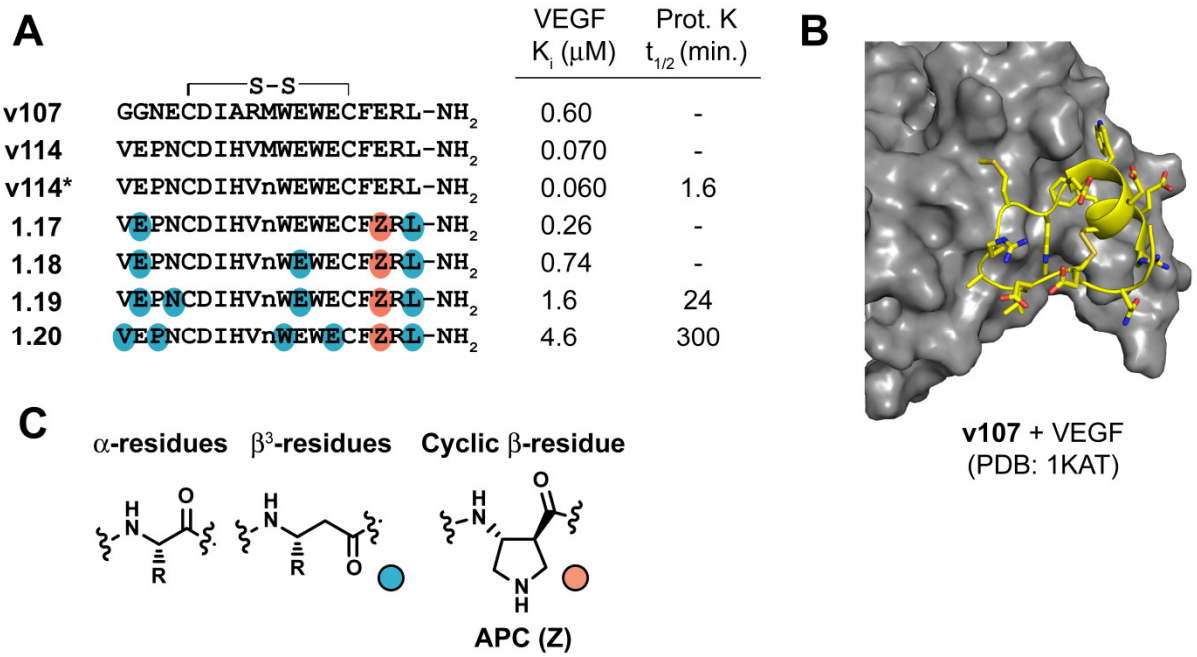

Figure 1.13 Design of α/β-peptides targeting VEGF, derived from phage-derived peptide **v114**.[243] (A) Primary sequences of α- and α/β-peptides, along with associated K_i values (as determined by competition FP assay) and susceptibility of 50 μM α- or α/β-peptide to 10 μg/mL proteinase K in 5% DMSO (from ref.[243]). (B) NMR structure of **v107** (yellow) in complex with $VEGF_{8-109}$ (gray) (PDB: 1KAT).[126] (C) Structures of a generic α-residue, a generic β^3-residue (teal), and the cyclic β-residue APC (Z) (orange).

Recently, Horne et al. designed foldameric analogues of the mini-protein GB1, which adopts a well-defined tertiary structure made up of a helical segment, loops, a four-stranded sheet, and turns.[245] Sequence-based design was used to replace α-residues in the helix and loop regions with β^3-residues, and the resulting α/β-peptides adopted a folded conformation, as determined by circular dichroism experiments. However, α→β^3-residue substitutions in β-sheet regions of the GB1 protein led to a complete loss of tertiary structure. Instead, substitutions with *N*-methyl-α-residues were employed in sheet regions, and Aib and D-proline were used in short turn segments. However, although substitutions in each type of secondary structure individually were minimally detrimental to tertiary structure stability, combining all of the identified

substitutions resulted in a dramatic loss of conformational stability relative to GB1 itself. Conformational stability in the foldamer was recovered through the incorporation of side chain modifications that had previously been identified to increase the thermal stability of the GB1 α-peptide scaffold. The effort ultimately resulted in a foldamer analogue of the GB1 mini-protein containing both backbone and side chain modifications that displayed thermal stability near that of the native GB1 protein. This effort, along with the **v114** example described above, highlight the difficulty in making α→β-residue replacements in non-helical secondary structures.

1.9 Limitations and challenges for α/β-peptides

α/β-Peptides can be designed as structural and functional mimics of α-peptides that adopt a single, contiguous α-helix. The sequence-based design approach, followed by conformational rigidification with cyclic β-residues, appears to be a general strategy for the mimicry of helical α-peptides that bind to specific protein surfaces. The resulting α/β-peptides can adopt helical structures closely resembling an α-helix, can interact with protein targets with affinity comparable to that of their parent α-peptides, can display low susceptibility to proteolysis, and can have enhanced pharmacokinetic properties *in vivo*. However, there are several limitations for α/β-peptide design that must be addressed.

First, thus far α/β-peptide mimicry has been limited primarily to mimicry of single α-helices that bind to their protein targets in hydrophobic clefts. This is a significant limitation given that many protein-protein interaction interfaces feature surfaces that are broader and significantly less regular than a single α-helix. Strategies to extend the α/β-peptide design principles that succeeded for α-helix mimicry toward the mimicry of less regular secondary structures, such as **v114*** and the GB1 scaffold, were largely unsuccessful. In the case of **v114***, for instance, the incorporation of multiple α→β-residue substitutions led to significant decrease

in affinity for the protein target VEGF. The inability to mimic α-peptide conformations beyond a single helix limits the protein surface topologies that can be targeted by α/β-peptides, reducing the number of therapeutically-relevant proteins that can be targeted. Thus, one important goal is to develop a strategy to design an α/β-peptide to target a protein surface, such as the receptor-binding site on VEGF, which is relatively large and irregular in its topology. This goal is addressed in Chapter 2 of this dissertation.

A second limitation of the current α/β-peptide design strategies is that each protein target must be approached *de novo*; the optimal α→β-residue substitution pattern must be experimentally determined for the mimicry of each α-peptide. While the sequence-based design approach provides a general framework for the incorporation of α→β-residue substitutions in helical peptides, this approach often requires the synthesis of sets of α/β-peptides exploring different substitution patterns (e.g., αααβ versus ααβααβ) in different registers, followed by experimental evaluation of affinity or activity, to achieve the optimal α/β-peptides. While this can be achieved with relatively small sets for the mimicry of helical α-peptides (< 20 α/β-peptides analogues), mimicry of secondary structures less regular than an α-helix will likely require the synthesis of many α/β-peptide analogues to determine the optimal substitution pattern. Furthermore, the α→β-residue substitution pattern identified as optimal for one irregular structure will not be directly applicable to the mimicry of an unrelated structure. At present, each new protein target with an irregular surface (i.e., not amenable to modulation by a single α-helix) may require the synthesis of a large library of α/β-peptides to identify the optimal placement of β-residues. Thus, a second important goal is to develop a general strategy to target diverse protein surfaces without needing to chemically synthesize large libraries of α/β-peptides. Ideally, this strategy would identify an optimal α→β-residue substitution pattern that could be translated

to the mimicry of different α-peptides targeting different protein surfaces. This goal is addressed in Chapter 3, and further expanded on in Chapter 4 of this dissertation.

A third limitation of α/β-peptides is that they cannot cross cell membranes. This constraint means that α/β-peptides that target intracellular proteins or protein-protein interactions will have no activity *in vivo*, and significantly limits the number of proteins that can be targeted with these compounds. Thus, a third important goal is to develop a strategy to deliver α/β-peptides into the cytosol of cells. This goal is addressed in Chapters 5 and 6 of this dissertation.

1.10 References

1. Wilson, A. J. (2009) Inhibition of protein-protein interactions using designed molecules, *Chemical Society Reviews 38*, 3289-3300.
2. Azzarito, V., Long, K., Murphy, N. S., and Wilson, A. J. (2013) Inhibition of alpha-helix-mediated protein-protein interactions using designed molecules, *Nature Chemistry 5*, 161-173.
3. Wells, J. A., and McClendon, C. L. (2007) Reaching for high-hanging fruit in drug discovery at protein-protein interfaces, *Nature 450*, 1001-1009.
4. Cochran, A. G. (2000) Antagonists of protein-protein interactions, *Chemistry & Biology 7*, R85-R94.
5. Milroy, L. G., Grossmann, T. N., Hennig, S., Brunsveld, L., and Ottmann, C. (2014) Modulators of Protein-Protein Interactions, *Chemical Reviews 114*, 4695-4748.
6. Fletcher, S., and Hamilton, A. D. (2006) Targeting protein-protein interactions by rational design: mimicry of protein surfaces, *Journal of the Royal Society Interface 3*, 215-233.
7. Jones, S., and Thornton, J. M. (1996) Principles of protein-protein interactions, *Proceedings of the National Academy of Sciences of the United States of America 93*, 13-20.
8. Lo Conte, L., Chothia, C., and Janin, J. (1999) The atomic structure of protein-protein recognition sites, *Journal of Molecular Biology 285*, 2177-2198.
9. Hwang, H., Vreven, T., Janin, J., and Weng, Z. (2010) Protein-protein docking benchmark version 4.0, *Proteins-Structure Function and Bioinformatics 78*, 3111-3114.
10. Keskin, O., Gursoy, A., Ma, B., and Nussinov, R. (2008) Principles of protein-protein interactions: What are the preferred ways for proteins to interact?, *Chemical Reviews 108*, 1225-1244.

11. Arkin, M. R., and Wells, J. A. (2004) Small-molecule inhibitors of protein-protein interactions: Progressing towards the dream, *Nature Reviews Drug Discovery 3*, 301-317.

12. Arkin, M. R., Tang, Y. Y., and Wells, J. A. (2014) Small-Molecule Inhibitors of Protein-Protein Interactions: Progressing toward the Reality, *Chemistry & Biology 21*, 1102-1114.

13. Leader, B., Baca, Q. J., and Golan, D. E. (2008) Protein therapeutics: A summary and pharmacological classification, *Nature Reviews Drug Discovery 7*, 21-39.

14. Mitragotri, S., Burke, P. A., and Langer, R. (2014) Overcoming the challenges in administering biopharmaceuticals: formulation and delivery strategies, *Nature Reviews Drug Discovery 13*, 655-672.

15. Vlieghe, P., Lisowski, V., Martinez, J., and Khrestchatisky, M. (2010) Synthetic therapeutic peptides: science and market, *Drug Discovery Today 15*, 40-56.

16. Nevola, L., and Giralt, E. (2015) Modulating protein-protein interactions: the potential of peptides, *Chemical Communications 51*, 3302-3315.

17. Diao, L., and Meibohm, B. (2013) Pharmacokinetics and Pharmacokinetic-Pharmacodynamic Correlations of Therapeutic Peptides, *Clinical Pharmacokinetics 52*, 855-868.

18. Ferrara, N., Gerber, H. P., and LeCouter, J. (2003) The biology of VEGF and its receptors, *Nature Medicine 9*, 669-676.

19. Carmeliet, P., and Jain, R. K. (2011) Molecular mechanisms and clinical applications of angiogenesis, *Nature 473*, 298-307.

20. Ferrara, N., and Kerbel, R. S. (2005) Angiogenesis as a therapeutic target, *Nature 438*, 967-974.

21. Kim, K. J., Li, B., Winer, J., Armanini, M., Gillett, N., Phillips, H. S., and Ferrara, N. (1993) Inhibititon of vascular endothelial growth factor-induced angiogenesis suppresses tumor growth in vivo, *Nature 362*, 841-844.

22. Grothey, A., and Galanis, E. (2009) Targeting angiogenesis: progress with anti-VEGF treatment with large molecules, *Nature Reviews Clinical Oncology 6*, 507-518.

23. Palladino, M. A., Bahjat, F. R., Theodorakis, E. A., and Moldawer, L. L. (2003) Anti-TNF-alpha therapies: The next generation, *Nature Reviews Drug Discovery 2*, 736-746.

24. Tracey, D., Klareskog, L., Sasso, E. H., Salfeld, J. G., and Tak, P. P. (2008) Tumor necrosis factor antagonist mechanisms of action: A comprehensive review, *Pharmacology & Therapeutics 117*, 244-279.

25. Locksley, R. M., Killeen, N., and Lenardo, M. J. (2001) The TNF and TNF receptor superfamilies: Integrating mammalian biology, *Cell 104*, 487-501.

26. Moore, J. P., and Doms, R. W. (2003) The entry of entry inhibitors: A fusion of science and medicine, *Proceedings of the National Academy of Sciences of the United States of America 100*, 10598-10602.

27. Matthews, T., Salgo, M., Greenberg, M., Chung, J., DeMasi, R., and Bolognesi, D. (2004) Enfuvirtide: The first therapy to inhibit the entry of HIV-1 into host CD4 lymphocytes, *Nature Reviews Drug Discovery 3*, 215-225.

28. Potts, J. T., and Gardella, T. J. (2007) Progress, paradox, and potential - Parathyroid hormone research over five decades, In *Skeletal Biology and Medicine, Pt B - Disease Mechanisms and Therapeutic Challenges* (Zaidi, M., Ed.), pp 196-208, Blackwell Publishing, Oxford.

29. Vilardaga, J. P., Romero, G., Friedman, P. A., and Gardella, T. J. (2011) Molecular basis of parathyroid hormone receptor signaling and trafficking: a family B GPCR paradigm, *Cellular and Molecular Life Sciences 68*, 1-13.

30. Neer, R. M., Arnaud, C. D., Zanchetta, J. R., Prince, R., Gaich, G. A., Reginster, J. Y., Hodsman, A. B., Eriksen, E. F., Ish-Shalom, S., Genant, H. K., Wang, O. H., and Mitlak, B. H. (2001) Effect of parathyroid hormone (1-34) on fractures and bone mineral density in postmenopausal women with osteoporosis, *New England Journal of Medicine 344*, 1434-1441.

31. Goke, R., Fehmann, H. C., Linn, T., Schmidt, H., Krause, M., Eng, J., and Goke, B. (1993) Exendin-4 is a high potency agonist and truncated exendin-(9-39)-amide an antagonist at the glucagon-like peptide 1-(7-36)-amide receptor of insulin-secreting beta-cells, *Journal of Biological Chemistry 268*, 19650-19655.

32. Lovshin, J. A., and Drucker, D. J. (2009) Incretin-based therapies for type 2 diabetes mellitus, *Nature Reviews Endocrinology 5*, 262-269.

33. Slamon, D. J., Clark, G. M., Wong, S. G., Levin, W. J., Ullrich, A., and McGuire, W. L. (1987) Human breast cancer: correlation of relapse and survival with amplification fo the HER-2/neu oncogene, *Science 235*, 177-182.

34. Slamon, D. J., Godolphin, W., Jones, L. A., Holt, J. A., Wong, S. G., Keith, D. E., Levin, W. J., Stuart, S. G., Udove, J., Ullrich, A., and Press, M. F. (1989) Studies of the HER-2/neu proto-oncogene in human breast and ovarian cancer, *Science 244*, 707-712.

35. Carter, P., Presta, L., Gorman, C. M., Ridgway, J. B. B., Henner, D., Wong, W. L. T., Rowland, A. M., Kotts, C., Carver, M. E., and Shepard, H. M. (1992) Humanization of an anti-P185HER2 antibody for human cancer therapy, *Proceedings of the National Academy of Sciences of the United States of America 89*, 4285-4289.

36. Slamon, D. J., Leyland-Jones, B., Shak, S., Fuchs, H., Paton, V., Bajamonde, A., Fleming, T., Eiermann, W., Wolter, J., Pegram, M., Baselga, J., and Norton, L. (2001) Use of chemotherapy plus a monoclonal antibody against HER2 for metastatic breast cancer that overexpresses HER2, *New England Journal of Medicine 344*, 783-792.

37. Orlova, A., Magnusson, M., Eriksson, T. L. J., Nilsson, M., Larsson, B., Hoiden-Guthenherg, I., Widstrom, C., Carlsson, J., Tolmachev, V., Stahl, S., and Nilsson, F. Y. (2006) Tumor Imaging using a picomolar affinity HER2 binding affibody molecule, *Cancer Research 66*, 4339-4348.

38. Baum, R. P., Prasad, V., Muller, D., Schuchardt, C., Orlova, A., Wennborg, A., Tolmachev, V., and Feldwisch, J. (2010) Molecular Imaging of HER2-Expressing

Malignant Tumors in Breast Cancer Patients Using Synthetic In-111- or Ga-68-Labeled Affibody Molecules, *Journal of Nuclear Medicine 51*, 892-897.

39. Sorensen, J., Sandberg, D., Sandstrom, M., Wennborg, A., Feldwisch, J., Tolmachev, V., Astrom, G., Lubberink, M., Garske-Roman, U., Carlsson, J., and Lindman, H. (2014) First-in-Human Molecular Imaging of HER2 Expression in Breast Cancer Metastases Using the In-111-ABY-025 Affibody Molecule, *Journal of Nuclear Medicine 55*, 730-735.

40. Cheng, A. C., Coleman, R. G., Smyth, K. T., Cao, Q., Soulard, P., Caffrey, D. R., Salzberg, A. C., and Huang, E. S. (2007) Structure-based maximal affinity model predicts small-molecule druggability, *Nature Biotechnology 25*, 71-75.

41. Gross, A., McDonnell, J. M., and Korsmeyer, S. J. (1999) BCL-2 family members and the mitochondria in apoptosis, *Genes & Development 13*, 1899-1911.

42. Cory, S., Huang, D. C. S., and Adams, J. M. (2003) The Bcl-2 family: roles in cell survival and oncogenesis, *Oncogene 22*, 8590-8607.

43. Willis, S. N., Fletcher, J. I., Kaufmann, T., van Delft, M. F., Chen, L., Czabotar, P. E., Ierino, H., Lee, E. F., Fairlie, W. D., Bouillet, P., Strasser, A., Kluck, R. M., Adams, J. M., and Huang, D. C. S. (2007) Apoptosis initiated when BH3 ligands engage multiple Bcl-2 homologs, not Bax or Bak, *Science 315*, 856-859.

44. Oltersdorf, T., Elmore, S. W., Shoemaker, A. R., Armstrong, R. C., Augeri, D. J., Belli, B. A., Bruncko, M., Deckwerth, T. L., Dinges, J., Hajduk, P. J., Joseph, M. K., Kitada, S., Korsmeyer, S. J., Kunzer, A. R., Letai, A., Li, C., Mitten, M. J., Nettesheim, D. G., Ng, S., Nimmer, P. M., O'Connor, J. M., Oleksijew, A., Petros, A. M., Reed, J. C., Shen, W., Tahir, S. K., Thompson, C. B., Tomaselli, K. J., Wang, B. L., Wendt, M. D., Zhang, H. C., Fesik, S. W., and Rosenberg, S. H. (2005) An inhibitor of Bcl-2 family proteins induces regression of solid tumours, *Nature 435*, 677-681.

45. Lessene, G., Czabotar, P. E., and Colman, P. M. (2008) BCL-2 family antagonists for cancer therapy, *Nature Reviews Drug Discovery 7*, 989-1000.

46. Tse, C., Shoemaker, A. R., Adickes, J., Anderson, M. G., Chen, J., Jin, S., Johnson, E. F., Marsh, K. C., Mitten, M. J., Nimmer, P., Roberts, L., Tahir, S. K., Mao, Y., Yang, X. F., Zhang, H. C., Fesik, S., Rosenberg, S. H., and Elmore, S. W. (2008) ABT-263: A potent and orally bioavailable Bcl-2 family inhibitor, *Cancer Research 68*, 3421-3428.

47. Roberts, A. W., Seymour, J. F., Brown, J. R., Wierda, W. G., Kipps, T. J., Khaw, S. L., Carney, D. A., He, S. Z., Huang, D. C. S., Xiong, H., Cui, Y., Busman, T. A., McKeegan, E. M., Krivoshik, A. P., Enschede, S. H., and Humerickhouse, R. (2012) Substantial Susceptibility of Chronic Lymphocytic Leukemia to BCL2 Inhibition: Results of a Phase I Study of Navitoclax in Patients With Relapsed or Refractory Disease, *Journal of Clinical Oncology 30*, 488-496.

48. Rudin, C. M., Hann, C. L., Garon, E. B., de Oliveira, M. R., Bonomi, P. D., Camidge, D. R., Chu, Q., Giaccone, G., Khaira, D., Ramalingam, S. S., Ranson, M. R., Dive, C., McKeegan, E. M., Chyla, B. J., Dowell, B. L., Chakravartty, A., Nolan, C. E., Rudersdorf, N., Busman, T. A., Mabry, M. H., Krivoshik, A. P., Humerickhouse, R. A.,

Shapiro, G. I., and Gandhi, L. (2012) Phase II Study of Single-Agent Navitoclax (ABT-263) and Biomarker Correlates in Patients with Relapsed Small Cell Lung Cancer, *Clinical Cancer Research 18*, 3163-3169.

49. Souers, A. J., Leverson, J. D., Boghaert, E. R., Ackler, S. L., Catron, N. D., Chen, J., Dayton, B. D., Ding, H., Enschede, S. H., Fairbrother, W. J., Huang, D. C. S., Hymowitz, S. G., Jin, S., Khaw, S. L., Kovar, P. J., Lam, L. T., Lee, J., Maecker, H. L., Marsh, K. C., Mason, K. D., Mitten, M. J., Nimmer, P. M., Oleksijew, A., Park, C. H., Park, C. M., Phillips, D. C., Roberts, A. W., Sampath, D., Seymour, J. F., Smith, M. L., Sullivan, G. M., Tahir, S. K., Tse, C., Wendt, M. D., Xiao, Y., Xue, J. C., Zhang, H. C., Humerickhouse, R. A., Rosenberg, S. H., and Elmore, S. W. (2013) ABT-199, a potent and selective BCL-2 inhibitor, achieves antitumor activity while sparing platelets, *Nature Medicine 19*, 202-208.

50. Pan, R. Q., Hogdal, L. J., Benito, J. M., Bucci, D., Han, L., Borthakur, G., Cortes, J., DeAngelo, D. J., Debose, L., Mu, H., Dohner, H., Gaidzik, V. I., Galinsky, I., Golfman, L. S., Haferlach, T., Harutyunyan, K. G., Hu, J. H., Leverson, J. D., Marcucci, G., Muschen, M., Newman, R., Park, E., Ruvolo, P. P., Ruvolo, V., Ryan, J., Schindela, S., Zweidler-McKay, P., Stone, R. M., Kantarjian, H., Andreeff, M., Konopleva, M., and Letai, A. G. (2014) Selective BCL-2 Inhibition by ABT-199 Causes On-Target Cell Death in Acute Myeloid Leukemia, *Cancer Discovery 4*, 362-375.

51. He, M. M., Smith, A. S., Oslob, J. D., Flanagan, W. M., Braisted, A. C., Whitty, A., Cancilla, M. T., Wang, J., Lugovskoy, A. A., Yoburn, J. C., Fung, A. D., Farrington, G., Eldredge, J. K., Day, E. S., Cruz, L. A., Cachero, T. G., Miller, S. K., Friedman, J. E., Choong, I. C., and Cunningham, B. C. (2005) Small-molecule inhibition of TNF-alpha, *Science 310*, 1022-1025.

52. Rettenmaier, T. J., Sadowsky, J. D., Thomsen, N. D., Chen, S. C., Doak, A. K., Arkin, M. R., and Wells, J. A. (2014) A small-molecule mimic of a peptide docking motif inhibits the protein kinase PDK1, *Proceedings of the National Academy of Sciences of the United States of America 111*, 18590-18595.

53. Kariolis, M. S., Kapur, S., and Cochran, J. R. (2013) Beyond antibodies: using biological principles to guide the development of next-generation protein therapeutics, *Current Opinion in Biotechnology 24*, 1072-1077.

54. Beck, A., Wurch, T., Bailly, C., and Corvaia, N. (2010) Strategies and challenges for the next generation of therapeutic antibodies, *Nature Reviews Immunology 10*, 345-352.

55. Ferrara, N., Hillan, K. J., Gerber, H. P., and Novotny, W. (2004) Discovery and development of bevacizumab, an anti-VEGF antibody for treating cancer, *Nature Reviews Drug Discovery 3*, 391-400.

56. Rosenfeld, P. J., Brown, D. M., Heier, J. S., Boyer, D. S., Kaiser, P. K., Chung, C. Y., Kim, R. Y., and Grp, M. S. (2006) Ranibizumab for neovascular age-related macular degeneration, *New England Journal of Medicine 355*, 1419-1431.

57. Heier, J. S., Brown, D. M., Chong, V., Korobelnik, J. F., Kaiser, P. K., Nguyen, Q. D., Kirchhof, B., Ho, A., Ogura, Y., Yancopoulos, G. D., Stahl, N., Vitti, R., Berliner, A. J., Soo, Y., Anderesi, M., Groetzbach, G., Sommerauer, B., Sandbrink, R., Simader, C.,

Schmidt-Erfurth, U., and Grp, V. V. S. (2012) Intravitreal Aflibercept (VEGF Trap-Eye) in Wet Age-related Macular Degeneration, *Ophthalmology 119*, 2537-2548.

58. Holash, J., Davis, S., Papadopoulos, N., Croll, S. D., Ho, L., Russell, M., Boland, P., Leidich, R., Hylton, D., Burova, E., Ioffe, E., Huang, T., Radziejewski, C., Bailey, K., Fandl, J. P., Daly, T., Wiegand, S. J., Yancopoulos, G. D., and Rudge, J. S. (2002) VEGF-Trap: A VEGF blocker with potent antitumor effects, *Proceedings of the National Academy of Sciences of the United States of America 99*, 11393-11398.

59. Papo, N., Silverman, A. P., Lahti, J. L., and Cochran, J. R. (2011) Antagonistic VEGF variants engineered to simultaneously bind to and inhibit VEGFR2 and alpha(v)beta(3) integrin, *Proceedings of the National Academy of Sciences of the United States of America 108*, 14067-14072.

60. Brooks, P. C., Clark, R. A. F., and Cheresh, D. A. (1994) Requirement of vascular integrin alpha(v)beta(3) for angiogenesis, *Science 264*, 569-571.

61. Passaniti, A., Taylor, R. M., Pili, R., Guo, Y., Long, P. V., Haney, J. A., Pauly, R. R., Grant, D. S., and Martin, G. R. (1992) Methods in laboratory investigation: a simple, quantitative method for assessing angiogenesis and antiangiogenic agents using reconstituted basement-membrane, heparin, and fibroblast growth factor, *Laboratory Investigation 67*, 519-528.

62. Hruby, V. J. (2002) Designing peptide receptor agonists and antagonists, *Nature Reviews Drug Discovery 1*, 847-858.

63. Stevenson, C. L. (2009) Advances in Peptide Pharmaceuticals, *Current Pharmaceutical Biotechnology 10*, 122-137.

64. Kilby, J. M., Hopkins, S., Venetta, T. M., DiMassimo, B., Cloud, G. A., Lee, J. Y., Alldredge, L., Hunter, E., Lambert, D., Bolognesi, D., Mathews, T., Johnson, M. R., Nowak, M. A., Shaw, G. M., and Saag, M. S. (1998) Potent suppression of HIV-1 replication in humans by T-20, a peptide inhibitor of gp41-mediated virus entry, *Nature Medicine 4*, 1302-1307.

65. Lagerstrom, M. C., and Schioth, H. B. (2008) Structural diversity of G protein-coupled receptors and significance for drug discovery, *Nature Reviews Drug Discovery 7*, 339-357.

66. Letai, A., Bassik, M. C., Walensky, L. D., Sorcinelli, M. D., Weiler, S., and Korsmeyer, S. J. (2002) Distinct BH3 domains either sensitize or activate mitochondrial apoptosis, serving as prototype cancer therapeutics, *Cancer Cell 2*, 183-192.

67. Chen, L., Willis, S. N., Wei, A., Smith, B. J., Fletcher, J. I., Hinds, M. G., Colman, P. M., Day, C. L., Adams, J. M., and Huang, D. C. S. (2005) Differential targeting of prosurvival Bcl-2 proteins by their BH3-only ligands allows complementary apoptotic function, *Molecular Cell 17*, 393-403.

68. Jochim, A. L., and Arora, P. S. (2009) Assessment of helical interfaces in protein-protein interactions, *Molecular Biosystems 5*, 924-926.

69. Jochim, A. L., and Arora, P. S. (2010) Systematic Analysis of Helical Protein Interfaces Reveals Targets for Synthetic Inhibitors, *Acs Chemical Biology 5*, 919-923.

70. Lao, B. B., Drew, K., Guarracino, D. A., Brewer, T. F., Heindel, D. W., Bonneau, R., and Arora, P. S. (2014) Rational Design of Topographical Helix Mimics as Potent Inhibitors of Protein-Protein Interactions, *Journal of the American Chemical Society 136*, 7877-7888.

71. Estieu-Gionnet, K., and Guichard, G. (2011) Stabilized helical peptides: overview of the technologies and therapeutic promises, *Expert Opinion on Drug Discovery 6*, 937-963.

72. Henchey, L. K., Jochim, A. L., and Arora, P. S. (2008) Contemporary strategies for the stabilization of peptides in the alpha-helical conformation, *Current Opinion in Chemical Biology 12*, 692-697.

73. Tyndall, J. D. A., Nall, T., and Fairlie, D. P. (2005) Proteases universally recognize beta strands in their active sites, *Chemical Reviews 105*, 973-999.

74. Oneil, K. T., and Degrado, W. F. (1990) A thermodynamic scale for the helix forming tendencies of the commonly occurring amino acids, *Science 250*, 646-651.

75. Huyghues-Despointes, B. M. P., Scholtz, J. M., and Baldwin, R. L. (1993) Helical peptides with 3 pairs of Asp-Arg and Glu-Arg residues in different orientations and spacings, *Protein Science 2*, 80-85.

76. Scholtz, J. M., Qian, H., Robbins, V. H., and Baldwin, R. L. (1993) The energetics of ion-pair and hydrogen-bonding interactions in a helical peptides, *Biochemistry 32*, 9668-9676.

77. Dwyer, J. J., Wilson, K. L., Davison, D. K., Freel, S. A., Seedorff, J. E., Wring, S. A., Tvermoes, N. A., Matthews, T. J., Greenberg, M. L., and Delmedico, M. K. (2007) Design of helical, oligomeric HIV-1 fusion inhibitor peptides with potent activity against enfuvirtide-resistant virus, *Proceedings of the National Academy of Sciences of the United States of America 104*, 12772-12777.

78. Lau, Y. H., De Andrade, P., Wu, Y. T., and Spring, D. R. (2015) Peptide stapling techniques based on different macrocyclisation chemistries, *Chemical Society Reviews 44*, 91-102.

79. Felix, A. M., Heimer, E. P., Wang, C. T., Lambros, T. J., Fournier, A., Mowles, T. F., Maines, S., Campbell, R. M., Wegrzynski, B. B., Toome, V., Fry, D., and Madison, V. S. (1988) Synthesis, biological activity and conformational analysis of cyclic GRF analogs, *International Journal of Peptide and Protein Research 32*, 441-454.

80. Murage, E. N., Gao, G. Z., Bisello, A., and Ahn, J. M. (2010) Development of Potent Glucagon-like Peptide-1 Agonists with High Enzyme Stability via Introduction of Multiple Lactam Bridges, *Journal of Medicinal Chemistry 53*, 6412-6420.

81. Okamoto, T., Zobel, K., Fedorova, A., Quan, C., Yang, H., Fairbrother, W. J., Huang, D. C. S., Smith, B. J., Deshayes, K., and Czabotar, P. E. (2013) Stabilizing the Pro-Apoptotic BimBH3 Helix (BimSAHB) Does Not Necessarily Enhance Affinity or Biological Activity, *Acs Chemical Biology 8*, 297-302.

82. Jo, H., Meinhardt, N., Wu, Y., Kulkarni, S., Hu, X., Low, K. E., Davies, P. L., DeGrado, W. F., and Greenbaum, D. C. (2012) Development of alpha-Helical Calpain Probes by

Mimicking a Natural Protein-Protein Interaction, *Journal of the American Chemical Society 134*, 17704-17713.

83. Cantel, S., Isaad, A. L. C., Scrima, M., Levy, J. J., DiMarchi, R. D., Rovero, P., Halperin, J. A., D'Ursi, A. M., Papini, A. M., and Chorev, M. (2008) Synthesis and conformational analysis of a cyclic peptide obtained via i to i+4 intramolecular side-chain to side-chain azide - Alkyne 1,3-dipolar cycloaddition, *Journal of Organic Chemistry 73*, 5663-5674.

84. Kawamoto, S. A., Coleska, A., Ran, X., Yi, H., Yang, C. Y., and Wang, S. M. (2012) Design of Triazole-Stapled BCL9 alpha-Helical Peptides to Target the beta-Catenin/B-Cell CLL/lymphoma 9 (BCL9) Protein-Protein Interaction, *Journal of Medicinal Chemistry 55*, 1137-1146.

85. Blackwell, H. E., and Grubbs, R. H. (1998) Highly efficient synthesis of covalently cross-linked peptide helices by ring-closing metathesis, *Angewandte Chemie-International Edition 37*, 3281-3284.

86. Blackwell, H. E., Sadowsky, J. D., Howard, R. J., Sampson, J. N., Chao, J. A., Steinmetz, W. E., O'Leary, D. J., and Grubbs, R. H. (2001) Ring-closing metathesis of olefinic peptides: Design, synthesis, and structural characterization of macrocyclic helical peptides, *Journal of Organic Chemistry 66*, 5291-5302.

87. Schafmeister, C. E., Po, J., and Verdine, G. L. (2000) An all-hydrocarbon cross-linking system for enhancing the helicity and metabolic stability of peptides, *Journal of the American Chemical Society 122*, 5891-5892.

88. Toniolo, C., Bonora, G. M., Bavoso, A., Benedetti, E., Diblasio, B., Pavone, V., and Pedone, C. (1983) Preferred conformations of peptides containing alpha, alpha-disubstituted alpha-amino acids, *Biopolymers 22*, 205-215.

89. Walensky, L. D., Kung, A. L., Escher, I., Malia, T. J., Barbuto, S., Wright, R. D., Wagner, G., Verdine, G. L., and Korsmeyer, S. J. (2004) Activation of apoptosis in vivo by a hydrocarbon-stapled BH3 helix, *Science 305*, 1466-1470.

90. Walensky, L. D., Pitter, K., Morash, J., Oh, K. J., Barbuto, S., Fisher, J., Smith, E., Verdine, G. L., and Korsmeyer, S. J. (2006) A stapled BID BH3 helix directly binds and activates BAX, *Molecular Cell 24*, 199-210.

91. Bernal, F., Tyler, A. F., Korsmeyer, S. J., Walensky, L. D., and Verdine, G. L. (2007) Reactivation of the p53 tumor suppressor pathway by a stapled p53 peptide, *Journal of the American Chemical Society 129*, 2456-2457.

92. Bernal, F., Wade, M., Godes, M., Davis, T. N., Whitehead, D. G., Kung, A. L., Wahl, G. M., and Walensky, L. D. (2010) A Stapled p53 Helix Overcomes HDMX-Mediated Suppression of p53, *Cancer Cell 18*, 411-422.

93. Gavathiotis, E., Suzuki, M., Davis, M. L., Pitter, K., Bird, G. H., Katz, S. G., Tu, H. C., Kim, H., Cheng, E. H. Y., Tjandra, N., and Walensky, L. D. (2008) BAX activation is initiated at a novel interaction site, *Nature 455*, 1076-1081.

94. Stewart, M. L., Fire, E., Keating, A. E., and Walensky, L. D. (2010) The MCL-1 BH3 helix is an exclusive MCL-1 inhibitor and apoptosis sensitizer, *Nature Chemical Biology 6*, 595-601.

95. Walensky, L. D., and Bird, G. H. (2014) Hydrocarbon-Stapled Peptides: Principles, Practice, and Progress, *Journal of Medicinal Chemistry 57*, 6275-6288.

96. Cromm, P. M., Spiegal, J., and Grossmann, T. N. (2015) Hydrocarbon Stapled Peptides as Modulators of Biological Function, *ACS Chemical Biology 10*, 1362-1375.

97. LaBelle, J. L., Katz, S. G., Bird, G. H., Gavathiotis, E., Stewart, M. L., Lawrence, C., Fisher, J. K., Godes, M., Pitter, K., Kung, A. L., and Walensky, L. D. (2012) A stapled BIM peptide overcomes apoptotic resistance in hematologic cancers, *Journal of Clinical Investigation 122*, 2018-2031.

98. Edwards, A. L., Gavathiotis, E., LaBelle, J. L., Braun, C. R., Opoku-Nsiah, K. A., Bird, G. H., and Walensky, L. D. (2013) Multimodal Interaction with BCL-2 Family Proteins Underlies the Proapoptotic Activity of PUMA BH3, *Chemistry & Biology 20*, 888-902.

99. Moellering, R. E., Cornejo, M., Davis, T. N., Del Bianco, C., Aster, J. C., Blacklow, S. C., Kung, A. L., Gilliland, D. G., Verdine, G. L., and Bradner, J. E. (2009) Direct inhibition of the NOTCH transcription factor complex, *Nature 462*, 182-188.

100. Takada, K., Zhu, D., Bird, G. H., Sukhdeo, K., Zhao, J. J., Mani, M., Lemieux, M., Carrasco, D. E., Ryan, J., Horst, D., Fulciniti, M., Munshi, N. C., Xu, W. Q., Kung, A. L., Shivdasani, R. A., Walensky, L. D., and Carrasco, D. R. (2012) Targeted Disruption of the BCL9/beta-Catenin Complex Inhibits Oncogenic Wnt Signaling, *Science Translational Medicine 4*, 148ra117.

101. Bird, G. H., Madani, N., Perry, A. F., Princiotto, A. M., Supko, J. G., He, X. Y., Gavathiotis, E., Sodroski, J. G., and Walensky, L. D. (2010) Hydrocarbon double-stapling remedies the proteolytic instability of a lengthy peptide therapeutic, *Proceedings of the National Academy of Sciences of the United States of America 107*, 14093-14098.

102. Hilinski, G. J., Kim, Y. W., Hong, J., Kutchukian, P. S., Crenshaw, C. M., Berkovitch, S. S., Chang, A., Ham, S., and Verdine, G. L. (2014) Stitched alpha-Helical Peptides via Bis Ring-Closing Metathesis, *Journal of the American Chemical Society 136*, 12314-12322.

103. Chu, Q., Moellering, R. E., Hilinski, G. J., Kim, Y. W., Grossmann, T. N., Yeh, J. T. H., and Verdine, G. L. (2015) Towards understanding cell penetration by stapled peptides, *Medchemcomm 6*, 111-119.

104. Glas, A., Bier, D., Hahne, G., Rademacher, C., Ottmann, C., and Grossmann, T. N. (2014) Constrained Peptides with Target-Adapted Cross-Links as Inhibitors of a Pathogenic Protein-Protein Interaction, *Angewandte Chemie-International Edition 53*, 2489-2493.

105. Bird, G. H., Gavathiotis, E., LaBelle, J. L., Katz, S. G., and Walensky, L. D. (2014) Distinct BimBH3 (BimSAHB) Stapled Peptides for Structural and Cellular Studies, *Acs Chemical Biology 9*, 831-837.

106. Li, Y. C., Rodewald, L. W., Hoppmann, C., Wong, E. T., Lebreton, S., Safar, P., Patek, M., Wang, L., Wertman, K. F., and Wahl, G. M. (2014) A Versatile Platform to Analyze Low-Affinity and Transient Protein-Protein Interactions in Living Cells in Real Time, *Cell Reports 9*, 1946-1958.

107. Baek, S., Kutchukian, P. S., Verdine, G. L., Huber, R., Holak, T. A., Lee, K. W., and Popowicz, G. M. (2012) Structure of the Stapled p53 Peptide Bound to Mdm2, *Journal of the American Chemical Society 134*, 103-106.

108. Chapman, R. N., Dimartino, G., and Arora, P. S. (2004) A highly stable short alpha-helix constrained by a main-chain hydrogen-bond surrogate, *Journal of the American Chemical Society 126*, 12252-12253.

109. Patgiri, A., Jochim, A. L., and Arora, P. S. (2008) A Hydrogen Bond Surrogate Approach for Stabilization of Short Peptide Sequences in alpha-Helical Conformation, *Accounts of Chemical Research 41*, 1289-1300.

110. Wang, D. Y., Liao, W., and Arora, P. S. (2005) Binding properties of artificial a helices derived from a hydrogen-bond surrogate: Application to Bcl-xL, *Angewandte Chemie-International Edition 44*, 6525-6529.

111. Wang, D. Y., Liao, W., and Arora, P. S. (2005) Enhanced metabolic stability and protein-binding properties of artificial a helices derived from a hydrogen-bond surrogate: Application to Bcl-xL, *Angewandte Chemie-International Edition 44*, 6525-6529.

112. Wang, D., Lu, M., and Arora, P. S. (2008) Inhibition of HIV-1 fusion by hydrogen-bond-surrogate-based alpha helices, *Angewandte Chemie-International Edition 47*, 1879-1882.

113. Henchey, L. K., Porter, J. R., Ghosh, I., and Arora, P. S. (2010) High Specificity in Protein Recognition by Hydrogen-Bond-Surrogate alpha-Helices: Selective Inhibition of the p53/MDM2 Complex, *Chembiochem 11*, 2104-2107.

114. Patgiri, A., Joy, S. T., and Arora, P. S. (2012) Nucleation Effects in Peptide Foldamers, *Journal of the American Chemical Society 134*, 11495-11502.

115. Henchey, L. K., Kushal, S., Dubey, R., Chapman, R. N., Olenyuk, B. Z., and Arora, P. S. (2010) Inhibition of Hypoxia Inducible Factor 1-Transcription Coactivator Interaction by a Hydrogen Bond Surrogate alpha-Helix, *Journal of the American Chemical Society 132*, 941-943.

116. Kushal, S., Lao, B. B., Henchey, L. K., Dubey, R., Mesallati, H., Traaseth, N. J., Olenyuk, B. Z., and Arora, P. S. (2013) Protein domain mimetics as in vivo modulators of hypoxia-inducible factor signaling, *Proceedings of the National Academy of Sciences of the United States of America 110*, 15602-15607.

117. Patgiri, A., Yadav, K. K., Arora, P. S., and Bar-Sagi, D. (2011) An orthosteric inhibitor of the Ras-Sos interaction, *Nature Chemical Biology 7*, 585-587.

118. Gallop, M. A., Barrett, R. W., Dower, W. J., Fodor, S. P. A., and Gordon, E. M. (1994) Applications of combinatorial technologies to drug discovery. 1. Background and peptide combinatorial libraries, *Journal of Medicinal Chemistry 37*, 1233-1251.

119. Smith, G. P. (1985) Filamentous fusion phage: novel expression vectors that display cloned antigens on the viron surface, *Science 228*, 1315-1317.

120. Cwirla, S. E., Peters, E. A., Barrett, R. W., and Dower, W. J. (1990) Peptides on phage: a vast library of peptides for identifying ligands, *Proceedings of the National Academy of Sciences of the United States of America 87*, 6378-6382.

121. Hamzeh-Mivehroud, M., Alizadeh, A. A., Morris, M. B., Church, W. B., and Dastmalchi, S. (2013) Phage display as a technology delivering on the promise of peptide drug discovery, *Drug Discovery Today 18*, 1144-1157.

122. Sidhu, S. S., Fairbrother, W. J., and Deshayes, K. (2003) Exploring protein-protein interactions with phage display, *Chembiochem 4*, 14-25.

123. Houghten, R. A., Pinilla, C., Blondelle, S. E., Appel, J. R., Dooley, C. T., and Cuervo, J. H. (1991) Generation and use of synthetic peptide combinatorial libraries for basic research and drug discovery, *Nature 354*, 84-86.

124. Houghten, R. A. (1985) General method for the rapid solid-phase synthesis of large numbers of peptides: specificity of antigen-antibody interaction at the level of individual amino acids, *Proceedings of the National Academy of Sciences of the United States of America 82*, 5131-5135.

125. Fairbrother, W. J., Christinger, H. W., Cochran, A. G., Fuh, C., Keenan, C. J., Quan, C., Shriver, S. K., Tom, J. Y. K., Wells, J. A., and Cunningham, B. C. (1998) Novel peptides selected to bind vascular endothelial growth factor target the receptor-binding site, *Biochemistry 37*, 17754-17764.

126. Pan, B., Li, B., Russell, S. J., Tom, J. Y. K., Cochran, A. G., and Fairbrother, W. J. (2002) Solution structure of a phage-derived peptide antagonist in complex with vascular endothelial growth factor, *Journal of Molecular Biology 316*, 769-787.

127. Foight, G. W., Ryan, J. A., Gulla, S. V., Letai, A., and Keating, A. E. (2014) Designed BH3 Peptides with High Affinity and Specificity for Targeting Mcl-1 in Cells, *Acs Chemical Biology 9*, 1962-1968.

128. Binz, H. K., Amstutz, P., and Pluckthun, A. (2005) Engineering novel binding proteins from nonimmunoglobulin domains, *Nature Biotechnology 23*, 1257-1268.

129. Gebauer, M., and Skerra, A. (2009) Engineered protein scaffolds as next-generation antibody therapeutics, *Current Opinion in Chemical Biology 13*, 245-255.

130. Gronwall, C., and Stahl, S. (2009) Engineered affinity proteins-Generation and applications, *Journal of Biotechnology 140*, 254-269.

131. Nygren, P. A., and Skerra, A. (2004) Binding proteins from alternative scaffolds, *Journal of Immunological Methods 290*, 3-28.

132. Skerra, A. (2007) Alternative non-antibody scaffolds for molecular recognition, *Current Opinion in Biotechnology 18*, 295-304.

133. Stahl, S., Kronqvist, N., Jonsson, A., and Lofblom, J. (2013) Affinity proteins and their generation, *Journal of Chemical Technology and Biotechnology 88*, 25-38.

134. Zoller, F., Haberkorn, U., and Mier, W. (2011) Miniproteins as Phage Display-Scaffolds for Clinical Applications, *Molecules 16*, 2467-2485.

135. Tashiro, M., Tejero, R., Zimmerman, D. E., Celda, B., Nilsson, B., and Montelione, G. T. (1997) High-resolution solution NMR structure of the Z domain of staphylococcal protein A, *Journal of Molecular Biology 272*, 573-590.

136. Eigenbrot, C., Ultsch, M., Dubnovitsky, A., Abrahmsen, L., and Hard, T. (2010) Structural basis for high-affinity HER2 receptor binding by an engineered protein, *Proceedings of the National Academy of Sciences of the United States of America 107*, 15039-15044.

137. Lofblom, J., Feldwisch, J., Tolmachev, V., Carlsson, J., Stahl, S., and Frejd, F. Y. (2010) Affibody molecules: Engineered proteins for therapeutic, diagnostic and biotechnological applications, *Febs Letters 584*, 2670-2680.

138. Nygren, P. A. (2008) Alternative binding proteins: Affibody binding proteins developed from a small three-helix bundle scaffold, *Febs Journal 275*, 2668-2676.

139. Nord, K., Gunneriusson, E., Ringdahl, J., Stahl, S., Uhlen, M., and Nygren, P. A. (1997) Binding proteins selected from combinatorial libraries of an alpha-helical bacterial receptor domain, *Nature Biotechnology 15*, 772-777.

140. Fedorova, A., Zobel, K., Gill, H. S., Ogasawara, A., Flores, J. E., Tinianow, J. N., Vanderbilt, A. N., Wu, P., Meng, Y. G., Williams, S. P., Wiesmann, C., Murray, J., Marik, J., and Deshayes, K. (2011) The Development of Peptide-Based Tools for the Analysis of Angiogenesis, *Chemistry & Biology 18*, 839-845.

141. Fleetwood, F., Klint, S., Hanze, M., Gunneriusson, E., Frejd, F. Y., Stah, S., and Lofblom, J. (2014) Simultaneous targeting of two ligand-binding sites on VEGFR2 using biparatopic Affibody molecules results in dramatically improved affinity, *Scientific Reports 4*, 7518.

142. Jonsson, A., Wallberg, H., Herne, N., Stahl, S., and Frejd, F. Y. (2009) Generation of tumour-necrosis-factor-alpha-specific affibody molecules capable of blocking receptor binding in vitro, *Biotechnology and Applied Biochemistry 54*, 93-103.

143. Kronqvist, N., Lofblom, J., Jonsson, A., Wernerus, H., and Stahl, S. (2008) A novel affinity protein selection system based on staphylococcal cell surface display and flow cytometry, *Protein Engineering Design & Selection 21*, 247-255.

144. Lofdahl, P. A., Nord, O., Janzon, L., and Nygren, P. A. (2009) Selection of TNF-alpha binding affibody molecules using a beta-lactamase protein fragment complementation assay, *New Biotechnology 26*, 251-259.

145. Lofdahl, P. A., and Nygren, P. A. (2010) Affinity maturation of a TNF alpha-binding Affibody molecule by Darwinian survival selection, *Biotechnology and Applied Biochemistry 55*, 111-120.

146. Wikman, M., Steffen, A. C., Gunneriusson, E., Tolmachev, V., Adams, G. P., Carlsson, J., and Stahl, S. (2004) Selection and characterization of HER2/neu-binding affibody ligands, *Protein Engineering Design & Selection 17*, 455-462.

147. Friedman, M., Nordberg, E., Hoiden-Guthenberg, I., Brisimar, H., Adams, G. P., Nilsson, F. Y., Carlss, J., and Stahl, S. (2007) Phage display selection of Affibody molecules with specific binding to the extracellular domain of the epidermal growth factor receptor, *Protein Engineering Design & Selection 20*, 189-199.

148. Friedman, M., Orlova, A., Johansson, E., Eriksson, T. L. J., Hoiden-Guthenberg, I., Tolmachev, V., Nilsson, F. Y., and Stahl, S. (2008) Directed evolution to low nanomolar

affinity of a tumor-targeting epidermal growth factor receptor-binding affibody molecule, *Journal of Molecular Biology 376*, 1388-1402.

149. Stumpp, M. T., Binz, H. K., and Amstutz, P. (2008) DARPins: A new generation of protein therapeutics, *Drug Discovery Today 13*, 695-701.

150. Lipovsek, D. (2011) Adnectins: engineered target-binding protein therapeutics, *Protein Engineering Design & Selection 24*, 3-9.

151. Skerra, A. (2008) Alternative binding proteins: Anticalins - harnessing the structural plasticity of the lipocalin ligand pocket to engineer novel binding activities, *Febs Journal 275*, 2677-2683.

152. Silverman, J., Lu, Q., Bakker, A., To, W., Duguay, A., Alba, B. M., Smith, R., Rivas, A., Li, P., Le, H., Whitehorn, E., Moore, K. W., Swimmer, C., Perlroth, V., Vogt, M., Kolkman, J., and Stemmer, W. P. C. (2005) Multivalent avimer proteins evolved by exon shuffling of a family of human receptor domains, *Nature Biotechnology 23*, 1556-1561.

153. Kim, B., Eggel, A., Tarchevskaya, S. S., Vogel, M., Prinz, H., and Jardetzky, T. S. (2012) Accelerated disassembly of IgE-receptor complexes by a disruptive macromolecular inhibitor, *Nature 491*, 613-617.

154. Getmanova, E. V., Chen, Y., Bloom, L., Gokemeijer, J., Shamah, S., Warikoo, V., Wang, J., Ling, V., and Sun, L. (2006) Antagonists to human and mouse vascular endothelial growth factor receptor 2 generated by directed protein evolution in vitro, *Chemistry & Biology 13*, 549-556.

155. Dineen, S. P., Sullivan, L. A., Beck, A. W., Miller, A. F., Carbon, J. G., Mamluk, R., Wong, H., and Brekken, R. A. (2008) The Adnectin CT-322 is a novel VEGF receptor 2 inhibitor that decreases tumor burden in an orthotopic mouse model of pancreatic cancer, *Bmc Cancer 8*, 352.

156. Tolcher, A. W., Sweeney, C. J., Papadopoulos, K., Patnaik, A., Chiorean, E. G., Mita, A. C., Sankhala, K., Furfine, E., Gokemeijer, J., Iacono, L., Eaton, C., Silver, B. A., and Mita, M. (2011) Phase I and Pharmacokinetic Study of CT-322 (BMS-844203), a Targeted Adnectin Inhibitor of VEGFR-2 Based on a Domain of Human Fibronectin, *Clinical Cancer Research 17*, 363-371.

157. Pollaro, L., and Heinis, C. (2010) Strategies to prolong the plasma residence time of peptide drugs, *Medchemcomm 1*, 319-324.

158. Gilbreth, R. N., and Koide, S. (2012) Structural insights for engineering binding proteins based on non-antibody scaffolds, *Current Opinion in Structural Biology 22*, 413-420.

159. Binz, H. K., Amstutz, P., Kohl, A., Stumpp, M. T., Briand, C., Forrer, P., Grutter, M. G., and Pluckthun, A. (2004) High-affinity binders selected from designed ankyrin repeat protein libraries, *Nature Biotechnology 22*, 575-582.

160. Koide, A., Wojcik, J., Gilbreth, R. N., Hoey, R. J., and Koide, S. (2012) Teaching an Old Scaffold New Tricks: Monobodies Constructed Using Alternative Surfaces of the FN3 Scaffold, *Journal of Molecular Biology 415*, 393-405.

161. Schonfeld, D., Matschiner, G., Chatwell, L., Trentmann, S., Gille, H., Hulsmeyer, M., Brown, N., Kaye, P. M., Schlehuber, S., Hohlbaum, A. M., and Skerra, A. (2009) An engineered lipocalin specific for CTLA-4 reveals a combining site with structural and conformational features similar to antibodies, *Proceedings of the National Academy of Sciences of the United States of America 106*, 8198-8203.

162. Gellman, S. H. (1998) Foldamers: A manifesto, *Accounts of Chemical Research 31*, 173-180.

163. Horne, W. S. (2011) Peptide and peptoid foldamers in medicinal chemistry, *Expert Opinion on Drug Discovery 6*, 1247-1262.

164. Goodman, C. M., Choi, S., Shandler, S., and DeGrado, W. F. (2007) Foldamers as versatile frameworks for the design and evolution of function, *Nature Chemical Biology 3*, 252-262.

165. Frackenpohl, J., Arvidsson, P. I., Schreiber, J. V., and Seebach, D. (2001) The outstanding biological stability of beta- and gamma-peptides toward proteolytic enzymes: An in vitro investigation with fifteen peptidases, *Chembiochem 2*, 445-455.

166. Steer, D. L., Lew, R. A., Perlmutter, P., Smith, A. I., and Aguilar, M. I. (2002) beta-amino acids: Versatile peptidomimetics, *Current Medicinal Chemistry 9*, 811-822.

167. Milton, R. C. D., Milton, S. C. F., and Kent, S. B. H. (1992) Total chemical synthesis of a D-enzyme: the enantiomers of HIV-1 protease show demonstration of a reciprocal chiral substrate specificity, *Science 256*, 1445-1448.

168. Miller, S. M., Simon, R. J., Ng, S., Zuckermann, R. N., Kerr, J. M., and Moos, W. H. (1995) Comparison of the proteolytic susceptibilities of homologous L-amino acid, D-amino acid, and N-substituted glycine peptide and peptoid oligomers, *Drug Development Research 35*, 20-32.

169. Schumacher, T. N. M., Mayr, L. M., Minor, D. L., Milhollen, M. A., Burgess, M. W., and Kim, P. S. (1996) Identification of D-peptide ligands through mirror-image phage display, *Science 271*, 1854-1857.

170. Zhao, L., and Lu, W. (2014) Mirror image proteins, *Current Opinion in Chemical Biology 22*, 56-61.

171. Eckert, D. M., Malashkevich, V. N., Hong, L. H., Carr, P. A., and Kim, P. S. (1999) Inhibiting HIV-1 entry: Discovery of D-peptide inhibitors that target the gp41 coiled-coil pocket, *Cell 99*, 103-115.

172. Welch, B. D., VanDemark, A. P., Heroux, A., Hill, C. P., and Kay, M. S. (2007) Potent D-peptide inhibitors of HIV-1 entry, *Proceedings of the National Academy of Sciences of the United States of America 104*, 16828-16833.

173. Welch, B. D., Francis, J. N., Redman, J. S., Paul, S., Weinstock, M. T., Reeves, J. D., Lie, Y. S., Whitby, F. G., Eckert, D. M., Hill, C. P., Root, M. J., and Kay, M. S. (2010) Design of a Potent D-Peptide HIV-1 Entry Inhibitor with a Strong Barrier to Resistance, *Journal of Virology 84*, 11235-11244.

174. Liu, M., Li, C., Pazgier, M., Li, C. Q., Mao, Y. B., Lv, Y. F., Gu, B., Wei, G., Yuan, W. R., Zhan, C. Y., and Lu, W. Y. (2010) D-peptide inhibitors of the p53-MDM2 interaction for targeted molecular therapy of malignant neoplasms, *Proceedings of the National Academy of Sciences of the United States of America 107*, 14321-14326.

175. Zhan, C., Zhao, L., Wei, X., Wu, X., Chen, X., Yuan, W., Lu, W.-Y., Pazgier, M., and Lu, W. (2012) An Ultrahigh Affinity D-Peptide Antagonist Of MDM2, *Journal of Medicinal Chemistry 55*, 6237-6241.

176. Mandal, K., Uppalapati, M., Ault-Riche, D., Kenney, J., Lowitz, J., Sidhu, S. S., and Kent, S. B. H. (2012) Chemical synthesis and X-ray structure of a heterochiral {D-protein antagonist plus vascular endothelial growth factor} protein complex by racemic crystallography, *Proceedings of the National Academy of Sciences of the United States of America 109*, 14779-14784.

177. Simon, R. J., Kania, R. S., Zuckermann, R. N., Huebner, V. D., Jewell, D. A., Banville, S., Ng, S., Wang, L., Rosenberg, S., Marlowe, C. K., Spellmeyer, D. C., Tan, R. Y., Frankel, A. D., Santi, D. V., Cohen, F. E., and Bartlett, P. A. (1992) Peptoids: a modular approach to drug discovery, *Proceedings of the National Academy of Sciences of the United States of America 89*, 9367-9371.

178. Fowler, S. A., and Blackwell, H. E. (2009) Structure-function relationships in peptoids: Recent advances toward deciphering the structural requirements for biological function, *Organic & Biomolecular Chemistry 7*, 1508-1524.

179. Miller, S. M., Simon, R. J., Ng, S., Zuckermann, R. N., Kerr, J. M., and Moos, W. H. (1994) Proteolytic studies of homologous peptide and N-substituted glycine peptoid oligomers, *Bioorganic & Medicinal Chemistry Letters 4*, 2657-2662.

180. Kwon, Y. U., and Kodadek, T. (2007) Quantitative evaluation of the relative cell permeability of peptoids and peptides, *Journal of the American Chemical Society 129*, 1508-1509.

181. Tan, N. C., Yu, P., Kwon, Y. U., and Kodadek, T. (2008) High-throughput evaluation of relative cell permeability between peptoids and peptides, *Bioorganic & Medicinal Chemistry 16*, 5853-5861.

182. Hara, T., Durell, S. R., Myers, M. C., and Appella, D. H. (2006) Probing the structural requirements of peptoids that inhibit HDM2-p53 interactions, *Journal of the American Chemical Society 128*, 1995-2004.

183. Udugamasooriya, D. G., Dineen, S. P., Brekken, R. A., and Kodadek, T. (2008) A peptoid "Antibody surrogate" that antagonizes VEGF receptor 2 activity, *Journal of the American Chemical Society 130*, 5744-5752.

184. Udugamasooriya, D. G., Ritchie, C., Brekken, R. A., and Kodadek, T. (2008) A peptoid antagonist of VEGF Receptor 2 recognizes a 'hotspot' in the extracellular domain distinct from the hormone-binding site, *Bioorganic & Medicinal Chemistry 16*, 6338-6343.

185. Lim, H. S., Archer, C. T., and Kodadek, T. (2007) Identification of a peptoid inhibitor of the proteasome 19S regulatory particle, *Journal of the American Chemical Society 129*, 7750-7751.

186. Lim, H. S., Archer, C. T., Kim, Y. C., Hutchens, T., and Kodadek, T. (2008) Rapid identification of the pharmacophore in a peptoid inhibitor of the proteasome regulatory particle, *Chemical Communications*, 1064-1066.

187. Trader, D. J., Simanski, S., and Kodadek, T. (2015) A Reversible and Highly Selective Inhibitor of the Proteasomal Ubiquitin Receptor Rpn13 Is Toxic to Multiple Myeloma Cells, *Journal of the American Chemical Society 137*, 6312-6319.

188. Tal-Gan, Y., Stacey, D., and Blackwell, H. (2014) *N*-Methyl and peptoid scans of an autoinducing peptide reveal new structural features required for inhibition and activation of AgrC quorum sensing receptors in *Staphylococcus aureus*, *Chemical Communications 50*, 3000-3003.

189. Laursen, J. S., Harris, P., Fristrup, P., and Olsen, C. A. (2015) Triangular prism-shaped beta-peptoid helices as unique biomimetic scaffolds, *Nature Communications 6*, 7013.

190. Seebach, D., and Gardiner, J. (2008) beta-Peptidic Peptidomimetics, *Accounts of Chemical Research 41*, 1366-1375.

191. Cheng, R. P., Gellman, S. H., and DeGrado, W. F. (2001) beta-peptides: From structure to function, *Chemical Reviews 101*, 3219-3232.

192. Seebach, D., Hook, D. F., and Glattli, A. (2006) Helices and other secondary structures of beta- and gamma-peptides, *Biopolymers 84*, 23-37.

193. Kritzer, J. A., Stephens, O. M., Guarracino, D. A., Reznik, S. K., and Schepartz, A. (2005) beta-Peptides as inhibitors of protein-protein interactions, *Bioorganic & Medicinal Chemistry 13*, 11-16.

194. Kritzer, J. A., Tirado-Rives, J., Hart, S. A., Lear, J. D., Jorgensen, W. L., and Schepartz, A. (2005) Relationship between side chain structure and 14-helix stability of beta(3)-peptides in water, *Journal of the American Chemical Society 127*, 167-178.

195. Hook, D. F., Bindschadler, P., Mahajan, Y. R., Sebesta, R., Kast, P., and Seebach, D. (2005) The proteolytic stability of 'designed' beta-peptides containing alpha-peptide-bond mimics and of mixed alpha,beta-peptides: Application to the construction of MHC-binding peptides, *Chemistry & Biodiversity 2*, 591-632.

196. Seebach, D., Overhand, M., Kuhnle, F. N. M., Martinoni, B., Oberer, L., Hommel, U., and Widmer, H. (1996) beta-peptides: Synthesis by Arndt-Eistert homologation with concomitant peptide coupling. Structure determination by NMR and CD spectroscopy and by X-ray crystallography. Helical secondary structure of a beta-hexapeptide in solution and its stability towards pepsin, *Helvetica Chimica Acta 79*, 913-941.

197. Seebach, D., Abele, S., Schreiber, J. V., Martinoni, B., Nussbaum, A. K., Schild, H., Schulz, H., Hennecke, H., Woessner, R., and Bitsch, F. (1998) Biological and pharmacokinetic studies with beta-peptides, *Chimia 52*, 734-739.

198. Hintermann, T., and Seebach, D. (1997) The biological stability of beta-peptides: No interactions between alpha- and beta-peptidic structures, *Chimia 51*, 244-247.

199. Werder, M., Hauser, H., Abele, S., and Seebach, D. (1999) beta-peptides as inhibitors of small-intestinal cholesterol and fat absorption, *Helvetica Chimica Acta 82*, 1774-1783.

200. Porter, E. A., Wang, X. F., Lee, H. S., Weisblum, B., and Gellman, S. H. (2000) Antibiotics - Non-haemolytic beta-amino-acid oligomers, *Nature 404*, 565-565.

201. Hamuro, Y., Schneider, J. P., and DeGrado, W. F. (1999) De novo design of antibacterial beta-peptides, *Journal of the American Chemical Society 121*, 12200-12201.

202. Karlsson, A. J., Pomerantz, W. C., Weisblum, B., Gellman, S. H., and Palecek, S. P. (2006) Antifungal activity from 14-helical beta-peptides, *Journal of the American Chemical Society 128*, 12630-12631.

203. Karlsson, A. J., Pomerantz, W. C., Neilsen, K. J., Gellman, S. H., and Palecek, S. P. (2009) Effect of Sequence and Structural Properties on 14-Helical beta-Peptide Activity against Candida albicans Planktonic Cells and Biofilms, *Acs Chemical Biology 4*, 567-579.

204. Lee, M. R., Raman, N., Gellman, S. H., Lynn, D. M., and Palecek, S. P. (2014) Hydrophobicity and Helicity Regulate the Antifungal Activity of 14-Helical beta-Peptides, *Acs Chemical Biology 9*, 1613-1621.

205. Gademann, K., Ernst, M., Hoyer, D., and Seebach, D. (1999) Synthesis and biological evaluation of a cyclo-beta-tetrapeptide as a somatostatin analogue, *Angewandte Chemie-International Edition 38*, 1223-1226.

206. Gademann, K., Kimmerlin, T., Hoyer, D., and Seebach, D. (2001) Peptide folding induces high and selective affinity of a linear and small beta-peptide to the human somatostatin receptor 4, *Journal of Medicinal Chemistry 44*, 2460-2468.

207. Kritzer, J. A., Lear, J. D., Hodsdon, M. E., and Schepartz, A. (2004) Helical beta-peptide inhibitors of the p53-hDM2 interaction, *Journal of the American Chemical Society 126*, 9468-9469.

208. Kritzer, J. A., Hodsdon, M. E., and Schepartz, A. (2005) Solution structure of a beta-peptide ligand for hDM2, *Journal of the American Chemical Society 127*, 4118-4119.

209. Harker, E. A., Daniels, D. S., Guarracino, D. A., and Schepartz, A. (2009) beta-Peptides with improved affinity for hDM2 and hDMX, *Bioorganic & Medicinal Chemistry 17*, 2038-2046.

210. Kritzer, J. A., Luedtke, N. W., Harker, E. A., and Schepartz, A. (2005) A rapid library screen for tailoring beta-peptide structure and function, *Journal of the American Chemical Society 127*, 14584-14585.

211. Harker, E. A., and Schepartz, A. (2009) Cell-Permeable beta-Peptide Inhibitors of p53/hDM2 Complexation, *Chembiochem 10*, 990-993.

212. Bautista, A. D., Appelbaum, J. S., Craig, C. J., Michel, J., and Schepartz, A. (2010) Bridged beta(3)-Peptide Inhibitors of p53-hDM2 Complexation: Correlation between Affinity and Cell Permeability, *Journal of the American Chemical Society 132*, 2904-2906.

213. Stephens, O. M., Kim, S., Welch, B. D., Hodsdon, M. E., Kay, M. S., and Schepartz, A. (2005) Inhibiting HIV fusion with a beta-peptide foldamer, *Journal of the American Chemical Society 127*, 13126-13127.

214. Bautista, A. D., Stephens, O. M., Wang, L. G., Domaoal, R. A., Anderson, K. S., and Schepartz, A. (2009) Identification of a beta(3)-peptide HIV fusion inhibitor with improved potency in live cells, *Bioorganic & Medicinal Chemistry Letters 19*, 3736-3738.

215. English, E. P., Chumanov, R. S., Gellman, S. H., and Compton, T. (2006) Rational development of beta-peptide inhibitors of human cytomegalovirus entry, *Journal of Biological Chemistry 281*, 2661-2667.

216. Yin, H., Slusky, J. S., Berger, B. W., Walters, R. S., Vilaire, G., Litvinov, R. I., Lear, J. D., Caputo, G. A., Bennett, J. S., and DeGrado, W. F. (2007) Computational design of peptides that target transmembrane helices, *Science 315*, 1817-1822.

217. Shandler, S. J., Korendovych, I. V., Moore, D. T., Smith-Dupont, K. B., Streu, C. N., Litvinov, R. I., Billings, P. C., Gai, F., Bennett, J. S., and DeGrado, W. F. (2011) Computational Design of a beta-Peptide That Targets Transmembrane Helices, *Journal of the American Chemical Society 133*, 12378-12381.

218. Denton, E. V., Craig, C. J., Pongratz, R. L., Appelbaum, J. S., Doerner, A. E., Narayanan, A., Shulman, G. I., Cline, G. W., and Schepartz, A. (2013) A beta-Peptide Agonist of the GLP-1 Receptor, a Class B GPCR, *Organic Letters 15*, 5318-5321.

219. Horne, W. S., and Gellman, S. H. (2008) Foldamers with Heterogeneous Backbones, *Accounts of Chemical Research 41*, 1399-1408.

220. Werner, H. M., and Horne, W. S. (2015) Folding and function in alpha/beta-peptides:targets and therapeutic applications, *Current Opinion in Chemical Biology 28*, 75-82.

221. Johnson, L. M., and Gellman, S. H. (2013) alpha-Helix Mimicry with alpha/beta-Peptides, *Methods in Protein Design 523*, 407-429.

222. Hayen, A., Schmitt, M. A., Ngassa, F. N., Thomasson, K. A., and Gellman, S. H. (2004) Two helical conformations from a single foldamer backbone: "Split personality" in short alpha/beta-peptides, *Angewandte Chemie-International Edition 43*, 505-510.

223. De Pol, S., Zorn, C., Klein, C. D., Zerbe, O., and Reiser, O. (2004) Surprisingly stable helical conformations in alpha/beta-peptides by incorporation of cis-beta-aminocyclopropane carboxylic acids, *Angewandte Chemie-International Edition 43*, 511-514.

224. Sadowsky, J. D., Schmitt, M. A., Lee, H. S., Umezawa, N., Wang, S. M., Tomita, Y., and Gellman, S. H. (2005) Chimeric (alpha/beta plus alpha)-peptide ligands for the BH3-recognition cleft of Bcl-x(L): Critical role of the molecular scaffold in protein surface recognition, *Journal of the American Chemical Society 127*, 11966-11968.

225. Sadowsky, J. D., Fairlie, W. D., Hadley, E. B., Lee, H. S., Umezawa, N., Nikolovska-Coleska, Z., Wang, S. M., Huang, D. C. S., Tomita, Y., and Gellman, S. H. (2007) (alpha/beta+alpha)-Peptide antagonists of BH3 Domain/Bcl-x(L) recognition: Toward general strategies for foldamer-based inhibition of protein-protein interactions, *Journal of the American Chemical Society 129*, 139-154.

226. Lee, E. F., Sadowsky, J. D., Smith, B. J., Czabotar, P. E., Peterson-Kaufman, K. J., Colman, P. M., Gellman, S. H., and Fairlie, W. D. (2009) High-Resolution Structural Characterization of a Helical alpha/beta-Peptide Foldamer Bound to the Anti-Apoptotic Protein Bcl-x(L), *Angewandte Chemie-International Edition 48*, 4318-4322.

227. Sadowsky, J. D., Murray, J. K., Tomita, Y., and Gellman, S. H. (2007) Exploration of backbone space in foldamers containing alpha- and beta-amino acid residues: Developing protease-resistant oligomers that bind tightly to the BH3-recognition cleft of Bcl-x(L), *Chembiochem 8*, 903-916.

228. Horne, W. S., Price, J. L., Keck, J. L., and Gellman, S. H. (2007) Helix bundle quaternary structure from alpha/beta-peptide foldamers, *Journal of the American Chemical Society 129*, 4178-4180.

229. Horne, W. S., Price, J. L., and Gellman, S. H. (2008) Interplay among side chain sequence, backbone composition, and residue rigidification in polypeptide folding and assembly, *Proceedings of the National Academy of Sciences of the United States of America 105*, 9151-9156.

230. Horne, W. S., Boersma, M. D., Windsor, M. A., and Gellman, S. H. (2008) Sequence-based design of alpha/beta-peptide foldamers that mimic BH3 domains, *Angewandte Chemie-International Edition 47*, 2853-2856.

231. Lee, E. F., Smith, B. J., Horne, W. S., Mayer, K. N., Evangelista, M., Colman, P. M., Gellman, S. H., and Fairlie, W. D. (2011) Structural Basis of Bcl-x(L) Recognition by a BH3-Mimetic alpha/beta-Peptide Generated by Sequence-Based Design, *Chembiochem 12*, 2025-2032.

232. Boersma, M. D., Haase, H. S., Peterson-Kaufman, K. J., Lee, E. F., Clarke, O. B., Colman, P. M., Smith, B. J., Horne, W. S., Fairlie, W. D., and Gellman, S. H. (2012) Evaluation of Diverse alpha/beta-Backbone Patterns for Functional alpha-Helix Mimicry: Analogues of the Bim BH3 Domain, *Journal of the American Chemical Society 134*, 315-323.

233. Horne, W. S., Johnson, L. M., Ketas, T. J., Klasse, P. J., Lu, M., Moore, J. P., and Gellman, S. H. (2009) Structural and biological mimicry of protein surface recognition by alpha/beta-peptide foldamers, *Proceedings of the National Academy of Sciences of the United States of America 106*, 14751-14756.

234. Johnson, L. M., Horne, W. S., and Gellman, S. H. (2011) Broad Distribution of Energetically Important Contacts across an Extended Protein Interface, *Journal of the American Chemical Society 133*, 10038-10041.

235. Johnson, L. M., Mortenson, D. E., Yun, H. G., Horne, W. S., Ketas, T. J., Lu, M., Moore, J. P., and Gellman, S. H. (2012) Enhancement of alpha-Helix Mimicry by an alpha/beta-Peptide Foldamer via Incorporation of a Dense Ionic Side-Chain Array, *Journal of the American Chemical Society 134*, 7317-7320.

236. Schmitt, M. A., Choi, S. H., Guzei, I. A., and Gellman, S. H. (2005) Residue requirements for helical folding in short alpha/beta-peptides: Crystallographic

characterization of the 11-helix in an optimized sequence, *Journal of the American Chemical Society 127*, 13130-13131.

237. Peterson-Kaufman, K. J., Haase, H. S., Boersma, M. D., Lee, E. F., Fairlie, W. D., and Gellman, S. H. (2015) Residue-Based Preorganization of BH3-Derived α/β-Peptides: Modulating Affinity, Selectivity and Proteolytic Susceptibility in α-Helix Mimics, *ACS Chemical Biology 10*, 1667-1675.

238. Pioszak, A. A., and Xu, H. E. (2008) Molecular recognition of parathyroid hormone by its G protein-coupled receptor, *Proceedings of the National Academy of Sciences of the United States of America 105*, 5034-5039.

239. Cheloha, R. W., Maeda, A., Dean, T., Gardella, T. J., and Gellman, S. H. (2014) Backbone modification of a polypeptide drug alters duration of action in vivo, *Nature Biotechnology 32*, 653-655.

240. Underwood, C. R., Garibay, P., Knudsen, L. B., Hastrup, S., Peters, G. H., Rudolph, R., and Reedtz-Runge, S. (2010) Crystal Structure of Glucagon-like Peptide-1 in Complex with the Extracellular Domain of the Glucagon-like Peptide-1 Receptor, *Journal of Biological Chemistry 285*, 723-730.

241. Johnson, L. M., Barrick, S., Hager, M. V., McFedries, A., Homan, E. A., Rabaglia, M. E., Keller, M. P., Attie, A. D., Saghatelian, A., Bisello, A., and Gellman, S. H. (2014) A Potent alpha/beta-Peptide Analogue of GLP-1 with Prolonged Action in Vivo, *Journal of the American Chemical Society 136*, 12848-12851.

242. Wiesmann, C., Fuh, G., Christinger, H. W., Eigenbrot, C., Wells, J. A., and deVos, A. M. (1997) Crystal structure at 1.7 angstrom resolution of VEGF in complex with domain 2 of the Flt-1 receptor, *Cell 91*, 695-704.

243. Haase, H. S., Peterson-Kaufman, K. J., Levengood, S. K. L., Checco, J. W., Murphy, W. L., and Gellman, S. H. (2012) Extending Foldamer Design beyond alpha-Helix Mimicry: alpha/beta-Peptide Inhibitors of Vascular Endothelial Growth Factor Signaling, *Journal of the American Chemical Society 134*, 7652-7655.

244. Guichard, G., Zerbib, A., Le Gal, F. A., Hoebeke, J., Connan, F., Choppin, J., Briand, J. P., and Guillet, J. G. (2000) Melanoma peptide MART-1(27-35) analogues with enhanced binding capacity to the human class I histocompatibility molecule HLA-A2 by introduction of a beta-amino acid residue: Implications for recognition by tumor-infiltrating lymphocytes, *Journal of Medicinal Chemistry 43*, 3803-3808.

245. Reinert, Z. E., Lengyel, G. A., and Horne, W. S. (2013) Protein-like Tertiary Folding Behavior from Heterogeneous Backbones, *Journal of the American Chemical Society 135*, 12528-12531.

Chapter 2: α/β-Peptide antagonists of the VEGF-VEGFR interaction derived from the Z-domain scaffold

Portions of this chapter have been published as:

Checco, J. W., Kreitler, D. F., Thomas, N. C., Belair, D. G., Rettko, N. J., Murphy, W. L., Forest, K. T., and Gellman, S. H. (2015) Targeting diverse protein–protein interaction interfaces with α/β-peptides derived from the Z-domain scaffold, *Proceedings of the National Academy of Sciences of the United States of America 112*, 4552–4557.

Respective contributions:

Research design: James W. Checco, Samuel H. Gellman

Peptide design: James W. Checco

Peptide synthesis: James W. Checco, Nicholas J. Rettko

FP assays: James W. Checco

Proteolysis: James W. Checco

Circular dichroism: James W. Checco

$VEGF_{8\text{-}109}$ expression: Nicole C. Thomas

Crystal structure: Dale F. Kreitler, James W. Checco, Katrina T. Forest

HUVEC assays: James W. Checco

HUVEC analysis: James W. Checco, David G. Belair, William L. Murphy

2.1 Preface

α/β-Peptides can mimic the recognition surface of an α-helix to modulate protein-protein interactions in which one partner contributes a single helix to the interface, while displaying a decreased susceptibility to protease degradation relative to their α-peptide counterparts. However, α/β-peptide design has been restricted to the mimicry of isolated α-helical peptides, which is a significant limitation given that most protein-protein interactions are mediated by surfaces than are broader than can be covered by a single, regular helix. For example, antagonizing the interaction between vascular endothelial growth factor (VEGF) and its receptors (VEGFRs) represents an attractive goal for the treatment of diseases related to misregulated angiogenesis, but designing molecules that block the VEGF-VEGFR interaction is challenging because the interaction interface is large and topologically complex.

The primary goal for the project described in this chapter was to design α/β-peptides that effectively target the receptor-recognition surface on VEGF to antagonize VEGF signaling, and display a low susceptibility to protease degradation. This goal was ultimately achieved by extending the principles for α/β-peptide mimicry of a single α-helix to mimic the multi-helical tertiary structure of the "Z-domain" mini-protein scaffold, which presents a binding surface that can recognize a relatively large region on a target protein. Importantly, because peptides derived from the Z-domain scaffold adopt very similar folded structures, the strategy developed in this chapter for the α/β-peptide mimicry of one Z-domain-derived α-peptide may provide a general framework to mimic Z-domain derivatives targeting other proteins. This concept is explored in Chapters 3 and 4.

2.2 Introduction

2.2.1 VEGF-VEGFR interaction and VEGF antagonists

Vascular endothelial growth factor (VEGF, also called VEGF-A) is a soluble homodimeric protein that plays a critical role in angiogenesis (the formation of new blood vessels from existing blood vessels).[1-5] The primary isoform of VEGF, $VEGF_{165}$, contains both a receptor binding domain and a heparin-binding domain.[2] $VEGF_{8-109}$, a construct of VEGF that lacks the heparin-binding domain, is often used for crystallization studies.[6] One of the principal activities of VEGF is to bind to two cell-surface receptor tyrosine kinases (VEGFRs), VEGFR1 (also called Flt-1) and VEGFR2 (also called KDR), that exist on the surface of vascular endothelial cells. These VEGFRs contain an intracellular tyrosine kinase domain, a transmembrane region, and an extracellular region consisting of seven immunoglobulin-like domains that project out from the cell surface (Figure 2.1). VEGF ligands bind primarily to domains 2 and 3 of the extracellular portion of the VEGFRs through an extended surface at the interface of the two VEGF monomers (Figure 2.2).[6-8] The antiparallel VEGF homodimer contains two equivalent receptor binding sites on opposite poles of the molecule, which allow it to bind to two molecules of VEGFR to cause receptor dimerization (Figures 2.1 and 2.2). Dimerization of the extracellular domains of the VEGFRs causes intracellular dimerization of the kinase domains, leading to phosphorylation and subsequent downstream signaling that promotes the survival, proliferation, and migration of endothelial cells.[1, 2] The receptor recognition site on VEGF is large and topologically complex, with over 800 $Å^2$ of the surface of VEGF buried upon receptor binding.[7] This flat, hydrophobic surface appears to be representative of many protein surfaces that mediate protein-protein interactions.[9]

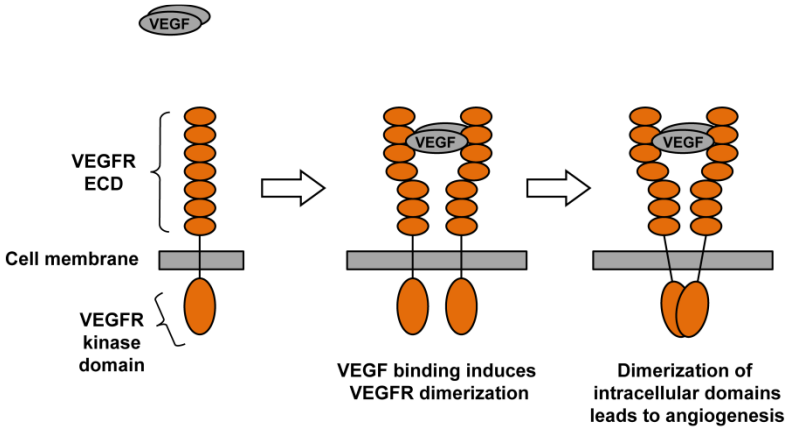

Figure 2.1 Cartoon depiction of VEGF signaling. The VEGF homodimer binds to the extracellular domain (ECD) of the membrane-bound VEGF receptor (VEGFR), leading to receptor dimerization and subsequent signaling to initiate angiogenesis.

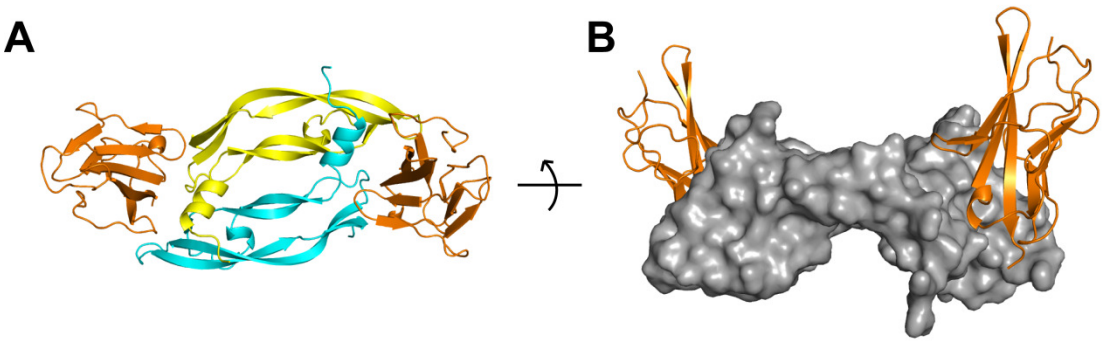

Figure 2.2 Crystal structure of the $VEGF_{8-109}$ homodimer in complex with domain 2 of VEGFR1 (PDB: 1FLT). (A) Two disulfide-crosslinked $VEGF_{8-109}$ monomers (shown in blue and yellow) form an anti-parallel homodimer that creates two equivalent surfaces to bind VEGFRs (domain 2 of VEGFR1 shown in orange). (B) $VEGF_{8-109}$ homodimer is depicted as a gray surface bound to two molecules of domain 2 of VEGFR1 (orange). Note that panel B is rotated 90° relative to panel A.

Because of the critical role of the VEGF-VEGFR interaction in angiogenesis, antagonists of this protein-protein interaction are currently used to treat both cancer and wet macular degeneration.[4, 10-13] In some cancers, VEGF appears to play an important role in the formation of the vasculature necessary to provide the growing tumor with the large amount of required nutrients. In age-related wet macular degeneration, neovascularization and vascular leakage in the eye caused by aberrant VEGF signaling can lead to vision loss and blindness.[12] Several engineered protein antagonists of the VEGF-VEGFR interaction are approved to treat various cancers and age-related wet macular degeneration, such as bevacizumab (anti-VEGF

antibody), ranibizumab (anti-VEGF antibody fragment), and aflibercept (soluble engineered VEGFR fragment).[4, 10, 11, 14] The proteins act by binding to the receptor recognition surface on the VEGF dimer. In addition, several smaller peptides have also been developed to bind VEGF, such as phage display-derived peptides **v107** and **v114** (Figure 2.3A),[15, 16] a D-peptide identified by mirror image phage display (Figure 2.3B),[17] and peptides derived from the "Z-domain" scaffold (Figures 2.3C and 2.4, described below).[18]

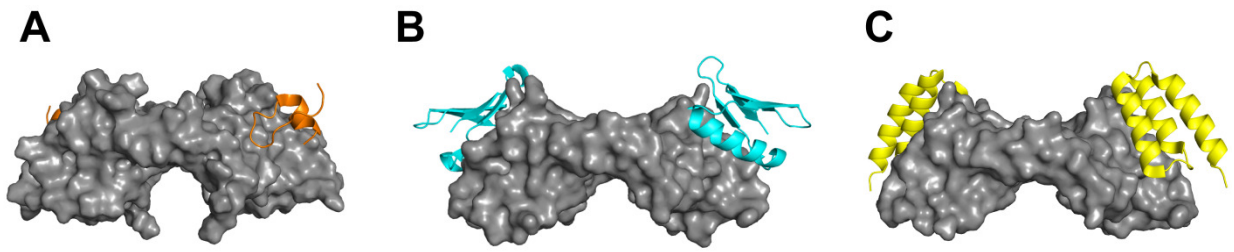

Figure 2.3 (A) NMR structure of $VEGF_{8-109}$ (gray) in complex with **v107** (orange) (PDB: 1KAT).[16] (B) Crystal structure of $VEGF_{8-109}$ (gray) in complex with a D-peptide identified by mirror image phage display (cyan), crystallized as a racemate (PDB: 4GLN).[17] (C) Crystal structure of $VEGF_{8-109}$ (gray) in complex with **Z-VEGF** (yellow), a peptide derived from the Z-domain scaffold (PDB: 3S1K).[18]

2.2.2 α/β-Peptides targeting VEGF

The primary goal of the project described in this chapter was to design protease-resistant α/β-peptides that bind to surfaces such as the VEGF receptor binding site. α/β-Peptide mimicry of helical peptides has been successful for modulating protein-protein interactions in a number of different systems, but the principles driving α/β-peptide design have been limited primarily to the mimicry of isolated α-helical peptides targeting relatively narrow, hydrophobic clefts on proteins.[19-24] Protein-protein interactions that feature broad and topologically complex interfaces covering large surface areas, such as the VEGF-VEGFR interaction, likely require a strategy distinct from prior α/β-peptide design efforts, since these interfaces may not be easily targeted by a single helix.[2, 12] Our group previously reported α/β-peptide analogues of phage-derived peptide **v114** (sequence = VEPNCDIHVMWEWECFERL-NH_2, Cys residues are engaged in a disulfide

bond), which adopts an irregular conformation when binding to the VEGF receptor binding region (Figure 2.3A).[25] However, this effort was only moderately successful. We found that α/β-peptide analogues of **v114** bound VEGF with modest affinity (K_i = ~2-5 μM by fluorescence polarization (FP) assay), antagonized $VEGF_{165}$-induced proliferation of human umbilical vein endothelial cells (HUVECs) in culture, and had a reduced susceptibility to proteolytic degradation relative to the parent α-peptide. However, while several individual α→β-amino acid substitutions were found to be tolerated in **v114** analogues using a "β-scanning" technique, the subsequent incorporation of multiple β-amino acid residues had a cumulative detrimental effect on affinity for VEGF (>60-fold loss in affinity for VEGF for the most proteolytically stable α/β-peptide relative to its parent α-peptide). These efforts ultimately suggest that the conformations required for binding of some irregularly-structured peptides, such as **v114,** may be negatively altered by the incorporation of multiple additional backbone atoms that result from α→β-amino acid residue substitutions.

2.2.3 Peptides that bind VEGF derived from the Z-domain scaffold

Several small proteins have been explored as scaffolds that can be adapted to interact with structurally diverse protein binding partners.[26, 27] The defined tertiary structures of such scaffolds allow them to present large binding surfaces that can engage large and complementary surfaces on target proteins. The "Z-domain" or "affibody" scaffold[28] is a widely studied example that is derived from domain B of staphylococcal protein A.[29] The parent Z-domain (**Z-IgG**, Figure 2.4) is a 58-residue engineered analogue of domain B that retains affinity for the Fc portion of immunoglobulin G (IgG), the natural binding partner of protein A.[30] **Z-IgG** adopts a three-helix bundle tertiary structure, with a large surface (>600 $Å^2$ buried in the interface with

Fc) formed by helices 1 and 2 contributing most of the Fc-contacting residues. Helix 3 stabilizes the Z-domain fold by packing against the other two helices.[29, 31]

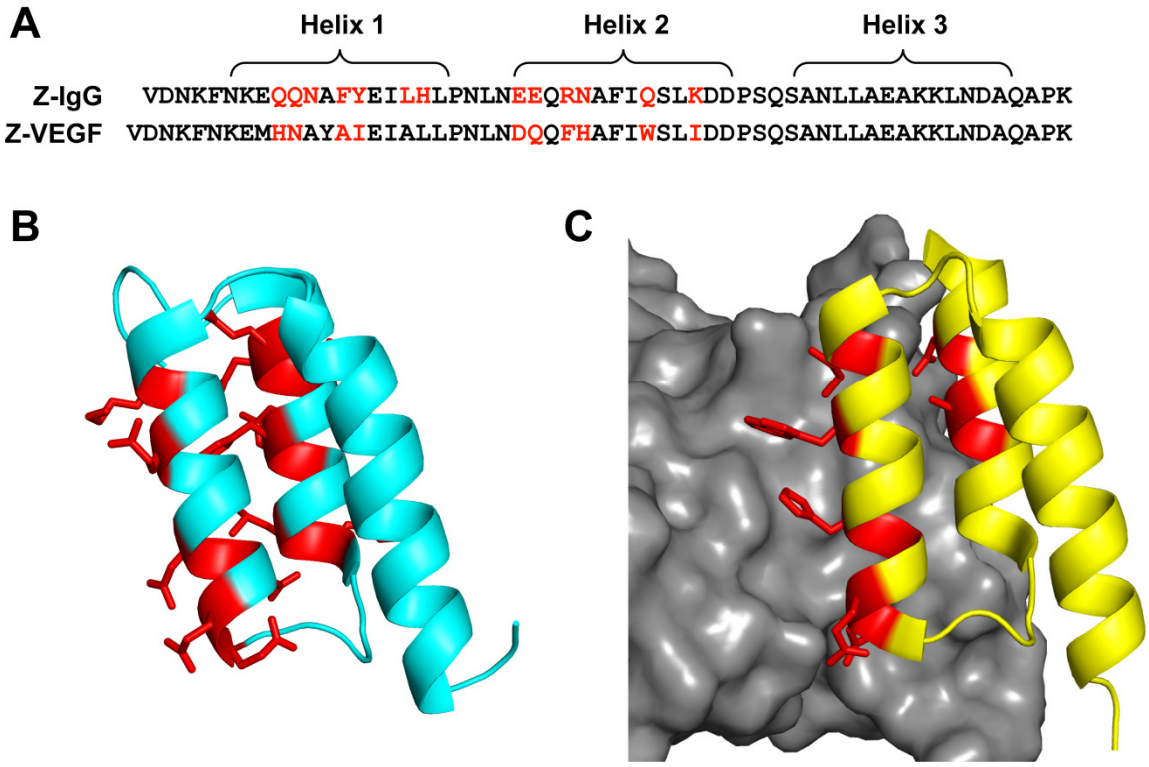

Figure 2.4 Z-VEGF is a three-helix peptide derived from **Z-IgG**, the parent Z-domain, using phage display and selection. (A) Primary sequences of previously reported peptides **Z-IgG** and **Z-VEGF** targeting IgG[30] and VEGF[18], respectively. Approximate positions of helices 1, 2, and 3 are indicated by brackets. Sequences are arranged based on structural alignment of helical regions. For **Z-IgG**, the parent Z-domain, red positions indicate the residues that contact IgG. For **Z-VEGF**, red residues indicate those on the protein-binding face of helices 1 and 2 that were identified via randomization and selection (including the unintentionally incorporated Ala14 in **Z-VEGF**). (B) NMR structure of **Z-IgG** (PDB: 2SPZ).[31] Red residues indicate those that contact IgG. (C) Crystal structure of **Z-VEGF** (yellow and red) with $VEGF_{8-109}$ (gray) (PDB: 3S1K).[18] Red residues indicate those that were randomized to derive binding to VEGF.

The composite surface displayed by helices 1 and 2 of the Z-domain scaffold can be crafted for specific binding to diverse protein partners because the three-helix bundle tertiary structure tolerates substitutions at solvent-exposed positions.[32] Combinatorial randomization of as many as 13 solvent-exposed positions on helices 1 and 2, followed by affinity-based selection, has identified Z-domain derivatives that bind to a variety of targets,[27, 28] including VEGF.[18] Z-domain analogues derived to bind other targets are described in more detail in Chapter 3.

Z-VEGF is a 59-mer that was developed by Fedorova *et al*. via phage display for use as an imaging agent (Figure 2.4).[18] Nine residues on the protein-binding face of helices 1 and 2 of the Z-domain scaffold were randomized, and favorable variants were identified by selecting for binding to the $VEGF_{8-109}$ homodimer.[18] A co-crystal structure shows that **Z-VEGF** occupies the receptor-binding region of $VEGF_{8-109}$ (PDB: 3S1K, Figures 2.3C and 2.4C).[7, 18] **Z-VEGF** adopts the three-helix bundle tertiary structure that is characteristic of the Z-domain family, and the surface defined by helices 1 and 2 makes contact with $VEGF_{8-109}$, as predicted. During the phage display/selection process, an alanine residue (Ala14) was unexpectedly incorporated, shifting the preceding N-terminal residues by one position in helix 1 relative to the parent **Z-IgG**.

2.2.4 Previous efforts to truncate Z-domain derivatives

Several prior studies have aimed to truncate three-helix Z-domain peptides to two-helix analogues (Figure 2.5). Because the protein-contacting residues in the Z-domain family are located on the surface formed by helix 1 and helix 2, the primary hypothesis behind these efforts has been that removal of helix 3 should yield a two-helix peptide that retains an intact protein-binding surface. These studies were pioneered by Wells et al., who successfully truncated the **Z-IgG** peptide (which binds to the Fc portion of IgG) to a two-helix analogue.[33, 34] The initial report by Wells et al. showed that the removal of helix 3 from **Z-IgG** leads to an abolition of affinity for IgG, presumably because of a loss of the conformational stability that was provided by helix 3. To overcome this loss of structural stability, these workers used phage display to identify favorable mutations in the context of the two-helix peptide that promoted the helix-loop-helix structure required for binding to IgG (Figure 2.5A, pink residues).[33] A subsequent study from the same group showed that the incorporation of a disulfide bond connecting the termini of helix 1 and helix 2 can provide further increases in affinity by promoting the helix-loop-helix

conformation.[34] A similar strategy was employed to design a two-helix analogue of a HER2-binding peptide derived from the Z-domain scaffold.[35] In this case, five of the helix-stabilizing substitutions mentioned above (those thought not to be involved in the binding interface) and an interhelical disulfide were employed to generate a two-helix Z-domain analogue that bound HER2 (Figure 2.5B).

In addition to the three-helix **Z-VEGF**, Fedorova et al. also reported a VEGF-binding two-helix peptide, termed **Mini-Z-1**.[18] **Mini-Z-1** was derived from phage display by randomizing nine residues of a helix-loop-helix scaffold (this scaffold is a hybrid of the two-helix **Z-IgG** analogue Z34C[34] and the HER2-binding peptide **Z-HER2**,[36] both shown in Figure 2.5) and selecting for binding to $VEGF_{8-109}$. **Mini-Z-1** did bind VEGF with an affinity constant similar to that of the full-length **Z-VEGF** by bio-layer interferometry (BLI). However, the **Mini-Z-1**+$VEGF_{8-109}$ co-crystal structure unexpectedly showed that this peptide required homodimerization to bind VEGF, indicating that the residue randomization process led to an alternative mode of binding by **Mini-Z-1** relative to that intended.[37, 38]

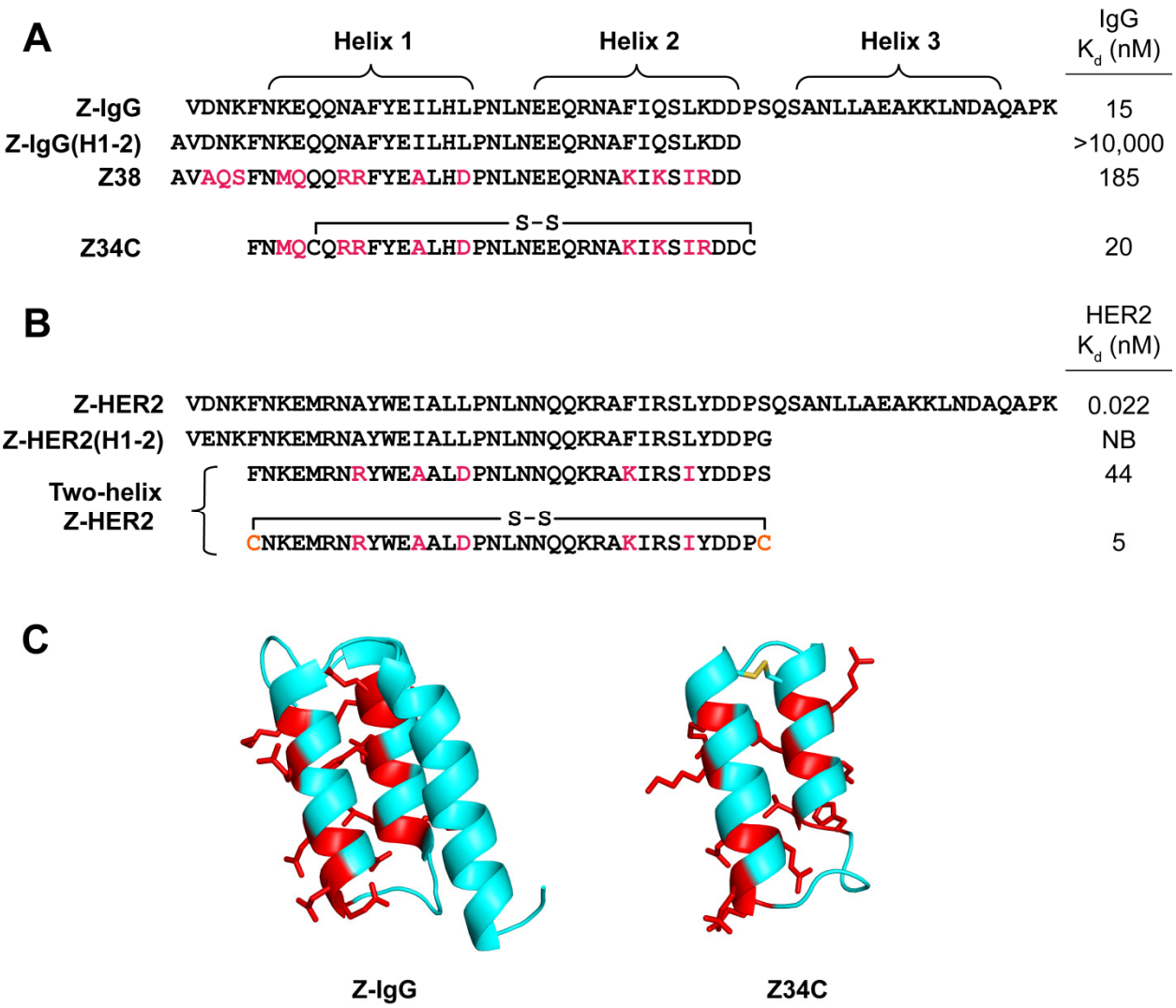

Figure 2.5 Previous strategies to truncate three-helix peptides derived from the Z-domain scaffold. (A) Truncation of **Z-IgG**. Residues in pink indicate those identified by phage display to stabilize the helix-loop-helix structure in the absence of helix 3. Cysteine residues are engaged in a disulfide. K_d values indicate binding to immobilized IgG, derived from SPR analysis, from refs [33, 34]. (B) Truncation of **Z-HER2**, a three-helix peptide derived from the Z-domain scaffold that binds HER2. Residues in pink indicate positions identified by phage display from the study in panel (A). Orange C indicates homocysteine residues, which are engaged in a disulfide. K_d values indicate binding to immobilized HER2, from ref [35]. (C) NMR structures of **Z-IgG** (left, PDB: 2SPZ)[31] and **Z34C** (right, PDB: 1ZDD).[34] Residues in red are those that contact IgG, as depicted in Figure 2.4A.

2.2.5 Z-VEGF as a starting point for α/β-peptide design

The high α-helix content of **Z-VEGF** led us to envision that α/β-peptide analogues could be developed that mimic **Z-VEGF**'s protein recognition properties while having reduced susceptibility to protease degradation. Furthermore, because the **Z-VEGF**+$VEGF_{8\text{-}109}$ co-crystal

structure shows that **Z-VEGF** binds to VEGF in the receptor contact region, we hypothesized that α/β-peptide analogues may be useful as VEGF antagonists.

Because the VEGF-binding residues of **Z-VEGF** are restricted to helices 1 and 2, we sought to remove helix 3 while retaining high affinity for VEGF (Figure 2.6, left arrow). This truncation strategy, pioneered by Wells et al.,[33, 34] should be beneficial since shorter oligomers are more amenable to chemical synthesis, which is required for access to α/β-peptides. In addition, the removal of helix 3 opens sites in helices 1 and 2 that are distal to the VEGF-binding face and therefore attractive for α→β replacement (Figure 2.6, right arrow). We decided that designing an α/β-peptide based on a truncated analogue of **Z-VEGF** would be preferred to using the VEGF-binding peptide **Mini-Z-1** as a starting point for α→β-residue replacement due to **Mini-Z-1**'s complex binding mode. By retaining the residues in **Z-VEGF** that make contact with the protein, we predicted we could retain the binding mode of this parent peptide even while making multiple α→β-residue substitutions, as depicted in Figure 2.6.

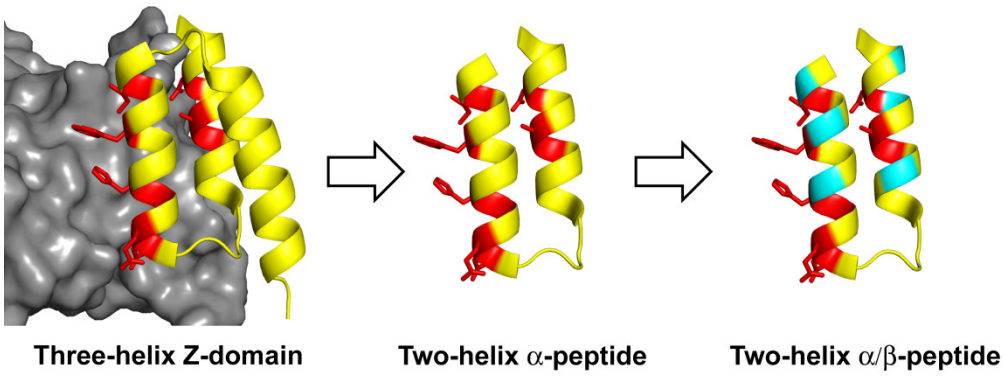

Figure 2.6 Strategy for the design of α/β-peptide mimics of **Z-VEGF** (shown in yellow and red). Red residues indicate selected residues that contact $VEGF_{8-109}$ (shown in gray) in the co-crystal structure. Several sites targeted for non-natural amino acid substitutions shown in teal. Figure based on PDB: 3S1K.

In this chapter, I describe the detailed design route that led to successful two-helix α/β-peptides targeting VEGF based on **Z-VEGF**, a route that utilized an iterative design strategy to

identify favorable sites for α→β-residue replacements while maintaining high affinity for the target protein. These α/β-peptides structurally and functionally mimic **Z-VEGF** in their protein-binding properties while having significantly increased protease stability. Furthermore, experiments on HUVECs show that these compounds can act as VEGF antagonists in cell culture. The strategy for α/β-peptide design described here is distinct from prior efforts to develop α/β-peptides that block protein-protein interactions, which have focused primarily on evaluating regular patterns of α→β-amino acid residue substitution throughout one single helix.[19-24] The principles underlying this strategy for α/β-peptide mimicry of a medium-sized, multi-helical tertiary structure may be applied to derive α/β-peptide mimics of other tertiary structures and peptide scaffolds to target a wide variety of protein surfaces.

2.3 Design of a helix-loop-helix α-peptide targeting the VEGF receptor binding site

2.3.1 Analysis of Z-VEGF binding to VEGF by FP assay

We began by synthesizing the previously reported α-peptide **Z-VEGF** and evaluating its ability to bind to the receptor recognition region of VEGF using a competition fluorescence polarization (FP) assay (Figure 2.7).[39] In this assay, **Z-VEGF** displayed an equilibrium inhibitory constant (K_i) of 0.41 μM affinity for $VEGF_{165}$ (Figure 2.8A). The measured K_i value of 0.41 μM for **Z-VEGF** to $VEGF_{165}$ by FP is ~10-fold higher than the value reported by Fedorova et al. using a direct-binding BLI experiment in which $VEGF_{8-109}$ binds to immobilized biotinylated **Z-VEGF** (reported K_d = 0.038 μM).[18] This type of discrepancy between calculated equilibrium constants can occur between results obtained from solution-based equilibrium binding assays (such as FP) and surface-based assays (such as BLI or surface plasmon resonance experiments).[40-42] Such discrepancies have been attributed to a number of phenomena arising

from surface-based measurements, such as a high uncertainty in equilibrium constants calculated from kinetic data (derived from surface-based experiments such as BLI or SPR data) due to protein rebinding and multivalency effects.[40, 42] It has also been suggested that the immobilization of a ligand onto a surface facilitates binding interactions by reducing the entropic cost associated with protein-ligand binding relative to solution-based experiments.[41] Another possible explanation for the discrepancy between our K_i value and the reported K_d value could be differences in protein construct used ($VEGF_{165}$ for FP versus $VEGF_{8-109}$ for BLI). Regardless, the measured K_i value of 0.41 μM by competition FP serves as a benchmark for competition FP evaluation of new α- and α/β-peptide **Z-VEGF** analogues.

As a further evaluation of **Z-VEGF**'s affinity for VEGF in a solution-based assay, we synthesized the 6-carboxyfluorescein-labeled analogue of **Z-VEGF** (peptide **2.1**) and evaluated its ability to bind $VEGF_{165}$ in a direct-binding FP assay. In this experiment, **2.1** displayed K_d = 0.088 μM (Figure 2.8B). The slightly lower K_d value for **2.1** versus **Z-VEGF** may reflect differences in experimental set-up (direct-binding versus competition FP). Alternatively, the difference between the K_i value (for **Z-VEGF**) and K_d value (for **2.1**) may indicate that the fluorophore present in **2.1** makes favorable contacts with $VEGF_{165}$, as has been previously reported for fluorophore-labeled peptides targeting VEGF.[39]

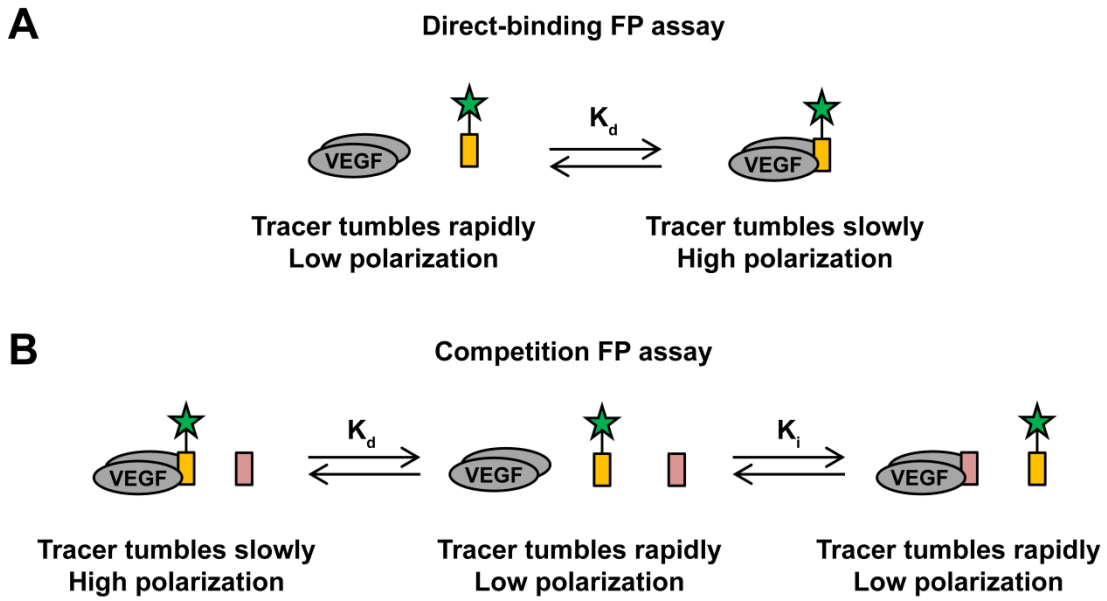

Figure 2.7 Cartoon depiction of the $VEGF_{165}$ fluorescence polarization (FP) assays used in this study. (A) In direct-binding FP, the decrease in tumbling rate (due to a higher apparent molecular weight) of a fluorophore-labeled "tracer" peptide (yellow) that is bound to $VEGF_{165}$ (gray) leads to an increase in polarization values. Fitting polarization values as a function of $VEGF_{165}$ concentration can be used to obtain the K_d value for this association. (B) In competition FP, binding of an unlabeled competitor peptide to the receptor-binding region of $VEGF_{165}$ displaces the tracer peptide, leading to a decrease in polarization. Titration of a potential competitor in the presence of a fixed concentration of tracer (with a known K_d, determined by direct-binding FP) and $VEGF_{165}$ allows calculation of the competitor's K_i for binding to $VEGF_{165}$.

A **Competitor peptide Z-VEGF, competition FP assay**

	K_i (μM)
VDNKFNKEMHNAYAIEIALLPNLNDQQFHAFIWSLIDDPSQSANLLAEAKKLNDAQAPK-NH_2	0.41

B **Labeled peptide 2.1, direct-binding FP assay**

	K_d (μM)
FAM-VDNKFNKEMHNAYAIEIALLPNLNDQQFHAFIWSLIDDPSQSANLLAEAKKLNDAQAPK-NH_2	0.088

Figure 2.8 Binding of **Z-VEGF** to $VEGF_{165}$ by fluorescence polarization (FP). (A) In competition FP, unlabeled **Z-VEGF** is able to compete with a tracer peptide for binding to the receptor binding site of $VEGF_{165}$. K_i values for $VEGF_{165}$ competition FP assays typically vary ~2-fold between independent experiments and so any values within this range are considered experimentally indistinguishable. See Table 2.1 for a list of K_i values obtained for each compound reported in this chapter from independent experiments. (B) In direct-binding FP, **2.1**, a labeled analogue of **Z-VEGF**, is able to bind directly to $VEGF_{165}$. FAM = 6-carboxyfluorescein.

2.3.2 Truncation of Z-VEGF

Z-VEGF is 59 residues in length. However, only residues 7-58 appear in the **Z-VEGF**+$VEGF_{8-109}$ co-crystal structure (Figure 2.4C).[18] Residues 1-6 are not present in the model, presumably because these residues are unstructured and do not make contact with $VEGF_{8-109}$. Removal of N-terminal residues in the two-helix **Z-IgG** analogue **Z34C** did not negatively affect affinity for IgG (Figure 2.5A).[33, 34] Together, these precedents suggest that residues 1-6 are likely not making critical contacts to VEGF and may not be required for high-affinity binding.

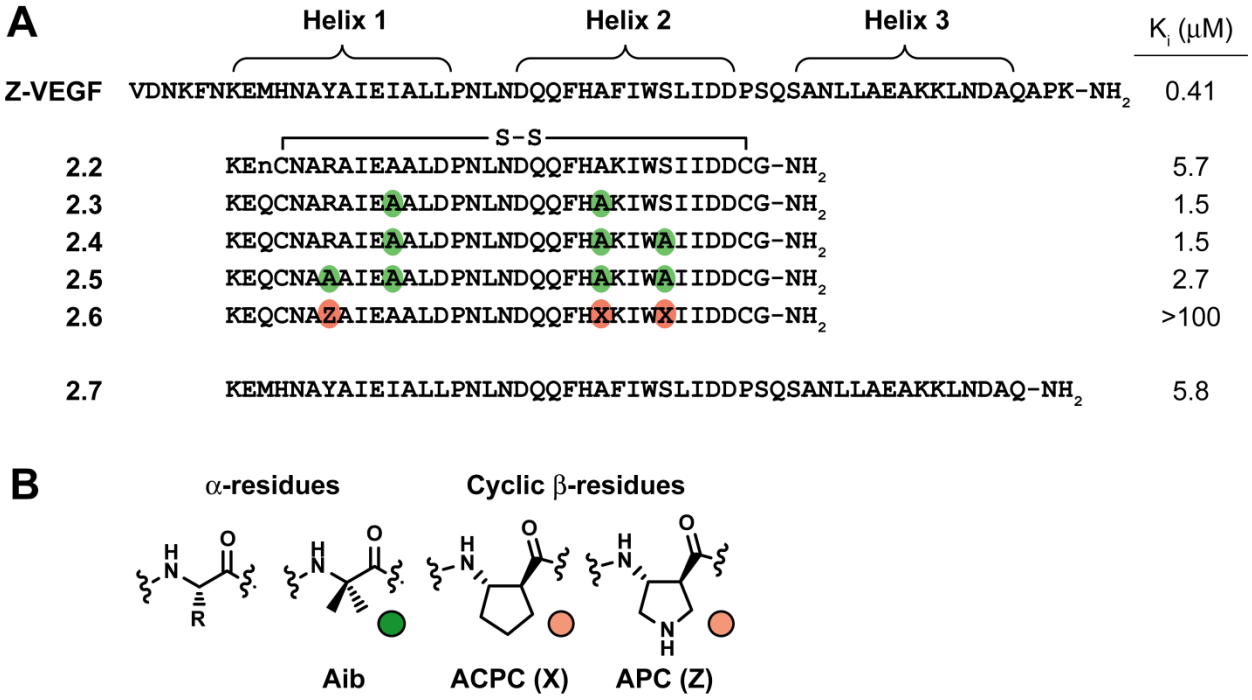

Figure 2.9 First generation of two-helix analogues of **Z-VEGF**. (A) Primary sequences of **Z-VEGF** and α- and α/β-peptide derivatives utilized in first generation designs, along with associated K_i values, as determined by $VEGF_{165}$ competition FP assay. K_i values for $VEGF_{165}$ competition FP assays typically vary ~2-fold between independent experiments and so any values within this range are considered experimentally indistinguishable. See Table 2.1 for a list of K_i values obtained for each compound reported in this chapter from independent experiments. Non-natural residues are indicated by colored circles, and "n" indicates norleucine. Each cysteine is engaged in an intramolecular disulfide bond. *(B)* Structures of a generic α-residue, the Aib residue (green), and the cyclic β-residues ACPC (X) and APC (Z) (orange).

With the hypothesis that residues 1-6 are likely not required for VEGF binding, we designed the helix-loop-helix α-peptide **2.2** corresponding to residues 7-39 of **Z-VEGF** (Figure 2.9). Peptide **2.2** included a norleucine residue in place of Met9 (numbering corresponds to full-length **Z-VEGF** sequence) to avoid undesired products resulting from methionine oxidation. We hypothesized that the removal of helix 3 would likely reduce the conformational stability of the resulting two-helix structure (which has been seen in prior truncation efforts based on Z-domain analogues[33-35]), and therefore **2.2** incorporates five of the α-amino acid residue substitutions mentioned above that were identified by phage display (Figure 2.5)[33, 35] to promote the intended helix-loop-helix structure (the analogous substitutions in **Z-VEGF**, based on structural alignment, are Tyr13→Arg, Ile17→Ala, Leu20→Asp, Phe31→Lys, and Leu35→Ile).

In an attempt to stabilize the intended two-helix structure in the absence of helix 3, we sought to incorporate the previously explored disulfide bond at the termini of the helices in **2.2**. We overlaid helices 1 and 2 of **Z-VEGF** in the co-crystal structure with $VEGF_{8-109}$ with the NMR structure of the two-helix **Z-IgG** analogue (PDB: 1ZDD);[34] this comparison suggested two sites in two-helix **Z-VEGF** analogues for cysteine substitution (Figure 2.10): His10, which occurs near the N-terminal side of helix 1, and Pro39, which lies at the C-terminus of helix 2. Peptide **2.2** contains the His10→Cys and Pro39→Cys substitutions. Finally, it is known that C-terminal cysteine residues can be problematic in peptide synthesis because of epimerization at the α-carbon of cysteine when it is bonded to the resin linker.[43] Although this side reaction does not significantly occur during the synthesis of C-terminal amides (it was reported for the synthesis of C-terminal acids), we included a glycine residue at the C-terminus as a spacer between the resin linker used for solid phase peptide synthesis and the last cysteine residue in

peptide **2.2** (as well as many other peptides described below) in order to ensure maximum yields of these relatively long sequences.

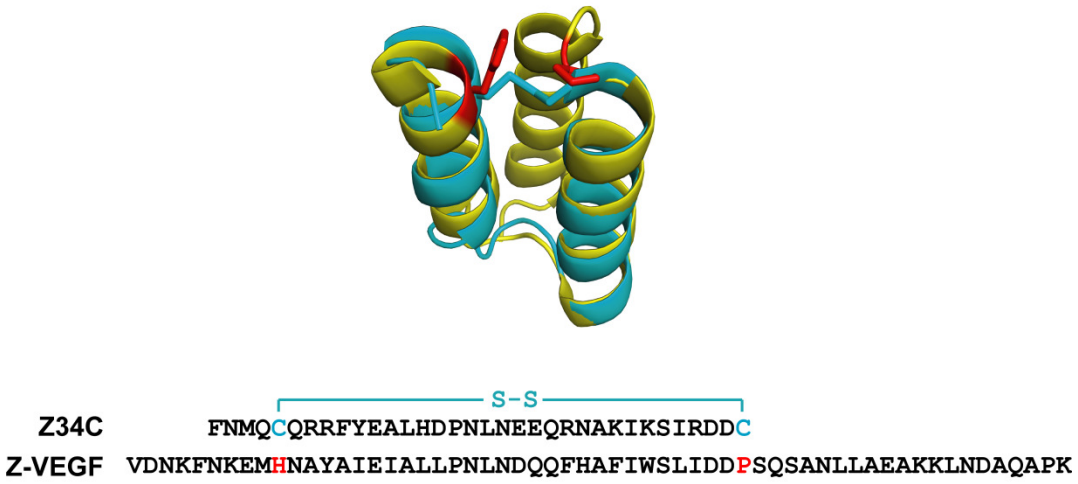

Figure 2.10 Overlay of cartoon representation of the crystal structure of **Z-VEGF** (yellow, from PDB: 3S1K) with the NMR solution structure of two-helix analogue of **Z-IgG** called **Z34C** (teal, PDB: 1ZDD). The disulfide bond is shown as sticks. Inspection of the overlay suggests that the location of Cys residues in **Z34C** corresponds well with His10 and Pro39 of **Z-VEGF**, highlighted in red.

Unexpectedly, **2.2** bound only weakly to VEGF, with an apparent K_i = 5.7 μM in the competition FP assay for binding to $VEGF_{165}$, a >13-fold decrease in affinity relative to the full-length **Z-VEGF** (Figure 2.9). We hypothesized that the decrease in affinity of **2.2** for VEGF may be due to a lack of conformational stability resulting from the absence of helix 3, even in the presence of the helix-stabilizing α-residue substitutions (Figure 2.5)[33, 35] and disulfide bond. In an attempt to increase the helical content of two-helix **Z-VEGF** derivatives, we designed analogues **2.3-2.6** containing helix-promoting substitutions (Aib[44] or cyclic β-amino acid residues[20, 22]) in regions that appeared helical in the **Z-VEGF**+$VEGF_{8-109}$ co-crystal structure but did not make direct contact with VEGF (Figure 2.9). Peptides **2.3-2.5** exhibited moderate improvements in VEGF affinity (~2- to 3-fold decrease in K_i relative to **2.2**), while α/β-peptide **2.6**, which contained cyclic β-residues at positions corresponding to those of the Aib

substitutions in **2.5**, showed no detectable binding to VEGF. Thus, while the incorporation of the helix-promoting Aib residue at several rationally-selected locations can modestly improve affinity of these two-helix designs, the resulting compounds were not able to match the affinity of the full-length parent peptide, **Z-VEGF**. Furthermore, our initial attempt at α→β-residue replacement in this scaffold (α/β-peptide **2.6**) was unsuccessful.

Residues 1-6 are not present in the **Z-VEGF**+$VEGF_{8-109}$ co-crystal structure, and so we predicted that these residues would not contribute significant contacts to VEGF. However, when we synthesized and evaluated peptide **2.7**, a peptide that corresponds to residues 7-56 of **Z-VEGF**, we were surprised to find that it displayed K_i = 5.8 μM for $VEGF_{165}$. This K_i value represents a >14-fold decrease in affinity for VEGF relative to the full-length **Z-VEGF**. The lower affinity of **2.7** relative to **Z-VEGF** suggests that a subset of residues 1-6 or 57-59 may be critical for high-affinity binding. This result emphasizes that caution should be exercised when using crystallographic data or data derived from analogous peptides as the sole guides in antagonist design. For example, just because a segment appears disordered in a crystal structure does not necessarily indicate that it does not contribute to protein binding.

To gain insight into the role of residues 1-6 and 57-59 on the conformation of **Z-VEGF** in solution, we compared the far-UV circular dichroism (CD) spectra of **Z-VEGF** and **2.7**, normalized both for peptide length (per residue) and concentration (Figure 2.11). The CD spectra of both peptides displayed minima at ~208 nm and 222 nm, which is consistent with the signatures of α-peptides adopting primarily an α-helical secondary structure. The CD spectra of **Z-VEGF** and **2.7** overlay very closely, which suggests that residues 1-6 and 57-59 do not play a critical role in stabilizing the overall structure of **Z-VEGF** in solution, despite their different affinities for VEGF. Alternatively, this could indicate that residues 1-6 and 57-59 in **Z-VEGF**

are relatively well-ordered under these conditions, since the CD signal (normalized "per residue") would be expected to be lower for **Z-VEGF** than **2.7** if these residue were random coil. Although it is unclear what role these residues play in the **Z-VEGF**+VEGF interaction, it is possible that one or more of these residues make(s) productive contacts with VEGF, despite not being resolved in the **Z-VEGF**+$VEGF_{8-109}$ co-crystal structure. Alternatively, it may be that some subset of residues 1-6 help to correctly position another critical contacting residue, such as Asn11, which is involved in a hydrogen bonding interaction to $VEGF_{8-109}$ in the **Z-VEGF**+$VEGF_{8-109}$ co-crystal structure.[18]

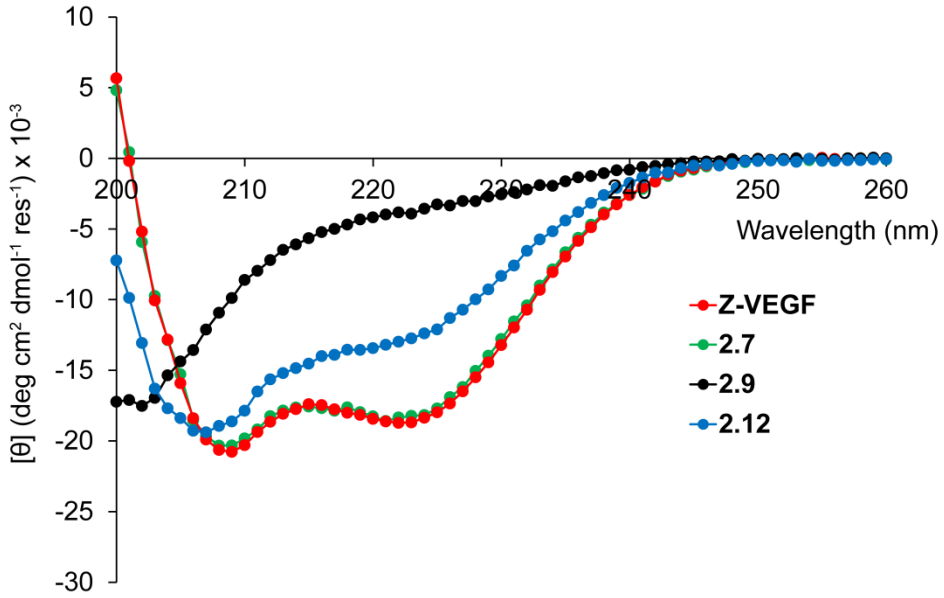

Figure 2.11 Far-UV circular dichroism data for α-peptides targeting VEGF based on **Z-VEGF**. All oligomers 75 μM in PBS, pH 7.5, 20°C.

With the hypothesis that residues 1-6 may play an important role in VEGF affinity in the context of the three-helix **Z-VEGF**, we designed a second generation of two-helix analogues of **Z-VEGF** that retained these residues (Figure 2.12). Simply removing helix 3 from **Z-VEGF**

gave peptide **2.8**. Peptide **2.8** showed no binding to $VEGF_{165}$, which is consistent with the loss of target affinity seen for other Z-domain derived peptides upon removal of helix 3.[33, 35] We next tried to incorporate into **2.8** the five helix-stabilizing substitutions[34, 35] mentioned above (Figure 2.5), along with a Met9→Gln substitution to avoid methionine oxidation. A glutamine residue appears at the analogous position in a two-helix **Z-IgG** derivative (**Z34C**, Figure 2.10), and so we hypothesized that it would be tolerated in the two-helix scaffold. However, these substitutions did not restore binding to $VEGF_{165}$ (peptide **2.9**). The far-UV circular dichroism (CD) spectrum of **2.9** suggests that this peptide is relatively unstructured in solution (Figure 2.12). This observation and the lack of affinity of **2.9** for $VEGF_{165}$ suggest that helix 3 of **Z-VEGF** plays a critical role in stabilizing the tertiary structure required for binding. In contrast to prior three-helix truncation approaches (**Z-IgG** and **Z-HER2** truncation, see Figure 2.5), this conformation destabilization brought about by removal of helix 3 cannot be reversed by incorporation of five of the phage-derived substitutions discovered by Wells et al.[33, 35]

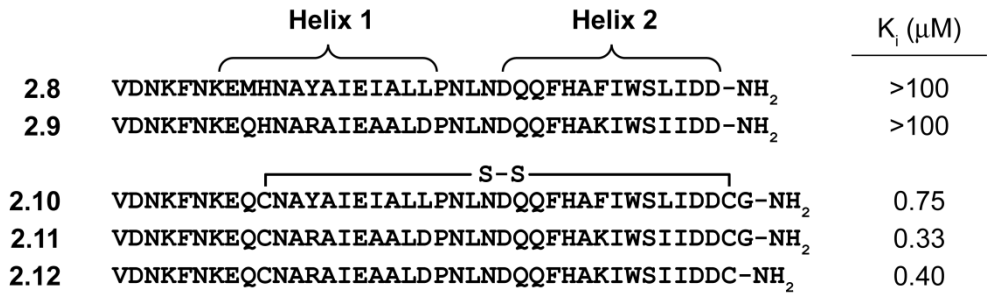

Figure 2.12 Primary sequences of two-helix α-peptides derived from **Z-VEGF** derivatives, along with associated K_i values, as determined by $VEGF_{165}$ competition FP assay. K_i values for $VEGF_{165}$ competition FP assays typically vary ~2-fold between independent experiments and so any values within this range are considered experimentally indistinguishable. See Table 2.1 for a list of K_i values obtained for each compound reported in this chapter from independent experiments. Each cysteine is engaged in an intramolecular disulfide bond.

We next incorporated the previously explored disulfide crosslink in an effort to stabilize the helix-loop-helix conformation,[34, 35] as described above for **2.2**. Peptides **2.10** and **2.11** are the

disulfide-constrained analogues of **2.8** and **2.9**, respectively. Both **2.10** and **2.11** showed high-affinity binding to VEGF, comparable to that of **Z-VEGF**. α-Peptide **2.11** displayed increased aqueous solubility relative to both **2.8** and **2.10**, likely due to the substitution of a number of hydrophobic residues for charged residues at sites expected to be distal to the VEGF-binding face. These solubility-enhancing substitutions were retained in subsequent designs. Finally, to evaluate the effect of the C-terminal glycine on VEGF affinity, we synthesized **2.12**, which lacks this residue. Peptide **2.12** was synthesized with comparable efficiency to those peptides containing the C-terminal glycine described above, indicating that the C-terminal glycine is not necessary for efficient peptide synthesis. Moreover, peptide **2.12** displayed K_i = 0.40 μM in the competition FP assay for VEGF, indicating that the C-terminal glycine has negligible effect on affinity. **2.12** showed an α-helical far-UV CD signature, which suggests that the incorporation of a disulfide into this two-helix scaffold promotes helical secondary structure, although the per-residue CD signal is not as intense as that for the full-length **Z-VEGF** (Figure 2.11). Peptides **2.11** and **2.12** bind to the $VEGF_{165}$ dimer with K_i values that are indistinguishable from the K_i for the full-length, three-helix 59-mer **Z-VEGF** binding to $VEGF_{165}$. This indicates that both **2.11** and **2.12** are successful two-helix mimics of **Z-VEGF**, despite the absence of the 20 residues of helix 3 that are critical for stabilizing tertiary structure required for VEGF binding.

2.3.3 Exploration of salt bridging interactions to stabilize helix-loop-helix conformation

Dense arrays of acidic and basic side chains can be used in combination to pre-organize helical conformations in α-peptides,[45-47] β-peptides,[48-50] and α/β-peptides.[51] Because the incorporation of salt bridges can increase conformational stability in such helical structures, this strategy can be useful both for enhancing protein affinity and for reducing protease susceptibility.

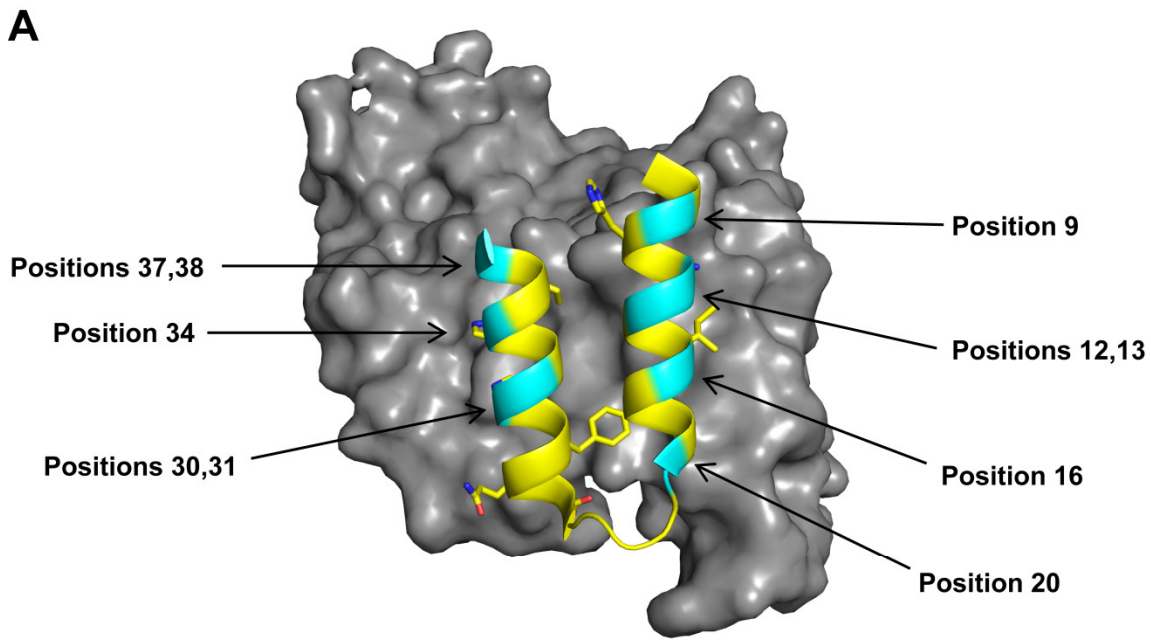

B

		K_i (μM)
	Helix 1 / Helix 2 (S–S)	
2.11	VDNKFNKEQCNARAIEAALDPNLNDQQFHAKIWSIIDDCG-NH_2	0.33
2.13	VDNKFNKEECNARAIEAALDPNLNDQQFHAKIWRIIDDCG-NH_2	0.35
2.14	VDNKFNKEECNRRAIEAALDPNLNDQQFHEKIWRIIEDCG-NH_2	0.13
2.15	VDNKFNKEECNRRAIEAALRPNLNDQQFHEEIWRIIEECG-NH_2	0.12
2.16	VDNKFNKEECNRRAIEAALRPNLNDQQFHRRIWEIIRRCG-NH_2	>40
2.17	VDNKFNKERCNEEAIRAALDPNLNDQQFHRRIWEIIRRCG-NH_2	1.5
2.18	VDNKFNKERCNEEAIRAALDPNLNDQQFHEEIWRIIEECG-NH_2	1.3

Figure 2.13 Design of two-helix **Z-VEGF** α-peptide analogues with additional ion pairing interactions (relative to **2.11**). (A) Sites targeted for substitution with acidic or basic residues are shown in cyan. Figure adapted from PDB: 3S1K. (B) Primary sequences of two-helix α-peptides derived from **Z-VEGF** derivatives, along with associated K_i values, as determined by $VEGF_{165}$ competition FP assay. K_i values for $VEGF_{165}$ competition FP assays typically vary ~2-fold between independent experiments and so any values within this range are considered experimentally indistinguishable. See Table 2.1 for a list of K_i values obtained for each compound reported in this chapter from independent experiments. Each cysteine is engaged in an intramolecular disulfide bond. Red and blue residues indicate acidic and basic residues, respectively, that may form salt bridging interactions in the positions indicated in panel (A).

To evaluate the effect of additional salt bridges in our helix-loop-helix tertiary structure, we explored analogues of **2.11** that contained additional acidic or basic side chain substitutions at positions opposite the VEGF-binding face (peptides **2.13**-**2.18**, Figure 2.13). Peptides **2.13**-**2.15**

contain a relatively small number of substitutions meant to impart one or two additional salt bridges, while peptides **2.16-2.18** make comparably more substantial substitutions (e.g., **2.16** and **2.17** swap the charge of most of the charged residues in helix 2 relative to **2.11**).

Peptides **2.13-2.18** were each synthesized and purified by reverse-phase HPLC. Although each peptide showed one major peak by reverse-phase analytical-scale HPLC (see "Experimental Methods" section), the MALDI-TOF MS spectra of peptides **2.15-2.17** showed multiple, successive -16 masses (-16, -32, -48, etc.) as minor peaks in addition to the major $[M+H]^+$ parent ion mass, suggesting the presence of additional species ionized in the spectrometer. It is unclear if these additional masses represent degradation products resulting from the ionization process in the spectrometer or stable species present in the purified peptide powder that co-elute with the desired product by analytical-scale HPLC. These masses likely result from successive loss of NH_2 groups; at the time of these experiments the University of Wisconsin-Madison Department of Chemistry did not have the advanced analytical mass spectrometry instrumentation required to definitively identify these species.

We evaluated the ability of **2.13-2.18** to bind to $VEGF_{165}$ by competition FP assay and compared affinities relative to **2.11**, the parent two-helix peptide containing no engineered salt-bridging residues other than those occurring in the Wells two-helix scaffold, from which **2.11** is modeled (Figure 2.13). In this experiment, we saw that **2.13** (K_i = 0.35 μM), **2.17** (K_i = 1.5 μM), and **2.18** (K_i = 1.3 μM) bound similarly to or slightly more weakly than **2.11** to $VEGF_{165}$. Peptide **2.16** showed only negligible binding to $VEGF_{165}$, even at the highest concentration tested, indicating that the placement of ionic side chains in this peptide is detrimental for VEGF affinity. In contrast, **2.14** and **2.15** showed moderately higher affinity for $VEGF_{165}$ relative to **2.11** (K_i = 0.13 μM for **2.14** and K_i = 0.12 μM for **2.15**), which suggests that the incorporation of additional

salt bridging interactions at certain positions increases the affinity for VEGF of peptides adopting the helix-loop-helix tertiary structure. This increase in affinity in **2.14** and **2.15** presumably is due to increased helix propensity as a result of productive placement of salt bridges on the back face of the helix-loop-helix structure. Consistent with this hypothesis, the far-UV CD spectrum of **2.15** showed an increase in intensity at ~208 nm and 222 nm relative to both **2.12** and **2.13** (Figure 2.14), which suggests that this peptide has increased helical character in solution. Interestingly, **2.17** and **2.18** also show an increased CD intensity relative to **2.12**, despite the fact that these peptides bind $VEGF_{165}$ with lower affinity than **2.12**. The overall shape of the CD signal for **2.17** and **2.18** is slightly different from that of **2.15**, which raises the possibility that the placement of additional ion pairs in these peptides may stabilize a somewhat different conformation from the one that is productive for binding VEGF. Unfortunately, we did not have sufficient material for CD analysis of **2.16**.

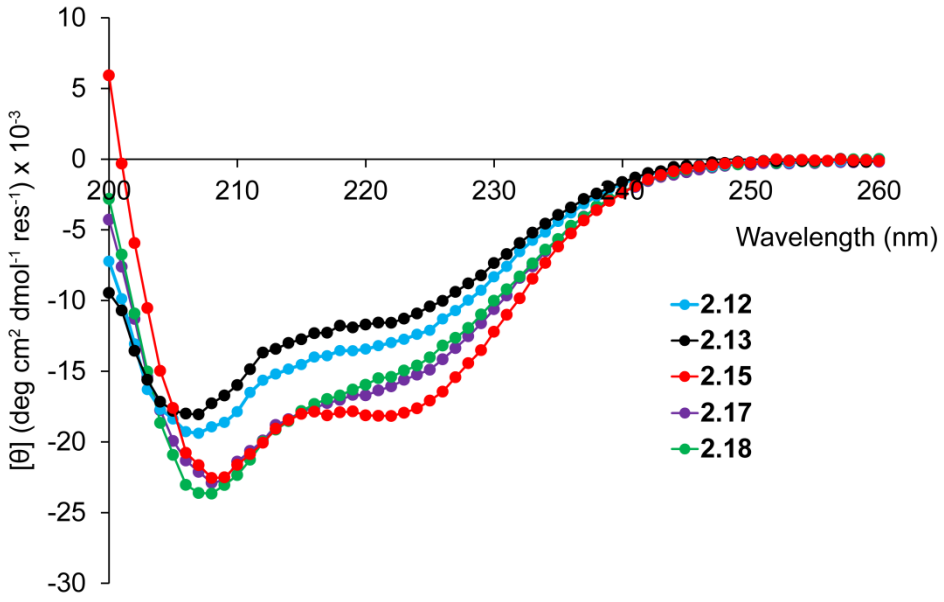

Figure 2.14 Far-UV circular dichroism data for two-helix α-peptides targeting VEGF based on **Z-VEGF**. All oligomers 75 μM in PBS, pH 7.5, 20°C.

2.4 α/β-Peptide design using iterative non-natural residue incorporation

We used peptide **2.11** as a starting point for α→β-amino acid residue substitutions with the goal of designing α/β-peptide mimics that bind VEGF with high affinity but display a decreased susceptibility to proteolysis. Our group has previously shown that the substitution of α-amino acid residues by their corresponding β^3-amino acid residues (bearing the same side chain) in an ααβααβ pattern can mimic helical peptides for protein recognition,[19, 21, 23] and we first sought to probe whether such substitutions into a single helix of the helix-loop-helix tertiary structure would be tolerated. α/β-Peptide **2.19** contains three α→β^3 substitutions in positions that are predicted not to make contact with VEGF or with helix 1 (i.e., on the solvent-exposed face of the peptide when bound to VEGF) (Figure 2.15). However, **2.19** showed very little affinity for VEGF by FP assay, with only limited binding at the highest concentration tested (100 μM).

Incorporation of β^3-amino acid residues into helical structures can sometimes lead to a decreased affinity for target proteins, likely due to the increased flexibility of the β^3-backbone relative to the backbone of an α-residue.[20, 24] In such cases, the incorporation of cyclically-constrained β-amino acid residues (e.g., ACPC, APC, sAPC, Figure 2.15B) sometimes increases affinity by restricting the Cα-Cβ torsion.[20, 22] We therefore incorporated single cyclic β-amino acid residues at solvent-exposed positions of helix 2, replacing uncharged Ala30 or Ser34 with ACPC to give α/β-peptides **2.20** and **2.21**, respectively. α/β-Peptide **2.20** showed very low affinity for $VEGF_{165}$ by FP (K_i > 100 μM), while **2.21** showed modest affinity (K_i = 0.99 μM). α/β-Peptide **2.22**, which contains both Ala30→ACPC and Ser34→ACPC, showed very weak binding to $VEGF_{165}$ (K_i >100 μM). These data suggest that certain positions in helix 2, such as position 30, do not tolerate α→β-residue substitutions even in the context of other potentially helix-stabilizing substitutions.

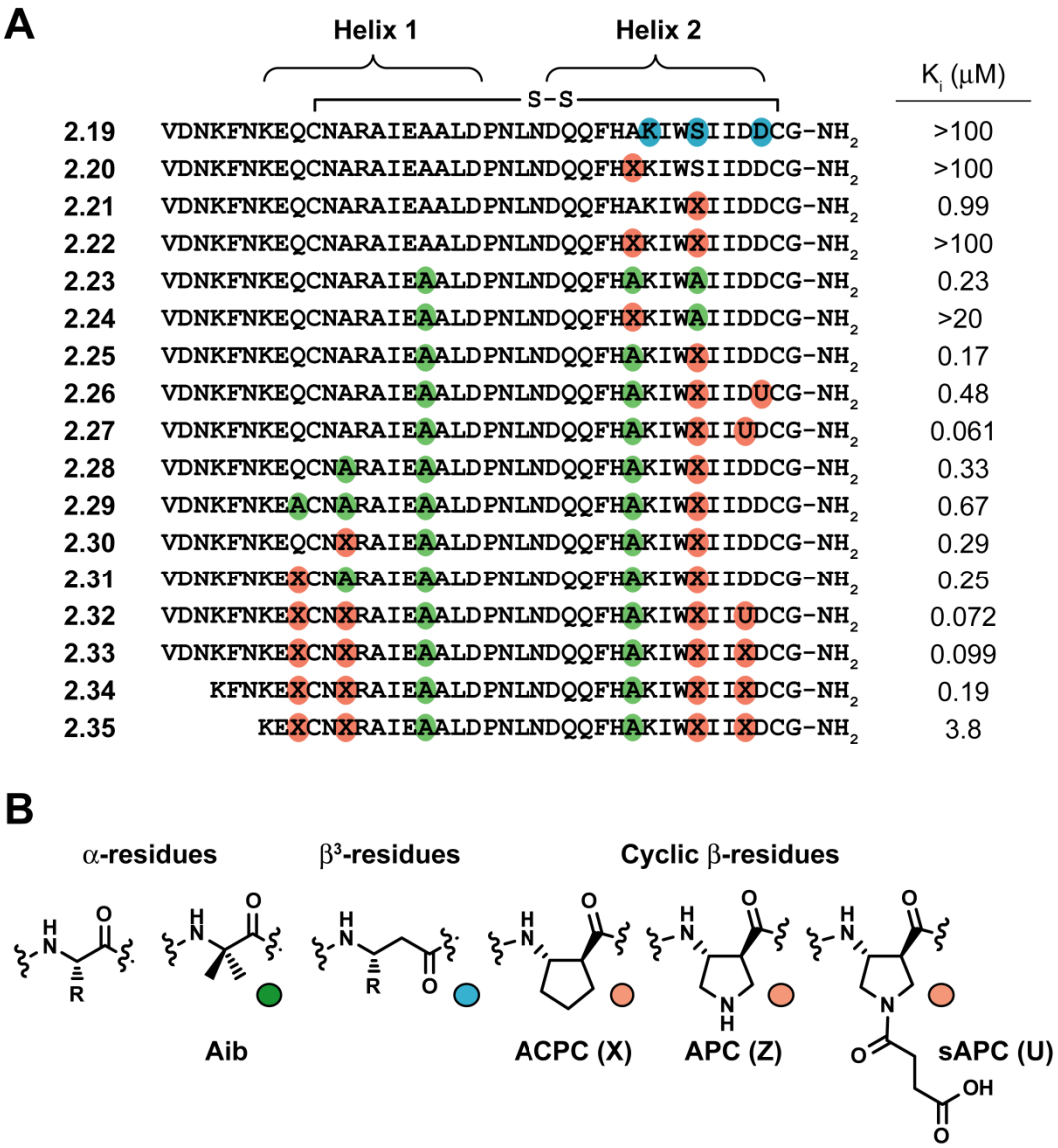

Figure 2.15 (A) Primary sequences of two-helix α/β-peptides derived from **2.11**, along with associated K_i values, as determined by $VEGF_{165}$ FP assay. K_i values for $VEGF_{165}$ competition FP assays typically vary ~2-fold between independent experiments and so any values within this range are considered experimentally indistinguishable. See Table 2.1 for a list of K_i values obtained for each compound reported in this chapter from independent experiments. Non-natural residues are indicated by colored circles. Each cysteine is engaged in an intramolecular disulfide bond. (B) Structures of a generic α-residue, the Aib residue (green), a generic β^3-residue (teal), and the cyclic β-residues ACPC (X), APC (Z), and sAPC (U) (orange).

Our initial studies on shorter two-helix **Z-VEGF** analogues (peptides **2.3-2.5**, Figure 2.9) suggested that the helix-promoting α-residue Aib may be better tolerated at the positions not amenable to α→β-residue substitution. Therefore, oligomers **2.23-2.25** contain Aib residues at rationally selected positions with either zero or one cyclic β-residue. Peptide **2.23**, which

contains three Aib residues, bound to $VEGF_{165}$ with high affinity (K_i = 0.23 μM), possibly because Aib residues at these positions increase the helicity of the two-helix peptide required. α/β-Peptide **2.24**, which contains the Ala30→ACPC substitution in addition to two Aib substitutions, showed very low affinity for VEGF, mirroring the results from **2.6**, **2.20**, and **2.22**, which also place ACPC at position 30. However, α/β-peptide **2.25**, which contains Ser34→ACPC in addition to two Aib residue replacements, showed high affinity for $VEGF_{165}$ (K_i = 0.17 μM).

Examination of the **Z-VEGF**+$VEGF_{8-109}$ co-crystal structure suggested that the Ala30 side chain may not play a critical role in VEGF binding or in interhelical tertiary packing. However, replacement of this residue with the cyclic β-amino acid residue ACPC in α/β-peptides **2.6**, **2.20**, **2.22,** and **2.24** led to a substantial loss in affinity for VEGF. In contrast, the helix-promoting α-residue Aib was tolerated at this position. Position 30 is located near the beginning of helix 2, close to the central loop region. Side chains from the loop and both helices are involved in packing interactions that may be critical for adopting the conformation necessary for VEGF-binding.[18, 52] One possible explanation for the low VEGF affinity of analogues that contain the Ala30→ACPC substitution is that the extra atom in the backbone of the β-residue shifts nearby side chains in a way that is detrimental to the tertiary packing in the loop region. Intramolecular side chain contacts involving residues further away from the loop may be less important for the overall helix-loop-helix conformation, which may be why cyclic β-residue incorporation was tolerated at position 34, more toward the terminus of helix 2 in α/β-peptides **2.21** and **2.25**.

We next used **2.25** as a starting point for additional replacements into the C-terminal end of helix 2 and into helix 1. We designed **2.26** and **2.27** with sAPC substitutions at either Asp37

or Asp38 in addition to those substitutions in **2.25**. While both **2.26** and **2.27** bound to $VEGF_{165}$ with high affinity, **2.27** bound tighter (K_i = 0.061 μM for **2.27** versus 0.48 μM for **2.26**), indicating that the Asp37→sAPC substitution is more favorable for VEGF-binding in the context of the substitution pattern of **2.25**. In parallel, we also used **2.25** as a starting point for probing non-natural substitutions into helix 1, and designed **2.28** and **2.29** with Aib substitutions at positions 9 and 12. Both **2.28** and **2.29** bound $VEGF_{165}$ with high affinity, suggesting that both positions 9 and 12 tolerate side chain substitution. α/β-Peptides **2.30** and **2.31** evaluate positions 9 or 12 for α→cyclic β-residue substitution; both α/β-peptides bound VEGF with high affinity. Residues within the central loop region (residues 21-24) form intramolecular hydrophobic contacts and hydrogen bonds to residues in both helix 1 and helix 2, and these interactions may be critical to the helix-loop-helix conformation; therefore, we did not make substitutions in the loop. Combining the β-residue substitutions identified as favorable in α/β-peptides **2.27**, **2.30**, and **2.31** gives α/β-peptide **2.32**, which displayed K_i = 0.072 μM in the competition FP assay for binding to $VEGF_{165}$.

We next sought to evaluate which residues at the N-terminus were necessary for high affinity, with the hopes of minimizing the sequence of the two-helix α/β-peptides further to provide the benefit of increased synthetic accessibility associated with shorter peptides. We first designed α/β-peptide **2.33** by substituting sAPC37 for the commercially-available ACPC, and found that this α/β-peptide retained high affinity for VEGF (K_i = 0.099 μM for **2.33** versus K_i = 0.072 μM for **2.32**). We designed analogues of **2.33** lacking residues 1-3 (α/β-peptide **2.34**, K_i = 0.19 μM) or 1-6 (α/β-peptide **2.35**, K_i = 3.8 μM). These results indicate that residues 1-3 may be removed from these two-helix analgoues, but some subset of residues 4-6 is required for high-affinity VEGF binding. It is notable that **2.33-2.35** qualitatively displayed significantly reduced

aqueous solubility compared to many previously designed analogues, likely due to the number of hydrophobic ACPC and Aib residue substitutions.

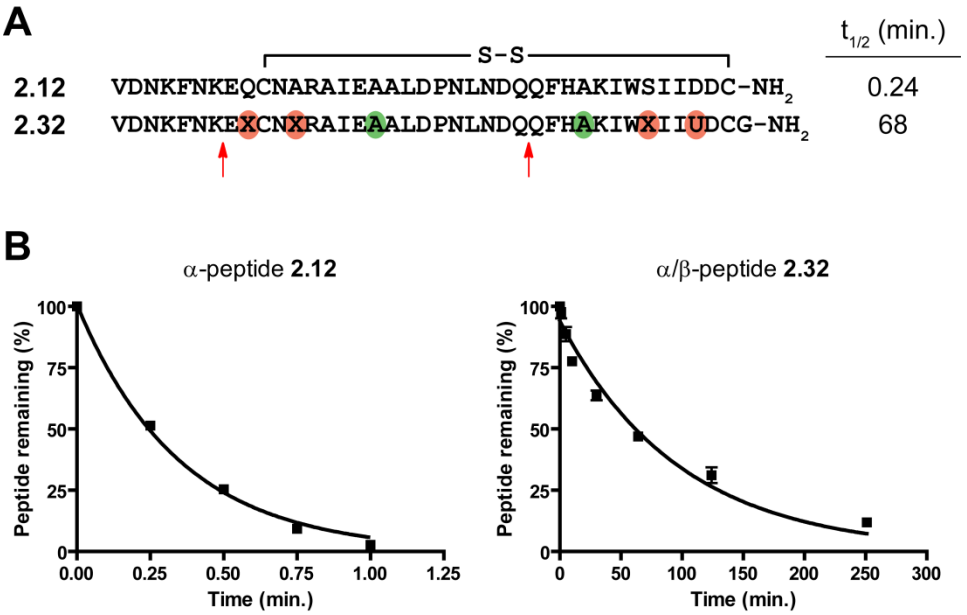

Figure 2.16 Susceptibility of 40 μM α-peptide **2.12** or α/β-peptide **2.32** to 10 μg/mL proteinase K in TBS, pH 7.5 with 5% DMSO at room temperature. (A) Sequences of peptides and associated half-life values. Red arrows indicate early cleavage sites for α/β-peptide **2.32**, as assessed by MALDI-TOF of the reaction mixture after 64 minutes. (B) Time course of α- or α/β-peptide degradation, as assessed by HPLC. Note the different scales on the horizontal axes.

α/β-Peptide **2.32** incorporates four α→cyclic β-residue and two Aib residue substitutions, each of which may reduce this oligomer's susceptibility to protease degradation.[20, 22, 53] In order to gain insight into how these non-natural substitutions affect protease susceptibility, we performed a protease digestion experiment. We incubated 40 μM of either **2.12** or **2.32** with 10 μg/mL proteinase K, a promiscuous and aggressive protease,[54] and quantified the amount of intact oligomer remaining by high performance liquid chromatography (HPLC) (Figure 2.16).

α-Peptide **2.12** was rapidly degraded by proteinase K, and displayed a half-life of 0.24 minutes in this assay. In contrast, α/β-peptide **2.32** showed substantial resistance to proteinase K degradation and displayed a half-life of 68 minutes under the same conditions (>280-fold

increase in half-life relative to **2.12**). We examined several quenched samples from the reaction of **2.32** with proteinase K by matrix-assisted laser desorption ionization time of flight mass spectrometry (MALDI-TOF MS) to identify putative protease cleavage sites by identifying masses that correspond to hydrolyzed fragments present in the mixture (Figure 2.17). Although we were not able to assign every fragment in the MALDI-TOF spectra of the protease reaction mixtures, we did observe masses that correspond to products resulting from hydrolysis of the Gln26-Gln27 amide bond and the Lys7-Glu8 amide bond (Figure 2.16A, red arrows). These results suggest that **2.32** may be most susceptible to proteolysis near the central loop in helix 2 (Gln26-Gln27) and near the N-terminus (Lys7-Glu8).

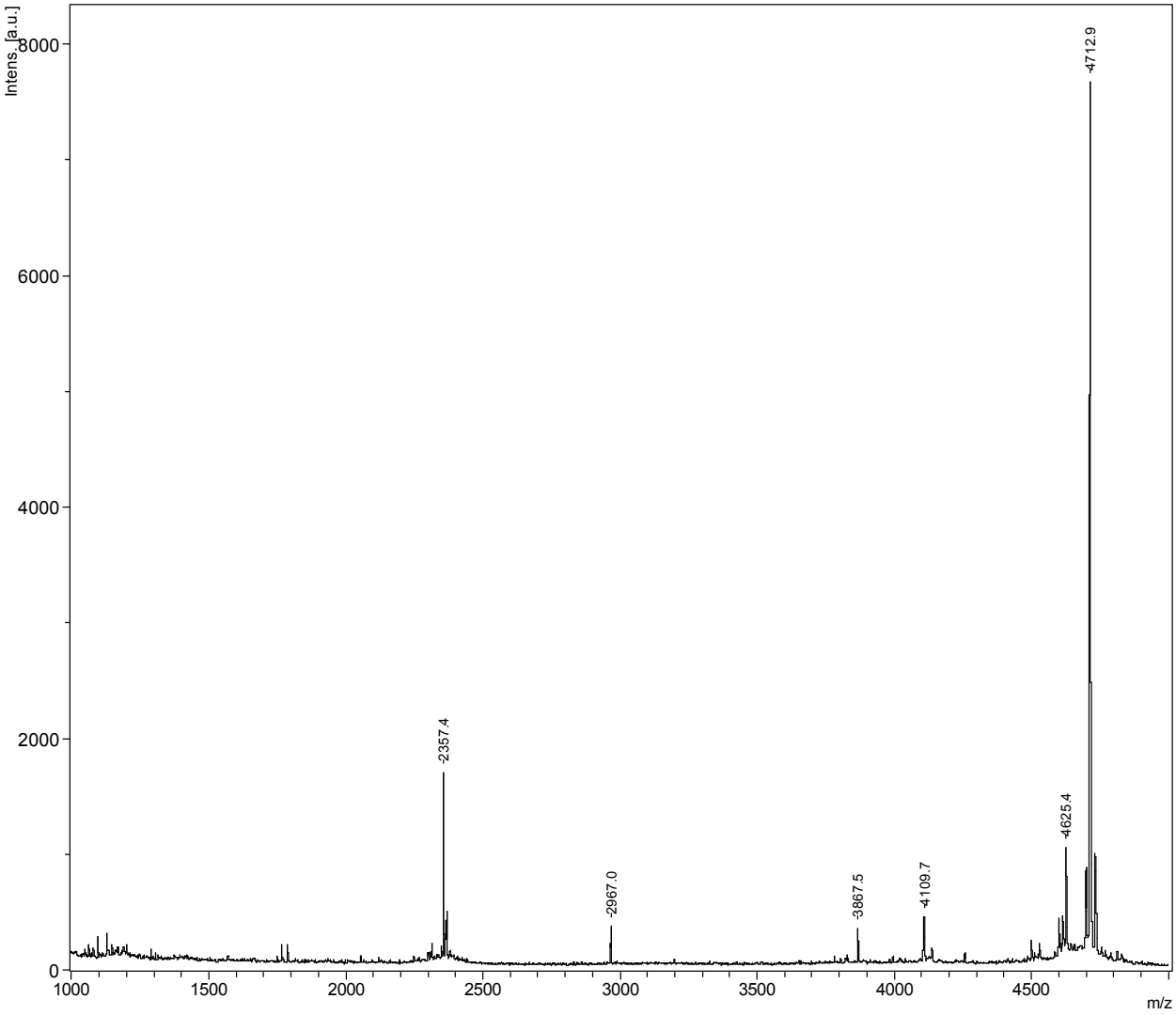

Figure 2.17 MALDI-TOF spectrum of the quenched proteinase K reaction mixture of α/β-peptide **2.32** after 64 minutes incubation with 10 μg/mL proteinase K. Each peak represents a species present in the mixture at that time point. For α/β-peptide **2.32**, calc. $[M+H]^+$ = 4713.3. Fragments resulting from hydrolysis of the Gln26-Gln27 bond (peptide sequence = VDNKFNKEXCNXRAIE(Aib)ALDPNLNDQ-OH, calc. $[M+H]^+$ = 2967.5) and the Lys7-Glu8 bond (peptide sequence = EXCNXRAIE(Aib)ALDPNLNDQQFH(Aib)KIWXIIUDCG-NH_2, calc. $[M+H]^+$ = 3867.9) are present in the spectrum. Other observed *m/z* values could not be assigned to specific fragments.

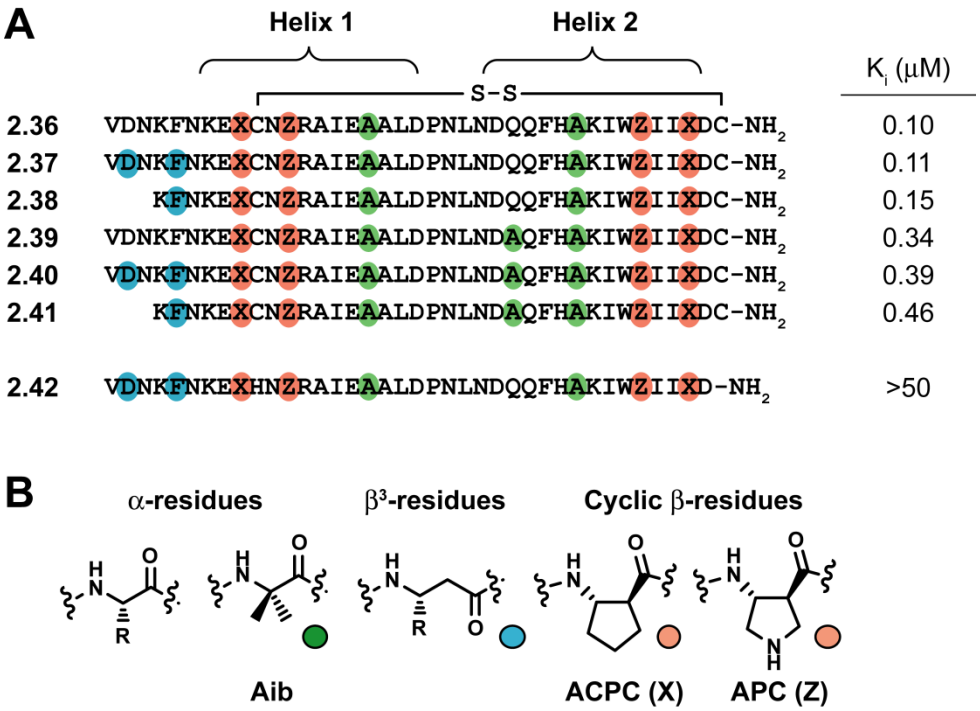

Figure 2.18 (A) Primary sequences of two-helix α/β-peptides derived from **2.32**, along with associated K_i values, as determined by $VEGF_{165}$ FP assay. K_i values for $VEGF_{165}$ competition FP assays typically vary ~2-fold between independent experiments and so any values within this range are considered experimentally indistinguishable. See Table 2.1 for a list of K_i values obtained for each compound reported in this chapter from independent experiments. Non-natural residues are indicated by colored circles. Each cysteine is engaged in an intramolecular disulfide bond. (B) Structures of a generic α-residue, the Aib residue (green), a generic β^3-residue (teal), and the cyclic β-residues ACPC (X) and APC (Z) (orange).

α/β-Peptide **2.32** showed high affinity for VEGF, yet was significantly less susceptible to protease degradation than its parent α-peptide, **2.12**. However, the high number of hydrophobic APC and Aib residues incorporated into **2.32** led to greatly reduced solubility in analogues **2.33**-**2.35**. (ACPC may be preferred to APC or sAPC for exploratory β-substitution efforts because ACPC is commercially available.) We therefore designed **2.36** as an analogue of **2.32** and **2.33** that contains ACPC at positions 9 and 37 and the positively charged APC at positions 12 and 34, and does not contain the C-terminal glycine (Figure 2.18). We suspected that the substitution of APC at positions 12 and 34 would be well tolerated due to the tolerance of Arg at these positions in peptides **2.14** and **2.15**. α/β-Peptide **2.36** bound to VEGF tightly, with K_i = 0.10 μM. Because we do not know what effect conformation and side chains have on

protein binding in the N-terminal region of the two-helix peptide, we incorporated two α→β^3-residue replacements into **2.36** within residues 1-6 to protect this region of the α/β-peptide from proteolysis yet retain the original side chains and conformational flexibility. The resulting α/β-peptide, **2.37**, bound to $VEGF_{165}$ with K_i = 0.11 μM. An analogue of **2.37** lacking residues 1-3, α/β-peptide **2.38**, also showed high-affinity binding to $VEGF_{165}$ (K_i = 0.15 μM), consistent with the observation that **2.34** bound $VEGF_{165}$ with a similar affinity to **2.33**.

The region from Ala18 to His29 in **2.37** contains only proteinogenic α-amino acid residues, and the proteolysis experiment described above suggested that the region near Gln26-Gln27 may be particularly susceptible to protease degradation (Figures 2.16 and 2.17). Therefore, we designed **2.39**, **2.40**, and **2.41** as analogues of **2.36**, **2.37**, and **2.38**, respectively, containing an additional Gln26→Aib substitution in an effort to protect this region from proteolysis.[53] These α/β-peptides each bound to VEGF with K_i = 0.34-0.46 μM, slightly weaker than the **2.36-2.38** series, yet experimentally indistinguishable from the full-length **Z-VEGF** and the parent two-helix α-peptide **2.12**.

Finally, in order to gain insight into the importance of the disulfide bond for affinity for VEGF in the presence of the helix-stabilizing cyclic β- and Aib residues, we designed **2.42**, an analogue of **2.37** that contains the native residue from **Z-VEGF** in place of the Cys10 (His10), and lacks Cys39. Interestingly, **2.42** showed very little binding to $VEGF_{165}$ in the competition FP assay (K_i > 50 μM).

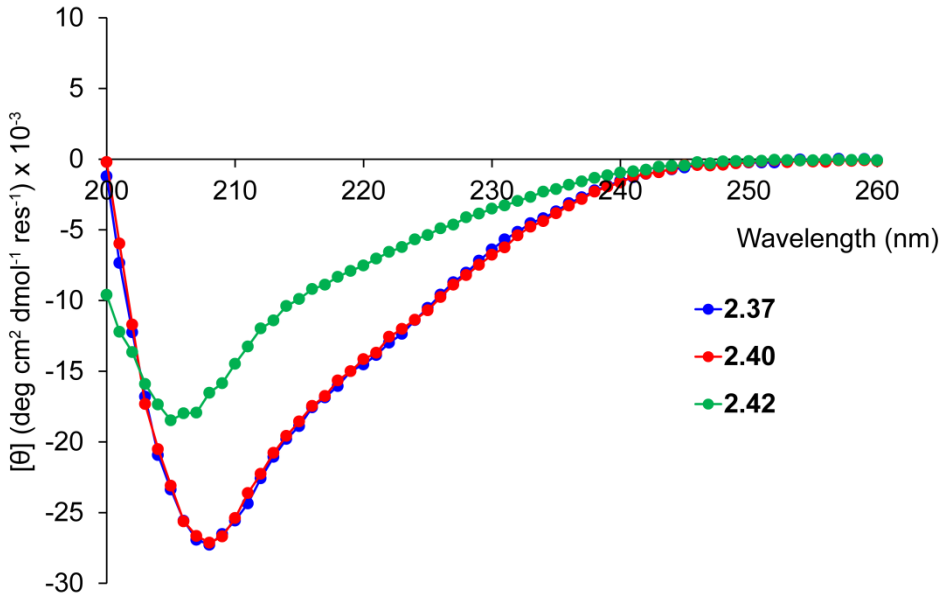

Figure 2.19 Far-UV circular dichroism data for α/β-peptides targeting VEGF based on **Z-VEGF**. All oligomers 75 μM in PBS, pH 7.5, 20°C.

The far-UV CD spectrum of **2.37** and **2.40** both showed a single intense minimum at ~209 nm, which is characteristic of an α/β-peptide adopting a helical conformation in solution.[55] The CD signals for **2.37** and **2.40** overlaid very well with one another, suggesting these two α/β-peptides have a similar fraction of folded population in solution. The far-UV CD spectrum of **2.42** also showed a single minimum at ~209 nm, indicating that this α/β-peptide also adopts a helical conformation in solution (Figure 2.19). However, the intensity of the normalized CD signal for **2.42** was weaker than that of **2.37** (its disulfide bonded analogue), which suggests that **2.42** is less structured in solution than **2.37**. This result suggests that the disulfide bond present in the two-helix α/β-peptides reported in this chapter is required for VEGF-binding through stabilization of the helix-loop-helix conformation.

The α/β-peptides presented above represent the first examples in which functional mimicry of an α-peptide prototype has been achieved with α/β-peptides that are significantly

shorter than the prototype (39 residues versus 59 residues for **Z-VEGF**). Moreover, these compounds highlight the successful extension of the principles for α/β-peptide mimicry of single helices[20, 56] to a multi-helical tertiary structure. In the case of the **2.36-2.38** series, the affinity for $VEGF_{165}$ was modestly improved relative to **Z-VEGF**, presumably because the non-natural residues promote the helical secondary structure required for binding. The slightly diminished affinity of the **2.39-2.41** series relative to the **2.36-2.38** series may reflect loss of a modestly stabilizing contact resulting from Gln26→Aib substitution.

2.5 Crystal structure of α/β-peptide 2.37 bound to $VEGF_{8-109}$

The two-helix α- and α/β-peptides described above were designed to mimic the helix-loop-helix structure adopted by helix 1 and helix 2 of **Z-VEGF** (as depicted in Figure 2.6). The results of the competition FP assays showing that many of these oligomers bind to $VEGF_{165}$ with affinity similar to that of the parent three-helix **Z-VEGF** are consistent with the hypothesis that these compounds accurately mimic the protein recognition properties of the parent. To gain high-resolution insight into the interaction of these oligomers with VEGF, we pursued crystallization experiments with the goal of obtaining an X-ray crystal structure of one of the Z-domain-derived α/β-peptides either alone or in complex with VEGF.

We began by attempting to crystallize **2.37** and **2.40** alone, using the Hampton Index reagent system (Hampton Research) to screen conditions for crystallization. These preliminary experiments did not result in any diffraction-quality crystals, so we moved to attempts to co-crystallize **2.37** with the $VEGF_{8-109}$ homodimer. $VEGF_{8-109}$ is a construct that corresponds to the receptor-binding domain of human VEGF, and lacks the highly basic heparin binding domain present in $VEGF_{165}$. Almost all reported crystal structures of VEGF are of the $VEGF_{8-109}$ construct, and so we reasoned that this construct would be more amenable to crystallization than

$VEGF_{165}$. Nicole C. Thomas (Gellman Laboratory, University of Wisconsin-Madison) constructed a pET-3d vector containing the $VEGF_{8-109}$ gene, and *Escherichia coli* BL21(DE3)-RIPL cells were transformed with this vector. $VEGF_{8-109}$ was then expressed, refolded, and purified using a protocols adapted from the expression of $VEGF_{165}$ by Peterson et al.[39] (see "Experimental Methods").

Initial crystallization screens were carried out by mixing the $VEGF_{8-109}$ homodimer with purified α/β-peptide **2.37** in a 1:3.2 molar ratio and screening conditions from the Hampton Index (a 1:3 molar ratio of $VEGF_{8-109}$:**Z-VEGF** was used for their crystallization).[18] Several conditions from the initial screen grew crystals, and we pursued multiple conditions for optimization. The most promising crystals grew from Condition 92 (0.1 M magnesium formate dihydrate, 15% (w/v) PEG3350) of the Hampton Index at various concentrations of protein+α/β-peptide. Importantly, crystals from Condition 92 did not grow in the presence of $VEGF_{8-109}$ alone, strongly suggesting the presence of the **2.37**+$VEGF_{8-109}$ complex in the crystal. Condition 92 was optimized to afford the final crystallization conditions, as described in the "Experimental Methods" section.

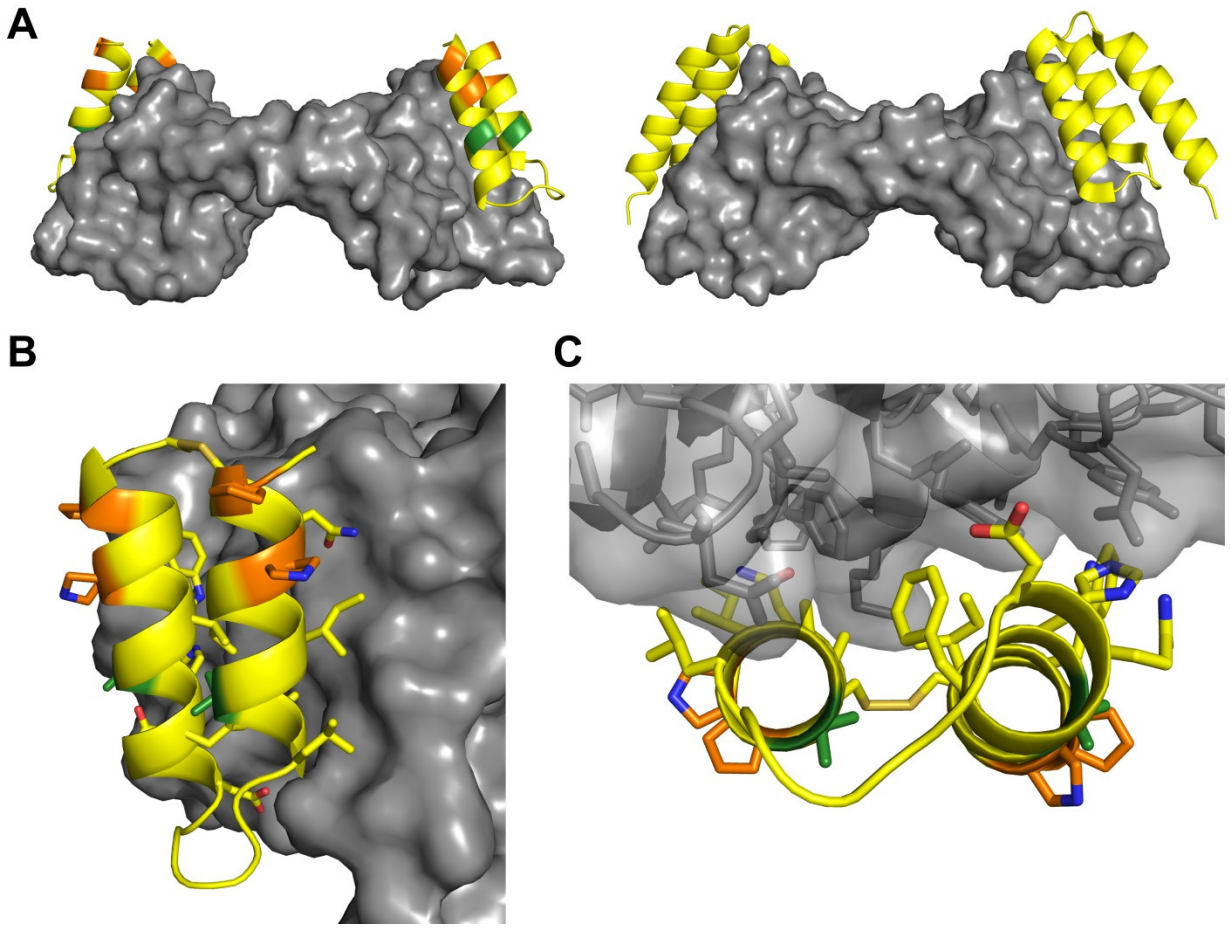

Figure 2.20 Crystal structure of α/β-peptide **2.37** in complex with $VEGF_{8-109}$ (PDB: 4WPB). Residues in **2.37** are colored by type of residue (yellow for α, green for Aib, and orange for cyclic β). $VEGF_{8-109}$ is depicted as a gray surface. (A) Left: Cartoon representation of **2.37** bound to $VEGF_{8-109}$. Right: Cartoon representation of α-peptide **Z-VEGF** bound to $VEGF_{8-109}$ (PDB: 3S1K)[18], for comparison. The α/β-peptide binds to the same surface of $VEGF_{8-109}$ as **Z-VEGF**. (B) Side view of **2.37**+$VEGF_{8-109}$ highlighting the interface between these molecules. The side chains are displayed as sticks for residues of **2.37** appearing to make contact with $VEGF_{8-109}$, for Aib and cyclic β residues, and for the disulfide bond. Carbon atoms are colored by residue type, blue atoms are nitrogen, red atoms are oxygen, and tan atoms are sulfur. (C) View of the **2.37**+$VEGF_{8-109}$ interface looking along the α/β-peptide helical axes. $VEGF_{8-109}$ shown as transparent surface with cartoon backbone and side chains represented as sticks.

The structure of α/β-peptide **2.37** in complex with the $VEGF_{8-109}$ homodimer was refined to 3.1 Å resolution, R = 24.5% (Figure 2.20, see also Table 2.2 in the Experimental Methods section for X-ray collection and refinement statistics, PDB: 4WPB). X-ray data collection, structure determination, and refinement were done in collaboration with Dale F. Kreitler (Gellman Laboratory, University of Wisconsin-Madison) and Professor Katrina T. Forest (Department of Bacteriology, University of Wisconsin-Madison). The crystal structure shows

two molecules of **2.37** bound to the equivalent receptor-binding sites of the $VEGF_{8-109}$ dimer; the same sites on $VEGF_{8-109}$ are occupied by **Z-VEGF** in its co-crystal structure (Figure 2.20).[18] Both **2.37** molecules adopt the anticipated helix-loop-helix conformation. As expected, the positions of the four cyclic β-amino acid residues and two Aib residues of **2.37** project away from $VEGF_{8-109}$ and toward the medium (Figure 2.20). Radiation damage was evident at the disulfide bonds, and a total of four side chains were disordered on the solvent-exposed face and at the helix 2 terminus, as well as at the N-terminus (residues 1-7), for each of the α/β-peptides (see Experimental Methods section). In contrast, most side chains from the α/β-peptides that contact $VEGF_{8-109}$ were well-ordered (Figure 2.20 and 2.21). Overall, the co-crystal structure indicates that **2.37** accurately mimics the binding mode of helices 1 and 2 of **Z-VEGF** with $VEGF_{8-109}$, confirming that the removal of helix 3 and incorporation of multiple α- and β-amino acid residue replacements distal to the VEGF-binding face does not alter recognition geometry.

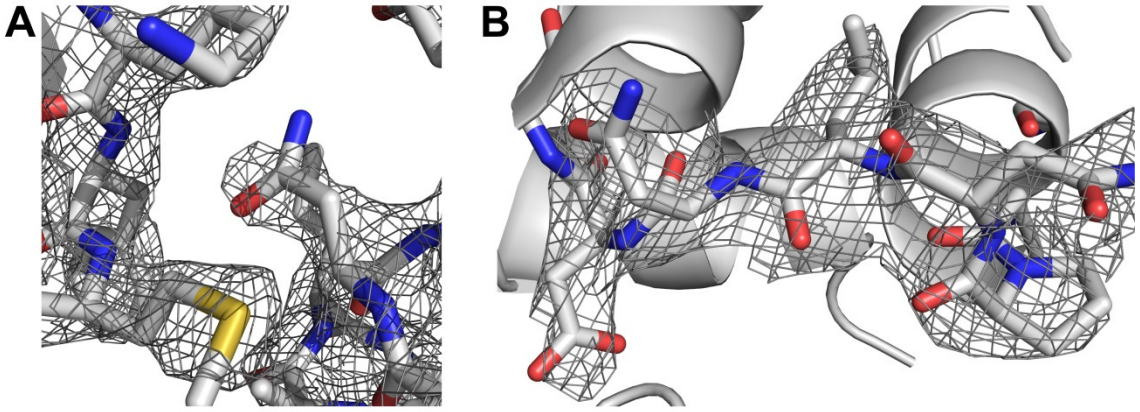

Figure 2.21(A) A contact between the side chain of α/β-peptide **2.37** Asn11 (chain C) and $VEGF_{8-109}$ (chain A), electron density is represented as a $2mF_o$-DF_c weighted map contoured at 1.2σ. (D) Residues 20-25 within the loop region of **2.37** (DPNLND, chain D), electron density is represented as a $2mF_o$-DF_c weighted map contoured at 1.2σ.

2.6 Protease susceptibility

2.6.1 Susceptibility to proteinase K degradation

We examined the impact of non-natural residue incorporation on susceptibility to degradation by proteinase K,[20, 54] a promiscuous and aggressive enzyme (Figure 2.22). The 59-mer **Z-VEGF** was rapidly degraded, displaying a half-life of 1.6 minutes under the assay conditions. **2.12**, the disulfide-constrained 39-mer α-peptide that matched the $VEGF_{165}$ affinity of **Z-VEGF**, was degraded even more rapidly (half-life = 0.20 minutes). The susceptibility trend for this pair may reflect decreased conformational stability of the two-helix scaffold relative to the three-helix scaffold. This trend is consistent with a previous report that the two-helix **Z-IgG** analogue (**Z34C**, Figure 2.5) manifests reduced conformational stability relative to full-length **Z-IgG** despite nearly identical affinities for IgG.[34] This half-life value for **2.12** of 0.20 minutes is also consistent with the preliminary proteinase K digestion experiment described above (Figure 2.16), despite slightly different experimental conditions. In contrast to the rapid degradation of **Z-VEGF** and **2.12** by proteinase K, 39-mer **2.37**, which contains six β-amino acid residues and two Aib residues, exhibited a half-life of 59 minutes, which represents a >290-fold increase relative to the analogous α-peptide, **2.12**. Indeed, **2.37** showed substantially greater resistance to proteinase K than the 59-mer α-peptide **Z-VEGF**. These observations are consistent with previous findings, involving other α- vs. α/β-peptide comparisons, that have shown that α→β replacements at multiple sites can substantially enhance polypeptide resistance to protease action.[19, 20, 22, 25] As predicted based on the proteinase K digest of **2.32** (Figure 2.16 and 2.17), the introduction of the Gln26→Aib substitution to convert **2.37** into **2.40** conferred additional resistance to proteinase K (half-life = 670 minutes; >400-fold increase relative to **Z-VEGF** and >3300-fold increase relative to **2.12**). Thus, despite having considerably fewer residues than **Z-**

VEGF, the α/β-peptides developed here match or exceed the target affinity of the initial 59-mer α-peptide while far surpassing this prototype in terms of resistance to proteolytic destruction.

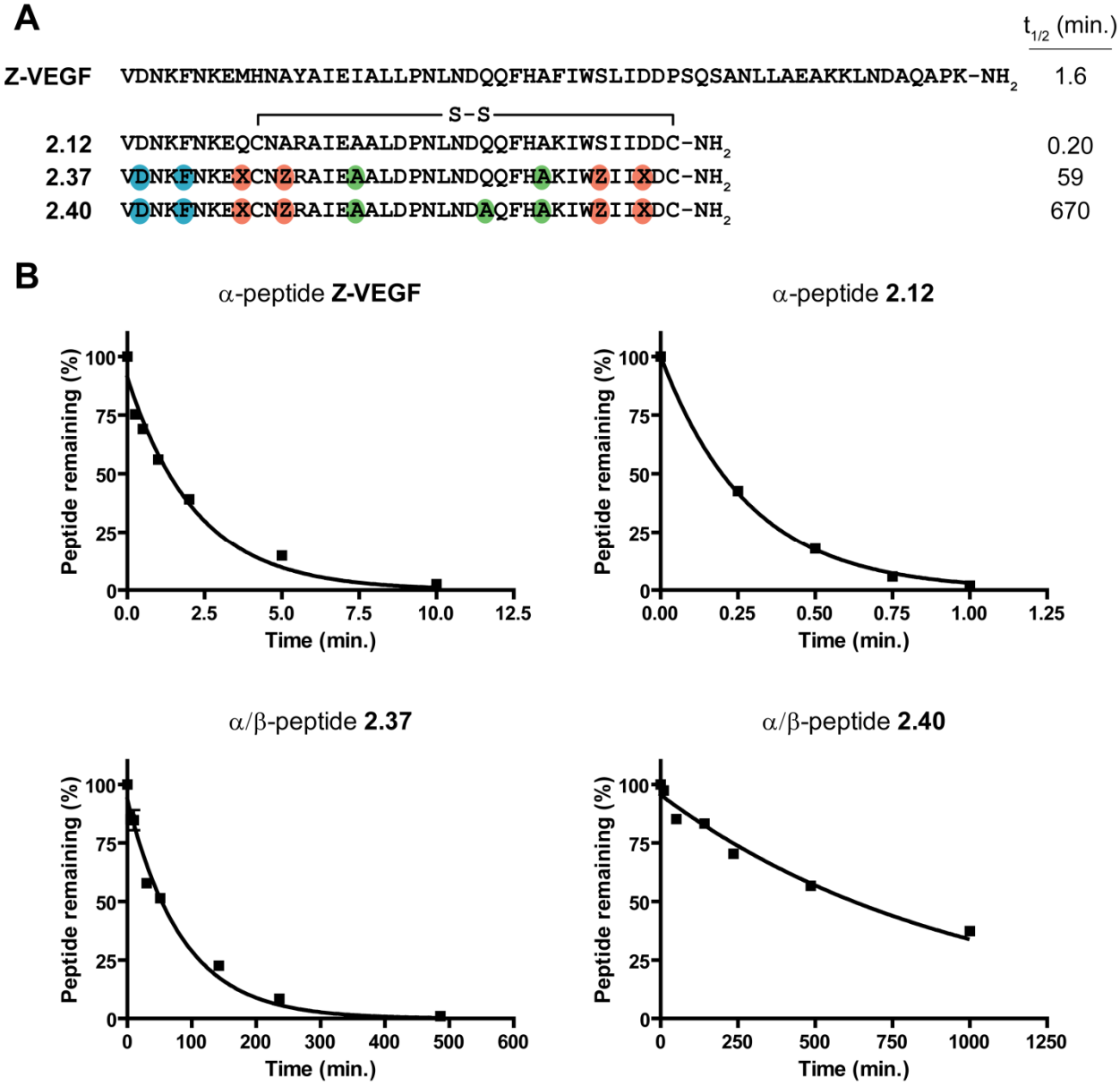

Figure 2.22 Susceptibility of 45 μM α- or α/β-peptide in the presence of 10 μg/mL proteinase K in TBS, pH 7.5 at room temperature. (A) Sequences of peptides and associated half-life values. (B) Time course of α- or α/β-peptide degradation, as assessed by HPLC. Note the different scales on the horizontal axes.

2.6.2 Susceptibility to degradation in simulated gastric fluid (SGF)

One potential advantage that α/β-peptides may have over conventional α-peptides is that the reduced proteolytic susceptibility of α/β-peptides may allow them to survive in the harsh protease-active environment of the gastrointestinal (GI) tract. Compounds that are able to survive long enough in such an environment may be absorbed into the blood stream to act in living systems. Thus, it is possible that the reduced susceptibility of α/β-peptides to protease degradation may allow them to be orally bioavailable, which is an attractive property for potential therapeutic agents since oral administration is often favored by patients over other forms of administration (e.g., injection).[57] To gain some insight into the relative stabilities of the α/β-peptides derived from **Z-VEGF** in a gastric-like environment, we evaluated the susceptibilities of **2.12**, **2.37**, and **2.40** to degradation in a simulated gastric fluid (SGF) test solution, as defined by the US Pharmacopeia (0.2% (w/v) NaCl, 0.32% (w/v) pepsin (800-2500 units/mg), 0.7% (v/v) conc. HCl, pH ~1.2, 37 °C).[58, 59] It is important to note that while the US Pharmacopeia calls for pepsin with activity of 800-2500 units/mg, the study described below used pepsin with activity defined at ≥2500 units/mg.

We incubated 30 μM of each α- or α/β-peptide in SGF solution and monitored oligomer degradation over time by HPLC and MALDI-TOF MS (Figures 2.23 and 2.24). The two-helix α-peptide **2.12** showed extremely rapid degradation in this assay, with no detectable peptide remaining at the 15 second time point by HPLC or MALDI-TOF. α/β-Peptide **2.37**, which showed a substantial increase in resistance to degradation by proteinase K relative to **2.12**, appeared to be degraded in the SGF test solution less rapidly, with a peak in HPLC corresponding to the same retention time as intact **2.37** present in the HPLC chromatogram after 2 minutes. However, when we analyzed the quenched reaction mixture of the 2 minute time

point for **2.37** by MALDI-TOF, we failed to detect the molecular ion peak corresponding to intact **2.37**. This result raises the possibility that the corresponding peak in the HPLC chromatogram may be a fragment of **2.37** rather than the intact oligomer. Alternatively, the absence of the parent peak in the MALDI spectrum may simply be due to this species being at a very low concentration. Regardless, this peak in the HPLC chromatogram is nearly absent at the 5 minute time point, indicating that **2.37** is essentially completely degraded within 5 minutes under these conditions.

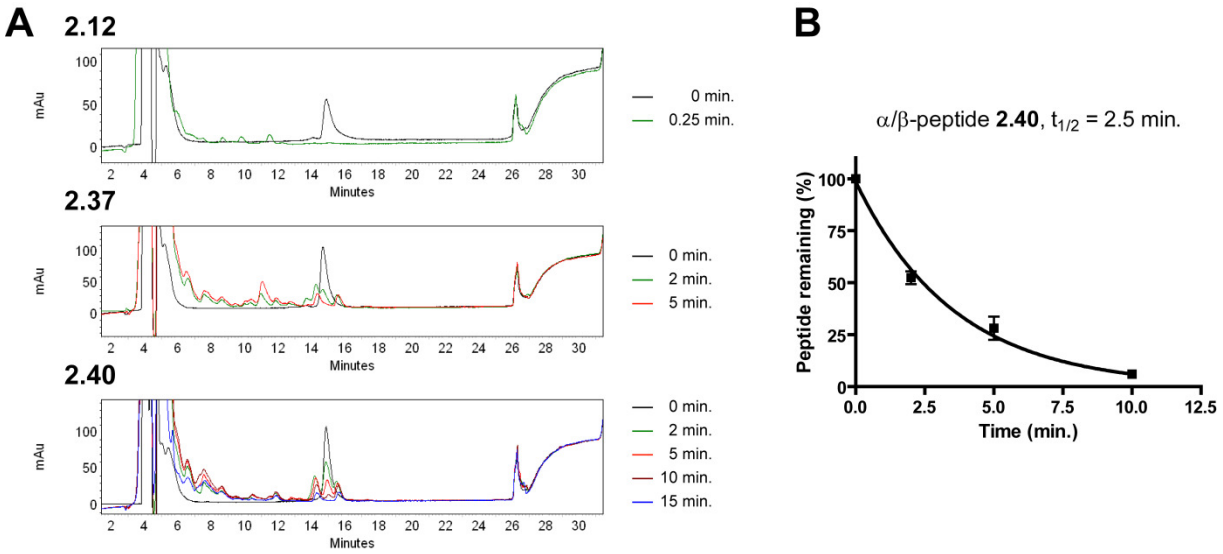

Figure 2.23 Digestion of 30 μM α- or α/β-peptide in simulated gastric fluid (SGF) test solution, 37 °C. (A) Overlay of HPLC chromatograms for the indicated oligomers at the indicated time points, monitoring UV absorbance at 220 nm. (B) Time course of α/β-peptide **2.40** degradation, as assessed by HPLC.

When α/β-peptide **2.40** was subjected to SGF conditions, the peak corresponding to the intact α/β-peptide was degraded over the course of 15 minutes at a rate significantly slower than the degradation of **2.12** (which displayed a half-life < 15 sec. in this assay) or **2.37**. In contrast to **2.37**, we were able to detect the parent ion corresponding to the intact **2.40** in the MALDI spectrum of the 2 minute time point, confirming that **2.40** survives at least 2 minutes under these conditions (Figure 2.24). An ion at *m/z* = 3262.7 is present in the MALDI spectrum for **2.40** after

2 minutes degradation by SGF. This mass likely corresponds to a relatively stable hydrolysis product under the SGF conditions, although we were unable to determine the identity of this species. At the five minute time point, the parent ion peak for **2.40** is no longer detectable by MALDI, although the corresponding peak in the HPLC chromatogram remains through the 10 minute time point. Fitting the area of the peak corresponding to **2.40** over time to an exponential decay model estimates the half-life of this compound as 2.5 minutes under these under these conditions (Figure 2.23B), which is at least a >10-fold increase in half-life relative to **2.12**, which was completely degraded at the first time point evaluated (15 seconds).

This preliminary degradation experiment suggests that **2.40** is significantly more stable under SGF conditions relative to the parent α-peptide **2.12**. The apparent stability trend for **2.12** versus **2.37** versus **2.40** matches the stability trend seen for the degradation of these compounds by proteinase K, although the rate of degradation for all compounds is much faster in SGF than in the proteinase K experiment. Overall, these results suggest that the incorporation of non-natural β-amino acid and Aib residues may be used to increase the stability of α/β-peptides in extremely harsh biological conditions such as gastric fluid and may offer promise for eventual oral bioavailability, if they can be further engineered to cross the intestinal membrane for absorption into the bloodstream.[60, 61] However, the rate of degradation seen in this SGF experiment, even for the most stable α/β-peptide **2.40**, is likely too rapid for these compounds to be effectively administered orally in animal models. The observation of a single, stable product during the degradation of **2.40** under SGF conditions (as determined by MALDI-TOF, Figure 2.24) suggests that **2.40** may be cleaved in a finite number of sites (e.g., the loop region, which contains only natural α-residues). It may be feasible to identify and target these sites for protection in future designs. It is important to note that the purified pepsin used in this study had

activity of ≥2500 units/mg, which is higher than the activity specified by the US Pharmacopeia of 800-2500 units/mg. Therefore, the SGF solution used in this experiment is likely more active than typical gastric fluid due to a higher concentration of the pepsin enzyme. Future studies with SGF test solution should include control peptides of known half-life values in this solution to ensure that the activity of the SGF is comparable to naturally occurring gastric fluid.

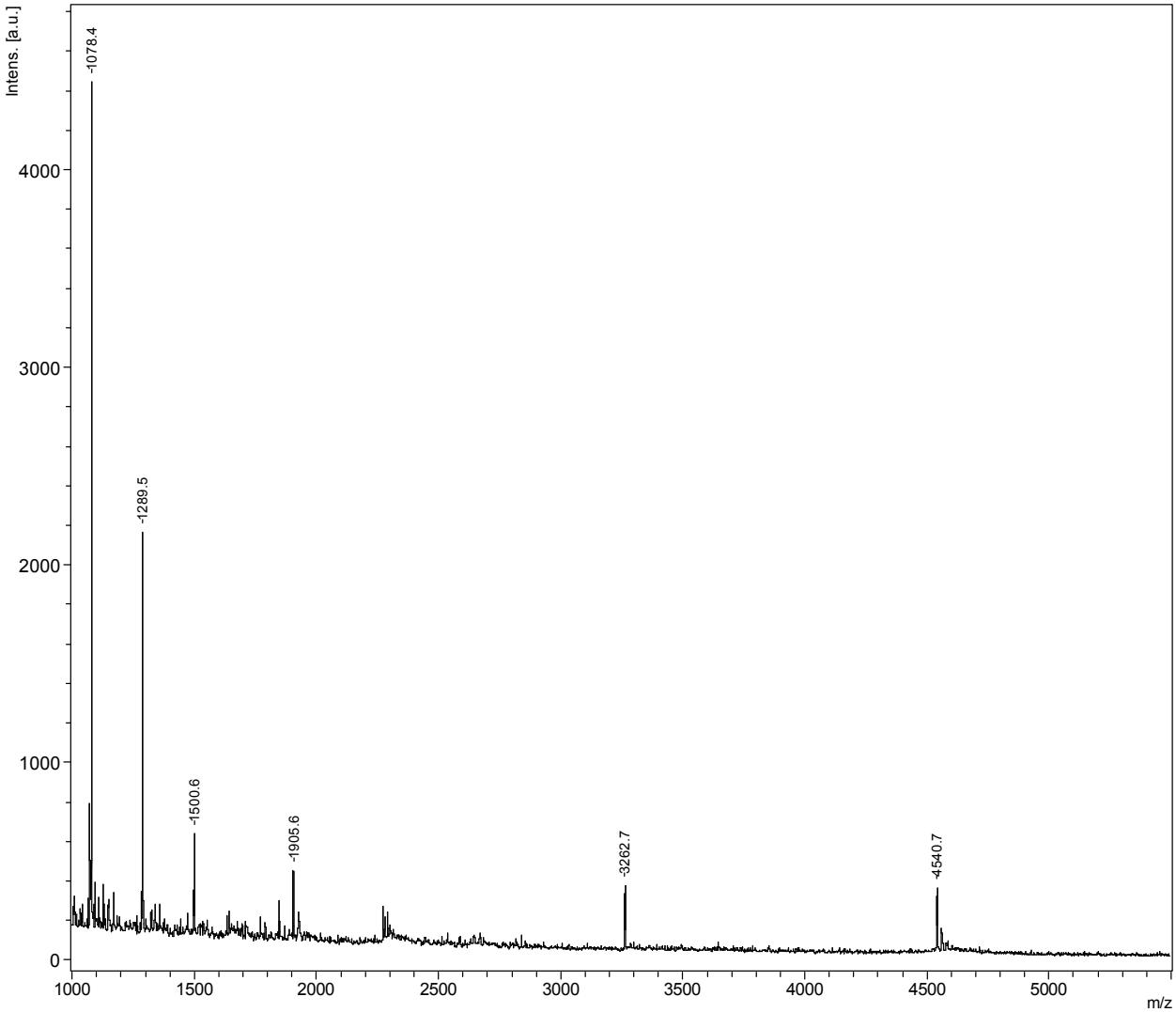

Figure 2.24 MALDI-TOF spectrum of the reaction mixture for α/β-peptide **2.40** after 2 minutes incubation under SGF conditions. Each peak represents a species present in the mixture at that time point. For α/β-peptide **2.40**, calc. $[M+H]^+ = 4542.3$.

2.7 Antagonism of VEGF signaling in cell culture

Human umbilical vein endothelial cells (HUVECs) proliferate when exposed to VEGF.[2] Because the α/β-peptide mimics of **Z-VEGF** bind VEGF at the receptor-recognition surface, we hypothesized that these α/β-peptides would act as VEGF antagonists in cell culture, attenuating the proliferation of HUVECs induced by treatment with exogenous VEGF. The parent three-helix peptide **Z-VEGF** also binds to the receptor binding region of $VEGF_{8-109}$, as revealed in its co-crystal structure; however, in the original report this peptide was not evaluated for its ability to inhibit VEGF signaling.[18] Thus it is unclear how effective Z-domain derived oligomers are at inhibiting VEGF signaling.

To test the hypothesis that the α/β-peptide mimics of **Z-VEGF** described above act as VEGF antagonists, we evaluated the ability **2.37** and **2.40** to attenuate the $VEGF_{165}$-induced proliferation of HUVECs, as determined using a Click-iT EdU proliferation assay, which measures the number of proliferating cells in response to stimulation by exogenous VEGF.[62] This work was performed in collaboration with David G. Belair (Department of Biomedical Engineering, Murphy Laboratory, University of Wisconsin-Madison) and Professor William L. Murphy (Department of Biomedical Engineering, University of Wisconsin-Madison).

Initial experiments evaluated the ability of the α/β-peptide **2.37** to attenuate $VEGF_{165}$-induced proliferation of HUVECs at various concentrations when compared to a positive control peptide, **v114*** (sequence VEPNCDIHVnWEWECFERL-NH_2, where n = norleucine and Cys residues are engaged in a disulfide bond). **v114*** is the Met10→norleucine variant of phage-derived peptide **v114**[15] and displays K_i = 0.060 μM in the competition FP assay for binding to $VEGF_{165}$ [25]; α-peptide **v114*** has previously been shown to antagonize $VEGF_{165}$-stimulated HUVEC proliferation,[25] as has **v114** itself.[15] An initial experiment evaluated an oligomer

concentration range from 6-50 μM, values far above the K_i for binding to $VEGF_{165}$ for both oligomers as determined by FP. α/β-peptide **2.37**, which bound $VEGF_{165}$ with K_i = 0.11 μM in the competition FP assay, was able to attenuate the proliferation of HUVECs down to the levels observed when no exogenous $VEGF_{165}$ was added (Figure 2.25) at most of the **2.37** concentrations tested. α-Peptide **v114*** was able to attenuate HUVEC proliferation in a similar manner. However, at the highest concentration of **v114*** (50 μM), the fraction of proliferating cells was lower than for the "No $VEGF_{165}$" control condition, suggesting that there may be some non-specific effects (e.g., toxicity) for this peptide at this high concentration. Based on these initial experiments, we focused subsequent experiments on evaluating **v114*** at a top concentration of 25 μM (approximately the concentration at which **v114*** was shown to attenuate HUVEC proliferation to "No $VEGF_{165}$" control levels and near the concentration range at which both **114** and **v114*** have previously been evaluated in this type of assay[15, 25]) and Z-domain derived α/β-peptides at a top concentration of 50 μM.

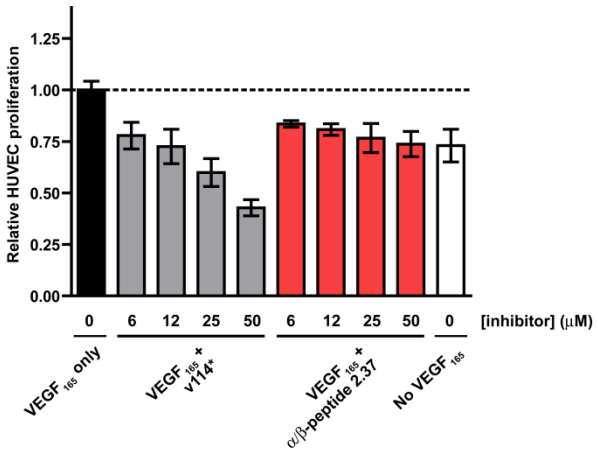

Figure 2.25 Representative experiment showing the relative proliferation of HUVECs treated with 10 ng/mL $VEGF_{165}$ and oligomers at the concentrations indicated. Columns represent mean ± SD from n = 8 replicate wells for each experimental condition on a single plate, as measured via Click-iT EdU assay. Values were normalized to the average value of the "$VEGF_{165}$ only" control (black bar, dotted line).

We next aimed to evaluate the effect of a variety of potential inhibitors on $VEGF_{165}$-induced proliferation of HUVECs. Representative experiments are shown in Figure 2.26. In these experiments, both α/β-peptides **2.37** and **2.40** showed a dose-dependent ability to attenuate proliferation of HUVECs. In contrast, peptide **2.9**, a Z-domain derived α-peptide that did not bind $VEGF_{165}$ in the competition FP assay (Figure 2.12), was not able to block HUVEC proliferation (Figure 2.26A). These results show that the ability of the Z-domain derived peptides to attenuate VEGF signaling is consistent with their ability to bind VEGF by competition FP assay. As an additional negative control, α/β-peptide **3.1**, an α/β-peptide that has a similar sequence to **2.37** but does not bind to $VEGF_{165}$ by competition FP, was not able to block HUVEC proliferation (Figure 2.26B). (The design of **3.1** is described in detail in Chapter 3.) This result further emphasizes that the VEGF antagonism seen for **2.37** and **2.40** arises from their ability to bind to the receptor-binding region of VEGF.

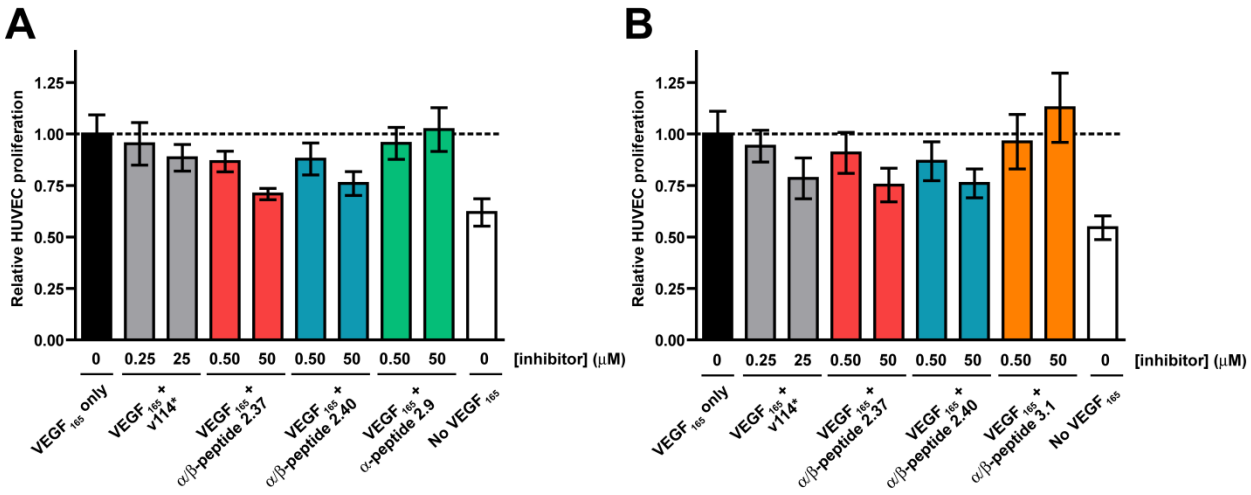

Figure 2.26 Representative experiments showing the relative proliferation of HUVECs treated with 10 ng/mL $VEGF_{165}$ and oligomers at the concentrations indicated. Columns represent mean ± SD from n = 8 replicate wells for each experimental condition and n = 16 replicate wells for "$VEGF_{165}$ only" control as measured via Click-iT EdU assay. Values were normalized to the average value of the "$VEGF_{165}$ only" control (black bar, dotted line).

We performed two preliminary experiments to ask whether α-peptide **2.12** (K_i = 0.40 μM by competition FP) could block $VEGF_{165}$-induced proliferation of HUVECs. HUVECs treated with **2.12** showed a significant and dose-dependent decrease in ratio of proliferating cells (Figure 2.27). However, in one of the two experiments, this compound reduced the ratio of proliferating cells to levels below the "No $VEGF_{165}$" control, suggesting that this peptide might be cytotoxic at this high concentration. There are at least three potential explanations that may account for this interesting result: i) **2.12** is a very effective inhibitor of $VEGF_{165}$ signaling, despite having affinity for VEGF similar to that of **2.37** or **2.40**; ii) **2.12** has some amount of an off-target (VEGF-independent) effect on cell viability or proliferation in addition to its on-target effects; or iii) the amount of **2.12** available for VEGF inhibition is higher than for **2.37** and **2.40**, potentially arising from slight amounts of aggregation or binding to serum proteins for **2.37** and **2.40**, which would reduce the amount of these α/β-peptides free in solution available to antagonize VEGF. Further studies are necessary to determine which of these possibilities, or combination of possibilities, accounts for the results seen here.

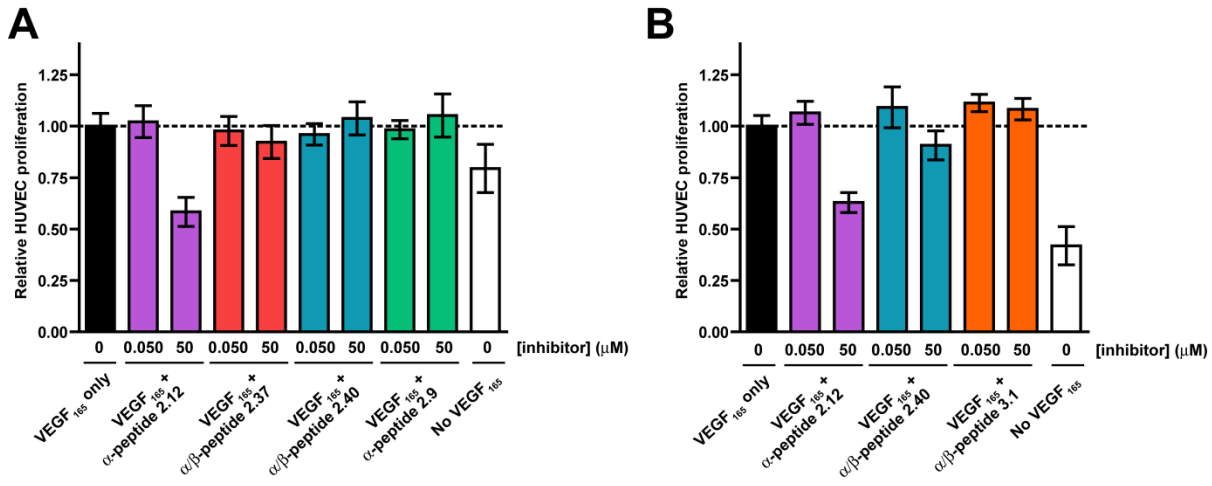

Figure 2.27 Representative experiments showing the relative proliferation of HUVECs treated with 10 ng/mL $VEGF_{165}$ and oligomers at the concentrations indicated. Columns represent mean ± SD from n = 8 replicate wells for each experimental condition and n = 16 replicate wells for "$VEGF_{165}$ only" control as measured via Click-iT EdU assay. Values were normalized to the average value of the "$VEGF_{165}$ only" control (black bar, dotted line).

Figures 2.25-2.27 show the results of experiments that highlight the ability of α/β-peptides derived from **Z-VEGF** to attenuate the signaling of $VEGF_{165}$ in cell culture. However, cell-based experiments are inherently more variable than protein-based experiments such as FP. In order to make meaningful statistical analyses to compare the relative effectiveness of these compounds, we combined the results experimental evaluations of 50 μM **2.9**, **2.37**, or **2.40**, along with 25 μM **v114*** as a positive control VEGF antagonist. An experiment was excluded from this analysis only if it failed to contain a positive control peptide to show the susceptibility of HUVECs in that particular experiment to VEGF inhibition. Together, this analysis combined data from eight independent experiments (Figure 2.28).

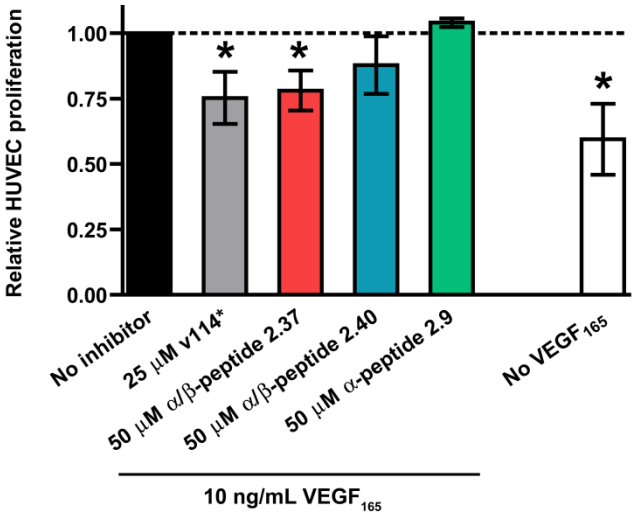

Figure 2.28 Proliferation of HUVECs after treatment with 10 ng/mL $VEGF_{165}$ and the indicated concentration of inhibitor: **v114*** (positive control, $n = 6$), α/β-peptide **2.37** ($n = 7$), α/β-peptide **2/40** ($n = 6$), or α-peptide **2.9** ($n = 3$). Each bar represents the mean ± SD collected from eight independent experiments. Note that each compound was not tested in every experiment, so $n = 8$ only for control conditions with no inhibitor. Data from each experiment were normalized to the respective "No inhibitor" control condition treated with $VEGF_{165}$ only (black bar, dotted line). White bar indicates relative levels of proliferation when no exogenous $VEGF_{165}$ is added ($n = 8$). Statistical differences are denoted for p-value ≤ 0.01 (*) relative to "No inhibitor" ($VEGF_{165}$ only) control using a two-tailed ratio t-test.

The aggregate analysis showed that **2.37** at 50 μM attenuated $VEGF_{165}$-induced HUVEC proliferation (Figure 2.28). The positive control α-peptide **v114*** at 25 μM attenuated

proliferation to about the same extent. Although we qualitatively observed that **2.40** seemed to attenuate $VEGF_{165}$-induced proliferation of HUVECs in many of the individual experiments (Figure 2.26), the response was not statistically different from the "$VEGF_{165}$ only" control condition when all the data from the independent experiments were combined. The apparently reduced activity of **2.40** relative to **2.37** is consistent with the lower affinity for $VEGF_{165}$ of **2.40** relative to **2.37** in the competition FP assay. The negative control peptide **2.9**, which did not bind to $VEGF_{165}$ according to the FP assay, showed no antagonism of proliferation at 50 μM.

To further evaluate the mechanism by which **2.37** and **2.40** reduce HUVEC proliferation, we evaluated their effect on cell viability under the experimental conditions used in the proliferation assays described above using a LIVE/DEAD viability assay. Neither **2.37** nor **2.40** reduced HUVEC viability at 50 μM under the assay conditions, which suggests that the decline in $VEGF_{165}$-stimulated proliferation was not due to non-specific cytotoxicity (Figure 2.29A). We also probed the mechanism of action of **2.37** by attempting to inhibit HUVEC proliferation that was induced by 10 ng/mL FGF-2 rather than $VEGF_{165}$;[15, 63] however, no attenuation was observed under these conditions (Figure 2.29B). Thus, the antagonistic properties of **2.37** are specific for proliferation induced by $VEGF_{165}$. Overall, the data presented in this section strongly suggest that α/β-peptides derived from **Z-VEGF** can function as specific inhibitors of $VEGF_{165}$-mediated signal transduction in the complex environment provided by cell-culture medium.

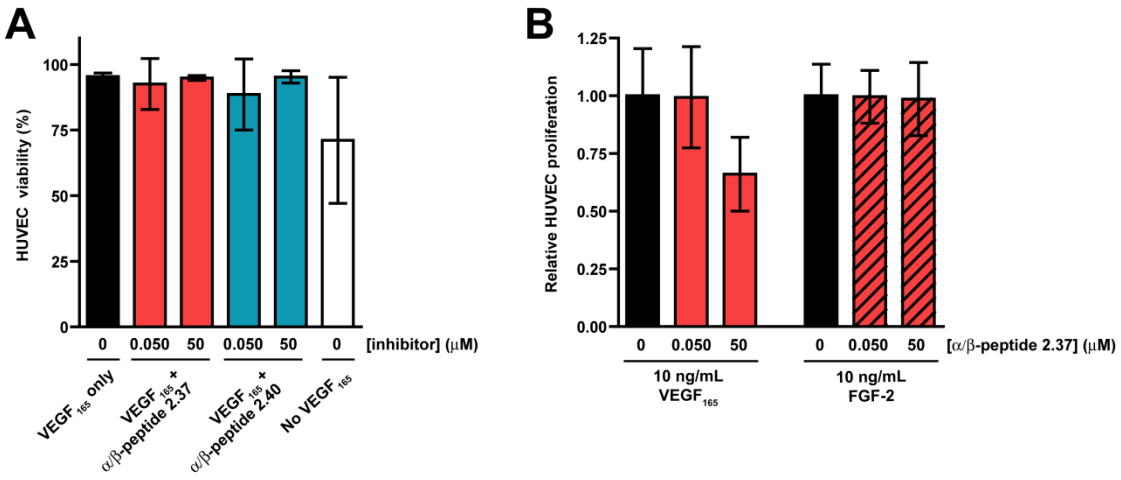

Figure 2.29 α/β-Peptides derived from **Z-VEGF** attenuate $VEGF_{165}$-mediated HUVEC proliferation in a VEGF-specific manner. (A) Representative experiment showing the viability of HUVECs treated with 10 ng/mL $VEGF_{165}$ and the indicated concentration of inhibitor, as determined by LIVE/DEAD viability assay (Life Technologies). Columns represent the mean ± SD from n = 6 replicate wells for each condition. (B) Representative experiment showing the relative proliferation of HUVECs treated with 10 ng/mL $VEGF_{165}$ or 10 ng/mL FGF-2 and the indicated concentration of **2.37**, as determined by Click-iT EdU assay. Columns represent the mean ± SD from n = 8 replicate wells for each condition. Data normalized to the average value for the "0 μM α/β-peptide **2.37**" control (black bars) for the respective growth factor.

2.8 Conclusions

One of the primary goals of α/β-peptide mimicry of protein-binding α-peptides is to make a sufficient number of α→β-residue replacements to retain high affinity for the target protein while providing a large increase in protease stability. Most previous efforts to mimic protein-modulating peptides using α/β-peptides have relied on several different strategies: synthesizing libraries surveying α→β substitutions in repeating patterns,[19-21, 23] "β-scanning" an entire sequence followed by combining the individual α→β substitutions that were best tolerated,[25] or rationally designing substitutions based on extensive structure-activity relationships known for the parent peptide.[24] The three-helix bundle Z-domain scaffold[28-30, 32] appeared to be a promising target for α/β-peptide mimicry due to its high α-helix content, but its large size, tertiary structure, and irregularly structured loop region provided challenges that we believed required a different approach successful for α/β-peptide mimicry. Indeed, several initial

attempts to rationally design α/β-peptides by incorporating multiple α→β replacements simultaneously were unsuccessful (e.g., α/β-peptides **2.6** and **2.19**).

In this chapter, I have described a strategy that complements the previous approaches for α/β-peptide design. Rather than survey all possible individual α→β substitutions or registers of regular substitution patterns, we instead relied on an iterative design approach. Inspired by previous efforts truncating other peptides derived from the Z-domain,[33-35] we first established a minimized analogue of **Z-VEGF** that retained binding for $VEGF_{165}$, as determined by competition FP assay. In contrast to previous attempts to truncate three-helix Z-domain-derived peptides,[33, 35] we unexpectedly found that removal of residues 1-6 from **Z-VEGF** led to a large loss in VEGF affinity. We found that the incorporation of a disulfide bond at the termini of the two helices was essential, as no analogue lacking a disulfide showed activity, even in the presence of structure-inducing non-natural residues (**2.42**).

To design an α/β-peptide mimic of the minimized two-helix scaffold, we began with a relatively small set of replacements rationally designed from inspection of crystallographic information, choosing positions that did not appear to make contact with VEGF (important for peptide-VEGF interaction) or to be involved in interhelical interactions (important for conformational stability). Based on these criteria, we first probed a small number of positions for non-natural residue substitution and found that some tolerated either cyclic β-residues or Aib residues, as assessed by evaluating the affinity for VEGF. Next, we iteratively added small numbers of non-natural residue substitutions and evaluated the resulting α/β-peptides' affinity for VEGF, in turn using this information to guide the next round of designs. In helix 1, we used the more conservative Aib residue substitution to first probe specific positions for tolerance to non-natural residue substitution, and then examined backbone-modified cyclic β-residues at those

positions. Initial attempts at α→β substitution near the central loop (Pro21 to Asn24) led to loss of affinity for $VEGF_{165}$ in **2.6**, **2.20**, **2.22,** and **2.24**, and we therefore employed the helix-promoting α-residue Aib at positions 17 and 30.[44, 53] Aib residues can protect peptides from proteolysis, but our group has observed that cyclic β-residues provide superior protection relative to Aib residues,[24] and so we employed Aib residues only in regions of the scaffold peptide that did not seem to tolerate cyclic β-residues (i.e., only near the central loop).

A protease digestion experiment was used at an intermediate stage of α/β-peptide design to identify regions that were particularly susceptible to degradation (which appeared to be regions with high proteinogenic α-residue content) for potential further modification with residues that discourage proteolysis. Protection of one of these sites (the Gln26-Gln27 amide bond) in α/β-peptide **2.40** did indeed lead to a significant decrease in susceptibility to both proteinase K degradation (Figure 2.22) and degradation in simulated gastric fluid (Figure 2.23). Overall, the α/β-peptides **2.37** and **2.40** showed greatly reduced susceptibility to proteinase K degradation relative to their parent α-peptide (**2.12**) and the parent three-helix peptide **Z-VEGF**. Thus, the incorporation of non-natural β-amino acid and Aib residues is able to significantly increase the stability of the helix-loop-helix scaffold over the parent **Z-VEGF**, despite the fact that the former has considerably fewer residues.

The co-crystal structure of **2.37** in complex with $VEGF_{8\text{-}109}$ shows that the helix-loop-helix α/β-peptide design developed here is able to accurately mimic the helix 1-helix 2 segment of **Z-VEGF** in its conformation, binding site, and binding geometry when complexed with VEGF. This result, together with the competition FP assay results showing that **2.37** and **2.40** match or exceed the affinity of **Z-VEGF** for $VEGF_{165}$, show that these α/β-peptides are presenting a protein-binding face which accurately mimics the protein-binding face presented by

Z-VEGF. Because the Z-domain is used as a scaffold for developing a variety of derivatives that bind selectively to different protein targets of biomedical interest,[27, 28] it is possible that the success of α/β-peptide mimicry of **Z-VEGF** by **2.37** may be directly translated to other Z-domain derivatives to yield α/β-peptides that selectively target other therapeutically interesting proteins, as well as other VEGF-binding Z-domain derivatives that bind VEGF with higher affinity. This possibility is explored in detail in Chapter 3.

Unlike in many prior α/β-peptide design efforts, the strategy of α/β-peptide mimicry outlined in this chapter is not limited to a regular pattern of α→β substitutions and does not rely on first making α→β^3 substitutions before incorporating cyclic β-residues.[20, 22] Although here we have mimicked helical regions in a helix-loop-helix tertiary structure, in principle this strategy can be applied to other, less regular tertiary structures to determine productive placement of β-amino acid residues in different parent α-peptides. Ultimately, this strategy for α/β-peptide design may be useful for mimicry of other small, tertiary structures utilized as scaffolds for deriving peptides that selectively bind to target protein surfaces.[26, 27, 64]

2.9 Future directions

Many of the two-helix α/β-peptides reported here bind to $VEGF_{165}$ with affinity similar to that of the parent three-helix **Z-VEGF**, indicating that they are good mimics of this parent peptide in spite of the considerably shorter length and unnatural backbone. However, the affinity of these compounds (~0.10-0.40 μM by competition FP assay) may not be high enough for potent inhibition of VEGF signaling in animal models for wet macular degeneration or cancer, two of the target therapeutic applications of VEGF inhibitors. Thus, one important future direction will be to increase the affinity of these two-helix α/β-peptide analogues for VEGF. One possible route to this goal may be to incorporate amino acid residue substitutions (either non-

natural or natural) on the protein-binding face. These substitutions could be rationally designed by inspection of the **2.37**+$VEGF_{8-109}$ or **Z-VEGF**+$VEGF_{8-109}$ co-crystal structures or determined by molecular modeling/computational efforts. Alternatively, it is possible that one can apply the α/β-peptide scaffold described here to mimic new three-helix Z-domain derivatives that may be developed by affinity maturation to bind VEGF with higher affinity (see Chapter 3 for a more detailed explanation of this affinity maturation strategy).[36, 65]

A preliminary experiment in simulated gastric fluid (SGF) suggested that the α/β-peptide **2.40** is much less susceptible to degradation under these conditions than the parent α-peptide **2.12**. However, the rate of degradation in the SGF was still relatively rapid and likely precludes administering this compound orally. It may be possible to optimize the two-helix α/β-peptide scaffold even further for stability in such a medium. If this goal were achieved, these stabilized two-helix α/β-peptides may serve as the starting point for the design of orally available α/β-peptides, although steps will likely need to be taken to increase absorption into the blood stream (e.g., formulation with oral absorption enhancers to facilitate transport across the intestinal membrane).[61, 66]

2.10 Experimental methods

2.10.1 General

Fmoc-protected α-amino acids with compatible side chain protecting groups and benzotriazole-1-yl-oxy-tris-pyrrolidino-phosphonium hexfluorophosphate (PyBOP) were purchased from Chem-Impex International and Novabiochem. Fmoc-protected β^3-amino acids with compatible side chain protecting groups were purchased from PepTech Corporation and Chem-Impex International. Fmoc-ACPC-OH was purchased from Chem-Impex International

(15073). Fmoc-sAPC(OtBu)-OH was synthesized as previously described.[22] Fmoc-APC(Boc)-OH was synthesized as previously described.[67]

2.10.2 Peptide synthesis and purification

α-Peptides were prepared by solid-phase peptide synthesis using NovaPEG Rink Amide resin (Novabiochem, 855047) either on a Symphony automated peptide synthesizer (Protein Technologies) as previously reported[68] or using microwave-assisted solid-phase methods, as described below. **Z-VEGF** was synthesized on a Symphony automated peptide synthesizer, double-coupling each amino acid, as previously described.[18] α/β-peptides were synthesized on NovaPEG Rink Amide resin using microwave-assisted solid-phase conditions[69] based on Fmoc protection of the main chain amine. Coupling reactions were carried out by treating the resin with a solution of protected amino acid (4 eq.), activated with PyBOP (4 eq.) and 0.1 M 1-hydroxybenzotriazole (HOBt) in the presence of *N,N*-diisopropylethylamine (DIEA) (8 eq.) in 1-methyl-2-pyrrolidone (NMP). Coupling reactions were irradiated by microwave to 70 °C for 6 minutes (2 minute ramp, 4 minutes hold) with a 5 minute cooldown (for α-residues) or for 14 minutes (2 minute ramp, 12 minute hold) with a 5 minute cooldown (for Aib residues, residues after Aib residues, and cyclic β-residues). Coupling reactions that were anticipated to be difficult (e.g., Arg or β-branched residues after Aib) could be coupled using the extended reaction time mentioned above or double-coupled to attempt to increase yield. Deprotection of the Fmoc protecting group was carried out using a solution of 5% piperazine, 0.1 M HOBt in *N,N*-dimethylformamide (DMF), irradiated by microwave to 80 °C for 4 minutes (2 minute ramp, 2 minute hold). All oligomers have a free amine at their N-terminus, except for **2.1** and the BODIPY-labeled **BODIPY-v114*$_{\Delta NT}$**, which was used as the tracer peptide for FP assays. Peptide **2.1** was labeled at its N-terminus by addition of 4 equivalents of 6-carboxyflourescein

(AnaSpec, AS-81004) under the above coupling conditions at room temperature overnight, protected from light. **BODIPY-v114*$_{\Delta NT}$** was synthesized in the same manner as the previously reported tracer peptide **BODIPY-v114$_{\Delta NT}$**.[39] After the completion of the synthesis on resin, α- and α/β-peptides containing no cysteine or methionine residues were cleaved from the resin using a solution of 95% trifluoroacetic acid (TFA), 2.5% H_2O, and 2.5% triisopropylsilane (TIS). α- and α/β-peptides containing cysteine or methionine residues were cleaved from the resin using a solution of 94% TFA, 2.5% H_2O, 2.5% 1,2-ethanedithiol, and 1% TIS. Excess TFA was removed under a stream of nitrogen, and the crude peptides were precipitated by the addition of cold diethyl ether. For α- and α/β-peptides without a disulfide bond, solutions of crude peptide were purified by reverse-phase HPLC. For α- and α/β-peptides containing a disulfide bond, crude ether-precipitated peptides were dissolved in DMSO (~10 mL for 50 μmol synthesis), and ammonium hydroxide (NH_4OH) was added to make the solution basic (approximately 25 drops for 50 μmol synthesis). These DMSO solutions were exposed to air and the oligomers allowed to oxidize over the course of 4-7 days, followed by purification by HPLC. Alternatively, disulfide-containing peptides could be purified as the bis-thiol immediately after cleavage (in the presence of reducing agent TCEP), subjected to oxidation using the above conditions, followed by repurification by HPLC. Final purity was assessed by analytical HPLC and identity confirmed by MALDI-TOF-MS ("Peptide characterization" section below).

2.10.3 Protein expression and purification

$VEGF_{165}$ used for FP assays was expressed and purified as previously reported.[39]

The gene encoding for the receptor-binding domain of human VEGF, residues 8-109, was sub-cloned from a pET-3d vector containing the gene for $VEGF_{165}$, residues 2-165. (Forward primer: 5'-GTTCCATGGGGCAGAATCATCAC-3' Reverse primer: 5'-

GGCGGATCCTCATCATCAATCTTTCTTT-3'). Sanger DNA sequencing confirmed the presence of the $VEGF_{8-109}$ gene in a pET-3d vector. The pET-3d vector containing the $VEGF_{8-109}$ gene was transformed into *Escherichia coli* BL21(DE3)-RIPL cells (Stratagene, 230280) using heat-shock transformation method. Cells were grown at 37°C in Luria-Bertani (LB) media supplemented with 50 μg/mL carbenicillin and 25 μg/mL chloramphenicol. $VEGF_{8-109}$ expression was induced with 0.4 mM isopropyl β-D-1-thiogalactopyranoside (IPTG) at an OD_{600} of approximately 0.6, and cells were grown for an additional 3 hours. The cells were pelleted by centrifugation at 3000g for 30 minutes at 4°C, washed with Tris-buffered saline (20 mM Tris-HCl, 150 mM NaCl, pH 7.5), and pelleted by centrifugation at 3000g for 30 minutes at 4°C.

The protocol for the isolation and refolding of $VEGF_{8-109}$ was adapted from Peterson et al.[39] Isolated inclusion bodies were solubilized in 27 mL dissolving buffer (20 mM Tris-HCl, 7.5 M Urea, 20 mM dithiothreitol [DTT], pH 7.5) overnight at 4°C. Solubilized inclusion bodies were clarified by centrifugation. Unfolded and reduced $VEGF_{8-109}$ was diluted in dissolving buffer to 0.75 mg/mL and dialyzed extensively against refolding buffer (20 mM Tris-HCl, 400 mM NaCl, 1 mM cysteine, pH 8.4) at 4°C. Purity of the $VEGF_{8-109}$ homodimer was confirmed by SDS-PAGE and analytical reverse-phase HPLC, with a final yield of ~48 mg/L for a three liter expression. A portion of the refolded $VEGF_{8-109}$ dimer was dialyzed against phosphate-buffered saline (PBS) for direct-binding fluorescence polarization assays (FP) to validate activity (protocol given below). The tracer in this assay has a dissociation constant (K_d) of 21 nM for $VEGF_{165}$. The K_d determined for the refolded $VEGF_{8-109}$ dimer was 14 nM. These data suggest that $VEGF_{8-109}$ is correctly folded and is able to bind the tracer peptide with essentially the same affinity as $VEGF_{165}$. For co-crystallization screens, $VEGF_{8-109}$ was dialyzed against crystallization buffer (20 mM Tris-HCl, 150 mM NaCl, pH 7.5) and concentrated to ~500 μM, as

determined by UV absorbance using an extinction coefficient of 12920 M^{-1} cm^{-1} for the $VEGF_{8-109}$ dimer, as determined by ExPASy Server.[70]

2.10.4 VEGF fluorescence polarization assays

Inhibitors of the $VEGF_{165}$-VEGFR interaction were evaluated using our $VEGF_{165}$ direct-binding and competition fluorescence polarization (FP) assays, as previously described.[39] The tracer used in the assays reported here was the Met→norleucine variant of the previously reported tracer (peptide **BODIPY-v114*$_{\Delta NT}$**, sequence ((BODIPY^{TMR})-X-CDIHVnWEWECFERL-NH_2, X = [2-(2-amino-ethoxy)-ethoxy]acetic acid, n = norleucine, where cysteines are linked in intramolecular disulfide; K_d = 21 nM). To account for slight variations in amount of active protein resulting from each expression, the K_d for **BODIPY-v114*$_{\Delta NT}$** was measured for each $VEGF_{165}$ expression stock solution by direct-binding FP assay, and the resulting K_d value was used for the determination of inhibitor dissociation constant (K_i) values derived from competition FP assays using that stock solution. Figure 2.30 shows representative direct-binding FP assays for the binding of **BODIPY-v114*$_{\Delta NT}$** and **2.1** to $VEGF_{165}$.

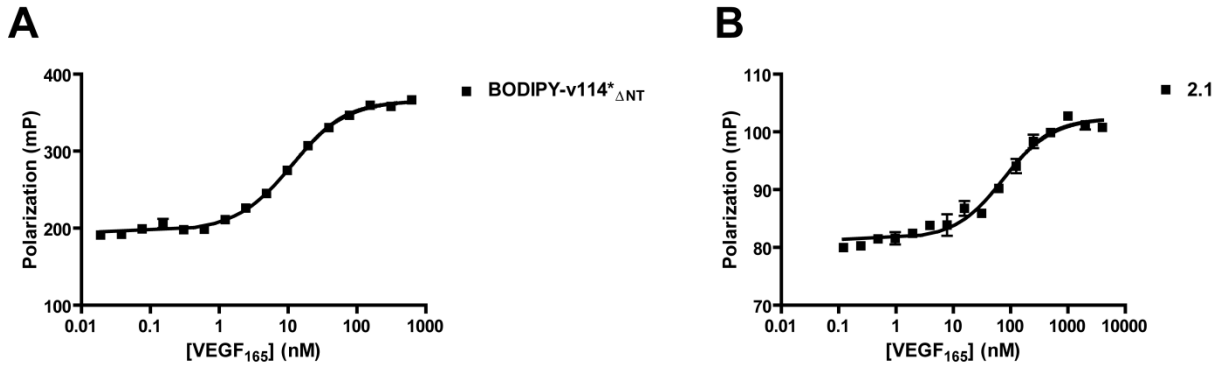

Figure 2.30 Representative $VEGF_{165}$ direct-binding FP assays. (A) Direct-binding of the tracer peptide **BODIPY-v114*** $_{\Delta NT}$ to $VEGF_{165}$. (B) Direct-binding of **2.1** to $VEGF_{165}$. Each data point represents the mean ± SEM for duplicate wells on the plate.

For competition FP assays, DMSO stock solutions of α- and α/β-peptide inhibitors were prepared and concentration determined by UV absorbance at 280 nm. Extinction coefficients for α- and α/β-peptides were calculated based on the number of tryptophan residues (ε_{280} = 5690 M^{-1} cm^{-1}), tyrosine residues (ε_{280} = 1280 M^{-1} cm^{-1}), and cystines (ε_{280} = 120 M^{-1} cm^{-1}) in each primary sequence.[71] Competition FP assays were performed by adding 2 μL of serial dilutions of inhibitor in DMSO to 48 μL of solution containing **BODIPY-v114*$_{\Delta NT}$** (final concentration = 10 nM) and $VEGF_{165}$ (final concentration = 40 nM) in FP buffer (50 mM NaCl, 16.2 mM Na_2HPO_4, 3.8 mM KH_2PO_4, 0.15 mM NaN_3, 0.15 mM EDTA, 0.5 mg/mL Pluoronic-F68, pH 7.5) in 384-well, black polystyrene plates (Costar). Plates were incubated at room temperature for more than 3 hours (usually 5-7 hours, although typically plates can be read after more time with little change in signal), then fluorescence polarization was read on either an Envision 2100 or a BioTek Synergy 2 microplate reader. Each condition was run in duplicate in each assay. Inhibition constants (K_i) were determined from FP data using methods described for a competitive binding model with GraphPad Prism 4.0,[39, 72] using Equation (1), described below:

(1) Y = BOTTOM+(TOP-BOTTOM)*((2*SQRT(a^2-3b)*COS(d/3)-a)/(3*KD1+2*SQRT(a^2-3b)*COS(d/3)-a))/e

Where:
a = KD1+KD2+LST+10^X-RT
b = KD1*(10^X-RT)+KD2*(LST-RT)+KD1*KD2
c = -KD1*KD2*RT
d = ARCCOS((-2*a^3+9*a*b-27*c)/(2*SQRT((a^2-3*b)^3)))
e = (LST+KD1+RT-sqrt[(LST+KD1+RT)^2-4*LST*RT])/(2*LST)

Y = mP reading
BOTTOM = mP of free tracer
TOP = mP of bound tracer
X = log concentration of inhibitor
KD1 = K_d for tracer binding to receptor (determined by direct-binding FP)
KD2 = K_i for inhibitor binding to receptor
LST = concentration of tracer
RT = concentration of receptor

Representative $VEGF_{165}$ competition FP assays for each of the compounds reported are shown below in Figure 2.31 and Table 2.1. Each data point represents the mean ± SEM of duplicate wells on the plate. Each panel in Figure 2.32 represents an independent experiment, and some compounds are tested multiple times in these representative experiments. K_i values for $VEGF_{165}$ competition FP assays typically vary ~2-fold between independent experiments and so any values within an ~4-fold range are considered experimentally indistinguishable. For example, for α/β-peptide **2.37**, fitted K_i values for three independent experiments range from 0.065 to 0.11 μM. This small variation highlights the variability we typically see in this FP assay with **2.37** or other active antagonists for fitted equilibrium constants between independent experiments. A complete table of K_i values calculated for each compound reported in Figure 2.31 is shown in Table 2.1. For weak-binding compounds in which the change in mP over the tested concentration range was too small to confidently fit the data to a competitive binding model (e.g., α/β-peptide **2.19,** Figure 2.31J), a lower bound for the K_i value is reported as the top concentration tested rounded to 1 significant figure. Some compounds showed an increase in mP values at higher concentrations (e.g., α/β-peptides **2.34** and **2.35**, Figure 2.31), which our group has previously observed with relatively hydrophobic peptides in these types of experiments.[73] We attribute this increase in mP at high peptide concentration to either association of the inhibitor with tracer or light scattering effects due to aggregation. In some of these cases, this effect precluded reasonable fitting of the data, so the data in these experiments were fit with a shared bottom value for all compounds in the panel, which was fit using all data on the plate. α-Peptide **v114***, sequence = VEPNCDIHVnWEWECFERL-NH_2, where Cys residues form an intramolecular disulfide bond and n = norleucine, reported K_i = 0.060 μM,[25] is included as a positive control in several experiments.

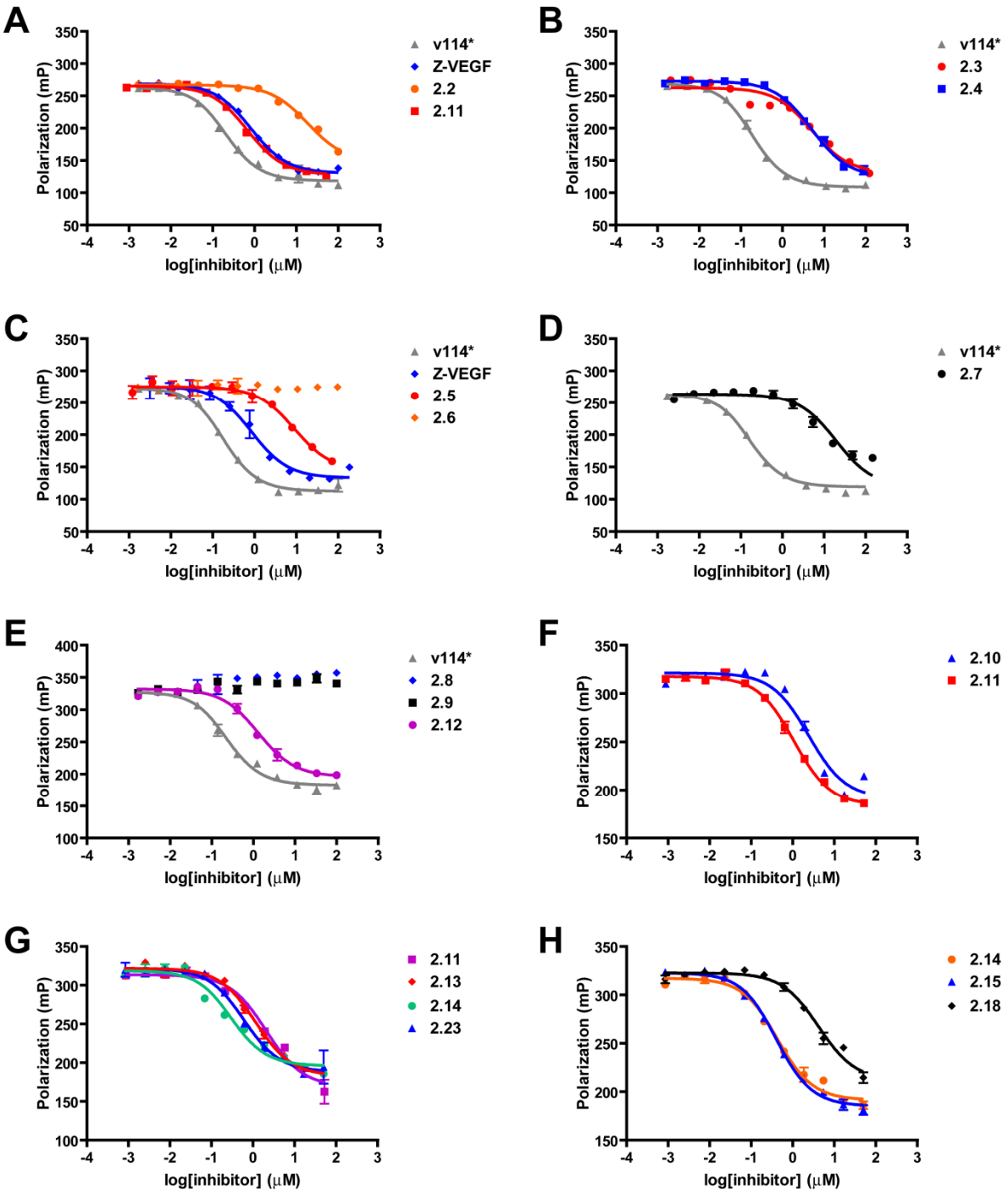

Figure 2.31 (A-H) Representative $VEGF_{165}$ competition FP assays for compounds reported in this chapter.

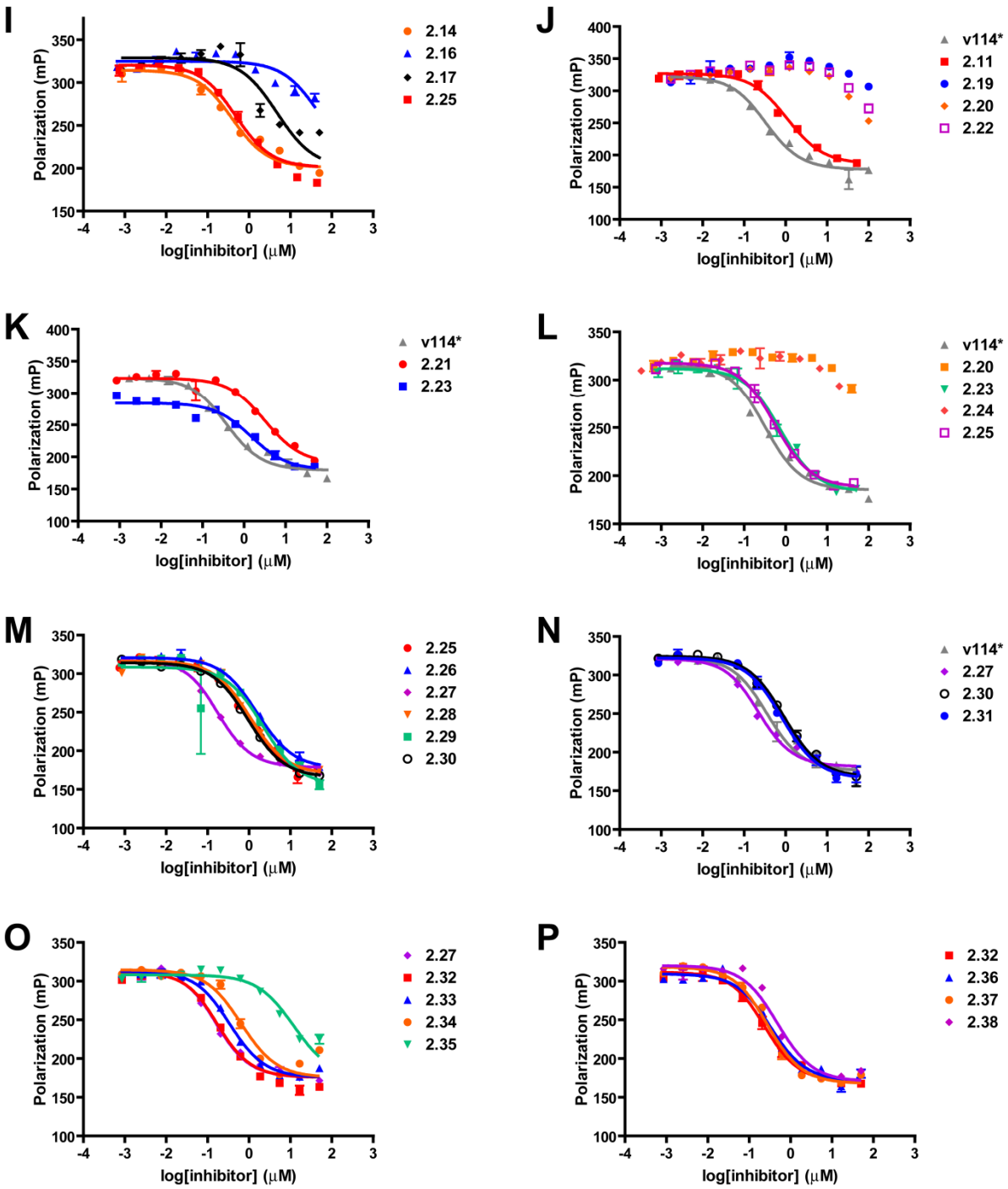

Figure 2.31 (I-P) Representative $VEGF_{165}$ competition FP assays for compounds reported in this chapter.

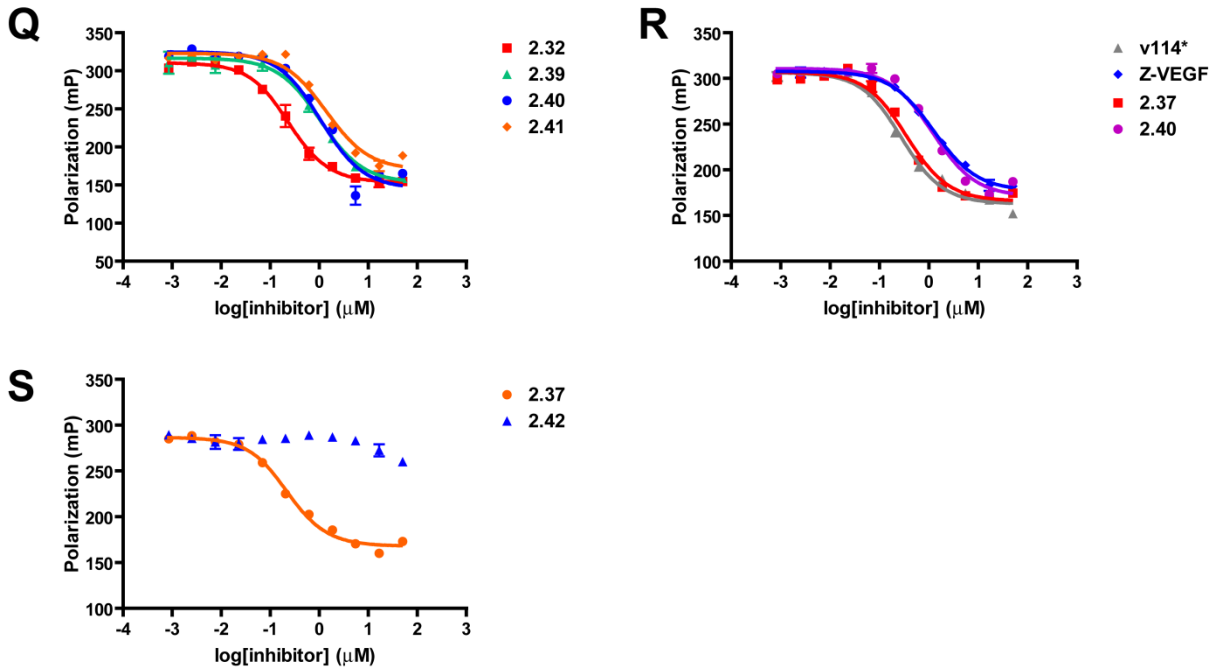

Figure 2.31 (Q-S) Representative $VEGF_{165}$ competition FP assays for compounds reported in this chapter.

		K_i (μM) (Panel from Figure 2.31 shown in parentheses)
Peptide	**v114***	0.050 (A), 0.049 (B), 0.046 (C), 0.041 (D), 0.062 (E), 0.096 (J), 0.11 (K), 0.093 (L), 0.10 (N), 0.086 (R)
	Z-VEGF	0.24 (A), 0.25 (C), 0.41 (R)
	2.2	5.7 (A)
	2.3	1.5 (B)
	2.4	1.5 (B)
	2.5	2.7 (C)
	2.6	>100 (C)
	2.7	5.8 (D)
	2.8	>100 (E)
	2.9	>100 (E)
	2.10	0.75 (F)
	2.11	0.20 (A), 0.33 (F), 0.64 (G), 0.33 (J)
	2.12	0.40 (E)
	2.13	0.35 (G)
	2.14	0.085 (G), 0.13 (H), 0.11 (I)
	2.15	0.12 (H)
	2.16	>40 (I)
	2.17	1.5 (I)
	2.18	1.3 (H)
	2.19	>100 (J)
	2.20	>100 (J), >40 (L)
	2.21	0.99 (K)
	2.22	>100 (J)
	2.23	0.18 (G), 0.45 (K), 0.23 (L)
	2.24	>20 (L)
	2.25	0.14 (I), 0.17 (L), 0.29 (M)
	2.26	0.48 (M)
	2.27	0.048 (M), 0.061 (N), 0.044 (O)
	2.28	0.33 (M)
	2.29	0.67 (M)
	2.30	0.29 (M), 0.28 (N)
	2.31	0.25 (N)
	2.32	0.046 (O), 0.072 (P), 0.070 (Q)
	2.33	0.099 (O)
	2.34	0.19 (O)
	2.35	3.8 (O)
	2.36	0.10 (P)
	2.37	0.085 (P), 0.11 (R), 0.065 (S)
	2.38	0.15 (P)
	2.39	0.34 (Q)
	2.40	0.35 (Q), 0.39 (R)
	2.41	0.46 (Q)
	2.42	>50 (S)

Table 2.1 K_i values of each oligomer from the $VEGF_{165}$ competition FP assays depicted in Figure 2.31. Letters in parentheses indicate from which panel the value is derived.

2.10.5 Circular dichroism spectroscopy

Circular dichroism measurements were performed on an Aviv Model 420 circular dichroism spectrometer. Solutions of α- and α/β-peptides were prepared in PBS, pH 7.5. Spectra were collected at 20 °C in a 0.1 cm quartz cell with a wavelength step size of 1 nm and a 10 second averaging time. Spectra were normalized to mean residue ellipticity, [θ] (deg cm^2 $dmol^{-1}$ res^{-1}) using the exact concentration determined by UV absorbance at 280 nm[71] to account for slight variations in concentration between solutions, using the Equation (2),[74] described below:

(2) $[\theta] = \theta/(l * c * \#res)$

Where:
θ = blank-corrected ellipticity value from CD spectrometer (in mdeg)
l = pathlength (in mm)
c = concentration of peptide (in M)
#res = the number of residues in the peptide

The mean residue ellipticity values ([θ]) obtained were then multiplied by 10^{-3} for plotting in the graphs shown in this chapter.

2.10.6 Crystallization

Crystallization screens were carried out by pre-mixing a solution of $VEGF_{8-109}$ dimer in crystallization buffer (20 mM Tris-HCl, 150 mM NaCl, pH 7.5) with a stock solution of **2.37** in water ($VEGF_{8-109}$ final concentration = 200 μM, **2.37** final concentration = 640 μM). After 40 minutes at room temperature, the protein+α/β-peptide solution was briefly centrifuged and then drops of 1 μL of the protein+α/β-peptide mixture with 1 μL of each precipitant condition from the Hampton Index (Hampton Research, HR2-144) were suspended over a 300 μL reservoir in 48-well crystallization trays. The final conditions were droplets of 1 μL of 110 μM $VEGF_{8-109}$ and 340 μM **2.37** (pre-mixed for 3 hours) with 1 μL of 0.1 M magnesium formate dihydrate, 15% PEG3350, 30% glycerol over 300 μL reservoir solution in a 48 well crystallization tray. The

addition of 30% glycerol in the optimized conditions was desired as a cryoprotectant. Crystals grew over the course of several days.

2.10.7 X-ray data collection and structure determination

Crystals were vitrified directly in liquid nitrogen on a nylon loop. Diffraction data were collected at the Life Sciences Collaborative Access Team (LS-CAT) beamline 21-ID-F at the Advanced Photon Source (APS), Argonne National Laboratory. 180 1º oscillation images with 8 second exposure time were collected. Data were indexed, integrated, scaled, and merged with the programs *XDS* and *XSCALE*.[75] Data were truncated at 3.1 Å resolution due to extreme anisotropy (Figure 2.32). A molecular replacement solution was found with the program *Phaser* using poly-alanine backbones of the $VEGF_{8-109}$ dimer (coordinates extracted from PDB ID: 3S1K) and the two-helix analogue of **Z-IgG** (PDB ID: 1ZDD) as search models (*TFZ*=9.5, *LLG*=856).[76] Anisotropic scaling and refinement were carried out in the program *phenix.refine*[77, 78] in combination with manual real-space model building and refinement in the program *Coot* (Crystallographic Object-Oriented Toolkit).[79] The initial refinement strategy comprised a combination of rigid-body refinement[80] and simulated annealing of torsion angles; intermediate rounds of refinement comprised coordinate, group atomic displacement parameter (ADP), and TLS refinement; final rounds of refinement comprised coordinate, group ADP, and TLS refinement with optimized ADP and coordinate weights. A composite omit map generated with the function *phenix.composite_omit_map* and simulated torsion annealing indicated weak electron density around each **2.37** disulfide bond, presumably due to radiation damage. A composite omit map generated from data collected in the first 120 degrees showed increased density around each **2.37** disulfide bond relative to the final model. Due to this radiation damage, sulfur occupancies were also refined in each **2.37** disulfide bond during the final round

of refinement. 18 TLS groups were assigned with the function *phenix.find_tls_groups* in *phenix.refine*. Residues 1-7 of each **2.37** molecule (chains C and D); residues 8-12, 108-109 for VEGF chain A; and residues 8-13, 107-109 of VEGF chain B were not modeled due to lack of electron density. For 34 residues within the structure (primarily within the loop regions and termini of $VEGF_{8\text{-}109}$ and the last two turns of the α/β-peptide C-terminal helix), side chains were not modeled in due to a lack of supporting electron density. NCS restraints were applied to torsion angles; secondary structure restraints and Ramachandran restraints were also applied to the model.[81] Standard peptide bond geometries were used to define custom restraints for links between α and β-amino acid residues. In addition to these custom link restraints the slack parameter feature in *phenix.refine* was used to define hydrogen bond restraints of 2.9 ± 0.2 Å corresponding to helical secondary structure in **2.37**. Figures depicting high-resolution structures were prepared using PyMOL molecular visualization software.

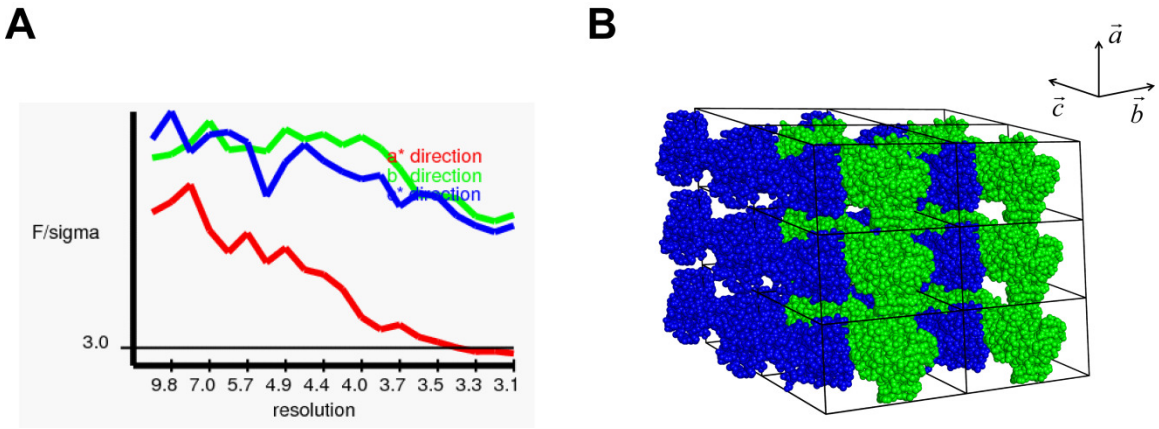

Figure 2.32 X-ray co-crystal structure of **2.37**+$VEGF_{8\text{-}109}$. (A) A graph of $|F_{obs}|/\sigma(|F_{obs}|)$ as a function of resolution, generated by the UCLA-MBI Diffraction Anisotropy Server (http://services.mbi.ucla.edu/anisoscale/). Magnitudes of $|F_{obs}|/\sigma(|F_{obs}|)$ corresponding to reciprocal axes a*, b*, and c* are indicated in red, green, and blue, respectively. (B) A block of 3x2x2 unit cells that illustrate the crystal packing of $VEGF_{8\text{-}109}$ dimers with the α/β-peptide **2.37**, crystallographic axes are indicated.

Data collection	
X-ray source	APS 21-ID-F
X-ray detector	MAR225
Wavelength (Å)	0.97872
Space group	$P2_1$
a / b / c (Å)	39.1 / 78.4 / 56.5
β (º)	102.8
Volume ($Å^3$)	169000
Matthews coefficient ($Å^3$/Da)	2.56
Solvent content (%)	51.9
Molecules per asymmetric unit	4
Resolution range (Å)*	45.08-3.11 (3.21-3.11)
Number of observations	22104 (2325)
Unique Reflections	6038 (616)
Completeness	99.6% (100%)
Redundancy	3.7 (3.8)
Mean I / σ(I)	14.2 (7.6)
$CC_{1/2}$	0.995 (0.978)
Wilson B factor ($Å^2$)	44.0
R_{merge}	0.083 (0.233)
R_{meas}	0.097 (0.272)
R_{pim}	0.050 (0.139)
Refinement statistics	
Refinement program	phenix.refine: 1.9_1692
Non-hydrogen protein atoms refined	1909
Resolution range (Å)	45.08-3.11 (3.42-3.11)
No. of reflections used in refinement	6017 (1492)
Completeness (%)	99.3 (99)
Reflections in cross-validation set	506
R-value (work, %)	24.1 (26.8)
R-value (free, %)	29.8 (36.1)
R-value (overall, %)	24.5
Overall mean ADP ($Å^2$)	66.8
Coordinate error (ML, Å)	0.41
RMSD	
Bond lengths (Å)	0.025
Bond angles (°)	1.475

Table 2.2 X-ray data collection and refinement statistics and parameters. *Highest resolution shell shown in parentheses.

2.10.8 Proteinase K susceptibility assay

For the preliminary proteinase K experiment in Figure 2.16, peptide stock solutions were prepared in Tris-buffered saline (TBS), pH 7.5 with 10% DMSO at 80 μM, as determined by UV absorbance. A stock solution of 50 μg/mL proteinase K (Novagen 70663-4) was prepared in TBS, pH 7.5 (without DMSO). Peptide stock solutions were diluted, and proteinase K stock solution was added to give final concentrations of 40 μM peptide, 10 μg/mL proteinase K, 5% DMSO in TBS, pH 7.5, and the reaction was allowed to proceed at room temperature. Reactions were run in duplicate and analyzed as described below. MALDI-TOF analysis to identify putative cleavage sites was performed directly on the quenched protease reaction mixtures without any further sample purification.

For the final proteolysis experiment shown in Figure 2.22, stock solutions of 50 μg/mL proteinase K were prepared in TBS, pH 7.5. Solutions of 90 μM α-peptide or α/β-peptide in TBS (no DMSO) were prepared, as determined by UV absorbance.[71] For each proteolysis reaction, the α- or α/β-peptide stock solution was diluted with TBS to achieve a final concentration of 45 μM. Proteinase K stock solution was added (final concentration = 10 μg/mL), and the reaction proceeded at room temperature. For each time point, 50 μL of the reaction mixture was removed and quenched by the addition of 100 μL of 1:1 H_2O/acetonitrile with 1% TFA. 125 μL of the resulting quenched solution was injected onto analytical reverse-phase HPLC. The relative amount of peptide remaining was quantified by integration of the peak at 220 nm in a series of HPLC chromatograms. Each reaction was run at least in duplicate. Half-lives were determined by fitting the time course of peptide degradation to an exponential decay model using GraphPad Prism 4.0.

2.10.9 Simulated gastric fluid (SGF) susceptibility assay

Simulated gastric fluid test solution was prepared by dissolving ~128 mg pepsin (>2500 units/mg, Sigma P7012), 80 mg NaCl, 280 μL conc. HCl in 40 mL water, pH ~1.2.[58, 59] Stock solutions of α- or α/β-peptides in TBS, pH 7.5 were prepared at 330 μM, as determined by UV absorbance.[71] For each proteolysis reaction, the peptide stock solution was diluted into the SGF test solution (final concentration = 30 μM α- or α/β-peptide), and the reaction was allowed to proceed at 37 °C. The reaction was quenched at various time points by removing 50 μL of the reaction mixture and adding 100 μL 1 M ammonium acetate. 125 μL of the resulting quenched solution was injected onto analytical reverse-phase HPLC. Each reaction was run in duplicate. Half-lives were determined by fitting the time course of peptide degradation to an exponential decay model using GraphPad Prism 4.0. MALDI-TOF analysis to confirm the presence of the intact peptide was performed directly on the quenched protease reaction mixtures without any further sample purification.

2.10.10 HUVEC proliferation assay

Stock solutions of α- or α/β-peptide in PBS were prepared at a concentration of 200 μM, as determined by UV absorbance. PBS stock solutions were sterile-filtered through 0.2 μm syringe filters prior to determining concentration. These PBS stock solutions of α- and α/β-peptides were stored at -20 °C between experiments and were used within ~1 month. Human umbilical vein endothelial cells (HUVECs) (Lonza, CC2519) were cultured using Medium 199 (M199) (Mediatech, 50-050-PB) supplemented with penicillin/streptomycin (HyClone, SV30010) and EGM-2 (Lonza, CC4176) at 37°C in 5% CO_2. Cells were grown to 60-80% confluence before beginning an experiment. On Day 0 of experiments, cells were serum-starved in Serum Starvation medium, consisting of M199 with 2 vol.% cosmic calf serum (CCS)

(HyClone, SH30087), overnight. On Day 1 of experiments, cells were trypsinized and reseeded in gelatin-coated 96-well plates at a density of 3000-4000 cells/well in Serum Starvation medium and allowed to attach for 6-8 hours. Appropriate dilutions of α- or α/β-peptide were made with PBS, and the resulting solutions were premixed with recombinant human $VEGF_{165}$ (R&D Systems, 293-VE-010) or recombinant human FGF basic (FGF-2) (R&D Systems, 233-FB-025) in Serum Starvation medium and incubated at room temperature for ~1 hour. For controls with no inhibitor, the same amount of PBS was pre-incubated with growth factor alone. After pre-incubation, these solutions were added to the cells to give a final concentration of 10 ng/mL growth factor (except in "no growth factor" controls), between 0 μM and 50 μM peptide, and 25 vol.% PBS. Cells were then cultured in the presence/absence of inhibitors and/or growth factor for 36 hours. Relative cell proliferation was quantified using the Click-iT EdU Alexa Flour 488 Assay (Life Technologies, C10337). After 24 hours of exposure to assay conditions (on Day 2), EdU was added (final concentration = 10 μM), and the cells were maintained at 37°C in 5% CO_2 for an additional 12 hours (36 hours total) before being fixed with 10% buffered formalin. EdU incorporation was detected using Life Technologies' assay protocol. All cell nuclei were counter-stained with the Hoechst 33342 stain supplied with the Click-iT EdU assay kit (1:1000 dilution in PBS) (some early experiments used DAPI, which also stains nuclei blue), and proliferating cells containing incorporated EdU were stained using copper-catalyzed alkyne-azide click addition of Alexa Fluor 488. Plates were imaged using a Nikon Ti-Eclipse inverted epifluorescence microscope with filters for FITC (detecting Alexa Fluor 488, EdU labeled cells) and DAPI (detecting Hoescht 33342, labeling all cells). Images were analyzed using NIS-Elements v3.2 Imaging Software to count the number of proliferating cells (EdU stained) and total number of cells (Hoechst stained).

Data presented in Figures 2.25-2.27 and 2.30 are from representative experiments, where values represent the mean ± SD for replicate wells on a given plate, and the value for each well is normalized relative to the average value of proliferating cells in the "No inhibitor" ($VEGF_{165}$ only) condition.

Data presented in Figure 2.28 represent the mean ± SD of relative proliferation collected from eight independent experiments. Because the maximum level of VEGF-induced proliferation varied for each independent experiment, each experimental condition was normalized to the relative "No inhibitor" ($VEGF_{165}$ only) control in its respective experiment (10 ng/mL $VEGF_{165}$ in Serum Starvation medium with 25 vol.% PBS with no inhibitor present). For statistical analysis, a two-tailed ratio t-test on the logarithmically transformed ratios was used to determine if the mean ratio for a given experimental condition differed from 1.0 (the "No inhibitor" control). To avoid false positives from making multiple comparisons, we used the Bonferroni correction to set a stricter significance threshold and required a given p-value $\leq 0.05/5 = 0.01$ for statistical significance.

2.10.11 LIVE/DEAD viability assay

HUVECs were cultured and treated with inhibitors and $VEGF_{165}$, as described above. After 36 hours in culture under the experimental conditions, cells were stained using LIVE/DEAD Viability/Cytotoxicity kit (Life Technologies, L3224). 4 μM calcein-AM and 2 μM ethidium homodimer-1 in M199 without serum was added to cells for 30 minutes at 37°C in 5% CO_2 to stain live and dead cells, respectively. After 30 minutes incubation with staining reagents, the medium was removed from wells and replaced with fresh M199 for imaging. Plates were imaged as above using filters for FITC (detecting calcein-AM, live cells) and TexasRed (detecting ethidium homodimer-1, dead cells). Images were analyzed using NIS-

Elements v3.2 AR Imaging Software to count the number of live and dead cells. The fraction of live cells was determined by dividing the number of live stained cells by the total number of cells (live stained cells + dead stained cells) (Figure 2.29A).

2.10.12 Peptide characterization

α-Peptide and α/β-peptide purity after purification was assessed by analytical scale reverse-phase HPLC, using solvent A: H_2O with 0.1% TFA, solvent B: acetonitrile with 0.1% TFA, with a flow rate of 1 mL/min. The solvent gradient for each peptide is specified in each panel. HPLC chromatograms at 220 nm are shown at the top of each panel. Peptide identity was confirmed by MALDI-TOF-MS, shown at the bottom of each panel. For each MALDI-TOF spectrum, the monoisotopic $[M+H]^+$, *m/z* is labeled.

Z-VEGF
HPLC: Gradient = 10-60% solvent B over 50 minutes
MALDI-TOF: Calculated monoisotopic $[M+H]^+$ = 6661.4

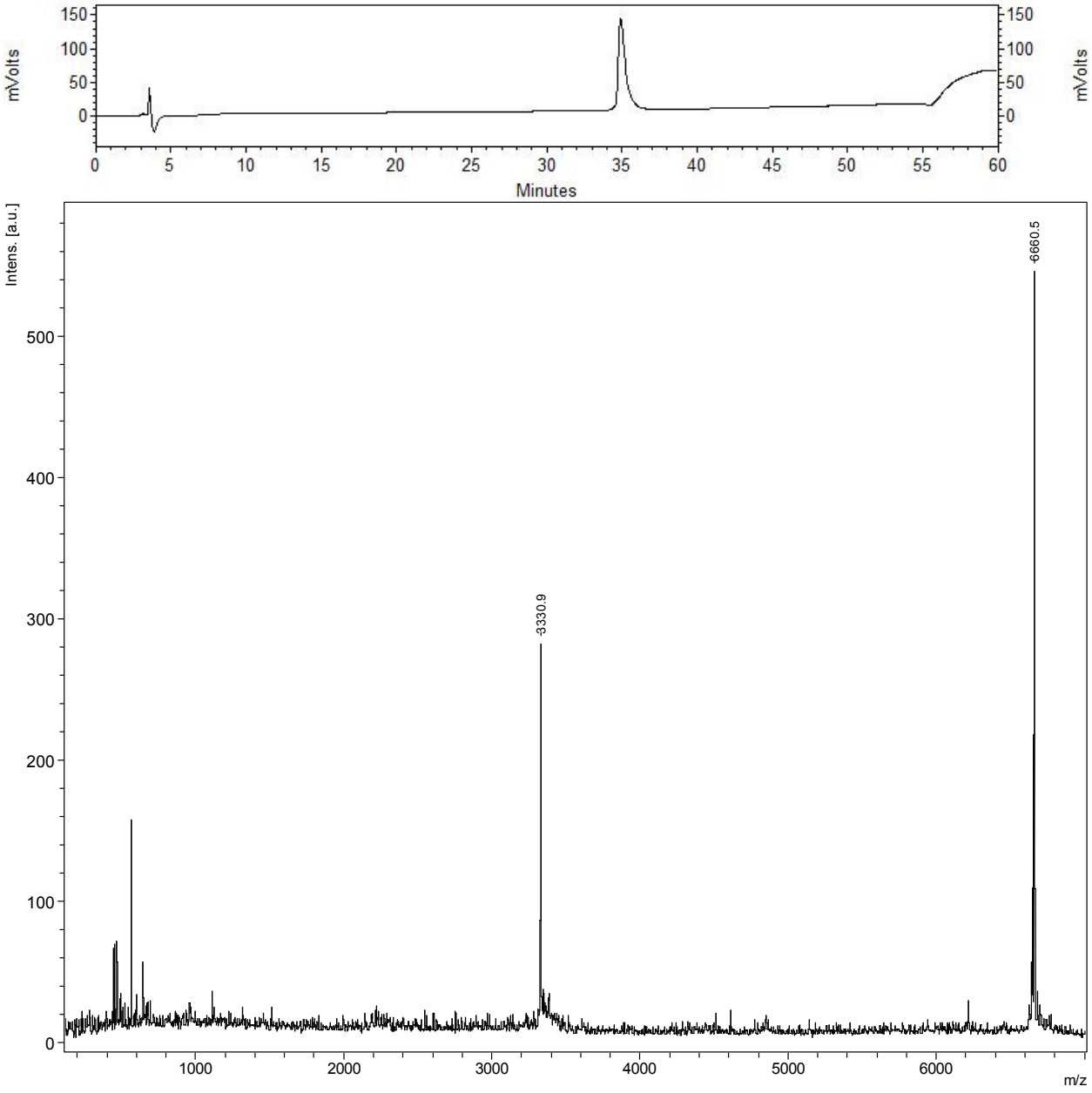

2.1

HPLC: Gradient = 10-60% solvent B over 50 minutes

MALDI-TOF: Calculated monoisotopic $[M+H]^+$ = 7019.4

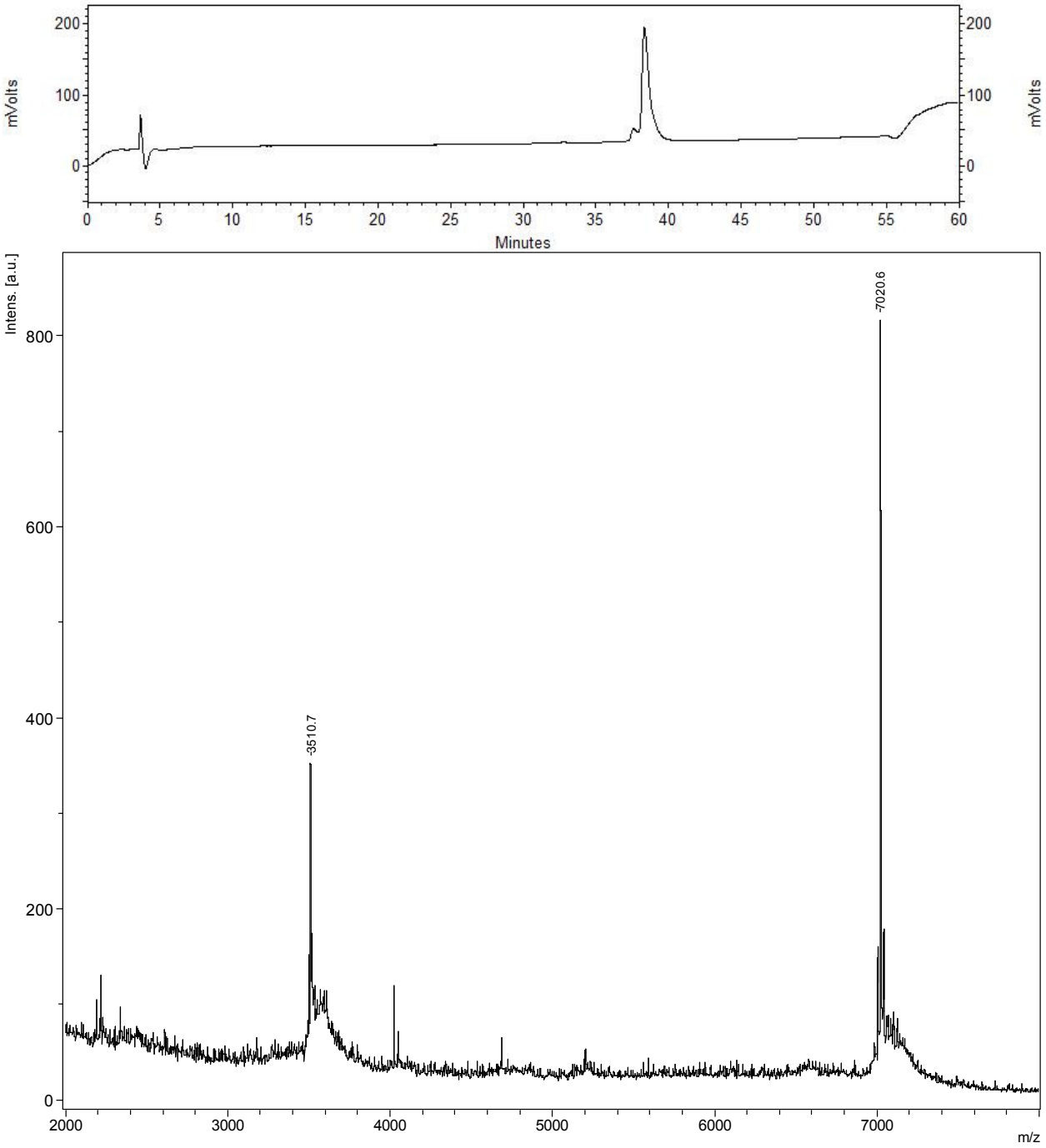

2.2

HPLC: Gradient = 10-60% solvent B over 50 minutes

MALDI-TOF: Calculated monoisotopic $[M+H]^+$ = 3808.9

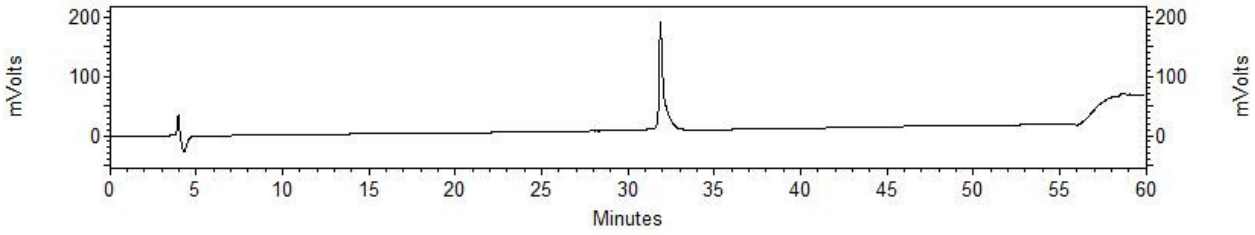

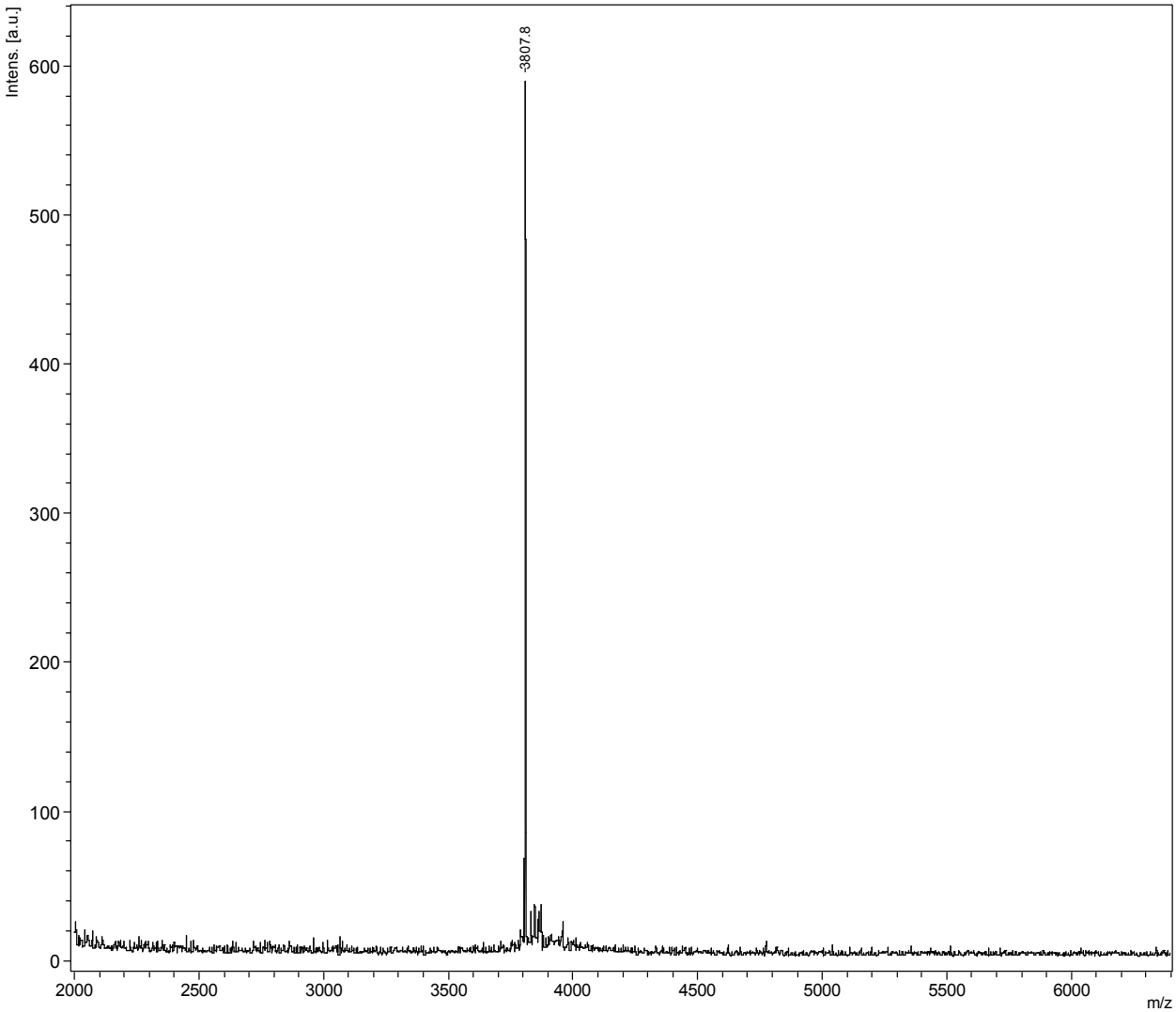

2.3

HPLC: Gradient = 10-60% solvent B over 50 minutes

MALDI-TOF: Calculated monoisotopic $[M+H]^+$ = 3851.9

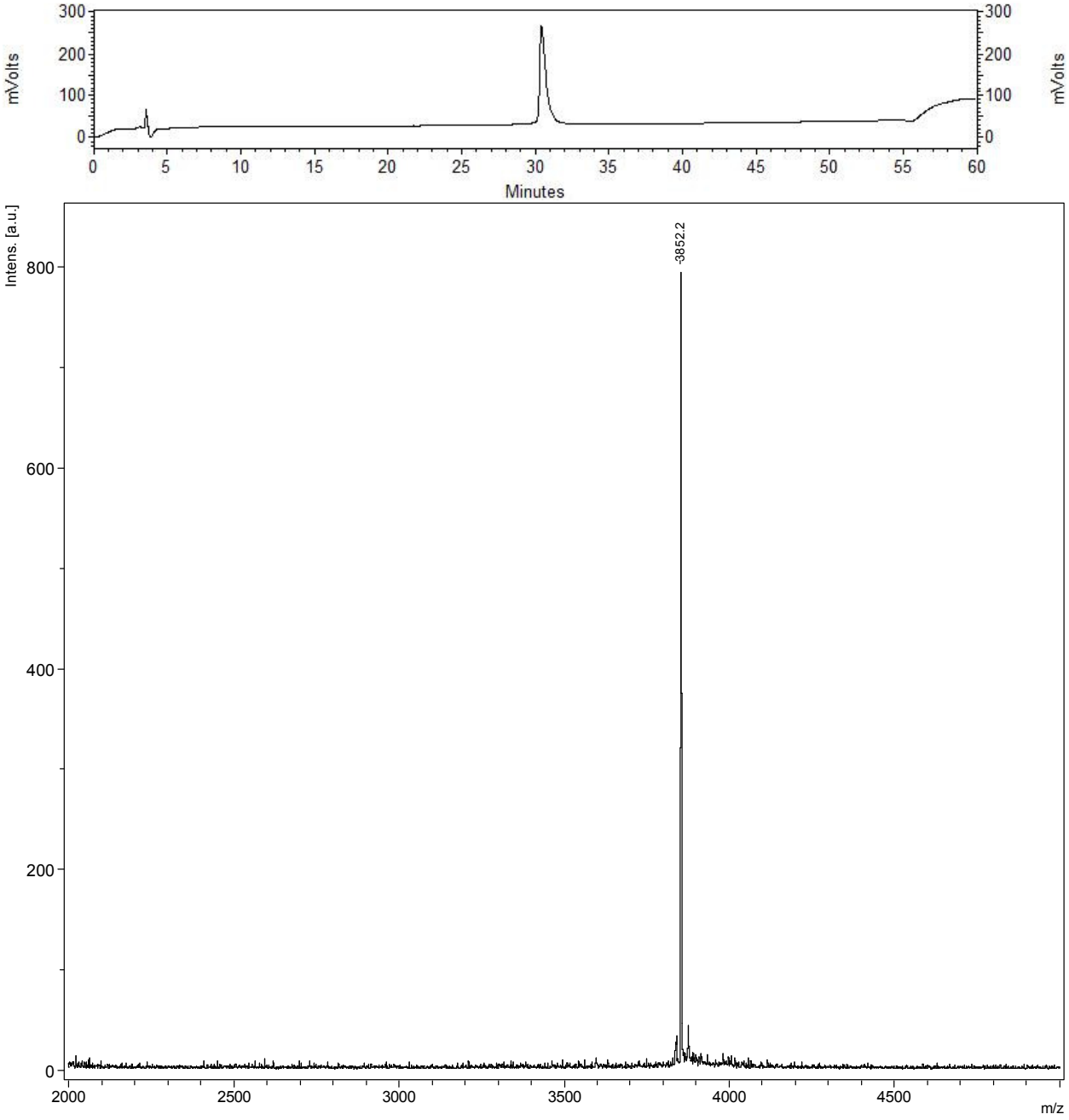

2.4

HPLC: Gradient = 10-60% solvent B over 50 minute

MALDI-TOF: Calculated monoisotopic $[M+H]^+$ = 3849.9

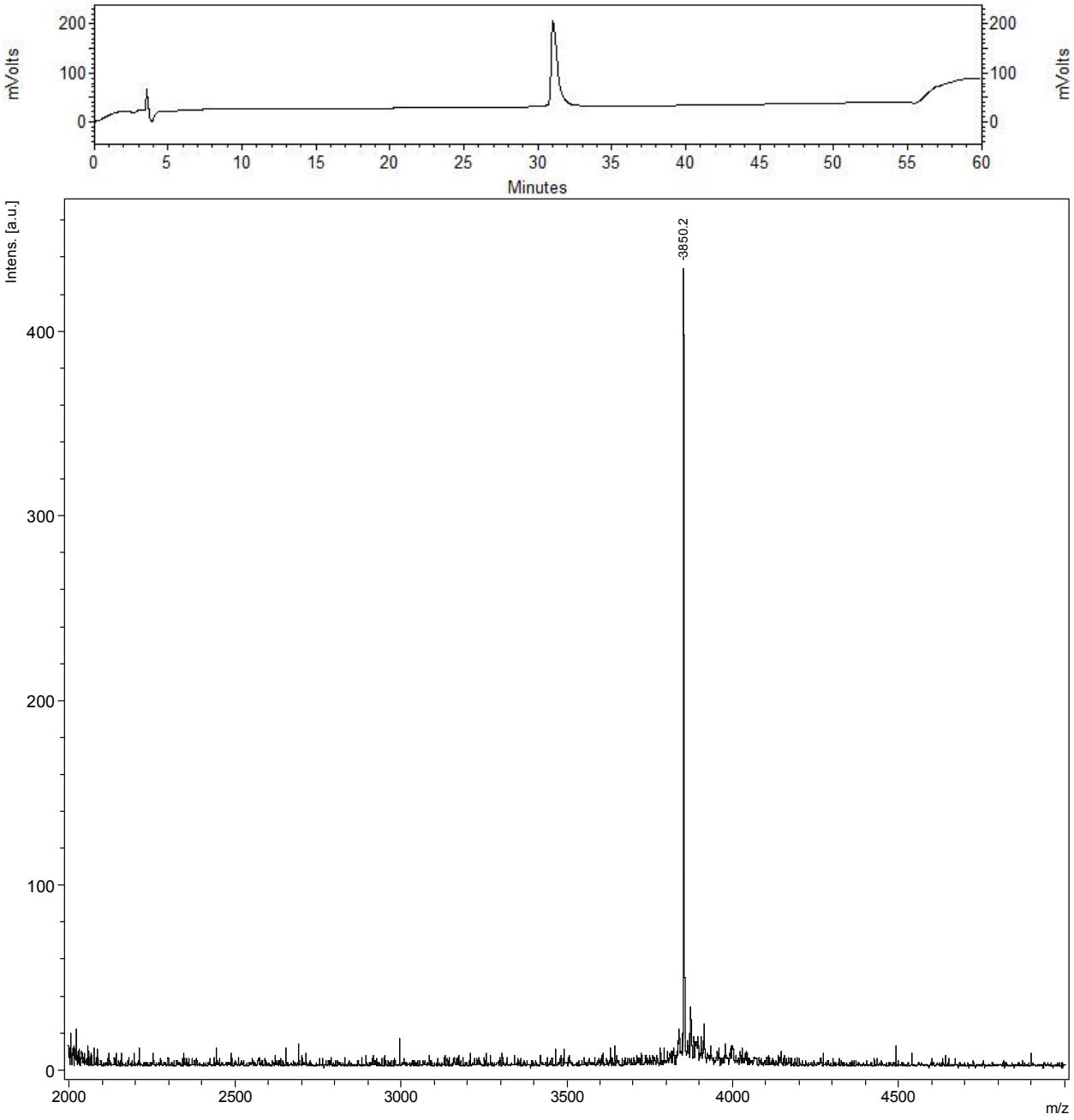

2.5

HPLC: Gradient = 10-60% solvent B over 50 minutes

MALDI-TOF: Calculated monoisotopic $[M+H]^+ = 3778.8$

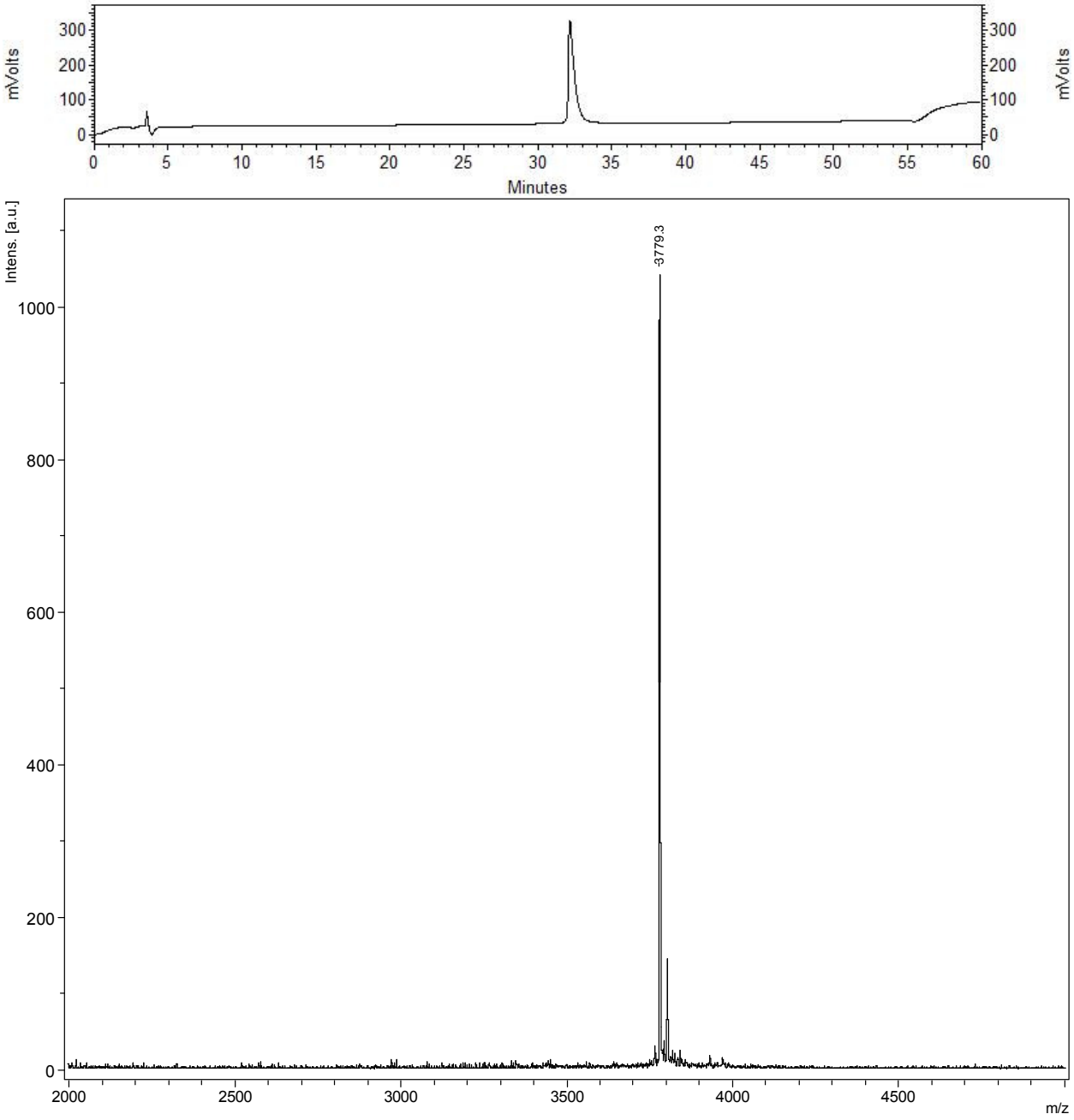

2.6

HPLC: Gradient = 10-60% solvent B over 50 minutes

MALDI-TOF: Calculated monoisotopic $[M+H]^+$ = 3843.9

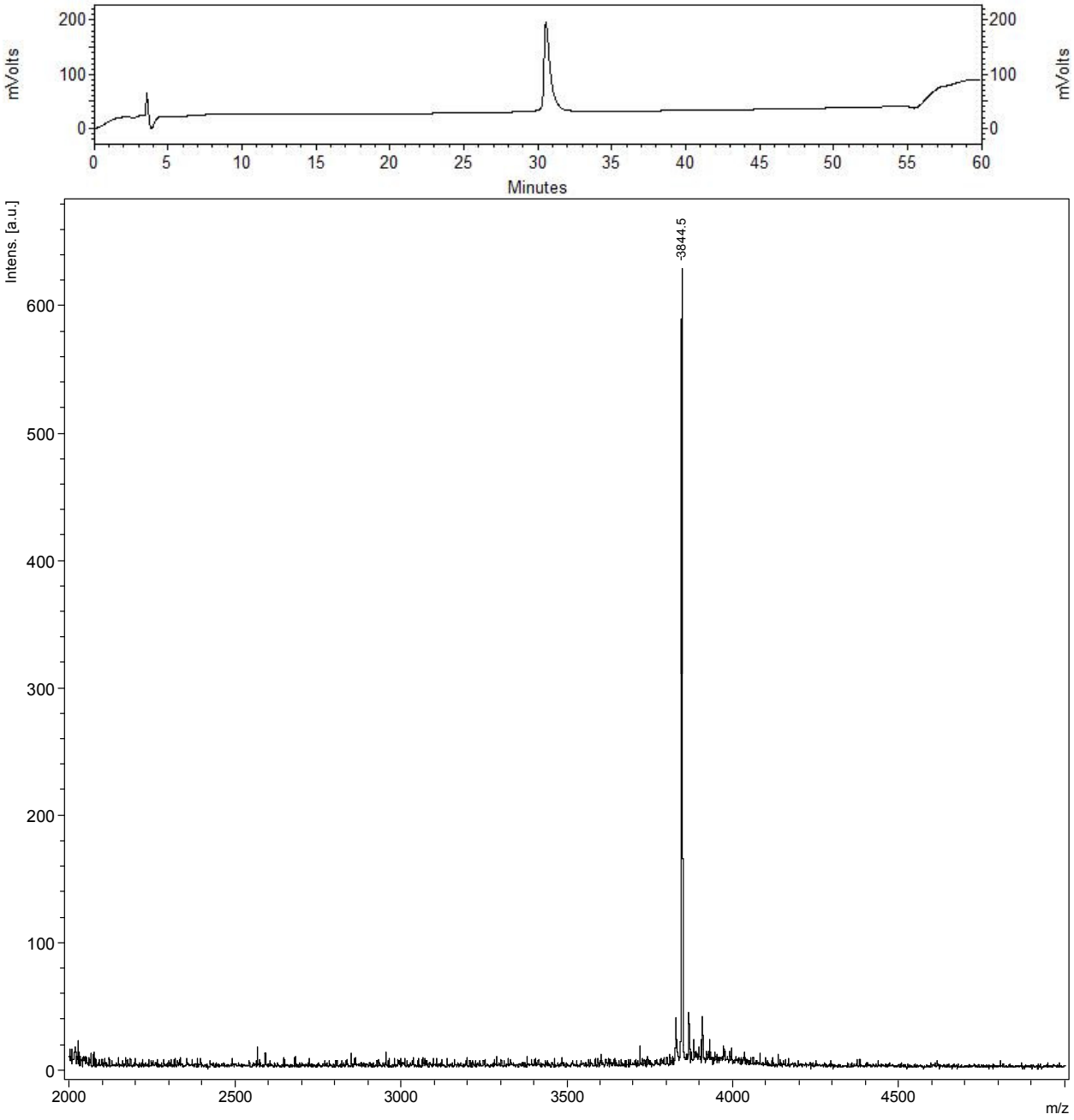

2.7

HPLC: Gradient = 10-60% solvent B over 50 minutes

MALDI-TOF: Calculated monoisotopic $[M+H]^+ = 5647.8$

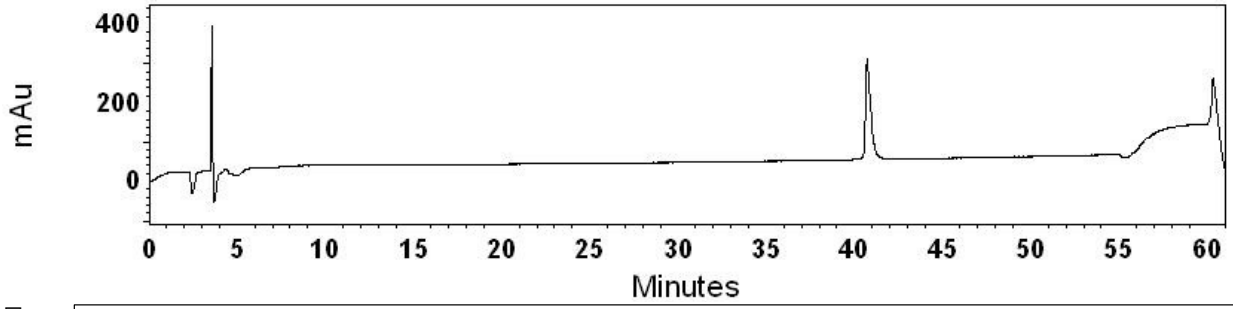

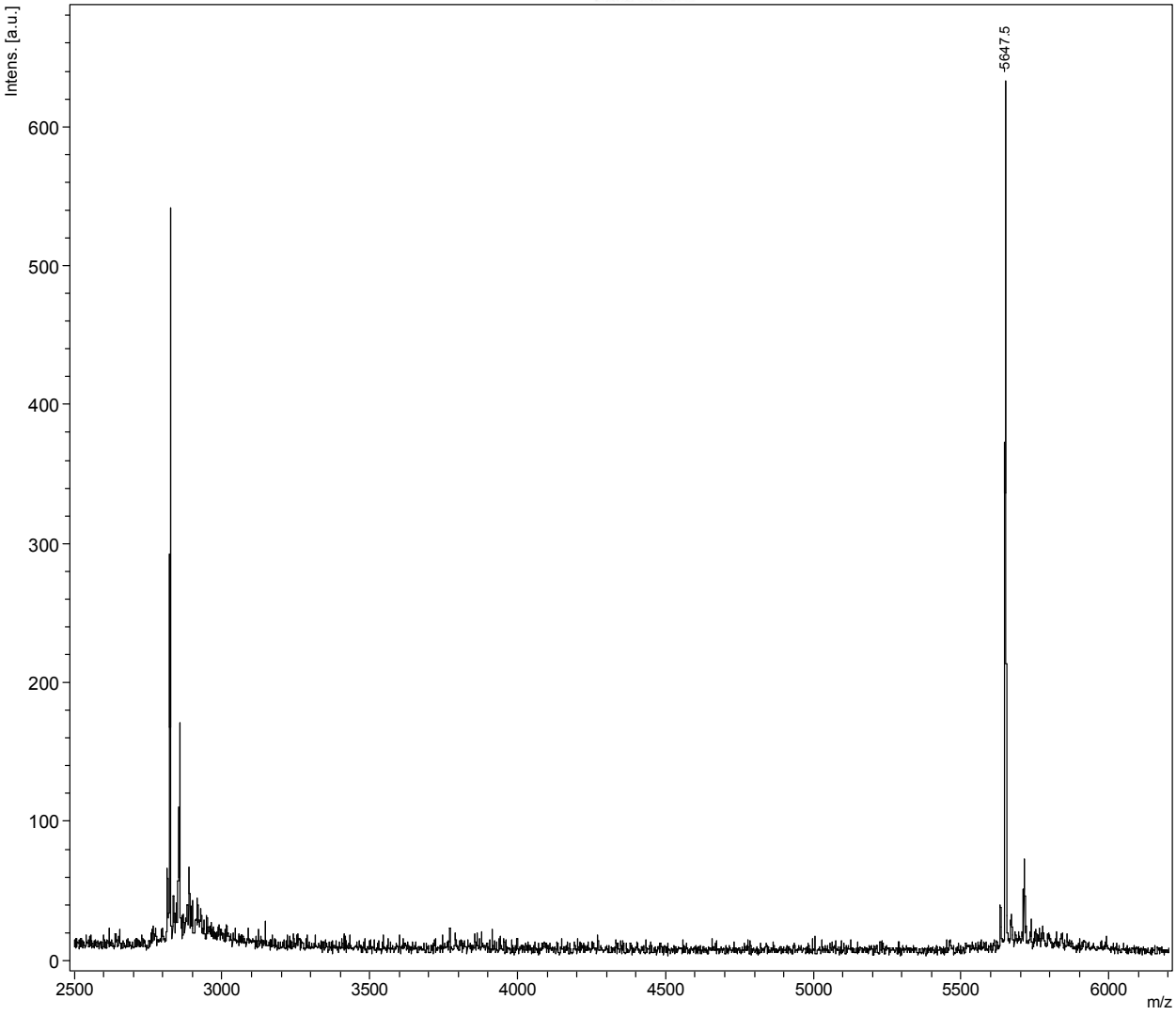

2.8

HPLC: Gradient = 10-60% solvent B over 50 minutes

MALDI-TOF: Calculated monoisotopic $[M+H]^+ = 4486.2$

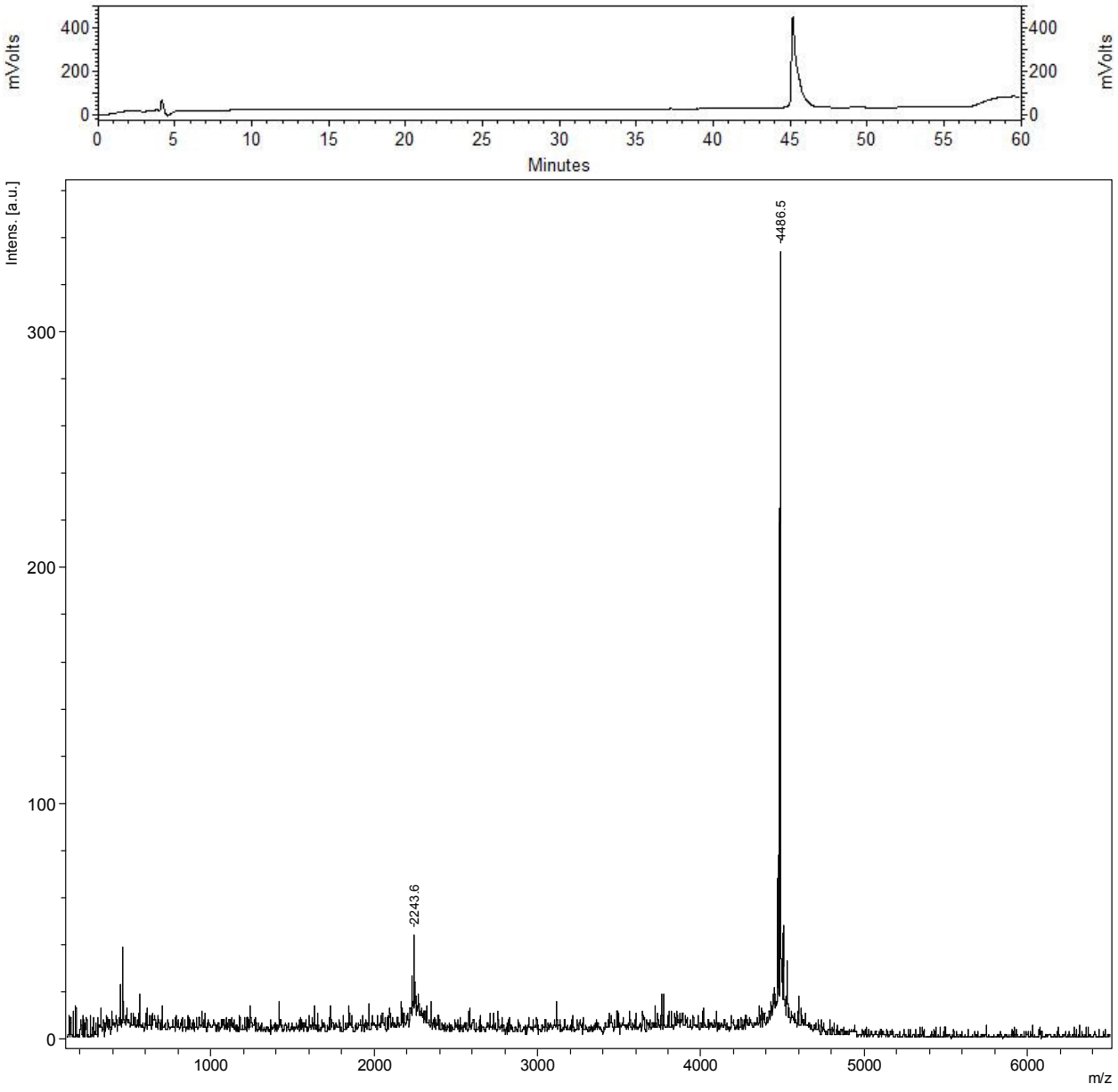

2.9

HPLC: Gradient = 10-60% solvent B over 50 minutes

MALDI-TOF: Calculated monoisotopic $[M+H]^+ = 4417.2$

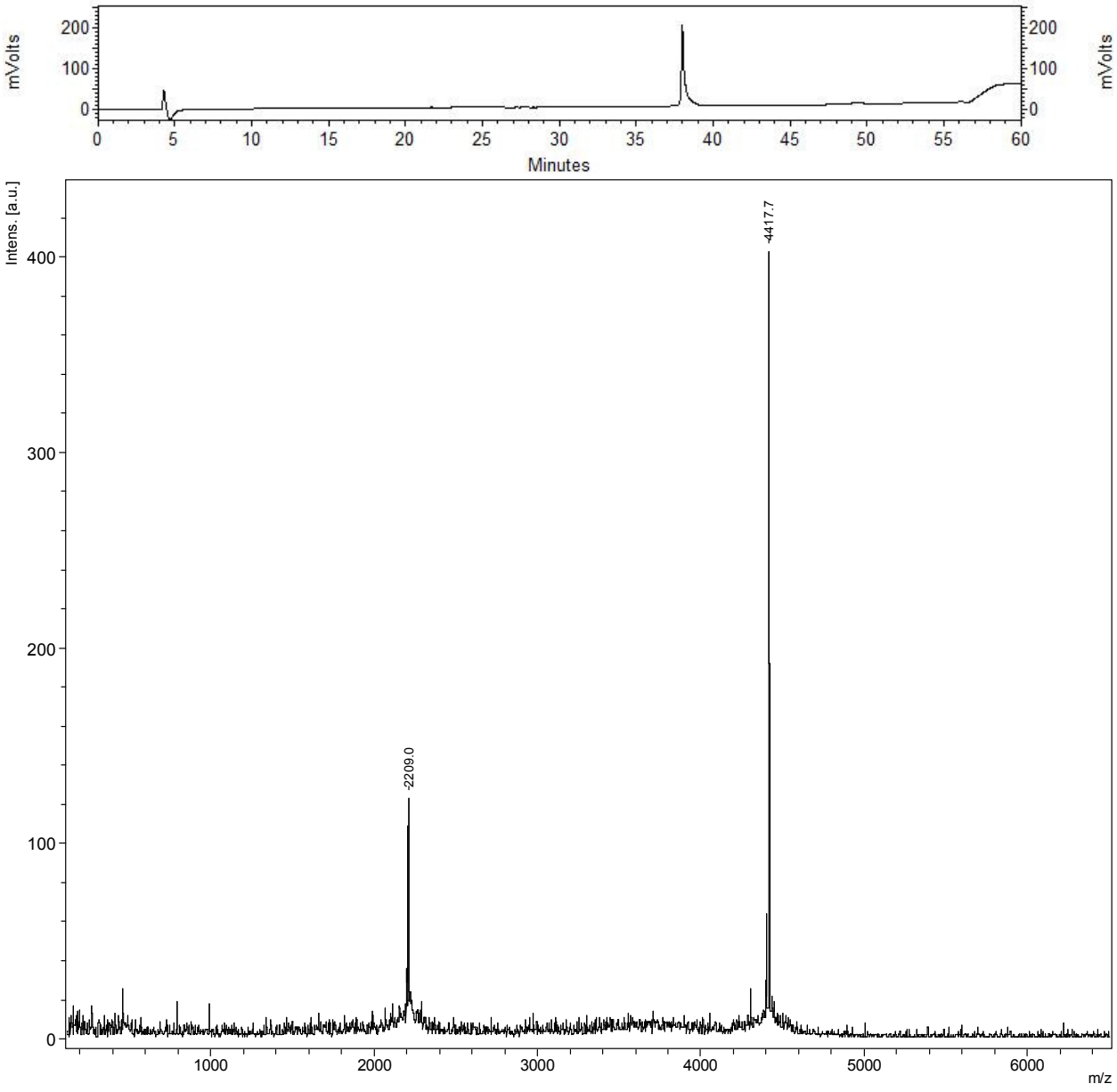

2.10

HPLC: Gradient = 10-60% solvent B over 50 minutes

MALDI-TOF: Calculated monoisotopic $[M+H]^+$ = 4607.2

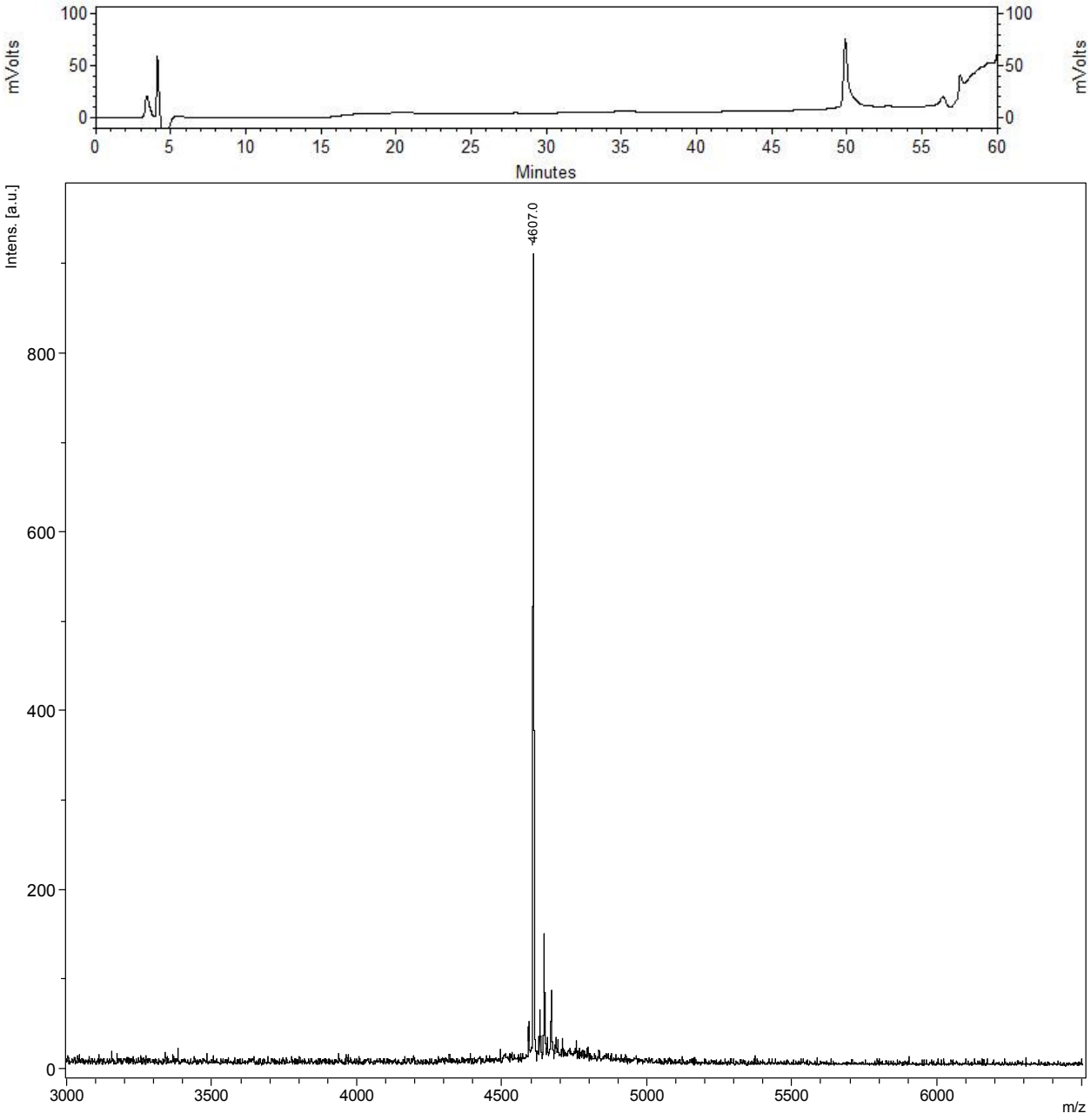

2.11

HPLC: Gradient = 10-60% solvent B over 50 minutes. Peak appearing at ~4 min is DMSO.
MALDI-TOF: Calculated monoisotopic $[M+H]^+$ = 4541.2

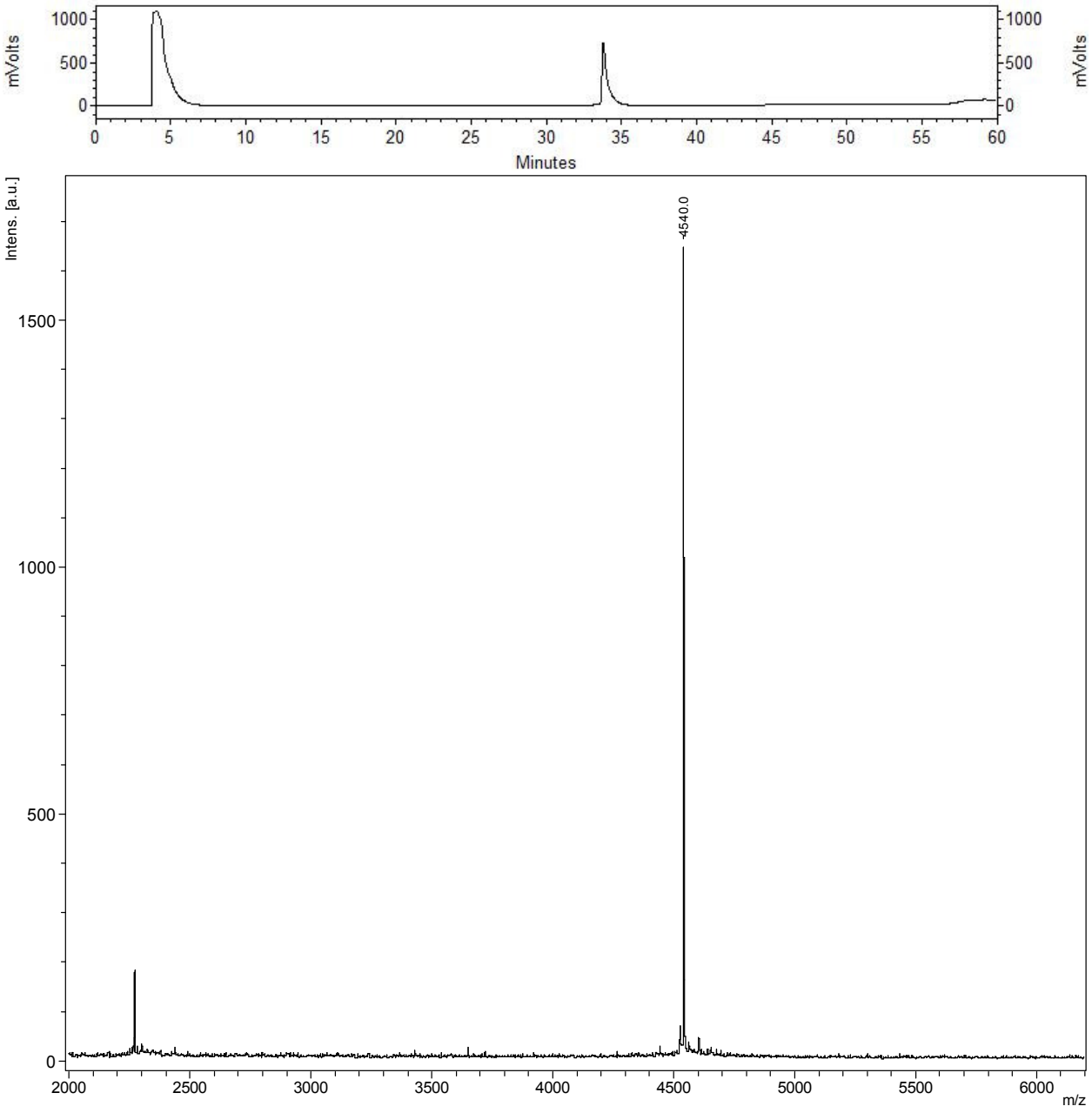

2.12

HPLC: Gradient = 10-60% solvent B over 50 minutes. Peak appearing at ~3 min is DMSO.
MALDI-TOF: Calculated monoisotopic $[M+H]^+$ = 4484.2

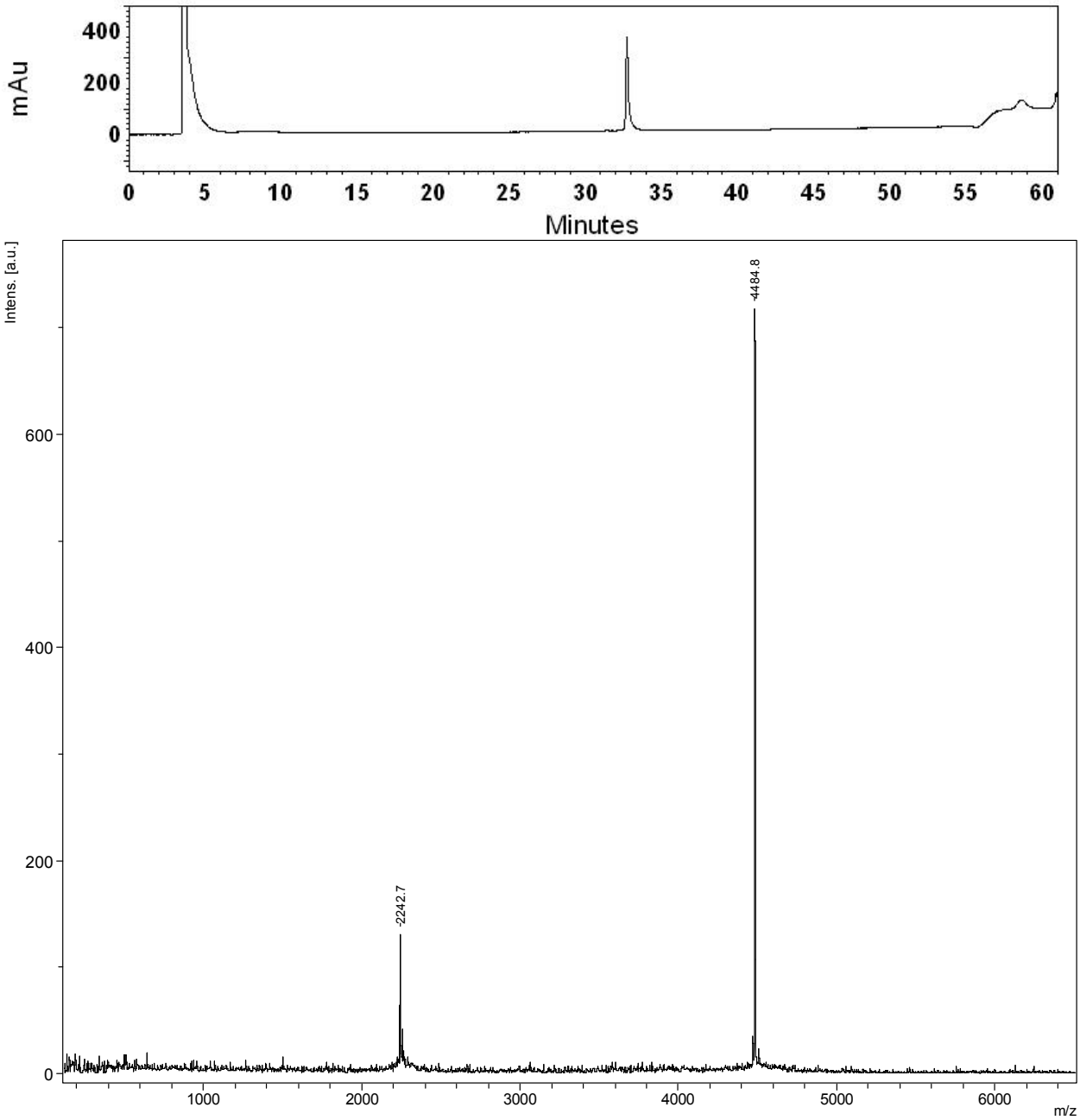

2.13

HPLC: Gradient = 10-60% solvent B over 50 minutes

MALDI-TOF: Calculated monoisotopic $[M+H]^+ = 4611.2$

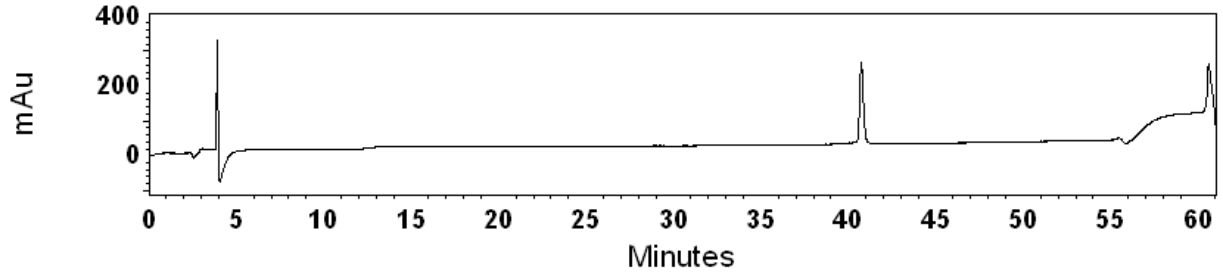

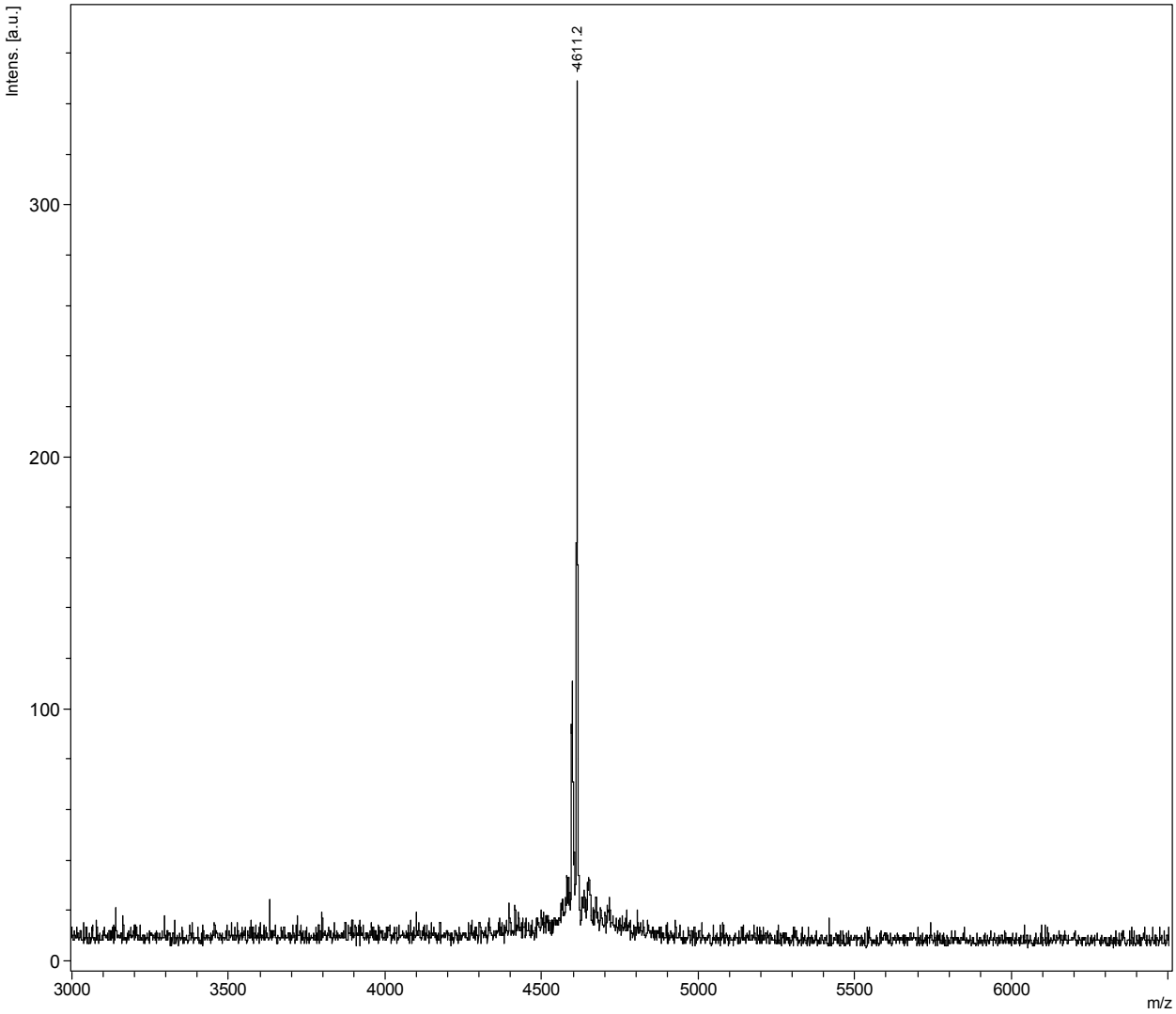

2.14

HPLC: Gradient = 10-60% solvent B over 50 minutes

MALDI-TOF: Calculated monoisotopic $[M+H]^+ = 4768.3$

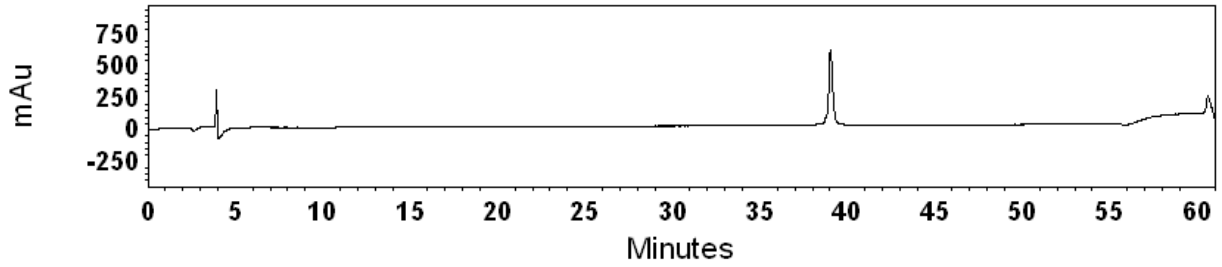

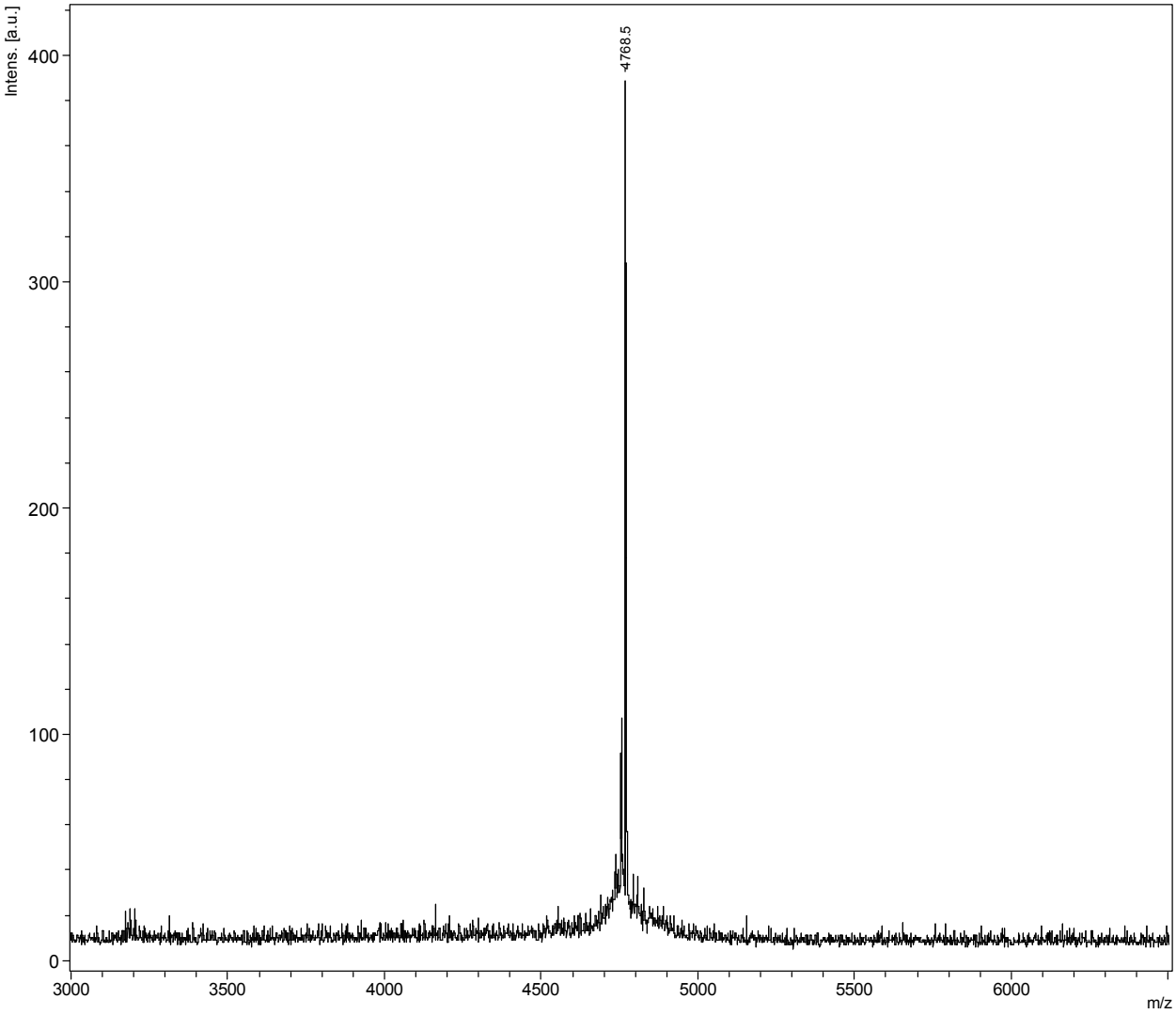

2.15

HPLC: Gradient = 10-60% solvent B over 50 minutes

MALDI-TOF: Calculated monoisotopic $[M+H]^+ = 4824.3$

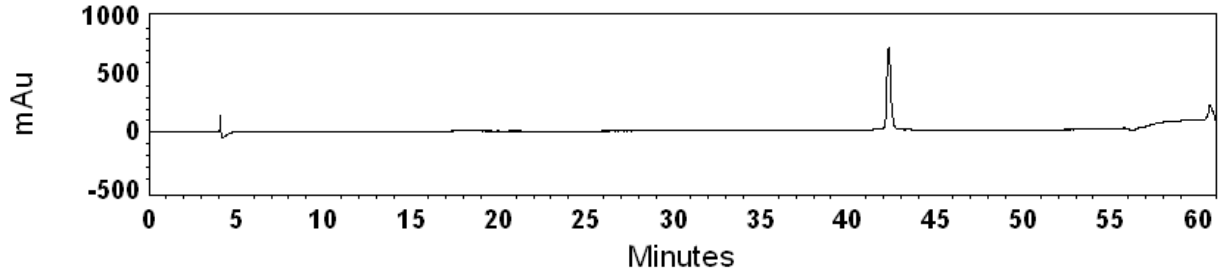

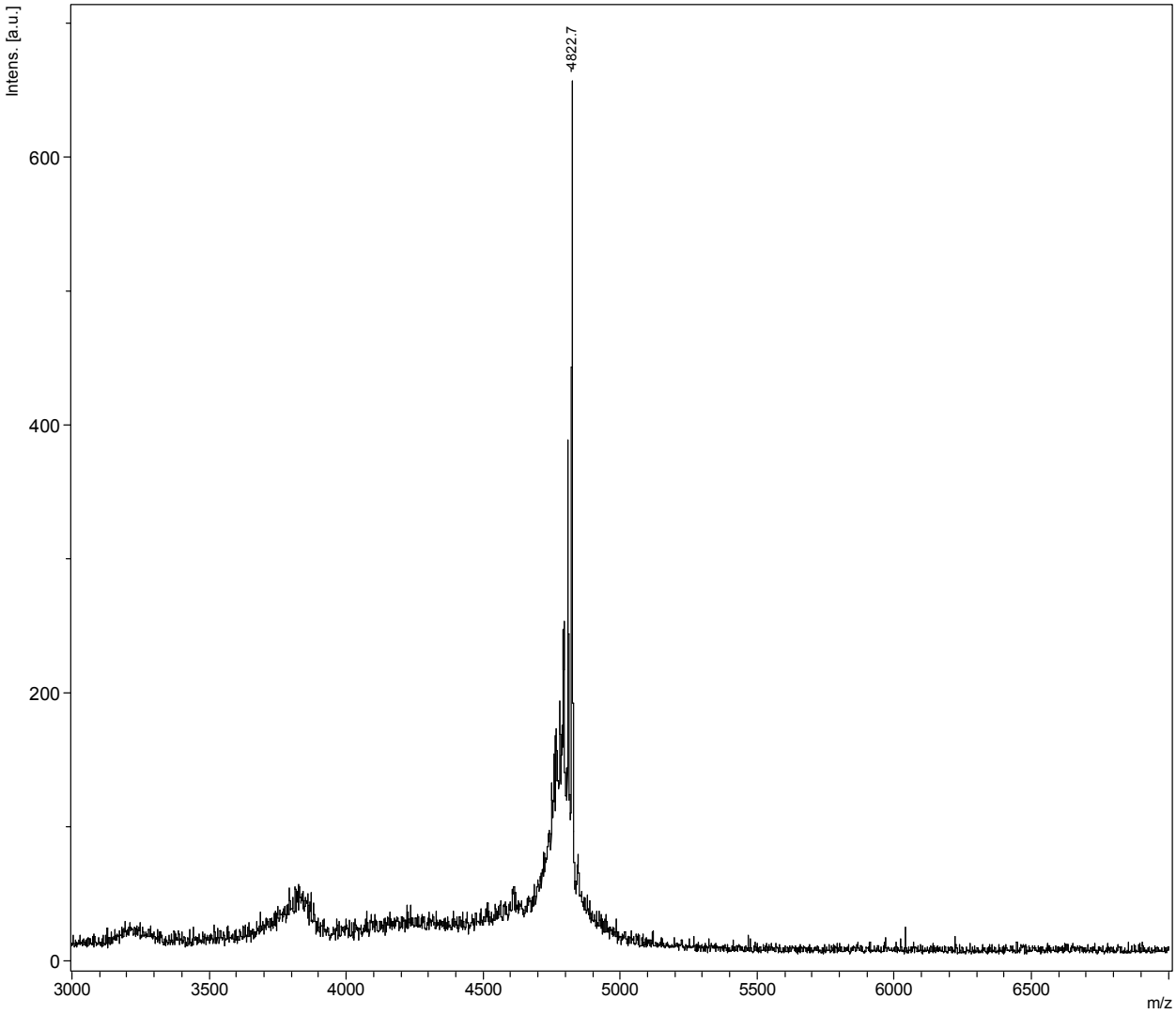

2.16

HPLC: Gradient = 10-60% solvent B over 50 minutes

MALDI-TOF: Calculated monoisotopic $[M+H]^+ = 4905.5$

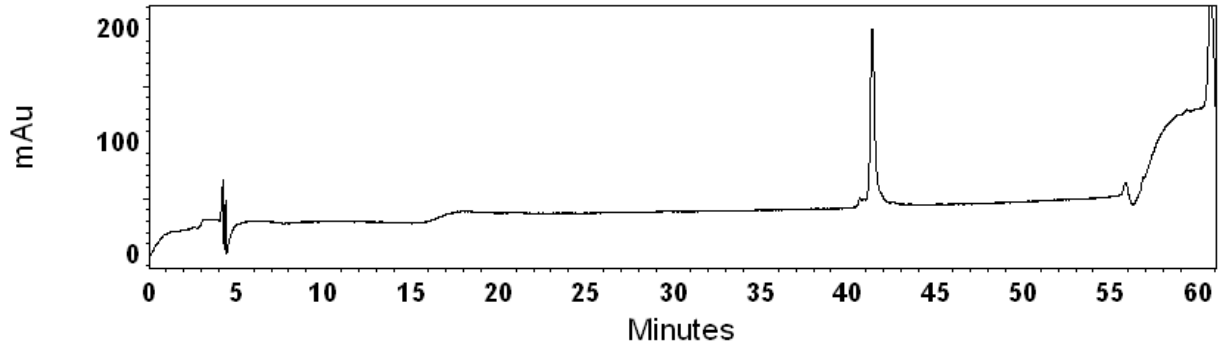

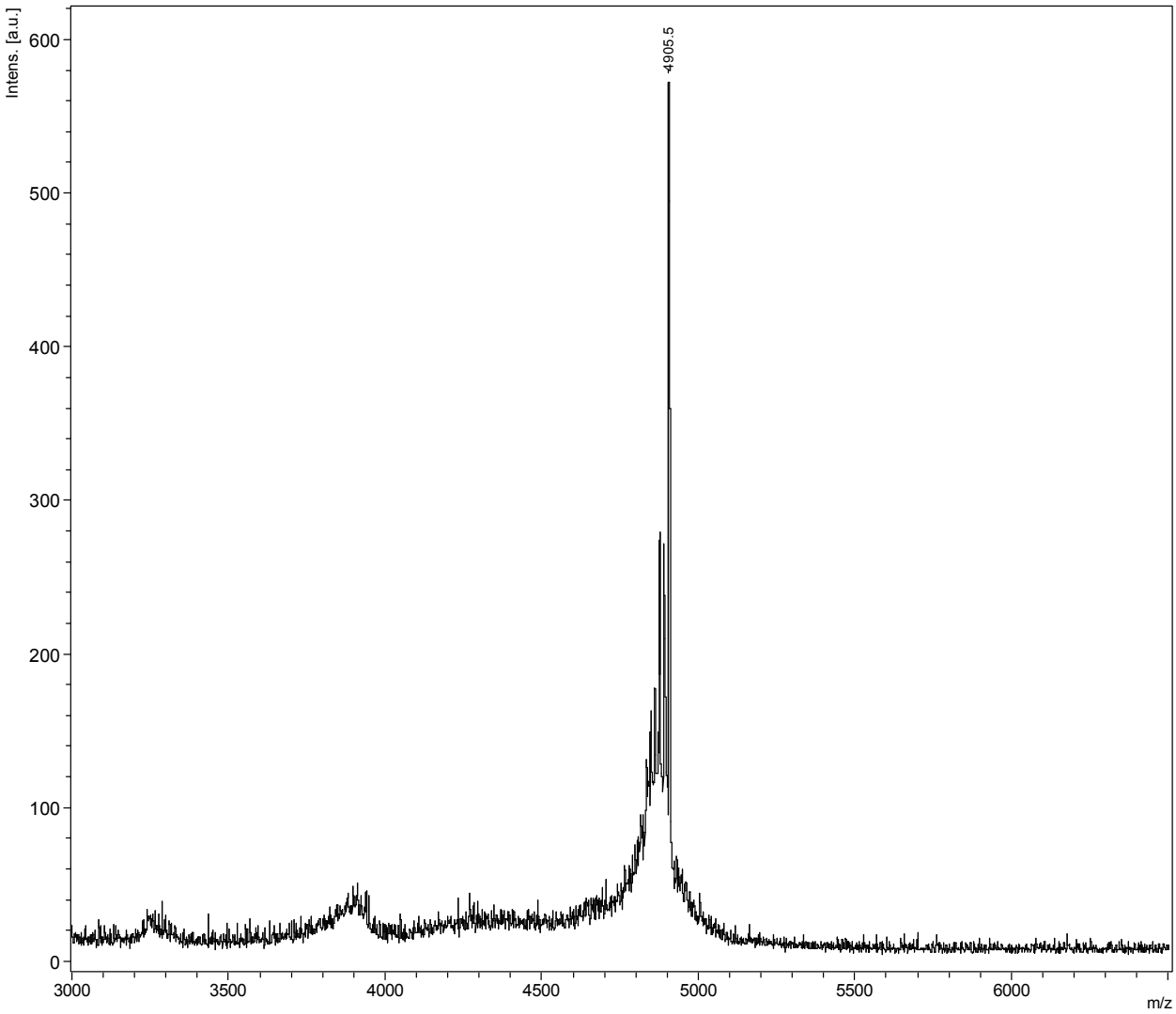

2.17

HPLC: Gradient = 10-60% solvent B over 50 minutes

MALDI-TOF: Calculated monoisotopic $[M+H]^+ = 4864.4$

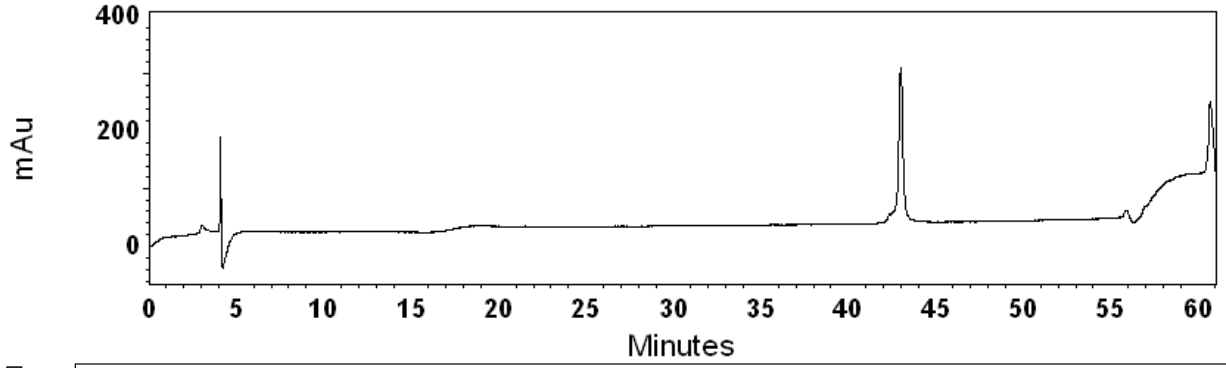

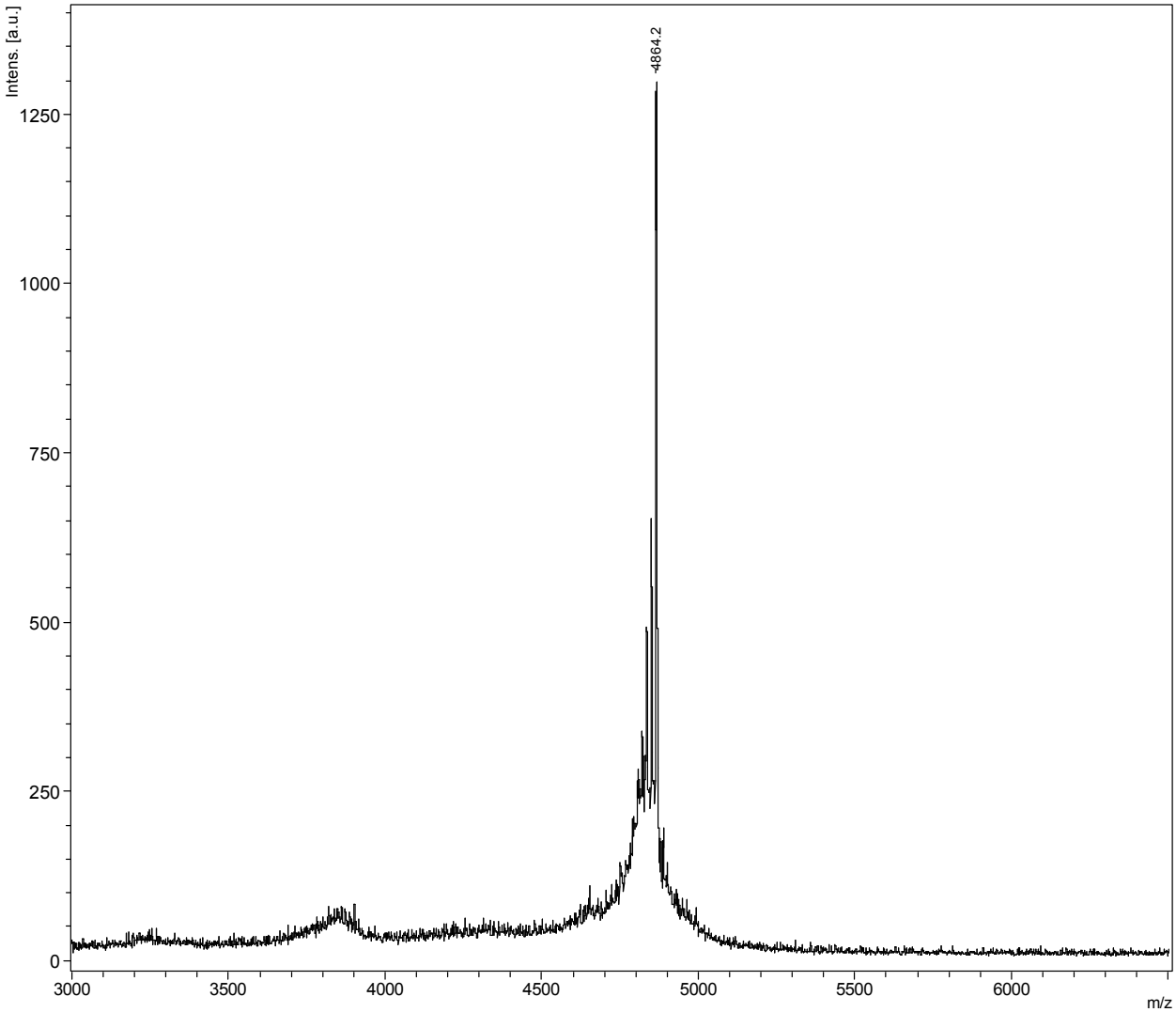

2.18

HPLC: Gradient = 10-60% solvent B over 50 minutes

MALDI-TOF: Calculated monoisotopic $[M+H]^+ = 4783.3$

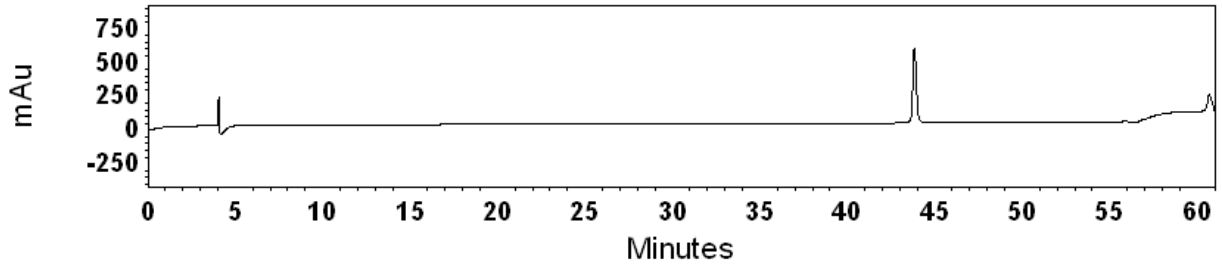

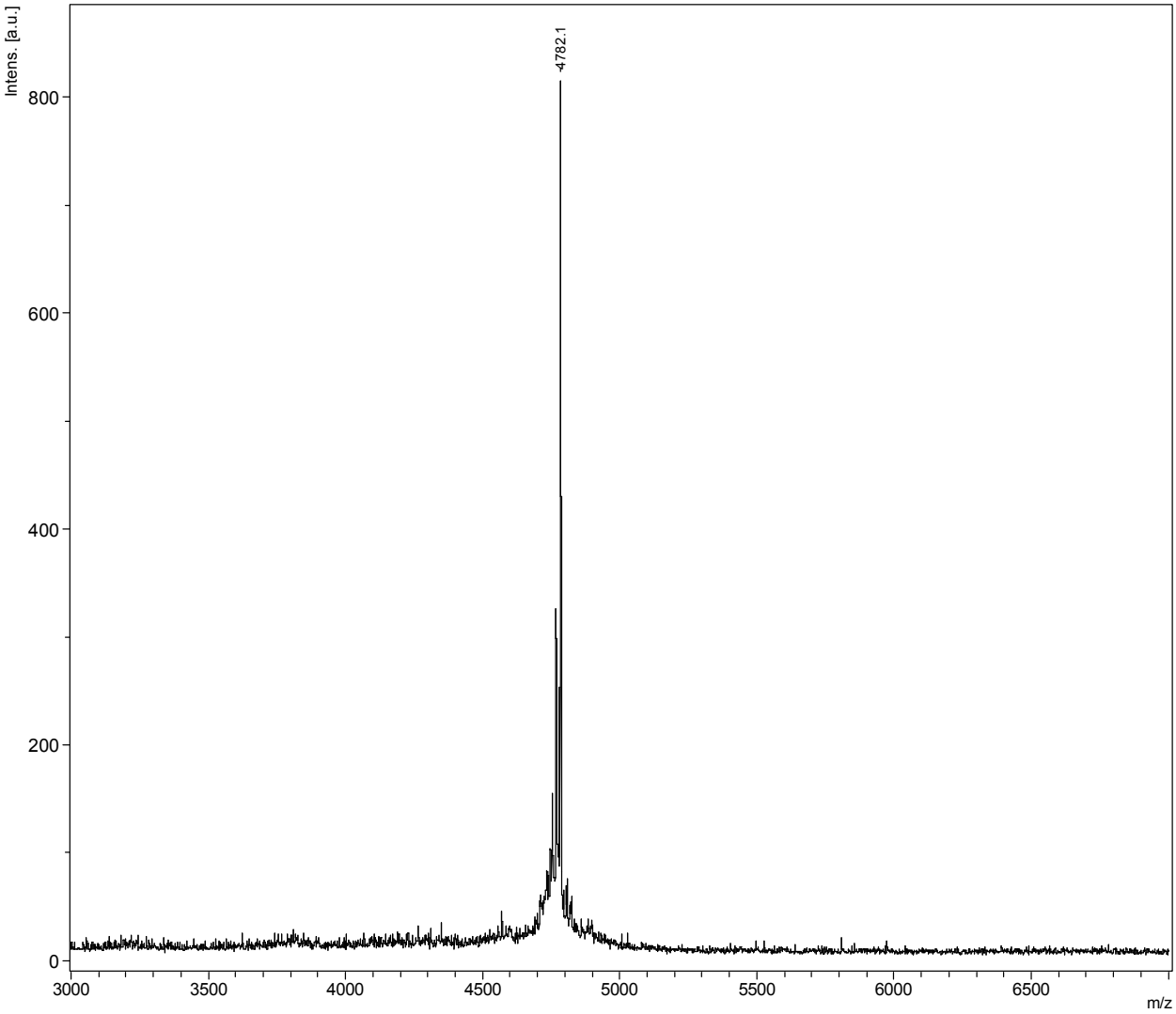

2.19

HPLC: Gradient = 10-60% solvent B over 50 minutes

MALDI-TOF: Calculated monoisotopic $[M+H]^+ = 4583.2$

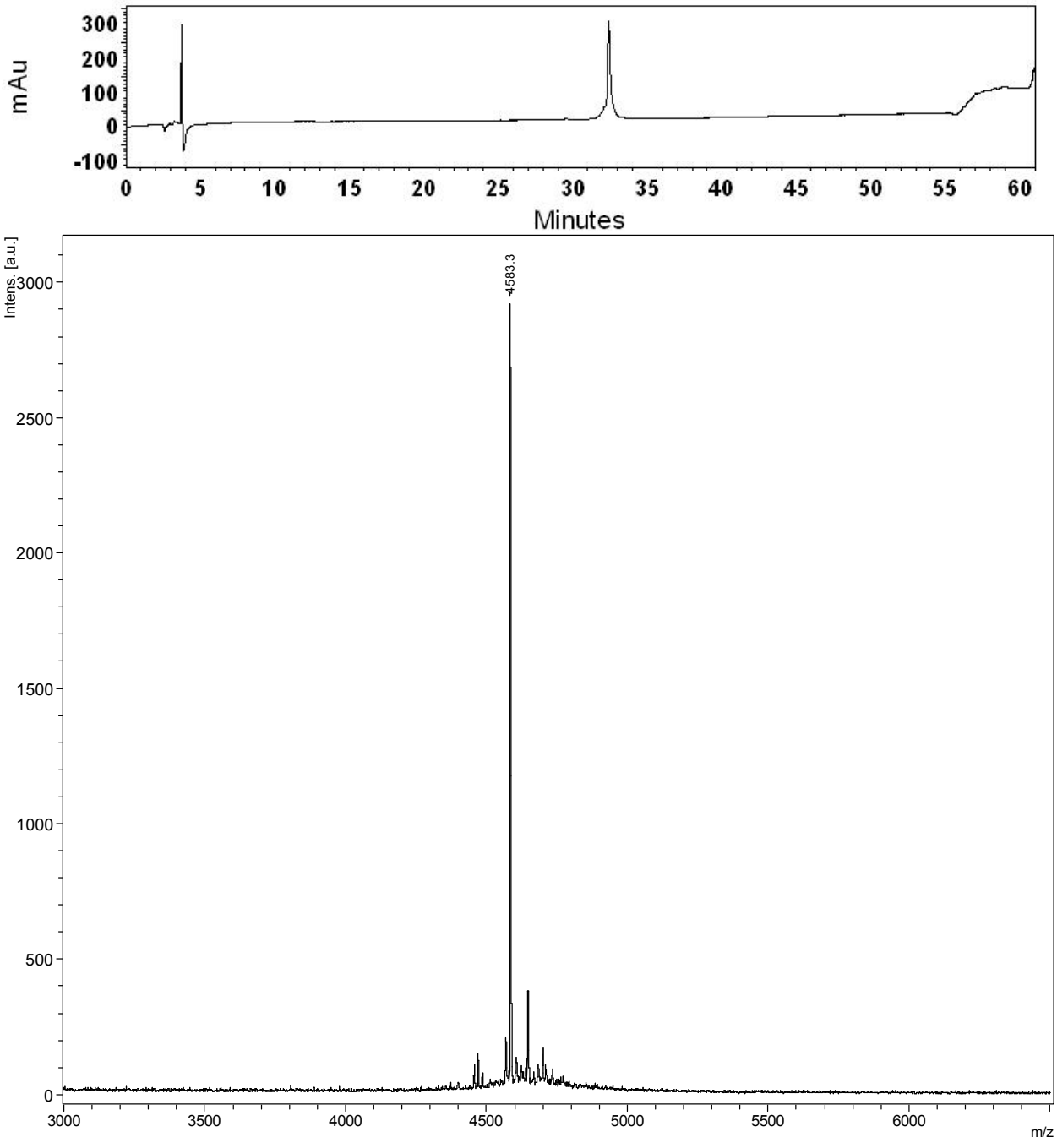

2.20

HPLC: Gradient = 10-90% solvent B over 80 minutes. Peak at ~4 min is DMSO.
MALDI-TOF: Calculated monoisotopic $[M+H]^+ = 4581.2$

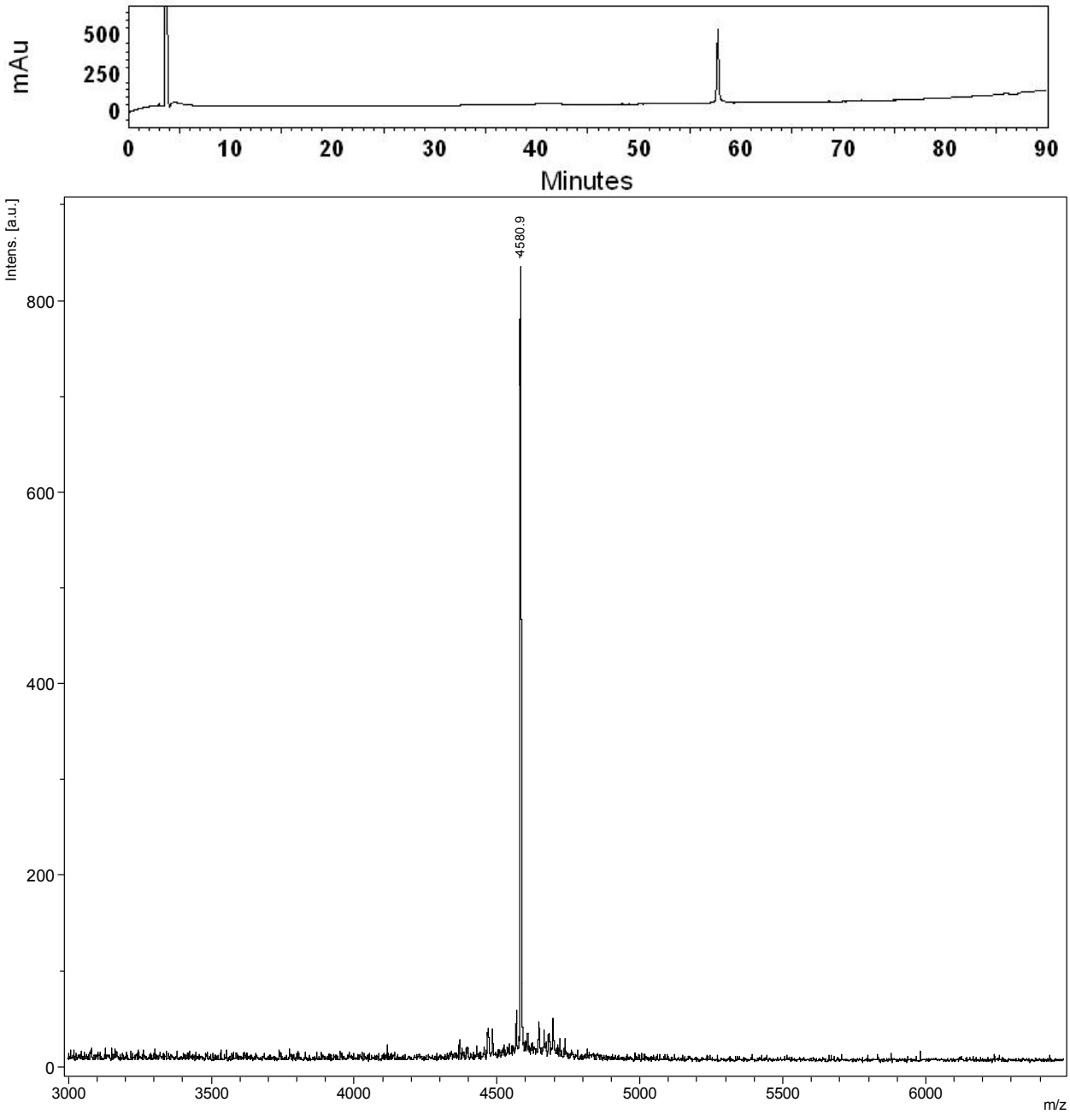

2.21

HPLC: Gradient = 10-60% solvent B over 50 minutes

MALDI-TOF: Calculated monoisotopic $[M+H]^+ = 4565.2$

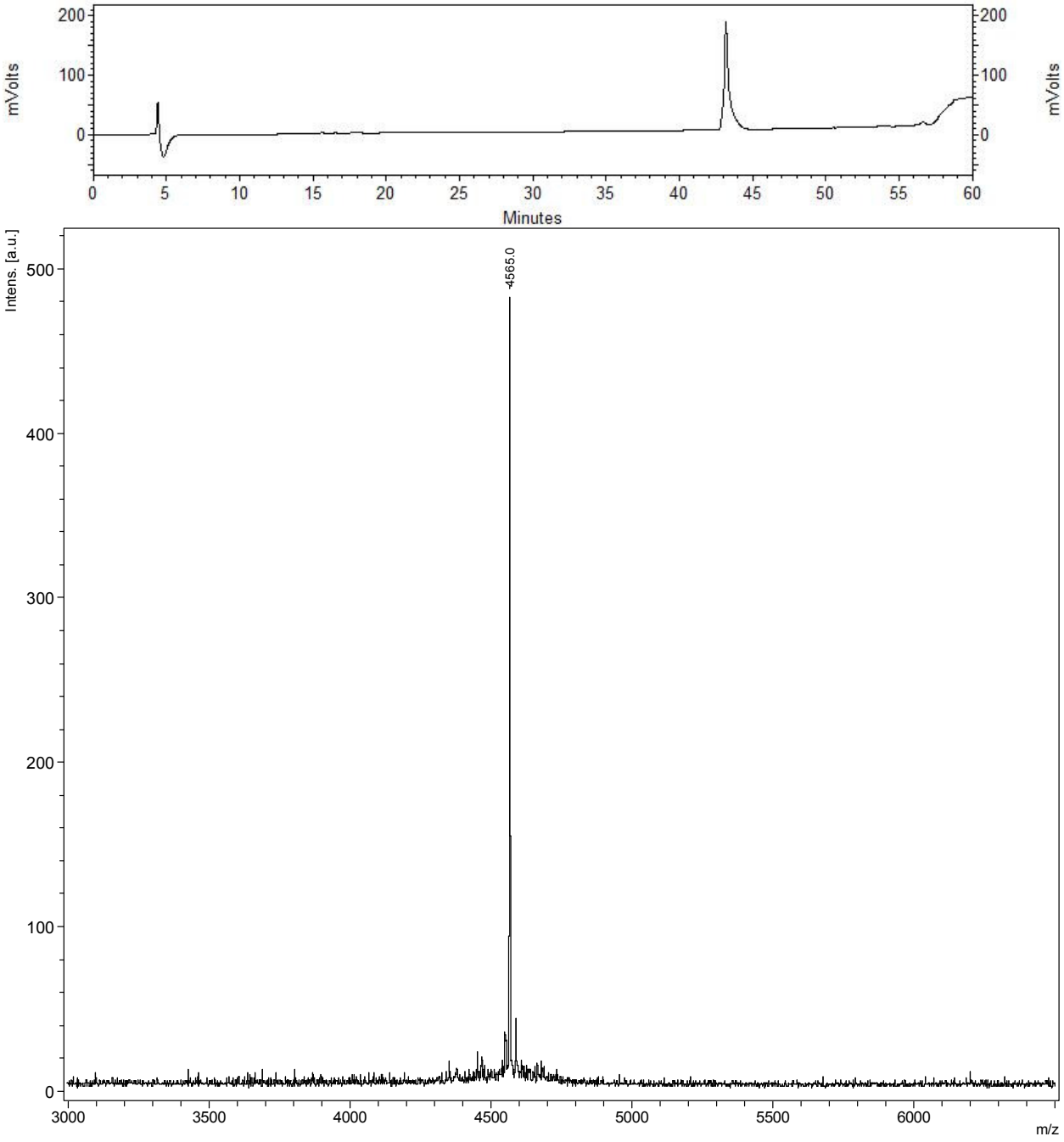

2.22

HPLC: Gradient = 10-60% solvent B over 50 minutes

MALDI-TOF: Calculated monoisotopic $[M+H]^+ = 4605.2$

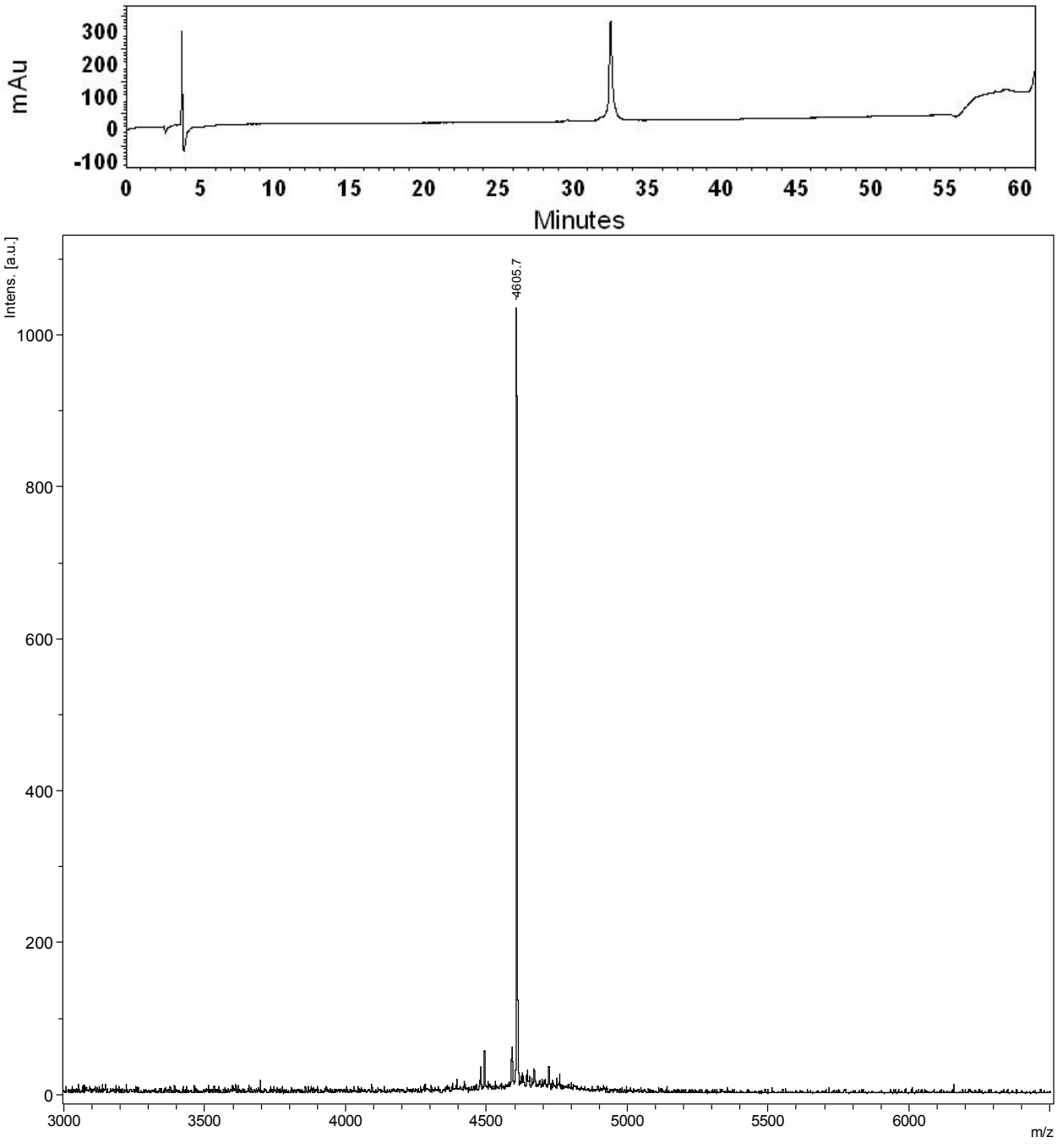

2.23

HPLC: Gradient = 10-90% solvent B over 80 minutes. Peak at ~4 min is DMSO.

MALDI-TOF: Calculated monoisotopic $[M+H]^+$ = 4567.2

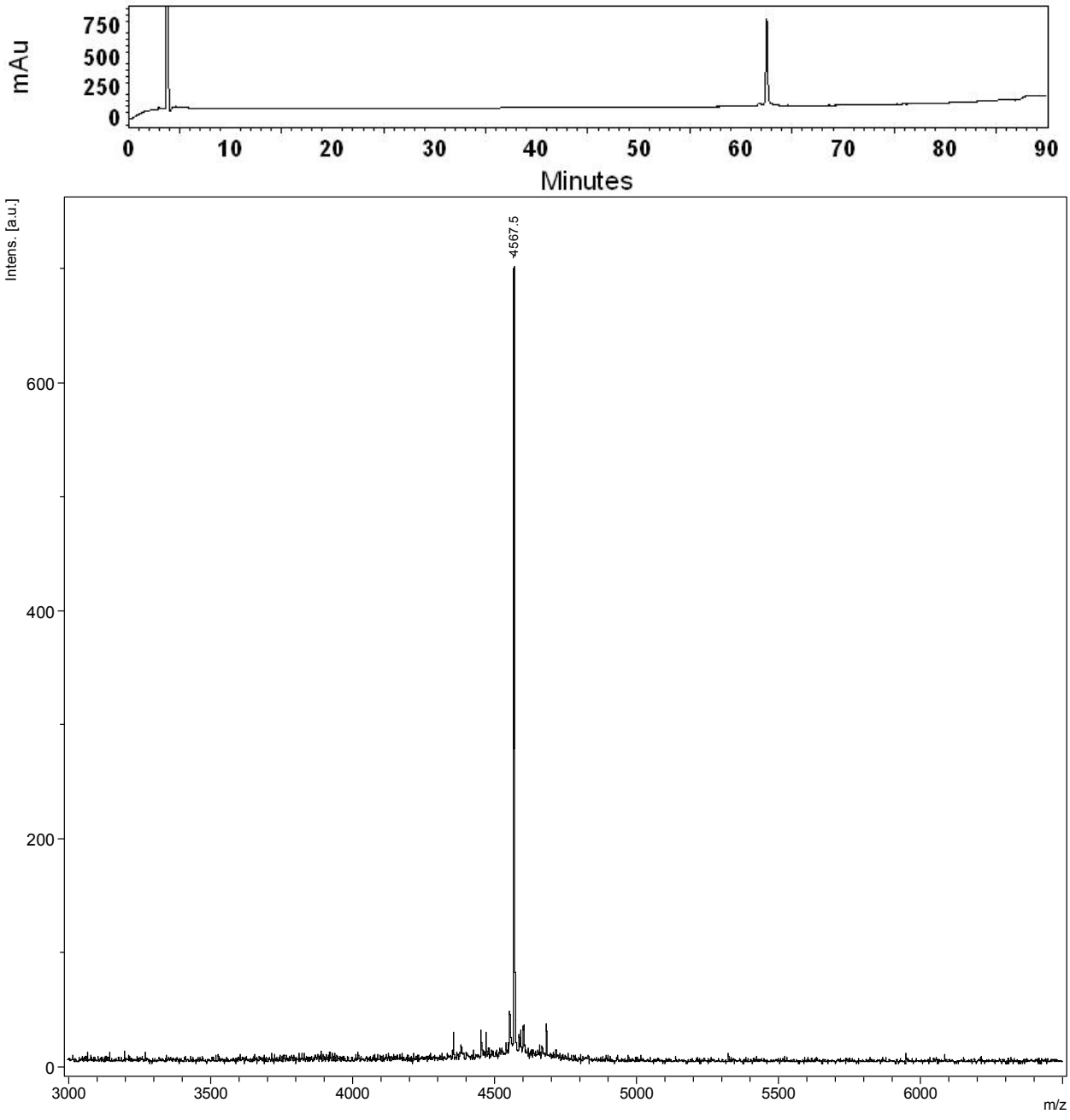

2.24

HPLC: Gradient = 10-90% solvent B over 80 minutes. Peak at ~4 min is DMSO.
MALDI-TOF: Calculated monoisotopic $[M+H]^+$ = 4593.2

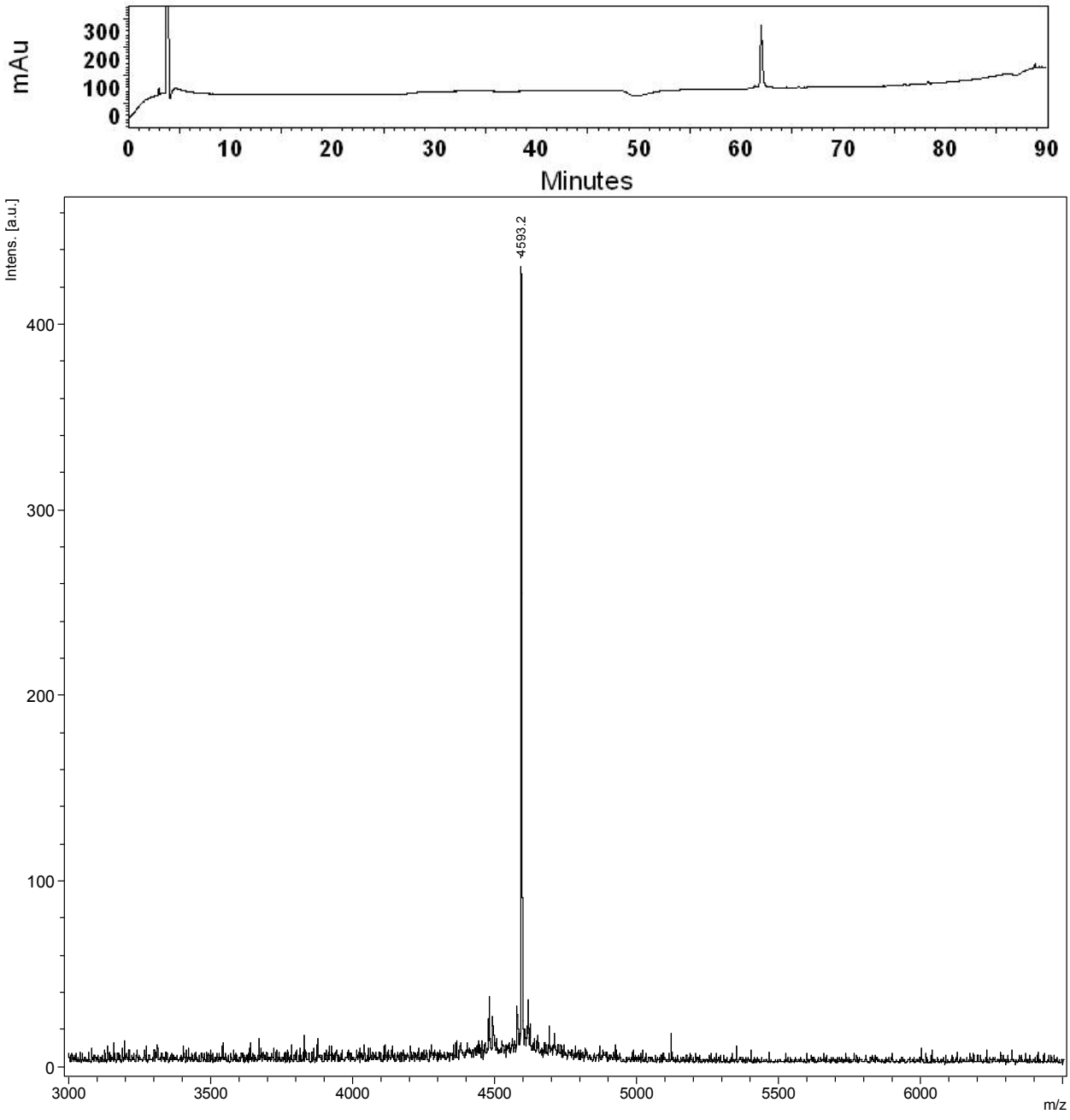

2.25

HPLC: Gradient = 10-90% solvent B over 80 minutes. Peak at ~4 min is DMSO.

MALDI-TOF: Calculated monoisotopic $[M+H]^+ = 4593.2$

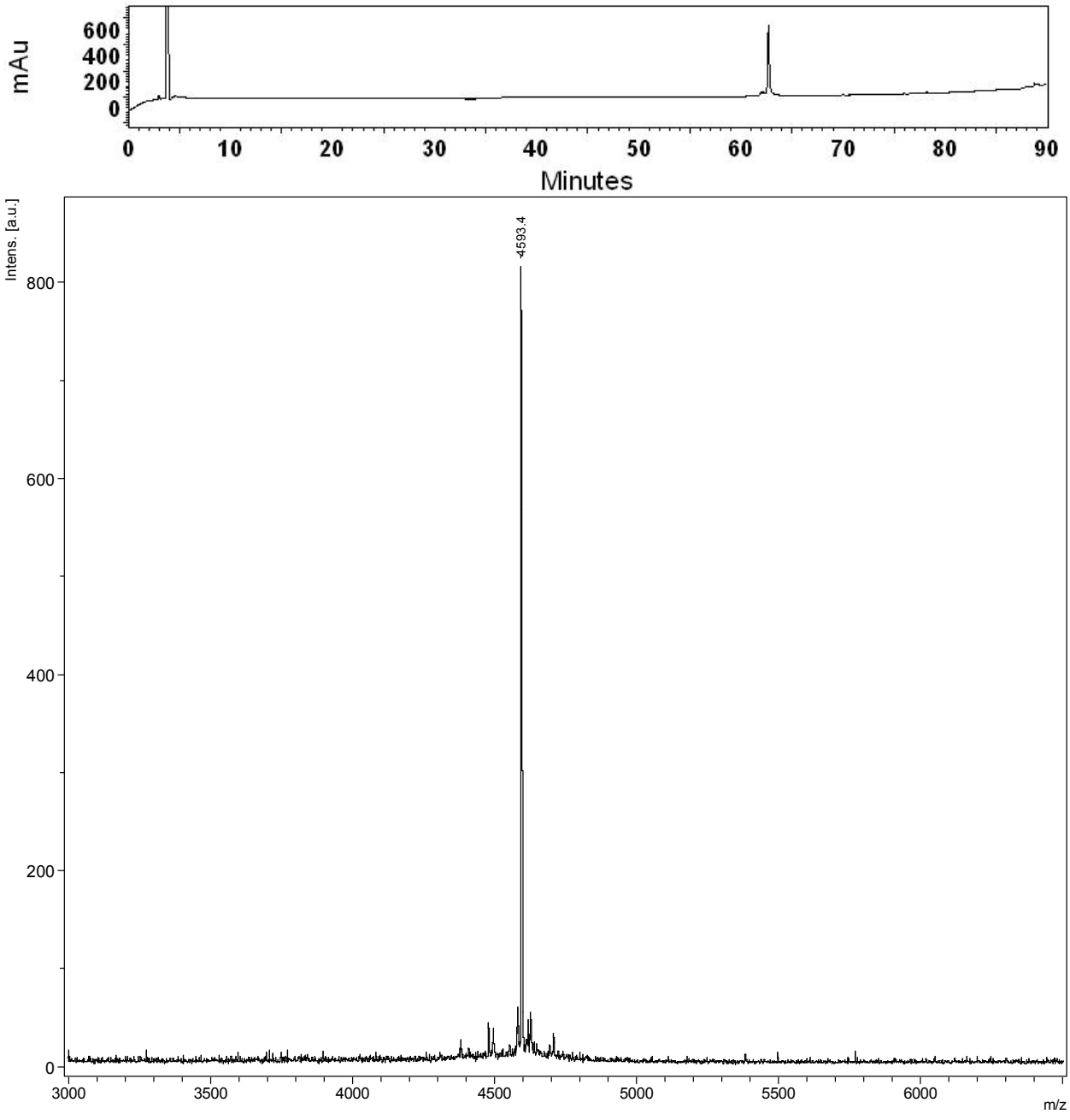

2.26

HPLC: Gradient = 10-60% solvent B over 50 minutes

MALDI-TOF: Calculated monoisotopic $[M+H]^+ = 4690.3$

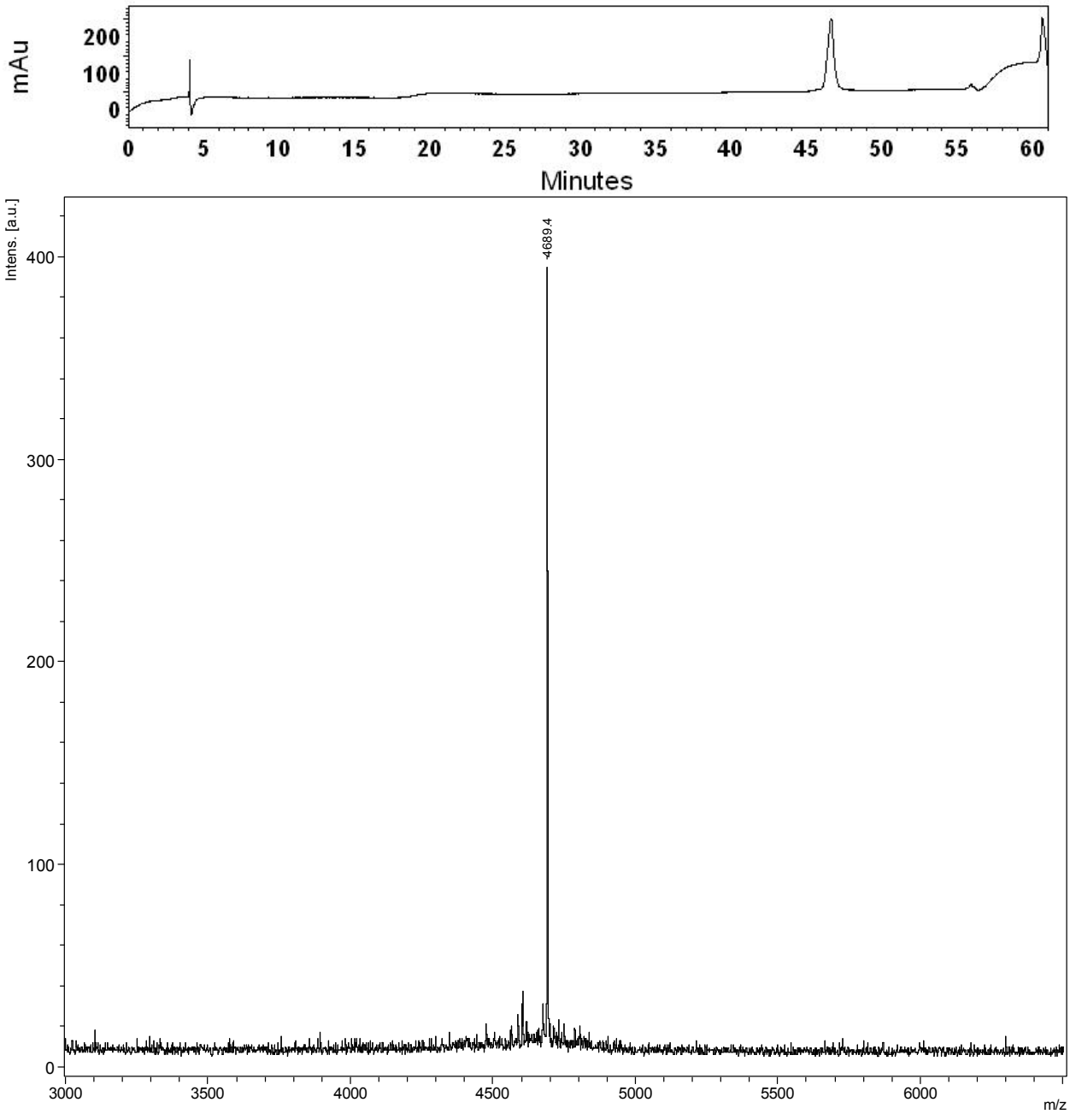

2.27
HPLC: Gradient = 10-60% solvent B over 50 minutes
MALDI-TOF: Calculated monoisotopic $[M+H]^+ = 4690.3$

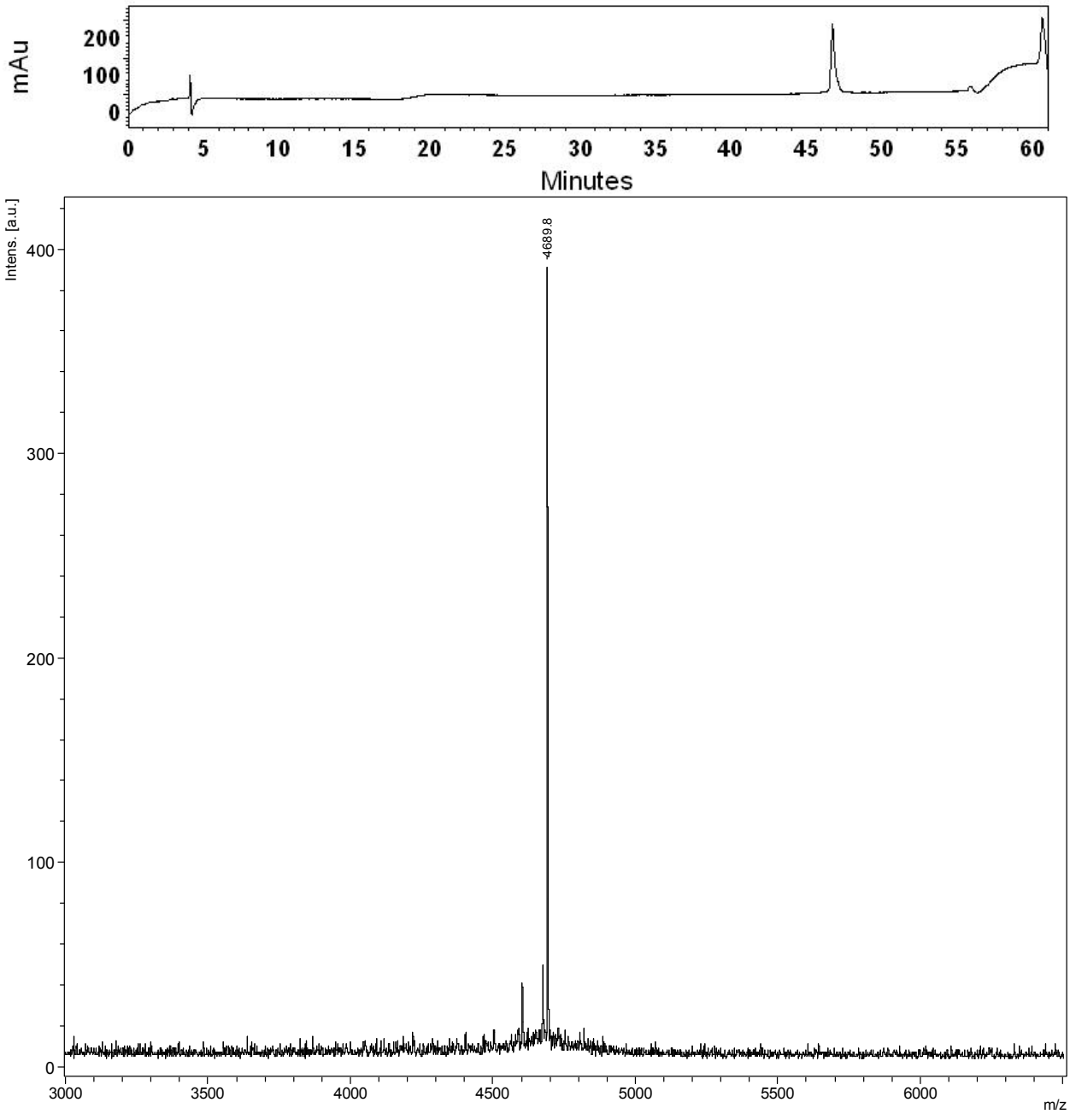

2.28

HPLC: Gradient = 10-60% solvent B over 50 minutes

MALDI-TOF: Calculated monoisotopic $[M+H]^+ = 4607.3$

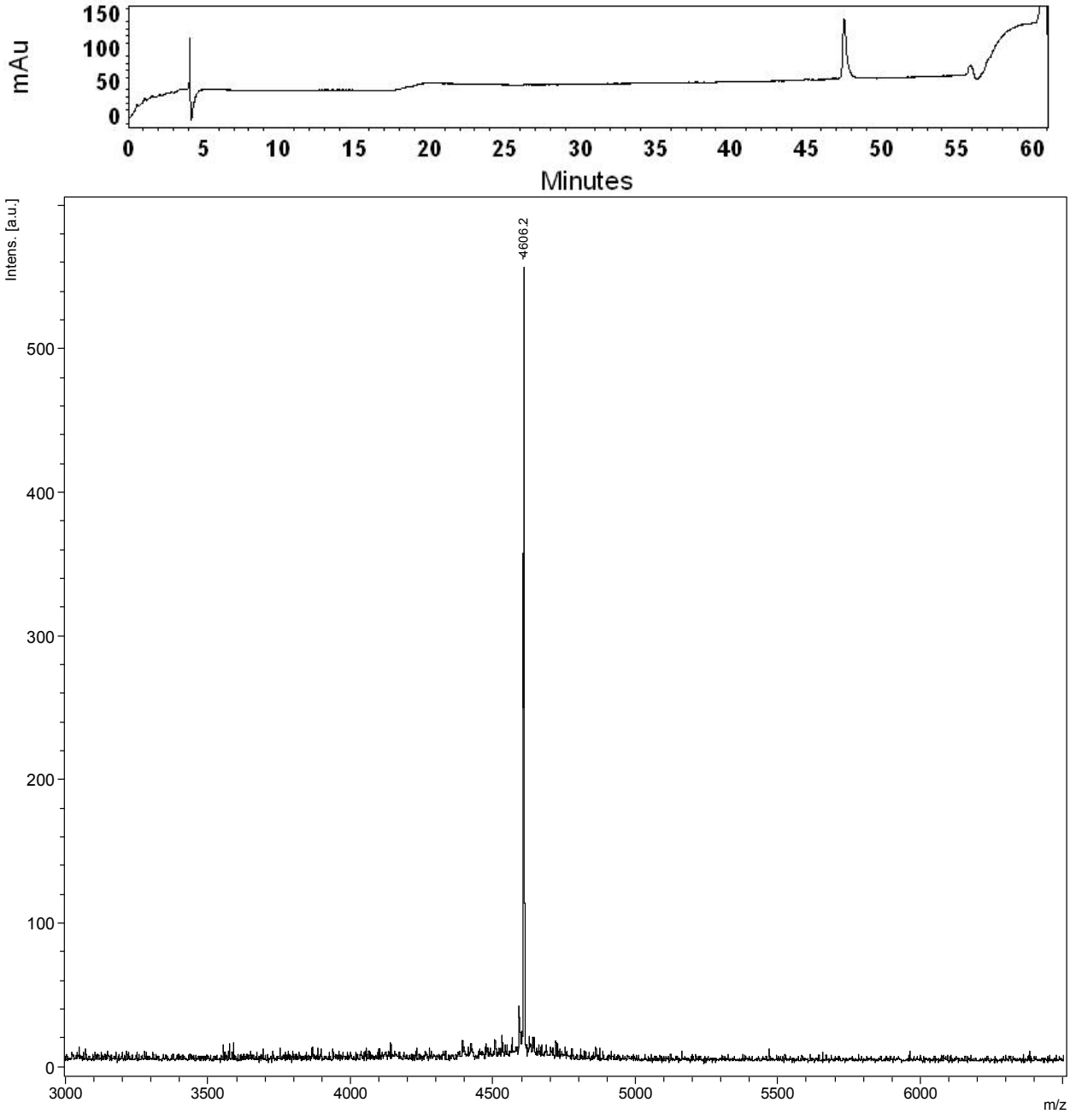

2.29

HPLC: Gradient = 10-60% solvent B over 50 minutes

MALDI-TOF: Calculated monoisotopic $[M+H]^+ = 4564.2$

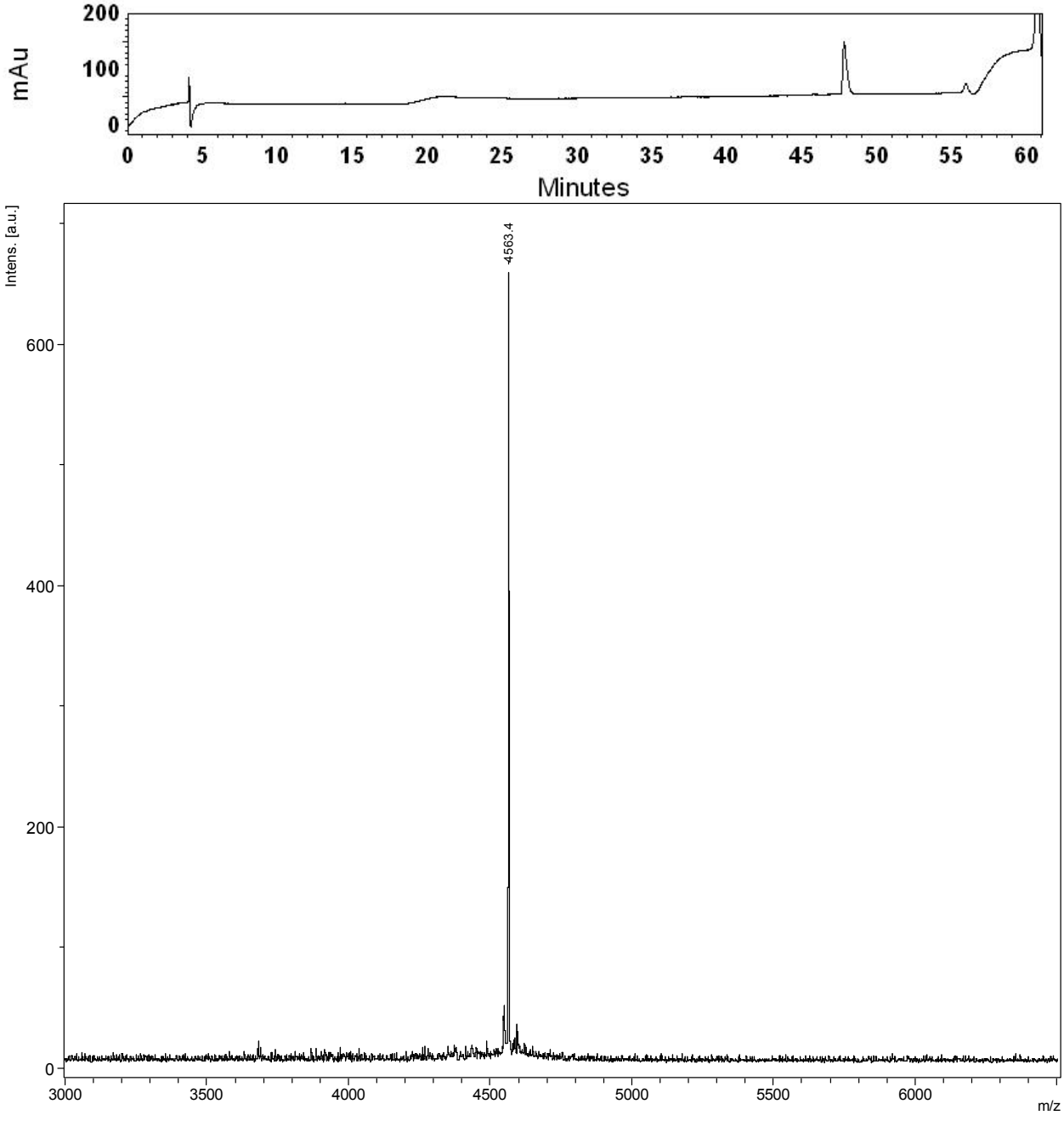

2.30

HPLC: Gradient = 10-60% solvent B over 50 minutes

MALDI-TOF: Calculated monoisotopic $[M+H]^+ = 4633.3$

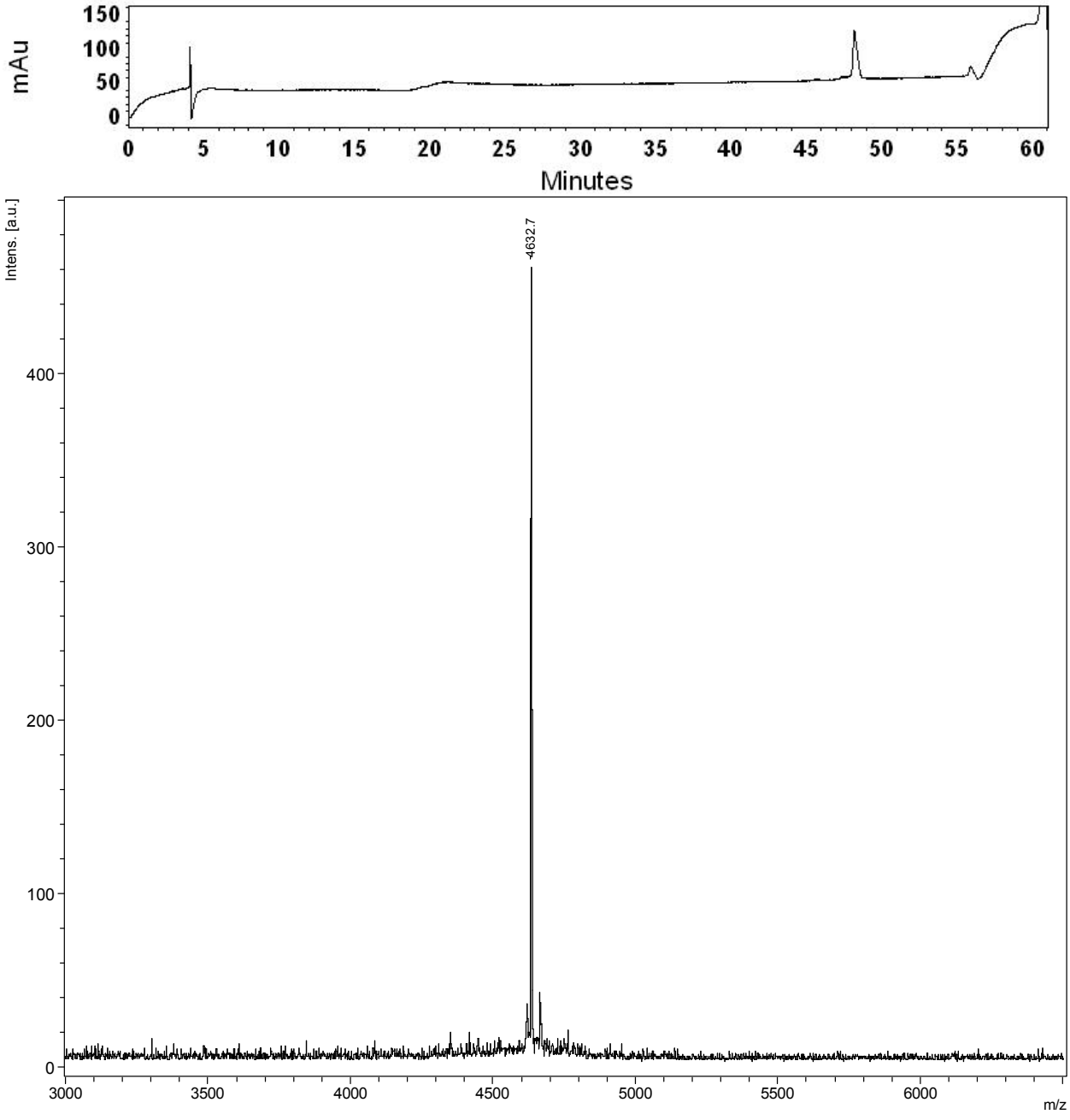

2.31

HPLC: Gradient = 10-60% solvent B over 50 minutes

MALDI-TOF: Calculated monoisotopic $[M+H]^+ = 4590.3$

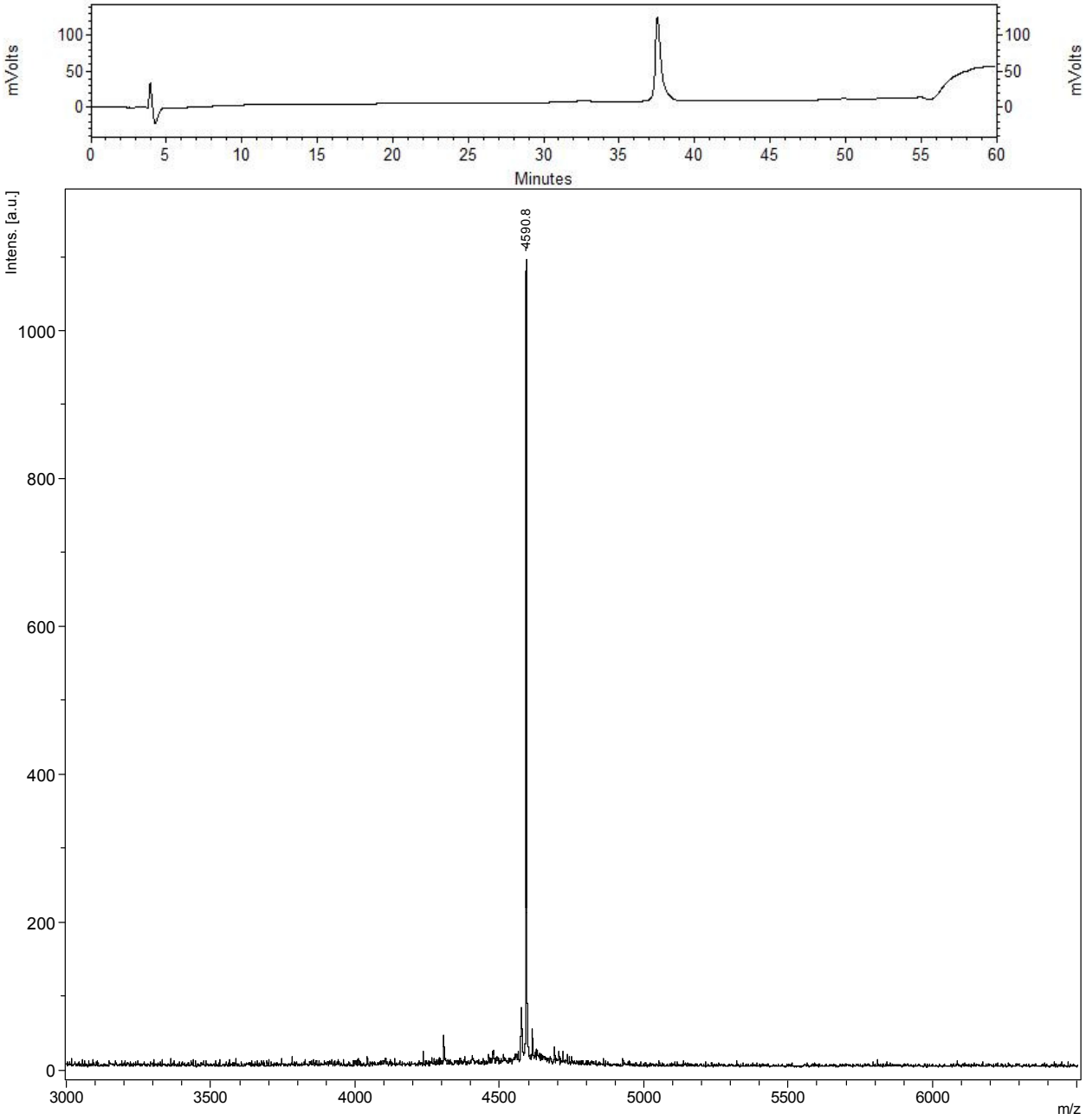

2.32

HPLC: Gradient = 10-60% solvent B over 50 minutes

MALDI-TOF: Calculated monoisotopic $[M+H]^+ = 4713.3$

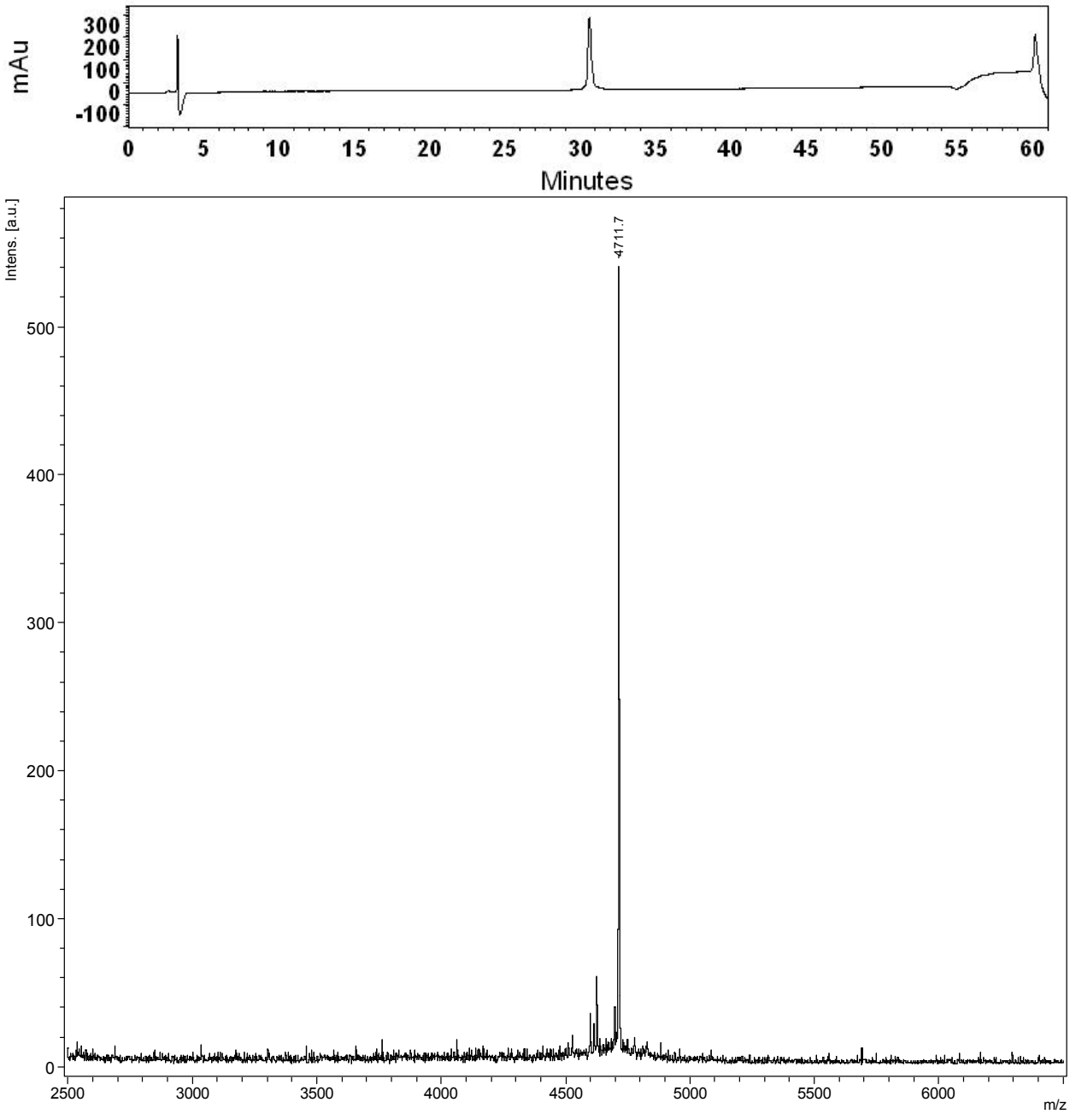

2.33

HPLC: Gradient = 10-60% solvent B over 50 minutes

MALDI-TOF: Calculated monoisotopic $[M+H]^+ = 4612.3$

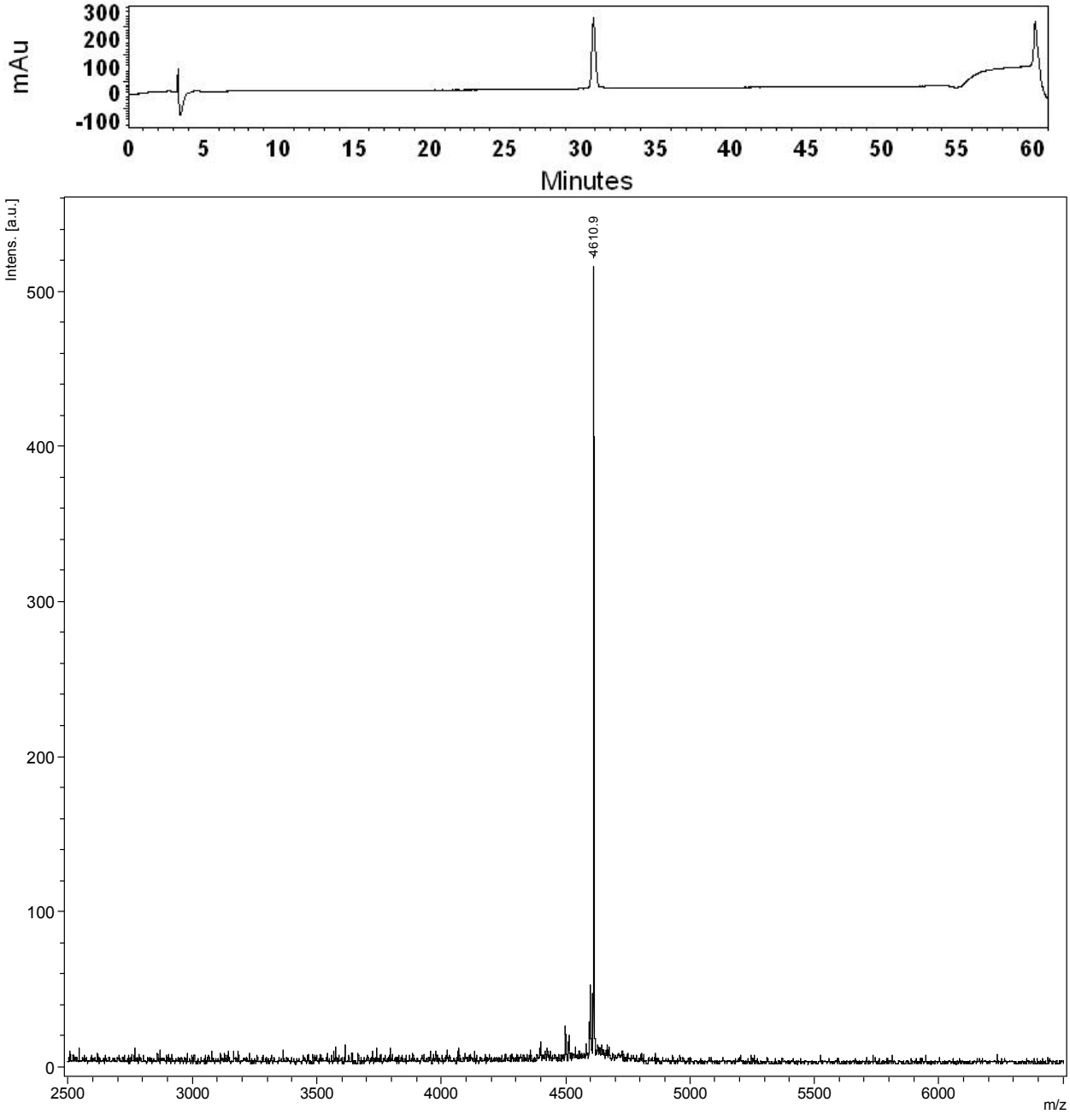

2.34

HPLC: Gradient = 10-60% solvent B over 50 minutes

MALDI-TOF: Calculated monoisotopic $[M+H]^+ = 4284.2$

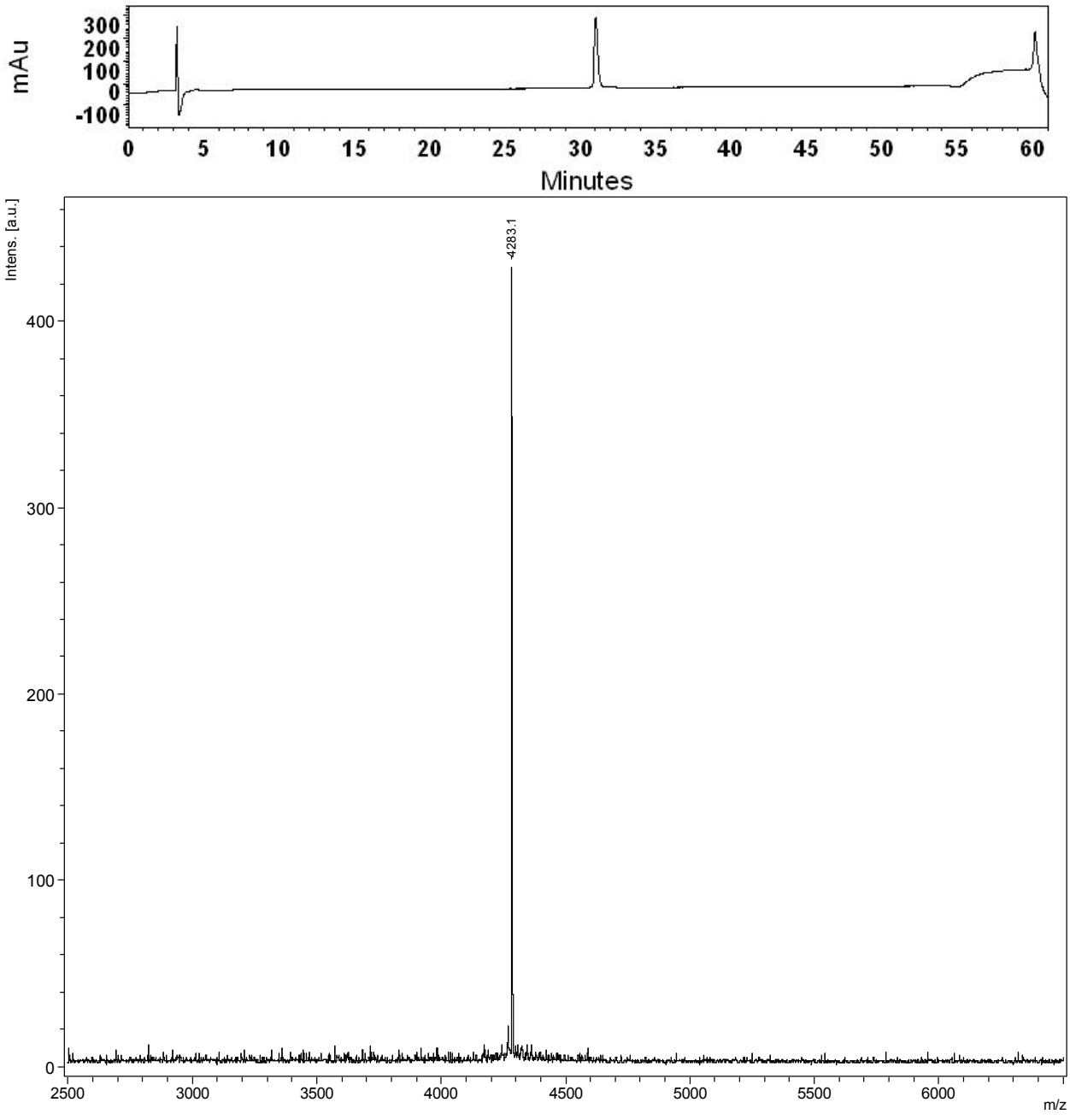

2.35

HPLC: Gradient = 10-60% solvent B over 50 minutes

MALDI-TOF: Calculated monoisotopic $[M+H]^+ = 3895.0$

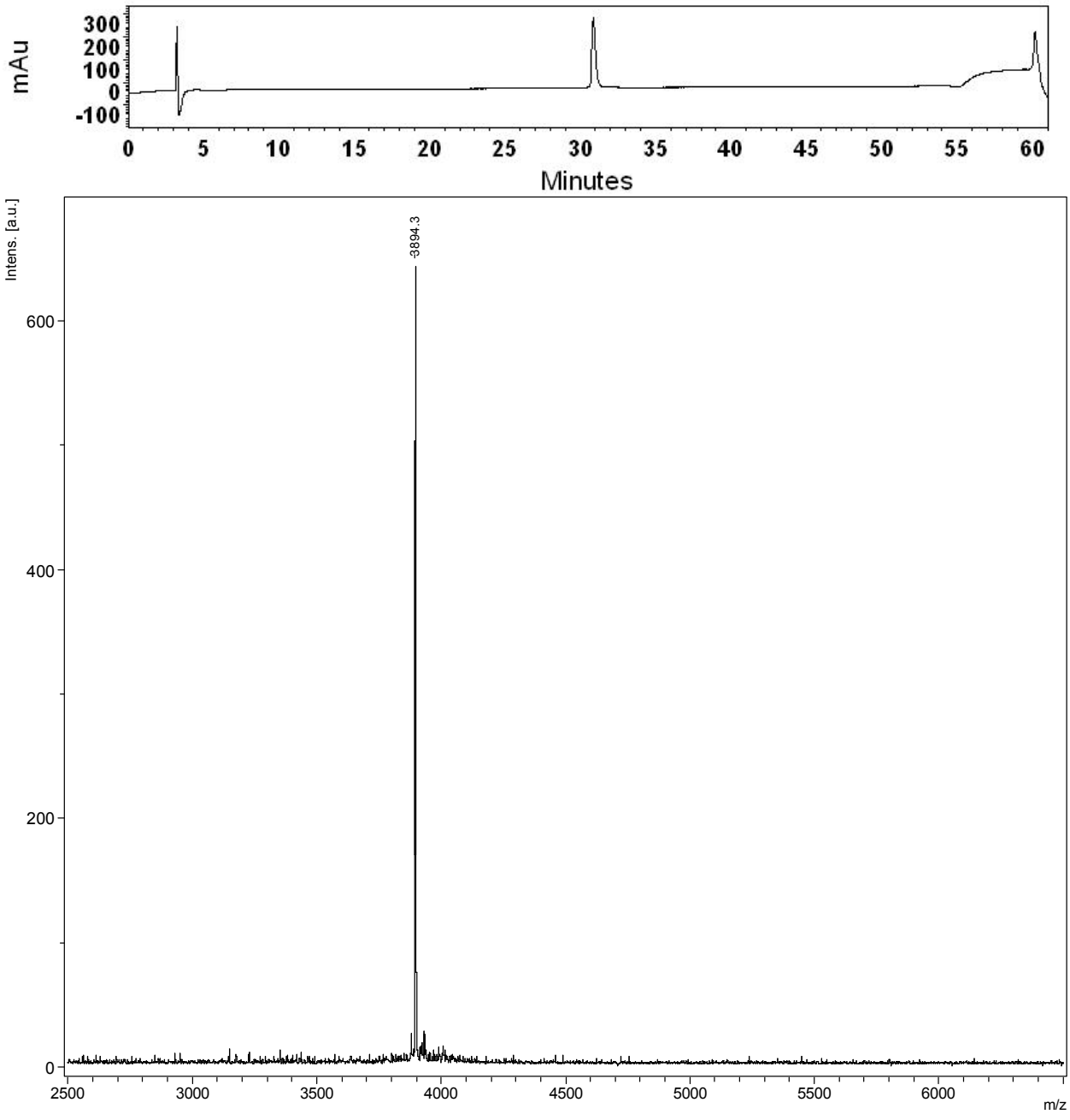

2.36

HPLC: Gradient = 10-60% solvent B over 50 minutes

MALDI-TOF: Calculated monoisotopic $[M+H]^+ = 4557.3$

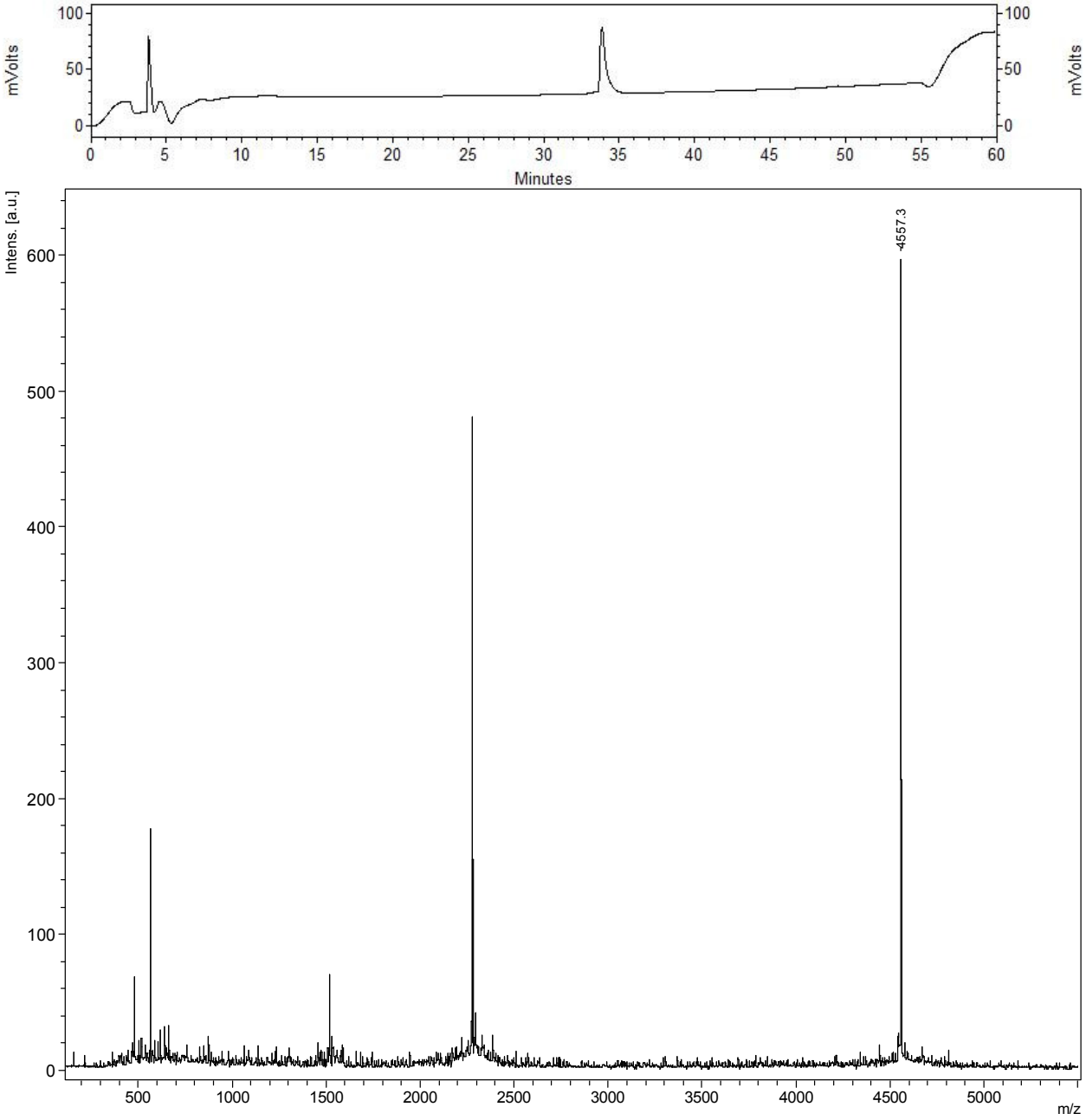

2.37

HPLC: Gradient = 10-60% solvent B over 50 minutes

MALDI-TOF: Calculated monoisotopic $[M+H]^+ = 4585.3$

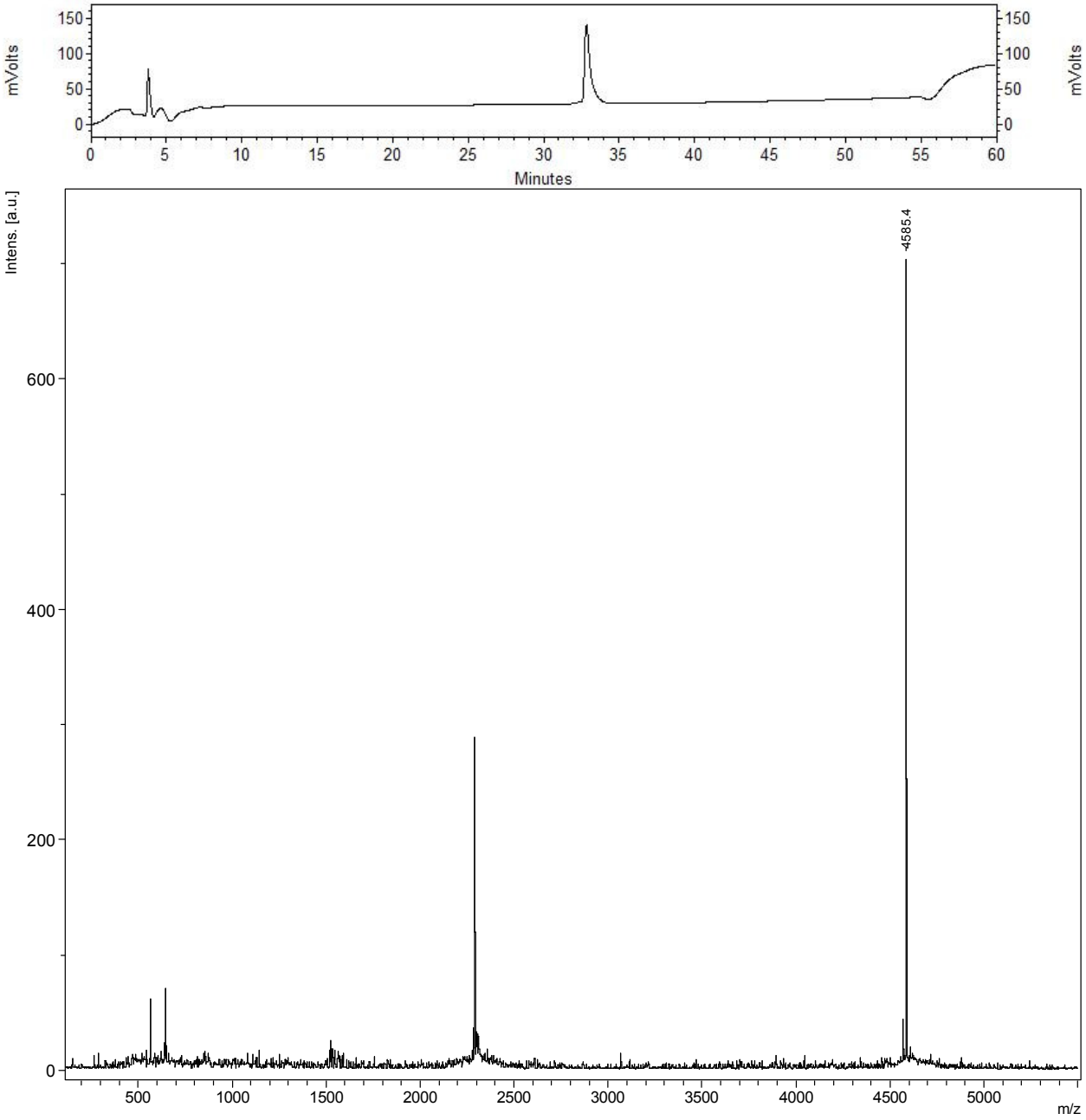

2.38

HPLC: Gradient = 10-60% solvent B over 50 minutes

MALDI-TOF: Calculated monoisotopic $[M+H]^+ = 4243.2$

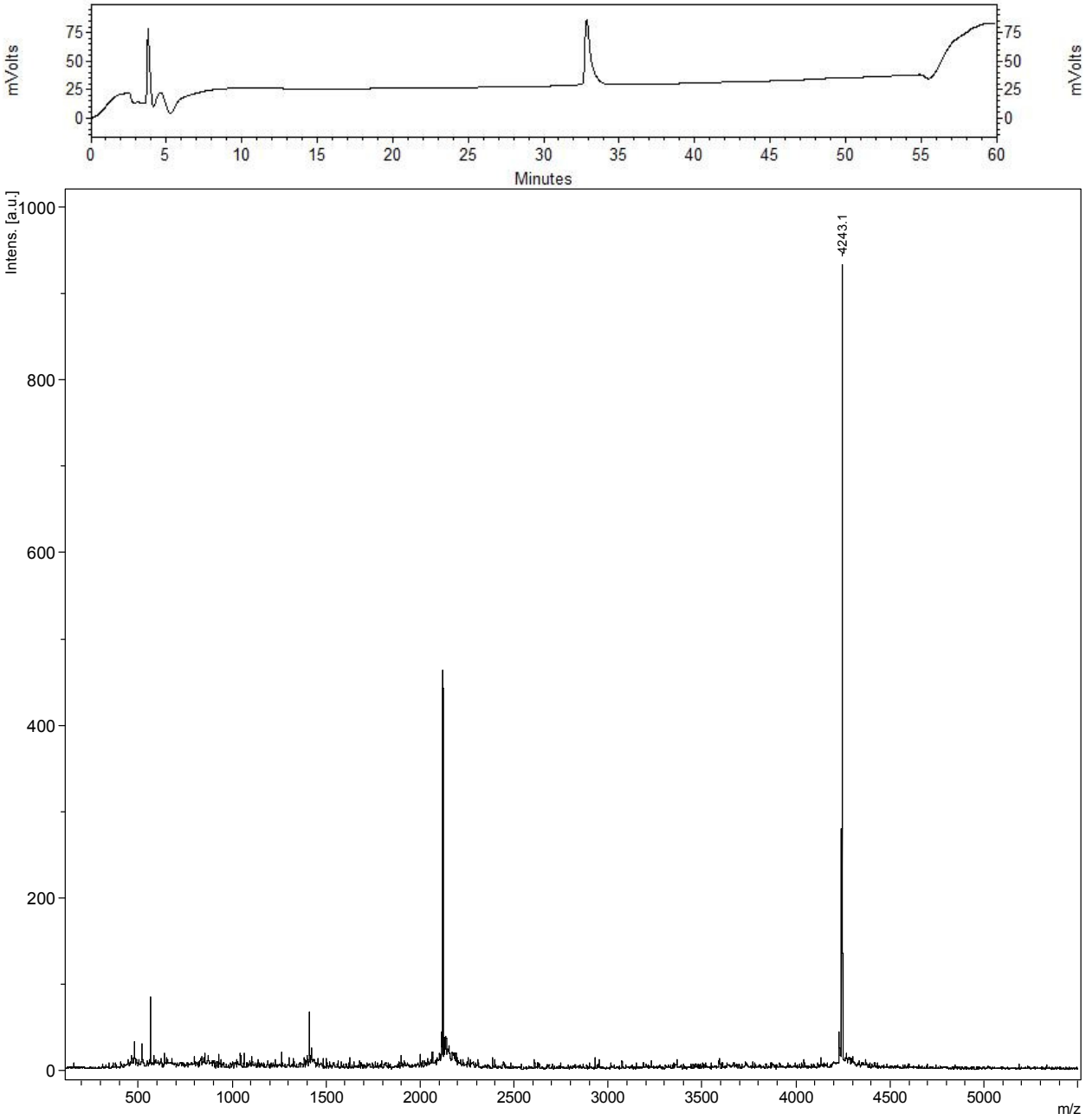

2.39

HPLC: Gradient = 10-60% solvent B over 50 minutes

MALDI-TOF: Calculated monoisotopic $[M+H]^+ = 4514.3$

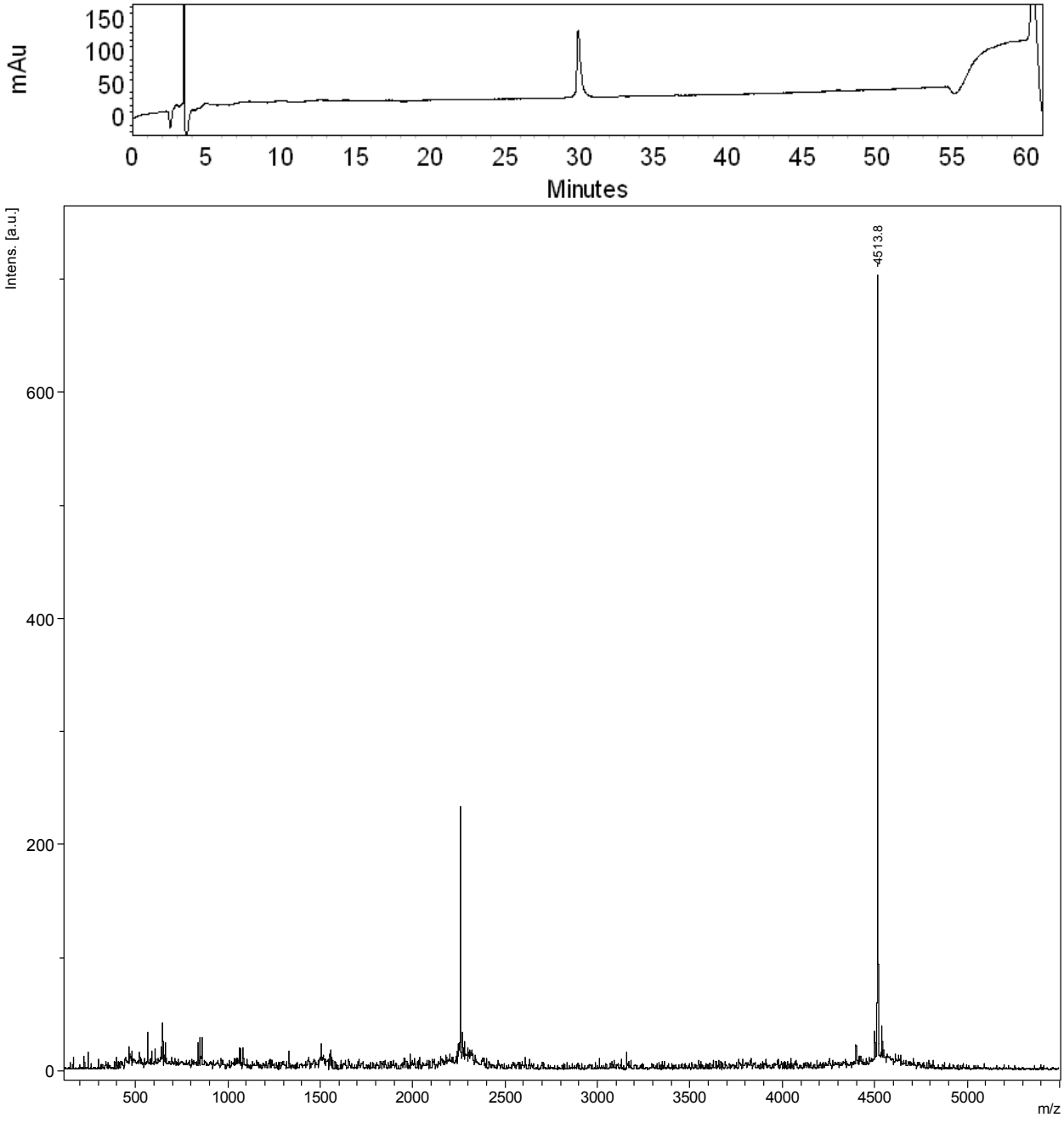

2.40

HPLC: Gradient = 10-60% solvent B over 50 minutes

MALDI-TOF: Calculated monoisotopic $[M+H]^+ = 4542.3$

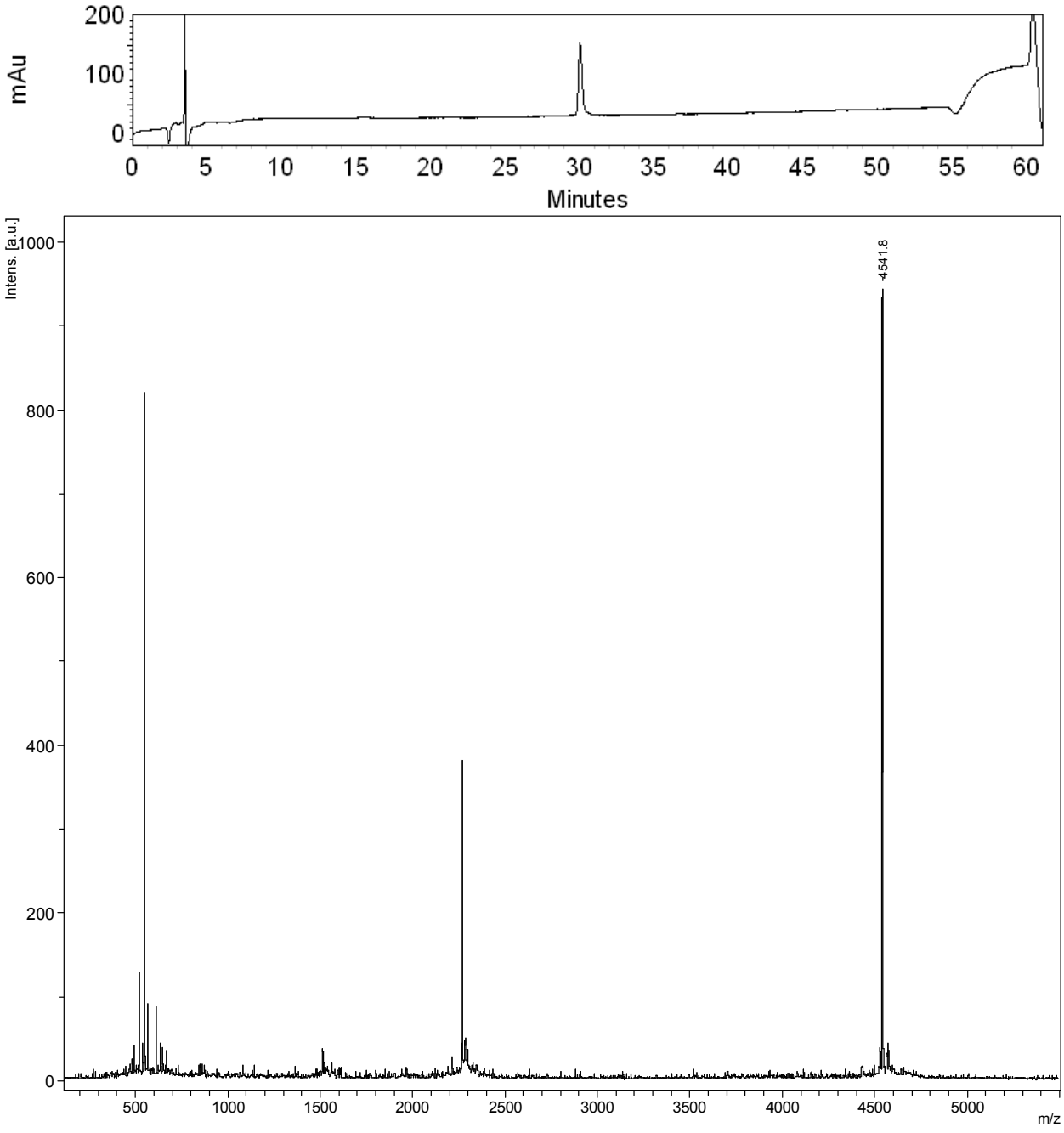

2.41

HPLC: Gradient = 10-60% solvent B over 50 minutes

MALDI-TOF: Calculated monoisotopic $[M+H]^+ = 4200.2$

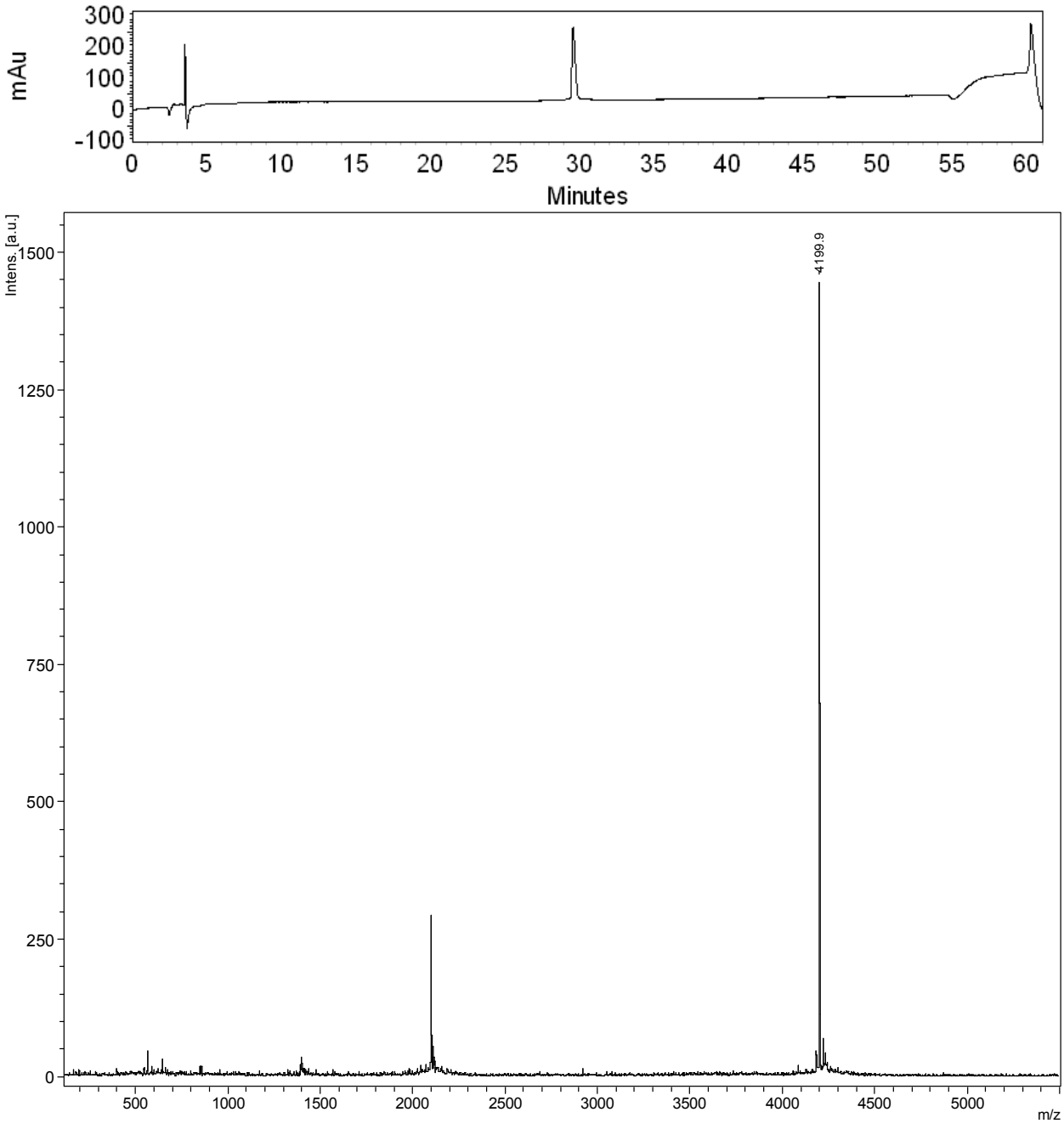

2.42

HPLC: Gradient = 10-60% solvent B over 50 minutes

MALDI-TOF: Calculated monoisotopic $[M+H]^+ = 4518.4$

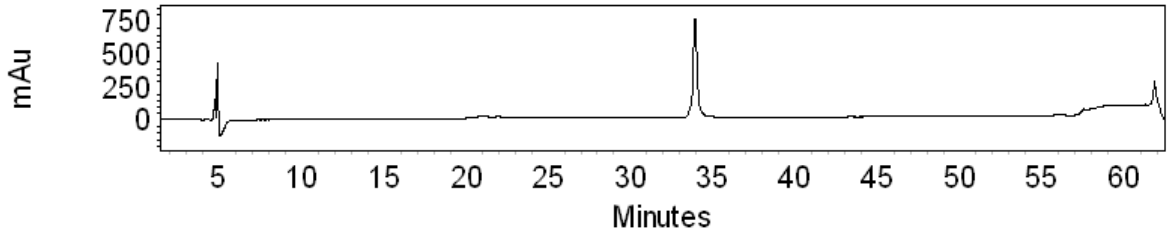

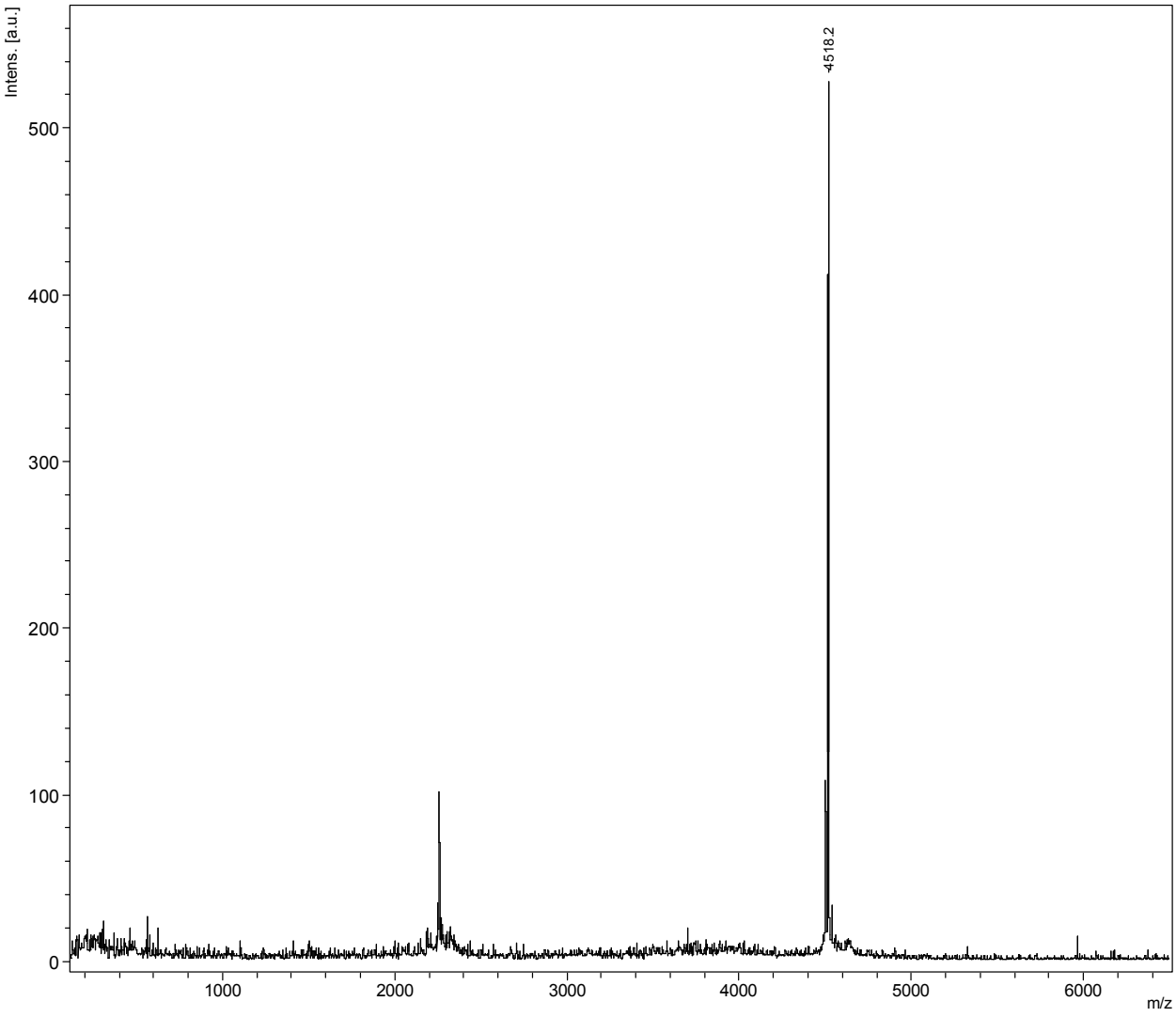

BODIPY-v114*$_{\Delta NT}$
HPLC: Gradient = 10-60% solvent B over 50 minutes
MALDI-TOF: Calculated monoisotopic $[M+H]^+$ = 2613.2

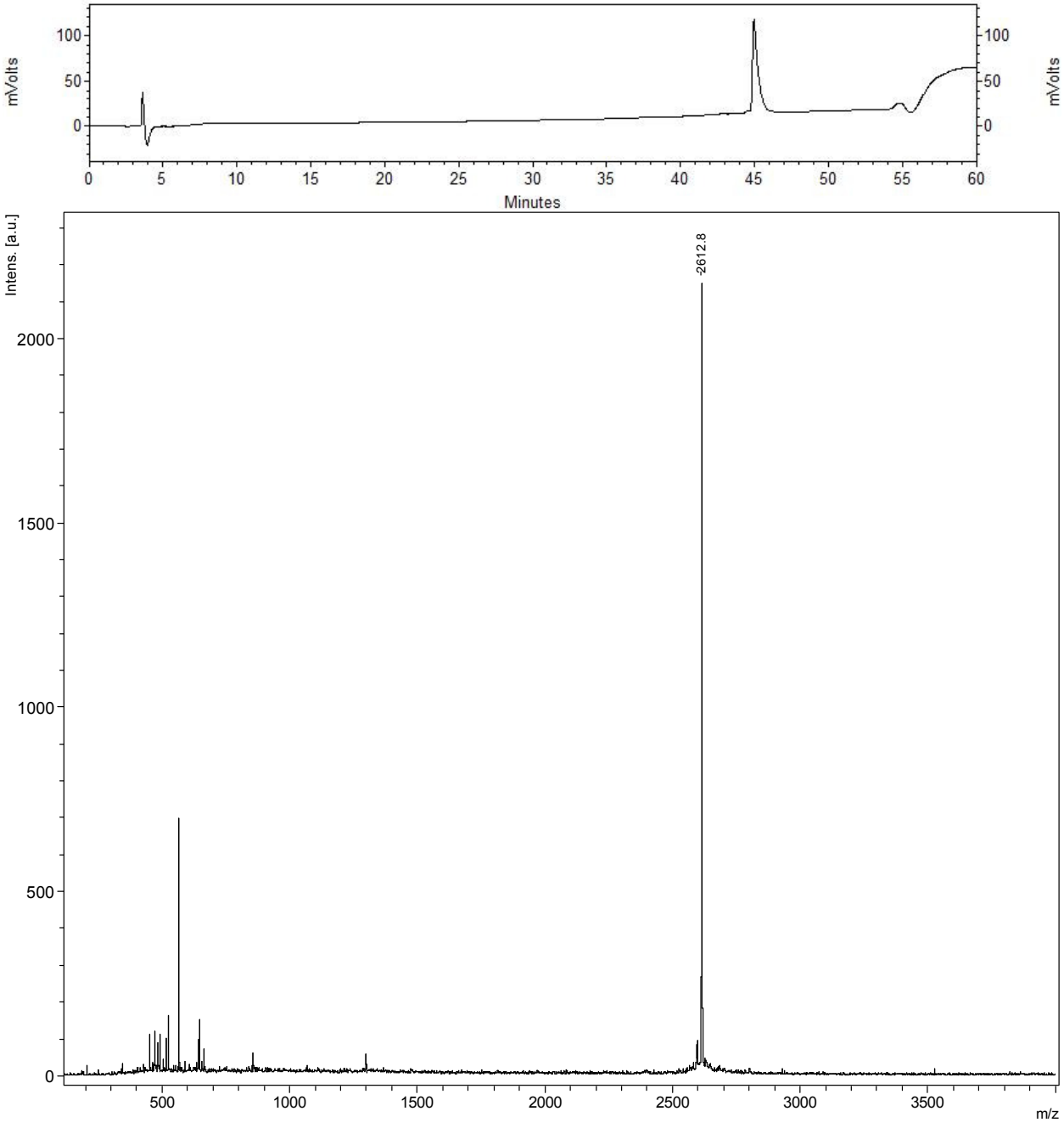

2.11 References

1. Ferrara, N., and DavisSmyth, T. (1997) The biology of vascular endothelial growth factor, *Endocrine Reviews 18*, 4-25.
2. Ferrara, N., Gerber, H. P., and LeCouter, J. (2003) The biology of VEGF and its receptors, *Nature Medicine 9*, 669-676.
3. Carmeliet, P. (2000) Mechanisms of angiogenesis and arteriogenesis, *Nature Medicine 6*, 389-395.
4. Carmeliet, P., and Jain, R. K. (2011) Molecular mechanisms and clinical applications of angiogenesis, *Nature 473*, 298-307.
5. Olsson, A. K., Dimberg, A., Kreuger, J., and Claesson-Welsh, L. (2006) VEGF receptor signalling - in control of vascular function, *Nature Reviews Molecular Cell Biology 7*, 359-371.
6. Muller, Y. A., Li, B., Christinger, H. W., Wells, J. A., Cunningham, B. C., and DeVos, A. M. (1997) Vascular endothelial growth factor: Crystal structure and functional mapping of the kinase domain receptor binding site, *Proceedings of the National Academy of Sciences of the United States of America 94*, 7192-7197.
7. Wiesmann, C., Fuh, G., Christinger, H. W., Eigenbrot, C., Wells, J. A., and deVos, A. M. (1997) Crystal structure at 1.7 angstrom resolution of VEGF in complex with domain 2 of the Flt-1 receptor, *Cell 91*, 695-704.
8. DavisSmyth, T., Chen, H., Park, J., Presta, L. G., and Ferrara, N. (1996) The second immunoglobulin-like domain of the VEGF tyrosine kinase receptor Flt-1 determines ligand binding and may initiate a signal transduction cascade, *Embo Journal 15*, 4919-4927.
9. Lo Conte, L., Chothia, C., and Janin, J. (1999) The atomic structure of protein-protein recognition sites, *Journal of Molecular Biology 285*, 2177-2198.
10. Kim, K. J., Li, B., Winer, J., Armanini, M., Gillett, N., Phillips, H. S., and Ferrara, N. (1993) Inhibititon of vascular endothelial growth factor-induced angiogenesis suppresses tumor growth in vivo, *Nature 362*, 841-844.
11. Ferrara, N., Hillan, K. J., Gerber, H. P., and Novotny, W. (2004) Discovery and development of bevacizumab, an anti-VEGF antibody for treating cancer, *Nature Reviews Drug Discovery 3*, 391-400.
12. Ferrara, N., and Kerbel, R. S. (2005) Angiogenesis as a therapeutic target, *Nature 438*, 967-974.
13. Grothey, A., and Galanis, E. (2009) Targeting angiogenesis: progress with anti-VEGF treatment with large molecules, *Nature Reviews Clinical Oncology 6*, 507-518.
14. Heier, J. S., Brown, D. M., Chong, V., Korobelnik, J. F., Kaiser, P. K., Nguyen, Q. D., Kirchhof, B., Ho, A., Ogura, Y., Yancopoulos, G. D., Stahl, N., Vitti, R., Berliner, A. J., Soo, Y., Anderesi, M., Groetzbach, G., Sommerauer, B., Sandbrink, R., Simader, C.,

Schmidt-Erfurth, U., and Grp, V. V. S. (2012) Intravitreal Aflibercept (VEGF Trap-Eye) in Wet Age-related Macular Degeneration, *Ophthalmology 119*, 2537-2548.

15. Fairbrother, W. J., Christinger, H. W., Cochran, A. G., Fuh, C., Keenan, C. J., Quan, C., Shriver, S. K., Tom, J. Y. K., Wells, J. A., and Cunningham, B. C. (1998) Novel peptides selected to bind vascular endothelial growth factor target the receptor-binding site, *Biochemistry 37*, 17754-17764.

16. Pan, B., Li, B., Russell, S. J., Tom, J. Y. K., Cochran, A. G., and Fairbrother, W. J. (2002) Solution structure of a phage-derived peptide antagonist in complex with vascular endothelial growth factor, *Journal of Molecular Biology 316*, 769-787.

17. Mandal, K., Uppalapati, M., Ault-Riche, D., Kenney, J., Lowitz, J., Sidhu, S. S., and Kent, S. B. H. (2012) Chemical synthesis and X-ray structure of a heterochiral {D-protein antagonist plus vascular endothelial growth factor} protein complex by racemic crystallography, *Proceedings of the National Academy of Sciences of the United States of America 109*, 14779-14784.

18. Fedorova, A., Zobel, K., Gill, H. S., Ogasawara, A., Flores, J. E., Tinianow, J. N., Vanderbilt, A. N., Wu, P., Meng, Y. G., Williams, S. P., Wiesmann, C., Murray, J., Marik, J., and Deshayes, K. (2011) The Development of Peptide-Based Tools for the Analysis of Angiogenesis, *Chemistry & Biology 18*, 839-845.

19. Horne, W. S., Boersma, M. D., Windsor, M. A., and Gellman, S. H. (2008) Sequence-based design of alpha/beta-peptide foldamers that mimic BH3 domains, *Angewandte Chemie-International Edition 47*, 2853-2856.

20. Horne, W. S., Johnson, L. M., Ketas, T. J., Klasse, P. J., Lu, M., Moore, J. P., and Gellman, S. H. (2009) Structural and biological mimicry of protein surface recognition by alpha/beta-peptide foldamers, *Proceedings of the National Academy of Sciences of the United States of America 106*, 14751-14756.

21. Boersma, M. D., Haase, H. S., Peterson-Kaufman, K. J., Lee, E. F., Clarke, O. B., Colman, P. M., Smith, B. J., Horne, W. S., Fairlie, W. D., and Gellman, S. H. (2012) Evaluation of Diverse alpha/beta-Backbone Patterns for Functional alpha-Helix Mimicry: Analogues of the Bim BH3 Domain, *Journal of the American Chemical Society 134*, 315-323.

22. Peterson-Kaufman, K. J., Haase, H. S., Boersma, M. D., Lee, E. F., Fairlie, W. D., and Gellman, S. H. (2015) Residue-Based Preorganization of BH3-Derived α/β-Peptides: Modulating Affinity, Selectivity and Proteolytic Susceptibility in α-Helix Mimics, *ACS Chemical Biology 10*, 1667-1675.

23. Cheloha, R. W., Maeda, A., Dean, T., Gardella, T. J., and Gellman, S. H. (2014) Backbone modification of a polypeptide drug alters duration of action in vivo, *Nature Biotechnology 32*, 653-655.

24. Johnson, L. M., Barrick, S., Hager, M. V., McFedries, A., Homan, E. A., Rabaglia, M. E., Keller, M. P., Attie, A. D., Saghatelian, A., Bisello, A., and Gellman, S. H. (2014) A Potent alpha/beta-Peptide Analogue of GLP-1 with Prolonged Action in Vivo, *Journal of the American Chemical Society 136*, 12848-12851.

25. Haase, H. S., Peterson-Kaufman, K. J., Levengood, S. K. L., Checco, J. W., Murphy, W. L., and Gellman, S. H. (2012) Extending Foldamer Design beyond alpha-Helix Mimicry: alpha/beta-Peptide Inhibitors of Vascular Endothelial Growth Factor Signaling, *Journal of the American Chemical Society 134*, 7652-7655.

26. Binz, H. K., Amstutz, P., and Pluckthun, A. (2005) Engineering novel binding proteins from nonimmunoglobulin domains, *Nature Biotechnology 23*, 1257-1268.

27. Gronwall, C., and Stahl, S. (2009) Engineered affinity proteins-Generation and applications, *Journal of Biotechnology 140*, 254-269.

28. Lofblom, J., Feldwisch, J., Tolmachev, V., Carlsson, J., Stahl, S., and Frejd, F. Y. (2010) Affibody molecules: Engineered proteins for therapeutic, diagnostic and biotechnological applications, *Febs Letters 584*, 2670-2680.

29. Deisenhofer, J. (1981) Crystallographic refinement and atomic models of a human Fc fragment and its complex with fragment B of Protein A from Staphylococcus aureus at 2.9-A and 2.8-A resolution, *Biochemistry 20*, 2361-2370.

30. Nilsson, B., Moks, T., Jansson, B., Abrahmsen, L., Elmblad, A., Holmgren, E., Henrichson, C., Jones, T. A., and Uhlen, M. (1987) A synthetic IgG-binding domain based on staphylococcal protein A, *Protein Engineering 1*, 107-113.

31. Tashiro, M., Tejero, R., Zimmerman, D. E., Celda, B., Nilsson, B., and Montelione, G. T. (1997) High-resolution solution NMR structure of the Z domain of staphylococcal protein A, *Journal of Molecular Biology 272*, 573-590.

32. Nord, K., Gunneriusson, E., Ringdahl, J., Stahl, S., Uhlen, M., and Nygren, P. A. (1997) Binding proteins selected from combinatorial libraries of an alpha-helical bacterial receptor domain, *Nature Biotechnology 15*, 772-777.

33. Braisted, A. C., and Wells, J. A. (1996) Minimizing a binding domain from protein A, *Proceedings of the National Academy of Sciences of the United States of America 93*, 5688-5692.

34. Starovasnik, M. A., Braisted, A. C., and Wells, J. A. (1997) Structural mimicry of a native protein by a minimized binding domain, *Proceedings of the National Academy of Sciences of the United States of America 94*, 10080-10085.

35. Webster, J. M., Zhang, R., Gambhir, S. S., Cheng, Z., and Syud, F. A. (2009) Engineered Two-Helix Small Proteins for Molecular Recognition, *Chembiochem 10*, 1293-1296.

36. Orlova, A., Magnusson, M., Eriksson, T. L. J., Nilsson, M., Larsson, B., Hoiden-Guthenherg, I., Widstrom, C., Carlsson, J., Tolmachev, V., Stahl, S., and Nilsson, F. Y. (2006) Tumor Imaging using a picomolar affinity HER2 binding affibody molecule, *Cancer Research 66*, 4339-4348.

37. Gilbreth, R. N., and Koide, S. (2012) Structural insights for engineering binding proteins based on non-antibody scaffolds, *Current Opinion in Structural Biology 22*, 413-420.

38. Hoyer, W., Gronwall, C., Jonsson, A., Stahl, S., and Hard, T. (2008) Stabilization of a beta-hairpin in monomeric Alzheimer's amyloid-beta peptide inhibits amyloid formation,

Proceedings of the National Academy of Sciences of the United States of America 105, 5099-5104.

39. Peterson, K. J., Sadowsky, J. D., Scheef, E. A., Pal, S., Kourentzi, K. D., Willson, R. C., Bresnick, E. H., Sheibani, N., and Gellman, S. H. (2008) A fluorescence polarization assay for identifying ligands that bind to vascular endothelial growth factor, *Analytical Biochemistry 378*, 8-14.

40. Nieba, L., Krebber, A., and Pluckthun, A. (1996) Competition BIAcore for measuring true affinities: Large differences from values determined from binding kinetics, *Analytical Biochemistry 234*, 155-165.

41. Pitter, K., Bernal, F., LaBelle, J., and Walensky, L. D. (2008) Dissection of the BCL-2 family signaling network with stabilized alpha-helices of BCL-2 domains, *Programmed Cell Death, the Biology and Therapeutic Implications of Cell Death, Part B 446*, 387-408.

42. Schuck, P. (1997) Reliable determination of binding affinity and kinetics using surface plasmon resonance biosensors, *Current Opinion in Biotechnology 8*, 498-502.

43. Chan, W. C., and White, P. D., (Eds.) (2000) *Fmoc solid phase peptide synthesis*, Oxford University Press, New York.

44. Karle, I. L., and Balaram, P. (1990) Structural characteristics of alpha-helical peptide molecules containing Aib residues, *Biochemistry 29*, 6747-6756.

45. Dwyer, J. J., Wilson, K. L., Davison, D. K., Freel, S. A., Seedorff, J. E., Wring, S. A., Tvermoes, N. A., Matthews, T. J., Greenberg, M. L., and Delmedico, M. K. (2007) Design of helical, oligomeric HIV-1 fusion inhibitor peptides with potent activity against enfuvirtide-resistant virus, *Proceedings of the National Academy of Sciences of the United States of America 104*, 12772-12777.

46. Huyghuesdespointes, B. M. P., Scholtz, J. M., and Baldwin, R. L. (1993) Helical peptides with 3 pairs of Asp-Arg and Glu-Arg residues in different orientations and spacings, *Protein Science 2*, 80-85.

47. Scholtz, J. M., Qian, H., Robbins, V. H., and Baldwin, R. L. (1993) The energetics of ion-pair and hydrogen-bonding interactions in a helical peptides, *Biochemistry 32*, 9668-9676.

48. Cheng, R. P., and DeGrado, W. F. (2001) De novo design of a monomeric helical beta-peptide stabilized by electrostatic interactions, *Journal of the American Chemical Society 123*, 5162-5163.

49. Kritzer, J. A., Tirado-Rives, J., Hart, S. A., Lear, J. D., Jorgensen, W. L., and Schepartz, A. (2005) Relationship between side chain structure and 14-helix stability of beta(3)-peptides in water, *Journal of the American Chemical Society 127*, 167-178.

50. Arvidsson, P. I., Rueping, M., and Seebach, D. (2001) Design, machine synthesis, and NMR-solution structure of a beta-heptapeptide forming a salt-bridge stabilised 3(14)-helix in methanol and in water, *Chemical Communications*, 649-650.

51. Johnson, L. M., Mortenson, D. E., Yun, H. G., Horne, W. S., Ketas, T. J., Lu, M., Moore, J. P., and Gellman, S. H. (2012) Enhancement of alpha-Helix Mimicry by an alpha/beta-Peptide Foldamer via Incorporation of a Dense Ionic Side-Chain Array, *Journal of the American Chemical Society 134*, 7317-7320.

52. Feldwisch, J., Tolmachev, V., Lendel, C., Herne, N., Sjoberg, A., Larsson, B., Rosik, D., Lindqvist, E., Fant, G., Hoiden-Guthenberg, I., Galli, J., Jonasson, P., and Abrahmsen, L. (2010) Design of an Optimized Scaffold for Affibody Molecules, *Journal of Molecular Biology 398*, 232-247.

53. Yamaguchi, H., Kodama, H., Osada, S., Kato, F., Jelokhani-Niaraki, M., and Kondo, M. (2003) Effect of alpha,alpha-dialkyl amino acids on the protease resistance of peptides, *Bioscience Biotechnology and Biochemistry 67*, 2269-2272.

54. Ebeling, W., Hennrich, N., Klockow, M., Metz, H., Orth, H. D., and Lang, H. (1974) Proteinase K from Tritirachium album limber, *European Journal of Biochemistry 47*, 91-97.

55. Horne, W. S., Price, J. L., Keck, J. L., and Gellman, S. H. (2007) Helix bundle quaternary structure from alpha/beta-peptide foldamers, *Journal of the American Chemical Society 129*, 4178-4180.

56. Johnson, L. M., and Gellman, S. H. (2013) alpha-Helix Mimicry with alpha/beta-Peptides, *Methods in Protein Design 523*, 407-429.

57. Antosova, Z., Mackova, M., Kral, V., and Macek, T. (2009) Therapeutic application of peptides and proteins: parenteral forever?, *Trends in Biotechnology 27*, 628-635.

58. Ezzat, K., Zaghloul, E. M., Andaloussi, S. E. L., Lehto, T., El-Sayed, R., Magdy, T., Smith, C. I. E., and Langel, U. (2012) Solid formulation of cell-penetrating peptide nanocomplexes with siRNA and their stability in simulated gastric conditions, *Journal of Controlled Release 162*, 1-8.

59. U.S.Pharmacopeia (2010) *The United States Pharmacopeia (USP 33) and The National Formulary (NF 28)*, United Book Press, Baltimore, MD.

60. Blaskovich, M. A., Lin, Q., Delarue, F. L., Sun, J., Park, H. S., Coppola, D., Hamilton, A. D., and Sebti, S. M. (2000) Design of GFB-111, a platelet-derived growth factor binding molecule with antiangiogenic and anticancer activity against human tumors in mice, *Nature Biotechnology 18*, 1065-1070.

61. Choonara, B. F., Choonara, Y. E., Kumar, P., Bijukumar, D., du Toit, L. C., and Pillay, V. (2014) A review of advanced oral drug delivery technologies facilitating the protection and absorption of protein and peptide molecules, *Biotechnology Advances 32*, 1269-1282.

62. Salic, A., and Mitchison, T. J. (2008) A chemical method for fast and sensitive detection of DNA synthesis in vivo, *Proceedings of the National Academy of Sciences of the United States of America 105*, 2415-2420.

63. Beenken, A., and Mohammadi, M. (2009) The FGF family: biology, pathophysiology and therapy, *Nature Reviews Drug Discovery 8*, 235-253.

64. Skerra, A. (2007) Alternative non-antibody scaffolds for molecular recognition, *Current Opinion in Biotechnology 18*, 295-304.

65. Gunneriusson, E., Nord, K., Uhlen, M., and Nygren, P. A. (1999) Affinity maturation of a Taq DNA polymerase specific affibody by helix shuffling, *Protein Engineering 12*, 873-878.

66. Park, K., and Kwon, I. C. (2011) Oral protein delivery: Current status and future prospect, *Reactive & Functional Polymers 71*, 280-287.

67. Lee, H. S., LePlae, P. R., Porter, E. A., and Gellman, S. H. (2001) An efficient route to either enantiomer of orthogonally protected trans-3-aminopyrrolidine-4-carboxylic acid, *Journal of Organic Chemistry 66*, 3597-3599.

68. Lee, E. F., Smith, B. J., Horne, W. S., Mayer, K. N., Evangelista, M., Colman, P. M., Gellman, S. H., and Fairlie, W. D. (2011) Structural Basis of Bcl-x(L) Recognition by a BH3-Mimetic alpha/beta-Peptide Generated by Sequence-Based Design, *Chembiochem 12*, 2025-2032.

69. Horne, W. S., Price, J. L., and Gellman, S. H. (2008) Interplay among side chain sequence, backbone composition, and residue rigidification in polypeptide folding and assembly, *Proceedings of the National Academy of Sciences of the United States of America 105*, 9151-9156.

70. Gasteiger, E., Hoogland, C., Gattiker, A., Duvaud, S., Wilkins, M. R., Appel, R. D., and Bairoch, A. (2005) Protein identification and analysis tools on the ExPASy server, In *The proteomics protocols handbook* (Walker, J. M., Ed.), pp 571-607, Humana Press.

71. Gill, S. C., and Vonhippel, P. H. (1989) Calculation of protein extinction coefficients from amino-acid sequence data, *Analytical Biochemistry 182*, 319-326.

72. Roehrl, M. H. A., Wang, J. Y., and Wagner, G. (2004) A general framework for development and data analysis of competitive high-throughput screens for small-molecule inhibitors of protein - Protein interactions by fluorescence polarization, *Biochemistry 43*, 16056-16066.

73. Kaufman, K. J. (2010) Investigations in Foldameric Inhibitors of Protein-Protein Interactions: Studies of the Bcl-2 Family of Proteins and Vascular Endothelial Growth Factor, In *Department of Chemistry*, p 220, University of Wisconsin-Madison, Madison, Wisconsin.

74. Greenfield, N. J. (2006) Using circular dichroism spectra to estimate protein secondary structure, *Nature Protocols 1*, 2876-2890.

75. Kabsch, W. (2010) XDS, *Acta Crystallographica Section D-Biological Crystallography 66*, 125-132.

76. McCoy, A. J., Grosse-Kunstleve, R. W., Adams, P. D., Winn, M. D., Storoni, L. C., and Read, R. J. (2007) Phaser crystallographic software, *Journal of Applied Crystallography 40*, 658-674.

77. Afonine, P. V., Grosse-Kunstleve, R. W., Adams, P. D., and Urzhumtsev, A. (2013) Bulk-solvent and overall scaling revisited: faster calculations, improved results, *Acta Crystallographica Section D-Biological Crystallography 69*, 625-634.

78. Afonine, P. V., Grosse-Kunstleve, R. W., Echols, N., Headd, J. J., Moriarty, N. W., Mustyakimov, M., Terwilliger, T. C., Urzhumtsev, A., Zwart, P. H., and Adams, P. D. (2012) Towards automated crystallographic structure refinement with phenix.refine, *Acta Crystallographica Section D-Biological Crystallography 68*, 352-367.

79. Emsley, P., and Cowtan, K. (2004) Coot: model-building tools for molecular graphics, *Acta Crystallographica Section D-Biological Crystallography 60*, 2126-2132.

80. Afonine, P. V., Grosse-Kunstleve, R. W., Urzhumtsev, A., and Adams, P. D. (2009) Automatic multiple-zone rigid-body refinement with a large convergence radius, *Journal of Applied Crystallography 42*, 607-615.

81. Headd, J. J., Echols, N., Afonine, P. V., Grosse-Kunstleve, R. W., Chen, V. B., Moriarty, N. W., Richardson, D. C., Richardson, J. S., and Adams, P. D. (2012) Use of knowledge-based restraints in phenix.refine to improve macromolecular refinement at low resolution, *Acta Crystallographica Section D-Biological Crystallography 68*, 381-390.

Chapter 3: Targeting diverse protein surfaces with α/β-peptides derived from the Z-domain scaffold

Portions of this chapter have been published as:

Checco, J. W., Kreitler, D. F., Thomas, N. C., Belair, D. G., Rettko, N. J., Murphy, W. L., Forest, K. T., and Gellman, S. H. (2015) Targeting diverse protein–protein interaction interfaces with α/β-peptides derived from the Z-domain scaffold, *Proceedings of the National Academy of Sciences of the United States of America 112*, 4552–4557.

Respective contributions:

Research design: James W. Checco, Samuel H. Gellman

Peptide design: James W. Checco, Takayuki Miki (HER2)

Peptide synthesis: James W. Checco, Takayuki Miki, Nicholas J. Rettko, Geoffrey A. Eddinger

ELISA design: James W. Checco (IgG, TNFα, EGFR), Takayuki Miki (HER2)

ELISA experiments: James W. Checco, Takayuki Miki, Nicholas J. Rettko

FP assays: James W. Checco

Pharmacokinetics in mice: James W. Checco, Jiang Zhisheng, Jill Kolesar

IgG1 Fc crystallography: James W. Checco, Dale F. Kreitler, Nicholas J. Rettko, Peter Coleman, W. Douglas Fairlie

Proteolysis: James W. Checco, Geoffrey A. Eddinger

Circular dichroism: Takayuki Miki

HER2 imaging in mice: Benjamin J. Hackel

3.1 Preface

In Chapter 2, I described the design of α/β-peptides that structurally and functionally mimicked the Z-domain-derived α-peptide **Z-VEGF**. α-Peptides derived from the Z-domain mini-protein scaffold are designed to adopt very similar three-helix bundle structures even if multiple changes are made on the protein binding face to derive selective protein binding. Because the α/β-peptide design strategy described in Chapter 2 was successful for the mimicry of one α-peptide derived from the Z-domain scaffold, we hypothesized the same strategy may successfully mimic other α-peptides from this scaffold family to rapidly derive α/β-peptides that target different protein surfaces. The primary goal for the research described in this chapter was to test this hypothesis by endeavoring to mimic other Z-domain-derived α-peptides with the same α/β-peptide design strategy outlined in Chapter 2. To this end, we successfully developed α/β-peptide mimics of Z-domain peptides targeting the Fc fragment of IgG and the inflammatory cytokine tumor necrosis factor-α (TNFα) using the exact same strategy of α→β-residue replacements that was successful for the mimicry of **Z-VEGF**. Furthermore, using a slightly modified design, we developed α/β-peptides targeting the growth factor receptor HER2, and these α/β-peptides localized to HER2-expressing tumors *in vivo*. These last molecules may have application as cancer diagnostic agents. Ultimately, the results described in this chapter suggest a general strategy for the development of α/β-peptides to target a protein surface of interest, regardless of topological complexity: select a Z-domain α-peptide from a large DNA-encoded library (e.g., from a phage display library) that binds to the intended protein surface, then develop a protease-resistant α/β-peptide that mimics the protein recognition surface of this Z-domain α-peptide using the design developed in Chapter 2.

3.2 Introduction

3.2.1 Non-immunoglobulin scaffolds for targeting protein surfaces

Designed molecules that bind selectively to specific sites on proteins may serve as inhibitors of medically important macromolecular interactions or diagnostic tools for biomarker detection. Small molecules often fail for these applications because of the relatively large and irregularly shaped target surfaces.[1-3] In contrast, large polypeptides (e.g., antibodies) can frequently be developed to recognize a protein surface with high affinity and selectivity, and represent the state-of-the-art for engineering ligands for specific biomacromolecular targets. Large polypeptides, however, suffer several disadvantages for *in vivo* applications, including costly production and low storage stability. Furthermore, many small to medium-sized peptides suffer from low bioavailability because of rapid proteolytic degradation.[4]

Mini-protein "scaffolds" are relatively small proteins (often isolated domains from larger proteins) that adopt defined tertiary structures.[5, 6] The tertiary structures of these proteins often tolerate a large number of substitutions at solvent exposed positions. This tolerance to substitutions can allow for combinatorial randomization of entire surfaces without disrupting the overall structure of the molecule. Creating combinatorial libraries of a given protein scaffold with randomized surfaces (e.g., using phage or yeast display) followed by affinity-based selection can lead to the discovery of new proteins derived from the parent scaffold that bind selectively to a wide variety of target proteins of interest.

3.2.2 The Z-domain scaffold

One of the most widely studied peptide scaffolds used to derive affinity proteins is the three-helix "Z-domain" scaffold (also called the "affibody" scaffold).[6, 7] The Z-domain scaffold

originates from protein A of *Staphylococcus aureus*, which binds tightly to mammalian IgG antibodies through several helical IgG-binding domains. Domain B from protein A binds to the region at the CH2/CH3 interface in the Fc fragment of IgG, and a co-crystal structure of domain B bound to IgG Fc shows that it binds to this protein primarily through 13 solvent exposed residues on the surface formed by helices 1 and 2 (Figure 3.1).[8] Formation of this complex buries ~1,300 Å^2 on the two partners (>600 Å^2 on the Fc fragment).

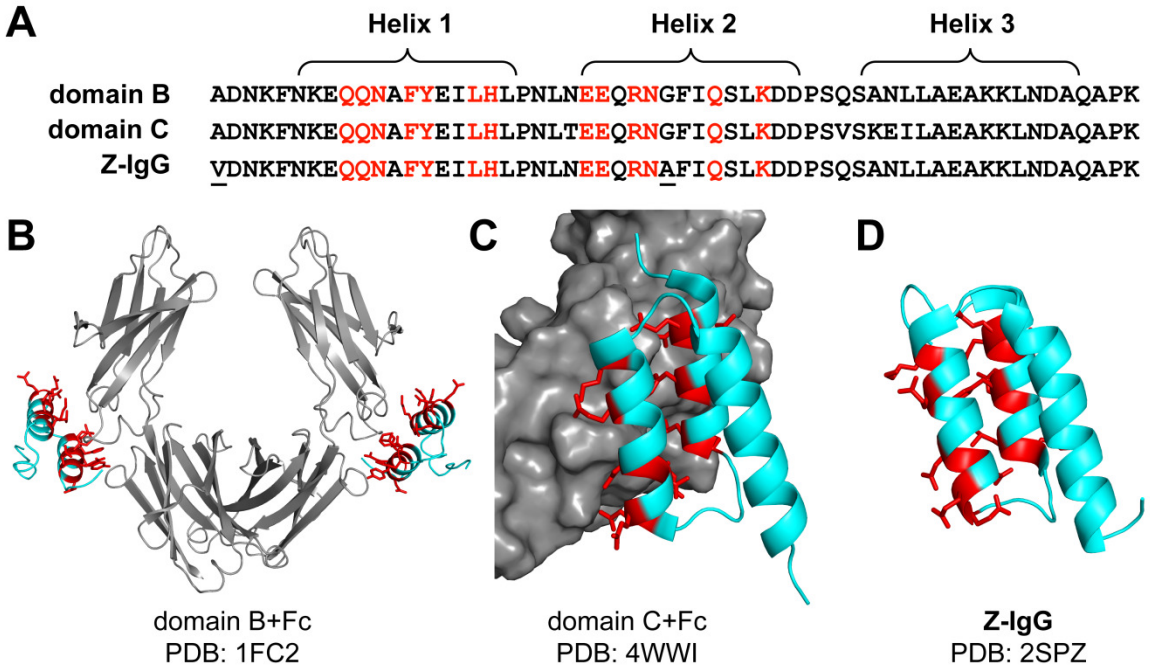

Figure 3.1 The parent Z-domain binds to the Fc fragment of IgG. (A) Sequences of domains B and C from staphylococcal protein A and synthetic analogue **Z-IgG**. Approximate positions of helices 1, 2, and 3 are indicated by brackets. Red residues indicate residues in helices 1 and 2 that contact IgG. Underlined residues indicate differences between the domain B and **Z-IgG**. (B) Crystal structure of domain B (cyan and red) in complex with Fc fragment of IgG dimer (gray) (PDB: 1FC2).[8] Residues in red correspond to those in panel A. In this structure, helix 3 did not appear fully folded. (C) Crystal structure of domain C (cyan and red) in complex with Fc fragment of IgG dimer (gray) (PDB: 4WWI).[9] Residues in red correspond to those in panel A. (D) NMR solution structure of **Z-IgG**. Red residues correspond to those in panel A (PDB: 2SPZ).[10]

A synthetic analogue of domain B, called the Z-domain (referred hereafter as **Z-IgG**), retains high affinity binding to IgG Fc (Figure 3.1A).[11] **Z-IgG** adopts a three-helix bundle conformation, with helices 1 and 2 contributing most of the Fc-contacting residues and helix 3

stabilizing the global Z-domain fold by packing against the other two helices (Figure 3.1D).[8, 10, 12, 13] Because **Z-IgG** has such a stable tertiary structure for a protein of its size, early studies discovered that solvent exposed positions of **Z-IgG** could be altered without dramatically destabilizing the three-helix structure.[14, 15] These studies culminated in the discovery that the randomization of up to 13 residues on the helix 1-helix 2 surface by phage display, followed by affinity-based selection to a target protein of interest, can be used to derive Z-domain analogues to a wide variety of different proteins (Figure 3.2A).[16] This technique has since been utilized to deliver high-affinity Z-domain derivatives that bind to a variety of targets, including VEGF (blocking the VEGF-VEGFR interaction),[17] VEGFR2 (blocking the VEGF-VEGFR2 interaction),[18] TNFα (blocking the TNFα-TNFR interaction),[19-22] HER2,[23, 24] EGFR,[25, 26] PDGFRβ (blocking the PDGF-PDGFRβ interaction),[27] CD25 (also called IL-2Rα, binding at the ligand binding site),[28] CD28 (blocking the CD28-CD80 interaction),[29] *Taq* polymerase,[16] human insulin,[16] and human IgA.[30] Such Z-domains might represent alternatives to antibodies for selective detection of disease-marker proteins or for blocking deleterious signal transduction.[5-7, 31] In many cases, selection from a phage library has identified Z-domain derivatives that display dissociation constants (K_d) in the nanomolar range for a chosen protein target. Affinity maturation has provided enhancements in binding, sometimes to K_d values in the picomolar range.[23] Recent clinical evaluations of radiolabeled Z-domain derivatives targeting HER2 (derived from peptide **Z-HER2**, Figure 3.2) reveal that peptides derived from this scaffold can be safely used to image HER2-overexpressing lesions in breast cancer patients,[32, 33] which highlights the medical promise of the Z-domain scaffold.

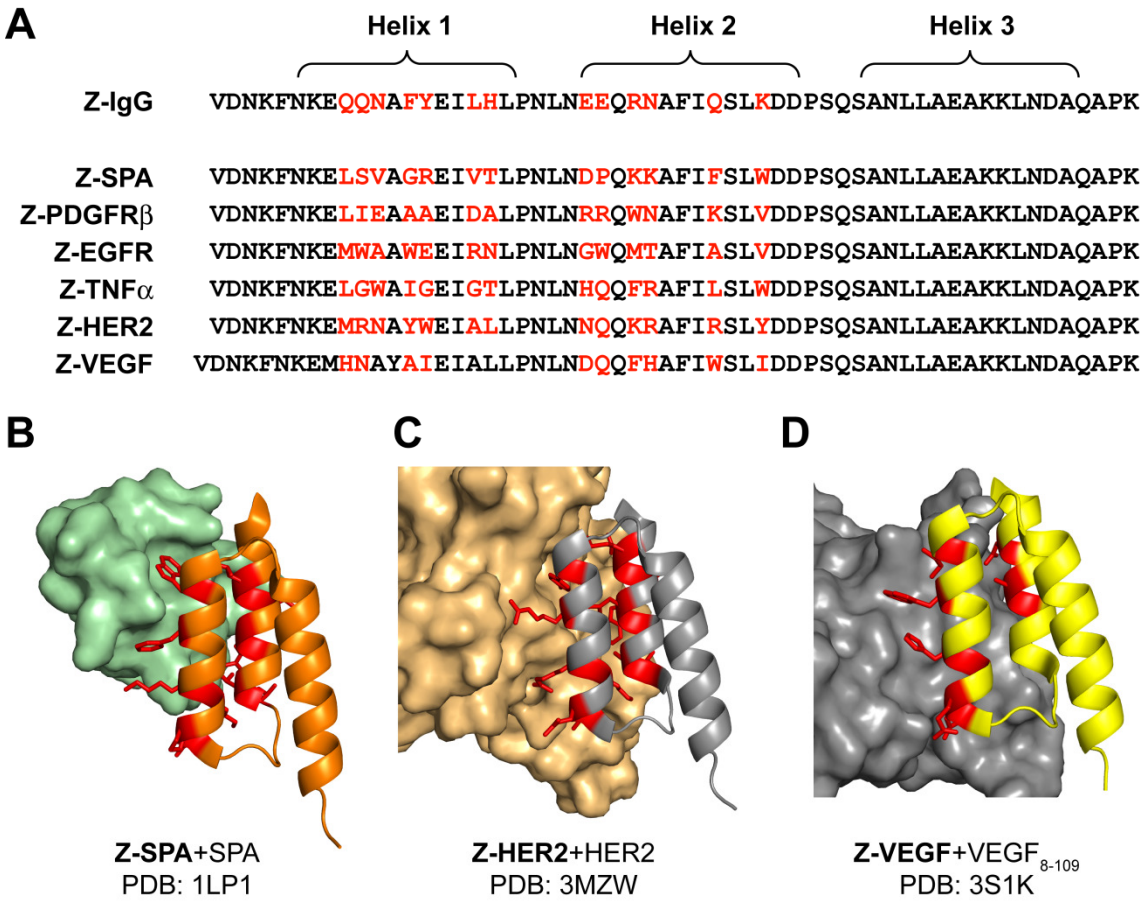

Figure 3.2 The Z-domain scaffold as a starting point for deriving peptides to target a wide-variety of protein surfaces. (A) Sequences of some peptides previously derived from the Z-domain scaffold. Z-domain peptides are named for the protein that they target (e.g., **Z-VEGF** binds to VEGF). Approximate positions of helices 1, 2, and 3 are indicated by brackets. For **Z-IgG**, the parent Z-domain, red positions indicate residues in helix 1 and 2 that contact IgG. For the other peptides, red residues indicate residues on the protein-binding face of helices 1 and 2 that were identified via randomization and selection (including the unintentionally incorporated Ala14 in **Z-VEGF**). Sequences are arranged based on structural alignment of helical regions. (B-D) Crystal structures of the indicated Z-domain peptides (orange, gray, and yellow cartoons) in complex with their respective proteins (green, tan, and gray surfaces). Side chains are shown for the residues in the Z-domain peptides that were randomized to derive protein binding (shown in red), which correspond to those in red in panel A.

3.2.3 α/β-Peptide mimicry of the Z-domain scaffold

In Chapter 2, I described the design of two-helix α/β-peptide mimics of **Z-VEGF**, a peptide derived from the Z-domain scaffold that binds to the receptor-binding region of VEGF. These α/β-peptides structurally mimicked the helix 1-helix 2 segment of **Z-VEGF** (as determined by a co-crystal structure with $VEGF_{8-109}$), bound to $VEGF_{165}$ with affinity

comparable to that of the parent **Z-VEGF**, and had greatly reduced proteolytic susceptibility relative to the parent α-peptides.

Three-helix α-peptides derived from the Z-domain scaffold are presumed to adopt very similar three-helix bundle tertiary structures even if multiple changes are made among residues that define the partner-binding surface (Figure 3.2B-D).[16, 17, 34] Because our α/β-peptide analogues of **Z-VEGF** accurately mimic the protein-binding surface of **Z-VEGF** itself, we anticipated that the strategy leading to these α/β-peptides could be extended to mimic the protein-binding surfaces of other Z-domain derivatives that bind to other target proteins. This approach could provide a general strategy to develop α/β-peptides that selectively target diverse protein surfaces: first by using display/selection technologies on the Z-domain scaffold to derive a three-helix α-peptide that targets a protein surface of interest, followed by α/β-peptide mimicry of this new Z-domain derivative to yield a protease-resistant α/β-peptide targeting that same surface.

In this chapter, we test the hypothesis that the α/β-peptide mimicry strategy that proved successful for mimicry of **Z-VEGF** can be extended to design α/β-peptides that mimic other Z-domain derivatives targeting other proteins. In support of this hypothesis, we show that our α/β-peptide design strategy can be rapidly extended to derive α/β-peptides that selectively target two other proteins: IgG Fc and TNFα. Furthermore, preliminary studies attempting to extend this strategy to design α/β-peptides targeting proteins for applications in the molecular imaging of tumor tissues (HER2 and EGFR) highlight the feasibility of this approach for these applications, but also suggest possible challenges that must be addressed to create a general strategy for targeting diverse protein surfaces using α/β-peptides.

3.3 α/β-Peptide mimicry of Z-IgG

3.3.1 Design of α/β-peptide mimics of Z-IgG

We began by attempting to design an α/β-peptide that mimics the first two helices of **Z-IgG**, the parent and most well-studied Z-domain peptide. As mentioned above, **Z-IgG** adopts a three-helix bundle structure and binds to the Fc portion of IgG through the surface defined by helix 1 and 2 (Figure 3.1).[8, 10, 11] Because this binding mode is so similar to the way in which **Z-VEGF** binds to $VEGF_{8-109}$,[17] we hypothesized that we could follow the same path that led to the successful α/β-peptide mimicry of **Z-VEGF** (described in detail in Chapter 2) to design an α/β-peptide mimic of **Z-IgG**.

We designed α/β-peptide **3.1** by removing helix 3 from **Z-IgG**, making five helix-stabilizing α-residue substitutions,[35, 36] introducing a disulfide constraint at positions 9 and 38, and implementing the corresponding Aib and α→β-residue replacements that were successful for the mimicry of **Z-VEGF** by **2.37** (one of the tightest VEGF-binding α/β-peptides), based on structural alignment of **Z-VEGF** and **Z-IgG** (Figure 3.3). Because **Z-IgG** contains one fewer residue than **Z-VEGF**, the two-helix α/β-peptide **3.1** correspondingly has one fewer residue than the analogous two-helix **2.37**. Within the helical regions that make contact with the protein (on the face formed by helices 1 and 2), α/β-peptide **3.1** differs from **2.37** at 11 residues, positions that differ between the corresponding three-helix parents, **Z-IgG** and **Z-VEGF**. These 11 differences account for the divergent protein-binding specificities of the α-peptides **Z-IgG** and **Z-VEGF**. By retaining these differences in the two-helix **3.1**, we anticipated that this α/β-peptide would retain its specificity for IgG, despite having a very similar sequence to **2.37** at the positions distal to the protein-binding surface.

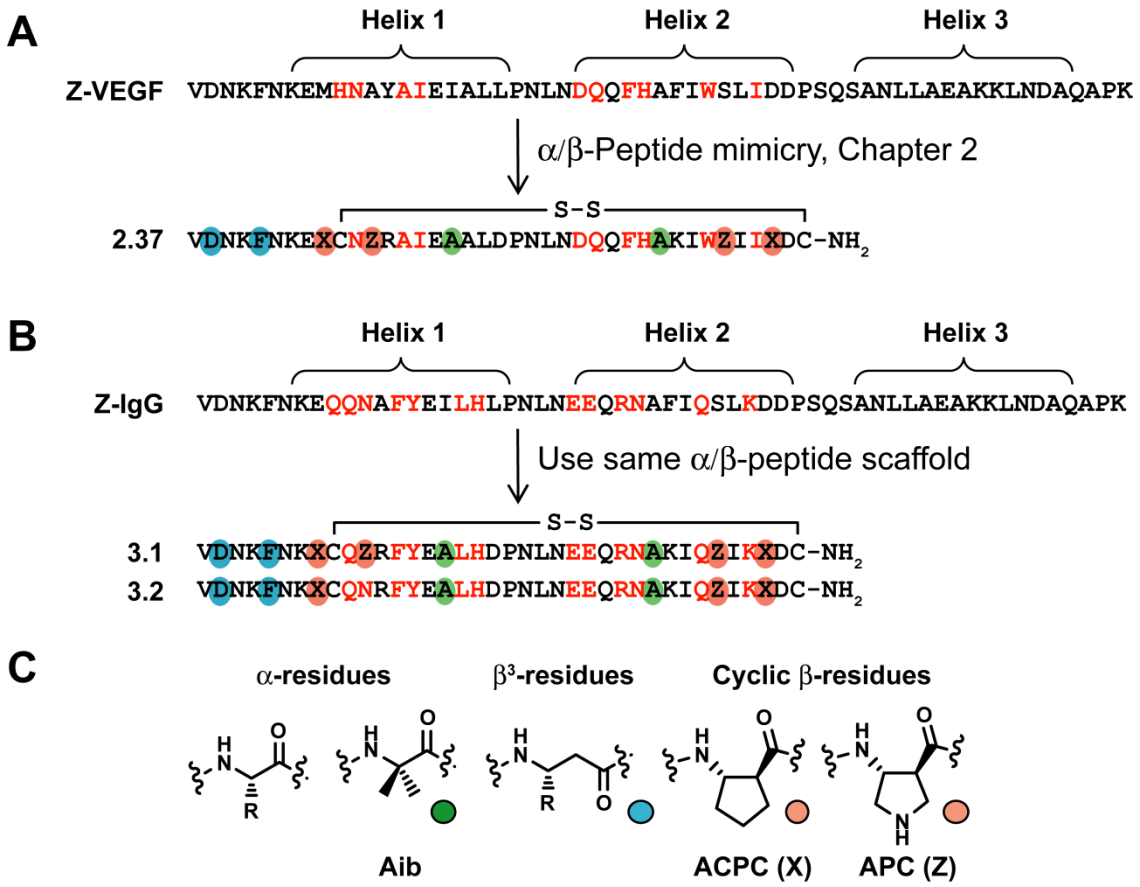

Figure 3.3 Extending α/β-peptide mimicry of the Z-domain scaffold to target a new protein surface. (A) Summary of the design of α/β-peptide **2.37** from the three-helix Z-domain peptide **Z-VEGF**, as described in Chapter 2. Helix 3 was removed, followed by the incorporation of a disulfide bond, several helix-promoting α-residue substitutions, and then by two Aib and six β-residue substitutions. Residues in red represent those that were randomized to derive VEGF binding, and most of these residues are retained in **2.37**. α/β-Peptide **2.37** mimicked the protein-recognition properties of **Z-VEGF** while having significantly decreased susceptibility to proteolysis. (B) The design of α/β-peptides **3.1** and **3.2** as derivatives of **Z-IgG**, following the same path shown in panel A. Residues in red indicate those in helices 1 and 2 that appear to contact IgG. (C) Structures of a generic α-residue, the Aib residue (green), a generic β^3-residue (teal), and the cyclic β-residues ACPC (X) and APC (Z) (orange).

In the development of **Z-VEGF**,[17] Ala12 was not a residue randomized to derive VEGF affinity, and Ala12 does not appear to make contact with VEGF in the **Z-VEGF**+$VEGF_{8-109}$ co-crystal structure. Because Ala12 did not appear to be important for VEGF binding of **Z-VEGF**, we placed the β-residue APC at position 12 in the design of **2.37**. α/β-Peptide **3.1** retains this APC residue at the corresponding position (position 11 in the **Z-IgG** sequence). However, the corresponding residue in the native domain B (Asn11) appears to make contact with the Fc portion of IgG in the co-crystal structure.[8] Thus, Asn11 of **Z-IgG** may contribute to affinity for

IgG, and so we designed **3.2** as an analogue of **3.1** that retains the native Asn at this position. Because our design strategy for the truncation of the Z-domain scaffold was inspired by efforts of Wells et al. involving truncation of **Z-IgG** to a two-helix analogue,[35, 37] **3.1** and **3.2** contain many of the same α-residue substitutions and the same disulfide bond as these previously reported analogues. Thus, **3.1** and **3.2** are also α/β-peptide analogues of these previously described two-helix IgG-binding α-peptides.

3.3.2 Evaluation of binding to IgG by ELISA

We evaluated binding of **3.1** and **3.2** to human IgG1-κ by indirect enzyme-linked immunosorbant assay (ELISA) (Figure 3.4). **3.1** and **3.2** were each conjugated to bovine serum albumin (BSA), and each conjugate was immobilized onto a Nunc Maxisorp ELISA plate. Both conjugates bound human IgG1-κ, as detected using goat anti-human IgG-alkaline phosphatase (Figure 3.5). When BSA alone was immobilized, no increase in ELISA signal over background was observed. In addition, no increase in signal was observed in the absence of human IgG1-κ, which indicates that neither **3.1** nor **3.2** bound to the goat antibody used for detection. These data indicate that **3.1** and **3.2** bind to human IgG1-κ, which is consistent with the hypothesis that these α/β-peptides mimic the protein binding surface of **Z-IgG**.

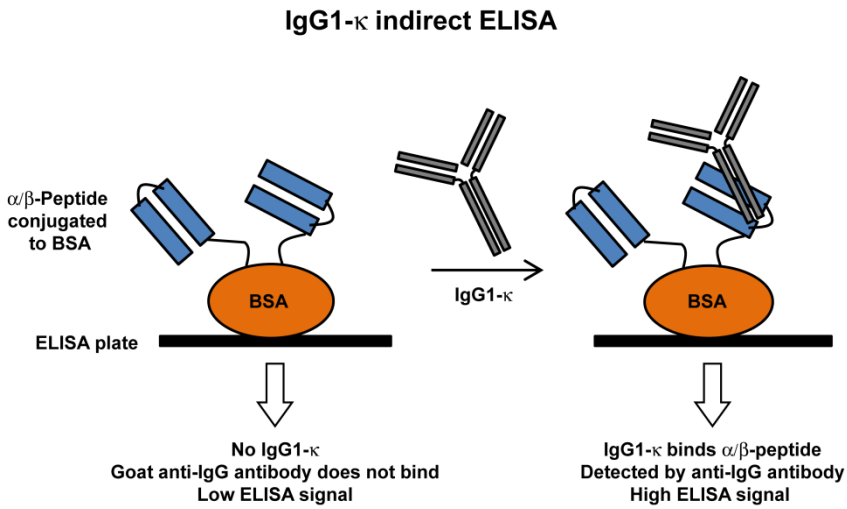

Figure 3.4 Cartoon depiction of the IgG1-κ indirect ELISA used to evaluate the binding of α/β-peptides **3.1** and **3.2** to IgG1-κ.

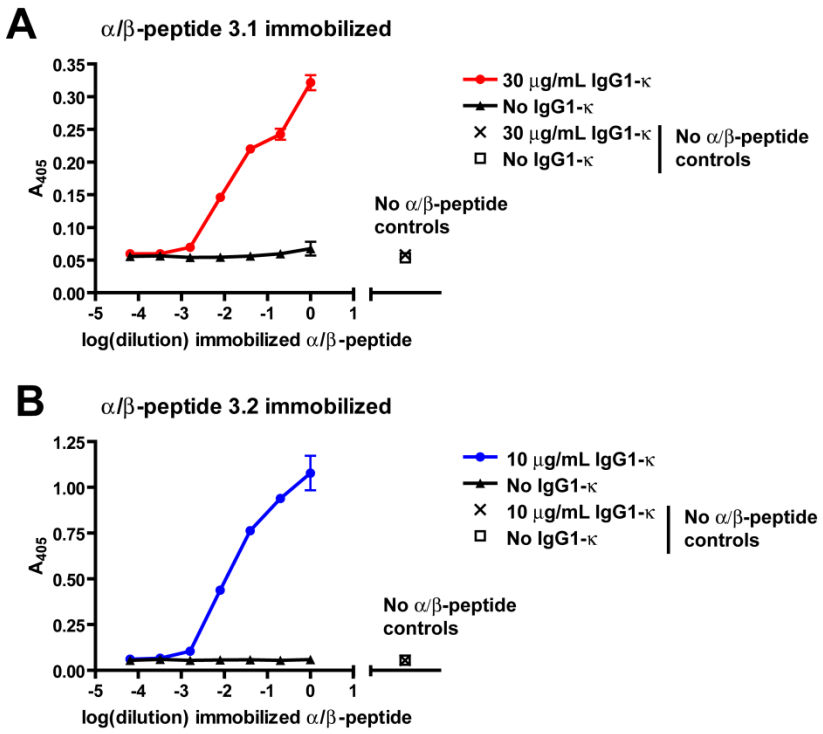

Figure 3.5 IgG1-κ indirect ELISA detecting the binding of human IgG1-κ to immobilized α/β-peptide+BSA conjugates (A) **3.1**+BSA conjugate with 30 μg/mL IgG1-κ and (B) **3.2**+BSA conjugate with 10 μg/mL IgG1-κ. Filled circles indicate signal when wells are incubated with respective amount of IgG1-κ. Black triangles indicate signal observed for the given dilution of immobilized α/β-peptide conjugate that is not incubated with IgG1-κ. Points labeled "No α/β-peptide controls" indicate wells incubated with or without IgG1-κ in which no α/β-peptide has been immobilized. Data points represent the mean ± SEM of duplicate wells on the plate.

The results from the indirect ELISA experiments described above show that both α/β-peptides **3.1** and **3.2** bind to IgG, as designed. However, because it is difficult to quantify the relative conjugation efficiency of **3.1** and **3.2** to BSA, these experiments cannot be used to compare the relative affinities of the different peptides because different amounts of peptide may be immobilized for each experiment. Therefore, a competition ELISA format was used to compare the affinities of **3.1** and **3.2** for IgG1-κ (Figure 3.6). Soluble forms of both **3.1** and **3.2** were able to compete with immobilized **3.2** for binding to human IgG1-κ, with IC_{50} values in this assay of 3.3 μM and 1.4 μM, respectively (Figure 3.7). (Note that these measurements of affinity for IgG are IC_{50} values for this particular experimental set-up, not equilibrium constants, and thus should not be compared to equilibrium constants determined using other methods.[38]) The approximately two-fold weaker affinity of **3.1** compared with **3.2** is consistent with the hypothesis that Asn11 makes favorable contacts with IgG, as observed in the domain B+IgG Fc co-crystal structure,[8] although the effect is very small.

We also immobilized **3.2** covalently to an ELISA plate by forming amide linkages through the free amines on the α/β-peptide (from the N-terminus or lysine side chain) and activated carboxylic acids on a Nunc Immobilizer Amino ELISA plate (in contrast to using a peptide+BSA conjugate for immobilization, as in the cases described above). We found that the directly immobilized α/β-peptide **3.2** was able to bind IgG1-κ and that soluble α/β-peptide **3.1** could compete with the directly immobilized **3.2** for binding, while several negative control peptides were not (Figure 3.25, in the "Experimental Methods" section).

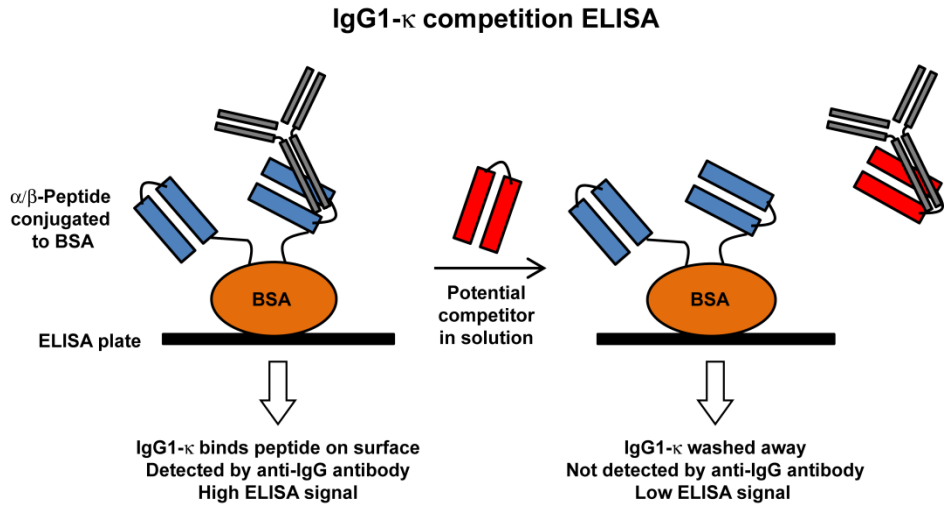

Figure 3.6 Cartoon depiction of the IgG1-κ competition ELISA experiment used to compare the ability of soluble α/β-peptides to block binding of IgG1-κ to an immobilized α/β-peptide.

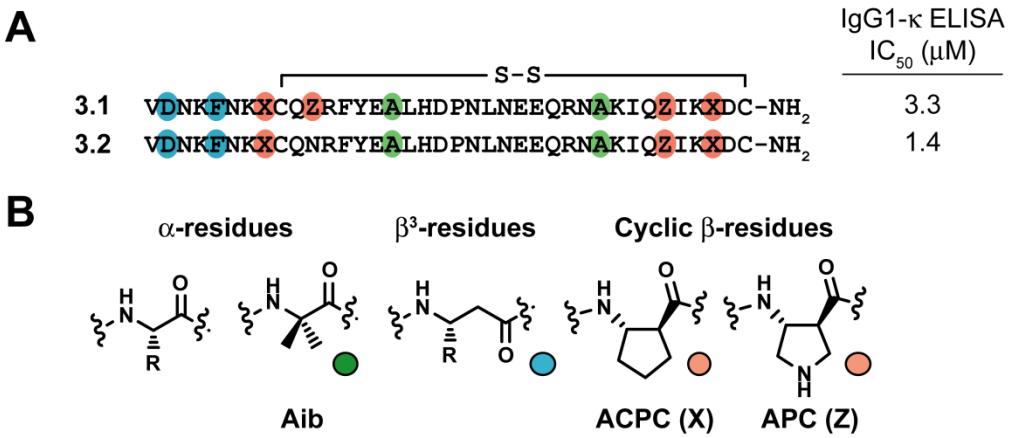

Figure 3.7 (A) Primary sequences of two-helix α/β-peptides **3.1** and **3.2** derived from **Z-IgG**, along with associated IC_{50} values, as determined by IgG1-κ competition ELISA. The uncertainty in the calculated IC_{50} values from ELISA is ~2-fold. Non-natural residues are indicated by colored circles. Each cysteine is engaged in an intramolecular disulfide bond. (B) Structures of a generic α-residue, the Aib residue (green), a generic β^3-residue (teal), and the cyclic β-residues ACPC (X) and APC (Z) (orange).

We did not synthesize the full-length **Z-IgG** for comparison in these experiments. Because the previous two-helix α-peptide reported by Wells et al.[37] (**Z34C**, Figure 2.5) binds to IgG with nearly the same affinity as **Z-IgG**, we anticipate that these α/β-peptides (which are close in sequence to **Z34C**) match the affinity of the parent three-helix. A competition ELISA experiment directly comparing **3.1** and **3.2** to **Z-IgG** will need to be performed to test this hypothesis. Overall, these experiments show that both **3.1** and **3.2** are able to bind to IgG, which

is consistent with the hypothesis that the strategy that proved successful for α/β-peptide mimicry of the protein-binding region of **Z-VEGF** can be extended to mimic other Z-domain derivatives.

3.3.3 Attempts at co-crystallization

To try to gain atomic-resolution information regarding how α/β-peptide analogues of **Z-IgG** interact with the Fc portion of IgG, we attempted to co-crystallize **3.2** (which binds IgG with higher affinity than does **3.1**) in complex with the Fc fragment of IgG1. We pre-incubated **3.2** with the Fc fragment from IgG1 and screened crystallization conditions from a variety of reagent screens. From this effort, we identified conditions to crystalize **3.2** with IgG1, Fc. Dale Kreitler (Gellman Laboratory, University of Wisconsin-Madison) collected low-resolution X-ray diffraction data on one crystal that diffracted to ~3.5 Å. We collaborated with Douglas Fairlie and Peter Colman (Walter and Eliza Hall Institute of Medical Research) to process and obtain a molecular replacement solution for this low-resolution data set using the Fc dimer (PDB: 1FC1) without sugars as a search model. Interestingly, after initial rounds of refinement the model for this data showed positive difference density at the hinge region of the Fc fragment where the α/β-peptide is predicted to bind (Figure 3.26, in Experimental Methods section). Furthermore, the shape of the positive difference density is roughly in the shape of the anticipated helix-loop-helix, consistent with the hypothesis that **3.2** mimics the helix 1-helix 2 segment of **Z-IgG** in its binding mode to IgG Fc. However, the quality of this data set was too low to refine the model any further. Future work could use these results as a starting point for obtaining better-diffracting crystals of **3.2** in complex with IgG Fc to gain insight into the interaction of this α/β-peptide with its protein binding partner.

3.3.4 Preliminary pharmacokinetics studies

To gain insight into how two-helix α/β-peptide analogues of Z-domain derivatives are processed in animals, we performed pharmacokinetics experiments in mice. These experiments were carried out in collaboration with Jiang Zhisheng and Jill Kolesar (3P Analytical Instrumentation Laboratory, University of Wisconsin-Madison). Female FVB mice were treated with an intraperitoneal (IP) injection of ~10 mg/kg α/β-peptide and sacrificed after the amount of time indicated in the specific experiments described below. Plasma and kidney homogenates were collected and analyzed by analytical reverse-phase HPLC and MALDI-TOF to look for intact α/β-peptides or α/β-peptide fragments. In these preliminary experiments, no attempt was made to quantify the amount of peptide remaining in the bloodstream at a given time, and the number of replicates for each condition was very low (1-2 mice per condition). The primary goals for these experiments were to determine effective procedures for the detection of peptides in the bloodstream after injection and to gain insight into the fate of these compounds. Thus, these experiments may form the basis for follow-up pharmacokinetics experiments.

In initial experiments, we found that we could detect α/β-peptides in kidney homogenates using MALDI-TOF for the two peptides tested (**3.2**, which targets IgG, and **2.39**, which targets VEGF), and we could detect **3.2** present in the plasma a mouse injected by IP with this compound and sacrificed ~20 minutes post-injection. We did not detect any **2.39** in the plasma of mice injected with this compound. The presence of both **3.2** and **2.39** in the kidneys suggests that these compounds may be readily removed from the bloodstream by renal filtration, which is a common mechanism of clearance for molecules of this size.[39, 40] Although very preliminary, this initial experiment suggested that **3.2** may be better at avoiding renal clearance than **2.39**. One potential explanation for this difference could be that **3.2**, which binds to

mammalian IgG, can evade renal filtration by binding to this common protein in the mouse bloodstream.

A

B

Mouse	Peptide	Kidney? (MALDI)	Plasma? (MALDI)	Plasma? (HPLC)
1	**3.2**	Obs.	Obs.	Not obs.
2	**3.2**	Not obs.	Not obs.	Not obs.
3	**3.3**	Obs.	Obs.	Obs.
4	**3.3**	Obs.	Obs.	Obs.
5	**2.39**	Not obs.	Not obs.	Not obs.

Figure 3.8 Analysis of preliminary pharmacokinetics experiments of α/β-peptides derived from the Z-domain in mice. (A) Primary sequences of α/β-peptides utilized in this study **3.2** and **3.3** (targeting IgG) and **2.39** (targeting VEGF). Each cysteine is engaged in an intramolecular disulfide. Non-natural residues are indicated by colored circles, with structures as depicted in Figure 3.7B. (B) Summary of the results obtained from MALDI-TOF and HPLC analysis of mouse kidney homogenates and plasma after injection with 10 mg/kg of the indicated compound by IP injection and sacrificed 20 minutes post-injection. Obs. = the intact compound was observed in the indicated biological sample using the indicated method (for MALDI, the parent mass was observed in the spectrum; for HPLC, a peak with the same elution time was observed in the chromatogram). Not obs. = the intact peptide was not observed in this sample. See Figures 3.27 and 3.28 in the Experimental Methods for HPLC and MALDI data for this experiment.

We next injected **2.39**, **3.2**, and **3.3** into five mice and analyzed the kidney homogenates and plasma, as described above (Figure 3.8). α/β-Peptide **3.3** is the β^3Phe5→β^3Ile5 analogue of **3.2**, and was designed based on a report showing that a Phe5→Ile5 substitution in the parent **Z-IgG** increases affinity for mouse IgG >10-fold.[41] Thus, we predicted that **3.3** may have higher affinity for mouse IgG than **3.2**, and therefore may stay in the bloodstream longer than **3.2** or **2.39** if IgG-binding does play a role in increasing plasma residence time. When injected into mice and analyzed 20 minutes post-injection, we detected **3.3** in both the kidney and plasma of both mice injected with this compound. The analysis for **3.2** was less consistent between mice

and analysis methods; α/β-peptide **3.2** was detected in the plasma of one mouse by MALDI, but not by HPLC analysis. This inconsistency for HPLC versus MALDI analysis of plasma and between mice may indicate that **3.2** was present at relatively low concentrations compared to **3.3**. Alternatively, the inconsistency could arise from a non-optimal protocol for sample preparation. α/β-Peptide **2.39**, which was only injected in one mouse in this experiment, was not detected in either the kidneys or the plasma. These results are consistent with the hypothesis that **3.3**, which is designed to bind to mouse IgG, remains in the bloodstream for longer periods of time, possibly by evading renal filtration through binding to native IgG in the bloodstream. However, the sample size for this study is very small (only two replicates for **3.2** and **3.3**, and only one mouse injected with **2.39**) and caution must be exercised when drawing conclusions. In particular, the reproducibility of these experiments from mouse to mouse appeared to be low.

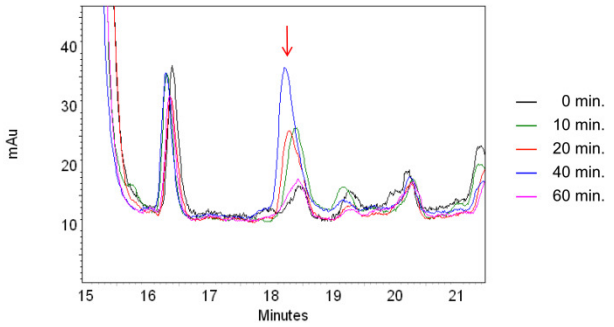

Figure 3.9 Monitoring of α/β-peptide **3.3** in the plasma of mice over time. Five mice were injected with 10 mg/kg **3.3** (or PBS for "0 min." time point) by IP injection, sacrificed at the indicated time point post-injection, and then their plasma analyzed by reverse-phase HPLC, monitoring UV absorbance at 220 nm. The red arrow indicates the peak in the chromatogram that corresponds to intact **3.3**.

We next injected α/β-peptide **3.3** into four mice (+ vehicle control) and sacrificed each mouse at a different time post-injection to monitor α/β-peptide presence in the bloodstream over time, as well as gain some insight into the reproducibility of this method of analysis (Figure 3.9). The goal of this experiment was to get preliminary data regarding the rate of clearance from the blood over time for **3.3**, the α/β-peptide that showed the most promising and reproducible results

above. In this experiment, we detected **3.3** in the isolated plasma samples from mice 10, 20, and 40 minutes post-injection by analytical HPLC. We did not detect a significant amount of **3.3** in the mouse sacrificed 60 minutes post-injection by HPLC, which suggests that the α/β-peptide was cleared from the bloodstream at this last time point.

Overall, the results reported in this section may be useful as a starting point for future pharmacokinetics studies of Z-domain-derived α/β-peptides in mice. These results suggest that renal filtration may be a major mechanism of clearance from the bloodstream for these compounds, as intact α/β-peptides could often be detected in kidney homogenates by MALDI-TOF. Furthermore, these initial experiments with **3.2** and **3.3** (relative to **2.39**) suggest that binding to IgG may be useful as a method for increasing circulation time in the blood. This raises the possibility that these α/β-peptides could find application as protease-resistant "tags" to reduce renal clearance of conjugated peptides or proteins. Indeed, three-helix peptides optimized to bind albumin are currently used as a technology to increase the circulation time of therapeutic Z-domain peptides.[42-44] Future work will need to explore these possibilities in more detail. In particular, the variability between individual mice may make the analysis of plasma residence time difficult using the current method (in which a mouse is sacrificed in order to isolate its plasma, preventing the monitoring of compound concentration over time in one animal). More reproducible results may be obtained by collaborating with a laboratory that has the capabilities to isolate blood samples from the same mouse over time. In addition, replicate experiments with more animals will need to be performed to draw meaningful conclusions.

3.4 α/β-Peptide mimicry of Z-TNFα

3.4.1 Design of α/β-peptide mimics of Z-TNFα

We further tested the generality of our α/β-peptide design strategy by endeavoring to mimic a Z-domain derivative that binds to tumor necrosis factor-α (TNFα). TNFα, a cytokine with a variety of functions, plays a key role in multiple inflammatory disorders.[45] Engineered proteins that bind to TNFα and inhibit association with its receptors (TNFRs) are currently used to treat rheumatoid arthritis, inflammatory bowel disease and other illnesses.[46] Using phage display, Jonsson *et al.* previously developed the 58-mer **Z-TNFα** (Figure 3.10), based on the Z-domain scaffold.[19] No crystallographic or other high-resolution characterization is available for this complex, in contrast to the **Z-VEGF**+VEGF interaction and the **Z-IgG**+IgG Fc interaction. **Z-TNFα** presumably adopts the characteristic three-helix bundle tertiary structure and contacts TNFα via the surface defined by helices 1 and 2. **Z-TNFα** has been reported to bind TNFα with an apparent dissociation constant (K_d) of 0.1-0.5 nM, as measured by surface plasmon resonance, and can block binding of TNFα to the receptor TNFR2 *in vitro*, as indicated by experiments with etanercept (a TNFR2+IgG1 Fc fusion protein).[19]

We designed **3.4** and **3.5** by removing helix 3 of **Z-TNFα**, introducing the five helix-stabilizing α-residue substitutions,[35, 36] adding a disulfide, and introducing α→β and Aib replacements at positions corresponding to those in the VEGF- and IgG-targeted α/β-peptides previously described (Figure 3.10). As in the α/β-peptide series based on **Z-IgG** (**3.1** and **3.2**), **3.4** contains the cyclic β residue APC at position 11, while **3.5** contains the native residue (Trp) at this position.

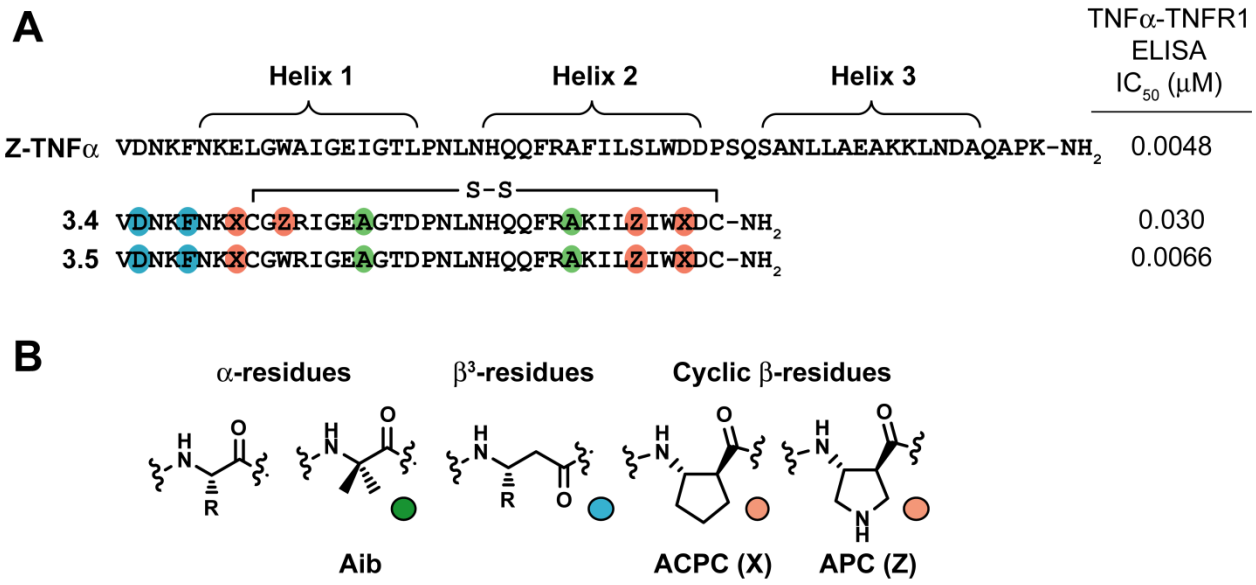

Figure 3.10 (A) Primary sequences three-helix α-peptide **Z-TNFα** and two-helix α/β-peptide derivatives **3.4** and **3.5**, along with associated IC_{50} values, as determined by TNFα-TNFR1 competition ELISA. The uncertainty in the calculated IC_{50} values from ELISA is ~2-fold, with a maximum deviation of ~7-fold for some experiments. Hypothesized positions of helices 1, 2, and 3 are indicated by brackets. Non-natural residues are indicated by colored circles. Each cysteine is engaged in an intramolecular disulfide bond. (B) Structures of a generic α-residue, the Aib residue (green), a generic β^3-residue (teal), and the cyclic β-residues ACPC (X) and APC (Z) (orange).

3.4.2 Evaluation of binding by competition ELISA

We used a competition ELISA experiment to determine whether **3.4** and **3.5** inhibit TNFα-TNFR1 complexation (Figure 3.11). The TNFR1 extracellular domain was immobilized onto an ELISA plate and allowed to interact with soluble TNFα in the presence of varying concentrations of a potential competitor. The relative amount of TNFα bound to the immobilized TNFR1 was then detected using a biotinylated anti-TNFα antibody and streptavidin-alkaline phosphatase. The three-helix parent α-peptide **Z-TNFα** had an IC_{50} value of 0.0048 μM in our assay (Figure 3.10), indicating that this peptide was able to disrupt the interaction between TNFα and the TNFR1 receptor fragment. Both α/β-peptides disrupted the TNFα-TNFR1 interaction as well, with IC_{50} values of 0.030 μM for **3.4** and 0.0066 μM for **3.5**. These results suggest that both α/β-peptides bound to TNFα with affinities comparable to that of the parent, **Z-TNFα**. The modestly lower IC_{50} value for **3.5** relative to **3.4** suggests that the residue at position 11 in **Z-**

TNFα (Trp11) makes favorable, but not essential, contacts with TNFα. This small advantage for the native residue at position 11 parallels our previous observations with **3.1** versus **3.2**. Taken together, these experiments show that **3.4** and **3.5** accurately mimic **Z-TNFα** in their ability to recognize the target protein TNFα and block binding to the cognate receptor. These results confirm that the α/β-peptide design strategy used to mimic both **Z-VEGF** (described in Chapter 2) and extended to mimic **Z-IgG** (described above) can also be applied to mimic the protein recognition surface of **Z-TNFα** to yield two-helix α/β-peptides that may be useful as TNFα antagonists. Studies to optimize α/β-peptides derived from **Z-TNFα**, as well as investigations into their mechanism of TNFα-TNFR inhibition, are explored in Chapter 4.

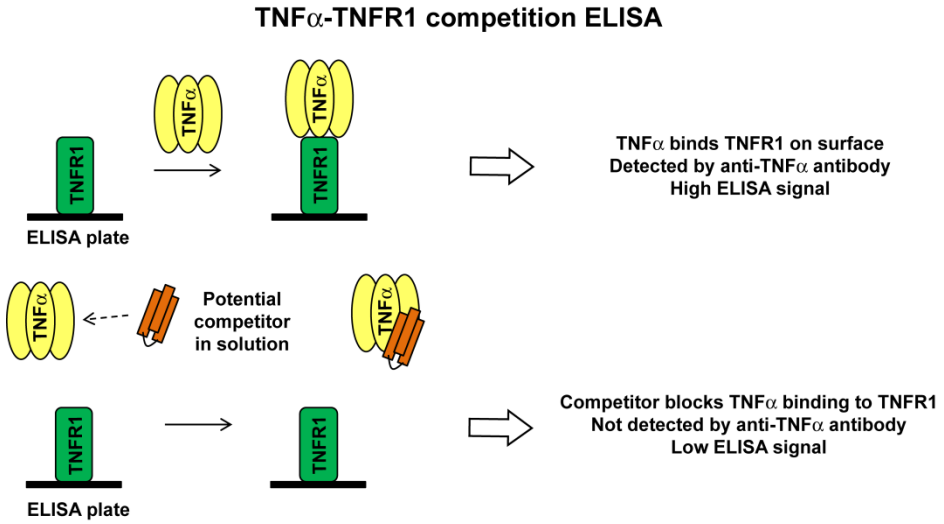

Figure 3.11 Cartoon representation of the TNFα-TNFR1 competition ELISA experiment to evaluate the ability of soluble α- and α/β-peptides to disrupt the TNFα-TNFR1 interaction.

3.5 Selectivity of α/β-peptides

Peptides derived from the Z-domain scaffold are designed to bind to their respective protein binding partners primarily through the composite surface formed by helices 1 and 2 from the residues randomized during the display/selection procedure. Thus, each different Z-domain peptide forms a different surface at this protein-binding face, despite having very similar overall

three-dimensional structures. Z-domain-derived peptides typically show very good specificity for the proteins for which they were selected to bind, often showing little to no binding to unrelated proteins, including IgG Fc, the protein targeted by the parent Z-domain (**Z-IgG**).[16] Because the α/β-peptide mimicry approach described here aims to mimic the protein-binding surface of the three-helix peptides in the context of the two-helix α/β-peptide scaffold, we hypothesized that the selectivity for the intended protein targets would be retained.

A

B

Peptide	Target	VEGF FP K_i (μM)	IgG1-κ ELISA IC_{50} (μM)	TNFα-TNFR1 ELISA IC_{50} (μM)
2.37	VEGF	0.11	>60	>10
2.40	VEGF	0.39	>60	-
3.1	IgG	>50	3.3	>10
3.2	IgG	>50	1.4	-
3.4	TNFα	>50	>60	0.030
3.5	TNFα	>50	>60	0.0066

Figure 3.12 α/β-Peptides derived from the Z-domain scaffold retain their selectivity for their intended protein target. (A) Sequences of α/β-peptides derived from **Z-VEGF** (**2.37**, **2.40**), **Z-IgG** (**3.1**, **3.2**), and **Z-TNFα** (**3.4**, **3.5**). Cysteine residues are engaged in an intramolecular disulfide. Colored circles indicate non-natural residues, as depicted in Figure 3.10B. (B) Evaluation of α/β-peptides for binding to $VEGF_{165}$ by competition FP assay, to IgG1-κ by IgG1-κ competition ELISA, and to TNFα by TNFα-TNFR1 competition ELISA. Values in red indicate no inhibition was observed at the highest concentration tested. A dash (-) indicates this compound was not tested in this experiment.

We evaluated the binding of several of the α/β-peptides derived from **Z-VEGF**, **Z-IgG**, and **Z-TNFα** for binding to $VEGF_{165}$ (by competition FP assay), IgG1-κ (by IgG competition ELISA), and TNFα (by TNFα-TNFR1 inhibition ELISA) (Figure 3.12). In these experiments, we

saw that each α/β-peptide bound to its intended protein target (as described in the respective sections above), but did not bind to the other proteins tested. For example, α/β-peptide **2.37**, which binds $VEGF_{165}$ with high affinity (K_i = 0.11 μM) did not bind to IgG1-κ and did not block the TNFα-TNFR1 interaction. The other α/β-peptides tested showed similar selectivity. These results show that the selectivity of the parent Z-domain peptides is retained in the α/β-peptide mimics.

3.6 α/β-Peptide mimicry of Z-HER2

3.6.1 Background

Human epidermal growth factor receptor 2 (HER2, also called ErbB2 and HER2/neu) is a membrane-bound growth factor receptor that is overexpressed in several types of human cancers. In particular, the gene encoding HER2 is amplified in 25-30% of breast cancers and is associated with increased tumor progression, decreased patient survival, and increased relapse.[47, 48] There is currently no known natural ligand for HER2, but this receptor is thought to stimulate tumor progression via ligand-induced heterodimerization with other epidermal growth factor receptor (EGFR) family proteins and through activation resulting from high receptor density.[49] Murine monoclonal antibodies directed against HER2 can reduce cancer cell proliferation *in vitro*[50] through mechanisms that are not well understood.[49] A humanized version of one of these antibodies, trastuzumab (Herceptin),[51] can reduce disease progression and increase survival in breast cancer patients with HER2-overexpressing tumors.[52]

Because HER2-overexpressing tumors respond to anti-HER2 treatments, it is of great clinical interest to determine the HER2 expression levels of a tumor before determining effective treatment strategies. To this end, several areas of research are focused on developing compounds

that bind selectively to HER2. Such compounds would find utility both in tumor imaging and in diagnosing the HER2 expression levels of a tumor. **Z-HER2** is a three-helix HER2-binding peptide derived from the Z-domain scaffold using phage display and selection,[24] followed by affinity maturation (Figures 3.2A and 3.13).[23] **Z-HER2** binds to HER2 with very high affinity (22 pM by SPR analysis) and a co-crystal structure of **Z-HER2** bound to HER2 shows that it binds adopts the three-helix bundle fold that is characteristic of Z-domain derivatives and interacts with HER2 through the surface formed by helices 1 and 2 (Figure 3.2C).[34] Labeled **Z-HER2** or its derivatives have been successfully used to image HER2-overexpressing tumors both in mouse models[23] and in humans.[32, 33]

There has been one previous attempt to truncate **Z-HER2** to a two-helix analogue (Figure 3.13).[36] This effort found that removal of helix 3 from **Z-HER2** led to a complete loss of affinity for HER2, as assessed by surface plasmon resonance (SPR) experiments. Incorporation of five α-residue substitutions discovered by phage display to stabilize the two-helix structure in the absence of helix 3[35] gave peptide **3.6**, which recovered its ability to bind to HER2, although with much weaker affinity than the parent three-helix **Z-HER2**. Incorporation of a disulfide bond to connect positions 5 and 39 modestly increased affinity for **Z-HER2** (peptide **3.7**), and substitution of Cys residues in **3.7** with homocysteine residues gave peptide **3.8**, which bound to HER2 with K_d = 5 nM by SPR. It is notable that the location of the disulfide bond, at positions 5 and 39, is not the same location utilized previously utilized in our prior Z-domain truncation strategies inspired by Wells et al. (positions 9 and 38).[37]

A

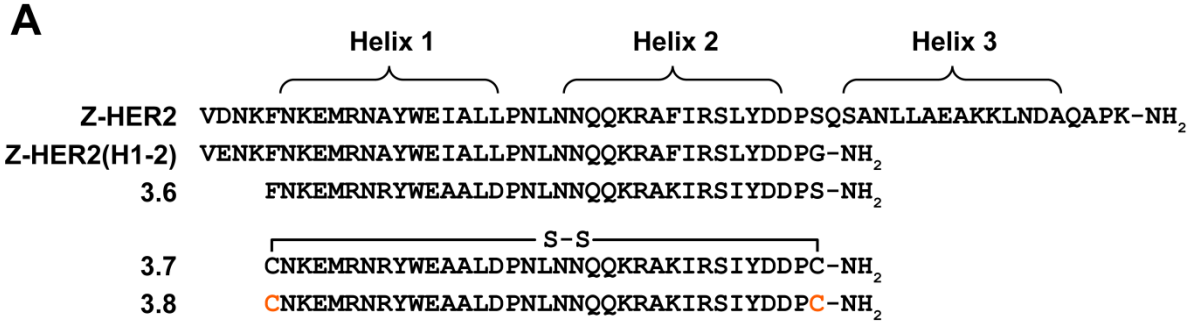

B

	K_d (nM) [SPR]*	Fold-change vs **Z-HER2**	IC_{50} (μM) [ELISA]	Fold-change vs **Z-HER2**
Z-HER2	0.022	1	0.024	1
Z-HER2(H1-2)	NB	-	-	-
3.6	44	2000	7.0	290
3.7	15	680	0.52	22
3.8	5	230	0.89	37

Figure 3.13 Previously reported truncation of **Z-HER2** to two-helix α-peptide analogues. (A) Primary sequences of **Z-HER2** and two-helix analogues reported by Webster et al.[36] The approximate positions of helix 1, 2, and 3 are indicated by brackets. Cysteine residues are engaged in an intramolecular disulfide bond. Orange C residues indicate homocysteine. (B) Affinity of **Z-HER2** and two-helix analogues to HER2 by SPR (left columns, *previously reported in ref.[36]) and HER2 competition ELISA, as described below (right columns). Based on TNFα-TNFR1 competition ELISA data (see Section 4.2.4 in Chapter 4), the uncertainty in the calculated IC_{50} values from ELISA is ~2-fold. Fold-changes represent the decrease in affinity for HER2 relative to **Z-HER2**. NB = No binding. For the IC_{50} column, a dash (-) indicates this compound was not tested in this experiment. For "fold-change" columns, a dash (-) indicates that this entry is not applicable.

Because **Z-HER2** binds HER2 through helices 1 and 2, we hypothesized that the α/β-peptide mimicry strategy described above may be used to design α/β-peptides that bind to HER2 for potential use in imaging HER2-overexpressing tumors, both for tumor detection and for diagnosis of HER2-expression levels. The small size of the two-helix α/β-peptide scaffold may provide benefits in terms of tumor and tissue penetration relative to both antibodies and the three-helix Z-domain scaffold.[36, 53, 54] It is worth noting that long plasma residence time is not necessarily desired for imaging applications, as this reduces the tumor:blood ratio and raises background signal. We hypothesize that rapid clearance by the kidneys will provide a mechanism by which these α/β-peptide compounds can be removed from the bloodstream to

reduce background, but the non-natural α/β-peptide backbone may provide advantages over α-peptides in enabling the imaging agent to survive long enough reach its target, as well as to survive once bound to HER2 on the tumor cell surface. Furthermore, the α/β-peptide backbone may also provide additional benefits in terms of immunogenic response, toxicity, or for targeted radiotherapy. The studies described below are focused on designing α/β-peptide mimics of **Z-HER2** for application in tumor imaging, and to evaluate whether the α/β-peptide backbone will provide any advantage (or disadvantage) over a natural α-peptide backbone for this application.

3.6.2 Initial designs and evaluation

The studies described in this subsection were carried out by Takayuki Miki (Gellman Laboratory, University of Wisconsin-Madison, visiting graduate student from Kyoto University) and undergraduate student Nicholas Rettko (Gellman Laboratory, University of Wisconsin-Madison).

We began by synthesizing the previously reported three-helix α-peptide **Z-HER2**, along with three of the two-helix α-peptide analogues reported by Webster et al. (**3.6**-**3.8**).[36] We evaluated the ability of these peptides to bind to HER2 using a competition ELISA format in which unlabeled peptide is allowed to compete with biotinylated **Z-HER2** (**Bt-Z-HER2**) for binding to immobilized HER2-Fc chimera. After the competition experiment, the amount of **Bt-Z-HER2** remaining bound to HER2 is detected with a streptavidin-conjugated alkaline phosphatase enzyme (Figure 3.14).

Using competition ELISA, we saw that **Z-HER2** competed with **Bt-Z-HER2** for binding to HER2 with an IC_{50} in this assay of 0.024 μM (Figure 3.13). The two-helix α-peptide **3.6**, which does not contain a disulfide constraint, also bound to HER2, with an IC_{50} = 7.0 μM. This ~300-fold decrease in affinity for HER2 relative to three-helix **Z-HER2** is consistent with

the large decrease in affinity previously reported by SPR analysis,[36] although the effect is not as dramatic in our experiments. Consistent with the previous report, **3.7** and **3.8**, which feature a disulfide bond near the termini of helices 1 and 2, bind with higher affinity than **3.6** (IC_{50} = 0.52 μM and 0.89 μM, respectively), but still weaker than **Z-HER2**.

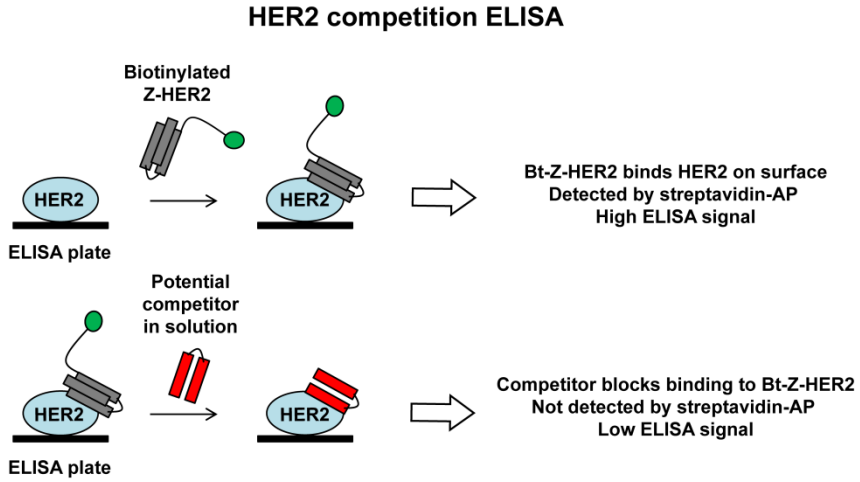

Figure 3.14 Cartoon representation of the HER2 competition ELISA used to evaluate the binding of α- and α/β-peptides to HER2. **Bt-Z-HER2** = Biotinylated **Z-HER2** peptide. AP = alkaline phosphatase.

We next aimed to design α/β-peptide analogues of **Z-HER2** using the strategy that proved successful for the mimicry of **Z-VEGF**, **Z-IgG**, and **Z-TNFα**. Inspired by these prior successes, we removed helix 3 from **Z-HER2**, added five helix-stabilizing α-residue substitutions,[35, 36] incorporated a disulfide bond at positions 9 and 38, and then incorporated the same pattern of Aib and β-residue substitutions (those found in **2.37**, **3.1**, and **3.4**) to generate **3.9** as a two-helix, disulfide-constrained α/β-peptide analogue of **Z-HER2** (Figure 3.15). We also designed **3.10** and **3.11** as analogues of **3.9** that lack several N-terminal residues in an effort to engineer shorter α/β-peptides. However, we found that **3.9**-**3.11** all failed to bind HER2, as judged by the competition ELISA (IC_{50} > 10 μM).

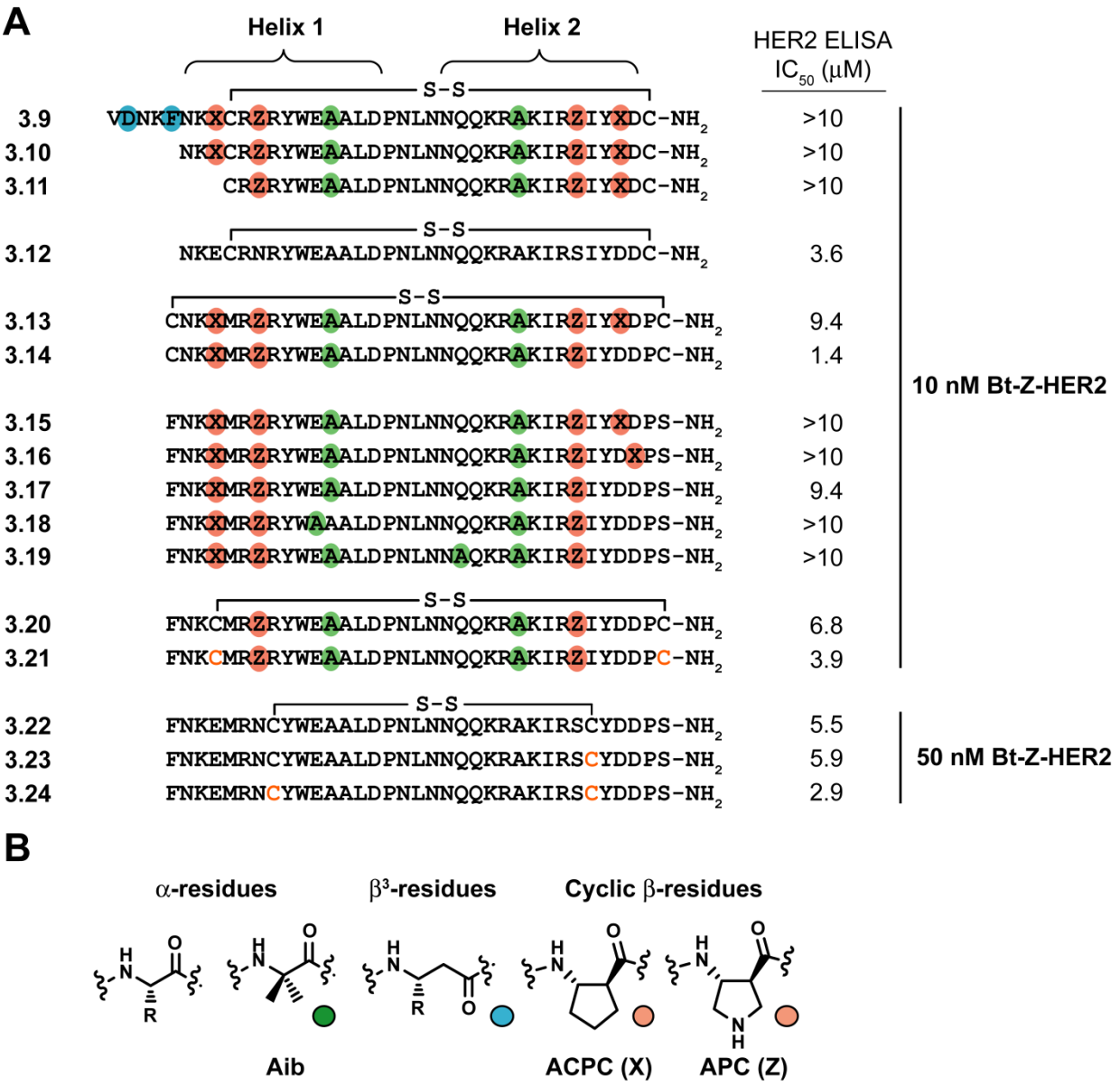

Figure 3.15 (A) Primary sequences of two-helix α- and α/β-peptides derived from **Z-HER2**, along with associated IC_{50} values, as determined by HER2 competition ELISA using the indicated concentration of **Bt-Z-HER2**. Based on calculated IC_{50} values for independent TNFα-TNFR1 competition ELISA experiments (see section 4.2.4 in Chapter 4), the uncertainty in the calculated IC_{50} values from ELISA is ~2-fold, with a maximum variation of up to ~7-fold for some experiments. Each cysteine is engaged in an intramolecular disulfide bond. Non-natural residues are indicated by colored circles. Orange C residues indicate homocysteine. (B) Structures of a generic α-residue, the Aib residue (green), a generic β^3-residue (teal), and the cyclic β-residues ACPC (X) and APC (Z) (orange).

The lack of binding for the α/β-peptide **3.9** was somewhat surprising given that its two-helix α/β-peptide scaffold was successful for the mimicry of three other Z-domain derivatives. However, close examination of the **Z-HER2**+HER2 crystal structure revealed two probable

origins for the much lower affinity of **3.9**. First, Met9 and Pro38, the residues that were replaced with Cys and form the disulfide in our α/β-peptide scaffold, make direct contacts with HER2 (Figure 3.16A). This contrasts both the **Z-VEGF**+$VEGF_{8-109}$ and domain B+Fc co-crystal structures, where the analogous positions do not make direct contacts to the respective proteins and project somewhat out into solution (Figure 3.16B). By replacing these residues with a disulfide bond, we may have removed critical contacts to HER2. A second possible origin of the lack of affinity for the two-helix α/β-peptides is that Asp36, which was replaced by the cyclic β-residue ACPC in **3.9-3.11**, makes a direct contact with HER2 in the co-crystal structure (Figure 3.16C), and removal of the Asp side chain may have been detrimental for affinity.

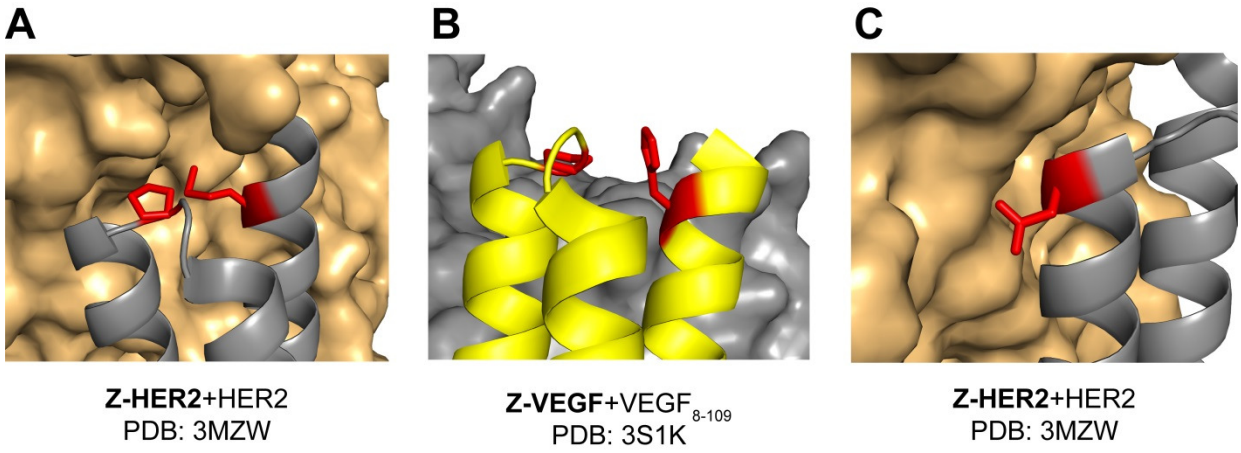

Figure 3.16 The **Z-HER2**+HER2 crystal structure (PDB: 3MZW) reveals possible reasons why α/β-peptides **3.9-3.11** did not bind HER2.[34] (A) Met9 and Pro38 in **Z-HER2**, highlighted in red, make direct contact with HER2 (tan). (B) The corresponding residues in **Z-VEGF**, His10 and Pro39, highlighted in red, do not make contact with $VEGF_{8-109}$ (gray) (PDB: 3S1K).[17] (C) Asp36 in **Z-HER2** (highlighted in red) appears to make contact with HER2 (tan).

To gain more insight into why **3.9-3.11** did not bind HER2, we synthesized **3.12** (the α-peptide analogue of **3.10**) and found that it bound HER2 with moderate affinity by competition ELISA (IC_{50} = 3.6 μM) (Figure 3.15). The IC_{50} value for **3.12** is higher than for both **3.7** and **3.8**, which both contain a disulfide bond at positions 5 and 39. This suggests that a disulfide bond at

positions 9 and 38 are not optimal for the two-helix **Z-HER2** scaffold, and that positions 5 and 39 may be better for mimicry of **Z-HER2**, likely because Met9 and Pro38 make contacts to HER2. However, the affinity of **3.12** is higher than that of its α/β-peptide analogue **3.10**, which strongly suggests that the incorporation of one of more of the non-natural residues in the α/β-peptide scaffold also was detrimental for HER2 affinity.

We designed α/β-peptide **3.13** as an analogue of **3.10** with the alternative disulfide bond at positions 5 and 39 (using **Z-HER2** numbering). Furthermore, we designed **3.14** as an analogue of **3.13** that contains the native residue (Asp) at position 36. While **3.13** showed only very weak binding to HER2, we found that **3.14** displayed IC_{50} = 1.4 μM, which indicates that Asp36 makes an important contact to HER2 in the context of the two-helix scaffold (Figure 3.15). Indeed, α/β-peptide **3.14**, which places the disulfide bond at positions 5 and 39 and has the native Asp36 residue, is a good functional mimic of the parent two-helix α-peptides **3.7** and **3.8**, binding with comparable affinity to HER2. However, the affinity of all two-helix analogues (both the α- and α/β-peptides) is lower than that of the parent three-helix **Z-HER2**, suggesting that this particular Z-domain scaffold is less amenable to truncation than are **Z-VEGF**, **Z-IgG**, and **Z-TNFα**, all three of which could be truncated to a two-helix α- or α/β-peptide without a significant loss of affinity.

One possible explanation for the loss of affinity of the two-helix **Z-HER2** analogues is that neither of the explored disulfide bond positions (linkage of positions 9,38 or positions 5,39) enforces the correct helix-loop-helix conformation nearly as well as the stabilization brought about from packing interactions by helix 3. Consistent with this hypothesis, we observed little difference in normalized, per residue far-UV CD signal for α-peptides **3.6** (no disulfide bond) versus **3.7** (disulfide at positions 5,39), and for α/β-peptides **3.15** (no disulfide bond) versus **3.13**

and **3.14** (disulfide at positions 5,39) (Figure 3.17). All of these compounds showed very little helical content in their far-UV CD signatures, suggesting that the placement of the disulfide bond at positions 5 and 39 does not promote a helical conformation in solution. To explore alternative two-helix scaffolds that may better mimic the correct binding conformation of the helix 1-helix 2 segment of **Z-HER2**, we designed several α- and α/β-peptide analogues that lacked a disulfide bond but contained helix-inducing Aib of cyclic β-substitutions (**3.15-3.19**) or contained alternative disulfide positions (**3.20-3.24**). However, none of these analogues displayed affinity for HER2 that was improved over that of α-peptides **3.7**, **3.8** or α/β-peptide **3.14** (Figure 3.15).

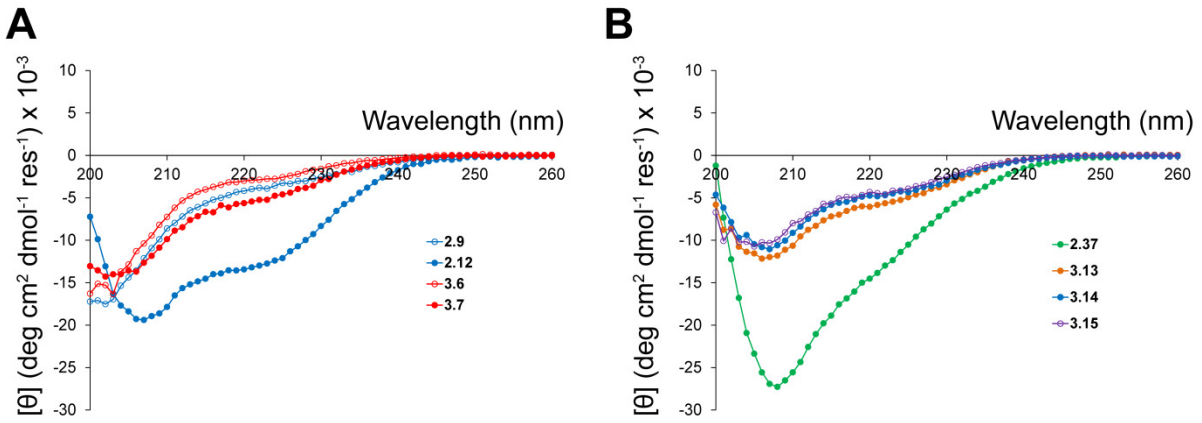

Figure 3.17 Far-UV circular dichroism data for α- and α/β-peptides shows that two-helix analogues of **Z-HER2** do not adopt a significant amount of helical content in solution. All oligomers 75 μM in PBS, 20°C. (A) α-Peptide **3.6** (no disulfide) and **3.7** (disulfide at positions 5,39) show little difference in CD signature. In contrast, the **Z-VEGF**-derived α-peptide **2.12** (disulfide at positions 10,39) shows significantly more helical content than **2.9** (no disulfide). (B) α/β-Peptides **3.13** and **3.14** (disulfide at positions 5,39) and **3.15** (no disulfide) show little difference in CD signature. In contrast, α/β-peptide **2.37** (disulfide at positions 10,39), derived from **Z-VEGF**, shows a strong helical CD signature.

Overall, **3.14** is an α/β-peptide mimic of the two-helix parent α-peptides **3.7** and **3.8**, but more work is necessary to identify alternative strategies to stabilize the intended helix-loop-helix conformation in the absence of helix 3. Prior truncation strategies relied on a disulfide bond at positions 9 and 38, but this position is likely not optimal in the **Z-HER2** context because this region of the peptide makes direct contact with the protein. Careful inspection of the **Z-**

HER2+HER2 co-crystal structure and creative peptide design may ultimately lead to a two-helix **Z-HER2** analogue that binds with affinity comparable to that of the full three-helix peptide.

3.6.3 Final designs

We next aimed to design two-helix α/β-peptide analogues of **Z-HER2** that could be used for *in vivo* tumor imaging. A 1,4,7,10-tetraazacyclododecane-1,4,7,10-tetraacetic acid (DOTA)-labeled analogue of two-helix α-peptide **3.25** (which is an extended analogue of **3.8**) has been used for tumor imaging in mice,[55] so we synthesized **3.25** as an α-peptide control for binding and proteolysis studies (Figure 3.18). Using **3.14** as a guide for the placement of Aib and β-residues, we also synthesized **3.26** as the α/β-peptide analogue of **3.25**. Finally, inspired by the large increase in protease stability manifested by a Gln26→Aib substitution in the α/β-peptide mimics of **Z-VEGF** (e.g., α/β-peptide **2.40**, described in Chapter 2), we also designed **3.27**, which contains the analogous Gln25→Aib substitution. We also synthesized derivatives of **3.25-3.27** bearing a DOTA-chelating group at their N-terminus for use in tumor imaging studies in mice (oligomers **3.28-3.30**). The synthesis of these compounds was carried out in collaboration with Geoffrey Eddinger (Gellman Laboratory, University of Wisconsin-Madison).

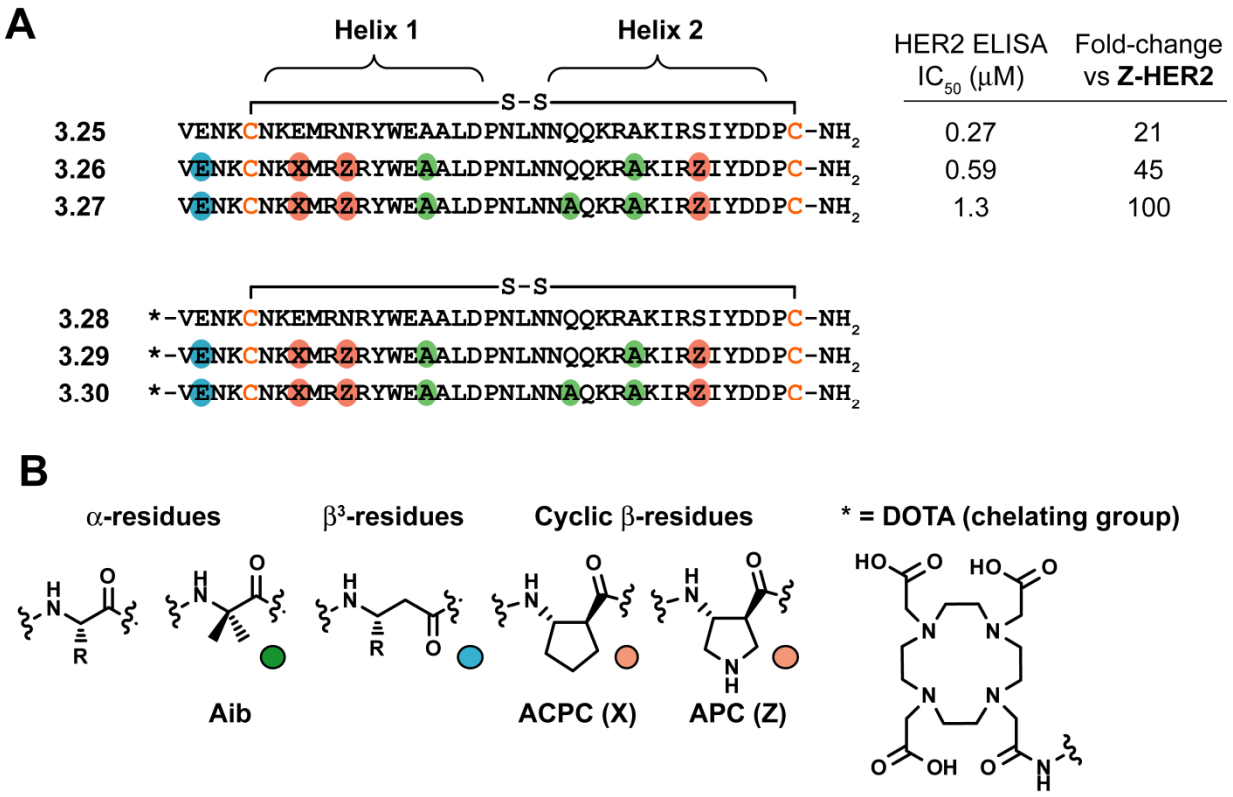

Figure 3.18 (A) Primary sequences of two-helix α- and α/β-peptides derived from **Z-HER2**, along with associated IC_{50} values, as determined by HER2 competition ELISA using 50 nM **Bt-Z-HER2**. The uncertainty in the calculated IC_{50} values from ELISA is ~2-fold. Fold-change indicates the decrease in affinity for HER2 relative to **Z-HER2** under these same conditions (**Z-HER2** IC_{50} = 0.013 μM in this same experiment). Each cysteine is engaged in an intramolecular disulfide bond. Non-natural residues are indicated by colored circles. Orange C residues indicate homocysteine. * = DOTA group for chelating to radioactive atoms for imaging applications. (B) Structures of a generic α-residue, the Aib residue (green), a generic β^3-residue (teal), the cyclic β-residues ACPC (X), APC (Z) (orange), and the DOTA chelating group (*).

We evaluated the binding of **3.25-3.27** to HER2 using competition ELISA (Figure 3.18). Here, we observed that **Z-HER2** bound HER2 with an IC_{50} = 0.013 μM and found that **3.25** bound to HER2 with an IC_{50} = 0.27 μM. The ~20-fold lower affinity of **3.25** versus **Z-HER2** is consistent with the **3.7**, **3.8** versus **Z-HER2** comparison described above. This ~20-fold drop in affinity is somewhat less dramatic than the ~200-fold drop in affinity previously reported for **3.8** versus **Z-HER2** by SPR analysis,[36] although it is unclear if Webster et al. actually performed a head-to-head comparison of **3.8** versus **Z-HER2** in their study, or if they simply reported the previously derived K_d for **Z-HER2** of 22 pM.[23] The α/β-peptides **3.26** and **3.27** (IC_{50} = 0.59 μM

and 1.3 μM, respectively) both bound to HER2 with similar affinity to that of α-peptide **3.25** (IC_{50} = 0.27 μM), suggesting that these α/β-peptides are both good functional mimics of the two-helix α-peptide. This trend is consistent with the results for **3.14** versus **3.7** and **3.8** described above. The slightly higher IC_{50} value for **3.27** versus **3.26** may be the result of the loss a productive contact from the Gln25 side chain, as was seen in the **Z-VEGF** α/β-peptide analogues **2.39-2.41**.

3.6.4 Proteolysis

We predicted that the incorporation of the non-natural Aib and β-amino acid residues would decrease the susceptibility of the α/β-peptides **3.26** and **3.27** to proteolytic degradation relative to the α-peptides **3.25** and **Z-HER2**. To test this hypothesis, we evaluated the relative susceptibilities of these oligomers to protease degradation in a proteinase K digestion assay (Figure 3.19). When 40 μM of α-peptide **3.25** was incubated with 10 μg/mL proteinase K, it was rapidly degraded, displaying a half-life of 0.27 minutes in this experiment. Surprisingly, the three-helix α-peptide **Z-HER2** was much more stable than **3.25**, showing much slower degradation than we typically see for α-peptides in this experiment. We saw ~75% **Z-HER2** remaining at 10 minutes, the last time point tested for this compound, and fitting this data to an exponential decay model gives an estimated half-life of ~25 minutes. For comparison, the three-helix **Z-VEGF** displayed a half-life of 1.6 minutes in the same experiment (reported in Chapter 2). The unusually high protease stability for the α-peptide **Z-HER2** may be due to a high conformational stability for this peptide, which may also be related to this peptide's high affinity for HER2.

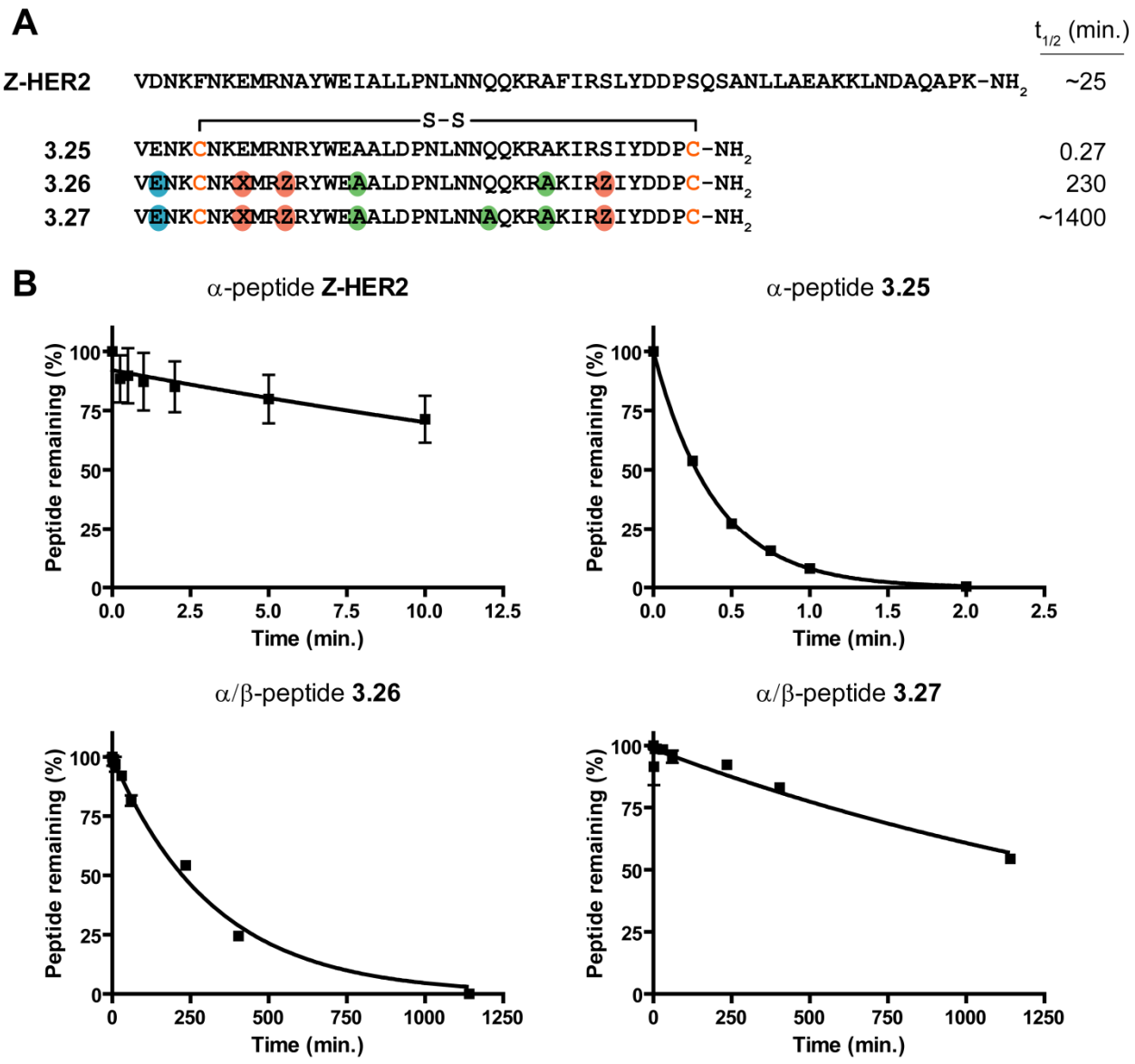

Figure 3.19 Susceptibility of 40 μM α- or α/β-peptide to 10 μg/mL proteinase K in TBS, pH 7.5 at room temperature. (A) Sequences of α- and α/β-peptides and associated half-life values. For **Z-HER2** and **3.27**, >50% of the intact oligomer remained at the final time point tested, so reported half-life values are approximate values obtained by fitting the data to an exponential decay model. (B) Time course of α- or α/β-peptide degradation, as assessed by HPLC. Note the different scales on the horizontal axes.

When the α/β-peptides **3.26** and **3.27** were subjected to proteinase K, they displayed half-lives of 230 minutes (for **3.26**) and ~1400 minutes (for **3.27**). These results indicate that the α/β-peptides have significantly reduced susceptibility to degradation by proteinase K relative to both the two-helix parent α-peptide **3.25** and the three-helix **Z-HER2**. However, this experiment

will need to be repeated to determine an accurate half-life value for both **Z-HER2** and **3.27**, as >50% of oligomer was remaining at the last time point evaluated for each compound (10 minutes for **Z-HER2** and 1100 minutes for **3.27**).

3.6.5 In vivo tumor imaging

We evaluated the utility of α/β-peptides **3.29** and **3.30** as molecular imaging agents in mice, and compared them to α-peptide **3.28** as a positive control. α-Peptide **3.28**, the DOTA-labeled analogue of **3.25**, has previously been used for imaging HER2-overexpressing tumors in mice using positron emission tomography (PET) to detect radioactive atoms chelated to the DOTA group.[53, 55] The imaging and biodistribution experiments described in this section were obtained by the Hackel Laboratory (Department of Chemical Engineering and Material Science, University of Minnesota).

Nu/nu mice were inoculated with MDA-MB-435 cells (low HER2 expression) and SKOV3 cells (high HER2 expression), in opposite shoulders. Tumors were allowed to grow from these implanted cells, and then ^{64}Cu-chelated **3.28**, **3.29**, or **3.30** were injected intravenously into the mice. PET/CT imaging was performed to monitor localization of peptides over time (Figure 3.20). Tissues and fluids were then collected by dissection, weighed, and counted for gamma radiation (Figure 3.21). This initial study showed ^{64}Cu-labeled α/β-peptides **3.29** and **3.30** localized to the HER2-overexpressing SKOV3 tumors, but not the MDA-MB-435 tumors, consistent with the hypothesis that these α/β-peptides are binding to HER2 on the tumor cell surface. All three compounds effectively targeted HER2-overexpressing tumors, with tumor:blood ratios of ~3-4 and tumor:muscle ratios ~8 for the SKOV3 tumors, in contrast to lower values for the MDA-MB-435 tumors (Figure 3.21C). High renal uptake was observed for each of **3.28-3.30**, which is commonly observed for this type of molecule,[23, 32, 55, 56] although α/β-

peptide **3.29** showed less renal uptake than **3.28** or **3.30** in this preliminary experiment (Figure 3.21B). Follow-up experiments are necessary to confirm if the lower kidney uptake observed for **3.29** is reproducible. Taken together, the imaging and biodistribution data (Figures 3.20 and 3.21) show that α/β-peptides **3.29** and **3.30** localize at HER2-overexpressing tumors, and perform as well as α-peptide **3.28** for imaging applications. Future experiments are necessary to investigate if the α/β-peptide backbone of **3.29** and **3.30** provide any benefits for this application over the α-peptide backbone of **3.28**.

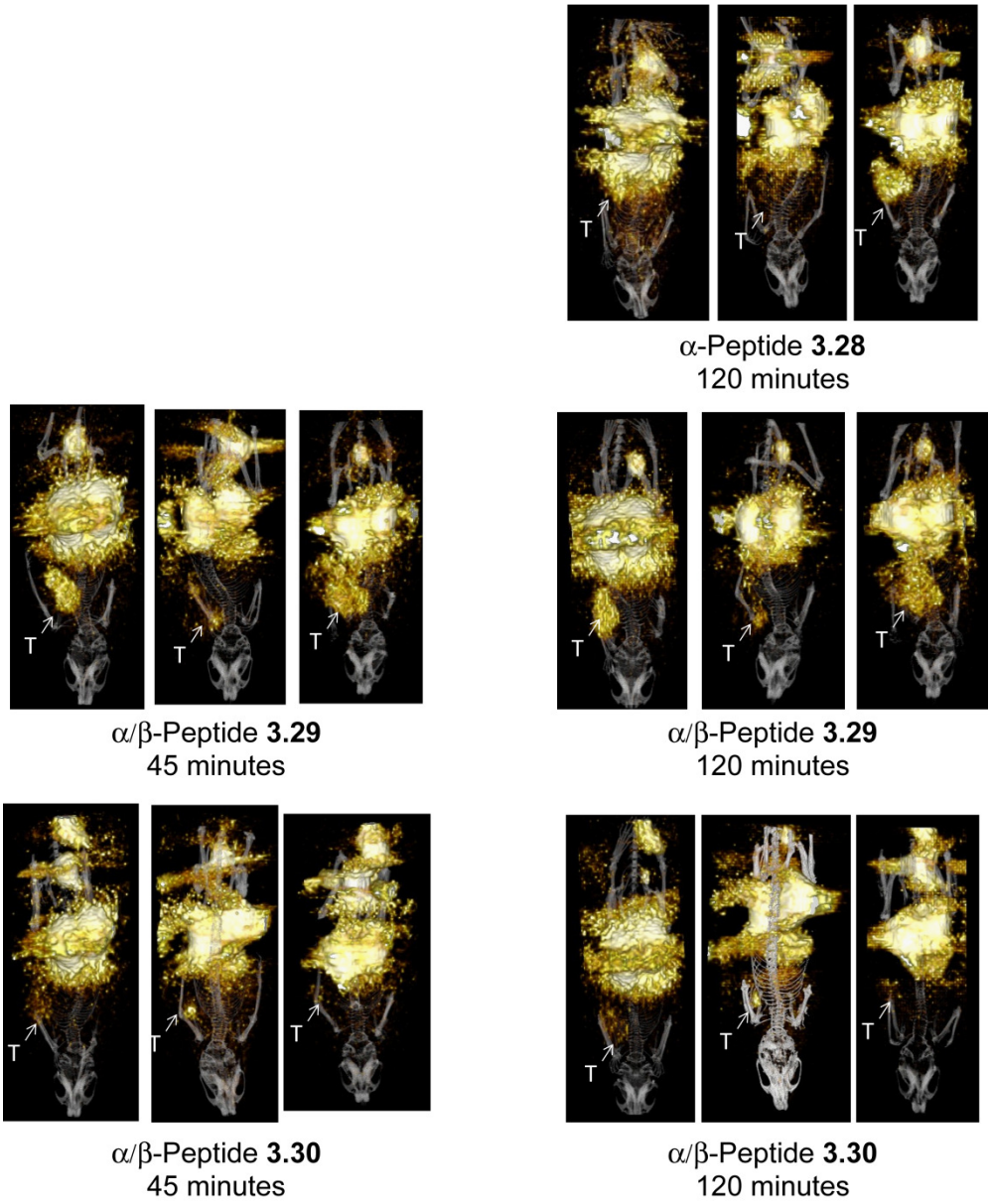

Figure 3.20 PET/CT imaging of mice bearing SKOV3 (high HER2 expression) tumors (labeled with "T" and arrow) with ^{64}Cu-**3.28**-**3.30**. Each compound was injected into three mice and imaged at 45 minutes and 120 minutes. α-Peptide **3.28** was only imaged at 120 minutes due to instrument error. High signal near in the center of each image arises from kidney, liver, etc. uptake.

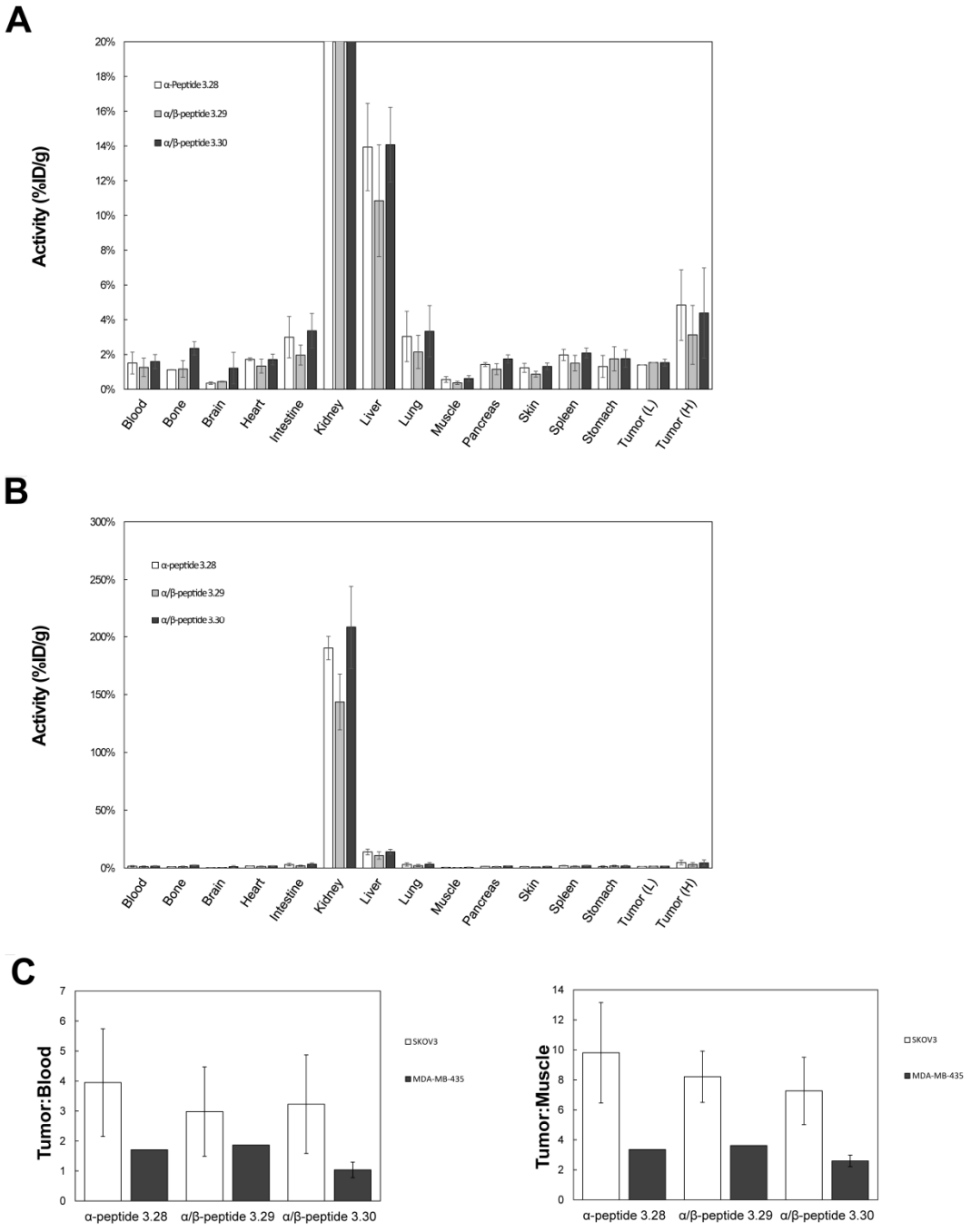

Figure 3.21 Biodistribution data for **3.28-3.30**. After imaging, mice were euthanized (~4 hours post-injection) and tissues and fluids were collected, weighed, and counted for gamma radiation (from ^{64}Cu). (A) Activity per mass is reported as percent of injected dose per gram of tissue or fluid. Values are presented as mean ± SD of three mice for each compound, except for the MDA-MB-435 tumor, in which only one mouse each for **3.28** and **3.29** generated this tumor. Tumor (L) indicates MDA-MB-435 (**L**ow HER2). Tumor (H) indicates SKOV3 (**H**igh HER2). (B) Zoomed out plot of the same data from panel A. (C) Tumor, blood, and muscle activities from panels A and B were evaluated as ratios for SKOV3 (high HER2) and MDA-MB-435 (low HER2) tumors.

3.7 Attempts at α/β-peptide mimicry of Z-EGFR

Epidermal growth factor receptor (EGFR, also called ErbB1) is a growth factor receptor that belongs to the same family as HER2. Like HER2, EGFR is overexpressed on certain tumors, and molecular imaging of EGFR may be useful as a diagnostic tool.[26, 49] **Z-EGFR** is a three-helix peptide derived from the Z-domain scaffold by selecting for binding to EGFR, followed by affinity maturation.[25, 26] To further test the generalizability of our α/β-peptide design strategy, as well as to create starting points for potential α/β-peptide imaging agents, we aimed to design α/β-peptide analogues of **Z-EGFR** following the α/β-peptide design strategy that proved successful for mimicry of **Z-VEGF**, **Z-IgG**, and **Z-TNFα**, removing helix 3 and incorporating the same disulfide and substitution patterns as successful for these cases (specifically, following the Aib and β-residue pattern of **3.2** and **3.5**). Following this path led us to design α/β-peptide **3.31**. α/β-Peptide **3.31** also included an N-terminal propargylglycine residue for eventual conjugation to chelating groups or dyes to be used in imaging experiments. We also designed **3.32** as an analogue of **3.31** bearing a Met27→norleucine substitution in an effort to avoid undesired methionine oxidation (Figure 3.22).

We evaluated the ability of **Z-EGFR**, **3.31**, and **3.32** to bind EGFR using a competition ELISA assay (Figure 3.23). In this experiment, we saw that the parent three-helix α-peptide **Z-EGFR** was able to compete with immobilized **Z-EGFR** for binding to soluble EGFR protein with an IC_{50} = 0.048 μM (Figure 3.22). In contrast, the two-helix α/β-peptides **3.31** and **3.32** both showed only very weak binding to EGFR, showing IC_{50} > 30 μM (estimated IC_{50} = ~40 μM for both α/β-peptides).

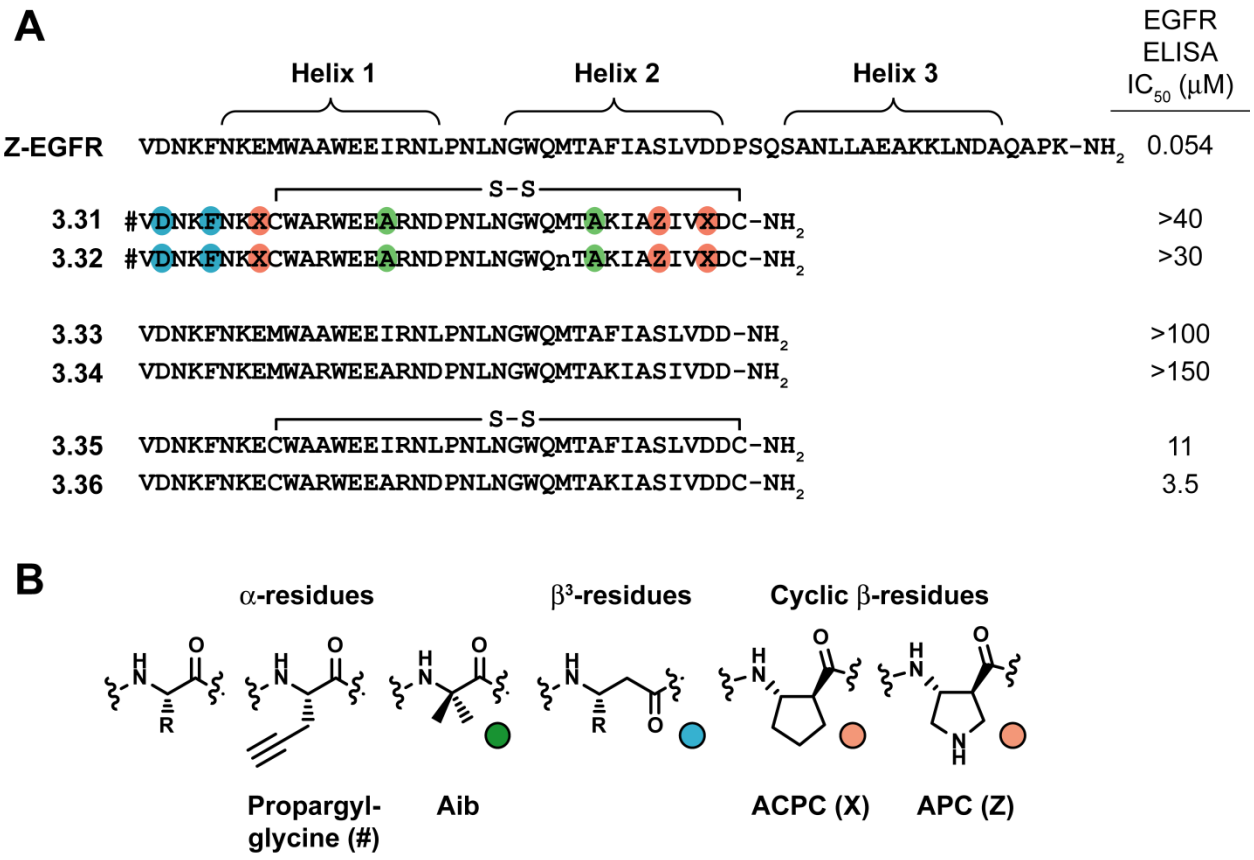

Figure 3.22 (A) Primary sequences of **Z-EGFR** and two-helix α- and α/β-peptide derivatives, along with associated IC_{50} values, as determined by EGFR competition ELISA. The uncertainty in the calculated IC_{50} values from ELISA is ~2-fold, with a maximum variation of up to ~7-fold for some experiments. Hypothesized positions of helices 1, 2, and 3 are indicated by brackets. Non-natural residues are indicated by colored circles. Each cysteine is engaged in an intramolecular disulfide bond. (B) Structures of a generic α-residue, the propargylglycine residue (#), the Aib residue (green), a generic β^3-residue (teal), and the cyclic β-residues ACPC (X) and APC (Z) (orange).

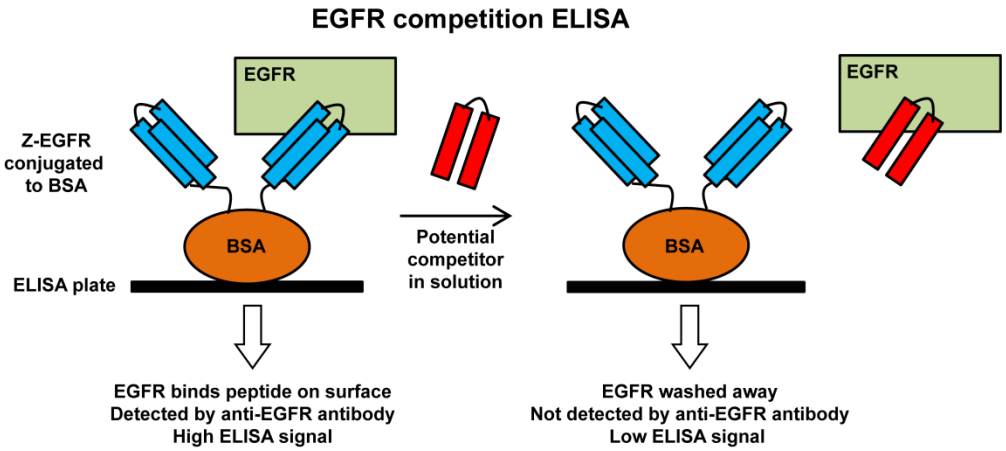

Figure 3.23 Cartoon representation of the EGFR competition ELISA used to evaluate the relative ability of α- and α/β-peptides to bind to EGFR.

To gain insight into why **3.31** and **3.32** bound to EGFR with so much lower affinity than **Z-EGFR**, we synthesized α-peptides **3.33-3.36**. α-Peptide **3.33** corresponds to residues 1-38 of **Z-EGFR**, and **3.34** is an analogue of **3.33** that contains five helix-stabilizing α-residue substitutions.[35, 36] α-Peptides **3.35** and **3.36** are disulfide-constrained analogues of **3.33** and **3.34**. When evaluated by competition ELISA, we saw that **3.33** and **3.34**, which contain no disulfide constraint, showed very little binding to EGFR (Figure 3.22). This is consistent with the results seen for the two-helix **Z-VEGF** α-peptide analogues (Chapter 2) in which two-helix peptides without a disulfide constraint lost all binding to the protein, likely because of a dramatic loss in conformational stability in the absence of helix 3. Both **3.35** and **3.36** bound to EGFR (IC_{50} = ~11 μM and 3.5 μM, respectively), but this binding was significantly weaker than that of three-helix **Z-EGFR**. This result is similar to the two-helix **Z-HER2** analogues described above, which all showed a decrease in affinity relative to full-length **Z-HER2**.

Taken together, the results from the **3.31-3.36** competition ELISA experiments suggest several explanations for the lack of affinity of the α/β-peptides **3.31** and **3.32**. First, because the two-helix α-peptides **3.33** and **3.34** lost almost all affinity for EGFR, it is essential to use some strategy, such as a disulfide bond, to stabilize the two-helix conformation in this system. Second, while **3.35** and **3.36** did regain binding to EGFR, their higher IC_{50} values compared to full-length **Z-EGFR** suggests that these two-helix α-peptide scaffolds are not optimal in this system, as is likely the case for **Z-HER2**, as described above. These trends could have a number of possible origins. Perhaps the residues replaced with the disulfide are critically important for EGFR binding, or perhaps helix 3 makes productive contacts with the protein. Because there is currently no crystal structure of **Z-EGFR** in complex with EGFR, it is difficult to predict which of these (or other) possibilities are true without further experimental efforts. Finally, because the

α/β-peptides **3.31** and **3.32** bound to EGFR more weakly than their α-peptide analogue **3.36**, it is likely that at least one of the non-natural substitutions in this α/β-peptide scaffold occurs at a site that is important for high affinity binding to EGFR.

Future efforts to develop EGFR-binding α/β-peptides based on **Z-EGFR** could explore different disulfide bond positions to attempt to stabilize the two-helix scaffold such that it binds with affinity comparable to that of **Z-EGFR**. Second, the results reported above suggest that one or more of the non-natural Aib or β-residue substitutions is detrimental for EGFR affinity in this system. This trend parallels the **Z-HER2** system described above, in which Asp36 made an important contact to HER2 that could not be replaced with a β-residue. Future α/β-peptide designs based on **Z-EGFR** should systematically evaluate each of these positions to determine which ones must remain native residues. Once these positions are determined, these residues can either be retained as α-residues in the final α/β-peptide designs (as we did for Asp36 in the **Z-HER2** analogues described above), or they may be replaced with β^3-residues to retain the native side chain while reducing protease susceptibility.

3.8 Conclusions

In this chapter, I have described a general strategy for creating peptidic oligomers with unnatural backbones that bind selectively to large surfaces on specific target proteins. This approach takes advantage of the very similar three-dimensional structures and binding modes of peptides derived from the Z-domain scaffold, binding to their target proteins primarily though the surface formed by helices 1 and 2. Because the α/β-peptide design strategy outlined in Chapter 2 for mimicry of **Z-VEGF** aimed to recapitulate this surface in the context of the two-helix α/β-peptide scaffold, we anticipated that the strategy could be readily adapted to mimic the analogous surfaces on other Z-domain derivatives. As shown here, this approach appears to be

relatively versatile: after optimizing the Z-domain-derived α/β-peptide scaffold for one protein partner (**Z-VEGF** analogues for binding to VEGF), we found that this unnatural backbone could be readily adapted, via modification of selected α-residue side chains, to two other protein targets for which Z-domain ligands were already known (IgG and TNFα). The unnatural backbone hinders proteolytic degradation of these α/β-peptides and therefore represents a substantial advantage relative to the conventional α-peptide backbone.

When we extended this approach to a fourth target, **Z-HER2**, we were able to obtain α/β-peptides that bound HER2 and could be used to image HER2-overexpressing tumors *in vivo*. The two-helix α/β-peptides targeting HER2 **3.26** and **3.27** bind to HER2 with comparable affinity to the parent two-helix α-peptide **3.25**, which suggests that the α→β and Aib substitutions are well-tolerated in this scaffold. However, the reduced affinity of all explored two-helix analogues compared to **Z-HER2** suggests we have not yet identified the optimal two-helix α-scaffold for this system, likely due to a non-optimal placement of the disulfide bond. Initial attempts to extend this approach to mimic **Z-EGFR** were unsuccessful, but the data described above strongly suggest that this failure may also be a result of a non-optimal two-helix α-peptide scaffold.

Our approach combines elements of two long-term polypeptide engineering initiatives: i) efforts from multiple laboratories to optimize the Z-domain (or "affibody") scaffold for selective binding to diverse partner proteins; and ii) efforts from our group to mimic information-bearing α-helices with oligomers that contain both α- and β-amino acid residues. Prior Z-domain scaffold efforts have identified a protein-binding face formed by two adjacent α-helical segments (helices 1 and 2 of the three-helix bundle tertiary structure). The recognition properties of this surface can be adapted to many different protein targets via randomization-selection protocols

focused on a specific set of residues from helices 1 and 2.[6, 7, 16] Moreover, polypeptide length can be minimized by eliminating helix 3 and incorporating compensatory features (including a disulfide) to stabilize the helix-loop-helix folding pattern.[35-37] Principles that have emerged from mimicry of individual α-helices with α/β-peptides[57, 58] enable α→β replacement at Z-domain sites that do not contact the target protein or interfere with tertiary packing. This integrated design strategy allows one to combine the benefits of large biosynthetically generated libraries, which offer profound advantages in terms of surveying vast regions of sequence space but are limited to the 20 proteinogenic α-amino acids, with the benefits in physiological stability provided by an unnatural backbone.

The availability of two-helix α/β-peptide analogues of Z-domains tailored to bind to three distinct protein partners (VEGF, IgG, and TNFα) allowed us demonstrate that high target specificity is maintained despite the unnatural backbones and despite high similarity in primary sequence. The data for analogues of **Z-VEGF** and **Z-TNFα** suggest that properly designed α/β-peptides can match the affinity of the prototype Z-domains for the target proteins. Therefore, we predict that the target affinity of two-helix α/β-peptide Z-domain analogues might be improved if phage display or some comparable technique were used to select a new two- or three-helix Z-domain with higher affinity for that target. Such an effort should, in principle, identify favorable changes to the set of target-contacting α-residues, and these changes could be transferred directly to the two-helix α/β-peptide scaffold.

The three-helix Z-domain α-peptide scaffold has proven to be very versatile, with customized variants reported for over twenty protein targets of biomedical interest.[6, 7] The resulting mini-proteins are attractive in terms of development of therapeutic antagonists of deleterious protein-protein associations and as starting points for highly specific imaging

agents.[5-7] Selection of new protein-binding molecules from Z-domain libraries usually generates polypeptides that maintain the characteristic Z-domain three-helix bundle tertiary structure and the two-helix interaction surface. The results reported here provide a strategy that should enable rapid creation of biostable two-helix α/β-peptide analogues of many Z-domain agents to target a wide variety of different types of protein surfaces.

3.9 Future directions

The results described in this chapter suggest a strategy to develop α/β-peptides that can target a diverse range of different proteins, first by selecting a Z-domain from a combinatorial library that binds to a target of interest, and then following the α/β-peptide design strategy outlined here (or a similar one) to mimic the protein-binding surface presented by the parent Z-domain. The generalizability of this α/β-peptide design approach to mimic many different Z-domain peptides suggests a method by which the affinity of α/β-peptides can be increased by first performing affinity maturation (using phage display and selection) on a parent three-helix α-peptide to derive higher affinity binders, followed by α/β-peptide mimicry. Long term goals are to extend this approach to other Z-domain targets of therapeutic and diagnostic interest. One potential new target is the recently reported biparatopic Z-domain dimer that targets VEGFR2 and blocks VEGF signaling.[18] This dimer could have application in the antagonism of VEGF signaling for the treatment of various diseases, or for molecular imaging of VEGFR2-overexpression in tumors.

Preliminary results with α/β-peptide analogues of **Z-IgG** suggest that these compounds may survive in the bloodstream for extended periods of time. This result may be useful for the development of α/β-peptide compounds designed to be administered in animal models. Alternatively, the increase in plasma residence time for these analogues may be due to IgG

binding, which suggests that these IgG-binding compounds may be used as tags on other molecules to reduce renal clearance. Finally, preliminary experiments with **3.2** suggest that this α/β-peptide may be amenable to co-crystallization with the Fc fragment of IgG1 to gain high-resolution information of this interaction. Solving and refining this structure will require higher quality crystals with better X-ray diffraction than those reported here, either through optimization of the conditions reported in this chapter or through screening and optimization of new crystallization conditions.

As exemplified by the **Z-HER2** and **Z-EGFR** cases, the exact same truncation and α→β substitution pattern does not work to mimic every Z-domain without some loss in affinity, perhaps due to subtle differences in the way that the Z-domains bind to their protein binding partners. Future work should attempt to broaden the "generalizability" of this strategy by outlining steps that a researcher can take to optimize the α/β-peptide scaffold for each new target. The two-helix α-peptide analogues of **Z-HER2** and **Z-EGFR** both showed a dramatic decrease in affinity for their respective protein targets relative to the parent three-helix peptides. Collectively, these results suggest that one two-helix scaffold is not universal for mimicry of all Z-domain peptides. Alternative disulfide positions or stabilization strategies should be explored with the goal of increasing the affinity of the two-helix α-peptide analogues to levels that match the parent three-helix peptides. Re-introduction of α→β and Aib substitutions can then be used to create a high-affinity α/β-peptide in these cases.

Preliminary results show that **3.29** and **3.30** can be used to image HER2-overexpressing tumors in mice and match the parent α-peptide **3.28** at their ability to localize at HER2-overexpressing tumors (Figures 3.20 and 3.21). This has direct application for the imaging of certain tumors and the diagnostic evaluation of their HER2 expression levels, which is an

important factor in determining the best treatment. It is not yet clear if the α/β-peptide backbone will provide significant benefits for this application. We predict that the unnatural backbone may have several potential advantages over a natural α-peptide backbone: i) The decreased protease susceptibility may allow the α/β-peptide to survive for long periods of time on a tumor surface. This would have applications for imaging at longer time points and for radiotherapy; ii) The decreased protease susceptibility for the α/β-peptide may reduce the immunogenicity of the α/β-peptide relative to the corresponding α-peptide; and iii) the α/β-peptides may have reduced toxicity due to proteolytic breakdown. Metabolic stability studies and imaging experiments spanning longer periods of time are currently under way to explore these possibilities.

Finally, because the results reported here also suggest that the α/β-peptide mimicry of one member of a family derived from a peptide scaffold (e.g., the "Z-domain") can be extended to mimic other members of that peptide family adopted from the same fold, future directions should explore the mimicry of other peptide scaffolds that may be of interest in targeting different types of protein surfaces or for different applications. For these experiments, one would choose a peptide derived from a non-immunoglobulin scaffold (e.g., the DARPin scaffold) and develop an α/β-peptide mimic of this peptide. α→β-Residue replacements in this peptide may be identified using an iterative β-residue incorporation strategy, as outlined in Chapter 2, or some other strategy. Once an α/β-peptide mimic of one peptide from the family is identified, it may be that the successful pattern of α→β-residue replacements can be transferred to design α/β-peptide mimics of other members of that particular family, as described in this chapter.

3.10 Experimental methods

3.10.1 General

Fmoc-protected α-amino acids with compatible side chain protecting groups and benzotriazole-1-yl-oxy-tris-pyrrolidino-phosphonium hexfluorophosphate (PyBOP) were purchased from Chem-Impex International and Novabiochem. Fmoc-protected β^3-amino acids with compatible side chain protecting groups were purchased from PepTech Corporation and Chem-Impex International. Fmoc-ACPC-OH was purchased from Chem-Impex International (15073). Fmoc-APC(Boc)-OH was synthesized as previously described.[59]

3.10.2 Peptide synthesis and purification

α- and α/β-peptides were prepared as described in Chapter 2. **Z-TNFα**, **Z-HER2**, and **Z-EGFR** were synthesized on a Symphony automated peptide synthesizer, double coupling each amino acid, as previously described for **Z-VEGF**.[17] **Bt-Z-HER2** was conjugated at the N-terminus with biotin by treating the peptide chain on resin with 4 equivalents of biotin activated with PyBOP and DIEA in the presence of 0.1 M HOBt in NMP for 2 x 1 hour at room temperature. α- and α/β-peptides **3.28-3.30** were labeled with DOTA by treating the peptide on resin with 4 equivalents of DOTA-tris(t-Bu ester) (Macrocyclics, B-260), activated with PyBOP and DIEA in the presence of 0.1M HOBt in NMP, stirred overnight at room temperature. The DOTA-labeled peptides were then cleaved from the resin and oxidized by DMSO+ammonium hydroxide, as described in Chapter 2. After purification, final peptide purity was assessed by analytical HPLC and identity confirmed by MALDI-TOF-MS ("Peptide characterization" section below).

3.10.3 IgG ELISA

The binding of α/β-peptides to human IgG1-κ was determined by indirect and competition ELISA. **3.1** and **3.2** were each conjugated to bovine serum albumin (BSA) by dissolving approximately 1 mg of purified α/β-peptide in a solution containing 3% BSA, 8 mM glutaraldehyde in 0.1 M NaOAc, pH 7.0, at a total volume of 330 μL. The conjugation reaction was allowed to proceed on a rocker at room temperature for 2 hours and quenched by the addition of 5-6 mg glycine and additional incubation for 1 hour. After quenching, the reaction solution was diluted to 3 mL with PBS, pH 7.0 and dialyzed overnight into PBS at 4 °C using 10,000 MWCO dialysis membrane. After dialysis, the α/β-peptide+BSA conjugates were concentrated to approximately 500 μL using 10,000 MWCO Amcon Ultra-15 centrifugal filter units (EMD Millipore, 901024). These concentrated solutions were stored at -20 °C, diluted and used directly for indirect and competition ELISA experiments.

For indirect ELISA using BSA-conjugated α/β-peptides, 50 μL of serial dilutions (starting with 1:50 dilution in PBS, pH 7.4) of **3.1** or **3.2** conjugated to BSA were immobilized onto a Nunc Maxisorp clear polystyrene 96-well ELISA plate (Thermo Scientific, 430341) in PBS, incubated overnight at 4 °C. After immobilization, the plate was washed with PBS+0.05% TWEEN20 (for this and all subsequent washes, wells were rinsed 3-5 times with 200 μL PBS+0.05% TWEEN20) and blocked with 1% BSA in PBS+0.05% TWEEN20 for 1-2 hours at room temperature. The plate was then washed with PBS+0.05% TWEEN20 and 100 μL of human IgG1-κ (Sigma, I5154) was added and incubated at room temperature for 1.5 hours. Because a stronger signal was observed for the **3.2**+BSA conjugate relative to the **3.1**+BSA conjugate (possibly due to a difference in affinity or in conjugation efficiency), 30 μg/mL human IgG1-κ in PBS+0.05% TWEEN20 was used for assays in which **3.1** was immobilized, and 10

μg/mL human IgG1-κ in PBS+0.05% TWEEN20 was used for assays in which **3.2** was immobilized. After immobilized α/β-peptide was allowed to bind human IgG1-κ, the plate was washed with PBS+0.05% TWEEN20, and the binding of human IgG1-κ detected by adding 100 μL of 1:2000 dilution of goat anti-human IgG (Fab specific)-alkaline phosphatase antibody (Sigma A8542) in PBS+0.05% TWEEN20 and the plate was incubated at room temperature for 1 hour. After washing with PBS+0.05% TWEEN20, 50 μL of SIGMA*FAST* p-Nitrophenyl phosphate (pNPP) solution (Sigma, N1891) was added to each well, and the alkaline phosphatase reaction allowed to proceed at room temperature. Plates were read (absorbance at 405 nm) during the time course of the reaction on a BioTek Synergy 2 microplate reader (Figure 3.5). Each condition was run in duplicate. No increase in signal over background was observed in wells in which no α/β-peptide was immobilized (negative control). In addition, no signal was observed for either immobilized α/β-peptide when no human IgG1-κ was incubated, indicating that the goat anti-human IgG (Fab specific)-alkaline phosphatase antibody does not bind non-specifically to the α/β-peptides or BSA.

For competition ELISA using BSA-conjugated α/β-peptides, 50 μL of a 1:100 dilution of the **3.2**+BSA conjugate in PBS was immobilized onto the ELISA plate and incubated at 4 °C overnight. After immobilization, the plate was washed with PBS+0.05% TWEEN20, blocked with 1% BSA for 1-2 hours, and then washed with PBS+0.05% TWEEN20. Serial dilutions of soluble α/β-peptides in DMSO were prepared, and 10 μL of each of these dilutions added to 240 μL of human IgG1-κ (final concentration = 10 μg/mL) in PBS+0.05% TWEEN20. The soluble α/β-peptides were allowed to pre-incubate with human IgG1-κ for 1-2 hours, and then 100 μL of each α/β-peptide+IgG1-κ mixture was added to the ELISA plate and the plate was incubated at room temperature for 2 hours. The binding of human IgG1-κ to the immobilized **3.2** was

measured using goat anti-human IgG (Fab specific)-alkaline phosphatase antibody, as described above. Each condition was run in duplicate. Plates were read (absorbance at 405 nm) during the time course of the reaction on a BioTek Synergy 2 microplate reader. Reactions were quenched with the addition of 100 μL of 1 M NaOH to each well. To compare the ability of each soluble α/β-peptide to bind human IgG1-κ and inhibit binding to the immobilized **3.2**, IC_{50} values were calculated by fitting the ELISA absorbance data to a sigmoidal dose-response equation using GraphPad Prism 4.0 (Figure 3.24). Based on the analysis of a large number of independent TNFα-TNFR1 competition ELISA experiments (Section 4.2.4 in Chapter 4), we believe that the believe the uncertainty in the calculated IC_{50} values from ELISA experiments is ~2-fold, with a maximum variation of up to ~7-fold for some experiments. The calculated IC_{50} values for each of the assays reported in Figure 3.24 are shown in Table 3.1. Thus, the reproducibility for calculated IC_{50} values in the competitors in the IgG1-κ ELISA is within this range, and perhaps even better.

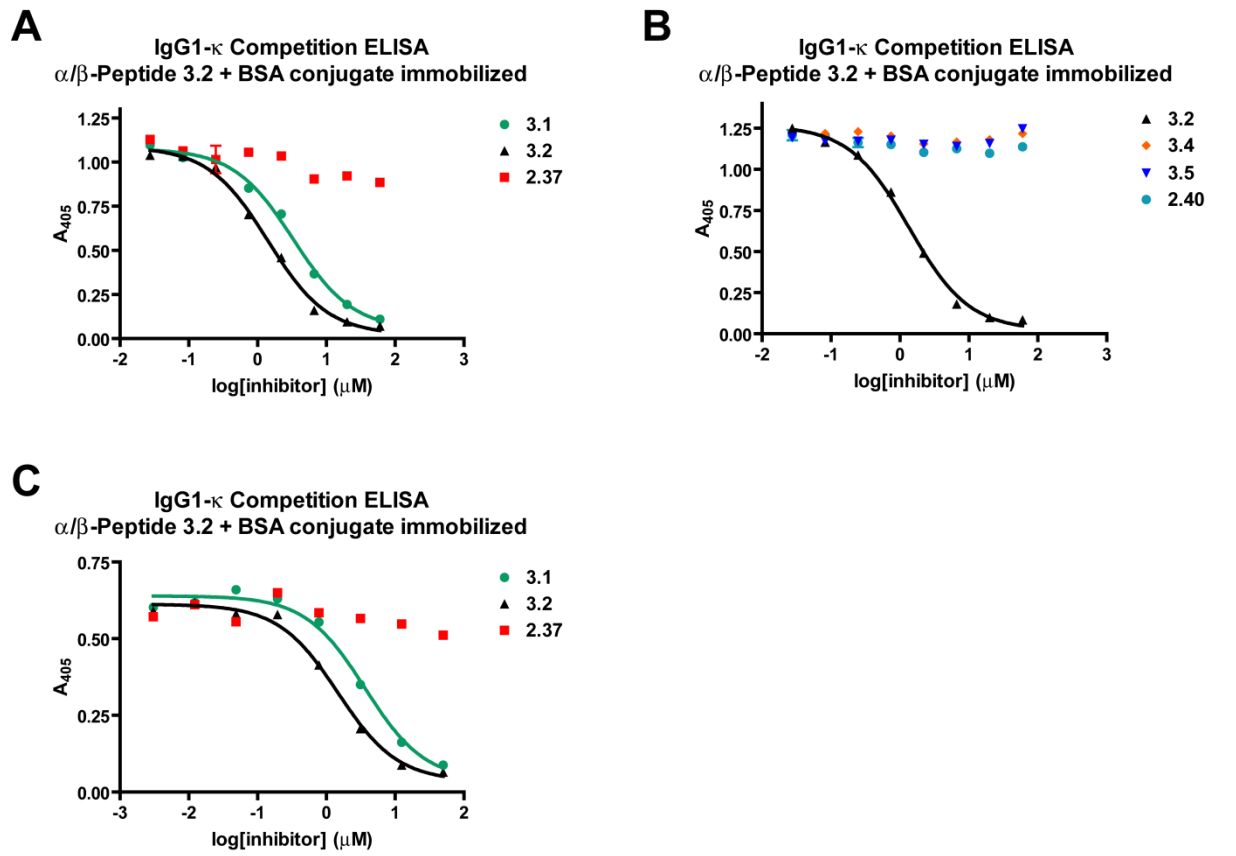

Figure 3.24 IgG1-κ competition ELISA comparing the relative ability of different α/β-peptides to inhibit binding of 10 μg/mL IgG1-κ to immobilized **3.2**+BSA conjugate. Each panel shows an independent experiments with soluble **3.2** used as an inhibitor in each assay to show reproducibility. Data points represent the mean ± SEM of duplicate wells on plate.

	IC_{50} (μM) (Panel from Figure 3.24 shown in parentheses)
3.1	3.3 (A), 3.7 (C)
3.2	1.4 (A), 1.4 (B), 1.5 (C)

Table 3.1 IC_{50} values obtained for each of the compounds reported in Figure 3.24.

For IgG competition ELISA using α/β-peptide **3.2** directly immobilized onto the ELISA plate (not as a BSA conjugate), a 3 μM α/β-peptide **3.2** solution was prepared in 100 mM sodium carbonate, pH ~9.6 (diluted from DMSO stock), and 100 μL of this solution was added to each well on a Nunc Immobilizer Amino ELISA plate, and the plate was shaken at room temperature for about 2 hours. The plate was then washed with PBS+0.05% TWEEN20 and blocked by the addition of 100 μL of 10 mM ethanolamine in 100 mM sodium carbonate, pH ~9.6, and this

blocking reaction allowed to proceed for 1 hour. The plate was then washed with PBS+0.05% TWEEN20, and then 100 μL of 20 μg/mL IgG1-κ was added to each well and allowed to incubate at room temperature for ~1 hour. The wells were washed with PBS+0.05% TWEEN20. Serial dilutions of soluble potential competitors in DMSO were prepared, and then diluted with PBS+0.05% TWEEN20 (final concentration = 4% DMSO), and 100 μL of this solution added to each well of the ELISA plate. The soluble potential inhibitors were allowed to compete with the immobilized α/β-peptide for binding to IgG1-κ over 3-4 hours. (This method of competition, in which IgG1-κ is first allowed to bind to immobilized α/β-peptide and then competed off by soluble peptide, produced the most reproducible results for this assay, in contrast to the other competition ELISA protocols described in this chapter.) After the competition reaction, the plate was washed with PBS+0.05% TWEEN20, and the binding of human IgG1-κ to the immobilized α/β-peptide was measured using goat anti-human IgG (Fab specific)-alkaline phosphatase antibody, as described above. Each condition was run in duplicate. Plates were read (absorbance at 405 nm) during the time course of the reaction on a BioTek Synergy 2 microplate reader. To compare the ability of each soluble α/β-peptide to bind human IgG1-κ and inhibit binding to the immobilized α/β-peptide, IC_{50} values were calculated by fitting the ELISA absorbance data to a sigmoidal dose-response equation using GraphPad Prism 4.0 (Figure 3.25).

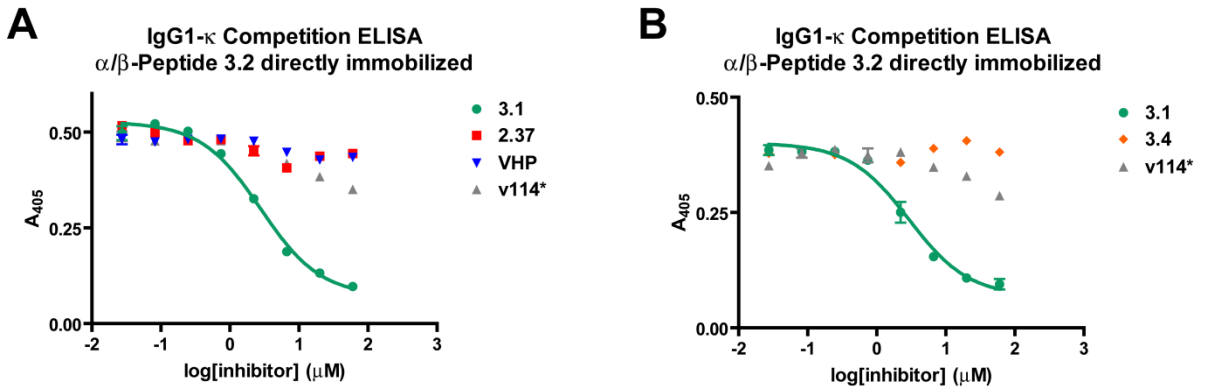

Figure 3.25 IgG1-κ competition ELISA comparing the relative ability of different α- and α/β-peptides to displace IgG1-κ from **3.2** covalently immobilized to Nunc Immobilizer Amino ELISA plates. Both (A) and (B) are independent experiments with soluble **3.1** used as an inhibitor in both assays to show reproducibility. **VHP** and **v114*** are unrelated α-peptides used as negative controls in this experiment. The sequence of **VHP** = LSDEDFKAVFGMTRSAFANLPLWKQQHLKKEKGLF-COOH, synthesized by Dale Kreitler (Gellman Laboratory, University of Wisconsin-Madison). The sequence of **v114*** = VEPNCDIHVnWEWECFERL-NH_2, where Cys residues are engaged in an intramolecular disulfide bond and n = norleucine. Data points represent the mean ± SEM of duplicate wells on plate.

3.10.4 Crystallization

Crystallization screens were performed by first dialyzing human IgG1-Fc fragment (Athens Research, 16-16-090707-1M-FC) against purified water using 2000 MWCO mini dialysis units (Thermo Scientific, 69580), and then mixing this protein solution with α/β-peptide solution in water. Initial screens were performed at ~5 mg/mL Fc fragment and between 200 and 900 μM α/β-peptide by mixing the protein/peptide solution with precipitant solution from various reagent screens offered from Hampton Research (Hampton Index, Crystal Screens 1 and 2, Low Ionic Strength Screen). A variety of protein/peptide concentrations and volumes were explored, both with IgG1-Fc fragment purchased from Athens Research, and with IgG1-Fc prepared by digestion of human IgG1 from myloma plasma (offered from a variety of companies, including Sigma) with papain and purification by protein A column using a Fab preparation kit (Pierce, 44985). (Although the kit is meant for the purification of Fab, the Fc fragment can also be isolated using the Protein A column.) Although we observed a number of initial crystallization hits through these screen, the most promising crystals grew from precipitant

solutions from the Low Ionic Strength Screen containing 0.05 mM glycine, pH 9.5 or pH 10.0, with 24% PEG3350. After some preliminary optimization, the conditions used to grow the crystals described in this chapter resulted from premixing 5 mg/mL IgG1, Fc fragment (Athens Research) with 600 μM **3.2** (~6:1 α/β-peptide/Fc ratio) in water and setting hanging drops with 2 μL of this solution, 1 μL of 0.05 mM glycine, pH 10.0, and 1 μL of reservoir solution containing 24% PEG3350 + 5% (+/-)-2-methyl-2,4-pentanediol (MPD) in 24-well crystallization trays over 1000 μL of reservoir solution covered with 600 μL Al's Oil (1:1 paraffin/silicon oil). The addition of Al's Oil appeared to slow crystal growth to produce larger crystals.

Crystals were mounted on a nylon loop and cryoprotected by dragging the crystal through a solution of 1:1 butandiol/32% PEG3350 and frozen at the beamline. Diffraction data were collected at the Life Sciences Collaborative Access Team (LS-CAT) beamline 21-ID-G at the Advanced Photon Source (APS), Argonne National Laboratory. 182 1° oscillation images with 5 second exposure time were collected at a wavelength of 0.97856 Å. At certain orientations background scattering from loop and ice was very significant, and we tried to find orientations that minimized this scattering during data collection. Frames 1-97 correspond to an oscillation range of 0-97 degrees, frames 98-182 correspond to an oscillation range of 256-340 degrees.

Numerous strategies for processing the data were attempted. The most promising results came from processing frames 1-95 in XDS[60] and finding an initial molecular replacement solution using *Phaser*[61] using the chains from PDB: 1FC1 containing the Fc dimer with sugar groups removed. Because of the low quality of the data, it was difficult to definitively determine the space group, but the most likely options were P31 or P3121. Initial refinements in Phenix[62]

used data processed as P31 using rigid body refinement. The model shown in Figure 3.26 is after several rounds of refinement with R_{work} = 34.4%, R_{free} = 43.7%.

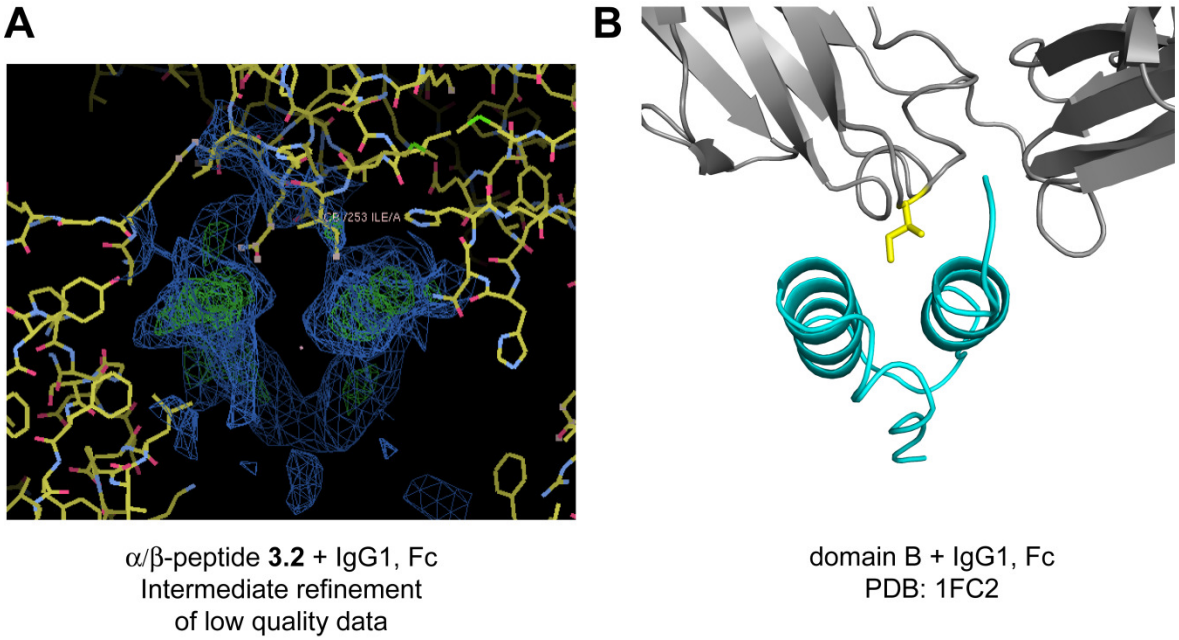

Figure 3.26 Preliminary crystallographic evidence shows that α/β-peptide **3.2** may accurately mimic the binding mode of the parent peptide **Z-IgG** (which is an analogue of domain B). (A) Intermediate refinement of data collected on a crystal of **3.2**+IgG1, Fc after molecular replacement using the Fc dimer (PDB: 1FC1) with sugars removed as a search model, as visualized in Coot. Modeled protein indicates the molecular replacement solution for the Fc fragment (note that multiple copies of the dimer are present in the asymmetric unit). Unmodeled density is present in the location where **3.2** is expected to bind, indicated in blue ($2F_o$-F_c, contoured to 1.02σ) and green (F_o-F_c, contoured to 3.0σ). Ile253 from the Fc fragment is labeled. (B) The co-crystal structure of domain B (cyan) in complex with IgG1, Fc (gray), for comparison (PDB: 1FC2).[8] The same Ile253 residue in Fc is highlighted in yellow.

3.10.5 Pharmacokinetics in mice

Peptide stocks were prepared in PBS at ~300 μM (~1-2 mg/mL), as determined by UV-absorbance.[63] Female FVB mice were weighed and injected with the appropriate volume of peptide stock to give ~10 mg/kg peptide (or comparable amount of PBS for controls), as indicated in the Figures above, using retro-orbital (RO) or intraperitoneal (IP) injection methods. Experiments shown in detail in the main text used IP injection. Initial experiments also used RO injection, although this injection method was less successful. After the indicated amount of time

post-injection, mice were anaesthetized with isoflurane and sacrificed by cervical dislocation. Blood and kidneys were collected immediately after death by dissection. Plasma was isolated from the blood and stored at -20 °C until analysis. Kidneys were homogenized in PBS and stored at -20 °C until analysis.

Analysis of plasma samples was performed by MALDI-TOF and analytical-scale reverse-phase HPLC. For MALDI-TOF analysis, plasma samples were diluted 1:1 with purified water and then dialyzed against water using 2000 MWCO mini dialysis units (Thermo Scientific, 69580) before being spotted onto the MALDI plate with α-cyana-4-hydroxycinnamic acid (CHCA) as the MALDI matrix. For HPLC analysis of plasma samples, plasma was diluted 1:2 with 1:1 water/acetonitrile + 0.1% trifluoroacetic acid (TFA), centrifuged for 2 minutes at 13,000 rpm to remove some precipitated plasma proteins, and then the supernatant was injected onto analytical-scale HPLC. (We suspect that some α/β-peptide may also co-precipitate under these conditions, and so further optimization of this protocol or addition of an internal standard may be necessary for rigorous quantitative analysis.) Kidney homogenates were analyzed by MALDI-TOF. Kidney homogenates were dialyzed against purified water using 2000 MWCO mini dialysis units (for ~1.5 hours) and then spotted onto the MALDI plate with CHCA matrix.

Figure 3.27 shows the HPLC analysis of plasma isolated from each mouse injected with 10 mg/kg of the indicated α/β-peptide, along with control injections of each α/β-peptide alone, for the experiment described in Figure 3.8.

Figure 3.28 shows the MALDI analysis of kidneys from each mouse (Panels A-E), and the plasma from each mouse (Panels F-J) for the experiment described in Figure 3.8.

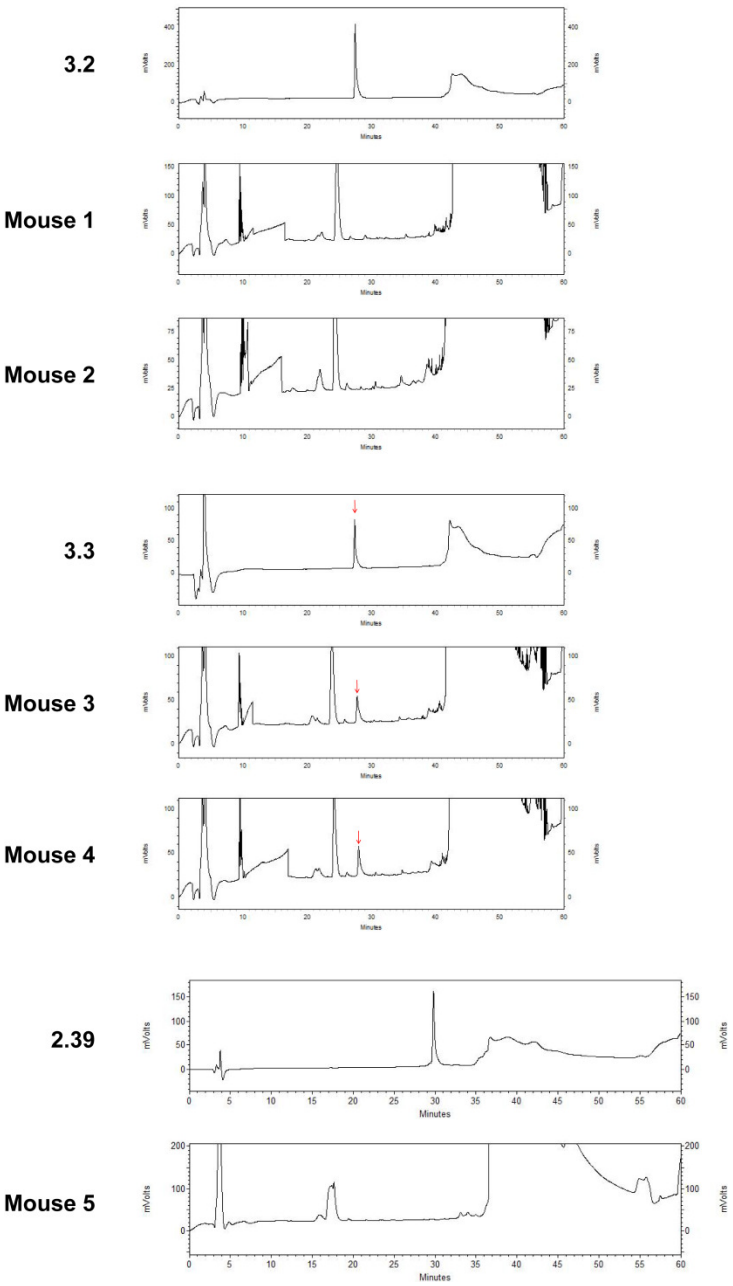

Figure 3.27 HPLC analysis of mouse plasma after injection with 10 mg/kg α/β-peptides **3.2**, **3.3**, or **2.39** using IP injection and analyzed 20 minutes post-injection, monitoring UV absorbance at 220 nm, from the experiment summarized in Figure 3.8. Chromatograms labeled with **3.2**, **3.3**, or **2.39** indicate chromatograms where pure peptide is injected onto HPLC to show retention time (note that the peaks eluting at >35 minutes in these chromatograms are residual serum proteins from previous injections). Chromatograms labeled "Mouse X" show the plasma analysis of that mouse, as indicated in Figure 3.8. The red arrow in Mouse 3 and Mouse 4 indicates the position of the peak corresponding to intact **3.3**.

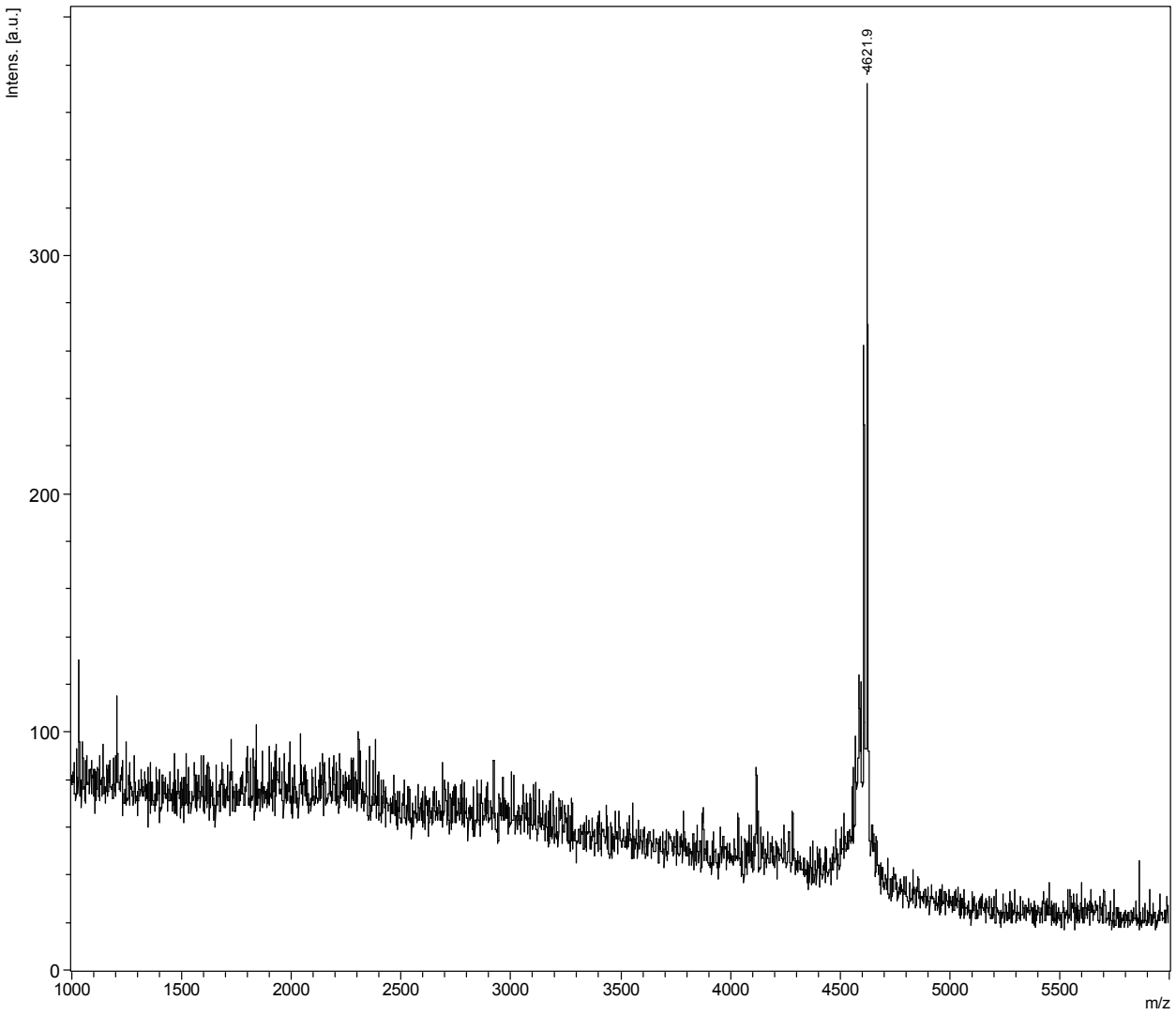

Figure 3.28 (A) MALDI-TOF analysis of kidney homogenates from Mouse 1. Expected $[M+H]^+$ for **3.2** = 4622.3.

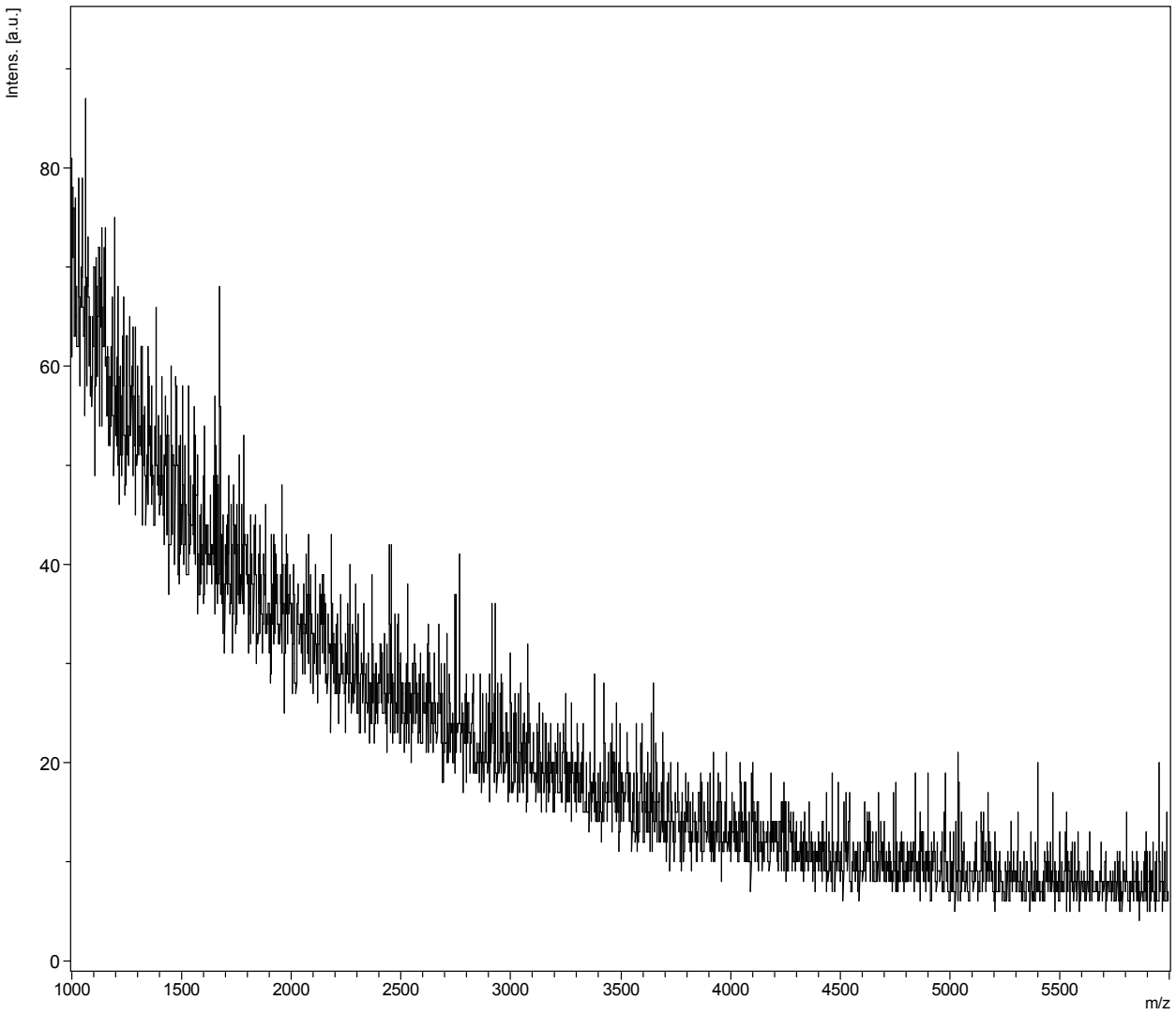

Figure 3.28 (B) MALDI-TOF analysis of kidney homogenates from Mouse 2. Expected $[M+H]^+$ for **3.2** = 4622.3.

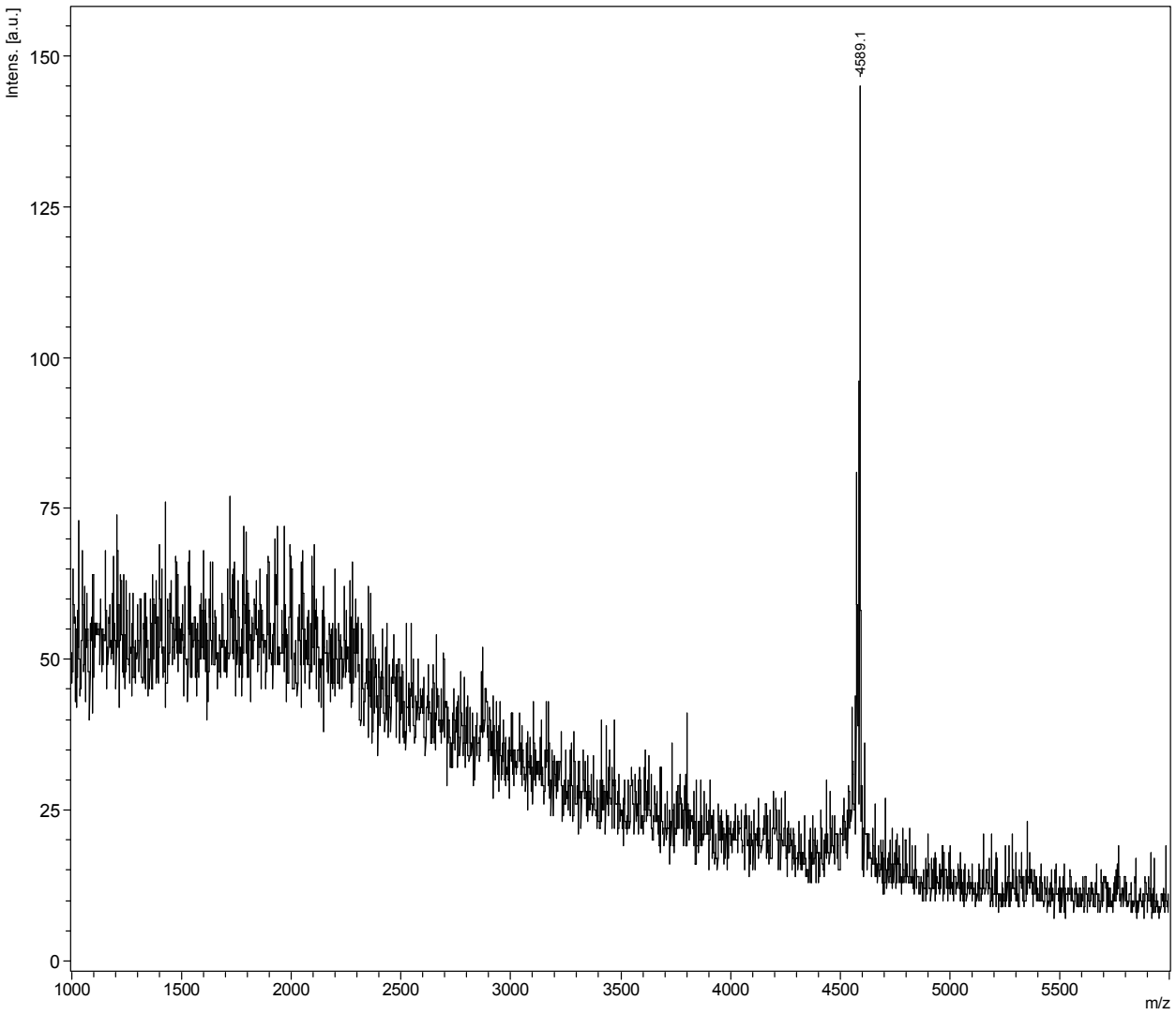

Figure 3.28 (C) MALDI-TOF analysis of kidney homogenates from Mouse 3. Expected $[M+H]^+$ for **3.3** = 4588.3.

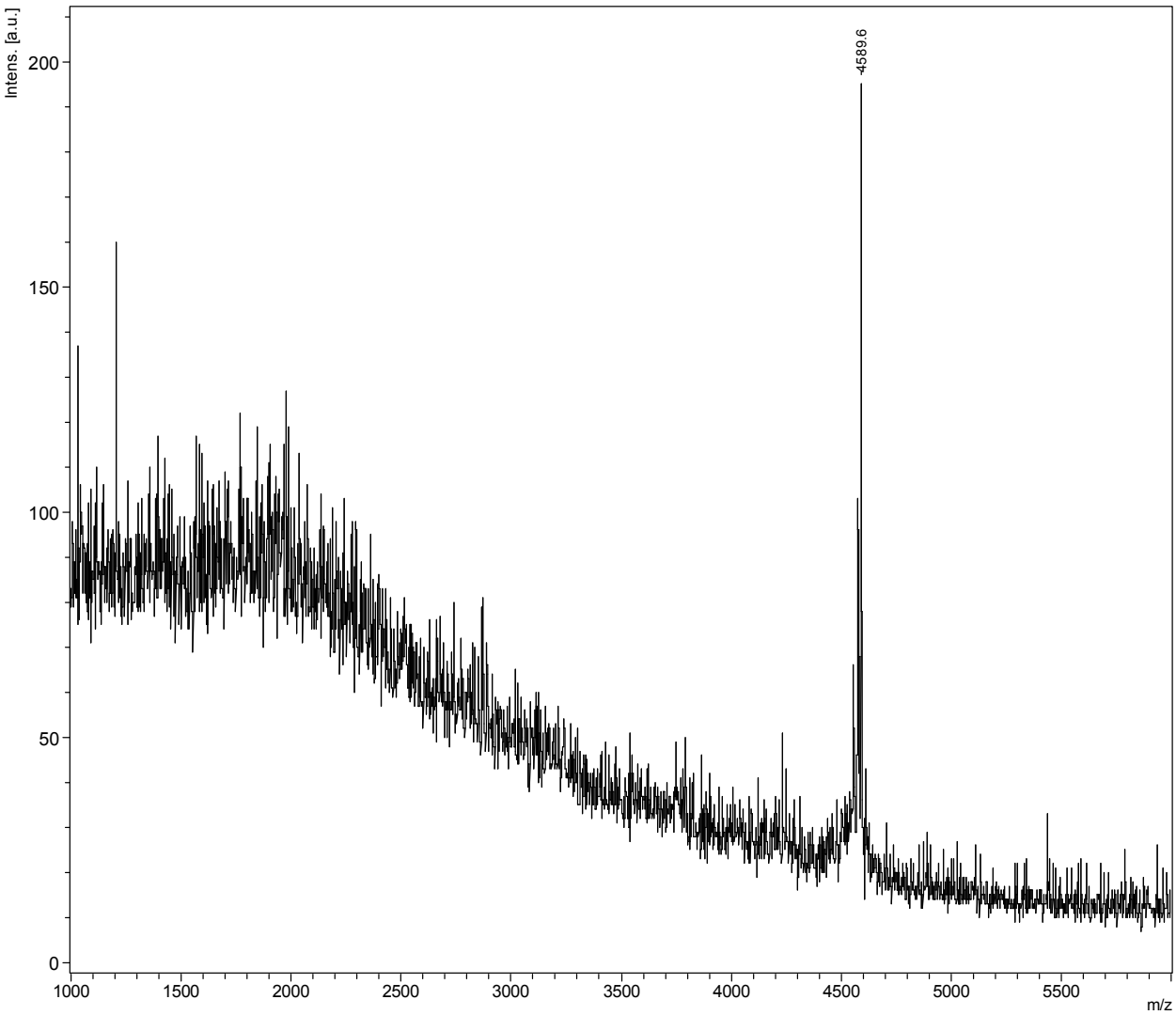

Figure 3.28 (D) MALDI-TOF analysis of kidney homogenates from Mouse 4. Expected $[M+H]^+$ for **3.3** = 4588.3.

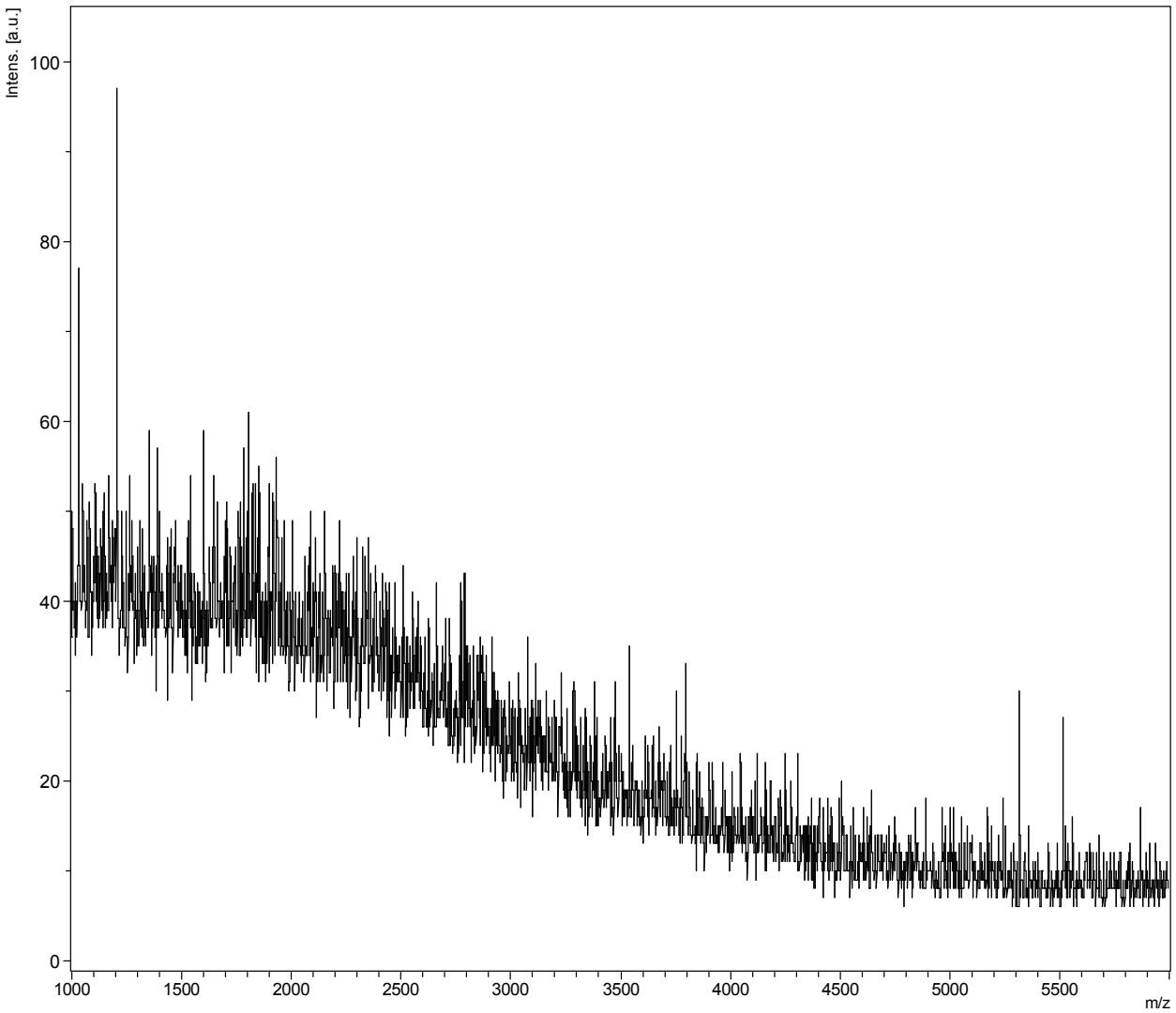

Figure 3.28 (E) MALDI-TOF analysis of kidney homogenates from Mouse 5. Expected $[M+H]^+$ for **2.39** = 4514.3.

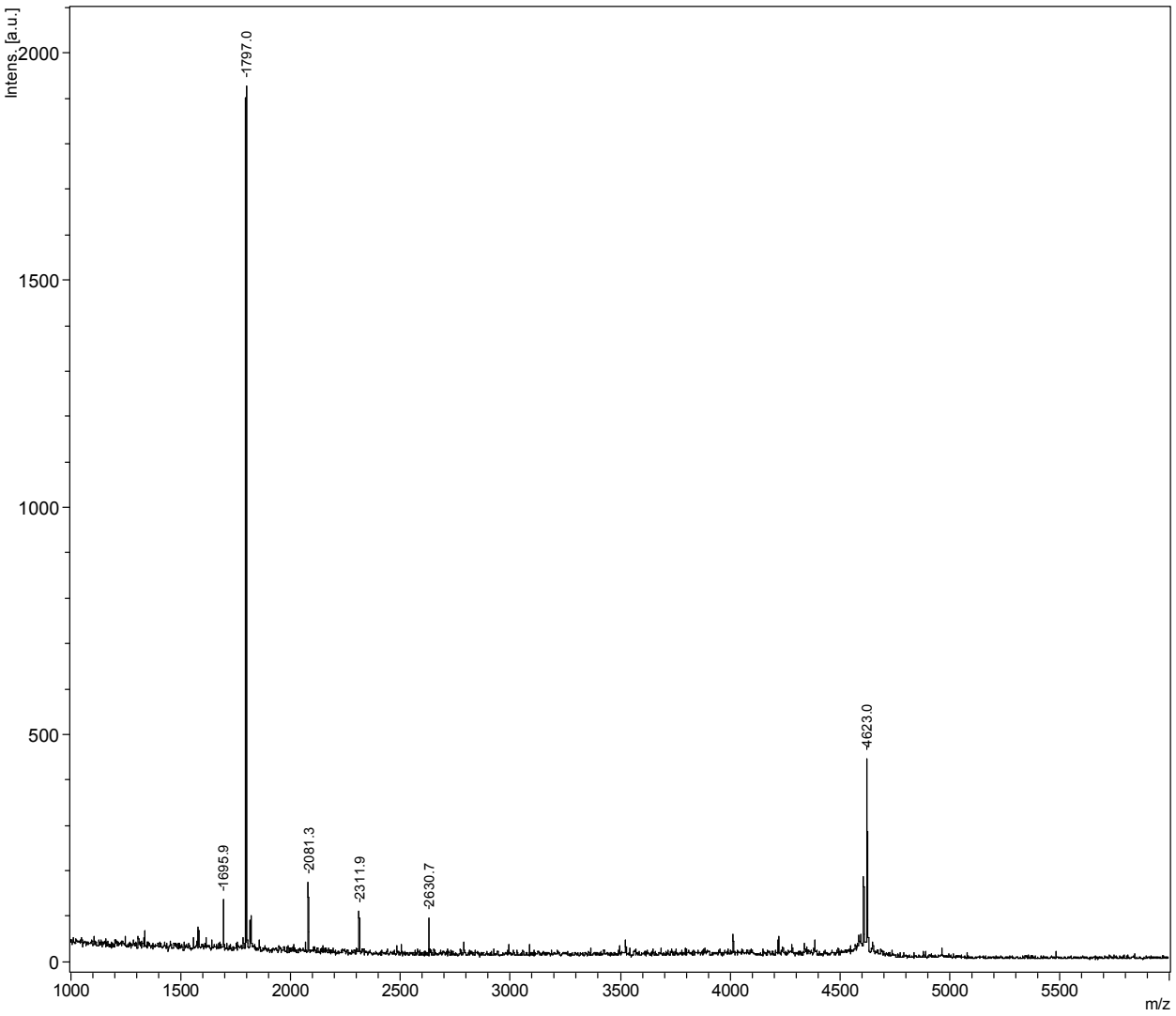

Figure 3.28 (F) MALDI-TOF analysis of plasma from Mouse 1. Expected $[M+H]^+$ for **3.2** = 4622.3.

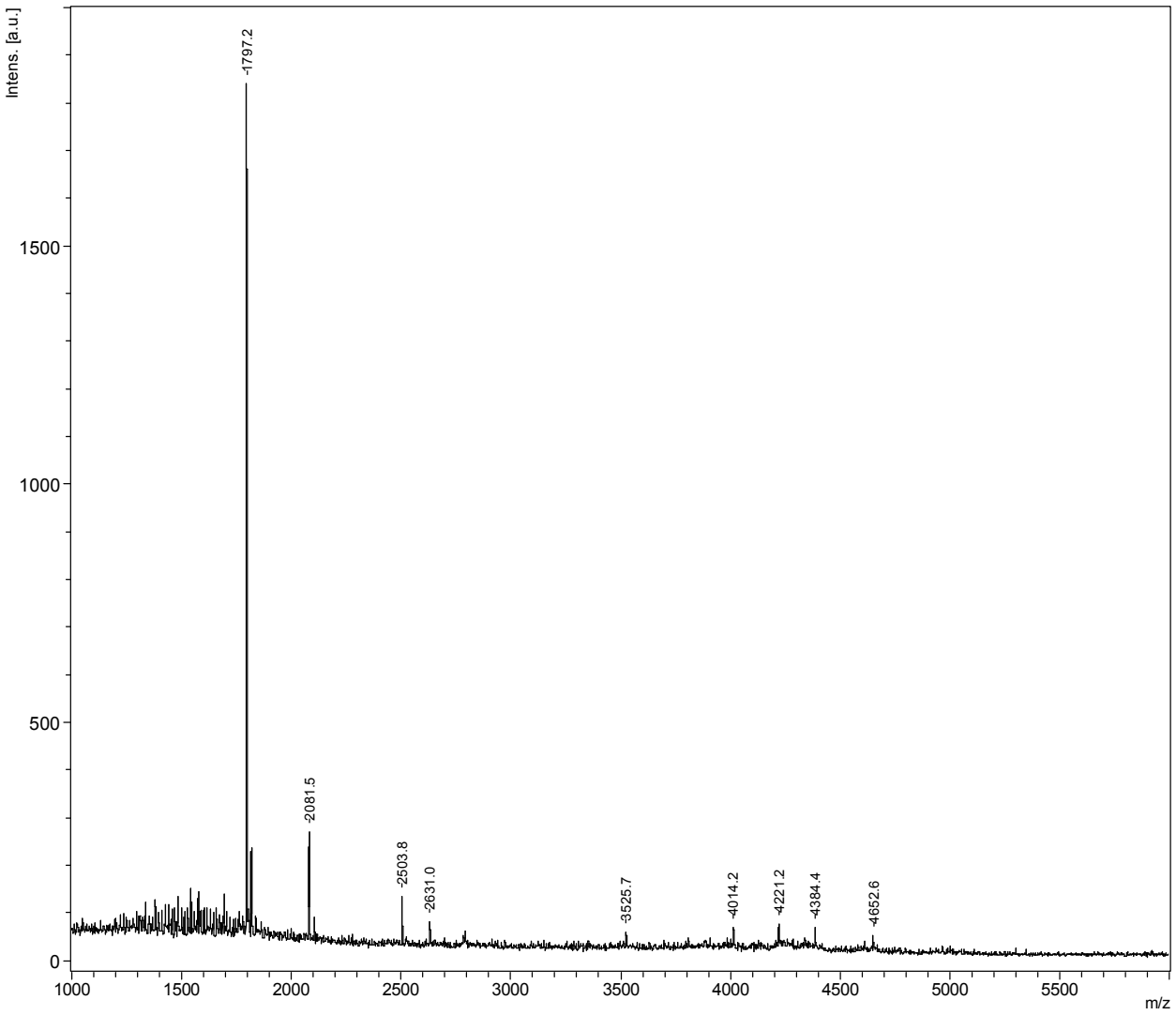

Figure 3.28 (G) MALDI-TOF analysis of plasma from Mouse 2. Expected $[M+H]^+$ for **3.2** = 4622.3.

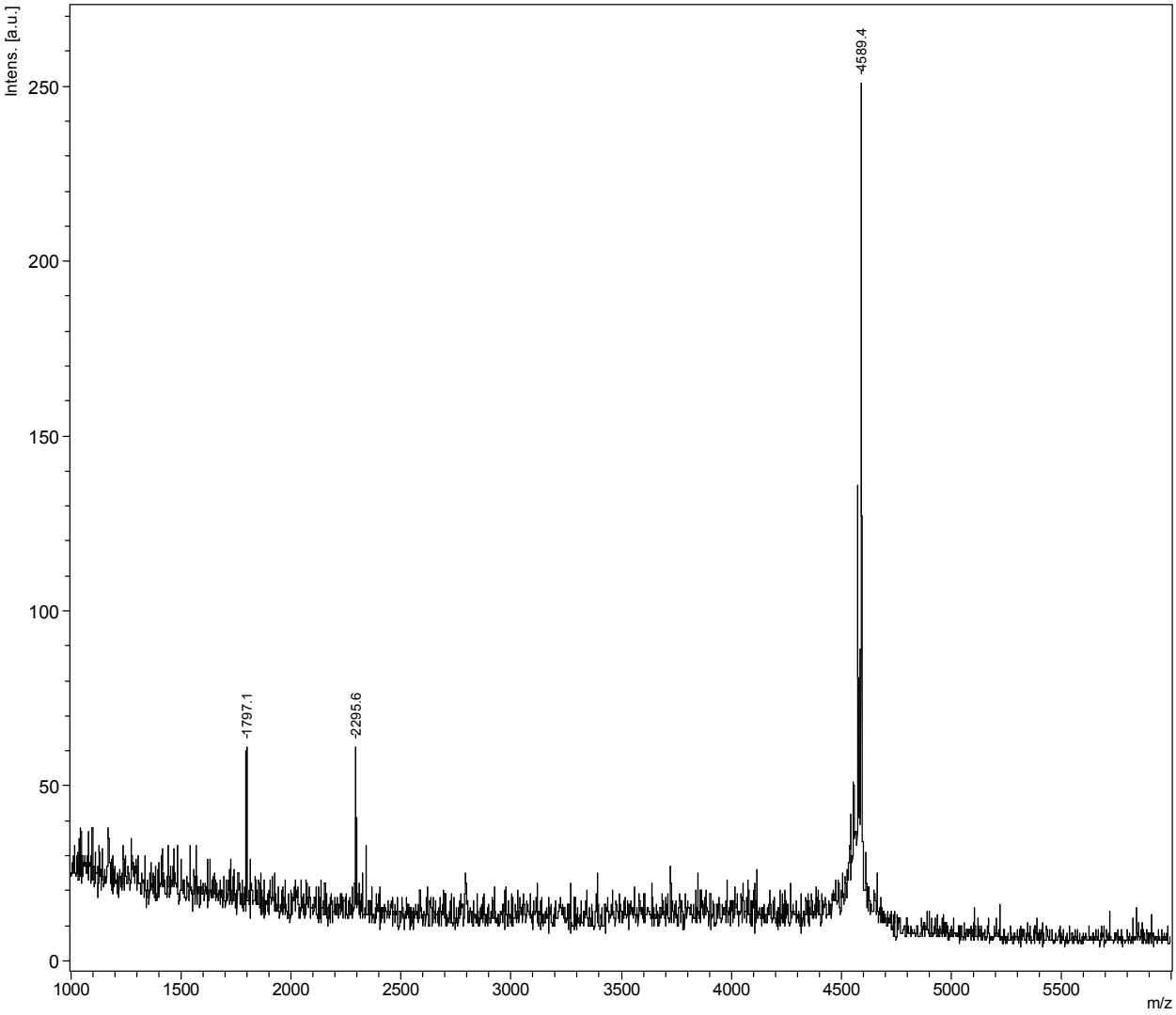

Figure 3.28 (H) MALDI-TOF analysis of plasma from Mouse 3. Expected $[M+H]^+$ for **3.3** = 4588.3.

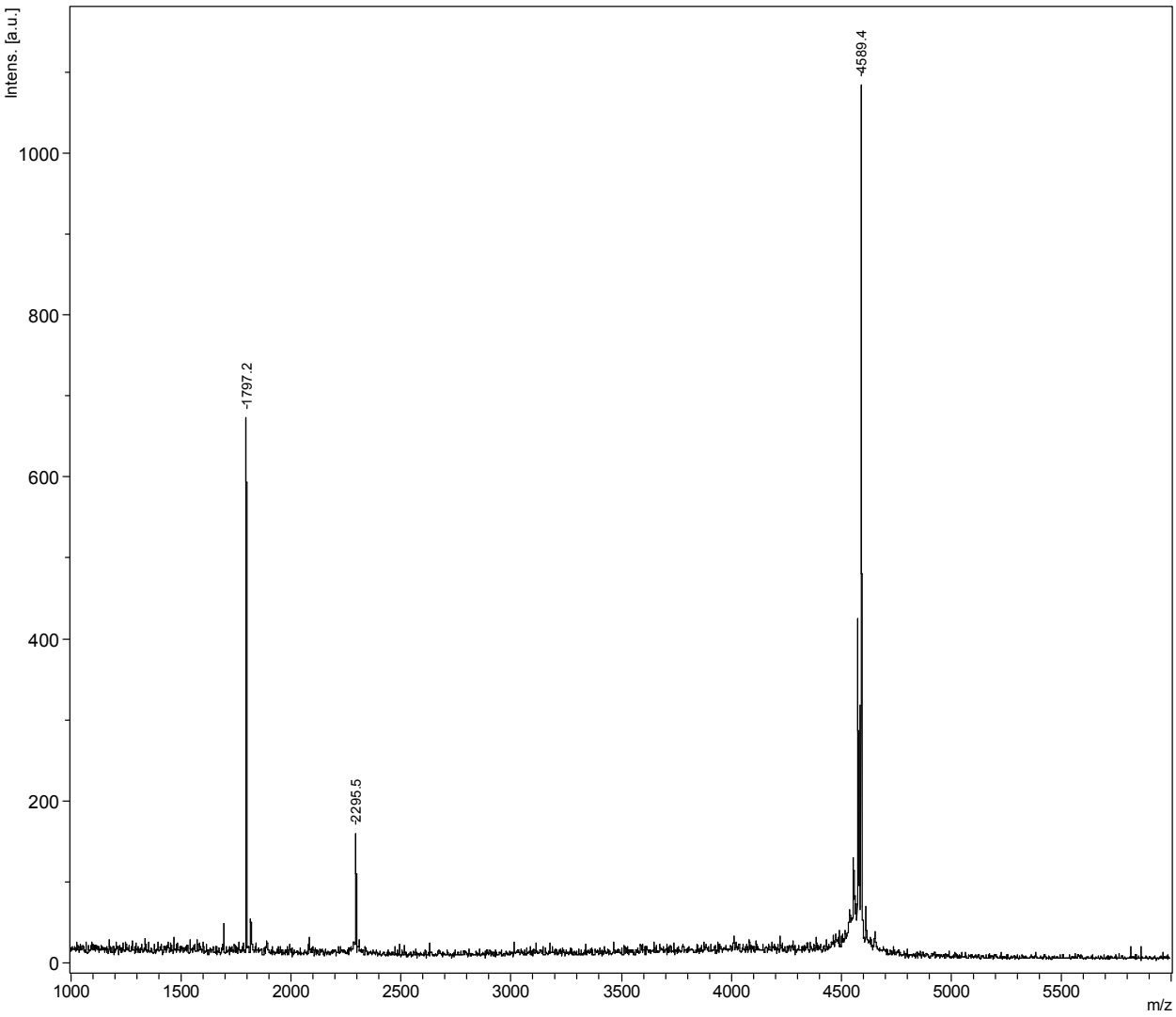

Figure 3.28 (I) MALDI-TOF analysis of plasma from Mouse 4. Expected $[M+H]^+$ for **3.3** = 4588.3.

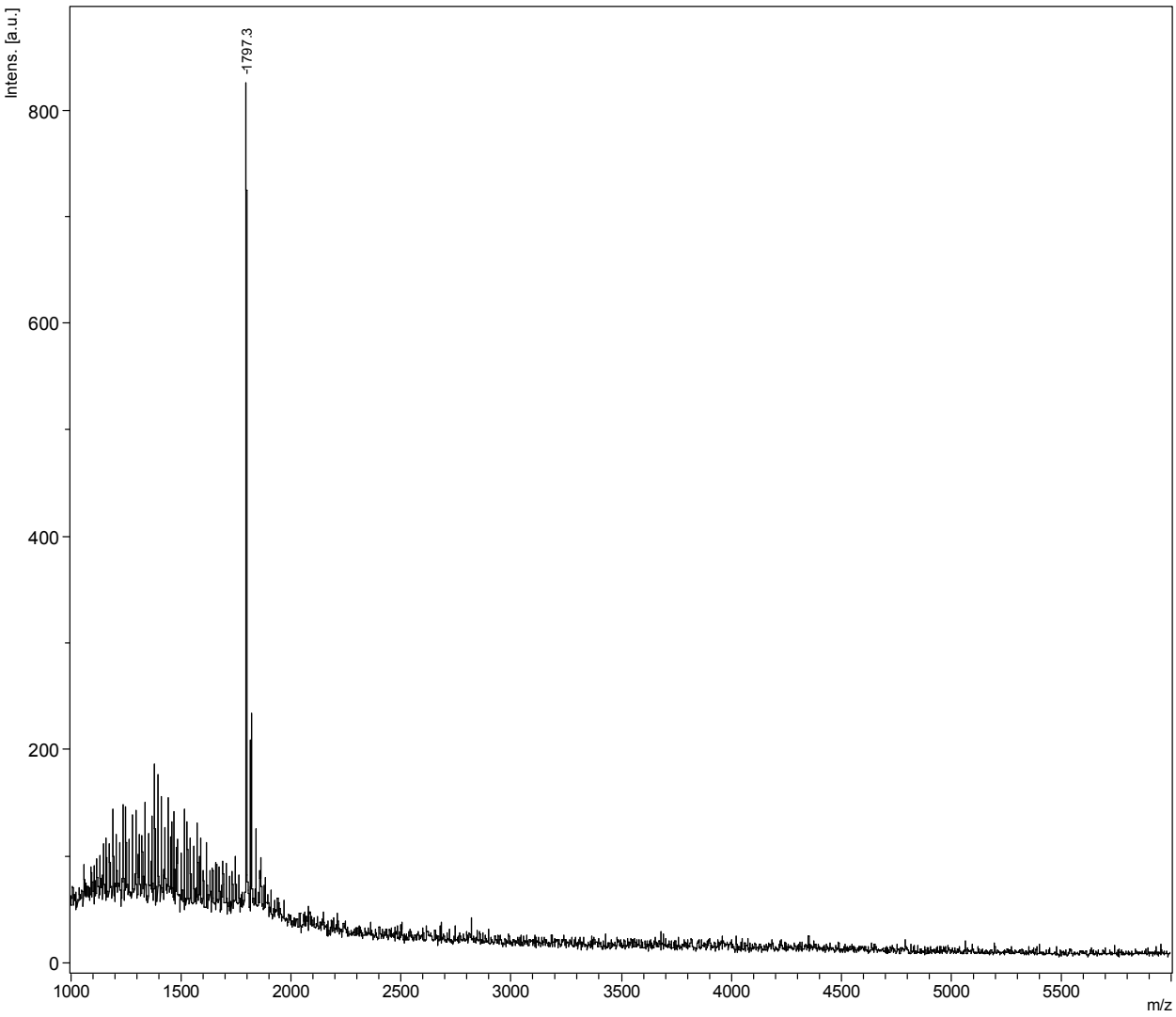

Figure 3.28 (J) MALDI-TOF analysis of plasma from Mouse 5. Expected $[M+H]^+$ for **2.39** = 4514.3.

3.10.6 TNFα-TNFR1 competition ELISA

The binding of α/β-peptides to TNFα to inhibit the binding of TNFα to TNFR1 was measured by competition ELISA. For each competition ELISA experiment, 50 μL of 1 μg/mL recombinant human sTNF RI/TNFRSF1A (TNFR1) (R&D Systems, 636-R1-025) in PBS was added to each well onto a Nunc Maxisorp ELISA plate and incubated at 4 °C overnight to immobilize TNFR1. After immobilization, the plate was washed with PBS+0.05% TWEEN20, blocked with 1% BSA in PBS for 2-4 hours, and then washed again with PBS+0.05% TWEEN20. Serial dilutions of soluble α/β-peptides in DMSO were prepared, and 10 μL of each of these solutions added to 240 μL of recombinant human TNFα (R&D Systems, 210-TA-020, final concentration = 0.081 μg/mL) in PBS+0.05% TWEEN20. The α/β-peptides were allowed to incubate with TNFα for 3 hours and then 100 μL of each α/β-peptide+TNFα mixture was added to wells on the ELISA plate and incubated at room temperature for 1 hour. The plate was then washed with PBS+0.05% TWEEN20 and the presence of TNFα detected by adding 100 μL of 0.40 μg/mL of human TNFα biotinylated antibody (R&D Systems, BAF210) in PBS+0.05% TWEEN20 and incubating at room temperature for 1 hour. The plate was washed with PBS+0.05% TWEEN20 and 100 μL of 1:1000 dilution of streptavidin-alkaline phosphatase (R&D Systems, AR001) in PBS+0.05% TWEEN20 was added and allowed to incubate at room temperature for 30 minutes. After washing with PBS+0.05% TWEEN20, 50 μL of pNPP solution was added to each well and the alkaline phosphatase reaction allowed to proceed at room temperature. Plates were read (absorbance at 405 nm) during the time course of the reaction on a BioTek Synergy 2 microplate reader. Each condition was run in duplicate. To compare the ability of each soluble α/β-peptide to inhibit the binding of TNFα to immobilized TNFR1, IC_{50} values were calculated by fitting the ELISA absorbance data to a sigmoidal dose-

response equation using GraphPad Prism 4.0 (Figure 3.29). Based on TNFα-TNFR1 competition ELISA data collected from a large number of independent experiments (see Section 4.2.4 in Chapter 4), we conclude that for most compounds with IC_{50} values <10,000 nM, the uncertainty in the calculated IC_{50} values is ~2-fold, with a maximum variation of up to ~7-fold for some experiments.

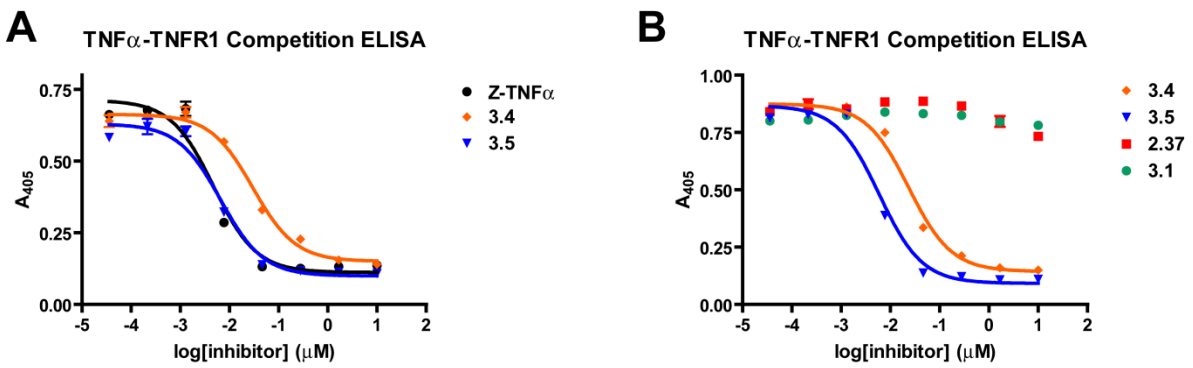

Figure 3.29 Representative TNFα-TNFR1 competition ELISA evaluating the ability of α- and α/β-peptides for the ability to block the binding of TNFα to immobilized TNFR1. Each panel represents an independent experiment with some oligomers present on multiple panels as positive controls and to show reproducibility. Data points represent the mean ± SEM from duplicate wells on plate.

3.10.7 VEGF$_{165}$ competition FP

VEGF$_{165}$ competition fluorescence polarization assays were carried out exactly as described in Chapter 2 (Figure 3.30).

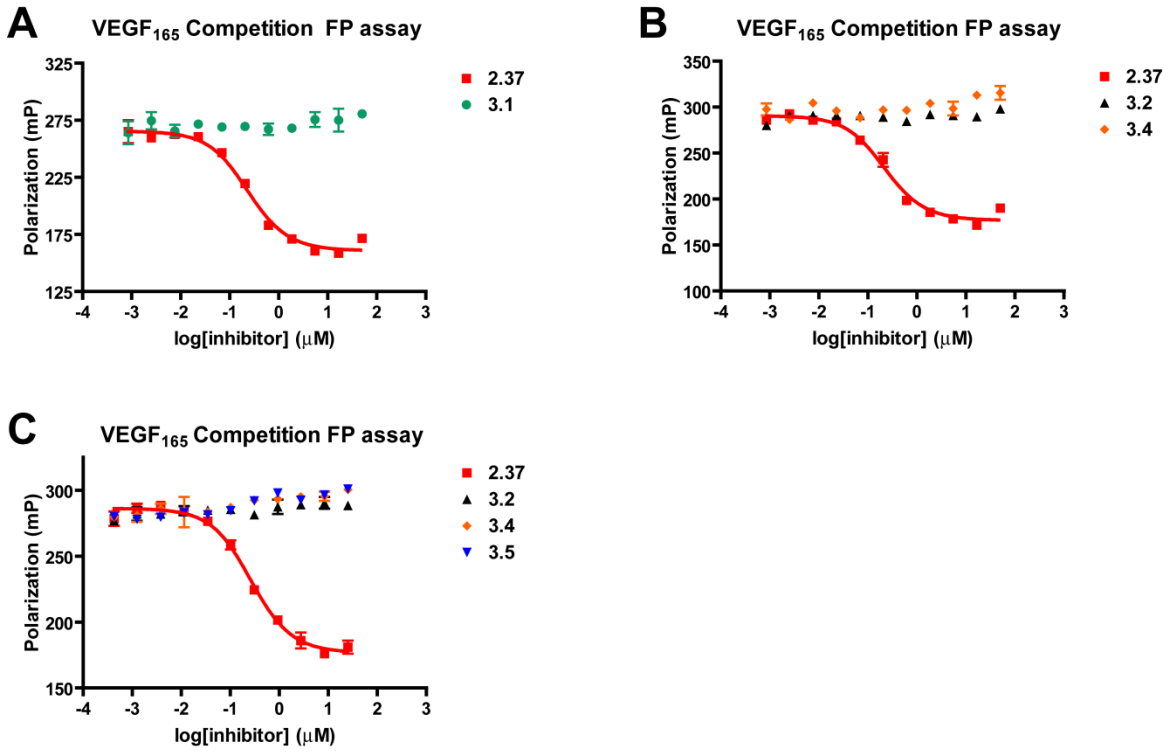

Figure 3.30 Representative VEGF$_{165}$ competition FP assays evaluating the binding of oligomers to VEGF$_{165}$. Each data point represents the mean ± SEM for duplicate wells on the plate.

3.10.8 HER2 competition ELISA

The binding of α- and α/β-peptides to HER2 was evaluated using a HER2 competition ELISA. For each ELISA experiment, 50 µL of 2-4 µg/mL recombinant human ErbB2/Her2 Fc chimera (HER2) (R&D Systems, 1129-ER-050) in PBS was added to each well on a Nunc Maxisorp ELISA plate and incubated at 4 °C overnight to immobilize HER2 onto the surface of the plate. After immobilization, the plate was washed with PBS+0.05% TWEEN20 and then blocked with 1% BSA in PBS for ~1-2 hours, and then washed again with PBS+0.05% TWEEN20. DMSO stock solutions of potential competitors were diluted into PBS (final

concentration = 2.5% DMSO, except for one experiment which used 5% DMSO) and serial dilutions of this stock were made into PBS with the same concentration of DMSO. A stock solution of **Bt-Z-HER2** was prepared by diluting a concentrated DMSO stock into PBS and this solution was then diluted 1:1 with competitor solution in PBS+DMSO (final concentrations = 10-50 nM **Bt-Z-HER2**, as indicated in the Figures and captions, final concentration of competitor = 10 μM top concentration with 6-fold dilutions), and then 50-100 μL of this mixture was added to each well on the ELISA plate and incubated at room temperature for ~2 hours. The plate was then washed with PBS+0.05% TWEEN20, and then 100 μL of 1:1000 of streptavidin-alkaline phosphatase in PBS+0.05% TWEEN20 was added and allowed to incubate at room temperature 1-2 hours. After washing with PBS+0.05% TWEEN20, 50 μL of pNPP solution (Sigma, N1891) was added to each well and the alkaline phosphatase reaction allowed to proceed at room temperature. Plates were read (absorbance at 405 nm) during the time course of the reaction on a BioTek Synergy 2 microplate reader. To compare the ability of each soluble α/β-peptide to inhibit the binding of **Bt-Z-HER2** to immobilized HER2, IC_{50} values were calculated by fitting the ELISA absorbance data to a sigmoidal dose-response equation using GraphPad Prism 4.0 (Figure 3.31). Because many of the compounds had relatively high IC_{50} values using the conditions of these experiments and did not reach the bottom of the competitive binding curve, the data were modeled with a shared bottom value (fit by modeling to compounds that did reach the bottom) to estimate the IC_{50} value.

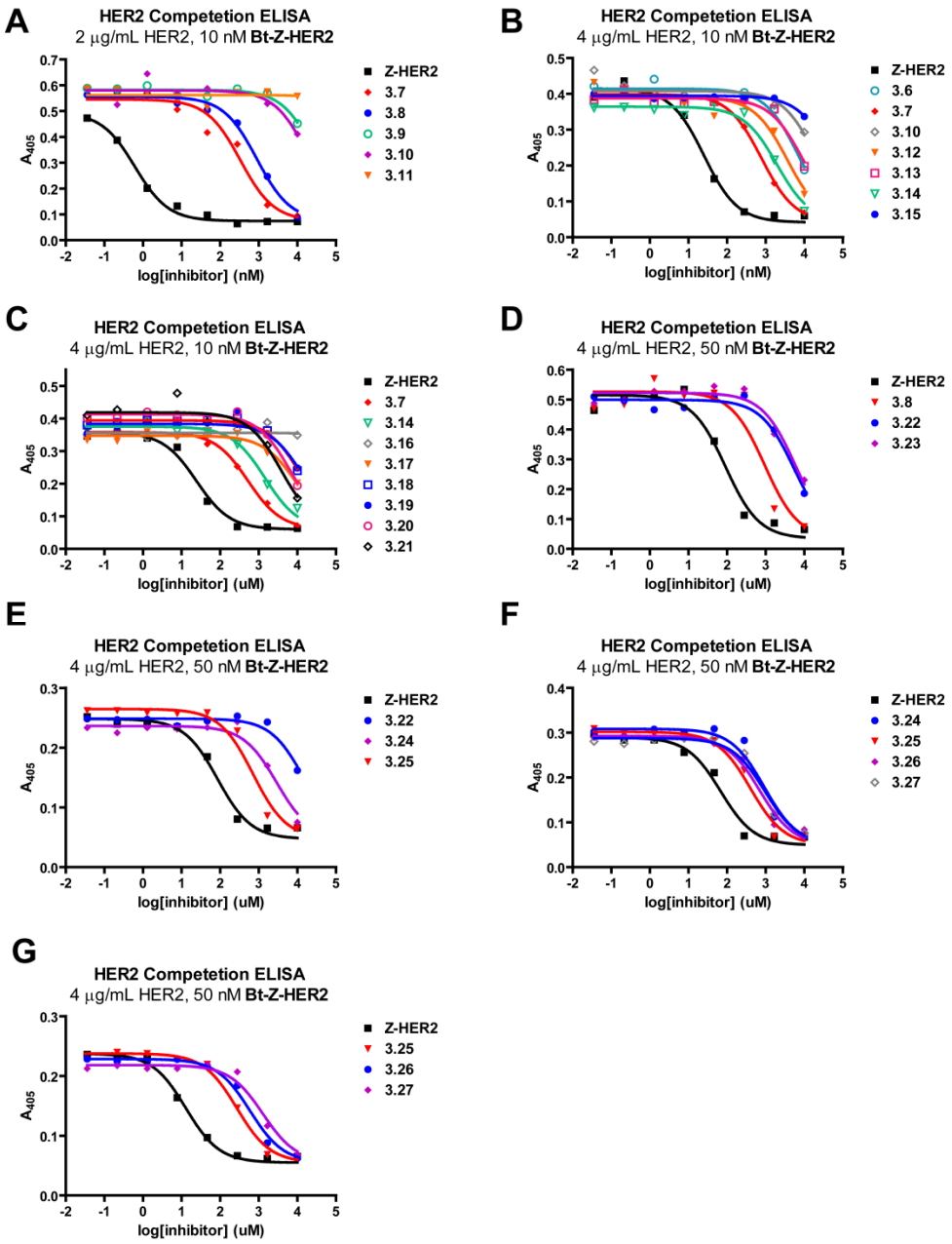

Figure 3.31 Representative HER2 competition ELISA experiments evaluating the ability of the indicated oligomers to block the binding of **Bt-Z-HER2** (10 nM **Bt-Z-HER2** for panels A-C, 50 nM **Bt-Z-HER2** for panels D-G) to immobilized HER2 (2 µg/mL HER2-Fc chimera immobilized for panel A, 4 µg/mL HER2-Fc chimera immobilized for all other panels). For panels A, B, C, D, and F, points represent single experiment at that given concentration. For panels E and G, data points represent mean ± SEM for duplicate wells on the plate.

3.10.9 Circular dichroism (CD) spectroscopy

Circular dichroism measurements were performed on an Aviv Model 420 circular dichroism spectrometer. Solutions of α- and α/β-peptides were prepared in PBS. Spectra were collected at 20 °C in a 0.1 cm quartz cell with a wavelength step size of 1 nm and a 5 second averaging time. Spectra were normalized to units of [θ] (deg cm^2 $dmol^{-1}$ res^{-1}) using the exact concentration determined by UV absorbance at 280 nm[63] to account for slight variations in concentration between solutions, using the Equation (1),[64] described below:

(1) $[\theta] = \theta/(l * c * \#res)$

Where:
θ = blank-corrected ellipticity value from CD spectrometer (in mdeg)
l = pathlength (in mm)
c = concentration of peptide (in M)
#res = the number of residues in the peptide

The mean residue ellipticity values ([θ]) obtained were then multiplied by 10^{-3} for plotting in the graphs shown in this chapter. CD spectra for **2.9**, **2.12**, and **2.37** are the same data as reported in Chapter 2.

3.10.10 Proteolysis

Stock solutions of 50 μg/mL proteinase K (Novagen, 70663-4) were prepared in TBS, pH 7.5. Solutions of 100 μM α- or α/β-peptide were prepared in TBS, and their concentrations were determined by UV absorbance.[63] For each proteolysis reaction, the stock of peptide was diluted with TBS (final concentration = 40 μM) and the proteinase K stock was added (final concentration = 10 μg/mL), and the reaction was allowed to proceed at room temperature. The reaction was quenched at each time point by removing 50 μL of the proteolysis reaction and adding 100 μL of 1:1 water/acetonitrile + 1% TFA. 5 μL of the resulting quenched solution were injected onto UPLC and analyzed by 10-60% [acetonitrile+0.1%TFA]/[water+0.1% TFA]

gradient over 5 minutes, 0.4 mL/min flow rate. The relative amount of peptide remaining was quantified by integration of the peak at 220 nm in a series of UPLC chromatograms. Each reaction was run in duplicate. Half-lives were determined by fitting the time course of peptide degradation to an exponential decay model using GraphPad Prism 4.0 (Figure 3.19).

3.10.11 In vivo tumor imaging

Tumor imaging and biodistribution studies were all performed in the Hackel Laboratory (Department of Chemical Engineering and Material Science, University of Minnesota).

Nu/nu mice immunocompromised were inoculated with SKOV3 cells (high HER2 expression) in one shoulder and MDA-MB-435 cells (low HER2 expression) in the opposite shoulder, which led to tumor development. DOTA-labeled α- or α/β-peptides **3.28-3.30** were mixed with ^{64}Cu in sodium acetate, pH 5.5 to chelate the metal to the DOTA group, and then the peptides were separated from unchelated metal using a size-exclusion column. Mice were injected intravenously with ~100 μCi of ^{64}Cu-DOTA-peptide. PET/CT imaging was performed (Figure 3.20). Mice were euthanized at ~4 hours post-injection. Tissues and fluids were collected via dissection, weighed, and counted for gamma radiation. Activity per mass in Figure 3.21 is reported as percent of injected dose per gram of tissue or fluid. Values are the average ± SD of three mice for each compound, except that only one mouse for **3.29** and **3.30** generated a MDA-MB-435 tumor.

3.10.12 EGFR competition ELISA

The binding of α- and α/β-peptides to EGFR was determined using a competition ELISA experiment similar to the competition ELISA experiment described above for IgG binding. **Z-EGFR** was conjugated to BSA by dissolving ~1 mg of **Z-EGFR** into 330 μL of 3% BSA, 8 mM

glutaraldehyde in PBS, pH 7 and allowing the conjugation reaction to proceed for ~3 hours at room temperature. The reaction was quenched by the addition of 5-6 mg glycine, and the mixture was incubated for an additional 2 hours at room temperature. This quenched solution was then diluted and dialyzed against PBS overnight at 4 °C in 10,000 MWCO dialysis cassettes. After dialysis, the **Z-EGFR**+BSA conjugate was removed from the dialysis cassette and concentrated to ~500 μL. This solution was then diluted and used directly in competition ELISA experiments.

For a competition ELISA experiment, the **Z-EGFR**+BSA conjugate solution described above was diluted 1:3000 into PBS and 50 μL of the resulting solution was added to a Nunc Maxisorp ELISA plate and incubated overnight at 4 °C to immobilize the **Z-EGFR**+BSA conjugate. After immobilization, the ELISA plate was washed with PBS+0.05% TWEEN20 and then blocked with 1% BSA in PBS for ~2-3 hours, and then washed with PBS+0.05% TWEEN20. Serial dilutions of α- or α/β-peptide competitors were prepared in DMSO, and 5 μL of each DMSO dilution was mixed with 120 μL of recombinant Human EGFR / HER1 / ErbB1 Protein (Fc Tag) (Sino Biological, 10001-H08H, final concentration = 2 μg/mL) in PBS+0.05%TWEEN20. These mixtures were allowed to pre-incubate for ~1-2 hours, and 50 μL of this EGFR/peptide mixture was added to the ELISA plate and allowed to incubate for ~1 hour, followed by washing with PBS+0.05% TWEEN20. The detection of bound EGFR was then carried out by subsequent addition of 100 μL of 1:500 dilution of Human EGF R Biotinylated Affinity Purified PAb, Goat IgG (R&D Systems, BAF231) in PBS+0.05% TWEEN20 (for ~1 hour), washing (with PBS+0.05% TWEEN20), and addition of 100 μL of 1:1000 dilution of Streptavidin-alkaline phosphatase in PBS+0.05% TWEEN20 (30 minutes), washing (with PBS+0.05% TWEEN20), and addition of 50 μL pNPP solution to each well and the alkaline phosphatase reaction allowed to proceed at room temperature. Plates were read (absorbance at

405 nm) during the time course of the reaction on a BioTek Synergy 2 microplate reader. Each condition was run in duplicate. To compare the ability of each soluble inhibitor to block the binding of EGFR to immobilized **Z-EGFR**+BSA conjugate, IC_{50} values were calculated by fitting the ELISA absorbance data to a sigmoidal dose-response equation using GraphPad Prism 4.0 (Figure 3.32).

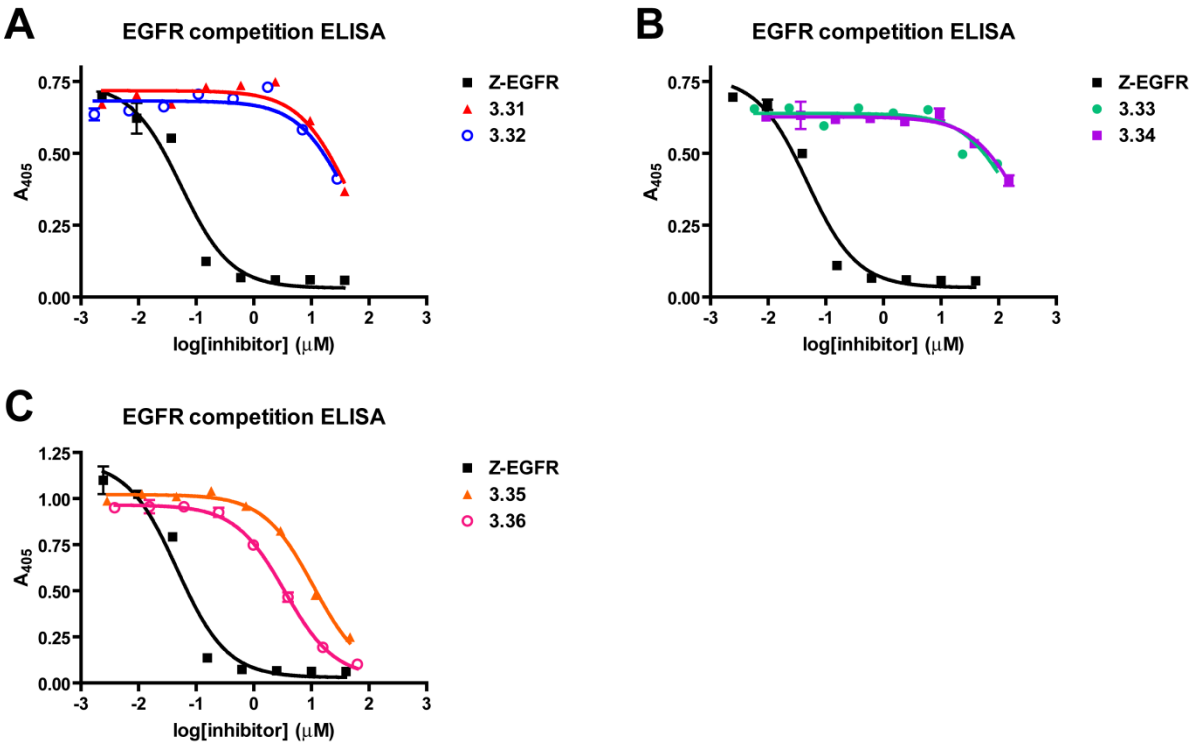

Figure 3.32 Representative EGFR competition ELISA experiments evaluating the ability for the indicated oligomers to block the binding of soluble EGFR fragment to immobilized **Z-EGFR**+BSA conjugate. Data points represent mean ± SEM for duplicate wells on the plate.

3.10.13 Peptide characterization

α-Peptide and α/β-peptide purity after purification was assessed by analytical scale reverse-phase HPLC, using solvent A: H_2O with 0.1% TFA, solvent B: acetonitrile with 0.1% TFA, with a flow rate of 1 mL/min. The solvent gradient for each peptide is specified in each panel. HPLC chromatograms at 220 nm are shown at the top of each panel. Peptide identity was

confirmed by MALDI-TOF-MS, shown at the bottom of each panel. For each MALDI-TOF spectrum, the monoisotopic $[M+H]^+$, *m/z* is labeled.

3.1

HPLC: Gradient = 10-60% solvent B over 50 minutes

MALDI-TOF: Calculated monoisotopic $[M+H]^+ = 4620.3$

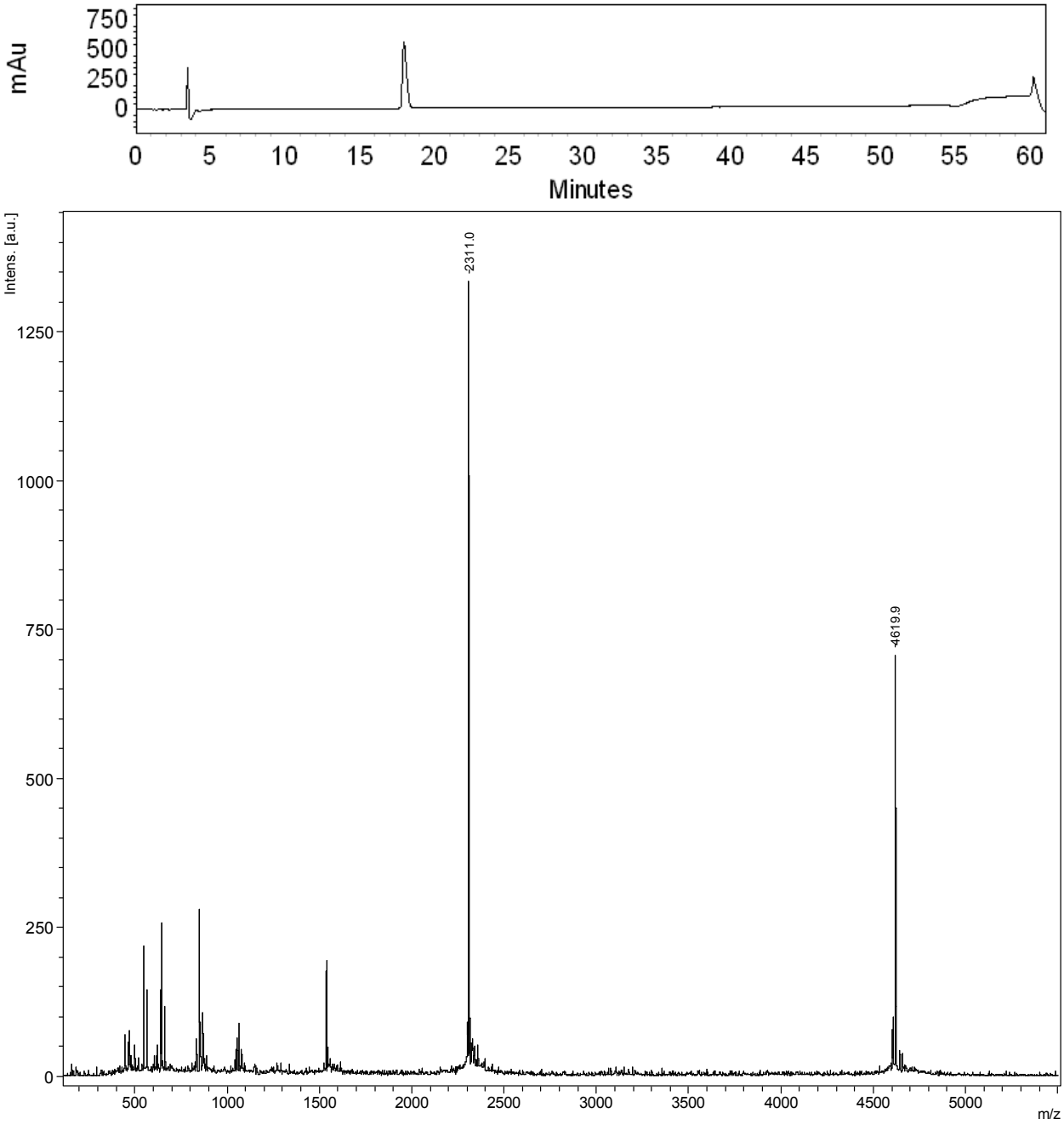

3.2

HPLC: Gradient = 10-60% solvent B over 50 minutes

MALDI-TOF: Calculated monoisotopic $[M+H]^+ = 4622.3$

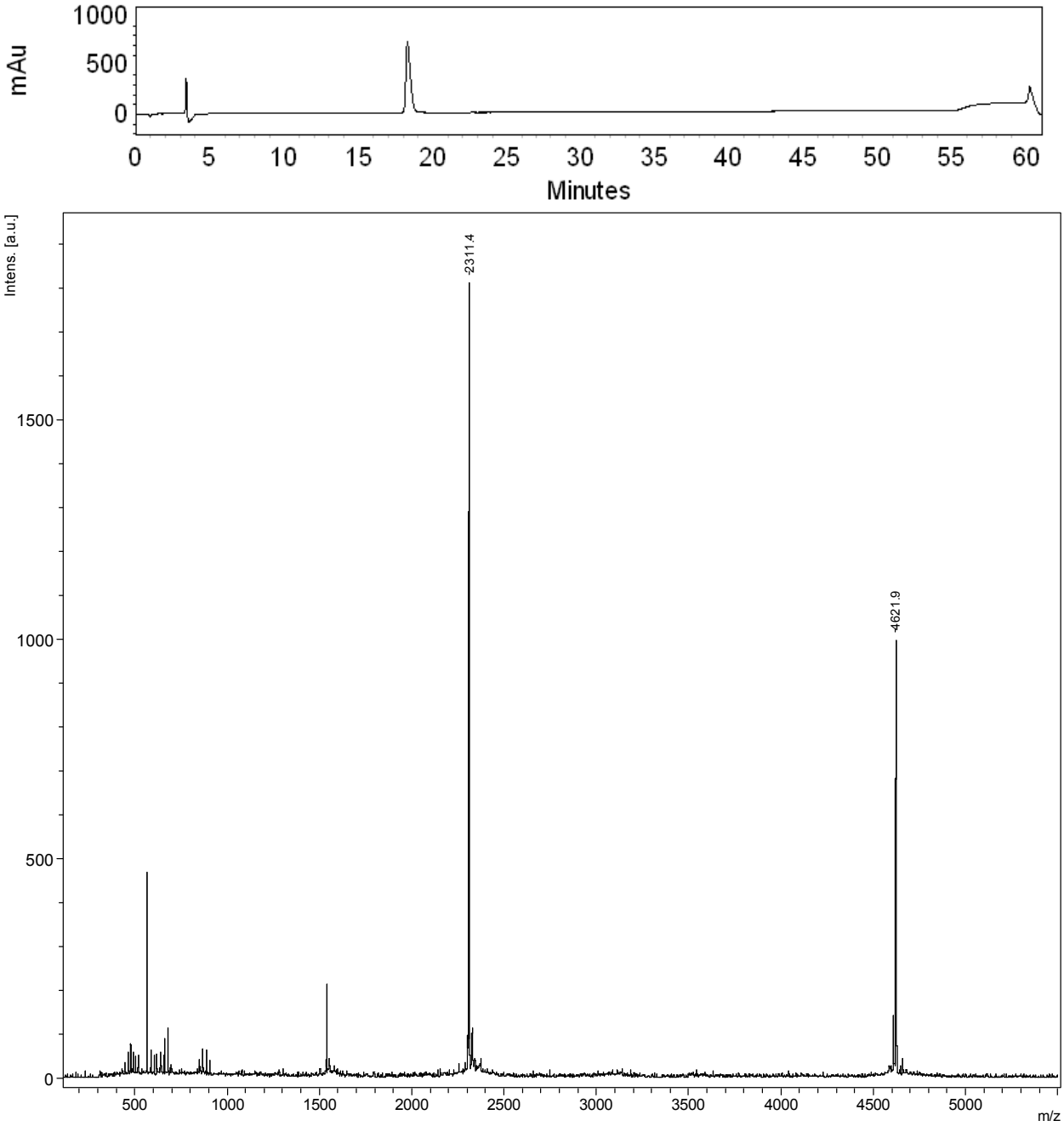

3.3

HPLC: Gradient = 10-60% solvent B over 50 minutes

MALDI-TOF: Calculated monoisotopic $[M+H]^+ = 4588.3$

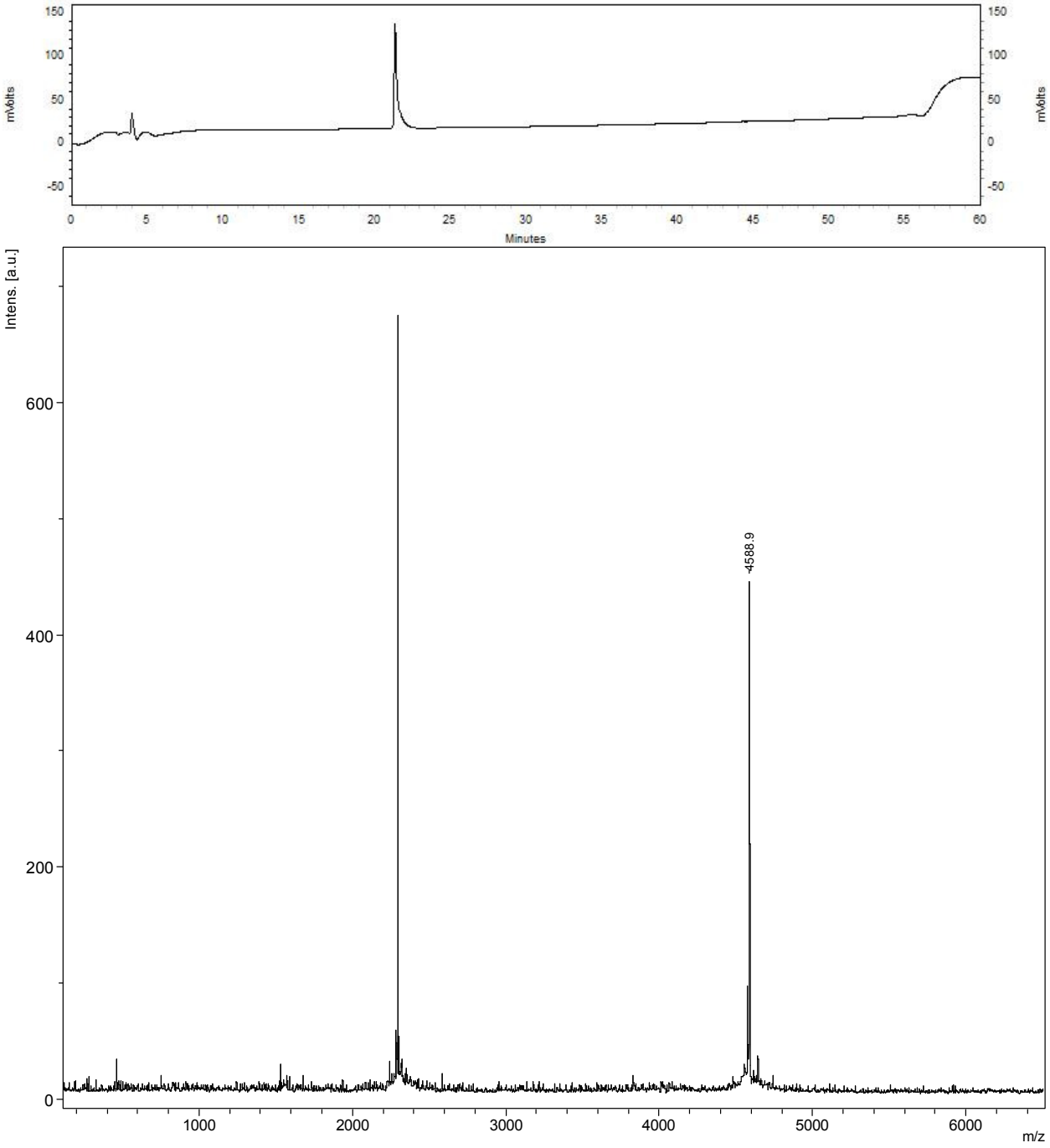

Z-TNFα
HPLC: Gradient = 10-60% solvent B over 50 minutes
MALDI-TOF: Calculated monoisotopic $[M+H]^+$ = 6473.4

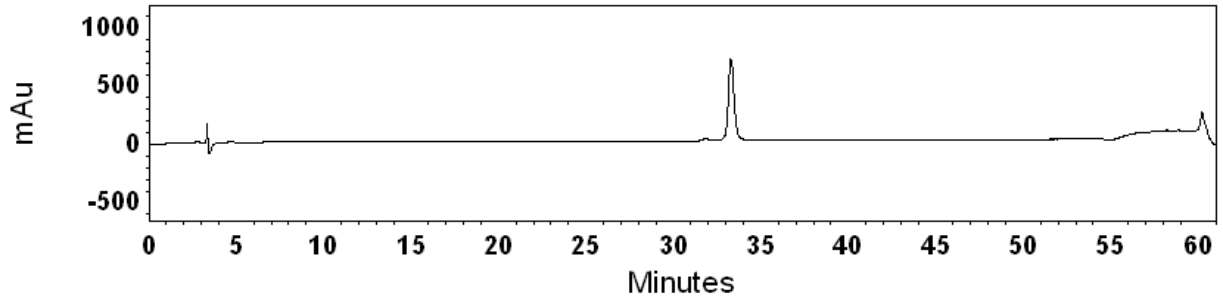

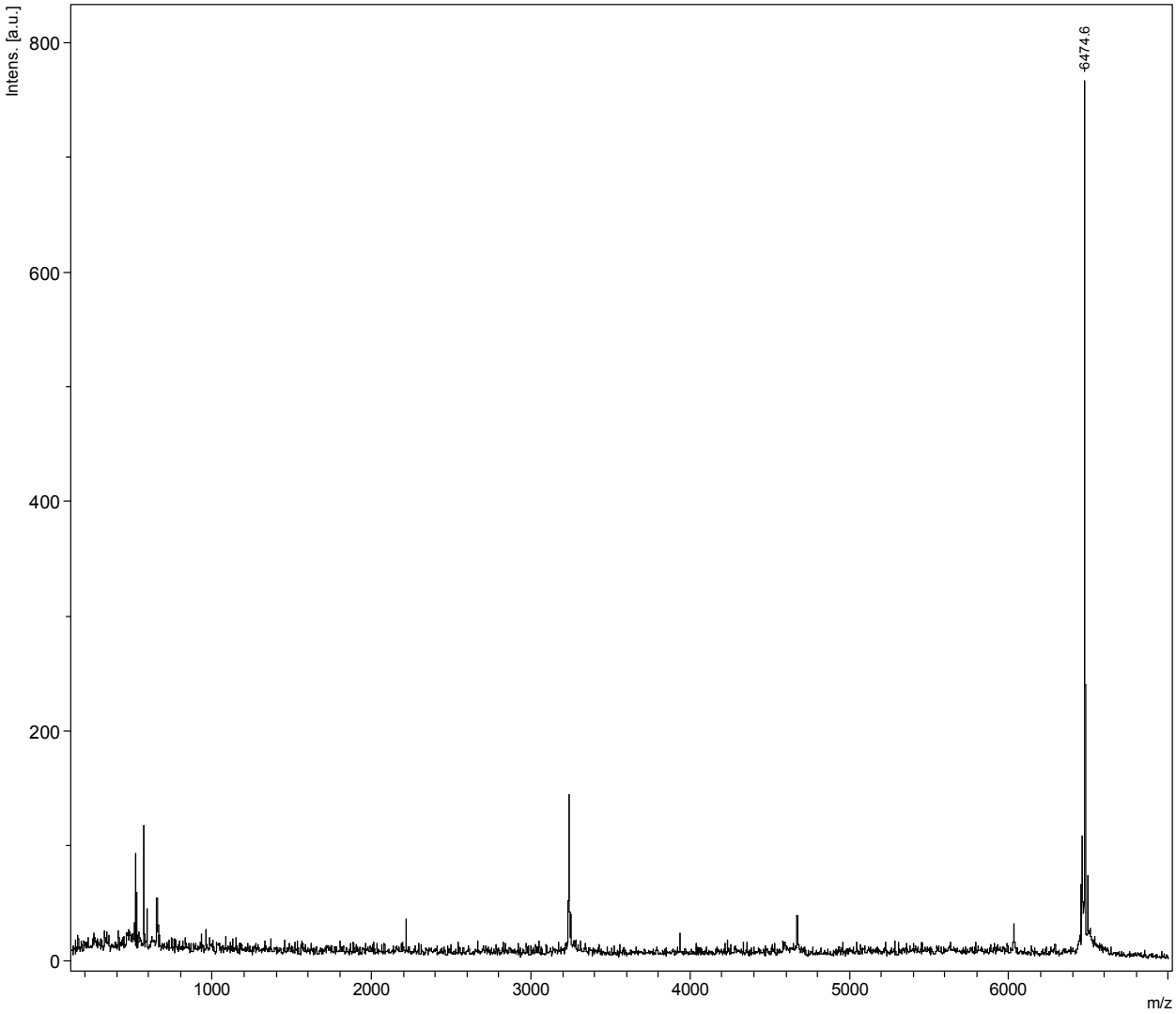

3.4

HPLC: Gradient = 10-60% solvent B over 50 minutes

MALDI-TOF: Calculated monoisotopic $[M+H]^+ = 4400.3$

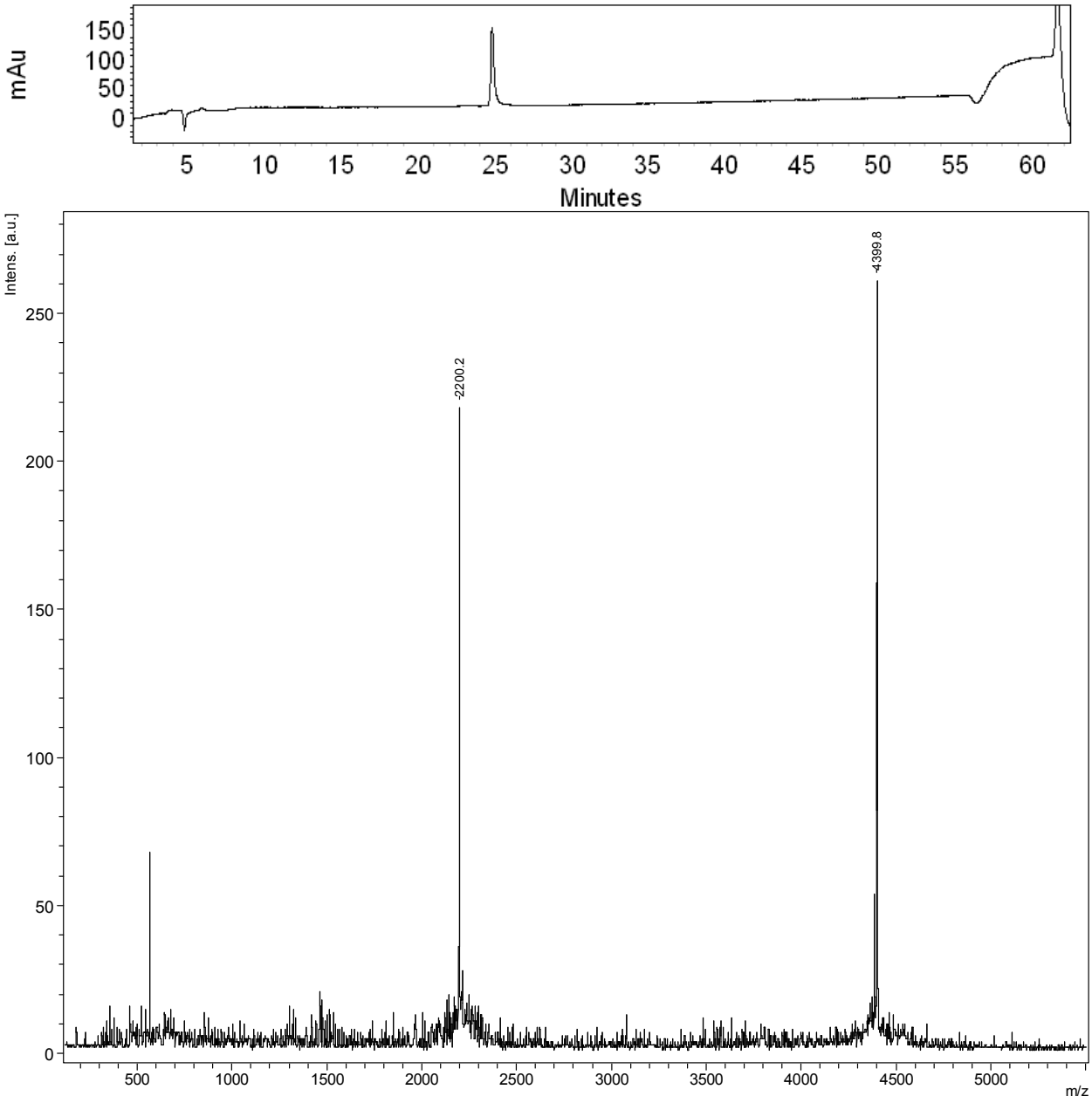

3.5

HPLC: Gradient = 10-60% solvent B over 50 minutes

MALDI-TOF: Calculated monoisotopic $[M+H]^+ = 4474.3$

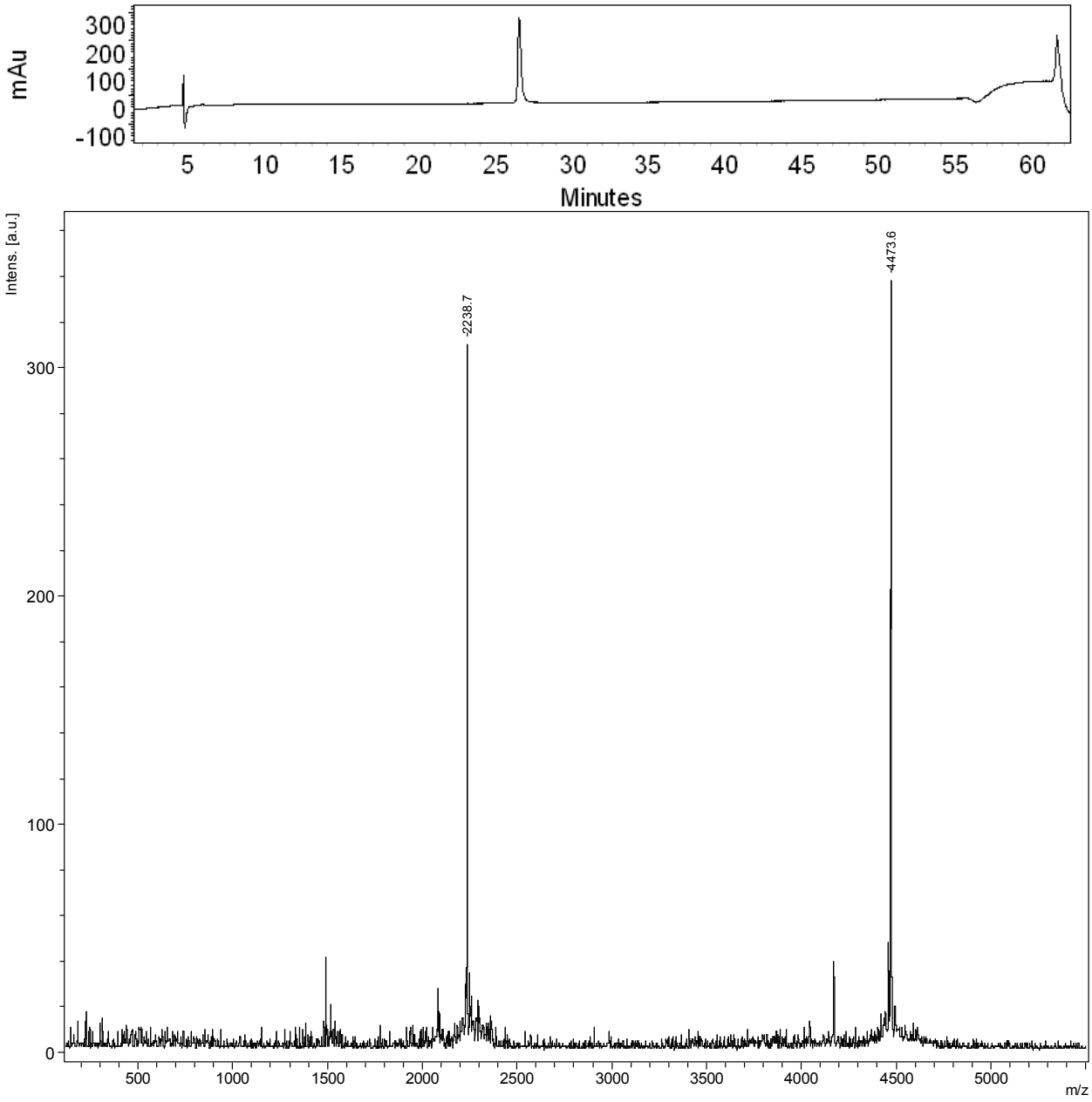

Z-HER2

HPLC: Gradient = 10-60% solvent B over 50 minutes

MALDI-TOF: Calculated monoisotopic $[M+H]^+$ = 6701.5

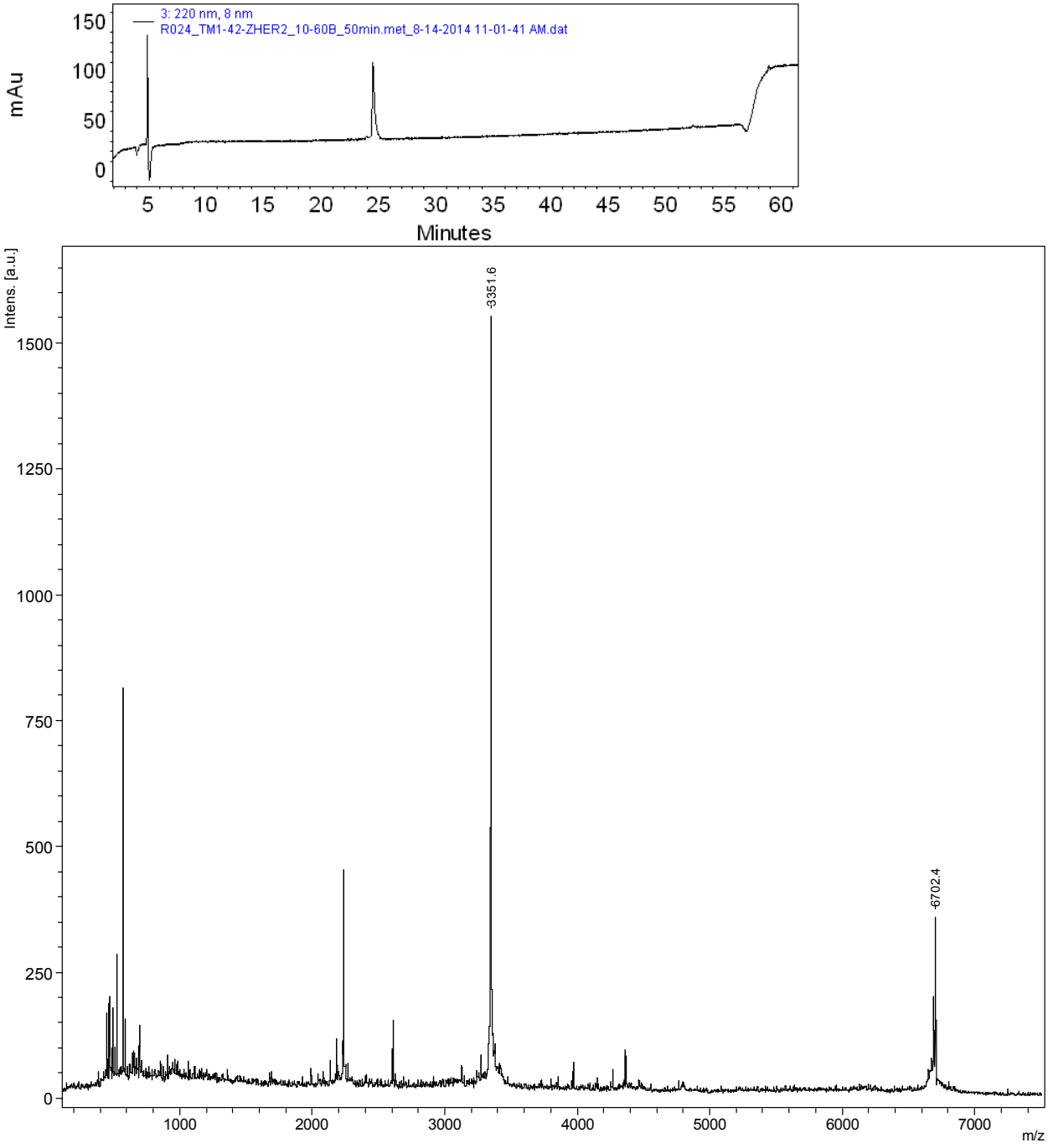

Bt-Z-HER2

HPLC: Gradient = 10-60% solvent B over 50 minutes

MALDI-TOF: Calculated monoisotopic $[M+H]^+$ = 6927.6

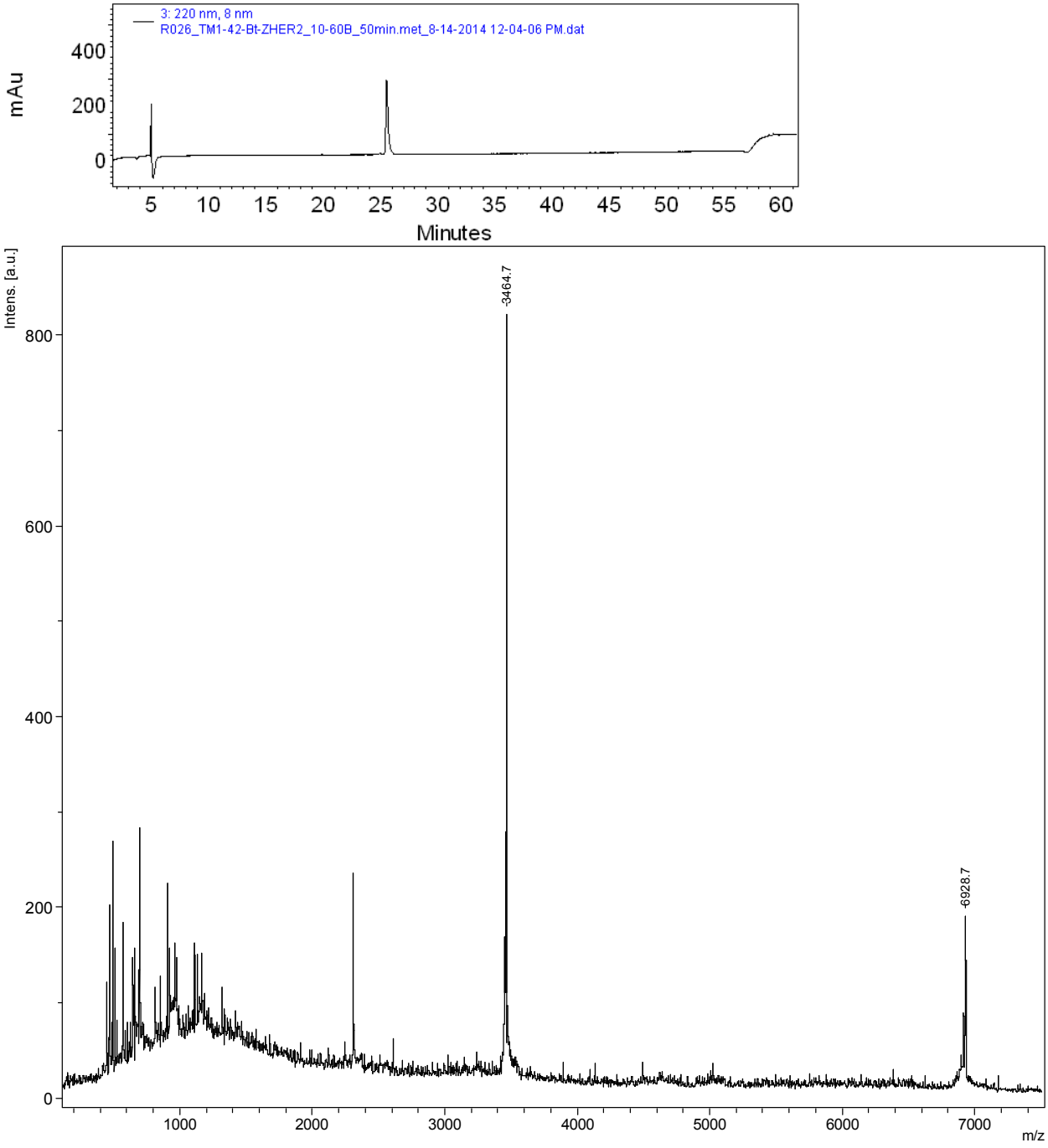

3.6

HPLC: Gradient = 10-60% solvent B over 50 minutes

MALDI-TOF: Calculated monoisotopic $[M+H]^+ = 4280.2$

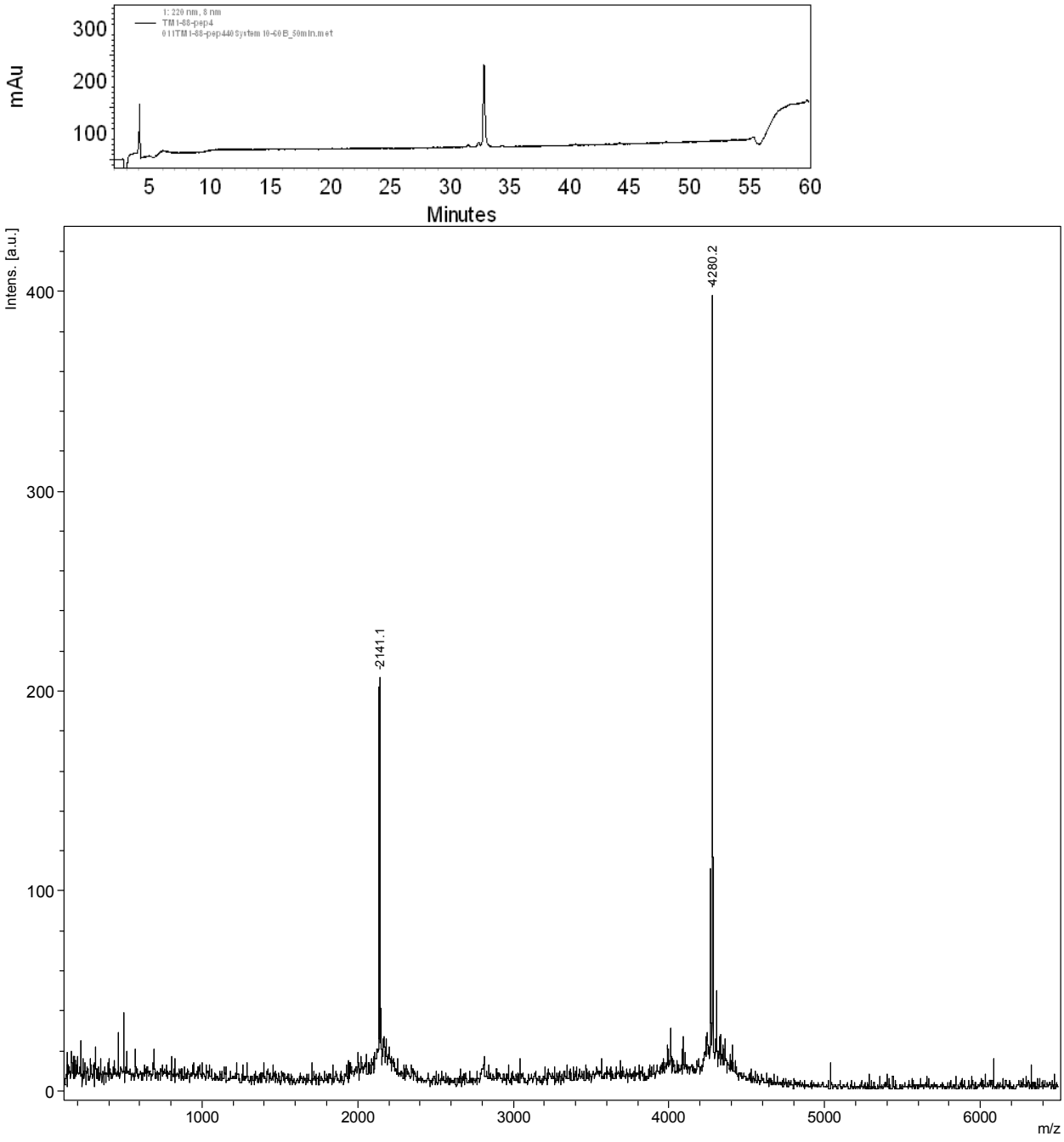

3.7

HPLC: Gradient = 10-60% solvent B over 50 minutes

MALDI-TOF: Calculated monoisotopic $[M+H]^+ = 4250.1$

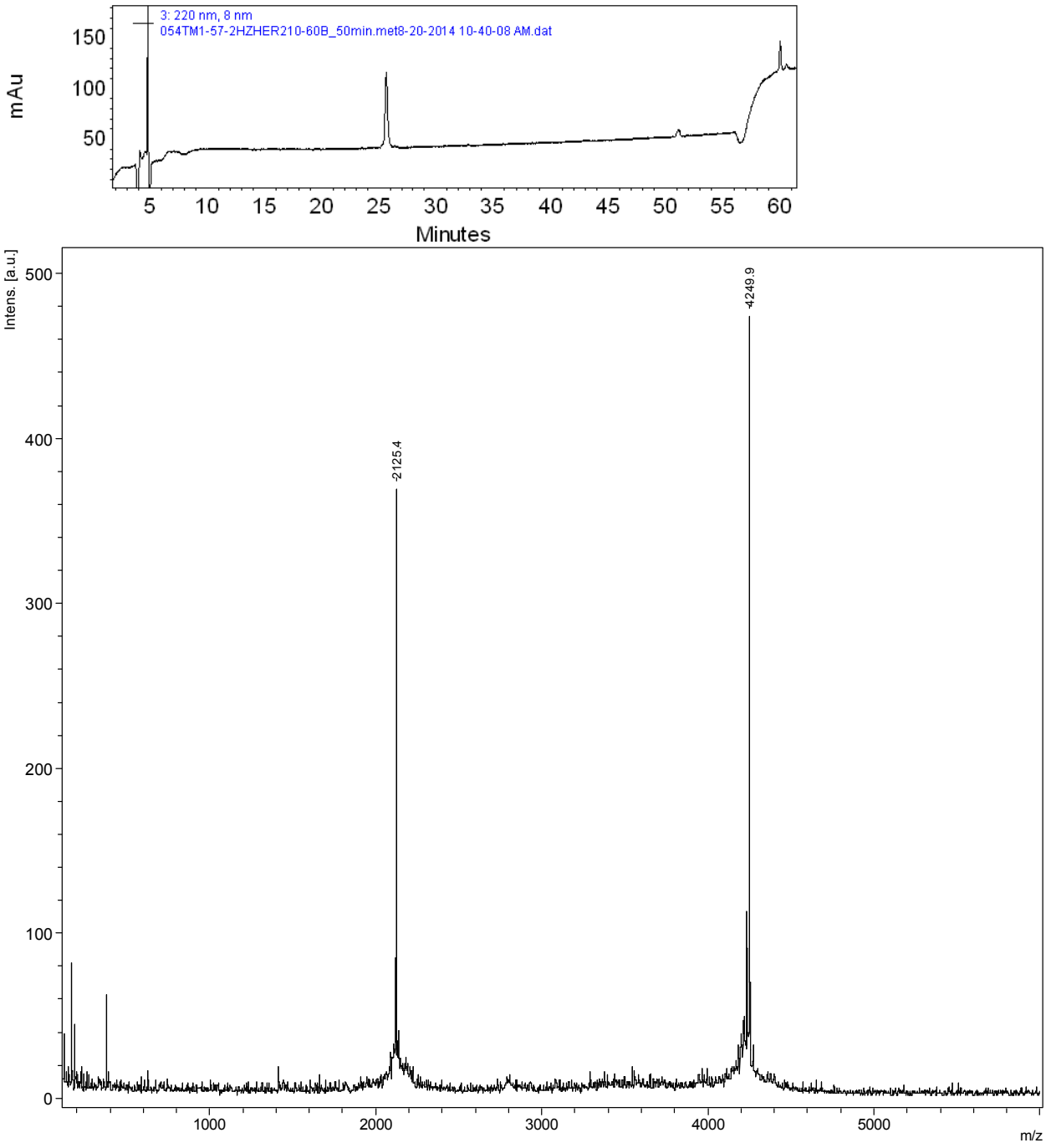

3.8

HPLC: Gradient = 10-60% solvent B over 50 minutes

MALDI-TOF: Calculated monoisotopic $[M+H]^+$ = 4278.1

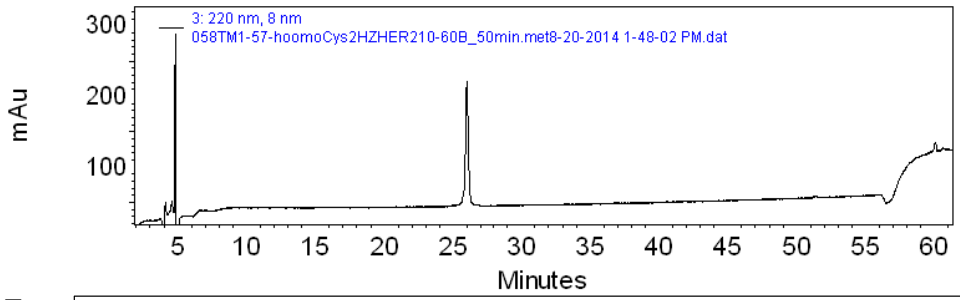

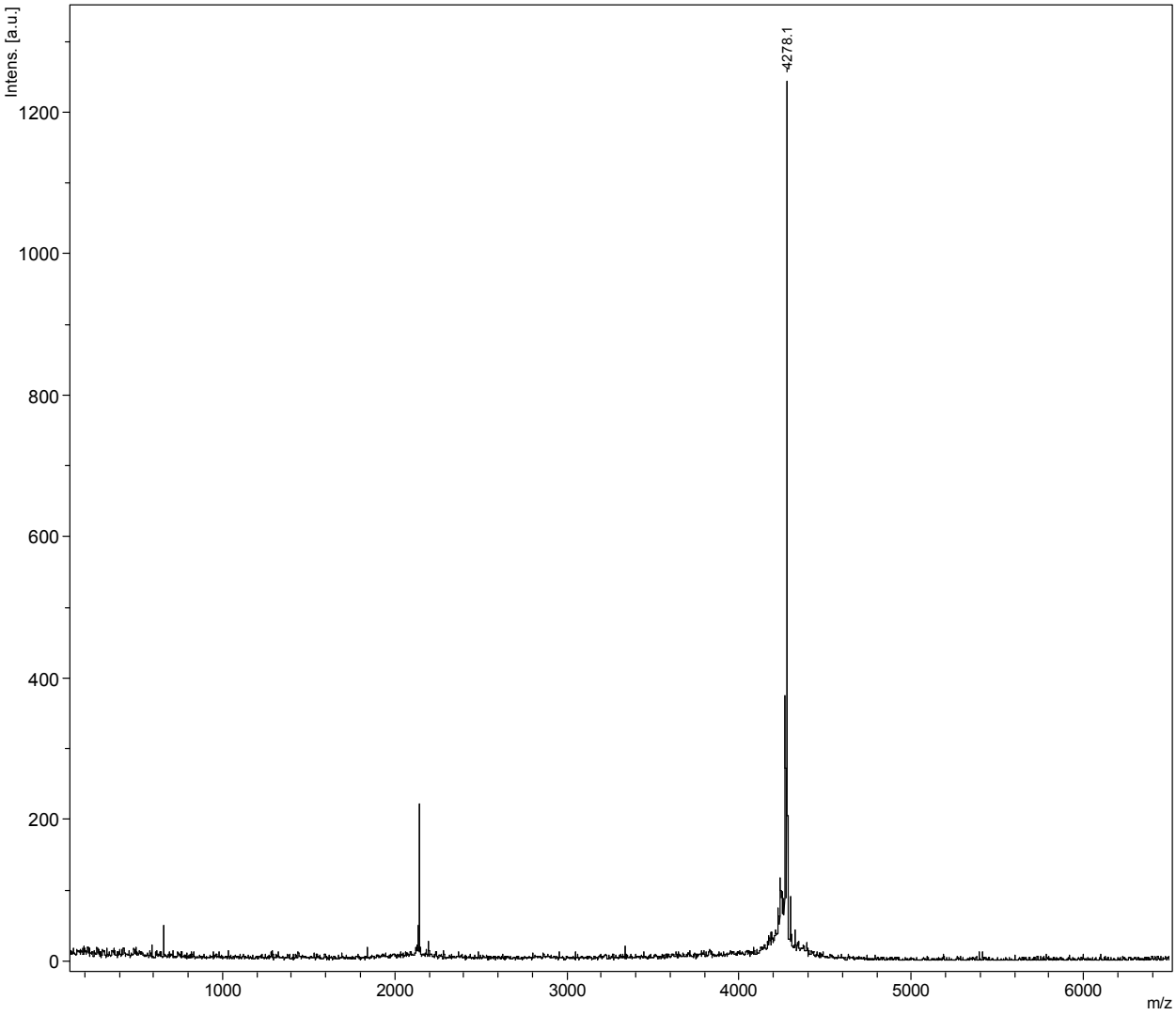

3.9

HPLC: Gradient = 10-60% solvent B over 50 minutes

MALDI-TOF: Calculated monoisotopic $[M+H]^+ = 4682.4$

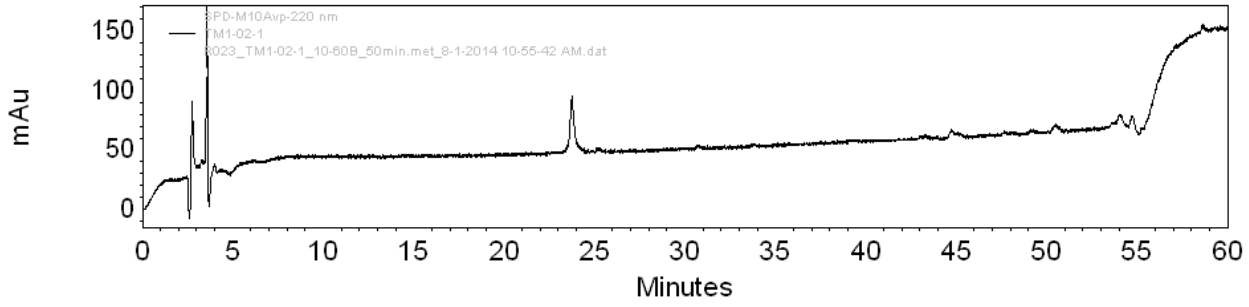

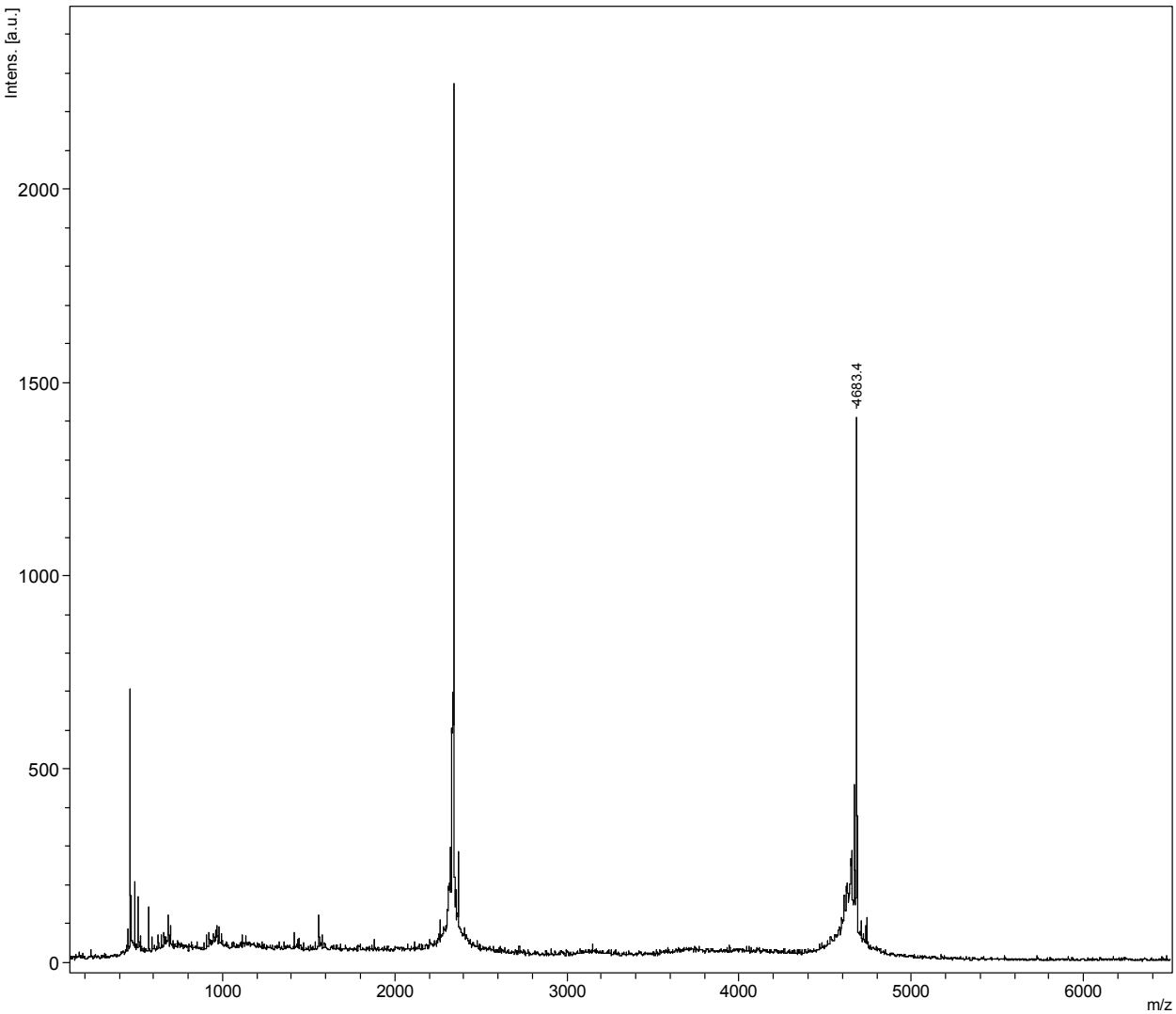

3.10

HPLC: Gradient = 10-60% solvent B over 50 minutes

MALDI-TOF: Calculated monoisotopic $[M+H]^+ = 4051.1$

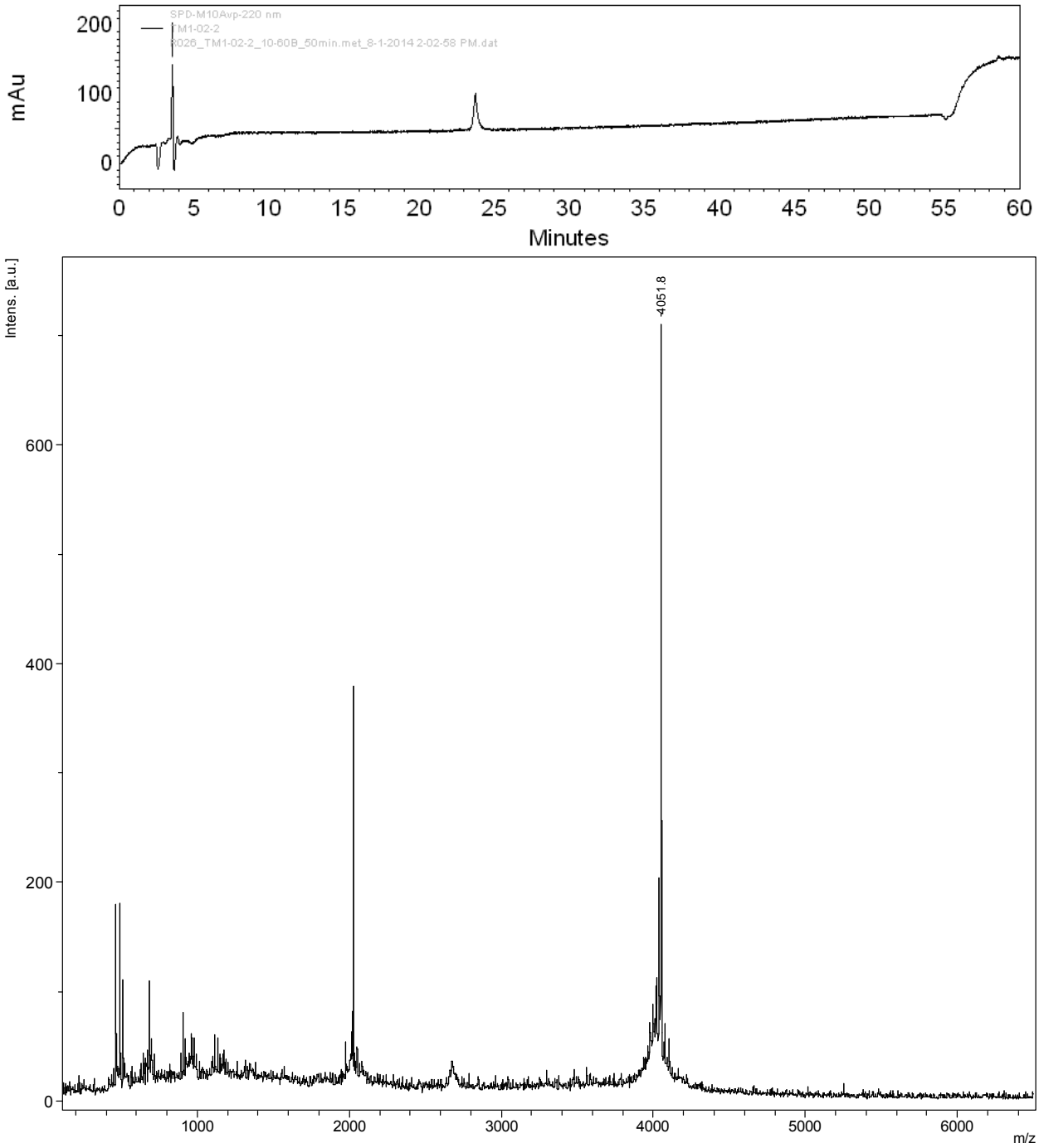

3.11

HPLC: Gradient = 10-60% solvent B over 50 minutes

MALDI-TOF: Calculated monoisotopic $[M+H]^+ = 3697.9$

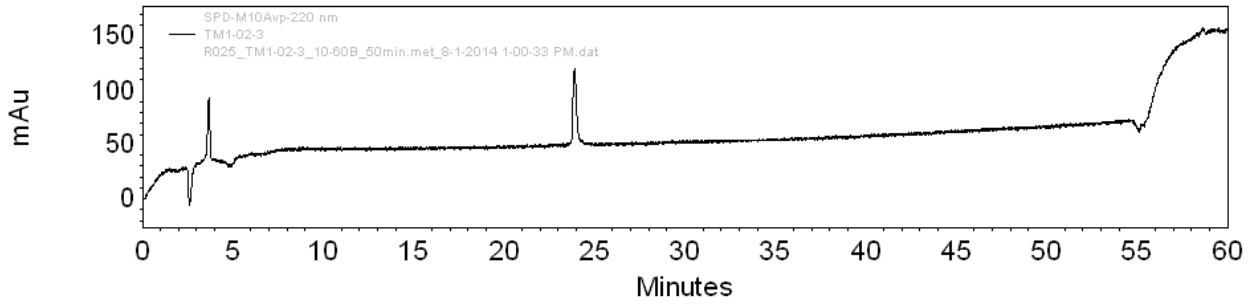

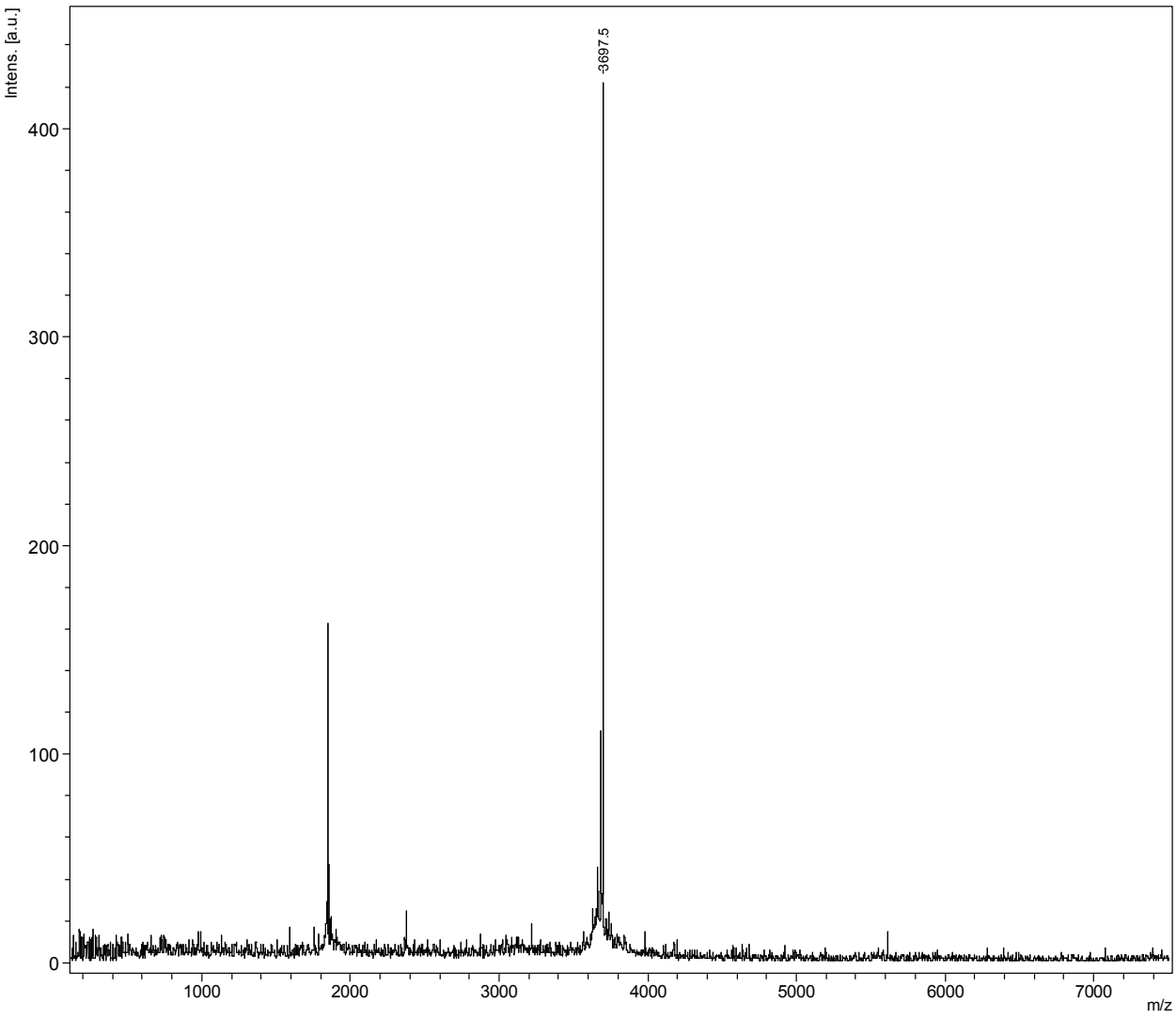

3.12

HPLC: Gradient = 10-60% solvent B over 50 minutes

MALDI-TOF: Calculated monoisotopic $[M+H]^+ = 4022.0$

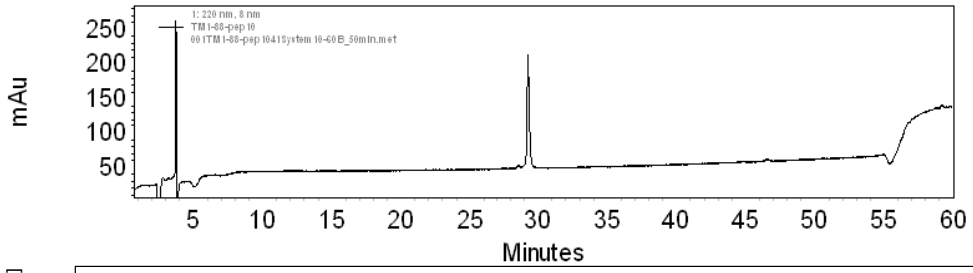

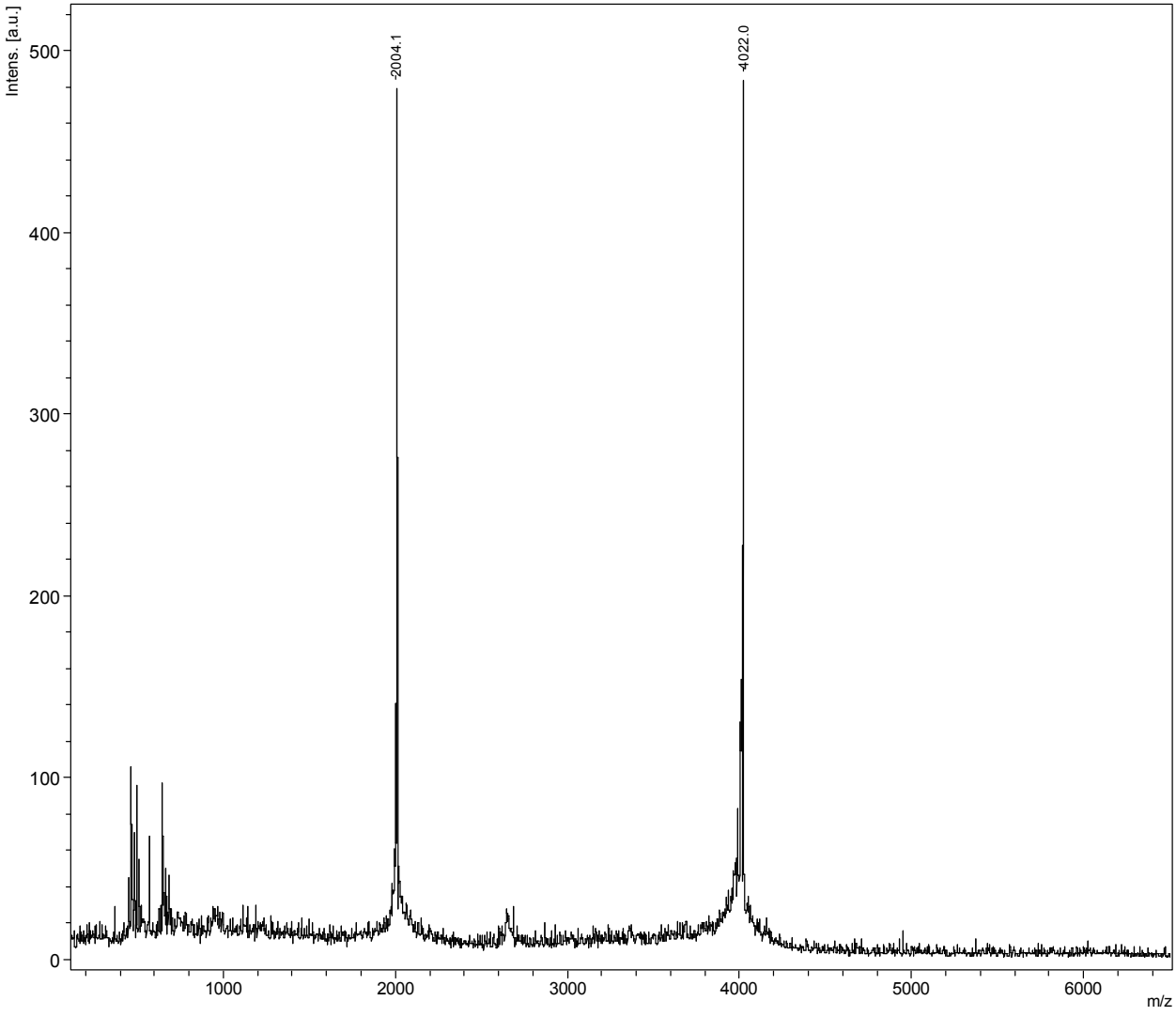

3.13

HPLC: Gradient = 10-60% solvent B over 50 minutes

MALDI-TOF: Calculated monoisotopic $[M+H]^+ = 4279.2$

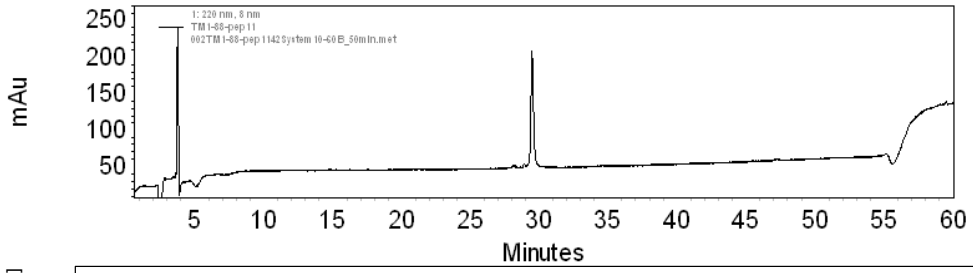

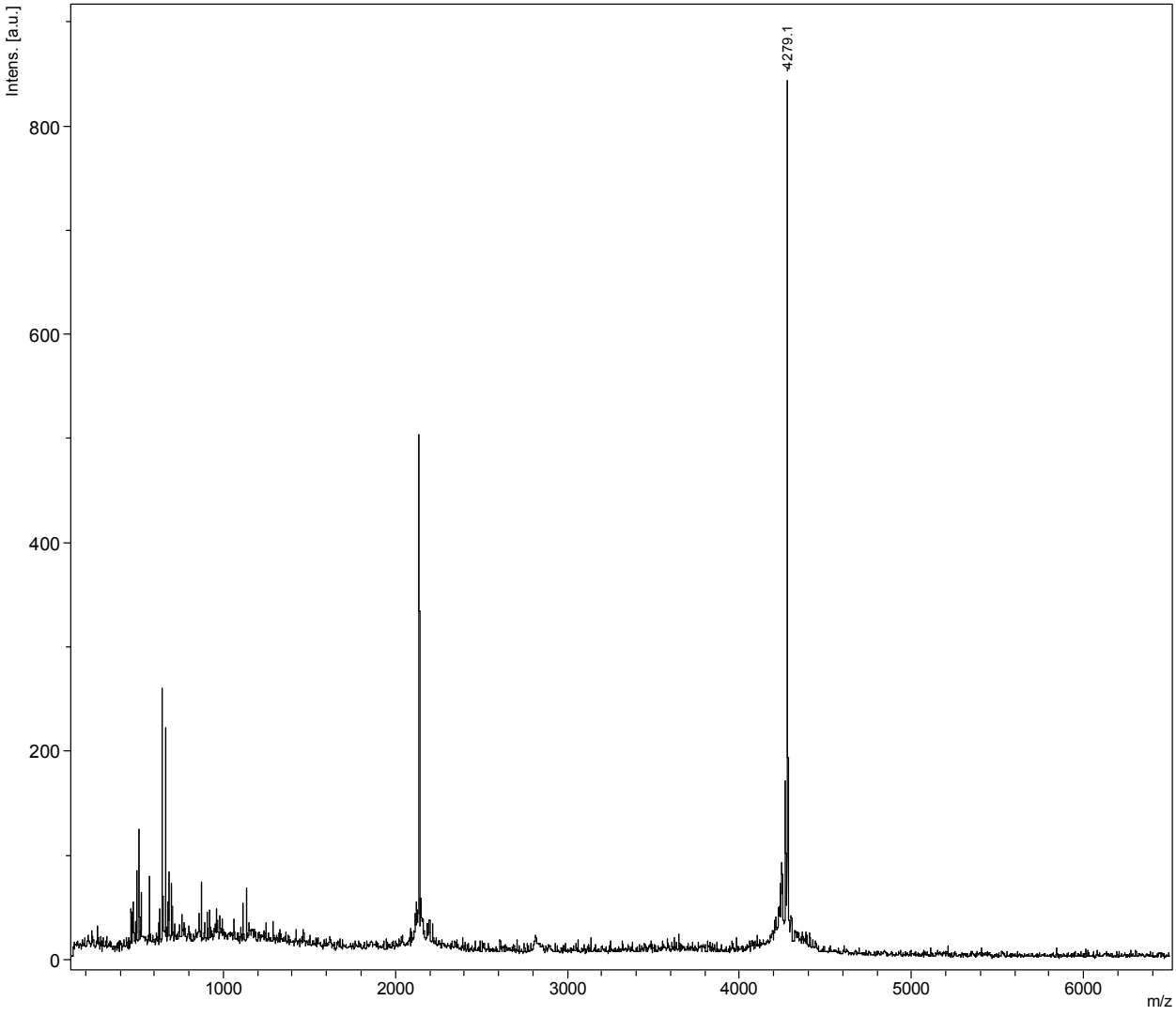

3.14

HPLC: Gradient = 10-60% solvent B over 50 minutes

MALDI-TOF: Calculated monoisotopic $[M+H]^+ = 4283.2$

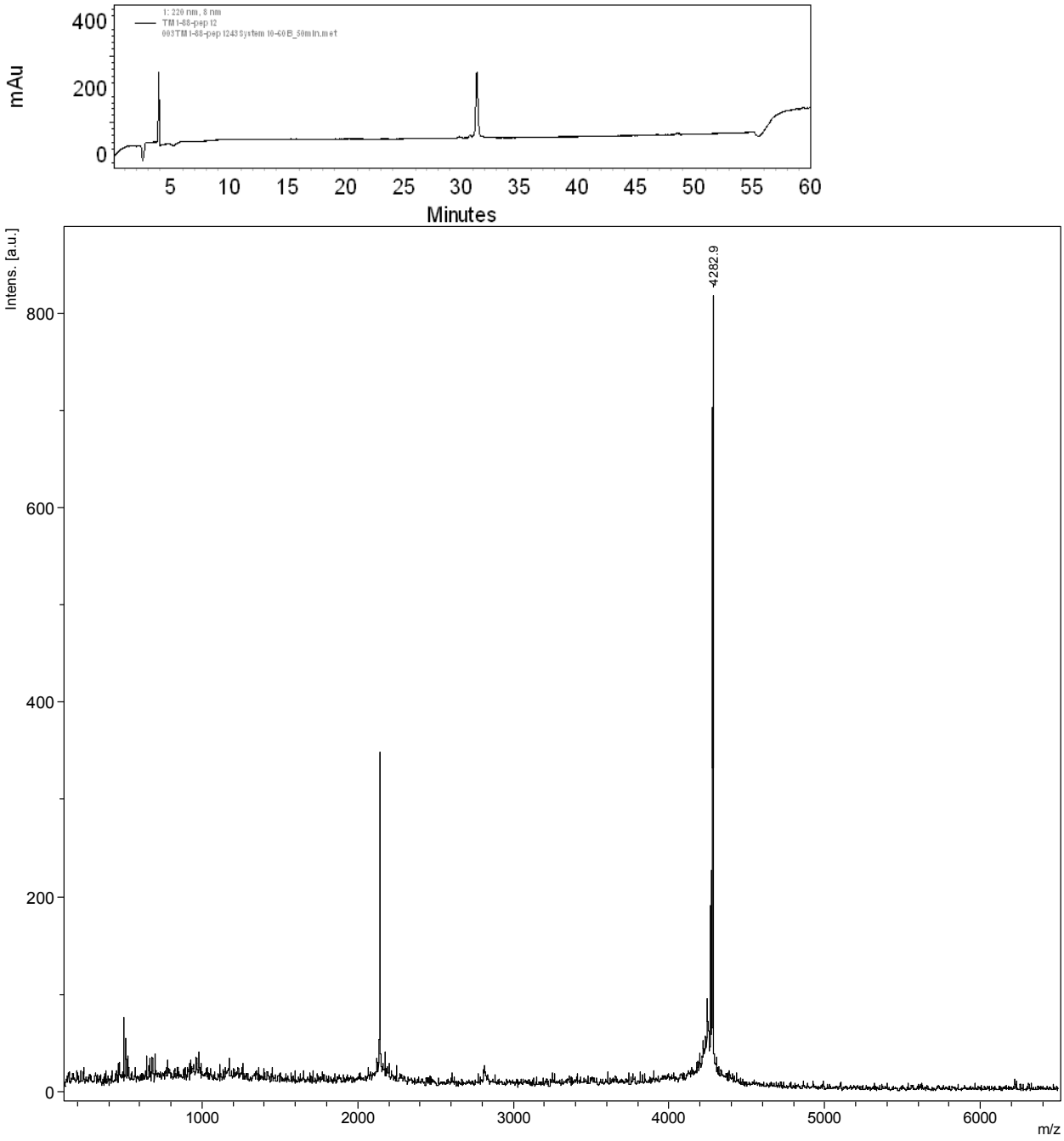

3.15

HPLC: Gradient = 10-60% solvent B over 50 minutes

MALDI-TOF: Calculated monoisotopic $[M+H]^+ = 4309.3$

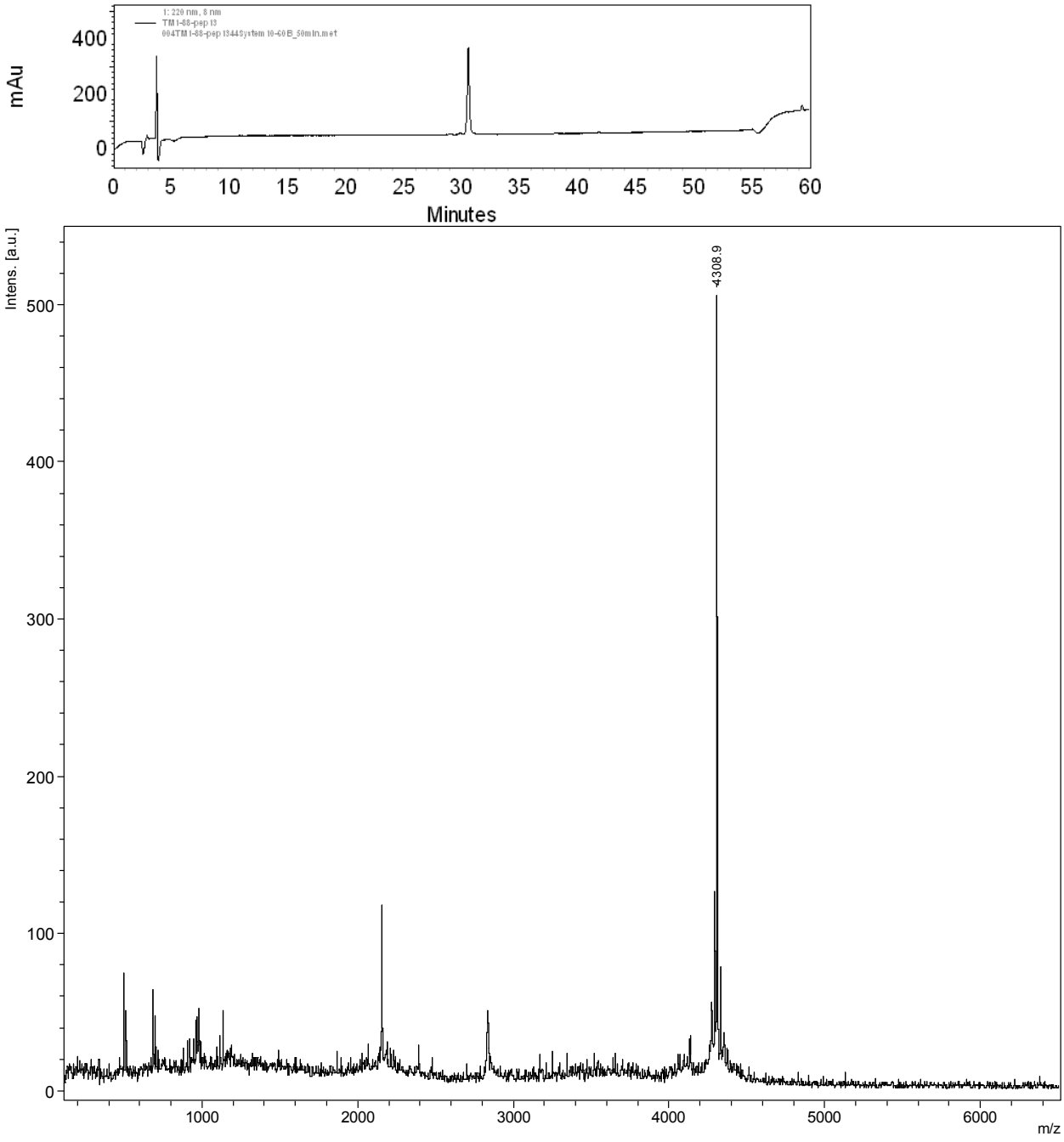

3.16

HPLC: Gradient = 10-60% solvent B over 50 minutes

MALDI-TOF: Calculated monoisotopic $[M+H]^+ = 4309.3$

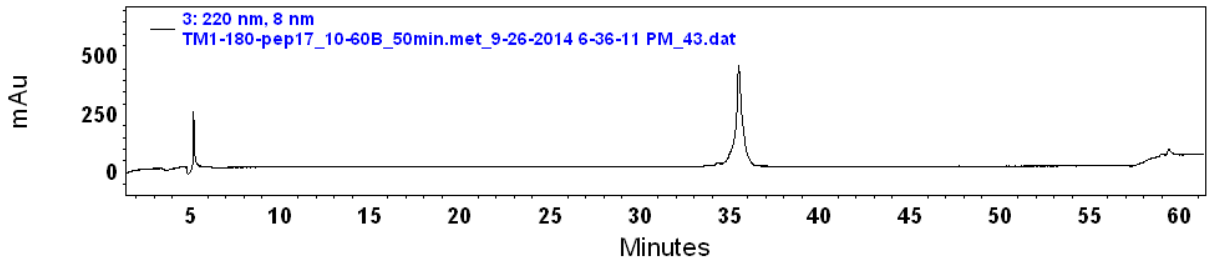

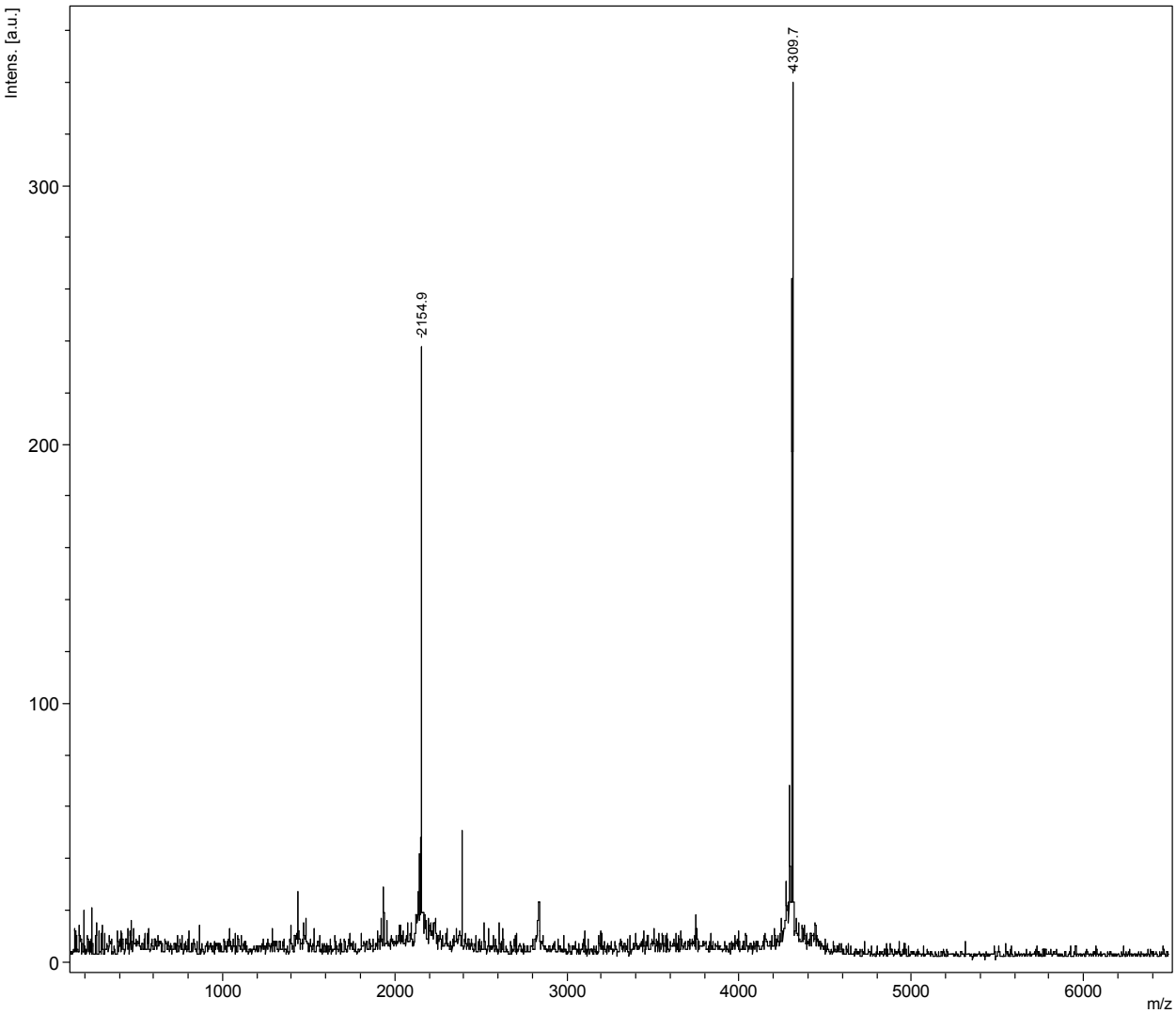

3.17

HPLC: Gradient = 10-60% solvent B over 50 minutes

MALDI-TOF: Calculated monoisotopic $[M+H]^+ = 4313.3$

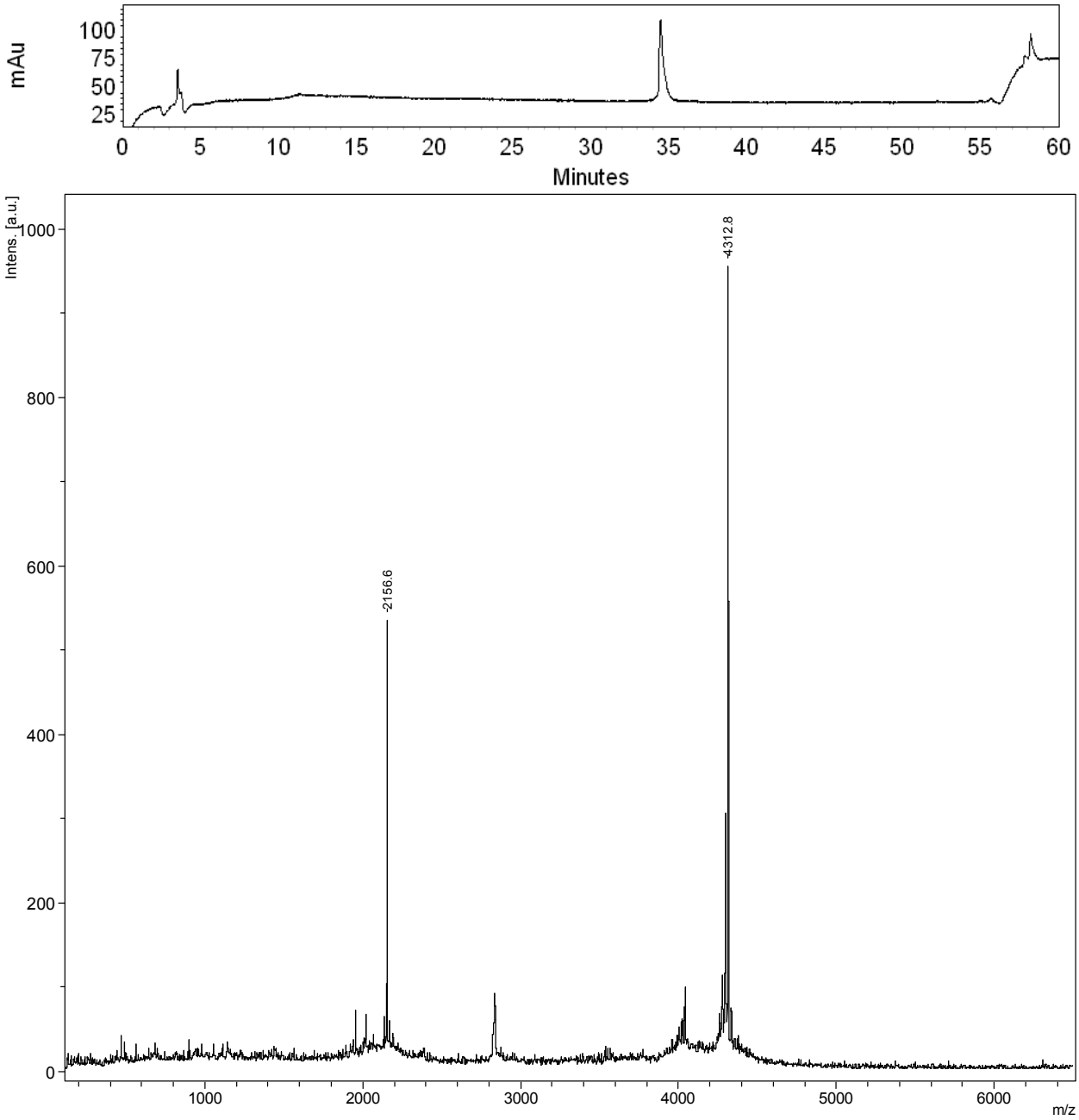

3.18

HPLC: Gradient = 10-60% solvent B over 50 minutes

MALDI-TOF: Calculated monoisotopic $[M+H]^+ = 4255.3$

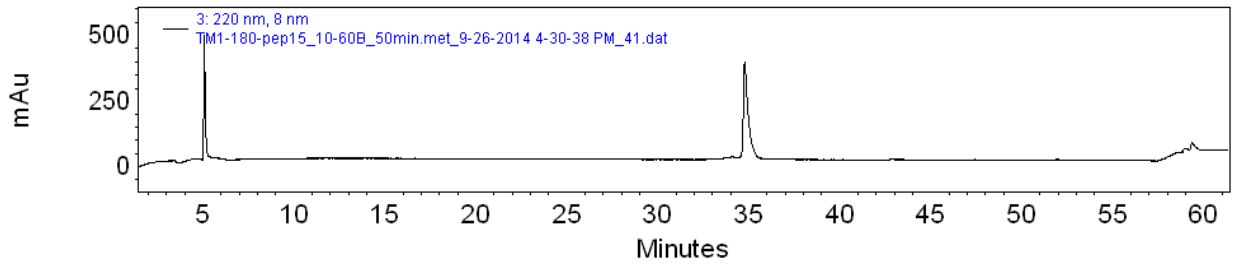

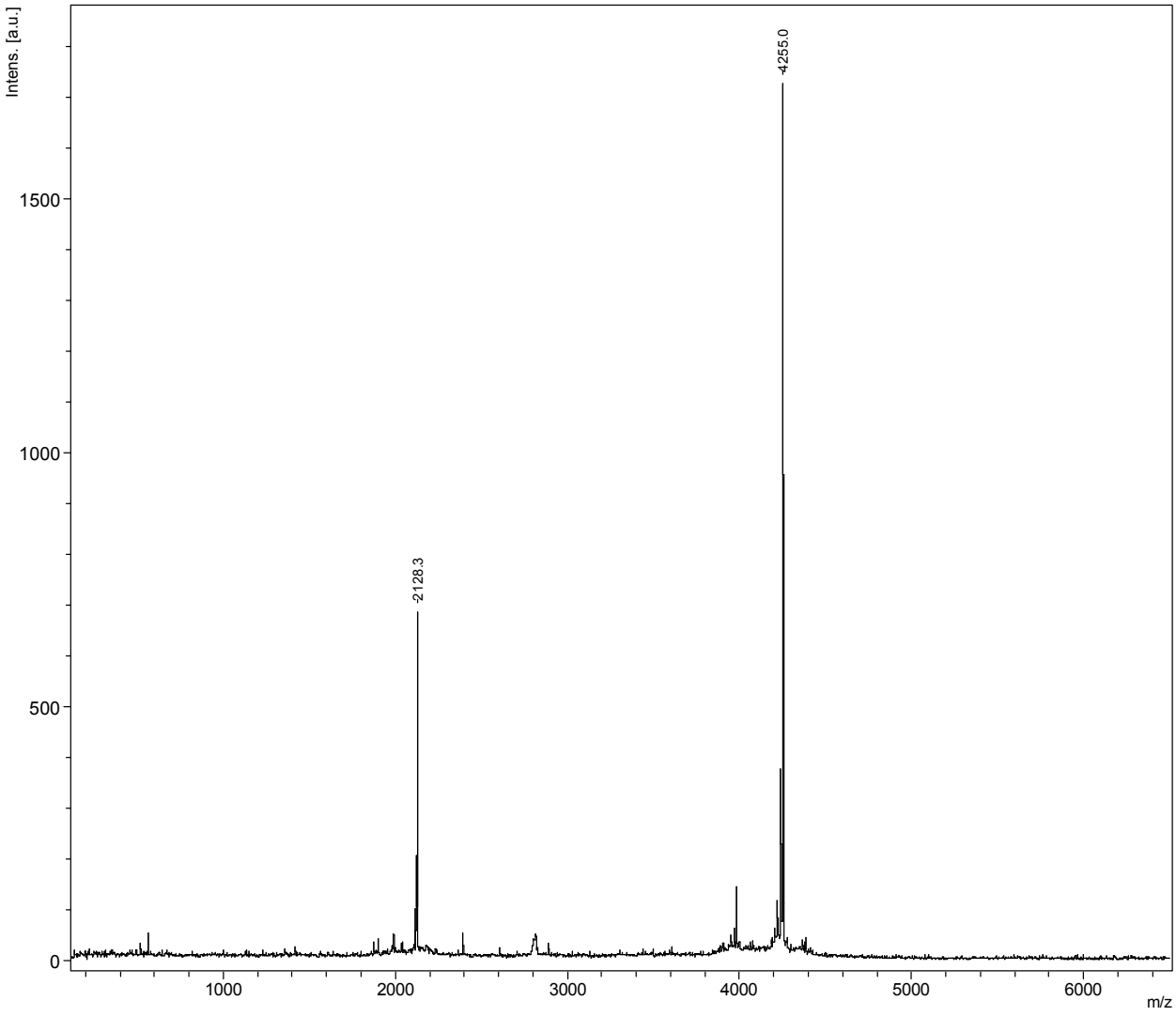

3.19

HPLC: Gradient = 10-60% solvent B over 50 minutes

MALDI-TOF: Calculated monoisotopic $[M+H]^+$ = 4270.3

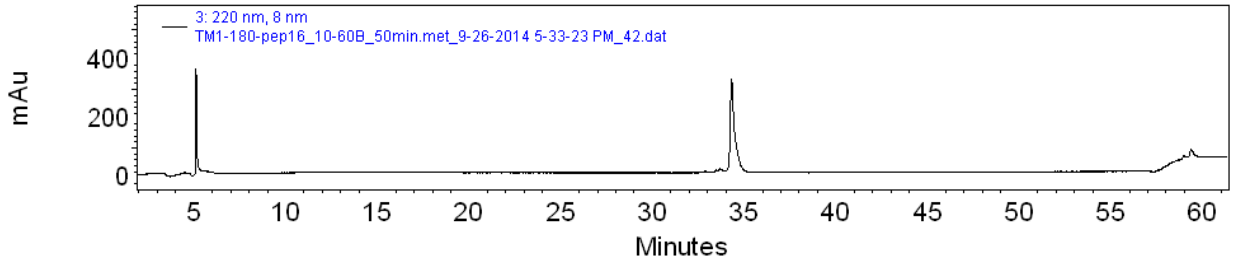

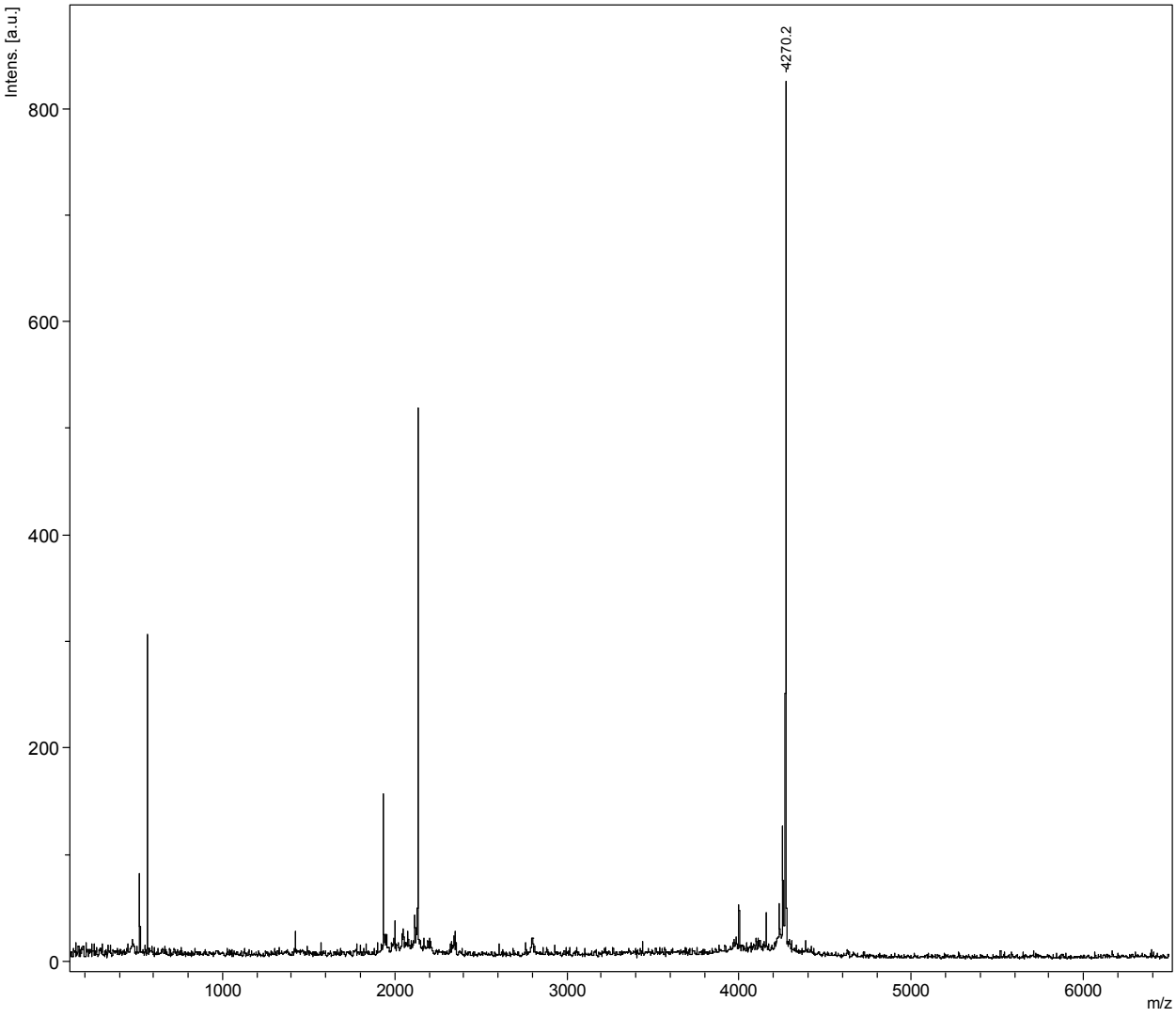

3.20

HPLC: Gradient = 10-60% solvent B over 50 minutes

MALDI-TOF: Calculated monoisotopic $[M+H]^+ = 4319.2$

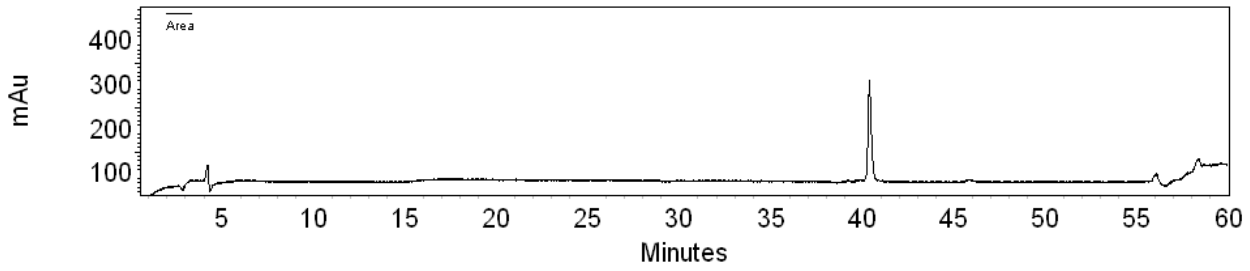

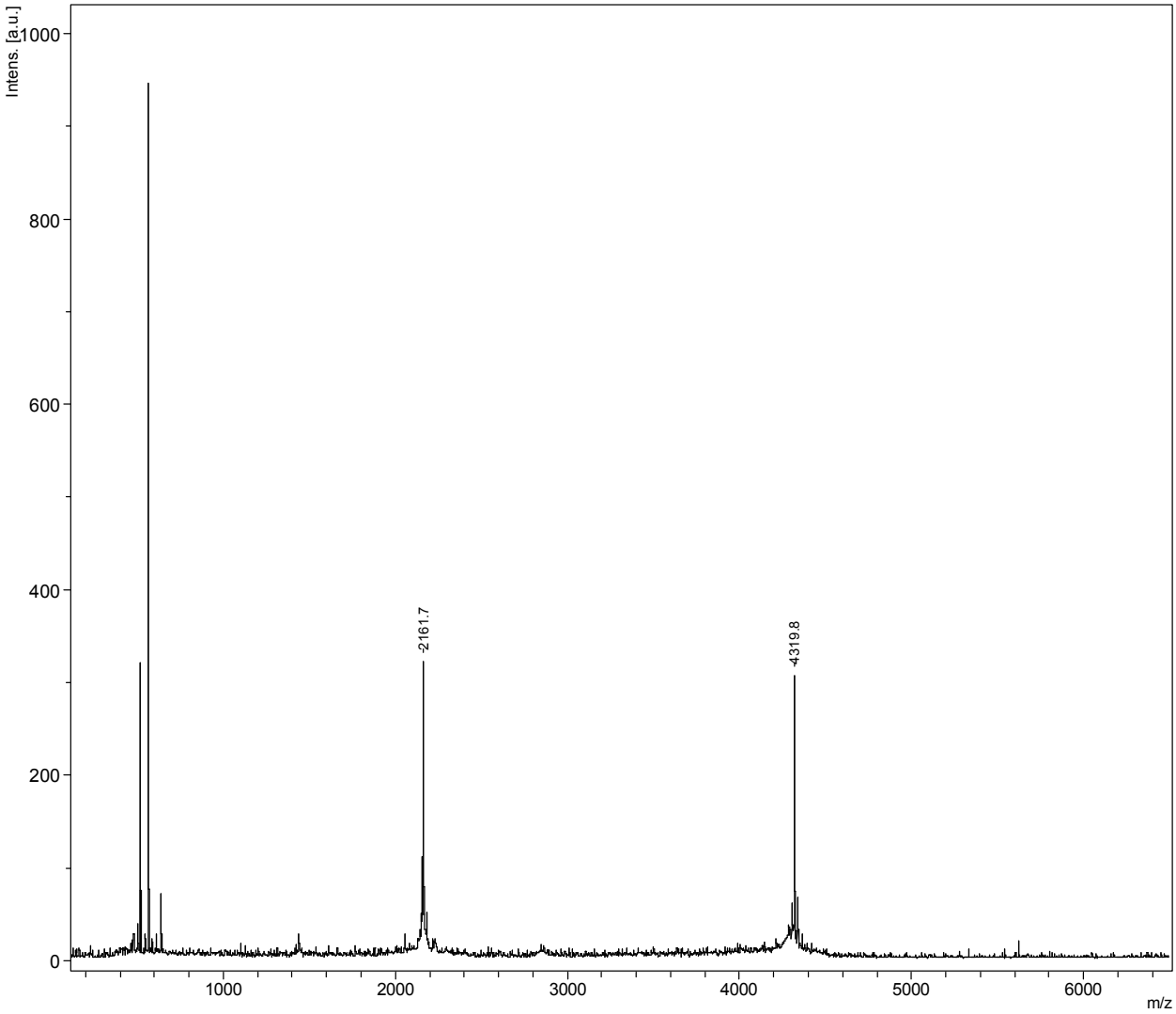

3.21

HPLC: Gradient = 10-60% solvent B over 50 minutes

MALDI-TOF: Calculated monoisotopic $[M+H]^+ = 4347.2$

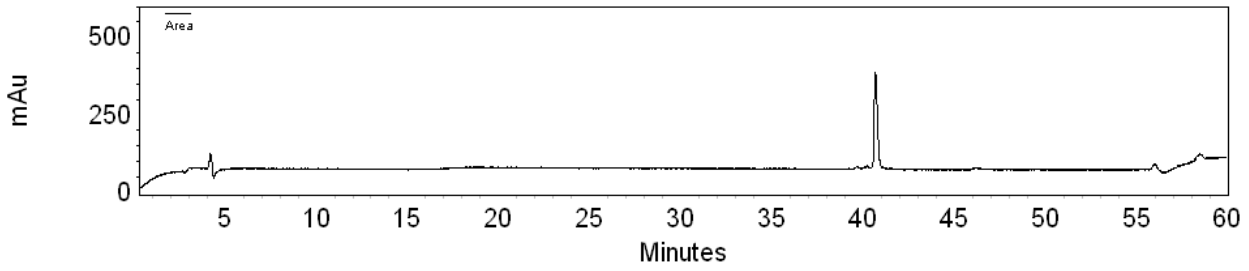

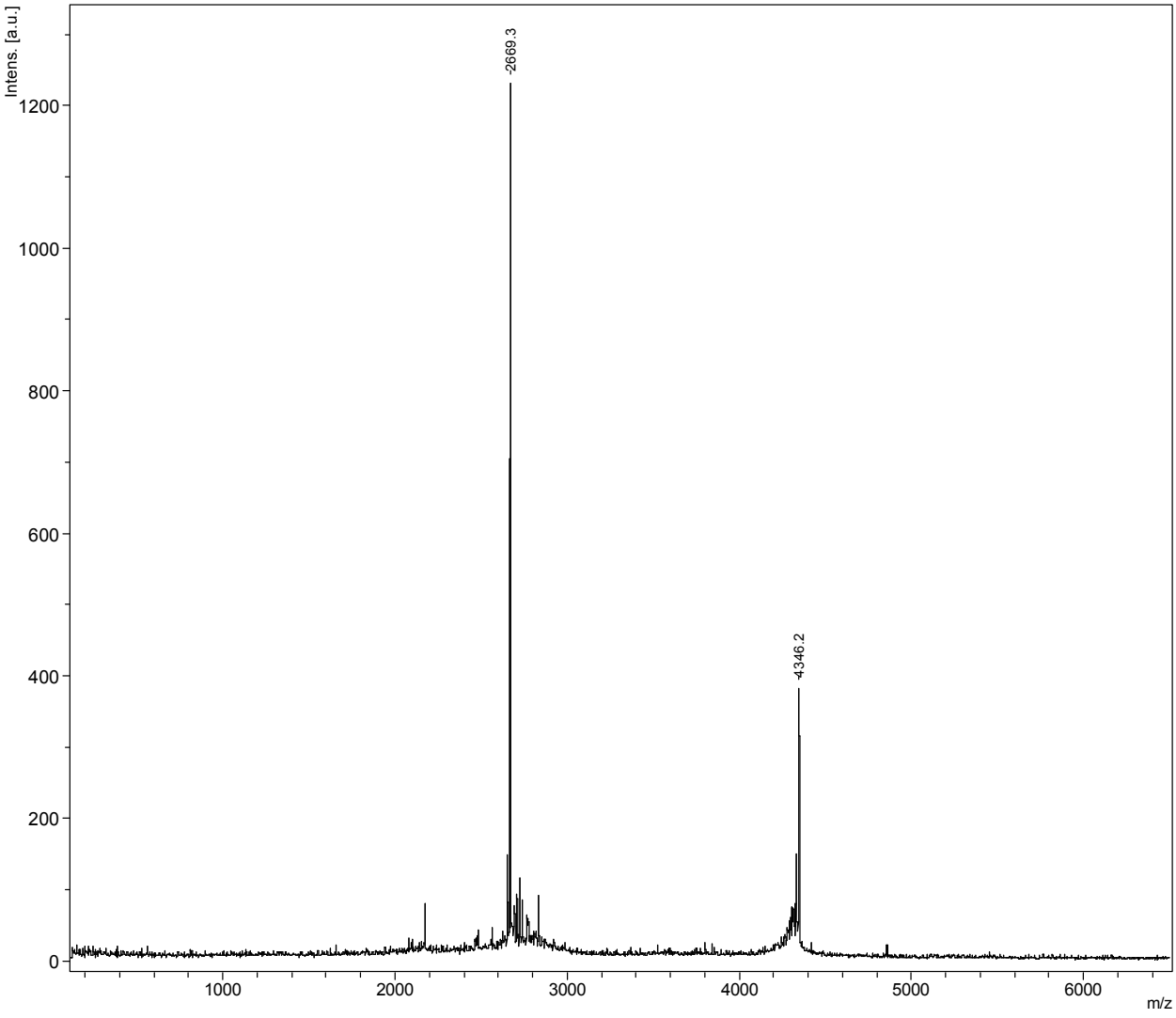

3.22

HPLC: Gradient = 10-60% solvent B over 50 minutes

MALDI-TOF: Calculated monoisotopic $[M+H]^+ = 4215.0$

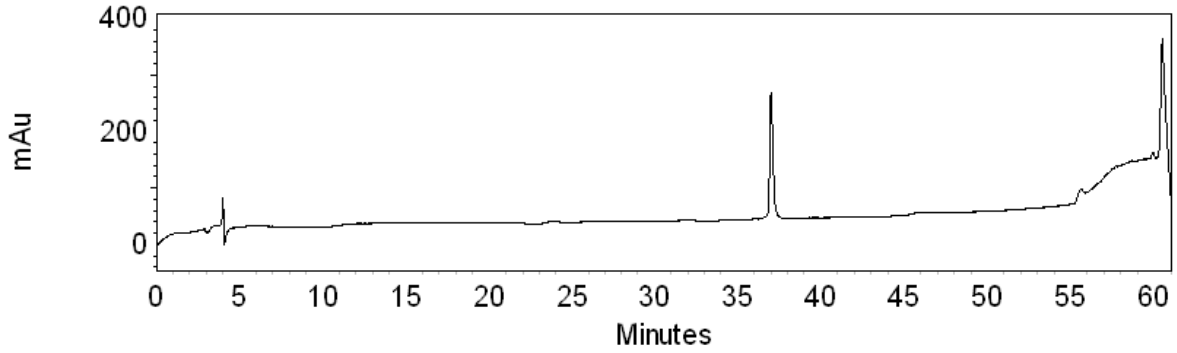

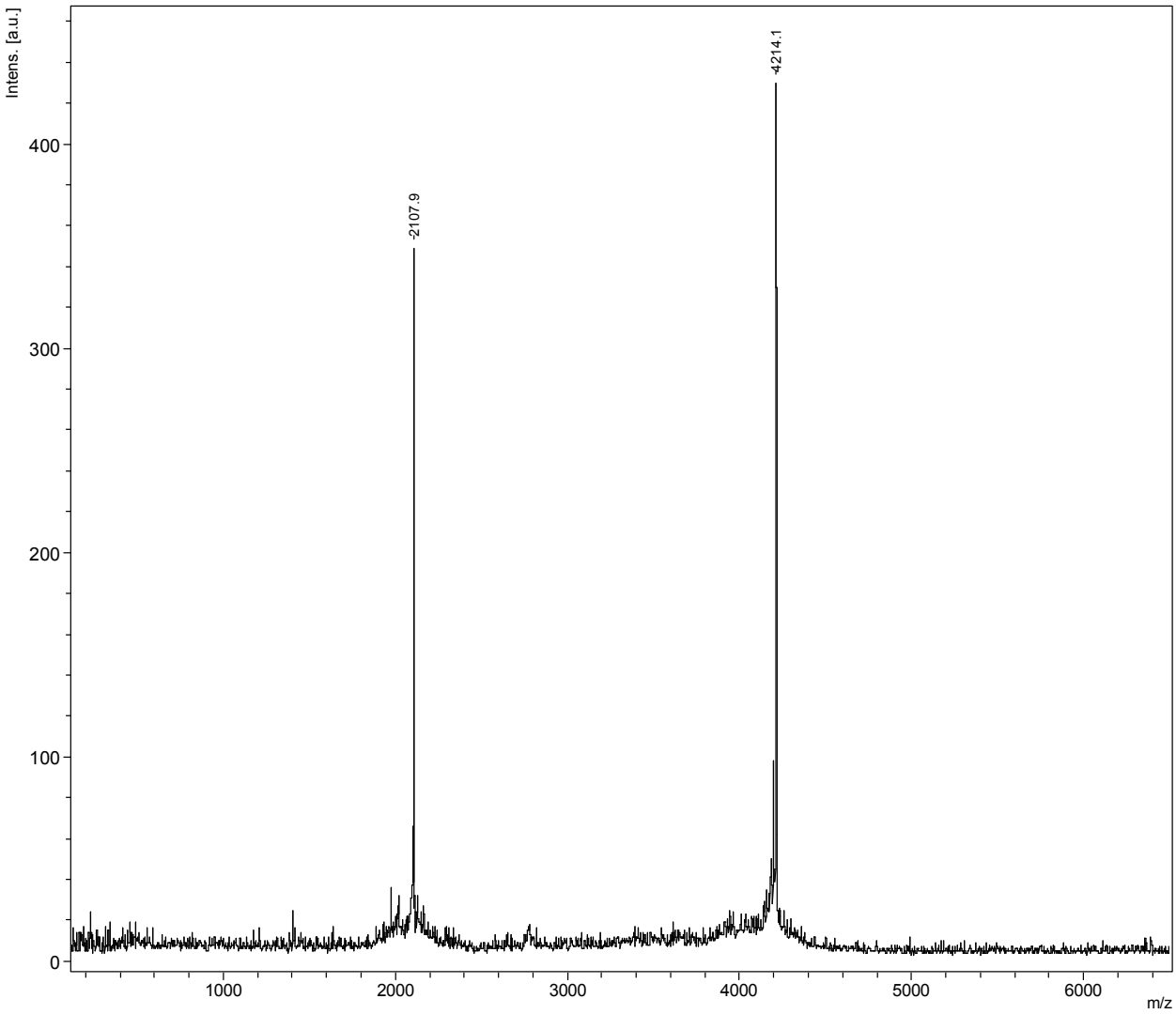

3.23

HPLC: Gradient = 10-60% solvent B over 50 minutes

MALDI-TOF: Calculated monoisotopic $[M+H]^+ = 4229.0$

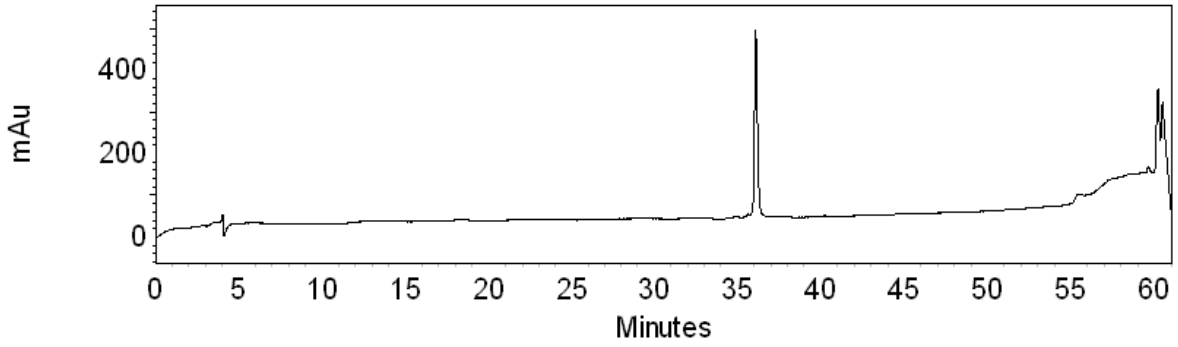

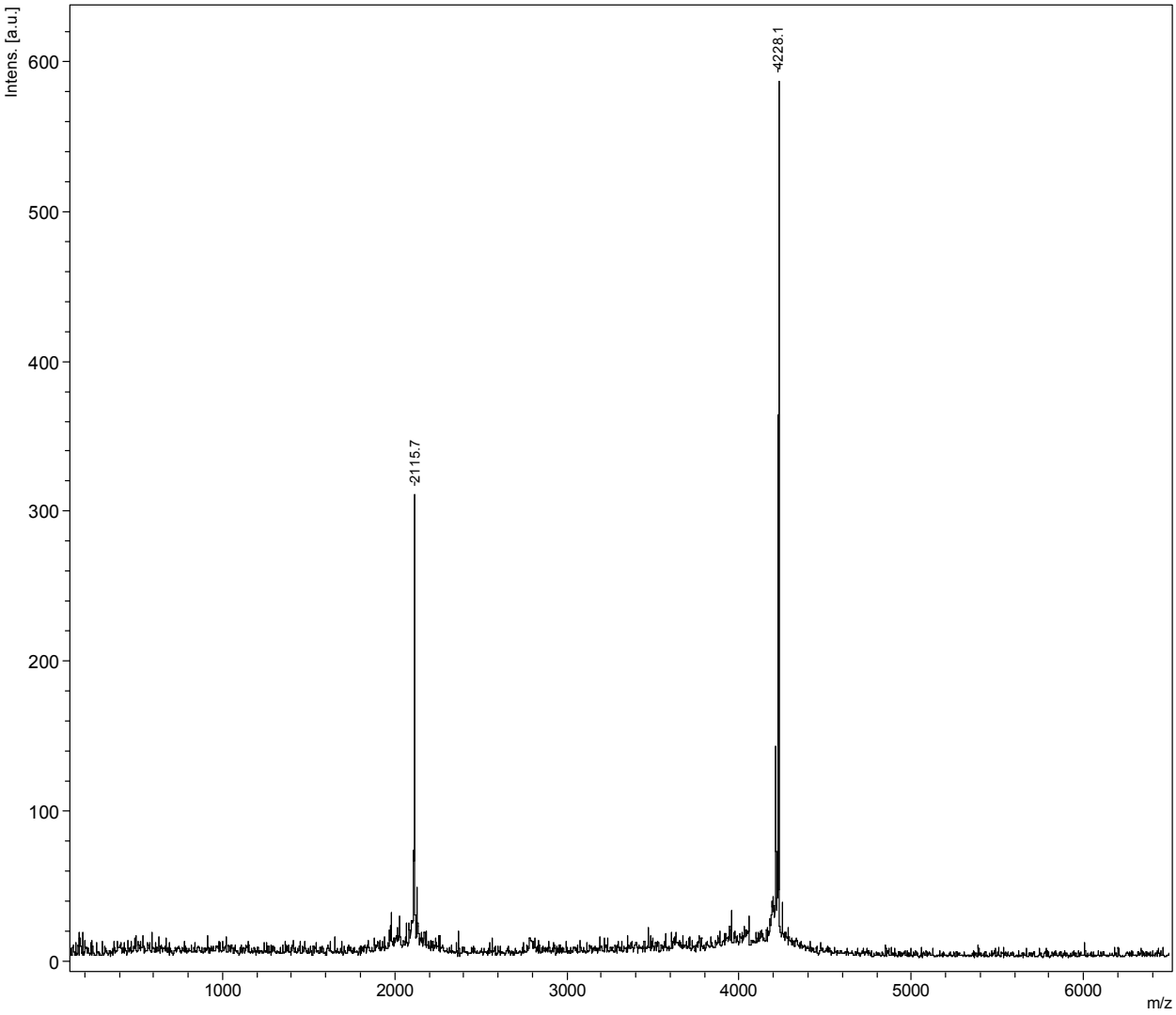

3.24

HPLC: Gradient = 10-60% solvent B over 50 minutes

MALDI-TOF: Calculated monoisotopic $[M+H]^+ = 4243.1$

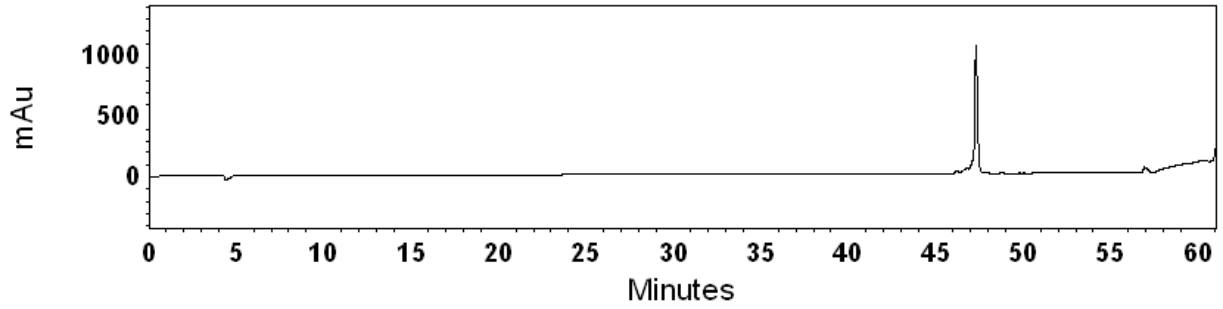

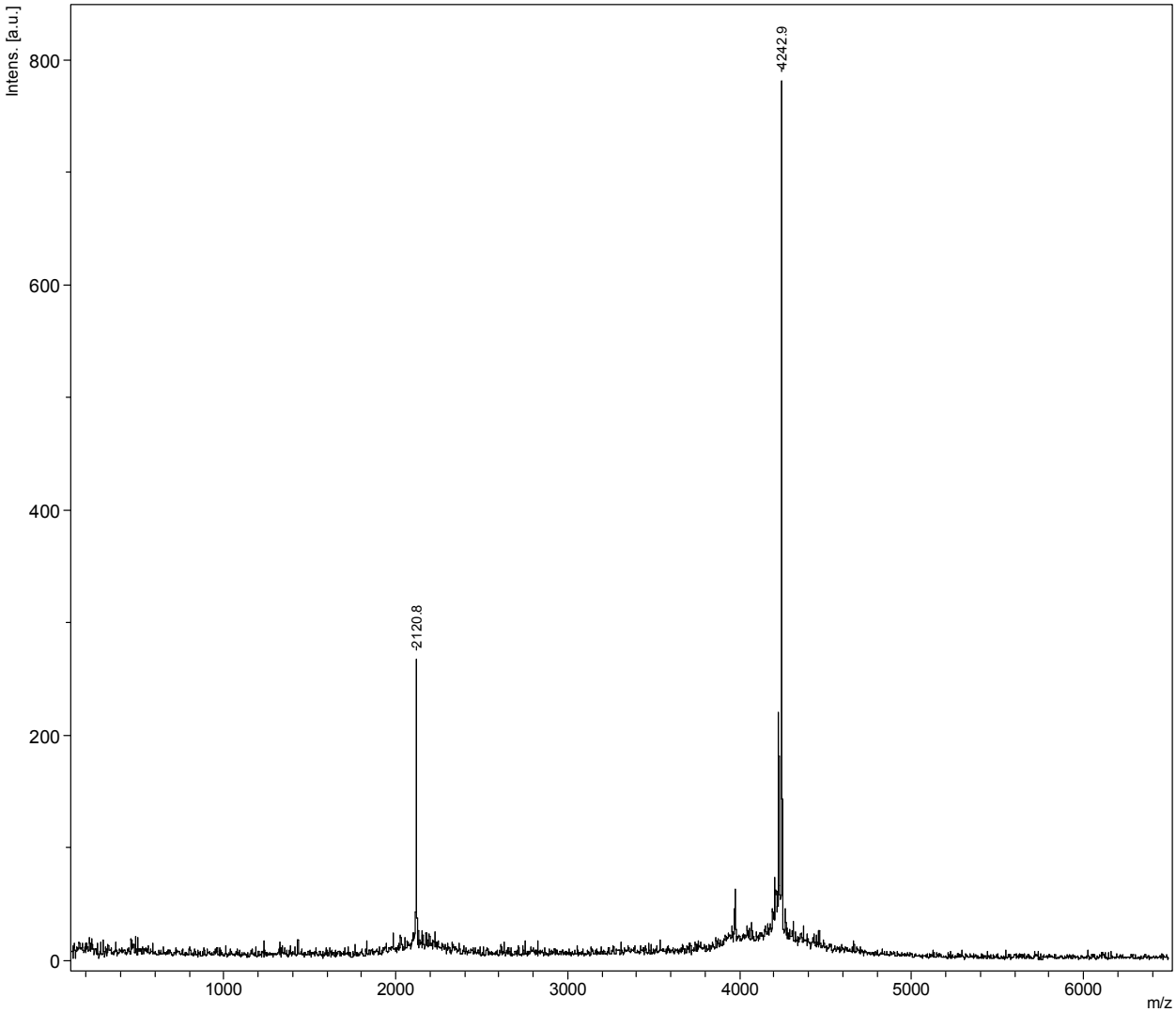

3.25

HPLC: Gradient = 10-60% solvent B over 50 minutes

MALDI-TOF: Calculated monoisotopic $[M+H]^+ = 4748.3$

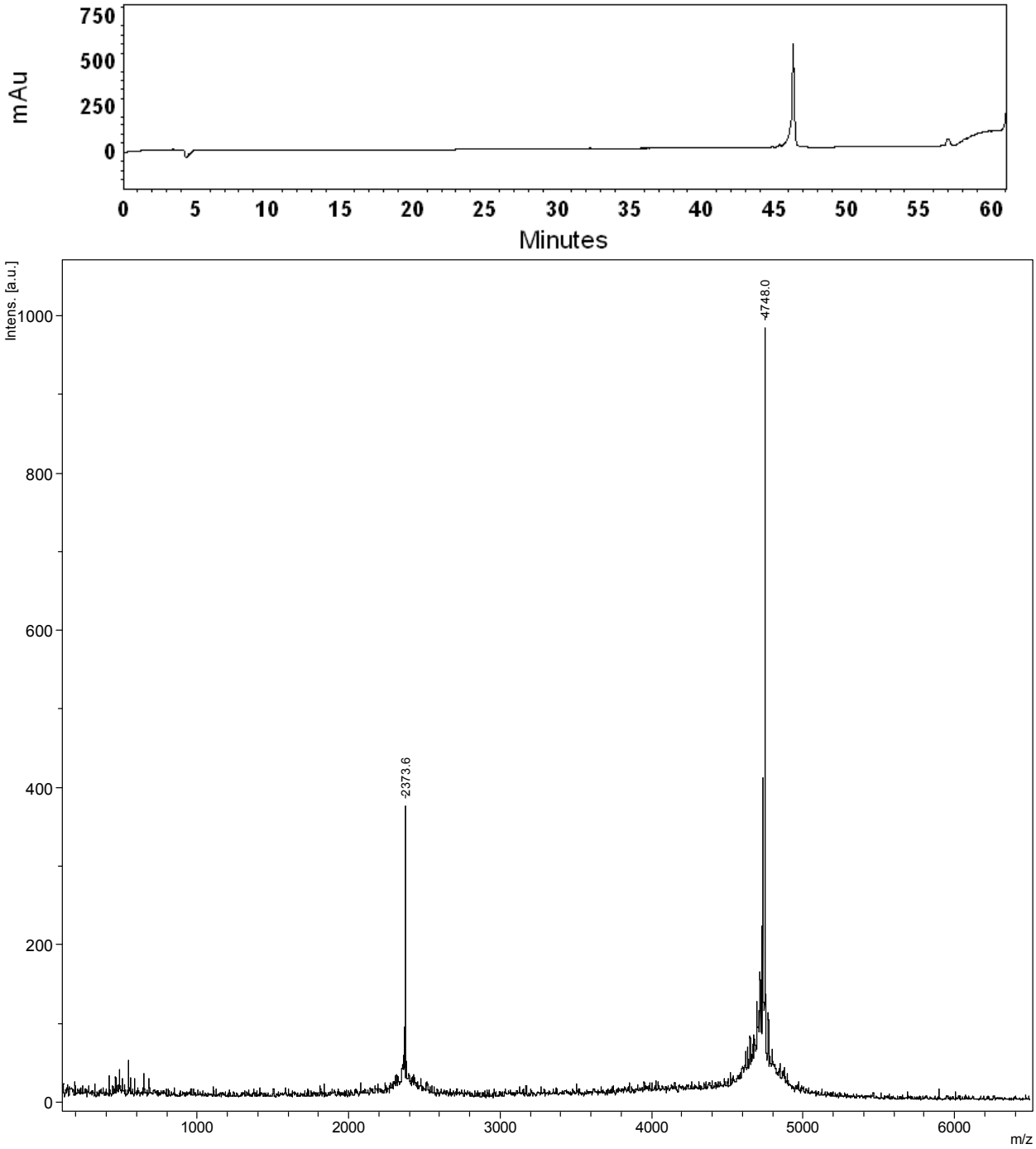

3.26

HPLC: Gradient = 10-60% solvent B over 50 minutes

MALDI-TOF: Calculated monoisotopic $[M+H]^+ = 4795.5$

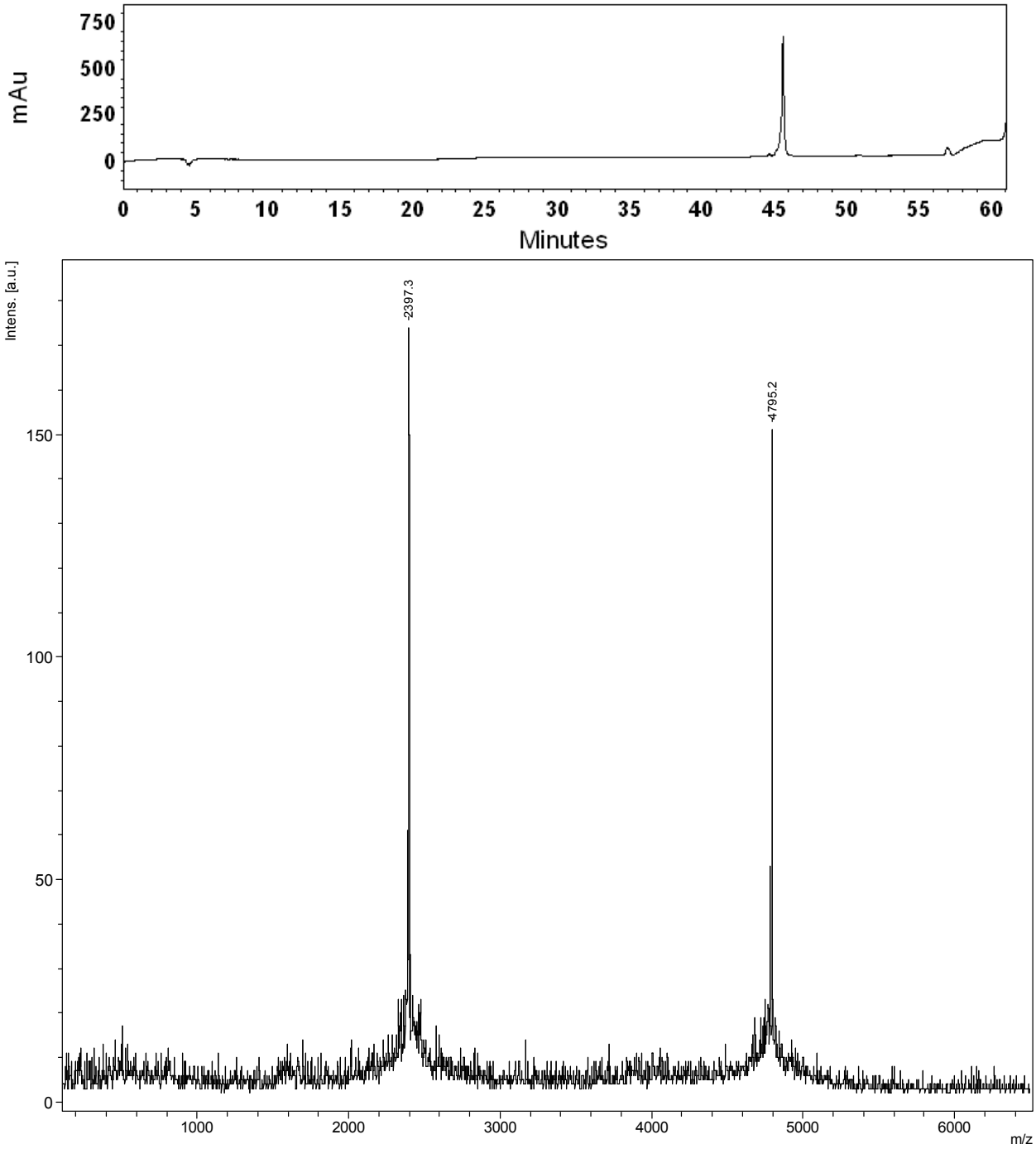

3.27

HPLC: Gradient = 10-60% solvent B over 50 minutes

MALDI-TOF: Calculated monoisotopic $[M+H]^+ = 4752.5$

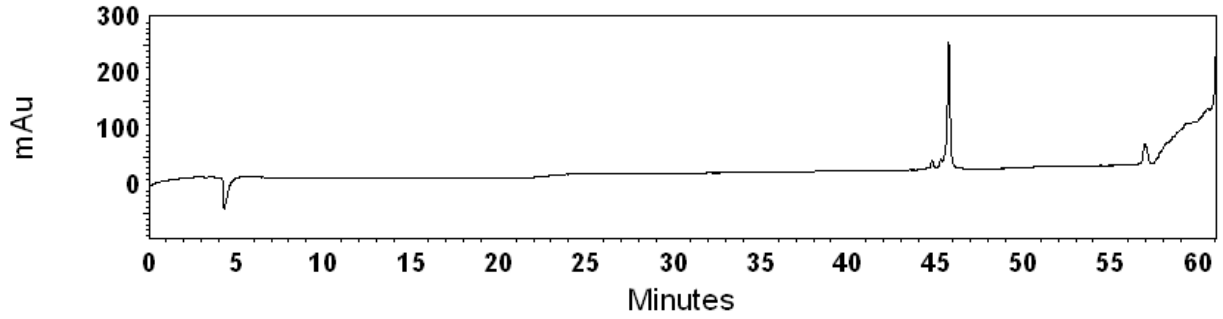

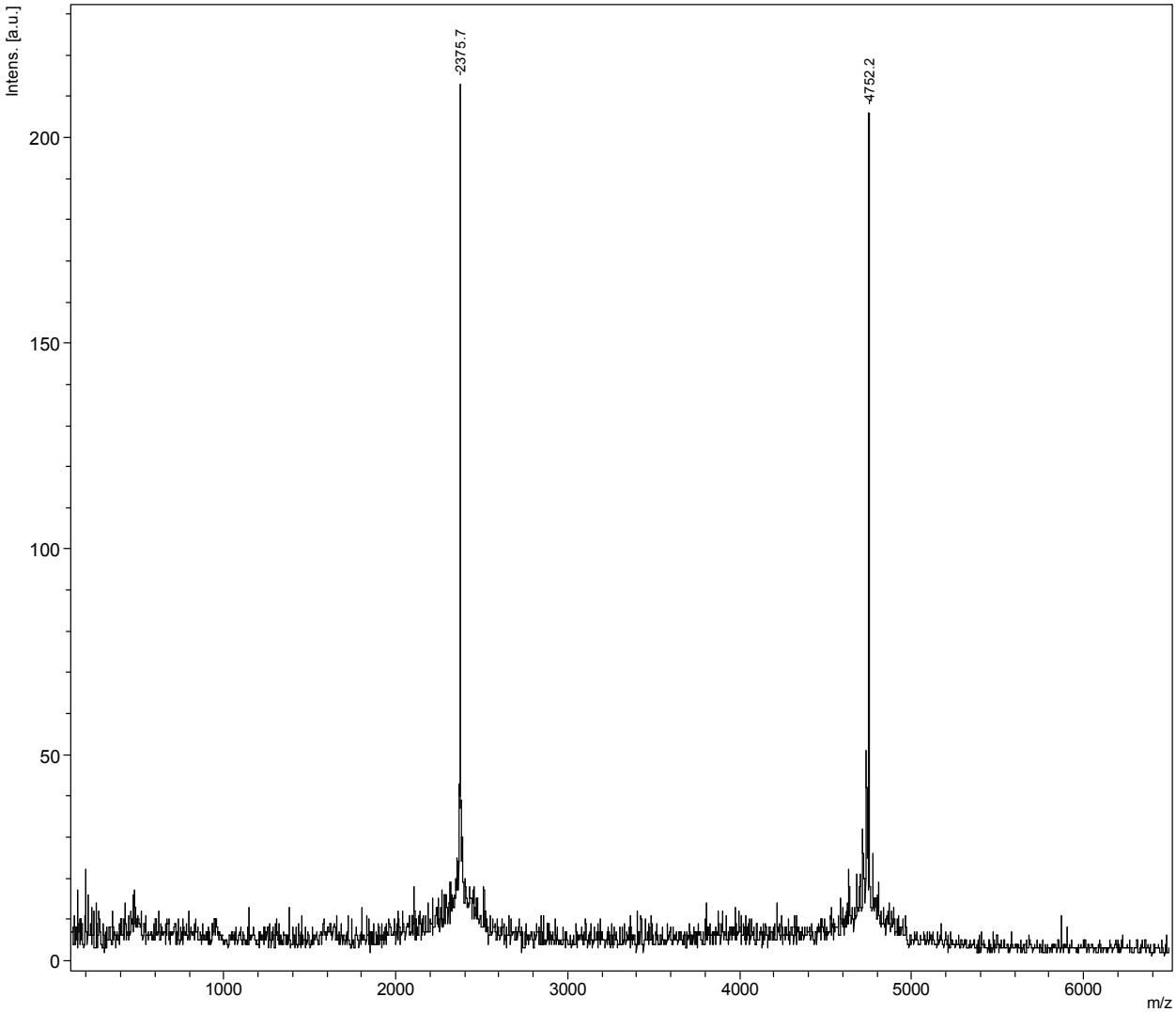

3.28

HPLC: Gradient = 10-90% solvent B over 80 minutes

MALDI-TOF: Calculated monoisotopic $[M+H]^+ = 5134.5$

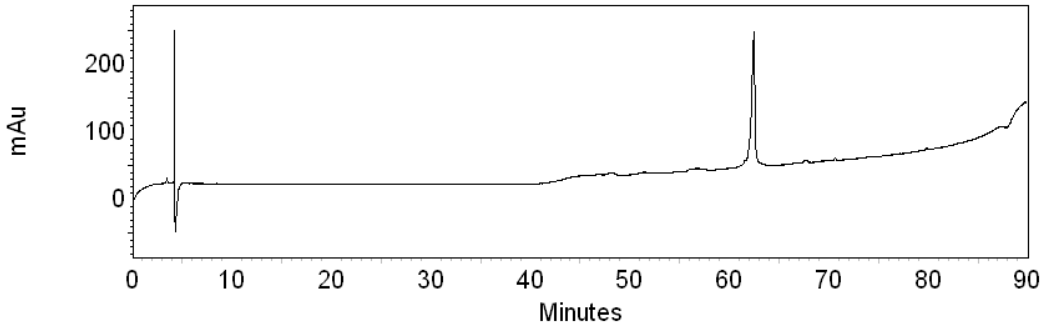

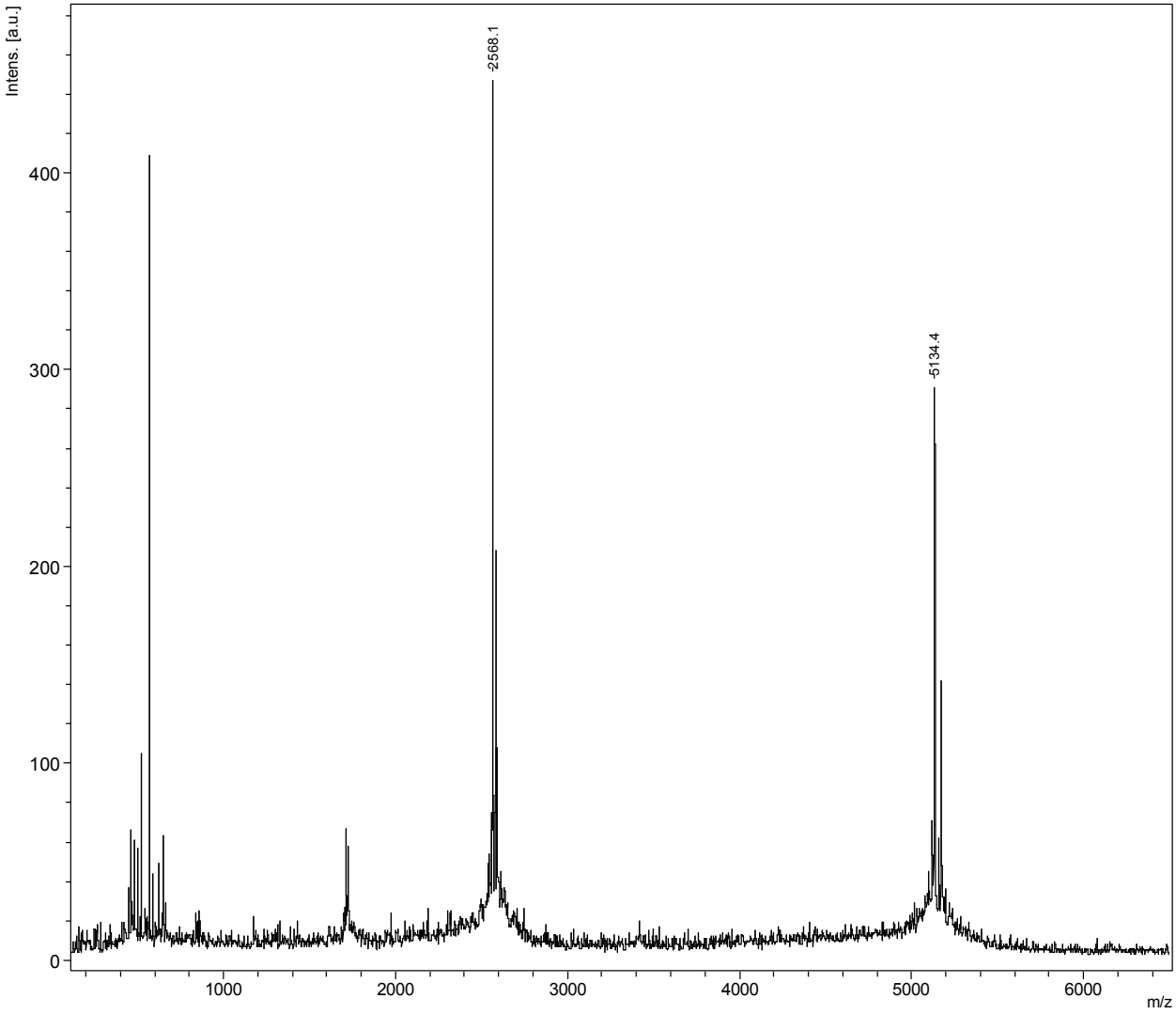

3.29

HPLC: Gradient = 10-90% solvent B over 80 minutes

MALDI-TOF: Calculated monoisotopic $[M+H]^+ = 5181.6$

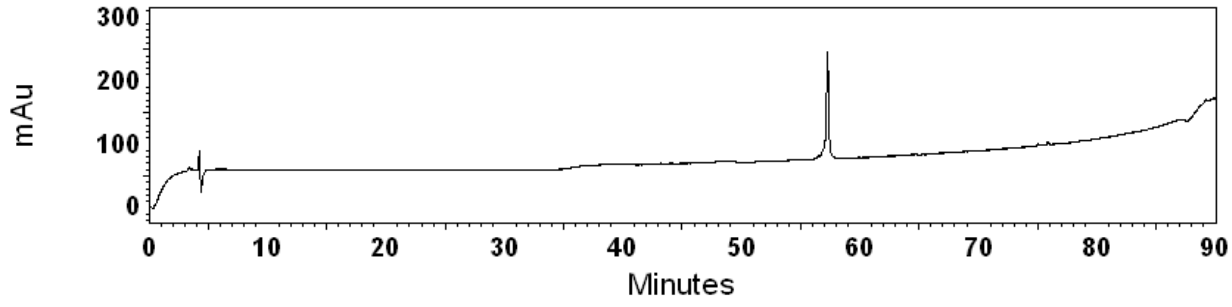

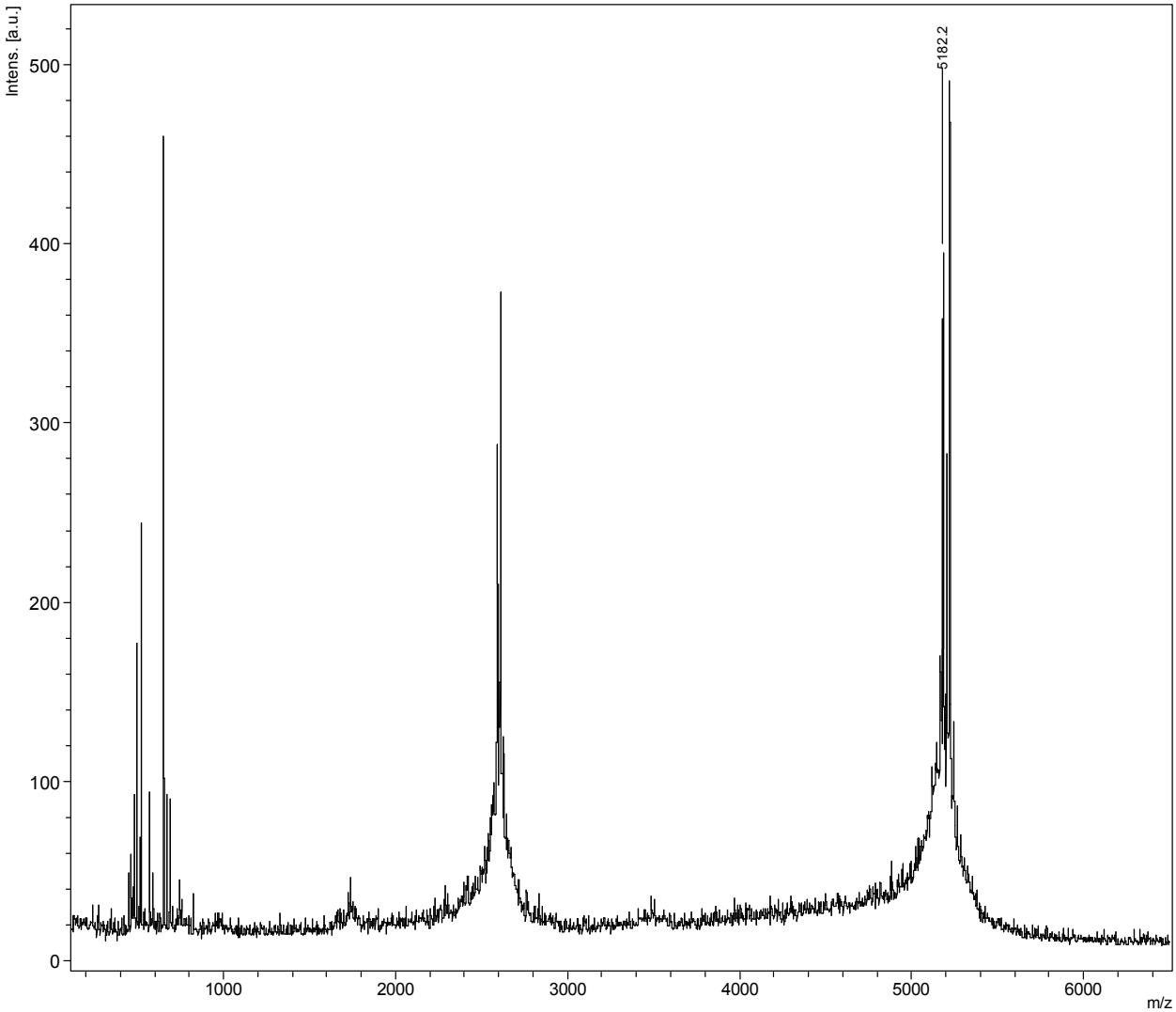

3.29

MALDI-TOF: Calculated monoisotopic $[M+H]^+$ = 5181.6, $[M+Na]^+$ = 5203.6, $[M+K]^+$ = 5219.7
(Expanded spectrum from previous page)

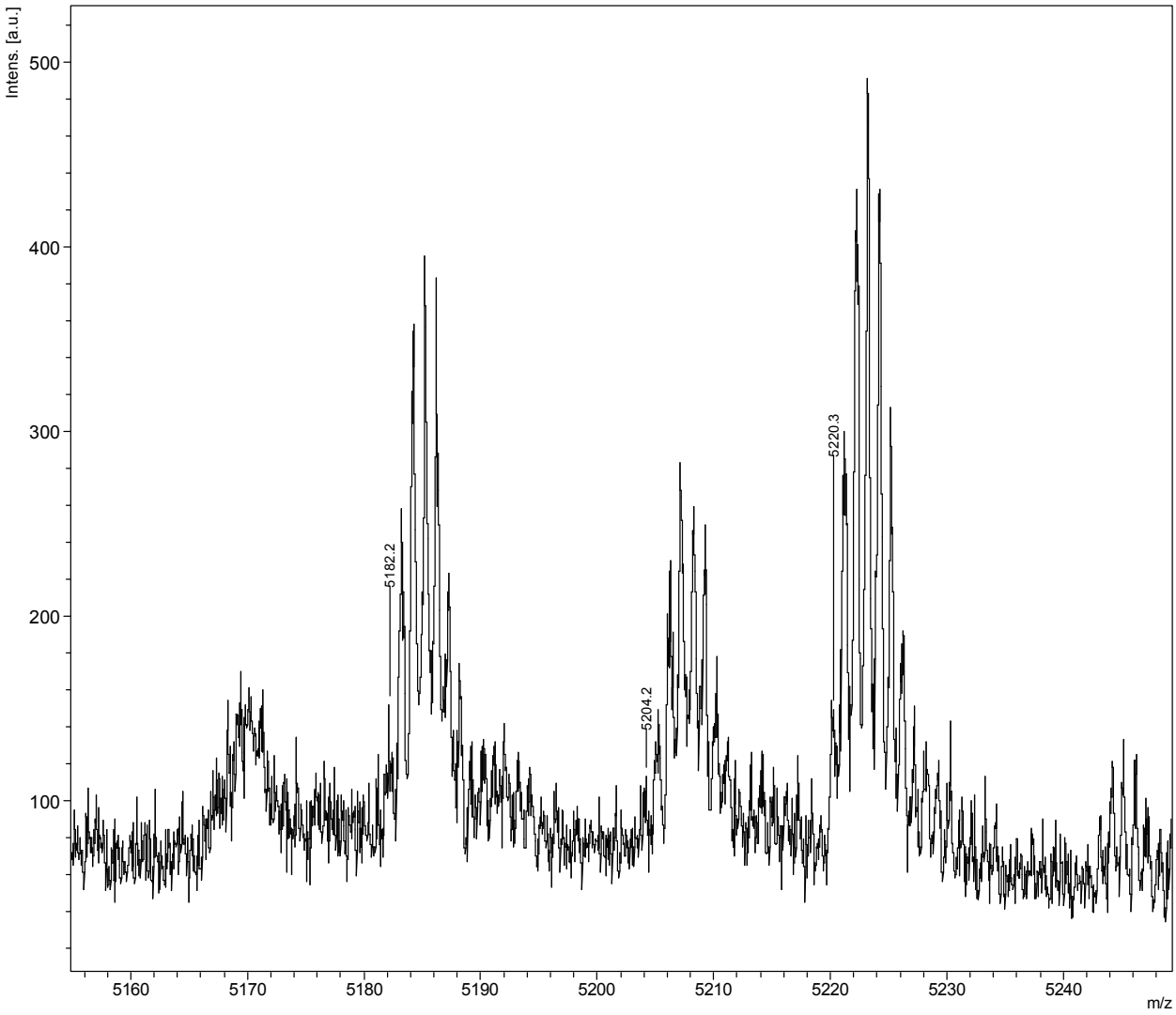

3.30

HPLC: Gradient = 10-90% solvent B over 80 minutes

MALDI-TOF: Calculated monoisotopic $[M+H]^+ = 5138.6$

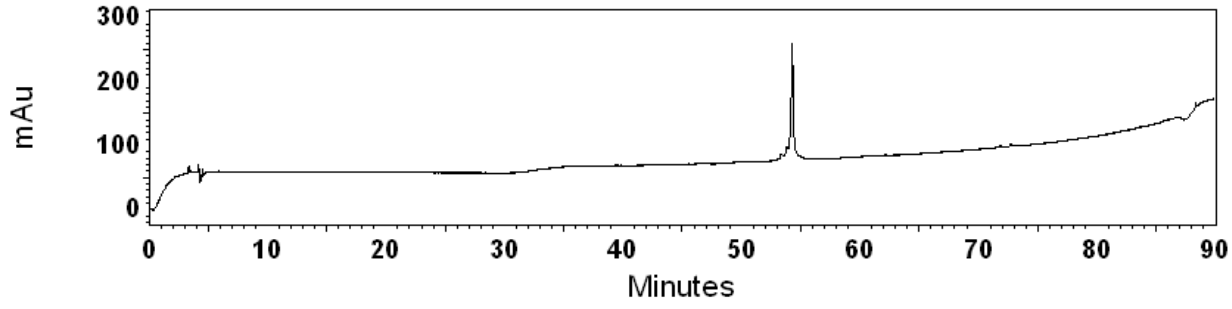

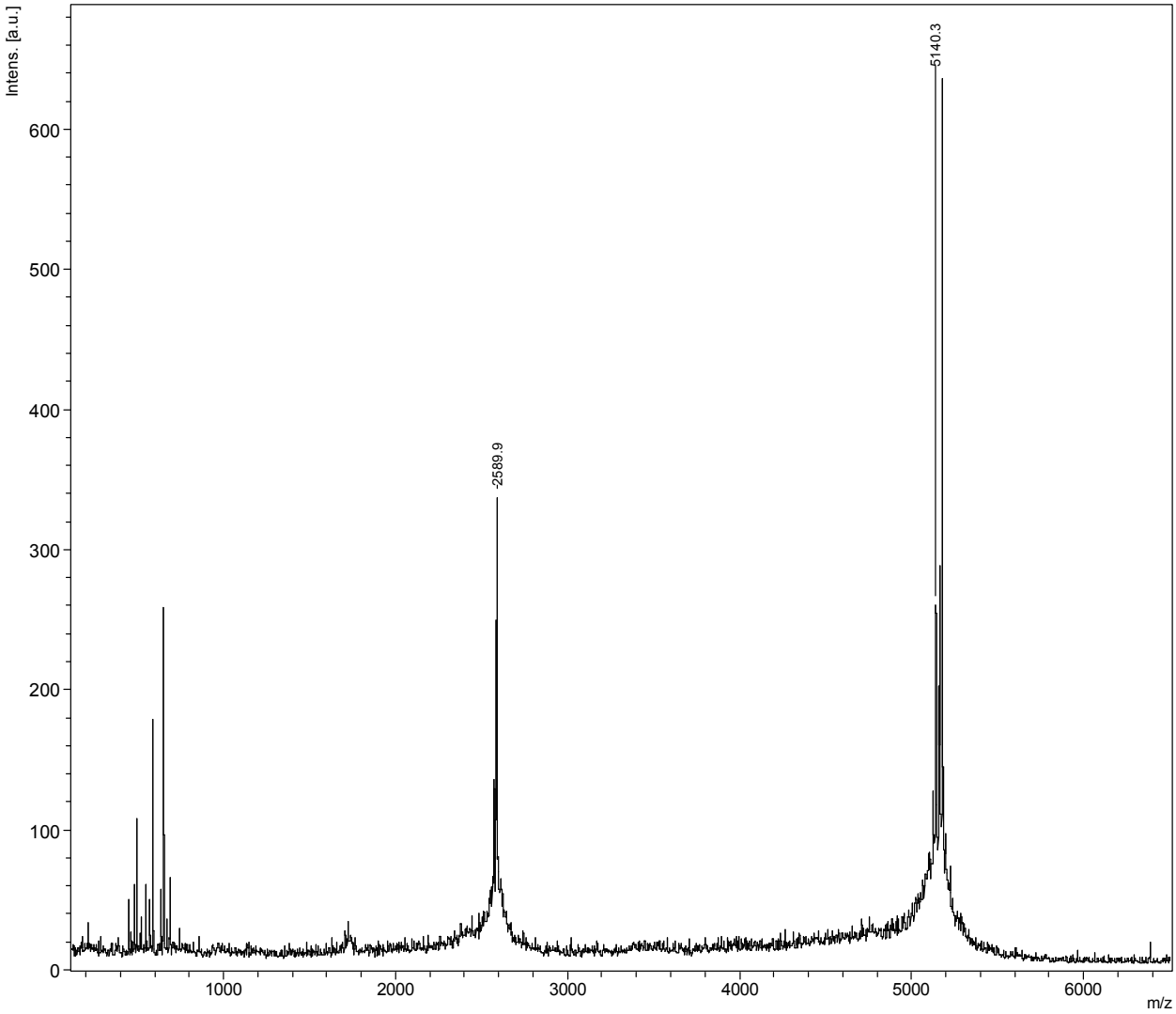

3.30

MALDI-TOF: Calculated monoisotopic $[M+H]^+$ = 5138.6, $[M+Na]^+$ = 5160.6, $[M+K]^+$ = 5176.7 (Expanded spectrum from previous page)

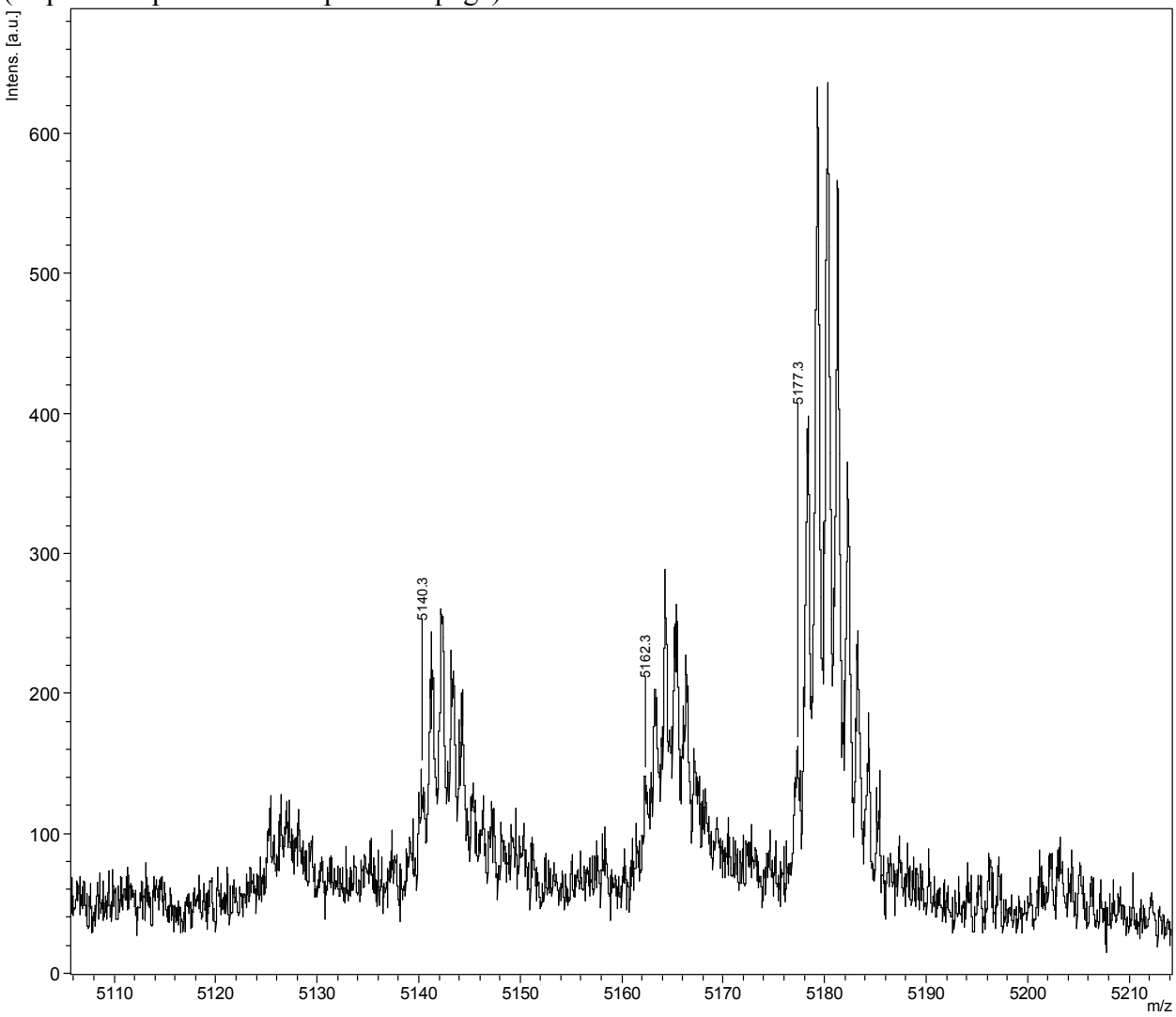

Z-EGFR
HPLC: Gradient = 10-60% solvent B over 50 minutes
MALDI-TOF: Calculated monoisotopic $[M+H]^+$ = 6540.3

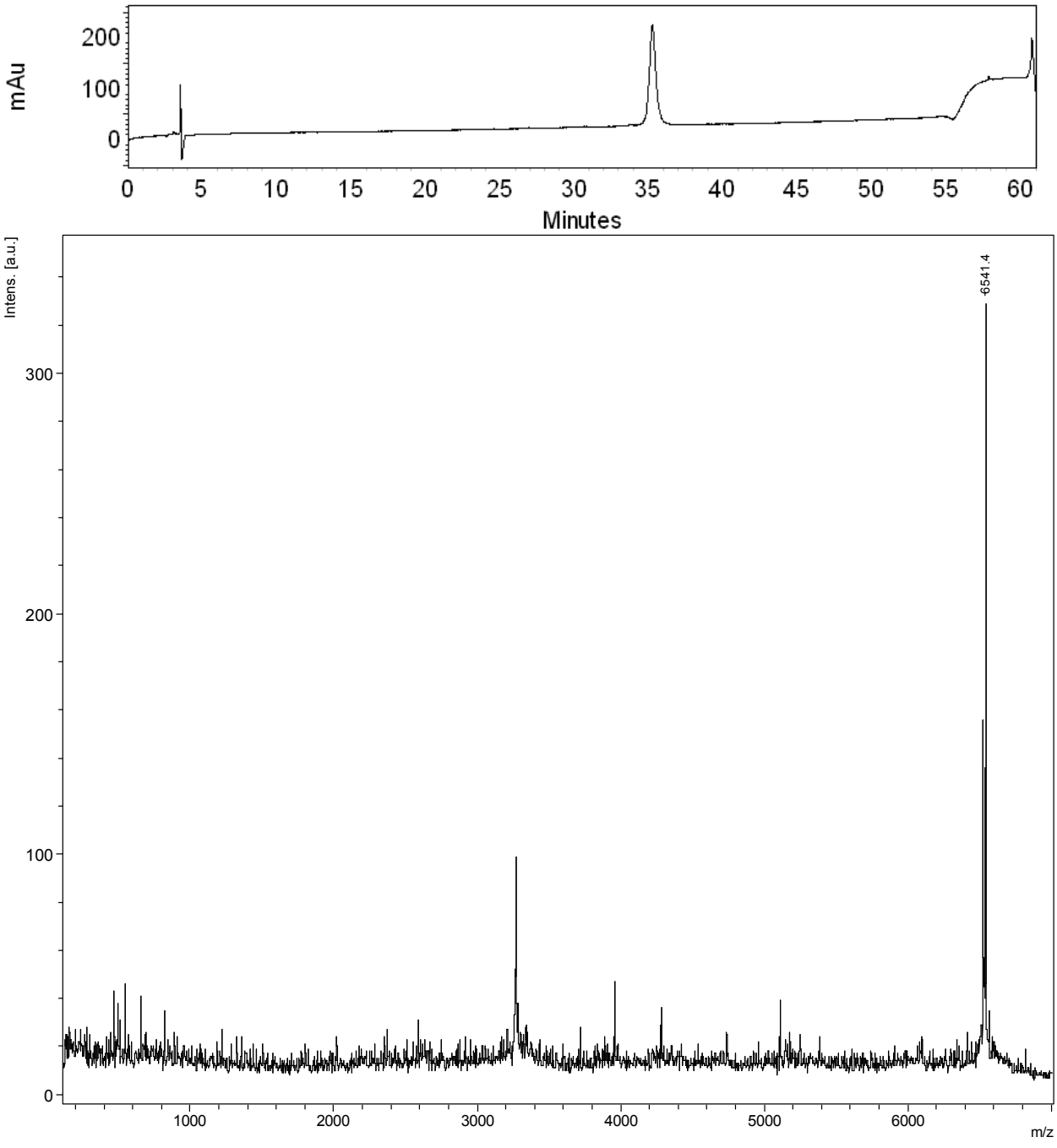

3.31

HPLC: Gradient = 10-60% solvent B over 50 minutes

MALDI-TOF: Calculated monoisotopic $[M+H]^+ = 4618.3$

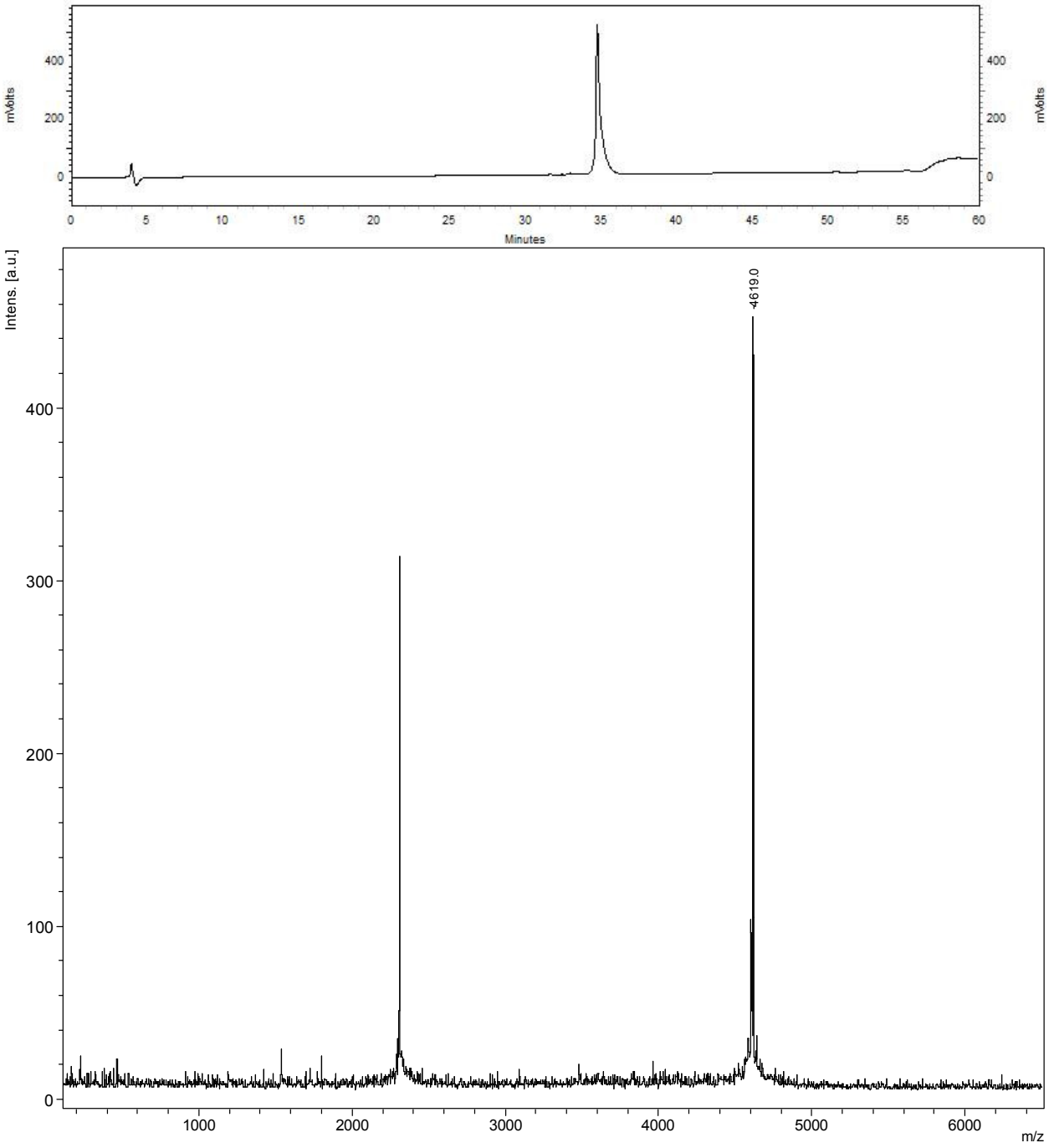

3.32

HPLC: Gradient = 10-60% solvent B over 50 minutes

MALDI-TOF: Calculated monoisotopic $[M+H]^+ = 4600.3$

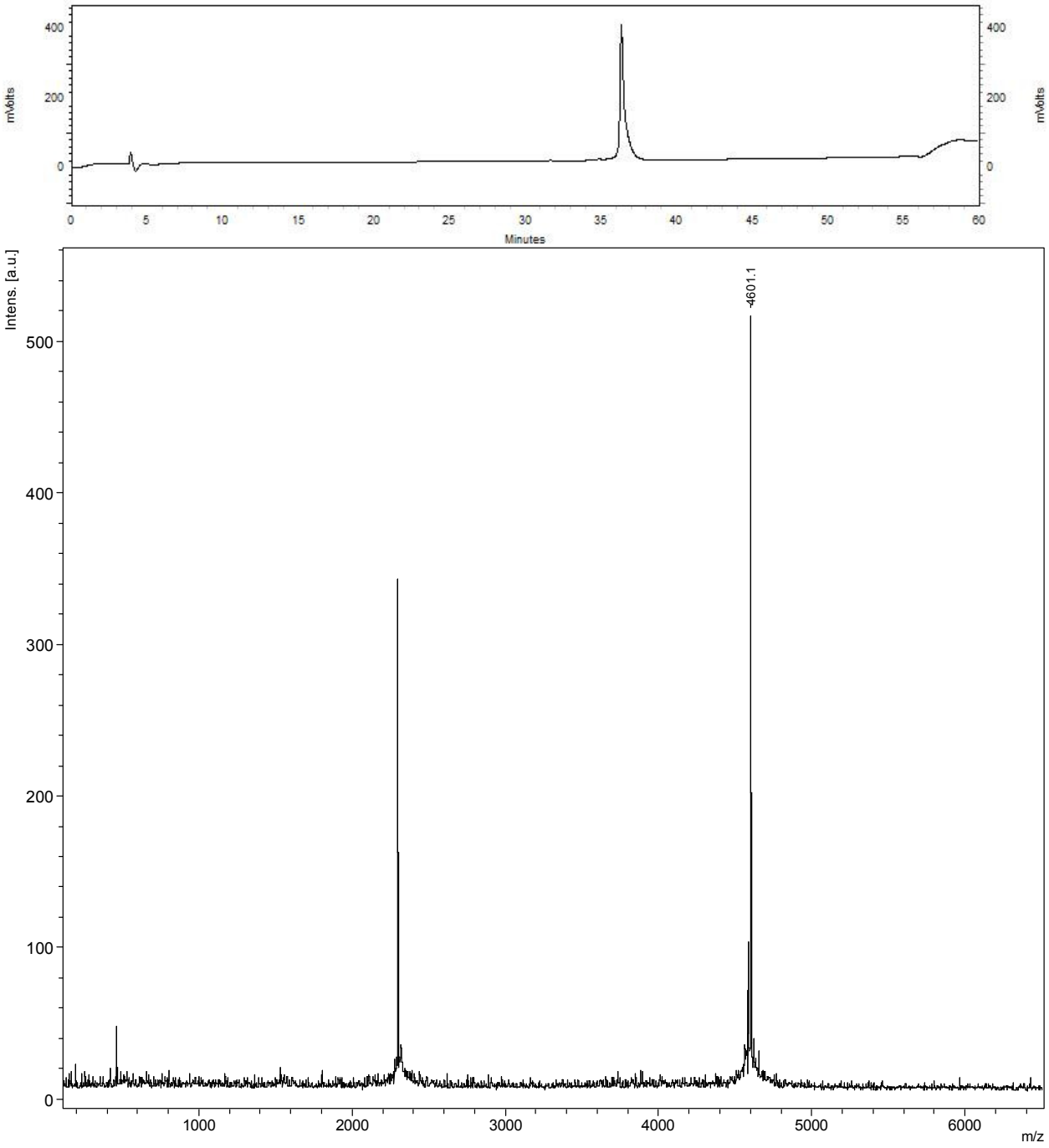

3.33

HPLC: Gradient = 10-60% solvent B over 50 minutes

MALDI-TOF: Calculated monoisotopic $[M+H]^+ = 4365.1$

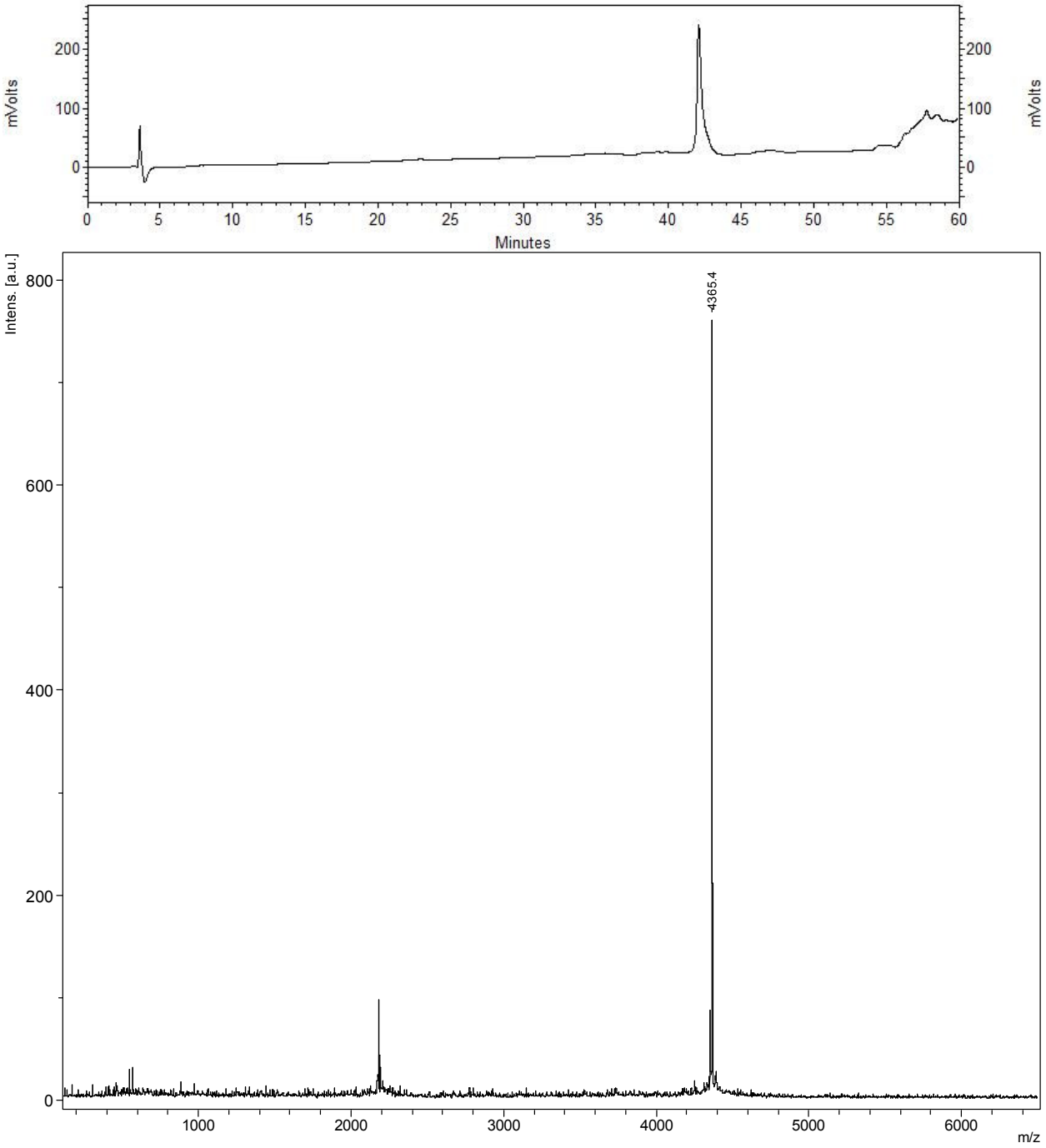

3.34

HPLC: Gradient = 10-60% solvent B over 50 minutes

MALDI-TOF: Calculated monoisotopic $[M+H]^+ = 4391.1$

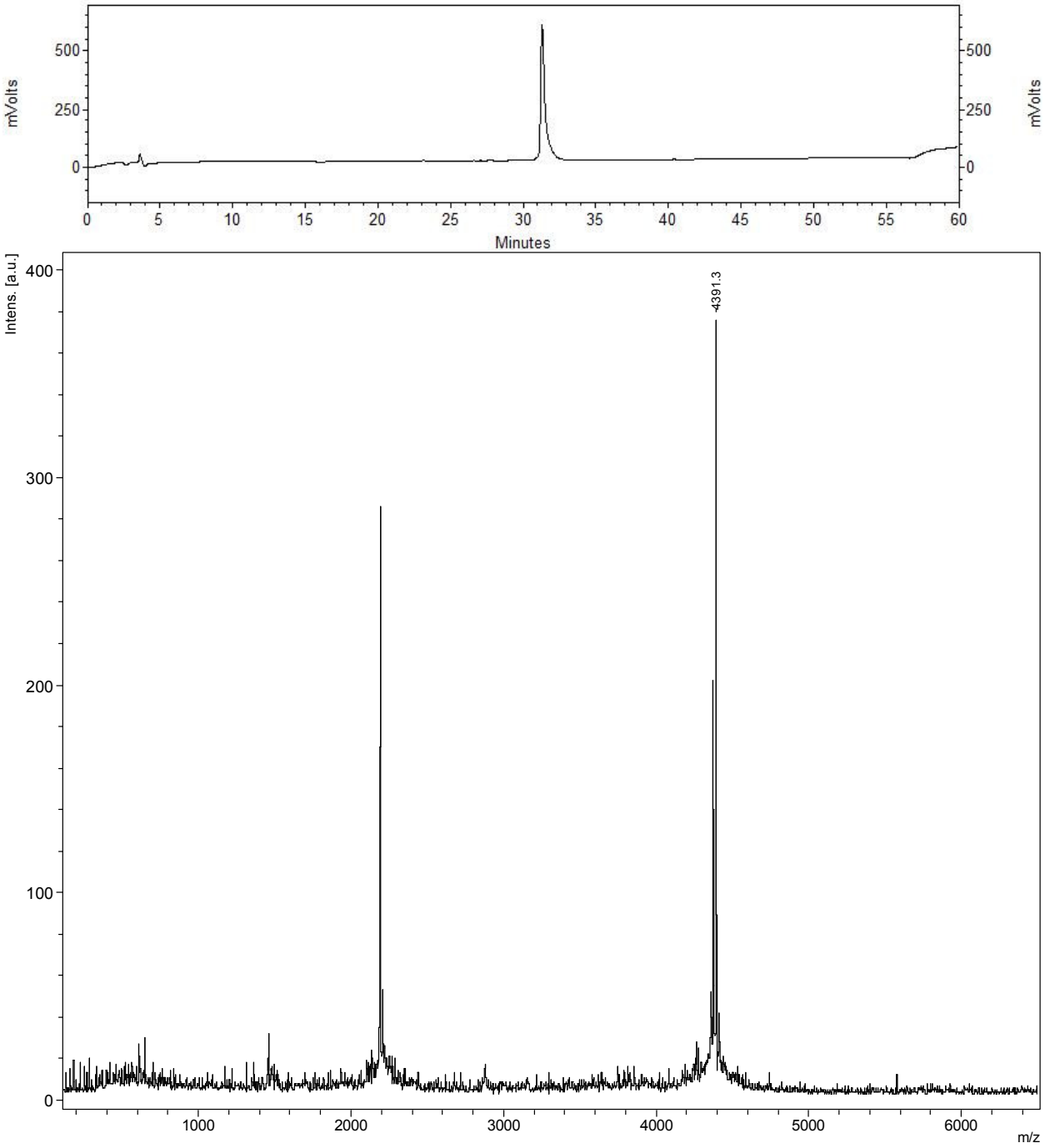

3.35

HPLC: Gradient = 10-75% solvent B over 65 minutes

MALDI-TOF: Calculated monoisotopic $[M+H]^+ = 4438.1$

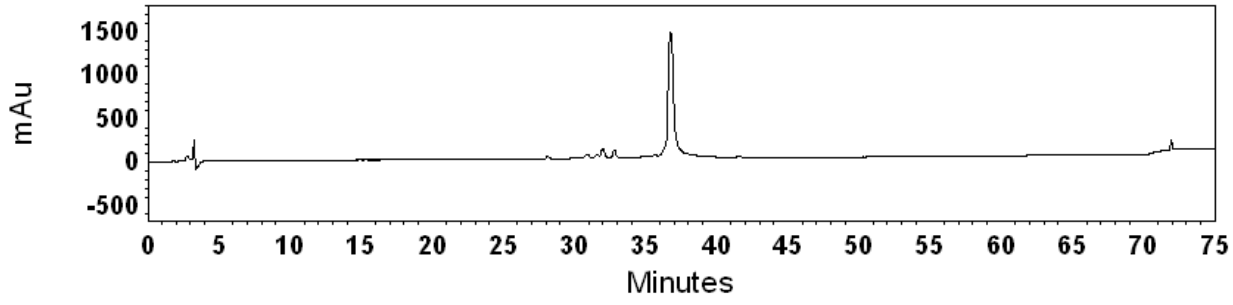

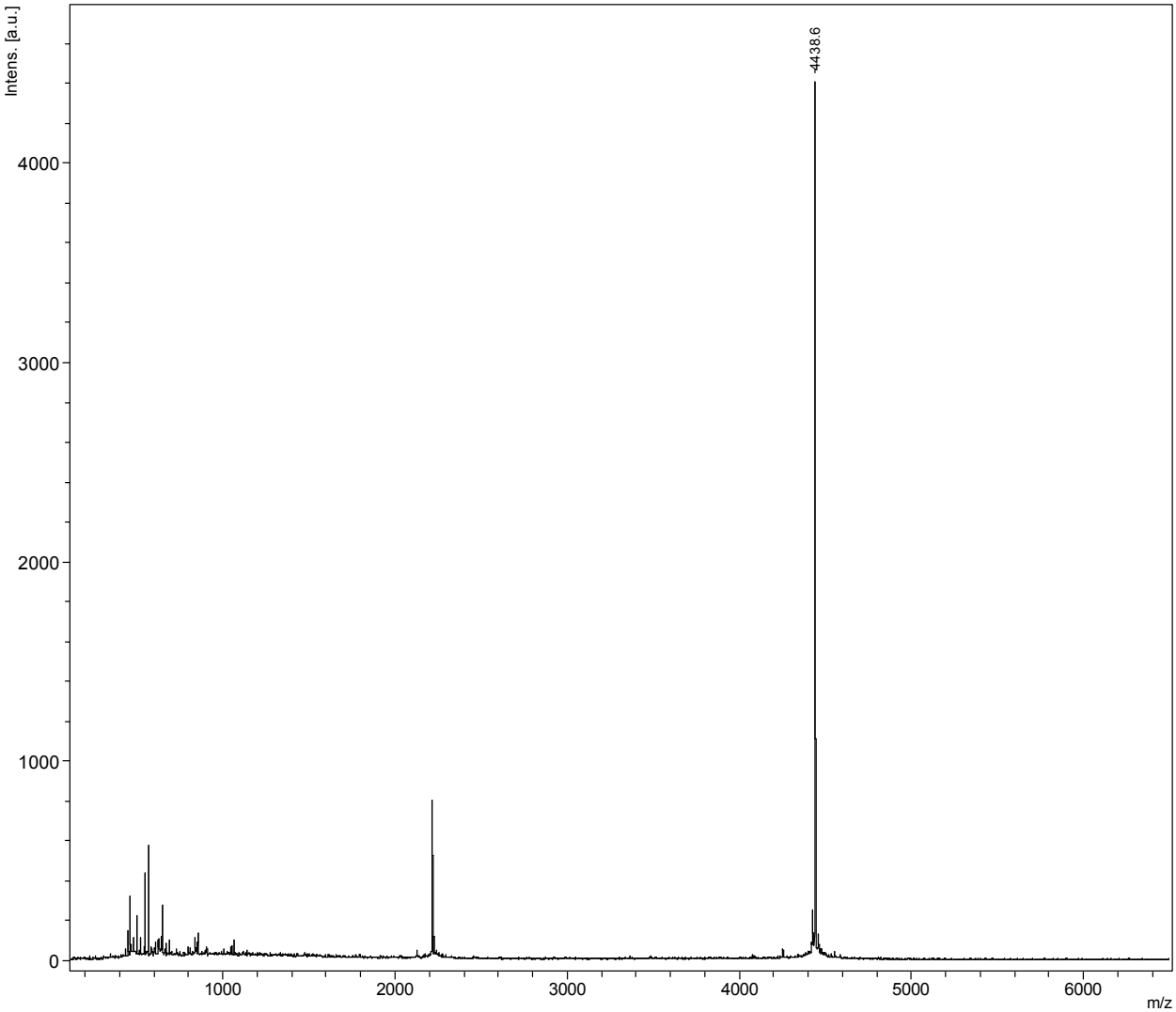

3.36

HPLC: Gradient = 10-75% solvent B over 65 minutes

MALDI-TOF: Calculated monoisotopic $[M+H]^+ = 4464.1$

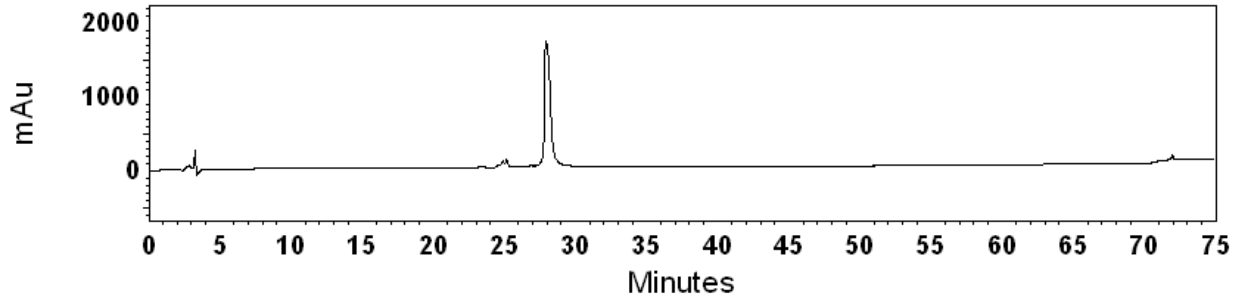

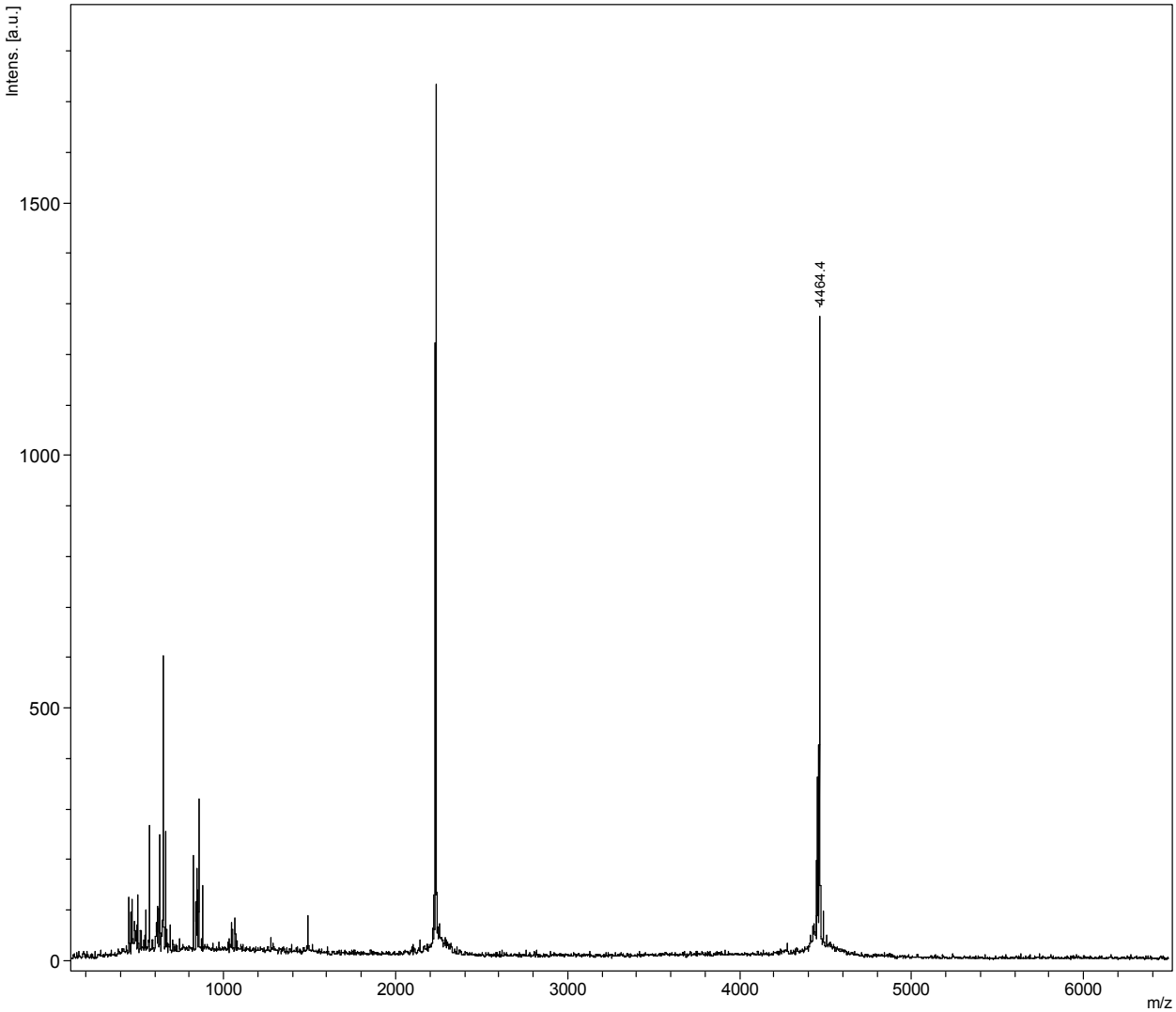

3.11 References

1. Wells, J. A., and McClendon, C. L. (2007) Reaching for high-hanging fruit in drug discovery at protein-protein interfaces, *Nature 450*, 1001-1009.
2. Arkin, M. R., Tang, Y. Y., and Wells, J. A. (2014) Small-Molecule Inhibitors of Protein-Protein Interactions: Progressing toward the Reality, *Chemistry & Biology 21*, 1102-1114.
3. Wilson, A. J. (2009) Inhibition of protein-protein interactions using designed molecules, *Chemical Society Reviews 38*, 3289-3300.
4. Vlieghe, P., Lisowski, V., Martinez, J., and Khrestchatisky, M. (2010) Synthetic therapeutic peptides: science and market, *Drug Discovery Today 15*, 40-56.
5. Binz, H. K., Amstutz, P., and Pluckthun, A. (2005) Engineering novel binding proteins from nonimmunoglobulin domains, *Nature Biotechnology 23*, 1257-1268.
6. Gronwall, C., and Stahl, S. (2009) Engineered affinity proteins-Generation and applications, *Journal of Biotechnology 140*, 254-269.
7. Lofblom, J., Feldwisch, J., Tolmachev, V., Carlsson, J., Stahl, S., and Frejd, F. Y. (2010) Affibody molecules: Engineered proteins for therapeutic, diagnostic and biotechnological applications, *Febs Letters 584*, 2670-2680.
8. Deisenhofer, J. (1981) Crystallographic refinement and atomic models of a human Fc fragment and its complex with fragment B of Protein A from Staphylococcus aureus at 2.9-A and 2.8-A resolution, *Biochemistry 20*, 2361-2370.
9. Deis, L. N., Wu, Q., Wang, Y., Qi, Y., Daniels, K. G., Zhou, P., and Oas, T. G. (2015) Suppression of conformational heterogeneity at a protein–protein interface, *Proceedings of the National Academy of Sciences of the United States of America 112*, 9028-9033.
10. Tashiro, M., Tejero, R., Zimmerman, D. E., Celda, B., Nilsson, B., and Montelione, G. T. (1997) High-resolution solution NMR structure of the Z domain of staphylococcal protein A, *Journal of Molecular Biology 272*, 573-590.
11. Nilsson, B., Moks, T., Jansson, B., Abrahmsen, L., Elmblad, A., Holmgren, E., Henrichson, C., Jones, T. A., and Uhlen, M. (1987) A synthetic IgG-binding domain based on staphylococcal protein A, *Protein Engineering 1*, 107-113.
12. Gouda, H., Torigoe, H., Saito, A., Sato, M., Arata, Y., and Shimada, I. (1992) Three-dimensional solution structure of the B domain of Staphlyococcal Protein A: Comparisons of the solution and crystal structures, *Biochemistry 31*, 9665-9672.
13. Jendeberg, L., Tashiro, M., Tejero, R., Lyons, B. A., Uhlen, M., Montelione, G. T., and Nilsson, B. (1996) The mechanism of binding staphylococcal protein A to immunoglobin G does not involve helix unwinding, *Biochemistry 35*, 22-31.
14. Cedergren, L., Andersson, R., Jansson, B., Uhlen, M., and Nilsson, B. (1993) Mutational analysis of the interaction between staphylococcal protein A and human IgG1, *Protein Engineering 6*, 441-448.

15. Nord, K., Nilsson, J., Nilsson, B., Uhlen, M., and Nygren, P. A. (1995) A combinatorial library of an alpha-helical bacterial receptor domain, *Protein Engineering 8*, 601-608.

16. Nord, K., Gunneriusson, E., Ringdahl, J., Stahl, S., Uhlen, M., and Nygren, P. A. (1997) Binding proteins selected from combinatorial libraries of an alpha-helical bacterial receptor domain, *Nature Biotechnology 15*, 772-777.

17. Fedorova, A., Zobel, K., Gill, H. S., Ogasawara, A., Flores, J. E., Tinianow, J. N., Vanderbilt, A. N., Wu, P., Meng, Y. G., Williams, S. P., Wiesmann, C., Murray, J., Marik, J., and Deshayes, K. (2011) The Development of Peptide-Based Tools for the Analysis of Angiogenesis, *Chemistry & Biology 18*, 839-845.

18. Fleetwood, F., Klint, S., Hanze, M., Gunneriusson, E., Frejd, F. Y., Stah, S., and Lofblom, J. (2014) Simultaneous targeting of two ligand-binding sites on VEGFR2 using biparatopic Affibody molecules results in dramatically improved affinity, *Scientific Reports 4*, 7518.

19. Jonsson, A., Wallberg, H., Herne, N., Stahl, S., and Frejd, F. Y. (2009) Generation of tumour-necrosis-factor-alpha-specific affibody molecules capable of blocking receptor binding in vitro, *Biotechnology and Applied Biochemistry 54*, 93-103.

20. Kronqvist, N., Lofblom, J., Jonsson, A., Wernerus, H., and Stahl, S. (2008) A novel affinity protein selection system based on staphylococcal cell surface display and flow cytometry, *Protein Engineering Design & Selection 21*, 247-255.

21. Lofdahl, P. A., Nord, O., Janzon, L., and Nygren, P. A. (2009) Selection of TNF-alpha binding affibody molecules using a beta-lactamase protein fragment complementation assay, *New Biotechnology 26*, 251-259.

22. Lofdahl, P. A., and Nygren, P. A. (2010) Affinity maturation of a TNF alpha-binding Affibody molecule by Darwinian survival selection, *Biotechnology and Applied Biochemistry 55*, 111-120.

23. Orlova, A., Magnusson, M., Eriksson, T. L. J., Nilsson, M., Larsson, B., Hoiden-Guthenherg, I., Widstrom, C., Carlsson, J., Tolmachev, V., Stahl, S., and Nilsson, F. Y. (2006) Tumor Imaging using a picomolar affinity HER2 binding affibody molecule, *Cancer Research 66*, 4339-4348.

24. Wikman, M., Steffen, A. C., Gunneriusson, E., Tolmachev, V., Adams, G. P., Carlsson, J., and Stahl, S. (2004) Selection and characterization of HER2/neu-binding affibody ligands, *Protein Engineering Design & Selection 17*, 455-462.

25. Friedman, M., Nordberg, E., Hoiden-Guthenberg, I., Brisimar, H., Adams, G. P., Nilsson, F. Y., Carlss, J., and Stahl, S. (2007) Phage display selection of Affibody molecules with specific binding to the extracellular domain of the epidermal growth factor receptor, *Protein Engineering Design & Selection 20*, 189-199.

26. Friedman, M., Orlova, A., Johansson, E., Eriksson, T. L. J., Hoiden-Guthenberg, I., Tolmachev, V., Nilsson, F. Y., and Stahl, S. (2008) Directed evolution to low nanomolar affinity of a tumor-targeting epidermal growth factor receptor-binding affibody molecule, *Journal of Molecular Biology 376*, 1388-1402.

27. Lindborg, M., Cortez, E., Hoiden-Guthenberg, I., Gunneriusson, E., von Hage, E., Syud, F., Morrison, M., Abrahmsen, L., Herne, N., Pietras, K., and Frejd, F. Y. (2011) Engineered High-Affinity Affibody Molecules Targeting Platelet-Derived Growth Factor Receptor beta In Vivo, *Journal of Molecular Biology 407*, 298-315.

28. Gronwall, C., Snelders, E., Palm, A. J., Eriksson, F., Herne, N., and Stahl, S. (2008) Generation of Affibody (R) ligands binding interieukin-2 receptor alpha/CD25, *Biotechnology and Applied Biochemistry 50*, 97-112.

29. Sandstrom, K., Xu, Z., Forsberg, G., and Nygren, P. A. (2003) Inhibition of the CD28-CD80 co-stimulation signal by a CD28-binding affibody ligand developed by combinatorial protein engineering, *Protein Engineering 16*, 691-697.

30. Ronnmark, J., Gronlund, H., Uhlen, M., and Nygren, P. A. (2002) Human immunoglobulin A (IgA)-specific ligands from combinatorial engineering of protein A, *European Journal of Biochemistry 269*, 2647-2655.

31. Skerra, A. (2007) Alternative non-antibody scaffolds for molecular recognition, *Current Opinion in Biotechnology 18*, 295-304.

32. Baum, R. P., Prasad, V., Muller, D., Schuchardt, C., Orlova, A., Wennborg, A., Tolmachev, V., and Feldwisch, J. (2010) Molecular Imaging of HER2-Expressing Malignant Tumors in Breast Cancer Patients Using Synthetic In-111- or Ga-68-Labeled Affibody Molecules, *Journal of Nuclear Medicine 51*, 892-897.

33. Sorensen, J., Sandberg, D., Sandstrom, M., Wennborg, A., Feldwisch, J., Tolmachev, V., Astrom, G., Lubberink, M., Garske-Roman, U., Carlsson, J., and Lindman, H. (2014) First-in-Human Molecular Imaging of HER2 Expression in Breast Cancer Metastases Using the In-111-ABY-025 Affibody Molecule, *Journal of Nuclear Medicine 55*, 730-735.

34. Eigenbrot, C., Ultsch, M., Dubnovitsky, A., Abrahmsen, L., and Hard, T. (2010) Structural basis for high-affinity HER2 receptor binding by an engineered protein, *Proceedings of the National Academy of Sciences of the United States of America 107*, 15039-15044.

35. Braisted, A. C., and Wells, J. A. (1996) Minimizing a binding domain from protein A, *Proceedings of the National Academy of Sciences of the United States of America 93*, 5688-5692.

36. Webster, J. M., Zhang, R., Gambhir, S. S., Cheng, Z., and Syud, F. A. (2009) Engineered Two-Helix Small Proteins for Molecular Recognition, *Chembiochem 10*, 1293-1296.

37. Starovasnik, M. A., Braisted, A. C., and Wells, J. A. (1997) Structural mimicry of a native protein by a minimized binding domain, *Proceedings of the National Academy of Sciences of the United States of America 94*, 10080-10085.

38. Burlingham, B. T., and Widlanski, T. S. (2003) An intuitive look at the relationship of K-i and IC50: A more general use for the Dixon plot, *Journal of Chemical Education 80*, 214-218.

39. Pollaro, L., and Heinis, C. (2010) Strategies to prolong the plasma residence time of peptide drugs, *Medchemcomm 1*, 319-324.

40. Lin, J. H. (2009) Pharmacokinetics of Biotech Drugs: Peptides, Proteins and Monoclonal Antibodies, *Current Drug Metabolism 10*, 661-691.

41. Yu, F. F., Jarver, P., and Nygren, P. A. (2013) Tailor-Making a Protein A-Derived Domain for Efficient Site-Specific Photocoupling to Fc of Mouse IgG(1), *Plos One 8*, e56597.

42. Jonsson, A., Dogan, J., Herne, N., Abrahmsen, L., and Nygren, P. A. (2008) Engineering of a femtomolar affinity binding protein to human serum albumin, *Protein Engineering Design & Selection 21*, 515-527.

43. Tolmachev, V., Orlova, A., Pehrson, R., Galli, J., Baastrup, B., Andersson, K., Sandstrom, M., Rosik, D., Carlsson, J., Lundqvist, H., Wennborg, A., and Nilsson, F. Y. (2007) Radionuclide therapy of HER2-positive microxenografts using a Lu-177-labeled HER2-specific affibody molecule, *Cancer Research 67*, 2773-2782.

44. Orlova, A., Jonsson, A., Rosik, D., Lundqvist, H., Lindborg, M., Abrahmsen, L., Ekblad, C., Frejd, F. Y., and Tolmachev, V. (2013) Site-Specific Radiometal Labeling and Improved Biodistribution Using ABY-027, A Novel HER2-Targeting Affibody Molecule-Albumin-Binding Domain Fusion Protein, *Journal of Nuclear Medicine 54*, 961-968.

45. Locksley, R. M., Killeen, N., and Lenardo, M. J. (2001) The TNF and TNF receptor superfamilies: Integrating mammalian biology, *Cell 104*, 487-501.

46. Palladino, M. A., Bahjat, F. R., Theodorakis, E. A., and Moldawer, L. L. (2003) Anti-TNF-alpha therapies: The next generation, *Nature Reviews Drug Discovery 2*, 736-746.

47. Slamon, D. J., Clark, G. M., Wong, S. G., Levin, W. J., Ullrich, A., and McGuire, W. L. (1987) Human breast cancer: correlation of relapse and survival with amplification fo the HER-2/neu oncogene, *Science 235*, 177-182.

48. Slamon, D. J., Godolphin, W., Jones, L. A., Holt, J. A., Wong, S. G., Keith, D. E., Levin, W. J., Stuart, S. G., Udove, J., Ullrich, A., and Press, M. F. (1989) Studies of the HER-2/neu proto-oncogene in human breast and ovarian cancer, *Science 244*, 707-712.

49. Mendelsohn, J., and Baselga, J. (2000) The EGF receptor family as targets for cancer therapy, *Oncogene 19*, 6550-6565.

50. Hudziak, R. M., Lewis, G. D., Winget, M., Fendly, B. M., Shepard, H. M., and Ullrich, A. (1989) P185HER2 monoclonal antibody has antiproliferative effects in vitro and sensitizes human breast tumor cells to tumor necrosis factor, *Molecular and Cellular Biology 9*, 1165-1172.

51. Carter, P., Presta, L., Gorman, C. M., Ridgway, J. B. B., Henner, D., Wong, W. L. T., Rowland, A. M., Kotts, C., Carver, M. E., and Shepard, H. M. (1992) Humanization of an anti-P185HER2 antibody for human cancer therapy, *Proceedings of the National Academy of Sciences of the United States of America 89*, 4285-4289.

52. Slamon, D. J., Leyland-Jones, B., Shak, S., Fuchs, H., Paton, V., Bajamonde, A., Fleming, T., Eiermann, W., Wolter, J., Pegram, M., Baselga, J., and Norton, L. (2001) Use of chemotherapy plus a monoclonal antibody against HER2 for metastatic breast cancer that overexpresses HER2, *New England Journal of Medicine 344*, 783-792.

53. Ren, G., Zhang, R., Liu, Z., Webster, J. M., Miao, Z., Gambhir, S. S., Syud, F. A., and Cheng, Z. (2009) A 2-Helix Small Protein Labeled with Ga-68 for PET Imaging of HER2 Expression, *Journal of Nuclear Medicine 50*, 1492-1499.

54. Schmidt, M. M., and Wittrup, K. D. (2009) A modeling analysis of the effects of molecular size and binding affinity on tumor targeting, *Molecular Cancer Therapeutics 8*, 2861-2871.

55. Ren, G., Webster, J. M., Liu, Z., Zhang, R., Miao, Z., Liu, H. G., Gambhir, S. S., Syud, F. A., and Cheng, Z. (2012) In vivo targeting of HER2-positive tumor using 2-helix affibody molecules, *Amino Acids 43*, 405-413.

56. Orlova, A., Tolmachev, V., Pehrson, R., Lindborg, M., Tran, T., Sandstrom, M., Nilsson, F. Y., Wennborg, A., Abrahmsen, L., and Feldwisch, J. (2007) Synthetic affibody molecules: A novel class of affinity ligands for molecular imaging of HER2-expressing malignant tumors, *Cancer Research 67*, 2178-2186.

57. Johnson, L. M., and Gellman, S. H. (2013) alpha-Helix Mimicry with alpha/beta-Peptides, *Methods in Protein Design 523*, 407-429.

58. Horne, W. S., Johnson, L. M., Ketas, T. J., Klasse, P. J., Lu, M., Moore, J. P., and Gellman, S. H. (2009) Structural and biological mimicry of protein surface recognition by alpha/beta-peptide foldamers, *Proceedings of the National Academy of Sciences of the United States of America 106*, 14751-14756.

59. Lee, H. S., LePlae, P. R., Porter, E. A., and Gellman, S. H. (2001) An efficient route to either enantiomer of orthogonally protected trans-3-aminopyrrolidine-4-carboxylic acid, *Journal of Organic Chemistry 66*, 3597-3599.

60. Kabsch, W. (2010) XDS, *Acta Crystallographica Section D-Biological Crystallography 66*, 125-132.

61. McCoy, A. J., Grosse-Kunstleve, R. W., Adams, P. D., Winn, M. D., Storoni, L. C., and Read, R. J. (2007) Phaser crystallographic software, *Journal of Applied Crystallography 40*, 658-674.

62. Adams, P. D., Grosse-Kunstleve, R. W., Hung, L. W., Ioerger, T. R., McCoy, A. J., Moriarty, N. W., Read, R. J., Sacchettini, J. C., Sauter, N. K., and Terwilliger, T. C. (2002) PHENIX: building new software for automated crystallographic structure determination, *Acta Crystallographica Section D-Biological Crystallography 58*, 1948-1954.

63. Gill, S. C., and Vonhippel, P. H. (1989) Calculation of protein extinction coefficients from amino-acid sequence data, *Analytical Biochemistry 182*, 319-326.

64. Greenfield, N. J. (2006) Using circular dichroism spectra to estimate protein secondary structure, *Nature Protocols 1*, 2876-2890.

Chapter 4: Optimization and mechanistic evaluation of α- and α/β-peptide tumor necrosis factor-α antagonists

Respective contributions:

Research design: James W. Checco, Nicholas J. Rettko, Samuel H. Gellman

Peptide design: James W. Checco, Nicholas J. Rettko, Alexander R. Chartier

Peptide synthesis: James W. Checco, Nicholas J. Rettko, Geoffrey A. Eddinger, Alexander R. Chartier, Mahmoud Matar (REU student)

ELISA experiments: James W. Checco, Nicholas J. Rettko, Alexander R. Chartier, Geoffrey A. Eddinger

Proteolysis: Geoffrey A. Eddinger

Circular dichroism: James W. Checco

Cell viability assays: James W. Checco

Size-exclusion chromatography: James W. Checco

4.1 Preface

Misregulated signaling of tumor necrosis factor-α (TNFα) plays a key role in many prominent inflammatory and autoimmune disorders, and antagonists of the interaction of TNFα and its receptors are valuable compounds for the treatment of these diseases. In Chapter 3, I described the design of α/β-peptides, derived from the Z-domain α-peptide **Z-TNFα**, which blocked the TNFα-TNFR interaction in protein binding experiments. The primary goals for the research described in this chapter were to optimize these TNFα-binding α/β-peptides for eventual application *in vivo*, and to evaluate their ability to antagonize TNFα signaling in cell culture.

We evaluated the affinity and protease susceptibility of a number of α/β-peptide analogues of **Z-TNFα** and identified optimized variants that were less than half the size of **Z-TNFα**, which may offer advantages in synthetic accessibility and tissue permeability, yet were over 150-fold more stable to protease action than this full-length α-peptide parent. The improved protease stability may give these α/β-peptides advantages for *in vivo* applications over their α-peptide counterparts. During experiments to evaluate the ability of our α/β-peptides to antagonize TNFα signaling in cell culture, we unexpectedly discovered that **Z-TNFα**, along with its α/β-peptide analogues, are dependent on a detergent used during the phage display/selection process for binding to TNFα. Follow-up experiments suggest a mechanism in which **Z-TNFα** binds TNFα at a site exposed only in the presence of detergent (or certain other small molecules) and dissociates the active trimer to block binding to the receptor. These efforts reveal a possible novel mechanism for targeting TNFα signaling for the treatment of a variety of diseases.

4.2 Introduction

4.2.1 Tumor necrosis factor-α (TNFα) signaling

Tumor necrosis factor-α (TNFα) is a cytokine that serves a variety of different functions for many cell types, including playing a critical role in the inflammatory response, regulating immune functions, and inducing apoptosis.[1-4] Misregulated TNFα signaling is associated with a variety of diseases, such as rheumatoid arthritis and inflammatory bowel disease. Because of the role of TNFα in these diseases, antagonists of the interaction of TNFα with its receptors (TNFRs) can be used for therapeutic treatment.[4, 5] Thus, it is of great interest to human health to identify molecules that can inhibit TNFα signaling.

TNFα is initially expressed in an extended, membrane-bound form that is enzymatically cleaved to yield a soluble 17 kDa TNFα protein.[1, 4] Three soluble TNFα monomers readily associate into a stable, non-covalent trimer in solution, which presents three equivalent receptor binding surfaces at each monomer-monomer interface (Figure 4.1).[6-9] The TNFα trimer can then bind to three molecules of membrane-bound receptor (TNFR1 or TNFR2), on the surface of most cell types, to initiate subsequent intracellular signaling (Figure 4.1C). A variety of disparate cellular responses (e.g., apoptosis, gene transcription) can occur as a result of these signaling events, and the ultimate response is dependent on many complex factors.[4] In cell culture, the addition of exogenous TNFα initiates apoptosis in many cell types, and antagonism of TNFα can rescue cells from this TNFα-mediated death, which provides a basis for evaluating potential TNFα inhibitors.[6, 10-12]

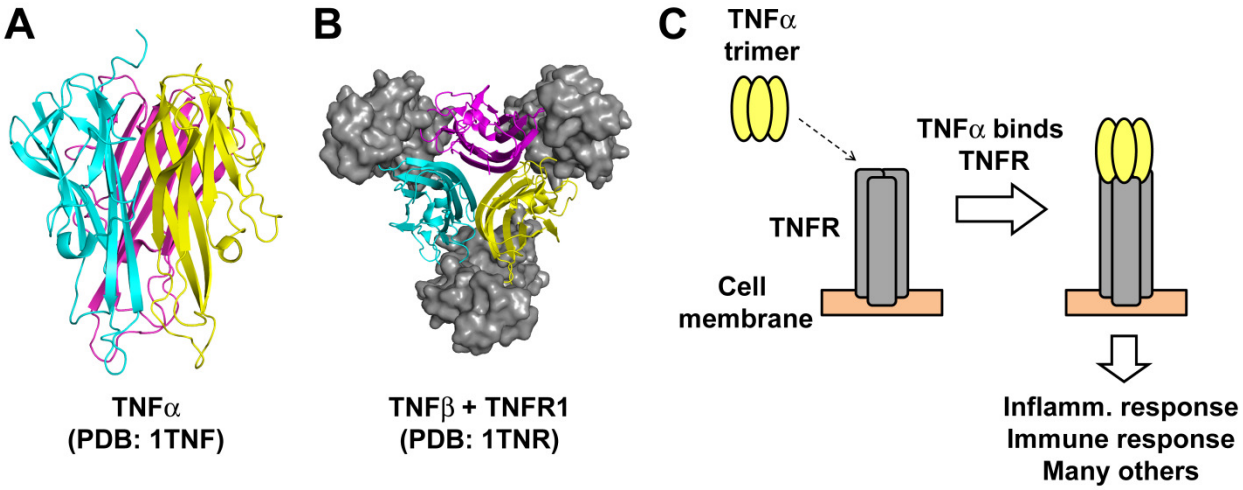

Figure 4.1 TNFα is a homotrimeric cytokine that signals through TNFRs. (A) Crystal structure of trimeric TNFα, with each monomer chain colored in yellow, cyan, and magenta (PDB: 1TNF).[8] (B) Crystal structure of tumor necrosis factor-β (TNFβ, monomers colored as in panel A), which is structurally similar to TNFα, in complex with soluble TNFR1 extracellular domain (gray). The receptor binding sites are located at each monomer-monomer interface (PDB: 1TNR).[9] (C) Cartoon depiction of TNFα signaling through TNFRs. Trimeric TNFα binds to trimeric receptor molecules (TNFR1 or TNFR2) to induce a variety of intracellular responses, including inflammatory and immune responses.

4.2.2 Antagonists of the TNFα-TNFR interaction

TNFα is an important target for the treatment of a variety of illnesses, and several anti-TNFα proteins are currently approved for therapeutic use, including etanercept (Enbrel, soluble TNFR2-Fc fusion protein), infliximab (Remicade, anti-TNFα antibody), and adalimumab (Humira, anti-TNFα antibody).[4, 5] These proteins bind TNFα at or near the receptor-binding site, which inhibits the active trimer from binding to the receptor to initiate signaling.[13]

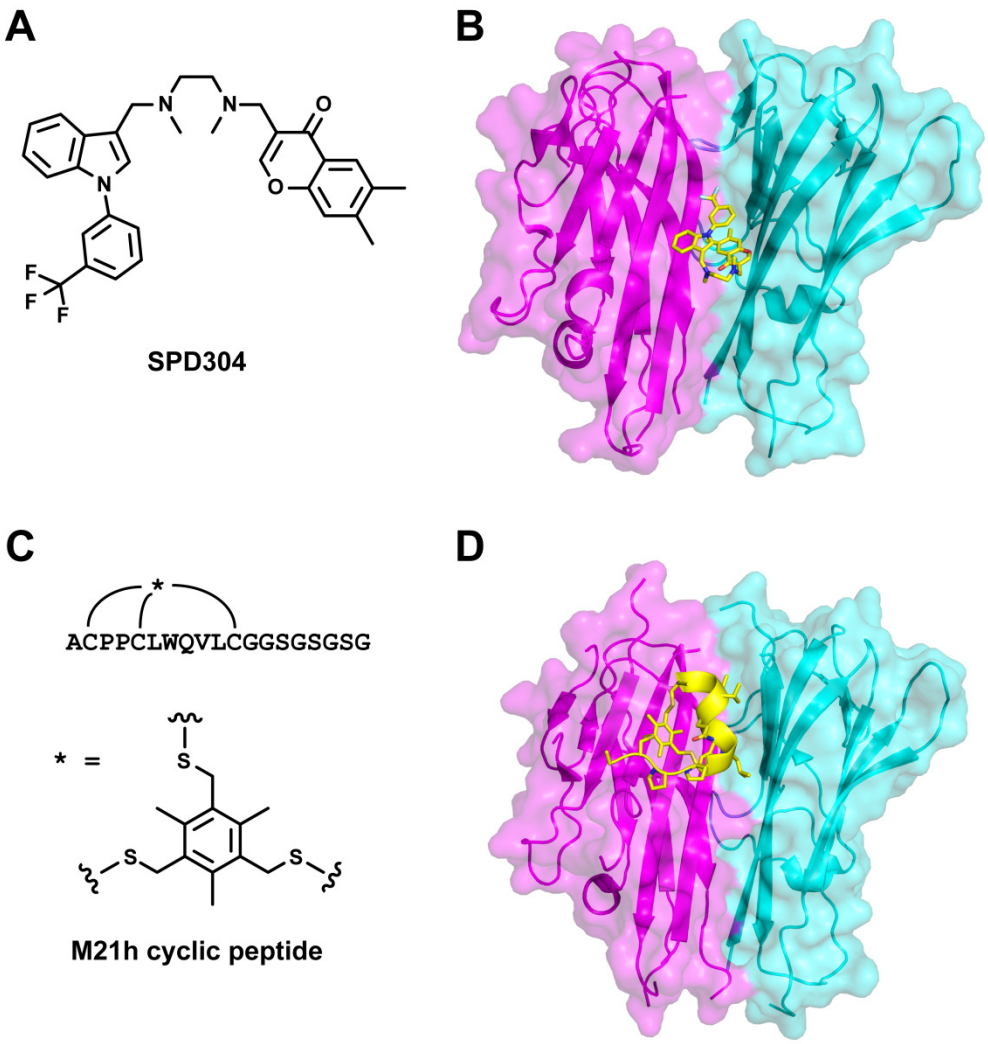

Figure 4.2 A small number of TNFα antagonists act by dissociating the active TNFα trimer. (A) SPD304 is a small molecule inhibitor of TNFα. (B) A crystal structure of SPD304 in complex with TNFα reveals that this small molecule (shown in yellow sticks) binds to dimeric TNFα (monomers shown in cyan and magenta) at the oligomerization interface, which dissociates the active trimer (PDB: 2AZ5).[14] (C) M21h (one-letter code sequence depicted) is a small peptide cyclized through a 2,4,6-trimethyl-mesitylene core (*). (D) A crystal structure of M21h (yellow cartoon and sticks) in complex with TNFα (monomers shown in cyan and magenta) reveals that this peptide binds to the TNFα dimer. M21h induces dissociation of the active TNFα trimer, consistent with this structure (PDB: 4TWT).[15]

In addition to large antibodies and receptor fragments, there are also several examples of smaller TNFα-binding molecules that antagonize TNFα signaling, including small peptides derived from TNFR1[12] and small cyclic peptides derived from combinatorial libraries built on small molecule scaffolds.[11, 15] Display and selection technologies have been used to develop TNFα-binding compounds derived from several mini-protein scaffolds, including the Z-domain

scaffold (**Z-TNFα**, described in Chapter 3),[16] the DARPin scaffold,[17] and the protein ubiquitin.[18] A small molecule, SPD304 (Figure 4.2A and B), has been reported to bind TNFα and block signaling.[14] Experiments investigating the interaction of SPD304 with TNFα revealed that this molecule blocks TNFα signaling by binding at TNFα's oligomerization interface and dissociating the active trimer. This unexpected mechanism for TNFα inhibition has since been shown to occur for several other molecules designed to bind TNFα, as revealed in oligomerization studies and co-crystal structures (Figure 4.2C and D).[15] Dissociation of the active TNFα trimer may represent an alternative strategy for blocking TNFα signaling *in vivo* that complements the traditional strategy of targeting the receptor-binding surface.

4.2.3 α/β-Peptides targeting TNFα

In Chapter 3, I described the design of α/β-peptides mimicking the three-helix Z-domain derivative **Z-TNFα**.[16] These two-helix α/β-peptides, **3.4** and **3.5**, mimicked **Z-TNFα**'s ability to block the TNFα-TNFR1 protein-protein interaction in enzyme-linked immunosorbent assay (ELISA) experiments, suggesting that these compounds may act as antagonists for TNFα-mediated signaling in cell culture or *in vivo*. In this chapter, I discuss the optimization of the sequences of **3.4** and **3.5** for applications in biological systems and their evaluation as antagonists of TNFα-mediated apoptosis in cell culture. Unexpectedly, we discovered that **Z-TNFα** and α/β-peptide analogues are dependent on the presence of the detergent TWEEN20 (used in both the phage display/selection process and in the competition ELISA experiments) for significant TNFα binding. Additional experiments using size exclusion chromatography and with a small molecule TNFα inhibitor strongly suggest that **Z-TNFα** and its α/β-peptide analogues act through binding to TNFα at the oligomerization interface and dissociating the active trimer, and that this event is facilitated by the presence of the detergent TWEEN20. These efforts highlight a

very critical and unexpected consequence of developing affinity proteins to non-covalent protein oligomers using techniques such as phage display, but also suggest a possible novel mechanism for targeting TNFα signaling for the treatment of a variety of diseases.

4.2.4 A note on affinity measurements

In Chapter 3, I reported TNFα-TNFR1 competition ELISA IC_{50} values for **Z-TNFα** (4.8 nM), **3.4** (30 nM), and **3.5** (6.6 nM), which are based on a representative competition ELISA experiment depicted in that chapter comparing these three compounds directly. These values are published in a report describing these compounds.[19] In this chapter, which serves as a follow-up to the preliminary work on TNFα-targeting α/β-peptides, I report IC_{50} values that are the average of at least two independent ELISA experiments. The IC_{50} values reported in this chapter for **Z-TNFα** (4.9 nM), **3.4** (28 nM), and **3.5** (5.1 nM) differ very slightly from those in the previous chapter. Figure 4.24 and Table 4.1 in "Experimental Methods" show data for each compound.

To determine the uncertainty in the ELISA measurements, we compared the lowest IC_{50} value obtained to the highest IC_{50} value obtained in independent experiments for each compound. The range of differences between these two values varied from ~1.1 to ~7.1-fold change, with an average variation of ~1.8-fold between the lowest and highest IC_{50} value obtained in the experiments reported. (This value excludes very weak binders with average IC_{50} values >10,000 nM, since these tend to vary widely in their calculated IC_{50} values due to too few points at the "bottom" of the competition curves). Based on this, we conclude that for most compounds with IC_{50} values <10,000 nM, the uncertainty in the calculated IC_{50} values is ~2-fold, with a maximum variation of up to ~7-fold for some experiments.

4.3 Optimization of α/β-peptides derived from Z-TNFα

4.3.1 Initial optimization attempts

α/β-Peptide **3.5** (described in Chapter 3) blocked the TNFα-TNFR1 interaction in a competition ELISA experiment with an IC_{50} value of 5.1 nM (Figure 4.3). This value is essentially identical to the IC_{50} value for the full-length **Z-TNFα** (4.9 nM), which suggests that the α/β-peptide **3.5** is a good functional mimic of **Z-TNFα** and binds to TNFα with nearly the same affinity. Here, we aimed to explore analogues of **3.4** and **3.5** that may be better suited for eventual applications in biological systems. To this end, the primary goal for the work described in this section was to design α/β-peptides that retained high affinity for TNFα (as judged by TNFα-TNFR1 competition ELISA), yet had additional benefits such as sequence length or no disulfide bond (both of which would provide higher synthetic accessibility) or increased protease stability. This work was done in collaboration with undergraduates Nicholas Rettko and Alexander Chartier (Gellman Laboratory, University of Wisconsin-Madison).

We began by synthesizing the two-helix α-peptides **4.1** and **4.2** to evaluate the effect of the disulfide constraint in the context of a natural α-peptide backbone (Figure 4.3). α-Peptide **4.1** corresponds to residues 1-38 of **Z-TNFα** and contains five α-residue substitutions (Ala12→Arg, Ile16→Ala, Leu19→Asp, Phe30→Lys, and Leu34→Ile)[20, 21] designed to stabilize the resulting helix-loop-helix structure in the absence of helix 3. We found that **4.1** blocked the TNFα-TNFR1 interaction, as judged by competition ELISA, with an IC_{50} value of 890 nM. This value represents an ~180-fold decrease in affinity for TNFα relative to the three-helix **Z-TNFα**. This result is consistent with the loss of affinity seen for two-helix α-peptide analogues of Z-domain peptides in the absence of helix 3.[20-22] However, this finding contrasts with the results from the

Z-VEGF family (described in Chapter 2), in which no two-helix analogue of **Z-VEGF** lacking an internal disulfide bound $VEGF_{165}$.

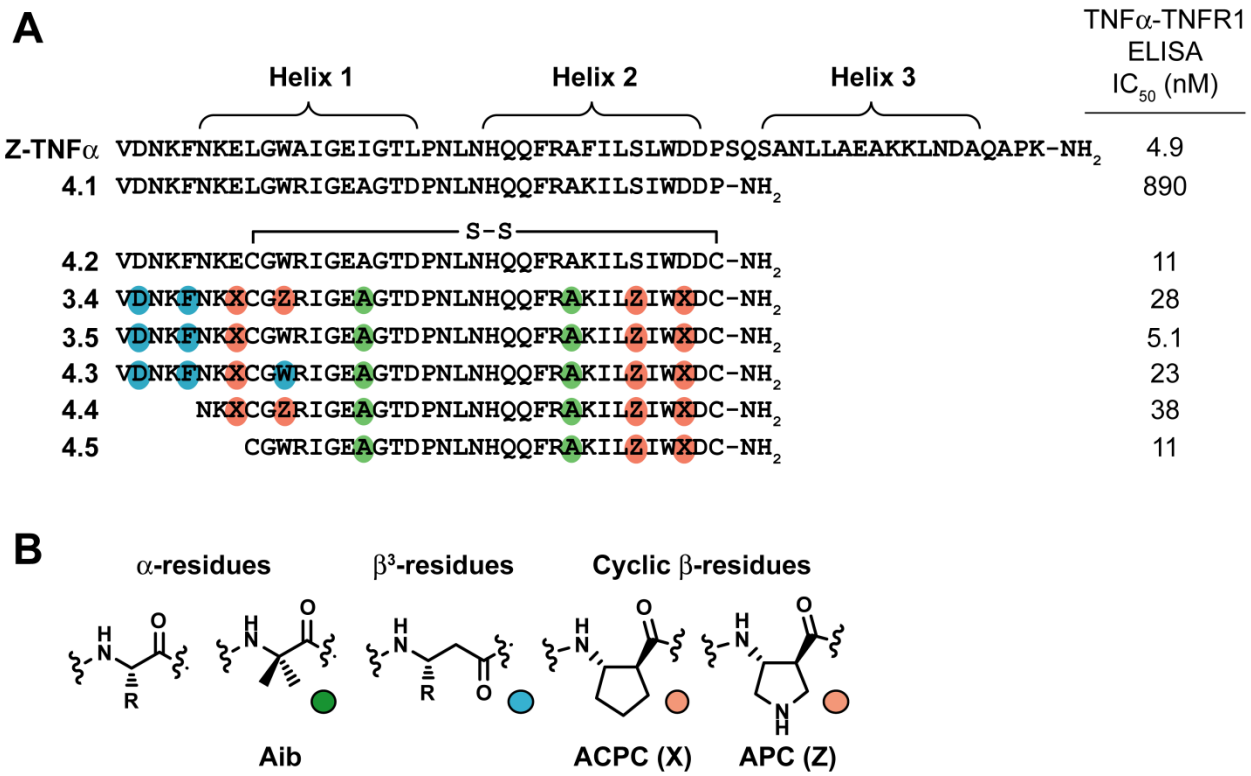

Figure 4.3 (A) Primary sequences of three-helix α-peptide **Z-TNFα** and two-helix α- and α/β-peptide derivatives, along with associated IC_{50} values, as determined by TNFα-TNFR1 competition ELISA. The uncertainty in the calculated IC_{50} values is ~2-fold, with a maximum variation of up to ~7-fold for some experiments. α/β-Peptide **3.4** and **3.5** were introduced in Chapter 3. Hypothesized positions of helices 1, 2, and 3 are indicated by brackets. Non-natural residues are indicated by colored circles. Each cysteine is engaged in an intramolecular disulfide bond. (B) Structures of a generic α-residue, the Aib residue (green), a generic β^3-residue (teal), and the cyclic β-residues ACPC (X) and APC (Z) (orange).

The α-peptide **4.2** is the analogue of **4.1** that contains a disulfide bond at positions 9 and 38, the same positions found in **3.4** and **3.5**. We found that α-peptide **4.2** disrupted the TNFα-TNFR1 interaction with an IC_{50} value of 11 nM. The lower IC_{50} value for **4.2** versus **4.1** indicates that the disulfide bond increases the affinity of the peptide for TNFα, presumably by stabilizing the two-helix structure that is required for productive TNFα binding. Indeed, **4.2** disrupts this interaction as well as **Z-TNFα**, indicating that the incorporation of the disulfide

constraint is able to recover nearly full affinity for TNFα after removal of helix 3. Overall, the evaluation of **4.1** and **4.2** indicate that the disulfide constraint plays an important, but not essential, role in TNFα binding for the two-helix analogues of **Z-TNFα**. We did not synthesize the analogue of **4.1** lacking the five α-residue substitutions mentioned above (which would correspond to the helix 1-helix 2 segment of **Z-TNFα**), so we do not know if these α-substitutions are playing a critical role in helix stabilization in the absence of the disulfide.

α/β-Peptide **3.5**, which contains the native residue Trp11 and binds to TNFα with modestly higher affinity than does α/β-peptide **3.4**, which places the cyclic β-residue APC at position 11. This difference in affinity likely arises because Trp11 makes productive contacts with TNFα, consistent with the fact that this residue is one that was randomized and selected for binding to TNFα.[16] To attempt to reduce the protease susceptibility of this region while preserving the native Trp side chain, we designed α/β-peptide **4.3**, which contains the Trp11→β^3Trp substitution (Figure 4.3). We found that **4.3** displayed an IC_{50} value of 23 nM in the competition ELISA, which is essentially identical to the IC_{50} value for **3.4** (28 nM). The lower affinity of **4.3** relative to **3.5** may mean that the side chain of the β^3-residue is not properly positioned to make the optimal contact to TNFα. It is possible that a β^2-residue (which places the side chain on the α-carbon) or an α-methyl-substituted α-tryptophan analogue may be better suited at this position to retain affinity of ~5-10 nM while decreasing protease susceptibility.

We next explored analogues of **3.4** and **3.5** that had fewer residues at their N-termini to attempt to minimize the sequence, which would provide benefits in terms of synthetic accessibility. In addition, exploring truncated analogues of **3.4** and **3.5** would provide insight into the role of the N-terminal residues (which were not randomized to derive **Z-TNFα**) into binding to TNFα. α/β-Peptide **4.4** is an analogue of **3.4** that lacks residues 1-5, and **4.4** blocked the

TNFα-TNFR1 interaction with IC_{50} = 38 nM (Figure 4.3). This result indicates that residues 1-5 do not make important contacts to TNFα. α/β-Peptide **4.5** is an analogue of **3.5** that lacks residues 1-8, and **4.5** blocked the TNFα-TNFR1 interaction with IC_{50} = 11 nM, indicating that residues 6-8 are also not essential. This result contrasts with the **Z-VEGF** family described in Chapter 2, in which removal of residues 4-6 led to a significant decrease in affinity for $VEGF_{165}$. Thus, α/β-peptide **4.5** is a high affinity analogue of **Z-TNFα** of 30 residues, just half the length of the full-length three-helix parent α-peptide. This molecule represents the shortest α/β-peptide analogue of **Z-TNFα** that contains a disulfide bond connecting positions 9 and 38. (Note that the residue numbering scheme used for all truncated α/β-peptides corresponds to the numbering for the full three-helix **Z-TNFα**, even if N-terminal residues are removed.)

4.3.2 α/β-Peptide analogues lacking a disulfide constraint

Based on the observation that α-peptide **4.1** (which contains no disulfide constraint) retained some affinity for TNFα, we next explored two-helix α/β-peptide analogues of **Z-TNFα** that lacked the disulfide bond. An optimized α/β-peptide containing no disulfide bond would be beneficial for several reasons: i) peptides that lack oxidation-prone cysteine residues, which can form complicated side-products, are easier to synthesize, purify, and store; and ii) removing the disulfide constraint may allow for the design of α/β-peptides that are even shorter than **4.5** (i.e., < 30 residues). To explore these possibilities, we designed analogues of **3.4** and **3.5** that lacked the disulfide bond (α/β-peptides **4.6** and **4.7**, respectively) (Figure 4.4). α/β-Peptide **4.6**, which contains the cyclic β-residue APC in place of Trp11, bound very weakly to TNFα (IC_{50} = 2100 nM). This result is consistent with the observation that **4.1**, which also lacks a disulfide bond, showed much lower affinity for TNFα than did the three-helix parent or the disulfide-constrained two-helix derivatives described above. Unexpectedly, however, the α/β-peptide **4.7**, which

features the native Trp11, blocked the TNFα-TNFR1 interaction with IC_{50} = 24 nM. The higher affinity of **4.7** versus **4.6** mirrors the increase in affinity seen for **3.5** versus **3.4**, indicating that the Trp11 residue makes important contacts with TNFα. Furthermore, the importance of Trp11 is much greater in the absence of the disulfide, as indicated by the much larger difference in affinity for **4.7** versus **4.6** than **3.5** versus **3.4**. The relative importance of Trp11 in the absence of the disulfide bond versus presence of the disulfide bond is surprising, and warrants further investigation. One possible explanation may be that the hydrophobic Trp11 makes a critical contact which initiates the binding to TNFα of the relatively unstructured **4.7**. In contrast, in the presence of the disulfide bond (e.g., in **3.4**), many other side chains are already in the correct positions for productive TNFα binding, and so the side chain of Trp11 is not as crucial. Interestingly, the much higher affinity of α/β-peptide **4.7** compared to its α-peptide analogue (**4.1**) shows that helix-promoting Aib and/or cyclic β-residues can be used to increase the affinity of α/β-peptides relative to their parent α-peptides, presumably by stabilizing the helical conformation required for TNFα binding.

We next designed analogues of **4.7** with residues removed from either terminus in an effort to identify a minimized α/β-peptide with no disulfide bond (Figure 4.4). Removing residues 1-5 of **4.7** (to generate **4.8**) was well tolerated, consistent with the results described above for the **4.3-4.5** series. However, further removal of residues 6-8 from the N-terminus led to a large drop in affinity (α/β-peptide **4.9**, IC_{50} = 1200 nM). This result suggests that these residues may play an important role in the absence of the disulfide bond, possibly through helix stabilization (as mentioned above) or through direct protein contact. α/β-Peptides **4.10-4.11** show that removal of additional residues from the C-terminus is modestly tolerated in the absence of the disulfide constraint, and α/β-peptide **4.12** shows that further removal of Leu10 and Gly11

leads to a substantial loss in affinity for TNFα. This result is consistent with the fact that both Leu10 and Gly11 are residues that were randomized and selected for TNFα binding and thus likely make contact with TNFα.

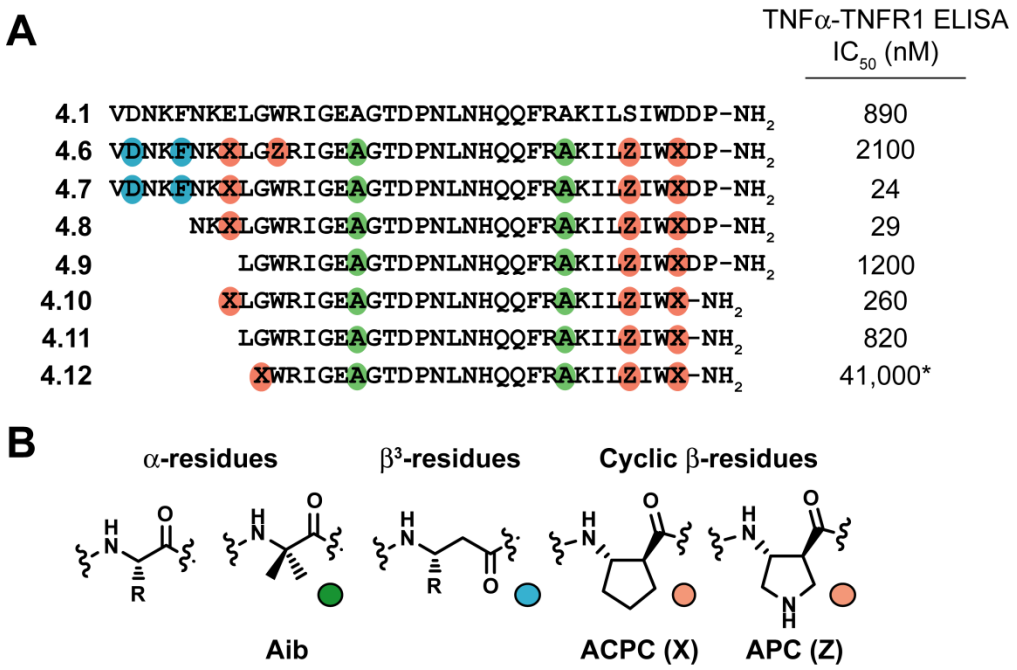

Figure 4.4 (A) Primary sequences of non-cyclized two-helix α- and α/β-peptides derived from **Z-TNFα**, along with associated IC_{50} values, as determined by TNFα-TNFR1 competition ELISA. The uncertainty in the calculated IC_{50} values is ~2-fold, with a maximum variation of up to ~7-fold for some experiments. For **4.12**, value is based on only one experiment (*). Non-natural residues are indicated by colored circles. (B) Structures of a generic α-residue, the Aib residue (green), a generic β^3-residue (teal), and the cyclic β-residues ACPC (X) and APC (Z) (orange).

4.3.3 Exploring alternative disulfide positions and final designs

Although several of the α/β-peptide analogues lacking a disulfide bond blocked the TNFα-TNFR1 interaction with high efficacy (e.g, **4.8**), shortening the sequence much beyond 33 residues led to a substantial loss in efficacy. In an effort to truncate the sequence further while maintaining high affinity for TNFα, we next explored disulfide bond positions that differed from the 9,38 position used for the **Z-VEGF**, **Z-IgG**, and **Z-TNFα** analogues described above and in Chapters 2 and 3. α/β-Peptide **4.13** places Cys residues at positions 16 and 30, which corresponds to a disulfide location central in the helices, somewhat near the loop region (Figure

4.5). **4.13** blocked the TNFα-TNFR1 interaction with IC_{50} = 160 nM. Thus, **4.13** does not bind TNFα any better than does its linear analogue **4.10**, which indicates that this position for a disulfide constraint is not productive for TNFα binding.

We next designed α/β-peptide **4.14**, which places Cys residues at positions 12 and 34. This disulfide position allowed for removal of residues 37 and 38 from the C-terminus to make this α/β-peptide slightly shorter than **4.5** (Figure 4.5). We found that **4.14** blocked the TNFα-TNFR1 interaction with IC_{50} = 6.9 nM, which indicates that this α/β-peptide binds with affinity comparable to that of **Z-TNFα** and the best of the α/β-peptides reported above. We designed α/β-peptide **4.15** and **4.16** by removing Leu9 and Gly10 individually from the N-terminus of **4.14**, and incorporating an N-terminal cyclic β-residue ACPC to reduce the susceptibility of the N-terminus from protease degradation. α/β-Peptide **4.15** (IC_{50} = 23 nM) blocked the TNFα-TNFR1 interaction with slightly decreased efficacy compared to **4.14** (IC_{50} = 6.9 nM), while **4.16** (IC_{50} = 5100 nM) was significantly less effective than both **4.14** and **4.15** at blocking this interaction. This result is consistent with the very large drop in affinity for **4.12** versus **4.11**, described above. The importance of Gly10 in both of these comparisons suggests that this residue either makes contact with TNFα or correctly positions a nearby residue to make a productive contact with the protein, consistent with the fact that Gly10 is a residue that was selected for during the phage display/selection process and likely resides on the protein-binding face of the helix 1-helix 2 surface. Consistent with its higher affinity, **4.14** showed an increased helical signature in its far-UV circular dichroism (CD) spectrum relative to both **4.13** and non-disulfide constrained analogues **4.8**, **4.10**, and **4.11** (Figure 4.6).

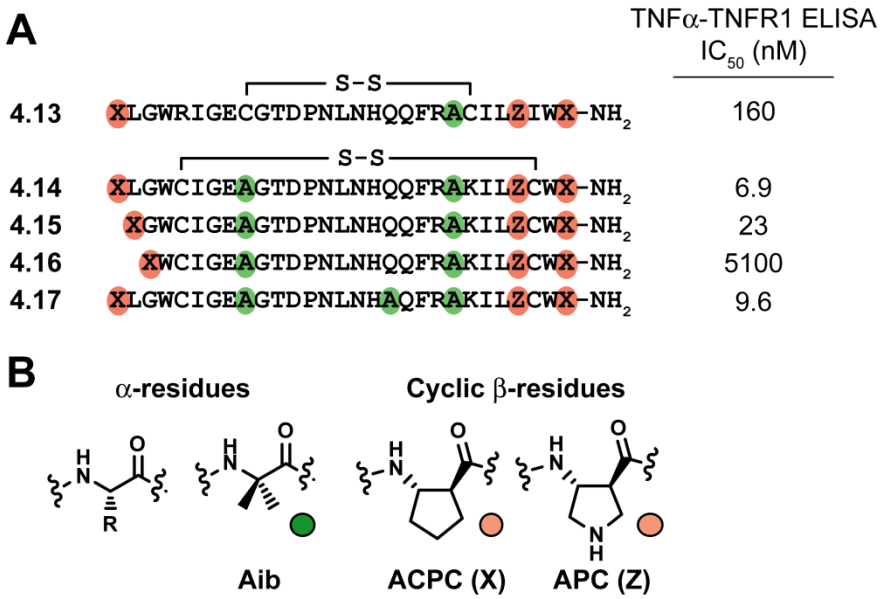

Figure 4.5 (A) Primary sequences of two-helix α/β-peptides derived from **Z-TNFα** containing novel disulfide bond positions, along with associated IC_{50} values, as determined by TNFα-TNFR1 competition ELISA. The uncertainty in the calculated IC_{50} values is ~2-fold, with a maximum variation of up to ~7-fold for some experiments. Non-natural residues are indicated by colored circles. Each cysteine is engaged in an intramolecular disulfide bond. (B) Structures of a generic α-residue, the Aib residue (green), a generic β^3-residue (teal), and the cyclic β-residues ACPC (X) and APC (Z) (orange).

Finally, in an effort to decrease the protease susceptibility of our optimized α/β-peptide, we designed **4.17**, an analogue of **4.14** that contains a Gln25→Aib substitution (Figure 4.5). The analogous substitution was found to dramatically reduce protease susceptibility in the α/β-peptide analogues of both **Z-VEGF** and **Z-HER2** (described in Chapters 2 and 3, respectively). α/β-Peptide **4.17** blocked the TNFα-TNFR1 interaction with IC_{50} = 9.6 nM, indicating that the Gln25 side chain was not particularly important for binding to TNFα. Overall, **4.17** represents an α/β-peptide of 29 residues (30 residues shorter than the three-helix parent **Z-TNFα** and 9 residues shorter than the two-helix parent α/β-peptide **3.5**) that binds to TNFα with affinity nearly identical to that of **Z-TNFα** and has a previously unexplored disulfide bond position.

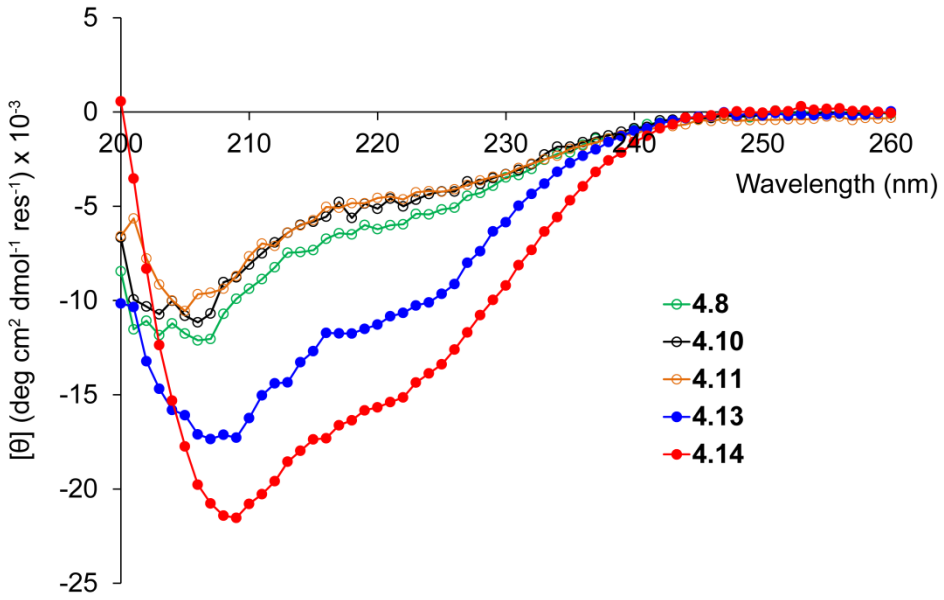

Figure 4.6 Far-UV circular dichroism (CD) data for two-helix α/β-peptides derived from **Z-TNFα** lacking (unfilled circles) and containing (filled circles) a disulfide bond. All oligomers 75 μM in PBS, pH 7.5.

4.4 Protease susceptibility

We evaluated the protease susceptibility of **Z-TNFα**, **3.5**, **4.2**, **4.7**, and **4.17** to degradation by proteinase K, a generic and aggressive protease (Figure 4.7). This work was performed in collaboration with Geoffrey Eddinger (Gellman Laboratory, University of Wisconsin-Madison). When incubated with proteinase K, the three-helix α-peptide **Z-TNFα** was rapidly degraded, with a half-life of 4.4 minutes under these assay conditions. The disulfide-constrained two-helix α-peptide **4.2**, which bound to TNFα with affinity nearly identical to that of **Z-TNFα**, was degraded even more rapidly and displayed a half-life of 0.18 minutes. The ~24-fold decrease in half-life for **4.2** versus **Z-TNFα** parallels the decrease in half-life seen for the analogous comparisons in the **Z-VEGF** and **Z-HER2** systems (described in Chapters 2 and 3, respectively). The higher protease susceptibility for the two-helix analogues relative to their three-helix parent Z-domains appears to be a general trend, likely resulting from decreased

conformational rigidity for the shorter peptides even in the presence of the structurally-stabilizing disulfide bond. Also paralleling these past observations, the incorporation of the non-natural Aib- and β-residues into the two-helix scaffold led to a significant decrease in protease susceptibility, with α/β-peptide **3.5** displaying a half-life of 78 minutes (~430-fold increase in half-life relative to **4.2** and ~18-fold increase relative to **Z-TNFα**).

Interestingly, α/β-peptide **4.7**, the analogue of **3.5** containing no disulfide bond, was significantly more susceptible to protease degradation, and displayed a half-life of 7.9 minutes in this experiment. The ~10-fold decrease in half-life for **4.7** versus **3.5** indicates that the disulfide bond plays a critical role in the high protease stability of **3.5**, likely by stabilizing the helical secondary structure of the two-helix α/β-peptide. Nonetheless, α/β-peptide **4.7** is ~40-fold more stable to protease degradation than is the disulfide-constrained α-peptide **4.2**, suggesting that the incorporation of non-natural residues greatly reduces susceptibility to proteolytic degradation, even in the absence of the disulfide. Finally, the optimized α/β-peptide **4.17**, which is 29 residues in length, features the novel disulfide position, and one additional Aib residue, displayed a half-life of 760 minutes in this experiment. The half-life value for **4.17** represents an >4000-fold increase relative to the two-helix **4.2** and a >170-fold increase relative to the parent three-helix **Z-TNFα**. The ~10-fold increase in half-life for **4.17** relative to **3.5** could be a result of the removal of sites particularly susceptible to proteolysis such as the N-terminal residues, near Trp11 (which is now near the new disulfide constraint), or substitution of Gln25 with Aib. Alternatively, the increase in half-life for **4.17** might arise from increased conformational rigidity, either from the new disulfide position or the additional Aib residue.

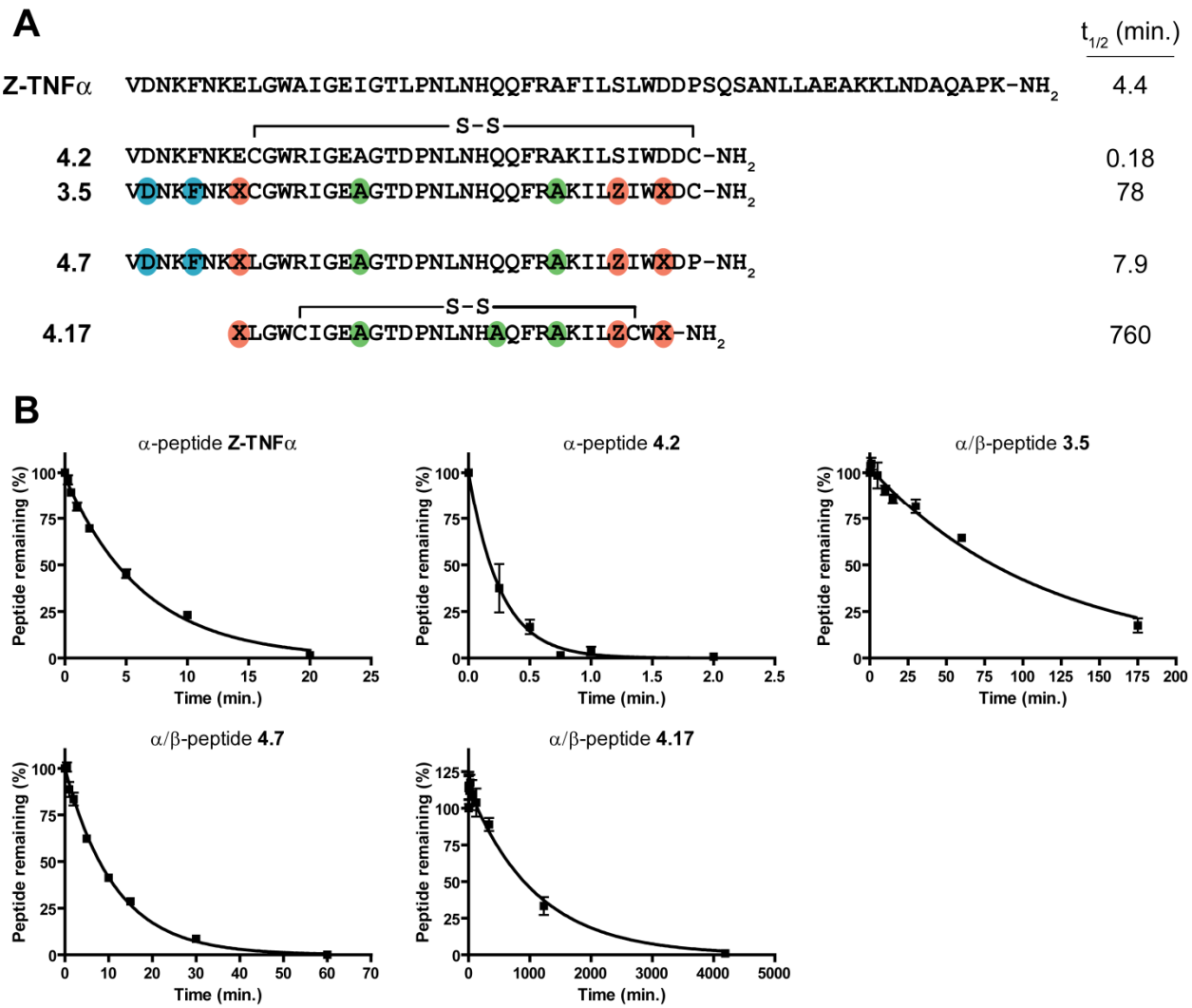

Figure 4.7 Susceptibility of 40 μM α- or α/β-peptide to 10 μg/mL proteinase K in TBS, pH 7.5 at room temperature. (A) Sequences of α- and α/β-peptides and associated half-life values. (B) Time course of α- or α/β-peptide degradation, as assessed by HPLC. Note the different scales on the horizontal axes.

4.5 Z-TNFα is dependent on TWEEN20 for binding to TNFα

TNFα signaling induces apoptosis in many cell types.[6, 10] **Z-TNFα** and our two-helix α/β-peptide analogues block the binding of TNFα to immobilized TNFR1 in competition ELISA experiments, which suggests that these compounds may be used as antagonists of TNFα signaling. To test this hypothesis, we evaluated the ability of **Z-TNFα** and several α/β-peptide analogues to block TNFα-mediated cell death of WEHI-13VAR mouse fibrosarcoma cells.[23]

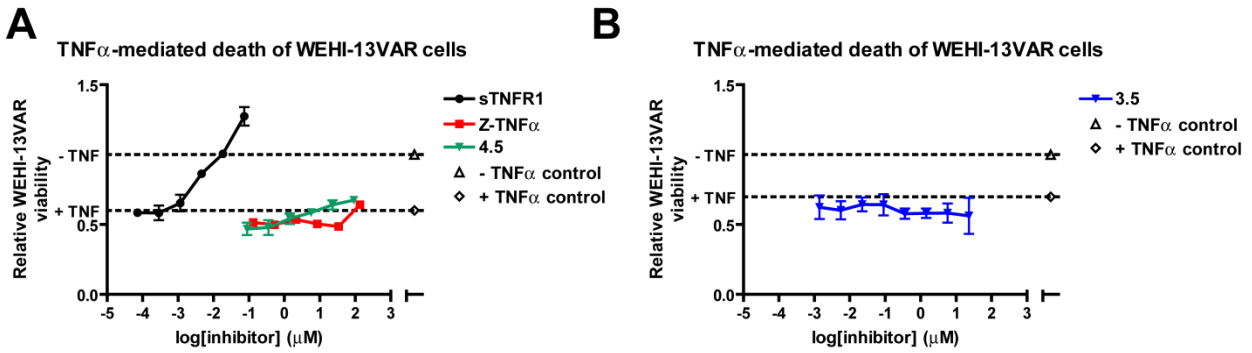

Figure 4.8 Evaluation of potential TNFα antagonists to inhibit TNFα-mediated death of WEHI-13VAR cells, as determined by CellTiter-Glo viability assay. Cells were treated with TNFα alone (unfilled diamond, "+ TNF" dotted line) to determine the dynamic range for each assay relative to untreated cells (unfilled triangle, "- TNF" dotted line). For evaluation of inhibitors, cells were treated with TNFα and the indicated concentration of compound. Luminescence data normalized to the average value for the "- TNFα" control to determine relative viability. Conditions for each assay were slightly different, as indicated: (A) Conditions: 10,000 cells/well seeded in 96-well tissue culture plate and allowed to recover overnight, 0.04 ng/mL TNFα, 0.4 μg/mL actinomycin D, 16% PBS/RPMI, 0.08% FBS, penicillin/streptomycin (P/S). Potential inhibitors were pre-incubated with TNFα for 2 hours in 50% PBS/RPMI, 1.2 μg/mL actinomycin D, 0.05% FBS, P/S at 37 °C, 5% CO_2 before being added to cells, and the plate was read after ~8 hours. Data points represent mean ± SEM for n = 2 wells (for inhibitors) or n = 4 wells (for controls). (B) Conditions: 10,000 cells/well seeded in 96-well tissue culture plate and allowed to recover overnight, 0.04 ng/mL TNFα, 1 μg/mL actinomycin D, 17% PBS/RPMI, 8% FBS, P/S. Potential inhibitors were pre-incubated with TNFα for 2 hours in 50% PBS/RPMI, 3 μg/mL actinomycin D, 5% FBS, P/S at 37 °C, 5% CO_2 before being added to cells, and the plate was read after ~15 hours. Data points represent mean ± SEM for n = 2 wells (for inhibitors) or n = 8 wells (for controls).

In initial experiments, we treated WEHI-13VAR cells with 0.04 ng/mL TNFα, in the presence of actinomycin D (which sensitizes this cell type to killing by TNFα),[23] and in the presence or absence of varying concentrations of α-peptide **Z-TNFα,** α/β-peptide **4.5**, or α/β-peptide **3.5**. After treatment with TNFα and potential antagonists, we evaluated cell viability using a CellTiter-Glo luminescent viability assay (Promega) to measure ATP levels, which corresponds to the number of metabolically active cells (Figure 4.8). Despite the fact that **Z-TNFα**, **4.5**, and **3.5** are each able to block the TNFα-TNFR1 interaction in competition ELISA, we saw that none of these oligomers could block the TNFα-mediated cell death of WEHI-13VAR cells under these cell culture conditions. In contrast, the recombinant soluble TNFR1 receptor fragment (sTNFR1) was able to rescue WEHI-13VAR cells from TNFα-mediated death under these conditions (Figure 4.8A).

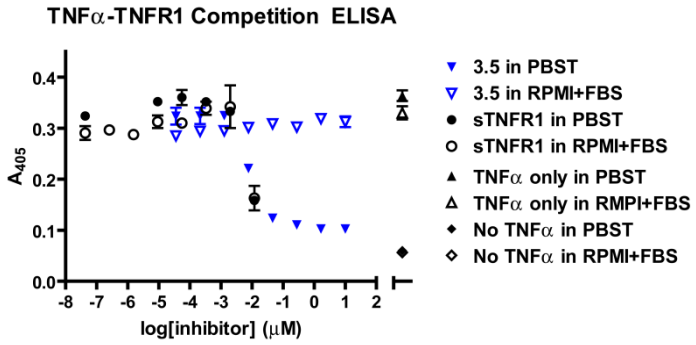

Figure 4.9 α/β-Peptide **3.5** blocks the binding of 0.08 μg/mL TNFα to immobilized TNFR1 in an ELISA experiment carried out in PBS+0.05% TWEEN20 (PBST, blue filled triangles), but not in RPMI+10% FBS (cell culture conditions, blue unfilled triangles). Recombinant soluble TNFR1 (sTNFR1) appears to be able to block this interaction under both conditions (unfilled and filled black circles), although the concentration of stock solution prevented evaluating higher concentrations. Note that for sTNFR1 in PBST, two serial dilutions were not tested due to an error in experimental set-up. Data points represent the mean ± SEM for duplicate wells on the plate.

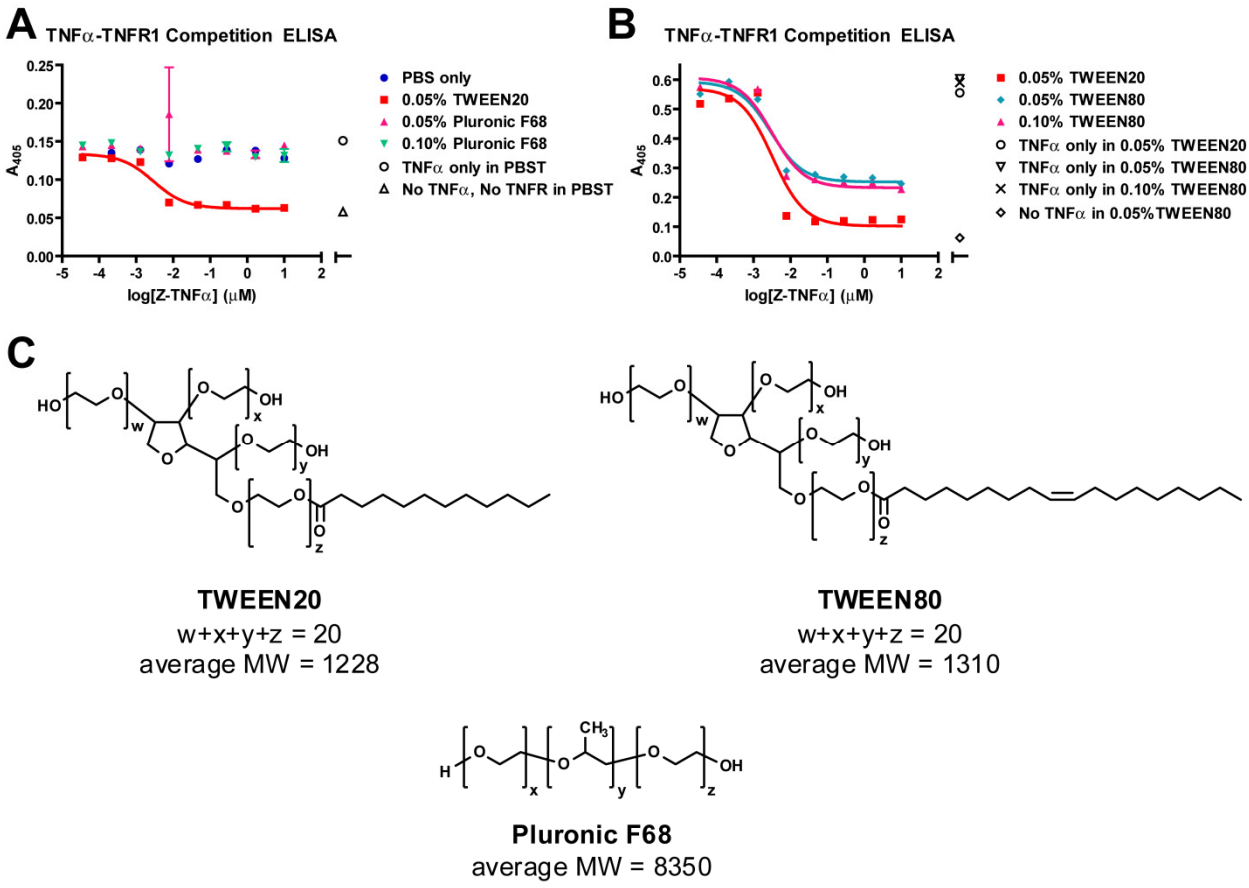

Figure 4.10 The binding of **Z-TNFα** to TNFα is dependent on the presence of TWEEN20. (A-B) TNFα-TNFR1 competition ELISAs evaluating the ability of **Z-TNFα** to block the binding of TNFα to immobilized TNFR1 in PBS with the indicated additives. For (A), data represent a single measurement for "0.05% TWEEN20", "PBS only", and the control conditions. All other conditions are the mean ± SEM of duplicate wells on the plate. (C) Chemical structures of TWEEN20, TWEEN80, and Pluronic F68.

The inactivity of **Z-TNFα** and its α/β-peptide analogues in our preliminary cell-based experiments led us to hypothesize that some component in the cell culture conditions was preventing the binding of these oligomers to TNFα, and that this component was not present in the ELISA conditions. Consistent with this hypothesis, we found that **3.5** was unable to block the TNFα-TNFR1 interaction in an ELISA experiment in which the TNFα-TNFR1 interaction step was carried out in RMPI media with 10% fetal bovine serum (FBS) (conditions typically used for cell culture experiments) rather than PBS+0.05% TWEEN20 (buffer typically used for ELISA) (Figure 4.9). Systematic evaluation of the components that differed between these two experimental conditions led to the unexpected observation that **Z-TNFα** is dependent on the detergent TWEEN20 to block the TNFα-TNFR1 interaction, as shown by the inability for this peptide to block the binding of TNFα to immobilized TNFR1 in PBS with no TWEEN20 in competition ELISA (Figure 4.10A). TWEEN20 is a nonionic detergent commonly used in selection protocols and ELISAs to reduce non-specific binding interactions (Figure 4.10C). To evaluate whether this effect was specific to TWEEN20, we explored other detergents in the competition ELISA experiment. We found that TWEEN80, which is similar in structure to TWEEN20, was able to promote the ability of **Z-TNFα** to block the TNFα-TNFR1 interaction, although not down to the same level as TWEEN20 (Figure 4.10B). In contrast, Pluronic F68, an unrelated non-ionic surfactant, was unable to promote **Z-TNFα**'s ability to block this interaction (Figure 4.10A). These results strongly suggest that TWEEN20, which was present during the phage display/selection procedure to derive **Z-TNFα**,[16] is facilitating the interaction of these oligomers with TNFα. The dependence on this detergent appears to be specific for this particular peptide-protein interaction, as the previously described Z-domain-derived peptides targeting

VEGF (**Z-VEGF** and its α/β-peptide analogues, Chapter 2) and HER2 (**Z-HER2** and its α/β-peptide analogues, Chapter 3) bound to their respective proteins in the absence of TWEEN20.

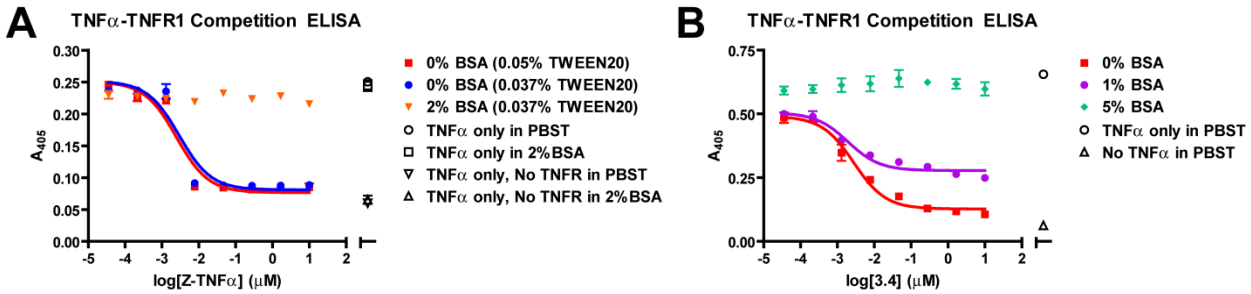

Figure 4.11 High concentrations of BSA attenuate the ability of **Z-TNFα** (A) and α/β-peptide **3.4** (B) to block the TNFα-TNFR1 interaction in a dose-dependent manner by competition ELISA. PBST = PBS + 0.05% TWEEN20.

Although the results described above suggest that TWEEN20 promotes the binding of **Z-TNFα** and its α/β-peptide analogues to TNFα, there are a number of other interesting observations from these experimental efforts that should be noted here. We found that high concentrations of bovine serum albumin (BSA) inhibited the ability of **Z-TNFα** and **3.4** to block the TNFα-TNFR1 interaction in competition ELISA experiments (Figure 4.11). This suggests that **Z-TNFα** analogues may be binding non-specifically to BSA, preventing them from binding to TNFα. However, in complementary experiments in which **3.5** was covalently immobilized directly onto the surface of Nunc Immobilizer Amino ELISA plates, we saw that BSA actually increased the binding of TNFα to the immobilized α/β-peptide (Figure 4.12, compare circles to squares). These results indicate that BSA does not inhibit the binding of TNFα to the Z-domain analogues, which suggests that the apparent loss of activity for these peptides in the TNFα-TNFR1 competition ELISA (Figure 4.11) is likely an artifact from the experimental conditions arising from the TNFα and TNFR1 interaction rather than due to non-specific binding of the peptides to BSA. Consistent with this hypothesis, BSA had no effect on the binding of a related two-helix α/β-peptide **3.2** to bind to IgG1-κ in its competition ELISA experiment, which

indicates this is effect is not inherent to the two-helix α/β-peptide scaffold (Figure 4.13). Importantly, the results in Figure 4.12 also show that the absence of TWEEN20 during the step in which TNFα is allowed to bind to directly immobilized α/β-peptide dramatically reduces the amount of TNFα that is detected on the ELISA plate (triangles), again indicating that TWEEN20 seems to be required for significant binding of the α/β-peptide to this protein.

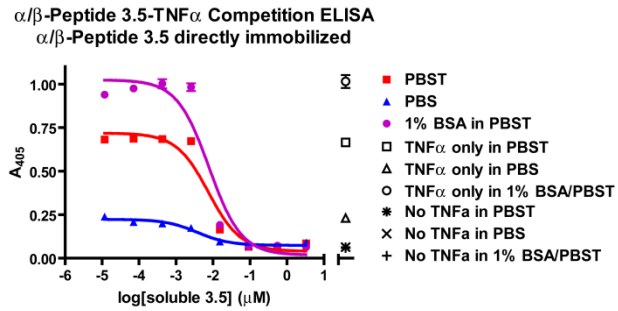

Figure 4.12 α/β-Peptide **3.5**-TNFα competition ELISA, in which **3.5** is covalently immobilized onto the ELISA plate, to evaluate the binding to TNFα directly to this α/β-peptide. Black points represent control conditions in which TNFα is allowed to bind to immobilized α/β-peptide **3.5** in the presence of no soluble competitor under various buffer conditions (PBST = PBS + 0.05% TWEEN20). Colored points and curves represent the binding of TNFα to immobilized **3.5** in the presence of soluble **3.5** as a competitor.

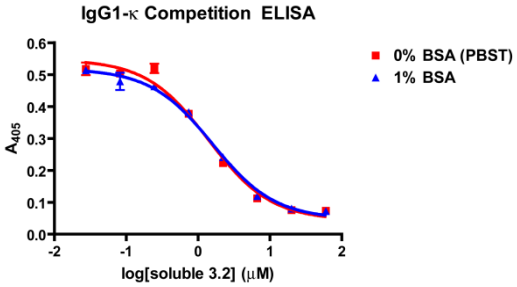

Figure 4.13 IgG1-κ competition ELISA comparing the relative ability of α/β-peptide **3.2** to inhibit binding of 9 μg/mL IgG1-κ to immobilized **3.2**+BSA conjugate in the presence (blue) or absence (red) of 1% BSA. PBST = PBS + 0.05% TWEEN20.

Detergents such as TWEEN20 can affect the oligomerization of TNFα in solution.[6, 24] This observation, in addition to a very recent report of a phage derived peptide that dissociates the TNFα trimer,[15] led us to speculate that perhaps **Z-TNFα** derivatives and TWEEN20 work together to dissociate the active TNFα trimer. To test this hypothesis, we monitored TNFα oligomerization over time under various buffer conditions using size exclusion chromatography

(SEC) on an ultra performance liquid chromatography (UPLC) instrument. When we injected TNFα in PBS, we observed a peak in the resulting chromatogram at ~3.2 minutes that appears to correspond to the TNFα trimer (Figure 4.14B, also see Figure 4.25 in the "Experimental Methods" section for chromatograms from other control injections). When we injected solutions containing 40 μg/mL TNFα in either PBS or PBS+0.05% TWEEN20 (PBST) with 4% DMSO, the area of this peak stayed constant over time (Figure 4.14A, blue and black, and Figure 4.14C), indicating that the addition of 0.05% TWEEN20 alone is not sufficient to dissociate the TNFα oligomer. Similarly, incubation of 40 μg/mL TNFα with 44 μM **4.17** in PBS (no TWEEN20) resulted in a peak at ~3.2 minutes that remained relatively constant over the course of the experiment (Figure 4.14A, green). In contrast, when we added 40 μg/mL TNFα to a solution containing 44 μM **4.17** in PBST with 4% DMSO, we saw the peak at ~3.2 minutes disappear over the course of the experiment and another peak with a smaller apparent mass (at ~4.2 minutes) grow in over time (Figure 4.14A, red and Figure 4.14D). This peak likely corresponds to the TNFα monomer, dimer, or some combination in complex with **4.17** and TWEEN20. In control experiments, we saw no decrease area of the TNFα oligomer peak when 40 μg/mL TNFα was incubated with 44 μM **4.17** in PBS alone (no TWEEN20), suggesting that **4.17** alone is not sufficient to dissociate the TNFα trimer. These results strongly suggest that the TNFα trimer nearly fully dissociates in the presence of both α/β-peptide **4.17** and 0.05% TWEEN20, but not in the presence of just one of these components. This suggests a mechanism in which **4.17** (and other **Z-TNFα** analogues) act by dissociating the active TNFα trimer, but that this dissociation is dependent on the presence of TWEEN20. One possible explanation for this may be that the binding site of **Z-TNFα** (and its analogues) is at the oligomerization interface, which is sufficiently exposed to allow peptide binding only in the presence of the detergent TWEEN20.

Once this binding site is partially exposed by TWEEN20, binding of **Z-TNFα** to this site dissociates the trimer into some combination of monomers and dimers. An alternative explanation is that TWEEN20 alters the kinetics of TNFα oligomerization and catalyzes TNFα trimer dissociation. Indeed, the dissociation rate of the TNFα trimer was found to be 2- to 3-fold higher in the presence of 0.0005% TWEEN20 in SPR experiments,[24] which is a 100-fold lower TWEEN20 concentration than we used in our ELISA experiments.

One interesting observation that may be explained by this mechanism is the fact that in some TNFα-TNFR1 competition ELISA experiments, **Z-TNFα** and its analogues were not able to fully block the TNFα-TNFR1 interaction, with a small amount of TNFα still bound to the plate even at high inhibitor concentrations compared to control conditions in which no receptor was immobilized to the plate or which were never exposed to TNFα (for an example, compare control conditions with no TNFα (diamonds) to "**3.5** in PBST" conditions (blue filled triangles) in Figure 4.9). The extent of this binding that was unable to be blocked by Z-domain-derived peptides varied between experiments. There are several possible explanations for this behavior: i) Oligomers derived from **Z-TNFα** fully dissociate the TNFα trimer into a combination of monomers and dimers, some of which are still able to bind the immobilized receptor fragment and are still recognized by the polyclonal anti-TNFα antibody mixture. Even a small amount of antibody bound will eventually lead to signal due to amplification by enzymatic reaction; ii) the concentration of TWEEN20 used in these experiments (0.05%) is not high enough to fully facilitate dissociation of every TNFα molecule. Future work can investigate this second possibility by designing experiments at different concentrations of TWEEN20 and/or different concentrations of TNFα; or iii) a small fraction of TNFα in some experiments is unable to be dissociated by the combination of TWEEN20+**Z-TNFα** derivatives. A very similar observation

has previously been reported for at least one other compound that is known to dissociate the TNFα trimer,[25] and this has been attributed to a small fraction of nondissociable trimer crosslinked through intermolecular disulfide bonds (each native TNFα monomer contains one intramolecular disulfide bond which is not critical for biological activity).[1]

Overall, the experiments described in this section indicate that TWEEN20, a detergent that is often included in affinity-based selection protocols and ELISA experiments to minimize non-specific interactions, is critically involved in the **Z-TNFα**-TNFα interaction. This effect is also evident for α/β-peptide analogues of **Z-TNFα**. Detergents, including TWEEN20, have been shown to alter the oligomerization state of TNFα in solution.[6, 24] Furthermore, dependence on the detergent TWEEN20 for binding has been noted in at least two other reports describing phage-derived peptides directed to TNFα.[17, 18] These observations raise the possibility that the selection of TNFα-binding peptides in the presence of certain detergents unintentionally returns binders to a site that is exposed only in the presence of these detergents. Together, the data presented here are consistent with a mechanism in which TWEEN20 exposes a site on TNFα (e.g., at the oligomerization interface) where **Z-TNFα** and its analogues bind and dissociate the active trimer.

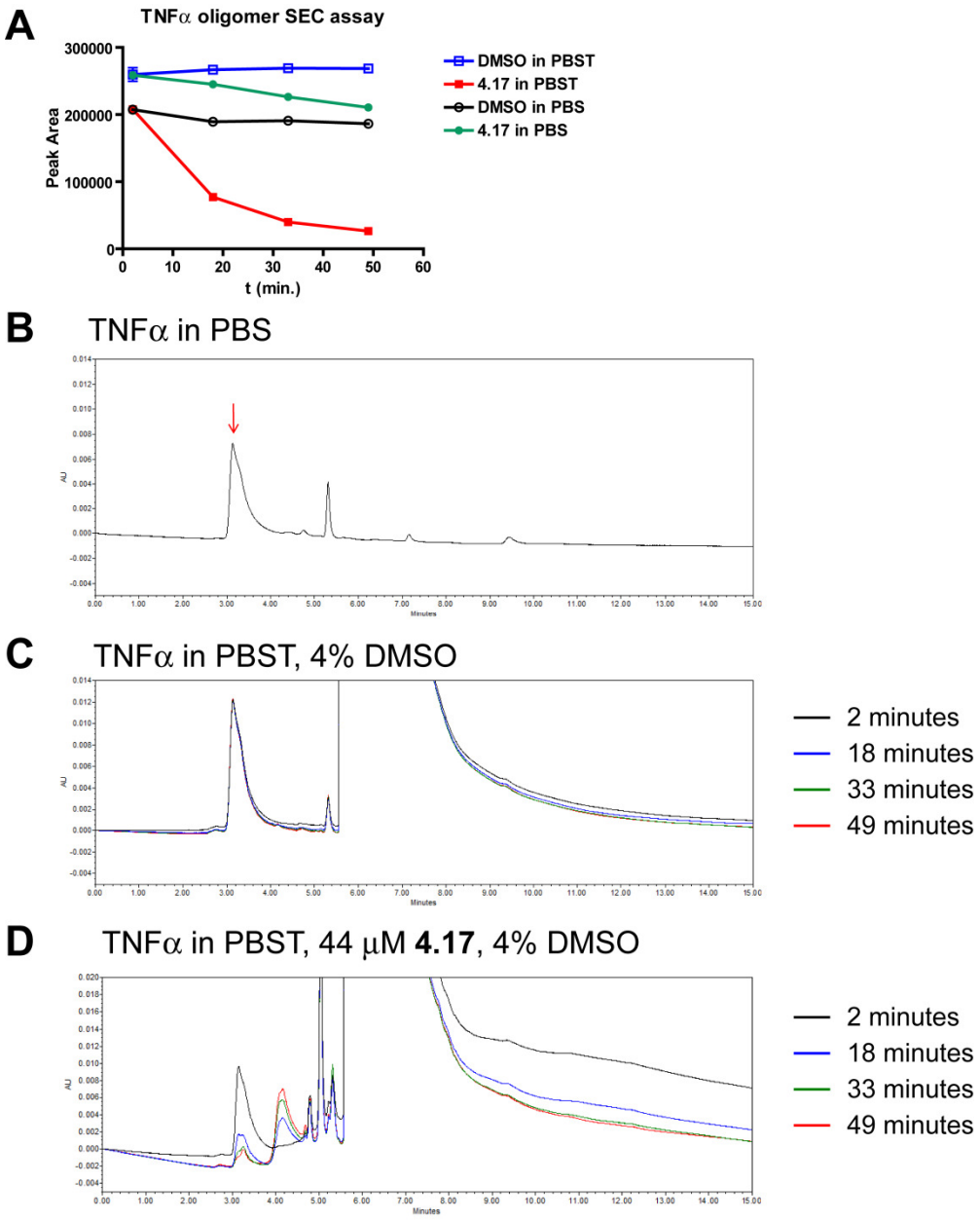

Figure 4.14 α/β-Peptide **4.17** acts with TWEEN20 to dissociate the TNFα oligomer. (A) Monitoring of the oligomeric TNFα peak over time by SEC, as determined by peak area at 220 nm. 40 μg/mL TNFα was incubated in PBS+0.05% TWEEN20 (PBST) with 4% DMSO (blue), with 44 μM **4.17** in PBST with 4% DMSO (red), in PBS with 4% DMSO (black), and with 44 μM **4.17** in PBS with 4% DMSO (green). Data points represent the mean ± SEM of duplicate experiments. (B) Chromatogram resulting from the injection of TNFα in PBS. The native TNFα oligomer peak is indicated by the red arrow. The peak at ~5.3 minutes is present in the blank run injecting PBS only. (C) Overlay of chromatograms resulting from monitoring 40 μg/mL TNFα in PBST with 4% DMSO over time (blue points in panel A). (D) Overlay of chromatograms resulting from monitoring 40 μg/mL TNFα with 44 μM **4.17** in PBST with 4% DMSO over time (red points in panel A).

4.6 Truncation of other Z-domains targeting TNFα

Z-TNFα and its α/β-peptide derivatives exhibited an unexpected mode of binding to TNFα that was dependent on the detergent TWEEN20. This detergent dependence likely precludes these molecules from eventual use *in vivo*, one of the major end goals of TNFα inhibitors. We sought to evaluate whether other Z-domain derivatives selected from combinatorial libraries to bind TNFα also showed this same detergent dependence, with the goal of identifying a peptide sequence that could block TNFα signaling in the absence of TWEEN20 to serve as the starting point for new α/β-peptide analogues. We chose seven peptides that have been previously reported from combinatorial libraries based on the Z-domain scaffold to bind TNFα[16, 26, 27] and designed α-peptides **4.18-4.24** as two-helix, disulfide-constrained analogues of these three-helix peptides (Figure 4.15). **4.18-4.21** each incorporate a disulfide bond as well as five helix-stabilizing and solubility-enhancing substitutions,[20, 21] while **4.22-4.24** contain only the additional disulfide bond. Most of the parent three-helix peptides were selected from display libraries in the presence of detergent (in an attempt to minimize non-specific binding), and thus may also show TWEEN20-dependence on TNFα binding.

A

Z-TNFα-1	VDNKFNKENIAAMTEITRLPNLNPYQRAAFIWSLSDDPSQSANLLAEAKKLNDAQAPK
Z-TNFα-2	VDNKFNKERGHAIGEIWELPNLNLAQIVAFIISLHDDPSQSANLLAEAKKLNDAQAPK
Z-TNFα-3	VDNKFNKELGGAFYEILELPNLNVLQKAAFIRSLYDDPSQSANLLAEAKKLNDAQAPK
Z-TNFα-P5	VDNKFNKESGEALGEIGELPNLNALQFRAFIISLWDDPSQSANLLAEAKKLNDAQAPK
Z-TNFα-200	VDNKFNKEKGRATGEIGALPNLNPQQYRAFILSLHDDPSQSANLLAEAKKLNDAQAPK
Z-TNFα-206	VDNKFNKERQQALGEISALPNLNLHQYYAFIRSLLDDPSQSANLLAEAKKLNDAQAPK
Z-TNFα-186	VDNKFNKESEGAMHEIVRLPNLNAWQRQAFIVSLWDDPSQSANLLAEAKKLNDAQAPK

B

S-S

4.18	VDNKFNKECIARMTEATRDPNLNPYQRAAKIWSISDDC-NH_2
4.19	VDNKFNKECGHRIGEAWEDPNLNLAQIVAKIISIHDDC-NH_2
4.20	VDNKFNKECGGRFYEALEDPNLNVLQKAAKIRSIYDDC-NH_2
4.21	VDNKFNKECGERLGEAGEDPNLNALQFRAKIISIWDDC-NH_2
4.22	VDNKFNKECGRATGEIGALPNLNPQQYRAFILSLHDDC-NH_2
4.23	VDNKFNKECQQALGEISALPNLNLHQYYAFIRSLLDDC-NH_2
4.24	VDNKFNKECEGAMHEIVRLPNLNAWQRQAFIVSLWDDC-NH_2

C

Three-helix Z-domain	SPR K_d (nM)*	Two-helix peptide	TNFα-TNFR1 ELISA IC_{50}(nM)
Z-TNFα-1	0.77	**4.18**	22
Z-TNFα-2	1.7	**4.19**	570
Z-TNFα-3	6.6	**4.20**	790
Z-TNFα-P5	0.84	**4.21**	5300
Z-TNFα-200	ND	**4.22**	21,000
Z-TNFα-206	ND	**4.23**	18,000
Z-TNFα-186	ND	**4.24**	79

Figure 4.15 Two-helix α-peptides derived from different Z-domain-derivatives selected from display libraries. (A) Sequences of three-helix Z-domain analogues (different from **Z-TNFα**) selected for binding to TNFα, from refs[16, 26, 27]. Residues in red are those that were randomized to derive TNFα binding. (B) Designs of two-helix α-peptide analogues of the three-helix peptides from panel A. (C) (Left) Previously reported affinities for TNFα of three-helix peptides, as determined by SPR analysis (ND = not determined), and (right) IC_{50} values for each of the two-helix analogues, as determined by TNFα-TNFR1 competition ELISA. For oligomers with IC_{50} values < 10,000 nM, The uncertainty in the calculated IC_{50} values is ~2-fold, with a maximum variation of up to ~7-fold for some experiments.

We evaluated the ability of **4.18-4.24** to bind TNFα by competition ELISA in the presence of TWEEN20 (Figure 4.15C, right columns). We found that each of these peptides showed some ability to block the TNFα-TNFR1 interaction, although they varied significantly in their effectiveness. The relative affinities of these compounds roughly correlated with the

previously reported affinities for the full three-helix Z-domain peptides, as determined by SPR analysis (Figure 4.15C, left columns). These results indicate that the two-helix α-peptide scaffold is fairly good at mimicking these other Z-domains, and are particularly significant because they further emphasize the generalizability of designing two-helix Z-domain derivatives based on three-helix prototypes identified via display/selection processes. This ultimately suggests that the two-helix truncation strategy originally developed by Wells et al.[20, 22] and utilized by us to derive two-helix α/β-peptide mimics of various Z-domain peptides should be fairly general for a large number of Z-domain derivatives regardless of their primary sequences (as discussed in Chapter 3).

When we evaluated α-peptides **4.18-4.24** in a competition ELISA in the absence of TWEEN20, none of these peptides showed an ability to block TNFα from binding to immobilized TNFR1, indicating that each of these peptides also was dependent on TWEEN20 for TNFα binding (Figure 4.16). This suggests that most of the Z-domain analogues selected for binding to TNFα in the presence of TWEEN20 bind to sites that are not exposed in the absence of TWEEN20 (e.g., the oligomerization interface rather than the receptor binding region).

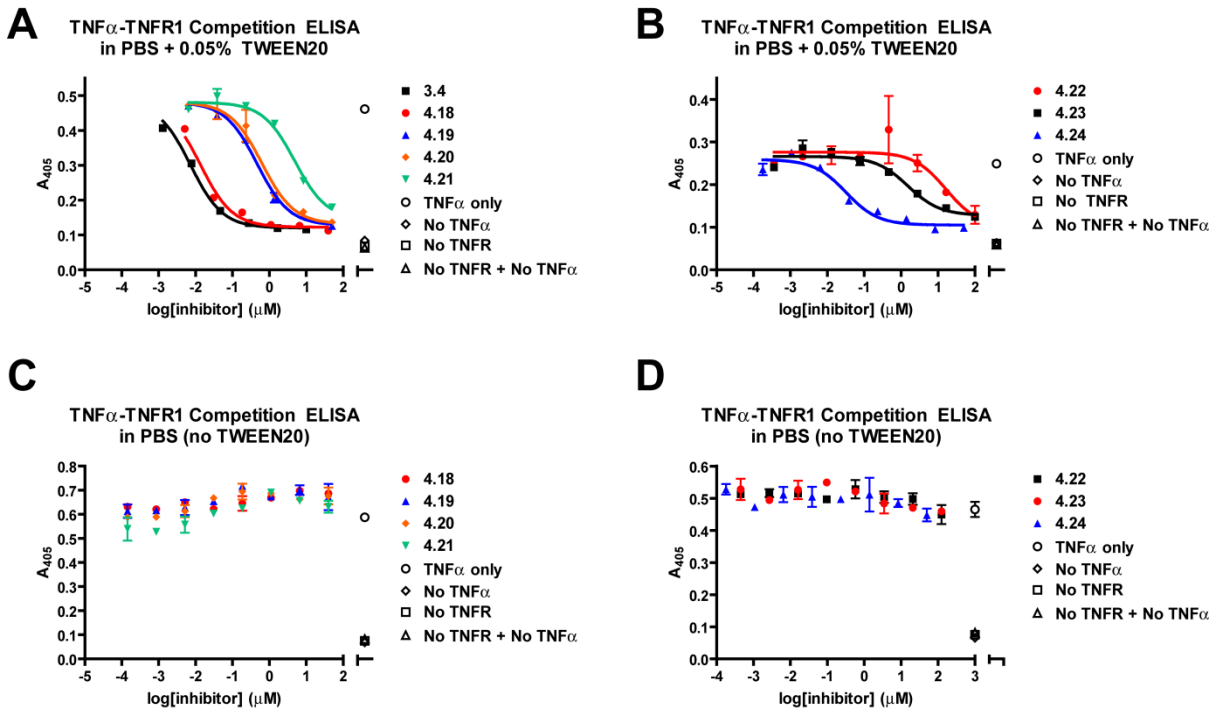

Figure 4.16 Representative TNFα-TNFR1 competition ELISA experiments evaluating the ability of **4.18-4.24** to block the TNFα-TNFR1 interaction in the presence of 0.05% TWEEN20 (A, B) and in the absence of TWEEN20 (C, D). In this experiment, all compounds are unable to block this interaction in the absence of TWEEN20.

4.7 Z-domain analogues synergize with TWEEN20 to block TNFα-mediated cell death

If **Z-TNFα** and its α/β-peptide analogues work with TWEEN20 to dissociate the TNFα trimer, then pre-incubation of TNFα under these conditions should inactivate the trimer from signaling in the WEHI-13VAR cytotoxicity experiments, since the full trimer is required for receptor activation by TNFα. To test this hypothesis, we pre-incubated TNFα in PBS+0.05% TWEEN20 in the presence or absence of potential inhibitors, conditions virtually identical to those utilized in the ELISA experiments, and then diluted this solution ~2000-fold so that the concentration for TNFα was in its active range (0.04 ng/mL), while the TWEEN20 concentration was negligible (0.000023%). When we performed the experiment in this manner, we saw that **Z-TNFα** and α/β-peptides derived from **Z-TNFα** were able to block TNFα-mediated death of WEHI-13VAR cells (Figure 4.17A and C), but not without pre-incubation in PBS+0.05%

TWEEN20 (Figure 4.17B). The antagonistic effect of these compounds was dose-dependent, and the relative potencies of these oligomers correlated to their potencies in the TNFα-TNFR1 ELISA experiments (Figure 4.17D), which is consistent with this being an on-target effect due to TNFα binding rather than some non-specific proliferative effect. For example, **Z-TNFα** and **4.5**, oligomers with low IC_{50} values by competition ELISA, each were relatively potent at inhibiting TNFα-mediated cell death (Figure 4.17). In contrast, **4.16** and **4.20**, α/β-peptides that displayed high IC_{50} values by ELISA, were significantly less potent at blocking TNFα signaling in cell culture, even though they were also pre-incubated in the PBS+TWEEN20 solution. Although in initial experiments (Figure 4.17A), the concentration of potential inhibitor was kept relatively high throughout the course of the experiment, we found that pre-incubation of TNFα with high concentrations of inhibitor in PBS+0.05% TWEEN20 was sufficient to rescue WEHI-13VAR cells from TNFα-mediated cell death, even after dilution ~2000-fold (Figure 4.17C). This suggests that this pre-incubation step inactivates TNFα and that this inactivation is not rapidly reversed upon dilution.

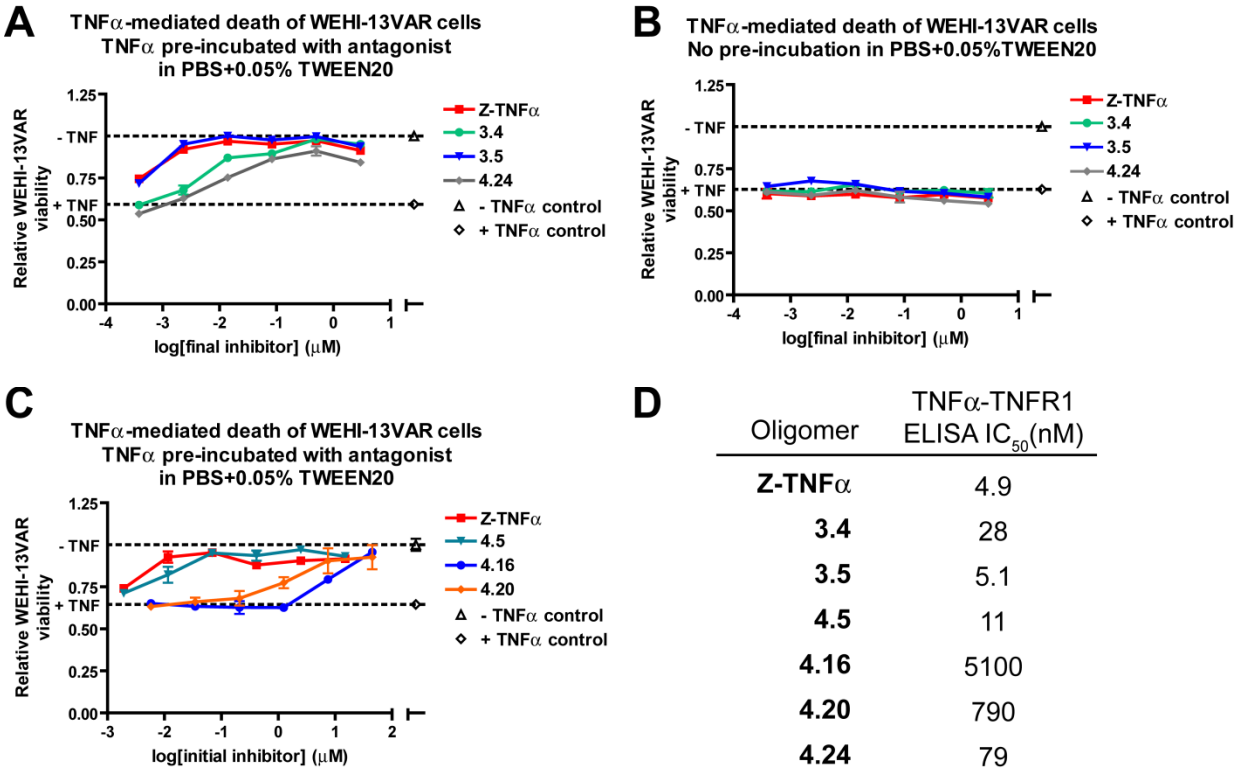

D

Oligomer	TNFα-TNFR1 ELISA IC_{50}(nM)
Z-TNFα	4.9
3.4	28
3.5	5.1
4.5	11
4.16	5100
4.20	790
4.24	79

Figure 4.17 Evaluation of potential TNFα antagonists to inhibit TNFα-mediated death of WEHI-13VAR cells, as determined by CellTiter-Glo viability assay. Cells were treated with TNFα (unfilled diamond, "+ TNF" dotted line) determine the dynamic range for each assay relative to untreated cells (unfilled triangle, "-TNF" dotted line). For evaluation of inhibitors, cells were treated with TNFα and the indicated concentration of compound. Luminescence data normalized to the average value for the "- TNFα" control to determine relative viability. Conditions for each assay were slightly different, as indicated: (A) Conditions: 8000 cells/well seeded in 96-well tissue culture plate and allowed to recover overnight, 0.04 ng/mL TNFα, 0.73 μg/mL actinomycin D, RPMI, 0.6% DMSO, 7% FBS, 0.000023% TWEEN20, penicillin/streptomycin (P/S). Potential inhibitors were pre-incubated with TNFα for 2 hours in PBS+0.05%TWEEN20 with 4% DMSO at 37 °C, 5% CO_2 with a top inhibitor concentration of 20 μM. After pre-incubation, conditions were diluted into RPMI ~2000-fold to achieve the final conditions, and additional peptide in DMSO was added to achieve the indicated final concentration, and the plate was read after ~20 hours. Data points represent mean ± SEM for n = 2 wells (for inhibitors) or n = 6 wells (for controls), and horizontal axis represents final peptide concentration. (B) Conditions: Same as in panel A, but potential inhibitors were mixed directly with TNFα in RPMI and a small amount of PBS/TWEEN (final concentration = 0.000023%) before adding to the plate, and the plate was read after ~20 hours. Data points represent mean ± SEM for n = 2 wells (for inhibitors) or n = 6 wells (for controls), and horizontal axis represents final peptide concentration. (C) Conditions: 8000 cells/well seeded in 96-well tissue culture plate and allowed to recover overnight, 0.04 ng/mL TNFα, 0.73 μg/mL actinomycin D, RPMI, 0.002% DMSO, 7% FBS, 0.000023% TWEEN20, P/S. Potential inhibitors were pre-incubated with TNFα for 1 hour in PBS+0.05%TWEEN20 with 4% DMSO at 37 °C, 5% CO_2. After pre-incubation, conditions were diluted into RPMI ~2000-fold to achieve the final conditions, and the plate was read after ~18 hours. Data points represent mean ± SEM for n = 2 wells (for inhibitors) or n = 6 wells (for controls), and horizontal axis represents initial peptide concentration during pre-incubation. (D) TNFα-TNFR1 competition ELISA IC_{50} values in the presence of PBS+0.05% TWEEN20, for comparison.

It is possible that TWEEN20 facilitates binding of these peptides by increasing the kinetics of subunit dissociation of the TNFα trimer, allowing the peptides to bind and prevent re-

association on the timescale of the experiments performed in this chapter.[24] To test this hypothesis, we attempted to incubate TNFα with peptides in medium without TWEEN20 for longer times (e.g., 24 hours) before evaluating them by ELISA or in cell-based experiments, but we saw a loss of TNFα activity under these conditions. Future experiments may be able to identify a protocol to observe the binding of **Z-TNFα** to TNFα after prolonged incubation in the absence of TWEEN20. Overall, these results show that pre-incubation of TNFα with Z-domain analogues in the presence of TWEEN20, but not TWEEN20 alone, inactivates TNFα and prevents this protein from inducing cell death. These results are consistent with the hypothesis that TWEEN20 and oligomers derived from TNFα-binding Z-domain peptides act synergistically to dissociate the active TNFα trimer.

4.8 Z-domain analogues synergize with SPD304

There are several reports of molecules that bind to the oligomerization interface of TNFα and dissociate the active trimer. One small molecule, SPD304 (Figure 4.2A), has been shown to act on TNFα by this mechanism.[14] However, SPD304 is not very potent and requires relatively high concentrations to block TNFα-mediated cell death. Because SPD304 dissociates the trimer and we believe that **Z-TNFα** and its analogues bind to a site on TNFα that is only exposed when the trimer is partially dissociated (e.g., by TWEEN20), we hypothesized that **Z-TNFα** and the analogues described in this chapter might work synergistically to inhibit the TNFα-TNFR interaction in the absence of TWEEN20. If this prediction were correct, this result would both provide further evidence in favor of our hypothesized mechanism for TNFα inhibition for this family of peptides and suggest a possible route for therapeutic utility of these compounds through co-administration with or conjugation to small molecules like SPD304.

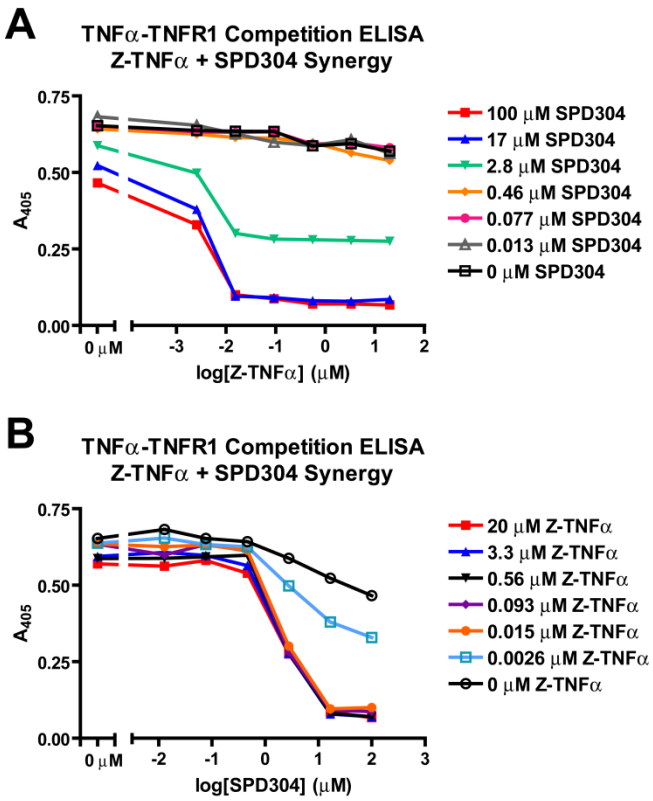

Figure 4.18 TNFα-TNFR1 competition ELISA evaluating the ability for **Z-TNFα** and SPD304 to synergize to block the binding of 0.09 μg/mL TNFα to immobilized TNFR1 in the absence of TWEEN20 (PBS only). Panels A and B show the same data, but plotted differently.

We first examined whether combinations of SPD304 and TNFα could block the TNFα-TNFR1 interaction in a competition ELISA experiment performed in the absence of TWEEN20. We titrated variable concentrations of both SPD304 and **Z-TNFα** and quantified the binding of TNFα to immobilized TNFR1 with an anti-TNFα antibody (Figure 4.18). In this experiment, we saw that SPD304 alone was a modest inhibitor of the TNFα-TNFR1 interaction, blocking ~70% of TNFα binding to TNFR1 at 100 μM (Figure 4.18B, "0 μM **Z-TNFα**" points). Consistent with our earlier findings, **Z-TNFα** alone showed essentially no ability to block the TNFα-TNFR1 interaction due to the absence of TWEEN20 from this experiment (Figure 4.18A, "0 μM SPD304" points). However, at 2.8 μM SPD304, **Z-TNFα** was able to block ~40% of TNFα

binding, and at concentrations ≥17 μM SPD304, **Z-TNFα** almost completely blocked the TNFα-TNFR1 interaction in a dose-dependent manner (Figure 4.18A).

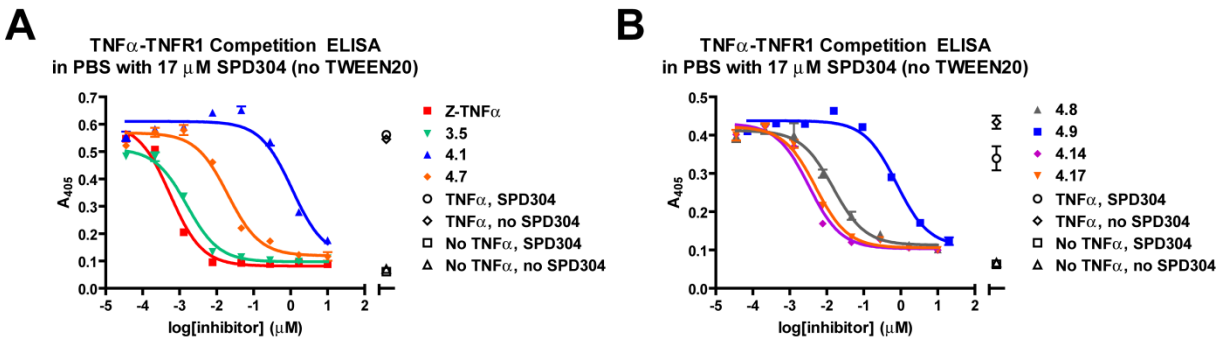

C

	TNFα-TNFR1 ELISA IC_{50}(nM)	
	Co-inhibitor:	
Oligomer	TWEEN20	SPD304
Z-TNFα	4.9	0.56
3.5	5.1	1.6
4.1	890	1100
4.7	24	20
4.8	29	15
4.9	1200	770
4.14	6.9	3.3
4.17	9.6	5.0

Figure 4.19 Z-TNFα and two-helix α- and α/β-peptide analogues block TNFα-TNFR1 interaction in the presence of 17 μM SPD304 as a "co-inhibitor". (A, B) Representative competition ELISA experiments showing the ability of several analogues to block the binding of 0.08 μg/mL TNFα to immobilized TNFR1. Points represent the mean ± SEM of duplicate wells on the plate. (C) Comparison of the IC_{50} values obtained for each oligomer in the presence of 0.05% TWEEN20 as co-inhibitor versus 17 μM SPD304 as co-inhibitor (derived from panels A and B).

We next evaluated several α- and α/β-peptides derived from **Z-TNFα** in competition ELISA experiments performed in the presence of 17 μM SPD304 without TWEEN20 (Figure 4.19). These experiments showed that each compound was able to block this protein-protein interaction in the presence of 17 μM SPD304 in a dose-dependent manner. The relative IC_{50} values for these α- and α/β-peptides agreed with the IC_{50} values seen in competition ELISA

experiments in the presence of TWEEN20, although these IC_{50} values were ~2-fold lower in the presence of SPD304 versus TWEEN20 for most of the Z-domain analogues. These results strongly suggest that SPD304 works via a mechanism similar to that of TWEEN20 to promote the binding of **Z-TNFα** and its derivatives to TNFα.

We evaluated the ability of SPD304 in combination with α/β-peptide **4.17** to dissociate the TNFα oligomer, as judged by SEC (Figure 4.20). When 40 μg/mL TNFα was incubated with 120 μM SPD304 in PBS with 4% DMSO, the area of the peak in the SEC corresponding to a higher order oligomer (trimer or dimer) remained constant over the course of ~50 minutes, suggesting that SPD304 alone is not sufficient to completely dissociate oligomeric TNFα under these conditions. Although the elution time was similar, we observed that the shape of this peak appeared to be slightly broader under these conditions than in many of the examples without SPD304 (Figure 4.25I in "Experimental Methods" section). This difference in peak shape could be a result of SPD304 binding to TNFα, either leading to a more heterogeneous mixture of TNFα+SPD304 species or dissociating some trimer into dimer. In contrast, in the presence of 44 μM α/β-peptide **4.17**, we saw almost a complete disappearance of this peak by the first time point (2 minutes) (Figure 4.20A). A comparison of the SEC chromatograms resulting from 49 minutes of incubation with 44 μM **4.17** in PBST versus 44 μM **4.17** in PBS with 120 μM SPD304 showed that these mixtures were very similar, both showing an additional peak at ~4.2 minutes that likely correspond to monomeric TNFα (Figure 4.20B). Ultimately, these results suggest that the combination of **4.17** with SPD304 (but not this concentration of SPD304 alone) leads to dissociation of the higher order oligomeric TNFα, likely in a very similar manner to the combination of **4.17** with TWEEN20 discussed above.

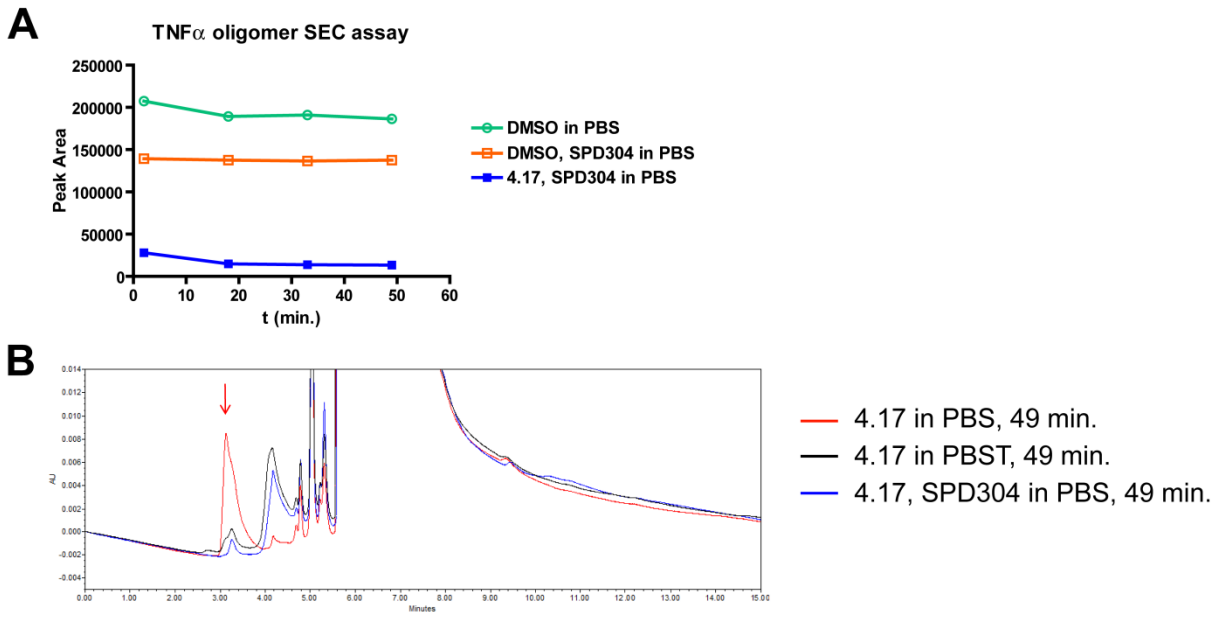

Figure 4.20 SPD304 acts synergistically with **4.17** to dissociate the TNFα oligomer. (A) Monitoring of the oligomeric TNFα peak over time by SEC, as determined by peak area at 220 nm. 40 μg/mL TNFα was incubated in PBS with 4% DMSO (green), with 120 μM SPD304 (orange), or with 44 μM **4.17** and 120 μM SPD304 (blue). Data for "DMSO in PBS" condition is the same as from Figure 4.14. For other conditions, data represent the area from a single experiment. (B) Overlay of the chromatograms resulting from incubating 40 μg/mL TNFα with 44 μM **4.17** in PBS with 4% DMSO for 49 minutes (red), 40 μg/mL TNFα with 44 μM **4.17** in PBST with 4% DMSO for 49 minutes (black), and 40 μg/mL TNFα with 44 μM **4.17** and 120 μM SPD304 in PBS with 4% DMSO for 49 minutes (blue). The native TNFα oligomer peak is indicated by the red arrow.

We next evaluated whether SPD304 could be used in combination with **Z-TNFα** or its α/β-peptide analogues to block the TNFα-mediated death of WEHI-13VAR cells. TNFα was pre-incubated in PBS with 17 μM SPD304 (no TWEEN20) in the presence of varying concentrations of Z-domain analogues, and then diluted this solution ~500-fold to reach final conditions of 0.17 ng/mL TNFα, 0.79 μg/mL actinomycin D, 36 nM SPD304, and 21 nM-0.0027 nM potential inhibitor. Following this protocol, we saw that pre-incubation with 17 μM SPD304 alone was not effective at blocking TNFα-mediated cell death (Figure 4.21, "TNFα, SPD304" controls). In contrast, **Z-TNFα**, α-peptide **4.1**, and α/β-peptides **3.5** or **4.17** in combination with SPD304 was effective at completely blocking cell death induced by TNFα in a dose-dependent manner (Figure 4.21). The relative effectiveness of these compounds at blocking TNFα-mediated cell death is in agreement with their relative IC_{50} values in the competition ELISA experiments

(Figure 4.19C). These observations indicate that these Z-domain peptides act synergistically with SPD304 to block TNFα signaling.

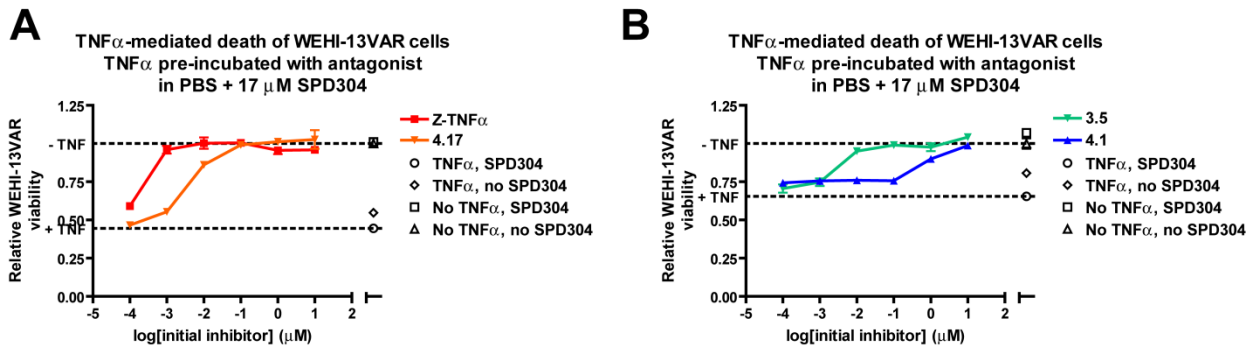

Figure 4.21 Evaluation of potential TNFα antagonists to inhibit TNFα-mediated death of WEHI-13VAR cells, as determined by CellTiter-Glo viability assay. Cells were treated with TNFα and SPD304 (unfilled circle, "+ TNF" dotted line) or without TNFα or SPD304 (unfilled triangle, "-TNF" dotted line) to determine the dynamic range for each assay. For evaluation of inhibitors, cells were treated with TNFα, SPD304, and the indicated concentration of compound. Luminescence data normalized to the average value for the "No TNFα, no SPD304" control to determine relative viability. Conditions for each assay were slightly different, as indicated: (A) Conditions: 8000 cells/well seeded in 96-well tissue culture plate and allowed to recover overnight, 0.17 ng/mL TNFα, 0.79 μg/mL actinomycin D, RPMI, 0.008% DMSO, 7% FBS, 36 nM SPD304, penicillin/streptomycin (P/S). Potential inhibitors were pre-incubated with TNFα for ~2 hours in PBS, 17 μM SPD304, 4% DMSO at room temperature. After pre-incubation, conditions were diluted into RPMI ~500-fold to achieve the final conditions, and the plate was read after ~20 hours. Data points represent mean ± SEM for n = 3 wells (for inhibitors) or n = 6 wells (for controls), and horizontal axis represents initial peptide concentration during pre-incubation. (B) Conditions: Same as in panel A, but the plate was read after ~15 hours.

4.9 Conclusions

In this chapter, I have described two studies focused on Z-domain-derived oligomers targeting TNFα. First, we have shown that we can significantly minimize two-helix α/β-peptide analogues of **Z-TNFα** derived from the "parent" scaffold developed in Chapter 2. Specifically, α/β-Peptide **4.17** contains a novel disulfide bond position that has not previously been used in two-helix Z-domain analogues and contains 29 residues, which is less than half the length of the parent **Z-TNFα** and 9 residues shorter than its direct two-helix parent **3.5**. In spite of its minimized length, α/β-peptide **4.17** blocks the TNFα-TNFR1 interaction with nearly identical affinity as **Z-TNFα**, yet is >4000-fold less susceptible to protease degradation than the two-helix α-peptide **4.2** and >150-fold less susceptible than the three-helix α-peptide **Z-TNFα**.

In contrast to the **Z-VEGF** system described in Chapter 2, properly designed two-helix analogues of **Z-TNFα** do not require a structure-stabilizing disulfide bond for effective blocking of the TNFα-TNFR1 interaction, although a disulfide does increase the affinity for TNFα and reduce the susceptibility to protease degradation of these compounds. This lack of requirement for a disulfide could mean that a relatively small number of side chains are critical for TNFα binding, and the rest of the peptide need not be fully folded to facilitate these interactions. Alternatively, the propensity of the residues in **Z-TNFα** to adopt the correct fold may be higher than those of **Z-VEGF**, allowing for an easier "induced fit" upon protein binding. Very intriguingly, the comparison between the competition ELISA IC_{50} values for α-peptide **4.1** (890 nM) versus α/β-peptides **4.7** and **4.8** (24 nM and 28 nM, respectively) suggests that the helix-promoting non-natural residues (Aib and cyclic β-residues) present in the α/β-peptides promote the correct TNFα-binding conformation more effectively than do the native α-residues that were replaced. This result suggests that the α/β-peptide design strategy described here may generally be used to increase affinity over that of the parent α-peptide containing a natural backbone. Indeed, this hypothesis is consistent with modestly higher K_i value for several **Z-VEGF** analogues (Chapter 2) over the parent α-peptide. However, the far-UV CD signature (mean residue ellipticity) for the unconstrained α/β-peptides **4.8**, **4.10**, and **4.11** do not adopt significant helical structure in solution (Figure 4.6). Thus, the reason for the higher affinity of some unconstrained analogues over others (e.g., **4.8** versus **4.11**) is likely more complex than simply having higher helix content in solution.

Efforts to optimize **Z-TNFα** ultimately show that although the general strategy for designing α/β-peptide mimics of Z-domains described in Chapter 3 can be used to rapidly obtain α/β-peptides targeting a diverse variety of protein surfaces, each system is slightly different and

may be amenable to further optimization. The modifications explored in this chapter (removing terminal residues, relaxing the disulfide constraint, incorporation of alternative disulfide positions, etc.) can be explored in the context of two-helix α/β-peptide analogues of other Z-domain peptides. For example, if the initial design of an α/β-peptide based on a three-helix Z-domain fails because the residues replaced by cysteine make critical contacts with the protein target, one can attempt the alternative disulfide bond positions identified in this chapter.

The second major study reported in this chapter investigates the mechanism by which **Z-TNFα** and its analogues bind to TNFα and block receptor binding. The experimental evidence reported here strongly suggests that **Z-TNFα** binds to TNFα prevents productive receptor binding by dissociating the active trimer. The binding of **Z-TNFα** to TNFα is dependent on TWEEN20, a detergent used during the selection of **Z-TNFα** from a phage library to reduce non-specific binding. Some detergents can dissociate the TNFα timer at low protein concentrations,[6, 24] and several peptides have been reported in the literature that are dependent on TWEEN20 for TNFα binding.[17, 18] Importantly, the small molecule SPD304, which is known to dissociate the TNFα trimer, can also work synergistically with **Z-TNFα** and its α/β-peptide analogues to block TNFα-TNFR binding. We propose a mechanism in which TWEEN20 (or SPD304) partially opens up the TNFα trimer to allow productive binding of **Z-TNFα** to a binding site on the interior of the trimer (possibly at the oligomerization interface on the monomer or the dimer), leading to dissociation of the active trimer (Figure 4.22).

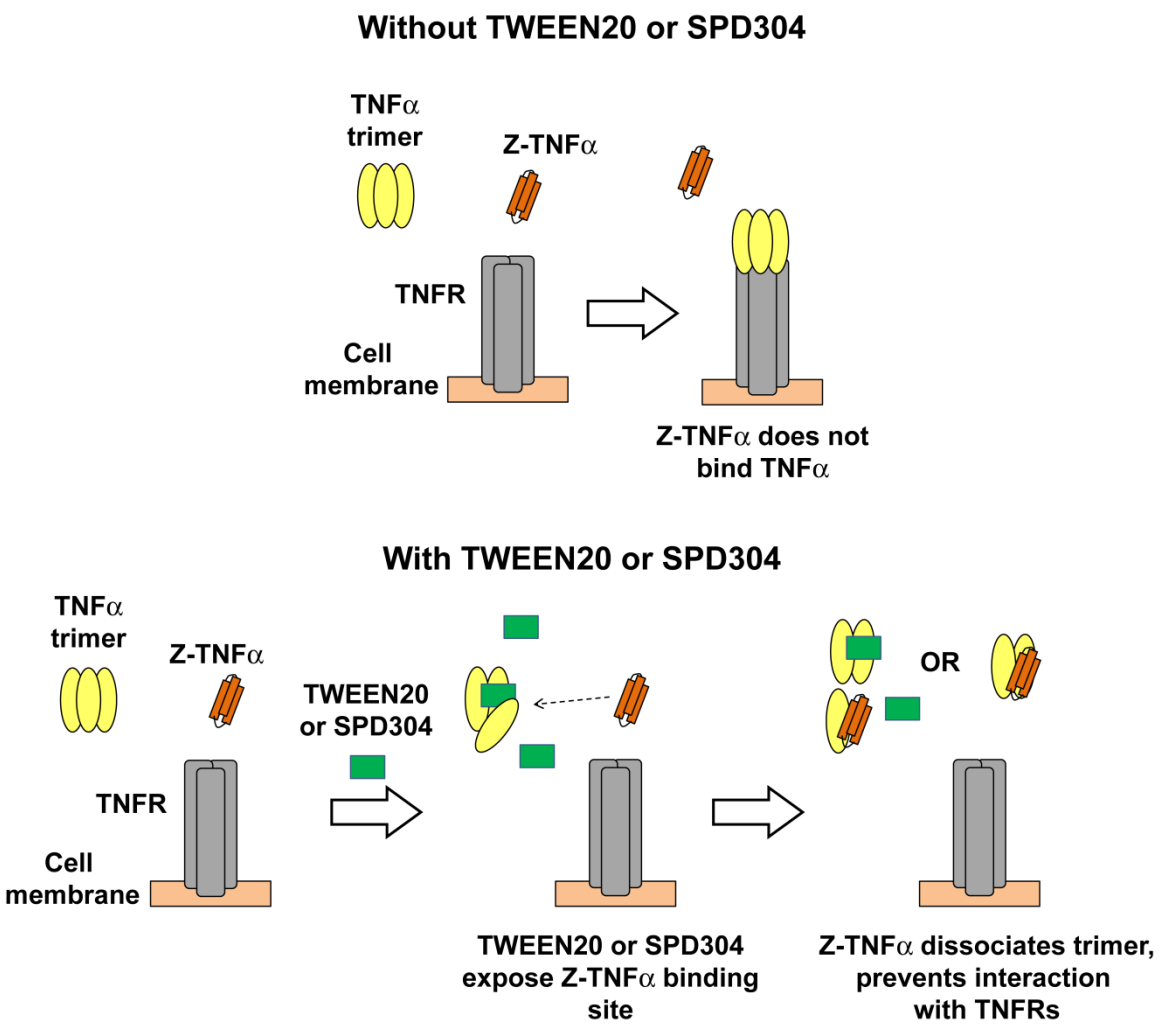

Figure 4.22 Proposed mechanism for the antagonism of TNFα by a combination of **Z-TNFα** and either TWEEN20 or SPD304, based on the experiments reported in this chapter.

The selection of **Z-TNFα** to bind to this alternative site, rather than to the intended site at which the TNFα trimer contacts the receptors, was most likely a result of carrying out all of the selection steps from the phage display library in the presence of TWEEN20,[16] which presumably opened up alternative binding sites on the non-covalent trimer during the selection procedure. The fact that two-helix analogues derived from seven different parent Z-domains all showed a dependence on TWEEN20 for binding (**Z-TNFα** and analogues, as well as α-peptides **4.18-4.24**) suggests that alternative binding sites revealed in the presence of such detergents resemble "hot spots" for derived affinity reagents,[28] possibly due to a high density of

hydrophobic side chains that are buried under normal physiological conditions. One interesting observation is that one of the truncated two-helix α-peptides, **4.21**, is derived from a three-helix parent Z-domain peptide (**Z-TNFα-P5**, Figure 4.15) that was selected not using display technologies in the presence of TWEEN20, but instead using a protein fragment complementation assay (PCA) which occurs inside an *E. coli* cell.[27, 29] In this PCA experiment, the Z-domain and TNFα are each expressed fused to a fragment of an enzyme. When a Z-domain binds to TNFα inside *E. coli* cell periplasm, the enzyme fragments come into close enough proximity to reconstitute enzymatic activity, giving an experimental readout for peptide+TNFα binding. TWEEN20 is not present in the periplasm of the *E. coli* cell, and so it is unclear why the two-helix analogue **4.21** still showed a dependence on TWEEN20 for binding in our TNFα-TNFR1 competition ELISA. Furthermore, **Z-TNFα**,[16] the parent Z-domain described in detail in both Chapter 3 and in this chapter, was also reported to have activity in this PCA experiment.[27] One possible explanation for this observation is that the TNFα protein expressed in the periplasm of the *E. coli* cells in the PCA assay is at a low enough concentration that it is monomeric rather than trimeric, which would facilitate the binding of **Z-TNFα** and other such Z-domain analogues to the alternative binding site hypothesized here. Consistent with this hypothesis, Lofdahl et al. reported an SDS-PAGE analysis of the *E. coli* periplasm from the PCA experiment which shows that the amount of TNFα present during selection is below the levels of detection by gel electrophoresis.[29]

Ultimately, the results reported here caution against using only one set of conditions for the selection of novel affinity proteins from randomized libraries, as this approach may select for binding under this condition only. This concern is especially critical for proteins of therapeutic interest such as TNFα, which often have an intended end use in biological systems. Many

research groups have attempted to derive novel peptides and proteins targeting TNFα using a variety of strategies,[11, 12, 15-18, 26, 27, 29] and perhaps are unaware of the unintentional consequences of using such additives during selection and characterization experiments. It is unclear if this behavior is unique to TNFα, is a phenomenon common to other non-covalent oligomers, or generally applies to many proteins for which binding molecules have been selected from display libraries.

4.10 Future directions

Alone, the TNFα-binding compounds described in this chapter are unlikely to be useful in biological systems due to their poor ability to bind TNFα in the absence of molecules like TWEEN20 or SPD304. However, the results described in this chapter suggest several immediate directions to pursue to derive α/β-peptides targeting TNFα that may be useful for future therapeutic applications.

Selection of new TNFα-binding Z-domain derivatives from phage/yeast display libraries in the absence of TWEEN20 should identify novel three-helix α-peptides that do not bind at the oligomerization interface. These new peptides may bind to the receptor binding surface of TNFα, and thus could be useful as TNFα antagonists under conditions of biological relevance, such as cell culture media or in animals. Because of the general nature of the α/β-peptide design strategy for mimicking three-helix Z-domain peptides (Chapter 3), it should then be relatively easy to derive two-helix α/β-peptides from these new peptides to target this same surface on the TNFα trimer. These compounds could be evaluated in cell culture in the absence of TWEEN20 or SPD304 pre-incubation. If these compounds blocked TNFα signaling, they could then be evaluated in animal models of inflammatory or autoimmune diseases caused by misregulated TNFα signaling.

Although the selection of entirely novel Z-domain derivatives represents one route toward deriving effective TNFα-binding α/β-peptides, the results described in this section also suggest a potentially different route for TNFα inhibition. **Z-TNFα** and its analogues appear to bind to a site that is accessible only in the presence of certain molecules (TWEEN20, SPD304). It may be possible to take advantage of this behavior to derive α/β-peptides that inhibit TNFα via a novel mechanism of action. One approach may be to conjugate one of the α/β-peptides described in this chapter (e.g., **4.17**) to SPD304 (Figure 4.23A). These SPD304+α/β-peptide conjugates may be able to access the internal α/β-peptide binding site through the SPD304 moiety then and efficiently dissociate the TNFα trimer.

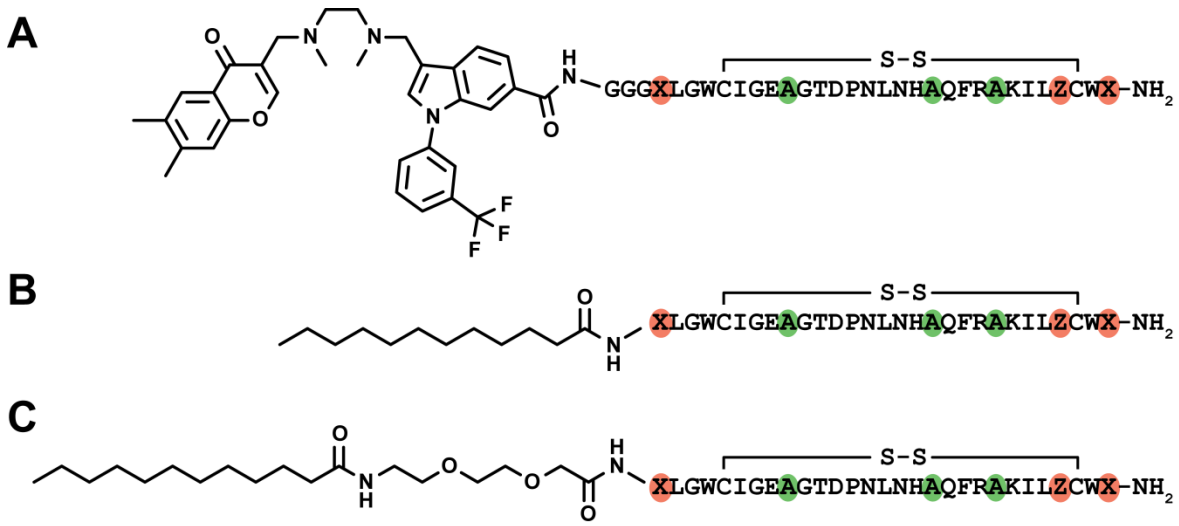

Figure 4.23 Proposed analogues of α/β-peptide **4.17** bearing groups that may allow for TNFα dissociation from a single agent. (A) Structure of an analogue of **4.17** conjugated to a modified SPD304 molecule. (B) Structure of an analogue of **4.17** conjugated to a 12-carbon fatty acid. (C) Structure of an analogue of **4.17** conjugated to a 12-carbon fatty acid with a small polyethylene glycol (PEG) spacer.

Inspection of the chemical structures of the detergents TWEEN20, TWEEN80, and Pluronic F68 (Figure 4.10C) suggests an additional strategy for developing an α/β-peptide antagonist of TNFα signaling. TWEEN20 features a 12-carbon fatty acid chain in addition to a large number of PEG groups and a central sugar. TWEEN80 differs from TWEEN20 in that it

has a different structure in its fatty acid tail, and this compound was only partially effective at facilitating binding of **Z-TNFα** to TNFα (Figure 4.10B). This result suggests that the identity of the fatty acid chain in these detergents may play a critical role in exposing **Z-TNFα**'s internal binding site. Consistent with this hypothesis, Pluronic F68, a detergent that has no fatty acid chain, does not facilitate binding of **Z-TNFα** to TNFα (Figure 4.10A). These observations suggest that the presence of a fatty acid group alone may be sufficient to promote exposure of **Z-TNFα**'s binding site, and that an α/β-peptide analogue containing an acyl chain (e.g., 12-carbon chain projecting from the N-terminus, as depicted in Figure 4.23B and C) may be able to access this binding site in the absence of other exogenous molecules. This strategy is especially intriguing as it would likely provide additional benefits such as increased plasma residence time due to reduced renal clearance.[30]

Finally, if none of the above directions yields positive results, co-injection of the α/β-peptides described in this chapter with SPD304 may be effective at blocking TNFα-based signaling in animal models. The ultimate goal is to identify α/β-peptide antagonists of TNFα and conditions for their administration that can be utilized in animals, and then to determine whether the non-natural backbone provides benefits (such as increased half-life due to decreased proteolytic susceptibility) relative to the natural α-peptide backbone that may be applied for the eventual design of therapeutic agents targeting the TNFα signaling pathway.

4.11 Experimental methods

4.11.1 General

Fmoc-protected α-amino acids with compatible side chain protecting groups and benzotriazole-1-yl-oxy-tris-pyrrolidino-phosphonium hexfluorophosphate (PyBOP) were

purchased from Chem-Impex International and Novabiochem. Fmoc-protected β^3-amino acids with compatible side chain protecting groups were purchased from PepTech Corporation and Chem-Impex International. Fmoc-ACPC-OH was purchased from Chem-Impex International (15073). Fmoc-APC(Boc)-OH was synthesized as previously described.[31]

4.11.2 Peptide synthesis and purification

The preparation of α- and α/β-peptides was carried out exactly as described in Chapter 2. After purification, final peptide purity was assessed by analytical HPLC, and identity was confirmed by MALDI-TOF-MS ("Peptide characterization" section below).

4.11.3 TNFα-TNFR1 competition ELISA

The binding of α- and α/β-peptides to TNFα to block the TNFα-TNFR1 interaction was assessed by competition ELISA, as described in Chapter 3. Unless otherwise noted, the final concentration of TNFα in these experiments was 0.08 μg/mL. For ELISA experiments in which the TNFα-TNFR1 interaction was evaluated under different buffer conditions (e.g., without TWEEN20 or in RMPI media), these conditions apply only to the solutions containing TNFα (specifically, the TNFα+inhibitor pre-incubation step and the subsequent addition of this solution onto the ELISA plate to allow TNFα to bind immobilized TNFR1). All subsequent steps, such as washes and incubation with antibodies, were performed with PBS+0.05% TWEEN20, as described in Chapter 3. To compare the abilities of soluble α- or α/β-peptides to inhibit the binding of TNFα to immobilized TNFR1, IC_{50} values were calculated by fitting the ELISA absorbance data to a sigmoidal dose-response equation using GraphPad Prism 4.0 (Figure 4.24). For some oligomers, there were not enough points either at the top or bottom of the curve to confidently fit these data. In these cases, the top or bottom was held constant as a shared value

for all data sets based on the value fit for other inhibitors in that same experiment. Experiments that were fit using shared top or bottom are indicated in the caption for Figure 4.24. In this chapter, the reported IC_{50} values represent the mean IC_{50} value for at least two independent competition ELISA experiments evaluating that particular compound. The uncertainty in the calculated IC_{50} values is ~2-fold, with a maximum variation of up to ~7-fold for some experiments (See section 4.2.4 above). A full table of IC_{50} values for each panel in Figure 4.24 is displayed in Table 4.1.

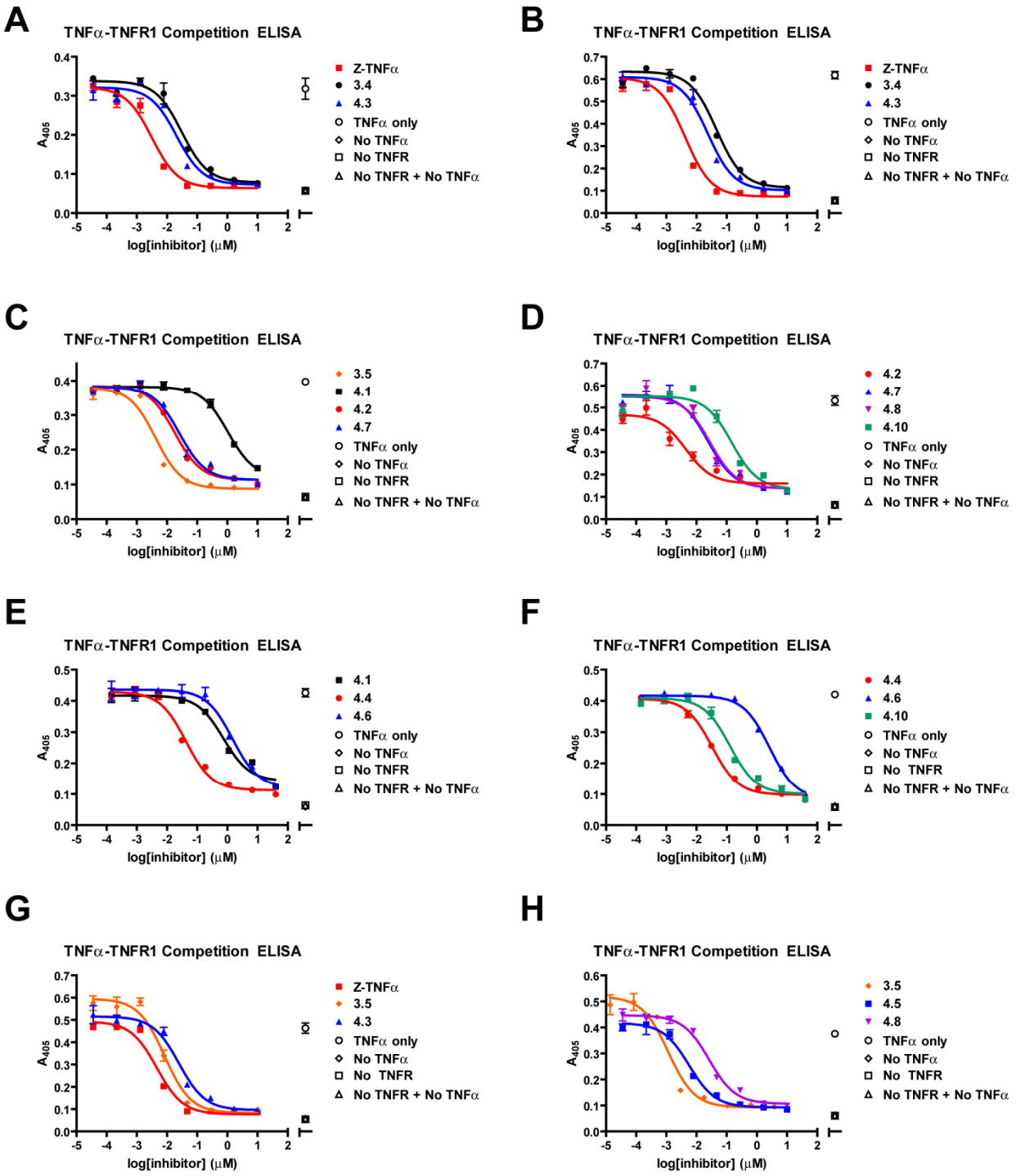

Figure 4.24 (A-H) Representative TNFα-TNFR1 competition ELISA assays for compounds reported in this chapter.

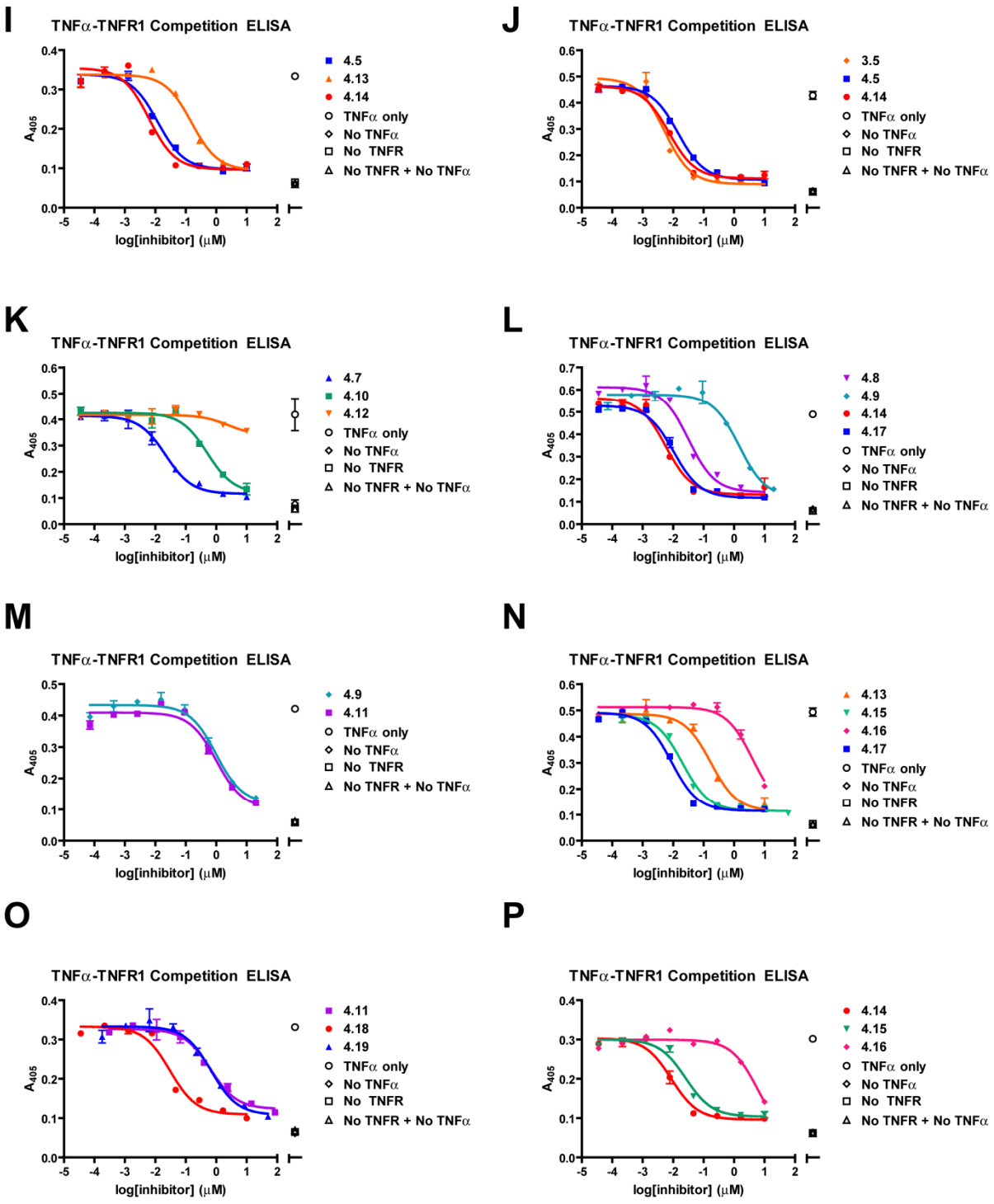

Figure 4.24 (I-P) Representative TNFα-TNFR1 competition ELISA assays for compounds reported in this chapter. In panel N, the bottom value is shared for all data sets.

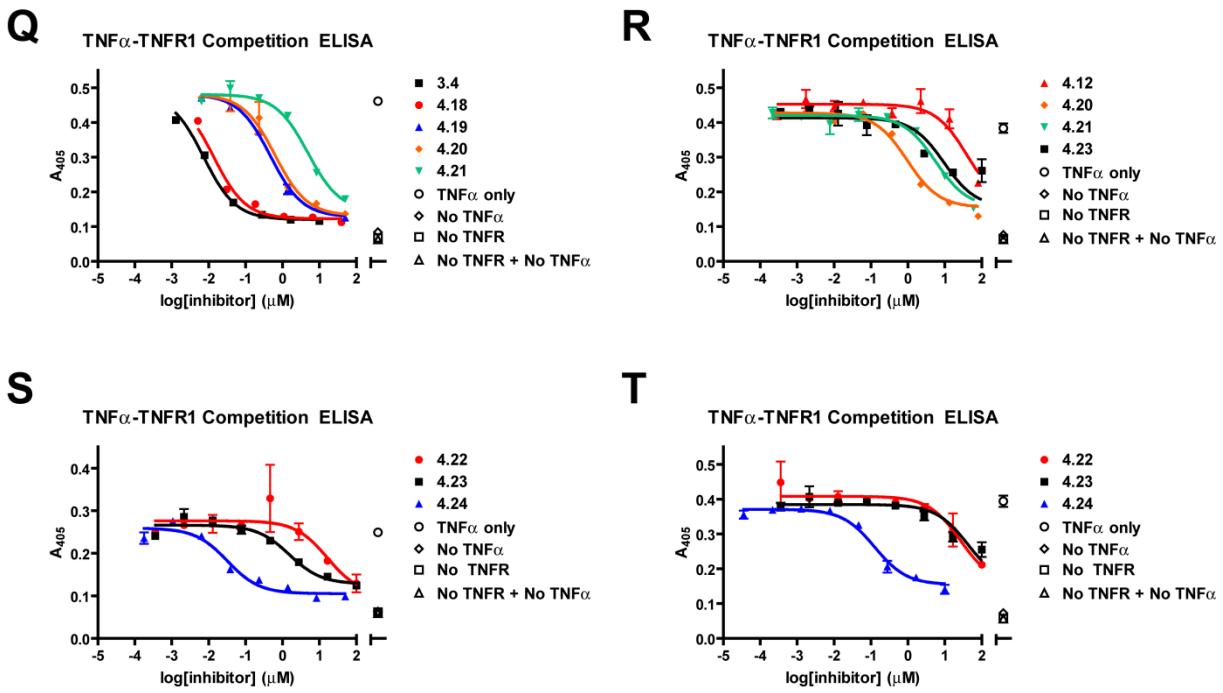

Figure 4.24 (Q-T) Representative TNFα-TNFR1 competition ELISA assays for compounds reported in this chapter. In panel Q, the top value is shared for all data sets. In panels R and T, the bottom value is shared for all data sets.

		IC_{50} (nM) (Panel from Figure 4.24 shown in parentheses)
Peptide	**Z-TNFα**	4.8 (Chapter 3, Figure 3.29A), 3.1 (A), 4.2 (B), 7.6 (G)
	3.4	30 (Chapter 3, Figure 3.29A), 30 (A), 46 (B), 7.3 (Q)
	3.5	6.6 (Chapter 3, Figure 3.29A), 4.1 (C), 8.2 (G), 1.1 (H), 5.2 (J)
	4.1	1030 (C), 740 (E)
	4.2	18 (C), 4.4 (D)
	4.3	21 (A), 24 (B), 25 (G)
	4.4	42 (E), 33 (F)
	4.5	5.6 (H), 12 (I), 14 (J)
	4.6	1500 (E), 2600 (F)
	4.7	26 (C), 25 (D), 22 (K)
	4.8	28 (D), 26 (H), 32 (L)
	4.9	1500 (L), 1000 (M)
	4.10	150 (D), 130 (F), 510 (K)
	4.11	1010 (M), 640 (O)
	4.12	>10,000 (K), 41,000 (R)
	4.13	150 (I), 170 (N)
	4.14	6.2 (I), 7.2 (J), 5.6 (L), 8.7 (P)
	4.15	20 (N), 26 (P)
	4.16	4100 (N), 6000 (P)
	4.17	10 (L), 8.9 (N)
	4.18	30 (O), 14 (Q)
	4.19	680 (O), 470 (Q)
	4.20	630 (Q), 960 (R)
	4.21	4900 (Q), 5600 (R)
	4.22	16,000 (S), 27,000 (T)
	4.23	9500 (R), 1500 (S), 42,000 (T)
	4.24	32 (S), 130 (T)

Table 4.1 IC_{50} values obtained for each of the compounds reported in Figure 4.24. Note that each value reported here is rounded to 2 significant figures. The averages reported in the main text were calculated using the values fit from the dose-response model, and then rounded to 2 significant figures.

4.11.4 α/β-Peptide 3.5-TNFα competition ELISA

For α/β-peptide **3.5**-TNFα Competition ELISA, α/β-peptide **3.5** was covalently immobilized to the plate by adding 100 μL of 1.15 μM **3.5** (diluted from DMSO stock solution) in sodium carbonate, pH 9.8 into each well of a Nunc Immobilizer Amino plate. The plate was incubated at room temperature for ~2 hours, and then washed with PBS+0.05% TWEEN20 and blocked with 10 mM ethanolamine in sodium carbonate, pH 9.8 at room temperature for ~1.5 hours. Solutions of TNFα (final concentration = 0.25 μg/mL) were prepared in various buffer conditions (in PBS+0.05%TWEEN20, in PBS with no TWEEN20, or in PBS+0.05% TWEEN20+1% BSA) and then mixed with serial dilutions of soluble **3.5** in DMSO (final DMSO concentration = 4%) and pre-incubated at room temperature for ~1 hour. After blocking of the ELISA plate and pre-incubation of soluble **3.5** with TNFα, the ELISA plate was washed with PBS+0.05% TWEEN20, and then 100 μL of each **3.5**+TNFα dilution was added to the ELISA plate, which was allowed to incubate at room temperature for ~2 hours. The plate was then washed with PBS+0.05% TWEEN20, and the bound TNFα was detected by the addition of 100 μL of 0.40 μg/mL of human TNFα biotinylated antibody (R&D Systems, BAF210) in PBS+0.05% TWEEN20, and the plate was then incubated at room temperature for ~1 hour. The plate was then washed with PBS+0.05% TWEEN20, and then 100 μL of 1:1000 dilution of streptavidin-alkaline phosphatase (R&D Systems, AR001) in PBS+0.05% TWEEN20 was added to each well, and the plate was incubated for 30 minutes. The plate was then washed with PBS+0.05% TWEEN20, and then 50 μL of SIGMA*FAST* p-nitrophenyl phosphate (pNPP) solution (Sigma, N1891) was added to each well, and the alkaline phosphatase reaction allowed to proceed at room temperature. Plates were read (absorbance at 405 nm) during the time course of the reaction on a BioTek Synergy 2 microplate reader.

4.11.5 IgG1-κ competition ELISA

The IgG competition ELISA experiment shown in Figure 4.13 was performed as described in Chapter 3 to determine the ability of soluble α/β-peptide **3.2** to compete with immobilized **3.2**+BSA conjugate for binding to 9 μg/mL IgG1-κ, as detected using goat anti-human IgG (Fab specific)-alkaline phosphatase antibody. For the "1% BSA" conditions, BSA was not included during washing steps or in the antibody solution.

4.11.6 Circular dichroism (CD) spectroscopy

Circular dichroism measurements were performed on an Aviv Model 420 circular dichroism spectrometer. Solutions of α- and α/β-peptides were prepared in PBS, pH 7.5. Spectra were collected at 20 °C in a 0.1 cm quartz cell with a wavelength step size of 1 nm and a 5 second averaging time. Spectra were normalized to mean residue ellipticity, [θ] (deg cm^2 $dmol^{-1}$ res^{-1}), using the exact concentration determined by UV absorbance at 280 nm[32] to account for slight variations in concentration between solutions, using the Equation (1),[33] described below:

(1) $[\theta] = \theta/(l * c * \#res)$

Where:
θ = blank-corrected ellipticity value from CD spectrometer (in mdeg)
l = pathlength (in mm)
c = concentration of peptide (in M)
#res = the number of residues in the peptide

The mean residue ellipticity values ([θ]) obtained were then multiplied by 10^{-3} for plotting in the graphs shown in this chapter.

4.11.7 Protease digestion assay

Stock solutions of 50 μg/mL proteinase K were prepared in Tris-buffered saline (TBS), pH 7.5. Solutions of ~200 μM α-peptide or α/β-peptide in TBS were prepared, and their

concentrations were determined by UV absorbance at 280 nm.[32] For each proteolysis reaction, the α- or α/β-peptide stock solution was diluted with TBS to achieve a final concentration of 40 μM. Proteinase K stock solution was added (final concentration = 10 μg/mL), and the reaction was allowed to proceed at room temperature. For each time point, an aliquot of the protease reaction was quenched 1:2 with 50% H_2O/acetonitrile with 1% TFA. The quenched solution (e.g., 5 μL) was then injected onto UPLC and eluted with a 10-60% [acetonitrile+0.1%TFA]/[water+0.1% TFA] gradient over 5 minutes, 0.3 mL/min flow rate. The relative amount of peptide remaining was quantified by integration of the peak at 220 nm in a series of UPLC chromatograms. Each reaction was run at least in duplicate. Half-lives were determined by fitting the time course of peptide degradation to an exponential decay model using GraphPad Prism 4.0.

4.11.8 WEHI-13VAR cell viability assays

Below is a general outline of the protocol used for WEHI-13VAR cell viability assays. Each experiment used slightly different conditions, which are explicitly indicated in the corresponding Figure captions above. WEHI-13VAR mouse fibrosarcoma cells (ATCC, CRL-2148) were cultured using RMPI-1640 medium (RPMI) (ATCC, 30-2001) supplemented with 10% fetal bovine serum (FBS) and penicillin/streptomycin (P/S) (HyClone, SV30010) at 37 °C in 5% CO_2. For a given experiment, cells were trypsinized and reseeded into sterile tissue culture treated clear bottom, white walled 96-well plates at a cell density of 8000-10,000 cells/well in 100 μL of RMPI+10% FBS+P/S (except for the experiment shown in Figure 4.8A, in which the cells were seeded in 100 μL in RPMI+0.1% FBS+P/S). Dilutions of TNFα (R&D Systems, 210-TA-020) were made into the appropriate media (PBS, PBS/TWEEN20, RPMI, etc.). These TNFα dilutions were then mixed with serial dilutions of potential inhibitor (in either PBS or

DMSO) and the TNFα+inhibitor mixtures were pre-incubated, as indicated in each Figure caption. For controls with no inhibitor candidate, the same amount of PBS or DMSO was diluted into TNFα solution. Controls without TNFα were treated in the same manner, using PBS instead of the TNFα stock solution. For experiments containing SPD304, a 3000 μM stock solution of SPD304 (Sigma, S1697) was prepared in water, and this solution was diluted appropriately for the pre-incubation steps. For SPD304 experiments, which contained both "TNFα, SPD304" and "TNFα, no SPD304" controls, we obtained the most reproducible results by preparing a 0.1 μg/mL TNFα solution in PBS, and then using this same solution for both of these control conditions as well as experimental conditions by adding inhibitor (or DMSO) and SPD304 (or water). After the appropriate pre-incubation, these solutions containing TNFα and inhibitors were serially diluted into RPMI, and then 50 μL of this solution was added to the appropriate wells (to make 150 μL total volume in each experimental well) to give the final experimental conditions indicated. Plates were then incubated at 37 °C, 5% CO_2 to allow TNFα to induce cell death. After this incubation, plates were removed from the incubator, and cooled to room temperature for ~20-30 minutes, and then 150 μL of CellTiter-Glo reagent (Promega, G7571) was added to each well. The plate was agitated for 2 minutes on an automated shaker, and then luminescence was read on a BioTek Synergy 2 microplate reader. The data displayed in each figure were normalized to "Relative WEHI-13VAR viability" by dividing the raw luminescence value for each well by the average luminescence value for the control wells containing cells not treated with TNFα (which represent the maximum amount of cell viability under these experimental conditions).

4.11.9 Monitoring the TNFα oligomer by SEC

Solutions of 40 μg/mL TNFα were prepared in PBS+0.05%TWEEN or PBS, with 4% DMSO, and with or without 44 μM α/β-peptide **4.17**. The time of the dilution was recorded, and 5 μL of the resulting solution was injected onto a Protein BEH SEC size exclusion column (Waters, 186006505) on a Waters Acquity UPLC H Class ultra performance liquid chromatography instrument, with PBS, pH 7.5 as the mobile phase running at 0.4 mL/min, for 15 total minutes. Each solution was injected four consecutive times to obtain successive chromatograms for the same solution as a function of time. Each time course for each condition was repeated in duplicate. For analysis, the area for the peak corresponding to the TNFα trimer (as determined by injection of TNFα in PBS alone and from MW standards) was monitored at 220 nm and plotted as a function of time.

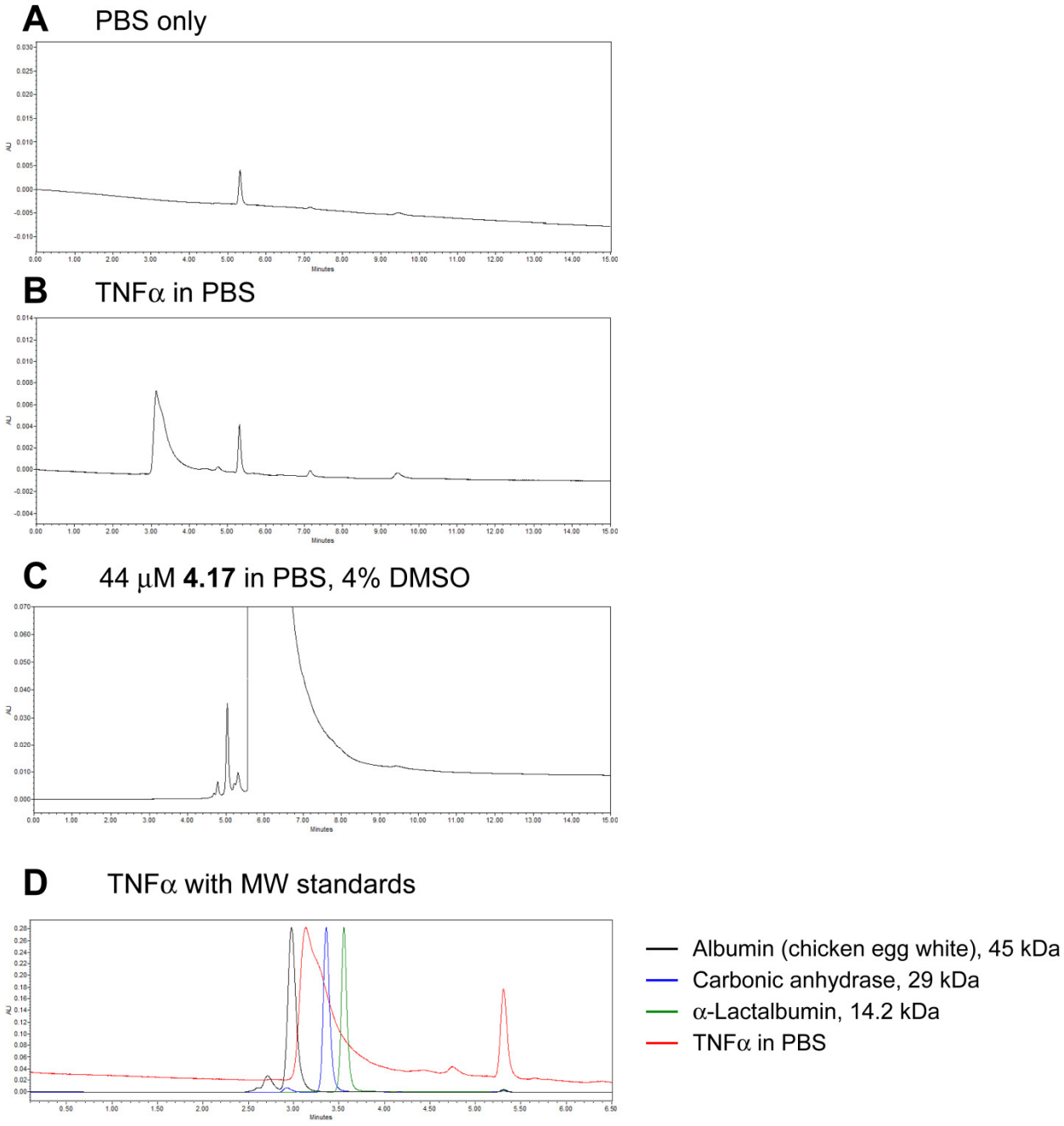

Figure 4.25 Analysis of TNFα oligomerization by size exclusion chromatography (SEC). (A) Injection of PBS. (B) Injection of TNFα in PBS. (C) Injection of α/β-peptide **4.17** in PBS, 4% DMSO. (D) Overlay of injection of TNFα from panel B with injections of MW standards, as indicated in the legend.

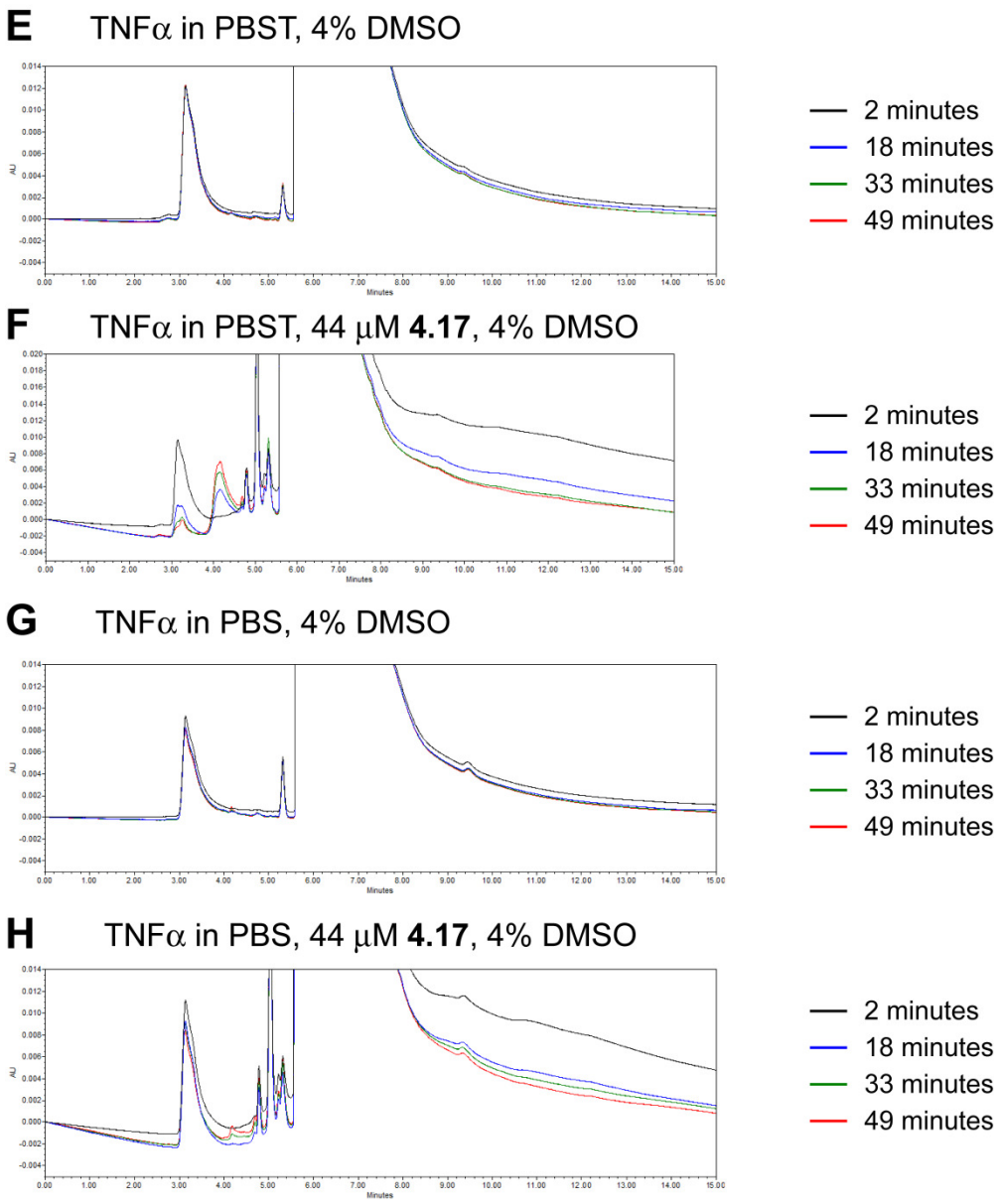

Figure 4.25 (E) Sequential injections of a solution of 40 μg/mL TNFα in PBS+0.05% TWEEN20 (PBST) with 4% DMSO over time. (F) Sequential injections of a solution of 40 μg/mL TNFα with 44 μM **4.17** in PBS+0.05% TWEEN20 (PBST) with 4% DMSO over time. (G) Sequential injections of a solution of 40 μg/mL TNFα in PBS with 4% DMSO over time. (H) Sequential injections of a solution of 40 μg/mL TNFα with 44 μM **4.17** in PBS with 4% DMSO over time.

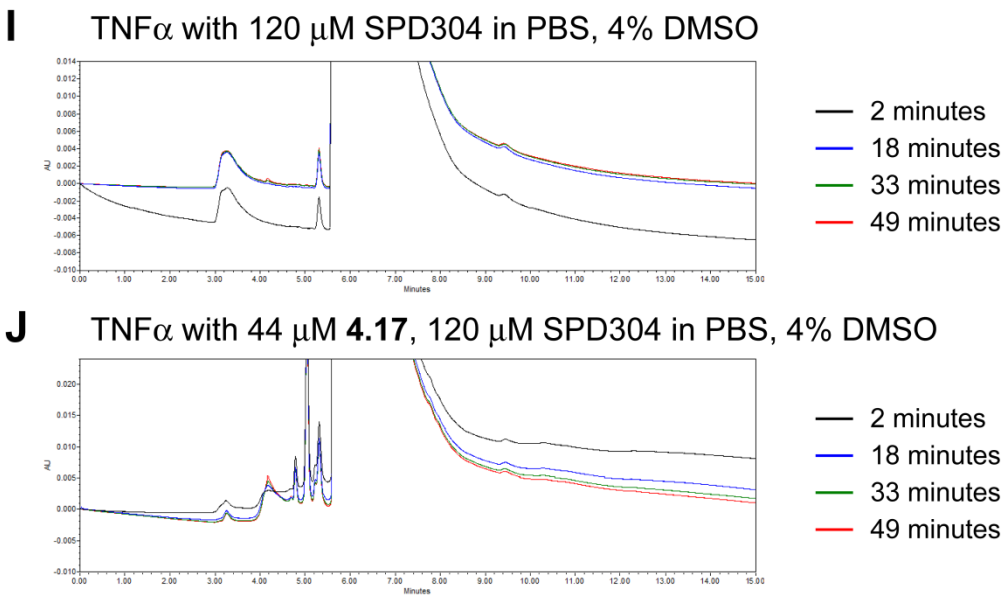

Figure 4.25 (I) Sequential injections of a solution of 40 μg/mL TNFα with 120 μM SPD304 in PBS with 4% DMSO over time. (J) Sequential injections of a solution of 40 μg/mL TNFα with 44 μM **4.17**, 120 μM SPD304 in PBS with 4% DMSO over time.

4.11.10 Peptide characterization

α-Peptide and α/β-peptide purity after purification was assessed by analytical scale reverse-phase HPLC, using solvent A: H_2O with 0.1% TFA, solvent B: acetonitrile with 0.1% TFA, with a flow rate of 1 mL/min (unless otherwise specified). The solvent gradient for each peptide is specified in each panel. HPLC chromatograms at 220 nm are shown at the top of each panel. Peptide identity was confirmed by MALDI-TOF-MS, shown at the bottom of each panel. For each MALDI-TOF spectrum, the monoisotopic $[M+H]^+$, *m/z* is labeled.

4.1

HPLC: Gradient = 10-60% solvent B over 50 minutes

MALDI-TOF: Calculated monoisotopic $[M+H]^+ = 4421.3$

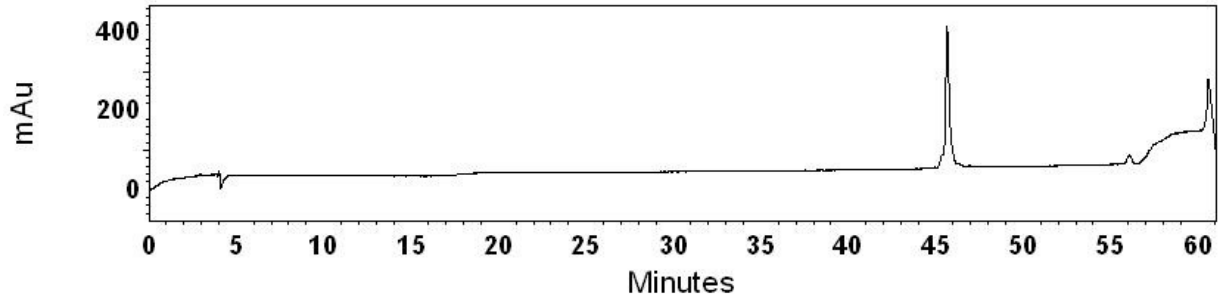

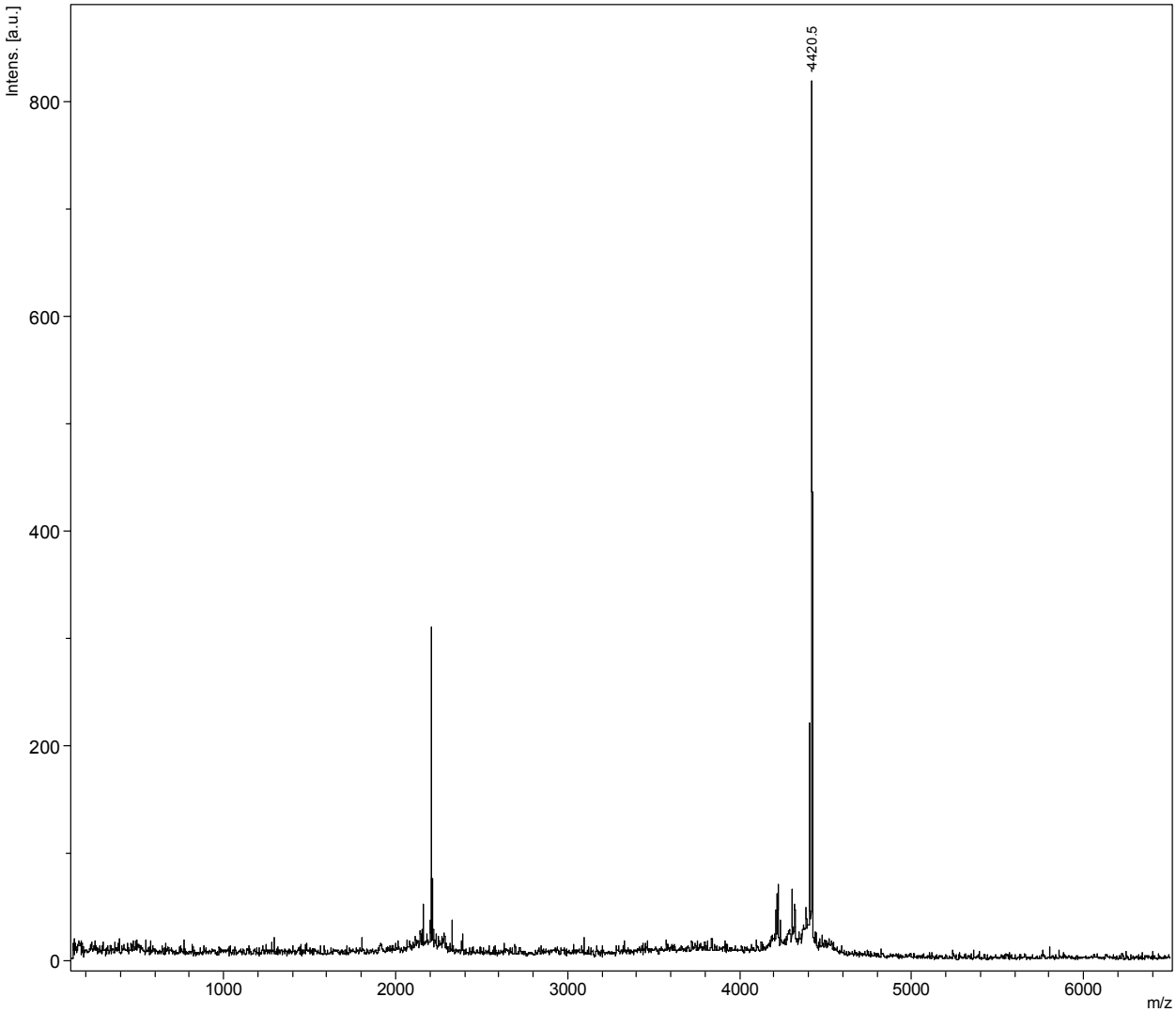

4.2

HPLC: Gradient = 10-60% solvent B over 50 minutes

MALDI-TOF: Calculated monoisotopic $[M+H]^+ = 4415.1$

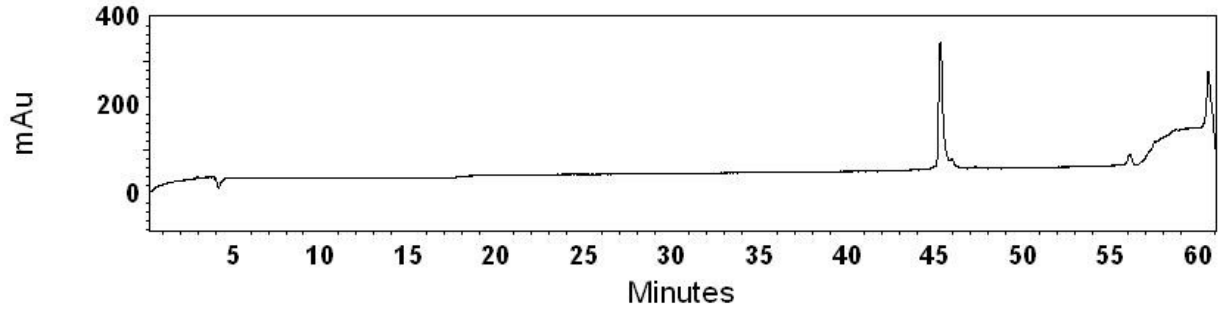

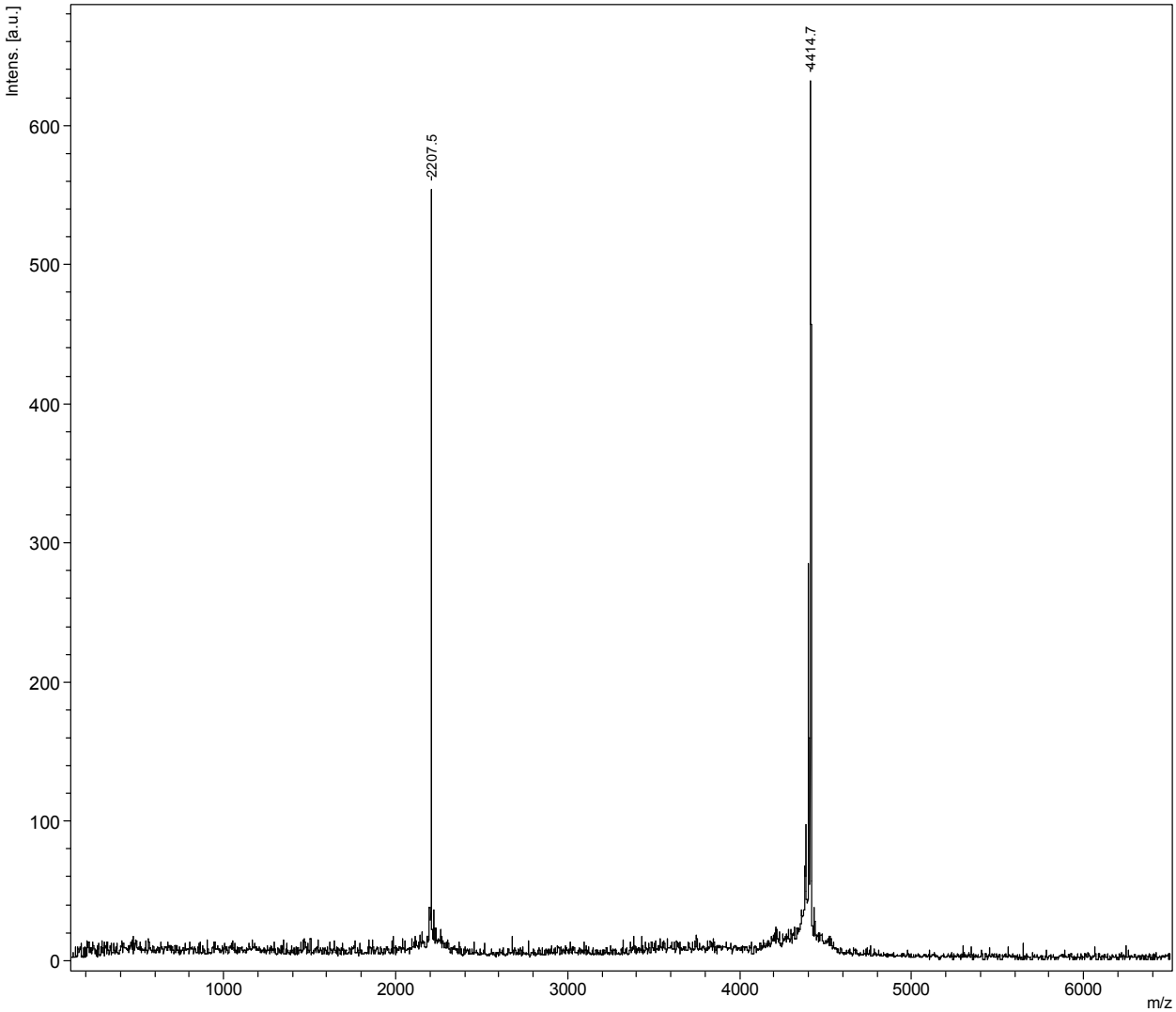

4.3

HPLC: Gradient = 10-60% solvent B over 50 minutes

MALDI-TOF: Calculated monoisotopic $[M+H]^+ = 4488.3$

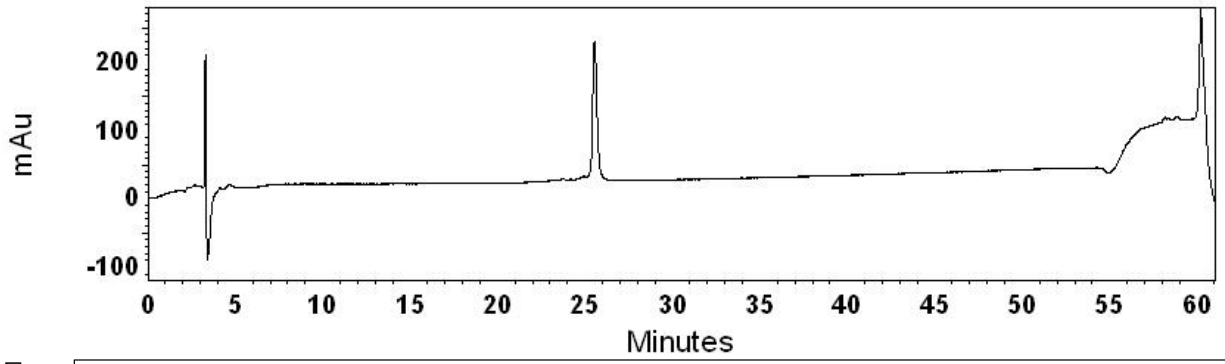

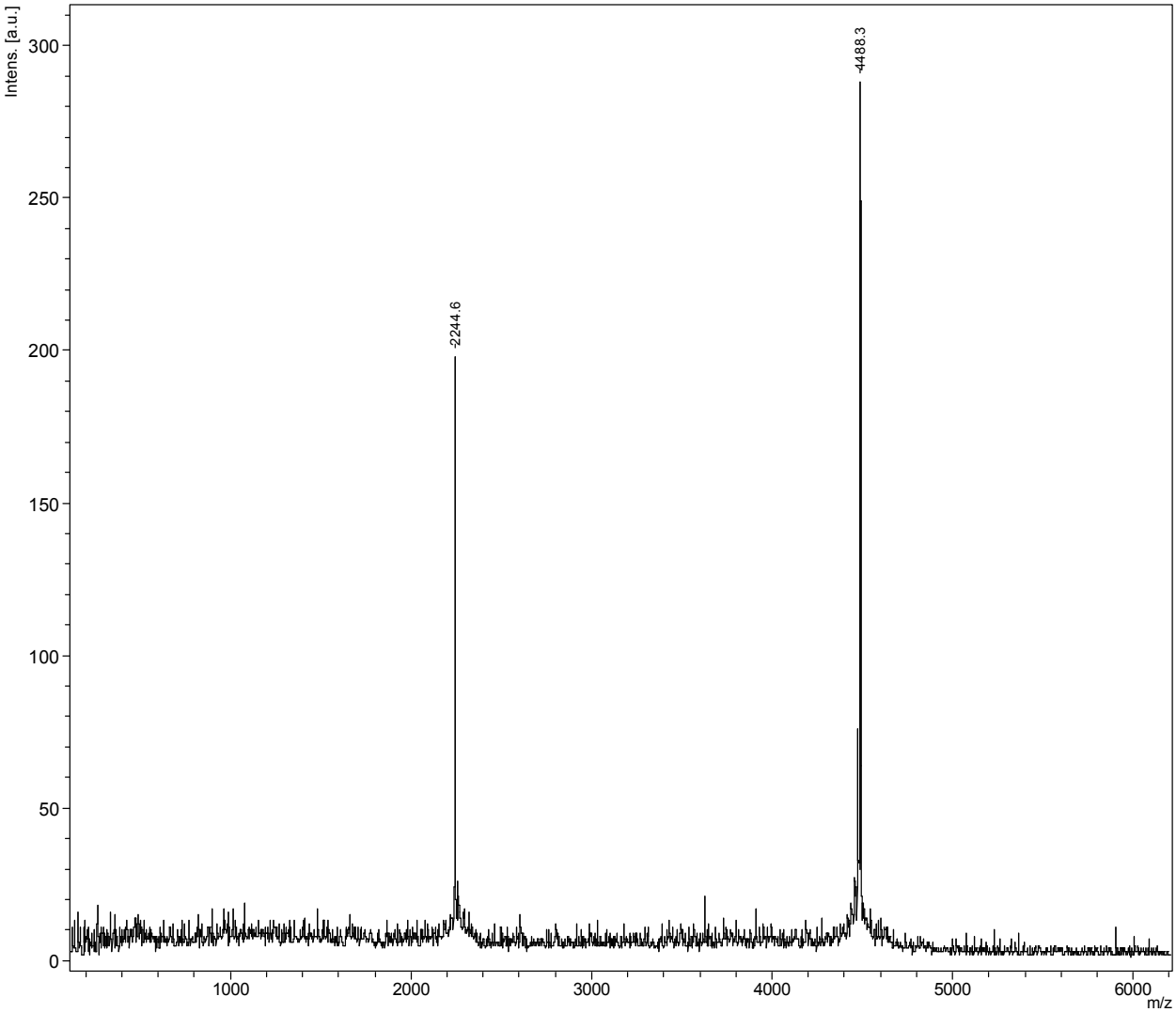

4.4

HPLC: Gradient = 10-60% solvent B over 50 minutes

MALDI-TOF: Calculated monoisotopic $[M+H]^+$ = 3768.9

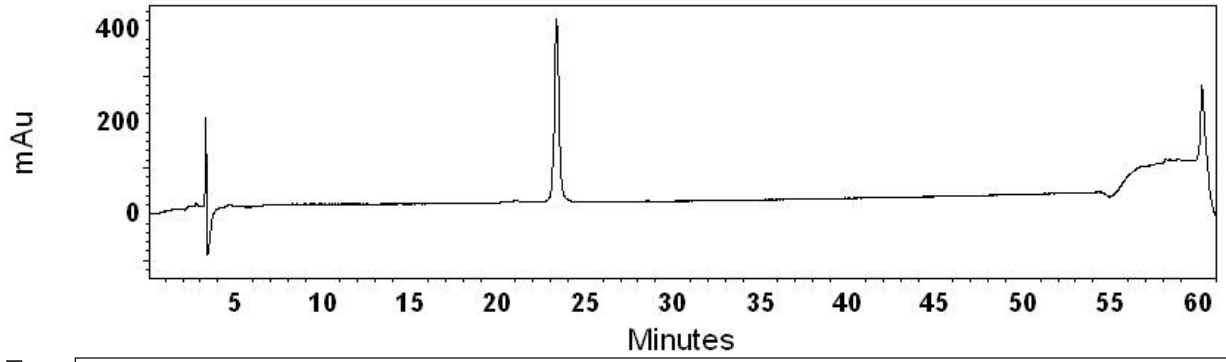

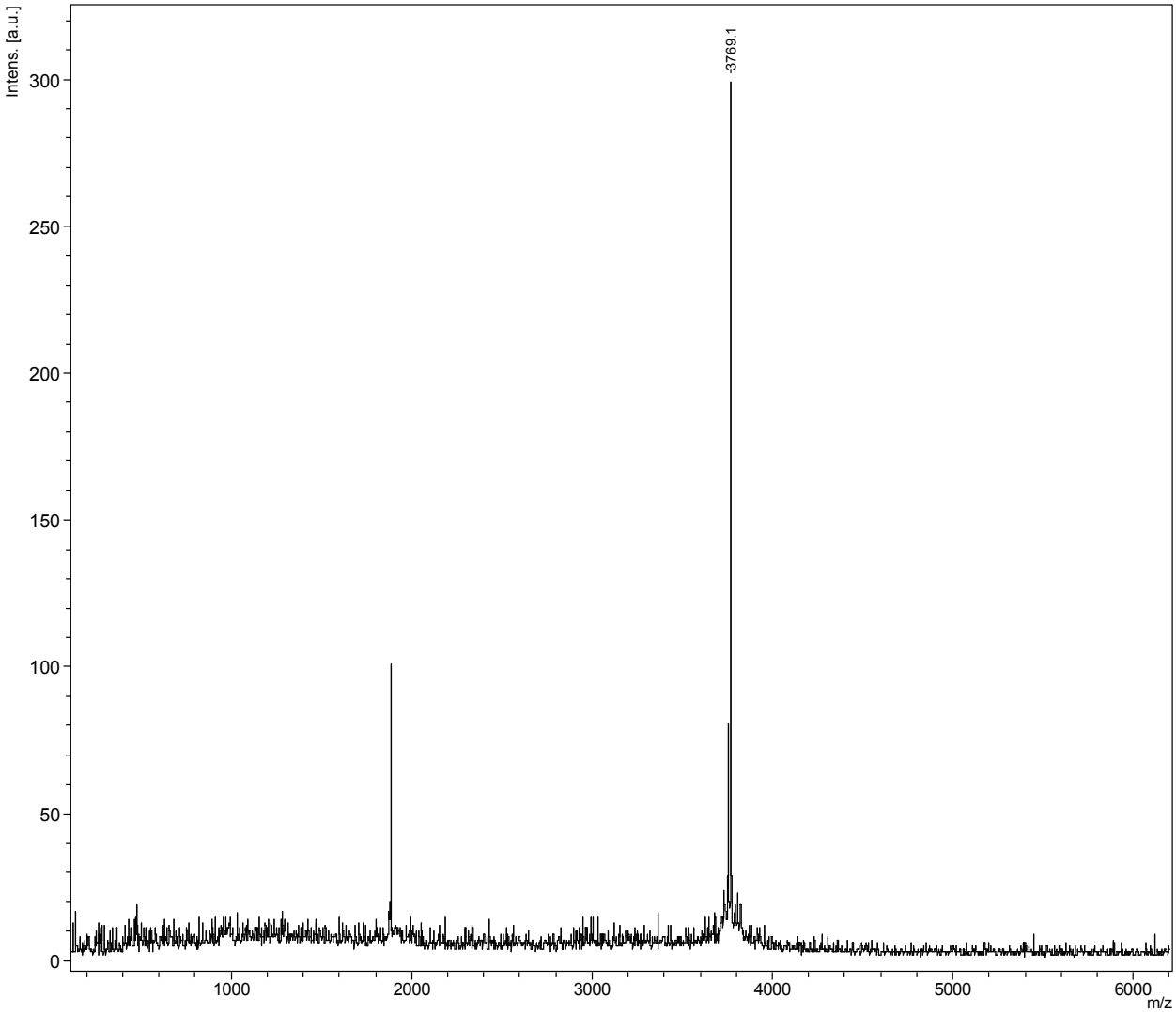

4.5

HPLC: Gradient = 10-60% solvent B over 50 minutes

MALDI-TOF: Calculated monoisotopic $[M+H]^+$ = 3489.7

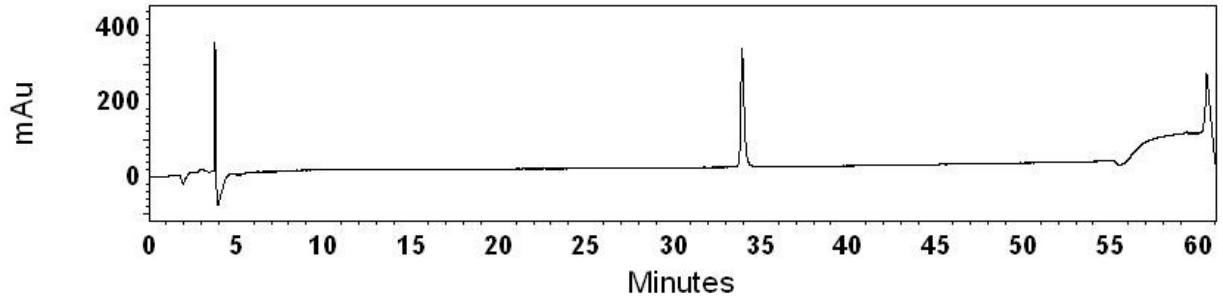

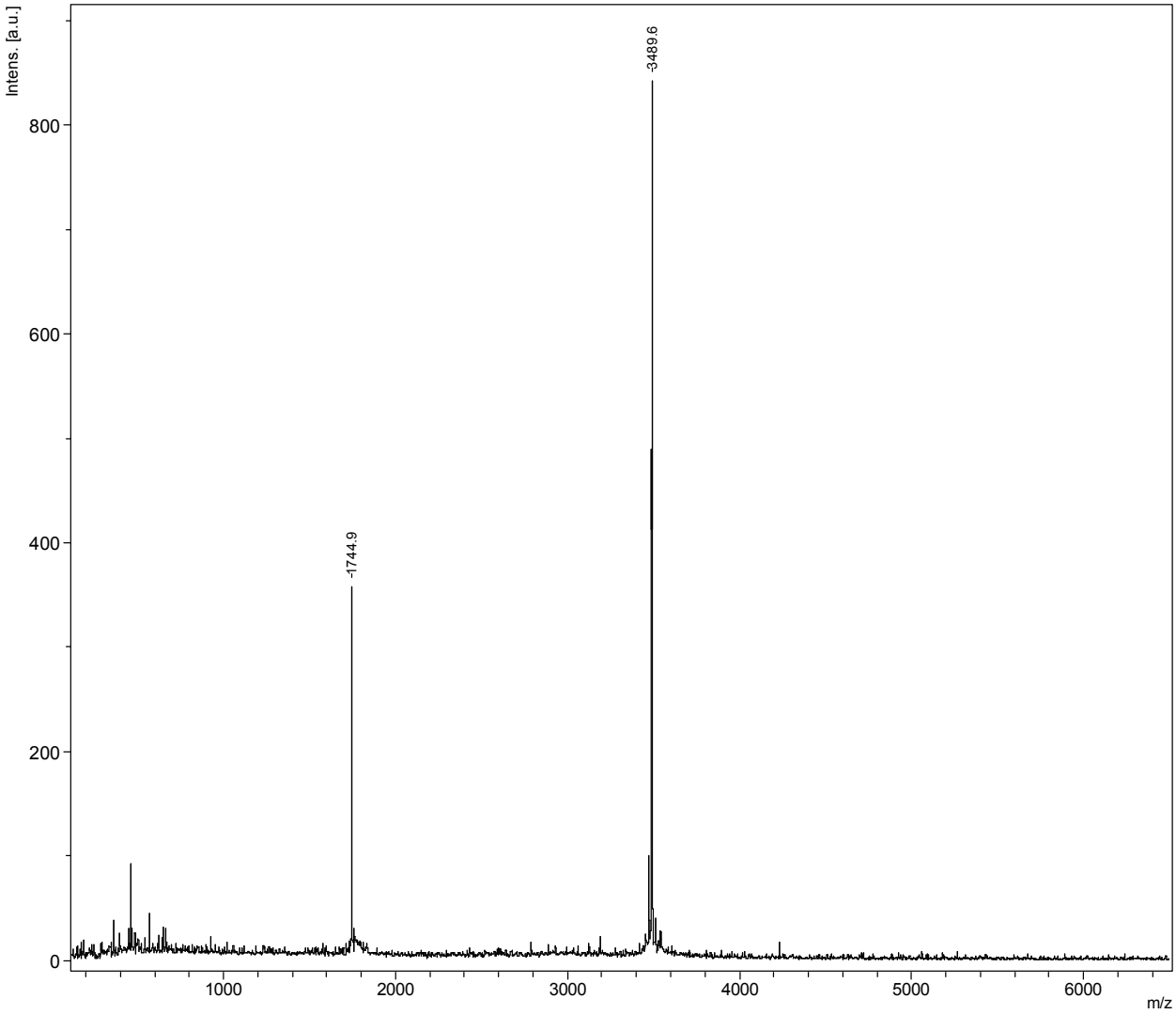

4.6

HPLC: Gradient = 10-60% solvent B over 50 minutes, peak at ~4 min. is DMSO

MALDI-TOF: Calculated monoisotopic $[M+H]^+ = 4406.4$

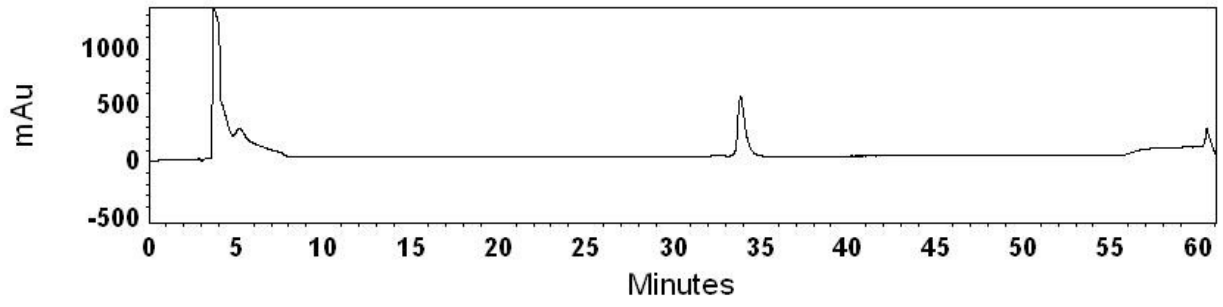

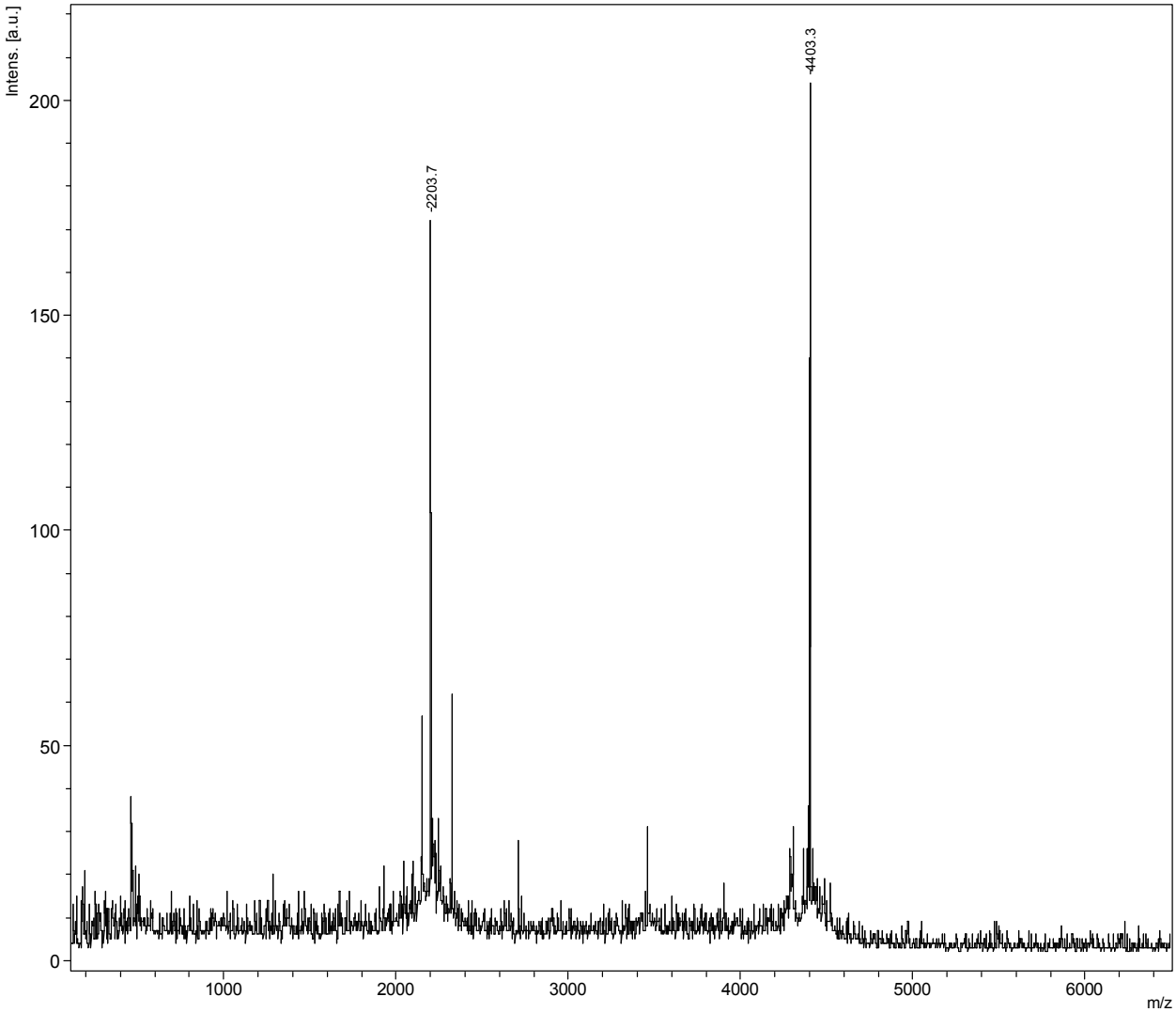

4.7

HPLC: Gradient = 10-60% solvent B over 50 minutes

MALDI-TOF: Calculated monoisotopic $[M+H]^+ = 4480.4$

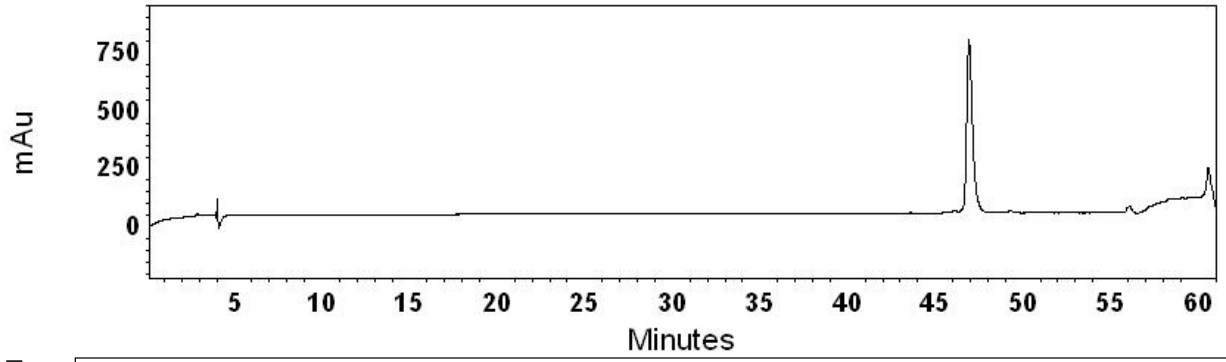

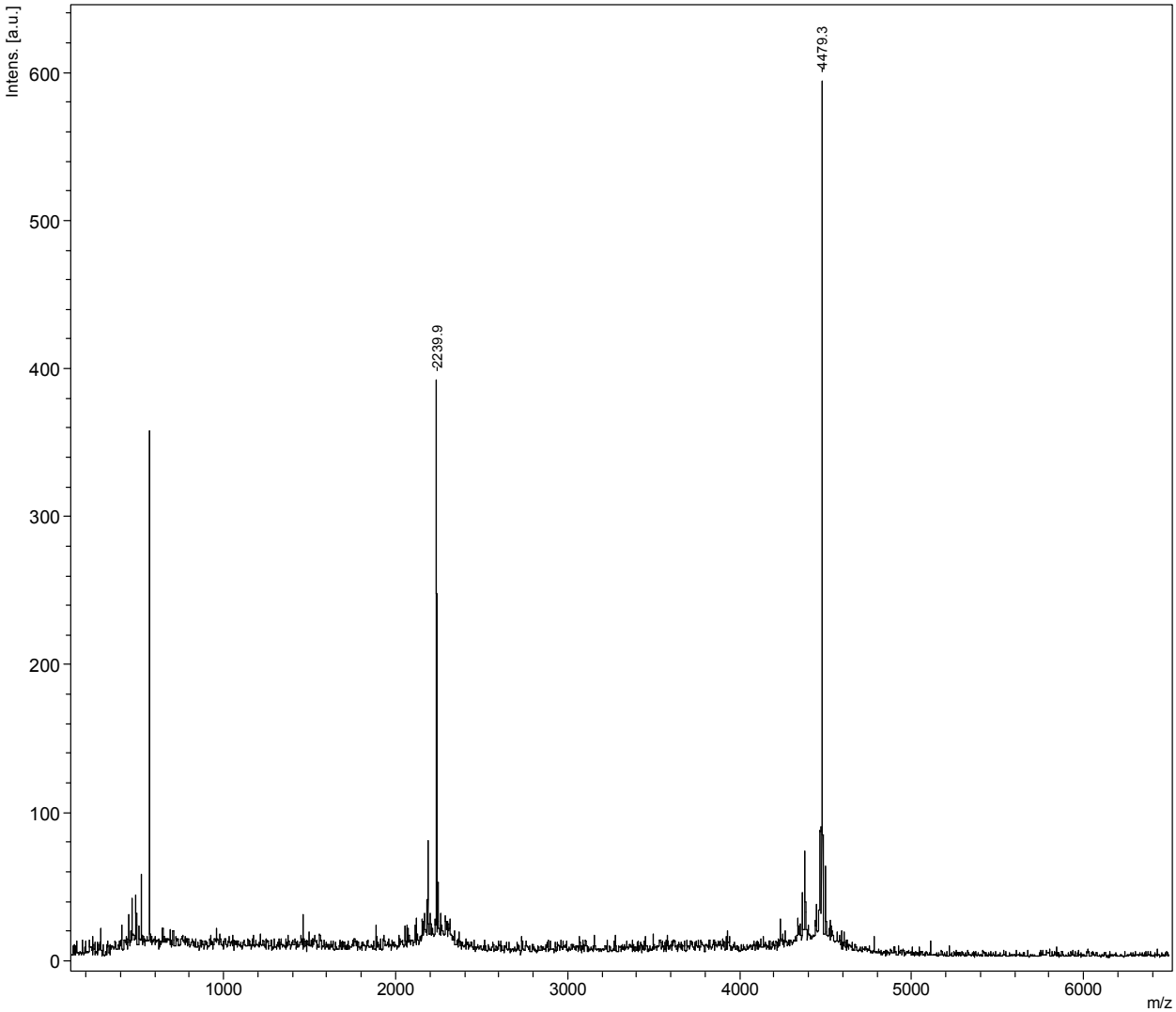

4.8

HPLC: Gradient = 10-60% solvent B over 50 minutes

MALDI-TOF: Calculated monoisotopic $[M+H]^+$ = 3849.1

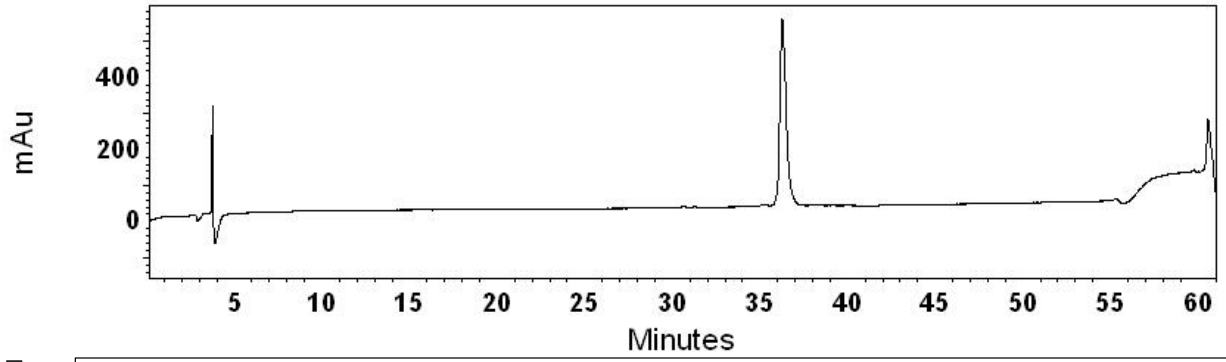

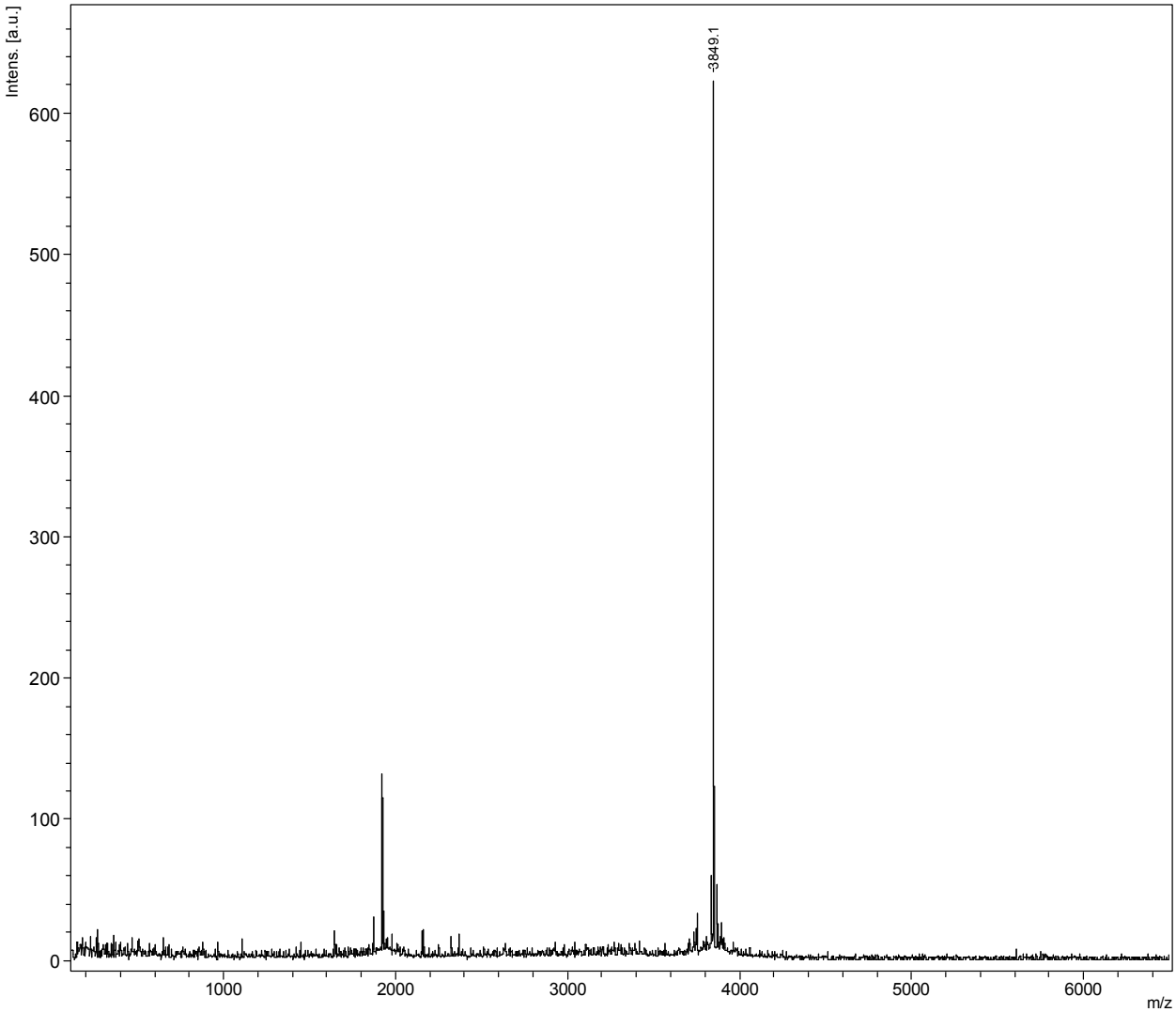

4.9

HPLC: Gradient = 10-60% solvent B over 50 minutes

MALDI-TOF: Calculated monoisotopic $[M+H]^+$ = 3495.9

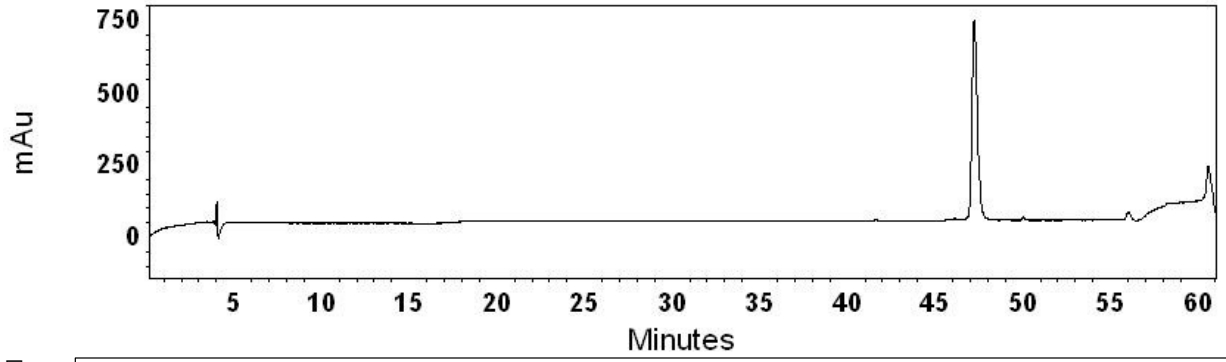

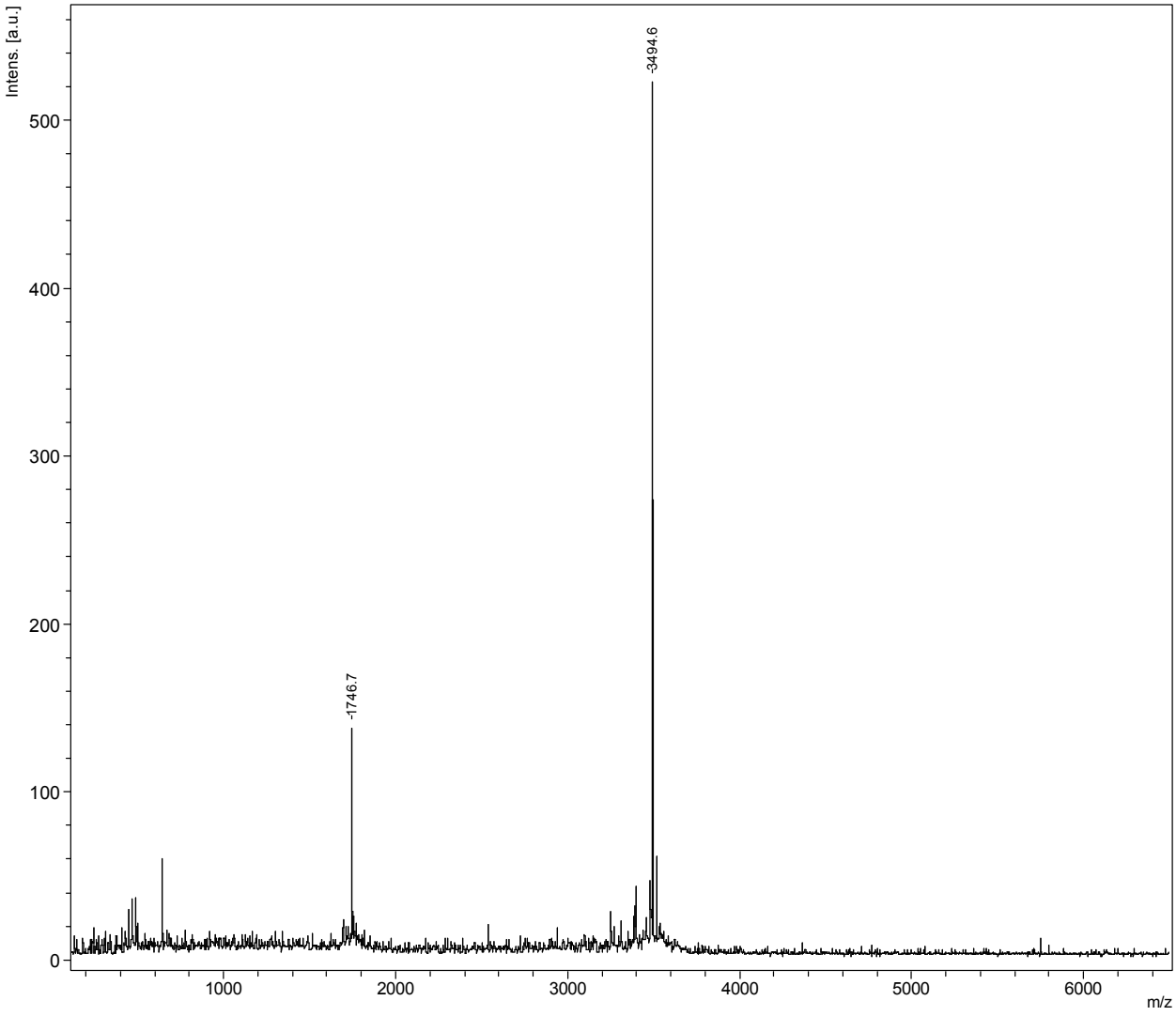

4.10

HPLC: Gradient = 10-60% solvent B over 50 minutes

MALDI-TOF: Calculated monoisotopic $[M+H]^+ = 3394.9$

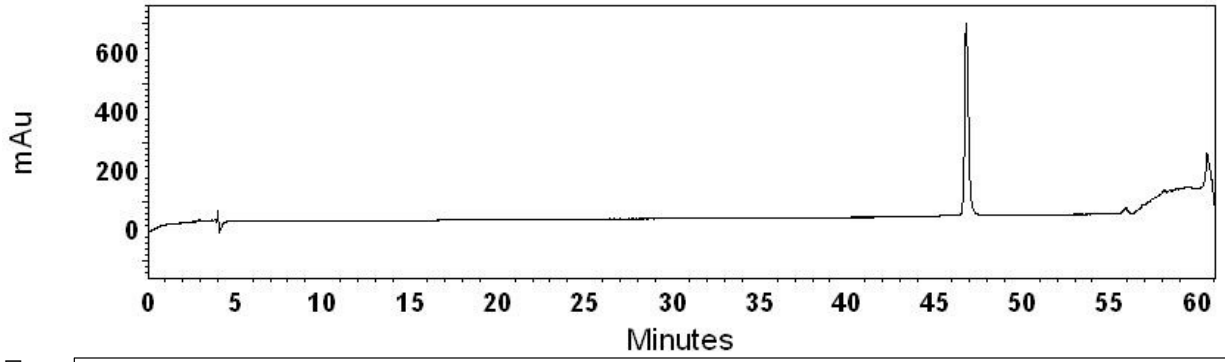

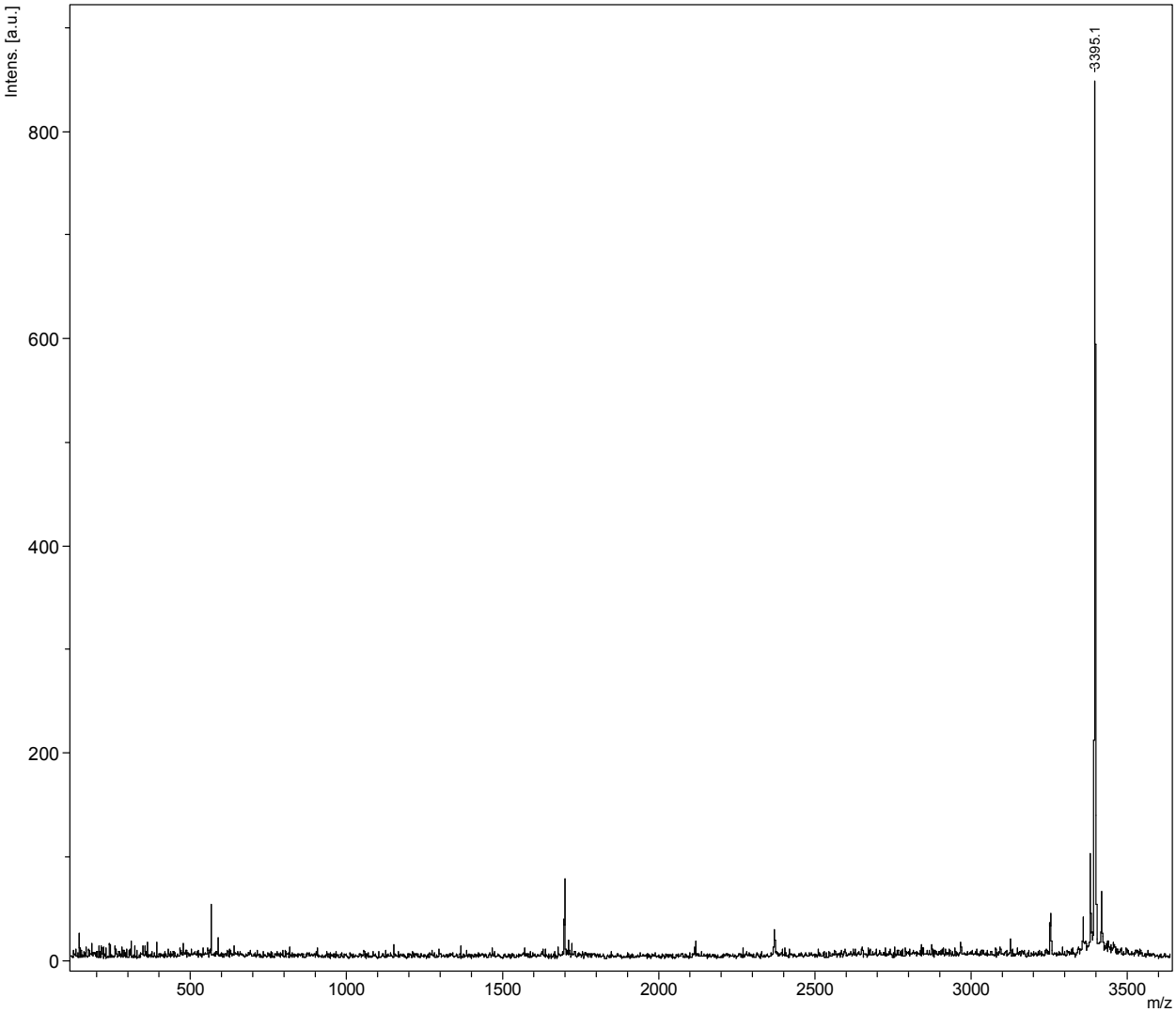

4.11

HPLC: Gradient = 10-60% solvent B over 50 minutes

MALDI-TOF: Calculated monoisotopic $[M+H]^+ = 3283.8$

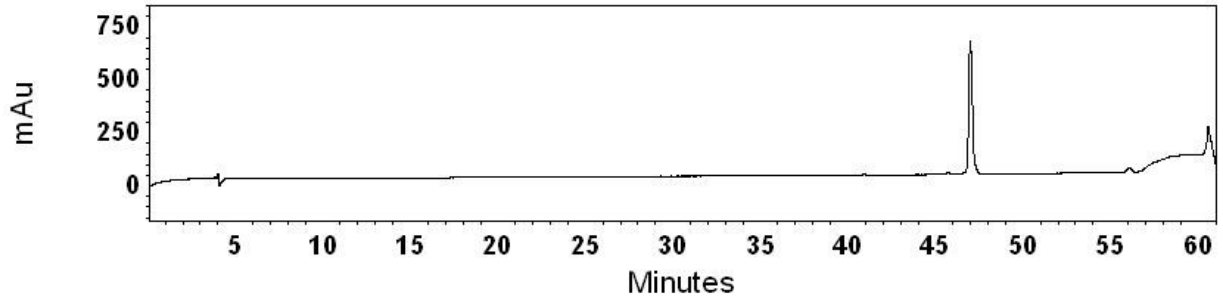

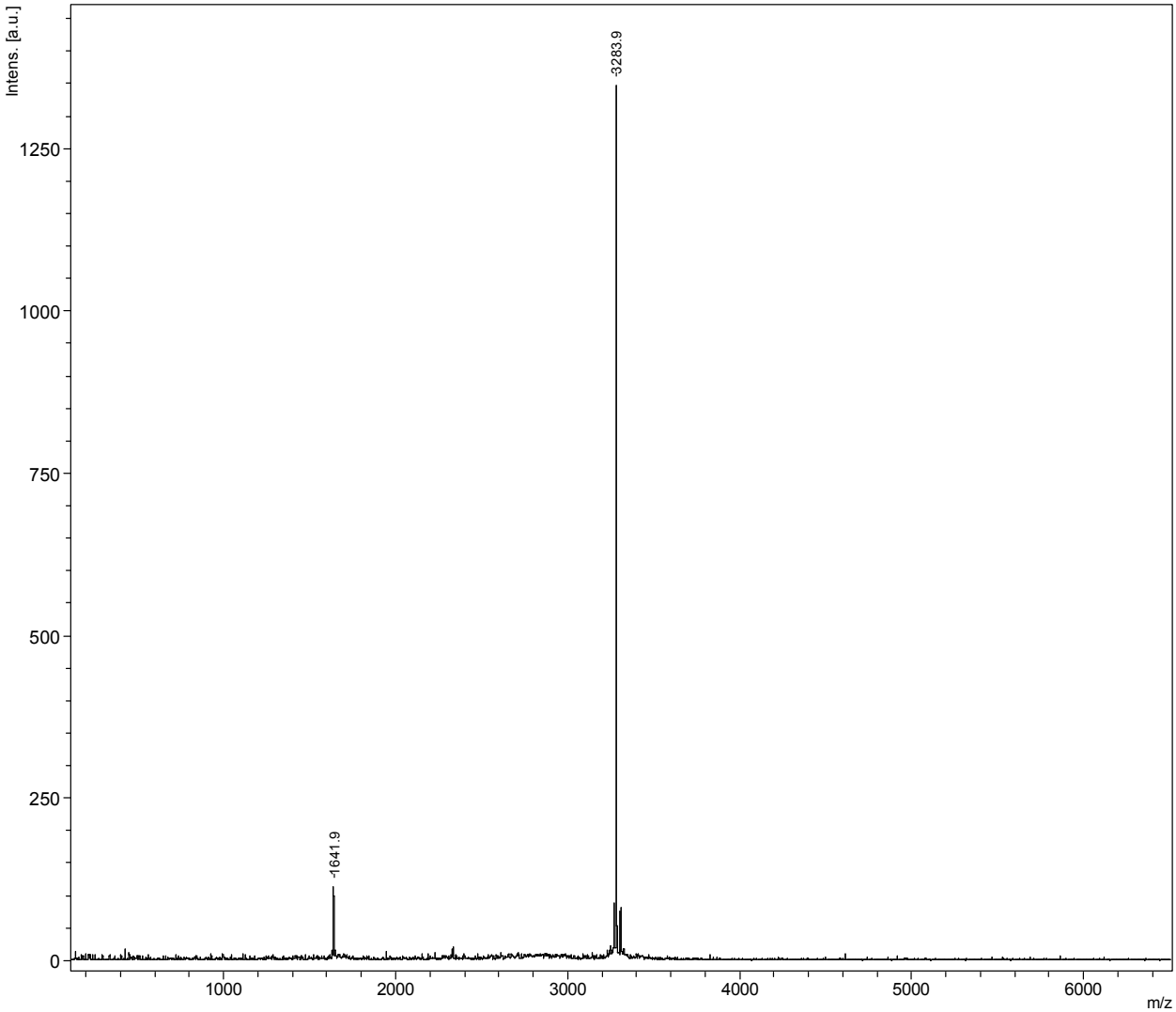

4.12

HPLC: Gradient = 10-60% solvent B over 50 minutes

MALDI-TOF: Calculated monoisotopic $[M+H]^+$ = 3224.8

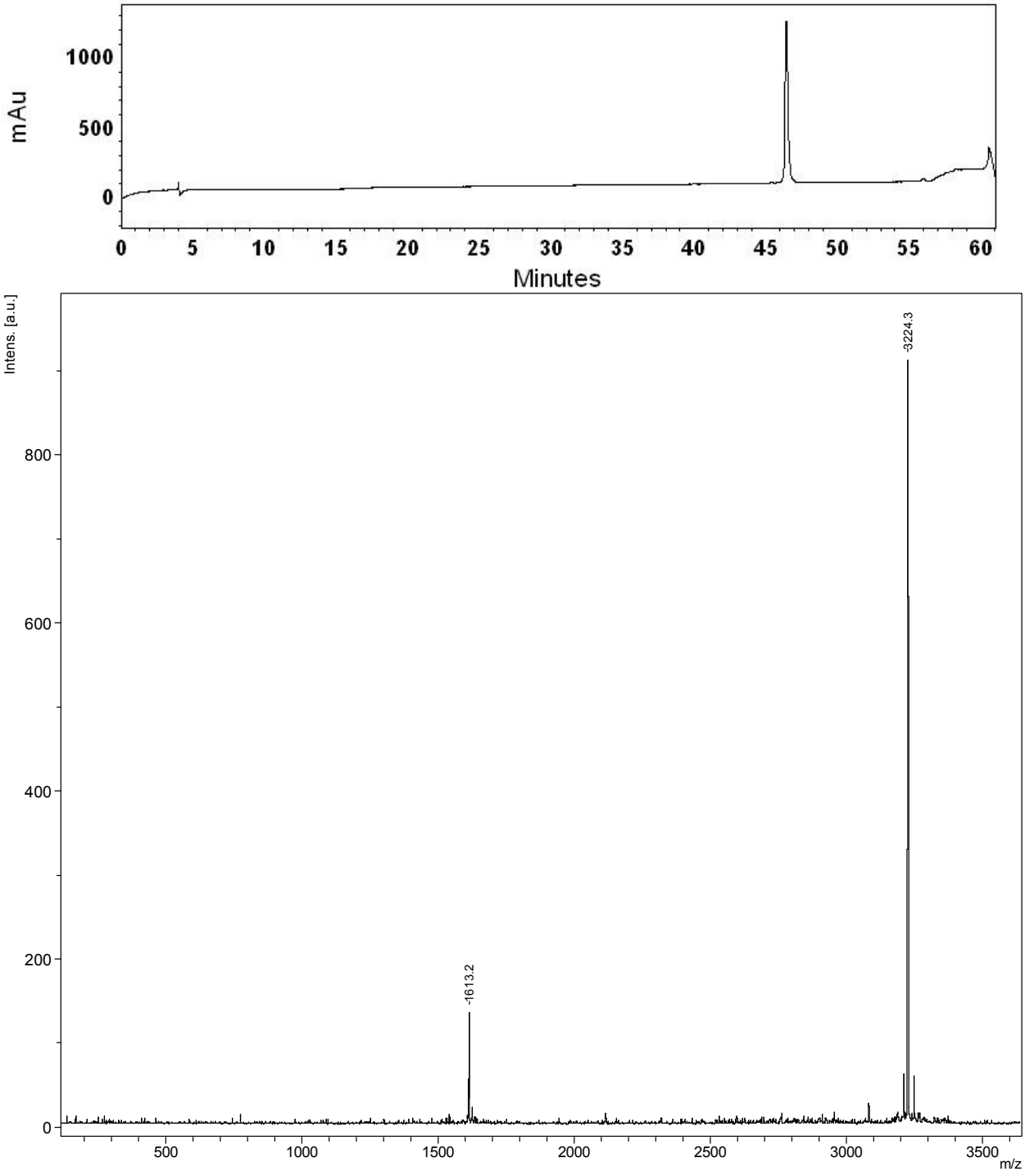

4.13

HPLC: Gradient = 10-60% solvent B over 50 minutes

MALDI-TOF: Calculated monoisotopic $[M+H]^+$ = 3385.7

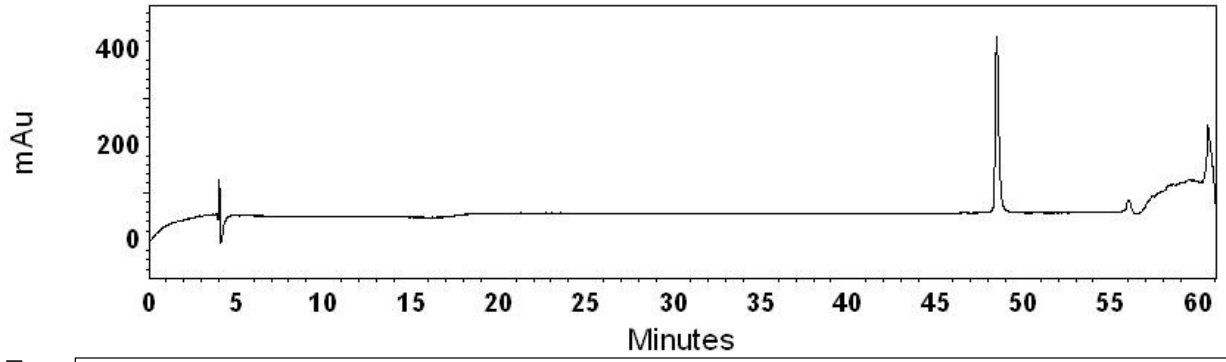

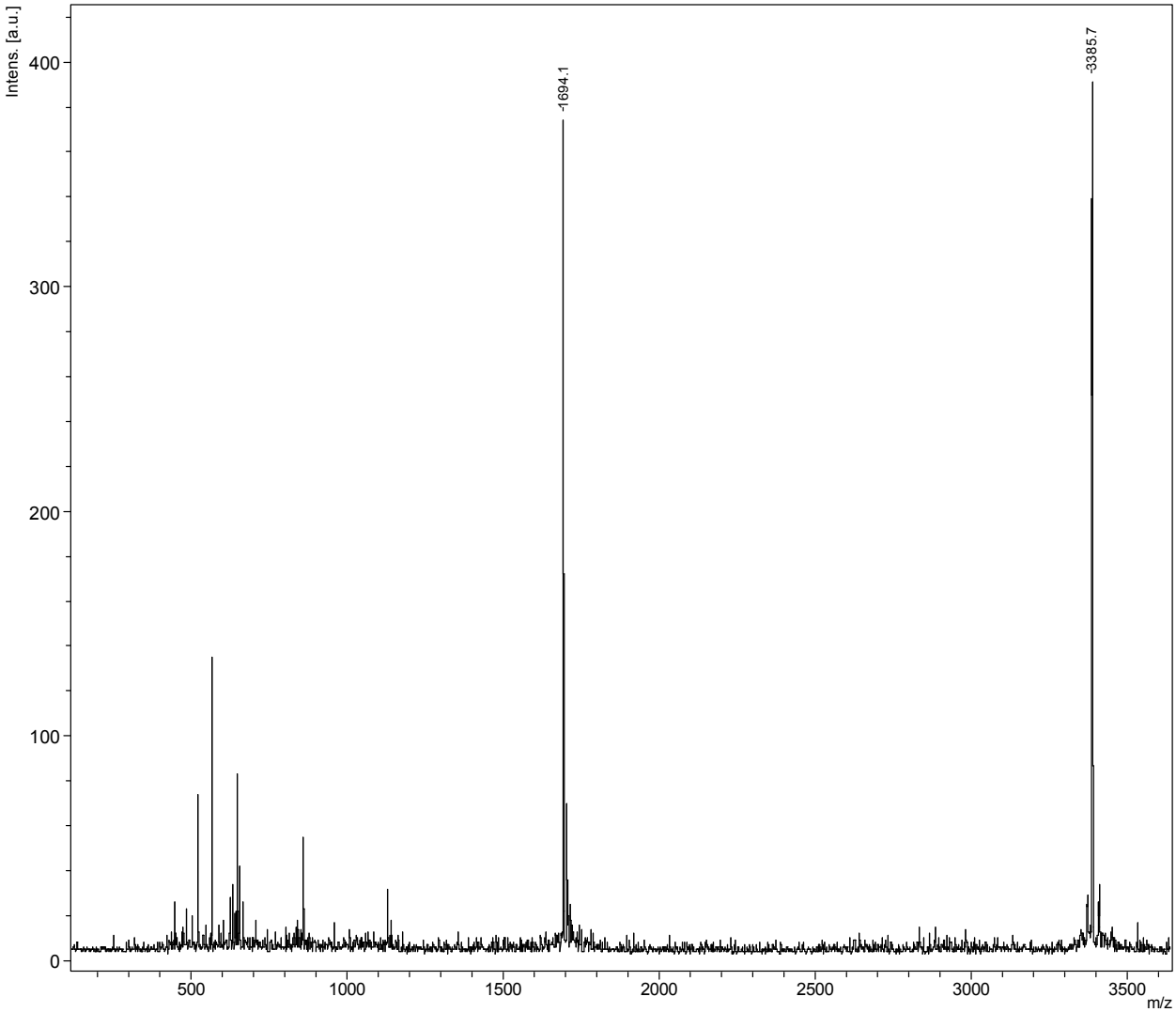

4.14

HPLC: Gradient = 10-60% solvent B over 50 minutes

MALDI-TOF: Calculated monoisotopic $[M+H]^+ = 3329.7$

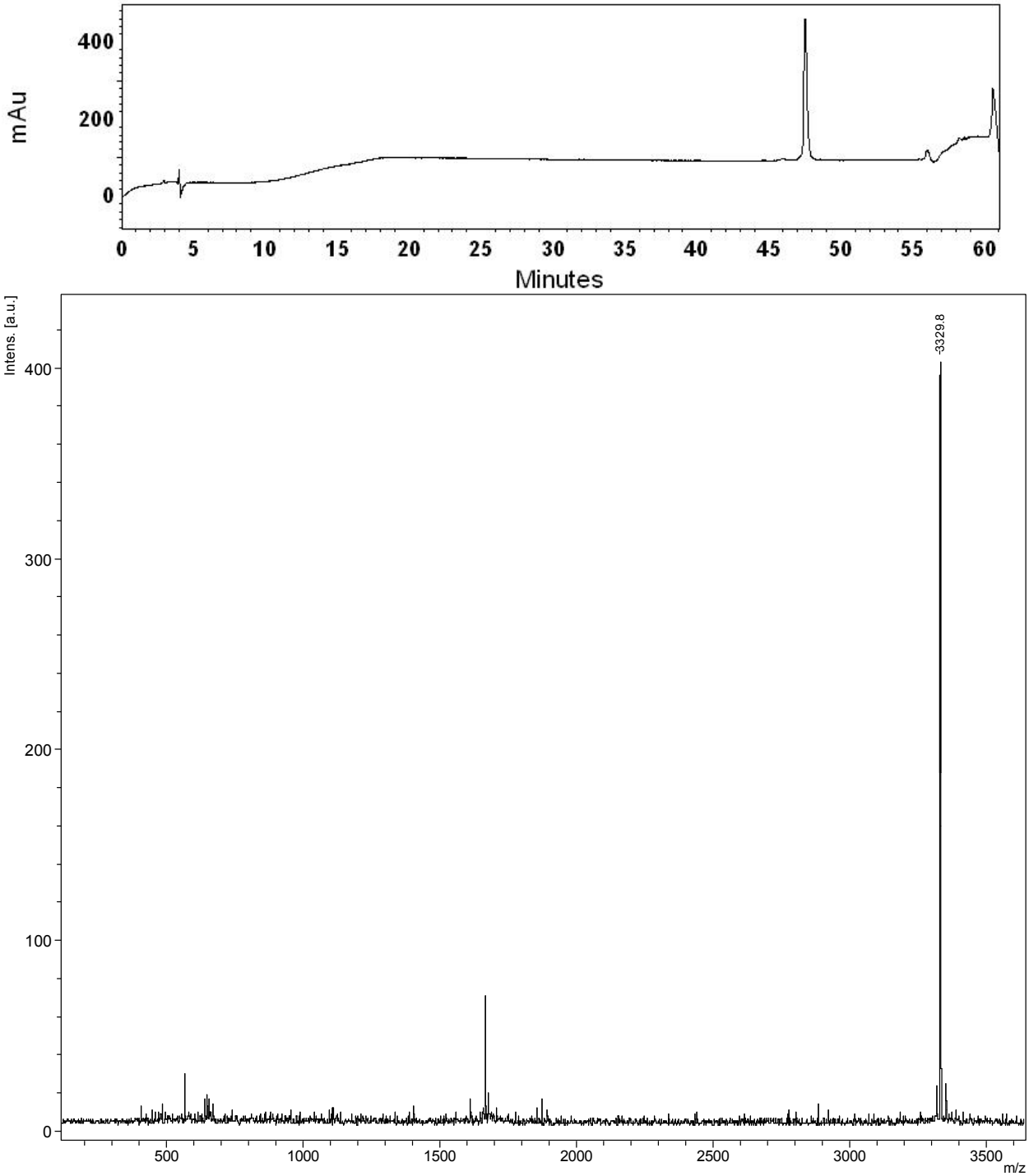

4.15

UPLC: Gradient = 10-95% solvent B over 4 minutes, 0.4 mL/min

MALDI-TOF: Calculated monoisotopic $[M+H]^+$ = 3216.6

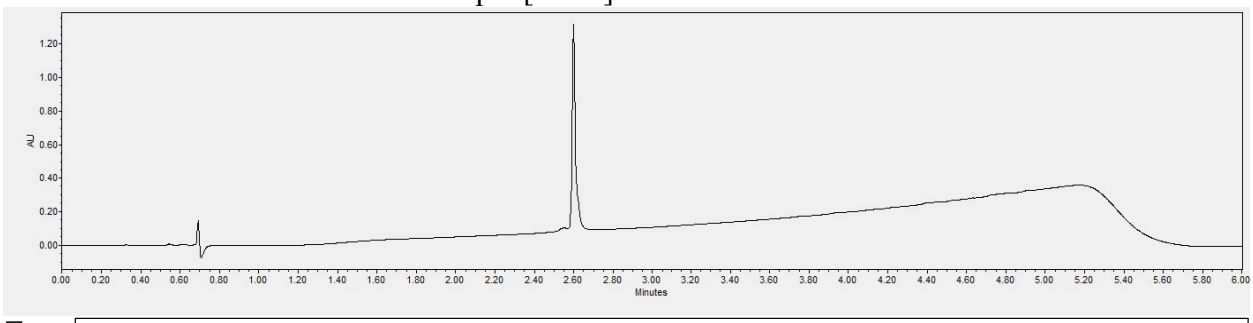

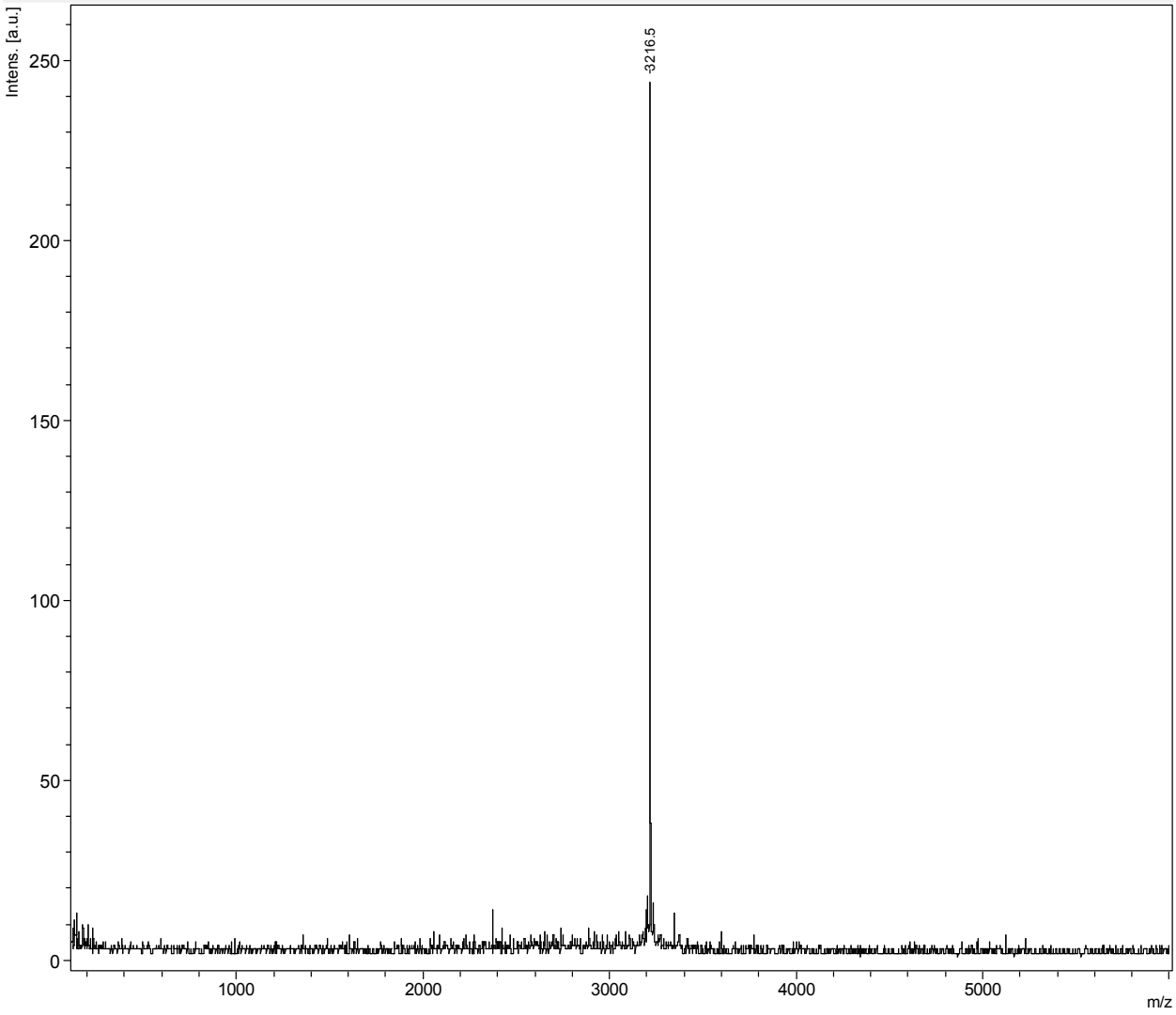

4.16

UPLC: Gradient = 10-95% solvent B over 4 minutes, 0.4 mL/min

MALDI-TOF: Calculated monoisotopic $[M+H]^+$ = 3159.6

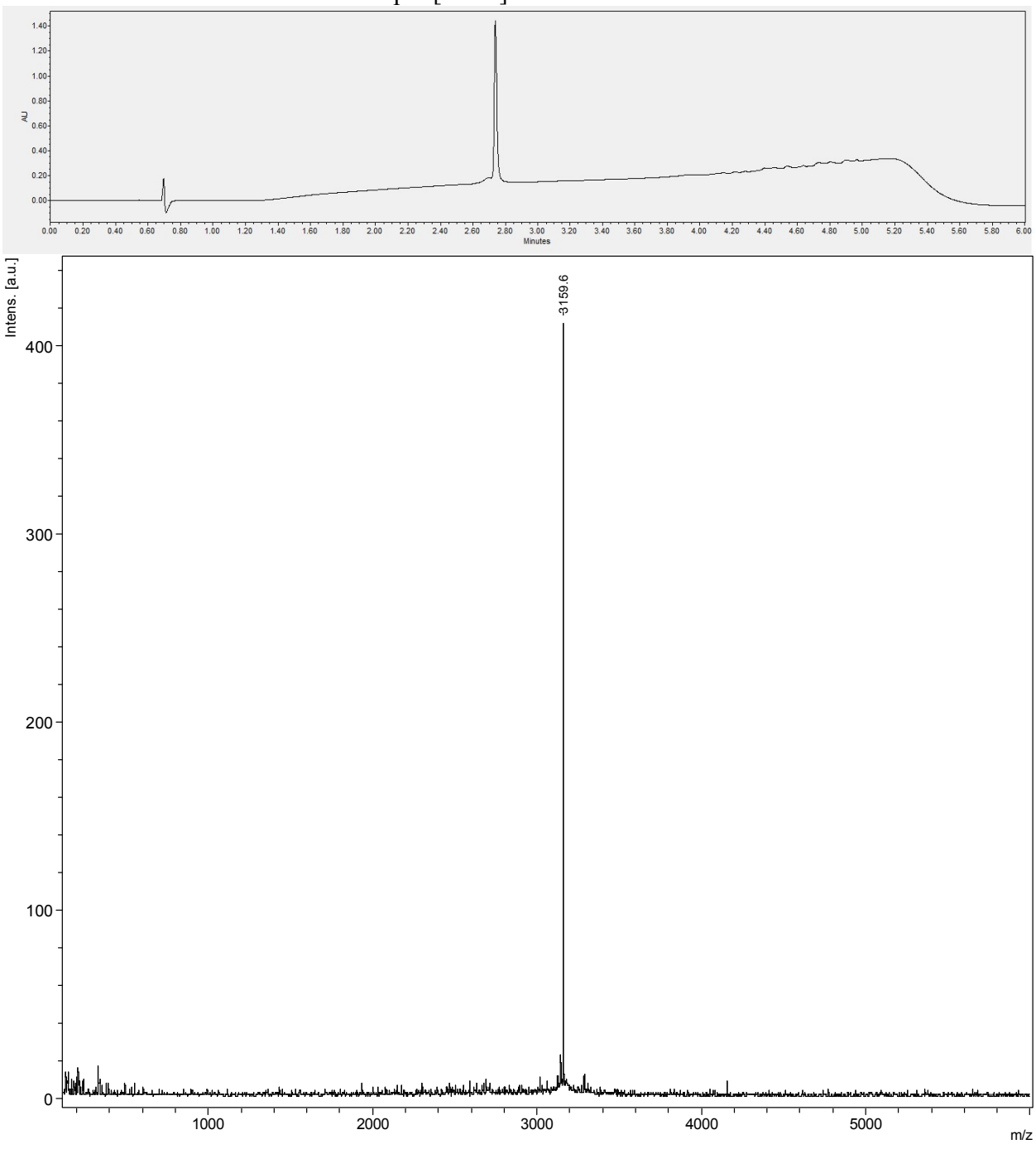

4.17

UPLC: Gradient = 10-60% solvent B over 5 minutes, 0.4 mL/min

MALDI-TOF: Calculated monoisotopic $[M+H]^+$ = 3286.7

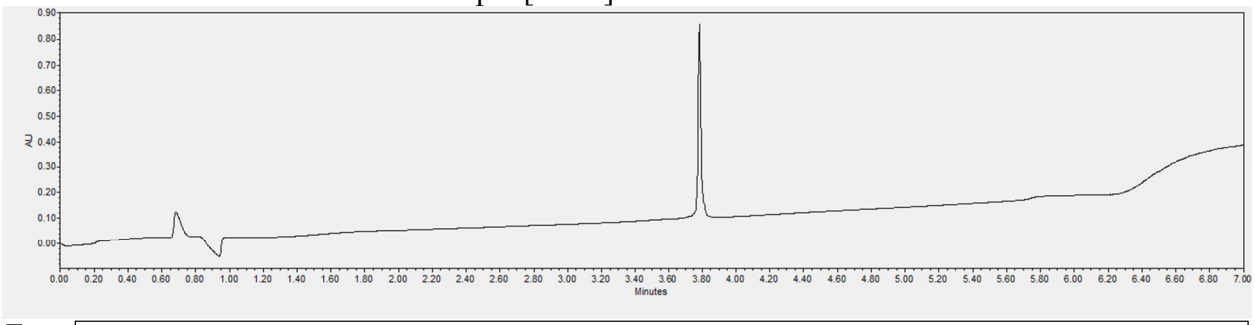

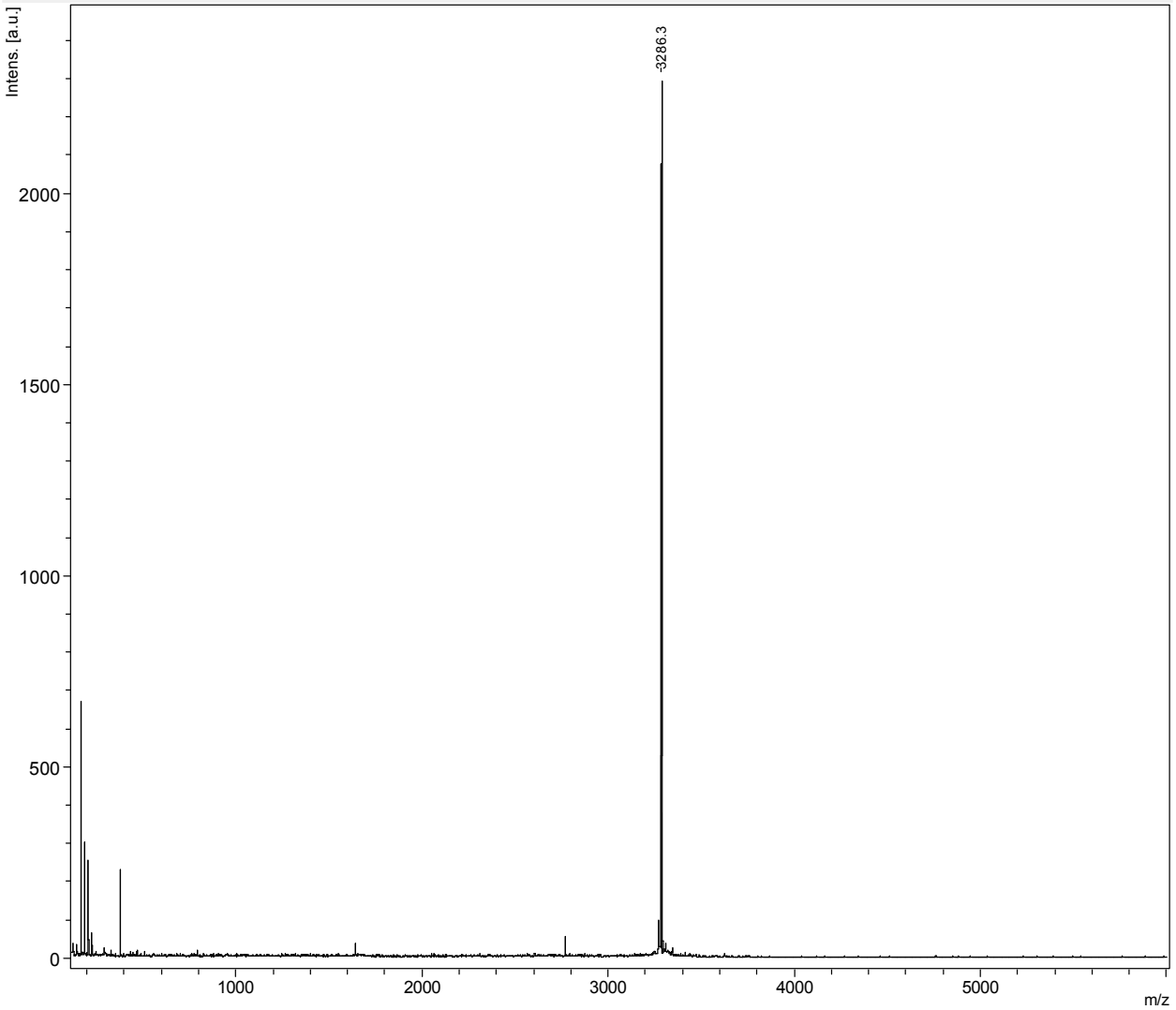

4.18

HPLC: Gradient = 10-90% solvent B over 80 minutes

MALDI-TOF: Calculated monoisotopic $[M+H]^+ = 4410.1$

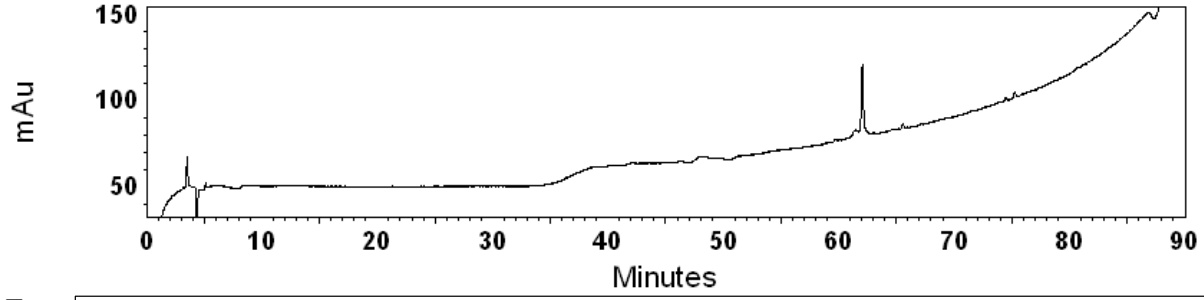

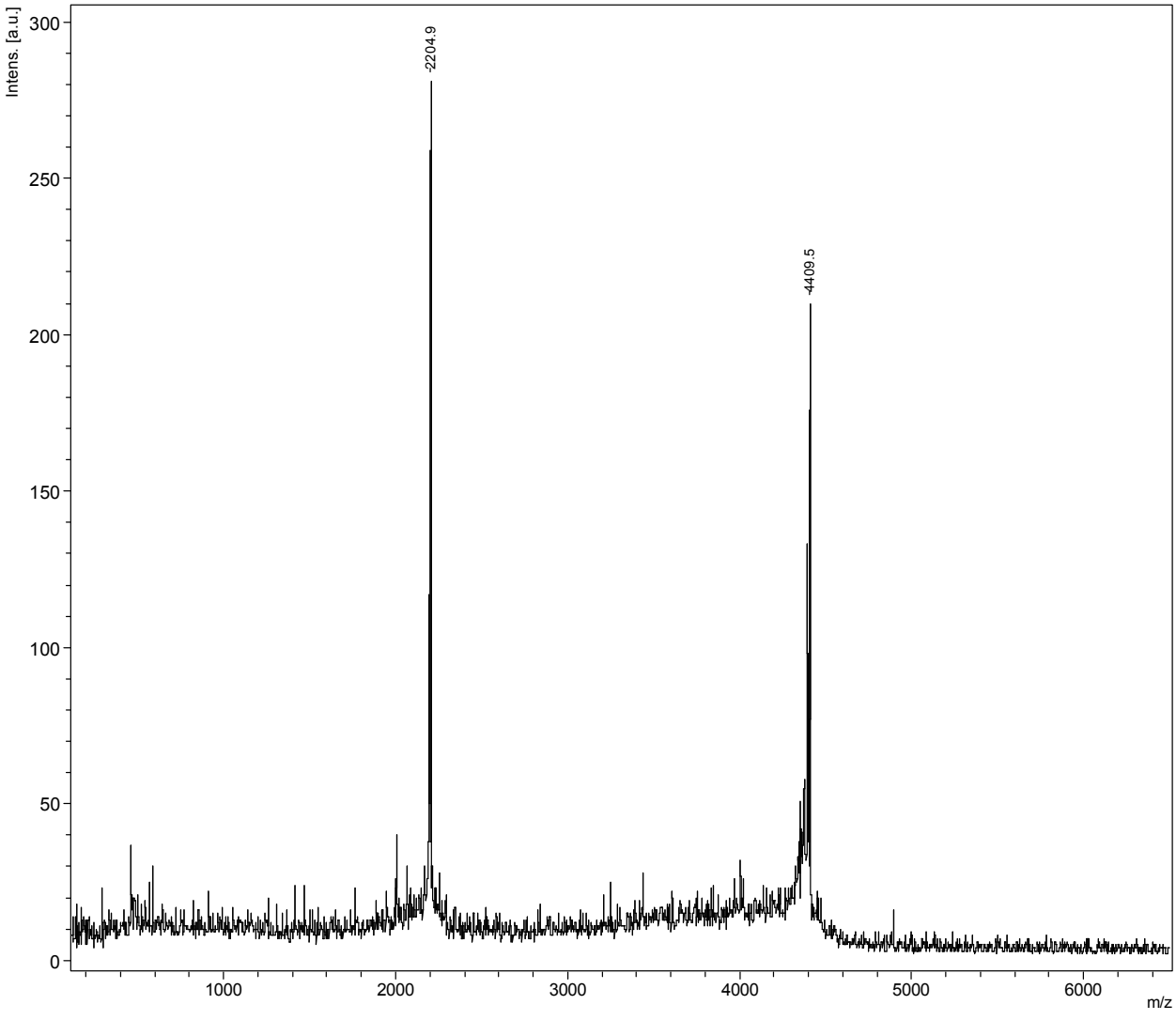

4.19

HPLC: Gradient = 10-90% solvent B over 80 minutes

MALDI-TOF: Calculated monoisotopic $[M+H]^+ = 4302.1$

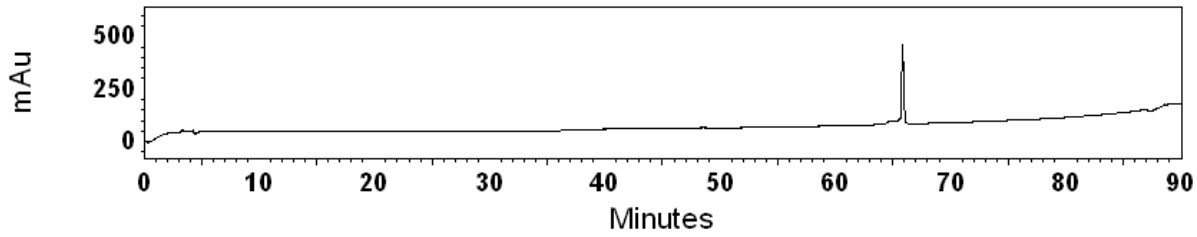

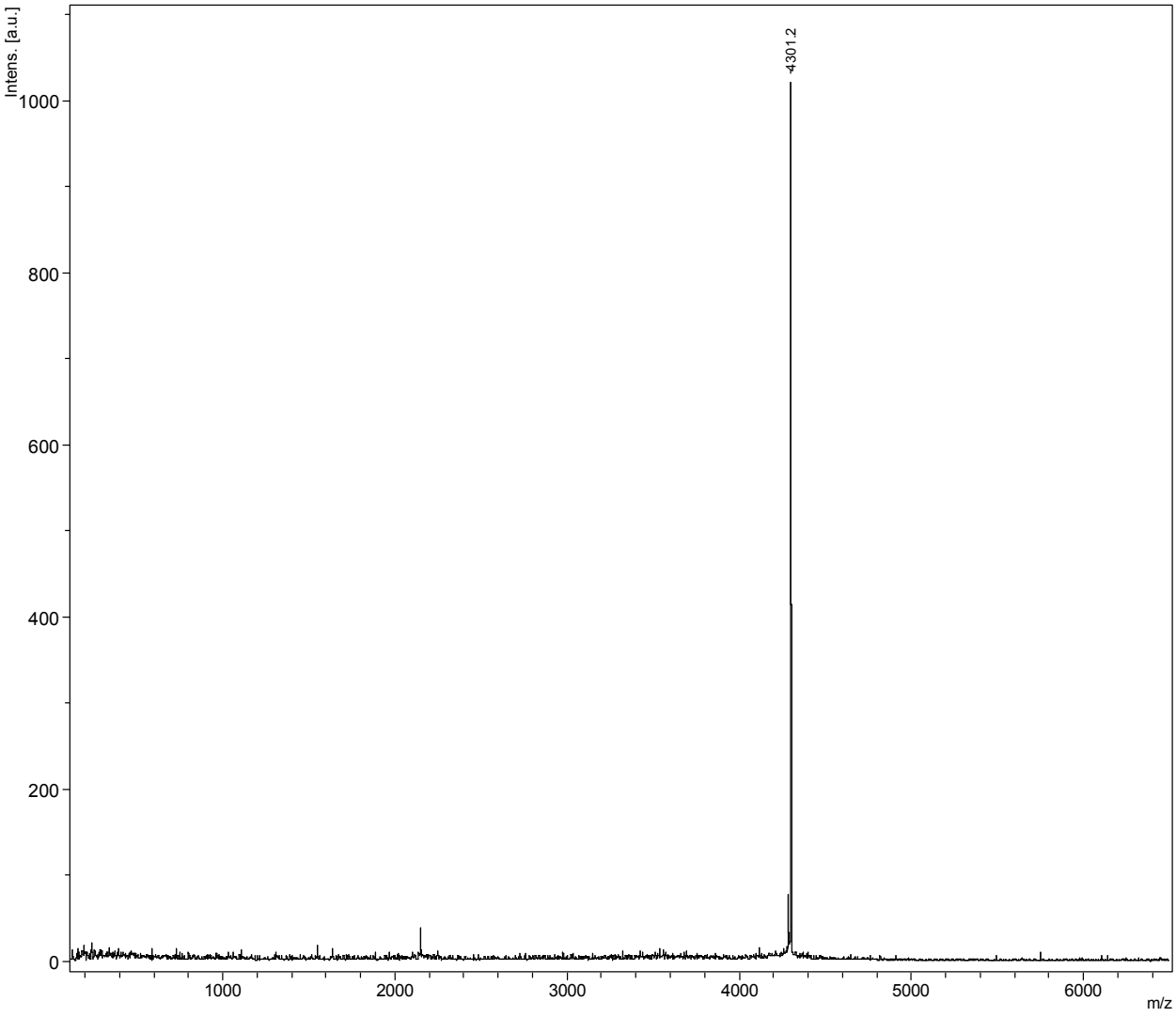

4.20

HPLC: Gradient = 10-90% solvent B over 80 minutes

MALDI-TOF: Calculated monoisotopic $[M+H]^+ = 4373.1$

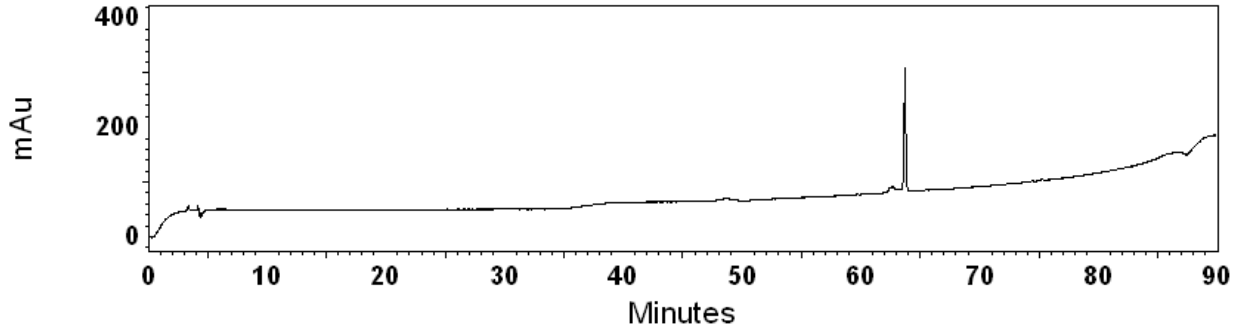

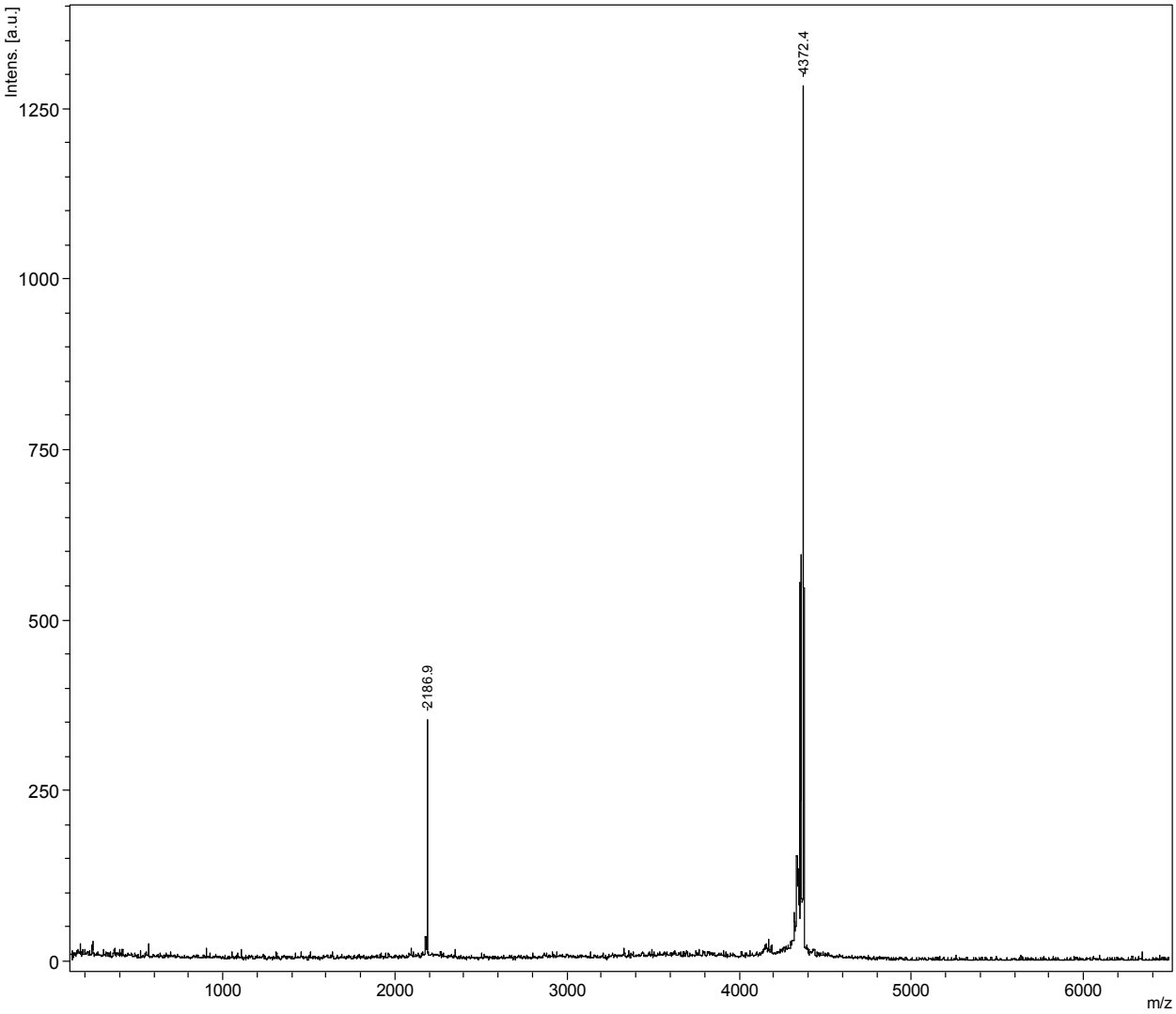

4.21

HPLC: Gradient = 10-90% solvent B over 80 minutes

MALDI-TOF: Calculated monoisotopic $[M+H]^+ = 4305.1$

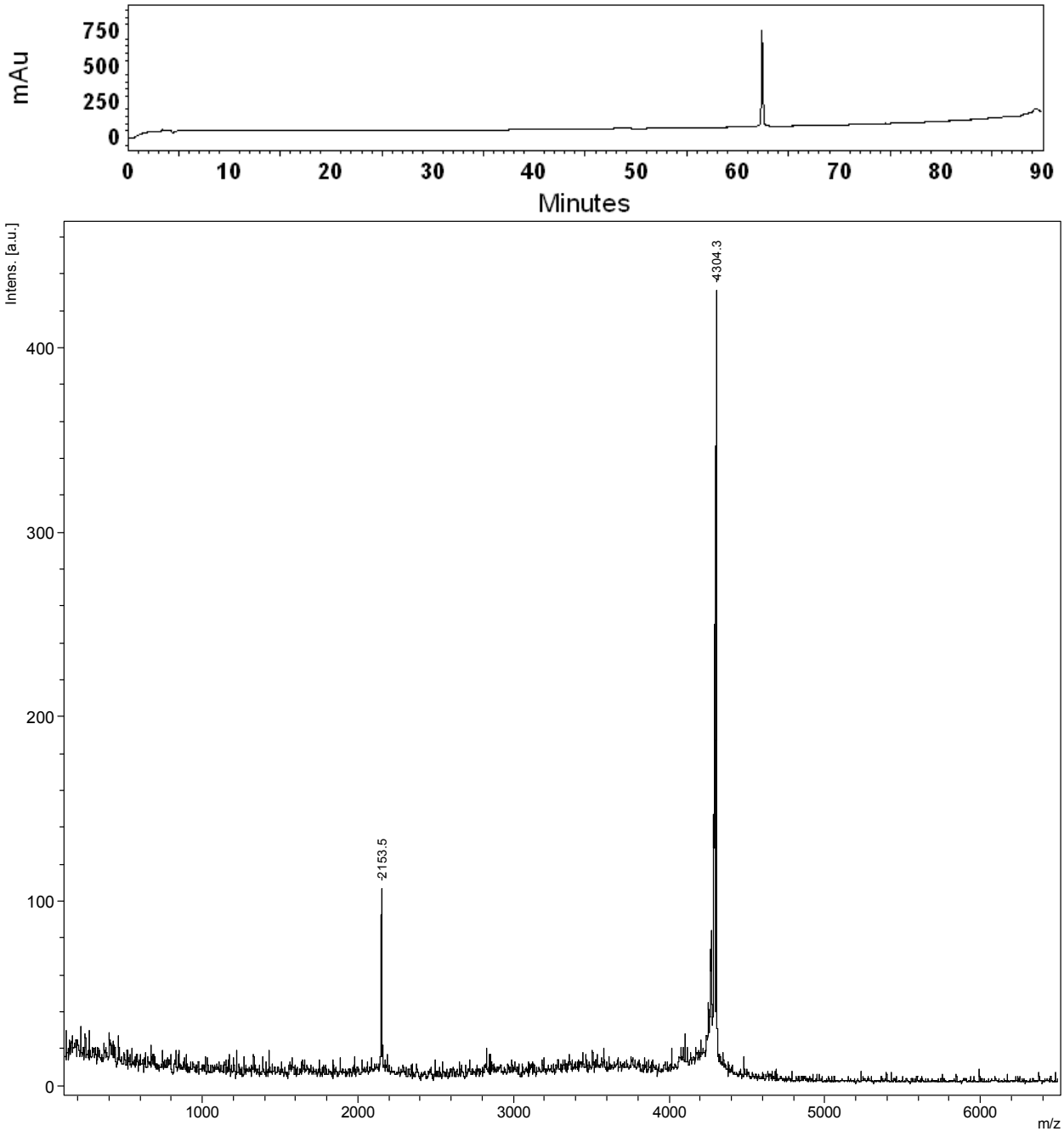

4.22

HPLC: Gradient = 10-90% solvent B over 80 minutes

MALDI-TOF: Calculated monoisotopic $[M+H]^+ = 4244.1$

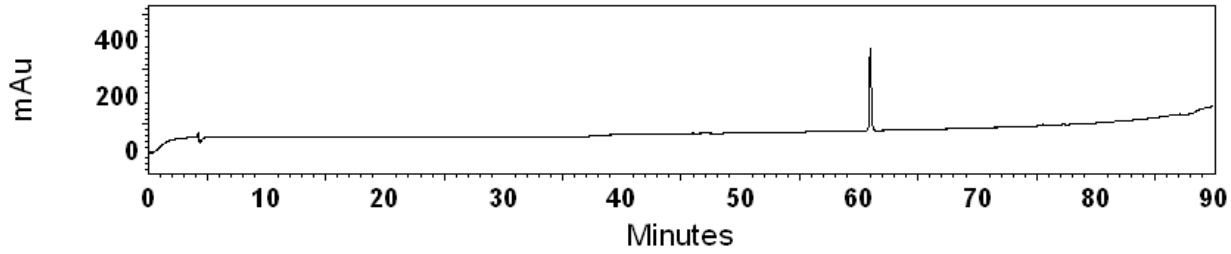

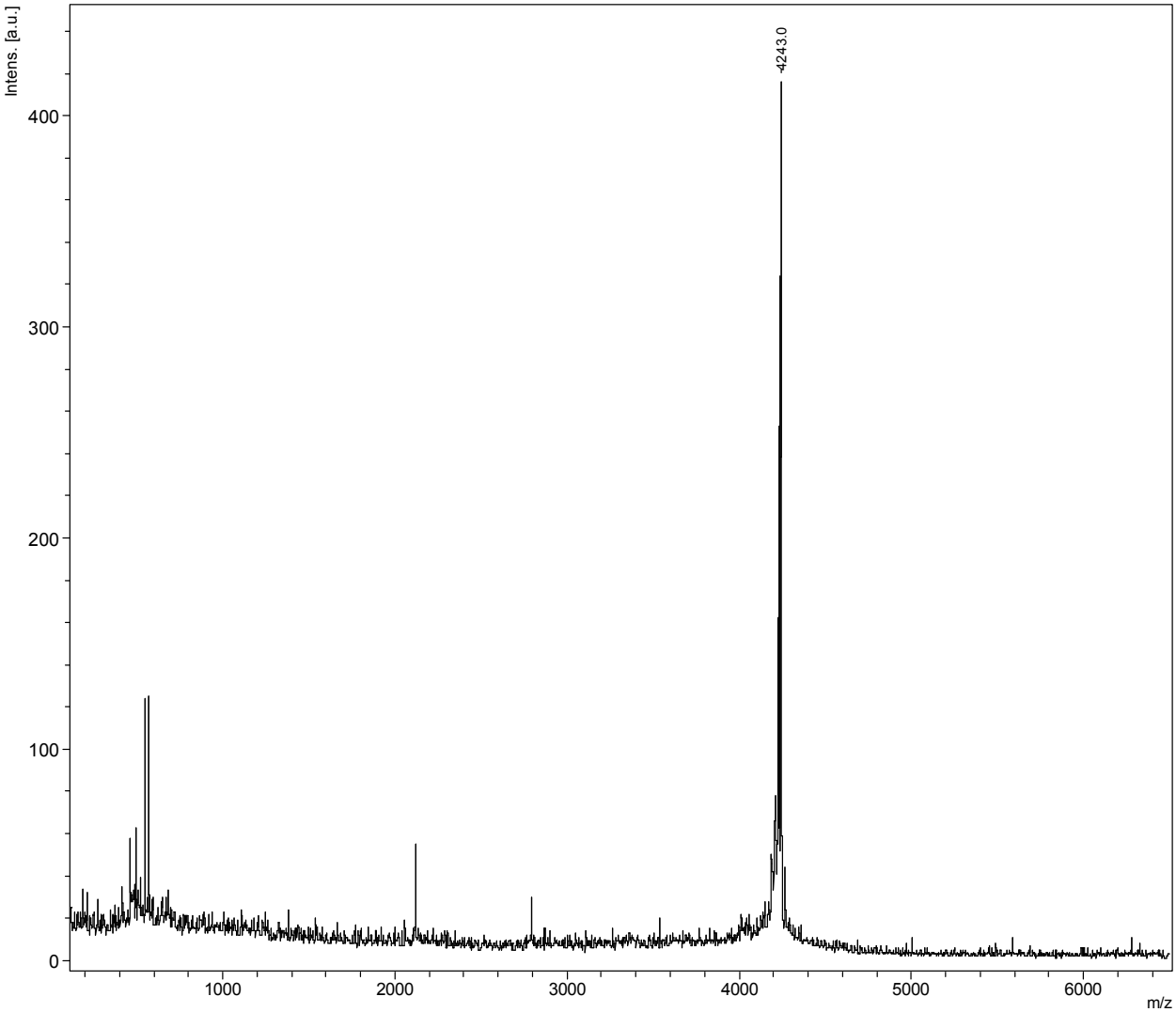

4.23

HPLC: Gradient = 10-90% solvent B over 80 minutes

MALDI-TOF: Calculated monoisotopic $[M+H]^+ = 4380.2$

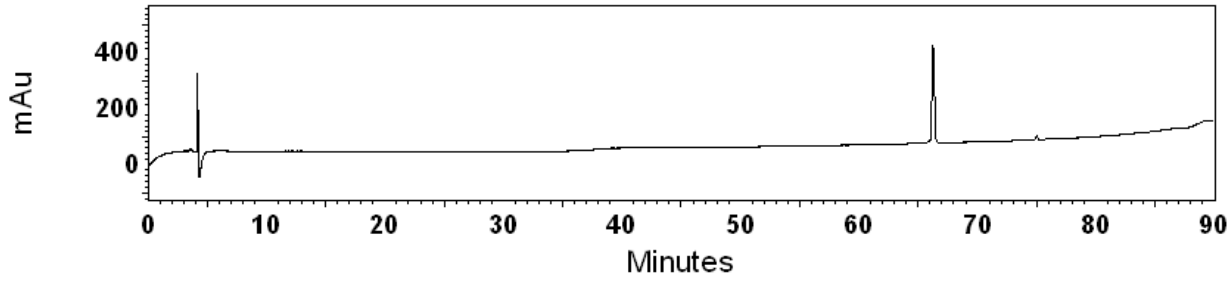

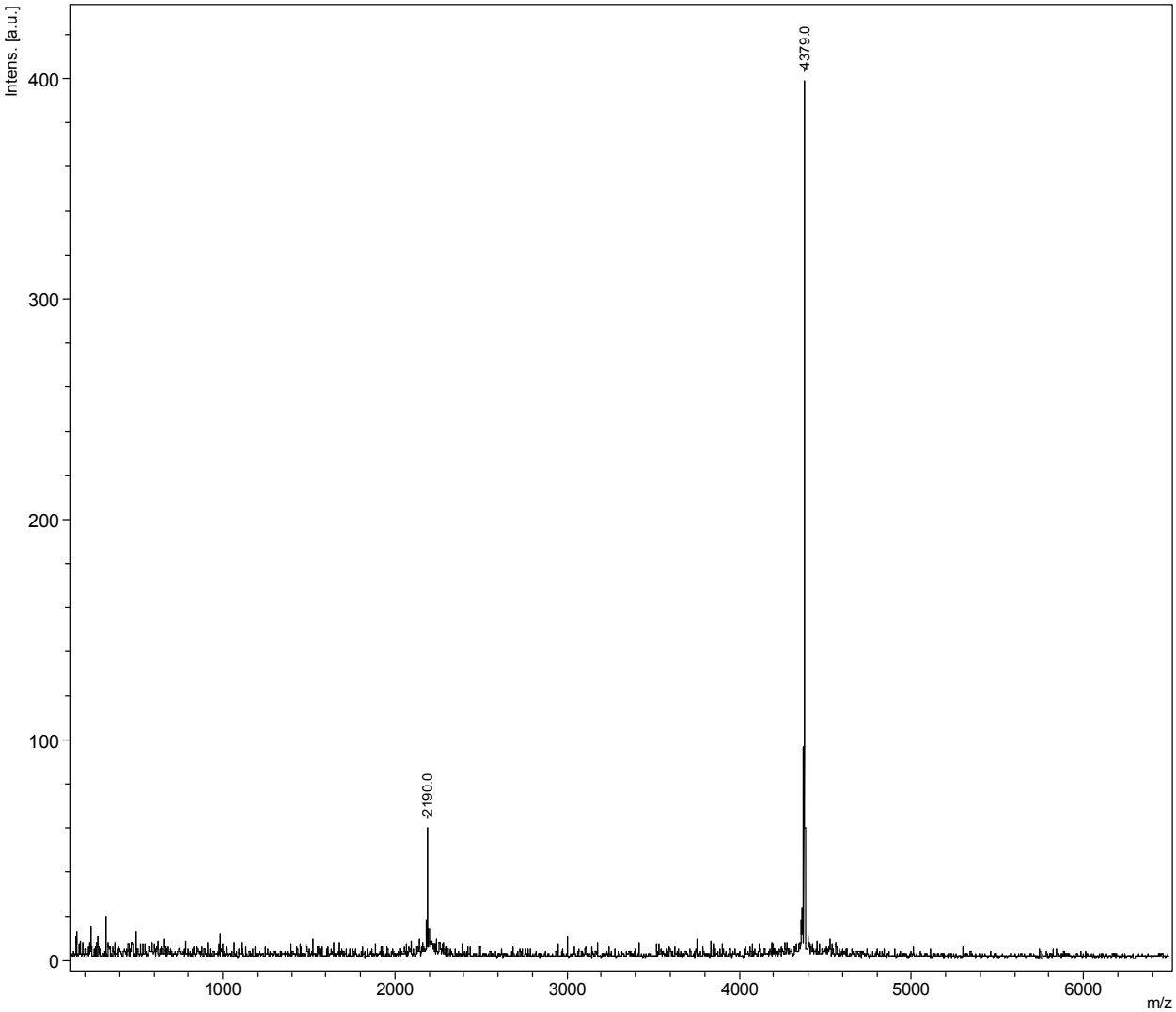

4.24

HPLC: Gradient = 10-90% solvent B over 80 minutes

MALDI-TOF: Calculated monoisotopic $[M+H]^+ = 4486.2$

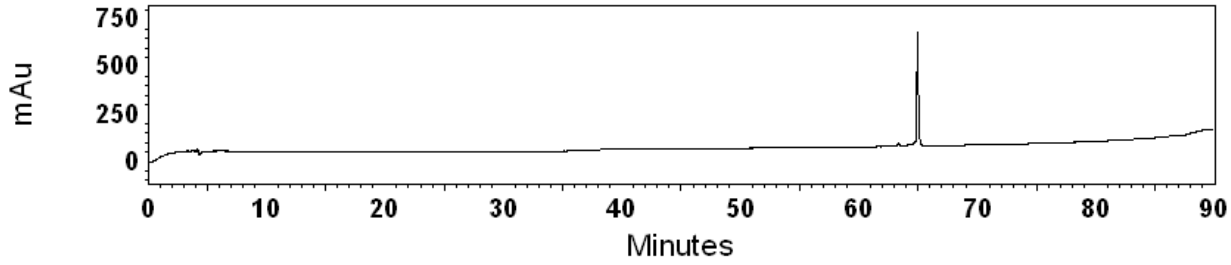

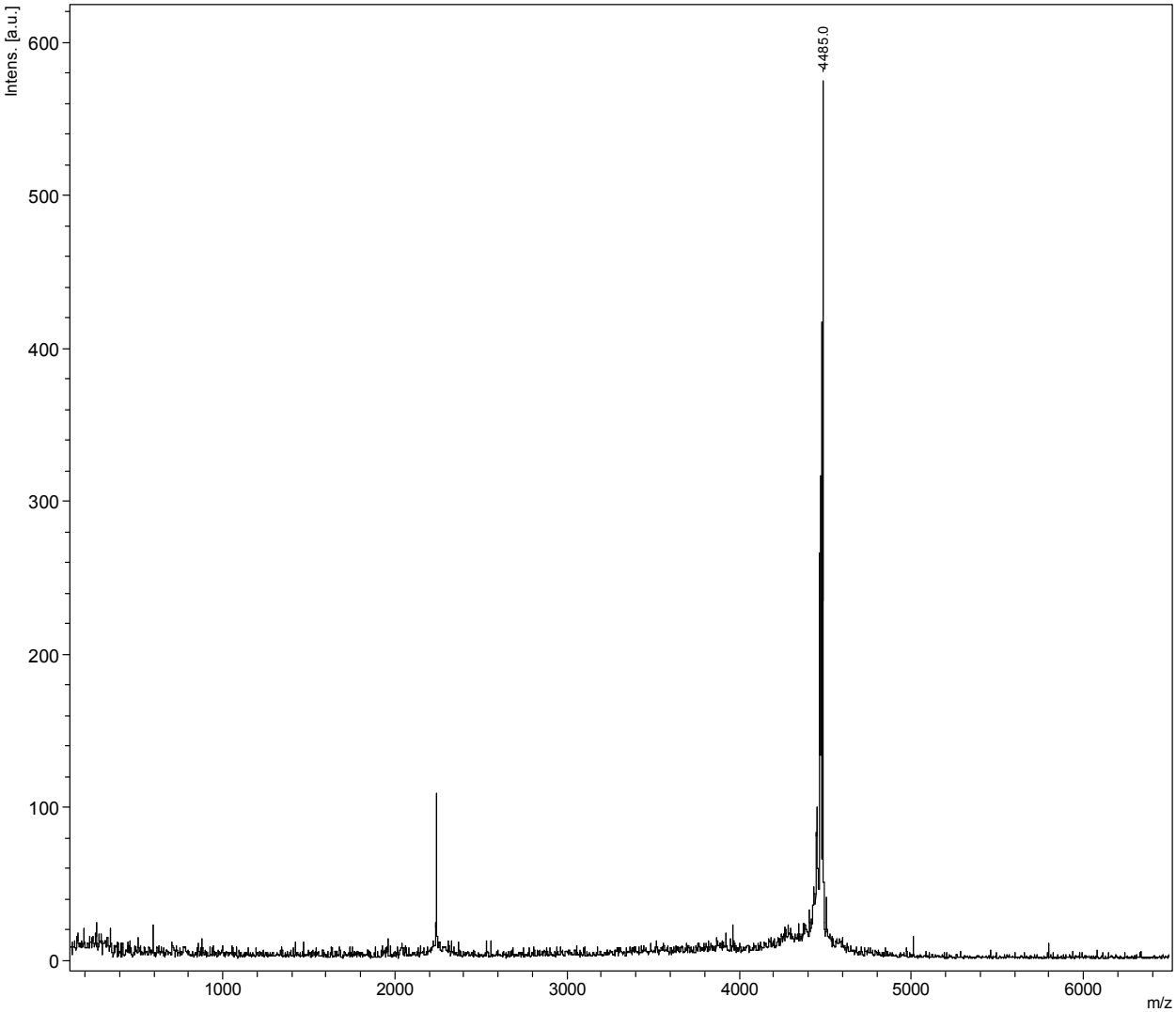

4.12 References

1. Idriss, H. T., and Naismith, J. H. (2000) TNF alpha and the TNF receptor superfamily: Structure-function relationship(s), Microscopy Research and Technique 50, 184-195.
2. Locksley, R. M., Killeen, N., and Lenardo, M. J. (2001) The TNF and TNF receptor superfamilies: Integrating mammalian biology, Cell 104, 487-501.
3. Chen, G. Q., and Goeddel, D. V. (2002) TNF-R1 signaling: A beautiful pathway, Science 296, 1634-1635.
4. Tracey, D., Klareskog, L., Sasso, E. H., Salfeld, J. G., and Tak, P. P. (2008) Tumor necrosis factor antagonist mechanisms of action: A comprehensive review, Pharmacology & Therapeutics 117, 244-279.
5. Palladino, M. A., Bahjat, F. R., Theodorakis, E. A., and Moldawer, L. L. (2003) Anti-TNF-alpha therapies: The next generation, Nature Reviews Drug Discovery 2, 736-746.
6. Smith, R. A., and Baglioni, C. (1987) The active form of tumor necrosis factor is a trimer, Journal of Biological Chemistry 262, 6951-6954.
7. Jones, E. Y., Stuart, D. I., and Walker, N. P. C. (1989) Structure of tumor necrosis factor, Nature 338, 225-228.
8. Eck, M. J., and Sprang, S. R. (1989) The structure of tumor necrosis factor-alpha at 2.6-A resolution: Implications for receptor binding, Journal of Biological Chemistry 264, 17595-17605.
9. Banner, D. W., Darcy, A., Janes, W., Gentz, R., Schoenfeld, H. J., Broger, C., Loetscher, H., and Lesslauer, W. (1993) Crystal structure of the soluble human 55 kd TNF receptor-human TNFbeta complex: Implications for TNFR receptor activation, Cell 73, 431-445.
10. Carswell, E. A., Old, L. J., Kassel, R. L., Green, S., Fiore, N., and Williamson, B. (1975) Endotoxin-induced serum factor that causes necrosis of tumors, Proceedings of the National Academy of Sciences of the United States of America 72, 3666-3670.
11. Lian, W. L., Upadhyaya, P., Rhodes, C. A., Liu, Y. S., and Pei, D. H. (2013) Screening Bicyclic Peptide Libraries for Protein-Protein Interaction Inhibitors: Discovery of a Tumor Necrosis Factor-alpha Antagonist, Journal of the American Chemical Society 135, 11990-11995.
12. Takasaki, W., Kajino, Y., Kajino, K., Murali, R., and Greene, M. I. (1997) Structure-based design and characterization of exocyclic peptidomimetics that inhibit TNF alpha binding to its receptor, Nature Biotechnology 15, 1266-1270.
13. Hu, S., Liang, S. Y., Guo, H. Z., Zhang, D. P., Li, H., Wang, X. Z., Yang, W. L., Qian, W. Z., Hou, S., Wang, H., Guo, Y. J., and Lou, Z. Y. (2013) Comparison of the Inhibition Mechanisms of Adalimumab and Infliximab in Treating Tumor Necrosis Factor alpha-Associated Diseases from a Molecular View, Journal of Biological Chemistry 288, 27059-27067.

14. He, M. M., Smith, A. S., Oslob, J. D., Flanagan, W. M., Braisted, A. C., Whitty, A., Cancilla, M. T., Wang, J., Lugovskoy, A. A., Yoburn, J. C., Fung, A. D., Farrington, G., Eldredge, J. K., Day, E. S., Cruz, L. A., Cachero, T. G., Miller, S. K., Friedman, J. E., Choong, I. C., and Cunningham, B. C. (2005) Small-molecule inhibition of TNF-alpha, Science 310, 1022-1025.

15. Luzi, S., Kondo, Y., Bernard, E., Stadler, L. K. J., Vaysburd, M., Winter, G., and Holliger, P. (2015) Subunit disassembly and inhibition of TNF alpha by a semi-synthetic bicyclic peptide, Protein Engineering Design & Selection 28, 45-52.

16. Jonsson, A., Wallberg, H., Herne, N., Stahl, S., and Frejd, F. Y. (2009) Generation of tumour-necrosis-factor-alpha-specific affibody molecules capable of blocking receptor binding in vitro, Biotechnology and Applied Biochemistry 54, 93-103.

17. Steiner, D., Forrer, P., and Pluckthun, A. (2008) Efficient Selection of DARPins with Sub-nanomolar Affinities using SRP Phage Display, Journal of Molecular Biology 382, 1211-1227.

18. Hoffmann, A., Kovermann, M., Lilie, H., Fiedler, M., Balbach, J., Rudolph, R., and Pfeifer, S. (2012) New Binding Mode to TNF-Alpha Revealed by Ubiquitin-Based Artificial Binding Protein, Plos One 7, e31298.

19. Checco, J. W., Kreitler, D. F., Thomas, N. C., Belair, D. G., Rettko, N. J., Murphy, W. L., Forest, K. T., and Gellman, S. H. (2015) Targeting diverse protein–protein interaction interfaces with α/β-peptides derived from the Z-domain scaffold, Proceedings of the National Academy of Sciences of the United States of America 112, 4552–4557.

20. Braisted, A. C., and Wells, J. A. (1996) Minimizing a binding domain from protein A, Proceedings of the National Academy of Sciences of the United States of America 93, 5688-5692.

21. Webster, J. M., Zhang, R., Gambhir, S. S., Cheng, Z., and Syud, F. A. (2009) Engineered Two-Helix Small Proteins for Molecular Recognition, Chembiochem 10, 1293-1296.

22. Starovasnik, M. A., Braisted, A. C., and Wells, J. A. (1997) Structural mimicry of a native protein by a minimized binding domain, Proceedings of the National Academy of Sciences of the United States of America 94, 10080-10085.

23. Khabar, K. S. A., Siddiqui, S., and Armstrong, J. A. (1995) WEHI-13VAR: a stable and sensitive variant of WEHI-164 clone 13 fibrosarcoma for tumor necrosis factor bioassay, Immunology Letters 46, 107-110.

24. Poiesi, C., Albertini, A., Ghielmi, S., Cassani, G., and Corti, A. (1993) Kinetic analysis of TNF-alpha oligomer-monomer transition by surface plasmon resonance and immunochemical methods, Cytokine 5, 539-545.

25. Alzani, R., Cozzi, E., Corti, A., Temponi, M., Trizio, D., Gigli, M., and Rizzo, V. (1995) Mechanism of suramin-induced deoligomerization of tumor necrosis factor alpha, Biochemistry 34, 6344-6350.

26. Kronqvist, N., Lofblom, J., Jonsson, A., Wernerus, H., and Stahl, S. (2008) A novel affinity protein selection system based on staphylococcal cell surface display and flow cytometry, Protein Engineering Design & Selection 21, 247-255.

27. Lofdahl, P. A., and Nygren, P. A. (2010) Affinity maturation of a TNF alpha-binding Affibody molecule by Darwinian survival selection, Biotechnology and Applied Biochemistry 55, 111-120.

28. DeLano, W. L., Ultsch, M. H., de Vos, A. M., and Wells, J. A. (2000) Convergent solutions to binding at a protein-protein interface, Science 287, 1279-1283.

29. Lofdahl, P. A., Nord, O., Janzon, L., and Nygren, P. A. (2009) Selection of TNF-alpha binding affibody molecules using a beta-lactamase protein fragment complementation assay, New Biotechnology 26, 251-259.

30. Pollaro, L., and Heinis, C. (2010) Strategies to prolong the plasma residence time of peptide drugs, Medchemcomm 1, 319-324.

31. Lee, H. S., LePlae, P. R., Porter, E. A., and Gellman, S. H. (2001) An efficient route to either enantiomer of orthogonally protected trans-3-aminopyrrolidine-4-carboxylic acid, Journal of Organic Chemistry 66, 3597-3599.

32. Gill, S. C., and Vonhippel, P. H. (1989) Calculation of protein extinction coefficients from amino-acid sequence data, Analytical Biochemistry 182, 319-326.

33. Greenfield, N. J. (2006) Using circular dichroism spectra to estimate protein secondary structure, Nature Protocols 1, 2876-2890.

Chapter 5: Attempts to design membrane-permeable analogues of a high-affinity α/β-peptide targeting Bcl-2 protein-protein interactions

Respective contributions:

Research design: James W. Checco, Samuel H. Gellman

Peptide design: James W. Checco, Samuel H. Gellman

Cyclic β-amino acid synthesis: James W. Checco, Timothy Choi

Peptide synthesis: James W. Checco, Timothy Choi

FP assays: James W. Checco

Peptide characterization: James W. Checco

Cell viability assays: Erinna F. Lee, W. Douglas Fairlie

Live-cell confocal microscopy: Chelcie H. Eller, James W. Checco, Ronald T. Raines

5.1 Preface

Chapters 2-4 highlight that properly designed α→β-residue substitutions can yield α/β-peptides adopting a well-folded tertiary structure that mimic the complex protein-recognition functions of their parent α-peptide. Ultimately, the efforts described in Chapters 2-4 suggest a general strategy to develop α/β-peptides to target a wide variety of proteins with irregular surface topologies. However, both α- and α/β-peptides are usually unable to cross cell membranes, which significantly limit the number of medically important proteins that can be targeted with these peptidic oligomers. The primary goal of the research described in this chapter was to develop a strategy to deliver an α/β-peptide, previously optimized for high affinity protein binding and decreased protease susceptibility, into the cytosol of cells to antagonize intracellular protein-protein interactions. Toward this goal, we designed and synthesized several novel cyclic β-amino acid residues hypothesized to increase the membrane-permeability of α/β-peptides, and evaluated their ability to enter cells and antagonize anti-apoptotic Bcl-2 family proteins to initiate apoptosis. The results from this effort were mixed. While several α/β-peptides appeared to enter cells, as designed, most did not appear to induce the intended cellular response. Rather than initiate apoptosis, many of the designed α/β-peptides appeared to kill cells in a non-specific manner at high concentrations, with no effect at lower concentrations. Ultimately, these results highlight the significant challenge of modifying optimized peptide oligomers for intracellular delivery and suggest that success may be more easily achieved by designing α/β-peptide mimics of an active α-peptide that is already known to enter cells, a direction explored in Chapter 6.

5.2 Introduction

5.2.1 Bcl-2 family protein-protein interactions

The B cell lymphoma-2 (Bcl-2) protein family mediates the initiation of apoptotic signaling, which plays an important role in a cell's response to internal damage.[1-3] The Bcl-2 family consists of three distinct classes of proteins: anti-apoptotic proteins (these include Bcl-2, Bcl-x_L, Bcl-w, and Mcl-1), pro-apoptotic multidomain proteins (Bax and Bak), and pro-apoptotic BH3-only proteins (these include Bim, Puma, and Bid) (Figure 5.1A). These proteins interact with each other in a complex network of protein-protein interactions to determine cell survival versus cell death. In many of the key protein-protein interactions in the Bcl-2 family, an anti-apoptotic member (e.g., Bcl-x_L) presents a hydrophobic groove on its surface which is engaged by an α-helix in the BH3 domain of a pro-apoptotic protein (Figure 5.1B-D).[4, 5]

The multidomain proteins Bax and Bak are the critical regulators of apoptosis.[6] When a cell is healthy, Bax and Bak are bound to anti-apoptotic members through their BH3 domains, preventing the initiation of apoptosis (Figure 5.2A). In the presence of cytotoxic signals (e.g., DNA damage), BH3-only proteins are expressed. The BH3 domain of the BH3-only proteins binds in the hydrophobic cleft presented by the anti-apoptotic proteins and displaces Bax and/or Bak (Figure 5.2A). Once free, Bax/Bak are "activated", leading to oligomerization and triggering the permeabilization of the mitochondrial outer membrane. This membrane disruption leads to the release of apoptotic molecules, such as cytochrome *c*, from the mitochondrial inner membrane space. These released apoptotic molecules subsequently activate caspases to initiate apoptosis (Figure 5.2B).[4, 5, 7, 8] The extent of the role BH3-only proteins play in activating Bax and Bak remains controversial. There is evidence that antagonizing the interaction between

Bax/Bak and anti-apoptotic proteins is sufficient for apoptosis initiation.[3] However, several studies that suggest some BH3-only proteins play additional roles by directly activating Bax/Bak.[9-11]

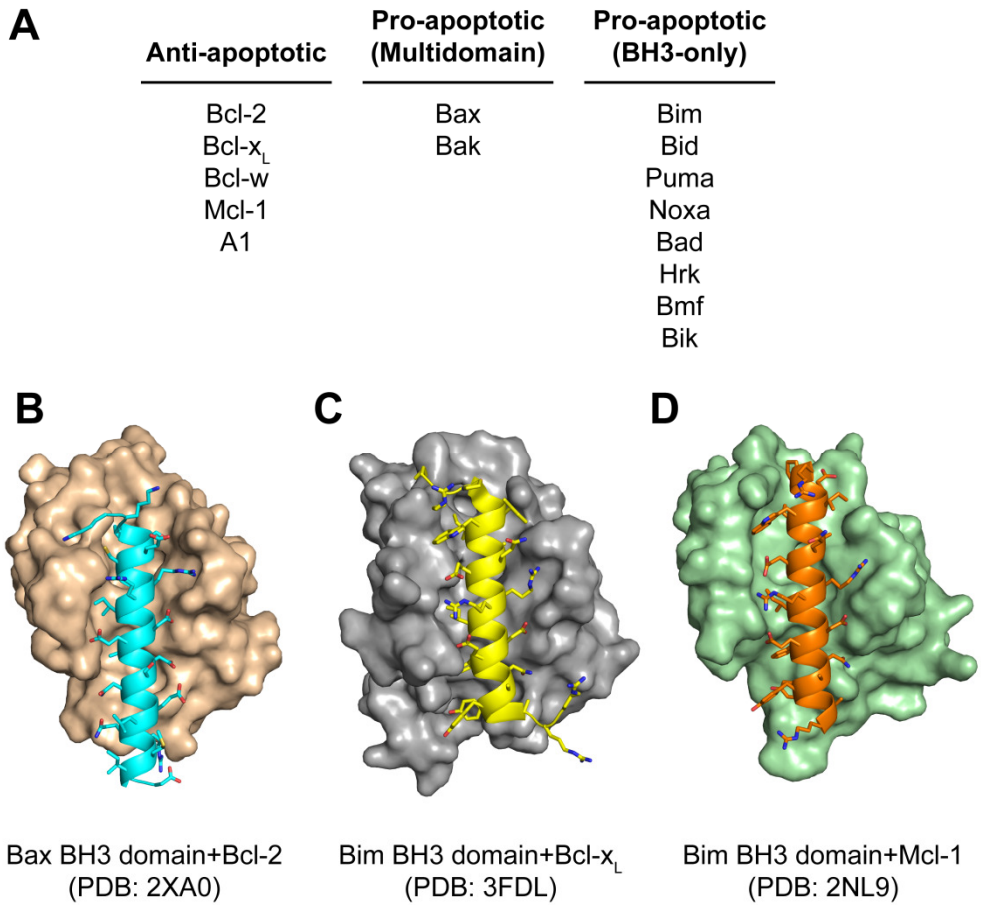

Figure 5.1 The Bcl-2 family of protein-protein interactions. (A) The Bcl-2 family is comprised of many different proteins that fall into three categories: anti-apoptotic, pro-apoptotic (multidomain), and pro-apoptotic (BH3-only). (B) X-ray crystal structure of the Bax BH3 domain (cyan) in complex with Bcl-2 (tan).[12] (C) X-ray crystal structure of the Bim BH3 domain (yellow) in complex with Bcl-x_L (gray).[13] (C) X-ray crystal structure of the Bim BH3 domain (orange) in complex with Mcl-1 (green).[14] The BH3 domain of these pro-apoptotic proteins forms an α-helix that binds to a hydrophobic cleft on the anti-apoptotic proteins.

Numerous forms of cancer take advantage of the Bcl-2 pathway by overexpressing anti-apoptotic family members.[15, 16] These overexpressed anti-apoptotic proteins are able to suppress apoptotic signaling by preventing the activation of Bax and Bak, either by directly sequestering these mutlidomain proteins or by sequestering pro-apoptotic BH3-only proteins. Freeing pro-

apoptotic proteins through the antagonism of these protein-protein interactions is a potential mechanism by which to initiate the apoptosis of unwanted cells.[5, 17] Certain types of cancers may be particularly susceptible to this inhibition due to a high dependence on Bcl-2 family proteins for survival and increased endocytic activity.[5, 10, 18] Indeed, several small molecules that bind anti-apoptotic proteins act as antagonists of these protein-protein interactions, can cause regression of tumors in mice,[17, 19] and have shown promising results in cancer patients.[20, 21] Peptides that mimic the helical BH3 domains of pro-apoptotic proteins are promising sources of high-affinity antagonists that may be able to target anti-apoptotic proteins not accessible to any currently known small molecules.[22, 23] However, peptides are usually not able to cross cell membranes, and so the application of these molecules as antagonists of Bcl-2 family proteins (which occur inside the cell) is severely limited in biological systems.

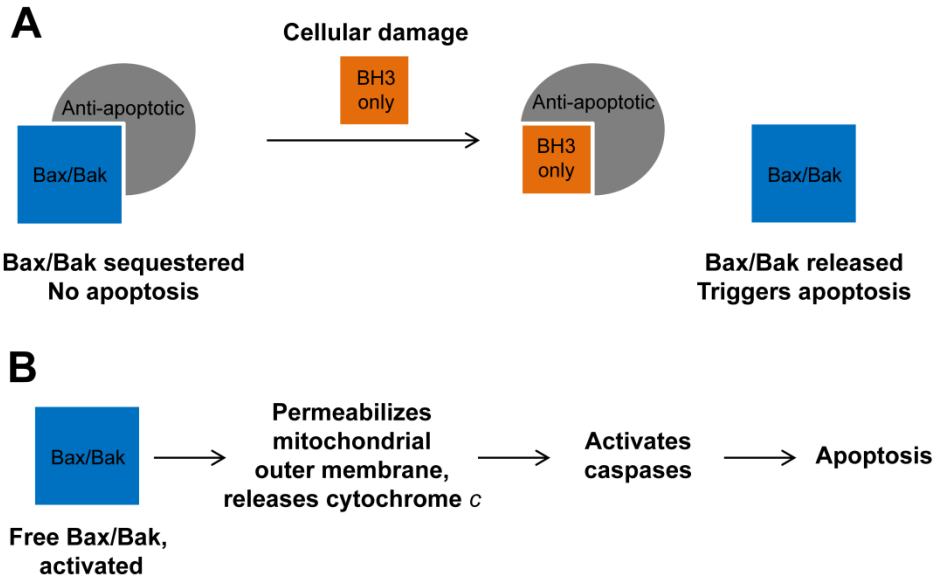

Figure 5.2 Cartoon depiction of a normal apoptotic response initiated by the Bcl-2 family of proteins.

5.2.2 α/β-Peptides targeting Bcl-2 proteins

Because BH3-only proteins engage anti-apoptotic proteins through short, α-helical segments, they represent a class of proteins well suited for mimicry by α/β-peptides. Our group has previously used these α-helical BH3 domains from Bcl-2 family proteins as model systems for exploring the effects of α→β-residue substitutions on the recognition of a helical ligand by partner proteins.[24-26] Early efforts to design foldamer mimics of helical BH3 domains ultimately led to the development of the "sequence-based design" strategy to develop α/β-peptides.[24] In sequence-based design, α-residues are systematically replaced with β^3-residues bearing the analogous side chains in a regularly spaced pattern. The first successful application of the sequence-based design strategy explored α/β-peptide analogues of the Puma BH3 domain.[24] α/β-Peptide analogues of the Puma BH3 peptide were designed exploring each register of the ααβαααβ substitution pattern, and some of the resulting α/β-peptides bound to anti-apoptotic proteins with high affinity while having a decreased susceptibility to proteolysis. Expanding on this approach, our group next explored α/β-peptide analogues of the Bim BH3 domain (Peptide **A**, Figure 5.3).[25] Incorporation of β^3-amino acids in an ααβαααβ pattern (as was employed for Puma), as well as in ααβ and αααβ patterns, led to two α/β-peptides that showed significant binding to anti-apoptotic proteins Bcl-x_L and Mcl-1 (one of these α/β-peptides, **B**, is shown in Figure 5.3). X-ray co-crystal structures of these α/β-peptides bound to Bcl-x_L revealed that these α/β-peptides adopt conformations very similar to the natural BH3 ligands when bound to their target protein.[25]

A

		FP K_i (nM)		
		Bcl-x_L	Mcl-1	$t_{1/2}$ (min.)
A	Ac-I W I A Q E L R R I G D E F N A Y Y-NH_2	23	26	1.7
B	Ac-I W I A Q E L R R I G D E F N A Y Y-NH_2	580	230	29
C	Ac-I X I A Q U L R Z I G D U F N X Y Y-NH_2	70	7.9	210
5.1	Ac-I X I A E U L R Z I G D U F N X K Y-NH_2	24	2.4	620

B

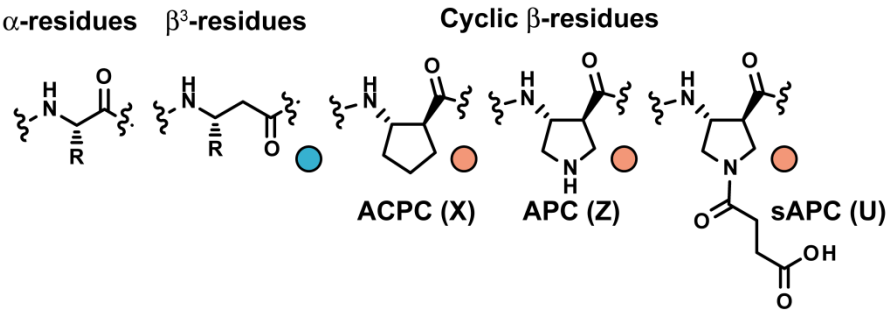

Figure 5.3 Sequences of α/β-peptides derived from the Bim BH3 domain, as previously reported.[25, 26] (A) Sequences of the Bim BH3 α-peptide **A** and α/β-peptides **B**, **C**, and **5.1**, along with K_i values, as determined by competition fluorescence polarization (FP) assay for binding to Bcl-x_L and Mcl-1, and half-life values ($t_{1/2}$) to degradation by 5 μg/mL proteinase K in TBS, pH 7.5 with 5% DMSO. Non-natural residues are indicated by colored circles. (B) Structures of a generic α-residue, a generic β^3-residue (teal), and the cyclic β-residues ACPC (X), APC (Z), and sAPC (U) (orange).

Replacing β^3-residues with cyclic β-residues can increase protein affinity and reduce protease susceptibility, presumably by restricting the flexibility about the Cα-Cβ torsion.[27] α/β-Peptide **B**, which features β^3-residues in an ααβααβ pattern, binds to target proteins Bcl-x_L and Mcl-1 with ~10-20-fold decreased affinity relative to the parent α-peptide, **A**. To attempt to increase the affinity of **B** for anti-apoptotic proteins, our group replaced the β^3-residues in **B** with cyclic β-residues, to yield **C** (Figure 5.3).[26] In this design, the hydrophobic cyclic β-residue ACPC (X) replaced β^3-Trp and β^3-Ala, the cationic cyclic β-residue APC (Z) replaced β^3-Arg, and the anionic sAPC (U) replaced β^3-Glu. Consistent with the design hypothesis, α/β-peptide **C** showed a greater affinity for Bcl-x_L and Mcl-1 relative to **B**. Furthermore, **C** also displayed

significantly decreased susceptibility to proteinase K degradation relative to both α/β-peptide **B** as well as the parent α-peptide **A**. Further optimization of **C**, based on the results of a "hydrophile" scan,[28] resulted in the most potent and proteolytically stable Bim-derived α/β-peptide, **5.1** (Figure 5.3).[26] Both **C** and **5.1** induced cytochrome *c* release from the mitochondria into the cytosol of mouse embryonic fibroblasts (MEFs) in which the outer membranes had been permeabilized, consistent with their intended biological effect as antagonists of anti-apoptotic proteins.[26] In contrast, α/β-peptide **B**, which bound to Bcl-x_L and Mcl-1 with lower affinity than **C** or **5.1**, did not induce cytochrome *c* release in permeabilized MEFs.[26] These results indicate that high affinity α/β-peptide analogues of **A** can engage Bcl-2 family proteins inside cells and may initiate apoptosis in living cells, if they can reach the cytosol. However, α/β-peptides are not expected to spontaneously cross intact cell membranes.

Because the α/β-peptide **5.1** binds to anti-apoptotic proteins with high affinity and is able to induce cytochrome *c* release in permeabilized MEFs, we hypothesized that it could be an antagonist of Bcl-2 family proteins in living cells, if a strategy could be identified to facilitate its transport across the outer cell membrane. The primary goal for the project described in this chapter was to design a method for delivering α/β-peptide **5.1** could be delivered into the cytosol of cells to antagonize intracellular Bcl-2 family proteins to initiate apoptosis.

5.2.3 Commonly utilized methods for increasing the membrane-permeability of peptides

Numerous strategies have been explored to attempt to impart cell-permeability into peptides. Fatty acid acylation of one terminus or side chain is commonly used in biological systems to target proteins to membranes, and it has been found that the attachment of hydrophobic sequences onto peptides can direct peptides to membranes.[29] Extended alkyl chains, generally 8-16 carbons in length, have been covalently attached to numerous peptide sequences

(including BH3 domains) to facilitate entry into cells.[30-33] This strategy can be used for many different types of targets, including peptide sequences that possess a net negative charge.[34] In a similar manner, prenylation has also been shown to grant cell-penetrating properties to peptides.[35, 36]

The stabilization of helical peptides, either through hydrocarbon-crosslinked "staples" or the hydrogen bond surrogate (HBS) strategy, has received attention as an additional method for targeting intracellular protein-protein interactions.[37-40] While these helix stabilizing strategies offer many of the same advantages as cyclic β-residue-containing α/β-peptides (such as an increased affinity and proteolytic stability over unconstrained analogues), it has been found that the presence of certain hydrocarbon bridges can also confer cell-penetrating properties to some peptides. For example, a series of hydrocarbon-crosslinked peptides derived from different BH3 domains were individually shown to enter cells and induce apoptosis.[18, 41, 42] A hydrocarbon-crosslinked peptide derived from the Bid BH3 domain was able to suppress tumor growth in mice by triggering apoptosis in tumor cells overexpressing Bcl-2 family proteins.[10] However, one important consequence of the addition of a permanent cell-penetrating group is that this group may significantly alter the biological activity of the resulting peptide. For example, hydrocarbon-crosslinks can make hydrophobic contacts with target proteins, affecting both affinity and selectivity of peptides containing the crosslinks.[42, 43]

In addition to covalent modification with hydrophobic groups, one of the most common approaches for delivering peptides into cells has been the attachment of cell-penetrating peptides (CPPs) to the molecules of interest. CPPs are short, often highly cationic peptide sequences that, when appended to a molecule of interest, facilitate its transport across the cell membrane. CPPs such as Tat from HIV, transportan, penetratin, and polyarginines are among the most common

sequences used, though many more exist.[44-47] In general, studies indicate that amphipathicity and a net positive charge are important for translocation of CPPs.

Oligomers containing β-amino acids can enter cells. Cationic β-peptides and hydrocarbon-crosslinked β-peptides have been shown to cross cell membranes in manners similar to those of their α-peptide counterparts.[48-52] These precedents indicate that the presence of β-amino acid residues in an α/β-peptide should not inherently prevent it from crossing the cell membrane.

5.3 Novel cyclic β-amino acid residues with labile ester side chains

We sought to design new cyclic β-amino acids bearing functional groups that may impart membrane permeability to the α/β-peptides in which they were incorporated. Furthermore, we envisioned that cell-penetrating functional groups linked through labile ester bonds would be stable enough to allow cellular entry, but would then be removed by intracellular esterases once in the cytosol (Figure 5.4). The removal of the cell-penetrating moiety upon cell entry would ensure that the functional groups used for membrane permeability do not interfere with α/β-peptide binding to target proteins inside the cell. Based on literature precedents described above, we hypothesized that linear alkyl groups may be used to facilitate cellular entry. This strategy, using labile alkyl esters to impart membrane permeability, has been explored in the context of short, cationic α-peptides,[53] but has not been explored in functional α/β-peptides.

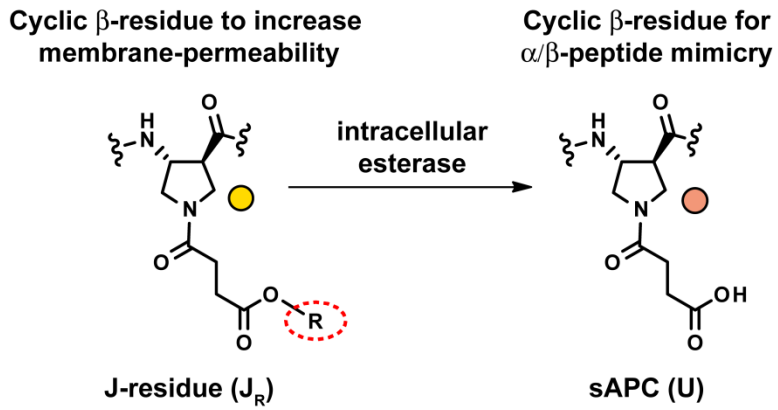

Figure 5.4 Design hypothesis behind the cyclic β-residues ("J-residues") described in this chapter. Each J-residue features a chemical group hypothesized to increase membrane permeability ("R", highlighted by red circle). If an α/β-peptide containing a J-residue enters the cell, intracellular esterases should hydrolyze the J-residue into sAPC, a residue used to replace anionic α- or β^3-residues in α/β-peptide design.

We designed analogues of the cyclic β-amino acid sAPC,[26] called "J-amino acids", featuring alkyl chains of various length linked through a succinyl ester (Figure 5.5). J-residues are designed to be hydrolyzed to sAPC residues once inside the cell. Therefore, we envisioned that any J-residue may be used to replace an sAPC residue in an optimized α/β-peptide, allowing for the release of this optimized α/β-peptide in the cell (Figure 5.4).

Fmoc-protected building blocks for the incorporation of J-amino acid residues via solid-phase peptide synthesis were synthesized from coupling of the corresponding alkyl succinate (e.g., mono-pentyl succinate) to the side chain nitrogen of Fmoc-APC-OH (Figure 5.6, and Figures 5.19 and 5.20 in "Experimental Methods"). Synthesis of these monomers was completed in collaboration with undergraduate Timothy Choi.

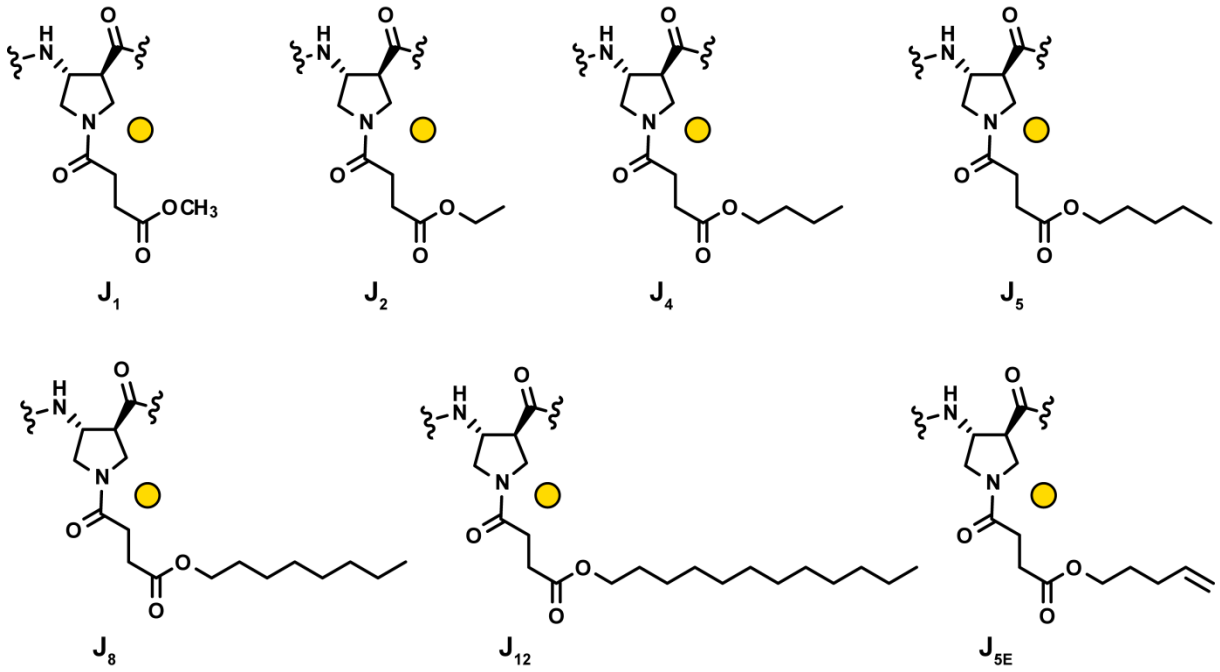

Figure 5.5 Library of J-residues. Each J-residue in this series is denoted "J_R", where R indicates the number of carbon atoms present in the alkyl ester (e.g., J_5 contains a pentyl ester functional group). J_{5E} contains an alkene for use in ring-closing metathesis. The corresponding monomer building blocks for use in solid-phase peptide synthesis are shown in Figure 5.19 in the "Experimental Methods" section.

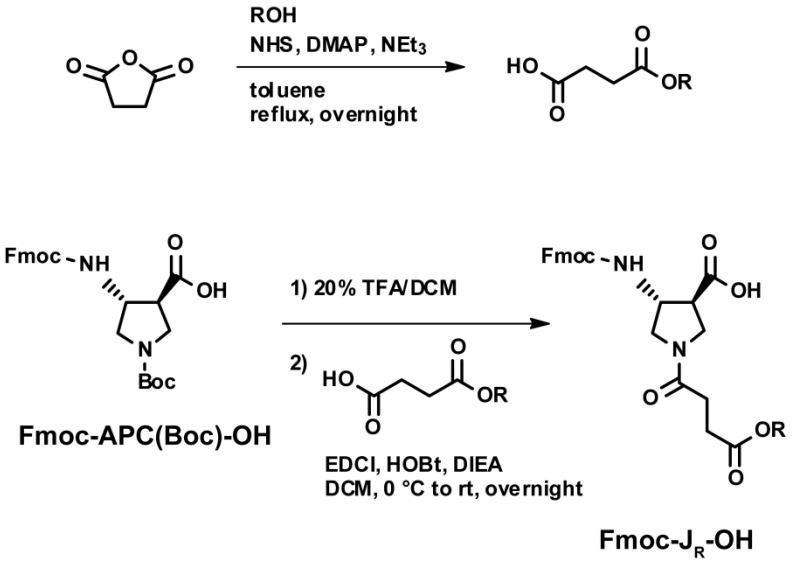

Figure 5.6 Scheme for the synthesis of J-amino acid monomers for use in solid-phase peptide synthesis.

5.4 Bim-derived α/β-peptides bearing J-amino acid residues for cell permeability

5.4.1 Initial α/β-Peptide designs

We used α/β-peptide **5.1**, derived from the Bim BH3 domain,[26] as the starting point for the design of cell-permeable α/β-peptides. This α/β-peptide was chosen because of its high affinity for anti-apoptotic proteins Bcl-x_L and Mcl-1 and its high stability to degradation by proteinase K. Starting from **5.1**, we designed analogues **5.2-5.6** by substituting the sAPC residues at positions 6 and 13 in **5.1** with J-residues bearing alkyl chains of varying lengths (Figure 5.7).

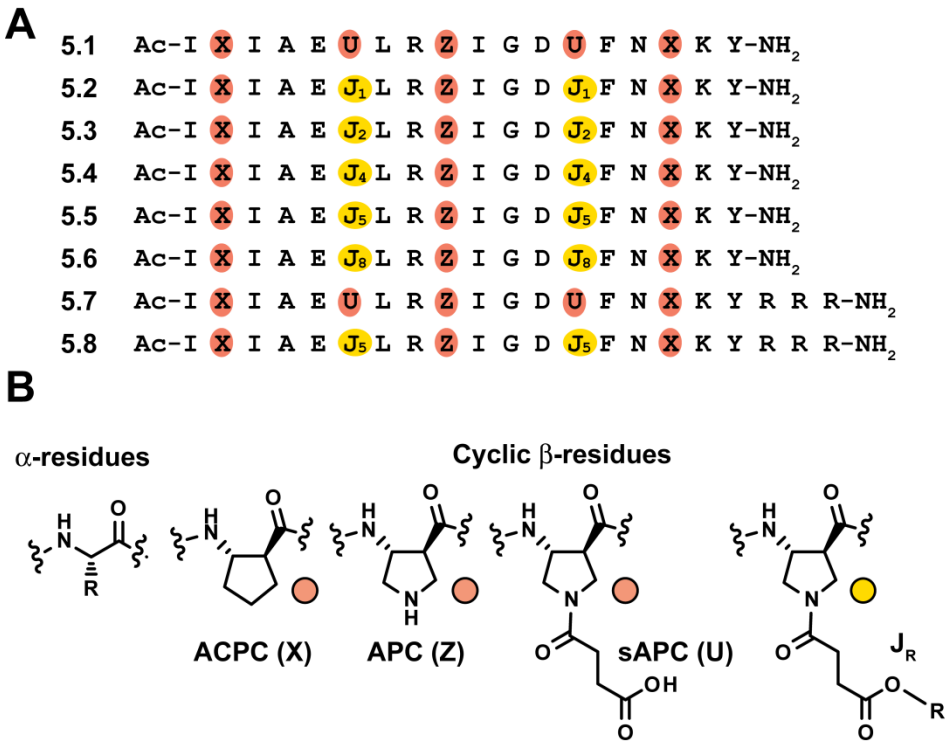

Figure 5.7 (A) Sequences of α/β-peptides derived from the Bim-derived α/β-peptide **5.1**.[26] Non-natural residues are indicated by colored circles. J-residues correspond to structures in Figure 5.5. (B) Structures of a generic α-residue, the cyclic β-residues ACPC (X), APC (Z), sAPC (U) (orange), and a generic J-residue (yellow).

As outlined above, we envisioned that if any of **5.2-5.6** entered cells (due to the inclusion of the hydrophobic alkyl side chains), then each of these would be hydrolyzed into **5.1**, which could target anti-apoptotic proteins inside the cell to initiate apoptosis.

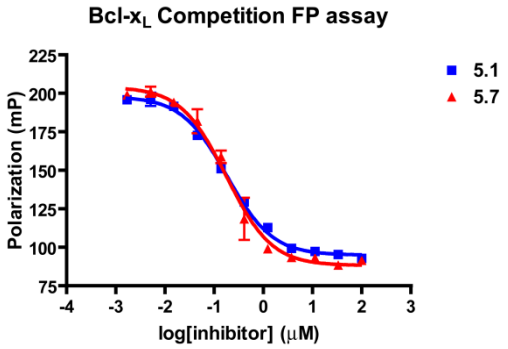

Figure 5.8 Representative Bcl-x_L competition FP assay evaluating the ability of **5.1** (blue, K_i = 49 nM) and **5.7** (red, K_i = 48 nM) to displace the binding of a tracer peptide from Bcl-x_L. Experimental uncertainly for calculated K_i values from competition FP assays is ~2-fold. α/β-Peptide **5.7** binds to Bcl-x_L with the same affinity as **5.1**.

Many peptides that are able to enter cells contain an overall net positive charge, often from multiple arginine residues.[44, 47, 54] The α/β-peptides **5.2-5.6** all have a net charge of -1, which may diminish or prevent membrane permeability even in the presence of the alkyl esters. To test the hypothesis that increasing positive charge may facilitate more efficient cell entry, we designed α/β-peptides **5.7** and **5.8** (analogues of **5.1** and **5.5**, respectively) bearing three additional arginine residues at their C-termini. To gain insight into how these additional residues affected the affinity of the resulting α/β-peptides for their anti-apoptotic proteins, we evaluated the affinity of **5.7** for Bcl-x_L by competition fluorescence polarization (FP) assay (Figure 5.8).[24, 25] In this experiment, we found that **5.7** bound to Bcl-x_L with affinity virtually identical to that of **5.1**, which indicates that the C-terminal arginine residues do not negatively affect the affinity of **5.7** for this protein. However, because we evaluated the binding of **5.7** to only Bcl-x_L, it may be that the addition of the three arginine residues may negatively affect binding to other anti-apoptotic proteins (e.g., Mcl-1), which would influence activity in cell-based assays.

5.4.2 Characterization of α/β-peptides

Each of the new J-amino acid monomers were incorporated into the α/β-peptides described above by microwave-assisted solid-phase peptide synthesis. The completed α/β-

peptides were cleaved from the solid phase using standard trifluoroacetic acid (TFA) cleavage conditions and purified by reverse-phase high performance liquid chromatography (HPLC) using a water+0.1%TFA/acetonitrile+0.1% TFA solvent system. The ester side chains of the J-residues survived the synthesis and purification process, as judged by mass spectrometry ("Peptide Characterization" section below).

As additional evidence in support of the presence of the ester functional group in the synthesized α/β-peptides, we subjected α/β-peptide **5.2**, which contains two J_1 residues, to basic conditions to chemically hydrolyze the methyl esters (Figure 5.9). After incubation overnight in 25 mM NaOH, we saw a shift to earlier retention time in the reverse-phase HPLC chromatogram, consistent with the removal of the hydrophobic methyl esters upon hydrolysis. Furthermore, MALDI-TOF analysis of the reaction mixture showed that the mass of the major product in the solution after the hydrolysis reaction corresponded to that of **5.1** (calc. $[M+H]^+$ = 2351.2, obs. $[M+H]^+$ = 2351.7), indicating that **5.2** had been hydrolyzed to **5.1**, as intended.

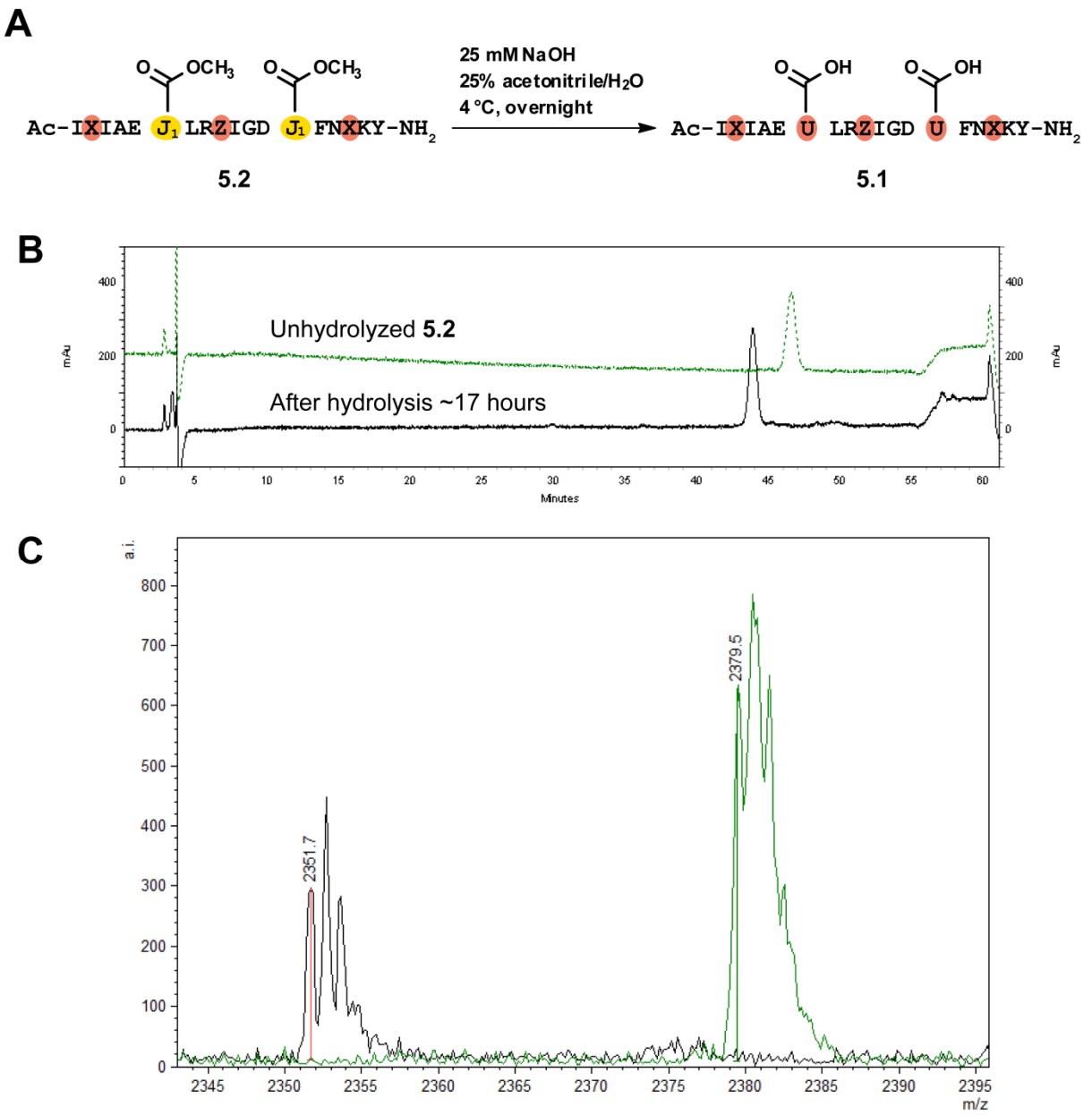

Figure 5.9 Chemical hydrolysis of α/β-peptide **5.2**. (A) Reaction conditions for the hydrolysis of **5.2** into **5.1**. (B) Overlay of the analytical-scale reverse-phase HPLC chromatograms resulting from the injection of **5.2** before (green) and after (black) subjection to hydrolysis conditions. (C) Overlay of MALDI-TOF MS spectra for **5.2** before (green) and after (black) subjection to hydrolysis conditions. **5.2** calc. $[M+H]^+ = 2379.3$; **5.1** calc. $[M+H]^+ = 2351.2$.

The ultimate goal for the research described in this chapter was to evaluate the ability of α/β-peptides bearing J-amino acid residues to cross cell membranes and initiate apoptosis by antagonizing Bcl-2 family proteins inside the cell. To gain insight into the stability and solubility of these compounds under conditions similar to those used in cell culture, we first incubated **5.2**

in Dulbecco's Modified Eagle's Medium (DMEM) with 1% fetal bovine serum (FBS) and 1% dimethylsulfoxide (DMSO) at 37 °C. At various times we centrifuged the mixture and injected the resulting supernatant onto reverse-phase analytical-scale HPLC to quantify the amount of intact, soluble peptide remaining in solution. (α/β-Peptide that precipitated over the course of the experiment would be pelleted by centrifugation and thus absent from the supernatant.) In this experiment, we found that the peak in the HPLC chromatogram corresponding to **5.2** remained relatively consistent over 16 hours (Figure 5.10). This indicates that α/β-peptide **5.2** is mostly soluble, and that the methyl ester functional group in the side chain of the J_1 residues is stable under cell culture conditions.

We next incubated 25 μM **5.5**, **5.6**, and **5.8** in DMEM with 1% FBS and 1% DMSO at 37 °C and monitored solubility over time, as described above (Figure 5.10). In this experiment, we found that **5.5** remained fully soluble for at least 2 hours, but at the 4 hour time point we observed a complete disappearance of the corresponding peak in the chromatogram, suggesting that **5.5** is removed from solution over that time. Thus, **5.5** is less soluble in aqueous solution than is **5.2**, which remained in solution for significantly longer in this experiment. α/β-Peptide **5.8**, the analogue of **5.5** containing three C-terminal arginine residues, disappeared from solution at a reduced rate, consistent with the hypothesis that this α/β-peptide would be more soluble than **5.5**. α/β-Peptide **5.6**, which contains two J_8 residues, was almost completely absent from the solution centrifuged after just 15 minutes of incubation, indicating that a substantial amount of this α/β-peptide is rapidly removed from solution, presumably due to the two hydrophobic octyl esters present in the J_8 residues (See also Figure 5.21 in "Experimental Methods"). Overall, these preliminary solubility experiments indicate that α/β-peptides containing J-residues with extended

alkyl esters are removed from solution over time. This could be due to aggregation/precipitation, association with serum proteins, or hydrolysis of the esters.

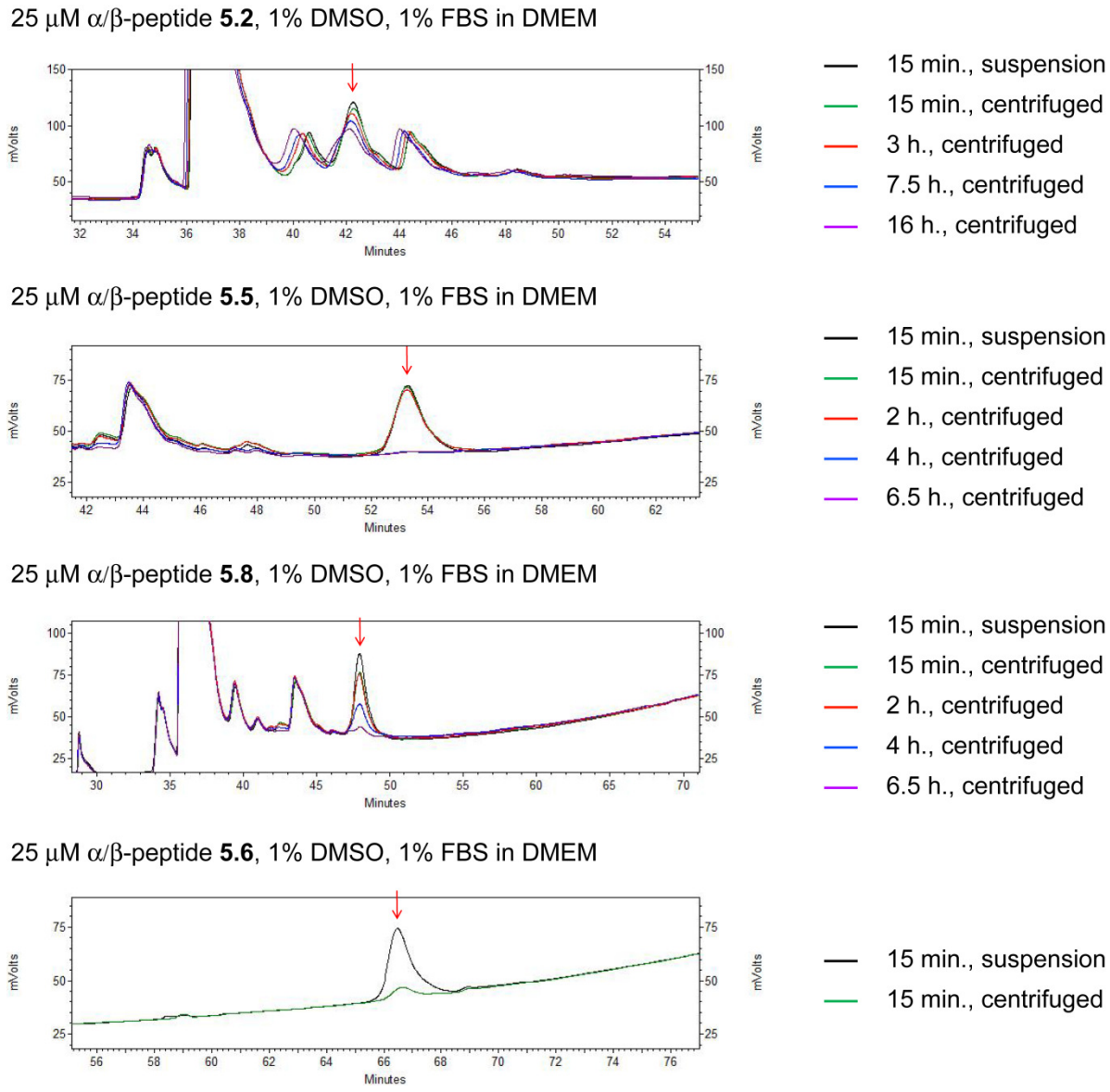

Figure 5.10 Evaluation of the presence of α/β-peptides containing J-residues in solution over time. α/β-Peptides were incubated in the indicated media at 37 °C. After 15 minutes, the suspension was injected onto analytical-scale reverse-phase HPLC (black chromatogram) to determine the amount of α/β-peptide present at that time point. After centrifuging at various time points, the supernatant was injected onto HPLC. The peak in each HPLC chromatogram corresponding to the α/β-peptide is indicated by the red arrow.

5.5 Evaluation of cellular uptake by confocal microscopy

Bim-derived peptides bearing two linear alkyl side chains with 5 carbon atoms can induce apoptosis in cells,[55] which suggests this amount of hydrophobicity is sufficient to grant cell permeability. To gain insight into how α/β-peptide analogues of **5.1** bearing two J_5 residues interact with cells, we synthesized fluorescein-labeled analogues of **5.1**, **5.5**, and **5.8** (**Flu-5.1**, **Flu-5.5**, and **Flu-5.8**, respectively) (Figure 5.11) and monitored cellular uptake by live-cell confocal microscopy. This work was completed in collaboration with Chelcie Eller (Raines Laboratory, University of Wisconsin-Madison).

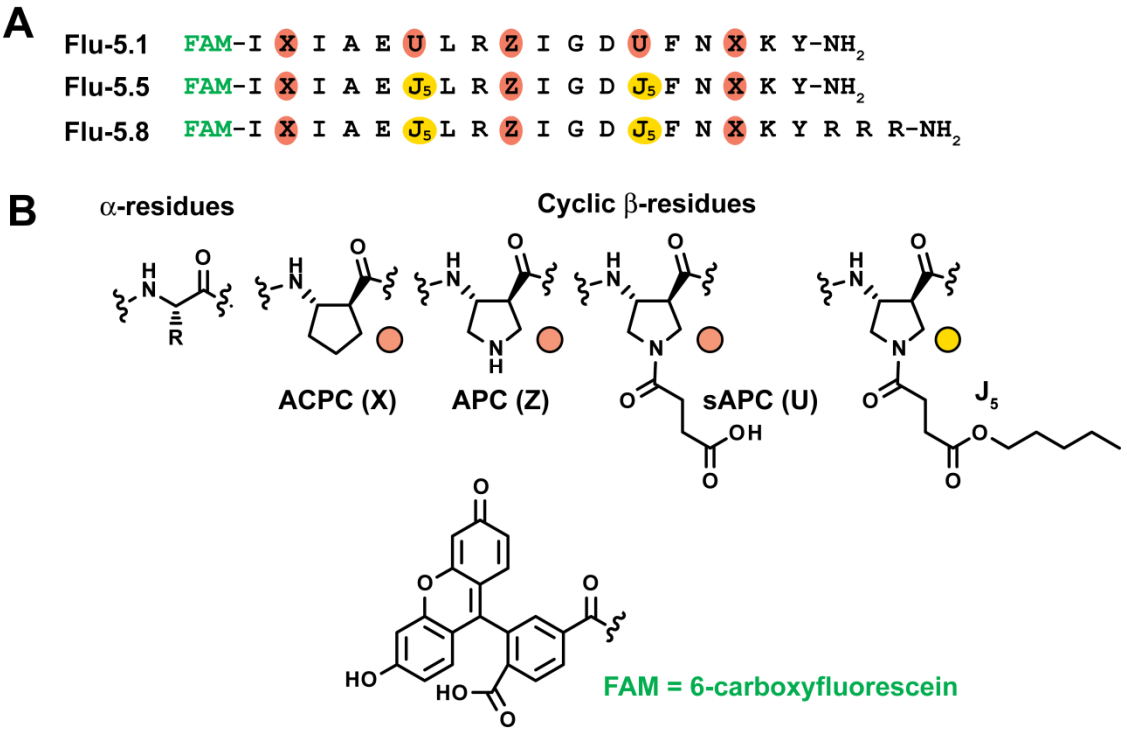

Figure 5.11 (A) Sequences of fluorescein-labeled analogues of α/β-peptides described in this chapter. Non-natural residues are indicated by colored circles. J-residues correspond to structures in Figure 5.5. FAM = 6-carboxyfluorescein. (B) Structures of a generic α-residue, the cyclic β-residues ACPC (X), APC (Z), sAPC (U) (orange), a generic J-residue (yellow), and the fluorophore 6-carboxyfluorescein.

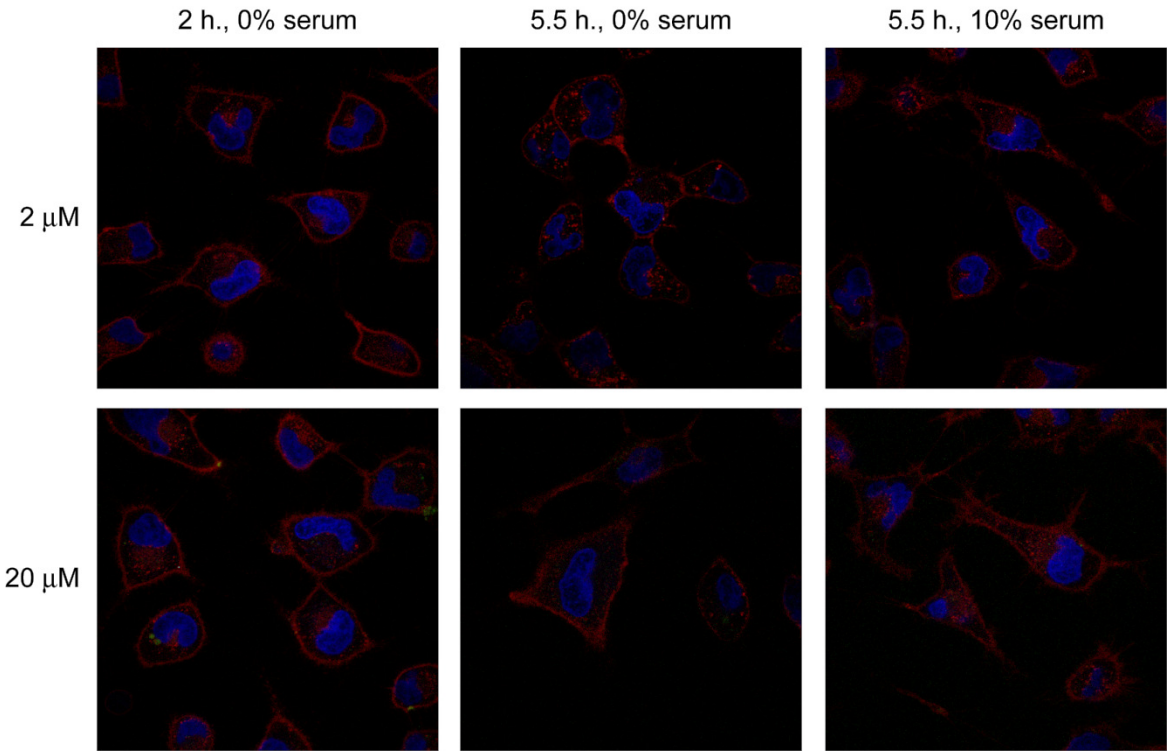

Figure 5.12 Analysis of HeLa cellular uptake of **Flu-5.1** by live-cell confocal microscopy. Images show channels for green (fluorescein, α/β-peptide), red (WGA488, outer membrane stain), and blue (Hoescht 33342, nuclear stain).

When HeLa cells were incubated with 20 μM **Flu-5.1** for 2 or 5.5 hours, either with or without serum, we saw no intracellular green fluorescence, indicating that this α/β-peptide did not enter cells (Figure 5.12). This is consistent with the predicted behavior for **5.1**, which is not expected to cross cell membranes. In contrast, when HeLa cells were incubated with **Flu-5.5**, we saw a dose-dependent increase in green fluorescence in the confocal images (Figure 5.13). In the absence of serum, most of this green fluorescence appeared on the outside of the cell at a higher concentration (≥10 μM), which we interpret as aggregated peptide strongly associated with the cell membrane that remained bound after multiple washing steps. In the presence of 10% serum, we saw substantially less of the α/β-peptide on the outside of the cells, and instead saw intracellular green fluorescence, suggesting that the α/β-peptide entered the HeLa cells under these conditions. The substantial difference in the localization of fluorescence in the images

obtained in the presence versus absence of serum may have resulted from the association of the hydrophobic **Flu-5.5** with serum proteins, reducing the tendency for the peptide to aggregate. It is unclear from these experiments if unlabeled **5.5** displays similar behavior.

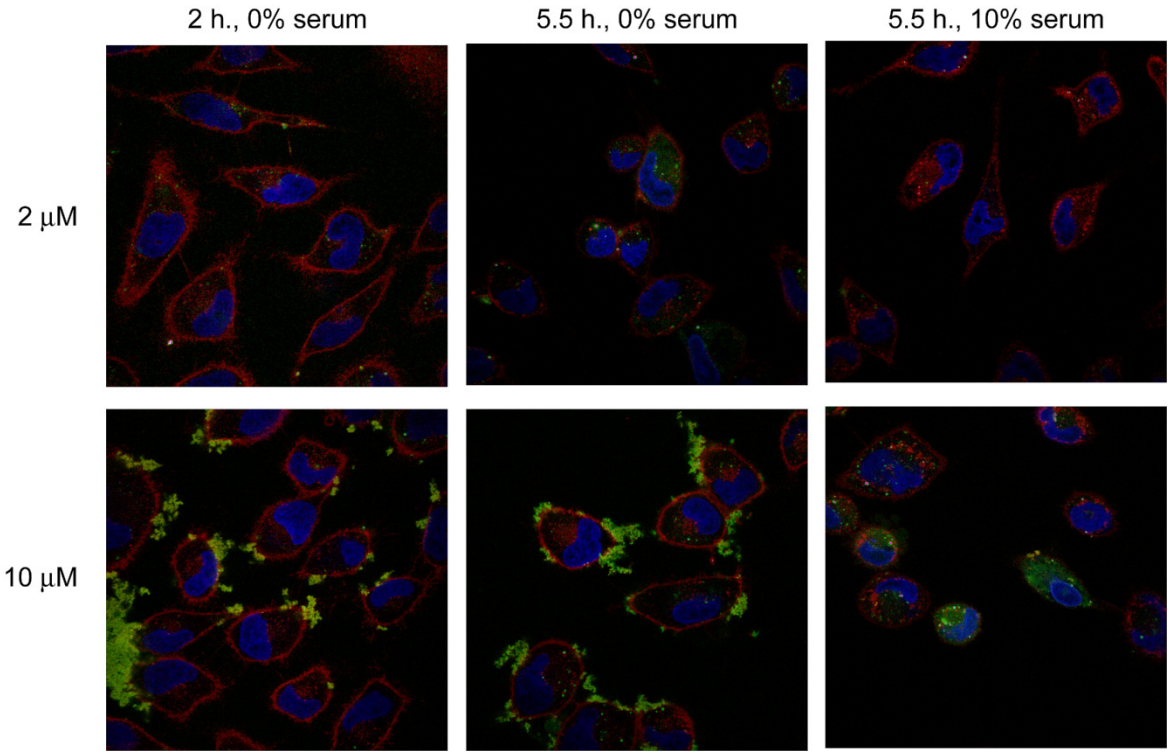

Figure 5.13 Analysis of HeLa cellular uptake of **Flu-5.5** by live-cell confocal microscopy. Images show channels for green (fluorescein, α/β-peptide), red (WGA488, outer membrane stain), and blue (Hoescht 33342, nuclear stain).

When HeLa cells were treated with **Flu-5.8**, we observed a significant amount of intracellular fluorescence in the confocal microscopy images, suggesting that this α/β-peptide is able to enter cells (Figure 5.14). The increased amount of intracellular fluorescence for **Flu-5.8** versus **Flu-5.5** indicates that the additional C-terminal arginine residues increase the efficiency of cellular uptake. Overall, the microscopy experiments suggest that α/β-peptides containing the J_5 residue associate with cells and, under some conditions, are able to cross the cell membrane. However, it is not clear from these experiments if these α/β-peptides can gain access to the cytosol (to antagonize their target proteins), or remain trapped in intracellular vesicles.

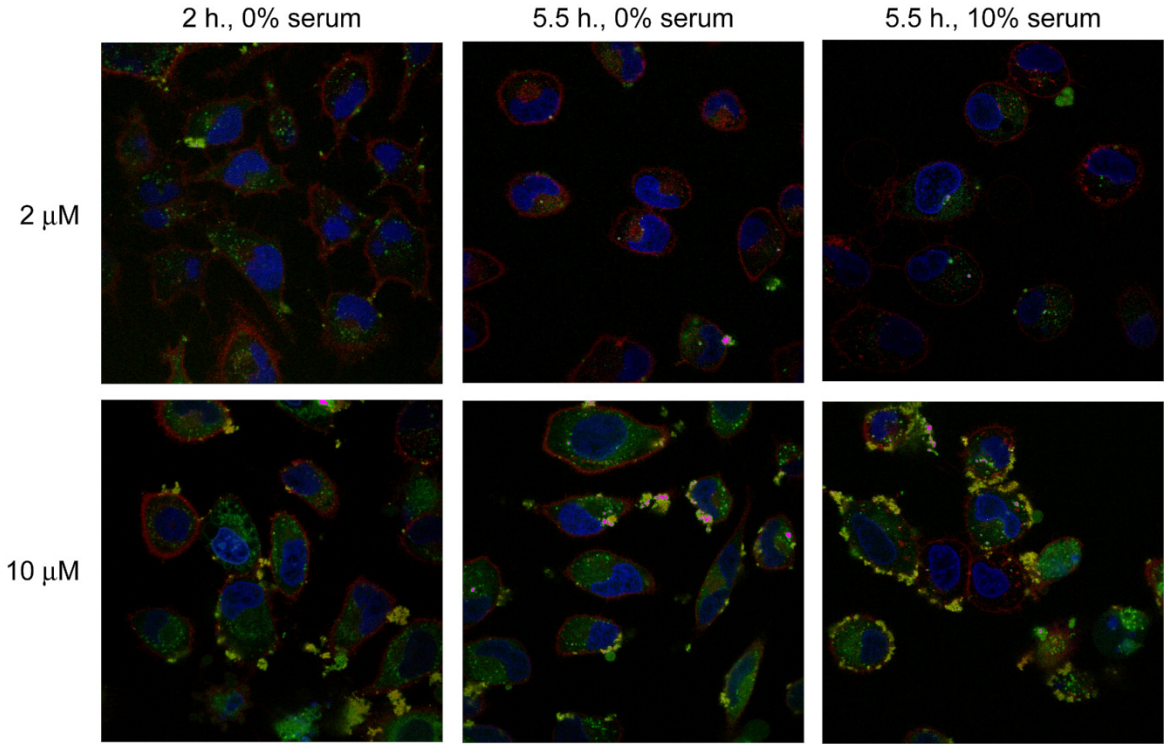

Figure 5.14 Analysis of HeLa cellular uptake of **Flu-5.8** by live-cell confocal microscopy. Images show channels for green (fluorescein, α/β-peptide), red (WGA488, outer membrane stain), and blue (Hoescht 33342, nuclear stain).

5.6 Evaluation of activity by cell-based assays

5.6.1 Initial cell killing assays

Our design hypothesis was that some α/β-peptide analogues of **5.1** containing J-residues may be membrane permeable, which might allow them to enter the cytosol of the cell. The J-residues are designed to be hydrolyzed into sAPC by intracellular esterases once inside the cell, yielding a potent α/β-peptide that may antagonize anti-apoptotic proteins (e.g., Bcl-x_L, Mcl-1) and initiate apoptosis. To evaluate the ability of these α/β-peptides to induce apoptosis, we treated a variety of cell types with α/β-peptide and measured cell viability using a CellTiter-Glo luminescent viability assay (Promega), which measures ATP levels. In this experiment, we hypothesized that **5.1** and analogues bearing J-residues with shorter alkyl groups (e.g., **5.2** or **5.3**) would not be membrane permeable and would not initiate apoptosis, while some analogues

bearing longer alkyl chains (e.g., **5.5** or **5.6**) might be able to enter cells, leading to a decrease in the population of viable cells. All cell killing assays were performed by Douglas Fairlie and Erinna Lee (Fairlie Laboratory, Division of Structural Biology, Walter and Eliza Hall Institute of Medical Research, Australia).

When non-cancerous mouse embryonic fibroblasts (MEFs) were treated with **5.1**-**5.4** (Figure 5.15), we saw no significant loss in cell viability even at the top concentration tested (20 μM), indicating that these α/β-peptides do not induce apoptosis in this cell type, consistent with the hypothesis that **5.1** and analogues bearing short alkyl chains are not membrane permeable. α/β-peptides **5.5** and **5.8**, which each feature two J_5 amino acid residues, showed a loss of cell viability at the highest concentration (20 μM). However, these α/β-peptides also killed *bax*$^{-/-}$/*bak*$^{-/-}$ double knock-out (DKO) cells, which lack the critical regulators of apoptosis Bax and Bak, and should not be susceptible to death through antagonism of Bcl-2 family protein-protein interactions. The observation that some of these α/β-peptides killed the DKO MEFs indicates that this loss in cell viability is due to an off-target effect rather than to antagonism of Bcl-2 protein-protein interactions. Similarly, **5.6**, which contains two J_8-residues, efficiently killed both wild type (wt) MEFs and DKO MEFs, suggesting that this α/β-peptide was killing by a non-specific effect.

Essentially identical results were seen for a variety of cancer cell lines tested: HeLa (cervical cancer), KM12 (colon cancer), MDA-MB-435 (breast cancer), and SK-MEL-2 (malignant melanoma) (Figure 5.16A-D). For **5.5**, **5.8**, and **5.6**, which all showed some amount of cell killing, toxicity was not effectively blocked by caspase inhibitor Q-VD-OPh. Because caspases are critical for apoptosis, the lack of inhibition by Q-VD-OPh strongly suggests that any cell death observed for these α/β-peptides is due to a non-specific cytotoxic effect. Interestingly,

when we added **5.6** to medium in these experiments, we noticed the formation of rod-like aggregate/precipitates over the course of the experiment (Figure 5.20 in "Experimental Methods" section). The only promising result came from MDA-MB-435 cells treated with **5.5** (Figure 5.16C), which appeared to show caspase-dependent cell death (attenuated by Q-VD-OPh) at 20 μM. Based on this preliminary result, we focused on the MDA-MB-435 cell line for follow-up studies.

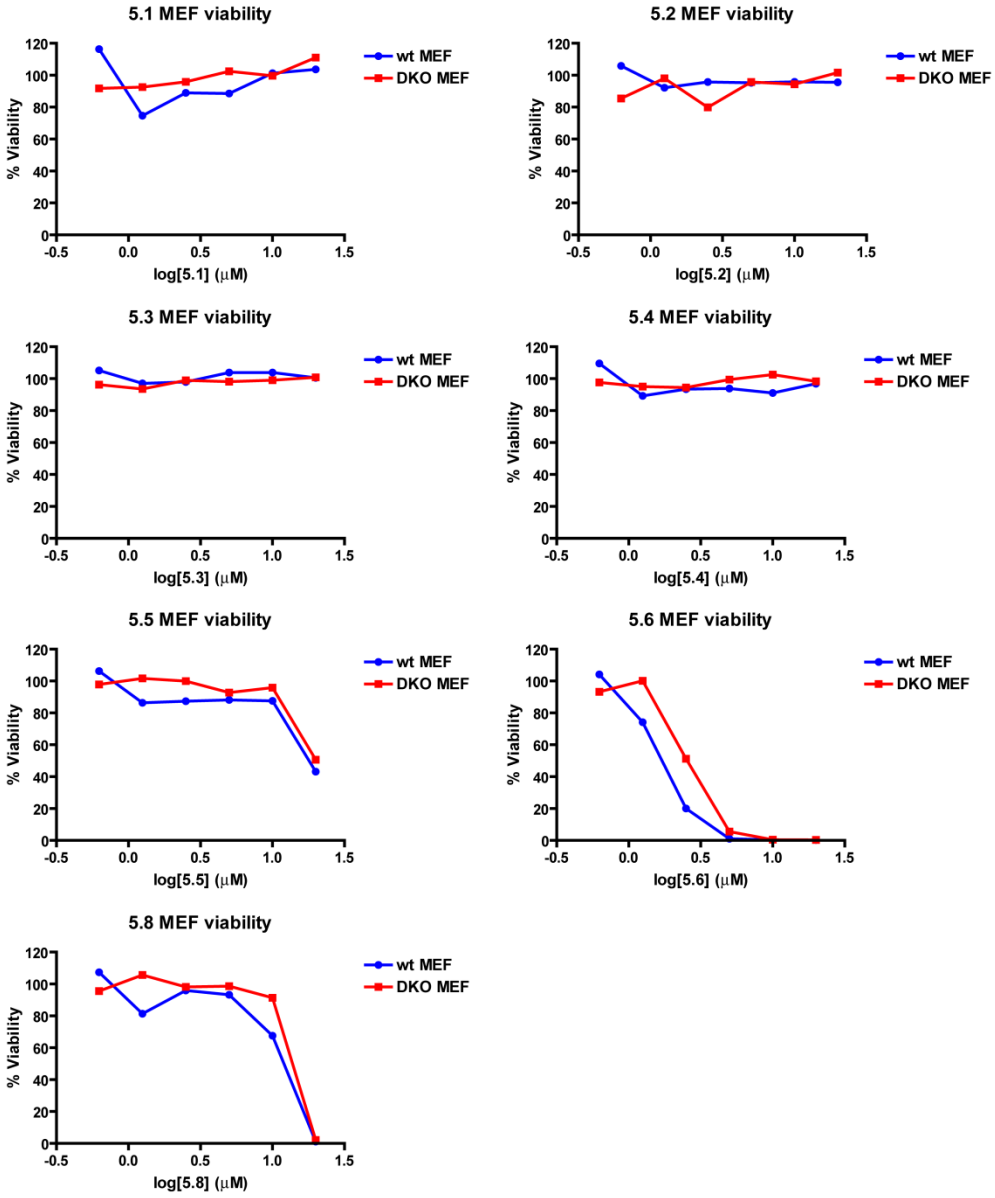

Figure 5.15 Viability of wild-type (wt, blue) or *bax*$^{-/-}$/*bak*$^{-/-}$ double knock-out (DKO) MEFs cells (relative to DMSO control) when treated with various concentrations of α/β-peptide, as determined by CellTiter-Glo assay. Cells were treated with the indicated α/β-peptide for 24 hours. Each data point represents a single well on a plate.

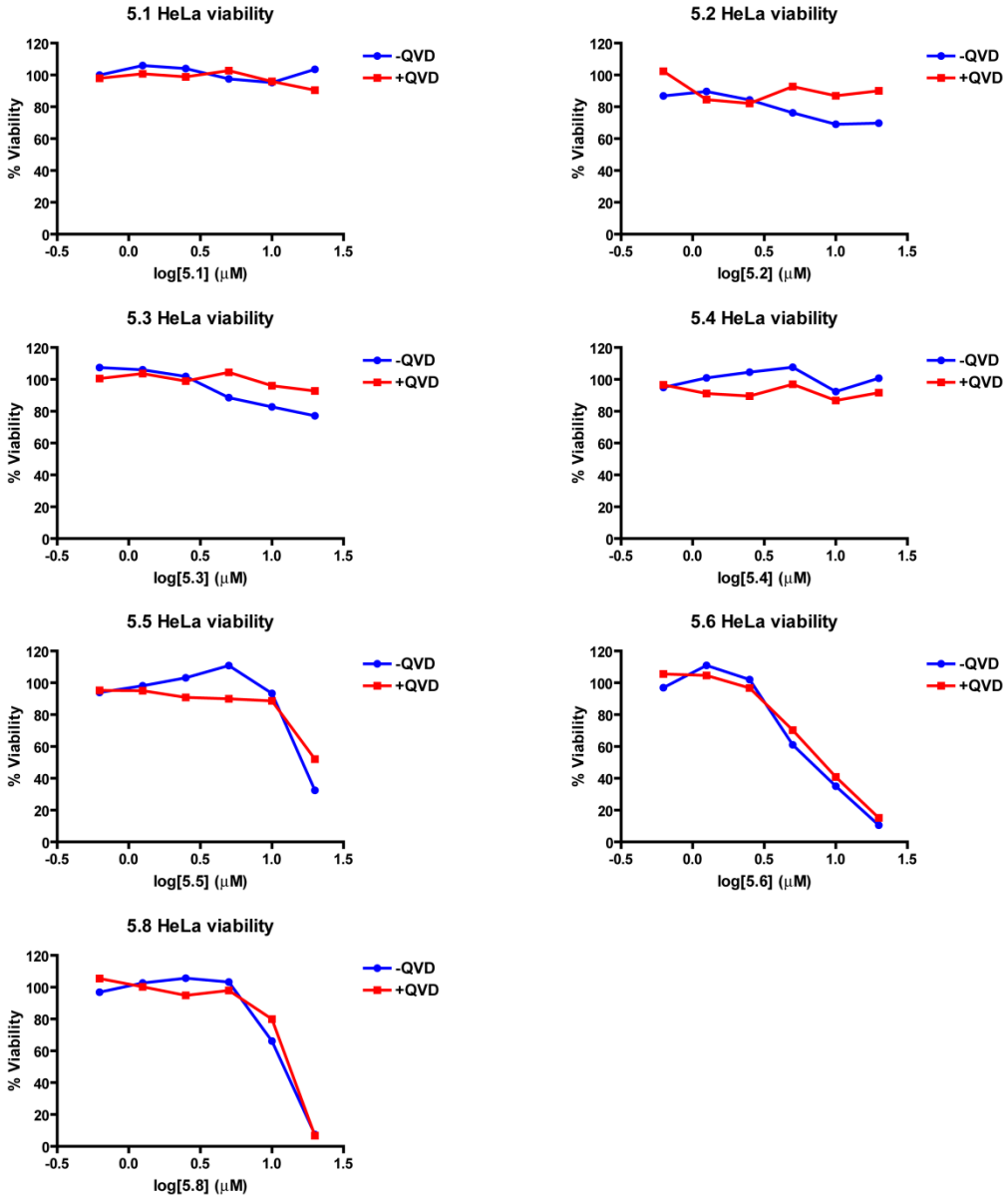

Figure 5.16 (A) Viability of HeLa cells (relative to DMSO control) when treated with various concentrations of α/β-peptide in the absence (blue) or presence (red) of caspase inhibitor Q-VD-OPh (QVD), as determined by CellTiter-Glo assay. Cells were treated with the indicated α/β-peptide for 24 hours. Each data point represents a single well on a plate.

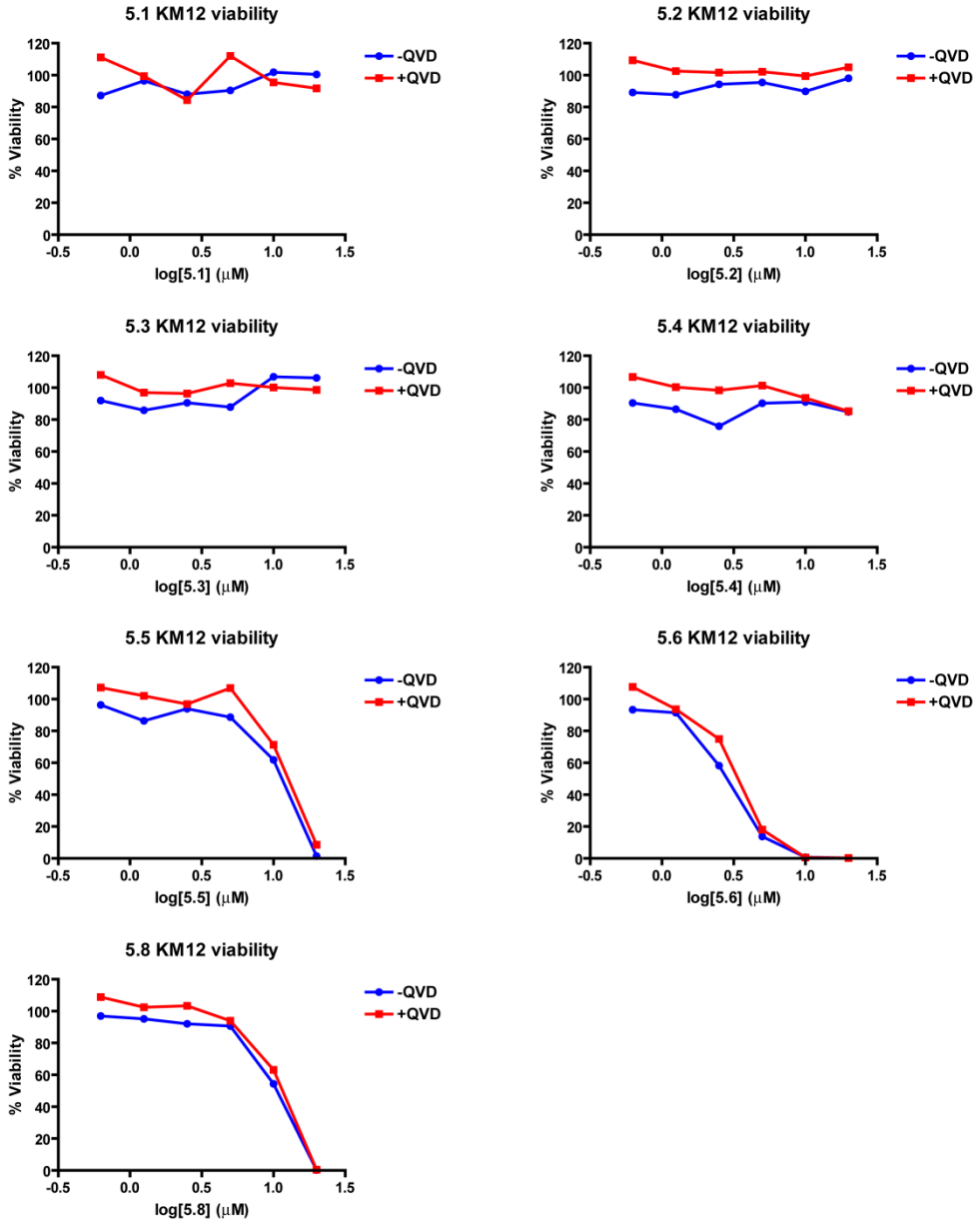

Figure 5.16 (B) Viability of KM12 cells (relative to DMSO control) when treated with various concentrations of α/β-peptide in the absence (blue) or presence (red) of caspase inhibitor Q-VD-OPh (QVD), as determined by CellTiter-Glo assay. Cells were treated with the indicated α/β-peptide for 24 hours. Each data point represents a single well on a plate.

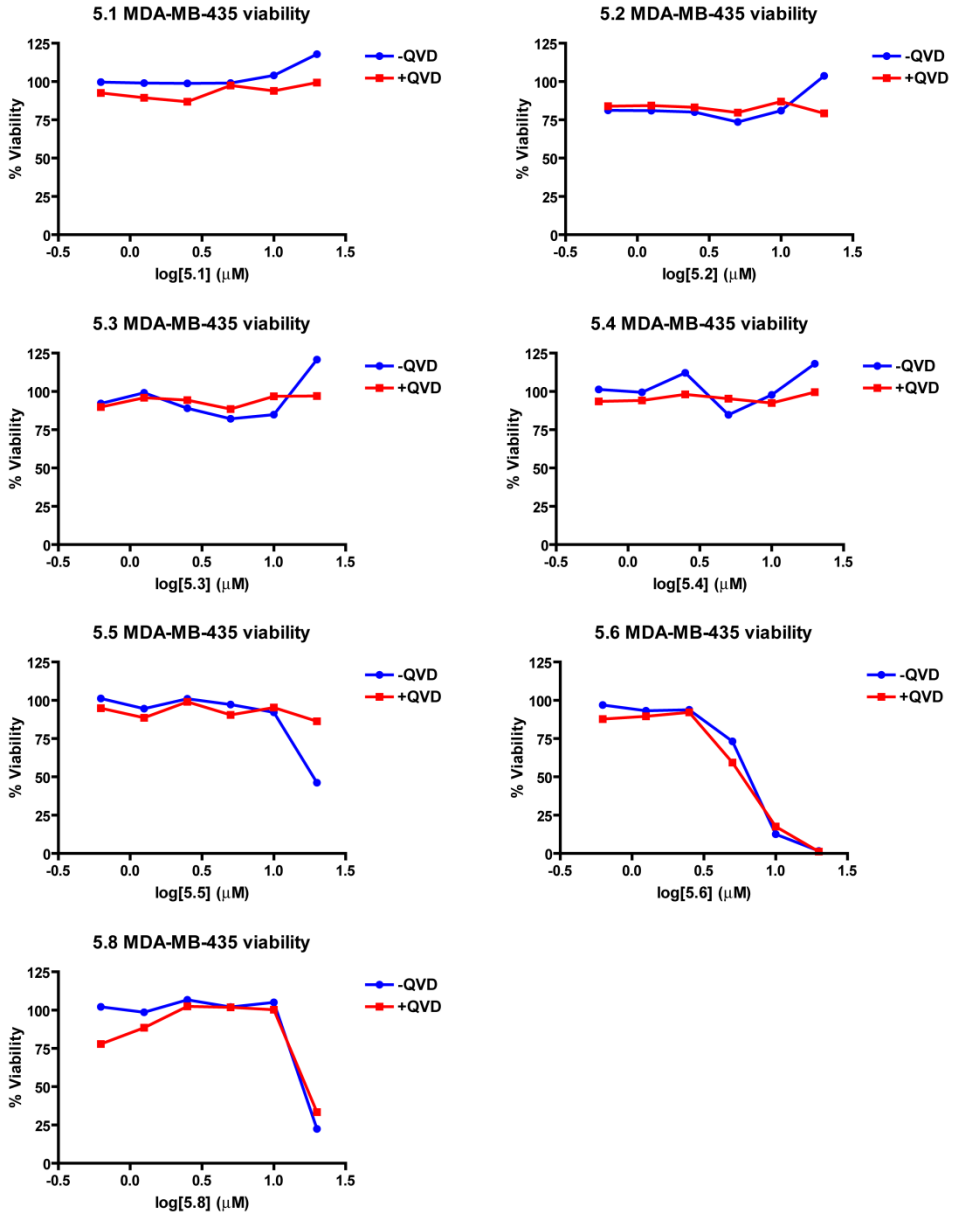

Figure 5.16 (C) Viability of MDA-MB-435 cells (relative to DMSO control) when treated with various concentrations of α/β-peptide in the absence (blue) or presence (red) of caspase inhibitor Q-VD-OPh (QVD), as determined by CellTiter-Glo assay. Cells were treated with the indicated α/β-peptide for 24 hours. Each data point represents a single well on a plate.

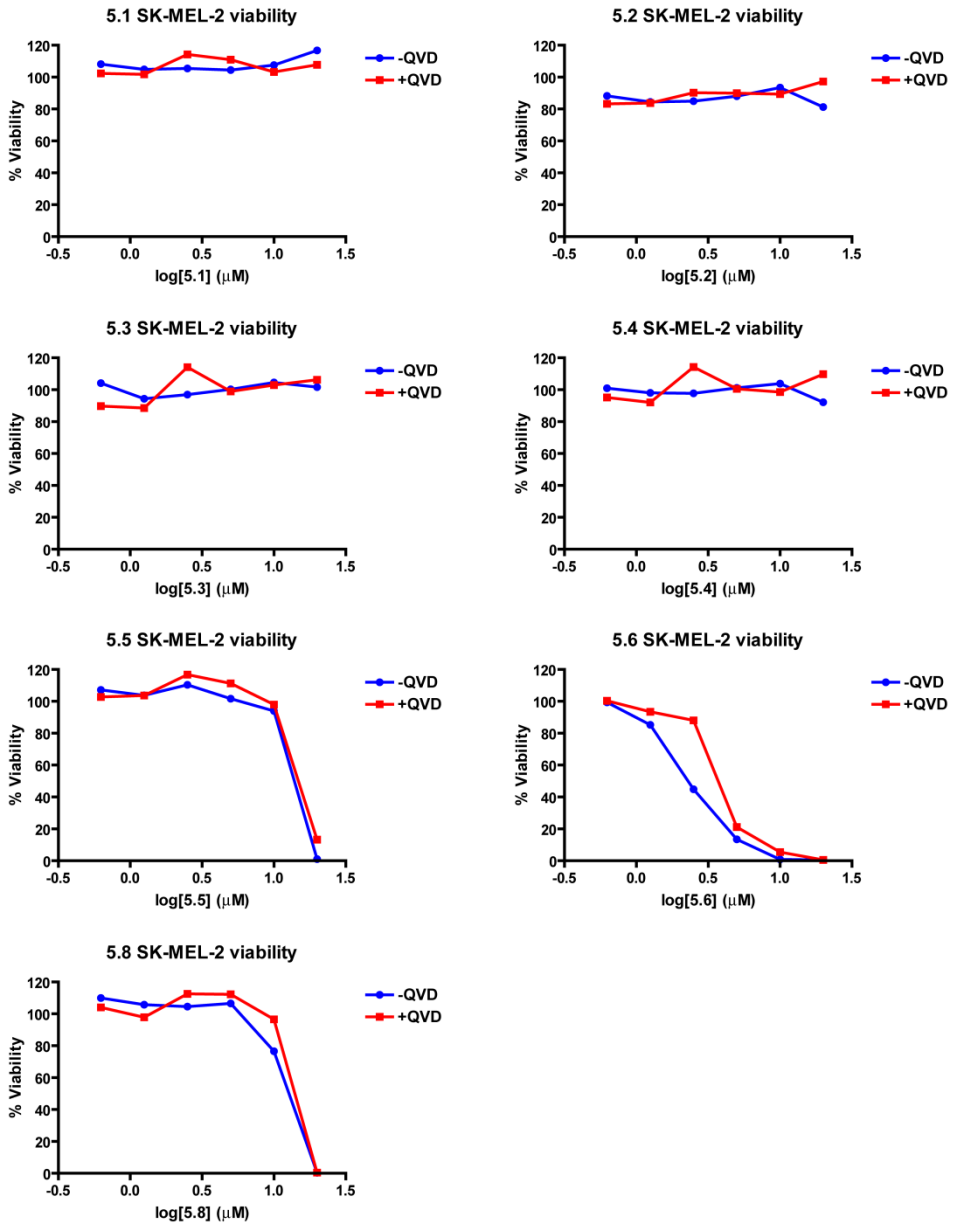

Figure 5.16 (D) Viability of SK-MEL-2 cells (relative to DMSO control) when treated with various concentrations of α/β-peptide in the absence (blue) or presence (red) of caspase inhibitor Q-VD-OPh (QVD), as determined by CellTiter-Glo assay. Cells were treated with the indicated α/β-peptide for 24 hours. Each data point represents a single well on a plate.

5.6.2 Second generation α/β-peptide designs

We were intrigued by the sharp contrast in behavior between α/β-peptides **5.4** (two J_4-residues; no cell killing activity) and **5.6** (two J_8-residues; significant non-specific cell killing), as well as the intermediate behavior showing that **5.5** (two J_5-residues) may be initiating apoptosis in MDA-MB-435 cells. Based on these observations, we designed a second generation of α/β-peptides with the hopes of exploring more of the "chemical space" between **5.4** and **5.6** (Figure 5.17). We designed **5.9**, an analogue of **5.5** with Leu7→Ala and Asp12→Ala substitutions. Leu7 and Asp12 are both critical for binding to anti-apoptotic proteins, so alanine substitutions at these positions should significantly reduce the affinity of **5.9** for these targets, allowing this α/β-peptide to serve as a negative control in cell-based assays. **5.10** is an analogue bearing one J_5 and one J_4 residue, and lies "in between" **5.4** and **5.5** in hydrophobicity. Because **5.8** appeared to kill cells non-specifically, we designed α/β-peptide **5.11**, which is an analogue of **5.8** with three lysine residues in place of the three C-terminal arginine residues to evaluate the effect of these different cationic residues on cell killing. α/β-Peptides **5.12-5.17** each contain one longer J-residue in place of sAPC6 and a J_1 residue in place of sAPC13, designed to present the saturated carbons in subtly different ways relative to the other α/β-peptides, which contain two identical J-residues. Finally, inspired by success using all-hydrocarbon-crosslinks to impart membrane permeability,[10, 18, 38] we synthesized **5.18** bearing two J_{5E} residues crosslinked by olefin metathesis.

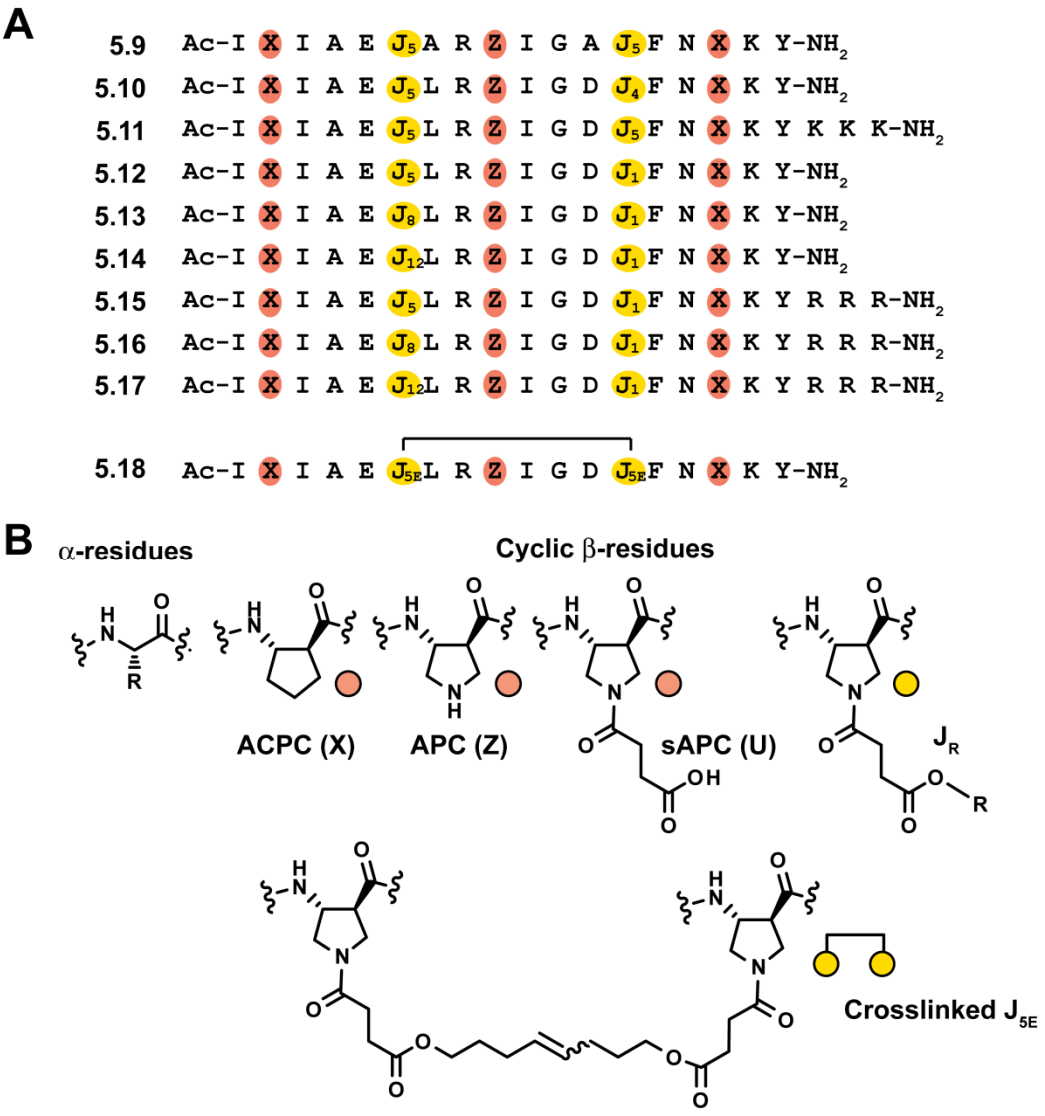

Figure 5.17 (A) Sequences of the second generation of α/β-peptides containing J-residues. Non-natural residues are indicated by colored circles. J-residues correspond to structures in Figure 5.5. (B) Structures of a generic α-residue, the cyclic β-residues ACPC (X), APC (Z), sAPC (U) (orange), a generic J-residue (yellow), and the crosslinked J_{5E} residues present in **5.18**.

5.6.3 MDA-MB-435 cell-killing experiments

We evaluated the second generation of α/β-peptides for their ability to kill MDA-MB-435 cells, and determined cell death from the analysis of Annexin V and propidium iodide staining by flow cytometry (Figure 5.18). In this experiment, we saw that **5.1** did not kill MDA-MB-435 cells, consistent with the results obtained from the CellTiter-Glo experiments described

above. Similarly, α/β-peptide **5.5**, which showed some ability to kill MDA-MB-435 cells at 20 μM in the CellTiter-Glo experiment, also showed killing of the MDA-MB-435 cells in this assay format. Interestingly, **5.10**, which differs from **5.5** only by one additional methylene unit in the side chain of one of the J-residues, did not kill the MDA-MB-435 cells. α/β-Peptide **5.11**, the analogue of **5.8** bearing three Arg→Lys substitutions, showed potent cell death. In contrast to every other α/β-peptide tested in this experiment, **5.11** showed cell death at the 10 μM concentration. α/β-Peptide **5.12** did not kill cells, while **5.13-5.17** each showed some ability to kill cells, especially after 48 hours. The negative control α/β-peptide **5.9** did not kill MDA-MB-435 cells in this experiment, which suggests that **5.5** might be killing by initiating apoptosis. However, α/β-peptide **5.9** did kill cells in a subsequent experiment, including *bax*$^{-/-}$/*bak*$^{-/-}$ DKO cells, which ultimately suggests that these peptides are killing by some non-specific interaction (e.g., rupturing the plasma membrane) rather than by antagonizing Bcl-2 protein-protein interactions (Figure 5.18C). Overall, the collected data for many of the α/β-peptides tested on multiple cell lines strongly indicate that most of the α/β-peptides bearing linear J-residues with alkyl chains ≥5 carbons kill cells at least partially in an off-target manner, although the mechanism for cell death is unclear.

Interestingly, the α/β-peptide **5.18**, which features the crosslinked J_{5E} residue, showed no ability to kill any of the cell types with which it was tested (Figure 5.18C). This indicates that **5.18** does not engage in the non-specific cell killing that is seen for **5.5** or **5.9**. However, the lack of cell death also indicates that this α/β-peptide does not initiate apoptosis in these cells. This could be for a variety of reasons, such as that **5.18** is unable to enter cells or does not engage the anti-apoptotic proteins critical for survival of this cell type with high affinity. (Crosslinked residues in cell-penetrating α- and α/β-peptides are explored in detail in Chapter 6.)

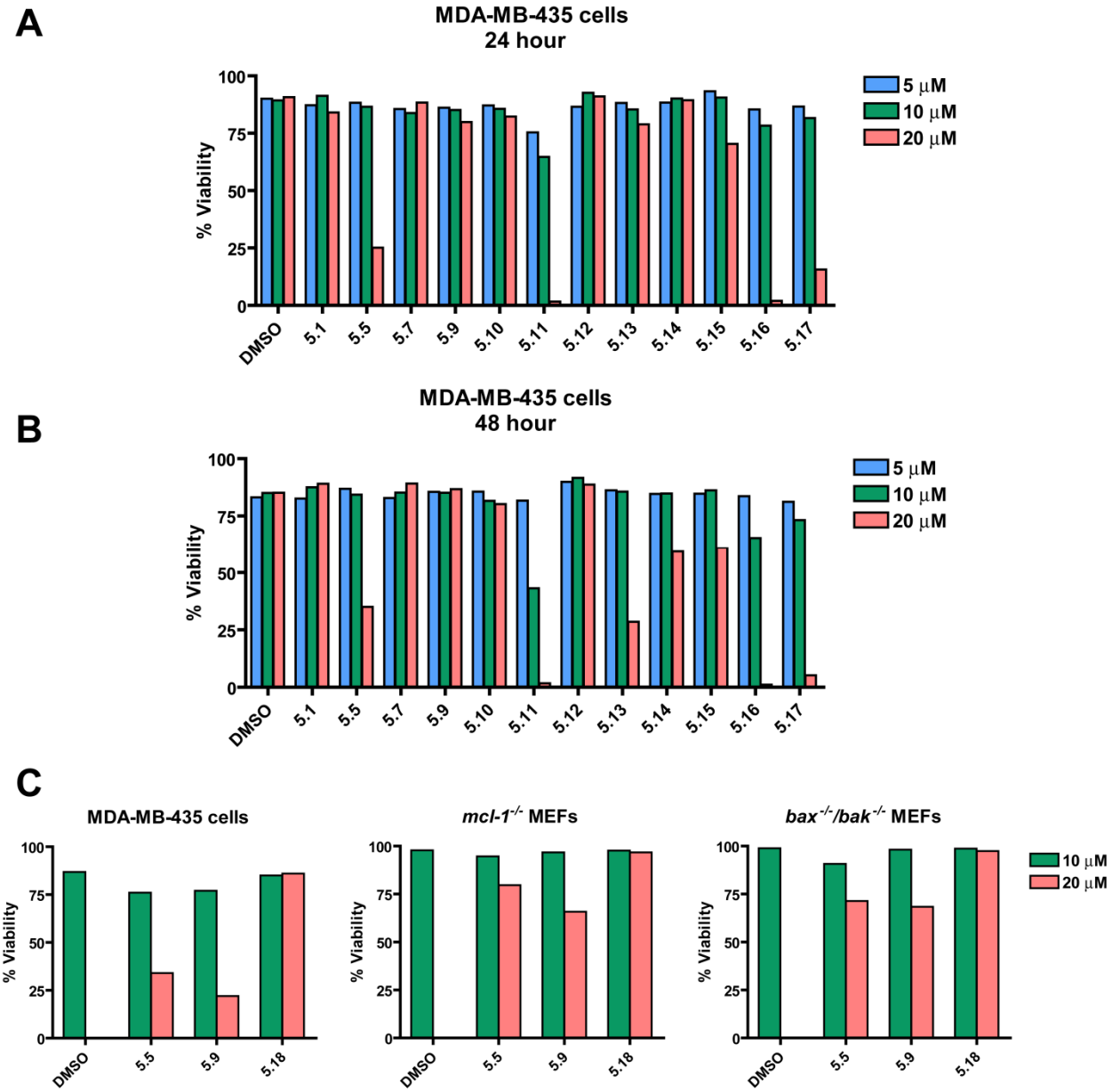

Figure 5.18 Analysis of cell viability when treated with Bim-derived α/β-peptides, as determined by flow cytometry. (A and B) MDA-MB-435 cells were treated with the indicated α/β-peptides and viability measured after (A) 24 hours and (B) 48 hours. "% viability" corresponds to the percentage of cells that excluded both Annexin V and propidium iodide (PI) staining. (C) Viability of various cell types, as determined by flow cytometry, after 24 hours.

5.7 Conclusions

In this chapter, I have described our attempts to impart membrane-permeability into an optimized α/β-peptide. Inspired by published successes showing that the covalent attachment of alkyl chains can facilitate the entry of short peptides (including BH3 domains) into cells,[30-33] we

designed novel cyclic β-amino acid residues ("J-residues") bearing alkyl esters of various lengths. Our hypothesis was that introducing one or more J-amino acid residues into an α/β-peptide could impart membrane-penetrating properties and that, once inside the cell, the ester of the J-residue would be hydrolyzed to the sAPC residue to yield an α/β-peptide that had been previously optimized to antagonize Bcl-2 family protein-protein interactions. The removal of the cell-penetrating moiety would be beneficial to ensure that this group did not interfere with protein binding.

We used the α/β-peptide **5.1**, derived from the Bim BH3 domain and previously optimized by our group for high-affinity binding to anti-apoptotic proteins and high protease stability,[26] as the starting point for J-residue incorporation. α/β-Peptide **5.1** contains two sAPC residues, and either or both of these could be substituted for a J-residue to attempt to derive membrane-permeable analogues. We designed J-amino acid residues with alkyl esters with chain length varying from 1 to 12 carbons and incorporated these into analogues of **5.1**. Peptides that are reported to have the ability to spontaneously cross cell membranes often have a net positive charge.[44, 47, 54, 56] Because **5.1** and its analogues with J-residues have a net charge of -1, we also designed **5.7**, bearing three C-terminal arginine residues, and incorporated J-residues into this sequence to evaluate whether increased overall charge would facilitate more efficient cell entry. The J-residues were all readily synthesized and incorporated using protocols routinely used for the synthesis and purification of α/β-peptides.

Fluorescein-labeled α/β-peptides **Flu-5.5** and **Flu-5.8**, each bearing two J_5 amino acid residues, were able to enter HeLa cells, as judged by confocal microscopy. In contrast, the α/β-peptide **Flu-5.1**, which contains two sAPC residues, did not enter HeLa cells according to the confocal microscopy results. These results are consistent with the hypothesis that the

incorporation of β-residues bearing medium-length alkyl chains into α/β-peptides can facilitate their entry into cells, as designed. It is unclear from the microscopy images whether these α/β-peptides are able to reach the cytosol, or remain trapped inside vesicles (e.g., endosomes). Fluorescence confocal microscopy co-localization experiments, involving labeling of different regions of the cell (endosomes, mitochondria, etc.), could be used to determine where the α/β-peptides localize upon cellular entry.

Most of the J-residue-containing α/β-peptides are designed to be hydrolyzed once inside the cell by intracellular esterases to generate **5.1** or **5.7**, both of which are able to bind tightly to anti-apoptotic proteins (though **5.7** was tested for binding to only Bcl-x_L). To evaluate the ability of α/β-peptides bearing J-residues to enter cells and antagonize Bcl-2 protein-protein interactions to initiate apoptosis, we treated a variety of cell types with α/β-peptides and monitored cell viability. Although several α/β-peptides were able to kill cells at the highest concentration tested (e.g., **5.5**, **5.6**, **5.8**), control experiments showing that these α/β-peptides also killed DKO MEFs (Figure 5.15) and were toxic in the presence of the caspase inhibitor Q-VD-OPh (Figure 5.16) strongly suggested that some or all of this cell death was due to a non-specific cytotoxic effect. Experiments evaluating solubility (Figure 5.10) and some microscopy images (Figures 5.13, 5.14, and 5.21) suggest that these hydrophobic α/β-peptides precipitate over time and may associate strongly with the cell membrane. This aggregation may lead to cell death over the extended periods of time evaluated in these experiments (24-48 hours).

It is unclear why the α/β-peptides explored in this chapter were unable to initiate apoptosis, despite the fact that some could enter cells. Recent reports show that only certain cell types (e.g., hematological cancers) are susceptible to the initiation of apoptosis by side chain crosslinked "stapled" BH3 domains, while other cell types (e.g., MEFs) are unaffected.[18] In light

of these results, it is possible that the inability of these α/β-peptides to initiate apoptosis may have arisen because the cell lines tested are not as sensitive to apoptosis through this mechanism, perhaps due to differing expression of anti-apoptotic Bcl-2 family members. Alternatively, although some these α/β-peptides may be able to cross the cell membrane, they may remain trapped inside intracellular vesicles and not released into the cytosol.

At high concentrations, some of the α/β-peptides that feature longer alkyl chains are able to kill cells by what appears to be a non-apoptotic mechanism. A recent report[57] suggests that certain peptides bearing hydrophobic groups (the so-called "stapled" peptides, described in detail in Chapter 6) can kill cells at high concentrations by disruption of the plasma membrane. It is possible that some of the J-residue-containing α/β-peptides described here are killing cells by a similar mechanism, although future studies into the mechanism of cell death will be required to test this hypothesis.

A series of recent reports highlight that small changes in primary sequence of a cell-permeable hydrocarbon crosslinked α-peptide can abolish its cell membrane permeability, even if the cell-penetrating moieties remain intact.[38, 55, 58, 59] Ultimately, these results suggests that the incorporation of hydrophobic groups is not sufficient to transform a peptide into a membrane-permeable peptide with activity toward intracellular protein-protein interactions. These results, together with the failures reported in this chapter to impart membrane-permeability to an α/β-peptide that has already been designed, suggest an alternative design strategy: rather than try to confer membrane permeability onto an already-designed α/β-peptide, success may be more easily achieved by attempting to design an α/β-peptide mimic of an α-peptide that is already known to enter cells and display activity. This direction is explored in Chapter 6.

5.8 Future directions

The novel cyclic β-residues ("J-residues") described in this chapter may ultimately be useful for conferring membrane permeability on α/β-peptides. Although the sequences described in this chapter did not successfully initiate apoptosis, this strategy may prove successful with different primary sequences. As noted above, primary sequence (particularly net charge) can have a very large impact on the ability of peptides to enter cells. Thus, incorporating J-residues into other primary sequences (e.g., Bim derivatives with a net positive charge, other BH3 domains, or entirely unrelated sequences) may yield α/β-peptides with higher membrane permeability than those described in this chapter. Furthermore, in this chapter, J-residues were all placed at positions 6 and 13 in **5.1** or **5.7**. Future work should explore other positions for J-residues, particularly spacing different from the *i,i+7* spacing explored here. Alternatively, other cell-penetrating groups (e.g., the "Tat" CPP) may be conjugated to an α/β-peptide through the side chain of a J-residue to facilitate cell entry.

Ultimately, the compounds reported in this chapter did not appear to induce apoptosis in the cell lines tested, although there were several promising leads. α/β-Peptide **5.11** showed a dose-dependent ability to kill MDA-MB-435 cells. This contrasts with many of the other α/β-peptides, which killed cells at only the very highest concentration. This dose-response for **5.11** may indicate an on-target mechanism for cell death (i.e., Bcl-2 family antagonism) at the lower concentrations, which is not seen for many of the other α/β-peptides explored. Future studies, such as viability experiments in the presence of a caspase inhibitor and confocal microscopy experiments with fluorescein-labeled analogues of **5.11**, would be required to determine if this compound is entering cells and initiating apoptosis.

Leukemia cell lines are particularly sensitive to the induction of apoptosis by cell-permeable BH3 domain peptides, while many other cell lines are not.[18, 30, 41] (See also Chapter 6 for additional examples.) None of the cell lines evaluated in this chapter were leukemia cells. Future work evaluating new analogues containing J-residues should evaluate the effect of these analogues on cell lines, such as Jurkat[41], U937[18], or HL-60[30] leukemia cells, that are known to be susceptible to apoptosis induced by similar peptides.

Finally, analogues of the J-residues may be useful for the installation of a wide variety of chemical groups into α/β-peptides, unrelated to the design of cell-permeable peptides, which can be removed either though chemical or enzymatic hydrolysis. This could be useful for the installation of temporary chemical moieties for a variety of applications, including synthesis or purification of difficult peptide sequences, masking of certain activity (analogous to an ester "prodrug"), or delivery to certain cell types by covalent attachment of a targeting ligand.

5.9 Experimental methods

5.9.1 General

Fmoc-protected α-amino acids with compatible side chain protecting groups and benzotriazole-1-yl-oxy-tris-pyrrolidino-phosphonium hexfluorophosphate (PyBOP) were purchased from Chem-Impex International and Novabiochem. Fmoc-ACPC-OH was purchased from Chem-Impex International (15073). Fmoc-APC(Boc)-OH was synthesized as previously described.[60] Fmoc-sAPC(tBu)-OH was synthesized as described previously.[26] Mono-methyl hydrogen succinate (M81101) and mono-ethyl succinate (475505) were purchased from Sigma-Aldrich. All other solvents and reagents used for peptide synthesis were purchased from Fisher Scientific or Sigma-Aldrich.

5.9.2 Synthesis of J-amino acid monomers

Mono-butyl succinate, mono-pentyl succinate, mono-octyl succinate, mono-dodecyl succinate, and mono-(4-penten-1-yl) succinate were synthesized based on a previously reported protocol.[61] Succinic anhydride (1 eq.) was suspended in toluene and N-hydroxysuccinimide (NHS, 0.3 eq), 4-(dimethylamino)pyridine (DMAP, 0.1 eq.), triethylamine (NEt_3, 0.3 eq.), and the appropriate linear alcohol (1-butanol, 1-pentanol, 1-octanol, 1-dodecanol, or 4-penten-1-ol; 1 eq.) were added. The reaction mixture was heated to reflux overnight. Upon completion of the reaction (as determined by TLC), the micture was cooled to room temperature. Ethyl acetate was added, and the organic phase was washed 3 times with 10% citric acid and 1 time with brine. The organic phase was dried over magnesium sulfate, and filtered. The solvent was removed by evaporation. The alkyl succinates were then used in the synthesis of J-amino acid monomers without further purification.

The synthesis of Fmoc-protected J-amino acid monomers for use in solid-phase peptide synthesis (Figures 5.19 and 5.20) was performed by dissolving Fmoc-APC(Boc)-OH in dichloromethane (DCM) with 20% TFA. The Boc deprotection reaction was allowed to proceed at room temperature and monitored by TLC. After complete deprotection of the Boc group, the solvent was removed by evaporation, and the product was dissolved in DCM and then evaporated to dryness multiple times to fully remove the TFA, until evaporation yielded a gray/white solid.

The coupling of the alkyl succinates to Fmoc-APC-OH (Fmoc protecting group on backbone amine) was performed by dissolving Fmoc-APC-OH (1 eq.) in DCM, followed by the addition of the appropriate alkyl succinate (1.1 eq.) pre-activated with 1.1 eq. of 1-ethyl-3-(3-dimethylaminopropyl)carbodiimide (EDCI), 1.1 eq. of 1-hydroxybenzotriazole (HOBt), and 6

eq. of N,N-diisopropylethylamine (DIEA) in an ice bath (Figure 6.18). The mixture was allowed to slowly warm from 4 °C to room temperature overnight, and was monitored by TLC. After completion of the reaction, the solvent was removed, and the Fmoc-protected J-amino acid monomer was then isolated, as detailed individually for each monomer below. For each monomer, acetic acid was included during purification by column chromatography to protonate the free acid and improve resolution. To remove acetic acid after purification, an azeotrope could be formed by adding toluene, followed by removing solvent with evaporation, and repeating as necessary.

Fmoc-J_1-OH. The crude mixture was dissolved in ethyl acetate, and the organic layer was extracted 3 times with 5% $NaHSO_4$, 1 time with brine, dried over magnesium sulfate, and filtered. The solvent was removed by evaporation. The product was then isolated via column chromatography (2% methanol in DCM, 2.5% acetic acid). The fractions containing the product were combined, and the solvent was removed by evaporation.

Fmoc-J_2-OH. The crude mixture was dissolved in ethyl acetate, and the organic layer was extracted 3 times with 5% $NaHSO_4$, 3 times with brine, dried over magnesium sulfate, and filtered. The solvent was removed by evaporation. The product was then isolated via column chromatography (2% methanol in DCM, 2.5% acetic acid). The fractions containing the product were combined, and the solvent was removed by evaporation.

Fmoc-J_4-OH. The crude mixture was dissolved in ethyl acetate, and the organic layer was extracted 3 times with 5% $NaHSO_4$, 2 times with saturated $NaHCO_3$, 2 times with 1 N HCl, 2 times with brine, dried over magnesium sulfate, and filtered. The solvent was removed by evaporation. The product was then isolated via column chromatography (1:1 ethyl

acetate/hexane, 5% acetic acid). The fractions containing the product were combined, and the solvent was removed by evaporation.

Fmoc-J_5-OH. The crude mixture was dissolved in ethyl acetate, and the organic layer was extracted 3 times with 5% $NaHSO_4$, 2 times with saturated $NaHCO_3$, 2 times with 1 N HCl, 2 times with brine, dried over magnesium sulfate, and filtered. The solvent was removed by evaporation. The product was then isolated via column chromatography (6:4 ethyl acetate/hexane, 5% acetic acid). The fractions containing the product were combined, and the solvent was removed by evaporation.

Fmoc-J_8-OH. The crude mixture was dissolved in ethyl acetate, and the organic layer was extracted 3 times with 5% $NaHSO_4$, 2 times with saturated $NaHCO_3$, 2 times with 1 N HCl, 2 times with brine, dried over magnesium sulfate and filtered. The solvent was removed by evaporation. The product was then isolated via column chromatography (first column with 4:6 ethyl acetate/hexane, 5% acetic acid→ethyl acetate, 5% acetic acid, followed by a second column with 1:1 ethyl acetate/hexane, 5% acetic acid). The fractions containing the product were combined, and the solvent was removed by evaporation.

Fmoc-J_{12}-OH. The crude mixture was dissolved in ethyl acetate, and the organic layer was extracted 3 times with 5% $NaHSO_4$, 2 times with saturated $NaHCO_3$, 2 times with 1 N HCl, 1 time with brine, dried over magnesium sulfate, and filtered. The solvent was removed by evaporation. The product was then isolated via column chromatography (1:1 ethyl acetate/hexane, 2.5% acetic acid). The fractions containing the product were combined, and the solvent was removed by evaporation.

Fmoc-J_{5E}-OH. The crude mixture was dissolved in ethyl acetate, and the organic layer was extracted 3 times with 5% $NaHSO_4$, 2 times with saturated $NaHCO_3$, 2 times with 1 N HCl,

1 time with brine, dried over magnesium sulfate, and filtered. The solvent was removed by evaporation. The product was then isolated via column chromatography (4:1 ethyl acetate/hexane, 2.5% acetic acid). The fractions containing the product were combined, and the solvent was removed by evaporation.

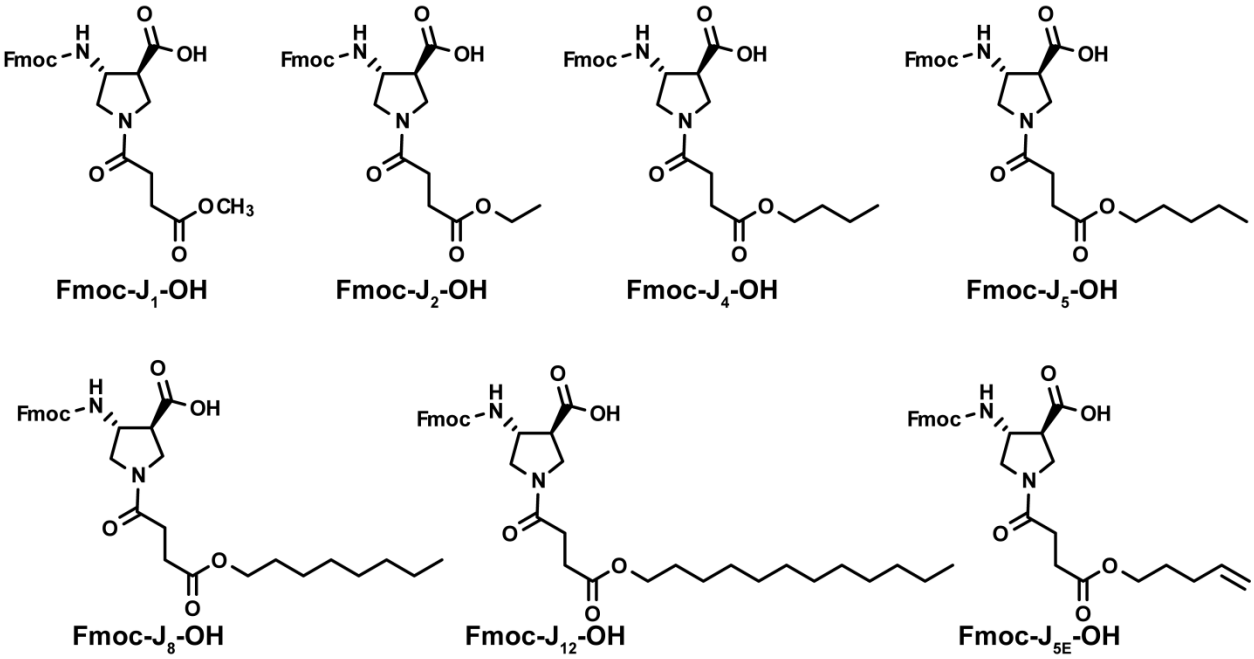

Figure 5.19 Protected J-amino acid building blocks for use in solid-phase peptide synthesis.

Figure 5.20 (below) shows ESI/EMM and ^{1}H-NMR data for each of the J-residue monomers reported in this chapter. Several of the NMR spectra contain residual solvent peaks and other minor impurities, but were still utilized for the synthesis of α/β-peptides.

Figure 5.20 (A) ESI/EMM data for Fmoc-J_1-OH, calc. $[M-H]^-$ = 465.2.
^{1}H-NMR for Fmoc-J_1-OH shown on the next page.

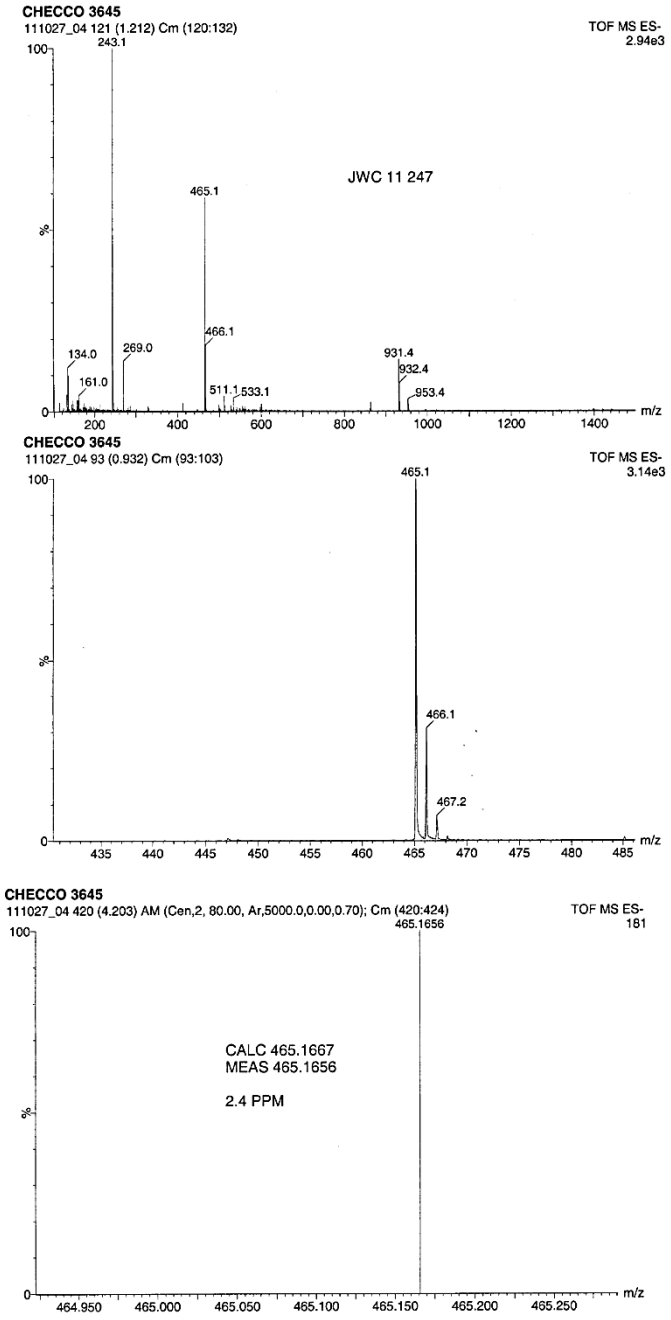

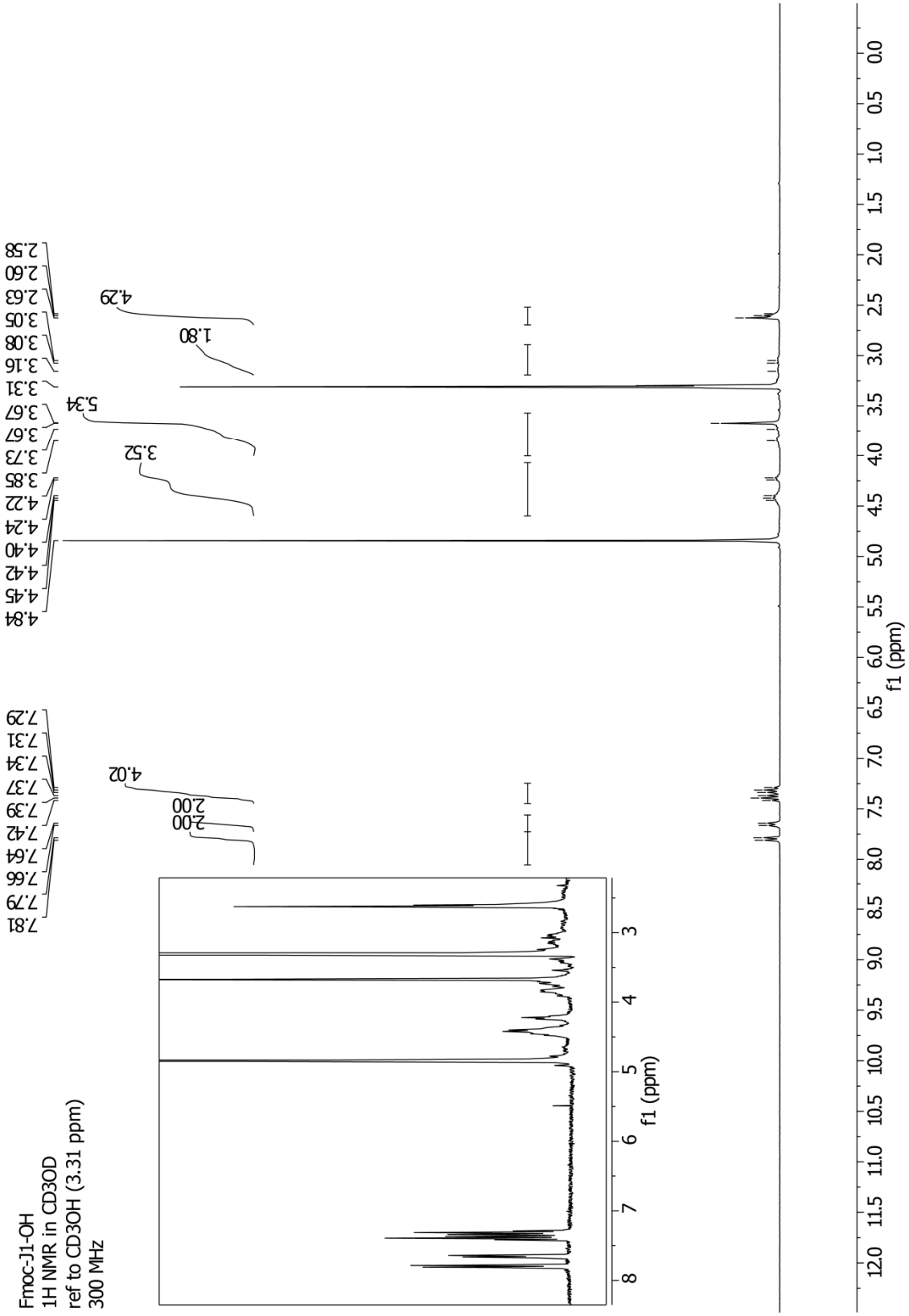
Fmoc-J1-OH
1H NMR in CD3OD
ref to CD3OH (3.31 ppm)
300 MHz
f1 (ppm)

Figure 5.20 (B) ESI/EMM data for Fmoc-J_2-OH, calc. $[M-H]^-$ = 479.2.
^{1}H-NMR for Fmoc-J_2-OH shown on the next page.

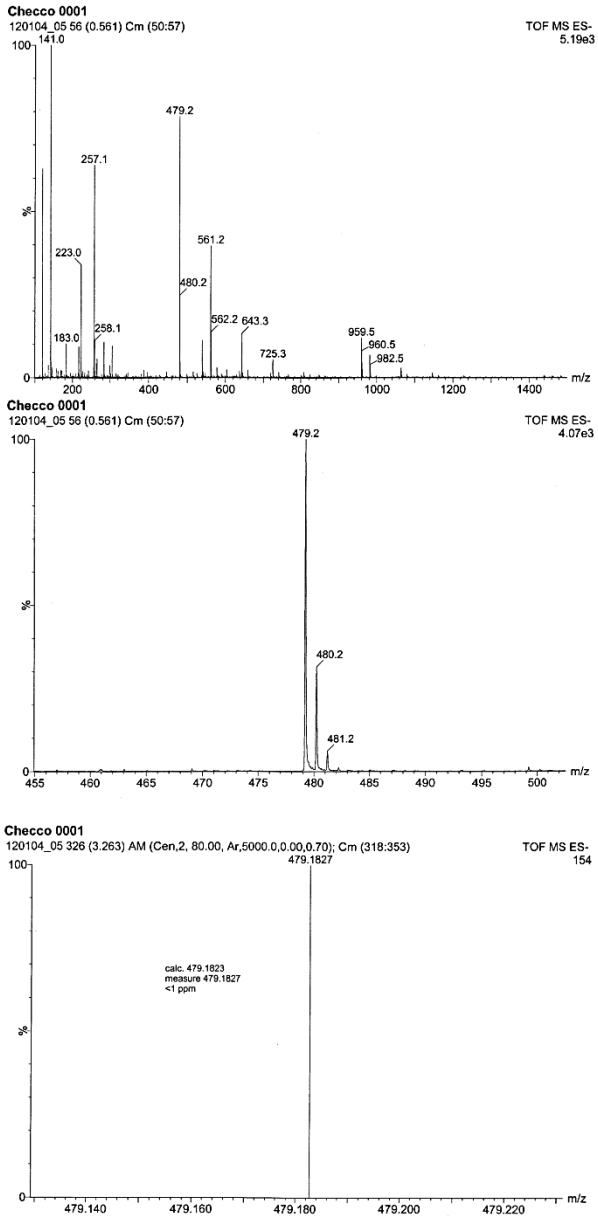

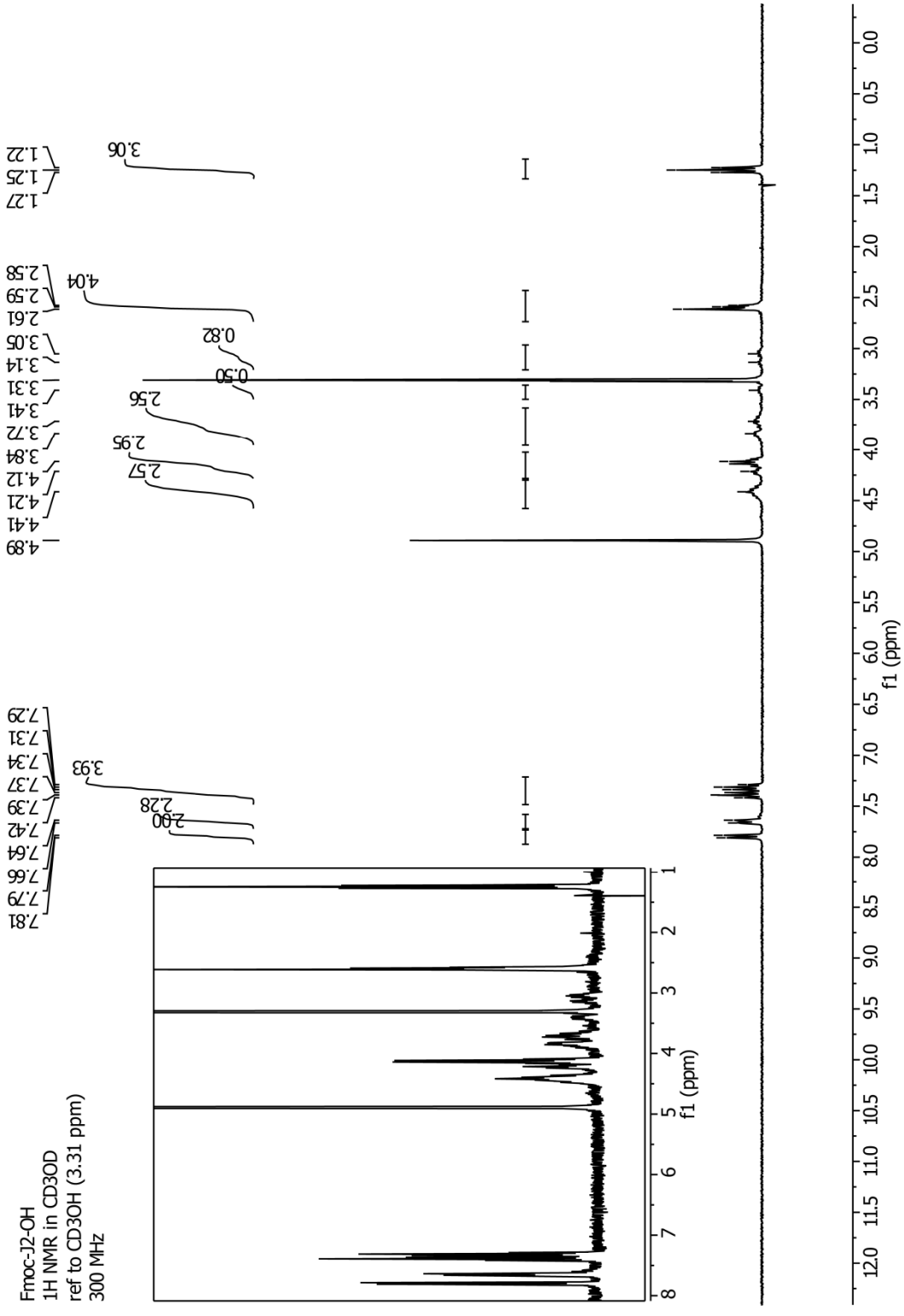
Fmoc-J2-OH
1H NMR in CD3OD
ref to CD3OH (3.31 ppm)
300 MHz
f1 (ppm)
7.81
7.79
7.66
7.64
7.42
7.39
7.37
7.34
7.31
7.29
3.93
2.28
2.00
4.89
4.41
4.21
4.12
3.84
3.72
3.41
3.31
3.14
3.05
2.61
2.59
2.58
4.04
2.57
2.95
2.56
0.50
0.82
3.06
1.27
1.25
1.22

Figure 5.20 (C) ESI/EMM data for Fmoc-J_4-OH, calc. $[M+H]^+ = 509.2$, $[M+Na]^+ = 531.2$. ^{1}H-NMR for Fmoc-J_4-OH shown on the next page.

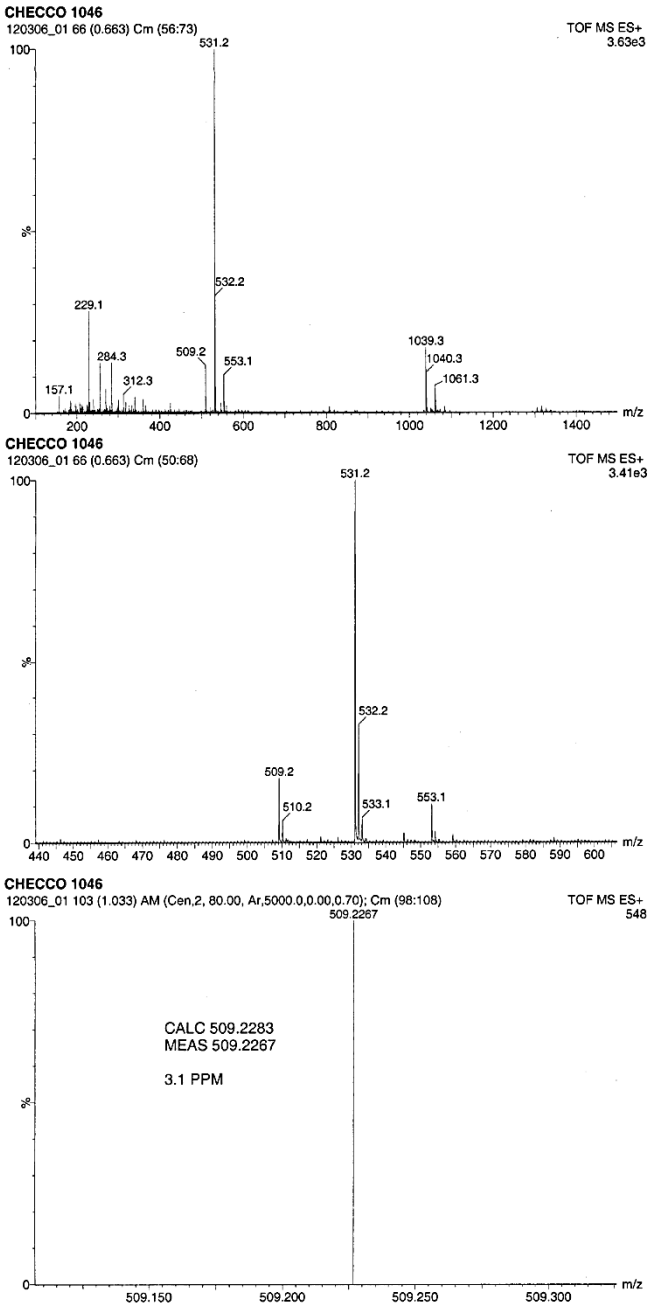

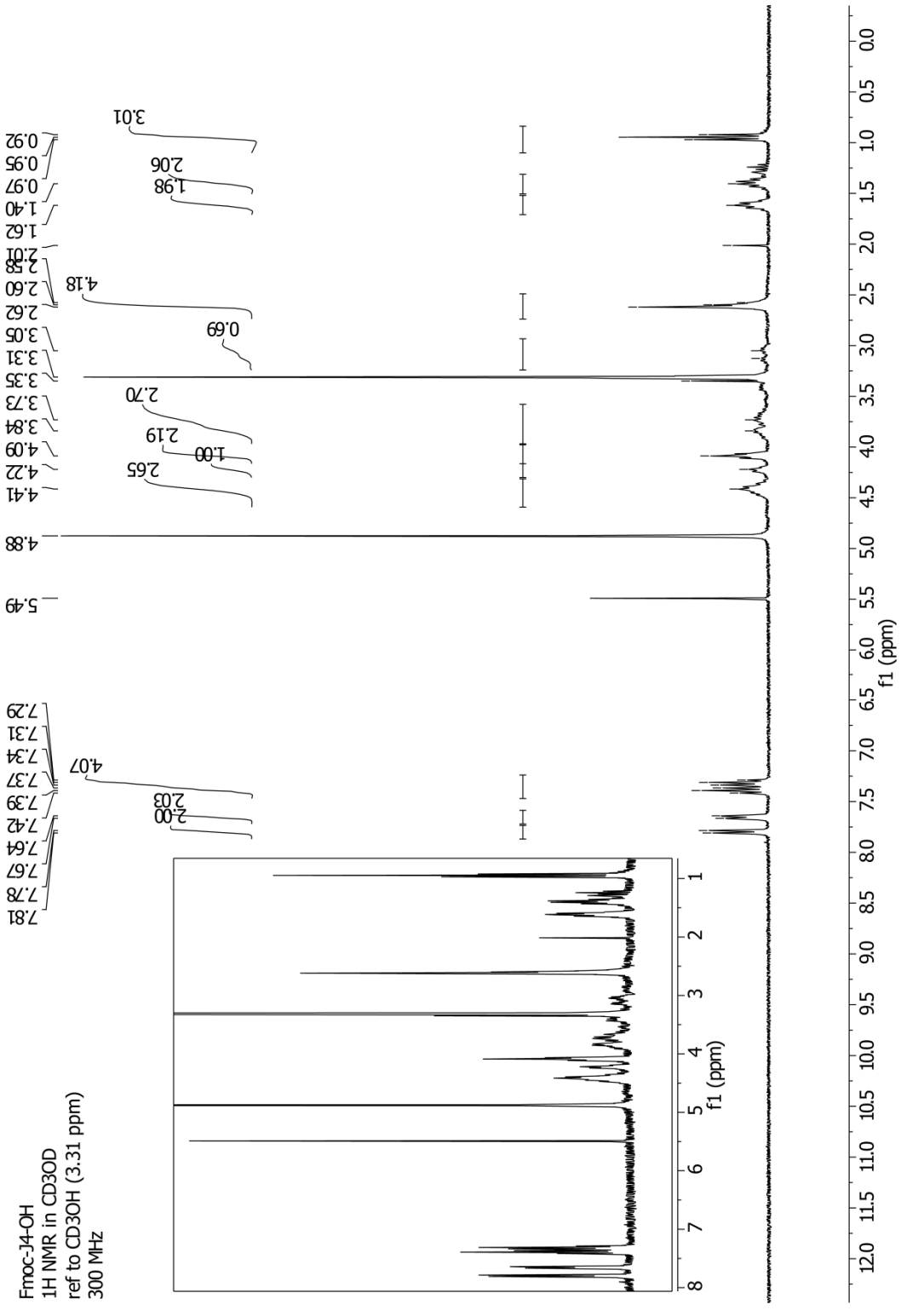
Fmoc-J4-OH
1H NMR in CD3OD
ref to CD3OH (3.31 ppm)
300 MHz
f1 (ppm)
7.81
7.78
7.67
7.64
7.42
7.39
7.37
7.34
7.31
7.29
4.07
2.00
2.03
5.49
4.88
4.41
4.22
4.09
3.84
3.73
3.35
3.31
3.05
2.62
2.60
2.58
2.01
1.62
1.40
0.97
0.95
0.92
3.01
2.06
1.98
4.18
0.69
2.70
2.19
1.00
2.65

Figure 5.20 (D) ESI/EMM data for Fmoc-J_5-OH, calc. $[M-H]^-$ = 521.2.
^{1}H-NMR for Fmoc-J_5-OH shown on the next page.

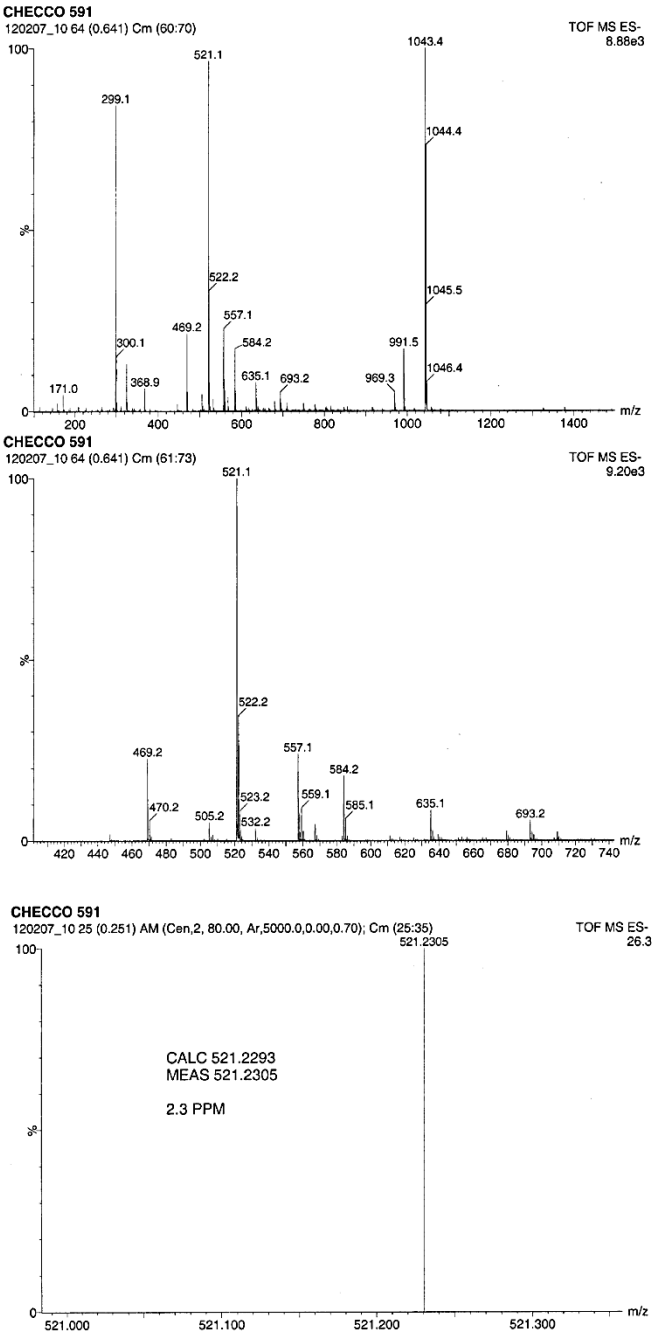

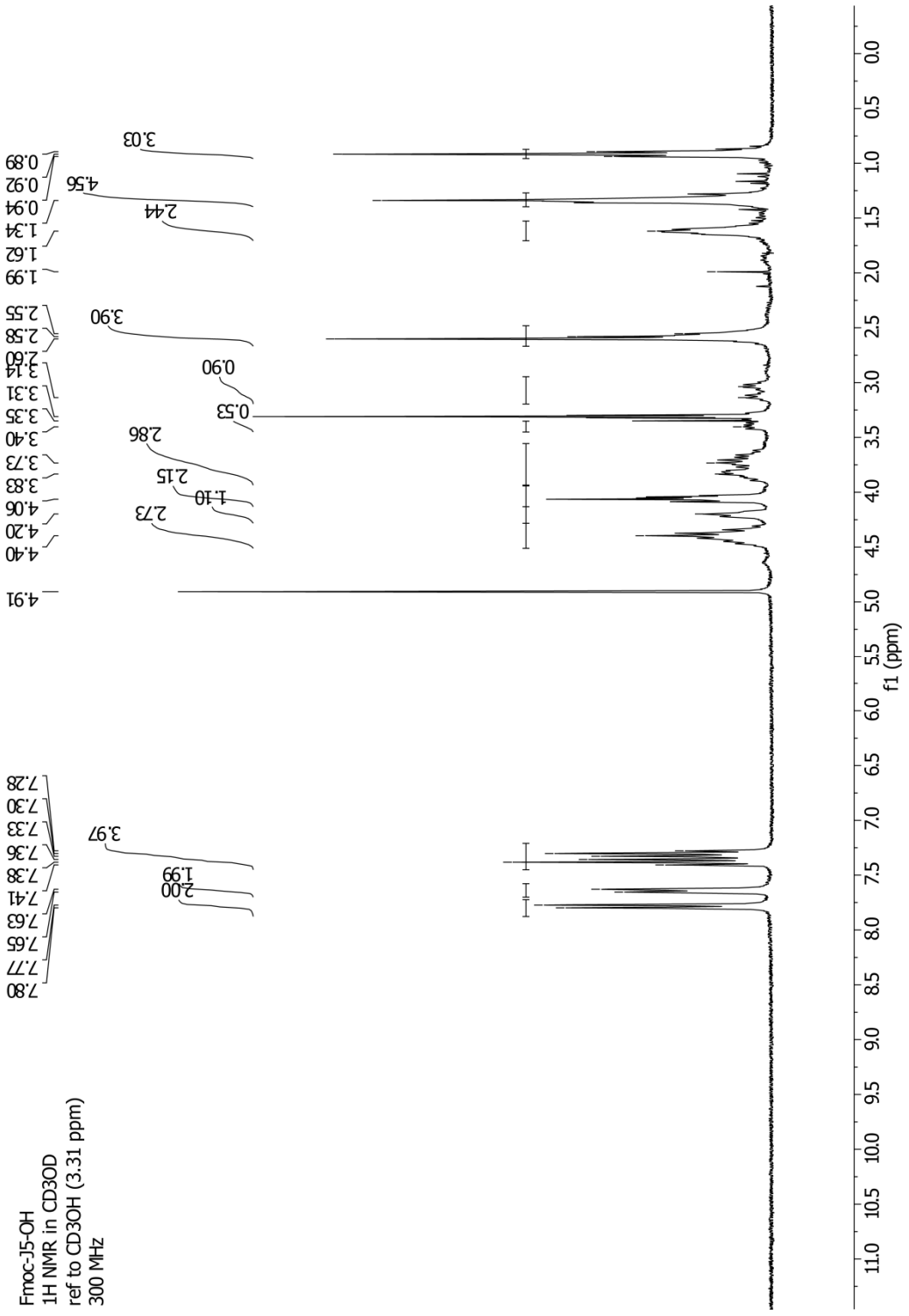
Fmoc-J5-OH
1H NMR in CD3OD
ref to CD3OH (3.31 ppm)
300 MHz
f1 (ppm)

Figure 5.20 (E) ESI/EMM data for Fmoc-J_8-OH, calc. $[M+H]^+ = 565.3$, $[M+Na]^+ = 587.3$. ^{1}H-NMR for Fmoc-J_8-OH shown on the next page.

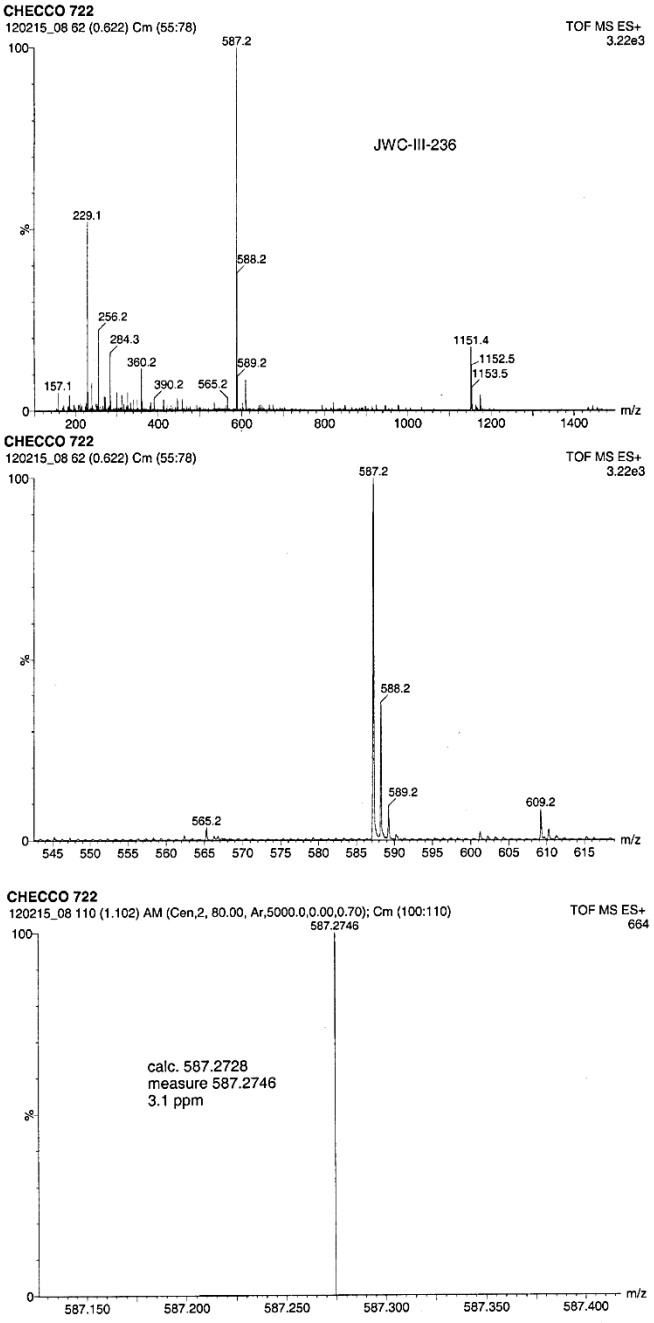

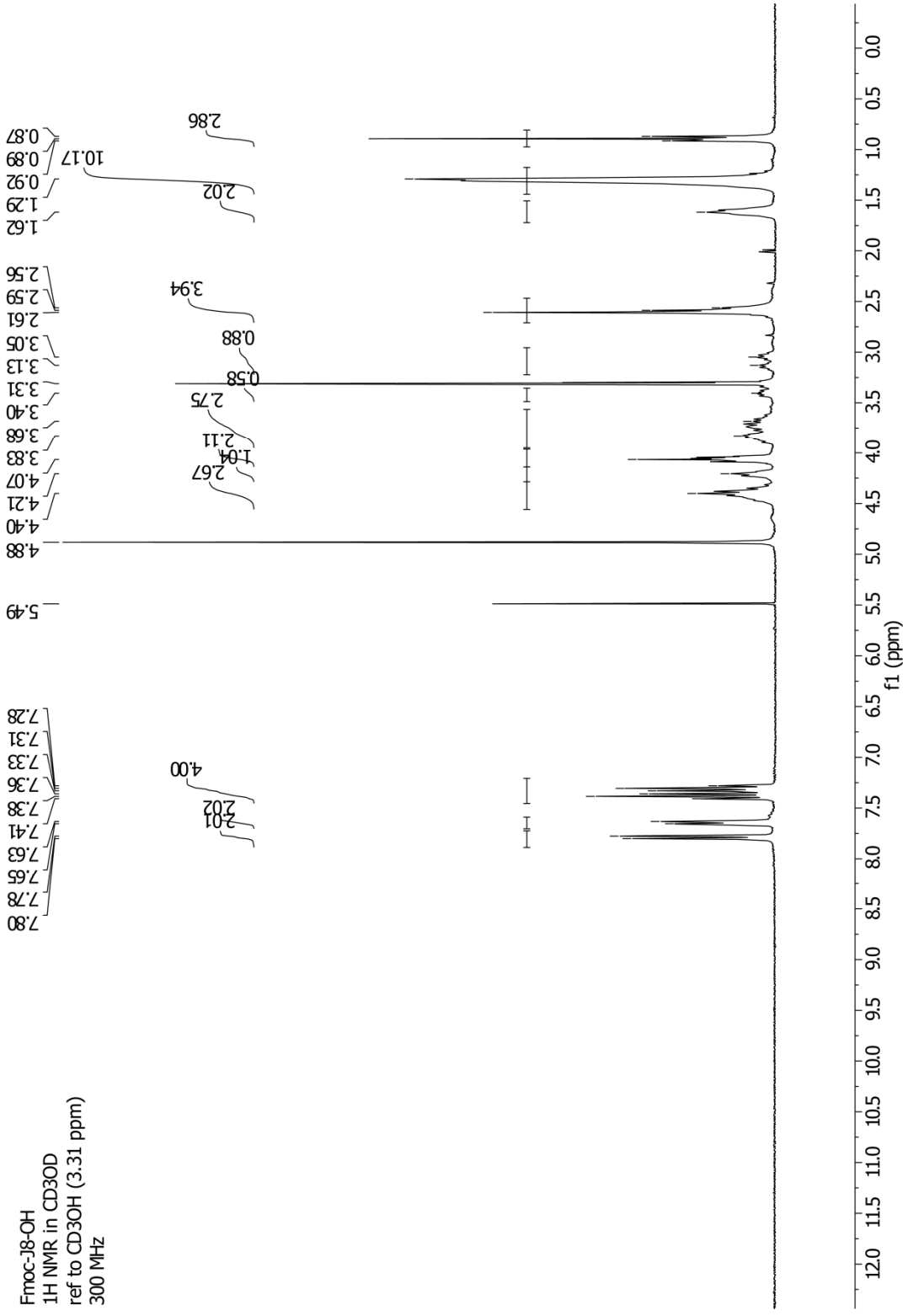
Fmoc-J8-OH
1H NMR in CD3OD
ref to CD3OH (3.31 ppm)
300 MHz
f1 (ppm)

Figure 5.20 (F) ESI/EMM data for Fmoc-J_{12}-OH, calc. $[M-H]^-$ = 619.3. ^{1}H-NMR for Fmoc-J_{12}-OH shown on the next page.

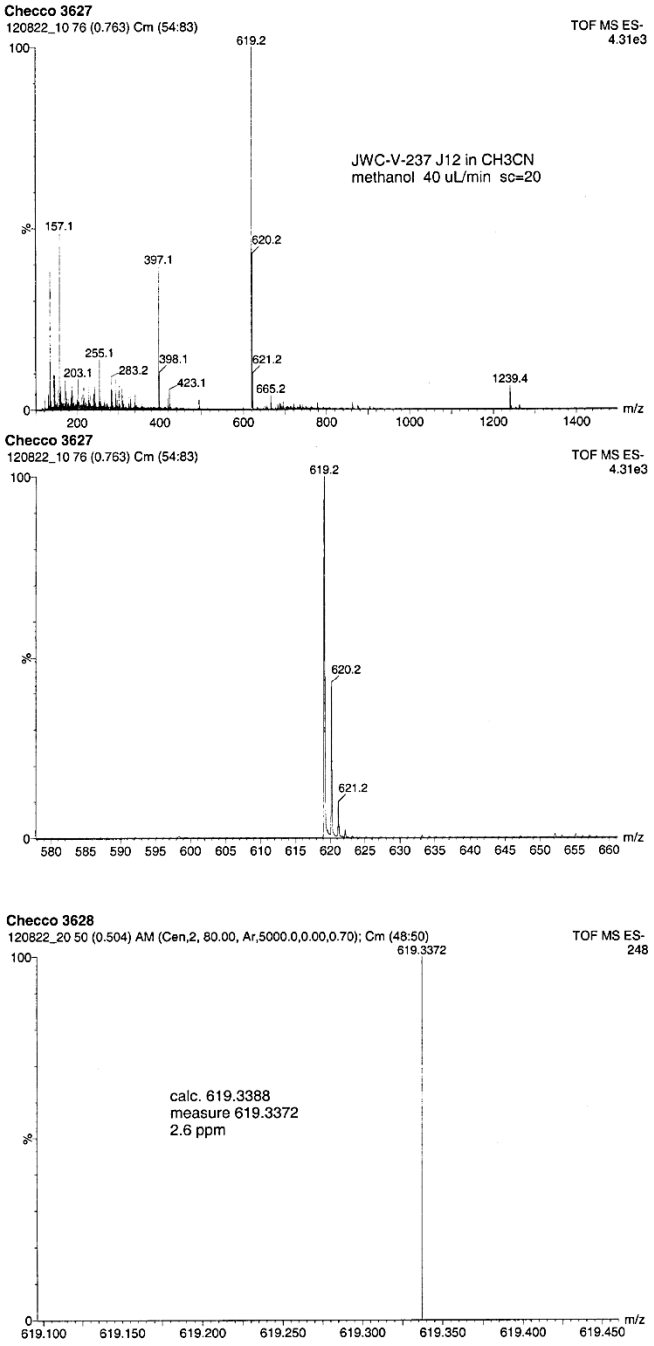

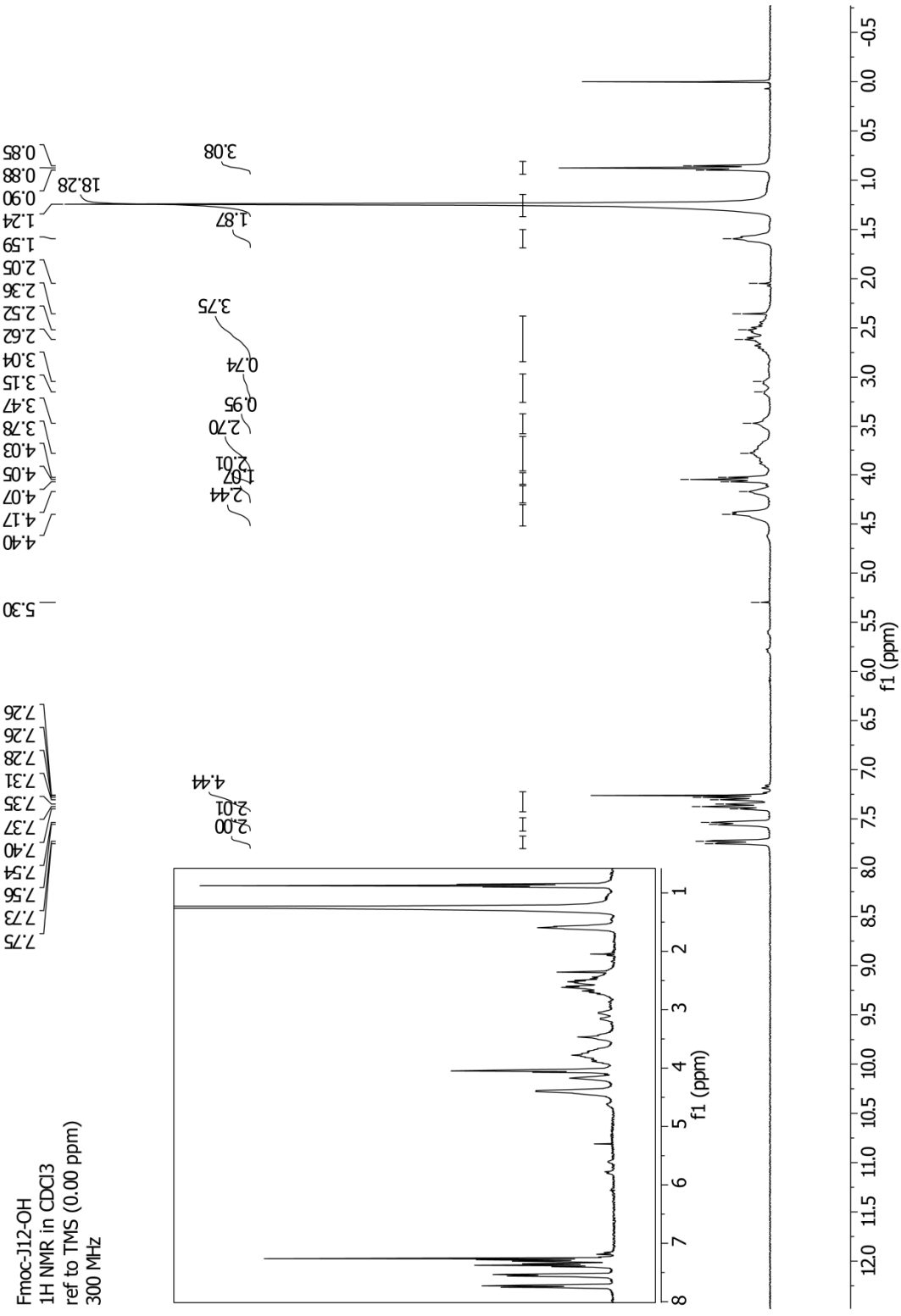
Fmoc-J12-OH
1H NMR in CDCl3
ref to TMS (0.00 ppm)
300 MHz
7.75
7.73
7.56
7.54
7.40
7.37
7.35
7.31
7.28
7.26
7.26
5.30
4.40
4.17
4.07
4.05
4.03
3.78
3.47
3.15
3.04
2.62
2.52
2.36
2.05
1.59
1.24
0.90
0.88
0.85
2.00
2.01
4.44
2.44
1.07
2.01
2.70
0.95
0.74
3.75
1.87
18.28
3.08
f1 (ppm)
f1 (ppm)

Figure 5.20 (G) ESI/EMM data for Fmoc-J_{5E}-OH, calc. $[M-H]^-$ = 519.2. ^{1}H-NMR for Fmoc-J_{5E}-OH shown on the next page.

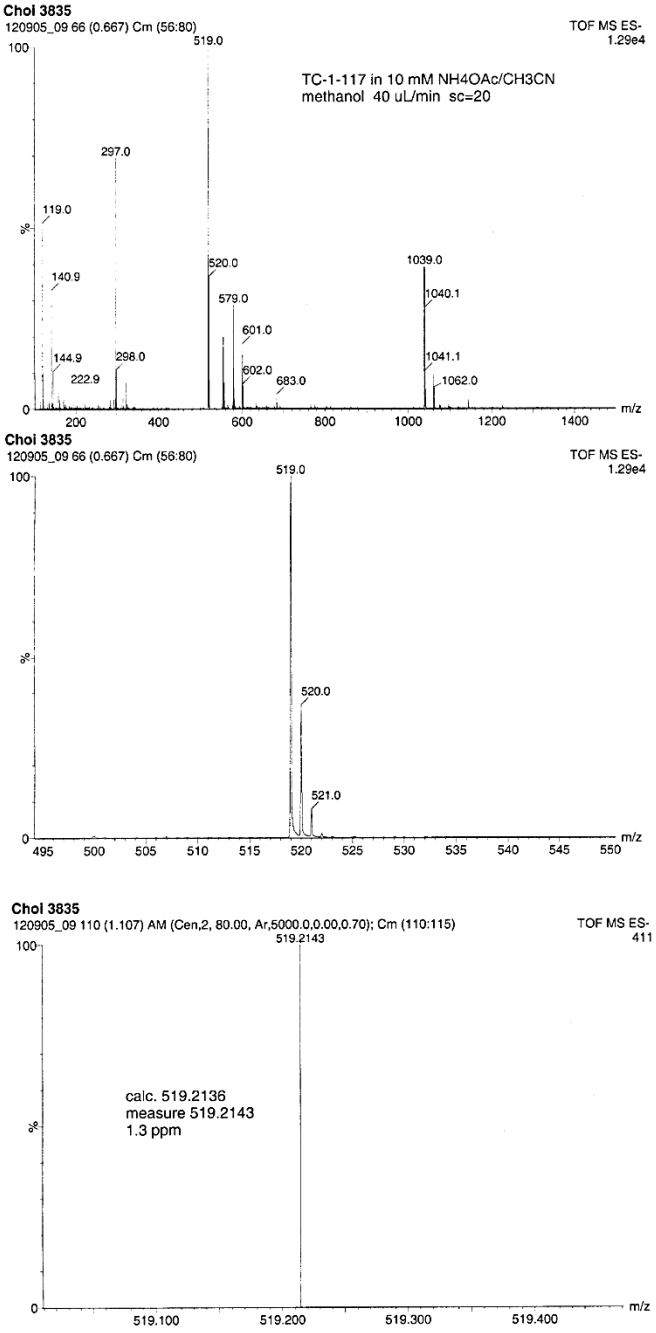

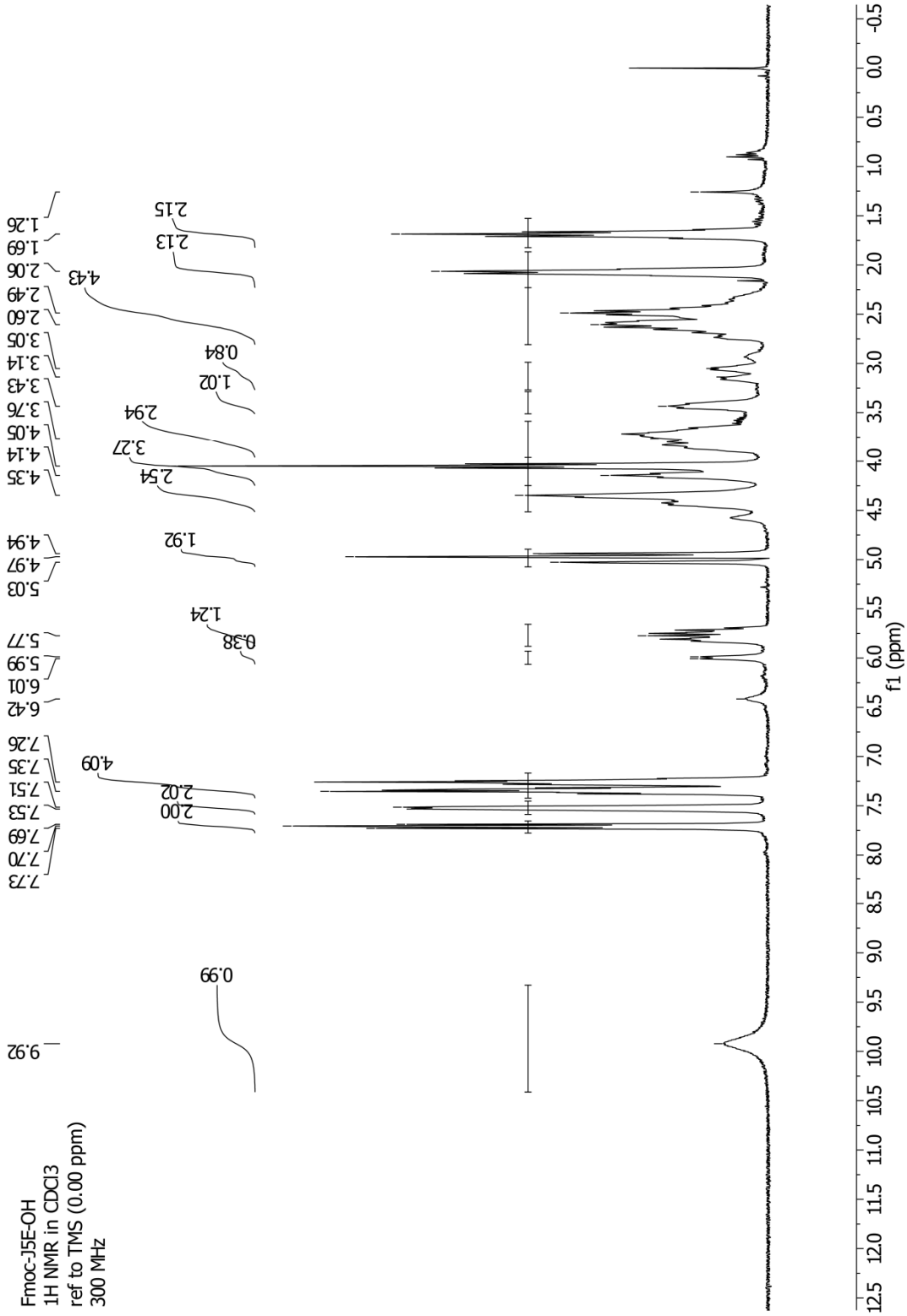
Fmoc-J5E-OH
1H NMR in CDCl3
ref to TMS (0.00 ppm)
300 MHz
9.92
0.99
7.73
7.70
7.69
7.53
7.51
7.35
7.26
4.09
2.00
2.02
6.42
6.01
5.99
5.77
0.38
1.24
5.03
4.97
4.94
1.92
4.35
4.14
4.05
3.76
3.43
3.14
3.05
2.60
2.49
2.06
4.43
2.54
3.27
2.94
1.02
0.84
2.13
2.15
1.69
1.26
f1 (ppm)

5.9.3 Peptide synthesis and purification

α-Peptides and α/β-peptides were synthesized by microwave assisted solid phase peptide synthesis on NovaPEG Rink Amide resin, as previously described.[62] Fmoc-protected amino acids (with standard compatible side chain protecting groups; 4 eq.) were activated with a solution of PyBOP (4 eq.), 0.1 M HOBt, and DIEA (8 eq.) in 1-methyl-2-pyrrolidone (NMP) and added to the resin. For the coupling of Fmoc-J-amino acids, 3 equivalents of monomer (with 3 eq. PyBOP and 6 eq. DIEA) was often used to conserve monomer. Coupling reactions were irradiated by microwave to 70 °C for 6 minutes (2 minute ramp, 4 minutes hold) with a 5 minute cooldown (for α-residues) or for 14 minutes (2 minute ramp, 12 minute hold) with a 5 minute cooldown (for cyclic β-residues). Fmoc deprotection reactions were carried out with a solution of 20% piperidine in N,N-dimethylformamide (DMF), irradiated by microwave at 80 °C for 4 minutes (2 minute ramp, 2 minute hold). After assembly of the linear chain, oligomers that were not fluorophore-labeled were acetylated by stirring the resin in a solution of 8:2:1 DMF:DIEA:acetic anhydride for about 10 minutes at room temperature. For oligomers labeled with 6-carboxyfluoroscein (6-FAM), resin was treated with 4 equivalents of 6-FAM (AnaSpec AS-81004) under the above coupling conditions at room temperature overnight, protected from light. For oligomers containing crosslinked J_{5E} residues, olefin metathesis was carried out on resin using a solution of ~10 mM Grubbs Catalyst, 1st Generation (Sigma, 579726) in dichloroethane (DCE) with stirring and bubbling nitrogen for 1-3 hours.[63] Reaction progress could be monitored by analysis of microcleavages of MALDI-TOF and HPLC, and the reaction was repeated until the majority of the product was crosslinked. Once the oligomer had been fully assembled on resin, peptides and α/β-peptides were cleaved using a solution of 95% trifluoroacetic acid (TFA), 2.5% water, 2.5% triisopropylsilane (TIS), concentrated under a

stream of nitrogen, and then precipitated with cold diethyl ether. Crude peptide mixtures were then purified by reverse-phase HPLC. After purification, final peptide purity was assessed by analytical HPLC and identity confirmed by MALDI-TOF-MS ("Peptide characterization" section below).

5.9.4 Bcl-x_L competition FP assay

Bcl-x_L for use in competition FP assays was expressed and purified as previously reported.[24]

Competition FP assays were carried out as previously reported, using the previously reported tracer (**BODIPY^{TMR}-Bak**).[25, 64] For competition FP assays, DMSO stock solutions of α/β-peptides were prepared and concentration determined by UV absorbance at 280 nm.[65] Competition FP assays were performed by adding 2 μL of serial dilutions of inhibitor in DMSO to 48 μL of solution containing **BODIPY^{TMR}-Bak** (final concentration = 3 nM) and Bcl-x_L (final concentration = 2 nM) in FP buffer (50 mM NaCl, 16.2 mM Na_2HPO_4, 3.8 mM KH_2PO_4, 0.15 mM NaN_3, 0.15 mM EDTA, 0.5 mg/mL Pluoronic-F68, pH 7.5) in 384-well, black polystyrene plates (Costar). The plate was incubated at room temperature for 4 hours, and fluorescence polarization values read on an Envision 2100 microplate reader. Each condition was run in duplicate. Inhibition constants (K_i) were determined from FP data using methods described for a competitive binding model with GraphPad Prism 4.0,[66, 67] using Equation (1), described below:

(1) Y = BOTTOM+(TOP-BOTTOM)*((2*SQRT(a^2-3b)*COS(d/3)-a)/(3*KD1+2*SQRT(a^2-3b)*COS(d/3)-a))/e

Where:
a = KD1+KD2+LST+10^X-RT
b = KD1*(10^X-RT)+KD2*(LST-RT)+KD1*KD2
c = -KD1*KD2*RT
d = ARCCOS((-2*a^3+9*a*b-27*c)/(2*SQRT((a^2-3*b)^3)))
e = (LST+KD1+RT-sqrt[(LST+KD1+RT)^2-4*LST*RT])/(2*LST)

Y = mP reading
BOTTOM = mP of free tracer
TOP = mP of bound tracer
X = log concentration of inhibitor
KD1 = K_d for tracer binding to receptor (determined by direct-binding FP)
KD2 = K_i for inhibitor binding to receptor
LST = concentration of tracer
RT = concentration of receptor

5.9.5 Chemical hydrolysis of α/β-peptide 5.2

Chemical hydrolysis was performed using an adapted protocol from Sohma et al.[68] A small amount of lyophilized **5.2** was dissolved in 25% acetonitrile/H_2O. NaOH (1 M) was added to achieve a final concentration of 25 mM NaOH. The reaction was stirred at 4 °C overnight, and analyzed by analytical-scale reverse-phase HPLC and MALDI-TOF MS.

5.9.6 Solubility experiments

DMSO stock solutions of α/β-peptides were prepared at 2500 μM, as determined by UV absorbance at 280 nm.[65] 10 μL of this DMSO stock solution was added to 980 μL DMEM and 10 μL FBS to give final conditions of 25 μM α/β-peptide, 1% DMSO, 1% FBS in DMEM. The mixture was then incubated at 37 °C with shaking. After 15 minutes of incubation, the solution was mixed thoroughly with a pipette (to ensure any insoluble peptide was fully suspended), and 125 μL of this solution was injected onto analytical-scale reverse-phase HPLC ("15 min., suspension", black chromatograms in Figure 5.10). The mixture was then centrifuged at 13,200 x

g, and 125 μL of the resulting supernatant was then injected onto HPLC ("15 min., centrifuged", green chromatograms in Figure 5.10). The mixture was then allowed to continue incubating at 37 °C with shaking. At various subsequent time points, the mixture was centrifuged and the supernatant was injected onto HPLC to determine the amount of α/β-peptide remaining in solution at that time.

5.9.7 Live-cell confocal microscopy

HeLa cells were plated in an 8-well microscopy slide at 50,000 cells/well in 200 μL DMEM containing 10% FBS supplemented with penicillin and streptomycin (P/S). Cells were allowed to recover overnight at 37 °C, 5% CO_2. Before an experiment, the media was removed and the replaced with 198 μL of fresh DMEM with 0% or 10% FBS. Fluorophore-labeled peptides in DMSO were added (final DMSO concentration = 1%) and the plates were incubated at 37 °C, 5% CO_2 for the 2-5.5 hours. After incubation, the media was removed, the cells were washed with PBS, and then fresh DMEM was added, followed by the addition of wheat germ agglutinin-Alexa Fluor 488 conjugate (WGA488) (Life Technologies) to each well at 5 μg/mL and incubated for 10-20 minutes. Subsequently, Hoechst 33342 (Life Technologies) was added to stain nuclei for 5 minutes. The media was then removed and the wells were washed 2 times with PBS, and then fresh PBS was added for imaging. Images were captured on Eclipse TE2000-U laser scanning confocal microscope (Nikon) equipped with an Axio Camdigital camera (Carl Zeiss). All images were contrast-adjusted uniformly across all conditions using Microsoft Word.

5.9.8 Cell-killing assays

All cell-killing assays were performed by Douglas Fairlie and Erinna Lee (Fairlie Laboratory, Division of Structural Biology, Walter and Eliza Hall Institute of Medical Research, Australia).

For CellTiter-Glo assays, wild-type (wt), *mcl-1*$^{-/-}$, or *bax*$^{-/-}$/*bak*$^{-/-}$ double knock-out (DKO) mouse embryonic fibroblasts (MEFs) were cultured in DMEM, supplemented with 10% FCS, 250 μM L-asparagine, and 50 μM 2-mercaptoethanol. On the day of experiments, cells were plated in opaque 96-well culture plates (~2000 cells/well) in DMEM, supplemented with 1% FCS, 250 μM asparagine, and 50 μM 2-mercaptoethanol, and allowed to recover for 4 hours. α/β-Peptides in DMSO were then diluted into media to make 2x stock solutions of α/β-peptides, and then added to cells. Cells were allowed to incubate at 37 °C, 5% CO_2 for 24-48 hours, and cell viability was determined by the addition of CellTiter-Glo chemiluminescence reagent (Promega). The percentage of viable cells was determined by dividing the luminescence signal from a well treated with α/β-peptide by the signal obtained from a control well with the same amount of DMSO. Similar protocols were followed for the analysis of cancer cell lines.

Interestingly, when α/β-peptide **5.6** was added to wells containing MDA-MB-435 cells, rod-like structures were rapidly formed that were visible under a microscope (Figure 5.21). This could be a potential source of the non-specific cell death observed for this α/β-peptide in many of the cell-based assays.

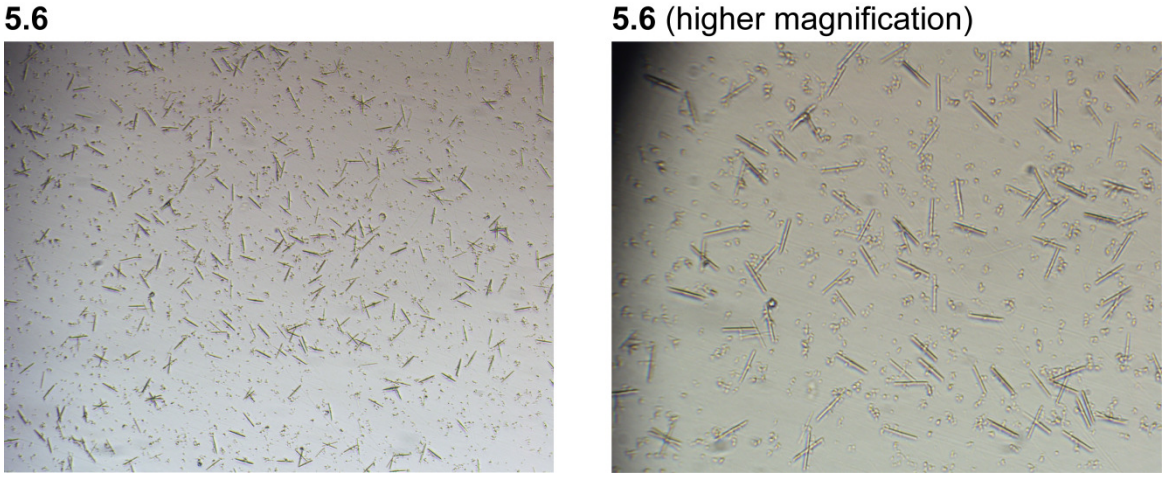

Figure 5.21 Images obtained under a light microscope of MDA-MB-435 cells treated with 20 μM **5.6**.

For flow cytometry analysis of MDA-MB-435 cells, $2x10^4$ cells/well were plated in HT-RPMI with 10% FCS and grown overnight. The media was removed and replaced with 500 μL of fresh HT-RPMI, 10% FCS, with α/β-peptides at the concentrations indicated in Figure 5.18. Cells were allowed to incubate at 37 °C, 5% CO_2 for 24 or 48 hours. Cells were then trypsinized and stained with 5 μg/mL propidium iodide (PI) and Annexin V-FITC. Flow cytometry analysis of MEFs was carried out in a similar manner. Cell viability was determined by flow cytometry analyses (FACSCalibur, Becton Dickinson) of cells that excluded PI and Annexin V-FITC (FL3-H and FL1-H, respectively). Figure 5.22 shows plots used to generate the viability graphs in Figure 5.18.

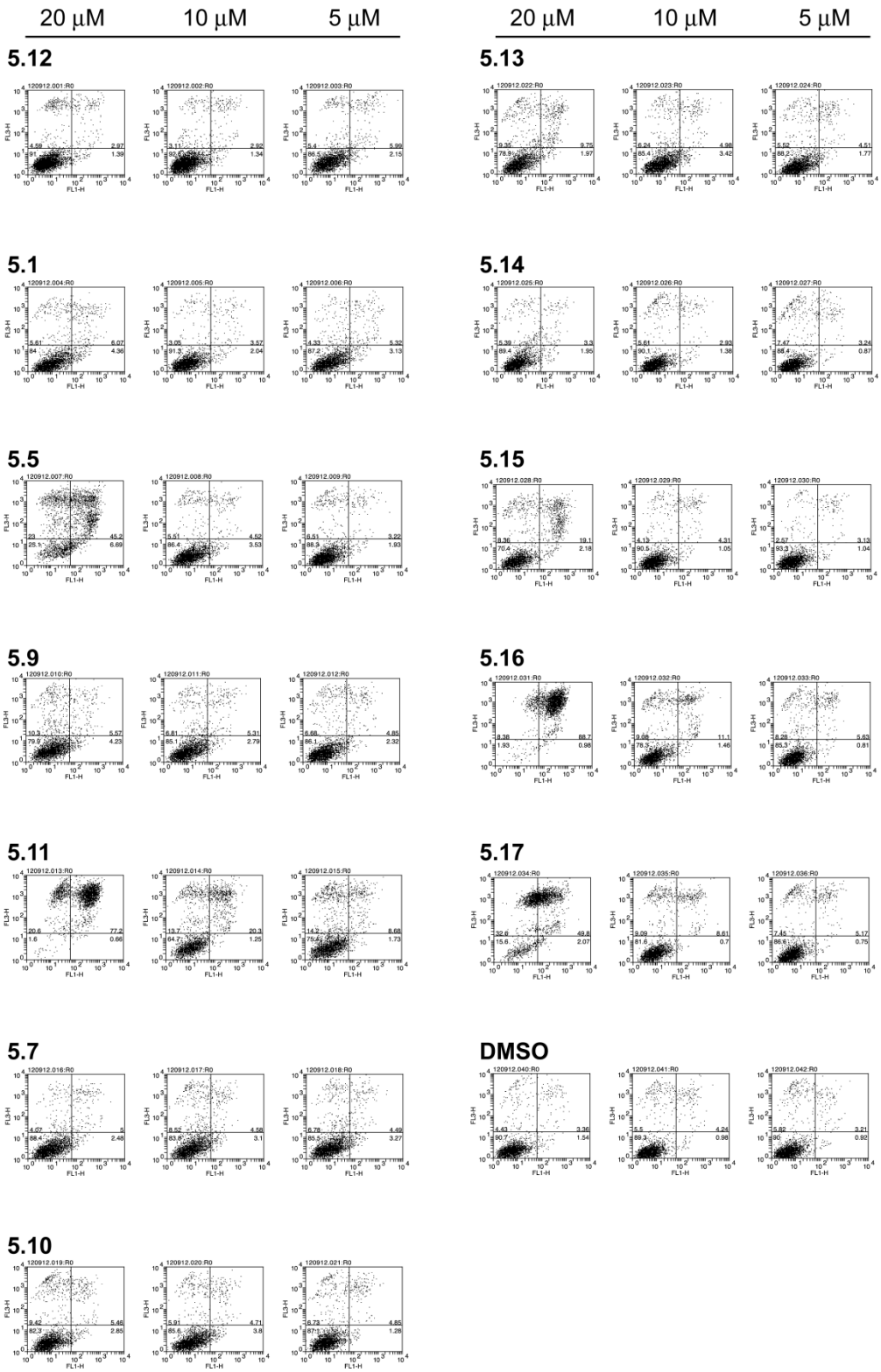

Figure 5.22 (A) Flow cytometry plots for MDA-MB-435 cells treated with the indicated α/β-peptide for 24 hours.

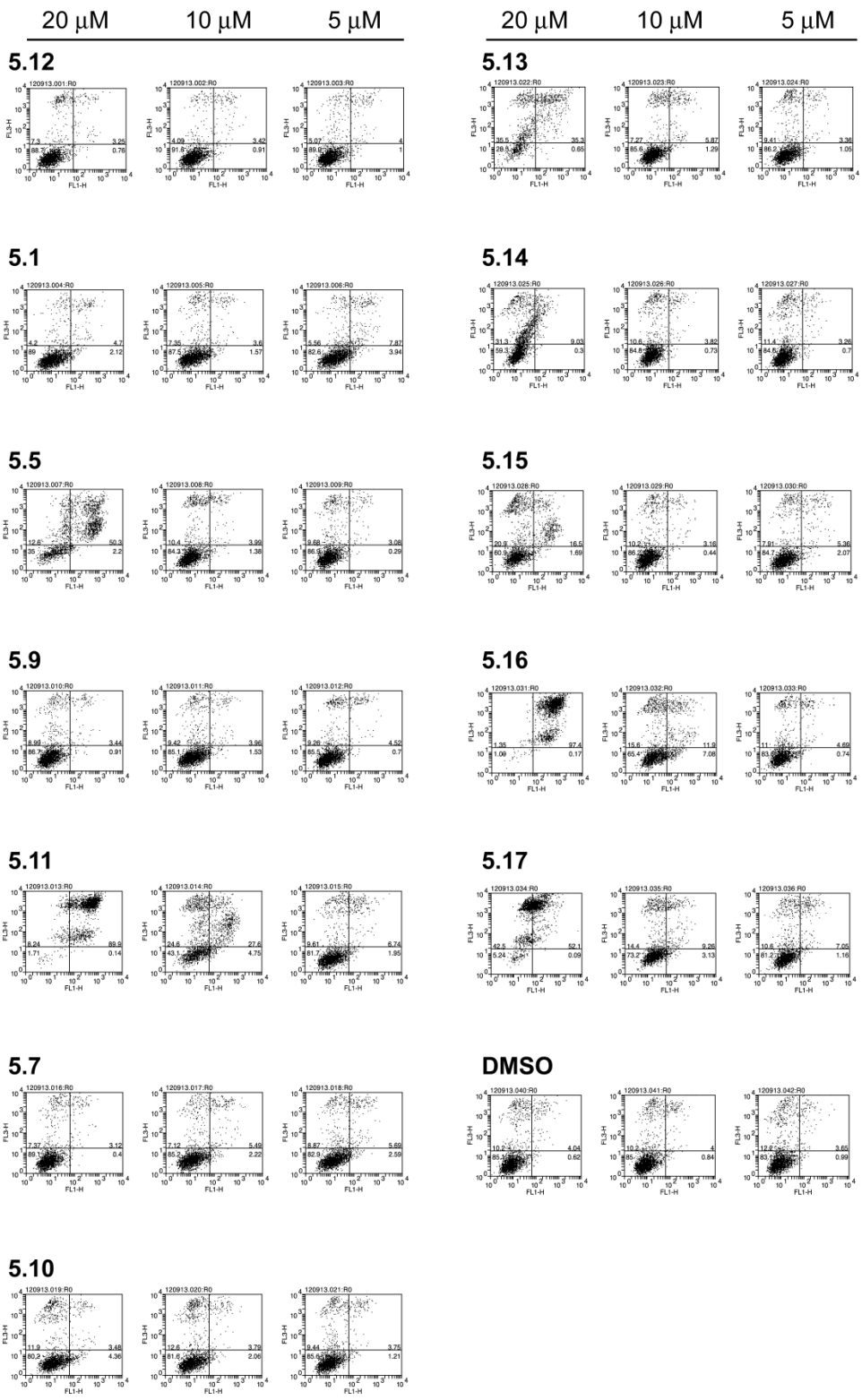

Figure 5.22 (B) Flow cytometry plots for MDA-MB-435 cells treated with the indicated α/β-peptide for 48 hours.

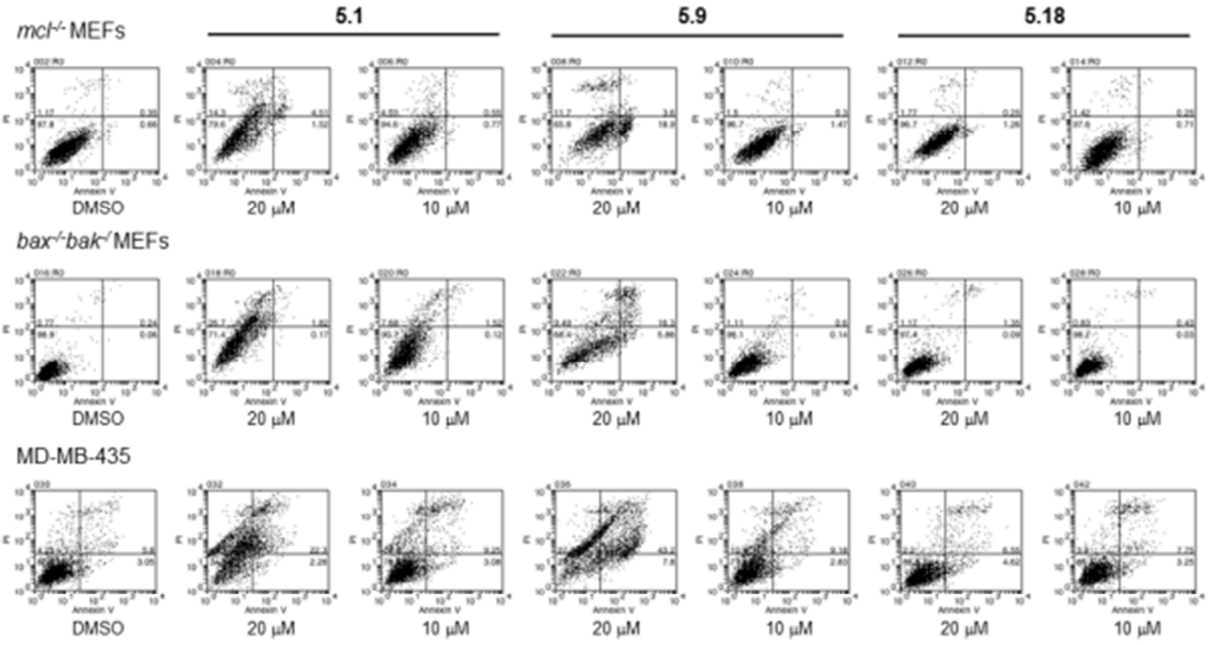

Figure 5.22 (C) Flow cytometry plots for various cell types treated with the indicated α/β-peptide for 24 hours.

5.9.9 Peptide characterization

α-Peptide and α/β-peptide purity after purification was assessed by analytical scale reverse-phase HPLC, using solvent A: H_2O with 0.1% TFA, solvent B: acetonitrile with 0.1% TFA, with a flow rate of 1 mL/min (unless otherwise specified). The solvent gradient for each peptide is specified in each panel. HPLC chromatograms at 220 nm are shown at the top of each panel. Peptide identity was confirmed by MALDI-TOF-MS, shown at the bottom of each panel. For each MALDI-TOF spectrum, the monoisotopic $[M+H]^+$, *m/z* is labeled.

5.1
HPLC: Gradient = 10-90% solvent B over 80 minutes
MALDI-TOF: Calculated monoisotopic $[M+H]^+$ = 2351.2

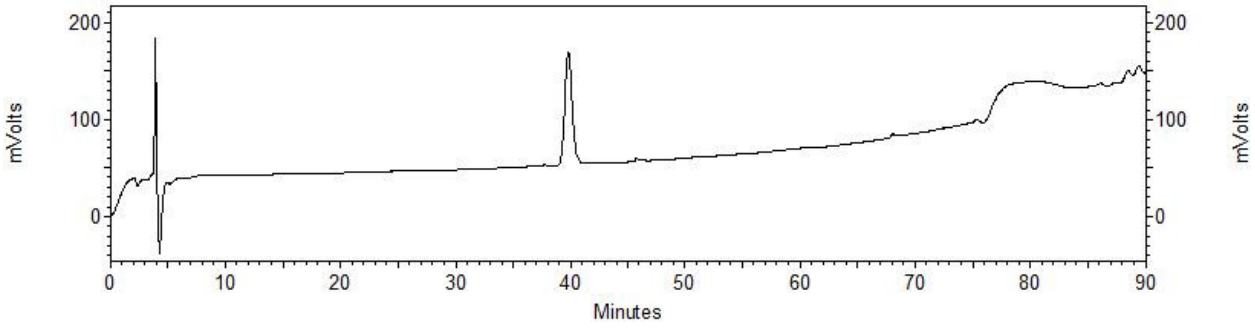

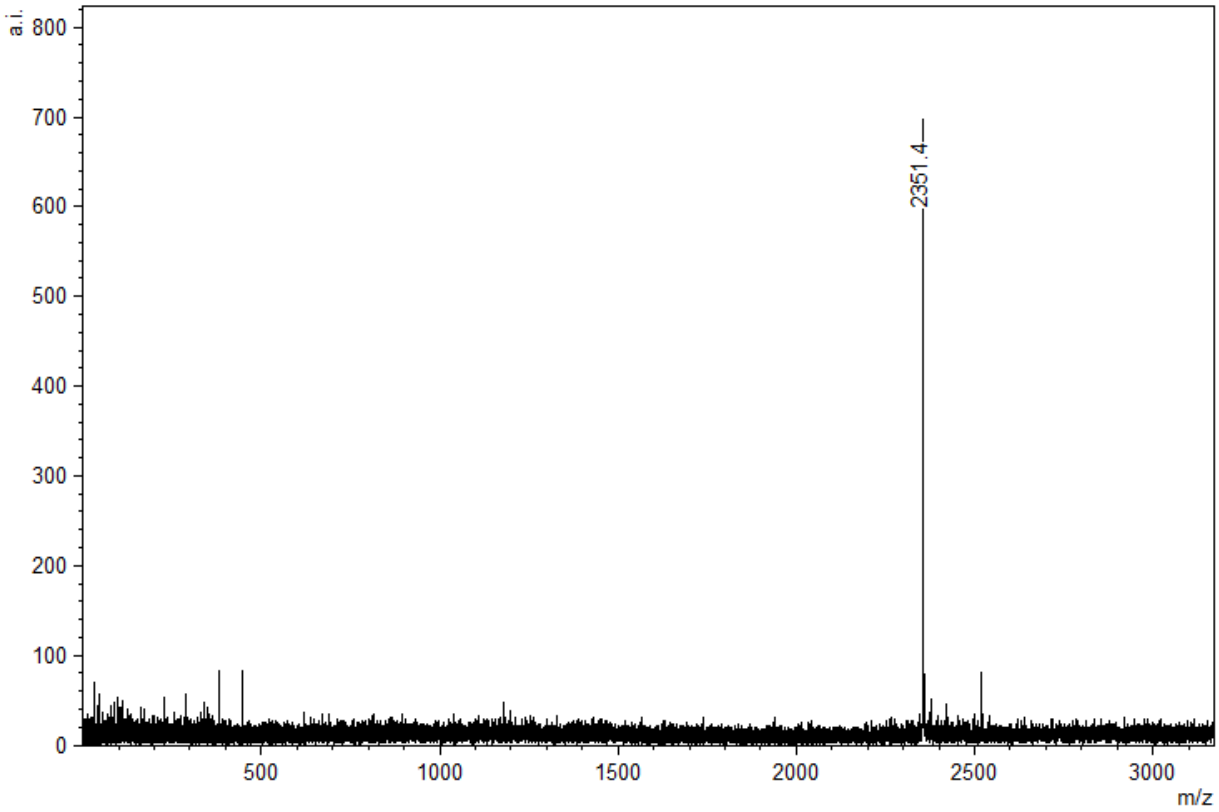

5.2

HPLC: Gradient = 10-90% solvent B over 80 minutes

MALDI-TOF: Calculated monoisotopic $[M+H]^+ = 2379.3$

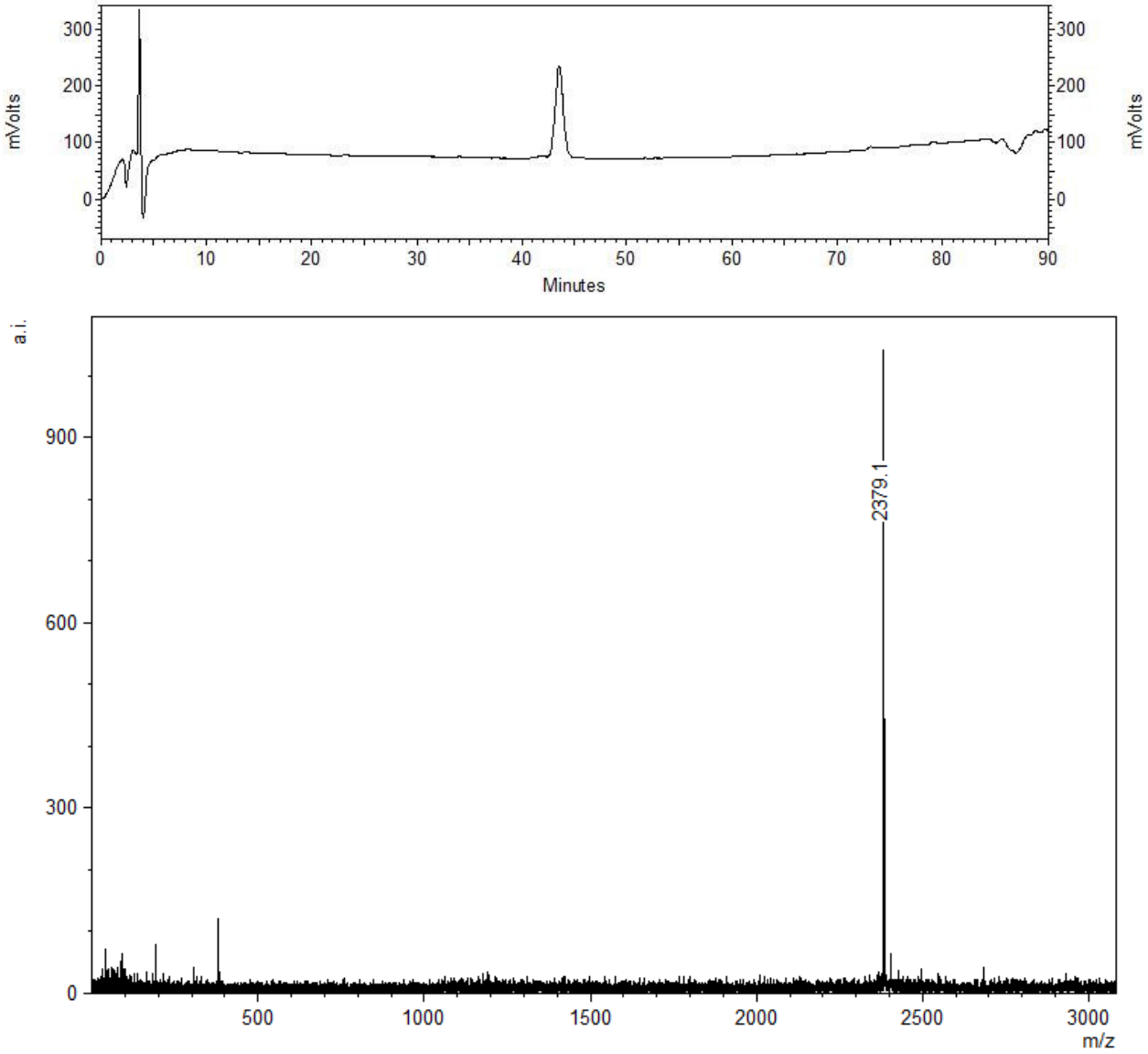

5.3
HPLC: Gradient = 10-60% solvent B over 50 minutes
MALDI-TOF: Calculated monoisotopic $[M+H]^+$ = 2407.3

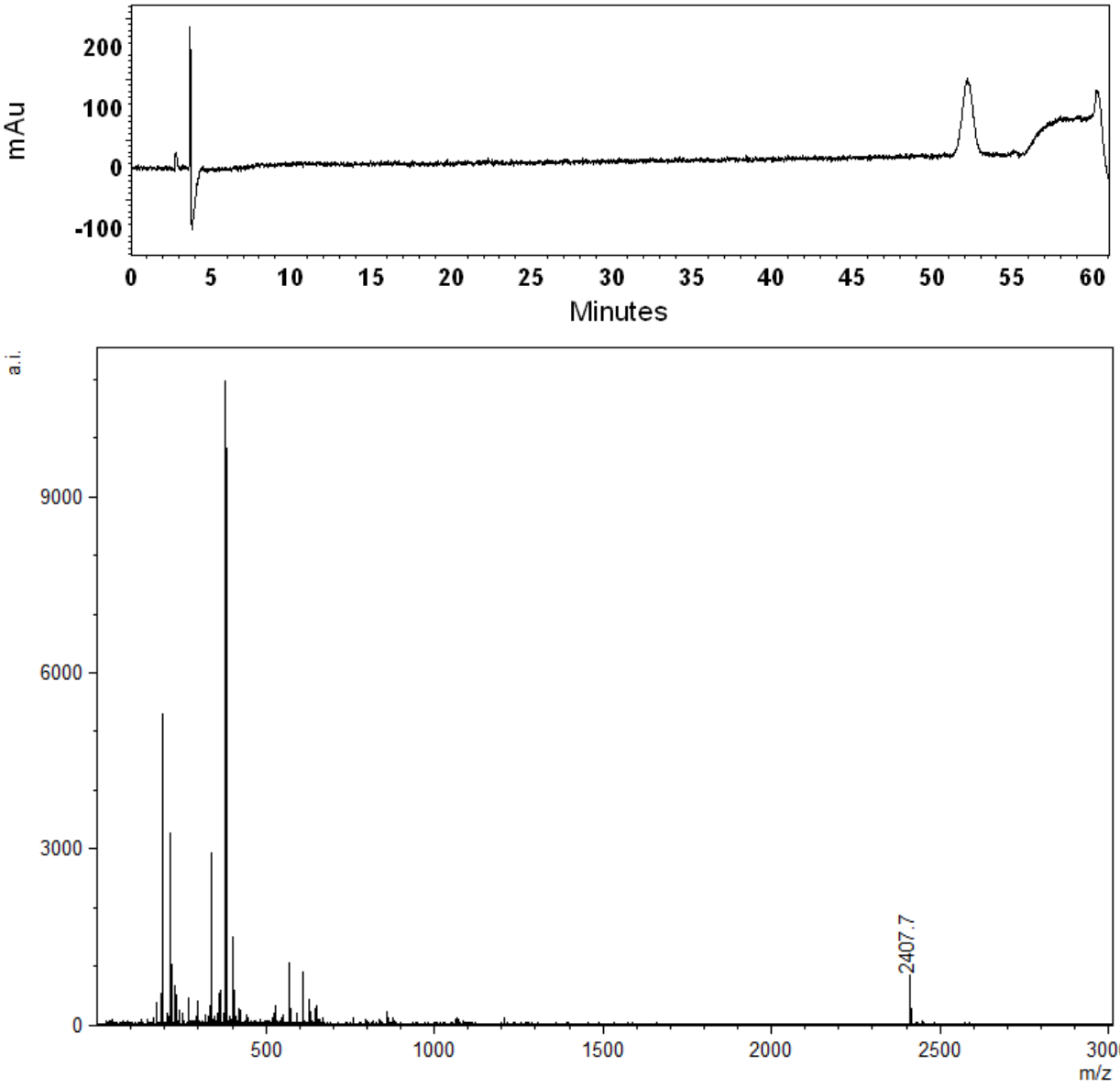

5.4

HPLC: Gradient = 10-90% solvent B over 80 minutes

MALDI-TOF: Calculated monoisotopic $[M+H]^+$ = 2463.4

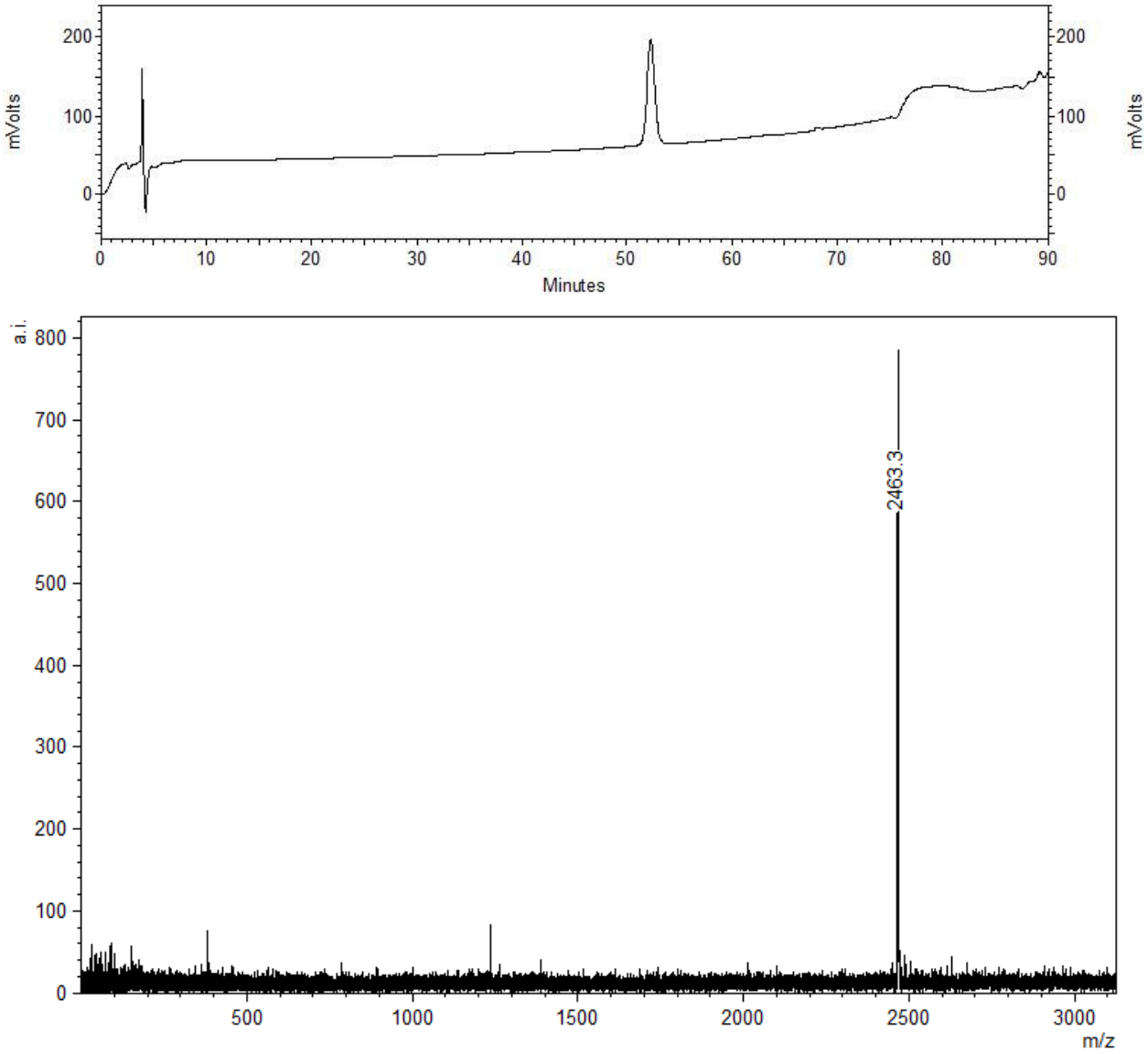

5.5

HPLC: Gradient = 10-90% solvent B over 80 minutes

MALDI-TOF: Calculated monoisotopic $[M+H]^+ = 2491.4$

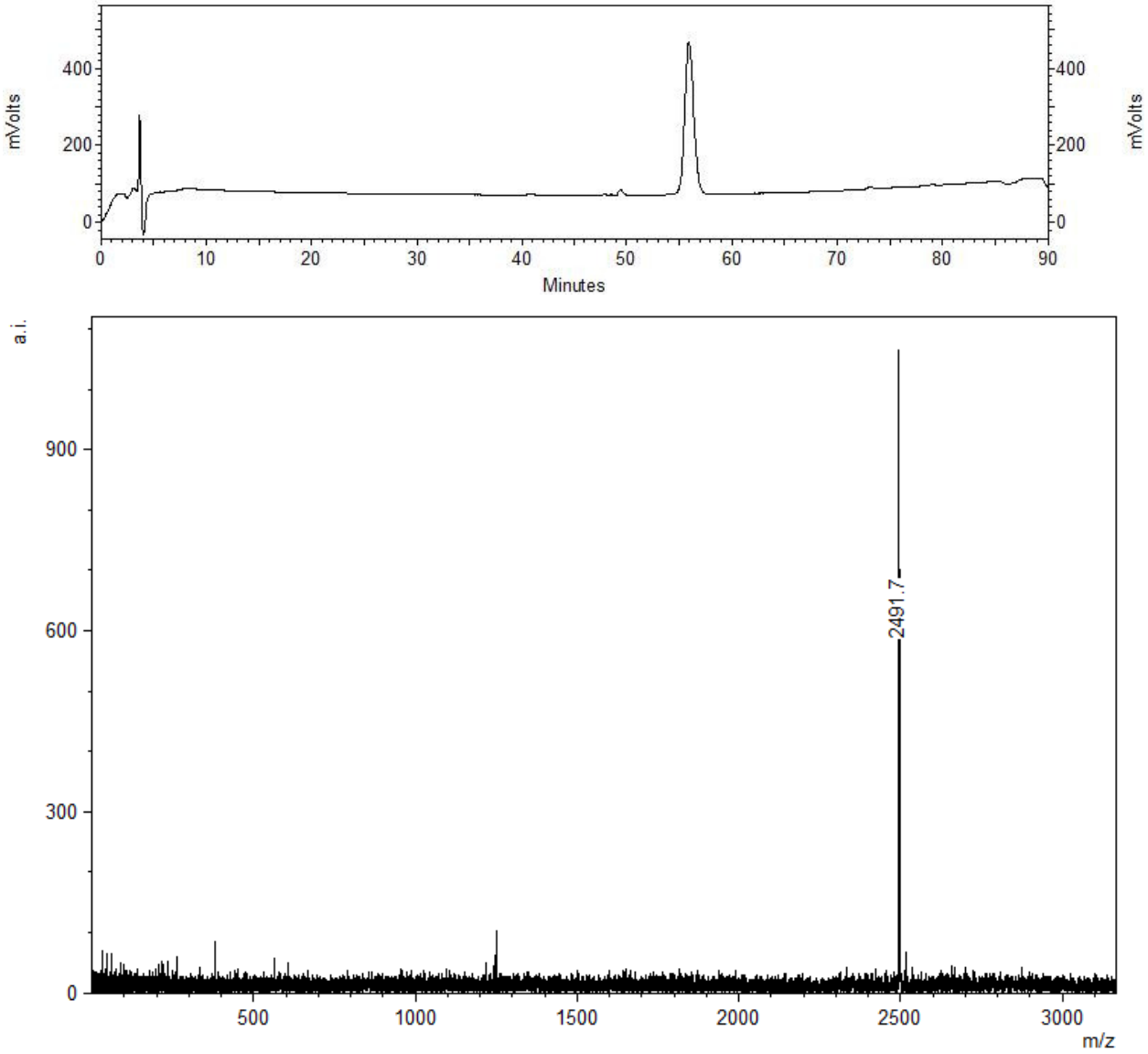

5.6

HPLC: Gradient = 10-90% solvent B over 80 minutes

MALDI-TOF: Calculated monoisotopic $[M+H]^+$ = 2575.5

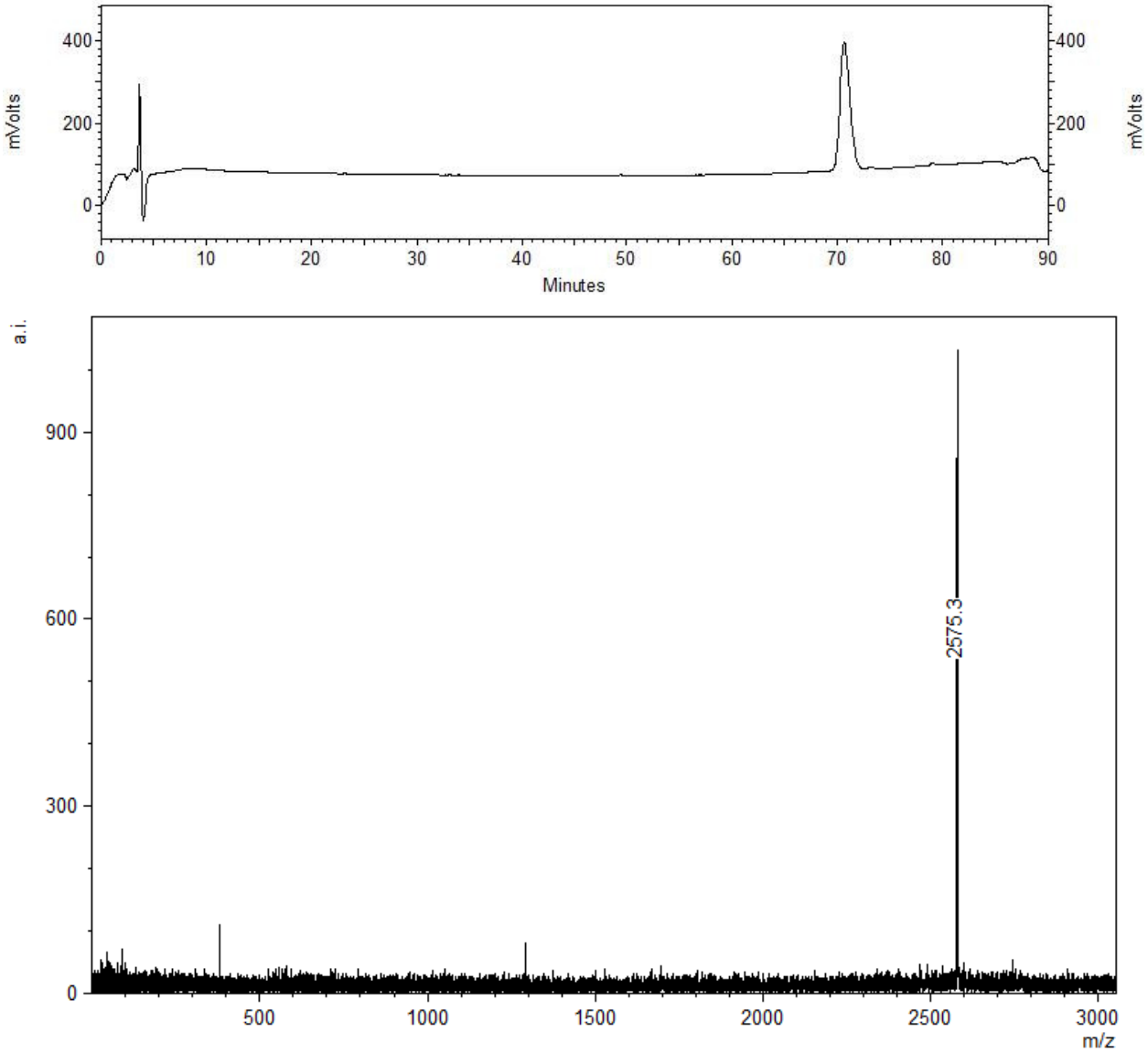

5.7

HPLC: Gradient = 10-90% solvent B over 80 minutes

MALDI-TOF: Calculated monoisotopic $[M+H]^+$ = 2819.5

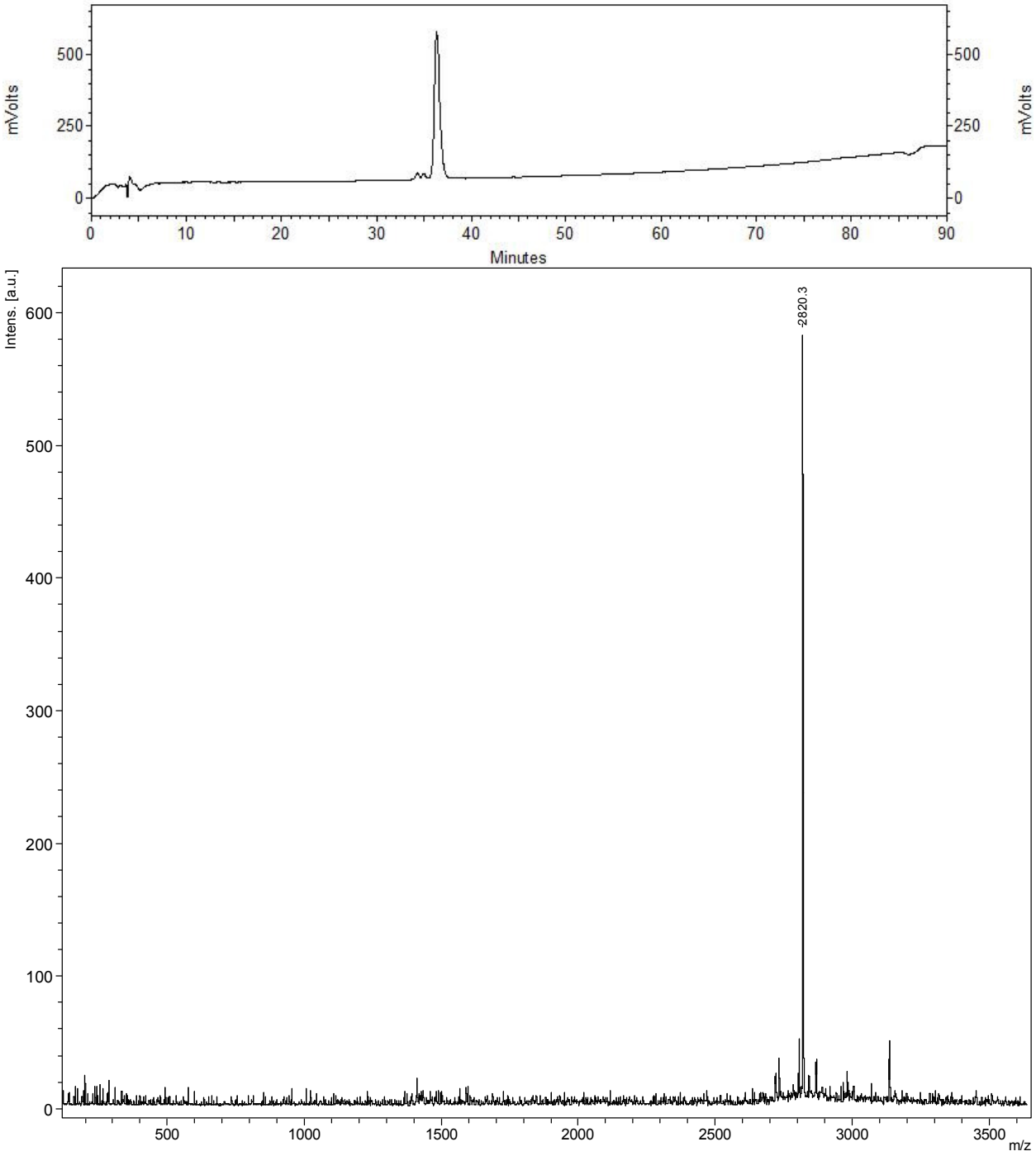

5.8

HPLC: Gradient = 10-60% solvent B over 50 minutes

MALDI-TOF: Calculated monoisotopic $[M+H]^+$ = 2959.7

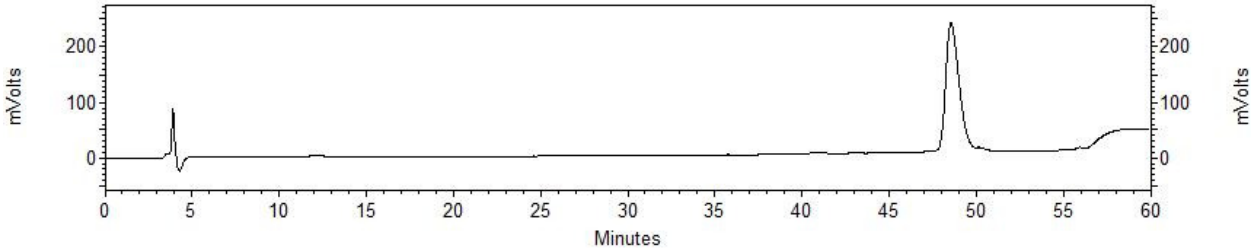

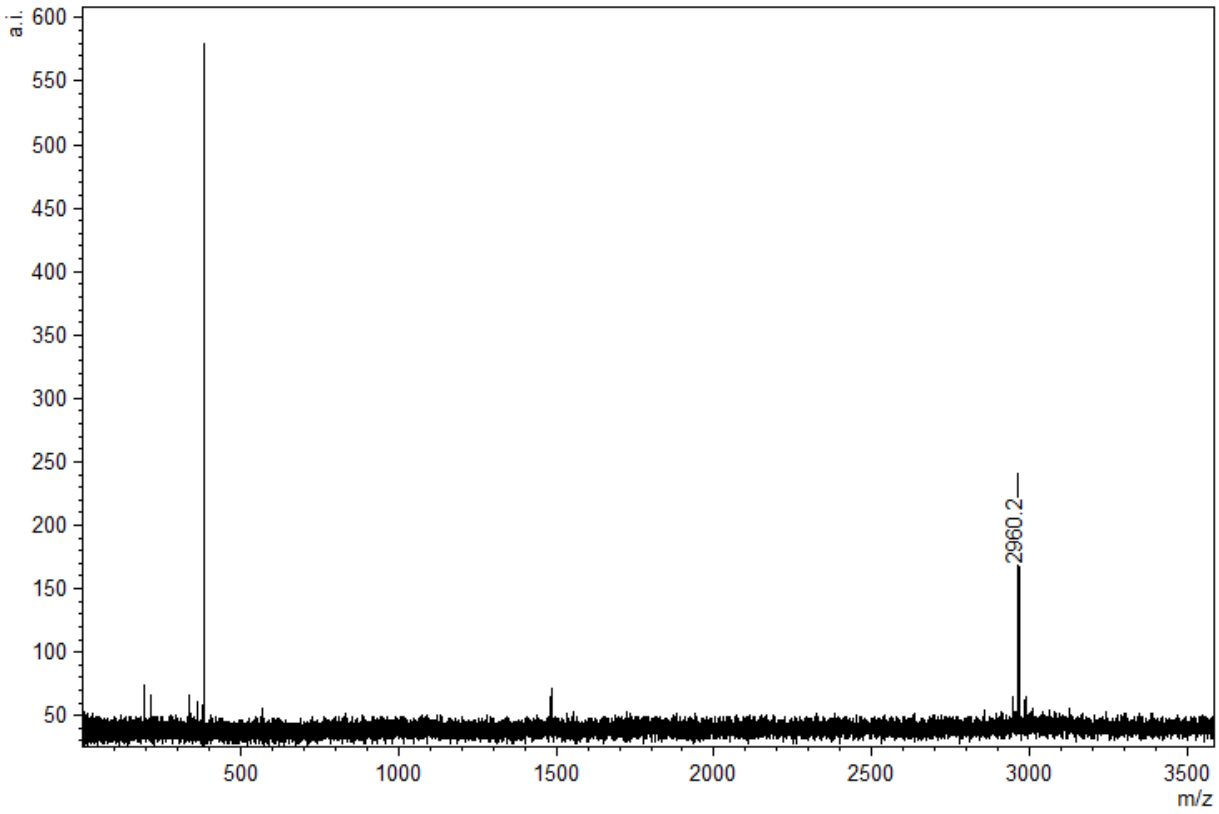

5.9

HPLC: Gradient = 10-90% solvent B over 80 minutes

MALDI-TOF: Calculated monoisotopic $[M+H]^+$ = 2405.4

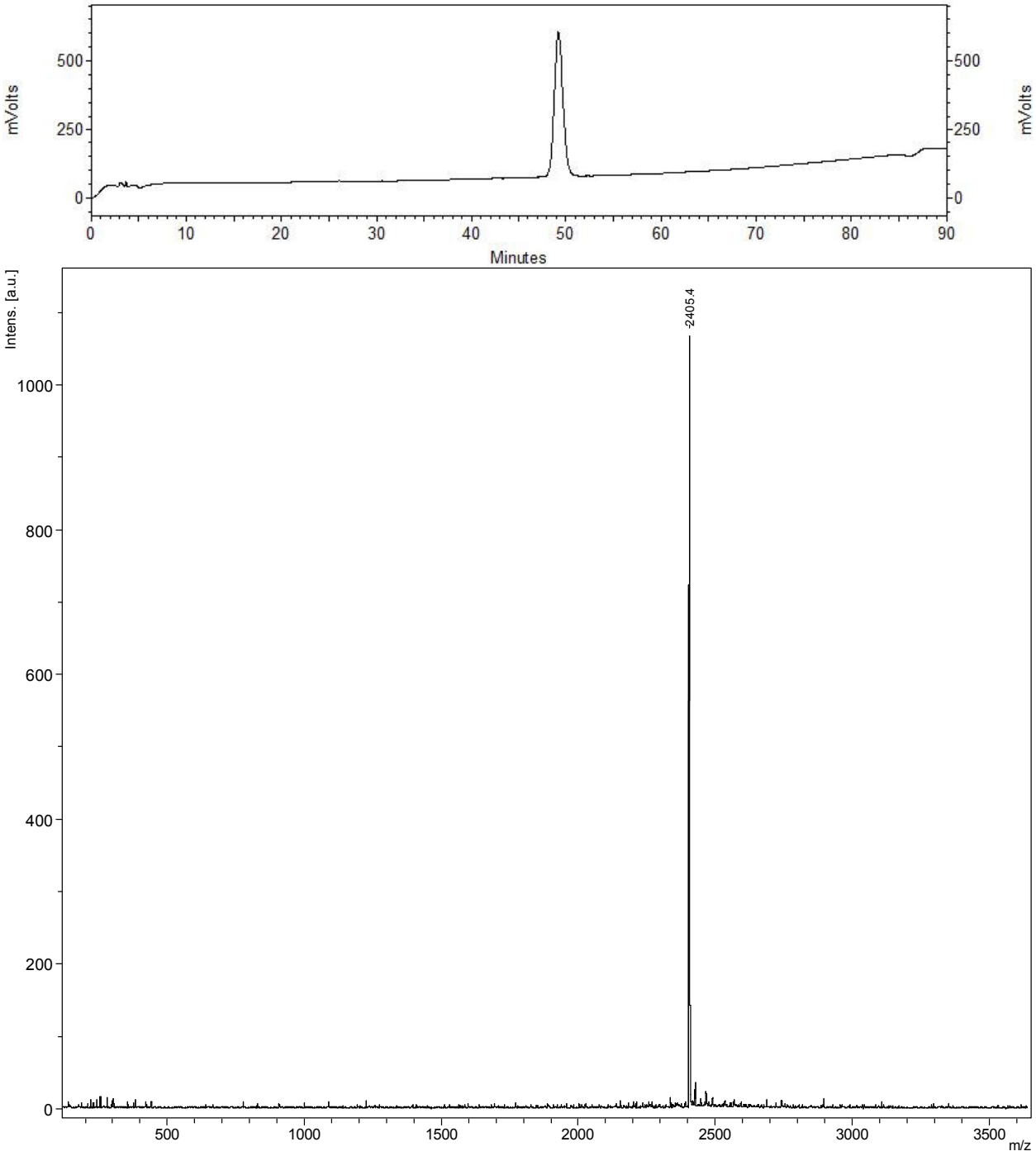

5.10

HPLC: Gradient = 10-90% solvent B over 80 minutes

MALDI-TOF: Calculated monoisotopic $[M+H]^+ = 2477.4$

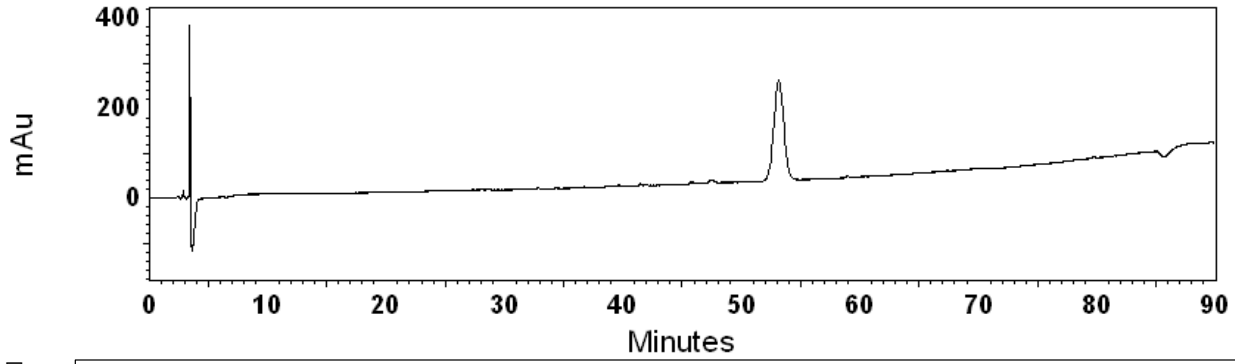

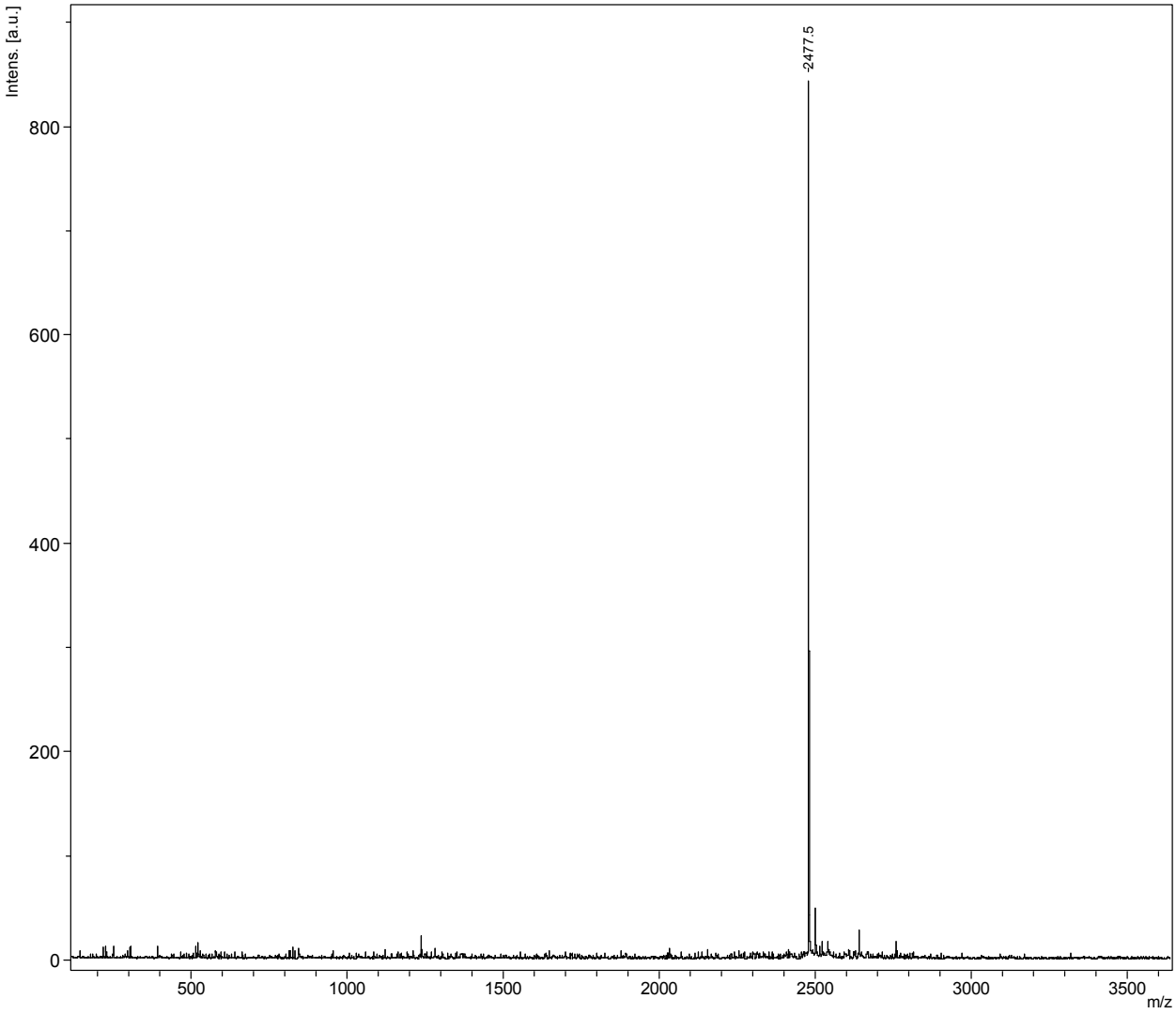

5.11

HPLC: Gradient = 10-90% solvent B over 80 minutes

MALDI-TOF: Calculated monoisotopic $[M+H]^+$ = 2875.7

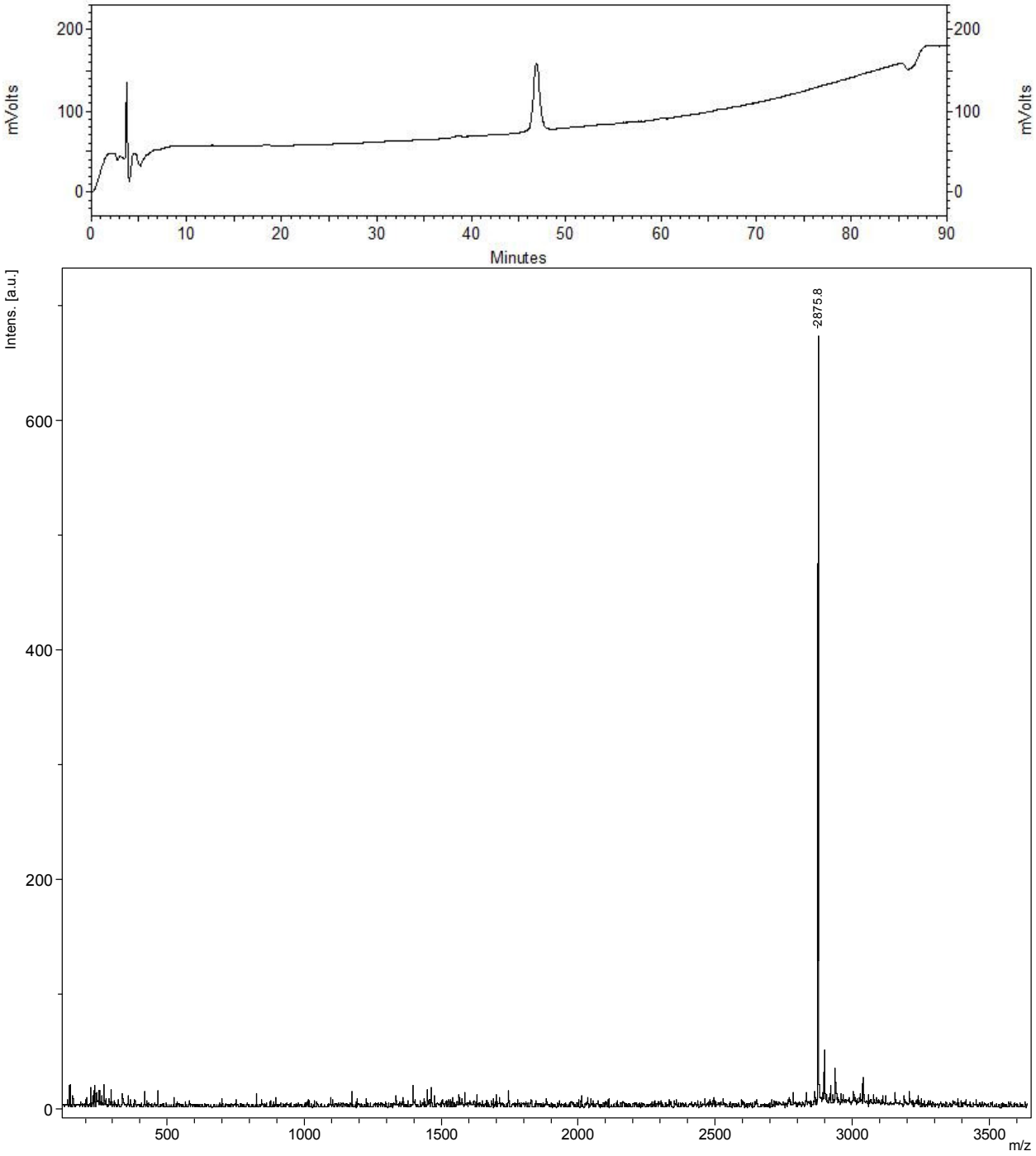

5.12

HPLC: Gradient = 10-90% solvent B over 80 minutes

MALDI-TOF: Calculated monoisotopic $[M+H]^+ = 2435.3$

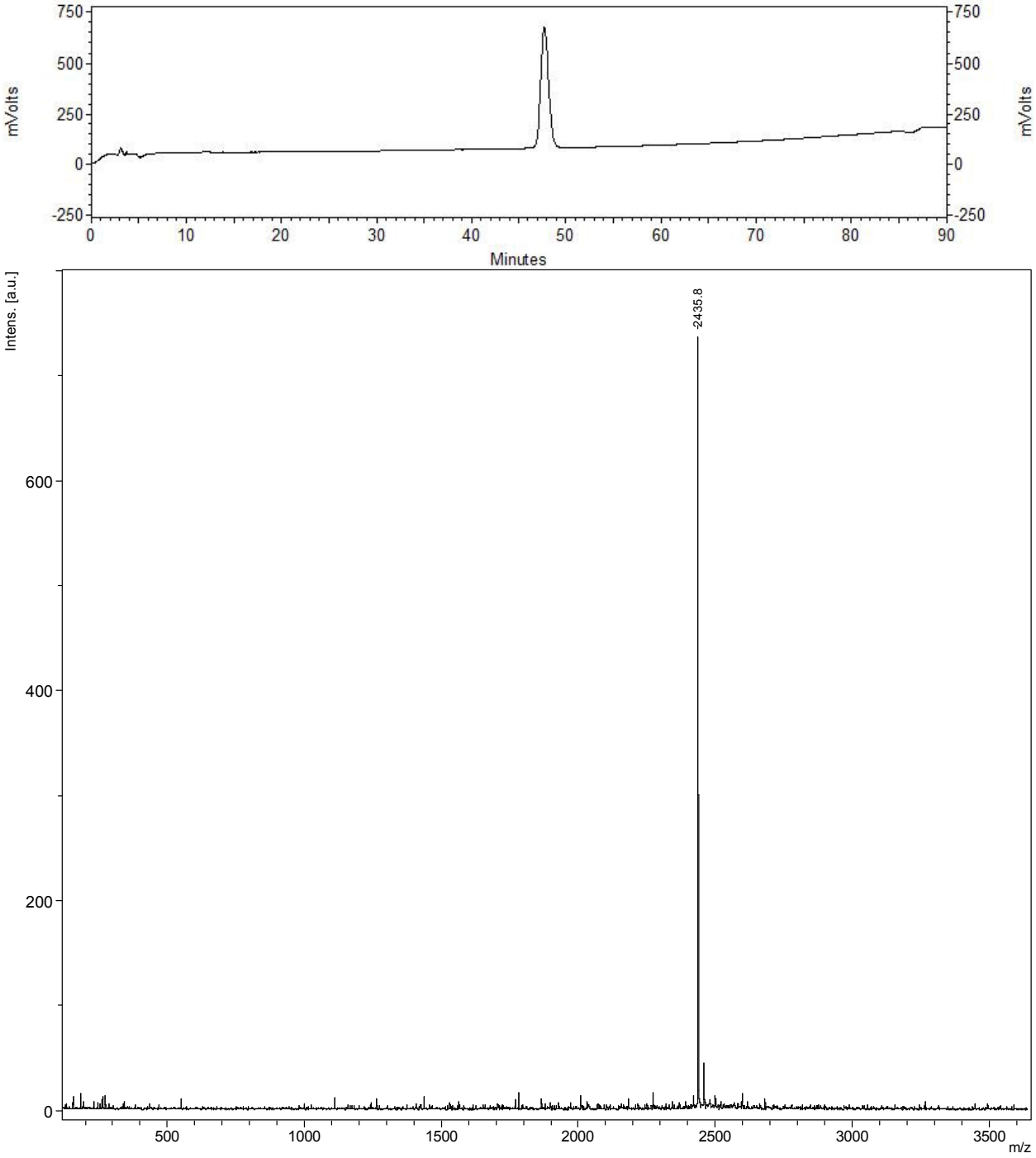

5.13

HPLC: Gradient = 10-90% solvent B over 80 minutes

MALDI-TOF: Calculated monoisotopic $[M+H]^+ = 2477.4$

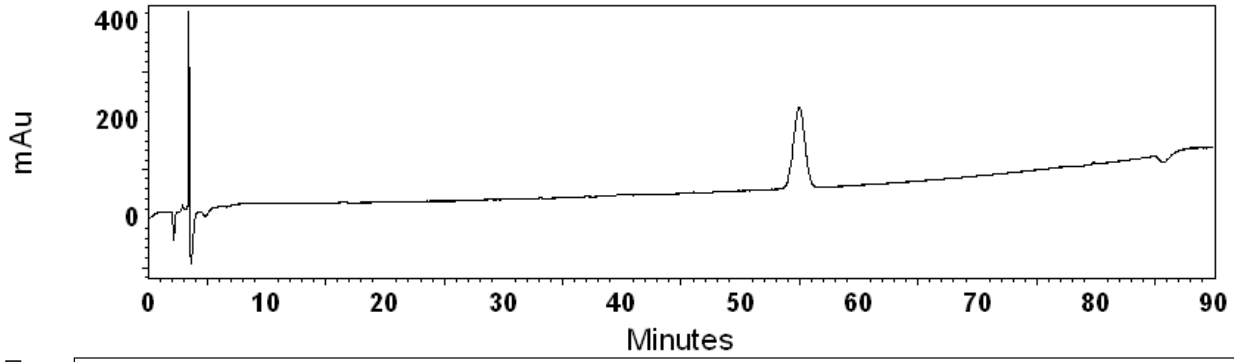

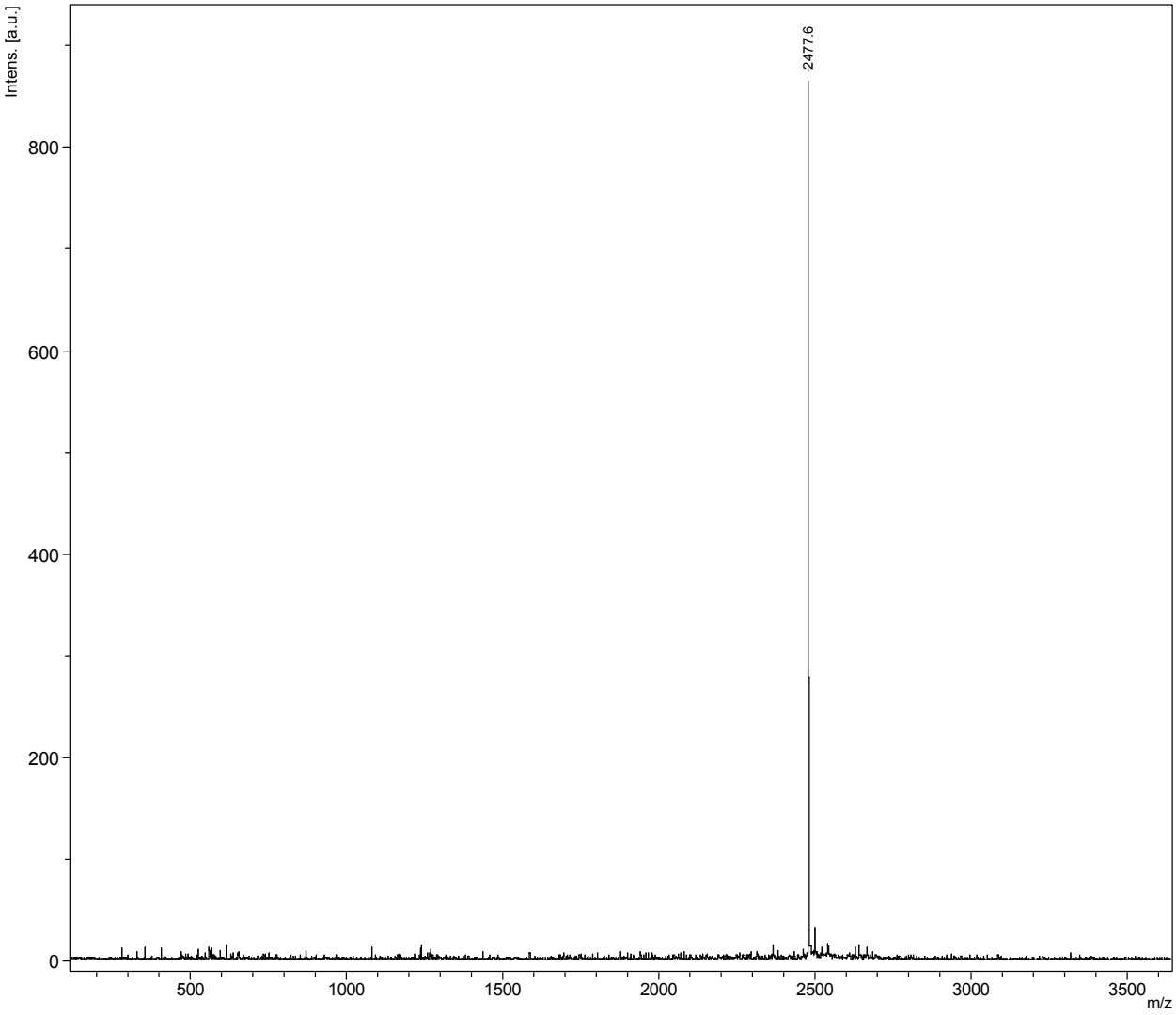

5.14

HPLC: Gradient = 10-90% solvent B over 80 minutes

MALDI-TOF: Calculated monoisotopic $[M+H]^+ = 2533.4$

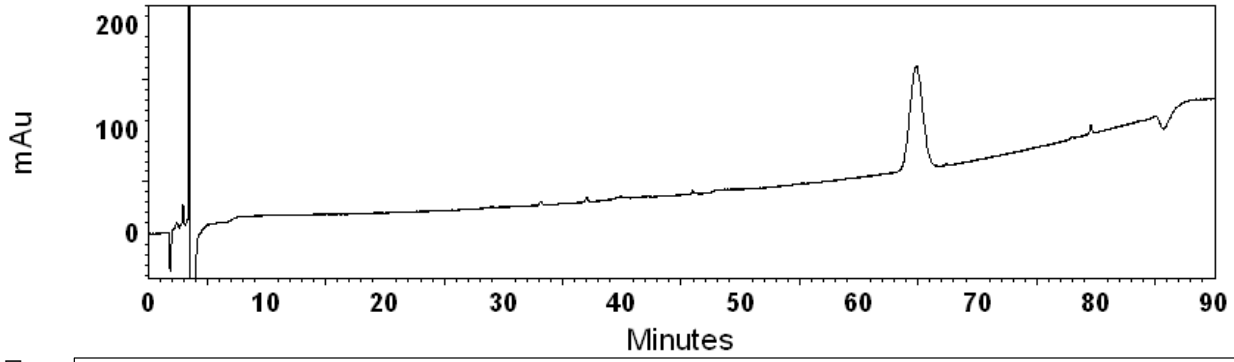

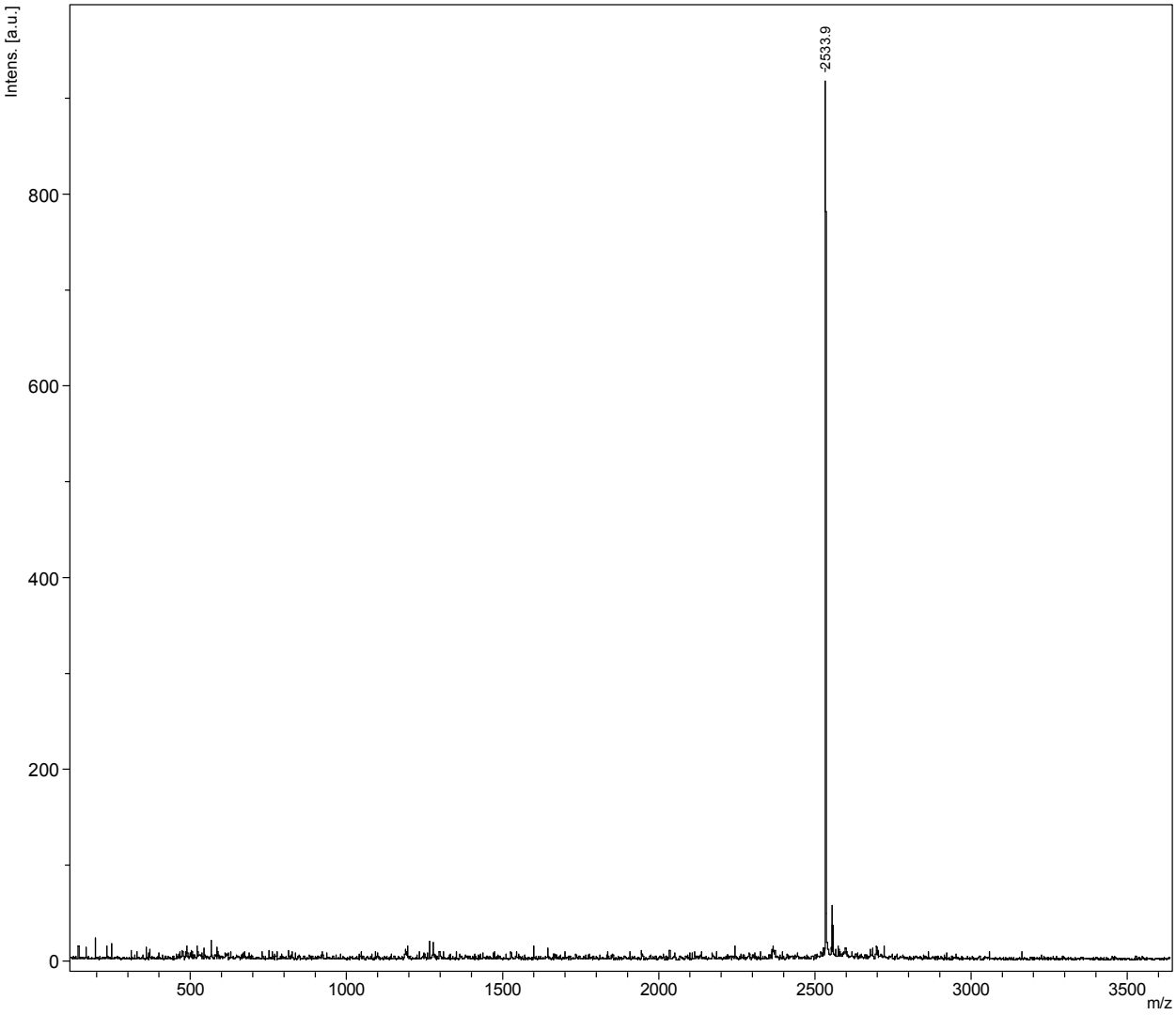

5.15

HPLC: Gradient = 10-90% solvent B over 80 minutes

MALDI-TOF: Calculated monoisotopic $[M+H]^+$ = 2903.6

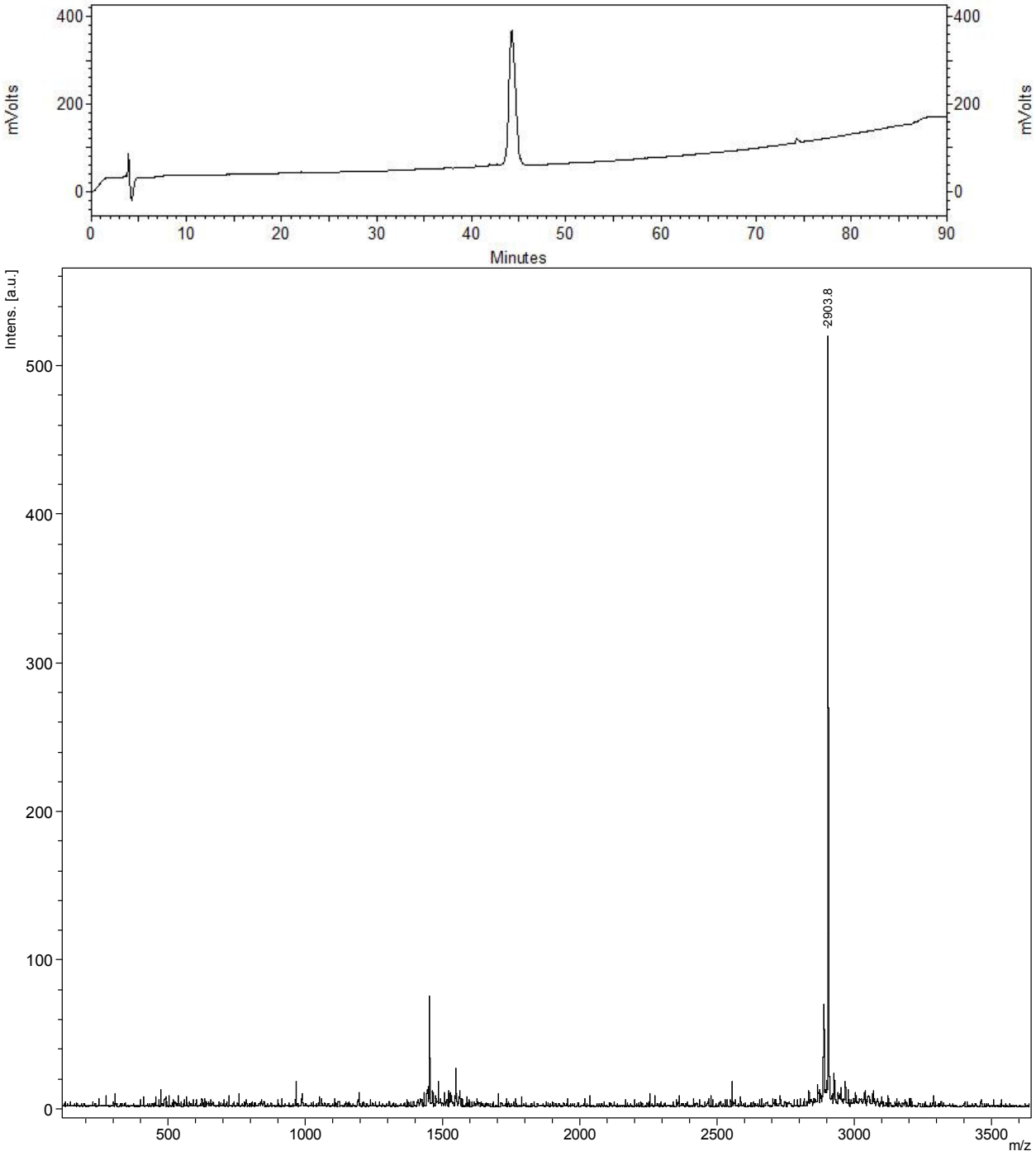

5.16

HPLC: Gradient = 10-90% solvent B over 80 minutes

MALDI-TOF: Calculated monoisotopic $[M+H]^+$ = 2945.7

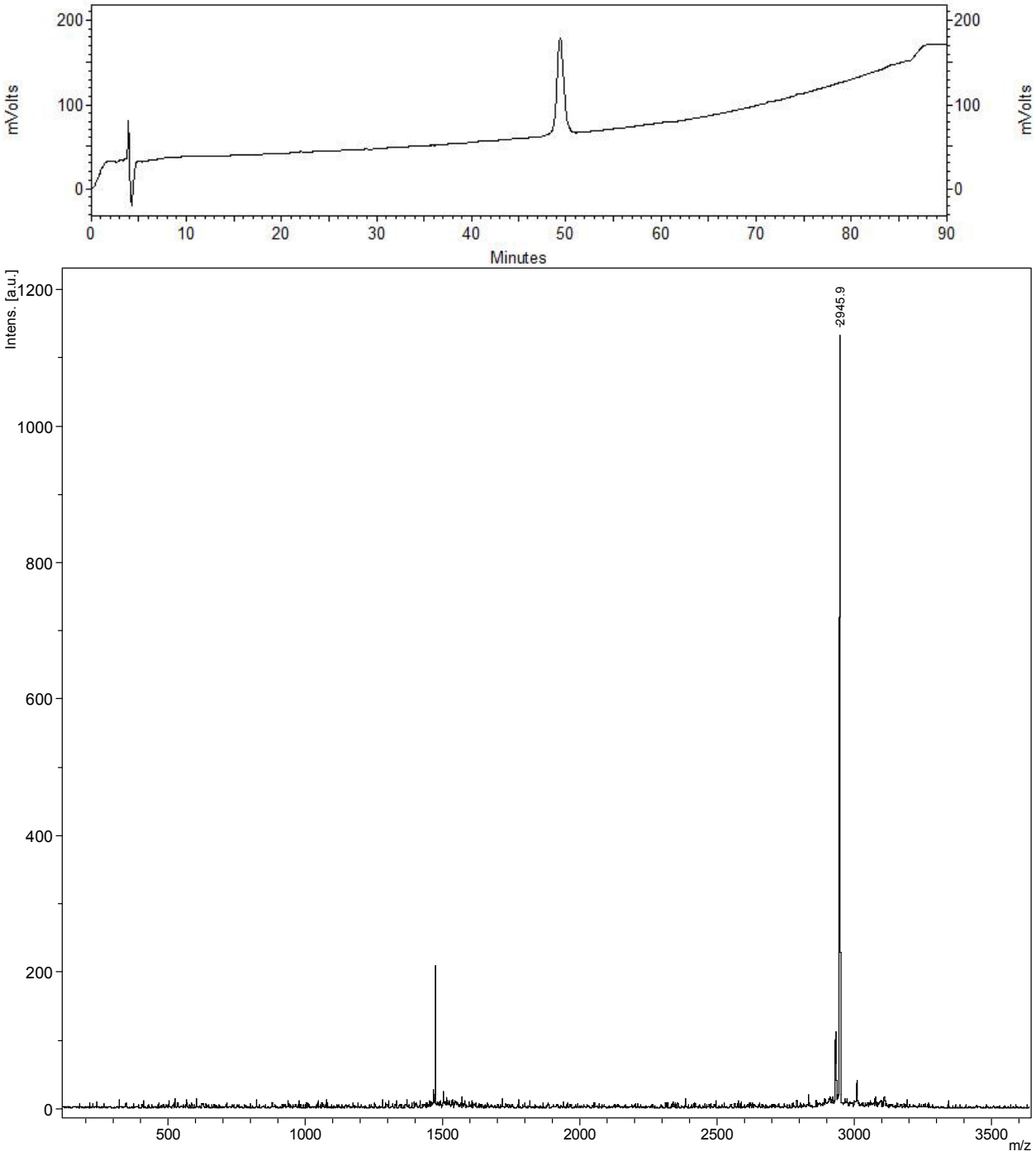

5.17
HPLC: Gradient = 10-90% solvent B over 80 minutes
MALDI-TOF: Calculated monoisotopic $[M+H]^+$ = 3001.7

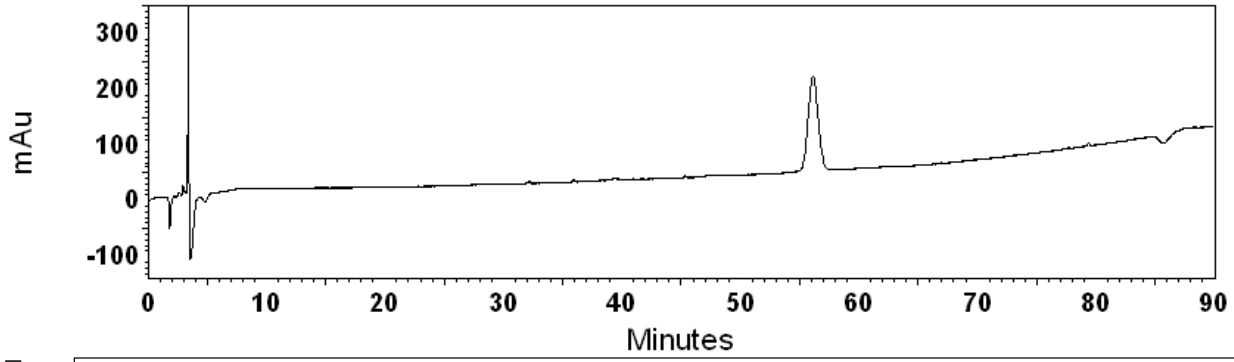

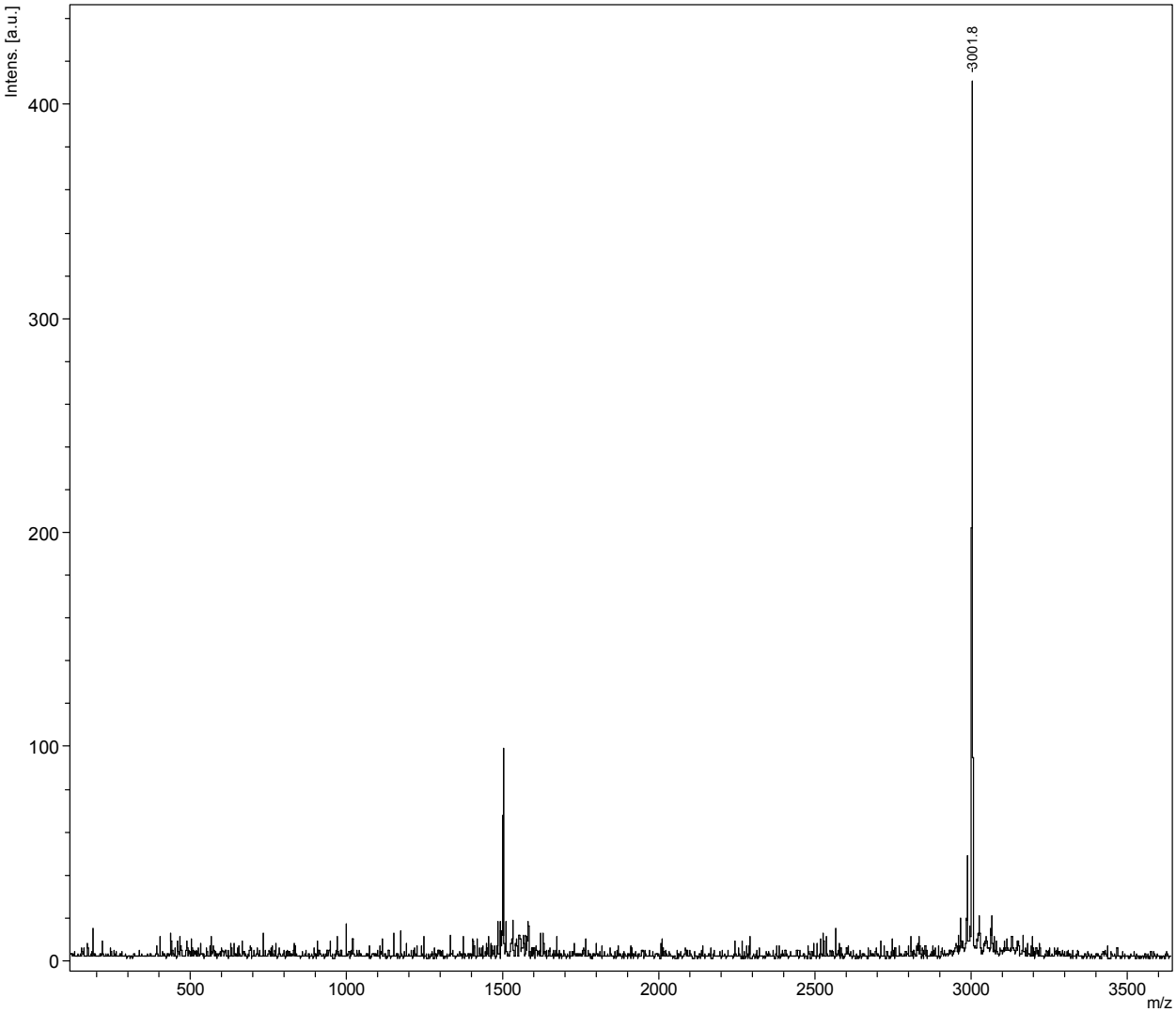

5.18

HPLC: Gradient = 10-90% solvent B over 80 minutes

MALDI-TOF: Calculated monoisotopic $[M+H]^+ = 2459.3$

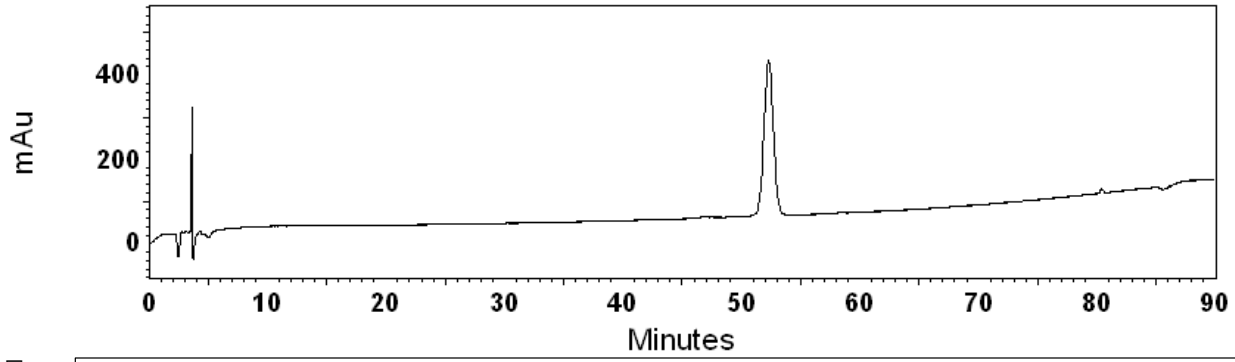

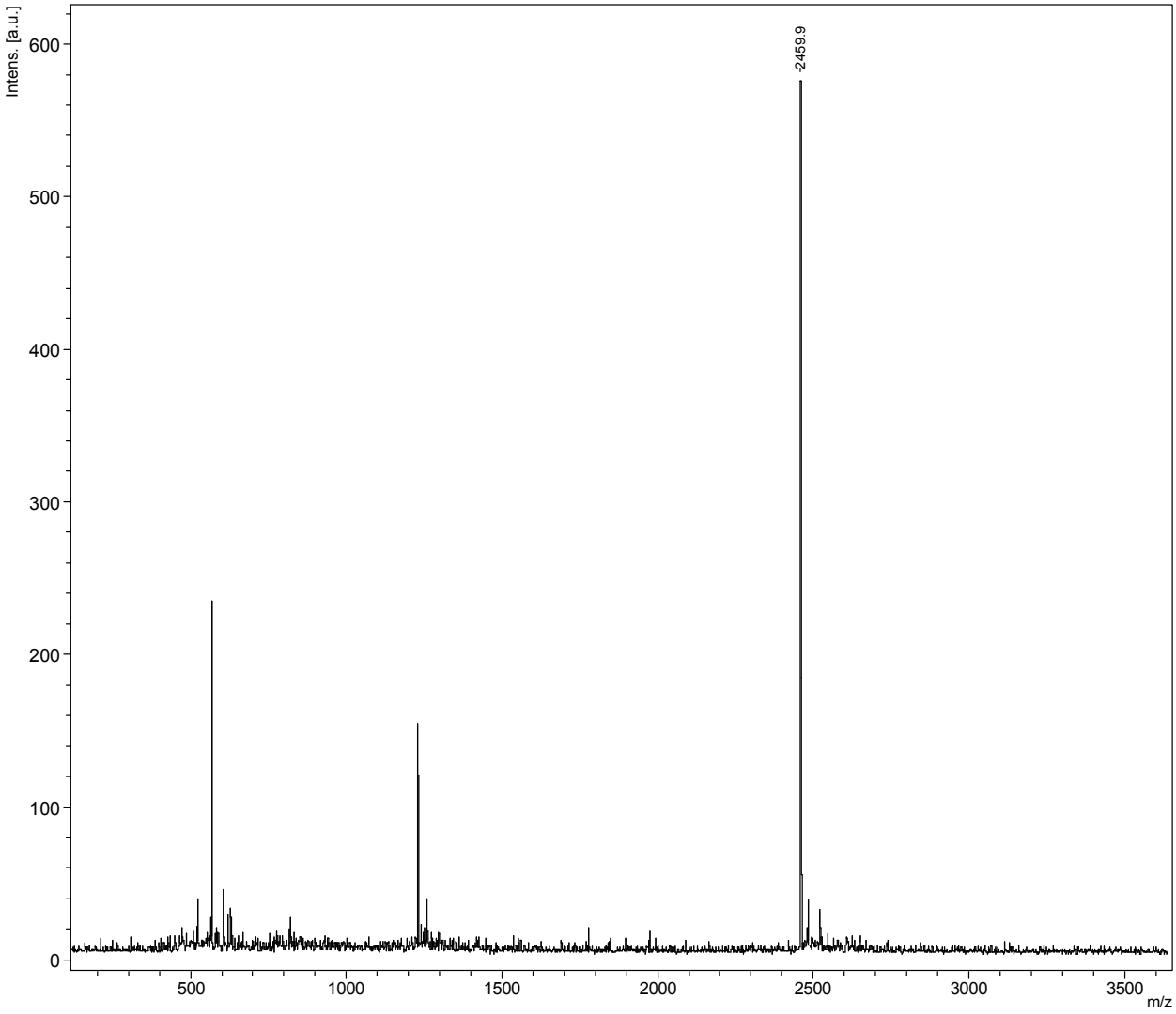

Flu-5.1
HPLC: Gradient = 10-90% solvent B over 80 minutes
MALDI-TOF: Calculated monoisotopic $[M+H]^+$ = 2667.3

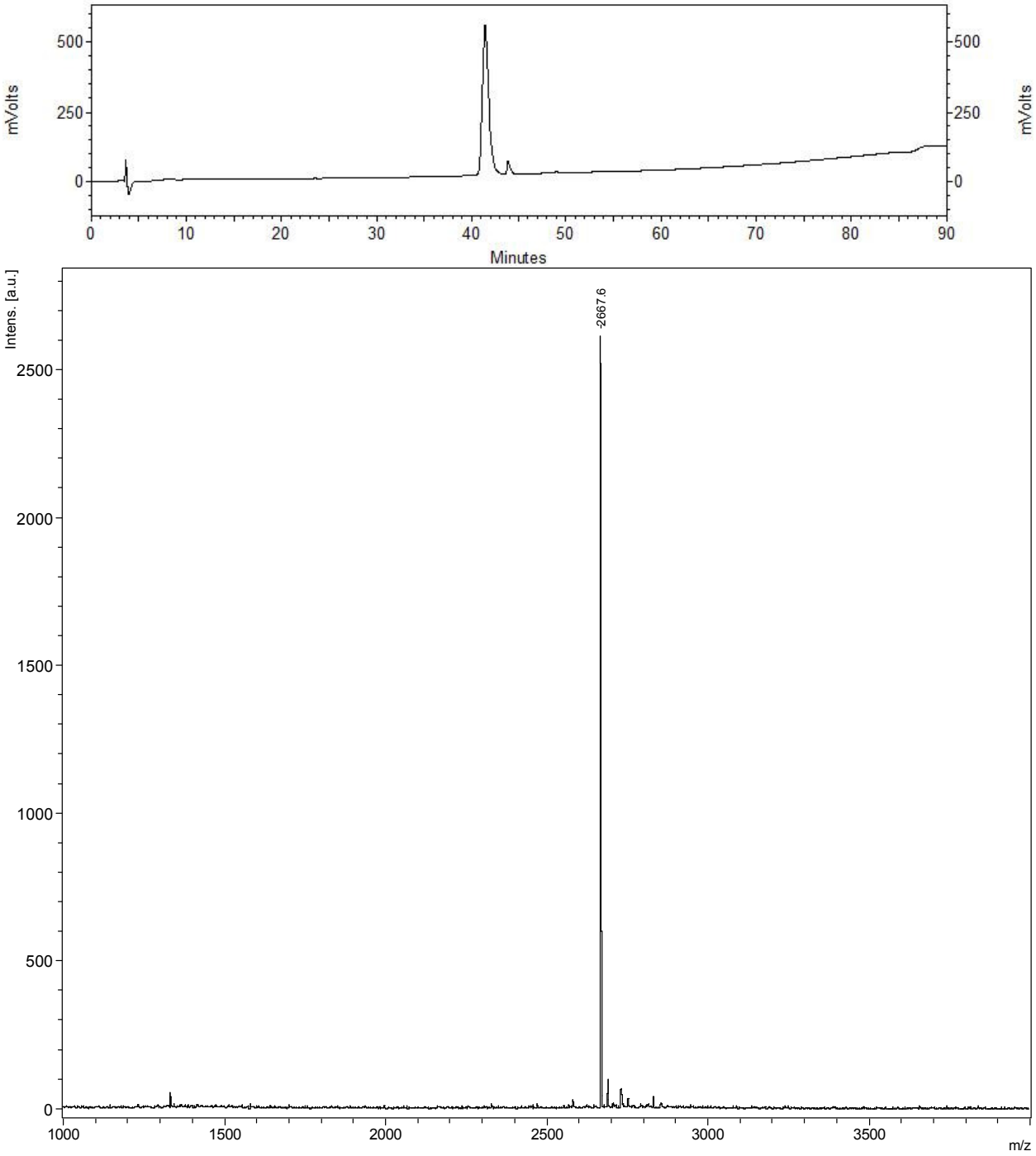

Flu-5.5
HPLC: Gradient = 10-90% solvent B over 80 minutes
MALDI-TOF: Calculated monoisotopic $[M+H]^+$ = 2807.4

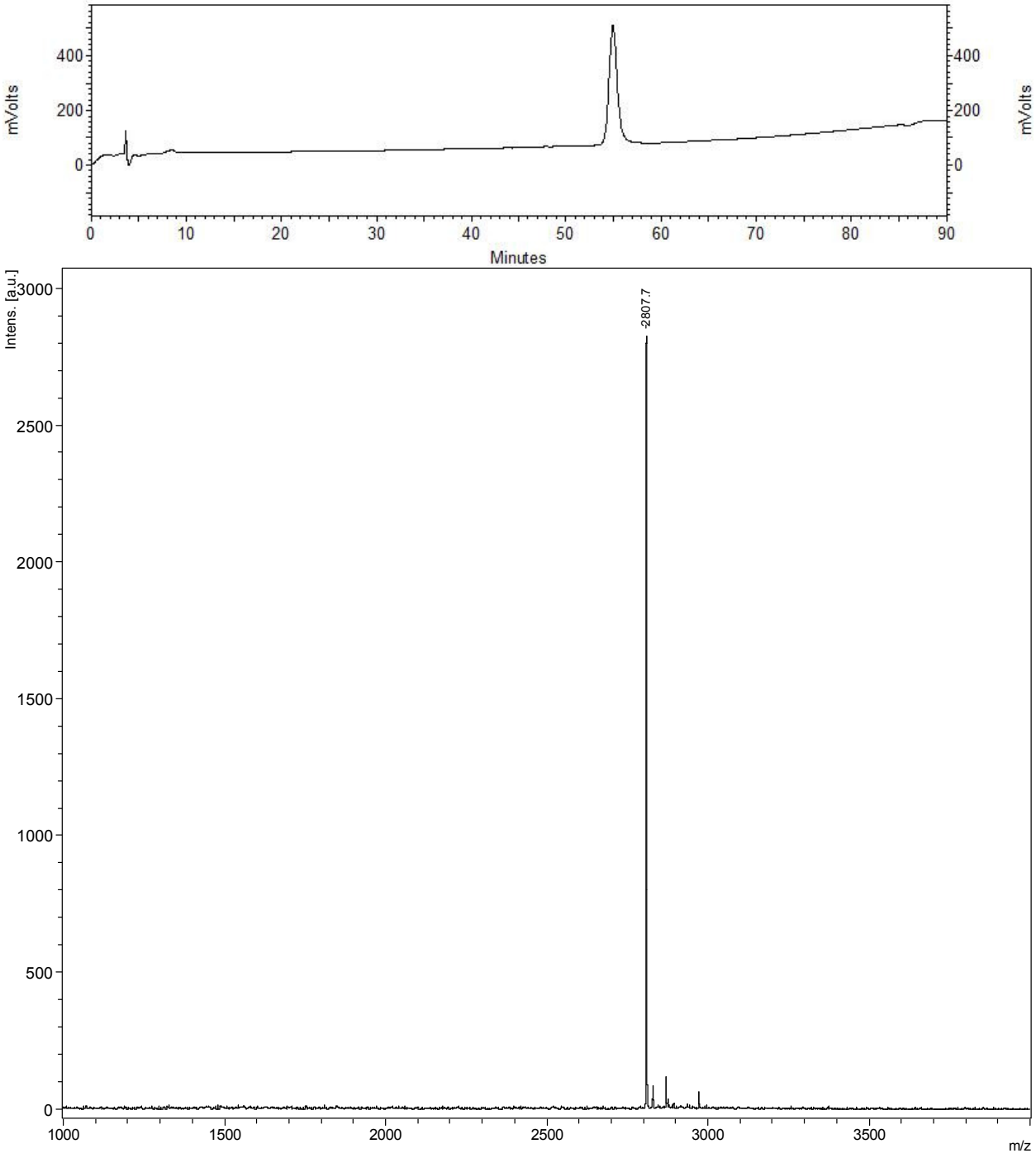

Flu-5.8
HPLC: Gradient = 10-90% solvent B over 80 minutes
MALDI-TOF: Calculated monoisotopic $[M+H]^+$ = 3275.7

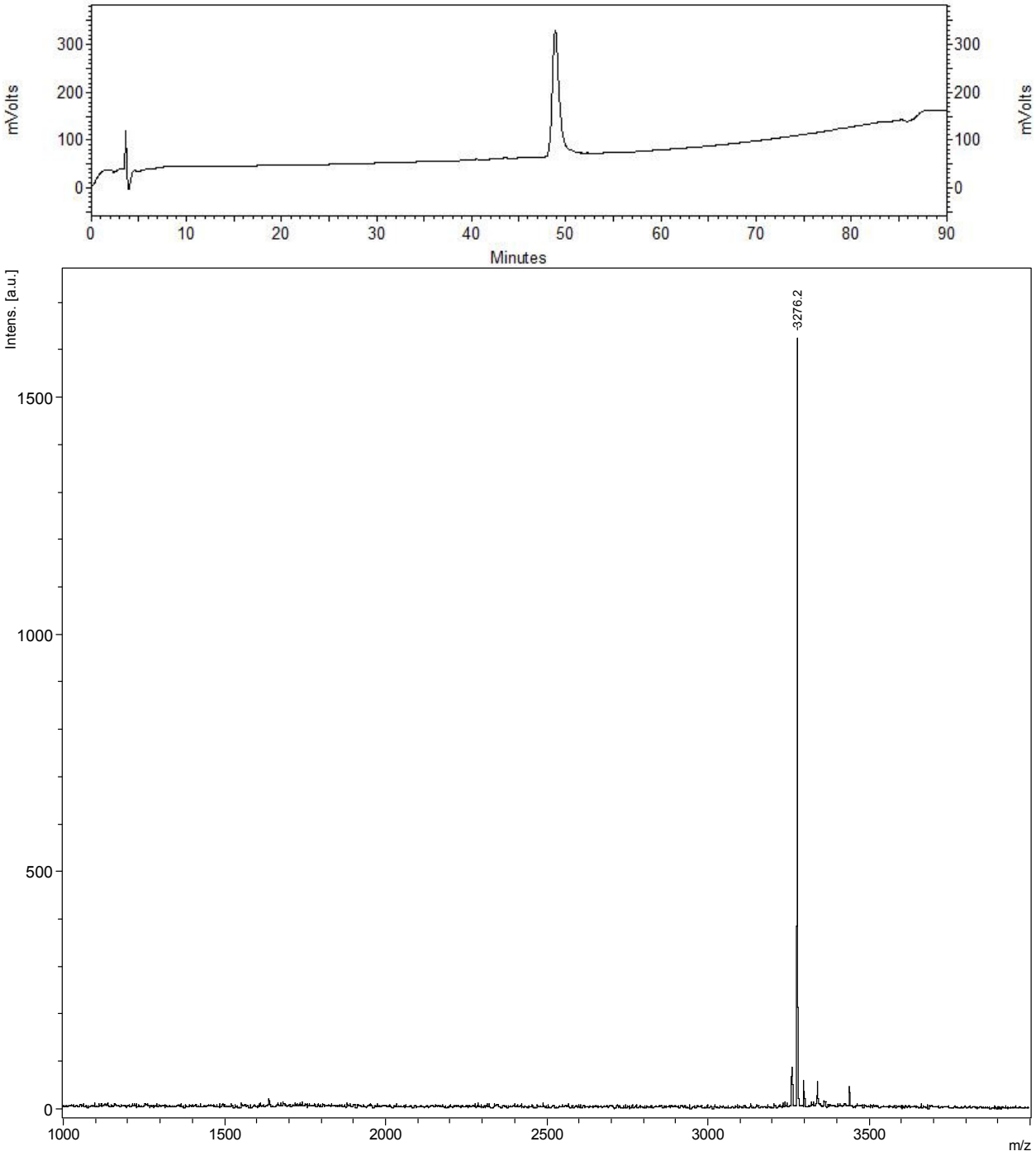

5.10 References

1. Gross, A., McDonnell, J. M., and Korsmeyer, S. J. (1999) BCL-2 family members and the mitochondria in apoptosis, *Genes & Development 13*, 1899-1911.
2. Cory, S., Huang, D. C. S., and Adams, J. M. (2003) The Bcl-2 family: roles in cell survival and oncogenesis, *Oncogene 22*, 8590-8607.
3. Willis, S. N., Fletcher, J. I., Kaufmann, T., van Delft, M. F., Chen, L., Czabotar, P. E., Ierino, H., Lee, E. F., Fairlie, W. D., Bouillet, P., Strasser, A., Kluck, R. M., Adams, J. M., and Huang, D. C. S. (2007) Apoptosis initiated when BH3 ligands engage multiple Bcl-2 homologs, not Bax or Bak, *Science 315*, 856-859.
4. van Delft, M. F., and Huang, D. C. (2006) How the Bcl-2 family of proteins interact to regulate apoptosis, *Cell Research 16*, 203-213.
5. Lessene, G., Czabotar, P. E., and Colman, P. M. (2008) BCL-2 family antagonists for cancer therapy, *Nature Reviews Drug Discovery 7*, 989-1000.
6. Wei, M. C., Zong, W. X., Cheng, E. H. Y., Lindsten, T., Panoutsakopoulou, V., Ross, A. J., Roth, K. A., MacCregor, G. R., Thompson, C. B., and Korsmeyer, S. J. (2001) Proapoptotic BAX and BAK: A requisite gateway to mitochondrial dysfunction and death, *Science 292*, 727-730.
7. Orzaez, M., Gortat, A., Mondragon, L., and Perez-Paya, E. (2009) Peptides and Peptide Mimics as Modulators of Apoptotic Pathways, *Chemmedchem 4*, 146-160.
8. Willis, S. N., Chen, L., Dewson, G., Wei, A., Naik, E., Fletcher, J. I., Adams, J. M., and Huang, D. C. S. (2005) Proapoptotic Bak is sequestered by Mcl-1 and Bcl-x(L), but not Bcl-2, until displaced by BH3-only proteins, *Genes & Development 19*, 1294-1305.
9. Gavathiotis, E., Suzuki, M., Davis, M. L., Pitter, K., Bird, G. H., Katz, S. G., Tu, H. C., Kim, H., Cheng, E. H. Y., Tjandra, N., and Walensky, L. D. (2008) BAX activation is initiated at a novel interaction site, *Nature 455*, 1076-1081.
10. Walensky, L. D., Pitter, K., Morash, J., Oh, K. J., Barbuto, S., Fisher, J., Smith, E., Verdine, G. L., and Korsmeyer, S. J. (2006) A stapled BID BH3 helix directly binds and activates BAX, *Molecular Cell 24*, 199-210.
11. Edwards, A. L., Gavathiotis, E., LaBelle, J. L., Braun, C. R., Opoku-Nsiah, K. A., Bird, G. H., and Walensky, L. D. (2013) Multimodal Interaction with BCL-2 Family Proteins Underlies the Proapoptotic Activity of PUMA BH3, *Chemistry & Biology 20*, 888-902.
12. Ku, B., Liang, C. Y., Jung, J. U., and Oh, B. H. (2011) Evidence that inhibition of BAX activation by BCL-2 involves its tight and preferential interaction with the BH3 domain of BAX, *Cell Research 21*, 627-641.
13. Lee, E. F., Sadowsky, J. D., Smith, B. J., Czabotar, P. E., Peterson-Kaufman, K. J., Colman, P. M., Gellman, S. H., and Fairlie, W. D. (2009) High-Resolution Structural Characterization of a Helical alpha/beta-Peptide Foldamer Bound to the Anti-Apoptotic Protein Bcl-x(L), *Angewandte Chemie-International Edition 48*, 4318-4322.

14. Czabotar, P. E., Lee, E. F., van Delft, M. F., Day, C. L., Smith, B. J., Huang, D. C. S., Fairlie, W. D., Hinds, M. G., and Colman, P. M. (2007) Structural insights into the degradation of Mcl-1 induced by BH3 domains, *Proceedings of the National Academy of Sciences of the United States of America 104*, 6217-6222.

15. Dharap, S. S., Chandna, P., Wang, Y., Khandare, J. J., Qiu, B., Stein, S., and Minko, T. (2006) Molecular targeting of BCL2 and BCLXL proteins by synthetic BCL2 homology 3 domain peptide enhances the efficacy of chemotherapy, *Journal of Pharmacology and Experimental Therapeutics 316*, 992-998.

16. O'Neill, J., Manion, M., Schwartz, P., and Hockenbery, D. M. (2004) Promises and challenges of targeting Bcl-2 anti-apoptotic proteins for cancer therapy, *Biochimica Et Biophysica Acta-Reviews on Cancer 1705*, 43-51.

17. Oltersdorf, T., Elmore, S. W., Shoemaker, A. R., Armstrong, R. C., Augeri, D. J., Belli, B. A., Bruncko, M., Deckwerth, T. L., Dinges, J., Hajduk, P. J., Joseph, M. K., Kitada, S., Korsmeyer, S. J., Kunzer, A. R., Letai, A., Li, C., Mitten, M. J., Nettesheim, D. G., Ng, S., Nimmer, P. M., O'Connor, J. M., Oleksijew, A., Petros, A. M., Reed, J. C., Shen, W., Tahir, S. K., Thompson, C. B., Tomaselli, K. J., Wang, B. L., Wendt, M. D., Zhang, H. C., Fesik, S. W., and Rosenberg, S. H. (2005) An inhibitor of Bcl-2 family proteins induces regression of solid tumours, *Nature 435*, 677-681.

18. LaBelle, J. L., Katz, S. G., Bird, G. H., Gavathiotis, E., Stewart, M. L., Lawrence, C., Fisher, J. K., Godes, M., Pitter, K., Kung, A. L., and Walensky, L. D. (2012) A stapled BIM peptide overcomes apoptotic resistance in hematologic cancers, *Journal of Clinical Investigation 122*, 2018-2031.

19. Pan, R. Q., Hogdal, L. J., Benito, J. M., Bucci, D., Han, L., Borthakur, G., Cortes, J., DeAngelo, D. J., Debose, L., Mu, H., Dohner, H., Gaidzik, V. I., Galinsky, I., Golfman, L. S., Haferlach, T., Harutyunyan, K. G., Hu, J. H., Leverson, J. D., Marcucci, G., Muschen, M., Newman, R., Park, E., Ruvolo, P. P., Ruvolo, V., Ryan, J., Schindela, S., Zweidler-McKay, P., Stone, R. M., Kantarjian, H., Andreeff, M., Konopleva, M., and Letai, A. G. (2014) Selective BCL-2 Inhibition by ABT-199 Causes On-Target Cell Death in Acute Myeloid Leukemia, *Cancer Discovery 4*, 362-375.

20. Rudin, C. M., Hann, C. L., Garon, E. B., de Oliveira, M. R., Bonomi, P. D., Camidge, D. R., Chu, Q., Giaccone, G., Khaira, D., Ramalingam, S. S., Ranson, M. R., Dive, C., McKeegan, E. M., Chyla, B. J., Dowell, B. L., Chakravartty, A., Nolan, C. E., Rudersdorf, N., Busman, T. A., Mabry, M. H., Krivoshik, A. P., Humerickhouse, R. A., Shapiro, G. I., and Gandhi, L. (2012) Phase II Study of Single-Agent Navitoclax (ABT-263) and Biomarker Correlates in Patients with Relapsed Small Cell Lung Cancer, *Clinical Cancer Research 18*, 3163-3169.

21. Souers, A. J., Leverson, J. D., Boghaert, E. R., Ackler, S. L., Catron, N. D., Chen, J., Dayton, B. D., Ding, H., Enschede, S. H., Fairbrother, W. J., Huang, D. C. S., Hymowitz, S. G., Jin, S., Khaw, S. L., Kovar, P. J., Lam, L. T., Lee, J., Maecker, H. L., Marsh, K. C., Mason, K. D., Mitten, M. J., Nimmer, P. M., Oleksijew, A., Park, C. H., Park, C. M., Phillips, D. C., Roberts, A. W., Sampath, D., Seymour, J. F., Smith, M. L., Sullivan, G. M., Tahir, S. K., Tse, C., Wendt, M. D., Xiao, Y., Xue, J. C., Zhang, H. C., Humerickhouse, R. A., Rosenberg, S. H., and Elmore, S. W. (2013) ABT-199, a potent

and selective BCL-2 inhibitor, achieves antitumor activity while sparing platelets, *Nature Medicine 19*, 202-208.

22. Foight, G. W., Ryan, J. A., Gulla, S. V., Letai, A., and Keating, A. E. (2014) Designed BH3 Peptides with High Affinity and Specificity for Targeting Mcl-1 in Cells, *Acs Chemical Biology 9*, 1962-1968.

23. Lee, E. F., Czabotar, P. E., Van Delft, M. F., Michalak, E. M., Boyle, M. J., Willis, S. N., Puthalakath, H., Bouillet, P., Colman, P. M., Huang, D. C. S., and Fairlie, W. D. (2008) A novel BH3 ligand that selectively targets Mcl-1 reveals that apoptosis can proceed without Mcl-1 degradation, *Journal of Cell Biology 180*, 341-355.

24. Horne, W. S., Boersma, M. D., Windsor, M. A., and Gellman, S. H. (2008) Sequence-based design of alpha/beta-peptide foldamers that mimic BH3 domains, *Angewandte Chemie-International Edition 47*, 2853-2856.

25. Boersma, M. D., Haase, H. S., Peterson-Kaufman, K. J., Lee, E. F., Clarke, O. B., Colman, P. M., Smith, B. J., Horne, W. S., Fairlie, W. D., and Gellman, S. H. (2012) Evaluation of Diverse alpha/beta-Backbone Patterns for Functional alpha-Helix Mimicry: Analogues of the Bim BH3 Domain, *Journal of the American Chemical Society 134*, 315-323.

26. Peterson-Kaufman, K. J., Haase, H. S., Boersma, M. D., Lee, E. F., Fairlie, W. D., and Gellman, S. H. (2015) Residue-Based Preorganization of BH3-Derived α/β-Peptides: Modulating Affinity, Selectivity and Proteolytic Susceptibility in α-Helix Mimics, *ACS Chemical Biology 10*, 1667-1675.

27. Horne, W. S., Johnson, L. M., Ketas, T. J., Klasse, P. J., Lu, M., Moore, J. P., and Gellman, S. H. (2009) Structural and biological mimicry of protein surface recognition by alpha/beta-peptide foldamers, *Proceedings of the National Academy of Sciences of the United States of America 106*, 14751-14756.

28. Boersma, M. D., Sadowsky, J. D., Tomita, Y. A., and Gellman, S. H. (2008) Hydrophile scanning as a complement to alanine scanning for exploring and manipulating protein-protein recognition: Application to the Bim BH3 domain, *Protein Science 17*, 1232-1240.

29. Resh, M. D. (2006) Trafficking and signaling by fatty-acylated and prenylated proteins, *Nature Chemical Biology 2*, 584-590.

30. Wang, J. L., Zhang, Z. J., Choksi, S., Shan, S. M., Lu, Z. X., Croce, C. M., Alnemri, E. S., Korngold, R., and Huang, Z. W. (2000) Cell permeable Bcl-2 binding peptides: A chemical approach to apoptosis induction in tumor cells, *Cancer Research 60*, 1498-1502.

31. Missirlis, D., Khant, H., and Tirrell, M. (2009) Mechanisms of Peptide Amphiphile Internalization by SJSA-1 Cells in Vitro, *Biochemistry 48*, 3304-3314.

32. Stephens, G., O'Luanaigh, N., Reilly, D., Harriott, P., Walker, B., Fitzgerald, D., and Moran, N. (1998) A sequence within the cytoplasmic tail of GpIIb independently activates platelet aggregation and thromboxane synthesis, *Journal of Biological Chemistry 273*, 20317-20322.

33. Ensenat-Waser, R., Martin, F., Barahona, F., Vazquez, J., Soria, B., and Reig, J. A. (2002) Direct visualization by confocal fluorescent microscopy of the permeation of myristoylated peptides through the cell membrane, *Iubmb Life 54*, 33-36.

34. Nelson, A. R., Borland, L., Allbritton, N. L., and Sims, C. E. (2007) Myristoyl-based transport of peptides into living cell, *Biochemistry 46*, 14771-14781.

35. Wollack, J. W., Zeliadt, N. A., Mullen, D. G., Amundson, G., Geier, S., Falkum, S., Wattenberg, E. V., Barany, G., and Distefano, M. D. (2009) Multifunctional Prenylated Peptides for Live Cell Analysis, *Journal of the American Chemical Society 131*, 7293-7303.

36. Wollack, J. W., Zeliadt, N. A., Ochocki, J. D., Mullen, D. G., Barany, G., Wattenberg, E. V., and Distefano, M. D. (2010) Investigation of the sequence and length dependence for cell-penetrating prenylated peptides, *Bioorganic & Medicinal Chemistry Letters 20*, 161-163.

37. Estieu-Gionnet, K., and Guichard, G. (2011) Stabilized helical peptides: overview of the technologies and therapeutic promises, *Expert Opinion on Drug Discovery 6*, 937-963.

38. Walensky, L. D., and Bird, G. H. (2014) Hydrocarbon-Stapled Peptides: Principles, Practice, and Progress, *Journal of Medicinal Chemistry 57*, 6275-6288.

39. Cromm, P. M., Spiegal, J., and Grossmann, T. N. (2015) Hydrocarbon Stapled Peptides as Modulators of Biological Function, *ACS Chemical Biology 10*, 1362-1375.

40. Patgiri, A., Yadav, K. K., Arora, P. S., and Bar-Sagi, D. (2011) An orthosteric inhibitor of the Ras-Sos interaction, *Nature Chemical Biology 7*, 585-587.

41. Walensky, L. D., Kung, A. L., Escher, I., Malia, T. J., Barbuto, S., Wright, R. D., Wagner, G., Verdine, G. L., and Korsmeyer, S. J. (2004) Activation of apoptosis in vivo by a hydrocarbon-stapled BH3 helix, *Science 305*, 1466-1470.

42. Stewart, M. L., Fire, E., Keating, A. E., and Walensky, L. D. (2010) The MCL-1 BH3 helix is an exclusive MCL-1 inhibitor and apoptosis sensitizer, *Nature Chemical Biology 6*, 595-601.

43. Baek, S., Kutchukian, P. S., Verdine, G. L., Huber, R., Holak, T. A., Lee, K. W., and Popowicz, G. M. (2012) Structure of the Stapled p53 Peptide Bound to Mdm2, *Journal of the American Chemical Society 134*, 103-106.

44. El-Andaloussi, S., Holm, T., and Langel, U. (2005) Cell-penetrating peptides: Mechanisms and applications, *Current Pharmaceutical Design 11*, 3597-3611.

45. Vives, E., Brodin, P., and Lebleu, B. (1997) A truncated HIV-1 Tat protein basic domain rapidly translocates through the plasma membrane and accumulates in the cell nucleus, *Journal of Biological Chemistry 272*, 16010-16017.

46. Vives, E., Schmidt, J., and Pelegrin, A. (2008) Cell-penetrating and cell-targeting peptides in drug delivery, *Biochimica Et Biophysica Acta-Reviews on Cancer 1786*, 126-138.

47. Fischer, P. M. (2007) Cellular uptake mechanisms and potential therapeutic utility of peptidic cell delivery vectors: Progress 2001-2006, *Medicinal Research Reviews 27*, 755-795.

48. Bautista, A. D., Appelbaum, J. S., Craig, C. J., Michel, J., and Schepartz, A. (2010) Bridged beta(3)-Peptide Inhibitors of p53-hDM2 Complexation: Correlation between Affinity and Cell Permeability, *Journal of the American Chemical Society 132*, 2904-2906.

49. Umezawa, N., Gelman, M. A., Haigis, M. C., Raines, R. T., and Gellman, S. H. (2002) Translocation of a beta-peptide across cell membranes, *Journal of the American Chemical Society 124*, 368-369.

50. Rueping, M., Mahajan, Y., Sauer, M., and Seebach, D. (2002) Cellular uptake studies with beta-peptides, *Chembiochem 3*, 257-259.

51. Potocky, T. B., Menon, A. K., and Gellman, S. H. (2003) Cytoplasmic and nuclear delivery of a TAT-derived peptide and a beta-peptide after endocytic uptake into HeLa cells, *Journal of Biological Chemistry 278*, 50188-50194.

52. Harker, E. A., and Schepartz, A. (2009) Cell-Permeable beta-Peptide Inhibitors of p53/hDM2 Complexation, *Chembiochem 10*, 990-993.

53. Carrigan, C. N., and Imperiali, B. (2005) The engineering of membrane-permeable peptides, *Analytical Biochemistry 341*, 290-298.

54. Schmidt, N., Mishra, A., Lai, G. H., and Wong, G. C. L. (2010) Arginine-rich cell-penetrating peptides, *Febs Letters 584*, 1806-1813.

55. Okamoto, T., Segal, D., Zobel, K., Fedorova, A., Yang, H., Fairbrother, W. J., Huang, D. C. S., Smith, B. J., Deshayes, K., and Czabotar, P. E. (2014) Further Insights into the Effects of Pre-organizing the BimBH3 Helix, *Acs Chemical Biology 9*, 838-839.

56. Mitchell, D. J., Kim, D. T., Steinman, L., Fathman, C. G., and Rothbard, J. B. (2000) Polyarginine enters cells more efficiently than other polycationic homopolymers, *Journal of Peptide Research 56*, 318-325.

57. Li, Y. C., Rodewald, L. W., Hoppmann, C., Wong, E. T., Lebreton, S., Safar, P., Patek, M., Wang, L., Wertman, K. F., and Wahl, G. M. (2014) A Versatile Platform to Analyze Low-Affinity and Transient Protein-Protein Interactions in Living Cells in Real Time, *Cell Reports 9*, 1946-1958.

58. Okamoto, T., Zobel, K., Fedorova, A., Quan, C., Yang, H., Fairbrother, W. J., Huang, D. C. S., Smith, B. J., Deshayes, K., and Czabotar, P. E. (2013) Stabilizing the Pro-Apoptotic BimBH3 Helix (BimSAHB) Does Not Necessarily Enhance Affinity or Biological Activity, *Acs Chemical Biology 8*, 297-302.

59. Bird, G. H., Gavathiotis, E., LaBelle, J. L., Katz, S. G., and Walensky, L. D. (2014) Distinct BimBH3 (BimSAHB) Stapled Peptides for Structural and Cellular Studies, *Acs Chemical Biology 9*, 831-837.

60. Lee, H. S., LePlae, P. R., Porter, E. A., and Gellman, S. H. (2001) An efficient route to either enantiomer of orthogonally protected trans-3-aminopyrrolidine-4-carboxylic acid, *Journal of Organic Chemistry 66*, 3597-3599.

61. Guzzo, P. R., and Miller, M. J. (1994) Catalytic, asymmetric synthesis of the carbacephem framework, *Journal of Organic Chemistry 59*, 4862-4867.

62. Horne, W. S., Price, J. L., and Gellman, S. H. (2008) Interplay among side chain sequence, backbone composition, and residue rigidification in polypeptide folding and assembly, *Proceedings of the National Academy of Sciences of the United States of America 105*, 9151-9156.

63. Kim, Y. W., Grossmann, T. N., and Verdine, G. L. (2011) Synthesis of all-hydrocarbon stapled alpha-helical peptides by ring-closing olefin metathesis, *Nature Protocols 6*, 761-771.

64. Sadowsky, J. D., Schmitt, M. A., Lee, H. S., Umezawa, N., Wang, S. M., Tomita, Y., and Gellman, S. H. (2005) Chimeric (alpha/beta plus alpha)-peptide ligands for the BH3-recognition cleft of Bcl-x(L): Critical role of the molecular scaffold in protein surface recognition, *Journal of the American Chemical Society 127*, 11966-11968.

65. Gill, S. C., and Vonhippel, P. H. (1989) Calculation of protein extinction coefficients from amino-acid sequence data, *Analytical Biochemistry 182*, 319-326.

66. Peterson, K. J., Sadowsky, J. D., Scheef, E. A., Pal, S., Kourentzi, K. D., Willson, R. C., Bresnick, E. H., Sheibani, N., and Gellman, S. H. (2008) A fluorescence polarization assay for identifying ligands that bind to vascular endothelial growth factor, *Analytical Biochemistry 378*, 8-14.

67. Roehrl, M. H. A., Wang, J. Y., and Wagner, G. (2004) A general framework for development and data analysis of competitive high-throughput screens for small-molecule inhibitors of protein - Protein interactions by fluorescence polarization, *Biochemistry 43*, 16056-16066.

68. Sohma, Y., Hua, Q. X., Whittaker, J., Weiss, M. A., and Kent, S. B. H. (2010) Design and Folding of Glu(A4)(O(beta)Thr(B30)) Insulin ("Ester Insulin"): A Minimal Proinsulin Surrogate that Can Be Chemically Converted into Human Insulin, *Angewandte Chemie-International Edition 49*, 5489-5493.

Chapter 6: α/β-Peptide mimics of cell-penetrating peptides targeting intracellular protein-protein interactions with activity in living cells

Portions of this chapter have been accepted for publication as:

Checco, J.W., Lee, E.F., Evangelista, M., Sleebs, N., Rogers, K., Pettikiriarachchi, A., Kershaw, N., Eddinger, G.A., Wilson, J.L., Belair, D.G., Eller, C.H., Raines, R.T., Murphy, W.L., Smith, B.J., Gellman, S.H., Fairlie, W.D. (2015) α/β-Peptide foldamers targeting intracellular protein-protein interactions with activity in living cells. *J. Am. Chem. Soc. — Accepted*

Respective contributions:

Research design: James W. Checco, Erinna F. Lee, Samuel H. Gellman, W. Douglas Fairlie

Peptide design: James W. Checco

Cyclic β-amino acid synthesis (5E-APC): Timothy Choi

Peptide synthesis: James W. Checco, Geoffrey A. Eddinger, Julia L. Wilson, Timothy Choi

Proteolysis: James W. Checco

Competition SPR assays: Erinna F. Lee, Marco Evangelista, Nerida J. Sleebs, Kelly Rogers, Anne Pettikiriarachchi, Nadia J. Kershaw, W. Douglas Fairlie

Circular dichroism: James W. Checco, Geoffrey A. Eddinger

Crystal structures: Erinna F. Lee, Brian J. Smith, W. Douglas Fairlie

Cytochrome *c* release assays: Erinna F. Lee, Marco Evangelista, Nerida J. Sleebs, Kelly Rogers, Anne Pettikiriarachchi, Nadia J. Kershaw, W. Douglas Fairlie

Cell viability assays: Erinna F. Lee, Marco Evangelista, Nerida J. Sleebs, Kelly Rogers, Anne Pettikiriarachchi, Nadia J. Kershaw, W. Douglas Fairlie

Live-cell confocal microscopy: David G. Belair, James W. Checco, Geoffrey A. Eddinger, William L. Murphy

6.1 Preface

Chapter 5 described attempts to increase the membrane permeability of α/β-peptides that had already been optimized for high-affinity protein binding and low protease susceptibility, with the end goal of developing α/β-peptides that can enter cells to modulate intracellular protein-protein interactions. In this chapter, we explore an alternative approach: rather than attempt to imbue an α/β-peptide with membrane permeability, instead we try design α/β-peptide mimics of an active α-peptide that is already known to enter cells. Toward this goal, we designed α/β-peptides based on a "stapled" Bim BH3 α-peptide, **BimSAHB,** which contains a hydrocarbon crosslink that allows this α-peptide to enter cells. We show that an α/β-peptide analogue of the crosslinked **BimSAHB** can structurally and functionally mimic the parent α-peptide in its ability to enter certain types of cells and block protein-protein interactions associated with apoptotic signaling. However, the α/β-peptide is nearly 100-fold more resistant to proteolysis than is the parent α-peptide because of the non-natural backbone. These results show that backbone modification, a strategy that has received relatively little attention in terms of peptide engineering for biomedical applications, can be combined with more commonly deployed peripheral modifications such as side chain crosslinking to produce synergistic benefits.

6.2 Introduction

6.2.1 BH3 domains

BH3 domains are short (~20-residues) α-helical domains that mediate interactions between pro- and anti-apoptotic Bcl-2 family proteins.[1-3] These domains bind to long, complementary grooves displayed by anti-apoptotic family members such as Bcl-x_L, Mcl-1 and Bcl-2. Binding of members of the BH3-only sub-class (e.g., Bim, Puma, Bad) to anti-apoptotic partners results in the initiation of apoptosis in damaged, redundant, or potentially dangerous cells. These interactions displace pro-apoptotic proteins such as Bax, Bak or "activator" BH3-only proteins from sequestration by the anti-apoptotic family members. This release of pro-apoptotic factors triggers mitochondrial membrane permeabilization, cytochrome *c* release, and caspase activation. The survival versus death decision is finely controlled by the balance of pro- and anti-apoptotic Bcl-2 family members within a cell. Several types of cancer cells rely on overexpression of certain anti-apoptotic Bcl-2 family proteins as a mechanism to evade cell death. This observation has engendered speculation that antagonism of anti-apoptotic Bcl-2 family proteins could be beneficial for cancer treatment.[4, 5] Indeed, several small molecule Bcl-2 protein antagonists have recently shown promising results in cancer patient samples and clinical trials.[6, 7] Bcl-2 family protein-protein interactions all occur inside the cell. Although short peptides mimicking BH3 domains can be developed to bind tightly to anti-apoptotic family members in protein binding experiments, the ability of unmodified peptides to antagonize this protein-protein interaction under conditions of biological relevance is limited because most peptides are not able to cross cell membranes.

6.2.2 "Stapled" α-helical mimics of BH3 domains

Several groups have sought to improve the properties of short peptides similar to BH3 domain-derived α-peptides by introducing side chain crosslinks that are intended to stabilize the binding conformation (an α-helix). A variety of different strategies have been employed,[8] including lactam crosslinking via amino acid residue side chains,[9-11] alkylation of cysteine residues with crosslinking groups,[12] and alkene crosslinking using olefin metathesis.[13-15] Use of a hydrocarbon crosslink, formed by ring-closing metathesis of two α,α-disubstituted pentenyl-containing amino acids (S5) at *i* and *i+4* positions (e.g., **BimSAHB**, Figure 6.1), has been the most intensively studied strategy.[16-18] The first report of this approach stems from studies by Blackwell et al., which utilized ring closing metathesis (RCM) to crosslink short helical peptides bearing non-natural amino acid residues with alkene ether side chains at the *i* and *i+4* positions.[13, 14] Inspired by this effort, Walensky et al. used α,α-disubstituted alkene amino acid residues (e.g., S5 residue, Figure 6.1A) to crosslink a short α-helical peptide derived from the Bid BH3 domain.[19] This "stapled" α-helix of a Bcl-2 domain ("SAHB") displayed increased helicity and decreased susceptibility to protease action relative to the analogous peptide containing only natural residues. Surprisingly, this all-hydrocarbon crosslinked Bid SAHB peptide was able to enter cells and induce apoptosis, consistent with the Bid BH3 domain's intended biological effect as an antagonist of anti-apoptotic Bcl-2 proteins. Since this report, this peptide "stapling" strategy has been applied to many other helical peptides and, in several exceptional cases, has imparted membrane permeability into other sequences as well.[17, 18, 20-33] In these reports, incorporation of the hydrocarbon crosslink can significantly increase helical content of the resulting "stapled" peptide, through the covalent crosslinking and the helix-promoting α-methyl substitution.[34, 35] The mechanism for cellular entry of stapled helical

peptides is not fully understood and not all stapled peptides can enter cells. It has been suggested that the hydrophobic crosslinker allows association of the peptide with the cellular membrane, with subsequent cell entry proceeding via energy-dependent endocytosis.[19, 36]

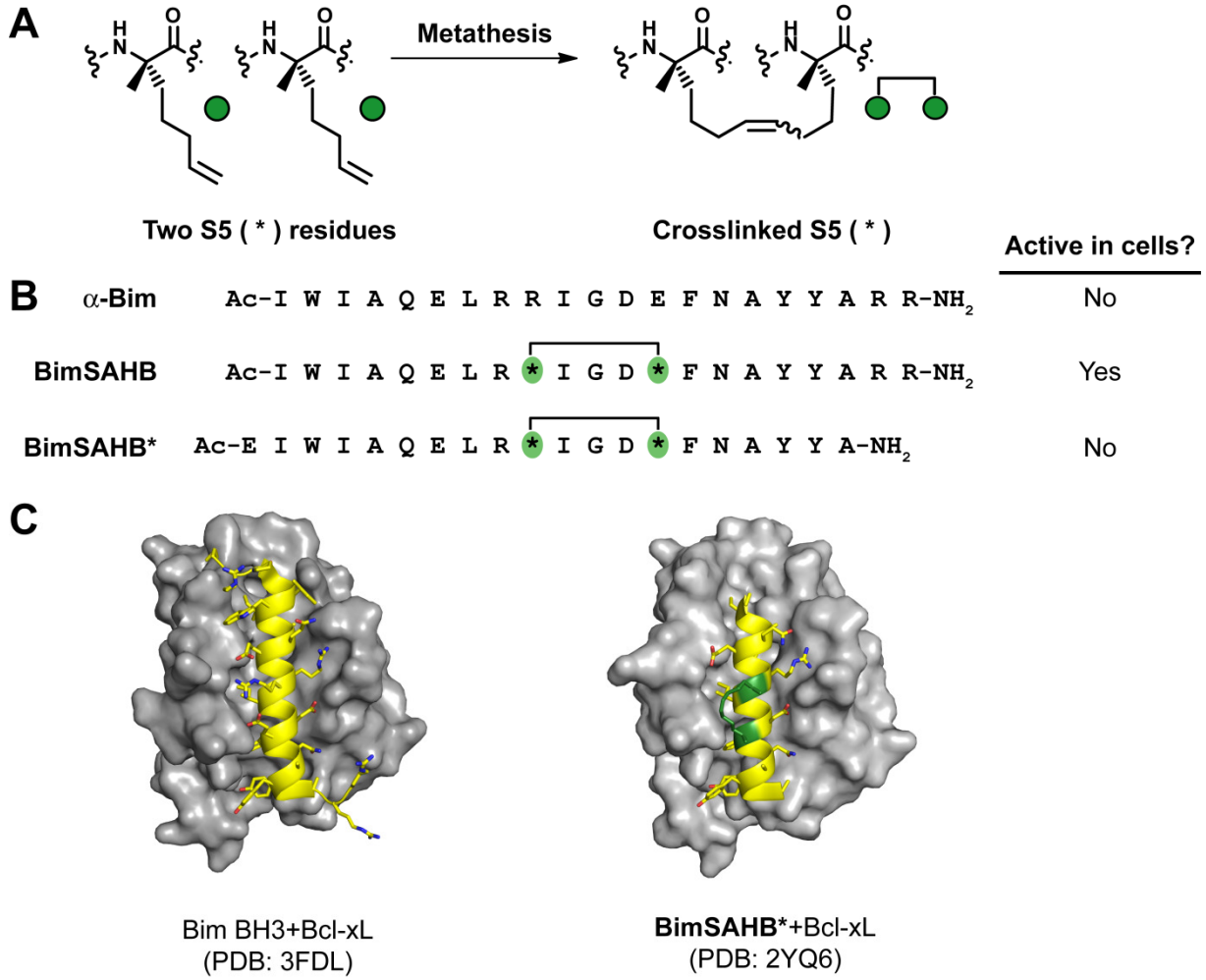

Figure 6.1 A "stapled" analogue of the Bim BH3 domain, **BimSAHB**, is active in living cells.[20, 26] (A) Schematic for the crosslinking reaction to connect two S5 residues (left) to form a hydrocarbon crosslink (right). (B) Sequence of **α-Bim**, **BimSAHB**, and **BimSAHB***. The crosslinked S5 (*) residues are indicated by green circles. Right column indicates if this sequence has been shown to spontaneously enter certain types of cells and initiate apoptosis. (C) Co-crystal structures of the Bim BH3 domain peptide (yellow) bound to Bcl-x_L (gray) (PDB: 3FDL)[37] and **BimSAHB*** (yellow) bound to Bcl-x_L (gray) (PDB:2YQ6).[11] The crosslinked S5 residues are shown in green.

6.2.3 BimSAHB is a crosslinked analogue of the Bim BH3 domain

An analogue of the Bim BH3 domain containing the all-hydrocarbon "staple" crosslink, **BimSAHB**, was first reported by Walensky et al. (Figure 6.1B).[20] In this report, **BimSAHB** was developed to test a hypothesis involving direct BH3 domain binding to Bax, and cellular studies were not performed. In a follow-up report by Gavathiotis et al.,[38] an analogue of **BimSAHB** with a slightly different sequence (denoted **BimSAHB*** in this chapter, Figure 6.1B) was developed for structural studies by NMR. Following this, a report from LaBelle et al.[26] showed that **BimSAHB** can enter certain hematological cancer cell lines (e.g., U937) and initiate apoptosis by antagonizing Bcl-2 family protein-protein interactions.

In 2013, Okamoto et al.[11] published a report showing that **BimSAHB*** did not induce apoptosis in cells, in apparent conflict with reports by LaBelle et al. using **BimSAHB**.[26] Confusion between these closely related peptides arose from the naming convention used by the original authors, in which both **BimSAHB** and **BimSAHB*** were designated "$BimSAHB_A$", even when used in the same paper.[38] Follow-up discussion[39, 40] and review articles[17] confirm that **BimSAHB** is active in certain cell types, while **BimSAHB*** is inactive, likely due to an overall negative charge and low helical character for this latter peptide. Overall, these findings demonstrate that small, seemingly trivial sequence changes in **BimSAHB** can lead to dramatic differences in cellular activity, likely due to a difference in cell-penetrating ability. Thus, the cell-penetrating ability of peptides bearing a hydrocarbon "staple" is extremely sensitive to the particular sequence of the peptide into which it is incorporated.

6.2.4 α/β-Peptide mimics of "stapled" peptides

Several reports have highlighted the significant impact of primary sequence on the activity of stapled α-peptides in living cells. Small changes in sequence or charge can

substantially alter the ability of these peptides to enter cells, which indicates that the presence of a hydrocarbon crosslinker alone does not ensure membrane transit or activity.[11, 17, 21, 25, 39] In light of these results, one primary goal of the work described in this chapter was to determine whether the replacement of a subset of α-amino acid residues with β-amino acid residues in a known, active cell-penetrating peptide (**BimSAHB**, Figure 6.1)[26] would alter the ability of the resulting α/β-peptides to cross cell membranes and initiate apoptosis. In contrast to Chapter 5, in which we attempted to introduce cell permeability into an optimized α/β-peptide, here we sought to design an α/β-peptide mimic of a peptide that is already known to be membrane-permeable.

Here we describe α/β-peptide analogues of **BimSAHB**,[20, 26] a crosslinked α-helical α-peptide derived from the Bim BH3 domain. The "stapled" α/β-peptide mimics the activity of the crosslinked parent α-peptide in cell-based experiments. However, the crosslinked α/β-peptide manifests greater resistance to proteolytic degradation than does the analogous crosslinked α-peptide. These results show that properly designed α/β-peptides can recapitulate favorable characteristics of stapled peptides (such as protein recognition, conformation stability, and membrane permeability) while providing additional benefits. Such compounds may be useful as chemical probes for studying interactions among Bcl-2 family proteins within cells or as starting points for the development of future therapeutic agents.

The studies described in this chapter were all performed in close collaboration with Douglas Fairlie and Erinna Lee (Fairlie Laboratory, Walter and Eliza Hall Institute of Medical Research, Australia).

6.3 Design and characterization of α/β-peptide mimics of BimSAHB

6.3.1 α/β-Peptide design

Our group recently reported α/β-peptide analogues of the Bim BH3 domain that contain cyclic β-amino acid residues (Figure 6.2) and bind to both Bcl-x_L and Mcl-1 with high affinity.[41] These α/β-peptides are significantly less susceptible to proteolytic degradation relative to α/β-peptides that contain only flexible, acyclic β-residues. Based on this precedent, we designed **6.1** (Figure 6.3), an analogue of **BimSAHB** that contains three α→cyclic β-residue substitutions (Trp2→ACPC, Glu6→sAPC, Ala16→ACPC) along with the side chain crosslink. We also synthesized linear "unstapled" analogues of **BimSAHB** and **6.1** (**6.2** and **6.3**, respectively) to evaluate the effect of the covalent crosslink on protein affinity and cellular activity.

A

		FP K_i (nM)		
		Bcl-x_L	Mcl-1	$t_{1/2}$ (min.)
A	Ac-I W I A Q E L R R I G D E F N A Y Y-NH_2	23	26	1.7
B	Ac-I W I A Q E L R I G D E F N A Y Y-NH_2	580	230	29
C	Ac-I X I A Q U L R Z I G D U F N X Y Y-NH_2	70	7.9	210

B

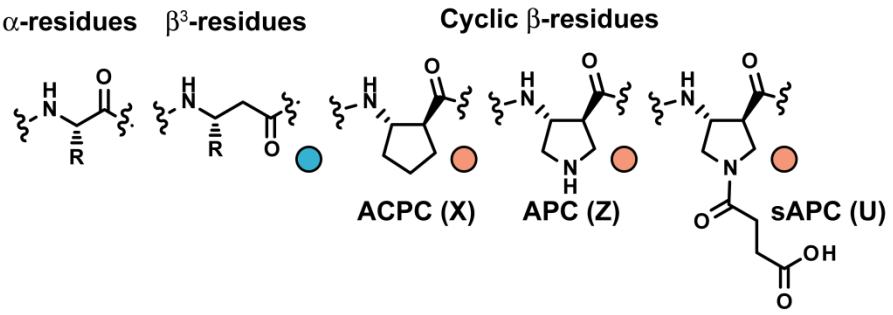

Figure 6.2 Previously reported α/β-peptide analogues of the Bim BH3 domain, from ref[41]. (A) Sequences of the Bim BH3 α-peptide **A** (note that **A** is a slightly different region of the Bim BH3 domain than **α-Bim**) and α/β-peptides **B** and **C**, along with K_i values, as determined by competition fluorescence polarization (FP) assay, for binding to Bcl-x_L and Mcl-1 and half-life values ($t_{1/2}$) to degradation by 5 μg/mL proteinase K in TBS, pH 7.5 with 5% DMSO. Non-natural residues are indicated by colored circles. (B) Structures of a generic α-residue, a generic β^3-residue (teal), and the cyclic β-residues ACPC (X), APC (Z), and sAPC (U) (orange).

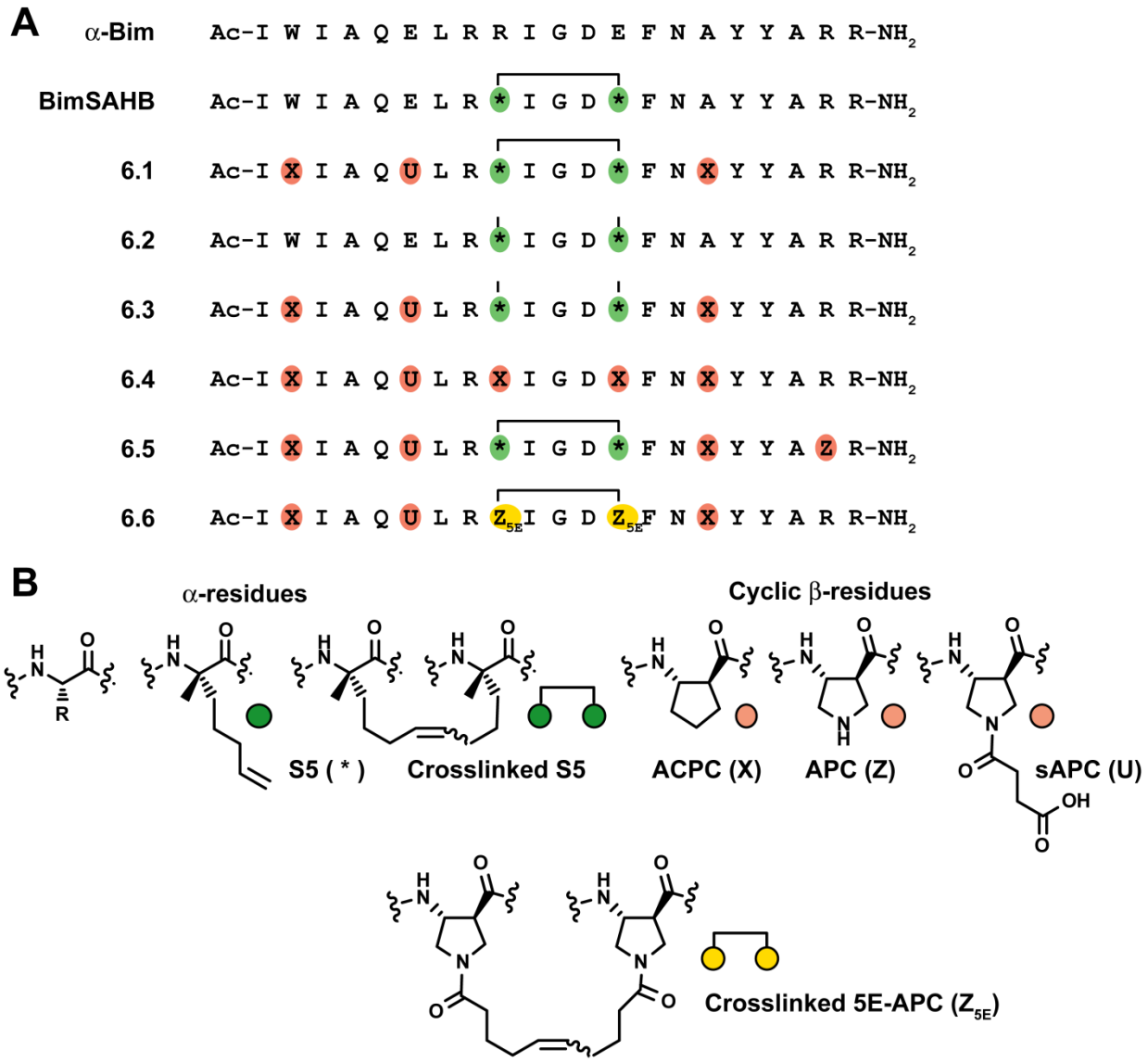

Figure 6.3 (A) Primary sequences of α- and α/β-peptides used in this study. The crosslinked α-peptide **BimSAHB** has been studied in prior reports.[20, 26] Non-natural amino acid residues are indicated by colored circles: green for S5 residue used for crosslinking, orange for cyclic β-residues, and yellow for 5E-APC residue. A horizontal line connecting two residues indicates that these residues have been crosslinked using olefin metathesis. (B) Structures of a generic α-residue, the S5 residue (*), two crosslinked S5 residues, the cyclic β-residues ACPC (X), APC (Z), sAPC (U), and the crosslinked 5E-APC (Z_{5E}) residue.

We synthesized several other α/β-peptide analogues to evaluate the effect of different types of substitutions in this system. To gain insight into the impact of the the S5 residues play on activity, we prepared **6.4**, an analogue of **6.3** that contains two hydrophobic ACPC cyclic β-residues in place of the S5 residues. We hypothesized that while both ACPC and S5 are

hydrophobic and helix-promoting, they present their hydrophobic surfaces in different ways, which may be important for biological activity. We hypothesized that **6.1**, which contains three cyclic β-residues in addition to the crosslink, would have a reduced susceptibility to proteolysis relative to both **α-Bim** and **BimSAHB**. In an effort to reduce the proteolytic susceptibility even further, we also designed **6.5**, which contains an additional Arg20→APC substitution. This substitution has not previously been explored in the context of the Bim BH3 peptide. Finally, we desired to design a β-residue that may mimic S5's remarkable ability to grant certain peptides cell permeability. With this goal, we designed an analogue of APC, called "5E-APC (Z_{5E})", bearing a pentenyl functional group. We designed **6.6**, an analogue of **6.1** bearing two 5E-APC residues in place of S5 and linking them via olefin metathesis (Figure 6.3).

6.3.2 Protein binding by SPR

We used a surface plasmon resonance (SPR) competition assay to evaluate the affinity of the Bim-derived α- and α/β-peptides to three key anti-apoptotic proteins: Bcl-x_L, Mcl-1, and Bcl-2 (Figure 6.4). **BimSAHB**, **6.1**, **6.2**, and **6.3** all bound to Mcl-1 as tightly as did the parent **α-Bim** sequence. α/β-Peptide **6.1** also bound to Bcl-x_L and Bcl-2 similarly to **α-Bim**, while **BimSAHB**, **6.2**, and **6.3** generally bound one or both of these anti-apoptotic proteins somewhat more weakly than did **α-Bim** (~5- to 50-fold decline in affinity, depending on the combination). Interestingly, **6.4**, an analogue of **6.3** that contains the cyclic β-residue ACPC in place of the S5 residues, retained relatively high affinity for Mcl-1 but displayed reduced affinity for Bcl-x_L and Bcl-2 compared to **6.3**. In a preliminary SPR competition experiment (separate from the more rigorous SPR analyses reported for the compounds above), the α/β-peptide **6.6**, bearing the crosslinked 5E-APC cyclic β-residues, also showed high affinity for both Bcl-x_L and Mcl-1, indicating that the 5E-APC residue does not significantly perturb protein binding. The protein

affinity of **6.5** was not determined. Overall, these data imply that **6.1** mimics the protein-recognition profiles of both **α-Bim** and **BimSAHB**, which suggests that the incorporation of cyclic β-amino acid residues into this sequence, in place of α-residues, does not negatively impact the affinity for anti-apoptotic proteins. Indeed, for some anti-apoptotic proteins, the affinity of **6.1** is stronger than is the affinity of **BimSAHB**.

	SPR IC_{50} (nM)		
Oligomer	Bcl-x_L	Mcl-1	Bcl-2
α-Bim	4.1 (0.5)	4.4 (0.4)	3.6 (0.6)
BimSAHB	22.2 (4.8)	3.3 (0.4)	66.6 (13.6)
6.1	4.5 (3.4)	4.1 (2.9)	10.2 (1.4)
6.2	80.0 (7.5)	4.0 (0.2)	189 (33)
6.3	5.5 (0.8)	4.0 (0.5)	50.5 (10.1)
6.4	579 (202)	15.7 (5.6)	1323 (234)
6.5	ND	ND	ND
6.6	25*	7.9*	ND

Figure 6.4 Relative binding of oligomers to anti-apoptotic proteins determined by competition SPR assays. Values are derived from 2-5 independent experiments, except for **6.6**, for which values reported were obtained from a single preliminary experiment (denoted with a *). Numbers in parentheses indicate standard deviation.

6.3.3 Structural analysis in solution by circular dichroism

To gain insight into the impact of the hydrocarbon crosslink on oligomer conformation in solution, we examined the far-UV circular dichroism (CD) spectra of Bim-derived α- and α/β-peptides (Figure 6.5). Consistent with previous reports,[20, 26] **α-Bim** showed little evidence of helicity in aqueous solution, while the stapled peptide **BimSAHB** showed a strong α-helical signature in the far-UV CD, with minima at ~208 and 222 nm. Interestingly, **6.2**, the "unstapled" analogue of **BimSAHB**, also showed a pronounced α-helical CD signature, although the minima were less intense than those of **BimSAHB**. This result suggests that incorporation of the α,α-disubstituted S5 residue alone is sufficient to promote a helical conformation, although

not to the extent observed with an intact crosslink. α/β-Peptides **6.1** and **6.3** both showed a single minimum at ~209 nm, consistent with the signal observed for α/β-peptides that adopt an α-helix-like conformation in solution.[42] As seen for the **6.2** versus **BimSAHB** comparison, **6.3** displayed a less intense helical signature relative to cyclized analogue **6.1**. The CD signal intensity for all of the peptides containing the S5 residue, with or without cyclization, was concentration-dependent in the range 5-50 μM (Figure 6.20 in the "Experimental Methods" section), which suggests that the molecules aggregate under these conditions. Hence, the relative differences in the signal intensities for the linear versus crosslinked peptides could reflect slightly altered propensities to aggregate rather than differences in helix stability.

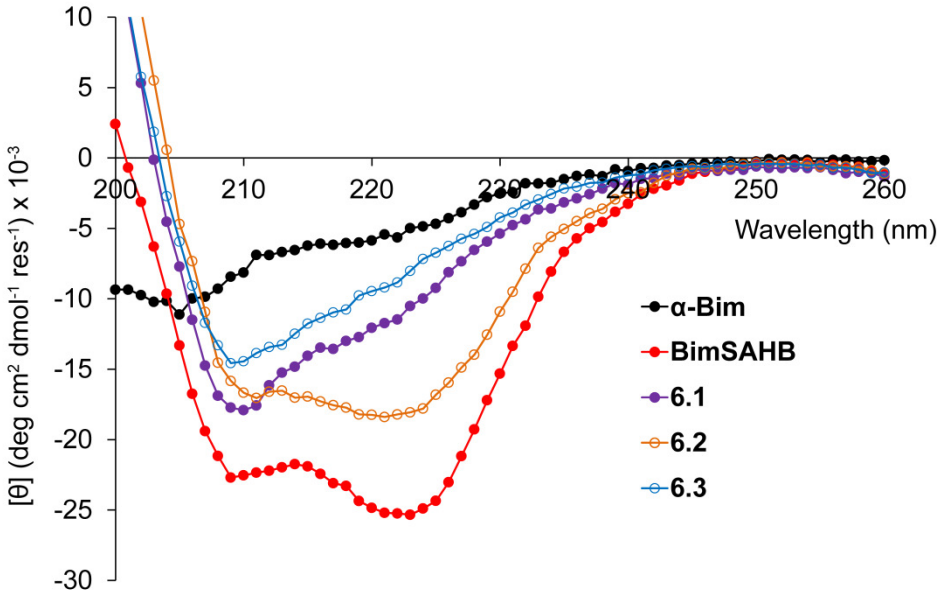

Figure 6.5 Far-UV circular dichroism spectra of α- and α/β-peptides at 50 μM in water at 20 °C.

6.3.4 Crystal structures

To gain atomic-resolution insight regarding the impact of the β-amino acid residues and the hydrocarbon crosslink on binding to an anti-apoptotic protein partner, we solved X-ray crystal structures of **6.1** (PDB: 5AGW) and **6.3** (PDB: 5AGX) in complex with Bcl-2 (Figure

6.6, Table 6.1 in the "Experimental Methods" section). The two α/β-peptides crystallized with Bcl-2 under similar conditions and produced similar crystal forms. No structure is available for the **α-Bim**:Bcl-2 complex for comparison, but both **6.1** and **6.3** engage Bcl-2 *via* the large hydrophobic groove (formed by helices α3, α4, and the N-terminal segment of α5) that is known to be the interaction site on Bcl-2 for BH3 peptide ligands (Figure 6.6A, B); comparable grooves are evident in structures of other anti-apoptotic proteins.[37, 43-47] The four conserved hydrophobic residues (h1-h4) on the buried face of the α/β-peptides project into the groove on Bcl-2 in a manner similar to that in which equivalent residues on **α-Bim** and **BimSAHB*** interact with the equivalent groove on Bcl-x_L (Figure 6.6C). The salt bridge between Asp12 of the α/β-peptides and Arg146 from the BH1 domain of Bcl-2 matches a salt-bridge observed in most reported structures of BH3 domains bound to anti-apoptotic proteins. As anticipated, the β-amino acid residues of **6.1** and **6.3** are aligned as a "stripe" along the solvent-exposed face of the helix formed by each α/β-peptide, although the long sAPC side chain projects close to the α3 helix of Bcl-2 and makes a hydrogen bond with Glu114 in the **6.1**:Bcl-2 complex structure. The hydrocarbon crosslink in the **6.1**:Bcl-2 complex overlays almost perfectly with the crosslink in the structure of **BimSAHB*** bound to Bcl-x_L (PDB:2YQ6).[11] Neither crosslink makes any contacts with the anti-apoptotic protein. In the **6.3** structure the S5 side chains project out to the solvent. Overall, the co-crystal structures indicate that both α/β-peptides **6.1** and **6.3** recapitulate the classic BH3 binding mode, and that incorporation of the S5 and cyclic β-amino acid residues does not dramatically alter the structure or binding mode of the resulting α/β-peptides relative to that of a classical α-helical BH3 domain.

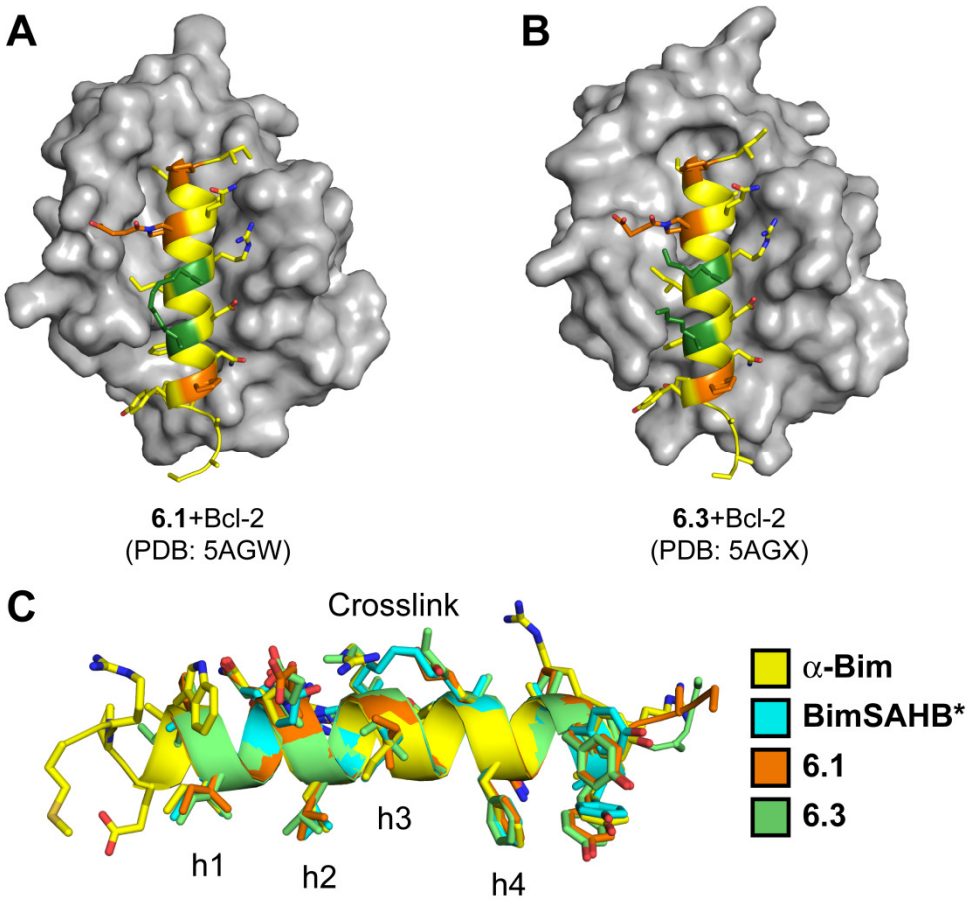

Figure 6.6 Crystal structures of α/β-peptides **6.1** and **6.3** bound to Bcl-2. (A) Structure of **6.1** bound to Bcl-2 (PDB: 5AGW). (B) Structure of **6.3** bound to Bcl-2 (PDB: 5AGX). In panels A and B, the α/β-peptide is colored by residue type (yellow for natural α-residues, green for S5 residues, and orange for cyclic β-residues) and the Bcl-2 surface is shown in gray. (C) Overlay of **6.1** and **6.3** with previously reported structures of an analogue of **α-Bim** (bound to Bcl-x_L, PDB: 3FDL)[37] and an analogue of **BimSAHB*** (bound to Bcl-x_L, PDB: 2YQ6).[11] Positions of key protein-contacting hydrophobic residues h1-h4 and the position of the crosslink (for **BimSAHB*** and **6.1**) are labeled.

6.4 Activity in cell culture

6.4.1 Cytochrome c release assay from permeabilized cells

To establish whether **6.1** could neutralize anti-apoptotic protein function in a cellular milieu, we tested whether this stapled α/β-peptide could induce cytochrome *c* release from mitochondria (a hallmark of cell death induction). These studies were conducted in wild-type mouse embryonic fibroblasts (MEFs) in which the plasma membrane was permeabilized by treatment with digitonin (Figure 6.7). This permeabilization approach is usually required to

enable BH3-derived peptides to reach the proteins that regulate apoptosis. Mouse embryonic fibroblasts are dependent on both Bcl-x_L and Mcl-1 for their survival,[48] and therefore both of these proteins must be neutralized to induce apoptosis.

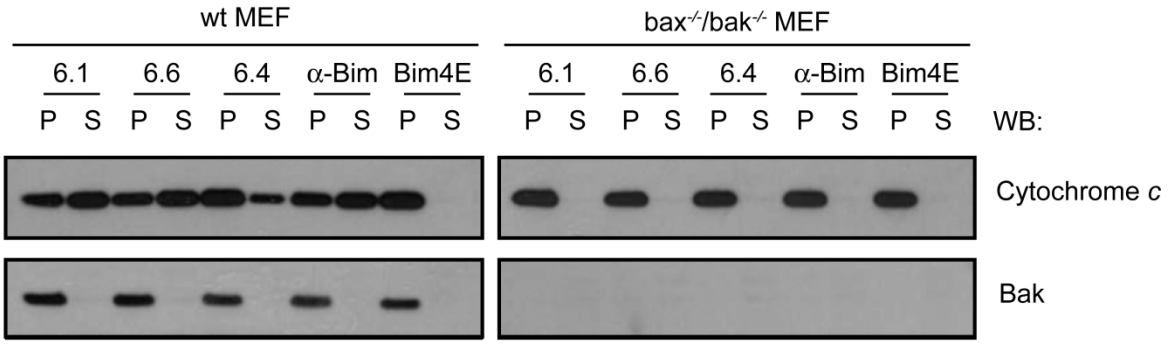

Figure 6.7 Cytochrome *c* release assay on permeabilized wild-type (wt) or *bax*$^{-/-}$/*bak*$^{-/-}$ mouse embryonic fibroblasts (MEFs) treated with 10 μM of the indicated α- or α/β-peptide for 1 hour. **6.1**, **6.6**, **6.4**, and **α-Bim** were able to induce cytochrome *c* release from the mitochondria-containing pellet fraction (P) to the soluble cytosolic fraction (S) in wt MEFs, but not in *bax*$^{-/-}$/*bak*$^{-/-}$ MEFs, as indicated by western blot for cytochrome *c*. No cytochrome *c* release was seen for negative control **Bim4E** (DMRPEIWEAQEERREGDEENAYYARR-OH). The lower panel shows western blot for Bak as a control for membrane permeabilization. Bak is a mitochondrial protein and therefore should not appear in the cytosolic fraction. *bax*$^{-/-}$/*bak*$^{-/-}$ MEFs do not have Bak, and therefore no band is apparent.

Consistent with the binding profile of α/β-peptide **6.1** for these anti-apoptotic proteins, treatment of permeabilized MEFs with **6.1** induced movement of cytochrome *c* from the pellet fraction (which contains the mitochondria) to the soluble cytosolic fraction. Comparable behavior was observed with the **α-Bim** peptide, which is comprised solely of α-residues (Figure 6.7). α/β-Peptide **6.6**, which contains crosslinked 5E-APC cyclic β-residues in place of the S5 α-residues also released cytochrome *c* in this assay. Slightly less cytochrome *c* release was observed with **6.4** relative to **6.1**, consistent with the difference in affinity for Bcl-x_L between these two α/β-peptides (Figure 6.4). No cytochrome *c* release was seen with a negative control Bim-derived α-peptide (**Bim4E**) in which key interacting residues (h1-h4) were substituted with glutamic acid, or in permeabilized MEFs derived from embryos deficient in Bax and Bak, the

essential mediators of apoptosis. Combined, these data suggest that **6.1** (and analogues) can neutralize Bcl-x_L and Mcl-1 in permeabilized cells, leading to the activation of Bax and/or Bak.

6.4.2 Cell killing assays

Previous studies have shown that some cell types, particularly hematological cancer cell lines, are either killed or are sensitized to apoptosis by treatment with stapled BH3 domain α-peptides, but that other cell lines (e.g., fibroblasts, HCT-116 colon cancer) are resistant to these stapled peptides.[11, 17, 26, 40] We therefore screened a panel of various cell lines to identify those cells that could be used in detailed functional analyses. The crosslinked α/β-peptide **6.1** was compared to the crosslinked α-peptide **BimSAHB** at a high concentration (10 μM) in a CellTiter-Glo assay (Promega), which measures intracellular ATP levels as an indicator of cell viability (Figure 6.8). Consistent with previous reports for **BimSAHB**, we saw essentially no effect of **6.1** or **BimSAHB** on MEFs, which are not cancer cells (Figure 6.8),[26] even though **6.1** can engage the apoptotic network when the MEF outer membrane has been permeabilized (Figure 6.7). Additionally, no significant cell death was induced by **6.1** or **BimSAHB** with any of the adherent cancer cell lines tested, including those derived from mammary (MDA-MB-231, MDA-MB-468), colon (LIM-2405, SW480), or lung (A549) tumors. In contrast, **6.1** potently impacted U937 lymphoma cell viability, similar to the effect previously observed with **BimSAHB** on these cells.[26] Overall, these data indicate that **6.1** mimics the highly selective cell-killing profile of **BimSAHB**, suggesting that the non-natural α/β backbone supports mimicry of the complex biological activity of the stapled α-peptide **BimSAHB**.

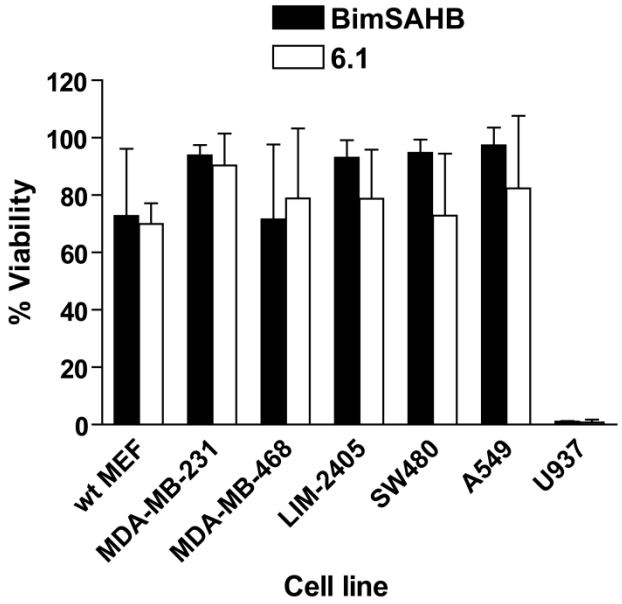

Figure 6.8 Viability of various cell lines (relative to DMSO control) when exposed to 10 μM α-peptide **BimSAHB** (black bars) or α/β-peptide **6.1** (white bars) for 24 hours, as measured using CellTiter-Glo assay. Each bar represents the mean ± SD for two independent experiments.

To gain insight into the relative potency of **6.1** versus **BimSAHB** toward U937 cells, and to establish whether the loss of cell viability observed following treatment was due to activation of the apoptotic cascade or to some non-specific effect (e.g., rupture of the plasma membrane), we performed titrations of **BimSAHB** or **6.1** in the presence or absence of the broad-spectrum caspase inhibitor Q-VD-OPh (Figure 6.9). Following just 2 hours of treatment with crosslinked oligomer in the absence of caspase inhibitor, a significant reduction in cell viability was observed for both **BimSAHB**- and **6.1**-treated cells. This loss in viability was attenuated by Q-VD-OPh for both the stapled α-peptide and the stapled α/β-peptide, suggesting that the cell killing was due to activation of the intrinsic cell death pathways (in which caspases play a critical role) rather than a non-specific effect. Additional caspase-dependent killing was seen after 6 hours of treatment for both oligomers; however, after treatment with peptides for 24 hours most of the cell death observed was not inhibited by Q-VD-OPh. **BimSAHB** was slightly more potent than **6.1** (EC_{50} = ~2 μM for **BimSAHB** versus ~4 μM for **6.1** at 6 hours), but there

appeared to be slightly more caspase-independent killing (not blocked by Q-VD-OPh) at the earlier time points for **BimSAHB** compared to **6.1**.

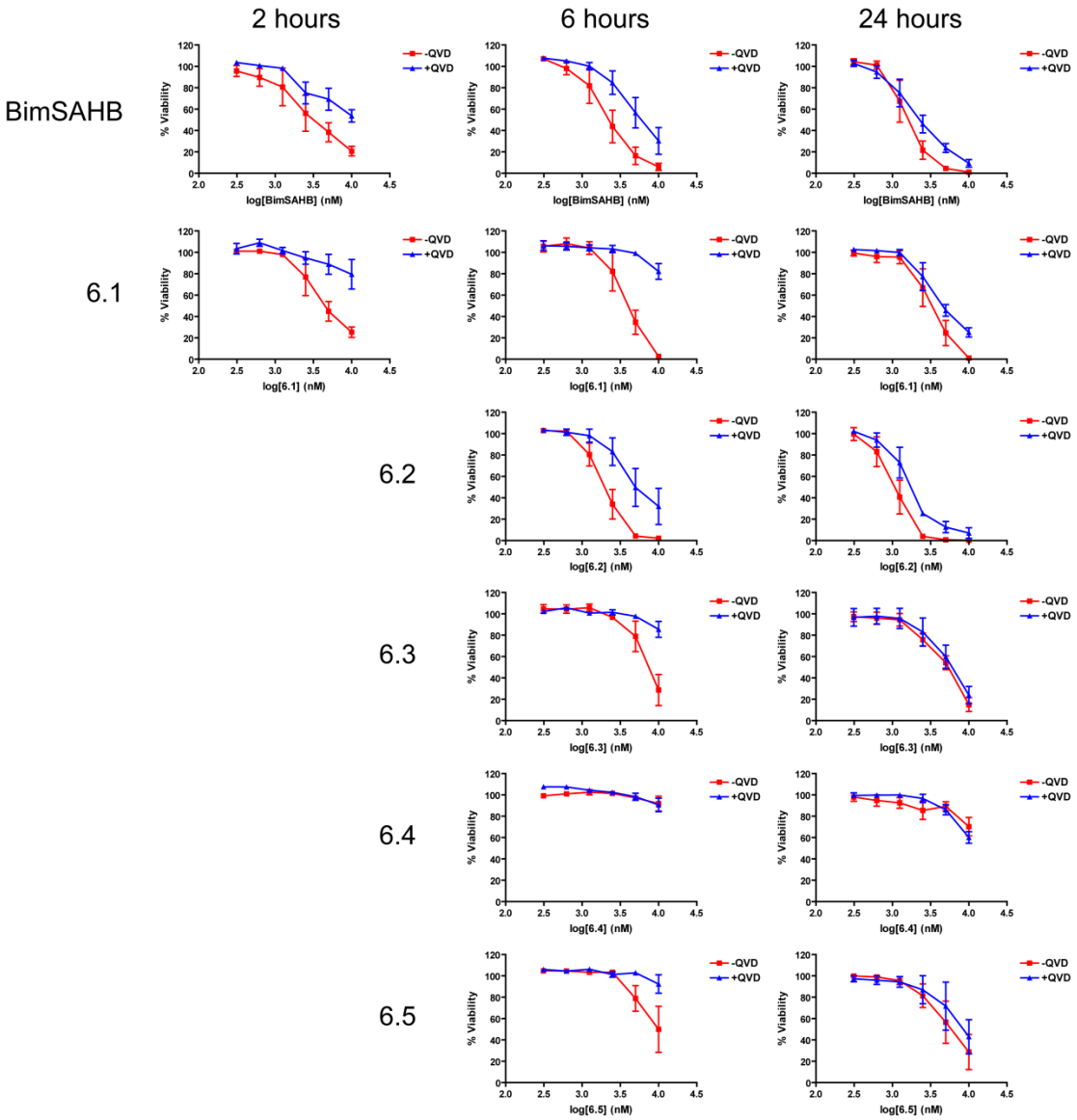

Figure 6.9 Viability of U937 cells (relative to DMSO control) when treated with various concentrations of α- or α/β-peptides in the absence (red) or presence (blue) of 50 μM caspase inhibitor Q-VD-OPh (QVD), as determined by CellTiter-Glo assay. Cells were treated with the indicated α- or α/β-peptide for 2 hours under serum-free conditions, followed by the addition of serum-containing media and additional incubation until the indicated time point. Each data point represents the mean ± SEM for 3-5 replicate measurements.

Recent reports[40, 49] suggest that the hydrocarbon crosslink *per se* may not be required for cell entry in some stapled peptides, but rather that the presence of the two S5 residues alone (no

cyclization via ring-closing metathesis) may be sufficient to facilitate cell entry and initiation of apoptosis. To evaluate the importance of the hydrocarbon crosslink in our system, we tested the linear peptides **6.2** and **6.3** for killing activity toward U937 cells. Consistent with an earlier report using **6.2**,[40] both linear oligomers were effective at reducing U937 cell viability in a caspase-dependent manner (Figure 6.9). In contrast, the α/β-peptide that contained ACPC residues in place of the hydrocarbon crosslink (**6.4**) had no significant effect on cell viability, even after 24 hours.

α/β-Peptide **6.5**, an analogue of **6.1** containing one additional Arg→APC substitution (designed to increase protease stability), appeared modestly active against U937 cells. It is unclear if this apparently reduced activity relative to **6.1** stems from reduced protein affinity (this α/β-peptide was not evaluated by SPR), reduced ability to enter the cell, or some alternative reason. It is possible that the removal of the guanidinium functional group resulting from this substitution negatively affected cellular entry, as the presence of arginine residues is correlated with cell entry in a number of contexts.[50, 51] If this is the case, substitution of the APC20 residue for an APC analogue bearing a guanidinium functional group[52] may facilitate cell permeability while protecting the C-terminal end of this α/β-peptide from protease degradation. Further studies are required to determine why this α/β-peptide appears to be less active in these cell-based studies relative to **6.1**.

Finally, α/β-peptide **6.6**, which featured two crosslinked 5E-APC residues, appeared inactive in preliminary cell-based experiments (Figure 6.10). α/β-Peptide **6.6** differs from **6.1** only in the identity of the hydrophobic crosslink, which indicates the 5E-APC residues are not adequate mimics of the S5 residues for cellular permeability. Because preliminary SPR analysis (Figure 6.4) indicated that **6.6** binds relatively well to Bcl-x_L and Mcl-1, the lack of activity of

6.6 may arise because this α/β-peptide does not enter cells. This could be due to the number of hydrophilic atoms in the side chain amide group of 5E-APC, which may reduce the α/β-peptide's interaction with the cell membrane. Further studies, such as careful SPR analysis and microscopy experiments, should be performed to determine why this α/β-peptide was inactive.

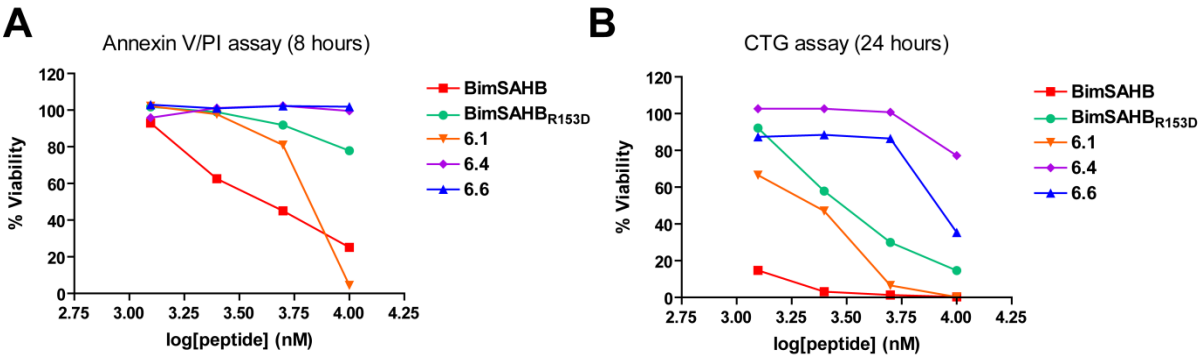

Figure 6.10 Viability of U937 cells (relative to DMSO control) when treated with various concentrations of α- or α/β-peptides, as determined by Annexin V/PI staining after 8 hours (A) and CellTiter-Glo assay after 24 hours (B). Cells were treated with the indicated α- or α/β-peptide for 2 hours under serum-free conditions, followed by the addition of serum-containing media and additional incubation until the indicated time point. Each data point represents a single measurement in this preliminary experiment. **BimSAHB$_{R153D}$** (sequence = Ac-IWIAQELD*IGD*FNAYYARR-NH_2, where * = crosslinked S5 residues), which binds weakly to most Bcl-2 family proteins (although still binds tightly to Mcl-1), was used as a negative control.[26]

We next used another marker of apoptosis, propidium iodide (PI) staining of DNA as detected with fluorescence microscopy, to monitor cell viability and morphology over time (Figure 6.11). U937 cells were treated with 5 μM of **6.1** or **BimSAHB** and imaged every 30 minutes. The results closely matched the CellTiter-Glo assay data, although cell killing appeared to proceed with slightly different kinetics, presumably due to the differences in experimental read-out between the two assays. These studies revealed a dependence on caspase activity for cell killing by both **6.1** and **BimSAHB**, particularly at the earlier time points, as indicated by the delay in cell death for conditions containing Q-VD-OPh (Figure 6.11A). These observations are fully consistent with those based on CellTiter-Glo assays. Close examination of the images reveals that even after just 1 hour of treatment, classical features of apoptotic cell death such as

membrane blebbing start to appear. These features are present in the majority of cells within 2 hours (Figure 6.11B), but are not seen in the presence of caspase inhibitor Q-VD-OPh. Significant PI staining (i.e., to >50% of cells) was slightly delayed in cells treated with **6.1** compared to **BimSAHB**, consistent with the CellTiter-Glo results, suggesting **BimSAHB** killed more rapidly than did **6.1** (Figure 6.11A). The majority of cells treated with either **6.1** or **BimSAHB**, however, were dead (PI^{+ve}) within 2-6 hours, and this cell death was accompanied by the prodigious release of small apoptotic bodies, another hallmark of apoptosis induction.

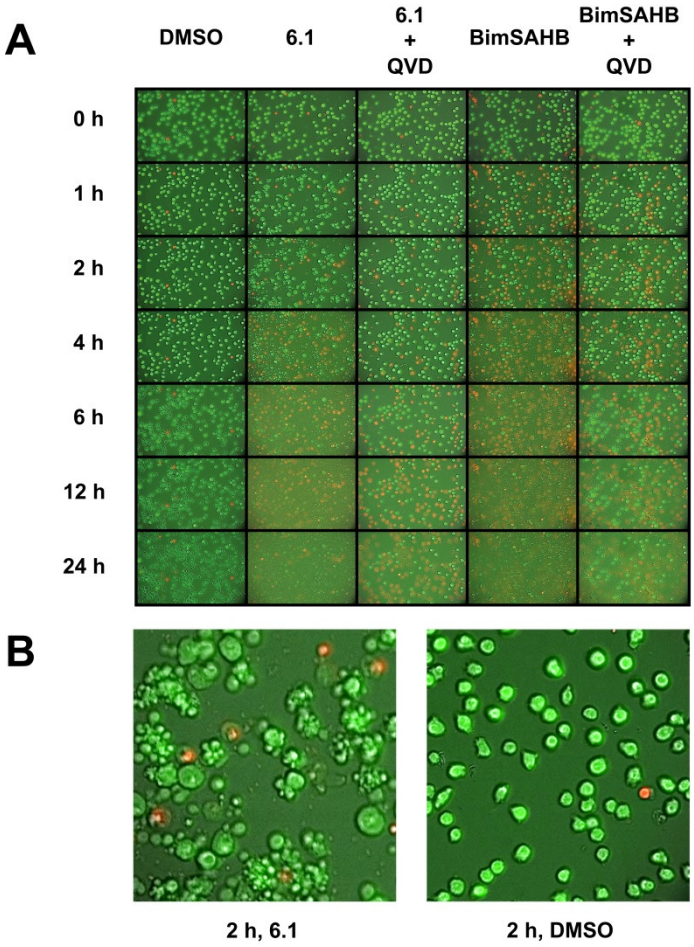

Figure 6.11 (A) Analysis of U937 cell killing over time induced by 5 μM **6.1** or **BimSAHB** in the absence or presence of 50 μM Q-VD-OPh (QVD). Green cells indicate those stained for CellTracker Green dye (living cells). Red cells indicate cells stained by propidium iodide (dead cells). (B) Close up of the indicated conditions from panel A, highlighting morphological changes resulting from treatment with **6.1** relative to DMSO control.

6.4.3 Effect of serum on cell killing effect

Stapled peptides bearing the crosslinked S5 residues are extremely hydrophobic and have been shown to associate with serum proteins.[17, 28] Binding to serum proteins can sometimes be beneficial for peptide therapeutics in living systems, as this can increase biological half-life *in vivo* through reducing both renal clearance and susceptibility to protease degradation.[53] However, very strong binding to serum proteins can also be detrimental as it may prevent the peptide from acting on its target. Indeed, some stapled peptides containing crosslinked S5

residues show reduced activity in cell culture in the presence of serum.[28] Indeed, in reports describing **BimSAHB**,[26, 40] this stapled α-peptide was evaluated in cell-based assays by treating cells with peptides in the absence of serum for 2 hours followed by the addition of serum to promote cell survival. This protocol was also used in our cell-based experiments above.

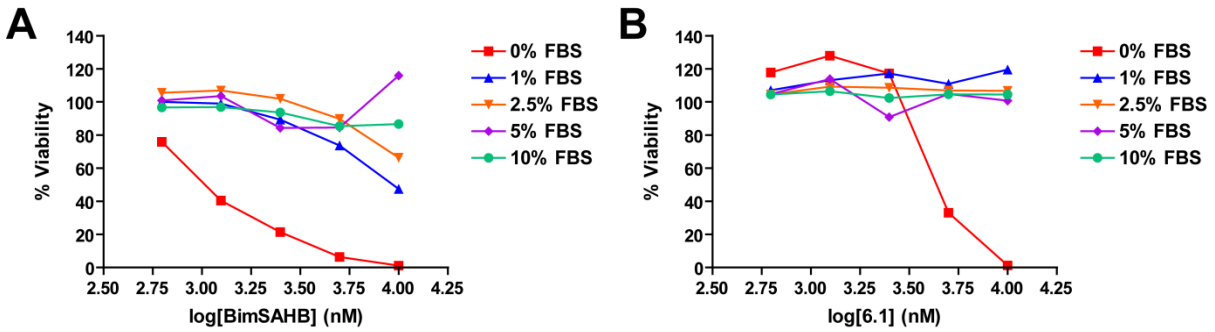

Figure 6.12 Effect of fetal bovine serum (FBS) on activity of **BimSAHB** (A) and **6.1** (B) on U937 cells, as judged by CellTiter-Glo. Cells were incubated with peptide for 2 hours in 0% serum followed by 6 hours in 10% serum (red) or in the presence of the indicated concentration of serum for 8 hours.

We evaluated the ability of **BimSAHB** and **6.1** to kill U937 cells in the presence of different amounts of serum (Figure 6.12). In this experiment, we found that the ability for both **BimSAHB** and **6.1** to induce apoptosis was virtually completely blocked even at 1% serum. This strongly suggests that these oligomers associate with serum proteins, likely through hydrophobic interactions, which prevents them from entering cells and inducing apoptosis. This observation is surprising given that **BimSAHB** was reported to show efficacy in animal models[26] and will certainly need to be addressed before compounds such as these can be used as therapeutic agents.

6.4.4 Cytochrome c release assay on unpermeabilized cells

To further assess whether cell killing by stapled **6.1** occurred *via* the mitochondrial pathway, we examined unpermeabilized U937 cells for cytochrome *c* release 3 hours after treatment (Figure 6.13). Here we observed that most of the cytochrome *c* was present in the

soluble fraction, which contrasted with the location of cytochrome *c* exclusively in the pellet after intact cells were treated with either **α-Bim** or **6.4**, neither of which is stapled. The absolute amount of cytochrome *c* detected in cells treated with **6.1** was somewhat lower than the amount in cells subjected to the other treatments; this trend may reflect some degree of leakage through the plasma membrane of the dying cells after treatment with **6.1**.

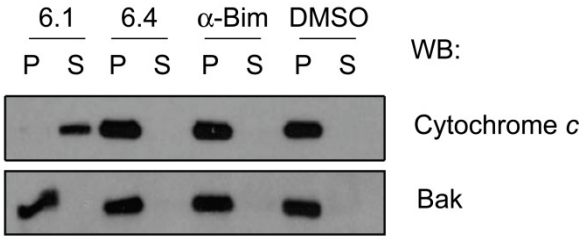

Figure 6.13 Cytochrome *c* release assay on unpermeabilized U937 cells treated with 10 μM of the indicated α- or α/β-peptide for 3 hours. **6.1**, but not **6.4** or **α-Bim**, was able to induce cytochrome *c* release from the mitochondria-containing pellet fraction (P) to the soluble cytosolic fraction (S). The lower panel indicates western blot for Bak as a control for membrane permeabilization.

6.4.5 Analysis of cellular uptake by live-cell confocal microscopy

We examined the cellular uptake of fluorescein (Flu)-labeled derivatives of **α-Bim, BimSAHB**, **6.1**, **6.2**, and **6.3** (Figure 6.14) in both U937 and MEF cells by live-cell confocal microscopy (Figures 6.15 and 6.16, Figures 6.21 and 6.22 in "Experimental Methods" section). These experiments were performed in collaboration with David Belair (Murphy Laboratory, University of Wisconsin-Madison), Geoffrey Eddinger (Gellman Laboratory, University of Wisconsin-Madison), and undergraduate Julia Wilson (Gellman Laboratory, University of Wisconsin-Madison).

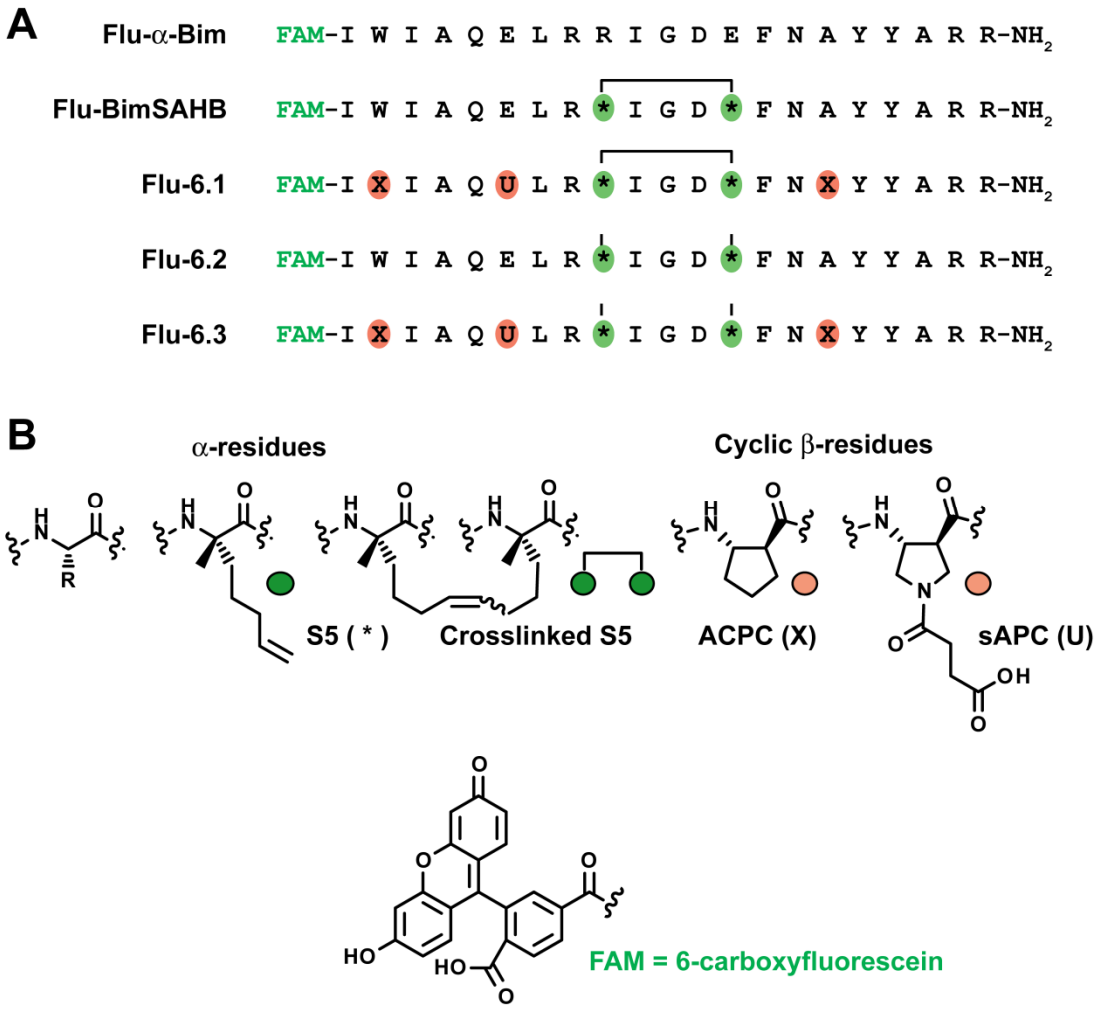

Figure 6.14 (A) Primary sequences of fluorescein-labeled α- and α/β-peptides used in this study. Non-natural residues are indicated by colored circles: green for S5 residue used for crosslinking, and orange for cyclic β-residues. A horizontal line connecting two S5 residues indicates that these residues have been crosslinked using olefin metathesis. FAM = 6-carboxyfluorescein coupled to the N-terminal amine. (B) Structures of a generic α-residue, the S5 residue, two crosslinked S5 residues, the cyclic β-residues ACPC (X) and sAPC (U), and 6-carboxyfluorescein (FAM).

When U937 cells were treated with Flu-labeled peptides at 2 μM for 3 hours under serum-free conditions, we observed intracellular green fluorescence for both **Flu-BimSAHB** and **Flu-6.1** (Figure 6.15), consistent with the hypothesis that **BimSAHB** and **6.1** can cross membranes spontaneously and gain access to targets within the cytosol of living cells. We observed similar intracellular fluorescence for **Flu-6.2** and **Flu-6.3**, which is consistent with our finding that both **6.2** and **6.3** can also initiate apoptosis in U937 cells. With all oligomers

containing the S5 residue, whether subjected to cyclization or not, we also observed significant green fluorescence associated with the outer membrane of some cells, which we interpret as aggregated peptide. These aggregates remained strongly associated with the cell membrane even after multiple washes prior to imaging. U937 cells treated with **Flu-α-Bim**, which does not contain the S5 residue, displayed negligible green fluorescence inside cells or associated with the outer membrane, consistent with the hypothesis that **α-Bim** does not enter cells.

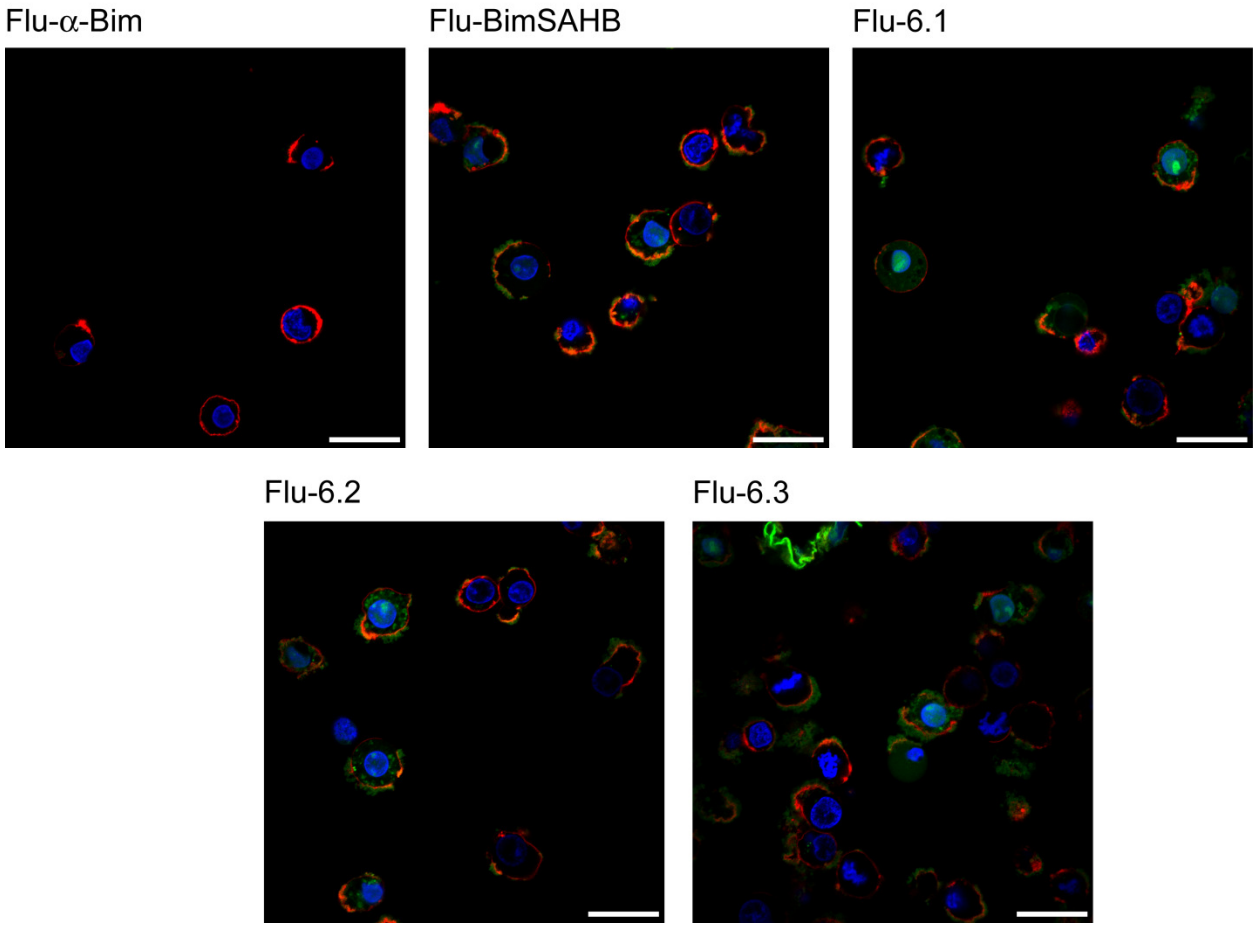

Figure 6.15 Analysis of U937 cellular uptake of fluorescein (Flu)-labeled analogues of α- and α/β-peptides by live-cell confocal microscopy. Cells were treated with 2 μM of the indicated α- or α/β-peptide in serum-free media for 3 hours prior to imaging. Images are obtained under 90x magnification, showing the channels for green (fluorescein, peptide), red (WGA488, outer membrane stain), and blue (Hoescht 33342, nuclear stain). Scale bars represent 25 μm.

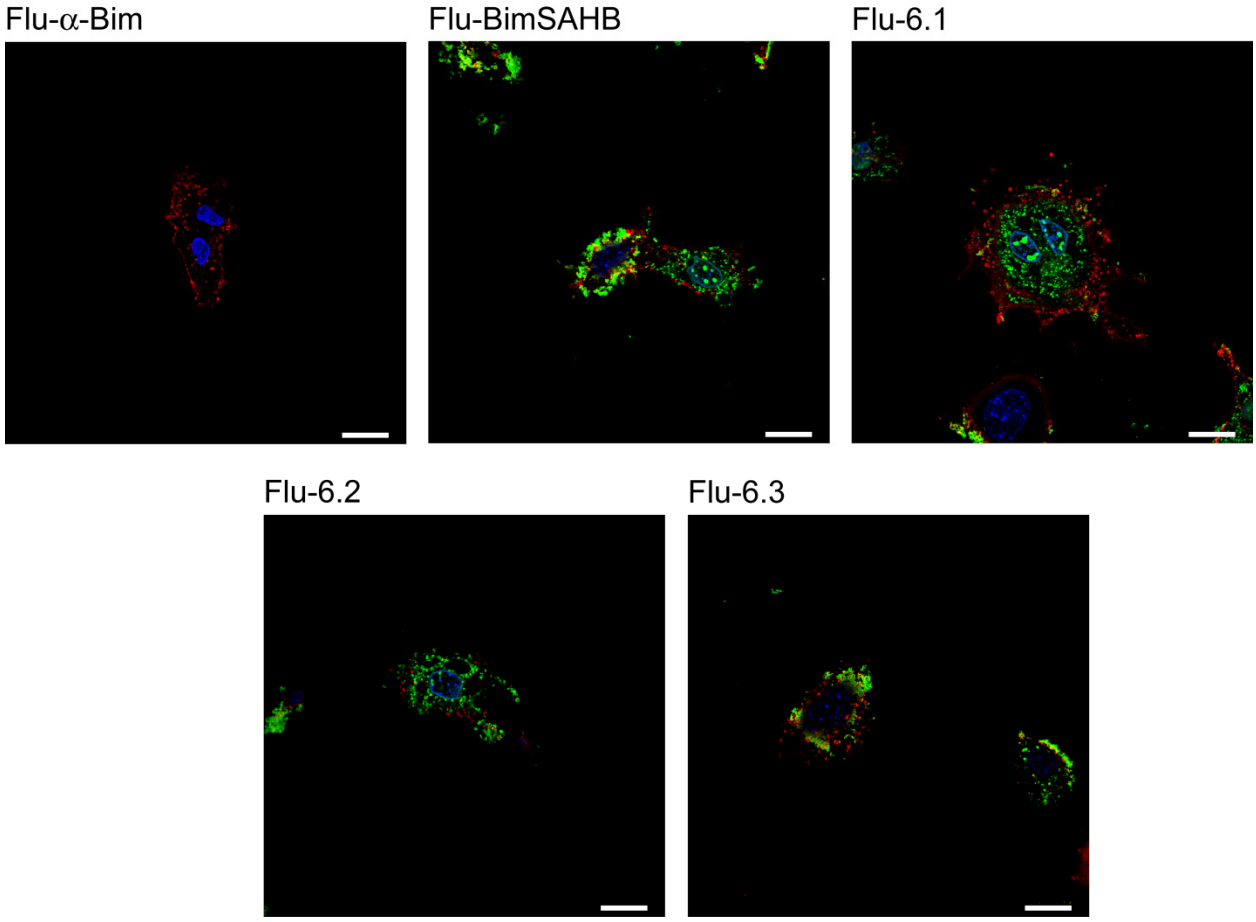

Figure 6.16 Analysis of MEF cellular uptake of fluorescein (Flu)-labeled analogues of α- and α/β-peptides by live-cell confocal microscopy. Cells were treated with 2 μM of the indicated α- or α/β-peptide in serum-free media for 3 hours prior to imaging. Images are obtained under 60x magnification, showing the channels for green (fluorescein, peptide), red (WGA488, outer membrane stain), and blue (Hoescht 33342, nuclear stain). Scale bars represent 25 μm.

When MEFs were treated with fluorescein-labeled analogues of Bim-based oligomers, the confocal microscopy images were similar to those seen with the U937 cells, with **Flu-BimSAHB**, **Flu-6.1**, **Flu-6.2**, and **Flu-6.3** all appearing to enter the MEFs (Figure 6.16). These observations are consistent with a previous report showing that labeled **BimSAHB** can enter MEFs, despite the stapled peptide's inability to kill these cells.[26] However, the fluorescent staining pattern appeared somewhat more punctate in the MEFs than was observed with the U937 cells. This result suggests that although the stapled and unstapled α- and α/β-peptides can

enter MEFs, these peptides may be unable to move into the cytoplasm in this cell type, in contrast to U937 cells.

6.5 Protease susceptibility

We evaluated a subset of the peptides for susceptibility to degradation by proteinase K, a generic and aggressive protease (Figure 6.17). In this assay, the linear α-peptide **α-Bim** was very rapidly degraded, showing a half-life of 0.27 minutes. **BimSAHB**, an α-peptide that contains the hydrocarbon crosslink, showed modestly diminished susceptibility to degradation by proteinase K, with a half-life of 1.6 minutes under the assay conditions. The ~6-fold increase in half-life for **BimSAHB** relative to **α-Bim** is consistent with previous reports in terms of the extent to which a hydrocarbon crosslink confers resistance to proteolytic destruction.[19, 22] This modest resistance to proteolysis presumably arises from the presence of the α,α-disubstituted residues and the crosslinking segment, both of which favor a helical conformation. α/β-Peptide **6.1**, which contains three cyclic β-amino acid residues in addition to the crosslink, showed a large improvement in resistance to proteolysis relative to **BimSAHB**, with a half-life of 150 minutes (>90-fold increase in relative to the stapled peptide **BimSAHB** and >500-fold increase relative to **α-Bim**). Finally, although α/β-peptide **6.5** (which contains an Arg→APC substitution near the C-terminus, relative to **6.1**) was not very active in the cell-based assays, we evaluated its susceptibility to proteinase K degradation and found that it was even more stable than **6.1**, with a half-life of 440 minutes, consistent with our design hypothesis. Overall, these results suggest that the incorporation of β-amino acid residues can be used to develop an α/β-peptide analogue (**6.1**) that mimics the complex functions of a stapled α-peptide (apoptosis initiation in certain cell types) while dramatically reducing susceptibility to protease degradation.

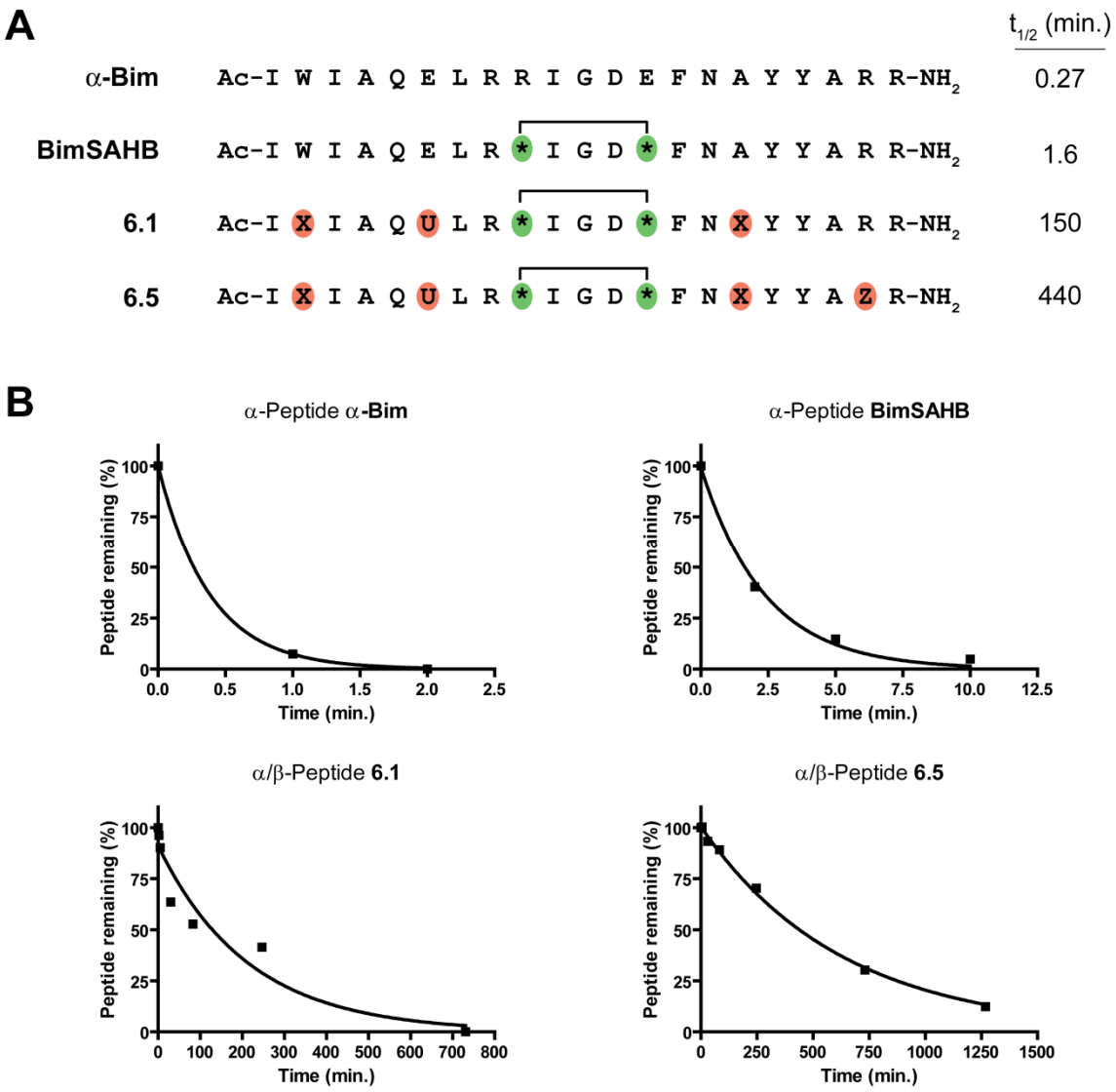

Figure 6.17 Susceptibility of 40 μM α- or α/β-peptide to 10 μg/mL proteinase K in TBS, pH 7.5 with 8% DMSO at room temperature. (A) Sequences of α- and α/β-peptides and associated half-life values. (B) Time course of α- or α/β-peptide degradation, as assessed by HPLC. Note the different scales on the horizontal axes.

6.6 Conclusions

Our group has previously shown that properly designed α/β-peptides, in which the peptidic backbone deviates from that of conventional peptides and proteins, are able to mimic analogous α-peptides structurally and functionally in terms of selective recognition of target proteins *in vitro*.[54-56] Furthermore, recent studies have shown that α/β-peptides can exhibit improved properties *in vivo* relative to analogous α-peptides, likely due to a decreased

susceptibility of the unnatural α/β backbone to proteolytic destruction.[57] However, the inability of most α- and α/β-peptides to cross cellular membranes has limited these compounds to extracellular targets for cellular and *in vivo* applications. The remarkable ability of the so-called "stapled" BH3 domain peptides (first reported by Walensky et al.) to penetrate cell membranes and initiate apoptosis[19, 26] led us to investigate whether α/β-peptide analogues of a hydrocarbon-crosslinked BH3 α-peptide could retain these interesting and useful characteristics.

To evaluate the impact of α→β-residue substitution on the activity of the α-peptide **BimSAHB**, we designed **6.1** using an α→β substitution pattern previously shown to be effective for mimicry of the Bim BH3 domain.[41] α/β-Peptide **6.1**, along with linear analogue **6.3** and an analogue bearing ACPC residues in place of the S5 residues (**6.4**), bound tightly to anti-apoptotic proteins (Figure 6.4), indicating that the α→β substitutions did not dramatically alter protein recognition (although **6.4** displayed reduced affinity for Bcl-xL and Bcl-2). α/β-Peptides **6.1**, **6.4**, and **6.6** all displayed activity similar to that of the prototype α-peptide **α-Bim** in promoting Bax/Bak-dependent cytochrome *c* release in membrane-permeabilized MEFs (Figure 6.7), indicating that each of these α/β-peptides can engage the apoptotic machinery in a cellular environment if the membrane barrier is removed. The crystal structures of **6.1** and **6.3** bound to Bcl-2 demonstrate that these α/β-peptides engage the BH3-recognition groove of the anti-apoptotic protein, making all of the expected side chain contacts to Bcl-2 (Figure 6.6).

When tested against a broad panel of non-cancerous and cancerous cell lines, **6.1** showed the same profile of activity as **BimSAHB**, efficiently killing U937 lymphoma cells while having negligible impact on the viability of the other cell lines tested (Figure 6.8). This very selective activity is consistent with the previous reports of **BimSAHB**[26, 40] and may be due to the high reliance on Mcl-1 for survival that is characteristic of acute myeloid leukemia cells such as

U937.[58] Both **6.1** and **BimSAHB** bind to Mcl-1 with high affinity (Figure 6.4). Live-cell confocal microscopy indicated that fluorescein-labeled analogues of **6.1**, **6.2**, and **6.3** were each able to enter U937 cells in a manner similar to the entry of fluorescein-labeled **BimSAHB** (Figures 6.15, 6.21, and 6.22). Our detailed viability studies indicated that the ability of **6.1** to kill U937 cells was dose-dependent, attenuated by caspase inhibitor Q-VD-OPh, and resulted in significant cell membrane blebbing and release of "apoptotic bodies", all consistent with the induction of apoptosis rather than an off-target cytotoxic effect (Figures 6.9 and 6.11). Furthermore, the release of cytochrome *c* from the mitochondria of unpermeabilized U937 cells is consistent with initiation of the apoptotic pathway by **6.1** (Figure 6.13). These data demonstrate that the on-target effects of **6.1** are in line with those documented in previous studies showing that stapled BH3 peptides, including **BimSAHB**, are able to initiate apoptosis in certain cell types.[19, 26, 40] Interestingly, at the 24 hour time point, the level of cell death that could be inhibited by Q-VD-OPh was significantly less than at the earlier time-points. This trend could indicate that the caspase inhibitor was "overwhelmed" due to the sustained apoptosis activation in the cells. An alternative explanation is that prolonged exposure of cells to the stapled (or non-stapled but S5-containing) peptides results in non-specific toxicity. This latter hypothesis is consistent with a recent report[59] showing that stapled helical α-peptides based on the N-terminal segment of p53 kill cells in a p53-independent manner because these peptides cause disruption of the plasma membrane, which leads to non-specific cell death at high peptide concentrations (>10 μM). Further studies will be required to establish whether either of these explanations accounts for the apparent non-caspase-dependent death after long-term exposure of U937 cells to the peptides discussed here.

Neither **BimSAHB** nor **6.1** demonstrated any significant killing activity toward MEFs, an observation that is consistent with previous reports regarding the effects of stapled BH3 peptides on these cells.[11, 26] These results are somewhat surprising given that: i) our binding assays showed that **6.1** and **BimSAHB** can engage both Mcl-1 and Bcl-x_L (the critical anti-apoptotic proteins in MEFs) with high affinity (Figure 6.4); ii) assays using permeabilized cells demonstrated that **6.1** can induce cytochrome *c* release in MEFs (Figure 6.7); and iii) live-cell imaging demonstrated that fluorescein-labeled analogues of both **BimSAHB** and **6.1** can enter these cells (Figure 6.16). One explanation for this lack of activity could be that the peptides do not reach the cytosol of MEF cells, and instead remain trapped within intracellular vesicles. This possibility is consistent with the punctate staining pattern revealed by our live-cell imaging of MEF cells. However, it is unclear why these peptides are able to enter the cytoplasm of U937 cells; the unique features that allow U937 cytoplasm entry merit further investigation. It is also unclear from our study why neither **BimSAHB** nor **6.1** caused toxicity toward other cancer cell lines tested (this behavior has been previously noted for **BimSAHB**).[40] One possibility is that the peptides become trapped within vesicles in these cells. A second possibility is that these peptides are not taken up via endocytosis in these cell types. A third possibility is that the peptides do not bind sufficiently tightly to the critical anti-apoptotic protein (e.g., Bcl-2) in these cell types.

Recent reports have highlighted examples of linear ("unstapled") analogues of stapled α-peptides that contain the S5 residue and manifest cell-killing activity.[40, 49] The experiments reported here are consistent with these precedents; we observe that the linear α-peptide **6.2** and the linear α/β-peptide **6.3** are able to enter cells (Figures 6.15 and 6.16) and initiate apoptosis in U937 cells (Figure 6.9). These results, together with the similar IC_{50} values displayed by pairs of

stapled and unstapled analogues (i.e., by **BimSAHB** and **6.2**, and by **6.1** and **6.3**) and the co-crystal structures of complexes formed by **6.1** or **6.3** with Bcl-2, suggest that the S5 residue is a critical determinant of biochemical and cellular activity, whether or not a covalent crosslink is formed. The role of this α,α-disubstituted α-amino acid residue could arise from the high intrinsic hydrophobicity and/or from the strong helix-promoting properties that are well-known for residues of this type, such as 2-aminoisobutyric acid (Aib).[60] Indeed, our CD data (Figure 6.5) show that the presence of two S5 residues leads to a significant enhancement in α-peptide helicity, even in the absence of a crosslink. The lack of cellular activity for **6.4**, which does not contain S5 residues, raises the possibility that some aspect of the α,α-disubstituted unit is important for cell entry. However, an alternative explanation for the lack of **6.4** activity is the low affinity of this α/β-peptide for some anti-apoptotic proteins (Figure 6.4), which is also reflected in this α/β-peptide's decreased ability to induce cytochrome *c* release in permeabilized MEFs relative to **6.1** (Figure 6.7).

One major motivation for the design of α/β-peptide analogues of α-helical α-peptides is to decrease susceptibility to proteolysis. Stapled α-helical α-peptides containing two S5 residues crosslinked by olefin metathesis are less prone to protease degradation relative to analogous non-stapled α-peptides containing only natural residues, presumably because of enhanced helicity conferred by introduction of the α,α-disubstituted S5 residues and the covalent crosslink.[16, 17, 19] The data presented here show that incorporating a small number of β-amino acid residues into the stapled α-peptide **BimSAHB** (to generate α/β-peptide **6.1**) leads to a much more pronounced protection from proteolysis than does introduction of the S5 α-residues and the staple alone (Figure 6.4). Thus, crosslinked α/β-peptides may be better suited for eventual *in vivo* applications than are crosslinked α-peptides. One caveat to these studies is that the incorporation of the S5

residue appears to result in a tendency for both α- and α/β-peptides to aggregate, as judged by CD experiments. This result is consistent with previous reports on α-peptides containing S5 residues.[61] Susceptibility to proteolysis is likely to be influenced by staple incorporation, by β-residue incorporation, and by aggregation, and it is not possible from our data to isolate the effect exerted by each of these factors. Nevertheless, the increase in protease resistance we observed for α/β-peptide **6.1** versus α-peptide **BimSAHB** is consistent with many prior reports from our groups involving α→β substitutions.[41, 54, 55, 62, 63] Other significant limitations of the stapling strategy, which we observed both for α-peptides and α/β-peptides, including low aqueous solubility, inactivation in the presence of serum, and activity toward only limited cell types, remain to be addressed.[17]

The success described in this chapter was ultimately achieved using α/β-peptide mimicry of a known cell-penetrating peptide, in contrast to the approach described in Chapter 5, in which we attempted to rationally incorporate cell-permeability into a previously designed α/β-peptide. The successful mimicry of **BimSAHB** by α/β-peptide **6.1** suggests that β-residue incorporation at certain positions can be tolerated without disrupting the ability of the S5 crosslink to impart cell-permeability to the resulting α/β-peptide. This is especially significant given the many examples in which seemingly benign sequence changes in stapled α-peptides completely abolished activity.[11, 17, 21, 25, 39]

I have described the design of an α/β-peptide analogue of a "stapled" α-helical α-peptide that structurally and functionally mimics the original stapled α-peptide and can kill one type of cancer cell by engaging anti-apoptotic protein targets. This report marks the first demonstration that an intracellular protein-protein interaction can be modulated by an α/β-peptide. Because α/β-peptides are less susceptible to proteolytic degradation than are their α-peptide analogues, stapled

α/β-peptides may be useful for probing the functional roles of specific protein-protein interactions in living cells. Ultimately such α/β-peptides might serve as starting points for the development of therapeutic agents. The results presented here show that backbone modification via periodic α→β-residue replacement can deliver oligomers that are highly resistant to proteolysis while retaining other desirable properties of the original α-peptide, particularly cell-permeability and specific protein recognition.

6.7 Future directions

In this chapter, I have described the design of a stapled α/β-peptide, **6.1**, which mimics the ability of the well-studied stapled α-peptide **BimSAHB** to enter U937 cells and initiate apoptosis. However, both of these peptides suffer from a number of disadvantages which would prevent their use *in vivo*, namely high insolubility and a lack of activity in the presence of serum. Future work in this area could work to address these limitations by redesigning either **BimSAHB** or **6.1**, possibly by introducing polar functional groups or residues, to decrease hydrophobicity. However, since hydrophobicity is certainly an important factor in cell permeability, any derivatives of these compounds will need to be carefully evaluated for efficacy in cell-based experiments.

The observation that the "unstapled" α- and α/β-peptide analogues **6.2** and **6.3** can also enter cells and initiate apoptosis reveals that the covalent crosslink is not essential for cellular activity. These results open up the intriguing possibility that we may be able to design a β-amino acid residue that recapitulates the remarkable properties of S5. However, the lack of activity for **6.6**, which contains two crosslinked 5E-APC residues in place of S5, suggests that such a novel residue may need to be relatively devoid of polar atoms. It is interesting to speculate that β^3-

norleucine, its five-carbon analogue (β^3-homonorleucine), or an analogue of ACPC bearing a linear alkyl chain may impart membrane permeability, based on these results.

The α/β-peptide **6.5** was significantly less susceptible to proteinase K degradation than was **6.1**, which contained one less cyclic β-residue (Figure 6.17). However, **6.5** was also less active in inducing apoptosis in U937 cells compared to **6.1**. Because **6.5** differs from **6.1** only in an Arg20→APC substitution, this difference in cellular activity may reflect the important role that guanidinium groups play in the association of peptides with membranes.[50, 51] Based on this, I hypothesize that substitution of Arg20 with an APC analogue bearing a guanidinium functional group[52] may result in an α/β-peptide that retains cellular activity while providing even greater resistance to protease degradation.

Ultimately, the most important result from this chapter is the demonstration that the α/β-peptide mimicry strategy developed by our group is compatible with another commonly used structural modification, side chain crosslinking, to provide synergistic benefits. This result demonstrates that careful placement of β-residues can be well-tolerated in a variety of contexts, despite the unnatural backbone. This opens up further possibilities for introducing α→β-residue substitutions in other highly modified peptides (e.g., other crosslinked peptides, backbone cyclized peptides, etc.) to produce α/β-peptides with significantly enhanced properties.

6.8 Experimental methods

6.8.1 General

NovaPEG Rink Amide resin was purchased from Novabiochem (855047). Fmoc-protected α-amino acids, benotriazole-1-yl-oxy-pyrrolidino-phosphonium hexafluorophosphate (PyBOP), and O-(7-Azabenzotriazol-1-yl)-N,N,N',N'-tetramethyluronium hexafluorophosphate

(HATU) were purchased from Chem-Impex International and Novabiochem. Fmoc-ACPC-OH was purchased from Chem-Impex International. Fmoc-APC(Boc)-OH was synthesized as previously reported.[64] Fmoc-sAPC(tBu)-OH was synthesized as described previously.[41] (S)-N-Fmoc-α-(4-Pentenyl)alanine (Fmoc-S5-OH) was purchased from Nagase & Co. (365023) and from Sigma-Aldrich (F6312). All other solvents and reagents used for peptide synthesis were purchased from Fisher Scientific or Sigma-Aldrich.

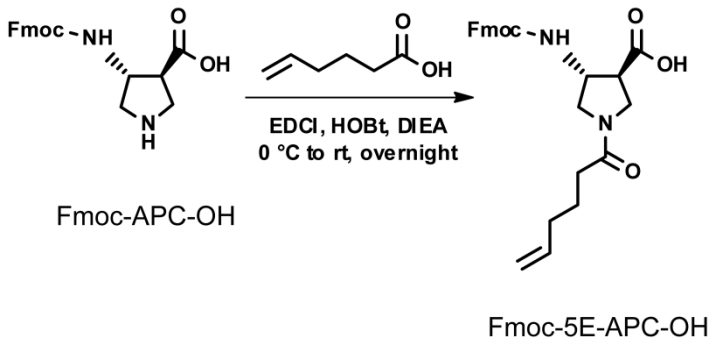

Figure 6.18 Scheme for the synthesis of Fmoc-5E-APC-OH.

The synthesis of 5E-APC was performed by dissolving Fmoc-APC-OH (no side chain Boc group; 1 eq.) in dichloromethane (DCM), followed by the addition of 5-hexenoic acid (1.1 eq.) pre-activated with 1.1 eq. of 1-Ethyl-3-(3-dimethylaminopropyl)carbodiimide (EDCI), 1.1 eq. of 1-hydroxybenzotriazole (HOBt), and 6 eq. of N,N-diisopropylethylamine (DIEA) while the reaction vessel was cooled in an ice bath (Figure 6.18). The reaction mixture was allowed to slowly warm from 4 °C → room temperature overnight. The solvent was removed from the reaction mixture, and the crude product was redissolved in ethyl acetate with a small amount of methanol and then purified on silica gel by column chromatography (7:3 ethyl acetate/hexane + 2.5% acetic acid). After purification by column, the product was dissolved in ethyl acetate and washed with sat. sodium bicarbonate, dried over magnesium sulfate, and the solvent was removed by rotary evaporation. Figure 6.19 shows the ^{1}H-NMR spectrum (panel A), and

ESI/EMM mass spectra (panel B) for 5E-APC. Synthesis and data collection for this compound were performed by undergraduate student Timothy Choi (Gellman Laboratory, University of Wisconsin-Madison).

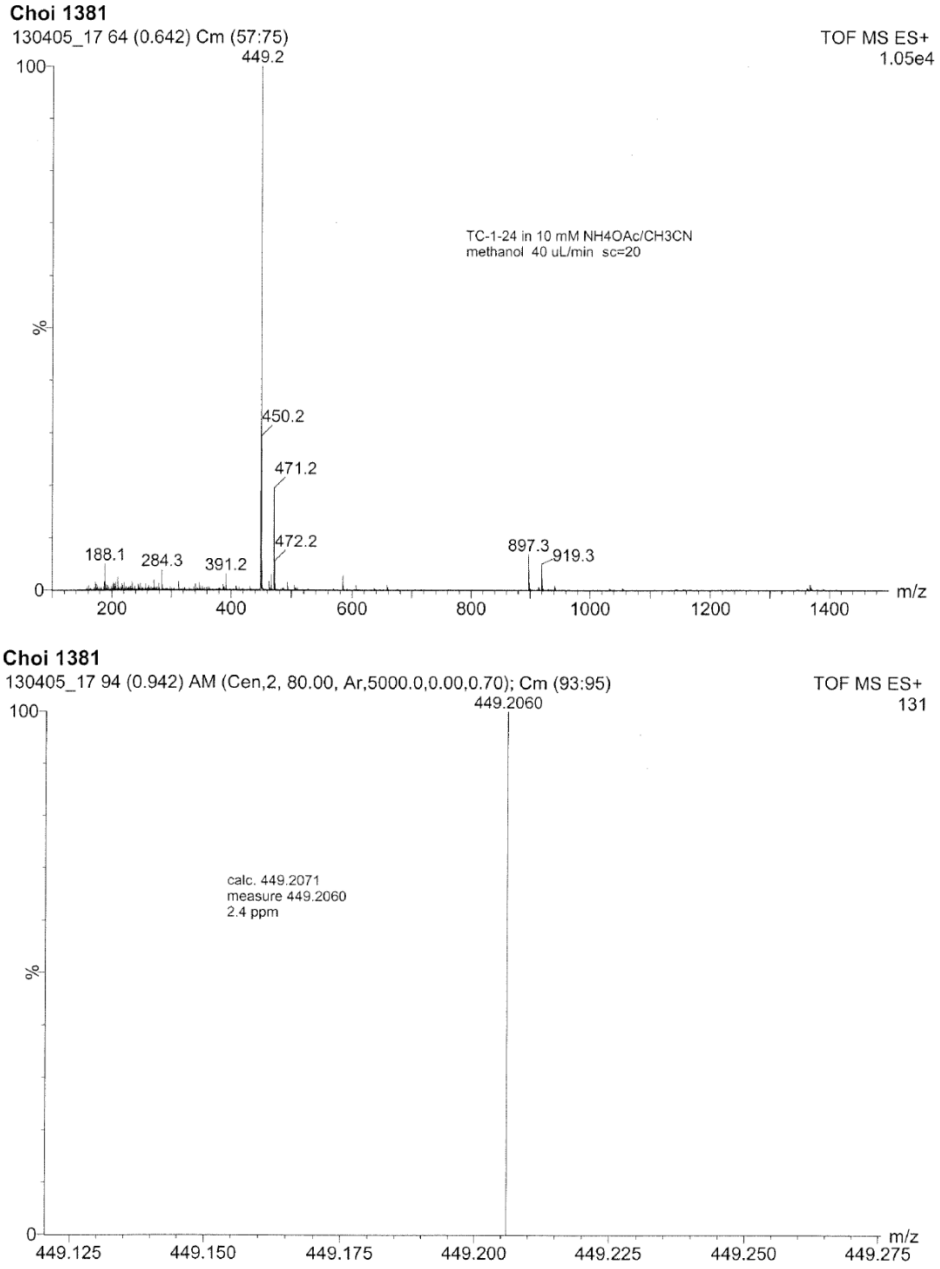

Figure 6.19 (A) Mass spectra for 5E-APC. The top panel shows ESI data, while the bottom panel shows EMM data. Calculated (calc.) and measured $[M+H]^+$ monoisotopic masses are displayed on the spectrum for EMM. (B, below) ^{1}H-NMR spectrum in D4-methanol of 5E-APC.

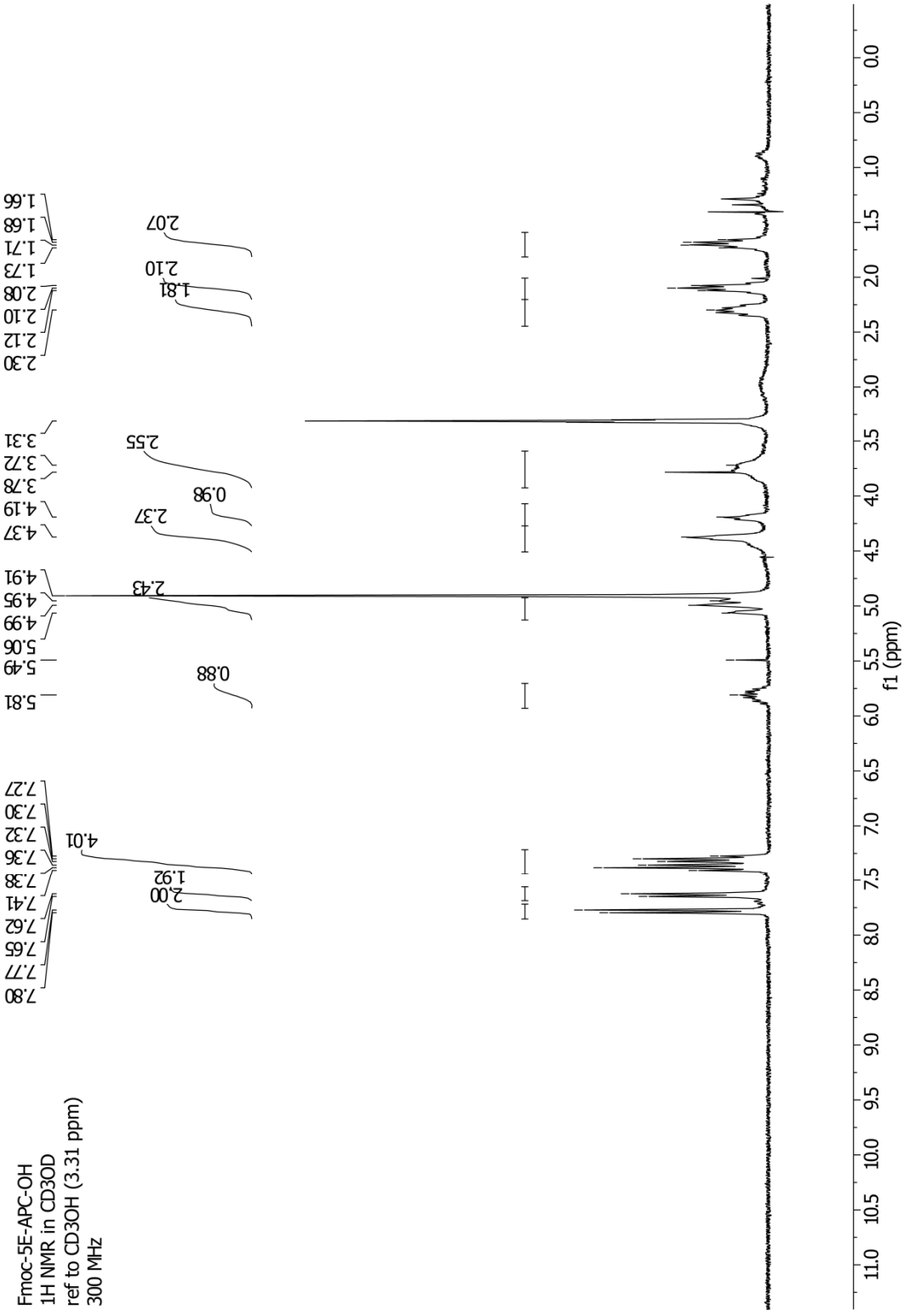
Fmoc-5E-APC-OH
1H NMR in CD3OD
ref to CD3OH (3.31 ppm)
300 MHz
7.80
7.77
7.65
7.62
7.41
7.38
7.36
7.32
7.30
7.27
5.81
5.49
5.06
4.99
4.95
4.91
4.37
4.19
3.78
3.72
3.31
2.30
2.12
2.10
2.08
1.73
1.71
1.68
1.66
4.01
2.00
1.92
0.88
2.43
2.37
0.98
2.55
1.81
2.10
2.07
f1 (ppm)

6.8.2 Peptide synthesis and purification

α-Peptides and α/β-peptides were synthesized by microwave assisted solid phase peptide synthesis on NovaPEG Rink Amide resin, as previously described.[65] Fmoc-protected amino acids (with standard compatible side chain protecting groups) were activated with a solution of PyBOP, 0.1 M HOBt, and DIEA in 1-methyl-2-pyrrolidone (NMP) and added to the resin. Coupling reactions were irradiated by microwave to 70 °C for 6 minutes (2 minute ramp, 4 minutes hold) with a 5 minute cooldown (for α-residues) or for 14 minutes (2 minute ramp, 12 minute hold) with a 5 minute cooldown (for S5, residues after S5 residues, and cyclic β-residues). In some syntheses, Arg8 (which is coupled after an S5 residue) was double-coupled with either PyBOP or HATU to improve yield. Fmoc deprotection reactions were carried out with a solution of 20% piperidine in N,N-dimethylformamide (DMF), irradiated by microwave at 80 °C for 4 minutes (2 minute ramp, 2 minute hold). After completion of the linear chain, oligomers that were not fluorophore-labeled were acetylated by stirring the resin in a solution of 8:2:1 DMF:DIEA:acetic anhydride for about 10 minutes at room temperature. For oligomers labeled with 6-carboxyfluoroscein (6-FAM), resin was treated with 4 equivalents 6-FAM (AnaSpec AS-81004) under the above coupling conditions at room temperature overnight, protected from light. For oligomers containing crosslinked S5 residues, olefin metathesis was carried out on resin using a solution of ~10 mM Grubbs Catalyst, 1st Generation (Sigma, 579726) in dichloroethane (DCE) with stirring and bubbling nitrogen for 1-3 hours.[66] Reaction progress could be monitored by MALDI-TOF, and the reaction was repeated until the majority of the product was crosslinked, as assessed by MALDI-TOF. Once the oligomer had been fully assembled on resin, peptides and α/β-peptides were cleaved using a solution of 95% trifluoroacetic acid (TFA), 2.5% water, 2.5% triisopropylsilane (TIS), concentrated under a

stream of nitrogen, and then precipitated with cold diethyl ether. Crude peptide mixtures were then purified by reverse-phase HPLC. After purification, final peptide purity was assessed by analytical HPLC and identity was confirmed by MALDI-TOF-MS ("Peptide characterization" section below).

6.8.3 Recombinant protein expression and purification

Recombinant Bcl-2 anti-apoptotic proteins with N- and/or C-terminal truncations for binding studies (Bcl-2ΔC22, Bcl-x_LΔC24, Mcl-1ΔN170ΔC23) were expressed and purified as described previously for hexahistidine tagged proteins (in the case of Bcl-2)[67] or GST tagged proteins (in the case of Bcl-x_L and Mcl-1).[46] The human Bcl-2 construct (Bcl-2ΔC32ΔLoop) used for crystallization was identical to that reported previously for structural studies.[68] This construct has the large unstructured loop between residues 35-91 replaced with residues 35-50 of Bcl-x_L. The C-terminal 32 residues corresponding to the hydrophobic transmembrane domain were also deleted to improve protein solubility. The protein was expressed as a GST fusion protein from a pGEX6P3 vector, and purified using a combination of glutathione-affinity chromatography followed by gel-filtration chromatography.

6.8.4 Surface plasmson resonance (SPR) competition assays

Solution competition assays were performed using a Biacore 3000 instrument exactly as described previously.[69]

6.8.5 Circular dichroism

CD measurements were carried out in purified water using an Aviv Model 420 circular dichroism spectrometer. Solutions of α- and α/β-peptides were prepared in pure water, briefly sonicated, and then centrifuged to remove insoluble oligomer. Attempts to collect CD spectra in

PBS and several other aqueous buffers failed due to insolubility of peptides containing the S5-residue. Oligomer concentration in solution was determined by measuring the UV absorbance at 280 nm, using the extinction coefficient calculated based on the number of tryptophan (ε_{280} = 5690 M^{-1} cm^{-1}) and tyrosine (ε_{280} = 1280 M^{-1} cm^{-1}) residues in the primary sequence.[70] Spectra were collected in a quartz cuvette (0.1 cm or 1 cm) at 20°C with a wavelength step size of 1 nm and a 10 second averaging time. Spectra units were normalized to mean residue ellipticity, [θ] (deg cm^2 $dmol^{-1}$ res^{-1}), using the concentration determined by UV absorbance to account for slight variations, using the Equation (1),[71] described below:

(1) $[\theta] = \theta/(l * c * \#res)$

Where:
θ = blank-corrected ellipticity value from CD spectrometer (in mdeg)
l = pathlength (in mm)
c = concentration of peptide (in M)
#res = the number of residues in the peptide

The mean residue ellipticity values ([θ]) obtained were then multiplied by 10^{-3} for plotting in the graphs shown in this chapter.

Figure 6.20 shows CD data for several α- and α/β-peptides described in this chapter.

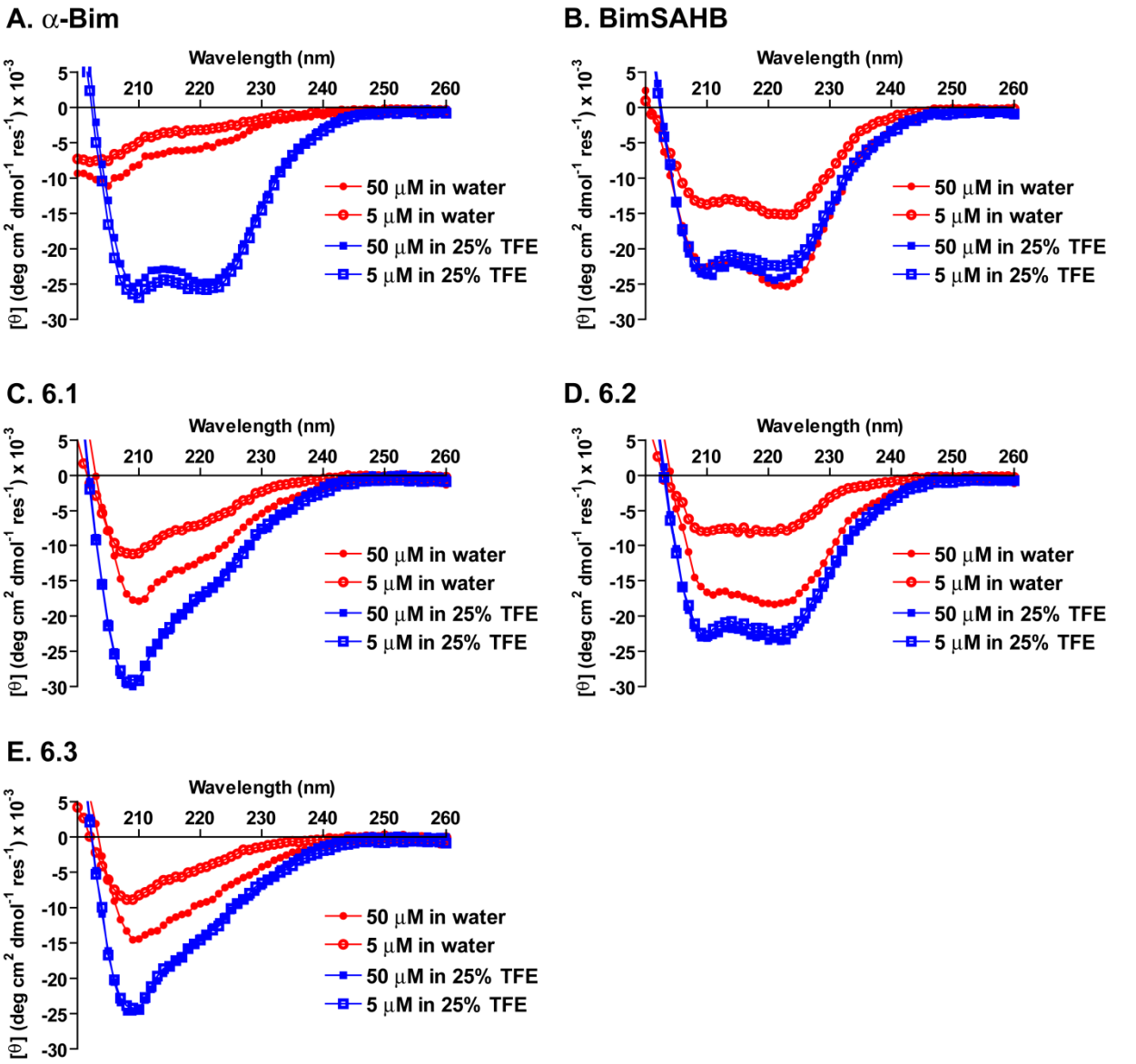

Figure 6.20 (A-E) Far-UV circular dichroism spectra for α- and α/β-peptides at 50 μM or 5 μM in pure water (red) or 25% trifluoroethanol (TFE) in water (blue). Solutions at approximately 50 μM were prepared in the indicated solvent, with the exact concentration determined by UV-absorbance at 280 nm. For each oligomer, the CD spectrum was first taken at 50 μM in a 0.1 cm cuvette, then that sample removed and diluted 10-fold in the indicated solvent to 5 μM and a second spectrum obtained in a 1 cm cuvette. All oligomers containing the S5 residue (panels B-E) show concentration dependence on CD signal in water, but not in 25% TFE.

6.8.6 Crystallography

Crystals were obtained by mixing Bcl-2ΔC32ΔLoop with each peptide at a molar ratio of 1:1.3 and then concentrating the sample to 10 mg/mL. Crystallization trials were performed at the Bio21 Collaborative Crystallization Centre. All crystals were grown by the sitting drop

method at room temperature. For the **6.1**:Bcl-2 structure, the crystals were grown in 20 mM $CaCl_2$, 0.1 M sodium MOPS pH 7.0, 10% (v/v) 2-propanol. For the **6.3**:Bcl-2 structure, the crystals were grown in 0.1 M $CaCl_2$, 0.1 M MES pH 6.5, 20% (v/v) ethanol. Prior to cryo-cooling in liquid N_2, crystals were equilibrated into cryoprotectant consisting of reservoir solution containing 15% (v/v) ethylene glycol. Crystals were mounted directly from the drop and plunge-cooled in liquid N_2.

6.8.7 Crystal diffraction data collection and structure determination

Diffraction data were collected at 100 K at the Australian Synchrotron MX2 beamline (Victoria, Australia) (wavelength for both structures was 0.9537 Å). The diffraction data were integrated and scaled with XDS.[72] The structure was obtained by molecular replacement with PHASER[73-75] using the crystal structure of the Bcl-2:Bax BH3 complex (PDB code 2XA0)[47] with the BH3 peptide removed as the search model. Multiple rounds of building in COOT[76] and refinement in PHENIX[77] led to the final model.

Data Set	α/β-1:Bcl-2 (PDB: 5AGW)	α/β-1-LIN:Bcl-2(PDB: 5AGX)
Crystal Parameters		
Space group	P43 21 1	P43 21 1
Unit Cell Parameters		
a, b, c (Å)	87.673, 87.673, 107.48	86.054, 86.054, 108.739
α, β, γ (°)	90.0, 90.0, 90.0	90.0, 90.0, 90.0
Data Collection		
Wavelength (Å)	0.9537	0.9537
Resolution (Å)	33.97-2.695 (2.791-2.695)	40.01-2.24 (2.32-2.24)
R_{merge}	0.1031 (2.067)	0.07313 (0.7821)
I/σ(I)	18.29 (1.038)	29.20 (3.89)
Completeness (%)	99.83 (98.27)	99.91 (99.25)
Redundancy	13.4 (9.3)	14.2 (14.0)
$CC_{1/2}$	0.999 (0.452)	1 (0.894)
No. of copies/a.s.u.	2	2
Temperature	100 K	100 K
Refinement		
Resolution (Å)	33.969-2.695 (2.965-2.694)	40.009-2.24 (2.358-2.240)
No. of reflections R_{work}	12081 (2764)	20250 (2665)
No. of reflections R_{free}	603 (145)	1013 (140)
R_{work}	0.2015 (0.3484)	0.1878 (0.2792)
R_{free}	0.2719 (0.4234)	0.2447 (0.3894)
No. of atoms		
Protein	2491	2627
Ligand	68	68
Solvent	6	44
R.M.S. Deviations		
Bond lengths (Å)	0.009	0.007
Bond angles (°)	1.274	1.105
Chiral ($Å^3$)	0.050	0.042

Table 6.1 Crystallographic data collection and refinement statistics. Values in parentheses represent statistics for highest resolution shell.

6.8.8 Cytochrome c release assays

Cytochrome *c* release assays with digitonin-permeabilized MEFs were performed as described previously.[69] For the cytochrome *c* release assay with the unpermeabilized U937 cells, $2x10^6$ cells were treated with peptides (10 μM) for 3 hours at 37 °C before pelleting by centrifugation. Cell pellets were then resuspended in digitonin-containing lysis buffer (20 mM HEPES pH 7.2, 100 mM KCl, 5 mM $MgCl_2$, 1 mM EDTA, 1 mM EGTA, 250 mM sucrose, 0.05% (w/v) digitonin (Calbiochem) supplemented with protease inhibitors (Roche)) for 45 minutes at 30 °C to permeabilize the plasma membrane, then pelleted again. The supernatant was retained (soluble fraction) and the pellet resuspended in cell-lysis buffer (20 mM Tris pH 7.4, 135 mM NaCl, 1.5 mM $MgCl_2$, 1 mM EDTA, 1% (v/v) Triton X-100, 10% (v/v) glycerol supplemented with protease inhibitors (Roche)) and incubated on ice for 1 hour before centrifugation. This supernatant was then retained as the pellet fraction. Both soluble and pellet fractions were subsequently analyzed by Western blotting using an anti-cytochrome *c* antibody (BD Biosciences, clone 7H8.2C12).

6.8.9 Cell killing assays

U937 and adherent cancer cells (MDA-MB-231, MDA-MB-468, LIM-2405, SW480 and A549) were maintained in RPMI medium supplemented with 10% (v/v) fetal bovine serum (FBS). MEFs were maintained in FMA medium (DME KELSO medium supplemented with 10% (v/v) FBS, 250 μM L-asparagine and 50 μM 2-mercaptoethanol). Cell killing assays were performed similarly to those described previously for testing stapled peptides.[26] U937 cells were aliquoted ($1x10^4$ cells in 50 μL) into 96-well opaque plates and incubated with serial dilutions of peptides or DMSO (+/- 50 μM Q-VD-OPh) in serum-free RPMI medium for 2 hours, followed by addition of 50 μL RPMI containing 20% FBS (final concentration FBS 10% (v/v) in 100 μL).

Cells were incubated for a further 0, 4, or 22 hours prior to addition of CellTiter-Glo chemiluminescence reagent (for a total time of 2, 6, or 24 hours incubation with peptide) and luminescence measured on Lumistar Optima (BMG Labtech) microplate reader. For assays using adherent cells, cells were plated in their respective media described above ($1.5x10^3$ cells/well) then 24 hours later were washed with the corresponding serum-free media prior to addition and incubation with the peptides, DMSO and Q-VD-OPh, as for the U937 cells.

6.8.10 Analysis of cell killing by live-cell confocal microscopy

Stock solutions of fluorescein-labeled peptides were prepared in DMSO. Concentration of DMSO stock solutions were determined by diluting into 10 mM Tris, pH 8.0 and measuring UV absorbance, using an extinction coefficient for fluorescein of ε_{494} = 68,000 M^{-1} cm^{-1}.

U937 cells (ATCC, CRL-1593.2) were maintained in medium containing RPMI-1640 (HyClone, SH30027.01) supplemented with 10% (v/v) FBS (Gibco), 10,000 units/mL Penicillin and 10,000 µg/mL Streptomycin (P/S) (HyClone, SV30010), 1 mM sodium pyruvate (HyClone, SH30239.01), and 10 mM HEPES pH 7.4 (Fisher). On the day of experiments, U937 cells (passage 2-4) were pelleted at 200 x g for 5 minutes and washed twice in U937 serum-free media (U-SFM), containing RPMI-1640 without phenol red (HyClone, SH30605.01) and supplemented with P/S and L-glutamine (HyClone, SH30034). After the final wash in U-SFM, U937 cells were pelleted, resuspended in U-SFM, counted, and added to loosely-capped conical tubes at $5x10^5$ cells in 10 mL containing 1% (v/v) DMSO with or without 2 µM peptide for 3 hours at 37°C and 5% CO_2 (normal culture conditions). After 2.5 hours of incubation, Hoechst 33342 (Invitrogen) was added to each tube at 0.1% (v/v) and incubated for 20 minutes under normal culture conditions. Subsequently, wheat germ agglutinin-Alexa Fluor 488 conjugate (WGA488) (Life Technologies) was added to each tube at 5 µg/mL, and the mixture was incubated for 10 minutes

at 4°C. Subsequently, U937 cells were pelleted at 200 x g for 5 minutes and washed three times with U-SFM. After the final wash, U937 cells were resuspended in 1 mL of U-SFM and plated in a coverslip-bottom 24 well plate (Greiner Bio) for imaging.

Adherent MEFs (isolated using standard protocol from WiCell) were maintained in MEF Growth Medium (M-GM) containing DMEM (CellGro, 50-003-PB) supplemented with 10% (v/v) FBS, MEM non-essential amino acids (NEAA) (Gibco, 11140-076), P/S, and sodium bicarbonate (Acros). On the day before experiments, MEFs (passage 1) were dissociated with 0.05% Trypsin (HyClone SH30236), pelleted as above, resuspended in M-GM, counted, and seeded at $2x10^4$ cells/cm^2 in coverslip-bottomed 24 well plates with M-GM. On the day of experiments, MEFs were washed thrice with MEF serum-free medium (M-SFM) containing DMEM without phenol red (CellGro, 90-013-PB) and supplemented with sodium pyruvate, L-glutamine, NEAA, P/S, and sodium bicarbonate. Subsequently, MEFs were incubated in 1 mL of M-SFM with 1% (v/v) DMSO with or without 2 μM of peptide for 3 hours under normal culture conditions. Hoechst and WGA488 were added to each well at the times, concentrations, and temperatures specified above. After staining, wells were aspirated, washed three times in M-SFM, and filled with 1 mL of M-SFM for imaging.

After treatment under the conditions indicated in the Figures, U937s and MEFs were washed and then imaged using an inverted Eclipse Ti-E A1R-Si laser scanning confocal microscope (Nikon) equipped with Plan Apo 10x DIC L, Plan Apo VC 20x DIC N2, and Plan Apo VC 60x Oil DIC N2 objectives, a 1.5x optical zoom, lasers for 405 nm (blue), 488 nm (green), and 561/594 nm (red) wavelengths, a dichroic mirror (405/488/561/640), filters for 450/50 nm, 525/50 nm, and 595/50 nm wavelengths, a galvano scanning head, and a computer running NIS Elements software. U937 cells were imaged at 10x and at 60x (with 1.5x magnifier)

with lasers for blue, green, and red. MEFs were imaged at 60x with lasers for blue, green, and red. Images were collected using 4x averaging, 6.4 ms dwell, and 1024x1024 image size. Images were brightness-adjusted uniformly across conditions at a given magnification using NIS Elements v4.1 software (Nikon).

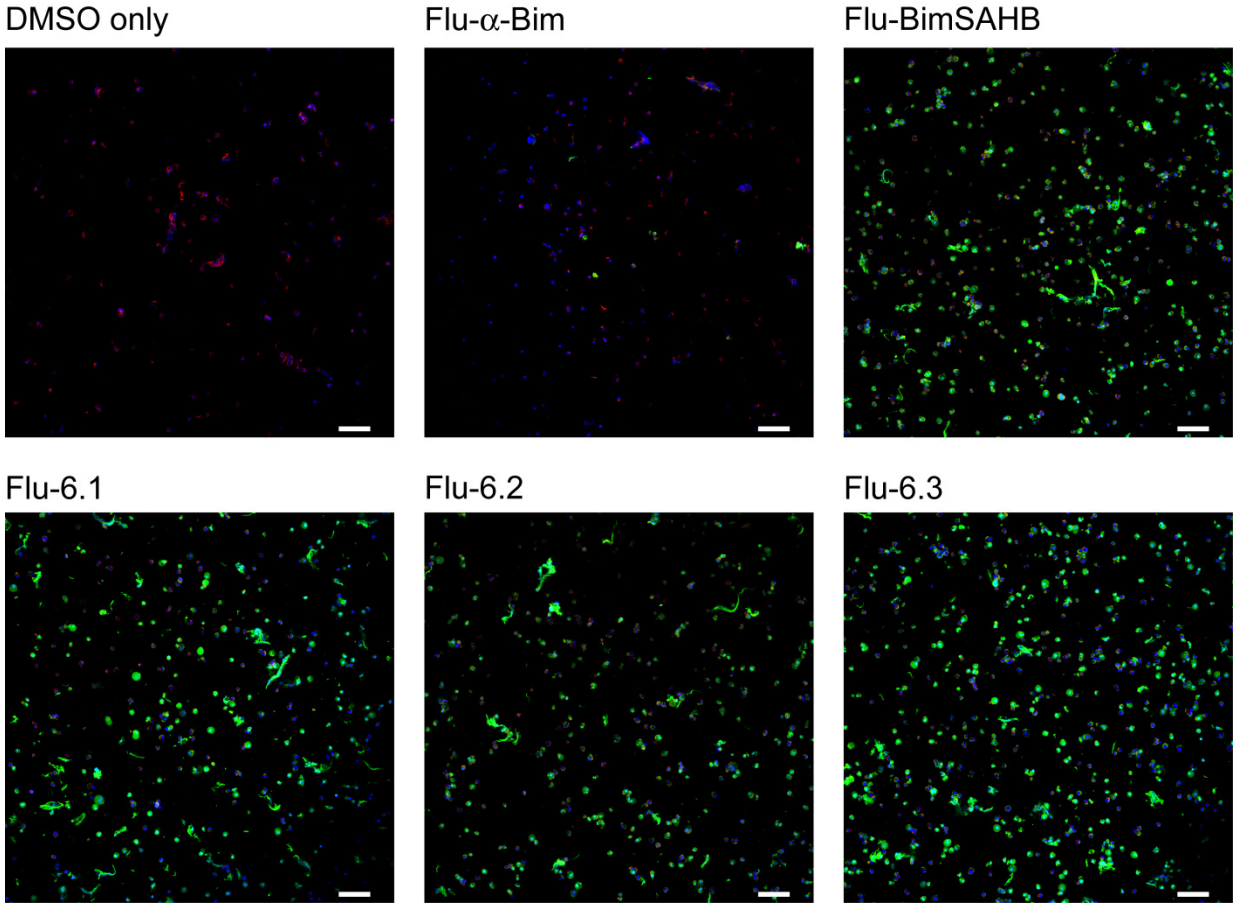

Figure 6.21 Analysis of U937 cellular uptake of fluorescein (Flu)-labeled analogues of α- and α/β-peptides by live cell confocal microscopy. Cells were treated with 2 μM of the indicated α- or α/β-peptide in serum-free media for 3 hours prior to imaging. Images were obtained under 10x magnification, showing the channels for green (fluorescein, peptide), red (WGA488 outer membrane stain), and blue (Hoescht 33342, nuclear stain). Scale bars represent 100 μm.

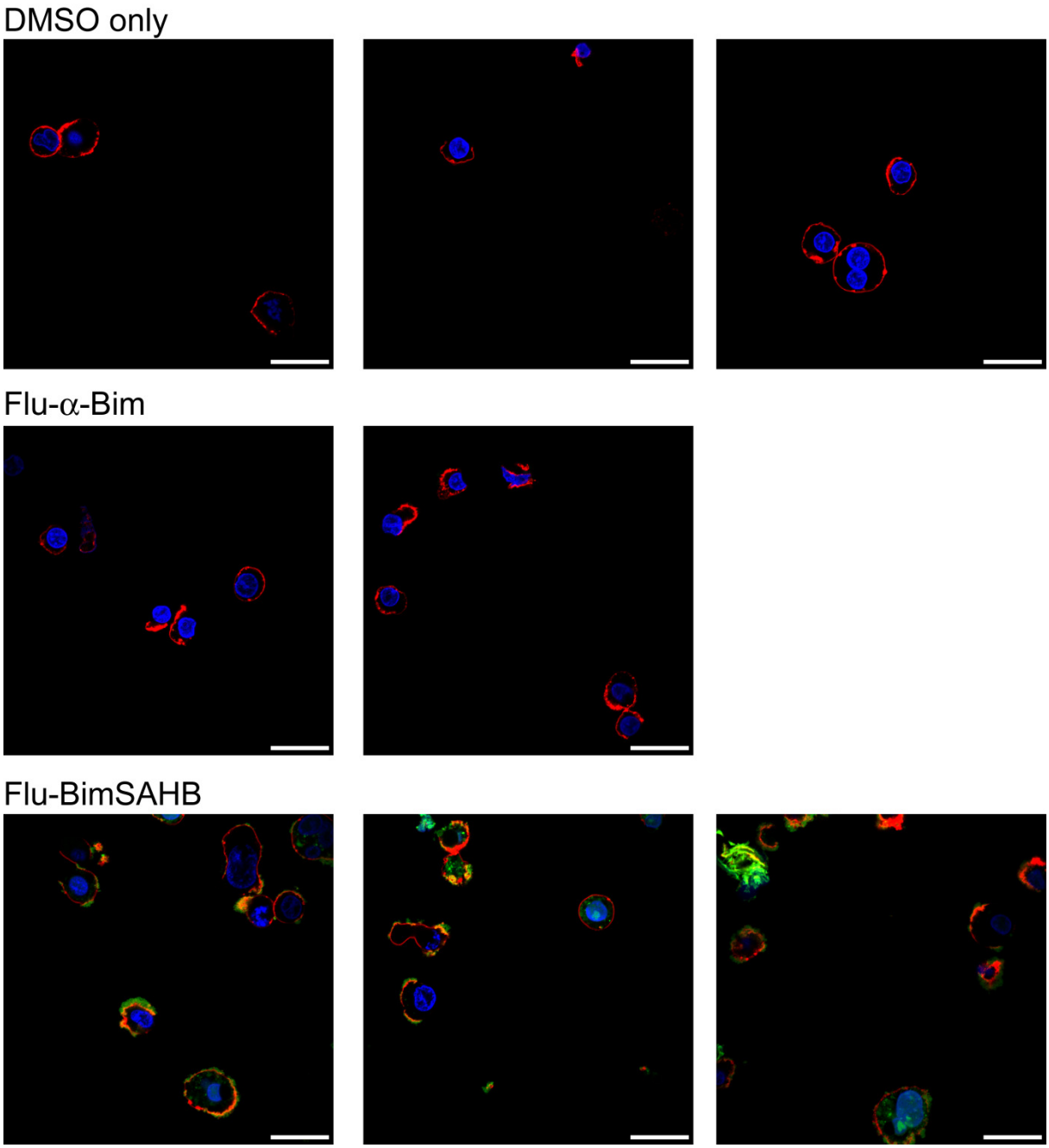

Figure 6.22 (A) Analysis of U937 cellular uptake of fluorescein (Flu)-labeled analogues of α- and α/β-peptides (or DMSO control) by live cell confocal microscopy. Cells were treated with 2 μM of the indicated α- or α/β-peptide in serum-free media for 3 hours prior to imaging. Images were obtained under 90x magnification, showing the channels for green (fluorescein, peptide), red (WGA488, outer membrane stain), and blue (Hoescht 33342, nuclear stain). Scale bars represent 25 μm.

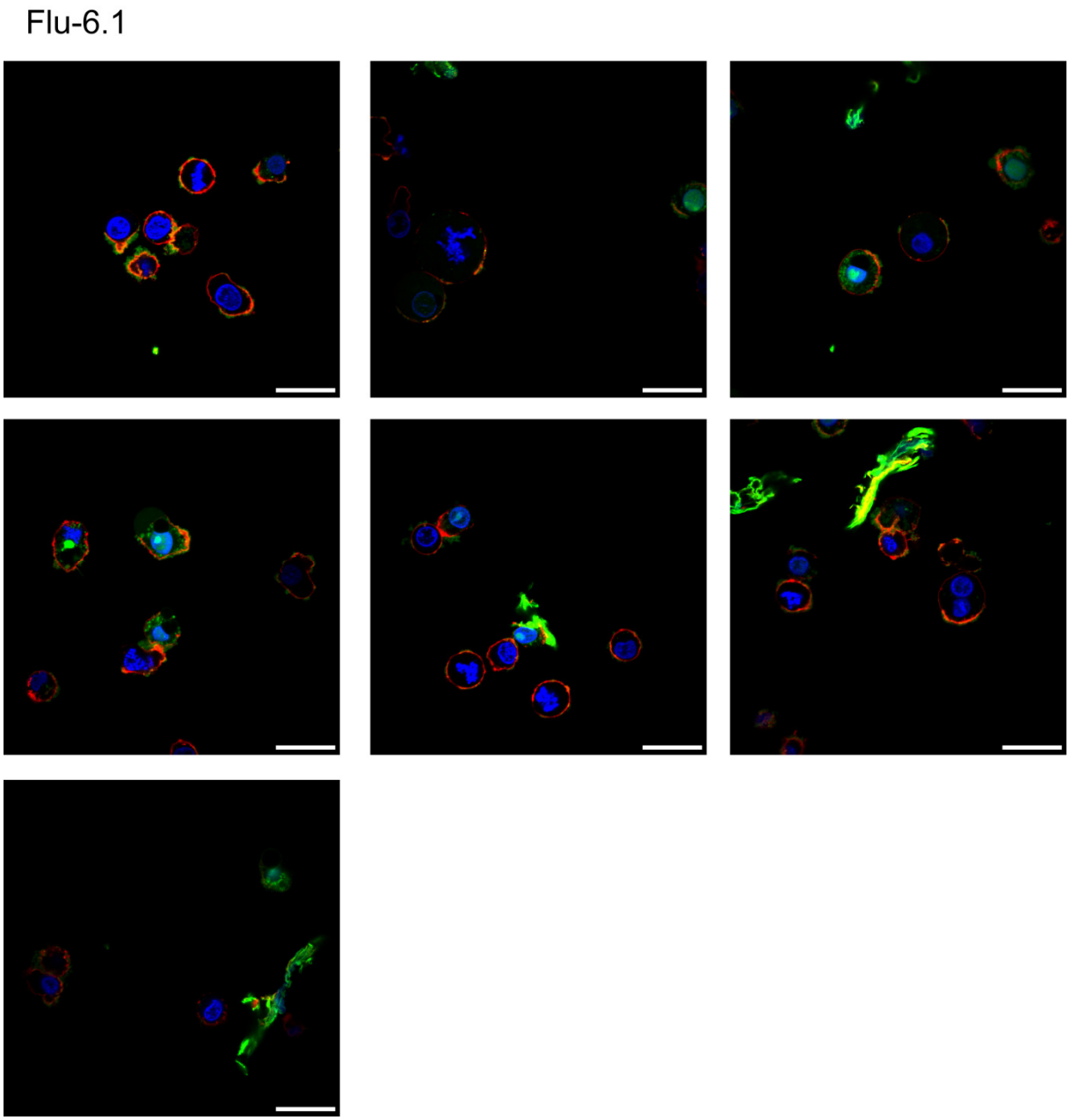

Figure 6.22 (B) Analysis of U937 cellular uptake of **Flu-6.1**. Cells were treated with 2 μM of **Flu-6.1** in serum-free media for 3 hours prior to imaging. Images were obtained under 90x magnification, showing the channels for green (fluorescein, peptide), red (WGA488, outer membrane stain), and blue (Hoescht 33342, nuclear stain). Scale bars represent 25 μm.

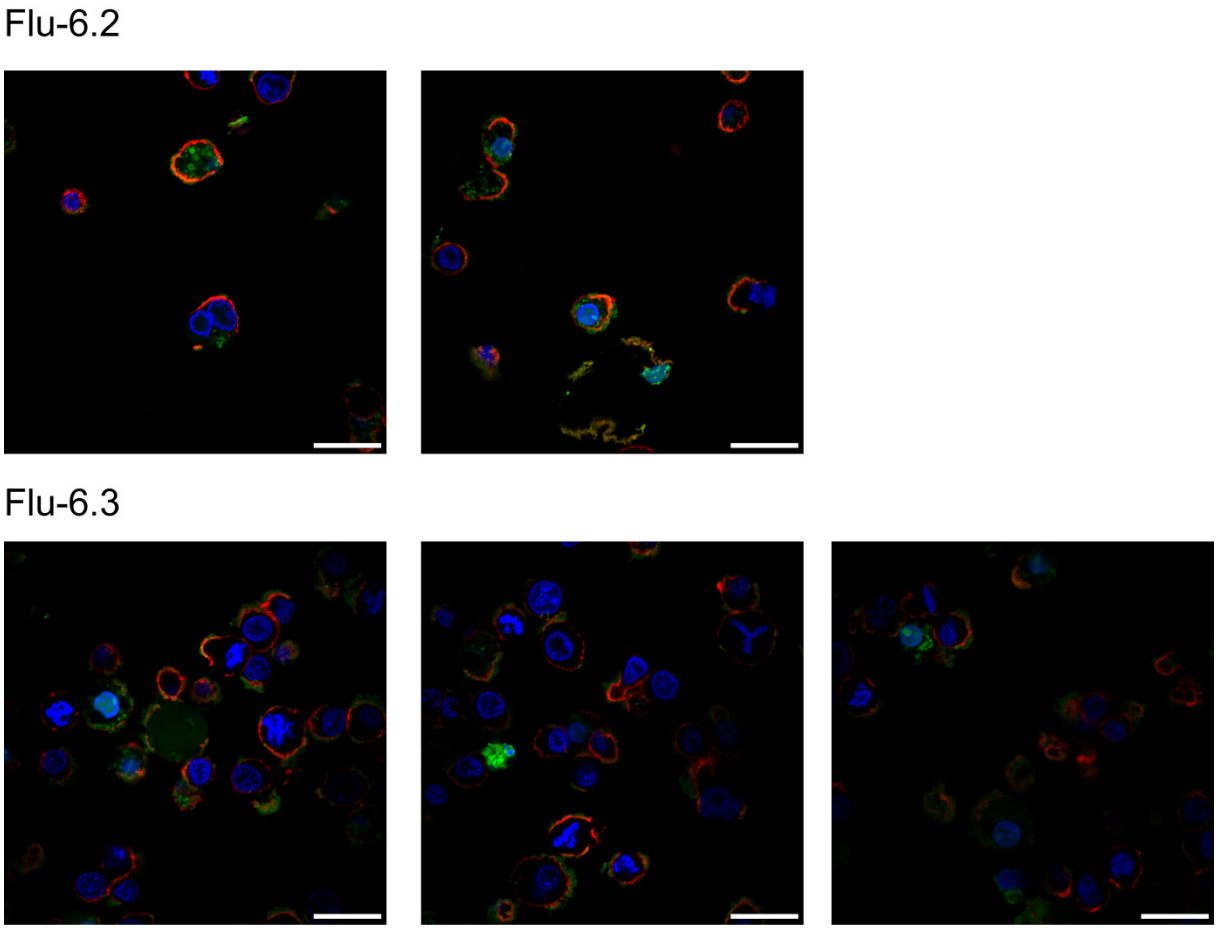

Figure 6.22 (C) Analysis of U937 cellular uptake of fluorescein (Flu)-labeled analogues of α- and α/β-peptides (or DMSO control) by live cell confocal microscopy. Cells were treated with 2 μM of the indicated α- or α/β-peptide in serum-free media for 3 hours prior to imaging. Images were obtained under 90x magnification, showing the channels for green (fluorescein, peptide), red (WGA488, outer membrane stain), and blue (Hoescht 33342, nuclear stain). Scale bars represent 25 μm.

6.8.11 Protease susceptibility assay

Stock solutions of ~100 μM peptide or α/β-peptide in water with 10% DMSO (for solubility) were prepared, as determined by UV-absorbance at 280 nm.[70] Solutions were then diluted in 10% DMSO/water to 50 μM and a solution of 50 μg/mL proteinase K in TBS (50 mM Tris pH 7.5, 200 mM NaCl) was added to give final concentrations = 40 μM peptide, 10 μg/mL proteinase K in 10 mM Tris, 40 mM NaCl, 8% DMSO. Protease reactions were allowed to proceed at room temperature and each reaction was run in duplicate. At each time point, 50 μL of the reaction was quenched with 125 μL of 1:1 water/acetonitrile + 1% TFA. The resulting

quenched solution (125 μL) was injected onto analytical HPLC. The amount of relative remaining oligomer at each time point was determined by integration of the peak at 220 nm in the resulting chromatogram. Half-lives were determined by plotting the amount of peptide remaining versus reaction time and fitting the data to an exponential decay model in GraphPad Prism 4.0.

6.8.12 Peptide characterization

α-Peptide and α/β-peptide purity after purification was assessed by analytical scale reverse-phase HPLC, using solvent A: H_2O with 0.1% TFA, solvent B: acetonitrile with 0.1% TFA, with a flow rate of 1 mL/min (unless otherwise specified). The solvent gradient for each peptide is specified in each panel. HPLC chromatograms at 220 nm are shown at the top of each panel. Peptide identity was confirmed by MALDI-TOF-MS, shown at the bottom of each panel. For each MALDI-TOF spectrum, the monoisotopic $[M+H]^+$, *m/z* is labeled.

α-Bim

HPLC: Gradient = 10-90% solvent B over 80 minutes

MALDI-TOF: Calculated monoisotopic $[M+H]^+ = 2681.4$

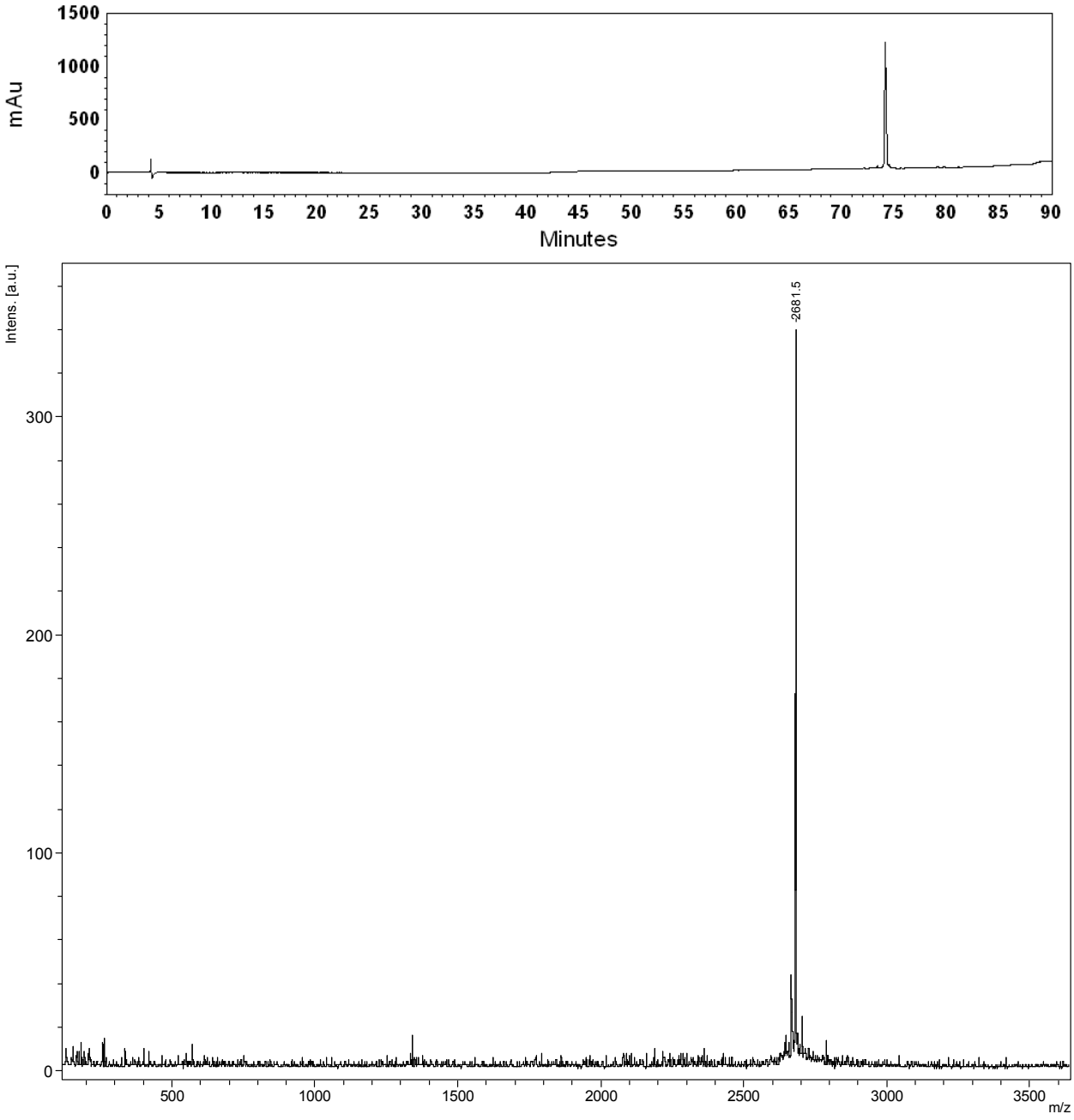

BimSAHB

HPLC: Gradient = 10-75% solvent B over 65 minutes

MALDI-TOF: Calculated monoisotopic $[M+H]^+$ = 2646.4

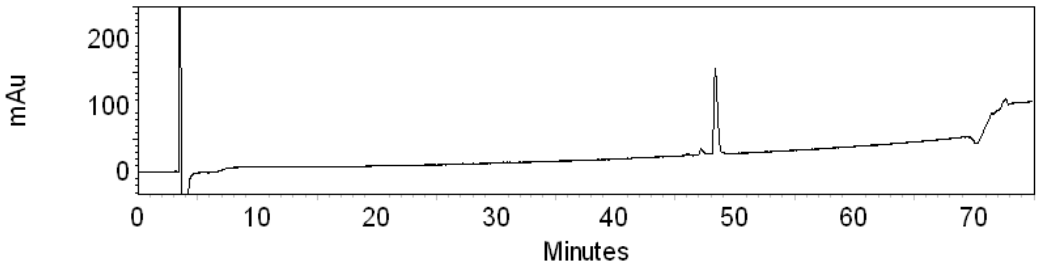

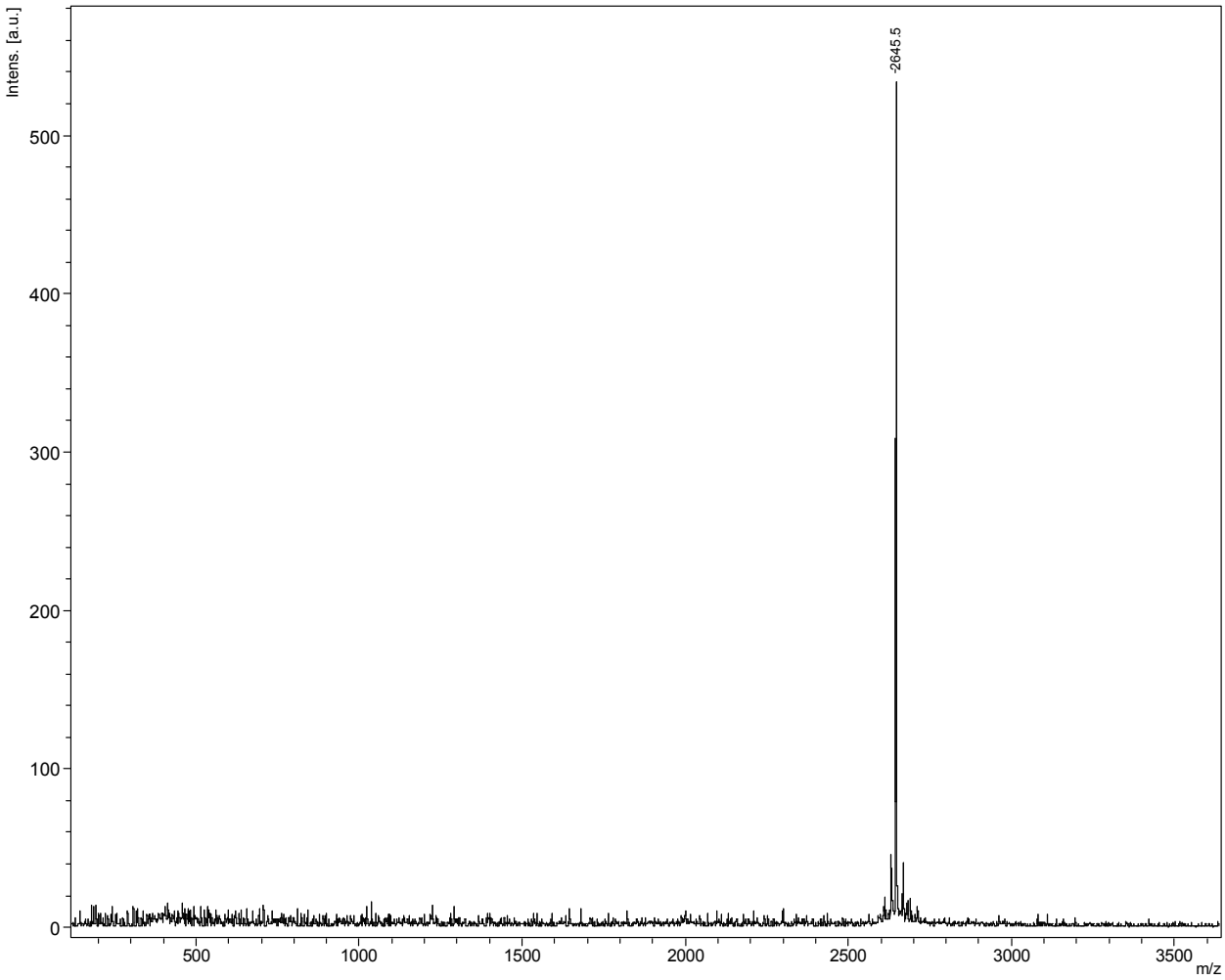

6.1

HPLC: Gradient = 10-75% solvent B over 65 minutes

MALDI-TOF: Calculated monoisotopic $[M+H]^+ = 2694.5$

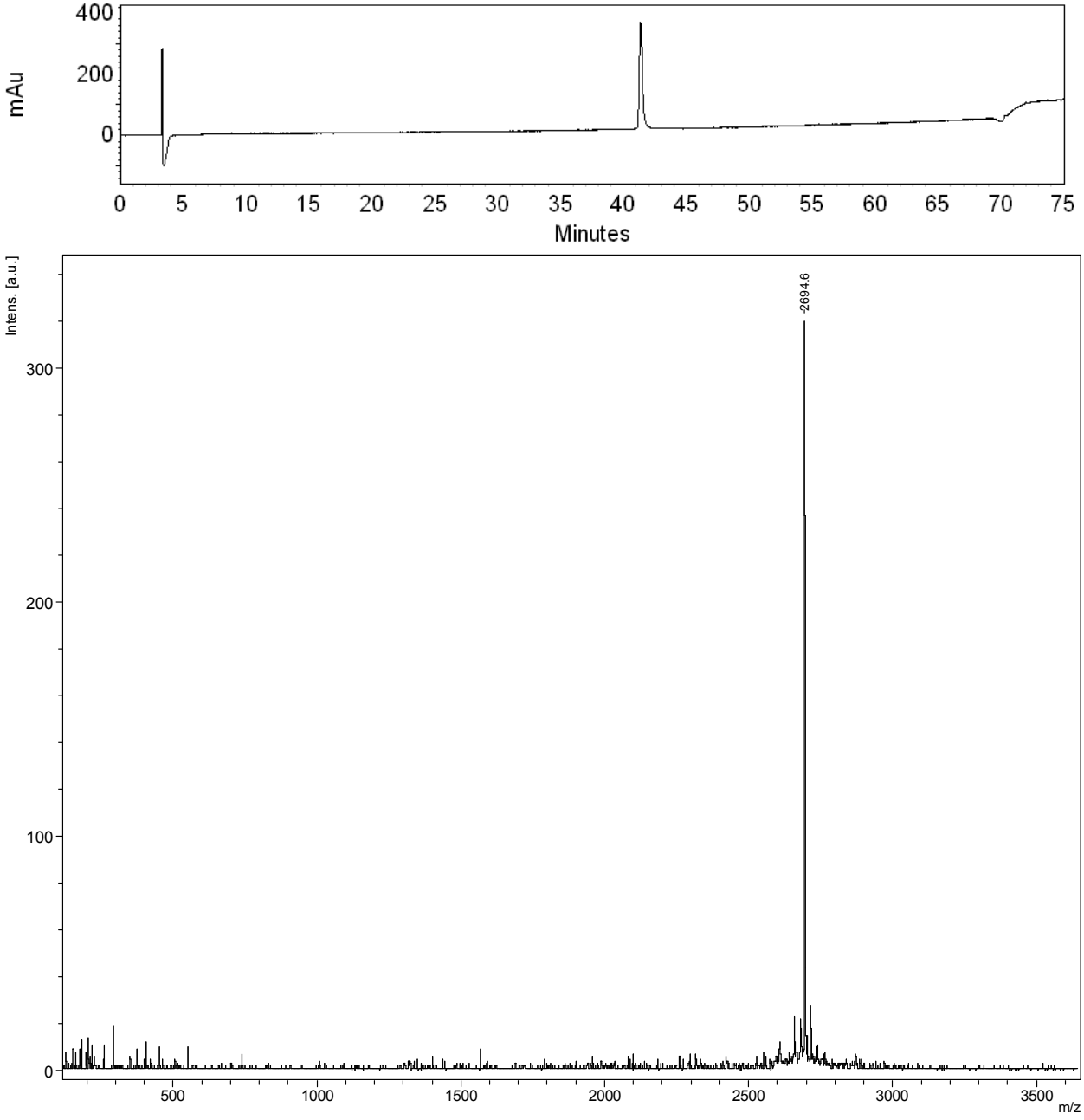

6.2

HPLC: Gradient = 10-75% solvent B over 65 minutes

MALDI-TOF: Calculated monoisotopic $[M+H]^+ = 2674.5$

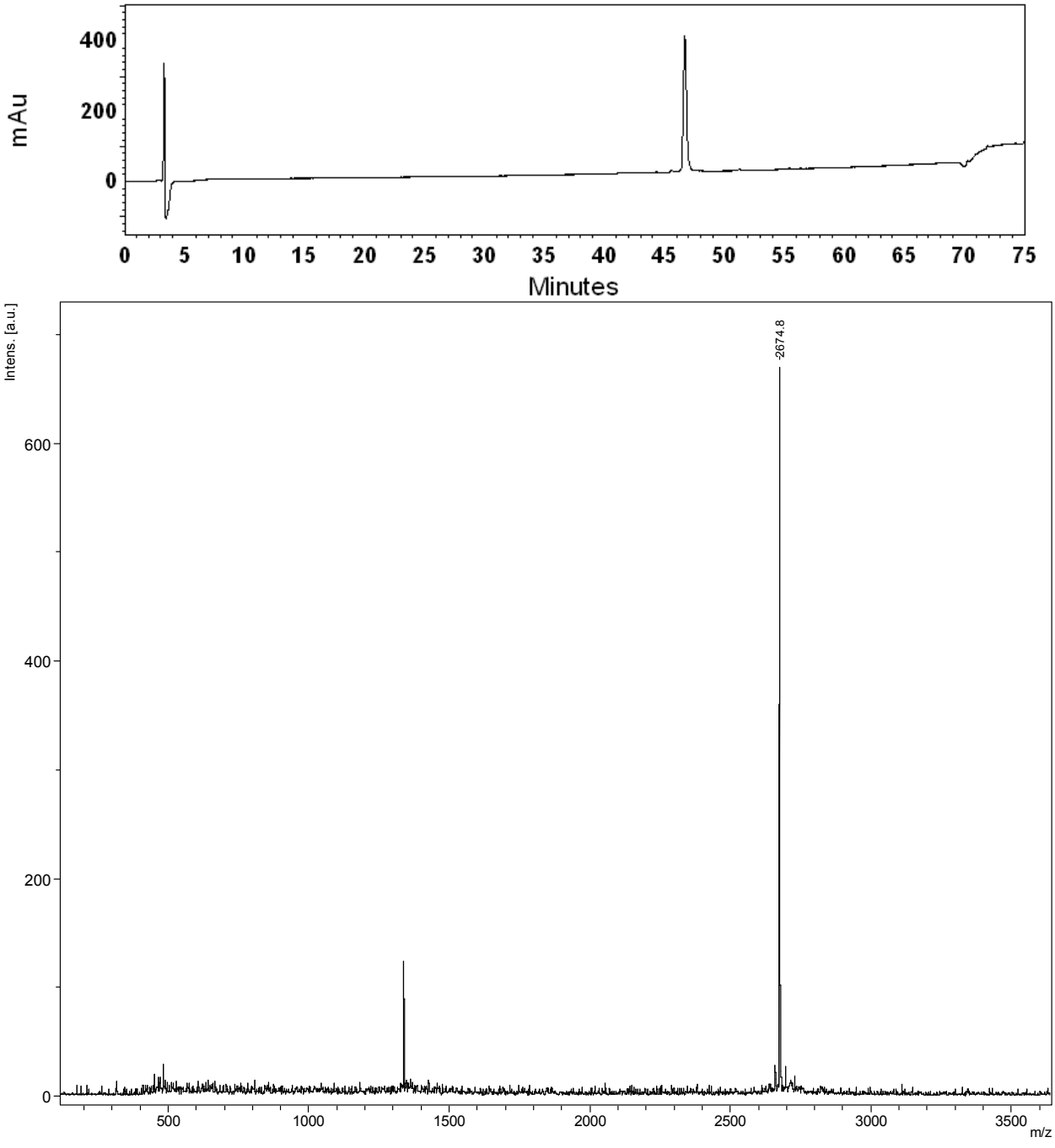

6.3

HPLC: Gradient = 10-75% solvent B over 65 minutes

MALDI-TOF: Calculated monoisotopic $[M+H]^+ = 2722.5$

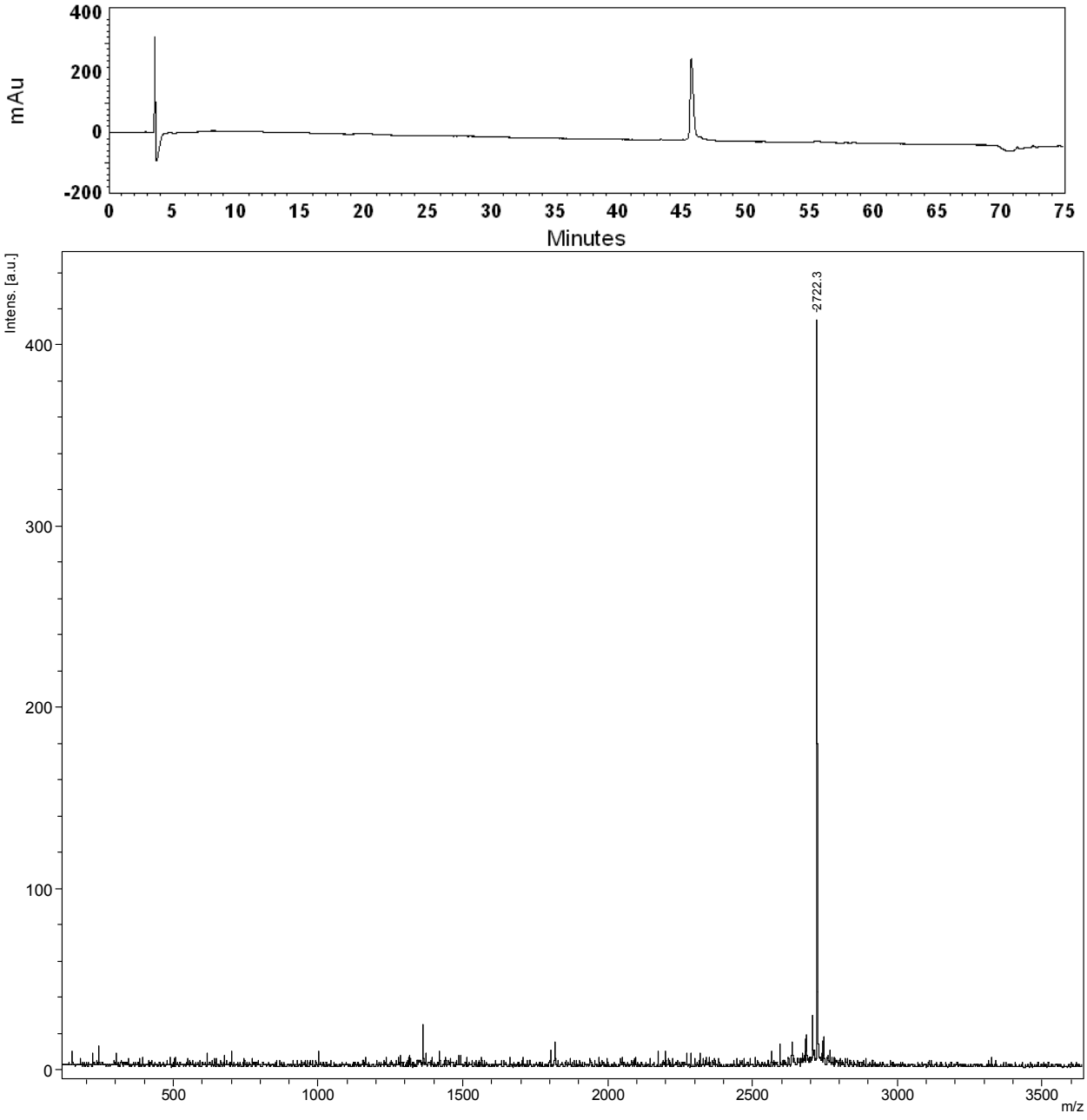

6.4

HPLC: Gradient = 10-75% solvent B over 65 minutes

MALDI-TOF: Calculated monoisotopic $[M+H]^+ = 2666.5$

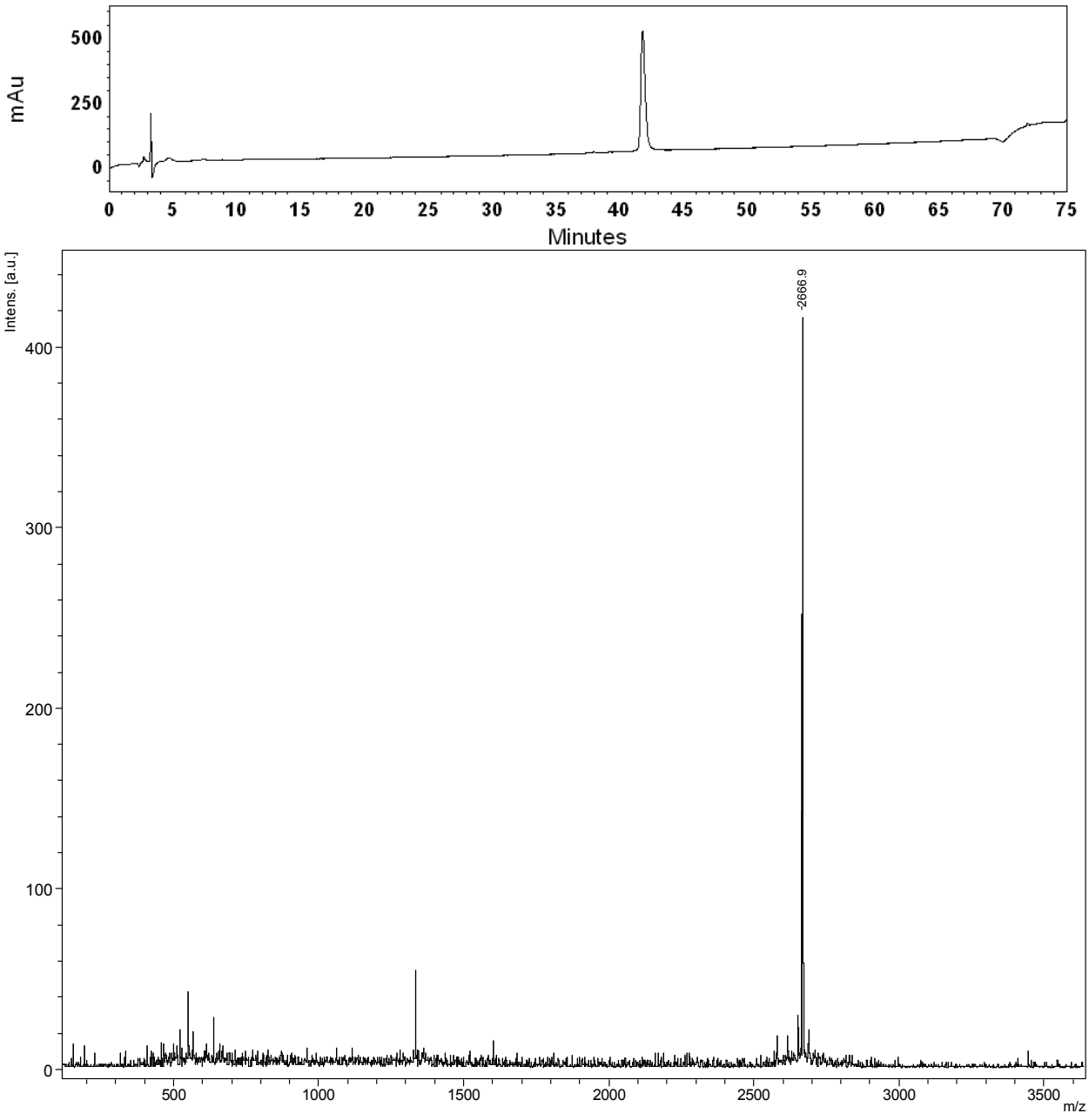

6.5

HPLC: Gradient = 10-75% solvent B over 65 minutes

MALDI-TOF: Calculated monoisotopic $[M+H]^+ = 2650.4$

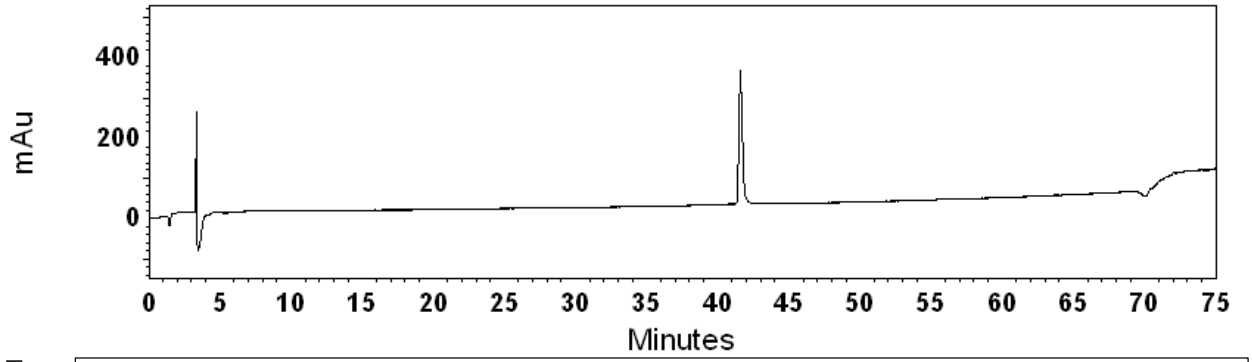

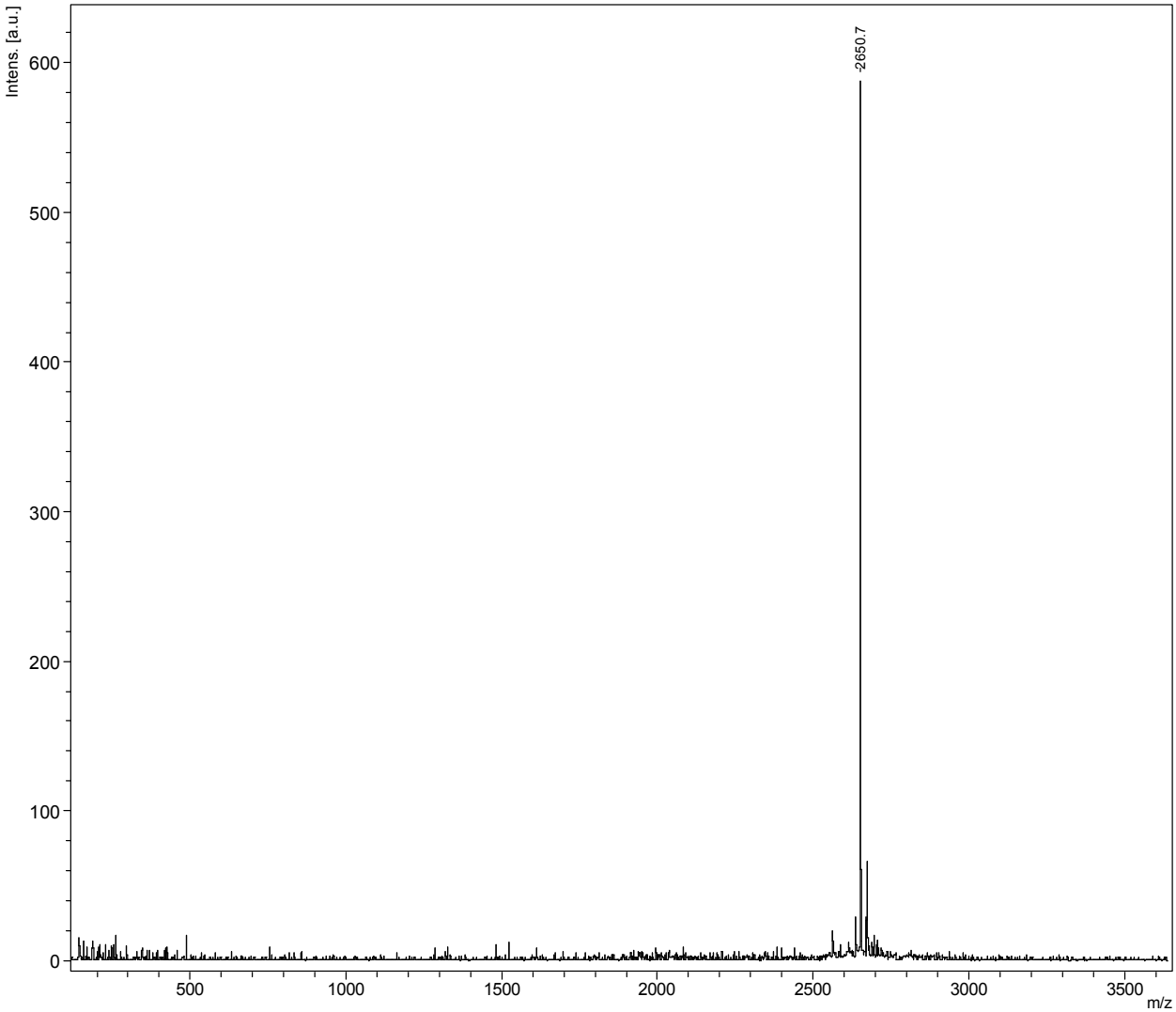

6.6

HPLC: Gradient = 10-90% solvent B over 80 minutes

MALDI-TOF: Calculated monoisotopic $[M+H]^+ = 2832.5$

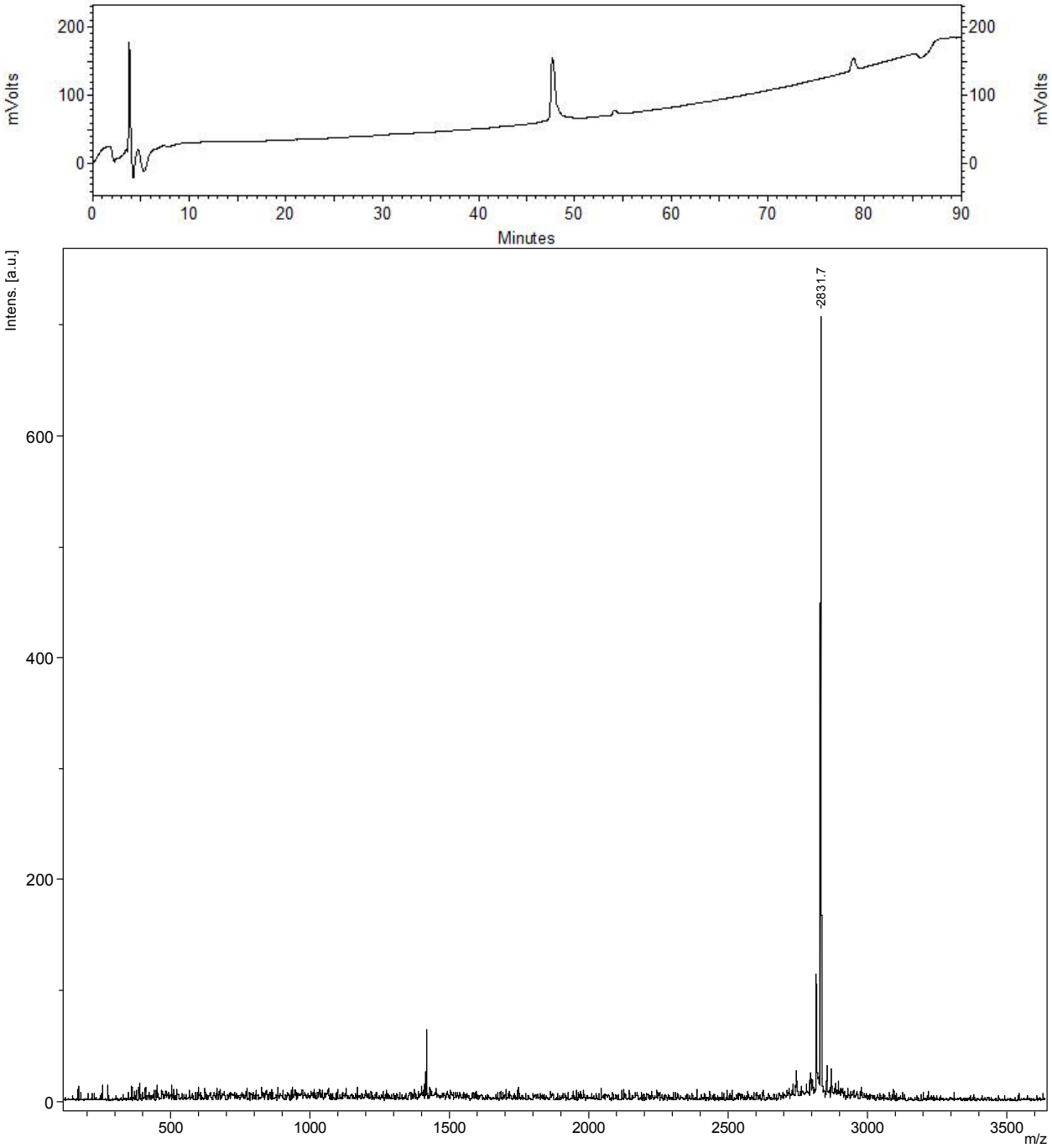

BimSAHB$_{R153D}$
HPLC: Gradient = 10-75% solvent B over 65 minutes
MALDI-TOF: Calculated monoisotopic $[M+H]^+$ = 2605.4

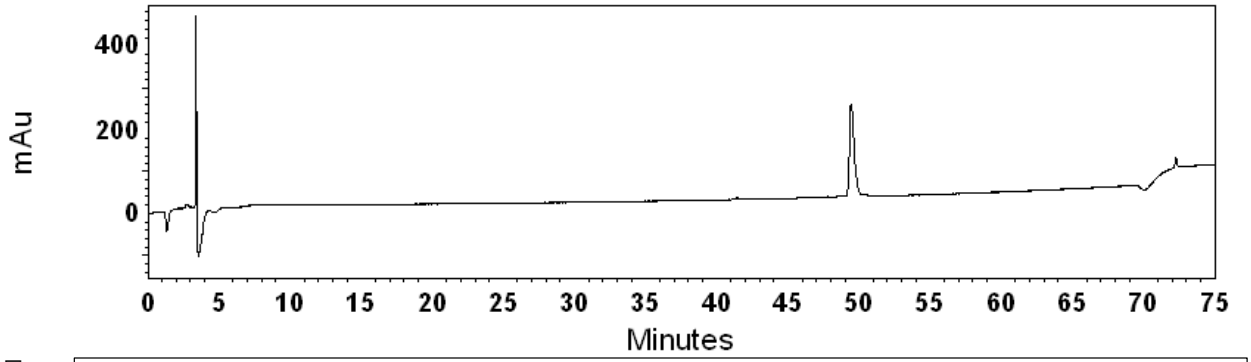

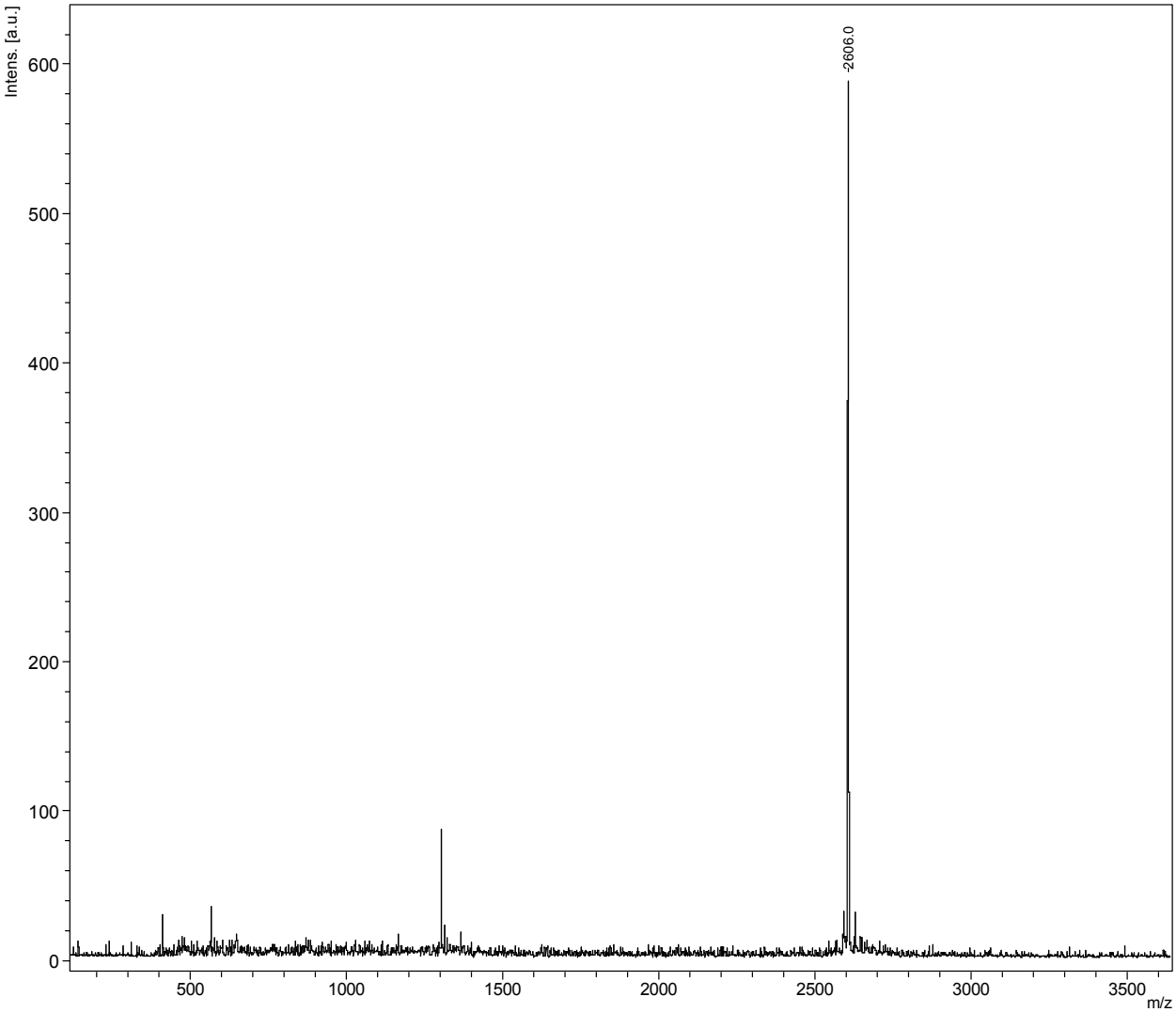

Flu-α-Bim

HPLC: Gradient = 10-75% solvent B over 65 minutes

MALDI-TOF: Calculated monoisotopic $[M+H]^+$ = 2997.4

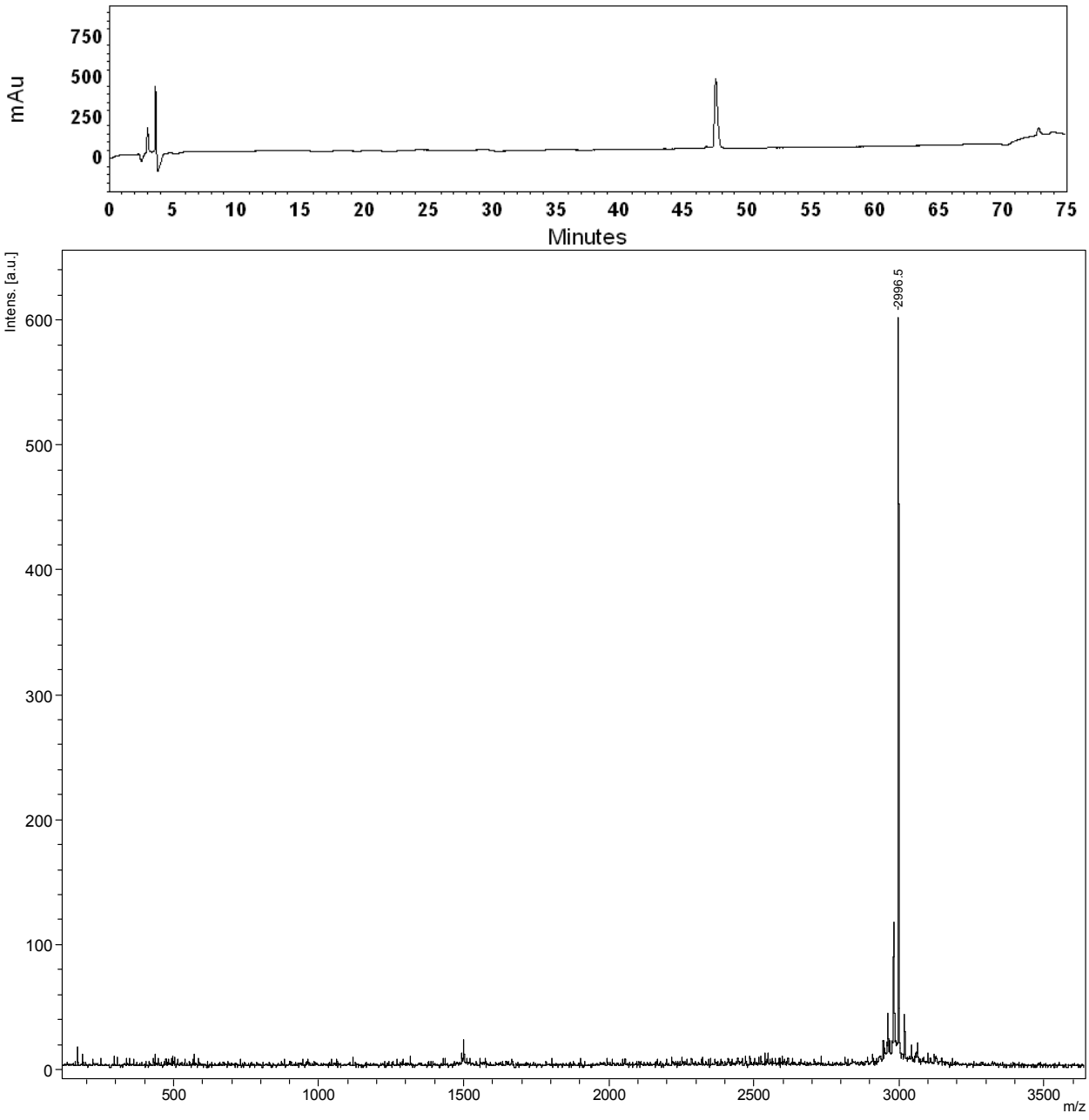

Flu-BimSAHB

HPLC: Gradient = 10-75% solvent B over 65 minutes

MALDI-TOF: Calculated monoisotopic $[M+H]^+$ = 2962.5

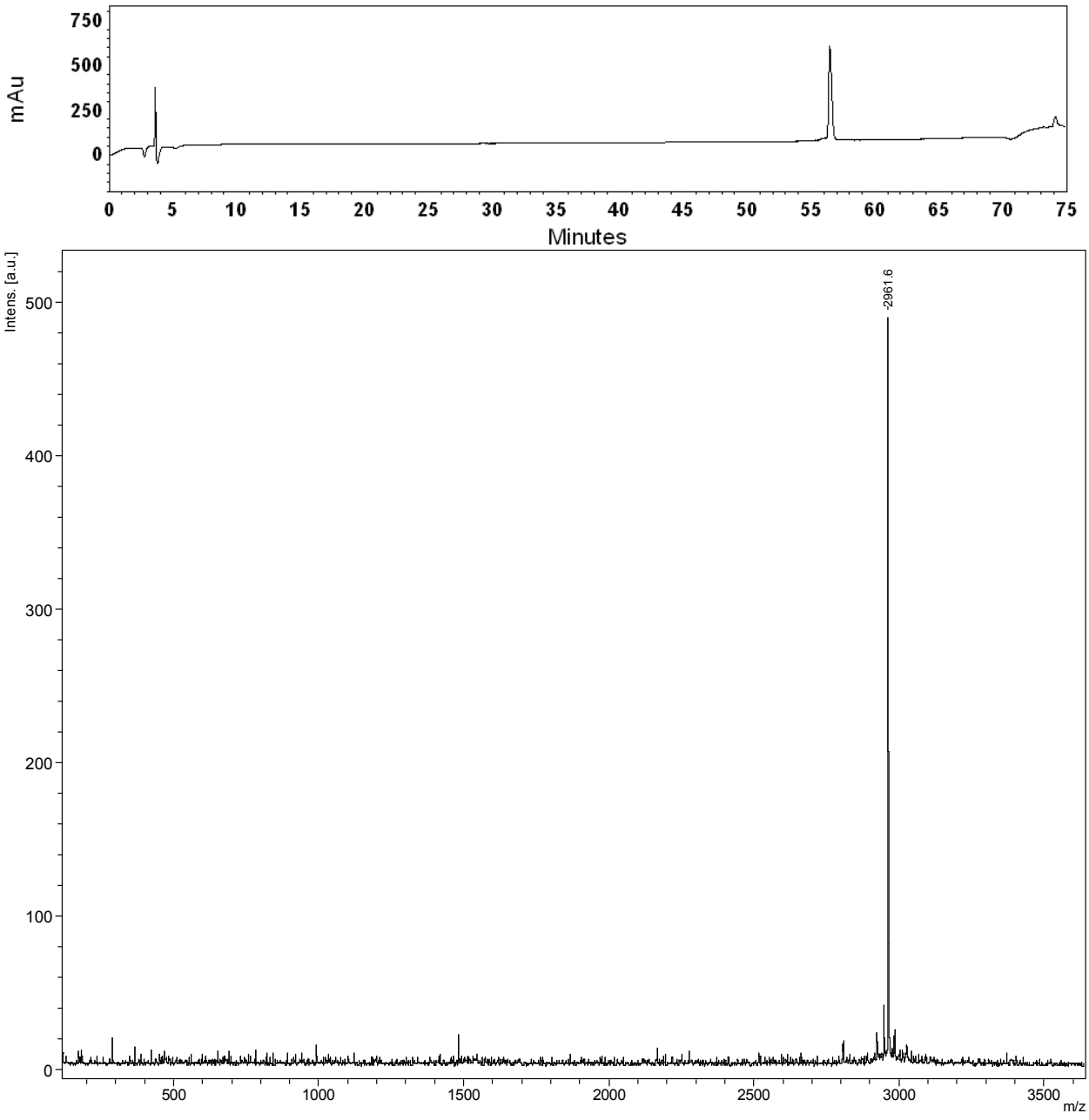

Flu-6.1
HPLC: Gradient = 10-80% solvent B over 70 minutes
MALDI-TOF: Calculated monoisotopic $[M+H]^+$ = 3010.5

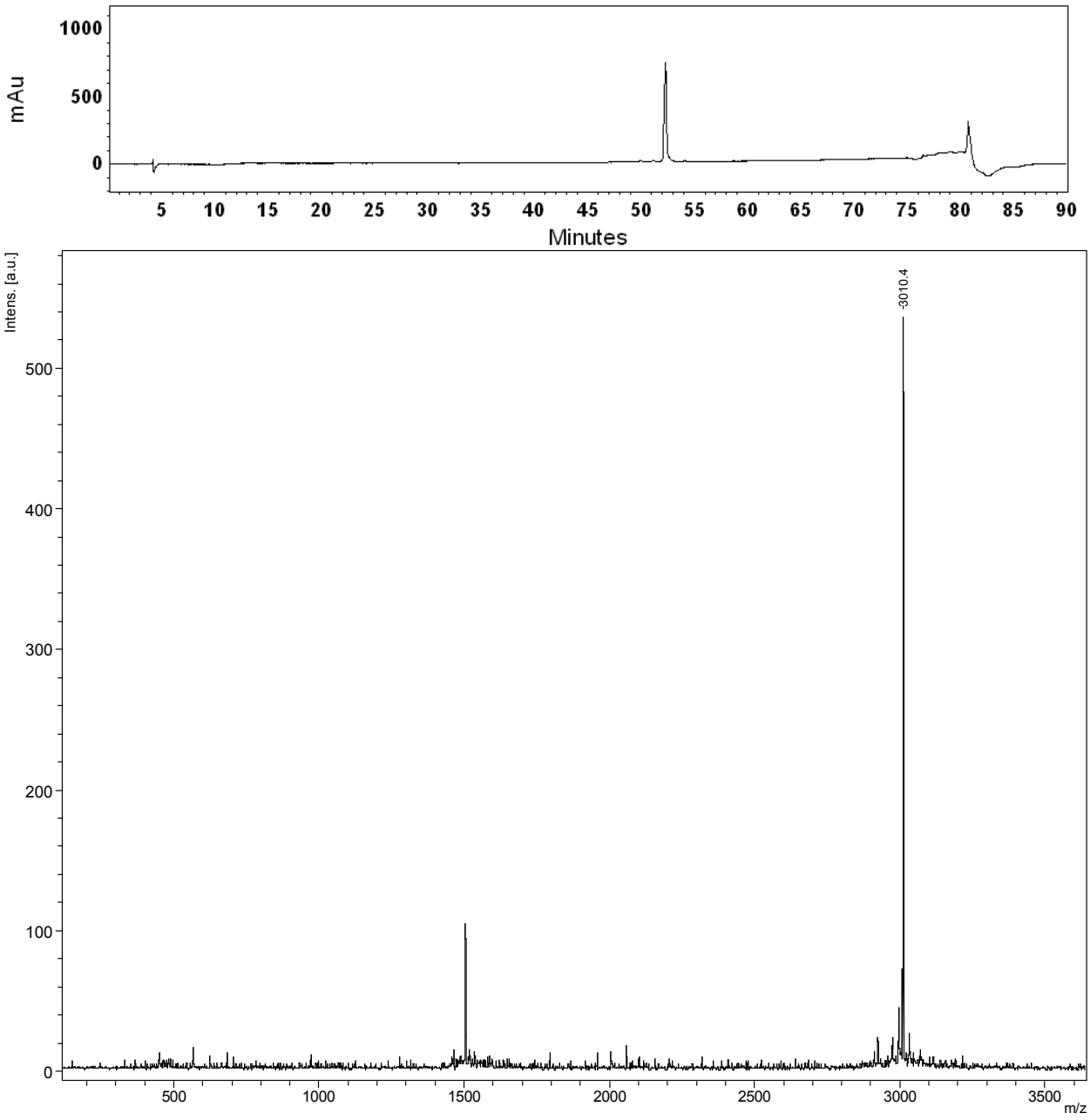

Flu-6.2
HPLC: Gradient = 10-75% solvent B over 65 minutes
MALDI-TOF: Calculated monoisotopic $[M+H]^+$ = 2990.5

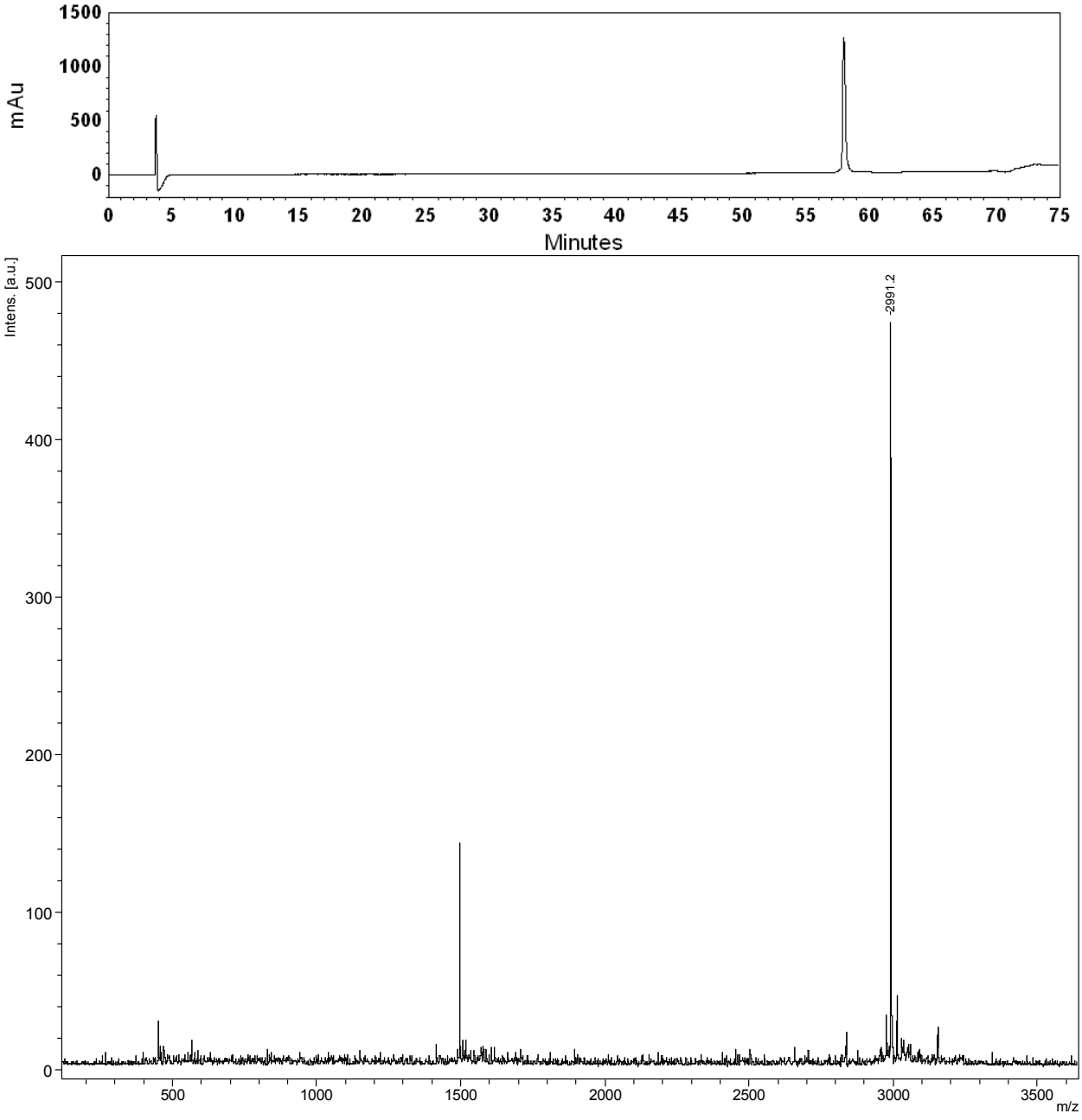

Flu-6.3
HPLC: Gradient = 10-80% solvent B over 70 minutes
MALDI-TOF: Calculated monoisotopic $[M+H]^+$ = 3038.6

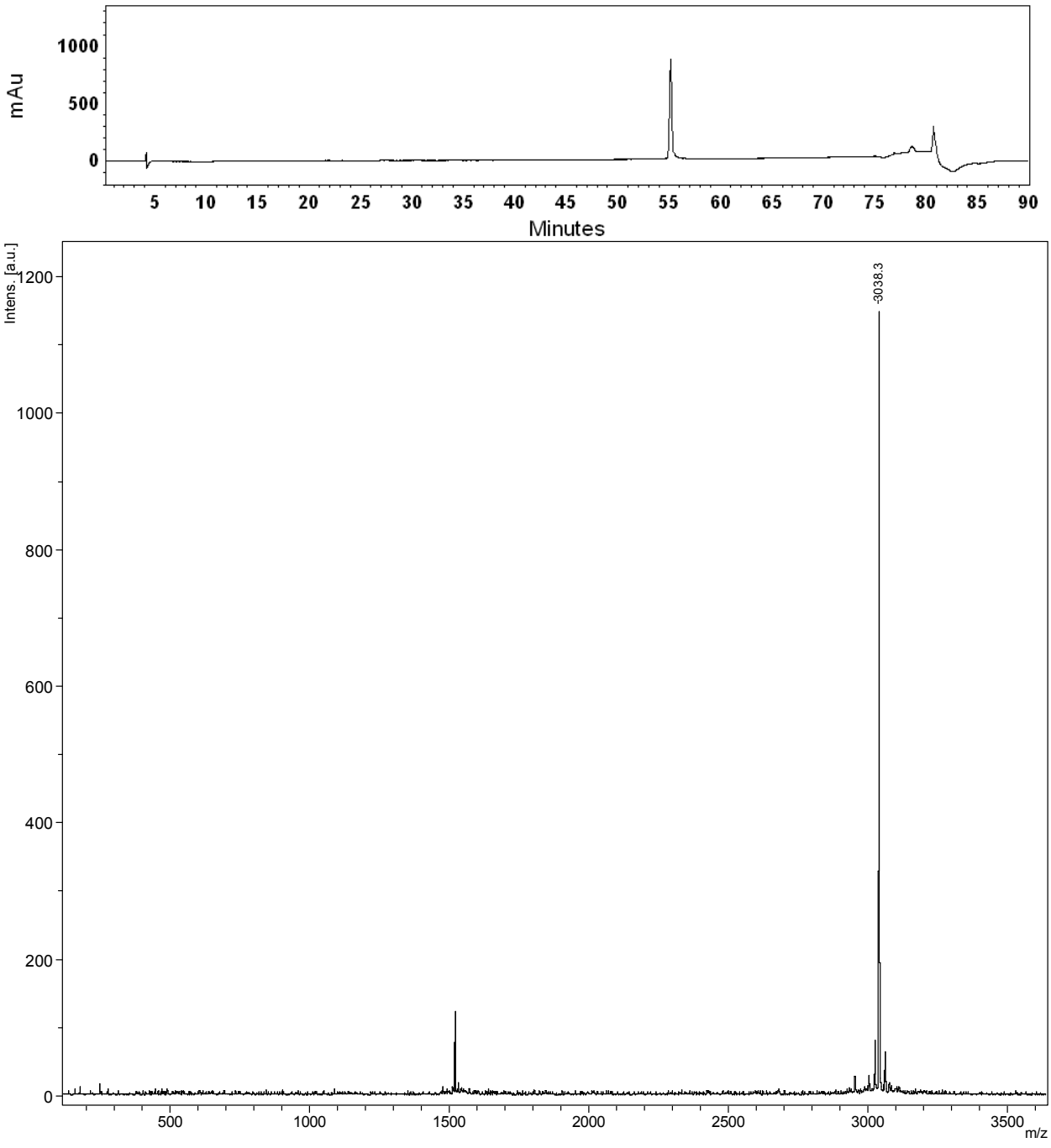

6.9 References

1. Gross, A., McDonnell, J. M., and Korsmeyer, S. J. (1999) BCL-2 family members and the mitochondria in apoptosis, *Genes & Development 13*, 1899-1911.

2. Cory, S., Huang, D. C. S., and Adams, J. M. (2003) The Bcl-2 family: roles in cell survival and oncogenesis, *Oncogene 22*, 8590-8607.

3. Willis, S. N., Fletcher, J. I., Kaufmann, T., van Delft, M. F., Chen, L., Czabotar, P. E., Ierino, H., Lee, E. F., Fairlie, W. D., Bouillet, P., Strasser, A., Kluck, R. M., Adams, J. M., and Huang, D. C. S. (2007) Apoptosis initiated when BH3 ligands engage multiple Bcl-2 homologs, not Bax or Bak, *Science 315*, 856-859.

4. Oltersdorf, T., Elmore, S. W., Shoemaker, A. R., Armstrong, R. C., Augeri, D. J., Belli, B. A., Bruncko, M., Deckwerth, T. L., Dinges, J., Hajduk, P. J., Joseph, M. K., Kitada, S., Korsmeyer, S. J., Kunzer, A. R., Letai, A., Li, C., Mitten, M. J., Nettesheim, D. G., Ng, S., Nimmer, P. M., O'Connor, J. M., Oleksijew, A., Petros, A. M., Reed, J. C., Shen, W., Tahir, S. K., Thompson, C. B., Tomaselli, K. J., Wang, B. L., Wendt, M. D., Zhang, H. C., Fesik, S. W., and Rosenberg, S. H. (2005) An inhibitor of Bcl-2 family proteins induces regression of solid tumours, *Nature 435*, 677-681.

5. Lessene, G., Czabotar, P. E., and Colman, P. M. (2008) BCL-2 family antagonists for cancer therapy, *Nature Reviews Drug Discovery 7*, 989-1000.

6. Rudin, C. M., Hann, C. L., Garon, E. B., de Oliveira, M. R., Bonomi, P. D., Camidge, D. R., Chu, Q., Giaccone, G., Khaira, D., Ramalingam, S. S., Ranson, M. R., Dive, C., McKeegan, E. M., Chyla, B. J., Dowell, B. L., Chakravartty, A., Nolan, C. E., Rudersdorf, N., Busman, T. A., Mabry, M. H., Krivoshik, A. P., Humerickhouse, R. A., Shapiro, G. I., and Gandhi, L. (2012) Phase II Study of Single-Agent Navitoclax (ABT-263) and Biomarker Correlates in Patients with Relapsed Small Cell Lung Cancer, *Clinical Cancer Research 18*, 3163-3169.

7. Pan, R. Q., Hogdal, L. J., Benito, J. M., Bucci, D., Han, L., Borthakur, G., Cortes, J., DeAngelo, D. J., Debose, L., Mu, H., Dohner, H., Gaidzik, V. I., Galinsky, I., Golfman, L. S., Haferlach, T., Harutyunyan, K. G., Hu, J. H., Leverson, J. D., Marcucci, G., Muschen, M., Newman, R., Park, E., Ruvolo, P. P., Ruvolo, V., Ryan, J., Schindela, S., Zweidler-McKay, P., Stone, R. M., Kantarjian, H., Andreeff, M., Konopleva, M., and Letai, A. G. (2014) Selective BCL-2 Inhibition by ABT-199 Causes On-Target Cell Death in Acute Myeloid Leukemia, *Cancer Discovery 4*, 362-375.

8. Lau, Y. H., De Andrade, P., Wu, Y. T., and Spring, D. R. (2015) Peptide stapling techniques based on different macrocyclisation chemistries, *Chemical Society Reviews 44*, 91-102.

9. Felix, A. M., Heimer, E. P., Wang, C. T., Lambros, T. J., Fournier, A., Mowles, T. F., Maines, S., Campbell, R. M., Wegrzynski, B. B., Toome, V., Fry, D., and Madison, V. S. (1988) Synthesis, biological activity and conformational analysis of cyclic GRF analogs, *International Journal of Peptide and Protein Research 32*, 441-454.

10. Murage, E. N., Gao, G. Z., Bisello, A., and Ahn, J. M. (2010) Development of Potent Glucagon-like Peptide-1 Agonists with High Enzyme Stability via Introduction of Multiple Lactam Bridges, *Journal of Medicinal Chemistry 53*, 6412-6420.

11. Okamoto, T., Zobel, K., Fedorova, A., Quan, C., Yang, H., Fairbrother, W. J., Huang, D. C. S., Smith, B. J., Deshayes, K., and Czabotar, P. E. (2013) Stabilizing the Pro-Apoptotic BimBH3 Helix (BimSAHB) Does Not Necessarily Enhance Affinity or Biological Activity, *Acs Chemical Biology 8*, 297-302.

12. Jo, H., Meinhardt, N., Wu, Y., Kulkarni, S., Hu, X., Low, K. E., Davies, P. L., DeGrado, W. F., and Greenbaum, D. C. (2012) Development of alpha-Helical Calpain Probes by Mimicking a Natural Protein-Protein Interaction, *Journal of the American Chemical Society 134*, 17704-17713.

13. Blackwell, H. E., and Grubbs, R. H. (1998) Highly efficient synthesis of covalently cross-linked peptide helices by ring-closing metathesis, *Angewandte Chemie-International Edition 37*, 3281-3284.

14. Blackwell, H. E., Sadowsky, J. D., Howard, R. J., Sampson, J. N., Chao, J. A., Steinmetz, W. E., O'Leary, D. J., and Grubbs, R. H. (2001) Ring-closing metathesis of olefinic peptides: Design, synthesis, and structural characterization of macrocyclic helical peptides, *Journal of Organic Chemistry 66*, 5291-5302.

15. Wang, D. Y., Liao, W., and Arora, P. S. (2005) Enhanced metabolic stability and protein-binding properties of artificial a helices derived from a hydrogen-bond surrogate: Application to Bcl-xL, *Angewandte Chemie-International Edition 44*, 6525-6529.

16. Schafmeister, C. E., Po, J., and Verdine, G. L. (2000) An all-hydrocarbon cross-linking system for enhancing the helicity and metabolic stability of peptides, *Journal of the American Chemical Society 122*, 5891-5892.

17. Walensky, L. D., and Bird, G. H. (2014) Hydrocarbon-Stapled Peptides: Principles, Practice, and Progress, *Journal of Medicinal Chemistry 57*, 6275-6288.

18. Cromm, P. M., Spiegal, J., and Grossmann, T. N. (2015) Hydrocarbon Stapled Peptides as Modulators of Biological Function, *ACS Chemical Biology 10*, 1362-1375.

19. Walensky, L. D., Kung, A. L., Escher, I., Malia, T. J., Barbuto, S., Wright, R. D., Wagner, G., Verdine, G. L., and Korsmeyer, S. J. (2004) Activation of apoptosis in vivo by a hydrocarbon-stapled BH3 helix, *Science 305*, 1466-1470.

20. Walensky, L. D., Pitter, K., Morash, J., Oh, K. J., Barbuto, S., Fisher, J., Smith, E., Verdine, G. L., and Korsmeyer, S. J. (2006) A stapled BID BH3 helix directly binds and activates BAX, *Molecular Cell 24*, 199-210.

21. Bernal, F., Tyler, A. F., Korsmeyer, S. J., Walensky, L. D., and Verdine, G. L. (2007) Reactivation of the p53 tumor suppressor pathway by a stapled p53 peptide, *Journal of the American Chemical Society 129*, 2456-2457.

22. Bird, G. H., Madani, N., Perry, A. F., Princiotto, A. M., Supko, J. G., He, X. Y., Gavathiotis, E., Sodroski, J. G., and Walensky, L. D. (2010) Hydrocarbon double-stapling remedies the proteolytic instability of a lengthy peptide therapeutic, *Proceedings of the National Academy of Sciences of the United States of America 107*, 14093-14098.

23. Stewart, M. L., Fire, E., Keating, A. E., and Walensky, L. D. (2010) The MCL-1 BH3 helix is an exclusive MCL-1 inhibitor and apoptosis sensitizer, *Nature Chemical Biology 6*, 595-601.

24. Bernal, F., Wade, M., Godes, M., Davis, T. N., Whitehead, D. G., Kung, A. L., Wahl, G. M., and Walensky, L. D. (2010) A Stapled p53 Helix Overcomes HDMX-Mediated Suppression of p53, *Cancer Cell 18*, 411-422.

25. Bautista, A. D., Appelbaum, J. S., Craig, C. J., Michel, J., and Schepartz, A. (2010) Bridged beta(3)-Peptide Inhibitors of p53-hDM2 Complexation: Correlation between Affinity and Cell Permeability, *Journal of the American Chemical Society 132*, 2904-2906.

26. LaBelle, J. L., Katz, S. G., Bird, G. H., Gavathiotis, E., Stewart, M. L., Lawrence, C., Fisher, J. K., Godes, M., Pitter, K., Kung, A. L., and Walensky, L. D. (2012) A stapled BIM peptide overcomes apoptotic resistance in hematologic cancers, *Journal of Clinical Investigation 122*, 2018-2031.

27. Chang, Y. S., Graves, B., Guerlavais, V., Tovar, C., Packman, K., To, K. H., Olson, K. A., Kesavan, K., Gangurde, P., Mukherjee, A., Baker, T., Darlak, K., Elkin, C., Filipovic, Z., Qureshi, F. Z., Cai, H. L., Berry, P., Feyfant, E., Shi, X. G. E., Horstick, J., Annis, D. A., Manning, A. M., Fotouhi, N., Nash, H., Vassilev, L. T., and Sawyer, T. K. (2013) Stapled alpha-helical peptide drug development: A potent dual inhibitor of MDM2 and MDMX for p53-dependent cancer therapy, *Proceedings of the National Academy of Sciences of the United States of America 110*, E3445-E3454.

28. Edwards, A. L., Gavathiotis, E., LaBelle, J. L., Braun, C. R., Opoku-Nsiah, K. A., Bird, G. H., and Walensky, L. D. (2013) Multimodal Interaction with BCL-2 Family Proteins Underlies the Proapoptotic Activity of PUMA BH3, *Chemistry & Biology 20*, 888-902.

29. Sinclair, J. K. L., Denton, E. V., and Schepartz, A. (2014) Inhibiting Epidermal Growth Factor Receptor at a Distance, *Journal of the American Chemical Society 136*, 11232-11235.

30. Hilinski, G. J., Kim, Y. W., Hong, J., Kutchukian, P. S., Crenshaw, C. M., Berkovitch, S. S., Chang, A., Ham, S., and Verdine, G. L. (2014) Stitched alpha-Helical Peptides via Bis Ring-Closing Metathesis, *Journal of the American Chemical Society 136*, 12314-12322.

31. Bird, G. H., Irimia, A., Ofek, G., Kwong, P. D., Wilson, I. A., and Walensky, L. D. (2014) Stapled HIV-1 peptides recapitulate antigenic structures and engage broadly neutralizing antibodies, *Nature Structural & Molecular Biology 21*, 1058-1067.

32. Pitter, K., Bernal, F., LaBelle, J., and Walensky, L. D. (2008) Dissection of the BCL-2 family signaling network with stabilized alpha-helices of BCL-2 domains, *Programmed Cell Death, the Biology and Therapeutic Implications of Cell Death, Part B 446*, 387-408.

33. Bird, G. H., Bernal, F., Pitter, K., and Walensky, L. D. (2008) Synthesis and biophysical characterization of stabilized alpha-helices of BCL-2 domains, *Programmed Cell Death, the Biology and Therapeutic Implications of Cell Death, Part B 446*, 369-386.

34. Karle, I. L., and Balaram, P. (1990) Structural characteristics of alpha-helical peptide molecules containing Aib residues, *Biochemistry 29*, 6747-6756.

35. Yamaguchi, H., Kodama, H., Osada, S., Kato, F., Jelokhani-Niaraki, M., and Kondo, M. (2003) Effect of alpha,alpha-dialkyl amino acids on the protease resistance of peptides, *Bioscience Biotechnology and Biochemistry 67*, 2269-2272.

36. Chu, Q., Moellering, R. E., Hilinski, G. J., Kim, Y. W., Grossmann, T. N., Yeh, J. T. H., and Verdine, G. L. (2015) Towards understanding cell penetration by stapled peptides, *Medchemcomm 6*, 111-119.

37. Lee, E. F., Sadowsky, J. D., Smith, B. J., Czabotar, P. E., Peterson-Kaufman, K. J., Colman, P. M., Gellman, S. H., and Fairlie, W. D. (2009) High-Resolution Structural Characterization of a Helical alpha/beta-Peptide Foldamer Bound to the Anti-Apoptotic Protein Bcl-x(L), *Angewandte Chemie-International Edition 48*, 4318-4322.

38. Gavathiotis, E., Suzuki, M., Davis, M. L., Pitter, K., Bird, G. H., Katz, S. G., Tu, H. C., Kim, H., Cheng, E. H. Y., Tjandra, N., and Walensky, L. D. (2008) BAX activation is initiated at a novel interaction site, *Nature 455*, 1076-1081.

39. Bird, G. H., Gavathiotis, E., LaBelle, J. L., Katz, S. G., and Walensky, L. D. (2014) Distinct BimBH3 (BimSAHB) Stapled Peptides for Structural and Cellular Studies, *Acs Chemical Biology 9*, 831-837.

40. Okamoto, T., Segal, D., Zobel, K., Fedorova, A., Yang, H., Fairbrother, W. J., Huang, D. C. S., Smith, B. J., Deshayes, K., and Czabotar, P. E. (2014) Further Insights into the Effects of Pre-organizing the BimBH3 Helix, *Acs Chemical Biology 9*, 838-839.

41. Peterson-Kaufman, K. J., Haase, H. S., Boersma, M. D., Lee, E. F., Fairlie, W. D., and Gellman, S. H. (2015) Residue-Based Preorganization of BH3-Derived α/β-Peptides: Modulating Affinity, Selectivity and Proteolytic Susceptibility in α-Helix Mimics, *ACS Chemical Biology 10*, 1667-1675.

42. Horne, W. S., Price, J. L., Keck, J. L., and Gellman, S. H. (2007) Helix bundle quaternary structure from alpha/beta-peptide foldamers, *Journal of the American Chemical Society 129*, 4178-4180.

43. Lee, E. F., Smith, B. J., Horne, W. S., Mayer, K. N., Evangelista, M., Colman, P. M., Gellman, S. H., and Fairlie, W. D. (2011) Structural Basis of Bcl-x(L) Recognition by a BH3-Mimetic alpha/beta-Peptide Generated by Sequence-Based Design, *Chembiochem 12*, 2025-2032.

44. Sattler, M., Liang, H., Nettesheim, D., Meadows, R. P., Harlan, J. E., Eberstadt, M., Yoon, H. S., Shuker, S. B., Chang, B. S., Minn, A. J., Thompson, C. B., and Fesik, S. W. (1997) Structure of Bcl-x(L)-Bak peptide complex: Recognition between regulators of apoptosis, *Science 275*, 983-986.

45. Smits, C., Czabotar, P. E., Hinds, M. G., and Day, C. L. (2008) Structural plasticity underpins promiscuous binding of the prosurvival protein a1, *Structure 16*, 818-829.

46. Czabotar, P. E., Lee, E. F., van Delft, M. F., Day, C. L., Smith, B. J., Huang, D. C. S., Fairlie, W. D., Hinds, M. G., and Colman, P. M. (2007) Structural insights into the

degradation of Mcl-1 induced by BH3 domains, *Proceedings of the National Academy of Sciences of the United States of America 104*, 6217-6222.

47. Ku, B., Liang, C. Y., Jung, J. U., and Oh, B. H. (2011) Evidence that inhibition of BAX activation by BCL-2 involves its tight and preferential interaction with the BH3 domain of BAX, *Cell Research 21*, 627-641.

48. Willis, S. N., Chen, L., Dewson, G., Wei, A., Naik, E., Fletcher, J. I., Adams, J. M., and Huang, D. C. S. (2005) Proapoptotic Bak is sequestered by Mcl-1 and Bcl-x(L), but not Bcl-2, until displaced by BH3-only proteins, *Genes & Development 19*, 1294-1305.

49. Sinclair, J. K. L., and Schepartz, A. (2014) Influence of Macrocyclization on Allosteric, Juxtamembrane-Derived, Stapled Peptide Inhibitors of the Epidermal Growth Factor Receptor (EGFR), *Organic Letters 16*, 4916-4919.

50. Schmidt, N., Mishra, A., Lai, G. H., and Wong, G. C. L. (2010) Arginine-rich cell-penetrating peptides, *Febs Letters 584*, 1806-1813.

51. Mitchell, D. J., Kim, D. T., Steinman, L., Fathman, C. G., and Rothbard, J. B. (2000) Polyarginine enters cells more efficiently than other polycationic homopolymers, *Journal of Peptide Research 56*, 318-325.

52. Demizu, Y., Oba, M., Okitsu, K., Yamashita, H., Misawa, T., Tanaka, M., Kurihara, M., and Gellman, S. H. (2015) A preorganized beta-amino acid bearing a guanidinium side chain and its use in cell-penetrating peptides, *Organic & Biomolecular Chemistry 13*, 5617-5620.

53. Pollaro, L., and Heinis, C. (2010) Strategies to prolong the plasma residence time of peptide drugs, *Medchemcomm 1*, 319-324.

54. Horne, W. S., Boersma, M. D., Windsor, M. A., and Gellman, S. H. (2008) Sequence-based design of alpha/beta-peptide foldamers that mimic BH3 domains, *Angewandte Chemie-International Edition 47*, 2853-2856.

55. Horne, W. S., Johnson, L. M., Ketas, T. J., Klasse, P. J., Lu, M., Moore, J. P., and Gellman, S. H. (2009) Structural and biological mimicry of protein surface recognition by alpha/beta-peptide foldamers, *Proceedings of the National Academy of Sciences of the United States of America 106*, 14751-14756.

56. Johnson, L. M., and Gellman, S. H. (2013) alpha-Helix Mimicry with alpha/beta-Peptides, *Methods in Protein Design 523*, 407-429.

57. Cheloha, R. W., Maeda, A., Dean, T., Gardella, T. J., and Gellman, S. H. (2014) Backbone modification of a polypeptide drug alters duration of action in vivo, *Nature Biotechnology 32*, 653-655.

58. Glaser, S. P., Lee, E. F., Trounson, E., Bouillet, P., Wei, A., Fairlie, W. D., Izon, D. J., Zuber, J., Rappaport, A. R., Herold, M. J., Alexander, W. S., Lowe, S. W., Robb, L., and Strasser, A. (2012) Anti-apoptotic Mcl-1 is essential for the development and sustained growth of acute myeloid leukemia, *Genes & Development 26*, 120-125.

59. Li, Y. C., Rodewald, L. W., Hoppmann, C., Wong, E. T., Lebreton, S., Safar, P., Patek, M., Wang, L., Wertman, K. F., and Wahl, G. M. (2014) A Versatile Platform to Analyze

Low-Affinity and Transient Protein-Protein Interactions in Living Cells in Real Time, *Cell Reports 9*, 1946-1958.

60. Toniolo, C., Bonora, G. M., Bavoso, A., Benedetti, E., Diblasio, B., Pavone, V., and Pedone, C. (1983) Preferred conformations of peptides containing alpha, alpha-disubstituted alpha-amino acids, *Biopolymers 22*, 205-215.

61. Bhattacharya, S., Zhang, H. T., Cowburn, D., and Debnath, A. K. (2012) Novel structures of self-associating stapled peptides, *Biopolymers 97*, 253-264.

62. Haase, H. S., Peterson-Kaufman, K. J., Levengood, S. K. L., Checco, J. W., Murphy, W. L., and Gellman, S. H. (2012) Extending Foldamer Design beyond alpha-Helix Mimicry: alpha/beta-Peptide Inhibitors of Vascular Endothelial Growth Factor Signaling, *Journal of the American Chemical Society 134*, 7652-7655.

63. Boersma, M. D., Haase, H. S., Peterson-Kaufman, K. J., Lee, E. F., Clarke, O. B., Colman, P. M., Smith, B. J., Horne, W. S., Fairlie, W. D., and Gellman, S. H. (2012) Evaluation of Diverse alpha/beta-Backbone Patterns for Functional alpha-Helix Mimicry: Analogues of the Bim BH3 Domain, *Journal of the American Chemical Society 134*, 315-323.

64. Lee, H. S., LePlae, P. R., Porter, E. A., and Gellman, S. H. (2001) An efficient route to either enantiomer of orthogonally protected trans-3-aminopyrrolidine-4-carboxylic acid, *Journal of Organic Chemistry 66*, 3597-3599.

65. Horne, W. S., Price, J. L., and Gellman, S. H. (2008) Interplay among side chain sequence, backbone composition, and residue rigidification in polypeptide folding and assembly, *Proceedings of the National Academy of Sciences of the United States of America 105*, 9151-9156.

66. Kim, Y. W., Grossmann, T. N., and Verdine, G. L. (2011) Synthesis of all-hydrocarbon stapled alpha-helical peptides by ring-closing olefin metathesis, *Nature Protocols 6*, 761-771.

67. Lee, E. F., Dewson, G., Smith, B. J., Evangelista, M., Pettikiriarachchi, A., Dogovski, C., Perugini, M. A., Colman, P. M., and Fairlie, W. D. (2011) Crystal Structure of a BCL-W Domain-Swapped Dimer: Implications for the Function of BCL-2 Family Proteins, *Structure 19*, 1467-1476.

68. Petros, A. M., Medek, A., Nettesheim, D. G., Kim, D. H., Yoon, H. S., Swift, K., Matayoshi, E. D., Oltersdorf, T., and Fesik, S. W. (2001) Solution structure of the antiapoptotic protein bcl-2, *Proceedings of the National Academy of Sciences of the United States of America 98*, 3012-3017.

69. Smith, B. J., Lee, E. F., Checco, J. W., Evangelista, M., Gellman, S. H., and Fairlie, W. D. (2013) Structure-guided rational design of alpha/beta-peptide foldamers with high affinity for BCL-2 family prosurvival proteins, *Chembiochem 14*, 1564-1572.

70. Gill, S. C., and Vonhippel, P. H. (1989) Calculation of protein extinction coefficients from amino-acid sequence data, *Analytical Biochemistry 182*, 319-326.

71. Greenfield, N. J. (2006) Using circular dichroism spectra to estimate protein secondary structure, *Nature Protocols 1*, 2876-2890.

72. Kabsch, W. (2010) XDS, *Acta Crystallographica Section D-Biological Crystallography 66*, 125-132.

73. McCoy, A. J., Grosse-Kunstleve, R. W., Storoni, L. C., and Read, R. J. (2005) Likelihood-enhanced fast translation functions, *Acta Crystallographica Section D-Biological Crystallography 61*, 458-464.

74. Read, R. J. (2001) Pushing the boundaries of molecular replacement with maximum likelihood, *Acta Crystallographica Section D-Biological Crystallography 57*, 1373-1382.

75. Storoni, L. C., McCoy, A. J., and Read, R. J. (2004) Likelihood-enhanced fast rotation functions, *Acta Crystallographica Section D-Biological Crystallography 60*, 432-438.

76. Emsley, P., and Cowtan, K. (2004) Coot: model-building tools for molecular graphics, *Acta Crystallographica Section D-Biological Crystallography 60*, 2126-2132.

77. Adams, P. D., Grosse-Kunstleve, R. W., Hung, L. W., Ioerger, T. R., McCoy, A. J., Moriarty, N. W., Read, R. J., Sacchettini, J. C., Sauter, N. K., and Terwilliger, T. C. (2002) PHENIX: building new software for automated crystallographic structure determination, *Acta Crystallographica Section D-Biological Crystallography 58*, 1948-1954.